Origine et évolution de la terrestrialité chez les crocodiliens altirostres

Yohan Pochat-Cottilloux

Université Claude Bernard Lyon 1

THESE de DOCTORAT DE
L'UNIVERSITE CLAUDE BERNARD LYON 1

Ecole Doctorale N° 341
Évolution, Écosystèmes, Microbiologie, Modélisation

Discipline : Sciences de l'Univers

Soutenue publiquement le 13/10/2023, par :
Yohan Pochat-Cottilloux

Origine et évolution de la terrestrialité chez les crocodiliens altirostres

---

Devant le jury composé de :

DELFINO, Massimo	Professeur	Università di Torino	Rapporteur
HOUSSAYE, Alexandra	Directrice de Recherche	MNHN	Rapporteur
CUNY, Gilles	Professeur	LEHNA	Président
BÖHME, Madeleine	Professeure	Universität Tübingen	Examinatrice
MARTIN, Jérémy	Chargé de Recherche	LGL-TPE	Directeur de thèse
AMIOT, Romain	Chargé de Recherche	LGL-TPE	Co-directeur de thèse

‘Traverse la rivière avant d’insulter le crocodile.’

Proverbe kenyan

‘I do not say this lightly; *Pristichampsus* is widely used. Its elimination may lead to confusion in the literature, and, in all likelihood, my own violent death at the hands of my colleagues. Taxonomic stability should be promoted, and I would rather not be killed.’

Christopher Brochu, when talking about the taxonomic status of *Pristichampsus*

Remerciements

Me voilà arrivé au terme de ces trois années de thèse. Cette aventure étant le résultat non seulement de mon travail, mais aussi du travail, de la collaboration et du soutien de nombreuses personnes, je souhaite ici les remercier, et essayer de n'en oublier aucune.

Je tiens en premier lieu à remercier mes encadrants de thèse, Jérémy et Romain, pour m'avoir fait confiance pendant ces trois années et avoir su, chacun à leur manière, m'enseigner de nouvelles choses, ou au contraire y apporter un regard nouveau. Nos discussions scientifiques et conseils professionnels ont pour moi toujours été très stimulants intellectuellement, mais vous avez aussi su mettre de côté le sérieux lorsque cela était nécessaire, et c'est cette flexibilité que j'ai tout particulièrement appréciée. J'espère que nous serons encore amenés à collaborer ensemble, pour ma part ce sera avec plaisir !

I would like to thank the members of the jury, Alexandra Houssaye (Muséum National d'Histoire Naturelle), Massimo Delfino (Università di Torino), Madeleine Böhme (Universität Tübingen) and Gilles Cuny (Université Lyon 1), for agreeing to read and devote some of their time to review my thesis. I hope you enjoy reading it.

Je me dois également de remercier le Laboratoire de Géologie de Lyon, l'Université Lyon 1 et l'ENS de Lyon pour m'avoir accueilli au sein de leurs locaux et m'avoir donné accès à leurs équipements, qui m'ont permis de mener à bien mes travaux de recherche. Je tiens également à remercier le CNRS, qui par le biais du financement ANR accordé à Jérémy Martin (Université Lyon 1), a permis de financer l'intégralité de mes recherches et des dépenses associées. Merci également à l'école doctorale E2M2 pour m'avoir permis d'effectuer mon doctorat dans les meilleures conditions.

Je remercie les membres de mon comité de suivi : Ronan Allain (Muséum National d'Histoire Naturelle), Fabrice Cordey, Stéphane Dray, Laurent Simon & Peggy Vincent (Université Lyon 1). Vous présenter l'avancement de mon travail chaque année m'a été très utile et nos discussions m'ont permis de mener cette thèse de manière sereine et logique.

Cette thèse étant le fruit d'une approche multidisciplinaire, l'implication de nombreuses personnes a été nécessaire pour la mener à bien.

Côté CT scan / données 3D, je tiens à remercier particulièrement Jérôme Adrien et Joël Lachambre (INSA Lyon) pour leur concours sur les tomographes, et d'avoir bien voulu jouer

le jeu de scanner ces dizaines de crânes de crocodiles, et ce toujours avec le sourire. Nos échanges pendant les temps de scan m'ont toujours été très agréables, et promis, plus de crocodiles ! (enfin jusqu'aux prochains…). Après avoir acquis ces données, il a bien fallu les traiter. Pour cela, je remercie Benjamin Dailh, Céline Salaviale, Davide Conedera, Gwendal Perrichon, Jérémy Martin, Jeanne Rolland-Guillard & Nicolas Rinder (Université Lyon 1), pour m'avoir donné un coup de main à la segmentation, au traitement et à l'impression 3D de tous ces scans. Sans eux, la base de données 3D présentée ici ne serait pas aussi complète. Merci également à Lionel Hautier (Université de Montpellier) pour ses conseils avisés en segmentation et géométrie morphométrique 3D.

Les scans utilisés au sein de cette thèse n'auraient cependant pas pu être acquis sans le concours et la confiance de nombreux et nombreuses gestionnaires de collections, qu'il me semble ici important de remercier : Ronan Allain & Nour-Eddine Jalil (Muséum National d'Histoire Naturelle, France), Blandine Bartschi & Emmanuel Robert (Université Lyon 1, France), Didier Berthet (Musée d'Histoire Naturelle de Lyon, France), Christophe Borrely (Muséum d'Histoire Naturelle de Marseille, France), Sébastien Bruaux (Institut Royal des Sciences Naturelles de Belgique, Belgique), Anne-Lise Charrault & Mehdi Mouana (Université de Montpellier, France), Stéphane Jouve (Sorbonne Université, France), Jean Le Loeuff (Musée des Dinosaures d'Espéraza, France), Elisabeth Ludes-Fraulob & Marie Meister (Musée Zoologique de Strasbourg, France), Margarethe Maillart (ENS Lyon, France), Laurent Picot (Paléospace), Baptiste Suchéras-Marx & Bruno Vila (Université d'Aix-Marseille, France), Jean-François Tournepiche (Musée d'Angoulême) et Xavier Valentin (Université de Poitiers).

Furthermore, I would also like to thanks all the colleagues over the world that allowed me access to more scans, either through Open Access data, or collaborations: David Blackburn (Florida Museum of Natural History, United States), Christopher Brochu (University of Iowa, United States), Mario Bronzati & Hussam Zaher (Universidade de São Paulo, Brazil), Patrick Campbell, Vincent Fernandez & Susannah Maidment (National History Museum of the United Kingdom, England), Gustavo Darlim (Universität Tubingen, Germany), Pedro Henrique Fonseca (Universidade Federal do Rio Grande do Sul, Brazil), Yanina Herrera (Universidad Nacional de La Plata, Argentina), Jessie Maisano (Jackson School of Geosciences, United States), Eduardo Puértolas-Pascual (Universidad de Zaragova, Spain), Irena Raselli (University of Fribourg, Switzerland), Jorgo Ristevski (University of Queensland, Australia), Timothy Rowe (University of Texas, United States), Julia Schwab (University of Manchester, England), Silke Schweiger & Viola Winkler (Natural History Museum Vienna, Austria), Cody Thompson

(University of Michigan, United States), Alan Turner & Eric Wilberg (Stony Brook University, United States), Thomas van der Kamp & Marcus Zuber (Staatliche Museum für Naturkunde Karlsruhe, Germany) and Lawrence Witmer (Ohio University, United States).

Côté géochimie, je remercie Florent Arnaud-Godet & Philippe Telouk (ENS Lyon) ainsi que François Fourel & Laurent Simon (Université Lyon 1) pour leur support technique et leur expertise sur les spectromètres en tout genre. Je remercie également Emmanuelle Albalat, Pierre-Jean Dodat, Samuel Le Goff & Auguste Hassler (ENS Lyon) ainsi que Thibault Clauzel, Vincent Luccisano, Jean Goedert & Nicolas Séon (Université Lyon 1) pour leur aide en salle de chimie et discussions géochimiques. Pour les autorisations d'échantillonnage, je remercie Blandine Bartschi (Université Lyon 1), Damien Becker (Jurassica Museum), Didier Berthet (Musée d'Histoire Naturelle de Lyon), Ricardo Cespedes (Museo de Historia Natural 'Alcide d'Orbigny'), Stéphane Jouve (Sorbonne Université), Yves Laurent (Musée d'histoire naturelle de Toulouse), Fabrice Lihoreau & Rodolphe Tabuce (Université de Montpellier) et Christian de Muizon (Muséum National d'Histoire Naturelle).

Thanks are also due to Julián Bayona, Ingo Braasch, Joschua Knüppe, Scott Hartman, Brian O'Meara, Armin Reindl and Roberto Diaz Sibaja for transferring their work to the public domain and making it available on PhyloPic, with which I was able to illustrate the graphics in Chapter 4.

Côté histologie, un merci tout particulier à Jorge Cubo (Sorbonne Université) pour m'avoir accueilli et guidé dans le cadre de l'étude des ostéodermes, ainsi qu'à Ronan Allain, Damien Germain et Séverin Morel (Muséum National d'Histoire Naturelle) pour leur appui technique.

Kop khun mak khrap to my thailandese colleagues for welcoming me in their beautiful country during a month on such short notice, allowing me to work on those beautiful atoposaurid specimens and taking me on the field. Thanks to Phornphen Chantasit and the team at the Sirindhorn Museum (Kalasin) as well as Komsorn Lauprasert, Sita Manitkoon and the team at the Paleontological Research Center (Maha Sarakham) for your friendship and facilitating my stay. I am also very pleased and thankful that you were able to come visit us in Lyon as well and scan those specimens. I hope I can see you again soon !

Les données exploitées au sein de cette thèse ont été mises à profit dans plusieurs publications. Je tiens donc ici à remercier les co-auteurs de ces dernières que je n'ai pas encore cités, et qui, chacun à leur façon, y ont participé : Vivian de Buffrénil (Muséum National d'Histoire

Naturelle), Mathieu Faure-Brac (Sorbonne Université), Stéphane Hua (Paléospace) et Christophe Lécuyer & Vincent Perrier (Université Lyon 1). Thanks also to the reviewers and editors not cited previously which have agreed to read and review those studies: Philip Cox & Philip Mannion (University College of London, England), Pedro Godoy (Stony Brook University, United States), Logan King (University of Bristol, England), Patrick O'Connor (Ohio University, United States), Timothy Smith (Slippery Rock University, United States), Matthias Starck (University of Munich, Germany) and Sally Thomas (Palaeontological Association, England), as well as anonymous ones. Thanks finally to Marco Auditore (Museo Civico di Storia Naturale, Italy), Eric Buffetaut (ENS Paris, France), Lilian Cazes, Florent Goussard & France de Lapparent de Broin (Muséum National d'Histoire Naturelle, France), Romain David (Max Planck Institute for Evolutionary Anthropology, Germany), Diego Pol (Museo Paleontologico Ediglio Feruglio, Argentina) and Nicolas Roumenoff (Université Lyon 1, France) for their contribution, in one way or another, to those manuscripts.

Merci aux collègues Montpelliérains (Anne-Lise Charrault, Lionel Hautier, Fabrice Lihoreau et Rodolphe Tabuce) de nous avoir accompagnés et m'avoir permis de fouiller sur un des sites étudiés dans cette thèse, celui d'Aumelas. J'espère que vous trouverez les résultats préliminaires présentés ici intéressants.

Special mention for Ronan Allain & Maxime Lasseron (Muséum National d'Histoire Naturelle) and Torsten Scheyer (University of Zurich), who have supervised my master research projects, and have thus contributed in some way in shaping the researcher I am today. It was a pleasure working with all of you, I hope we will collaborate again soon and finish what we started !

Je tenais aussi à remercier les trois 'ex-stagiaires' que j'ai eu la chance d'encadrer au cours de ma thèse, pour la qualité de leur travail et leur sympathie : Benjamin, Davide et Gwendal.

Finally, huge thanks also to Alexandra Elbakyan and her initiative for allowing free access to so many scientific papers and knowledge for everyone.

Voilà pour les remerciements 'scientifiques'. Cependant, cette thèse n'aurait pu arriver à son terme sans plusieurs personnes que je tenais à remercier ici, pour leur soutien durant ces trois années et pour me supporter depuis plus ou moins longtemps.

Tout d'abord, je pense à mes collègues et camarades de labo, sans qui l'ambiance quotidienne ne serait pas aussi bonne, qui m'ont permis de penser à autre chose lorsque cela était nécessaire et de râler un bon coup. Merci donc à Arnauld, Eve, Gilles, Gwendal, Hugo, Jeanne, Jiashun,

Mickaël, les trois Nicolas, Sébastien, Ségolène, Thibault, Thomas et Vincent. Mention spéciale à Ibrahim pour tout l'alcool gratuit.

Mes camarades de promo de master (et depuis plus longtemps pour certains), à savoir Antoine, Erwan, Guillaume, Lazare, Pénélope, Rachel et Rodolphe sont aussi à remercier pour m'avoir aidé à survivre à ces deux années précédant la thèse. Petite clin d'œil aussi aux fouilleurs et fouilleuses d'Angeac, qu'il m'est toujours agréable de recroiser en congrès ou au labo, j'espère pouvoir retourner patauger dans la boue bientôt !

Je remercie également Lokan, Nagg, Pierre, Valentin et le serveur Discord 8.6 non officiel, pour la bonne humeur qui y règne et toutes ces journées/soirées/WE de jeux terribles.

Un énorme merci à Alexandre, Alexis, Aymeric, Elise et Manon pour avoir toujours été là dans les bons comme dans les mauvais moments, et ce encore pour longtemps. Vivement le prochain Hellfest !

Les copains d'Annecy (François, Maxence, Nicolas, Niels, Paul-Louis et Yann), je suis content que notre amitié résiste à la distance qui nous sépare chacun. On se voit au prochain kebab chez Ali !

Samuel, j'ai calculé ça fait plus de la moitié de ma vie que l'on se connaît, ça ne nous rajeunît pas ! Merci d'avoir été et d'être toujours là pour moi (et vivement les vacances).

Merci à Elise, Erwan, Jérémy & Romain d'avoir eu le courage de relire tout ou partie de ma thèse.

Finalement, je tiens à remercier du fond du cœur mes parents et mon frère, qui m'ont toujours soutenu et accompagné dans mes projets, m'ont permis et m'ont donné les moyens d'arriver là où je suis et d'être la personne que je suis.

J'espère n'avoir oublié personne, si tel est le cas, mes excuses, et puis vous savez bien que j'écris ces remerciements bien trop tard, comme tout bon thésard qui se respecte.

Taxonomic note

Following the International Code of Zoological Nomenclature and general guidelines of systematic publications, each scientific name used in this thesis main text will be followed by its taxonomic authority (author(s) and date) at its first mention.

Résumé étendu

Les crocodiliens actuels, selon la systématique et les méthodes phylogénétiques utilisées, comprennent neuf genres et 23 à 28 espèces (McAliley *et al*., 2006 ; Willis *et al*., 2007 ; Hekkala *et al*., 2011 ; Oaks, 2011 ; Shirley *et al*., 2014 ; Murray *et al*., 2019). Ces organismes sont des prédateurs semi-aquatiques que l'on trouve en Afrique, en Asie, en Océanie et en Amérique du Nord et du Sud (voir Grigg & Kirshner, 2015). Ces taxons sont classiquement subdivisés en trois clades principaux (Brochu, 2003) : Gavialoidea Hay, 1930, Alligatoroidea Gray, 1844 et Crocodyloidea Fitzinger, 1826, bien que certains conflits subsistent, notamment entre les approches phylogénétiques morphologiques et moléculaires (Poe, 1996 ; Brochu, 1997, 1999, 2000, 2001 ; Janke *et al.,* 2005 ; Roos *et al*., 2007 ; Meredith *et al*., 2011 ; Oaks, 2011 ; Groh *et al*., 2019 ; Milián-García *et al*., 2020 ; Hekkala *et al*., 2021 ; Pan *et al*., 2021 ; Rio & Mannion, 2021). Ces conflits sont principalement centrés sur le positionnement des gavialidés et de *Tomistoma* Müller, 1846, dans le cadre de la convergence morphologique longirostre (Brochu, 2003 ; Gatesy *et al*., 2003 ; Lee & Yates, 2018 ; Groh *et al*, 2019 ; Rio & Mannion, 2021) et de la délimitation entre certaines espèces (Hekkala, 2004 ; Hekkala *et al*., 2010, 2011, 2015, 2021 ; Shirley *et al*., 2014, 2018 ; Milián-García *et al*., 2015, 2020 ; Carr *et al*., 2021).

Étant donné qu'ils sont les seuls représentants vivants d'un groupe autrefois beaucoup plus important, Crocodylomorpha Hay, 1930, et qu'ils constituent, avec les oiseaux, les deux lignées d'archosauriens actuels, les crocodiliens modernes ont souvent été considérés comme des fossiles vivants. Cependant, ce n'est pas le cas, et les crocodylomorphes étaient autrefois beaucoup plus diversifiés d'un point de vue écologique et taxonomique. Cela inclut des taxons entièrement pélagiques (dyrosauridés et la plupart des thalattosuchiens), ainsi que des formes terrestres (notosuchiens, planocraniidés, sphénosuchiens et protosuchiens). Depuis le Trias, les crocodylomorphes ont survécu à de nombreuses crises biologiques, ce qui en fait un groupe très résistant. Par exemple, ils sont les seuls pseudosuchiens à avoir survécu à l'extinction de la fin du Trias (Nesbitt, 2011) et certaines lignées sont retrouvées avant et après la crise Crétacé - Paléogène (Pol *et al*., 2012 ; Sellés *et al*., 2020).

Des transitions évolutives majeures vers de nouveaux modes et environnements de vie se sont produites à de nombreuses reprises dans tous les grands clades d'organismes, et induisent des modifications du comportement, de la physiologie et de l'organisation corporelle. Ce type de transition est bien connu, par exemple lors du passage des poissons aux tétrapodes (Niedźwiedzki *et al*., 2010), des mammifères terrestres aux cétacés (Gatesy *et al*., 2013) ou que

certains dinosaures ont acquis la capacité de voler (Witmer, 2009a, b). Chez les crocodylomorphes, le moment exact et le nombre de transitions entre le milieu terrestre et le milieu aquatique sont encore inconnus et évoluent au fur et à mesure que de nouveaux fossiles sont découverts (Wilberg *et al*., 2019). L'un des principaux aspects de ces changements à travers ces adaptations est la forme du crâne : cette caractéristique est en effet liée au mode de vie (Brochu, 2001 ; Wilberg, 2017). Par exemple, le long rostre des thalattosuchiens (Pierce *et al*., 2009 ; Ballel *et al*., 2019 ; aussi appelé morphologie longirostre) est adapté à la vie et à l'alimentation en milieu aquatique, tandis que le crâne haut et court des sébécosuchiens et d'autres formes terrestres (morphologie altirostre) n'est pas viable dans un tel environnement. Il semble en effet plus adapté à la vie terrestre, comme l'indiquent la position des narines et des orbites et sa plus grande résistance au stress mécanique (Balouet & Buffetaut, 1987 ; Gasparini, 1984 ; Gasparini *et al*., 1993 ; Rossmann *et al*., 2000). Dans le cadre de cette thèse, je vais donc m'intéresser de plus près aux adaptations au mode de vie terrestre de certains crocodylomorphes, en me focalisant sur les questions suivantes : comment évaluer le mode de vie terrestre chez les formes fossiles de crocodylomorphes ? La terrestrialité est-elle la condition ancestrale des crocodylomorphes, ou a-t-elle évolué de manière convergente à travers différents clades ? La morphologie altirostre est-elle toujours associée à des taxons entièrement terrestres ?

Pour répondre à ces questions, je résumerai tout d'abord les différentes adaptations à un mode de vie non semi-aquatique trouvées dans les archives fossiles des crocodylomorphes, en mettant l'accent sur la terrestrialité et les informations essentielles pour comprendre et évaluer la paléoécologie de ces organismes. Puis, des clarifications phylogénétiques de certaines lignées clés seront présentées, car il est important de comprendre les relations entre les taxons terrestres pour évaluer la chronologie et l'évolution de ce trait. Ensuite, les structures endocrâniennes d'une sélection de taxons supposément terrestres seront étudiées et permettront de nombreuses interprétations paléoécologiques, avec un accent particulier sur les implications ontogénétiques, phylogénétiques et écologiques de l'oreille interne chez les crocodylomorphes. Ceci sera fait avec des données complémentaires provenant de crocodiliens actuels, ainsi que de formes fossiles adaptées au domaine aquatique. Une deuxième approche complémentaire sera consacrée à des études de cas en géochimie isotopique, impliquant des taxons similaires. Grâce à une approche multi-isotopique, les caractéristiques alimentaires, physiologiques et écologiques de ces organismes fossiles seront déduites, tout en gardant un point de vue global sur l'ensemble de la faune impliquée dans chaque localité et un regard sur des données actuelles.

Enfin, une autre approche histologique prometteuse portant sur les ostéodermes sera évaluée dans une étude préliminaire, ces résultats devant être confirmés dans de futures études. Les données présentées dans cette thèse sont sous la forme de manuscrits publiés ou soumis à des revues à comité de lecture, ainsi que de données non publiées.

Ainsi, dans le 1er chapitre, un examen des différentes adaptations non semi-aquatiques dans le registre fossile des crocodylomorphes est proposé. Les crocodylomorphes "primitifs" (sphénosuchiens et protosuchiens) étaient ancestralement terrestres, avec une posture érigée. La plupart des notosuchiens (uruguaysuchidés, peirosauridés, mahajangasuchidés, sphagésauriens, sébécidés et baurusuchidés) sont également considérés comme terrestres, avec diverses adaptations à l'omnivorie et à l'herbivorie, ou à un comportement fouisseur. Les adaptations à la terrestrialité se retrouvent également chez certains néosuchiens (le clade qui comprend les crocodiliens actuels), avec des groupes tels que les atoposauridés, les paralligatoridés, les mékosuchinés et les planocraniidés, présentant une morphologie altirostre liée à ce mode de vie. D'autre part, tout au long de son histoire évolutive, le clade Crocodylomorpha a également inclus des formes entièrement aquatiques, telles que les thalattosuchiens ou les dyrosauridés, certains spécimens présentant même des adaptations à un mode de vie entièrement pélagique. La déduction du milieu de vie de tous ces organismes est dans la littérature principalement basée sur la morphologie de leur crâne (orientation des orbites et des narines externes), la morphologie de leurs membres et de leurs ceintures (liée à la posture) et leur dentition (liée aux régimes alimentaires possibles).

Bien que ces observations soient valables, il est nécessaire de mieux comprendre les relations phylogénétiques de tous ces organismes, ce qui est une condition préalable à toute comparaison à grande échelle et à toute étude des tendances évolutives. Cette question est abordée dans le chapitre 2, où je remarque que les relations entre les peirosauridés, les sébécidés et les baurusuchidés sont complexes à évaluer. À partir d'une revue bibliographique des analyses phylogénétiques réalisées sur le sujet, je conclus que ni le regroupement des sébécidés avec les peirosauridés (Sebecia) ni celui des sébécidés avec les baurusuchidés (Sebecosuchia) en tant que taxons frères ne sont étayés par des synapomorphies non ambiguës et, comme ces deux taxons sont également étayés dans la littérature par une combinaison complète de caractères, il est difficile de favoriser l'un ou l'autre. Ensuite, je présente une étude publiée focalisée sur le statut et le contenu taxonomique d'*Hamadasuchus*, un peirosauridé du Crétacé du Maroc. Une nouvelle demi-mandibule et des séries ontogénétiques de crocodiliens actuels permettent d'amender la diagnose de *H. rebouli* (la seule espèce valide du genre), ainsi que de réduire son

contenu taxonomique. Enfin, une étude complète et une évaluation phylogénétique de nouveaux spécimens d'atoposauridés du Crétacé de Thaïlande m'ont permis d'ériger un nouveau taxon, *Varanosuchus sakonnakhonensis*. Il s'agit de la deuxième occurrence d'atoposauridés en Thaïlande, qui vient s'ajouter à l'énorme diversité des crocodylomorphes du Crétacé en Asie du Sud-Est et permet de réévaluer les relations phylogénétiques de certains clades de néosuchiens. L'accent a également été mis sur les adaptations paléoécologiques de ces derniers spécimens, dont de nombreuses caractéristiques suggèrent un mode de vie terrestre mais avec des affinités semi-aquatiques (soit un mode de vie semi-terrestre).

Le chapitre 3 est ensuite consacré à une méthode permettant d'évaluer la paléoécologie d'organismes éteints : la reconstruction des structures internes du crâne. À partir d'une mise en perspective des progrès des techniques de tomodensitométrie, qui ont permis d'obtenir tant de données depuis le début du 21e siècle, les structures internes de trois taxons représentatifs de trois clades supposément terrestres différents sont étudiées : les sébécidés (*Zulmasuchus*), les peirosauridés (*Hamadasuchus*) et les atoposauridés (*Varanosuchus*). Chez les crocodylomorphes, l'endocaste et les nerfs crâniens sont associés à plusieurs sens tels que l'olfaction ou la vision ; les labyrinthes endo-osseux apportent des informations sur la posture de la tête et ses capacités de mouvement, ainsi que sur les capacités auditives ; le développement de la pneumaticité crânienne particulière de ces organismes pourrait être lié au mode de vie. Par conséquent, en se basant sur ces données, *Zulmasuchus* est considéré comme un notosuchien entièrement terrestre, tandis que *Hamadasuchus* aurait pu avoir également des affinités semi-aquatiques et que *Varanosuchus* était probablement semi-terrestre. L'oreille interne des crocodylomorphes est ensuite examinée de plus près, en utilisant une approche morphométrique géométrique en 3D sur un vaste ensemble de données concernant les crocodylomorphes existants et éteints, et comprenant la plupart des modes de vie connus de ce groupe. Comme l'ont souligné des études récentes, un lien étroit entre la forme et l'ontogenèse a été trouvé, ainsi qu'un signal phylogénétique minimal. Cependant, la forme de ces structures ne semble pas être en corrélation avec l'écologie.

Une autre méthode indépendante a ensuite été utilisée dans le chapitre 4, la géochimie isotopique, avec un accent particulier sur les sébécidés. La combinaison des compositions isotopiques de l'oxygène, du carbone, du calcium et du strontium a été étudiée dans plusieurs faunes du Paléogène, dans le but de comprendre comment ce clade s'est adapté à la suite de la crise biologique du Crétacé/Paléogène. Les compositions isotopiques de l'oxygène et du strontium fournissent des informations sur le milieu de vie d'un organisme, tandis que les

compositions isotopiques du carbone et du calcium sont liées à son régime alimentaire. Les sébécidés étaient déjà au sommet de la chaîne alimentaire terrestre peu après le début du Paléogène, comme le montre la faune de Tiupampa (Bolivie), et ont conservé cette position tout au long de cette période, comme le montrent les faunes d'Aumelas et de Réalmont (France). Cependant, le mystérieux sébécidé *Eremosuchus elkoholicus* de la faune d'El Kohol (Algérie) se révèle semi-aquatique, ce qui justifie une réévaluation de ce taxon. Bien que ces travaux confirment que les sébécidés ont rempli la niche écologique de grand prédateur laissée vacante par la disparition des dinosaures théropodes non aviens, les raisons de leur survie à la transition Crétacé/Paléogène restent inconnues. De plus, l'enregistrement géochimique de la dentine par échantillonnage sérié pourrait aussi être une approche intéressante, notamment pour détecter les changements écologiques sur une courte période (c'est-à-dire le temps de développement de la dent ou taux de remplacement dentaire). En mesurant les compositions isotopiques de l'oxygène et du strontium (indicateur du milieu de vie) et du calcium et de l'azote (indicateur du régime alimentaire) de quatre dents appartenant à trois espèces différentes de crocodiliens actuels, j'ai observé que ces variations sont anti corrélées entre le calcium et l'azote et corrélées entre l'oxygène et le strontium. Le spécimen d'*Osteolaemus* présente les changements les plus drastiques dans les compositions isotopiques, ce qui correspond aux changements saisonniers de son mode de vie. Bien que plusieurs limitations doivent être prises en compte, ce protocole pourrait apporter des résultats intéressants sur les formes fossiles.

Enfin, dans le chapitre 5, une étude préliminaire utilisant un autre proxy qui pourrait être intéressant pour évaluer la paléoécologie d'un organisme éteint est présentée. Cette étude histologique porte sur des ostéodermes d'une sélection de crocodylomorphes ayant des modes de vie différents. Un sébécidé présente des structures particulières, correspondant à une implantation plus profonde de l'ostéoderme dans le derme chez ce taxon, qui pourrait être liée à sa posture et à son mode de vie terrestre. En outre, nous avons observé que l'ornementation des ostéodermes avait disparu chez les notosuchiens dérivés, et que son absence pourrait donc être liée à un mode de vie terrestre, avec les problèmes de thermorégulation qui y sont associés.

En tenant compte de tous ces résultats, les principales conclusions qui viennent en réponse aux problématiques posées sont les suivantes :

- En plus des observations morphologiques, le mode de vie peut être évalué indépendamment chez un organisme éteint par l'étude de ses structures internes crâniennes et des compositions isotopiques de ses éléments squelettiques ;

- La terrestrialité est la condition ancestrale des crocodylomorphes, avec plusieurs adaptations convergentes ultérieures aux environnements semi-aquatiques et aquatiques (comme les crocodiliens actuels, qui ne sont donc pas des "fossiles vivants") tout au long de leur histoire évolutive ;

- Les sébécidés avaient déjà atteint la niche écologique de grand prédateur (remplaçant les dinosaures théropodes non aviens) à la suite de la transition Crétacé - Tertiaire, et l'ont conservée pendant la plus grande partie du Paléogène ;

- La morphologie altirostre en elle-même n'est pas nécessairement associée à un mode de vie entièrement terrestre, avec des clades présentant une écologie aux affinités semi-aquatiques, que l'on pourrait qualifier de semi-terrestre.

Cette thèse a également mis en lumière plusieurs perspectives intéressantes, qui pourront être abordées dans de futures études :

- Outre la description de nouveaux spécimens et la réévaluation de taxons clés, des données alternatives postcrâniennes ou internes pourraient aider à résoudre les conflits phylogénétiques et taxonomiques qui subsistent au sein des crocodylomorphes. Les variations ontogénétiques doivent également être prises en compte et devraient s'appuyer sur l'étude des représentants actuels (en particulier chez les crocodylomorphes) ;

- La fonction et les implications ontogénétiques, phylogénétiques et écologiques de la pneumaticité crânienne et de l'endocaste chez les crocodylomorphes doivent être mieux comprises et pourraient potentiellement apporter des preuves supplémentaires aux interprétations paléoécologiques des formes fossiles. De même, la relation entre les labyrinthes endo-osseux et les oreilles internes (c'est-à-dire les tissus durs par rapport aux tissus mous) doit également être étudiée ;

- Les études multi-isotopiques bénéficieraient de l'inclusion d'un plus grand nombre d'éléments indépendants, tels que le zinc, le magnésium, l'azote ou l'hydrogène. De telles études devraient être menées sur des faunes terrestres du Crétacé (formation Adamantina du Brésil, groupe Kem Kem du Maroc ou faune de Phu Sung de Thaïlande, par exemple), afin de comprendre comment les crocodylomorphes se sont intégrés dans des environnements dominés par les dinosaures, voir si leurs relations interfaunales étaient les mêmes qu'au cours du Paléogène ou non et comment certaines lignées, comme les sébécidés, ont survécu à la crise Crétacé - Paléogène ;

- L'amélioration des techniques analytiques et une meilleure compréhension des flux de calcium entre les différents tissus des reptiles pourront permettre des études détaillées et précises de restes d'organismes éteints pendant une période très courte, correspondant à leur taux de remplacement dentaire.

Mots-clés : Crocodylomorpha – CT scan – géochimie – paléontologie – phylogénie.

Abstract

Extant crocodylians are semi-aquatic organisms, but, throughout their evolutionary history, crocodylomorphs have adapted to various living environments, such as water or land, and have survived numerous biological crises. The lifestyle of those extinct forms has been inferred from their postcranial anatomy, their dentition, and their cranial shape. For example, terrestrial crocodylomorphs often display an altirostral morphology (i.e., high rostrum).

In this thesis, a closer look is taken at the adaptations to a terrestrial lifestyle of several clades of crocodylomorphs with the following questions in mind: are there any other proxies that can be used to assess a terrestrial lifestyle in those organisms? How has terrestriality originated and evolved in Crocodylomorpha? Is the altirostral morphology always linked with such a lifestyle?

First, a review of the different non-semi-aquatic adaptations in the fossil record of crocodylomorphs is proposed and I confirm that a terrestrial lifestyle is in fact the ancestral condition of the group, with subsequent adaptations to the semi-aquatic and aquatic environment. In order to propose a large-scale evolutionary study, the phylogenetic relationships of the different taxa must first be understood as best as possible. As a result, I then show through a literature review that neither of the phylogenetic hypotheses concerning the relationships of some notosuchians clades can be favoured, and this issue would benefit from the addition of other data (postcranium, internal structures). A first publication is focused on the phylogenetic and taxonomic status of *Hamadasuchus*, a peirosaurid from the Cretaceous of Morocco. New specimens allow to amend the diagnosis of *Hamadasuchus rebouli*, the only species included in *Hamadasuchus* and reduce its taxonomic content. A second submitted manuscript presents new specimens of atoposaurids from the Cretaceous of Thailand, allowing to erect the new taxon *Varanosuchus sakonnakhonensis*. This taxon is shown to be adapted to a semi-terrestrial lifestyle.

A powerful proxy to assess the paleoecology of extinct organisms is the study and reconstruction of their internal structures, via CT scan analyses. A review of the different structures with their associated ecological implications is presented, and the study of *Zulmasuchus* (Sebecidae), *Hamadasuchus* (Peirosauridae) and *Varanosuchus* (Atoposauridae) allows to infer their lifestyle (respectively from fully terrestrial to semi-terrestrial). A special emphasis is put on the ontogenetic, phylogenetic, and ecological signal of the inner ear, through a 3D geometric morphometric study on an extensive dataset of extant and extinct taxa. The

shape of this structure is heavily linked to ontogeny and minimally to phylogeny, but not to ecology.

A second proxy is then put forward, the isotope compositions of skeletal tissues. Multi-isotopic studies of different independent elements allow to understand the lifestyle and dietary habits of extinct organisms, as well as the trophic relationships they had with other organisms from the same fauna and propose a paleoenvironmental reconstruction. Several faunas from the Paleogene of South America, Africa and Europe are studied and confirm that sebecids were already apex predators in the aftermath of the Cretaceous - Paleogene transition and throughout this period. Furthermore, the geochemical recording of dentine by serial sampling could also be an interesting approach, particularly for detecting ecological changes over a short period (i.e., tooth development time or tooth replacement rate), as evidenced by measures on extant specimens.

Finally, the osteoderm histology of selected crocodylomorphs is presented and represent an interesting prospect for future studies, both internally and externally.

Keywords: Crocodylomorpha – CT scan – geochemistry – paleontology – phylogeny.

Figure captions

Table captions:

List of institutional abbreviations

AMNH: American Museum of Natural History (New York, United States)

AMU: Aix-Marseille Université (Marseille, France)

BMNH: British Museum of Natural History (London, England)

BP: Evolutionary Studies Institute (formerly Bernard Price Institute for Palaeontological Research; Johannesburg, South Africa)

BRLSI: Bath Royal Literary and Scientific Institute (Bath, England)

BSPG: Bavarian State Collection for Paleontology and Geology (Munich, Germany)

CHE: Cherves-de-Cognac, Musée d'Angoulême (Angoulême, France)

CM: Carnegie Museum of Natural History (Pittsburgh, United States)

CMC: Chinchilla Museum Collection (Queensland, Australia)

CMN: Canadian Museum of Nature (Ottawa, Canada)

CMNH: Cleveland Museum of Natural History (Cleveland, United States)

CNRST-SUNY: Centre National de la Recherche Scientifique et Technologique, Mali – Stony Brook University (New York, United States)

CPPLIP: Centro de Pesquisas Paleontológicas L. I. Price (Uberaba, Brazil)

DGM: Divisão de Geologia e Mineralogia (Rio de Janeiro, Brazil)

DVZ-M: Department of Vertebrate Zoology, Morphological Collection (Saint Petersburg, Russia)

FEF-PV: Fernandópolis Educational Foundation (São Paulo, Brazil)

FMNH: Field Museum of Natural History (Chicago, United States)

FUP: University of Brasília (Federal District, Brazil)

HUE: Museo de Paleontología de Castilla-La Mancha, Lo Hueco Collection (Cuenca, Spain)

IFSP-VTP: Federal Institute of Education, Science and Technology (São Paulo, Brazil)

IGM: Mongolian Institute of Geology (Ulaan Bataar, Mongolia)

INSA: Institut National des Sciences Appliquées (Lyon, France)

IRSNB: Institut Royal des Sciences Naturelles de Belgique (Bruxelles, Belgique)

IVPP: Institute of Vertebrate Paleontology and Paleoanthropology (Beijing, China)

LPP: Institut de Paléoprimatologie, Paléontologie Humaine, Evolution et Paléoenvironnements (Poitiers, France)

LPRP: Laboratório de Paleontologia de Ribeirão Preto (São Paulo, Brazil)

Mal: Malawi Department of Antiquities (Lilongwe, Malawi)

MACN: Museo Argentino de Ciencias Naturales 'Bernardino Rivadavia' (Buenos Aires, Argentina)

MAÑE: Museo de Ciencias de Añelo (Añelo, Argentina)

MAU: Museo Municipal Argentino Urquiza (Rincón de los Sauces, Argentina)

MCD: Museu de la Conca Dellà (Lleida, Spain)

MCF: Museo Municipal Carmen Funes (Plaza Huincul, Argentina)

MCT: Museu de Ciencias da Terra (Rio de Janeiro, Brazil)

MCZ: Museum of Comparative Zoology (Cambridge, United States)

MDA: Museo del Desierto de Atacama (Antofagasta, Chile)

MDE: Musée des Dinosaures d'Espéraza (Espéraza, France)

MJML: Museum of Jurassic Marine Life (Kimmeridge, England)

ML: Museu de Lourinhã (Lourinhã, Portugal)

MLP: Museo de La Plata (La Plata, Argentina)

MM: Minden Museum (Minden, Germany)

MN: Museu Nacional (Rio de Janeiro, Brazil)

MNB: National Museum of the Bahamas (Nassau, The Bahamas)

MNN: Musée National du Niger (Niamey, Niger)

MHNC: Museo de Historia Natural 'Alcide d'Orbigny' (Cochabamba, Bolivia)

MHNL: Musée d'Histoire Naturelle de Lyon (Lyon, France)

MHNM: Musée d'Histoire Naturelle de Marseille (Marseille, France)

MHNT: Muséum d'Histoire Naturelle de Toulouse (Toulouse, France)

MNA: Museum of Northern Arizona (Arizona, United States)

MNHN: Muséum National d'Histoire Naturelle (Paris, France)

MOZ : Museo Provincial de Ciencias Naturales « Profesor-Dr. Juan A. Olsacher » (Zapala, Argentina)

MPCA: Museo Paleontológico Carlos Ameghino (Cipolletti, Argentina)

MPEF: Museo Paleontológico Egidio Feruglio (Chubut, Argentina)

MPMA: Museo de Paleontologia de Monte de Alto (Monte Alto, Brazil)

MPV: Paléospace de Villers-sur-Mer (Villers-sur-Mer, France)

MPZ: Museo de Ciencias Naturales de la Universidad de Zaragoza (Zaragoza, Spain)

MUC: Museo de la Universidad Nacional del Comahue y Centro Paleontológico 'Lago Los Barreales' – Proyecto Dino (Lago Los Barreales, Argentina)

MZB: Museu Zoològie de Barcelona (Barcelona, Spain)

MZS: Musée Zoologique de Strasbourg (Strasbourg, France)

MZSP: Museu de Zoologia da Universidade de São Paulo (São Paulo, Brazil)

NHMLA: National History Museum of Los Angeles County (Los Angeles, United States)

NHMUK: Natural History Museum of the United Kingdom (London, England)

NHMW: Naturhistorisches Museum Wien (Vienna, Austria)

NMC: Canadian Museum of Nature (Ottawa, Canada, now CMN)

NMS: National Museum Scotland (Edinburgh, Scotland)

OUVC: Ohio University Vertebrate Collection (Athens, United States)

QMF: Queensland Museum (Brisbane, Australia)

ROM: Royal Ontario Museum (Toronto, Canada)

RRBP: Rukwa Rift Basin Project (Dar es Salaam, Tanzania)

RVC: Royal Veterinary College (London, England)

SAM PK: Iziko South African Museum (Cape Town, South Africa)

SCR: Paléontologie A16 collections (Porrentruy, Switzerland)

SM: Sirindhorn Museum (Non Buri, Thailand)

SMC: Sedgwick Museum (Cambridge, England)

SMNK: Staatliche Museum für Naturkunde Karlsruhe (Karlsruhe, Germany)

SNSB-BSPG: Staatliche Naturwissenschaftliche Sammlungen Bayerns-Bayerische Staatssammlung für Paläontologie und Geologie (Munich, Germany)

STUS: Salas de las Tortugas 'Emiliano Jiménez' de la Universidad de Salamanca (Salamanca, Spain)

SVSTUA: Collections pédagogiques du Département de Biologie de l'Ecole Normale Supérieure de Lyon (Lyon, France)

TCH: Paléontologie A16 collections (Porrentruy, Switzerland)

TCWC: Biodiversity Research and Teaching Collections (College Station, United States)

TMM: Texas Memorial Museum (Austin, United States)

UA: University of Antananarivo (Antananarivo, Madagascar)

UCBL: Université Claude Bernard Lyon 1 (Villeurbanne, France)

UCMP: University of California Museum of Paleontology (Berkeley, United States)

UCRC: University of Chicago Research Collection (Chicago, United States)

UF: University of Florida (Gainesville, United States)

UFRGS-PV-Z: Laboratório de Paleontologia de Vertebrados, Universidade Federal do Rio Grande do Sul, Zoological Collection (Porto Alegre, Brazil)

UFRJ: Universidade Federal do Rio de Janeiro (Rio de Janeiro, Brazil)

UM: Université de Montpellier (Montpellier, France)

UMZC: University Museum of Zoology (Cambridge, England)

UMMZ: University of Michigan Museum of Zoology (Ann Arbor, United States)

UNM: University of New Mexico (New Mexico, United States)

UNPSJB-PV: Universidad Nacional de la Patagonia San Juan Bosco-Paleontología de Vertebrados (Comodoro Rivadavia, Argentina)

USNM: United States National Museum of Natural History (Washington DC, United States)

YPM: Yale Peabody Museum (New Haven, United States)

ZIN: Zoological Institute (Saint Petersburg, Russia)

ZMMU MSU R: Zoological Museum of Moscow State University (Moscow, Russia)

Table of contents

General introduction

Extant crocodylians, depending on the systematics and phylogenetic methods used, comprise nine genera and 23 to 28 species (McAliley *et al*., 2006; Willis *et al*., 2007; Hekkala *et al*., 2011; Oaks, 2011; Shirley *et al*., 2014; Murray *et al*., 2019). Those organisms are semi-aquatic ambush predators and are found in the sub-tropical belt of Africa, Asia, Oceania and North and South America (for a complete review, see Grigg & Kirshner, 2015). These taxa are classically subdivided in three main clades (Brochu, 2003): Gavialoidea Hay, 1930, Alligatoroidea Gray, 1844 and Crocodyloidea Fitzinger, 1826, although some conflicts remain, especially between morphological and molecular phylogenetic approaches (Poe, 1996; Brochu, 1997, 1999, 2000, 2001; Janke *et al*., 2005; Roos *et al*., 2007; Meredith *et al*., 2011; Oaks, 2011; Groh *et al*., 2019; Milián-García *et al*., 2020; Hekkala *et al*., 2021; Pan *et al*., 2021; Rio & Mannion, 2021). Those conflicts are mainly centered around the placement of gavialids and *Tomistoma*, within the framework of convergence to longirostry (Brochu, 2003; Gatesy *et al*., 2003; Lee & Yates, 2018; Groh *et al*., 2019; Rio & Mannion, 2021) and the delimitation between certain species (Hekkala, 2004; Hekkala *et al*., 2010, 2011, 2015, 2021; Shirley *et al*., 2014, 2018; Milián-García *et al*., 2015, 2020; Carr *et al*., 2021).

Because they are the only living representatives of a once much larger group, Crocodylomorpha Hay, 1930, and together with Aves constitute the two extant archosaurian lineages, modern crocodylians could be seen as living fossils. However, this is not the case, and crocodylomorphs were once much more ecologically and taxonomically diverse. This includes fully pelagic taxa (dyrosaurids and thalattosuchians), as well as terrestrial forms (notosuchians, planocraniids, sphenosuchians and protosuchids). From the Triassic, crocodylomorphs have evolved continuously and have survived numerous biological crises, making it a very resilient group. For example, they are the only pseudosuchians to survive the end-Triassic extinction (Nesbitt, 2011) and some lineages are found before and after the Cretaceous-Paleogene crisis (Pol *et al*., 2012; Sellés *et al*., 2020; Fig. 1).

Major evolutionary transitions into new lifestyles and living environments have occurred numerous times in all major clades of organisms, and induce modifications in behavior, physiology, and body plan. This type of transition is well known, for example from fishes to tetrapods (Niedźwiedzki *et al*., 2010), terrestrial mammals to cetaceans (Gatesy *et al*., 2013) or when some dinosaurs acquired the ability to fly (Witmer, 2009a, b). In crocodylomorphs,

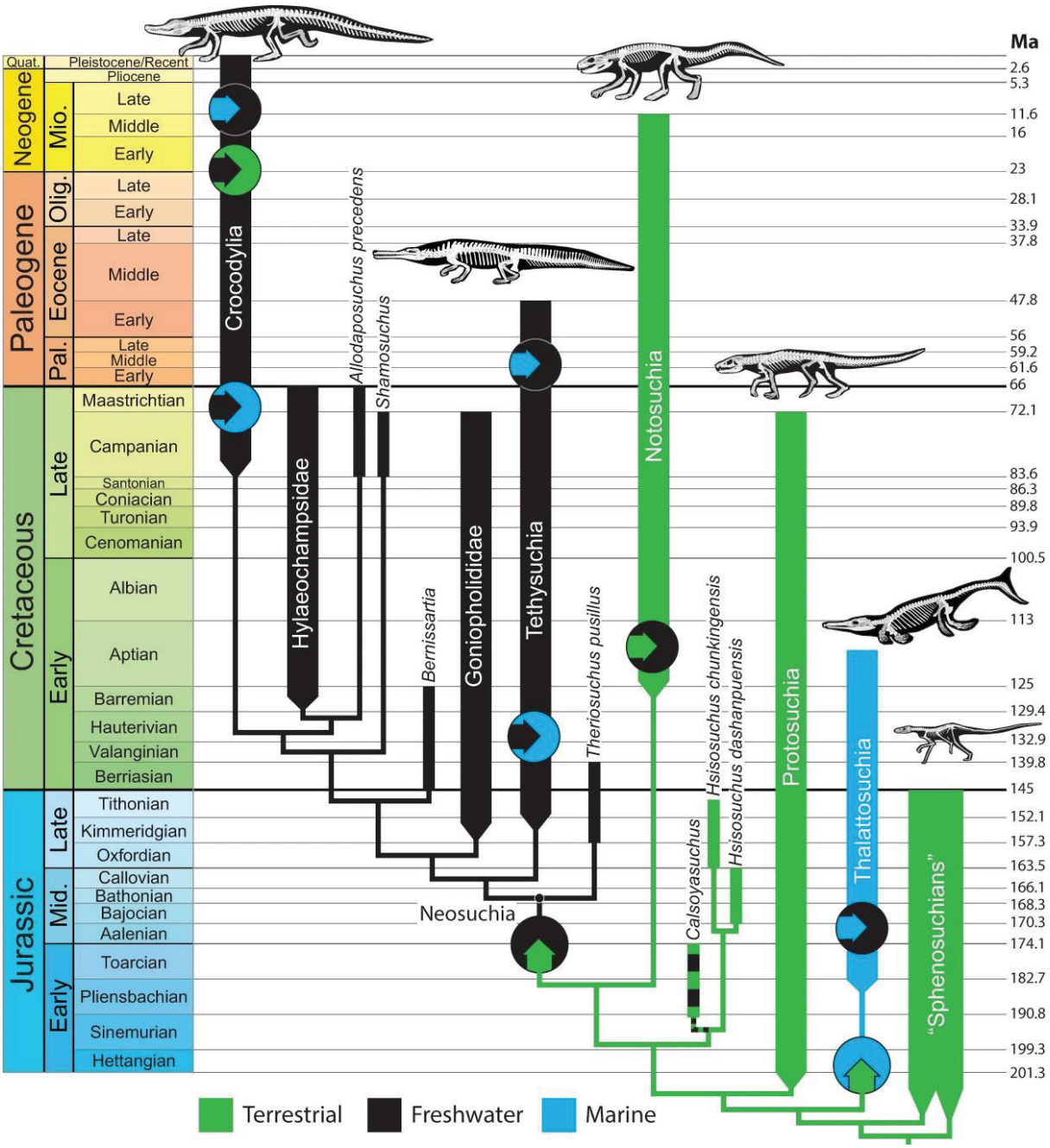

Figure 1: Hypothetic phylogenetic and temporal pattern of ecological shifts in Crocodylomorpha. Arrows indicate shifts. Note that the position of Thalattosuchia Fraas, 1901 is subject to debate, see also Chapter 1. Taken from Wilberg *et al*. (2019; fig. 2).

the exact timing and number of transitions between land and water is still under investigation as new fossils are found (Wilberg *et al*., 2019; Fig. 1). One of the main aspects of change across those adaptations is cranial shape: this characteristic is indeed linked to lifestyle (Brochu, 2001; Wilberg, 2017). For example, the long rostrum of thalattosuchians (Pierce *et al*., 2009; Ballel *et al*., 2019 or longirostral morphology) is adapted to living and feeding in the aquatic environment, while the high and short skull of sebecosuchians and other terrestrial forms

(altirostral morphology) is not viable in such an environment. It is more suitable for life on land, as indicated by the position of the nares and the orbits and its higher resistance to stress (Balouet & Buffetaut, 1977; Gasparini, 1984; Gasparini *et al*., 1993; Rossmann *et al*., 2000).

I will first summarize in Chapter 1 the different adaptations to a non-semi-aquatic lifestyle found in the fossil record of crocodylomorphs, with a focus on terrestriality and which further information are key to understand and assess the paleoecology of those organisms.

Chapter 1: Crocodylomorpha: evolution, taxonomy and paleobiology with a focus on non-semi-aquatic adaptations

Crocodylomorpha Hay, 1930 is a superorder of sauropsids dating back to the Late Triassic (Carnian; Irmis *et al*., 2013; Lecuona *et al*., 2016; Leardi *et al*., 2020a), and includes all taxa more closely related to crocodylians than to phytosaurs, ornithosuchids, aetosaurs, poposauroids, and rauisuchids (Nesbitt, 2009, 2011; Irmis *et al*., 2013; To *et al*., 2022; Fig. 1.1). Throughout their evolutionary history, members of this clade have adapted to a wide range of environments, from fully aquatic (such as metriorhynchids; see Young *et al.,* 2010 for a review) to fully terrestrial (such as sebecosuchians; see Rossmann *et al.,* 2000 for a review). Today, modern crocodylians are the only representatives of this once much more diverse group, with 23 to 28 taxa recognized (see Grigg & Kirshner, 2015 for a complete review). Contrary to popular belief, extant crocodylians are thus not 'living fossils' but rather extremely derived representatives of a diverse clade that survived three major biological crises. In this chapter, I provide an overview of the taxonomic and ecological occurrences of crocodylomorphs with a focus on non-semi-aquatic adaptations, and especially terrestrial ones, which will be important in situating the different groups studied in this thesis.

I- Sphenosuchians

Sphenosuchia were a diverse group of archosaurs with a global repartition. *Hesperosuchus agilis* Colbert, 1952 was the earliest known member from the late Carnian - early Norian of the Chinle Formation (United States; Fig. 1.2; Clark *et al*., 2001). Other fossils have also been found in China (Wu & Chatterjee, 1993; Harris *et al*., 2000; Clark *et al.,* 2004), Europe (Crush, 1984; Sereno & Wild, 1992; Knoll & Rohrberg, 2012), South America (Bonaparte, 1969; Lecuona *et al*., 2016; Mamani *et al*., 2022), and South Africa (Walker, 1990; Clark & Sues, 2002). The lineage extends until at least the Late Jurassic, with *Macelognathus vagans* Marsh, 1884 and *Hallopus victor* Marsh, 1877 from the Morrison Formation (Kimmeridgian, United States; Walker, 1970; Göhlich *et al*., 2005).

The phylogenetic relationships and monophyly of the group are still highly debated: several synapomorphies could support the clade (Sereno & Wild, 1992; Wu & Chatterjee, 1993); however, these characters are secondarily lost in derived crocodylomorphs, effectively reducing the support of the clade (Clark *et al*., 2004). Therefore, in some studies, sphenosuchians are retrieved as the sister group of Crocodyliformes (Sereno & Wild, 1992; Wu & Chatterjee, 1993;

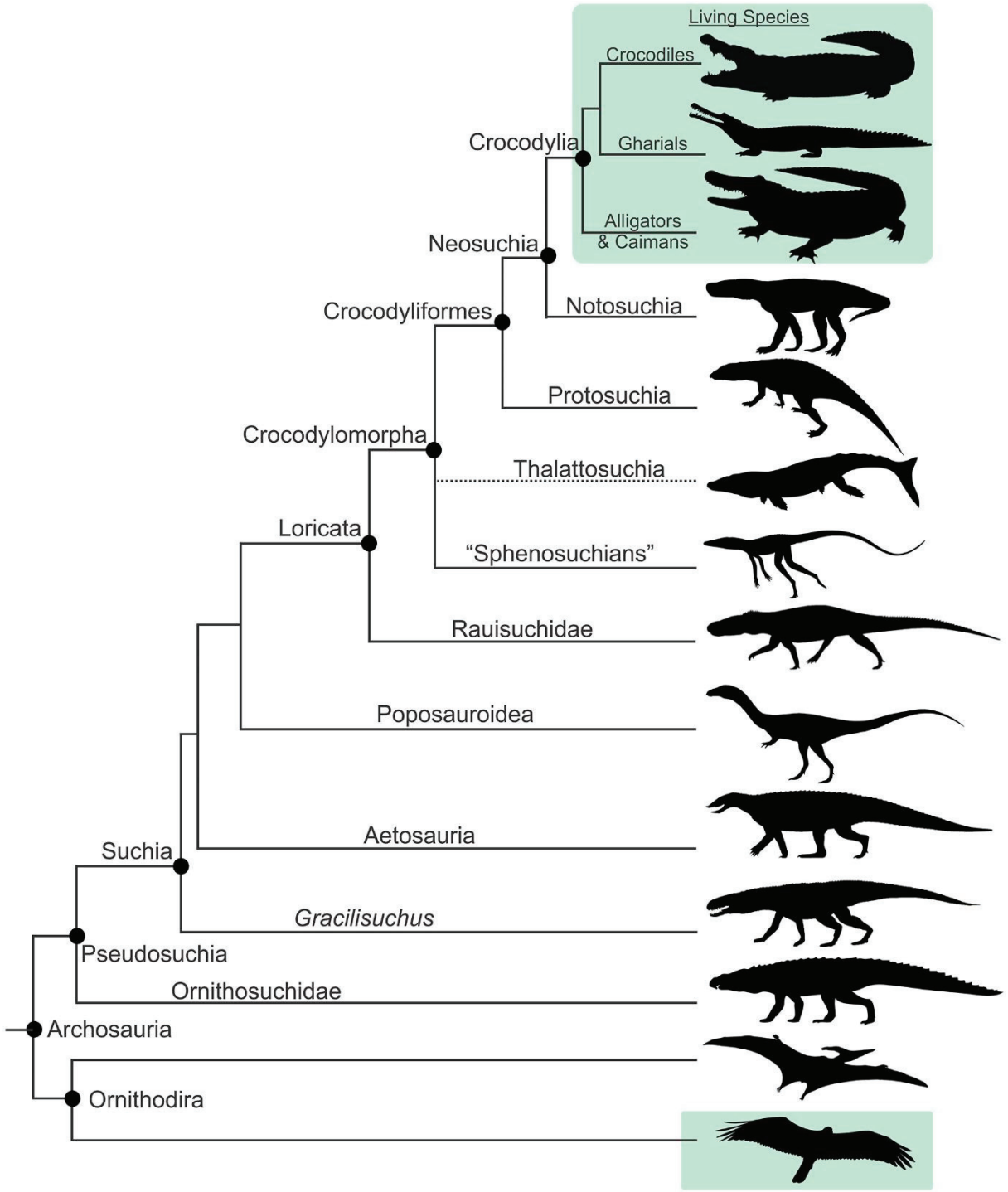

Figure 1.1: Phylogenetic placement of Crocodylomorpha among other archosaurs. Taken from Holliday & Schachner (2022; fig. 1).

Sues *et al*., 2003), whereas in others (Benton & Clark, 1988; Parrish, 1991; Clark *et al*., 2001; Clark & Sues, 2002; Clark *et al*., 2004; Nesbitt, 2009, 2011; Mamani *et al*., 2022, Spiekman, 2023), they are retrieved as paraphyletic taxa, forming the "non-crocodyliforms crocodylomorphs". This issue could be related to outgroup choice, which is very important in phylogenetic analyses and influences the obtained topologies (Irmis *et al*., 2013). As the

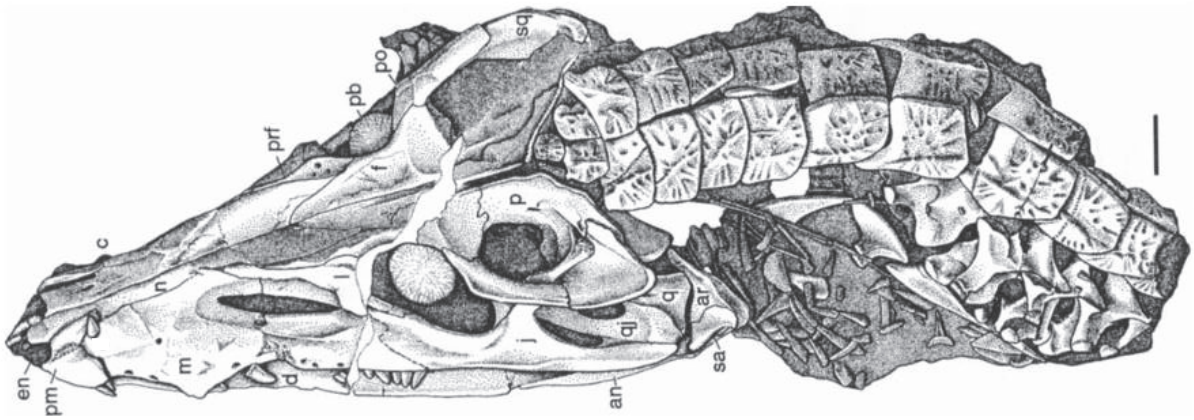

Figure 1.2: *Hesperosuchus agilis* (CM 29284), skull and cervical region in dorsal view. Modified from Clark *et al.* (2001; fig. 1). an: angular, ar: articular, c: caniniform tooth, d: dentary, en: external nares, f: frontal, m: maxilla, n: nasal, p: parietal, pb: palpebral, pm: premaxilla, po: postorbital, prf: prefrontal, q: quadrate, qj: quadratojugal, sa: surangular, sq: squamosal. Scale bar is 1 cm.

phylogenetic relationships of early archosaurians are poorly understood, there is no consensus on which outgroup(s) to choose, resulting in different character polarizations.

Sphenosuchians are found from the equator (Sues *et al*., 2003; Nesbitt *et* al., 2005; To *et al*., 2021) to mid paleolatitudes (40-50°) in the southern and northern hemispheres (Bonaparte, 1969; Walker, 1990; Sereno & Wild, 1992; Clark & Sues, 2002; Lecuona *et al*., 2016; Mamani *et al*., 2022). This indicates that they were able to withstand various climates: for example, during the Late Triassic to Early Jurassic, equatorial regions were warm and humid, middle latitudes were warm and arid and high latitudes were cool and humid (Kent & Tauxe, 2005; Sellwood & Valdes, 2006; Whiteside *et al*., 2011). Fossils have also been found in fluvial and floodplain depositional environments (Dubiel *et al.*, 1989; Schwartz & Gillette, 1994; Smith & Kitching, 1997; Caselli *et al*., 2001; Hester *et al*., 2001; Eberth *et* al., 2001; Arcucci *et al*., 2004; Bordy *et al*., 2004a, b; Currie *et al*., 2009; Smith *et al*., 2009), with the exception of *Terrestrisuchus gracilis* Crush, 1984 (Fraser & Sues, 1994; Whiteside & Marshall, 2008). This observation probably has a taphonomic origin, as these environments are ideal for the conservation of such organisms but could also indicate a lifestyle with terrestrial affinities.

Non-crocodyliforms crocodylomorphs display altirostral skulls, adapted to a terrestrial lifestyle and *Junggarsuchus sloani* Clark, Xu, Forster & Wang, 2004, the most derived 'sphenosuchian', has smaller supratemporal fenestrae and a large area of insertion for the *M. pterygoideus* on the mandible, suggesting powerful biting abilities (Schumacher, 1973). Furthermore, their tooth crows are labiolingually flattened and have serrated carinae, indicating a carnivorous diet (Abler, 1992). After the decline of 'rauisuchians' and their replacement by theropods dinosaurs

(Nesbitt *et al*., 2013), early crocodylomorphs were not apex predators, as highlighted by *Phyllodontosuchus lufengensis* Harris, Lucas, Estep & Li, 2000 which displays a heterodont dentition with posterior leaf-shaped crowns, implying a diet more inclined towards omnivory (Irmis *et al*., 2013). Abdominal content (Nesbitt *et al*., 2006) and predation marks (Walker, 1990; Sues *et al*., 2003) provide further evidence that early crocodylomorphs were not at the top of the food chain.

Early crocodylomorphs have a limited dorsal armour, elongated slender limbs in an erect posture, and procoelous vertebrae with short transverse processes corresponding to a terrestrial lifestyle (Parrish, 1987; Clark *et al*., 2004; Fig. 1.3). In its detailed study of *Hallopus*, Walker (1970) also noted that the narrow distal end of the humerus and the short olecranon process of the ulna allowed full extension of the forelimb, with a horizontally-fixed carpal and tarsal region (i.e., digitigrade). The absence of a greater trochanter on the femur implies that hindlimb movement was restricted to the parasagittal plane. The extended iliac blade (and thus extended *iliofemoralis* and *iliotibialis* musculature) is further evidence to this stance, maybe even allowing the gallop. Recently, Spiekman (2023) showed through a histological study that *Saltoposuchus* had a high growth rate, associated with a high resting metabolic rate and active lifestyle.

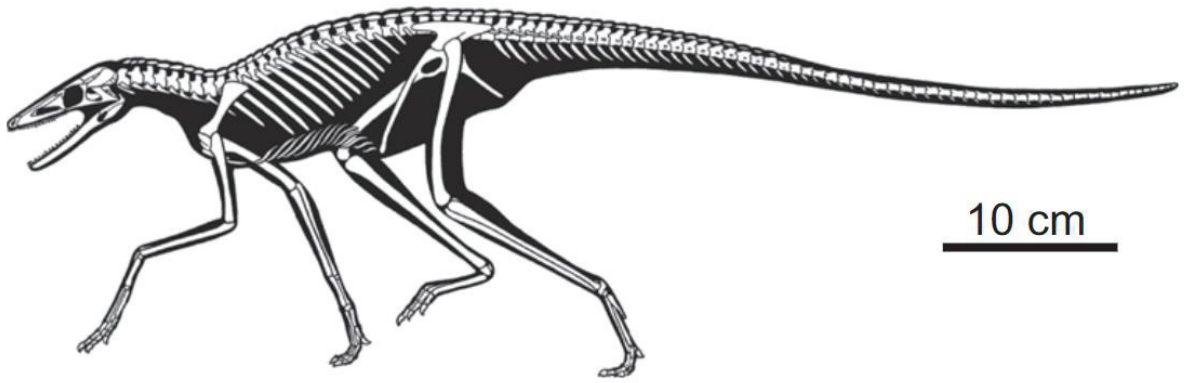

Figure 1.3: Hypothetical reconstitution of *Terrestrisuchus gracilis*. Taken from Irmis *et al*. (2013; fig. 5), modified from Currie (1984) and Sereno & Wild (1992; fig. 11).

II- Protosuchians

'Protosuchians', or non-mesoeucrocodylians crocodyliforms, are also most probably a paraphyletic group (Wu & Li, 1994; Clark & Sues, 2002; Pol & Norell, 2004a, b; Pol *et al*., 2004, 2013; Fiorelli & Calvo, 2007; Clark, 2011; Buscalioni, 2017; Lio *et al*., 2018; Martínez *et al*., 2018; Dollman *et al*., 2021; Melstrom *et al*., 2022). However, similarly to

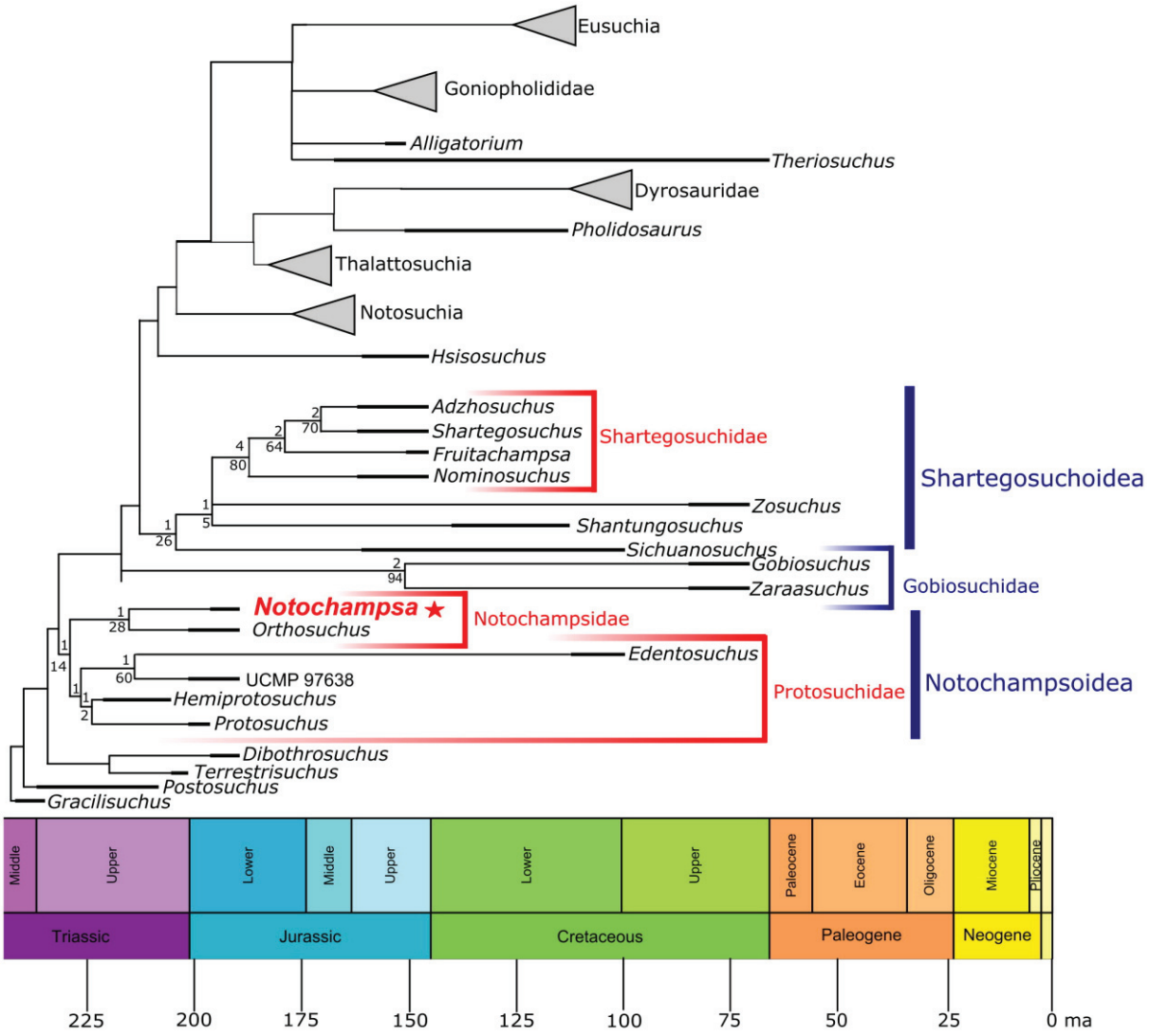

Figure 1.4: Phylogenetic tree of 'protosuchians'. Taken from Dollman *et al.* (2021; fig. 9).

'sphenosuchians' and probably for the same reasons, some other studies have supported the monophyly of the group (Wu *et al.*, 1994a, 1997; Dollman *et al.*, 2018). Recently, Dollman *et al.* (2021) proposed to incorporate those taxa into three monophyletic clades and four families (Fig. 1.4).

The earliest occurrences of the group are from the Norian (early Triassic) of Argentina: *Coloradisuchus abelini* Martínez, Alcober & Pol, 2018 and *Hemiprotosuchus leali* Bonaparte, 1969 from the Los Colorados Formation, as well as a putative unnamed specimen from the Quebrada del Barro Formation (Martínez *et al.*, 2015). After the Triassic/Jurassic biological crisis, 'protosuchians' are then quickly widespread throughout the Jurassic: in the south of Africa, there are at least three different taxa during the early Jurassic (van Hoepen, 1915; Nash, 1968; Raath, 1981; Busbey & Gow, 1984; Dollman *et al.*, 2019, 2021); in North America, those

organisms are also well-known, with at least five different taxa (Brown, 1933; Colbert & Mook, 1951; Galton, 1971; Hunt & Lockley, 1995; Sues *et al*., 1996; Clark & Sues, 2002; Clark, 2011; Melstrom *et al*., 2022); as well as in central Asia (Li *et al*., 1994; Wu & Sues, 1996a; Kurzanov *et al*., 2003; Peng & Shu, 2005; Wu *et al*., 2023). One exquisitely preserved specimen is known from the Oxfordian of Argentina (Pol *et al*., 2013) and there could also be some occurrences in Europe (Gierliński & Potemska, 1985; Moreau *et al*., 2019). During the Cretaceous, 'protosuchians' are reported from Asia (Young, 1961; Osmólska, 1972; Osmólska *et al*., 1997; Wu *et al*., 1994a, 1997; Pol & Norell, 2004 a, b; Pol *et al*., 2004; Hangjae *et al*., 2005), Europe (Buscalioni, 2017) and South America (Fiorelli & Calvo, 2007; Lio *et al*., 2018). It is especially interesting to see that there is no report of 'protosuchians' in North America and the south of Africa during the Cretaceous and that *Neuquensuchus universitas* from South America probably had an Asian origin (Fiorelli & Calvo, 2007), implying that 'protosuchians' underwent different paleobiogeographical processes compared to notosuchians, as will be underlined later.

Unfortunately, and as will be seen in other crocodylomorph groups, there are most probably a plethora of other forms and specimens from the Mesozoic of Central Asia in the Russian and Chinese paleontological literature, described in the works of Mikhail Efimov (Paleontological Institute, Russian Academy of Sciences) or the early works of Yang Zhongjian (Institute of Vertebrate Paleontology and Paleoanthropology). Those references are very hard to obtain and are often not translated in English, which is why I could not include most of them in this thesis. However, the reassessment of specimens and taxa has begun (Halliday *et al*., 2013; Turner, 2015; Kuzmin *et al*., 2019; Kuzmin, 2022a) and will be amplified. This is for example the case of the genera *Hsisosuchus* Young & Chow, 1953 and *Sichuanosuchus* Peng, 1995 from the Jurassic of the Sichuan basin in China, whose phylogenetic relationships and paleoecological traits remain to be ascertained, but have a skull morphology reminiscent of other terrestrial forms (Young & Chow, 1953; Li *et al*., 1994; Wu *et al*., 1994b, 1997; Peng, 1995; Gao, 2001; Peng & Shu, 2005; Wu *et al*., 2023).

As for 'sphenosuchians', 'protosuchians' are inferred to have had an erect stance (Fig. 1.5), as evidenced by the hinge-like articulations, elongated pubis and long distal carpals of *Cassissuchus sanziuami* (Buscalioni, 2017), the articular heads and shafts of the humerus and the development of appendicular osteoderms in *Gobiosuchus kielanae* (Osmólska *et al*., 1997) and the proportionally long limbs of *Protosuchus richardsoni* (Colbert & Mook, 1951) and *Neuquensuchus universitas* (Fiorelli & Calvo, 2007; Lio *et al*., 2018). However, a restricted neck flexibility is inferred from the overlapping cervical vertebrae of *Neuquensuchus*

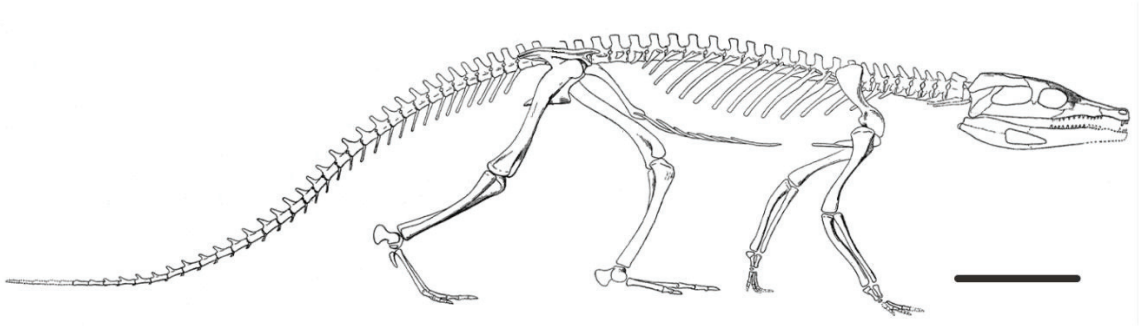

Figure 1.5: Reconstruction of *Protosuchus richardsoni*, based on AMNH 3024. Modified from Colbert & Mook (1951; fig. 4). Scale bar is 5 cm.

universitas (Lio *et al*., 2018) and the successive transverse rows of osteoderms (with laterally expanded nuchals) and elongated cervical ribs in *Gobiosuchus kielanae* (Osmólska *et al*., 1997), although it has also been hypothesized to be the results of defence mechanisms (Colbert & Mook, 1951).

In those taxa, we also see the first definitive appearance of a connection between the quadrate and the braincase (Pol *et al*., 2013), which is of pivotal importance in the acquisition of the strong bite force observed today in extant crocodylians and gave way to different adaptations, as will be seen in notosuchians. 'Protosuchians' thus would have displayed several different diets. Gobiosuchids, with their sharp and pointed teeth associated with small body size, could have fed preferentially on insects or other small invertebrates (Osmólska *et al*., 1997; Buscalioni, 2017), while *Edentosuchus* could have been herbivorous, with its rounded and columnar post canine teeth (Li *et al*., 1994). Those different ecological adaptations and the adaptative plasticity of the group are a good explanation as to why 'protosuchians' are known until the late Cretaceous, surviving two major biological crises.

III- Notosuchians

Notosuchians are a monophyletic clade which has achieved a huge diversity during the Cretaceous and is recognized as one of the only two groups of crocodylomorphs to survive the end Cretaceous biological crisis, with some taxa found until the Miocene (Paolillo & Linares, 2007). Here, I will describe with more details the several families that constitute this clade, as it is very diversified and especially important when studying the terrestrial adaptations of crocodylomorphs and their transition to a semi-aquatic lifestyle in the Cenozoic.

A- Uruguaysuchidae Gasparini, 1971

Uruguaysuchids form a family of notosuchian crocodylomorphs exclusively known from Gondwana during the Cretaceous (Pol & Leardi, 2015). Those little organisms are known simultaneously in several Cenomanian to Maastrichtian African deposits (Buffetaut, 1981; Turner, 2006; Sereno *et al*., 2003; Sereno & Larsson, 2009) and Barremian-Santonian of South America (Price, 1959; Ortega *et al*., 2000; Pol & Apesteguía, 2005; Soto *et al*., 2011; Dumont *et al*., 2020a). Since the early work of Buffetaut (1981), they have thus been taken as great examples of the paleobiogeographic vicariance event of terrestrial faunas that occurred between South America and Africa during the opening of the South Atlantic Ocean (Barremian to middle Albian; Pletsch *et al*., 2001; Turner, 2004), with subaerial connections that may have existed until the late Cretaceous (Sereno *et al*., 2003). This was also highlighted in other crocodylians (Buffetaut & Taquet, 1977; Souza *et al*., 2020a) and microvertebrate remains (Pochat-Cottilloux *et al*., 2022a).

Although their monophyly is not contested, the relationships of the different uruguaysuchids are still subject to debate and the taxonomic affinities of some *Araripesuchus* members could be reassessed. For example, *Araripesuchus rattoides* Sereno & Larsson, 2009 was erected from two dentary fragments of the Kem Kem group (Morocco) with no true diagnostic characters. The phylogenetic position of uruguaysuchids also remains enigmatic, either close to neosuchians (Buckley & Brochu, 1999; Buckley *et al*., 2000; Ortega *et al*., 2000; Brochu *et al*., 2002; Turner, 2006) or at the base of Notosuchia (Wu *et al*., 1997; Pol, 2003; Pol & Norell, 2004b; Pol & Apesteguía, 2005; Dumont *et al*., 2020a).

Recently, Nieto *et al*. (2022), through a finite element analysis of *Araripesuchus gomesii* Price, 1959, proposed that this organism would have suffered less mechanic stress in a head-twist feeding movement than a head-shake (as is seen today in *Alligator mississippiensis*), in relation with the difference in snout morphology of the two taxa. Given the size of the specimens, this could imply a diet focused on small preys such as insects and small vertebrates, which is corroborated by the anatomical dental studies of Ösi (2014) and Figueiredo & Kellner (2021). *Anatosuchus minor* Sereno, Sidor, Larsson & Gado, 2003 has been inferred to be a scratcher type feeder, based on its elongate flat-tipped manual unguals, adapted for feeding on small vertebrates with its hook-shaped tooth crowns and duck-shaped snout (Sereno & Larsson, 2009).

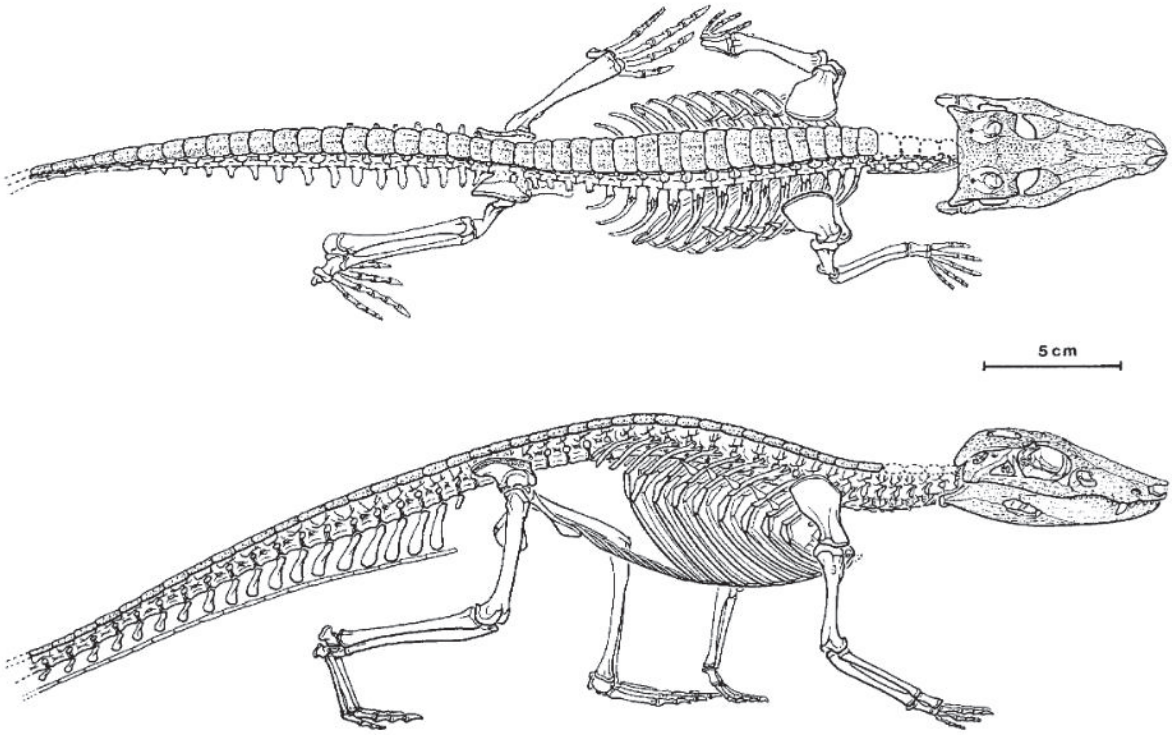

Figure 1.6: Skeletal reconstruction of *Araripesuchus gomesii* (from AMNH 24450). Taken from Hecht (1991).

Considering some exquisitely preserved specimens, relatively little is known about the stance of uruguaysuchids. Hecht (1991) figured and interpreted a semi-erect stance for *Araripesuchus gomesii*, adapted from a yet undescribed specimen (AMNH 24450; Fig. 1.6), while Sereno & Larsson (2009) infer an upright posture for *Anatosuchus minor* and *Araripesuchus wegeneri* Buffetaut & Taquet, 1979 based on their straight-shafted bones. A detailed biomechanical analysis would help to understand this aspect better.

B- Peirosauridae Gasparini, 1982

As uruguaysuchids, peirosaurids have a Gondwanan repartition and are known from Cretaceous deposits. The oldest record is *Amargasuchus minor* from the La Amarga Formation (Hauterivian, Argentina; Chiappe, 1988). However not much is known about this taxon, and it is very rarely included in phylogenies due to its incompleteness: only the right maxilla is preserved. Then, peirosaurids are known from the Aptian to the Maastrichtian in South America (Price, 1955; Buffetaut, 1985a; Chiappe, 1988; Gasparini *et al*., 1991; Carvalho *et al*., 2004, 2007; de Vasconcellos, 2006; Leardi & Pol, 2009; Calvo & Porfiri, 2010, Iori *et al.*, 2011) with a plethora of new forms described in the last decade (Iori & Garcia, 2012; Martinelli *et al.*, 2012; Lio *et al*., 2016; Barrios *et al*., 2016; Filippi *et al*., 2018; Pinheiro *et al.*, 2018, 2023; Coria *et al.*, 2019; Geroto & Bertini, 2019; Lamanna *et al*., 2019; Queiroz, 2022). Those

organisms are also known from the Aptian to the Maastrichtian of Africa (Buffetaut, 1974a, b, 1976a, 1994; Larsson & Sidor, 1999; Larsson & Sues, 2007; Rasmusson Simons & Buckley, 2009; Sertich & O'Connor, 2014; Ibrahim *et al*., 2020; Nicholl *et al*., 2021). Finally, teeth from the Naskal beds of India (Maastrichtian) could be referred to *Hamadasuchus* (Prasad & de Lapparent de Broin, 2002), but this occurrence would need to be confirmed by additional material. The origin of peirosaurids is thus difficult to assess, but it is probably from a Gondwanan ancestor that has evolved in separate lineages after the separation of South America and Africa (Chiappe, 1988).

The interrelationships of peirosaurids are poorly understood and subject to numerous debates. In his early works, Buffetaut created the clade Trematochampsidae, based on numerous fossils from the In Beceten Formation (Niger, Senonian; Buffetaut, 1974a, b, 1976a), however a recent revision of those specimens instead advocates for the presence of numerous taxa and for *Trematochampsa taqueti* to be considered as a nomen dubium as it is deemed non autapomorphic, warranting the abandon of the family Trematochampsidae as well (Meunier & Larsson, 2018). More generally, the taxonomic content of north African peirosaurids is subject to debate (Cavin *et al*., 2010; Ibrahim *et al*., 2020; Nicholl *et al*., 2021). Itasuchidae Carvalho, Ribeiro & Avilla, 2004 was originally proposed as a clade uniting some south American and African forms, but posterior contributions failed to recover this clade and it was thus abandoned. However, Pinheiro *et al*. (2018) has recently reproposed and redefined Itasuchidae, as part of the reassessment of "*Goniopholis*" *paulistanus* Roxo, 1936, which was confirmed in Pinheiro *et al*. (2023). Numerous taxa of peirosaurids are only known from very fragmentary mandibular remains, and many specimens were unfortunately illegally smuggled from South America or destroyed in the 2018 fire of Museu Nacional (UFRJ; Pinheiro *et al*., 2023), so those issues remain open.

Although little is known about the post cranial anatomy of peirosaurids, some exquisitely preserved specimens have allowed the assessment of some of their paleobiological traits (Fig. 1.7). The histological studies of Sena (2017) and Sena *et al.* (2018, 2023) have highlighted that MN 7466-V, a *Pepesuchus deiseae* specimen, was a mature female individual, which had already performed some ovogenetic cycles, as well as having a probable semi-aquatic lifestyle because of osteosclerosis observed in the metacarpals. Furthermore, Sharpey's fibers observed perpendicularly to the outer layer of the external cortex on osteoderms of *Itasuchus jesuinoi* Price, 1955 and *Uberabasuchus terrificus* Carvalho, Ribeiro & Avilla, 2004 indicate a tight attachment to the dermis and an overlying layer of skin, increasing the flexibility of their armor.

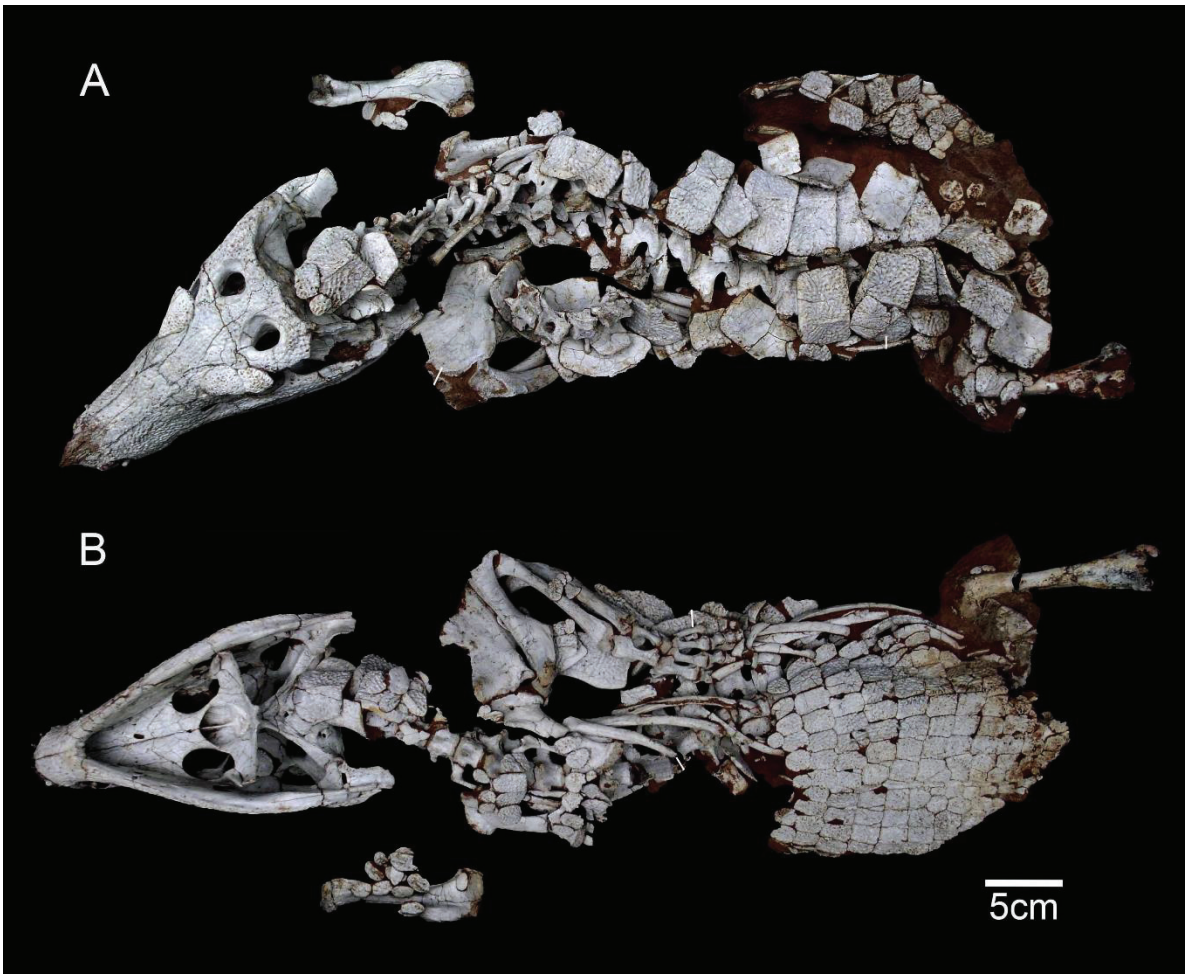

Figure 1.7: Skeleton of *Montealtosuchus arrudacamposi* (MPMA-16-0007/04) from the Turonian - Santonian of Adamantina Formation (Brazil). A: dorsal view, B: ventral view. Modified from Tavares *et al*. (2017; fig. 1).

Comparatively to *Peirosaurus* or *Uberabasuchus*, *Itasuchus* has a larger and heavier osteoderm skeleton with longitudinal keels, which would make it more fitted to a semi-aquatic lifestyle according to Marinho *et al.* (2006). On the other hand, the study of the post cranium of *Uberabasuchus* indicates an upright posture and terrestrial lifestyle, through a particular articular structure between the femur and the ilium and the imbrication of the dorsal osteoderms (de Vasconcellos, 2006). The exceptional preservation of this taxon (contrary to other fossils from the same assemblage) indicates that it could also have had burrowing habits, as observed nowadays on some extant crocodiles (de Vasconcellos & Carvalho, 2006). Osteoderms of *Montealtosuchus arrudacamposi* Carvalho, de Vasconcellos & Tavares, 2007 also indicate a lighter armor corresponding with terrestrial habits, as they display a reduced number of dorsal osteoderms rows and disarticulated accessory osteoderms (Tavares *et al*., 2015). A couple of years later, Tavares *et al*. (2017) published an extensive study of the skeletal remains of the same taxon, further advocating for the terrestrial lifestyle of this organism, through the rearticulation of its limbs in living position and observation of the cursorial movement

necessarily associated, especially because the anterior limbs were interpreted to be in a more upright position than in extant crocodiles, as well as the observed elongated metacarpals (as in sphenosuchians and some protosuchians). de Vasconcellos *et al.* (2004) further argue that the slender and laminated claws of *Uberabasuchus terrificus* would have been used for tearing carcasses or seize small preys.

Finally, *Roxochampsa paulistanus* could have had a more generalist diet (maybe durophageous), as evidenced by its posterior molariform teeth that are also observed today in alligators and caimans (Pinheiro *et al*., 2018). On the other hand, bite marks recently found on a sauropod epiphysis from the Presidente Prudente Formation (Campanian - Maastrichtian of Brazil) could indicate carnivory or necrophagy in itasuchids (Da Costa Pereira *et al*., 2022).

C- Mahajangasuchidae Sereno & Larsson, 2009

There are only two known taxa of mahajangasuchids: *Mahajangasuchus insignis* Buckey & Brochu, 1999 from the Campanian-Maastrichtian Maevarano Formation of Madagascar (Buckley & Brochu, 1999; Tuner & Buckley, 2008) and *Kaprosuchus saharicus* Sereno & Larsson, 2009 from the Cenomanian Echkar Formation of Niger (Sereno & Larsson, 2009).

The first one was originally described on mostly post cranial remains (Buckley & Brochu, 1999), which were later completed by cranial remains (Turner & Buckley, 2008; Fig. 1.8). The occurrence of this taxon corresponds with paleobiogeographical models in which Madagascar and Africa were still connected during the Early Cretaceous (Hay *et al*., 1999). It also provides interesting perspectives on the evolution of the crocodylian palate: as this taxon has an Eusuchian-style palate (fully pterygoid bound choanae) without being part of Eusuchia, it hints to this character being more linked to functional constraints together with the occurrence of platyrostry rather than to a phylogenetic signal (Turner & Buckley, 2008).

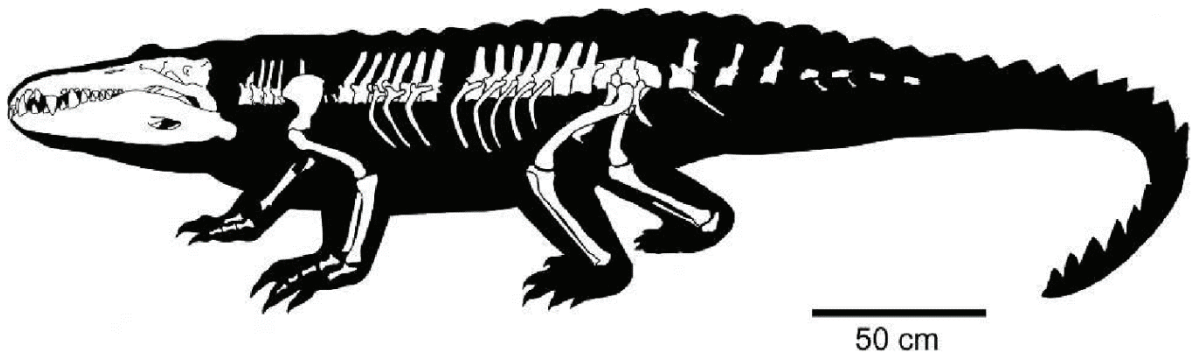

Figure 1.8: Skeletal reconstruction of *Mahajangasuchus insignis* (taken from Turner & Buckley, 2008, fig. 2).

The description of *Kaprosuchus saharicus* allowed to confirm the close links of those taxa, with important characters on the cranial, palate and mandibular regions (Sereno & Larsson, 2009). *Kaprosuchus* has sharp-edge hypertrophied caniniform teeth, associated with a retroarticular process allowing a rapid opening of the mouth. The fusion of the nasals could also be interpreted as an accommodation to a powerful bite. Those characters, along with the lateral orientation of the orbits, indicate a terrestrial rather than aquatic predator (Sereno & Larsson, 2009).

D- Sphagesaurians

Among notosuchians, sphagesaurians are historically very well-known with the first fossil of this clade described, *Notosuchus terrestris* Woodward, 1896, also being the first ever described notosuchian. However, although described in great details with numerous exquisitely preserved specimens, a consensus among their intra and inter relationships was only reached quite recently, with the proposed clade Sphagesauria Ruiz, Bronzati, Ferreira, Martins, Queiroz, Langer & Montefeltro, 2021 (Pinheiro *et al*., 2021), comprising both the original family Sphagesauridae Kuhn, 1968 and a paraphyletic group previously called "advanced notosuchians" (Pol *et al*., 2014).

The known fossil remains of this clade make it endemic to South America during the Late Cretaceous and apart from a taxon in the Turonian - Santonian Cajones Formation in Bolivia (Novas *et al*., 2009; Leardi *et al*., 2015) and two taxa from the Campanian Los Llanos Formation (Fiorelli *et al*., 2016) and Santonian Bajo de la Carpa Formation (Woodward, 1896; Gasparini, 1971; Pol, 2005; Fiorelli & Calvo, 2007; Barrios *et al*., 2018), most of the occurrences are from the Bauru Group of Brazil (Fig. 1.9). At least ten different taxa are found in the Campanian - Maastrichtian Adamantina Formation (Price, 1950; Pol, 2003; de Vasconcellos & Carvalho, 2005; Nobre & Carvalho, 2006, 2013; Zaher *et al*., 2006; Nobre *et al*., 2007; Marinho & Carvalho, 2009; Iori & Carvalho, 2009, 2011; Kellner *et al.*, 2011a; Pol *et al.*, 2014; Iori *et al*., 2016, 2018; Martinelli *et al*., 2018; Cunha *et al*., 2020), one from the Turonian - Campanian Santo Anastácio Formation (Ruiz *et al*., 2021), one from the Campanian Uberaba Formation (Martinelli *et al*., 2019), one from the Maastrichtian Marilia Formation (Kellner *et al*., 2011b) and one from the Turonian Araçatuba Formation (Pinheiro *et al*., 2021).

The relatively high number of specimens has allowed a lot of different paleobiological studies, focused on different areas. Using histological proxies, Sena (2017), Sena *et al*. (2022) and Navarro *et al*. (2023) have showed that *Mariliasuchus amarali* and *Notosuchus terrestris* have

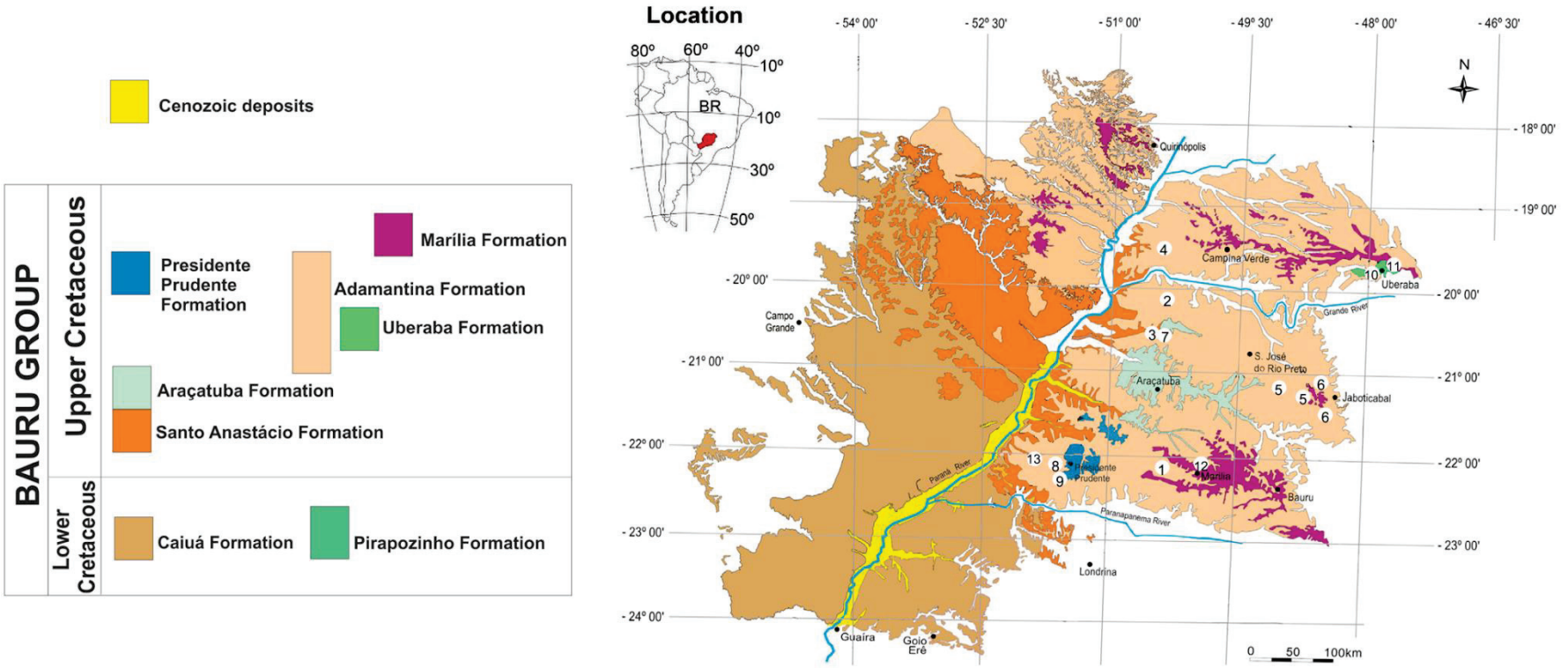

Figure 1.9: Map of the different formations of the Bauru Group (Brazil) showing the repartition of the different sphagesaurian taxa. 1: *Adamantinasuchus navae* Nobre & Carvalho, 2006, 2: *Armadillosuchus arrudai* Marinho & Carvalho, 2009, 3: *Caipirasuchus attenboroughi* Ruiz, Bronzati, Ferreira, Martins, Queiroz, Langer & Montefeltro, 2021, 4: *Caipirasuchus mineiri* Martinelli, Marinho, Iori & Ribeiro, 2018, 5: *Caipirasuchus montealtensis* de Andrade & Bertini, 2008, 6: *Caipirasuchus paulistanus* Iori & Carvalho, 2011, 7: *Caipirasuchus stenognathus* Pol, Nascimento, Carvalho, Riccomini, Pires-Domingues & Zaher, 2014, 8: *Caryonosuchus pricei* Kellner, Campos, Riff & de Andrade, 2011, 9: *Coronelsuchus civali* Pinheiro, de Souza, Bandeira, Brum, Pereira, de Castro, Ramos & Simbras, 2021, 10: *Eptalofosuchus viridi* Marinho, Martinelli, Basilici, Soares, Marconato, Ribeiro & Iori, 2022, 11: *Labidiosuchus amicum* Kellner, Figueiredo, Azevedo & Campos, 2011, 12: *Mariliasuchus amarali* Carvalho & Bertini, 1999 and *Mariliasuchus robustus* Nobre, Carvalho, de Vasconcellos & Nava, 2007, 13: *Sphagesaurus huenei* Price, 1950. Modified and adapted from Pinheiro *et al*. (2018; fig. 2) and Cunha *et al*. (2020; fig. 1).

retained the ancestral moderate growth pattern of archosaurs. The heterodont dentition of those organisms has also been extensively studied: for example, Pol (2003), Pol *et al*. (2014) and Iori *et al*. (2016) infer an herbivorous feeding mode of *Sphagesaurus huenei* and *Caipirasuchus* through the tooth-tooth occlusion, fore-aft jaw movements and unilateral jaw occlusion pattern induced from the wear facets of the teeth. The tooth battery of *Caipirasuchus montealtensis*, together with the concave and ornamented palate, have also been inferred to be the result of an herbivorous diet (de Andrade & Bertini, 2008; Fig. 1.10). Fiorelli & Calvo (2008) further showed that the specialized dentition (procumbent incisiform and posterior molariform with wear facets) and snout morphology (wide central depression of the nasal possibly indicative of nasolabial muscles) of *Notosuchus terrestris* were adapted for an herbivorous diet. The bite of *Caipirasuchus paulistanus* was reconstructed and observed experimentally from the fossil remains by Iori & Carvalho (2011) and two regions were observed: the anterior one, in which the teeth pierce and seize and the posterior one, where the teeth process the food, inducing a propalinal jaw movement. On the other hand, the molariform dentition but without possibility of anteroposterior jaw movement of *Adamantinasuchus navae* could also indicate an adaptation to a carnivorous/necrophagous diet (Nobre & Carvalho, 2006). In *Morrinhosuchus luziae*, Iori *et al.* (2018) infer an omnivorous diet linked with both caniniform teeth with an inferred robust bite force and molariform processing teeth. This hypothesis has been further reinforced when Nobre *et al*. (2008) chemically analysed coprolites attributed to *Mariliasuchus amarali*,

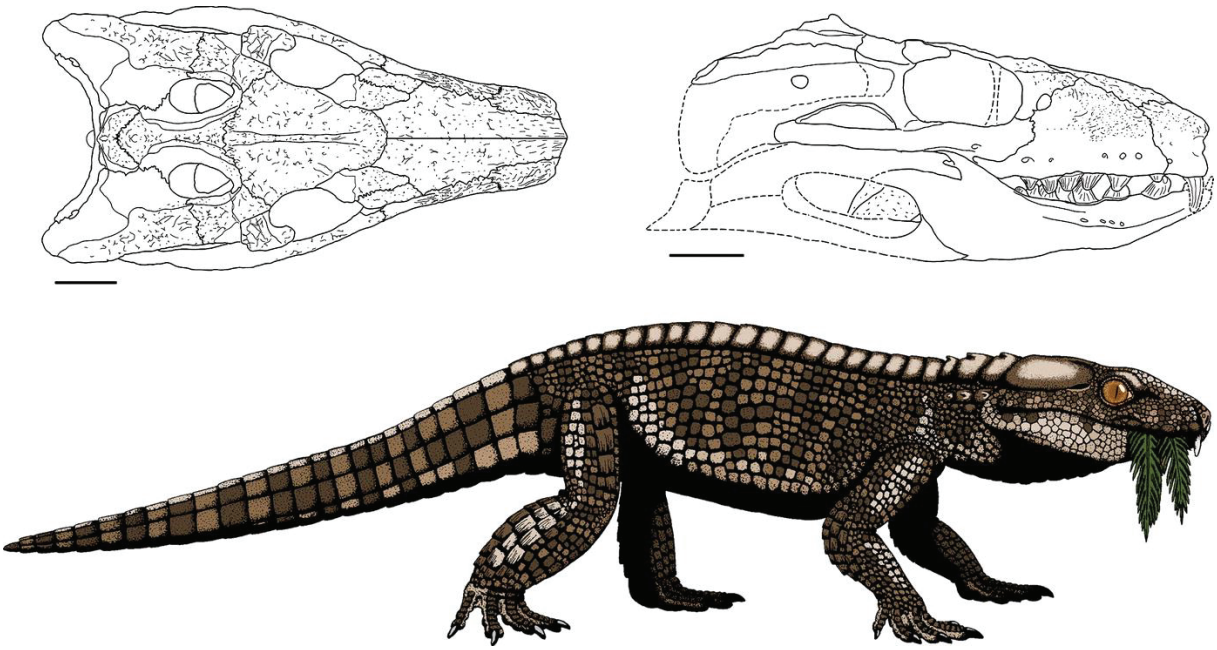

Figure 1.10: Proposed life reconstruction of *Caipirasuchus montealtensis*. Top: skull in dorsal and lateral view, scale bars are 2 cm. Bottom: restoration of complete specimen. Taken from de Andrade & Bertini (2008; fig. 15).

showing the presence of apatite and calcite corresponding to a carnivorous diet (Rodriguez de la Rosa *et al*., 1998) but also potassium that is linked with herbivory and omnivory (Hallgren, 1987). Indeed, the enamel of *Mariliasuchus* is truly unique among crocodylomorphs so far, with a unique combination of true and false denticles in the same tooth (zipomorph; Augusta & Zaher, 2019). This last study further proves that the heterodonty of this taxon is kept in all ontogenetic stages. In the histological study of Ricart *et al.* (2021), the teeth development and structure of baurusuchids, *Mariliasuchus* and a large sphagesaurid were compared. Baurusuchids exhibit a thin enamel layer, indicative of a carnivorous diet, whereas the large sphagesaurid has much thicker enamel indicative of a more herbivorous diet (Hwang, 2005; D'Emic *et al*., 2013), while *Mariliasuchus* has an intermediate thickness. Furthermore, enamel thickness variation is observed in the large sphagesaurid and the posterior teeth of *Mariliasuchus* but not in the baurusuchids, bringing a further argument to their difference in diets (Hwang, 2005; D'Emic *et al*., 2013). Finally, de Vasconcellos & Carvalho (2005) infer a terrestrial lifestyle from the reduced and specialized dental formula of *Mariliasuchus amarali*. This study on an ontogenetic series of this taxon is of particular interest, because it shows a thickening of the skull during ontogeny, corresponding to a caudal migration of the laterotemporal fenestra and a size increase of the supratemporal fenestra, indicating a stronger use of the adductor muscles during feeding in adults, maybe corresponding to different diets through the development of the organism and contradicting Augusta & Zaher (2019) hypothesis. A definite consensus on the exact ecology throughout ontogeny of *Mariliasuchus* and other sphagesaurians has thus yet to be reached.

Sphagesaurians were thus not at the top of the food chain, as evidenced in Godoy *et al*. (2014): sphagesaurian remains were found in the stomach of a baurusuchid, a top predator from the Adamantina Formation. Iori *et al*. (2016) hypothesize through the slender limbs of *Caipirasuchus* a cursorial habit, with this form of crocodylomorph relying on speed. The erect posture linked with a terrestrial lifestyle of sphagesaurians was also hypothesized through the deep acetabulum of *Notosuchus terrestris* (Pol, 2005), as well as the slender limbs and the probable reduction of the dorsal armor of *Caipirasuchus mineiri* (Martinelli *et al*., 2018). On the other hand, Nobre & Carvalho (2013) attributed a more amphibious lifestyle comparable to extant crocodylians to *Mariliasuchus amarali*, based on the morphology of its ilium and acetabular fossa, and robustness of its limb bones, which would be linked to a sprawling rather erect posture.

Martinelli *et al*. (2019) described a tetrapod burrow in the Marilia Formation (Brazil) that could correspond to the inferred size and habits of a small sized sphagesaurian, such as *Labidiosuchus amicum*, and which would also be linked with the robust forelimb observed in *Notosuchus terrestris* (Fiorelli & Calvo, 2008) and the abrasion pattern of the procumbent incisiform of *Mariliasuchus amarali* (Nobre *et al*., 2008). This hypothesis, although interesting, will have to be evidenced deeper.

Recently, Dias *et al*. (2020) have shown the presence of a pterygoid chamber in *Caipirasuchus* which they link to an enhanced vocalization ability (similarly to the pterygoid bulla of the extant *Gavialis gangeticus*; Martin & Bellairs, 1997), and perhaps sociality, as evidenced by other observations of egg clutches in association with *Yacarerani* (Novas *et al*., 2009).

E- Sebecidae Savage, 1951

Sebecids form a family of notosuchians that has been known since almost a century (Astre, 1931; Simpson, 1937; Colbert, 1946a; Rusconi, 1946). It is mostly known from the Paleogene of South America (Simpson, 1937; Colbert, 1946a; Langston, 1965; Buffetaut & Hoffstetter, 1977; Gasparini, 1984; Busbey, 1986; Buffetaut & Marshall, 1992; Gasparini *et al.*, 1993; Paolillo & Linares, 2007; Pol & Powell, 2011; Pol *et al*., 2012; Kellner *et al*., 2014; Bravo *et al*., 2021) and Europe (Astre, 1931; Antunes, 1975, 1986; Ortega *et al.*, 1996; Rossmann *et al.*, 2000; Ortega, 2004; Martin, 2014, 2016; Martin *et al*., 2023). *Eremosuchus elkoholicus* was also reported from the Eocene of Algeria (Buffetaut, 1982a, 1989) but is quite fragmentary and in need of a reassessment, together with a partial dentary from the Eocene Birket Qarun Formation in Egypt (Stefanic *et al*., 2019). Finally, there is also a recent report of a sebecid from the Maastrichtian of Spain (Sellés *et al*., 2020), which is very interesting because it implies that this family survived through the Cretaceous/Paleogene biological crisis and allows to ask the following question: why and how did these organisms survived through the crisis, whereas others with a similar inferred ecology (such as non-avian dinosaurs) did not?

This last occurrence also reopens another debate which is about the origin and paleobiogeographical history of Sebecidae. This family probably originated from sebecosuchians common ancestors that have dispersed in Gondwana in the Jurassic (*Razanandrongobe sakalavae*; Maganuco *et al*., 2006; Dal Sasso *et al*., 2017) and evolved independently in South America and Europe after the splitting of the two continents (Sellés *et al*., 2020), the European forms being linked to the reports from Africa following the Eurogondwana model (migration of some Gondwanan groups to Late Cretaceous archipelagos

via intermittent land bridges; Ezcurra & Agnolin, 2012; Csiki-Sava *et al*., 2015; Rabi & Sebök, 2015). Whether the close phylogenetic affinities of the South American and African/European forms are the result of an ecomorphological convergence or can be confirmed (Buffetaut, 1982a, b; Sellés *et al*., 2020; Martin *et al*., 2023) will hopefully be answered by a better knowledge of the African forms and sampling of the African Cretaceous strata.

The lifestyle of sebecids has been extensively studied: terrestriality was inferred once again from the long and slender limbs, the lateral compression of the snout with lateral orbits and anteriorly directed external nares, the powerful femur and development of the fourth trochanter and the ziphodont teeth reminiscent of those of terrestrial non-avian theropods (Gasparini, 1984, Buffetaut, 1986, 1989; Gasparini *et al*., 1993; Rossmann *et al*., 2000; Pol *et al*., 2012; Sellés *et al*., 2020). From the altirostral morphology of the skull of *Sebecus huilensis* Langston, 1965, Busbey (1986) further inferred a hypothetic ambush behavior of sebecids, based on comparison with the extant *Varanus komodoensis* Ouwens, 1912, the strongly bent pterygoid allowing a rapid closure of the mouth and a powerful bite (Gasparini *et al*., 1993). This interpretation is also supported by the detailed jaw musculature studies of Colbert (1946a) and Molnar (2012) on the skull of *Sebecus icaeorhinus* Simpson, 1937 which infer more powerful jaw adductors and a greater mandibular gape (Fig. 1.11). Finally, Bravo *et al*. (2022) recently showed that the morphological disparity of the palatal region of sebecids is higher than in any other notosuchian group, which these authors put into perspective with the diet of those organisms: as they exhibit palatal conformations between those of sphagesaurians (some of them inferred to be herbivorous; Pol, 2003; Fiorelli & Calvo, 2008; Pol *et al*., 2014; Iori *et al*., 2016; Ricart *et al*., 2021) and baurusuchids (hyper carnivorous; Montefeltro *et al*., 2020), sebecids would have had a carnivorous to omnivorous diet.

F- Baurusuchidae Price, 1945

Like sphagesaurians, baurusuchids are known exclusively from the Late Cretaceous of South America. At least nine taxa have been found in the Bauru group in Brazil (Price, 1945; Manzini *et al.*, 1996; Campos *et al*., 2001; Riff, 2003; de Vasconcellos *et al*., 2004; Carvalho *et al*., 2005, 2011a,b; Pinheiro *et al*., 2008; Montefeltro *et al*., 2011; Nascimento & Zaher, 2010, 2011; Geroto & Bertini, 2012; Marinho *et al*., 2013; Godoy, 2014; Godoy *et al*., 2014, 2016; Cotts *et al*., 2017; Darlim *et al*., 2021a,b; Martins, 2021; dos Santos *et al*., 2022) and two from the Bajo de La Carpa Formation, Argentina (Woodward, 1896; Martinelli & Pais, 2008; Leardi *et al*., 2018).

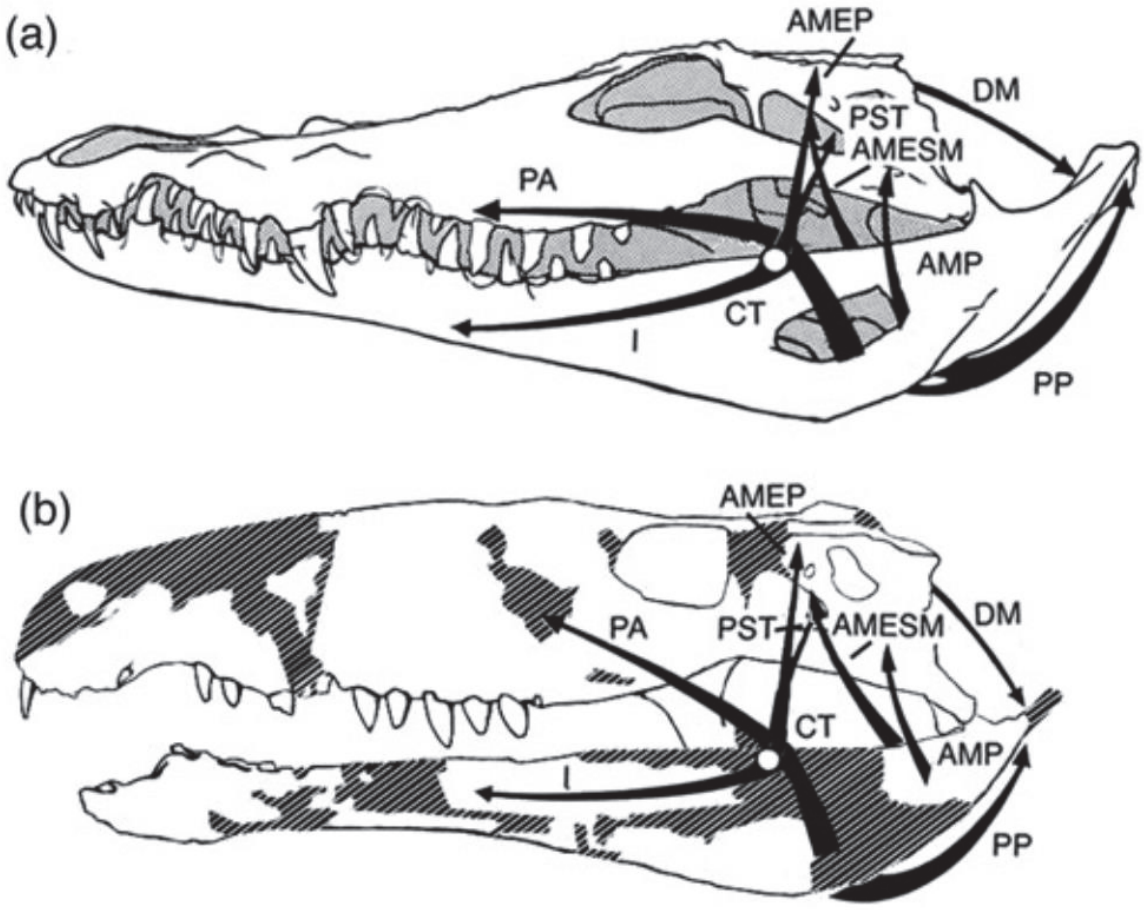

Figure 1.11: Jaw musculatures of *Crocodylus niloticus* (a) and *Sebecus icaeorhinus* (b). AMEP: *adductor mandibulae externus profundus*, AMESM: *adductor mandibulae externus superficialis et medialis*, AMP: *adductor mandibulae posterior*, CT: cartilago transiliens, DM: *depressor mandibulae*, I: *pars intramandibularis*, PA: *pterygoideus dorsalis*, PP: *pterygoideus ventralis*, PST: *pesudotemporalis*. Not to scale. Modified from Molnar (2012, fig. 15).

The terrestrial lifestyle of baurusuchids has been inferred from multiple observations, mainly on the skull shape (combined with increased skull resistance during biting; Carvalho *et al*., 2005; Marinho *et al*., 2013; Montefeltro *et al*., 2020) and position of the external nares and orbits (Riff, 2003). The ornamentation of the supraoccipital in *Stratiotosuchus maxhechti* has been linked with a developed nuchal musculature to support the head weight without the mitigation brought by water (Riff, 2003). In *Baurusuchus*, the close articulation of the dorsal vertebrae hinting at a robust and rigid dorsal spine, the high and expanded dorsal and sacral neural spines related to peculiar muscle attachment, the long and straight limb bones with a pronounced fourth trochanter on the femur, the peculiar deltopectoral crest on the humerus, the reduced space between the ulna and the radius, the laterally developed supraacetabular crest, the well-developed tarsal bones and the light exoskeleton, all point to a limb-driven, erect and terrestrial locomotion (de Vasconcellos *et al*., 2007; Nascimento & Zaher, 2010; Riff & Kellner, 2011; Godoy *et al*., 2016; Cotts *et al*., 2017). The surprising absence of osteoderms in

Pissarachampsa sera Montefeltro, Larsson & Langer, 2011 could represent a case of extreme adaptation to a terrestrial locomotion, where those structures are no longer needed to support the body; however, the potential impact of taphonomic processes cannot be ruled out (Godoy *et al*., 2016; Montefeltro, 2019). Nevertheless, the dermal armour conformation in baurusuchids is, with unsutured medial osteoderms and a cervicodorsal gap, and warrants future phylogenetic and/or ecological assessments (Montefeltro, 2019). Finally, a recent histological study of *Stratiotosuchus maxhechti* Campos, Suarez, Riff & Kellner, 2001, hints at the fast growth of this taxon, with a microstructure similar to those of theropods (de Andrade *et al*., 2023).

Baurusuchids are inferred to be apex predators. In this regard, their serrated carinae would have acted as lethal blades delivering powerful bites (Riff, 2003; Carvalho *et al*., 2005; Pinheiro *et al*., 2008; Marinho *et al*., 2013), while their robust and curved claws would be related to prey gripping (de Vasconcellos *et al.*, 2004). The size, orientation, and robustness of the pterygoid wings, as well as the enlarged supratemporal fenestrae, are, like in sebecids, indicative of a powerful and prolonged bite (Pinheiro *et al*., 2008). Definitive evidence came when Godoy *et al.* (2014) observed sphagesaurian remains in the abdominal cavity of *Aplestosuchus sordidus* Godoy, Montefeltro, Norell & Langer, 2014: baurusuchids were thus part of a complex food web (Fig. 1.12). Furthermore, coprolites referred to baurusuchids contain bone fragments, once again corroborating their carnivorous diet compared to contemporaneous sphagesaurians (de Oliveira *et al*., 2021). However, de Vasconcellos *et al.* (2008) and de Vasconcellos & Carvalho (2010) report on possible gastroliths found in association with baurusuchids remains, which is not in line with a carnivorous diet and are used nowadays by extant crocodylians to increase diving duration (Uriona *et al*., 2019). Bite marks on the tail of *Baurusuchus pachecoi* were even

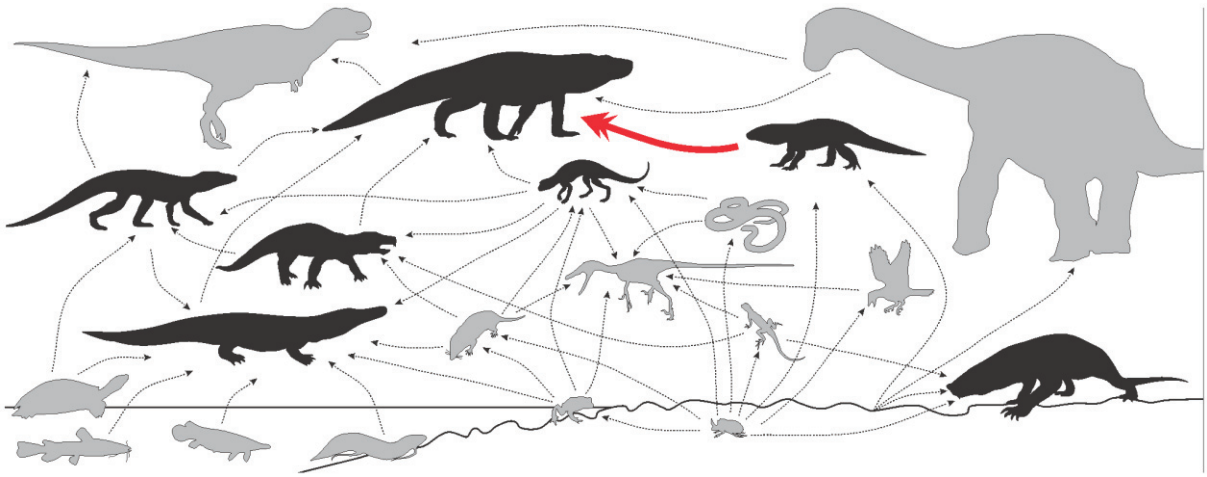

Figure 1.12: Inferred food web reconstruction of the ecosystem from the Adamantina Formation (Brazil) during the Late Cretaceous. The red arrow relates to the direct observation of the predatory habits of *Aplestosuchus sordidus* on a sphagesaurian (Godoy *et al*., 2014). Modified from Godoy *et al*. (2014; fig. 10).

attributed to individuals from the same species, as part of a male-to-male competition (de Vasconcellos & Carvalho, 2010).The hypothesis of baurusuchids (and sebecosuchians in general) being in competition with large non-avian theropods in South America during the Late Cretaceous has been extensively put forward (Gasparini *et al*., 1993; Carvalho *et al*., 2005; Marinho *et al*., 2013), based notably on their similarities in term of pelvic and limb anatomy (Riff & Kellner, 2011). This approach needs to be nuanced, as taphonomic and time averaging processes must also be considered, thus the apparent overabundance of crocodyliforms might indeed be a preservation artifact (Aráujo Jùnior & Marinho, 2013; Bandeira *et al*., 2018; de Celis *et al*., 2021; de Andrade *et al*., 2023).

From a developmental point of view, a recent histological study showed that baurusuchids alternated between periods of fast and slow growth, possibly correlated to seasonal changes and resources availibility (Marchetti *et al*., 2022), while osteoderm structure indicate an overlying thick layer of skin with impact for thermoregulation strategies (Sena *et al*., 2023).

G- Other forms

Some notosuchians cannot be attributed to specific groups, because of peculiar characteristics or the limited number of remains assigned to them. In the first case, an interesting clade is the taxa assigned to Candidodontidae Carvalho, Ribeiro & Avilla, 2004 from the Early to ‘middle’ Cretaceous of Africa (Clark *et al*., 1989; Gomani, 1997; O’Connor *et al*., 2010; Martin & de Lapparent de Broin, 2016) and Brazil (Carvalho, 1994; Nobre, 2004; Santos *et al*., 2011; Santos, 2014), representative of the Gondwanan affinities of notosuchians before the opening of the South Atlantic Ocean. The extremely diversified dentition of those small organisms has led to infer an omnivorous diet (Ösi, 2014) in a quite similar way to some sphagesaurians, with the ability of a fore and aft jaw movement (Clark *et al*., 1989; Gomani, 1997; O’Connor *et al*., 2010; Santos *et al*., 2011; Ösi, 2014). Martin & de Lapparent de Broin (2016) infer that *Lavocatchampsa sigogneaurussellae* Martin & de Lapparent de Broin, 2016 fed on abrasive materials (maybe insects), based on the extreme abrasion of some of its teeth. An erect posture was further inferred from the limb bones, cervical and calcaneal anatomy of *Malawisuchus mwakasyungutiensis* Gomani, 1997 and *Candidodon itapecuruense* Carvalho & Campos, 1988 (Gomani, 1997; Santos, 2014).

Another interesting taxon is *Simosuchus clarki* Buckley, Brochu, Krause & Pol, 2000 from the Maastrichtian of Madagascar: the high number of specimens assigned to this taxon allows to infer with high confidence an herbivorous diet and a terrestrial lifestyle, through its head

posture, peculiar dentition, and mandibular conformation (Kley *et al*., 2010). *Simosuchus* further possessed appendicular osteoderms and a developed dorsal and ventral armour, further indicating its non-aquatic habits and making it similar to armadillos (Hill, 2010; Fig. 1.13).

The second case highlights taxa such as *Doratodon* Seeley, 1881 from the Campanian of Europe or *Pehuenchesuchus* Turner & Calvo, 2005 from the Turonian - Coniacian of Argentina, which could be allied to Sebecidae but lacks anatomical data to do so (Bunzel, 1871; Company *et al*., 2005; Turner & Calvo, 2005; Rabi & Sebök, 2015; Filippi *et al*., 2021), hinting at a possible greater diversity than observed and having important paleobiogeographical implications (Rabi & Sebök, 2015). Similarly, *Chimaerasuchus* Wu, Sues & Sun, 1995 and *Wanosuchus* Zhang, 1981 (Zhang, 1981; Wu *et al*., 1995; Wu & Sues, 1996b) could represent notosuchian remains in Asia during the Cretaceous-Paleocene with similar habits to candidodontids (Wu & Sues, 1996b), but those reports must be confirmed by more better-preserved material. *Pabweshi pakistanensis* Wilson, Malkani & Gingerich, 2001 from the Maastrichtian Pab Formation (Wilson *et al*., 2001) could also be related to baurusuchids but its remains are very scarce.

IV- Neosuchians

Neosuchia Benton & Clark, 1988 forms a very widespread clade of crocodylomorphs that are all more closely related to extant crocodylians than to notosuchians. They are known since the Early Jurassic, with the occurrence of *Calsoyasuchus valliceps* Tykoski, Rowe, Ketcham & Colbert, 2002 (Kayenta Formation, United States). Here, as in notosuchians, I will go into more details in several families that constitute this clade, as some of them display adaptations for a terrestrial lifestyle.

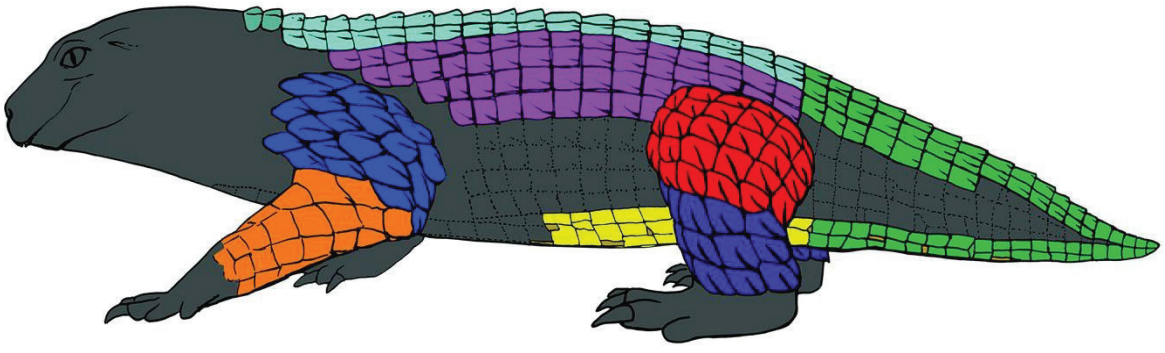

Figure 1.13: Reconstruction of *Simosuchus clarki* in lateral view. Light blue: nuchal and paravertebral shield, light green: caudal shield, purple: accessory dorsal shield, red: femoral osteoderms, dark blue: tibiofibular and humeral osteoderms, orange: radioulnar osteoderms, yellow: gastral shield. Scale bar is 10 cm. Modified from Hill (2010, fig. 1).

a- Atoposauridae Gervais, 1871

Atoposaurids are little crocodylomorphs that are known exclusively from the Jurassic and Cretaceous of Europe (Buffetaut, 1983; Buscalioni & Sanz, 1990; Brinkmann, 1992; Schwarz & Salisbury, 2005; Karl *et al*., 2006; Martin *et al*., 2010, 2014a; Tennant & Mannion, 2014; Tennant *et al*., 2016; Young *et al*., 2016b; Schwarz *et al*., 2017; Venczel & Codrea, 2019; Eijkelboom, 2020) and Southeast Asia (Lauprasert *et al*., 2011). *Brillanceausuchus babouriensis* Michard, de Lapparent de Broin, Brunet & Hell, 1990 from the Late Cretaceous of Cameroon and *Theriosuchus morrisonensis* Foster, 2018 from the Late Jurassic of the United States could also be atoposaurids, although their phylogenetic relationships are highly debated and the specimens are in need of a reassessment (Tennant *et al*., 2016). This is also the case for the remains attributed to cf. *Theriosuchus* sp. from the Early Cretaceous of China (Wu *et al*., 1996a). Furthermore, numerous microremains and teeth have been assigned to Atoposauridae throughout Europe (Cuny *et al*., 1991; Kriwet *et al*., 1997; Thies *et al*., 1997; Pouech *et al*., 2006, 2014; Schwarz *et al*., 2009; Néraudeau *et al*., 2012; Knoll *et al*., 2013; Vullo *et al*., 2014; Allain *et al*., 2022), Southeast Asia (Cuny *et al*., 2010), Africa (Haddoumi *et al*., 2016; Lasseron *et al*., 2020) and North America (Fiorillo, 1999), but those will also have to be confirmed by more complete remains.

The diet of atoposaurids has been inferred from their dentition and analogies with modern lizards and iguanas. Since these latter display various diets, paleoecological interpretations have been equally various. In the study of *Sabresuchus ibericus* Brinkmann, 1989, Brinkmann (1991) highlights that this organism may have been specialized in eating small vertebrates because of its lacertiform dentition, as do Schwarz & Salisbury (2005) and Schwarz *et al*. (2017) due to its small size. Buscalioni & Sanz (1990) assumed an entomophagous diet for *Theriosuchus* Owen, 1878, due to the similarity in dentition with iguanas, while Brinkmann (1992) proposed an herbivorous diet, although there are no signs of fore-aft jaw movements in the fossils. Thies *et al*. (1997) infer a piscivorous diet through comparisons with the dentition of fossil fishes and close occurrences of the two groups in fossil deposits.

Following their inferred diet, Brinkmann (1992) also proposes a terrestrially oriented lifestyle for *Theriosuchus*, in association with a large palpebral bone that is also found in the extant genus *Paleosuchus* Gray, 1862, one of the most terrestrially adapted extant crocodile (Campos & Magnusson, 2013). Although numerous skeletons are well known (Fig. 1.14), no detailed locomotor studies have been published, apart from the work of Eijkelboom (2020), which

Figure 1.14: Skeleton of *Alligatorellus beaumonti* (MNHN 15639) in dorsolateral view. Top: line drawing, bottom: photograph, scale bar is 1 cm. Modified from Tennant & Mannion (2014; fig. 3).

observes that the limb bones of *Knoetschkesuchus guimarotae* Schwarz & Salisbury, 2005 fall into the values of similar semi-aquatic taxa (Rooney, 2018).

b- Paralligatoridae Konzhukova, 1954

Paralligatorids are also small neosuchians but have been mostly known and better described since the beginning of the 21st century. They are found exclusively in Asia (Efimov, 1975; Wu *et al*., 2001; Pol *et al*., 2009; Turner, 2015; Kuzmin *et al*., 2019; Rummy *et al*., 2022) and North America (Adams, 2014, 2019; Noto *et al*., 2020; Noto, 2022). *Batrachomimus pastosbonensis* Montefeltro, Larsson, França & Langer, 2013 from the Late Jurassic of Brazil (Montefeltro *et*

al., 2013) would drastically extend the stratigraphic and geographic range of Paralligatoridae, but this occurrence is controversial and in need of a reassessment (Hester *et al*., 2016).

Paralligatorids and atoposaurids are either assumed to be sister taxa (Turner, 2015; Turner & Pritchard, 2015; Tennant *et al*., 2016; Schwarz *et al*., 2017; Leite & Fortier, 2018; Venczel & Codrea, 2019; Noto *et al*., 2020) or more distantly related with atoposaurids at the base of Neosuchia (Pol *et al*., 2009; Martin *et al*., 2010, 2020a; Adams, 2014), although this is probably the result of conflicting datasets being used repeatedly (for example, both results are found with two different datasets in Kuzmin *et al*., 2019). As the remains associated with this clade are mostly incomplete, paleoecological interpretations have been scarce. Adams (2019) infers a terrestrial lifestyle for *Tarsomordeo winkleri* Adams, 2019 based on its straight and gracile limb bones, compatible with an erect posture (Fig. 1.15). The feeding strategy of *Scolomastax sahlsteini* Noto, Drumheller, Adams & Turner, 2020 is inferred to have relied on an omnivorous/durophageous diet corresponding with its heterodont dentition and inferred enlarged adductor musculature (Noto *et al*., 2020; Noto, 2022). Those interpretations need to be better supported and broadened to other paralligatorid taxa.

c- Eusuchians

Eusuchia Huxley, 1875 is a wide clade comprising extant crocodiles (Alligatoridae, Gavialidae and Crocodylidae), as well as numerous fossils forms, with debated phylogenetic relationships and origin (Salisbury *et al*., 2006; Turner & Pritchard, 2015; Tennant *et al*., 2016; Leite & Fortier, 2018; Montefeltro *et al*., 2019; Martin *et al*., 2020a). Some of those fossil forms could exhibit adaptations to a terrestrial lifestyle.

1- Crocodylia Owen, 1842

Among the clade Crocodylia, a specimen from the phosphorites of Quercy (Eocene, France; de Stefano, 1905; Kälin, 1939; Rauhe, 1990; Brochu, 2004) is of particular interest. *Arambourgia*

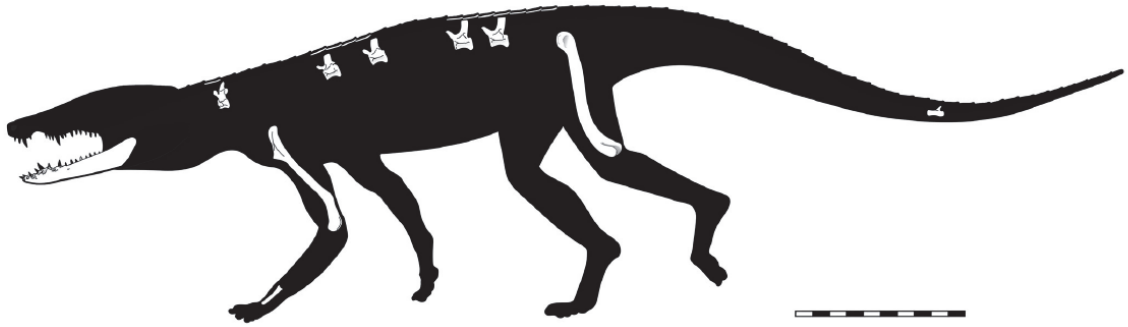

Figure 1.15: Reconstruction of *Tarsomordeo winkleri*, scale bar is 10 cm. Taken from Adams (2019; fig. 11).

gaudryi de Stefano, 1905, an inferred alligatoroid consists of a single altirostral specimen (Fig. 1.16) and could thus exhibit adaptations to a terrestrial lifestyle. However, it is in serious need of a reassessment.

2- Mekosuchinae Balouet & Buffetaut, 1987

Mekosuchins form a recently reviewed group (Ristevski *et al*., 2023b), are endemic to Australasia and are found in deposits dated from the Eocene (Willis *et al*., 1993; Salisbury & Willis, 1996; Holt *et al*., 2005; Buchanan, 2008, 2009) to the Holocene (Balouet & Buffetaut, 1987; Mead *et al*., 2002). They are known in mainland Australia (Molnar, 1981, 1982; Willis *et al*., 1990, 1993; Willis, 1993; Megirian *et al*., 1991; Willis & Molnar, 1991; Megirian, 1994; Willis & Mackness, 1996; Salisbury & Willis, 1996; Holt *et al*., 2005; Buchanan, 2008, 2009; Stein *et al*., 2015, 2016; Yates, 2017; Yates & Pledge, 2017; Ristevski *et al*., 2020, 2023a) but also from New Caledonia (Balouet & Buffetaut, 1987), Fiji (Molnar *et al*., 2002) and Vanuatu (Mead *et al*., 2002) .

This groups represents taxa with diverse inferred ecologies (Willis, 1997) with different snout morphologies and dentition (Fig. 1.17). Balouet & Buffetaut (1987) suggest that the position of the external nares, the short rostrum, and the morphology of the post cranium of *Mekosuchus*

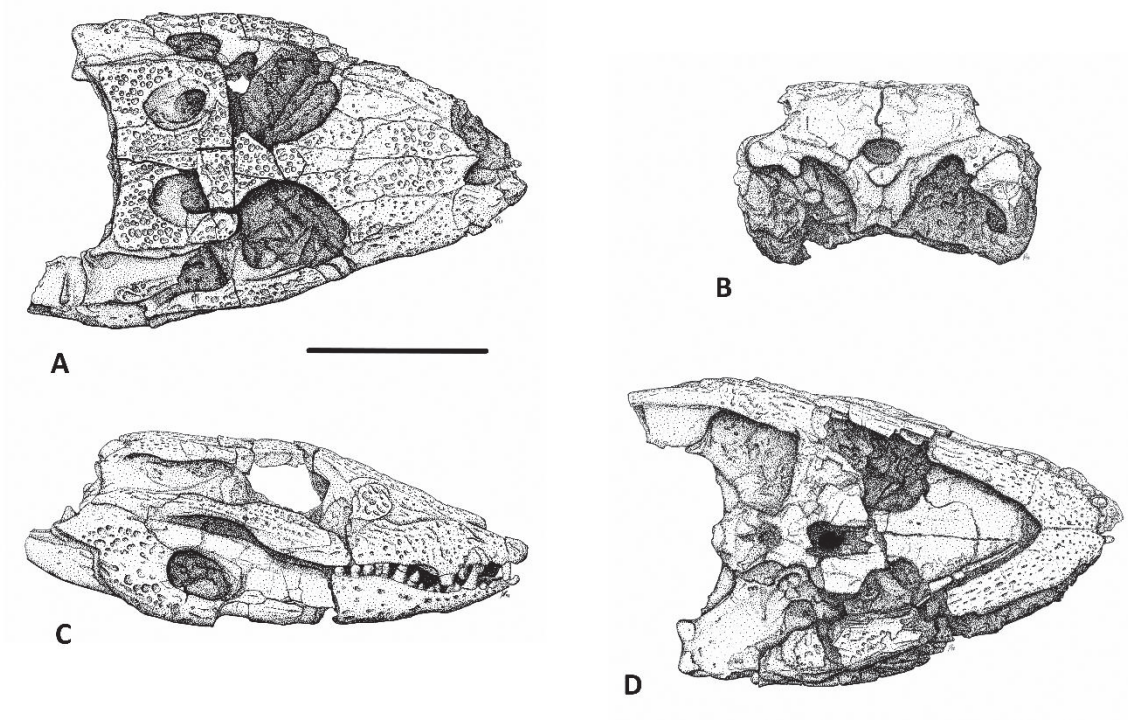

Figure 1.16: Skull of *Arambourgia gaudryi* (MNHN QU17155) from the Eocene of Quercy. A: dorsal view, B: posterior view, C: lateral view, D: ventral view. Scale bar is 5 cm.

inexpectatus Balouet & Buffetaut, 1987 correspond to a terrestrial lifestyle. Willis (1993) also observes that the neck musculature in *Trilophosuchus rackhami* Willis, 1993 implies that the cervical vertebrae were positioned more ventrally that in extant crocodylians and provided a greater role of the lateral flexion of the head, corresponding with a terrestrial erect posture and a specialized feeding strategy. The lack of torsion of the humeri of *Kambara* Willis, Molnar & Scanlon, 1993 specimens compared to extant forms, as well as the differences in condyles morphology imply a different resistance to mechanical stress, compatible with both a terrestrial or semi-aquatic with enhanced paraxial swimming lifestyle, according to Stein *et al*. (2012). Further specimens of *Mekosuchus whitehunterensis* Willis, 1997 also indicate an enlarged epaxial musculature, facilitating de-fleshing or scavenging in a terrestrial context (Stein *et al*., 2016). Stein *et al*. (2017) observe that the pelvic and pectoral girdles of forms related to *Quinkana* Molnar, 1982 are adapted for an erect, terrestrial lifestyle, notably through the enclosed and ventrally oriented acetabulum in the ilium. Those observations were then confirmed through a geometric morphometric approach coupled with a finite element analysis, clustering mekosuchins forms adapted to a terrestrial lifestyle away from more generalist forms (Stein *et al*., 2020). However, Wroe (2002) disagrees with those hypotheses, pointing out methodological issues in estimating body sizes, the lack of postcranial data and the competition with large terrestrial mammals and birds. Buchanan (2008) further points out that the postcranial anatomy of *Kambara taraina* Buchanan, 2009 does not show the specializations that other inferred terrestrial taxa display, especially regarding the ilium, femur, fibula, tibia

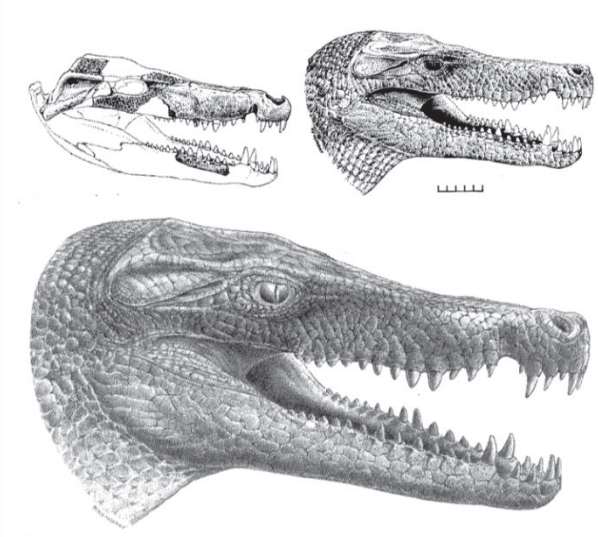

Figure 1.17: Reconstruction of the skull of *Quinkana timara.* Top left: preserved parts of the skull, top right and bottom: reconstructions. Scale bar is 5 cm. Modified from Megirian (1994, fig. 4).

and astragalus morphology (Parrish, 1987), and rather attributes a generalized lifestyle to this taxon.

In terms of diet, *Kambara taraina* could have been a chelonivour, based on taphonomic evidence of contemporaneous turtle remains (Buchanan, 2008). On the other hand, Stein *et al*. (2016) put forward a generalist diet for *Ultrastenos willisi* Stein, Hand & Archer, 2016, based on its longirostral morphology.

3- Planocraniidae Li, 1976

Planocraniids constitute a clade of crocodylomorphs with ziphodont dentition whose systematic and taxonomic content has been recently reassessed in Brochu (2012). It now comprises only three genera: *Boverisuchus*, Kuhn, 1938 from the Eocene of Europe and North America (Troxell, 1925; Kuhn, 1938; Langston, 1975; Brochu, 2012), *Planocrania* Li, 1976 from the Paleocene of China (Li, 1976, 1984) and *Duerosuchus* Santiago & Andrés, 2009 (Santiago & Andrés, 2009; Narváez *et al*., 2021). There may also be the presence of other taxa in those three continents, but those need to be confirmed or reassessed (Sacco, 1896; Buffetaut, 1985b; Efimov, 1988, 1993; Rauhe & Rossmann, 1995; Rossmann, 1998; Zonneveld *et al*., 2000; Blas *et al*., 2004; Kotsakis *et al*., 2004; Brochu, 2012; Venczel *et al*., 2021).

Nothing much is known of their paleoecology, apart from their ziphodont dentition, that could be related to the slicing of flesh, as in the extant Komodo monitor (*Varanus komodoensis*; D'Amore & Blumenschine, 2009).

V- Aquatic forms

Here, I also present crocodylomorphs that are fully adapted to an aquatic lifestyle, as they will be widely used as comparisons for assessing terrestriality throughout this thesis.

a- Thalattosuchians

Thalattosuchians were already described in the early works of Cuvier, Geoffroy Saint-Hilaire, and Eudes-Deslongchamps (father and son) on the French coastlines of the Channel (Cuvier, 1800, 1808, 1824; Geoffroy Saint-Hilaire, 1825, 1831; Eudes-Deslongchamps & Blainville, 1853; Eudes-Deslongchamps, 1849, 1866, 1867-1869, 1868a, b, c, 1869, 1870, 1896). As such, those organisms are wildly known and described from Jurassic and Cretaceous deposits from all over the world (see Young *et al*., 2021; Wilberg *et al*., 2022 for recent reviews). Thalattosuchia phylogenetic position within Crocodylomorpha, intra-group phylogeny and

taxonomy are quite complex and still not fully understood, with many studies published in the last two decades tackling difficulties such as redescription of centuries old taxa, sometimes erected on non-diagnostic characters, missing holotypes, ontogenetic variation, but also application of the International Code of Zoological Nomenclature (Gasparini *et al.*, 2000, 2008; Mueller-Töwe, 2005, 2006a; Pierce & Benton, 2006; Wilkinson *et al*., 2008; Jouve, 2009; Pol & Gasparini, 2009; Young & de Andrade, 2009; de Andrade *et al*., 2010; Young *et al*., 2010, 2012a, 2014a, b, 2015a, b, 2021; Cau & Fanti, 2011; Martin & Vincent, 2013; Cau, 2014, 2019; Young, 2014; Herrera *et al*., 2015; Martin *et al*., 2015a; Wilberg, 2015a; Barrientos-Lara *et al*., 2016; Foffa *et al*., 2018b ; Johnson *et al*., 2018, 2019, 2020a, b, 2022a; Foffa *et al*., 2019; Johnson, 2019; Sachs *et al*., 2019, 2020, 2021; Hua, 2020; Hua *et al*., 2021; Le Mort *et al*., 2022; Wilberg *et al*., 2022).

Thalattosuchians were adapted to life in the aquatic realm, with two families that coexisted: Teleosauridae Geoffroy Saint-Hilaire, 1831 and Metriorhynchidae Fitzinger, 1843 that were both adapted to different environments. Although they were mostly longirostrine organisms, their skull morphology is unique and non-comparable to other longirostrine clades in Crocodylomorpha and well-distinguishable in terms of evolutionary rate (Pierce *et al*., 2009; Ballel *et al*., 2019). They could even have had a specific thermoregulation strategy, assessed through geochemistry (Séon *et al*., 2020) and computed tomography scans (Young *et al*., 2023). Metriorhynchids possessed salt glands (Fernández & Gasparini, 2000, 2008; Gandola *et al*., 2006; Buchy *et al*., 2007; Herrera *et al*., 2013b), a uniform skin type (Spindler *et al*., 2021) and likely hunted small invertebrates and fishes, as evidenced by the stomachal content of *Metriorhynchus* von Meyer, 1830 (Hua & Buffetaut, 1997; Walker & Brett, 2002). However, detailed biomechanical, body size, dentition and niche partitioning studies show that, in fact, different taxa of metriorhynchids were probably adapted to different diets and lifestyles, with associated snout length and dentition (Wilkinson *et al*., 2008; de Andrade *et al*., 2010; Young *et al*., 2010, 2011a, b, 2012b, 2014b, c, d, 2020b; Cau & Fanti, 2011; Buchy *et al*., 2013; Foffa & Young, 2014; Waskow *et al*., 2018; Foffa *et al*., 2018a, b; Madzia *et al*., 2021; Sachs *et al*., 2021). Some taxa are even hypothesized to have had the ability to scavenge on the sea floor (Forrest, 2003; Le Mort, 2019) or suction-feed (Young *et al*., 2012a). These hypotheses are associated with a cranial musculature adapted for a quick closure of the mouth, with inferred elongated muscles (Buchy, 2008). This group of organisms also displays a progressive reduction of the dorsal armour and the fore limbs (forming flippers), with a hypocercal caudal fin sometimes developed (Hua & Buffrénil, 1996; Caldwell, 2002; Herrera *et al*., 2013a; Ösi *et*

al., 2018), progressively posteriorly displaced external nares (Hua *et al*., 2000; Young *et al*., 2020a), and 'smooth' dermatocranium to reduce drag (Young *et al*., 2013a), making them adapted to swimming in open sea (Fig. 1.18). Histologically, the long bones of metriorhynchids are relatively lighter, which brings further evidence to their fully aquatic adaptation (Talevi *et al*., 2016). Finally, the ventrally deflected sacral ribs and reduced pelvic girdle of metriorhynchids could be evidences of viviparity, whereas their oviparity laying eggs out the water seems less probable (Herrera *et al*., 2017).

This comes in contrast with teleosaurids that could probably lived in more diverse environments (Buffetaut & Thierry, 1977; Wilkinson *et al*., 2008; Wilberg, 2015b; Le Mort, 2019; Fig. 1.19). Teleosaurids, based on their reconstructed jaw musculature, had a slightly higher bite force compared to similar extant longirostrine taxa and a dentition adapted to piscivory, like *Gavialis gangeticus* Gmelin, 1789 (Mueller-Töwe, 2006a, b). Similar habits are also inferred between teleosaurids and *Gavialis gangeticus* based on comparison of the integument (Spindler *et al*., 2021) but also because of the anterodorsal position of the orbit, making it possible to stalk preys situated above in the water column (Mueller-Töwe, 2006); remains of fishes were also found in the stomachal contents of *Pelagosaurus* Bronn, 1841 (Pierce & Benton, 2006). However, some taxa also display a denticulated dentition, which might indicate a diet directed towards flesh slicing (Young *et al*., 2013b). In a recent study, Johnson *et al*. (2022b) showed that the ecomorphological range of teleosaurids was indeed more diversified than previously thought, although it remains less diverse than in metriorhynchids. More generally, their body shape and flexibility are very similar to extant crocodiles, although slight differences exist, between *Steneosaurus* and *Pelagosaurus* for example (Mueller-Töwe, 2006; Pierce & Benton, 2006). Their locomotion was based mostly on lateral tail undulation (Frey, 1988), as they could reach, as metriorhynchids, large sizes (Johnson *et al*., 2015, 2018; Young *et al*., 2016a). Some taxa

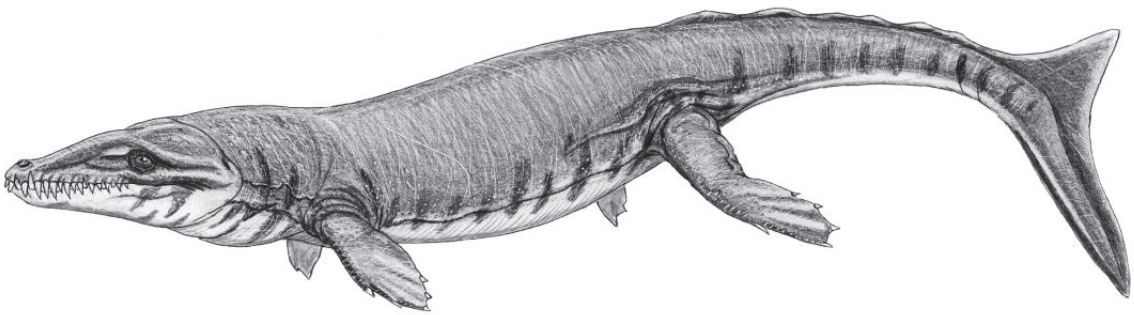

Figure 1.18: Life reconstruction of *Dakosaurus maximus* Plieninger, 1846, a metriorhynchid from the Late Jurassic. Drawing by Dmitry Bogdanov (modified from de Andrade *et al*., 2010, fig. 4).

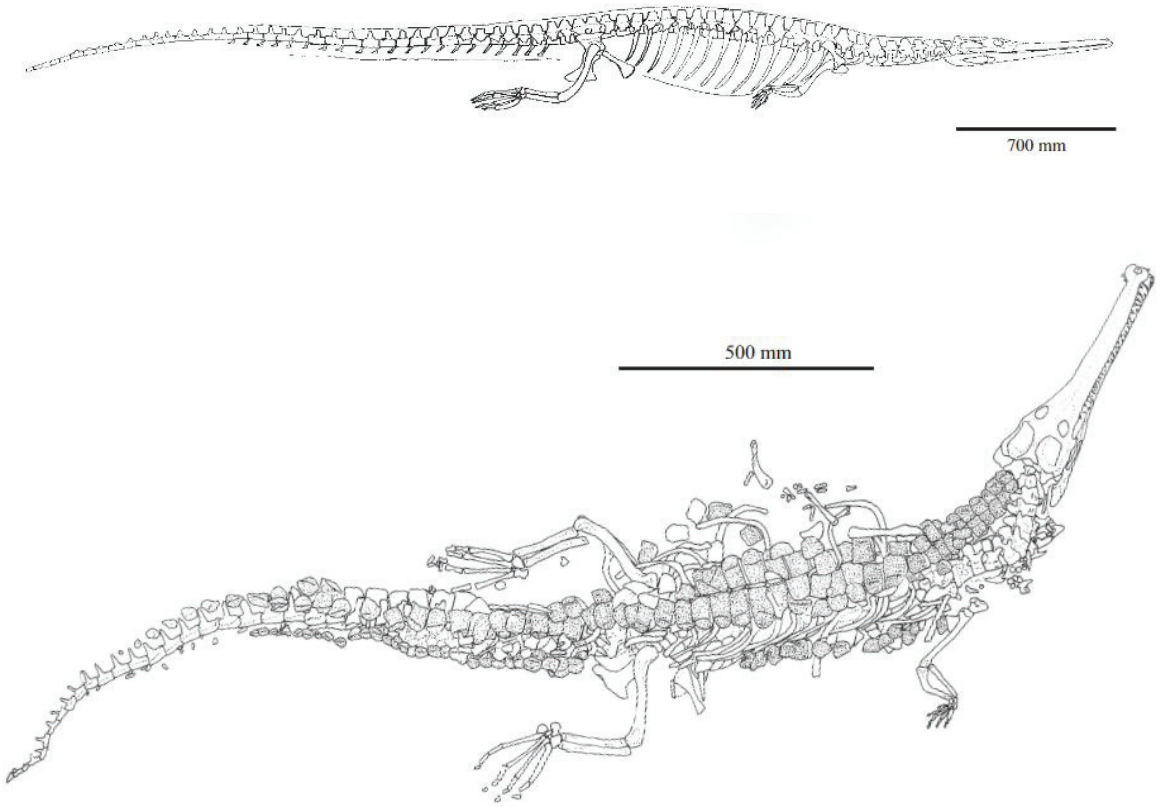

Figure 1.19: Skeletal reconstruction of Early Jurassic teleosaurids. Top: *Platysuchus multicrobiculatus* Berckhemer, 1929, bottom: '*Steneosaurus*' *bollensis* Cuvier, 1824. From Mueller-Töwe (2006b; fig. 3.24 & 8.9).

were probably more adapted to a pelagic lifestyle based on their reduced ornamentation and reduced limbs and recovery in deep-water sediments (Foffa *et al*., 2019), although others, like *Platysuchus* Westphal, 1961, exhibit a curved lateral femoral head and a well-developed iliac crest better suited for terrestrial locomotion (Mueller-Töwe, 2006). Little is known about the reproductive habits of teleosaurids, and it could either be an egg laying process or a viviparous behaviour (Mueller-Töwe, 2006).

As thalattosuchians were mainly marine organisms, they were probably more sensitive to transgressive-regressive phases and changes in marine ecosystem composition, which could be the reasons why they went extinct during the Cretaceous (Young *et al*., 2010), but the two families could possibly have disappeared at a different time and for different reasons (Young *et al*., 2014a).

b- Dyrosauridae de Stefano, 1903

Dyrosaurids form a clade of mostly exclusively aquatic crocodylomorphs, which thrived during the Late Cretaceous (Lamanna *et al*., 2004; Salih *et al*., 2022) to Early Paleogene (Jouve, 2005; Jouve *et al*., 2006; Amoudji *et al*., 2021). As such, they represent one of the few lineages of crocodiles to survive the Cretaceous/Paleogene biological crisis. They are known exclusively from North America (Denton *et al*., 1997; Schwarz *et al*., 2006; Jouve, 2007; Souza *et al*., 2020b); South America (Barbosa *et al*., 2008; Hastings *et al*., 2010, 2011, 2015; Shiller *et al*., 2016; Sena *et al*., 2017; Jouve *et al*., 2020; Scavezzoni & Fisher, 2021) and Africa (Buffetaut, 1976b, 1979; Brochu *et al*., 2002; Jouve & Schwarz, 2004; Jouve, 2005; Jouve *et al*., 2005, 2006, 2008; Schwarz *et al*., 2006; Jouve, 2007; Hill *et al*., 2008; Amoudji *et al*., 2021; Salih *et al*., 2022). There are also reports from Asia, but those are quite scarce and difficult to identify (Storrs, 1986; Rana & Sati, 2000; Khosla *et al*., 2009; Smith *et al*., 2016). This repartition could be explained by an adaptation to a slightly different climate between the Gondwanan and Laurasian landmasses dominated by dyrosaurids and gavialoids respectively, as well as a marine diversification of dyrosaurids subsequently to the Cretaceous/Paleogene biological crisis (Jouve, 2021).

Dyrosaurids have orbits located more laterally than dorsally, a long and flattened tail (numerous high caudal neural spines), an elongate and narrow snout with numerous homodont teeth and a light dorsal armour, which make them adapted to the marine environment (Denton *et al*., 1997; Schwarz *et al*., 2006; Fig. 1.20). The morphology of the ribs, femur and pelvis provides expanded musculature for active swimming, while differences in ischium conformation might indicate adaptation to fluvial to terrestrial settings in South American dyrosaurids (Hastings *et al*., 2011). This is also evidenced by recent histological studies that observe an open medullary cavity and the absence of microstructure specializations into the long bones of dyrosaurids, linked with a near-shore marine ambush predator lifestyle (de Andrade & Sayão, 2014; Pellegrini *et al*., 2021).

Furthermore, their limbs and large transverse processes do not seem adapted for deep swimming, contrary to what is seen in thalattosuchians for example, but could have allowed part-time access to semi-aquatic environments, probably for reproduction (Denton *et al*., 1997; Scavezzoni & Fisher, 2021). In terms of feeding, the inferred enlarged mandibular muscles and observed longer retroarticular process of dyrosaurids induce a quicker and more forceful contraction and enhanced capability of movement in the vertical plane (Schwarz, 2014),

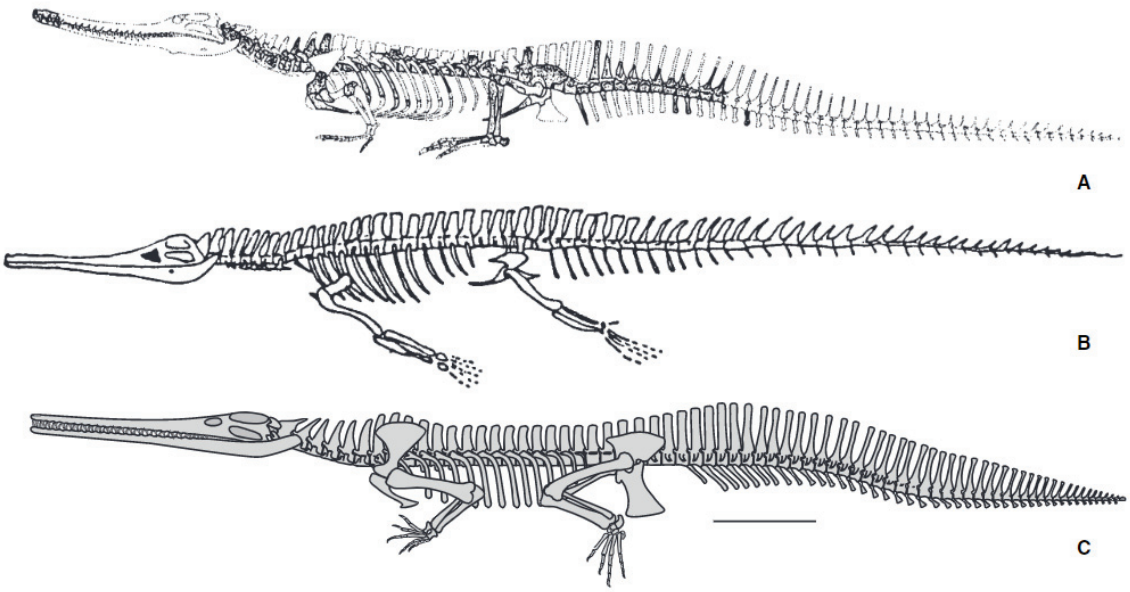

Figure 1.20: Postcranial reconstructions of dyrosaurids. A: cf. *Rhabdognathus* Swinton, 1930 (Langston, 1995); B: generalized dyrosaurid (Hua, 1997); C: *Congosaurus bequaerti* Dollo, 1914 (Schwarz, 2003). Scale bar is 0.5 m. Taken from Schwarz *et al*. (2006; fig. 1).

corresponding to a fish oriented. Gastroliths are found associated with some dyrosaurid skeletons, but their use as ballast is controversial (Denton *et al*., 1997; Martin *et al*., 2019) and there is also evidence of aggressive behaviors between individuals (Martin, 2013).

VI- Conclusions and perspectives

As notified throughout this chapter, crocodylomorphs are not living fossils, and, during their evolutionary history, they have developed numerous adaptations to drastically different environments. The primitive lifestyle of the clade seems to have been a terrestrial one, with adaptations to semi-aquatic and completely aquatic environments occurring as derived states, with a lot of lineages retaining this 'primitive' terrestrial lifestyle, even in 'advanced' neosuchians.

However, one must keep in mind that the inferences made above, however strong they might seem, remain hypothetical, and the reality was probably much more complex. The shift from the terrestrial to the aquatic realm (and vice-versa) is a long process and requires several adaptations, that are acquired throughout numerous generations. At some point in their evolutionary history, crocodylomorphs lineages must have exhibited lifestyle that were not simply fully terrestrial, semi-aquatic or fully aquatic, but rather a mix with subsequent adaptations (Wilberg *et al*., 2019). A good example is the one of extant genera *Paleosuchus* and *Osteolaemus* Cope, 1860 on one hand, and *Gavialis* Oppel, 1811 on the other hand. The first

ones, although they are mainly semi-aquatic, display a terrestrial lifestyle at certain periods, due to a shift of resources in their natural environment or different ontogenetic stages (Waitkuwait, 1989; Magnusson & Lima, 1991; Pauwels *et al*., 2007; Shirley & Austin, 2017; Shirley *et al*., 2017). The second one, although mostly adapted to the aquatic realm and piscivorous, still spends some time out of the water (Lang, 2015; Neupane *et al*., 2020). As a result, the impact of climate and temperature throughout time must also be considered in the ecology and repartition of fossil crocodylomorphs and their resilience to major biological crisis (Carvalho *et al*., 2010; Stubbs *et al*., 2013; Bronzati *et al*., 2015; Puértolas-Pascual *et al*., 2016; Jouve, 2021; Stockdale & Benton, 2021; see also subsequent discussion in Benson *et al*., 2022 and Stockdale & Benton, 2022; Aubier *et al*., 2023).

The inference of the terrestrial lifestyle of different groups of fossil crocodylomorphs is mainly based on their altirostral skull morphology, with subsequent orientation of the orbits and external nares, on their limb and girdle morphology, sometimes enabling an erect posture, and on their ziphodont dentition, adapted to a meat slicing carnivorous diet. Those observations, although robust and valid, call for other, independent proxies to serve as confirmation, so that the terrestrial lifestyle of those taxa can be inferred even more robustly, especially for clades where studies on those aspects are still needed. Furthermore, there is also the need for the phylogenetic relationships of those taxa to be understood better, to enable for large scale comparisons and evolutionary trends studies with a robust backbone, as well as to account for uncomplete sampling biases (Mannion *et al*., 2019; de Celis *et al*., 2021; Aubier *et al*., 2023).

In the framework of this thesis, I will thus take a closer look at the adaptations to a terrestrial lifestyle of certain crocodylomorphs, asking the following remaining questions: how can a terrestrial lifestyle be additionally assessed in fossil forms of crocodylomorphs? Is the altirostral morphology always associated with fully terrestrial taxa?

To answer those questions, I have first summarized in Chapter 1 the different adaptations to a non-semi-aquatic lifestyle found in the fossil record of crocodylomorphs, with a focus on which information are key to understand and assess the paleoecology of those organisms. Chapter 2 will be dedicated to phylogenetic clarifications of key lineages, as the understanding of the relationships of terrestrial taxa is important to assess the timing and evolution of this trait. In Chapter 3, the endocranial structures of a selection of putative terrestrial taxa will be studied and allow numerous paleoecological interpretations, with a special emphasis on the ontogenetic, phylogenetic, and ecological implications of the inner ear in crocodylomorphs.

This will be done with complementary data from extant crocodylians, as well as fossil forms adapted to the aquatic realm. Chapter 4 will be devoted to isotopic geochemistry applied to paleoecological and paleoenvironmental questions, involving similar taxa than in Chapter 3. Through a multi-isotopic approach, the dietary, physiological, and ecological characteristics of those organisms will be inferred, and compared with those of the rest of the fauna involved in several fossil localities. Furthermore, the geochemical recording of dentine by serial sampling could also be an interesting approach, particularly for detecting ecological changes over a short period (i.e., tooth development time or tooth replacement rate), as evidenced by measures on extant specimens. Finally, in Chapter 5 a preliminary study will show the usefulness of osteoderms histology and ornamentation to assess the lifestyle of extinct forms, but will have to be confirmed in future studies. I will then put forward general conclusions and perspectives. The data used and interpretations presented in this thesis are under the form of published or submitted manuscripts to peer-reviewed journals, as well as unpublished data.

VII- Altirostry: a tentative definition

During the preparation of this thesis, I realized that there is not a clear definition of the altirostrine condition, as well as the brevirostrine (short rostrum of extant alligators and caimans), mesorostrine (medium to long and broad rostrum of extant crocodiles) and longirostrine (long rostrum of extant gavialids and extinct thalattosuchians and dyrosaurids) conditions. The altirostral morphology is sometimes also designated as “oreinirostral” by some authors (in contrast with platyrostral skulls of extant crocodylians) which was first put forward by Busbey (1997). However, the term “altirostral” was first proposed as a peculiar morphology of phytosaur skulls, designating narrow snouts with rostral crests (Hunt, 1989; Hunt *et al*., 2006) and has been widely used in crocodylomorph studies to describe a dorsoventrally tall and laterally compressed snout (Salisbury & Willis, 1996; Rossmann *et al*., 2000; Mead *et al*., 2002; Brochu, 2003, 2007, 2012; Bickelmann & Klein, 2009; Hastings *et al*., 2013; Rabi & Sebök, 2015; Stein *et al*., 2016; Yates, 2017; Yates & Pledge, 2017; Narváez *et al*., 2021; Ristevski *et al*., 2021, 2023a). Here, I studied three measurements pertaining to the development of the rostrum in crocodylomorphs to see if the different conditions are truly different or not (Fig. 1.21A). The rostrum length (RL) is represented by the length between the anterior tip of the premaxilla and the anterior tip of the orbit, the rostrum width (RW) is the width of the skull at the anterior level of the orbits, and the rostrum height (RH) is the dorsoventral height of the snout anteriorly to the orbits. I then chose several adult specimens representative of the different snout morphologies put forward in the literature and compared their RL/RW, RL/RH and

RW/RH ratios (Fig. 1.21B & 1.21C); the full dataset of measurements is available here: https://mycore.core-cloud.net/index.php/s/vFk8aYpSLa8ihKR .

The altirostral morphology can be significantly distinguished from the brevirostral, mesorostral and longirostral one using the ratio of rostrum length to rostrum height (p-value < 0.02), but not significantly using the other metrics (Figure 1.21B & 1.21C). The values of altirostral organisms are equal or lower than three, whereas they are higher in the other groups. As a result, I propose that the altirostral morphology be defined as a skull possessing a rostrum length equal to or lower than three times its height. It is also interesting to observe that, in that case, the brevirostrine and mesorostrine condition are statistically undistinguishable, whereas the longirostrine condition is distinguished by the extreme length of the skull. Finally, according to those metrics, altirostral specimens are therefore not present in the extant crocodylians.

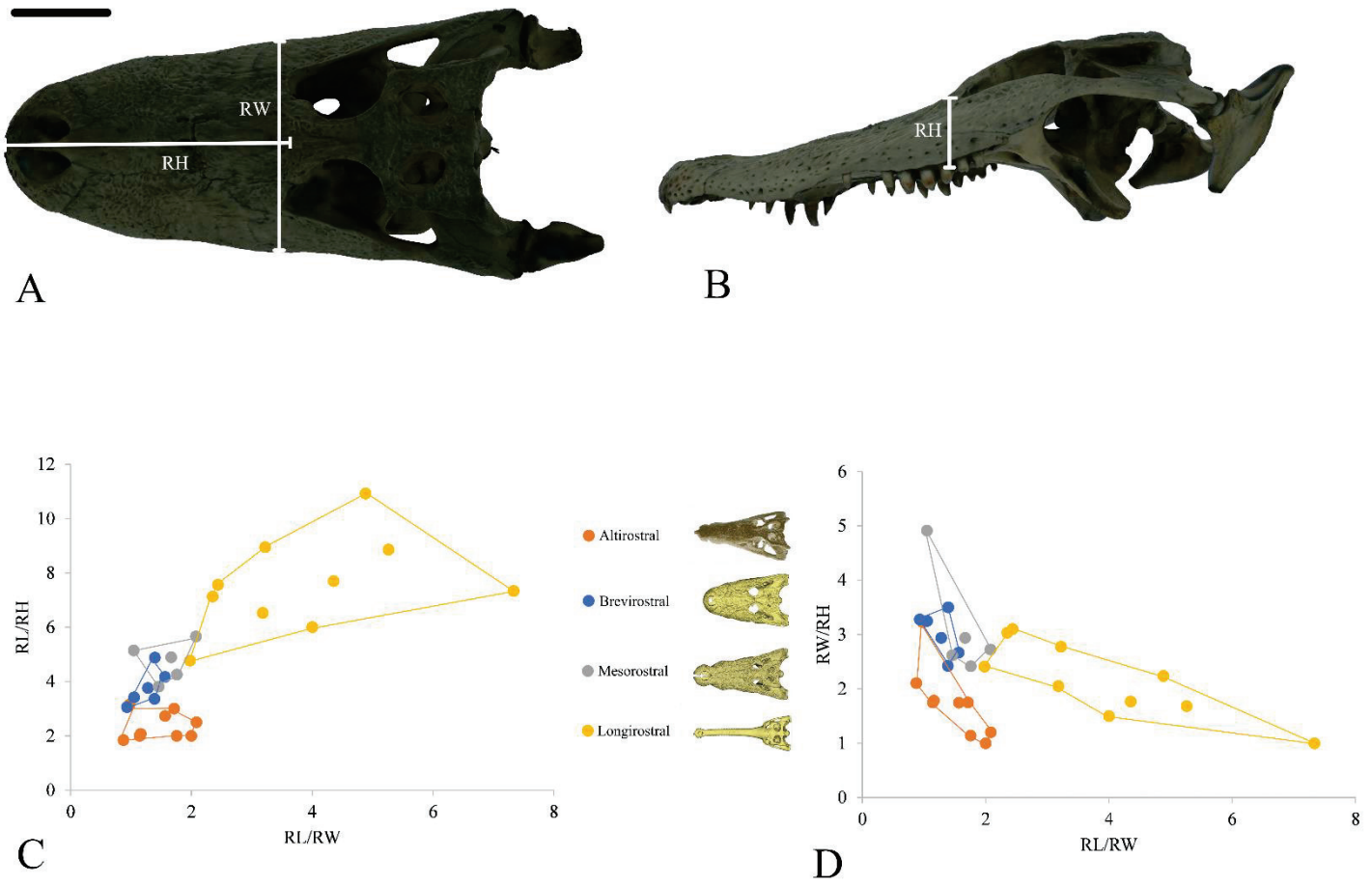

Figure 1.21: The different snout morphologies. Top: *Alligator mississippiensis* Daudin, 1801 (UCBL WB35) in dorsal (A) and lateral (B) views. Bottom: graphs presenting RL/RW against RL/RH (C) and RL/RW against RW/RH (D). RH: rostrum height, RL: rostrum length, RW: rostrum width. Skulls in dorsal view of the graph legend are as follow from top to bottom: *Hamadasuchus* Buffetaut, 1994 (UCBL FSL 532408), *Caiman latirostris* Daudin, 1801 (UMMZ herp 155287), *Crocodylus niloticus* Laurenti, 1768 (MHNL 50001405) and *Gavialis gangeticus* (MHNL 50001407). Scale bar is 5 cm.

Chapter 2: Phylogenetic and taxonomic clarification of key lineages with terrestrial-like morphologies

As stated previously, paleoecological inferences on terrestrial crocodylomorphs can only be made if the phylogenetic and taxonomic status of those group is understood. Although a phylogenetic topology must not be taken for more than it really is, that is to say a hypothesis based on morphological observations including all known evidence as best as possible, a general consensus of the relationships of the different taxa is necessary to make assumptions across different groups, sometimes separated by several million years. In this chapter, I will try to tackle this situation in different clades, which will be the subject of the subsequent chapters.

I- Sebecia Larsson & Sues, 2007 vs sebecosuchians

Among crocodylomorphs, the phylogenetic position of Sebecidae and Peirosauridae with each other as well as with other clades of notosuchians is debated. Two hypotheses are predominant: either sebecids and peirosaurids form a clade named Sebecia (Fig. 2.1; Sereno & Larsson, 2009; Young & de Andrade, 2009; de Andrade *et al*., 2011; Riff & Kellner, 2011; Pinheiro *et al*., 2018, 2021, 2023; Geroto & Bertini, 2019; Martins, 2021; Ruiz *et al*., 2021; Queiroz, 2022) or they are separated, with sebecids and baurusuchids forming a monophyletic group, Sebecosuchia Colbert, 1946a (Fig. 2.2; Gasparini *et al.*, 1991, 1993; Ortega *et al*., 1996, 2000; Gomani, 1997; Buckley & Brochu, 1999; Buckley *et al*., 2000; Tykosky *et al*., 2002; Pol, 2003; Sereno *et al*., 2001, 2003; Carvalho *et al*., 2004; Pol & Norell, 2004a, b; Pol *et al*., 2004; Company *et al*., 2005; Pol & Apesteguia, 2005; Turner & Calvo, 2005; Turner, 2006; Zaher *et al*., 2006; Fiorelli & Calvo, 2007; Turner & Buckley, 2008; Novas *et al*., 2009; Pol *et al*., 2009, 2012, 2014; Turner & Sertich, 2010; Iori & Carvalho, 2011; Nascimento & Zaher, 2011; Pol & Powell, 2011; Soto *et al*., 2011 ; Adams, 2013, 2014; Iori *et al*., 2013; Kellner *et al*., 2014; Sertich & O'Connor, 2014; Leardi *et al*., 2015, 2018; Fiorelli *et al*., 2016; Godoy *et al*., 2016; Martin & de Lapparent de Broin, 2016; Dal Sasso *et al*., 2017; Martinelli *et al*., 2018; Coria *et al*., 2019; Cunha *et al*., 2020 ; Dumont *et al*., 2020a; Sellés *et al*., 2020; Bravo *et al*., 2021; Nicholl *et al*., 2021; Marinho *et al*., 2022; Martin *et al*., 2023). Although both clades are widely used and referred to in the literature, they have never received a formal definition.

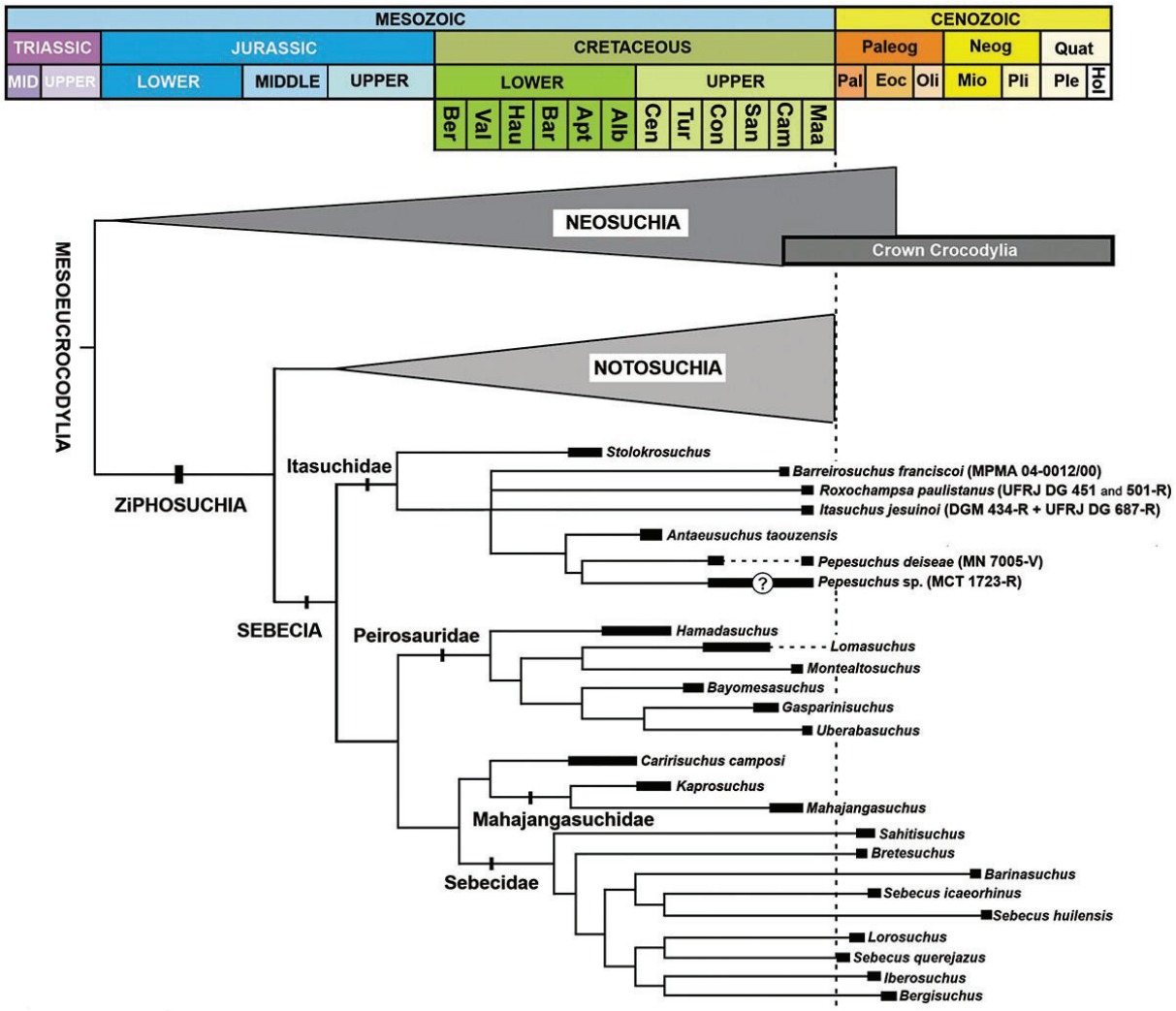

Figure 2.1: Consensus tree obtained in Pinheiro *et al*. (2023; fig. 17).

Here, I have undergone a thorough review of all the publications where a phylogenetic analysis highlighting either the Sebecia or Sebecosuchia hypothesis has been performed (see Appendix 1), extracting the phylogenetic datasets that served as the basis of each study and the diagnostic characters of either Sebecia or Sebecosuchia. Several points can be noticed:

1- As can be seen in Figure 2.3, all phylogenetic analyses are mostly based on groundbreaking general archosaur phylogeny works from the 1990's, with subsequent additions of new characters in later studies. It is interesting to notice that both phylogenetic 'paradigms' rely on similar datasets, as there are no clusters based on one phylogenetic hypothesis or the other in Figure 2.3. Furthermore, the chosen phylogenetic search procedure does not seem to have an impact on the resulting phylogenetic hypothesis (see Appendix 1). I would thus argue that the observed difference between Sebecosuchia and Sebecia hypotheses most probably comes from character and taxon sampling, as well as different or conflicting codings, which

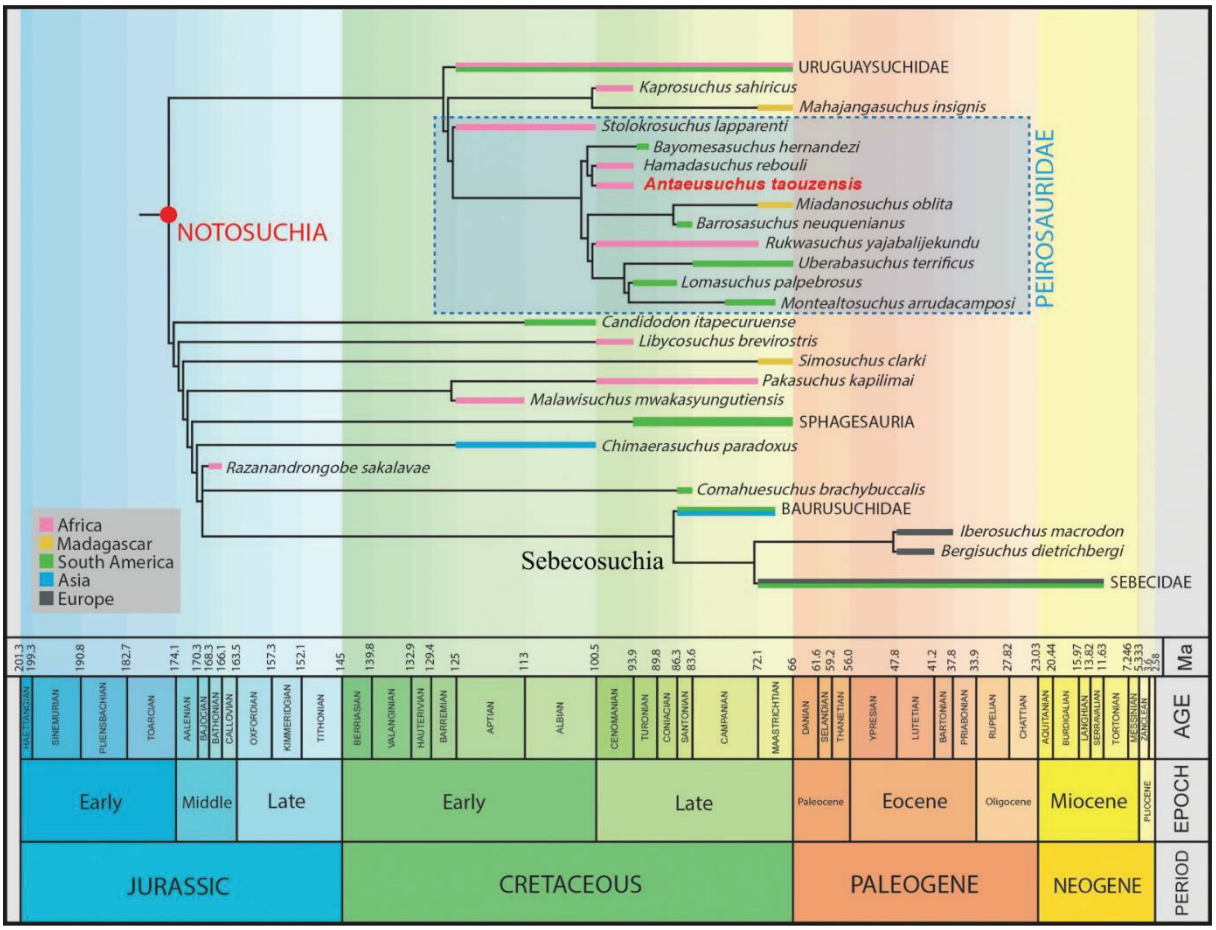

Figure 2.2: Time-calibrated phylogeny topology obtained in Nicholl *et al*. (2021; modified from fig. 11).

unfortunately cannot be resolved without taking a closer look at the data itself and is out of scope here.

2- Based on this thorough review, I identify several conflicting characters that are either hypothesized to be synapomorphies of Sebecosuchia or Sebecia but with different states in different publications or hypothesized to be synapomorphies of both clades in different publications. Those characters thus cannot be considered true synapomorphies of either clades and include the serrated carinae of the teeth (Fig. 2.4-1); the constricted cheek teeth crown base (Fig. 2.4-2); the size of the anterior dentary tooth opposite to the premaxilla-maxilla contact (Fig. 2.4-3); the splenial robust posteriorly to the mandibular symphysis (Fig. 2.4-4); the shape of the mandibular symphysis in lateral view (Fig. 2.4-5); the deep, well-defined groove on the lateral surface of the anterior region of the surangular and the posterior section of the dentary (Fig. 2.4-6); the lateral concavity of the dentary for the reception of the enlarged maxillary teeth (Fig. 2.4-7); the shape of the dorsal edge of the dentary (Fig. 2.4-7); the unsculpted region in the dentary below

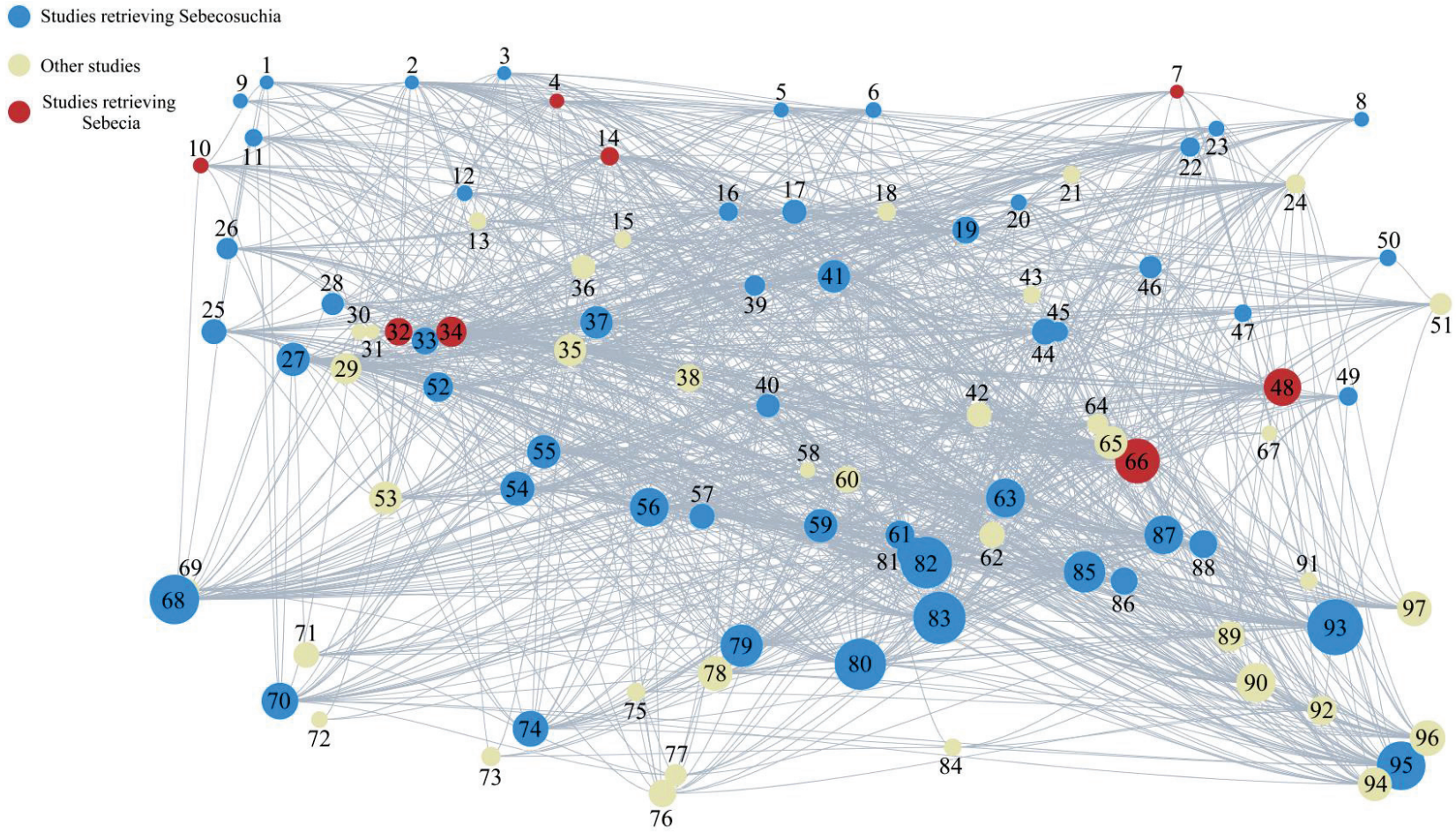

Figure 2.3: References network involved in the Sebecosuchia/Sebecia debate. Size of the circles represent the relevance of the reference (number of citations within the whole reference map). Vertical axis represents date of publication, horizontal axis clusters publications by citations to improve legibility. Reference numbers are available in Appendix 2. Made with Litmaps (www.litmaps.com).

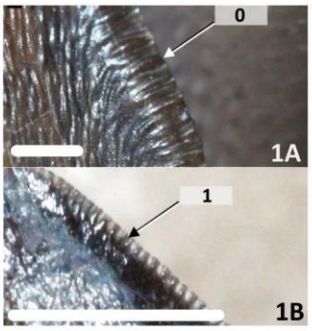
0
1A
1
1B


2


3


4

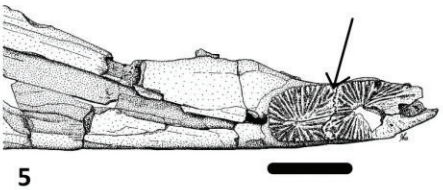
5


6

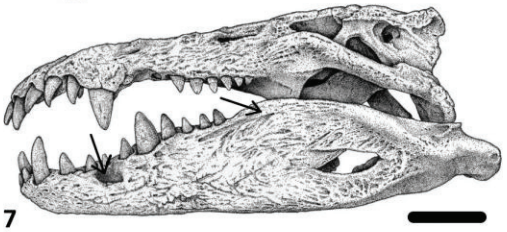
7


8


9


10

Figure 2.4: Different conflicting characters among sebecosuchians/sebecians. 1: serrated carinae of the teeth (0: absent, 1: present) in *Purussaurus neivensis* Mook, 1940 (A: UCMP 38932) and *Boverisuchus vorax* Troxell, 1925 (B: UCMP 170767). Taken from Rio & Mannion (2021; fig. S65B & D). 2: teeth of *Simosuchus clarki* (UA 8679) constricted at crown base. Taken from Buckley *et al*. (2000; fig. 1I-L). 3: hypertrophied fourth dentary teeth of a baurusuchid skull (FEF-PV-R-1/9). Taken from Dumont *et al*. (2020b; fig. 1B). 4: splenial robust posteriorly to the mandibular symphysis of *Dentaneosuchus crassiproratus* Astre, 1931 (MHNT.PAL.2006.0.53). Taken from Martin *et al*. (2023; fig. 13A). 5: mandibular symphysis of *Hamadasuchus* cf. *rebouli* Buffetaut, 1994 (MNHN-SAM 136). Taken from Pochat-Cottilloux *et al*. (2023a; fig. 3C). 6: deep, well-defined groove on the mandible of *Gavialis gangeticus* (UCBL WB39). 7: lateral concavity on the dentary and dorsal edge of the dentary with a single dorsal expansion of the reconstruction of the skull of *Mahajangasuchus insignis*. Taken from Turner & Buckley (2008; fig. 9). 8: unsculpted region below the dentary toothrow with the lateral surface of the dentary vertically oriented on the mandible of *Caipirasuchus mineiri* (CPPLIP 1463). Taken from Martinelli *et al*. (2018; fig. 14A). 9: premaxillary palate circular paramedian depression on the snout of *Campinasuchus dinizi* Carvalho, Teixeira, Ferraz, Ribeiro, Martinelli, Neto, Sertich, Cunha, Cunha & Ferrza, 2011 (CPPLIP 1236). Taken from Carvalho *et al*. (2011a; plate 5-2). 10: jugal part of the postorbital bar inset from the lateral surface of the jugal on the skull of *Mariliasuchus amarali* (MZSP-PV 50). Taken from Zaher *et al*. (2006; fig. 3B). Scale bars are 1mm in 1; 5 cm in 2, 3, 5, 6, 9; 2 cm in 4, 8; 10 cm in 7; and 1 cm in 10.

the toothrow (Fig. 2.4-8); the premaxillary palate circular paramedian depressions (Fig. 2.4-9), the shape of the lateral surface of the dentary (Fig. 2.4-8) and the position of the jugal portion of the postorbital bar relative to the lateral surface of the jugal (Fig. 2.4-10).

3- On the other hand, I can highlight several characters that are consistently retrieved as a combination diagnostic of Sebecia using different datasets and phylogenetic search procedure. Those include the first and second premaxillary teeth being nearly confluent (Fig. 2.5-1); the premaxilla-maxilla lateral fossa excavating the alveolus of the last premaxillary tooth (Fig. 2.5-2); the snout sinusoidal in dorsal view (Fig. 2.5-3); the maxillae sagittal contact bearing a longitudinal series of foramina (Fig. 2.5-4); the quadratojugal posteroventral extension forming a lateral extension until the quadrate condyles and participating in the articulation with the mandible, linked with the participation of the surangular in the glenoid fossa (Fig. 2.5-5); the anterior half of the palatines flared anteriorly between the suborbital fenestrae (Fig. 2.5-6); the primary pterygoidean palate forming the posterior, lateral and part of the anterior margin of the choanae (Fig. 2.5-7); the pterygoid flanges relatively short and not reaching the level of the quadrate medial condyle (Fig. 2.5-6); the mandibular symphysis clearly constricted at the fifth-sixth alveoli (Fig. 2.5-8) and the retroarticular process projecting posterodorsally (Fig. 2.5-9). However, among those, there are no unambiguous synapomorphies (i.e., that only apply to Sebecia among Crocodylomorpha), so this list should rather be taken as a diagnostic combination of features.

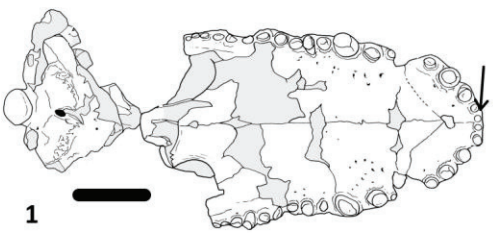

1

2

3

4

5

6

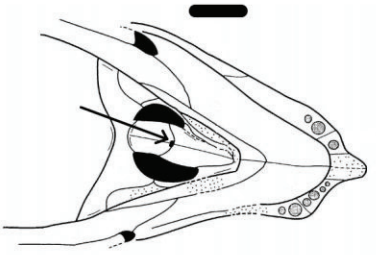

7

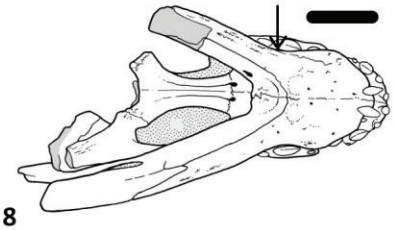

8

9

Figure 2.5: Combination of characters diagnostic of Sebecia. 1: first and second premaxillary teeth of *Gasparinisuchus peirosauroides* Martinelli, Sertich, Garrido & Praderio, 2012 (MOZ 1750 PV) almost confluent. Modified from Martinelli *et al*. (2012; fig. 3B). 2: premaxilla-maxilla lateral fossa excavating the last premaxillary alveolus of *Kaprosuchus saharicus* (UCRC PVC8). Modified from Sereno & Larsson (2009; fig. 33C). 3: sinusoidal snout in dorsal view of *Araripesuchus buitreraensis* Pol & Apesteguía, 2005 (MPCA PV 242). Taken from Dumont *et al*. (2020a; fig. 3A). 4: maxillae sagittal contact of *Pissarachampsa sera* (LPRP/USP 0019) bearing a series of longitudinal foramina. Modified from Montefeltro *et al*. (2011; fig. 3C). 5: quadratojugal reaching the quadrate condyle in *Araripesuchus buitreraensis* (MPCA PV 243). Taken from Dumont *et al*. (2020a; fig. 4C). 6: anteriorly flared palatines and short pterygoid flanges of *Caipirasuchus paulistanus* (MPMA 67-0001/00). Taken from Iori & Carvalho (2011; fig. 2C). 7: pterygoidean palate forming the posterior, lateral and part of the anterior margin of the choanae of *Malawisuchus mwakasyungtiensis* (Mal-45). Modified from Gomani (1997; fig. 2B). 8: constricted mandibular symphysis of *Campinasuchus dinizi* (CPP 1234). Modified from Carvalho *et al*. (2011a; plate 4-2). 9: posterodorsally projecting retroarticular process of *Hamadasuchus* cf. *rebouli* (MNHN-SAM 136). Modified from Pochat-Cottilloux *et al*. (2023a; fig. 2D).

4- Consequently, I am also able to identify the following combination of characters that is diagnostic of Sebecosuchia: an altirostral rostrum (Fig. 2.6-1); a sigmoidal toothrow in dorsal view (Fig. 2.6-1); one wave of enlarged maxillary teeth (Fig. 2.6-2); the second or third maxillary alveoli enlarged (Fig. 2.6-2); evaginated maxillary alveolar edges present as a continuous sheet (Fig. 2.6-2); a notch at the premaxilla-maxilla contact ventrally opened as a large fenestra (Fig. 2.6-2); no unsculpted region along the alveolar margin on the lateral surface of the maxilla (Fig. 2.6-2); an absence of antorbital fenestra (Fig. 2.6-2); the nasal lateral edges nearly parallel (Fig. 2.6-2); infratemporal fenestra elongated anteroposteriorly (Fig. 2.6-3); a jugal higher in its antorbital region rather than its infrorbital region with a lateral surface not visible in ventral (i.e., straight jugal; Fig. 2.6-3); the ventral margin of the jugal at the posterior end of the contact with the ectopterygoid is separated by a notch from the infratemporal bar of the jugal (Fig. 2.6-4); a strongly concave palate (Fig. 2.6-5); very large choanae (Fig. 2.6-5); vertical pterygoids (Fig. 2.6-5); the outer surface of the squamosal along the site of attachment of the ear valve groove reduced and vertically oriented (Fig. 2.6-3); the suture between the postorbital and the squamosal is convex anteriorly in lateral view (Fig. 2.6-3); a skull roof trapezoidal-shaped in dorsal view (Fig. 2.6-5); a long development of the paraoccipital process lateral to the cranioquadrate passage (Fig. 2.6-6); a big, slot-like foramen *intramandibularis oralis* (Fig. 2.6-2) and maxillary teeth that are set in isolated alveoli (Fig. 2.6-2). As for Sebecia, none of those characters are unique to Sebecosuchia within Crocodylomorpha, thus this list must also be taken as a combination diagnostic of Sebecosuchia.

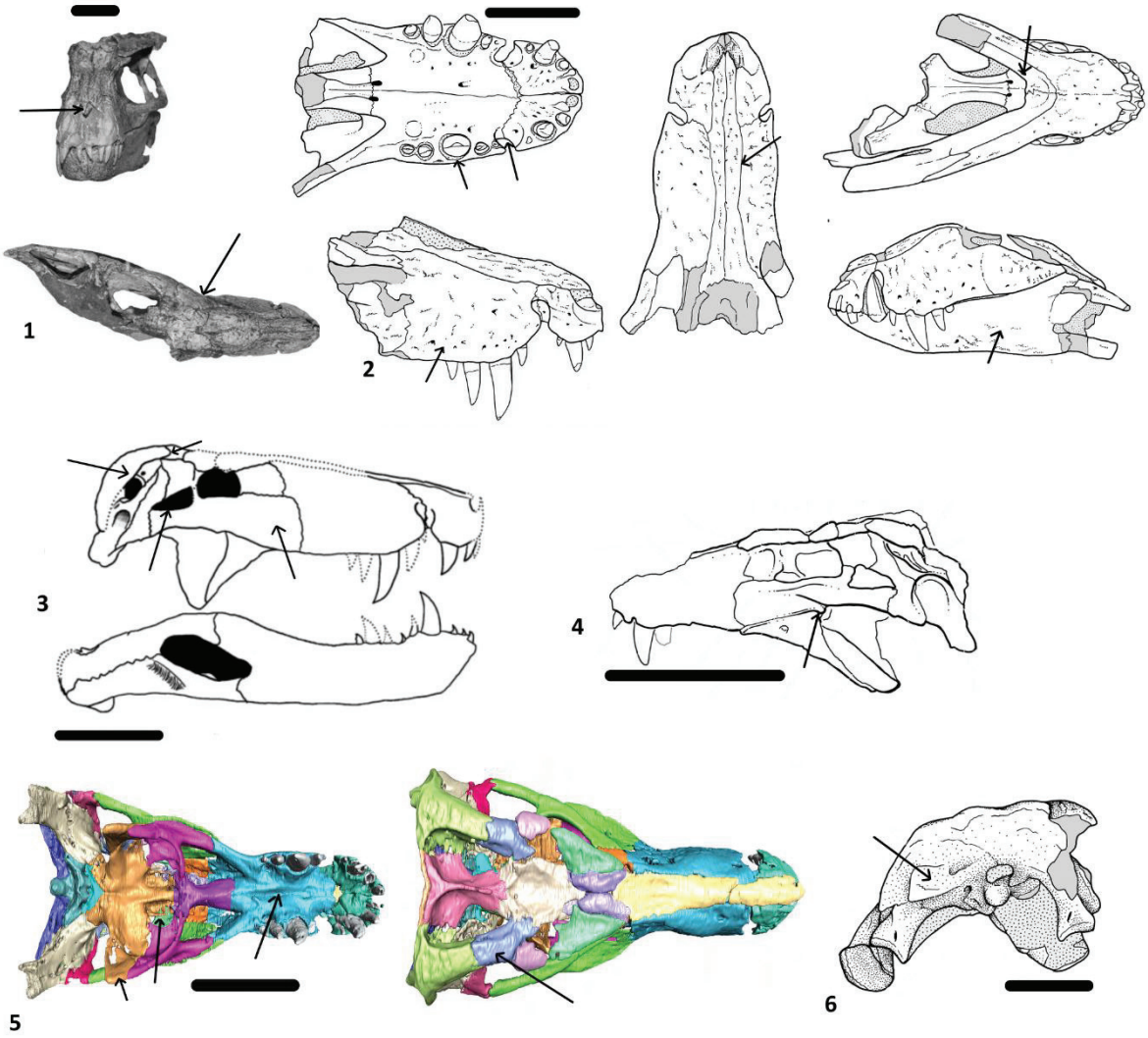

Figure 2.6: Combination of characters diagnostic of Sebecosuchia. 1: altirostral rostrum with a sigmoidal toothrow in dorsal view of *Gondwanasuchus scabrosus* Marinho, Iori, Carvalho & de Vasconcellos, 2013 (UFRJ DG 408-R). Taken from Marinho *et al*. (2013; fig. 2B & D). 2: one wave of enlarged maxillary teeth with third maxillary tooth enlarged and evaginated maxillary alveolar edges of *Campinasuchus dinizi* (CPP 1236). This specimen also has a notch at the premaxilla-maxilla contact opened ventrally as a large fenestra, nearly parallel lateral edges of the nasals, no antorbital fenestra, maxillary teeth set in isolated alveoli and no unsculpted region along the maxillary alveolar margin in lateral view. The other specimen (CPP 1234) has a big, slot-like foramen *intramandibularis oralis*. Modified from Carvalho *et al*. (2011a; plates 4-2, 4-3 & 6). 3: infratemporal fenestra more expanded anteroposteriorly than dorsoventrally with the jugal being higher in its antorbital region than in its infraorbital region, the suture between the squamosal and the postorbital anteriorly convex and the outer surface of the squamosal along the site of attachment of the ear valve groove reduced and vertically oriented in *Baurusuchus pachecoi* Price, 1945. Reconstruction taken from Nascimento & Zaher (2011; fig. 1). 4: notch at the posterior part of the ectopterygoid-jugal contact in *Pissarachampsa sera* (LPRP/USP 0019). Modified from Montefeltro *et al*. (2011; fig. 4A). 5: strongly concave palate, vertical pterygoids, trapezoidal-shaped skull roof and very large choanae of *Aphaurosuchus escharafacies* Darlim, Montefeltro & Langer, 2021 (LPRP 0697), digital reconstruction. Modified from Darlim *et al*. (2021b; fig. 5A & B). 6: long lateral development of the paraoccipital process of *Campinasuchus dinizi* (CPP 1235). Modified from Carvalho *et al*. (2011a; plate 2-4).

As a result, I cannot favour either phylogenetic hypotheses, as none of them rely on true synapomorphies and both are equally supported in the literature and by a complete combination of characters. However, it can be noticed that the characters put forward here only rely on cranial and mandibular traits, no postcranial or internal features are either used or found important. Thus, one way of tackling this conflict might reside in the further addition of such characters in the datasets, as they have been proven to also bear phylogenetic signal and could thus bring a new light to the debate (Pol *et al*., 2012, 2014; Godoy *et al*., 2016; Blanco, 2021).

II- Scientific publication: 'A peirosaurid mandible from the Albian/Cenomanian (Lower Cretaceous) of Algeria and the taxonomic content of *Hamadasuchus* (Crocodylomorpha, Peirosauridae)'

This publication was published in December 2022 in *Papers in Palaeontology*. Reference: Pochat-Cottilloux Y., Perrier V., Amiot R. & Martin J. E. (2023). A peirosaurid mandible from the Albian/Cenomanian (Lower Cretaceous) of Algeria and the taxonomic content of *Hamadasuchus* (Crocodylomorpha, Peirosauridae)'. *Papers in Palaeontology*, 9(2): e1485. https://doi.org/10.1002/spp2.1485

A peirosaurid mandible from the Albian/Cenomanian (Lower Cretaceous) of Algeria and the taxonomic content of *Hamadasuchus* (Crocodylomorpha, Peirosauridae)

Yohan Pochat-Cottilloux [A], Vincent Perrier [A], Romain Amiot [A], Jeremy E. Martin [A]

A: Univ Lyon, Univ Lyon 1, ENSL, CNRS, LGL-TPE, F-69622, Villeurbanne, France

Corresponding author: Yohan Pochat-Cottilloux, yohan.pochat-cottilloux@univ-lyon1.fr

Abstract

Peirosaurids form an extinct clade of terrestrial crocodylomorphs known from the Cretaceous of Africa and South America. Here, we describe a new mandibular ramus attributable to *Hamadasuchus* cf. *rebouli* from the Albian - Cenomanian of La Gara Samani (Algeria). We propose an emended diagnosis for this taxon, originally described from a left dentary fragment from the Kem Kem Group of Morocco and discuss the assignation of the specimens currently referred to it. Using ontogenetic series of extant crocodylians, we show that several mandibular characters commonly used to differentiate between close taxa instead record intraspecific or ontogenetic variability. On the other hand, reliable mandibular characters allow us to propose that the current taxonomic content of *Hamadasuchus rebouli* should be reduced to three specimens, pending future description of relatable cranial remains that will confirm or not this hypothesis. Finally, we demonstrate the importance of mandibular characters in phylogenies, by recovering the new specimen from La Gara Samani as closely related to North African peirosaurids on the basis of a data matrix designed solely on mandibular characters.

Keywords: Algeria – Crocodylomorpha – *Hamadasuchus* – mandible – middle Cretaceous – Peirosauridae.

Introduction

Peirosauridae belongs to Crocodylomorpha, and forms an extinct family known at least from the Aptian to the Maastrichtian (Price, 1955; Leardi & Pol, 2009). Their relationships to other groups of mesoeucrocodylians, as well as the taxonomic content of this group are highly debated. Some studies place them as closely related to the uruguaysuchids and the

mahajangasuchids from the Cretaceous of South America and Africa (Carvalho *et al*., 2004; Turner & Calvo, 2005; Turner, 2006; Turner & Sertich, 2010; Pol *et al*., 2012, 2014; Kellner *et al*., 2014; Sertich & O'Connor, 2014; Leardi *et al*., 2015, 2018; Barrios *et al*., 2016; Fiorelli *et al*., 2016; Godoy *et al*., 2016; Martinelli *et al*., 2018; Coria *et al*., 2019; Dumont *et al*., 2020a; Nicholl *et al*., 2021); other studies depict them as closely related to neosuchians (Sereno *et al*., 2003; Pol & Norell, 2004b; Company *et al*., 2005; Pol & Apesteguia, 2005; Zaher *et al*., 2006; Turner & Buckley, 2008; Leardi & Pol, 2009; Sereno & Larsson, 2009; Nascimento & Zaher, 2011; Pol & Powell, 2011); and they have also been united with sebecids forming the clade Sebecia (Larsson & Sues, 2007; Meunier & Larsson, 2017; Geroto & Bertini, 2019; Ruiz *et al*., 2021). Inside the peirosaurid clade, relationships are also poorly defined and, depending on the inclusion of yet imperfectly understood taxa, such as *Stolokrosuchus lapparenti* Larsson & Gado, 2000 or *Miadanasuchus oblita* Rasmusson Simons & Buckley, 2009, results do vary.

Several new taxa have been described recently and attributed to Peirosauridae, mostly on the basis of mandibular fragments (Barrios *et al*., 2016; Lio *et al*., 2016; Filippi *et al*., 2018; Coria *et al*., 2019; Lamanna *et al*., 2019; Nicholl *et al*., 2021). Such morphological representativity could be an explanation as to why this group is still poorly understood in terms of taxonomy and systematics. As phylogenetic matrices are mostly defined on cranial characters (only 13% of mandibular characters in Leardi *et al*., 2018 and Ruiz *et al*., 2021, for example), the unsettled relationships of peirosaurids may partly be explained by this lack of information.

Since the recognition of *Hamadasuchus rebouli*, from the Kem Kem Group of Morocco, the formation has regionally yielded numerous and far more complete peirosaurid specimens (Rauhut & Lopez-Arbarello, 2005; Larsson & Sues, 2007; Ibrahim *et al*., 2020; Nicholl *et al*., 2021). African peirosaurids are also known in East Africa, suggesting a wider distribution during the Cretaceous (Sertich & O'Connor, 2014). Because the holotype of *Hamadasuchus* consists of a mandibular fragment, taxonomic assignment of subsequent cranial discoveries has proven difficult (Cavin *et al*., 2010; Ibrahim *et al*., 2020; Nicholl *et al*., 2021). Moreover, and specifically for the Kem Kem Group of Morocco, the uncertain tracing of commercially acquired specimens and the high number of fossiliferous localities add difficulties in addressing the contemporaneity of the various specimens.

Here, we describe a left mandibular ramus (MNHN-SAM 136) from regionally slightly older stratigraphic deposits of the Albian - Cenomanian of Algeria that we attribute to Peirosauridae. Then, we discuss the taxonomic composition of North African peirosaurids in an attempt to

clarify the identity of the taxon *Hamadasuchus rebouli,* propose an emended diagnosis for the species and refer this fossil to it. Using a new matrix of mandibular characters only, we also attempt to better understand the phylogenetic relationships of peirosaurids from the middle to late Cretaceous.

Geological setting

The specimen was found at La Gara Samani locality (Algeria), on the north-western border of the Tademaït, between Timimoun and El Menia (Fig. 2.7; de Lapparent de Broin *et al*., 1971), during a fieldtrip involving C. Grenot and R. Vernet in 1970. This locality is part of the Saharan "Continental Intercalaire" and is considered as late Albian to early Cenomanian in age (de Lapparent de Broin *et al*., 1971; Lefranc & Toutin, 1971; Lefranc & Guiraud, 1990; Busson & Cornée, 1991; de Lapparent de Broin, 2002; Meunier & Larsson, 2017; Benyoucef *et al*., 2022). La Gara Samani has provided a diverse fauna including crocodylomorphs (de Lapparent de Broin *et al*., 1971; de Lapparent de Broin, 2002; Meunier & Larsson, 2017), dinosaurs (Taquet & Russell, 1998), dipnoi (Busson & Cornée, 1991), osteichthyes and turtles (de Lapparent de Broin *et al*., 1971) and molluscs (Busson & Cornée, 1991).

Material and methods

A well-preserved and uncrushed left hemi-mandible (MNHN-SAM 136, Fig. 2.8, 2.9 & 2.10) is described here for the first time. A surface scan of the mandible was obtained using an Artec Space Spider and the softwares Artec Studio (version 15) and MeshLab (version 2020.07). The 3D surface model is available in Supplementary File S1 & S2 (the video was made and rendered via Blender version 2.91).

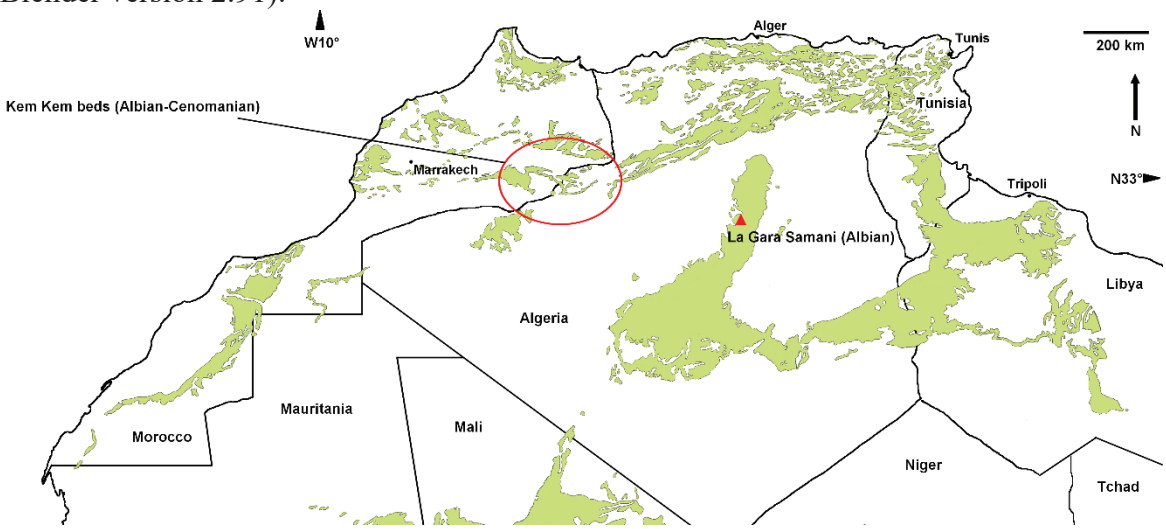

Figure 2.7: Location of La Gara Samani, Algeria and Kem Kem Group, Morocco. Cretaceous outcrops are highlighted in green. Modified after Choubert *et al*. (1976).

Phylogenetic analyses

A matrix of 92 characters and 65 taxa was built on the basis of Pol *et al*. (2014) and Geroto & Bertini (2019) (and references therein; Supplementary File S3 & S4) in order to sample as many notosuchian taxa as possible. *Dibothrosuchus elaphros* Simmons, 1965 was used as the operational outgroup and *Hamadasuchus rebouli* was separated in two different OTU (Operational Taxonomic Unit) because of the differences observed between the specimens assigned to it (see Discussion and Supplementary File S3). As our aim was to study the impact of mandibular characters, the matrix used here includes only this type of characters. We want to clarify here that those analyses are not meant to redefine clades or create new ones, but rather to assess the impact of mandibular characters on the phylogeny of notosuchians, and more precisely of peirosaurids. The results were then compared to those from more "classic" matrices (Supplementary file S5). Another set of analyses was then conducted on taxa usually attributed to Peirosauridae only, using *Kaprosuchus saharicus* as the operational outgroup, to better understand their relationships. Of the 92 equally weighted characters, 2 are continuous and were not discretized because the raw data linked to them did not reveal clear partitions. The matrix also has 9 ordered characters. Three new characters on the mandibular symphysis, splenial and diastema were formulated based on personal observation of specimens. The definition of 13 characters were modified and the coding was evaluated and modified when necessary for the other 76 characters if the data were available (see Supplementary File S3). The matrix is also available on Morphobank (project 4104; http://dx.doi.org/10.7934/P4104).

The analyses were made in parsimony, without phylogenetically uninformative characters and removing taxa with a significant amount of missing data (more than 80%, see also Supplementary file S5 for more details).

Analyses were run on TNT 1.5 (Goloboff & Catalano, 2016). New Technology Search was used enabling all search algorithms (Sectorial Search, Ratchet, Drift and Tree Fusing; Goloboff, 1999; Nixon, 1999). The default settings for these advanced search methods were only changed to increase the iterations of each method, it now features 100 sectorial search drifting cycles, 100 ratchet iterations, 100 drift cycles and 100 rounds of tree fusion per replicate. This tree-space search procedure was repeated for five different random start seeds (following the procedure in Jouve, 2016) using driven search to find the minimum length ten times. Otherwise, the default parameters were kept. Extended implied weighting (Goloboff, 2014) was not used as its utility remains controversial (Congreve & Lamsdell, 2016; Groh *et al*., 2019). Bootstrap

scores were then calculated. When necessary, the ACCTRAN optimization was used (Accelerated Transformation; Farris, 1970; Swofford & Maddison, 1987).

FigTree 1.4.4 was used to visualize the phylogenetic trees obtained.

Results

Systematic paleontology

Crocodylomorpha Hay, 1930

Crocodyliformes Hay, 1930 (*sensu* Benton & Clark, 1988)

Mesoeucrocodylia Whestone & Whybrow, 1983

Notosuchia Gasparini, 1971

Peirosauridae Gasparini, 1982 (*sensu* Geroto & Bertini, 2019)

Hamadasuchus Buffetaut, 1994

Diagnosis – a crocodylomorph characterized by the following unique combination of features: at least fifteen dentary alveoli; all alveoli are very close-set; at least four very small alveoli posterior to the large fourth alveolus; posterior dentary alveoli visible in lateral view; eleven completely involved alveoli in the mandibular symphysis; symphyseal region shallow dorsoventrally and narrow mediolaterally; dorsal and ventral dentary-splenial sutures directed anteromedially to posterolaterally (V-shaped if both hemimandibles were assembled); ventrolateral dentary surface anterior to mandibular fenestra transversely compressed; dentary extends posteriorly beneath the mandibular fenestra; anterior alveoli of dentary procumbent; concavity for the reception of the enlarged maxillary tooth lateral to the 7^{th} - 8^{th} alveolus of the dentary; surangular overlaps dentary above the external mandibular fenestra.

Locality and horizon – "Hamada du Guir", near Taouz, southern Morocco, red beds of late Albian to early Cenomanian age; La Gara Samani, Algeria, late Albian to early Cenomanian.

Hamadasuchus cf. *rebouli* Buffetaut, 1994

Holotype – incomplete left dentary (MDE C001).

Referred specimens – MNHN-MRS 3110, mandibular symphysis (Ibrahim *et al*., 2020, fig. 82A-C); MNHN-SAM 136 (Fig. 2.8, 2.9, 2.10 & 2.11).

Revised diagnosis – as for genus + heavily sculpted mandible; seven alveoli completely involved in the dentary part of the symphysis; surangular forms lateral margin of articular fossa; prominent posterolateral ridge on lateral surface of surangular.

Locality and horizon – as for genus.

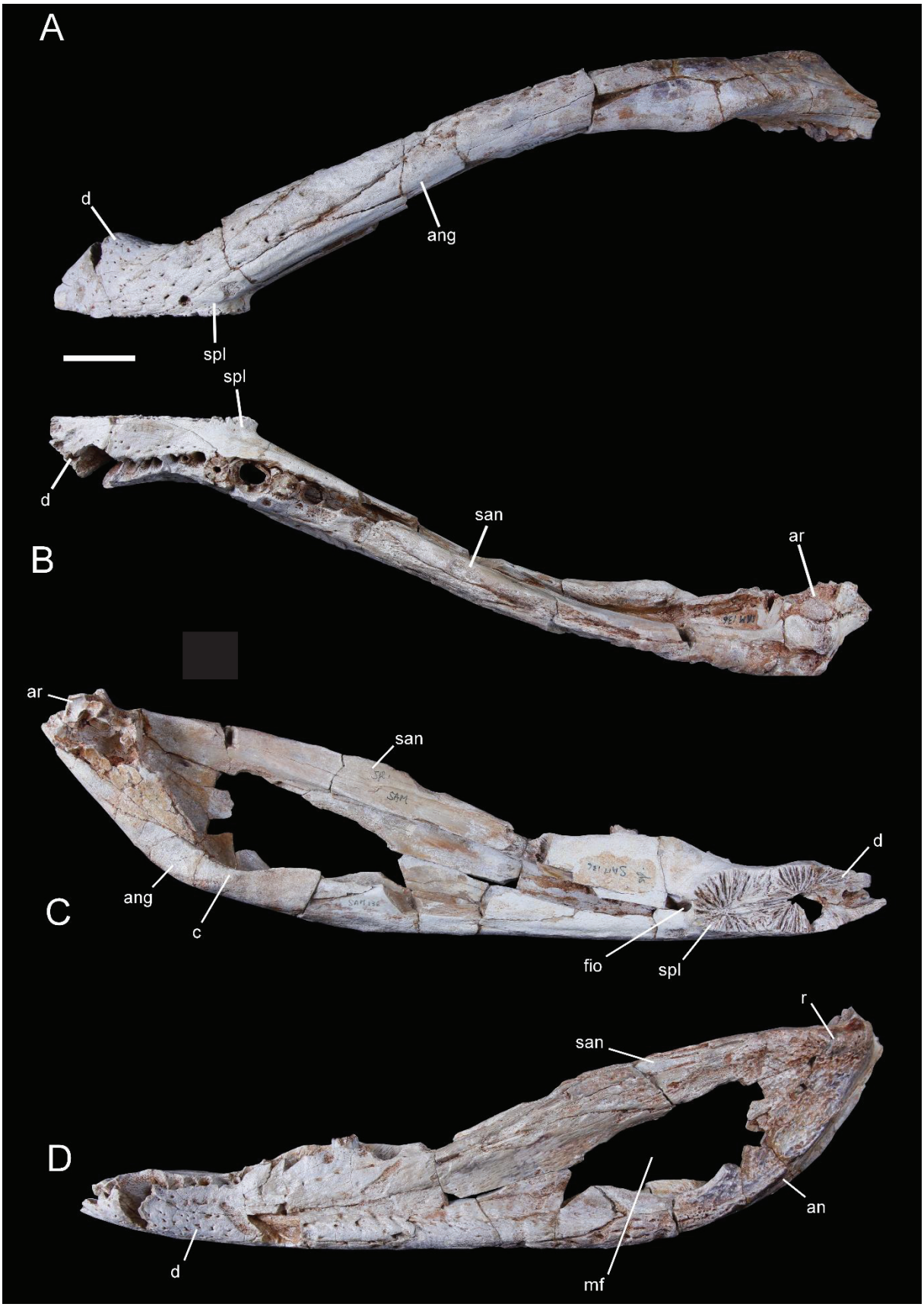

Figure 2.8: Pictures of MNHN-SAM 136 in ventral view (A), dorsal view (B), medial view (C) and lateral view (D). ang: angular, ar: articular, c: crest, d: dentary, fio: foramen *intermandibularis oralis*, mf: external mandibular fenestra, r: ridge, san: surangular, spl: splenial. Scale bar is 5 cm.

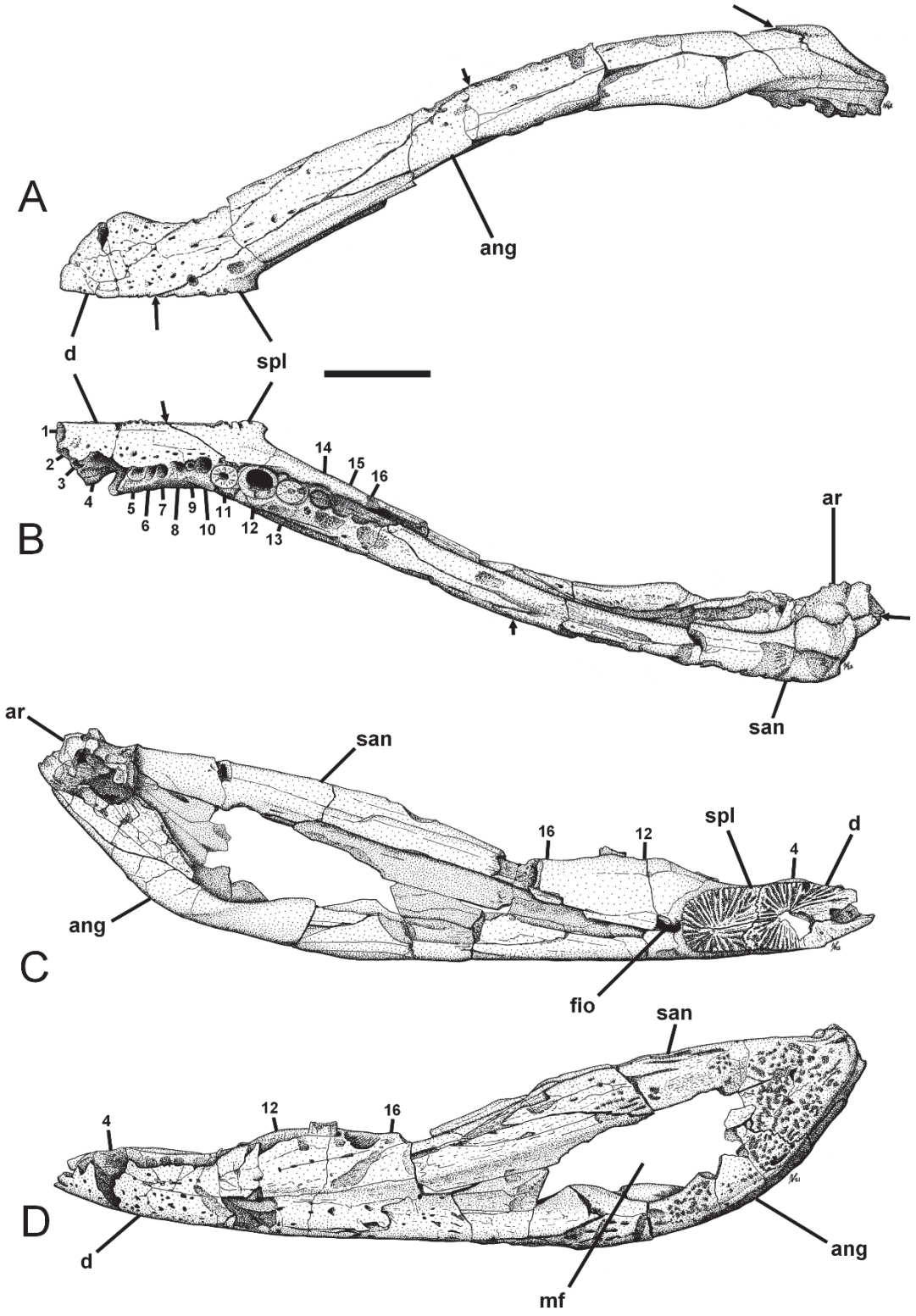

Figure 2.9: Interpretative drawings of MNHN-SAM 136 in ventral view (A), dorsal view (B), medial view (C) and lateral view (D). 1-16: alveolus one to sixteen; ang: angular, ar: articular, d: dentary, fio: foramen *intermandibularis oralis*, mf: external mandibular fenestra, san: surangular, spl: splenial. Arrows indicate bone sutures. Scale bar is 5 cm.

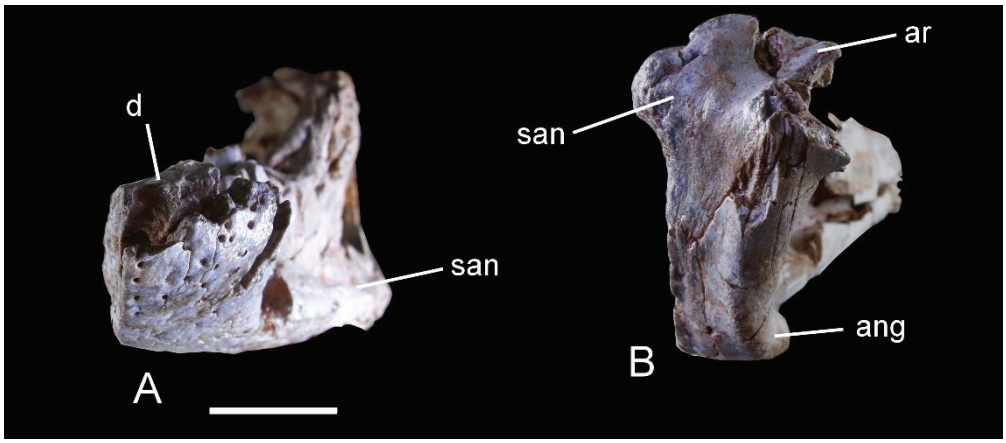

Figure 2.10: Pictures of MNHN-SAM 136 in anterior (A) and posterior view (B). ang: angular, ar: articular, d: dentary, san: surangular. Scale bar is 2 cm.

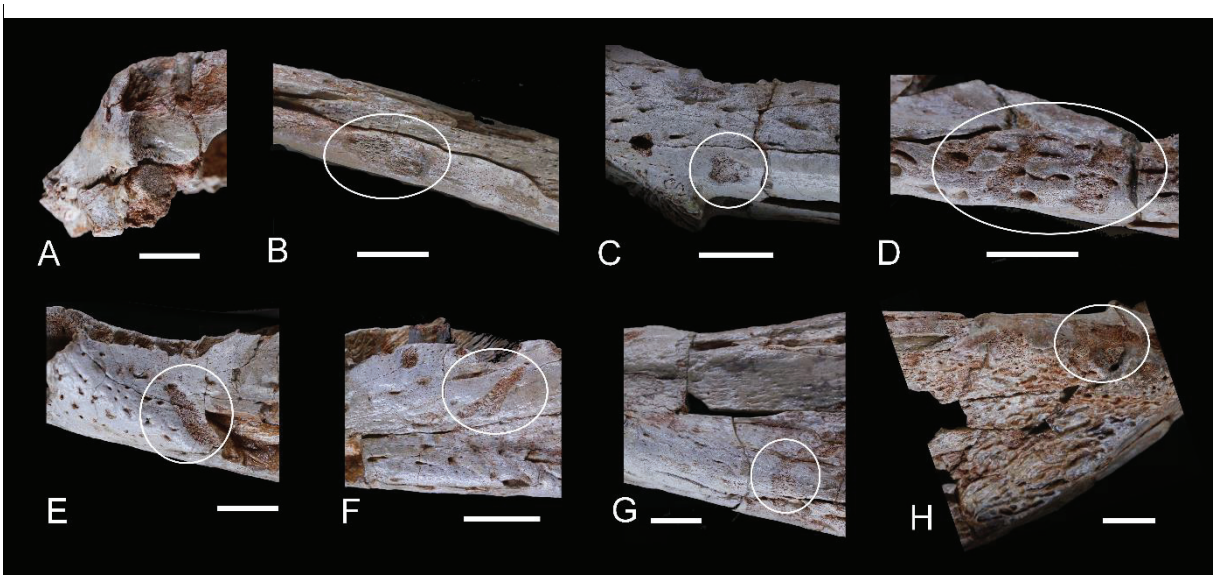

Figure 2.11: Close ups on MNHN-SAM 136 in dorsal view (A & B), ventral view (C & D) and lateral view (E-H). White circles are dermestid traces. Scale bars are 2 cm.

Description

MNHN-SAM 136 is a left mandibular ramus. Apart from the coronoid and the retroarticular process, all the bones are preserved and almost complete. The margins of the external mandibular fenestra are imperfect in some places, but the general outline is well-preserved. This fenestra is directed anteroposteriorly and is triangular-shaped in lateral view, with the longest side dorsally and parallel to the dorsal edge of the surangular. In lateral view, the mandible is arched anterodorsally. The outer surface of the mandible is ornamented with nutrient foramina in its anterior portion and shallow pits in its posterior area, corresponding to the ventral margin of the surangular and the angular. The mandible is nearly smooth and devoid of ornamentation in the anterior area of the external mandibular fenestra.

Dentary:

The mandibular symphysis is extensive and involves completely the first eleven alveoli (Fig. 2.8B & 2.9B). Both dentaries firmly suture to each other along a medial contact until the level of the 7th dentary alveolus (Fig. 2.8B & 2.9B). The symphyseal region is shallow dorsoventrally and narrow mediolaterally (Fig. 2.10A). In dorsal view, the suture with the splenial is oblique anteriorly (directed posterolaterally to anteromedially) up until the 11th dentary alveolus then it straightens posteriorly (Fig. 2.8B & 2.9B). In ventral view, the dentary-splenial suture is oblique all the way (Fig. 2.8A & 2.9A). In medial view, it is interdigitated and directed posteroventrally (Fig. 2.8C & 2.9C). The dentaries remain uniform in width up to their point of divergence, where they begin to taper off. Posteriorly, in lateral view, the dentary bone divides into a long posterodorsal process and a shorter posteroventral process (Fig. 2.8D & 2.9D) that contribute respectively to the anterodorsal and anteroventral margins of the external mandibular fenestra. The posteroventral process lies down against the angular. The posterior end of the toothrow seems to connect with one of the anterior processes of the surangular, but it is difficult to assess because the area is damaged. There are 17 alveoli, of which the 4th is the largest. Some alveoli preserve the root of a tooth, namely the 5th, 9th, and 11th to 13th, which are laterally moderately and variably compressed (precise measurements of each alveolus are available in Table 1). The first four alveoli are gradually directed anteriorly to anterolaterally and the dentary narrows medially at the level of the 8th/9th alveoli. Although this area may be deformed, this anatomical trait is still prominent. In lateral view, the mandibular dentition shows a sinuous margin, marked by two sets of waves (Fig. 2.8D & 2.9D). The apex of the first wave culminates at the large 4th alveolus, whereas the second wave culminates at the 12th/13th alveoli, which are also large. In between, dentary alveoli are distinctly but variably small (Table 1). The fourth alveolus is not dorsally elevated from the first one. The ventral surface of the dentary of MNHN-SAM 136 is anterolaterally curved dorsally and bears small but deep foramina (Fig. 2.8A). The ventrolateral margin of the dentary presents a very developed prominence, that stretches anteroposteriorly from the 4th alveolus to the ventral margin of the external mandibular fenestra (Fig. 2.8D & 2.9D). This gives a nearly flat ventral profile to the dentary, as observed in lateral view.

Splenial:

The splenial is mostly exposed medially where it forms a vertical plate that sutures with the dentary. In its anterior portion, the splenial contributes to the mandibular symphysis and

Table 1: Labiolingual and mesiodistal measurements of each mandibular alveolus of peirosaurid taxa (in mm).

Tooth position	*Hamadasuchus rebouli*		*Bayomesasuchus hernandezi*		*Pepesuchus deiseae*		*Montealtosuchus arrudacamposi*		*Barrosasuchus neuquenianus*		*Kinesuchus overoi*	
	ROM 49282		MCF PVPH-822		MN 7005-V		MPMA-16-0007-04		MCF-PVPH-413		MAUV-Pv-CO-583	
	LL	MD	LL	MD	LL	MD	LL	MD	LL	MD	LL	MD
d1	8	9	?	?	?	4.4	4	4	12.6	?	5.9	5.3
d2	5	5.5	?	?	7.6	3.1	3.2	4	8.4	10	6.5	5.3
d3	4.5	5	4.2	?	7.1	4.4	4	4	12.6	11.6	4.7	4.1
d4	9.5	11.5	6	10.1	7.6	11.1	6	6.8	10.5	5.2	8.8	10.6
d5	6	6.5	3.6	4.2	8.9	?	2.6	4	?	?	4.7	6.5
d6	4.5	4.5	3	3.6	?	?	3.2	3.6	10.5	?	5.3	5.9
d7	4	4	3	3.6	3.6	?	2.8	2.8	6.3	5.3	4.1	5.3
d8	4	4	3	4.2	4.4	4.4	3.2	4	5.3	8.4	3.5	5.3
d9	4	4	?	?	6.2	6.7	2.8	4	8.4	8.4	4.7	5.3
d10	5	5.5	?	?	5.3	?	3.2	4	7.4	7.4	?	5.9
d11	5.5	6	?	?	8.9	6.7	3.2	4.8	7.4	11.6	5.9	5.9
d12	7	7.5	?	?	8.9	?	4	6	9.5	12.6	6.5	7.1
d13	7.5	11	?	?	8.9	7.1	4	6	7.4	9.5	7.1	8.8
d14	5	7	?	?	8.9	?	2.4	4	5.3	8.4	5.9	8.2
d15	?	?	?	?	5.3	?	3.6	5.6	5.3	8.4	4.1	8.2
d16	?	?	?	?	8.9	6.2	3.7	4	?	?	3.5	5.9
d17	?	?	?	?	?	4	3.2	4	?	?	4.1	5.9
d18	?	?	?	?	3.1	?	2.8	4.8	?	?	?	?

LL, labiolingual; MD, mesiodistal.

Lomasuchus palpebrosus		*Patagosuchus anielensis*		*Gasparinisuchus peirosauroides*		*Itasuchus jesuinoi*		*Colhuehuapi-suchus lunai*		New specimen	
MOZ 4084 PV		MAÑE-PV 1		MOZ 1750 PV		DGM 434-R		UNPSJB-PV 961		MNHN-SAM 136	
LL	MD	LL	MD	LL	MD	LL	MD	LL	MD	LL	MD
8	?	?	?	?	?	?	12.8	5	7.3	?	16
5	5	4	?	7	8.8	15.3	17.9	5.1	5.5	12	10
8	10	3	?	?	?	12.8	15.3	6	5.4	10	8
?	?	7.7	?	?	14.7	9	12.8	8.3	9.7	19	21
?	?	4.7	4.7	5.9	7.6	7.8	10.2	?	?	11	9
?	?	4	3	4.1	5.9	?	?	3	4.1	8	5
?	?	5	4	5.9	6.5	10.2	?	3	3.9	9	7
?	?	4	4.3	4.1	5.3	12.8	15.3	?	?	8	7
?	?	3	5.7	4.7	3.5	?	16.6	?	?	5	5
?	?	5	4	5.9	5.9	17.9	19.2	?	?	10	11
?	?	5	6	8.2	7.6	11.5	14.1	2.8	4.3	12	14
?	?	?	?	7.6	11.2	15.3	15.3	4.7	6.4	17	24
?	?	?	?	10	14.1	14.1	16.6	?	?	13	15
?	?	?	?	5.3	7.1	12.8	14.1	?	?	11	11
?	?	?	?	4.1	5.9	11.5	12.8	?	?	10	?
?	?	?	?	3.5	7.1	11.5	10.2	?	?	10.5	?
?	?	?	?	4.1	7.6	?	?	?	?	?	?
?	?	?	?	2.9	5.3	?	?	?	?	?	?

would have sutured medially with the corresponding right splenial (Fig. 2.8A, 2.8B, 2.8C, 2.9A, 2.9B & 2.9C). Here, the splenial reaches anteriorly to the level of the 7th alveolus, dorsally and ventrally (Fig. 2.8A, 2.8B, 2.9A & 2.9B). The dorsal and ventral exposure of the splenial is strictly triangular-shaped and makes more than one third of the mandibular symphysis. In posterior view, the foramen *intermandibularis oralis* is displaced laterally, indicating the paired condition for the complete mandibular rami (Fig. 2.8C & 2.9C). Posteriorly, the splenial becomes thin and plate-like along the medial surface of the dentary taking part in the medial wall for the last seven dentary alveoli, until it tapers off dorsally and probably contacts the surangular medially. The area of insertion can be seen in medial view (Fig. 2.8C & 2.9C). The splenial also meets with the angular ventrally (Fig. 2.8A, 2.8C, 2.9A & 2.9C). Overall, all the surfaces of the splenial are smooth.

Angular:

The angular is the ventralmost mandibular element, it makes about two thirds of the mandibular ramus. In lateral view, it is elongated and curved posterodorsally (Fig. 2.8D & 2.9D). Medially, it is convex with a prominent crest twisting anterodorsally to posteroventrally just ventral to the external mandibular fenestra forming the posterodorsal part of the adductor fossa (Fig. 2.8C & 2.9C). Anteriorly, a long process sutures with the splenial medially and the dentary laterally up to the level of the 16th alveolus. The anterior part of the adductor fossa is formed ventrally and medially by the angular and medially by the splenial, whereas the posterior part of the medial wall of the adductor fossa is missing. The angular forms the ventral margin of the external mandibular fenestra laterally (Fig. 2.8D & 2.9D). The foramen *intermandibularis caudalis* is either absent or not preserved on the medial side. Posteriorly to the external mandibular fenestra, and for the rest of its length, the angular sutures with the surangular, reaching ventrally to the articulation surface of the articular as a sharp process and curving inwards and up (Fig. 2.8C, 2.9C & 2.10B). The lateral surface of the angular bears the prolongation of the pronounced lateral crest observed on the dentary (Fig. 2.8B, 2.8D, 2.9B & 2.9D), which becomes a groove in dorsolateral view, just ventral to the external mandibular fenestra. The posteroventral margin of the angular shows a developed area for the insertion of the *musculus pterygoideus*, which is visible in lateral and ventral views (Fig. 2.8A, 2.8D, 2.9A & 2.9D).

Surangular:

This bone is robust and elongated. Anteriorly, the suture with the dentary is complex: the dentary has two posterior processes that interlock with two anterior processes of the surangular

(Fig. 2.8B & 2.9B). In lateral view, the surangular curves dorsally at the level of the external mandibular fenestra (Fig. 2.8D & 2.9D). The surangular forms the posterior and posterodorsal margins of the external mandibular fenestra (Fig. 2.8C, 2.8D, 2.9C & 2.9D). Posteriorly to this fenestra, the surangular sutures with the angular for the rest of its length and it also becomes thinner mediolaterally and ventrally. The suture is linear anteriorly and curves dorsally toward the posterior end. The bone also curves dorsally and forms the lateral margin of the glenoid fossa (Fig. 2.8B, 2.10A, 2.10B & 2.11A). Laterally to this, there is a tiny ridge followed by a huge depression that is located beneath the level of the glenoid surface corresponding to the articulation with the quadratojugal condyle, indicating a double mandibular articulation (Fig. 2.8B & 2.9B). The posteriormost part of the surangular is broken. The dorsal surface is overall convex but flattens considerably just before the glenoid surface with the quadrate. The lateral surface is not as well preserved as the other parts of the mandible, but it bears a prominent posterolateral ridge (Fig. 2.8D & 2.9D). On the medial surface, the suture with the articular is directed posterodorsally to anteroventrally.

Articular:

The articular is contained laterally by the posterior parts of the angular and surangular. Only the anterior part as well as a part of the dorsal surface of the articular are preserved. The anterodorsal surface is separated from the posterodorsal surface by a mediolateral ridge and would have articulated with the quadrate. This ridge is tall and dorsally edged (Fig. 2.8B, 2.8C, 2.9B, 2.9C, 2.10B & 2.11A). The articular fossa is divided into a lateral and a medial portion separated by a small ridge oriented anteroposteriorly. Both seem to be of the same size; however, the medialmost part is broken (the foramen aërum is not preserved). The preserved part of the posterior surface is concave, curved ventromedially. The retroarticular process is broken but would have been directed posterodorsally. Ventromedially, the articular forms the posterior wall of the adductor chamber. It sutures with the surangular at its lateral margin and with the angular at its ventral margin (Fig. 2.8B, 2.8C, 2.9B, 2.9C, 2.10B & 2.10A).

Dentition:

The best partially preserved root is the 13th (Fig. 2.8B & 2.9B). It is broken at the exit of the toothrow. The root is compressed laterally (ovoid shape in dorsal view), no carinae can be seen and it bears apicobasal striations (Fig. 2.8D & 2.9D).

Phylogenetic analyses

The analysis generated 94 most parsimonious trees and a consensus tree with a length of 436 steps (Fig. 2.12; consistency index = 0.33, retention index = 0.79). Our results show that some groups within Crocodylomorpha are retrieved (Fig. 2.12) compared to recent phylogenetic studies on this subject (Pol *et al*., 2014; Godoy *et al*., 2016; Leardi *et al*., 2018; Dumont *et al.*, 2020a; see also Supplementary File S5). Here, based on ACCTRAN optimization, Baurusuchidae is separated from all other notosuchians on the basis of lacking posteroventral symphyseal depressions (char. 42), an anterior portion of the mandibular symphysis with an anteriorly verticalized angle of more than 45° (char. 43), a surangular that does not participate in the quadrate articulation (char. 50), a surangular anterior border clearly bifurcated and divergent (char. 54), a lateral flange of the retroarticular process that is shorter than the mediolateral width of the glenoid facets of the articular (char. 85), a small bulge located proximally on the medial flange of the retroarticular process that is absent (char. 88) and an anteromedial end of the medial flange of the retroarticular process that projects anteroventrally as a deep pendant process (char. 89). Sphagesauridae (and "advanced" notosuchians or Sphagesauria; Kuhn, 1968; Pol *et al*., 2014; Ruiz *et al*., 2021) are monophyletic on the basis of having a posterior region of alveolar margins facing dorsally, forming a broad alveolar shelf that is strongly inset medially from the lateral surface of the dentaries (char. 13), middle and posterior dentary teeth with a transverse circular to subcircular section without significant lateral compression (char. 24), the dentary symphysis tapering anteriorly forming an angle (V-shaped; char. 36) and having well developed coronoid tuberosities on the medial surface of the surangular, forming prominent crests (char. 45). Finally, Uruguaysuchidae (with the inclusion of *Comahuesuchus brachybuccalis* Bonaparte, 1991) is retrieved as monophyletic on the basis of an unsculpted region on the dentary below the toothrow (char. 11), a dentary that overlaps the surangular above the external mandibular fenestra (char. 16), middle and posterior dentary teeth with a transverse section circular to subcircular without significant lateral compression (char. 24), a splenial that forms close to 30% of the symphyseal length (char. 29), a straight shape of the splenial-dentary suture adjacent to the dentary toothrow (char. 39), an

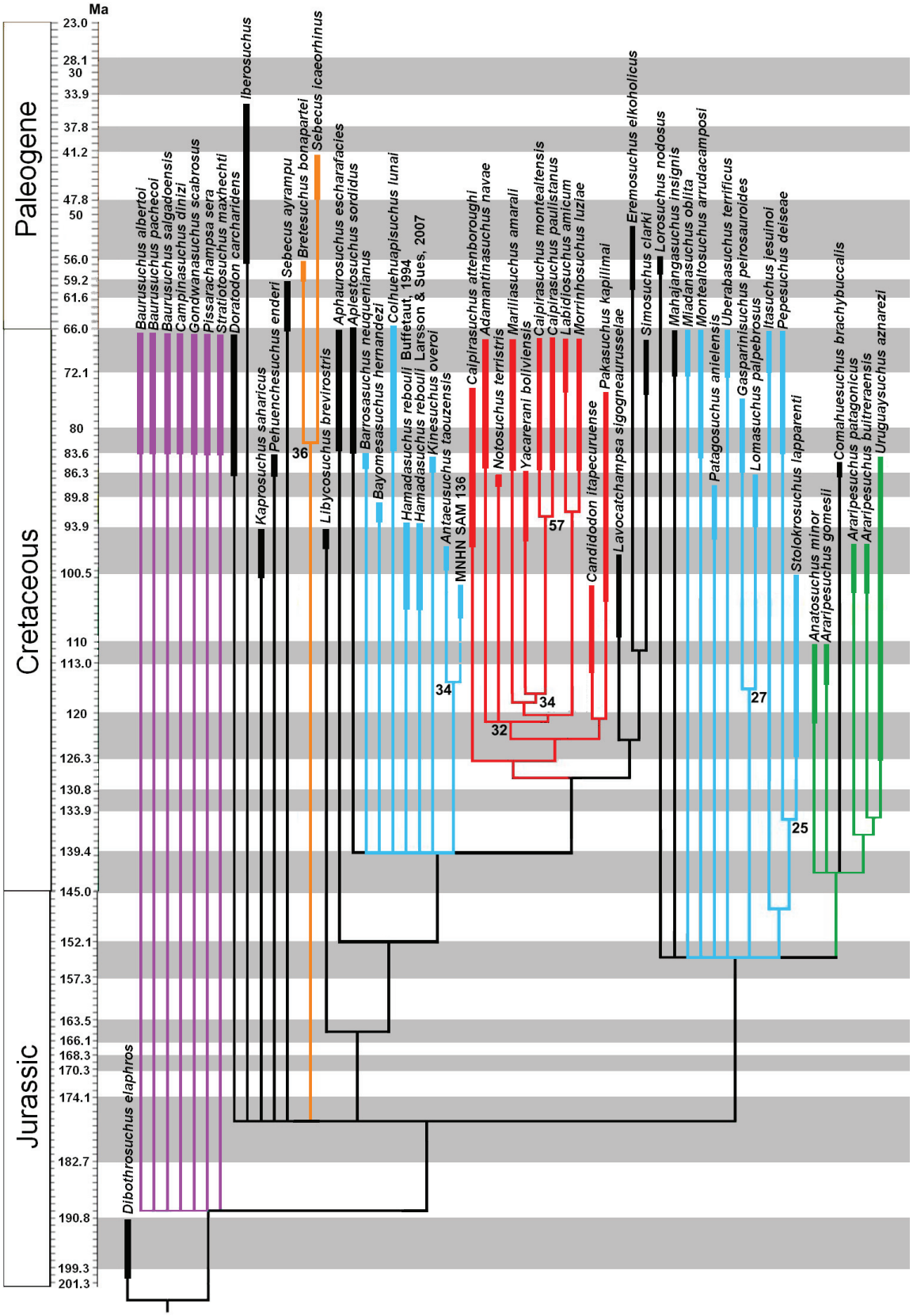

Figure 2.12: Time-calibrated phylogenetic tree on the full set of notosuchian taxa sampled here, result obtained with mandibular characters only (colours represent taxa usually attributed to different clades; purple: Baurusuchidae, orange: Sebecidae, red: Sphagesauridae and "advanced" notosuchians, green: Uruguaysuchidae, blue: Peirosauridae). Bootstrap scores are indicated where superior to 25%.

insertion area for the *M. pterygoideous posterior* that extends on the lateral surface of the angular (char. 66) and a retroarticular process that has a rounded surface, is longer than wide, flat and is posteroventrally oriented and facing dorsomedially (char. 84). Interestingly, the taxa usually attributed to the monophyletic family Peirosauridae are split into two groups: one is close to sphagesaurids and "advanced" notosuchians and composed of *Barrosasuchus neuquenianus* Coria, Ortega, Arcucci & Currie, 2019, *Bayomesasuchus hernandezi* Barrios, Paulina-Carabajal & Bona, 2016, *Colhuehuapisuchus lunai* Lamanna, Casal, Ibiricu & Martínez, 2019, *H. rebouli* (*sensu* Buffetaut, 1994 and Larsson & Sues, 2007), *Kinesuchus overoi* Filippi, Barrios & Garrido, 2018*, Antaeusuchus taouzensis* Nicholl, Hunt, Ouarhache & Mannion, 2021 & MNHN-SAM 136 whereas the other one is closely related to uruguaysuchids and composed of *Miadanasuchus oblita* Buffetaut & Taquet, 1979*, Montealtosuchus arrudacamposi, Patagosuchus anielensis* Lio, Agnolín, Juarez Valieri, Filippi & Rosales, 2016*, Uberabasuchus terrificus, Gasparinisuchus peirosauroides, Lomasuchus palpebrosus* Gasparini, Chiappe & Fernandez, 1991*, Itasuchus jesuinoi* Price, 1955*, Pepesuchus deiseae* Campos, Oliveira, Figueiredo, Riff, Azevedo, Carvalho & Kellner, 2011 and *Stolokrosuchus lapparenti* (Fig. 2.12).

The first taxa mentioned are grouped based on having procumbent, anteriorly inclined dentary teeth (char. 14), having a surangular that overlaps the dentary above the external mandibular fenestra (char. 16), having middle dentary teeth disposed in a groove, originally only separated from each other by soft tissue (char. 23), the surangular participating in the quadrate articulation and forming approximately one-third of the glenoid fossa with the quadratojugal bearing an articular condyle (char. 50) and a surangular-angular suture intersecting with the external mandibular fenestra at the posterodorsal angle (char. 59)

The remaining peirosaurids are related to uruguaysuchids on the basis of having a foramen *intermandibularis oralis* that is small or absent (char. 4), the posterior portion of the external mandibular fenestra that is sculpted (char. 7), a pattern of mandibular dentition after the fourth dentary teeth that is composed of 3-4 caniniforms, followed by molariforms (char. 22), a mandibular symphysis that is shallow and tapering anteriorly in lateral view (char. 37), a splenial-dentary suture on the ventral surface that is transverse (char. 38), a surangular posterior edge bent downward, forming a convexity (char. 56), a strong pitted pattern on the angular and the posterior pat of the surangular (char. 64), a posterior border of the articular glenoid fossa that is well developed, with a ridge limiting the posterior mandibular moves (char. 78), a retroarticular process that is elongated posteriorly, in triangular shape and facing dorsally (char.

84) and a medial edge of the medial flange of the retroarticular process that is straight or slightly convex (char. 91). Another set of analyses were conducted using taxa attributed to Peirosauridae only from the complete dataset and using *Kaprosuchus saharicus* as an outgroup. Here, this allows to include for the first time *K. overoi, P. anielensis* or *C. lunai.* This analysis generated three most parsimonious trees and a consensus tree of 114 steps (Fig. 2.13, see also Supplementary File S5; consistency index = 0.66, retention index = 0.53). The same dichotomy as in the general analysis is found. Using mandibular characters, the groups Pepesuchinae and Peirosaurinae *sensu* Geroto & Bertini, 2019 are not retrieved. However, *S. lapparenti* and *M. oblita*, which are two taxa whose position has been greatly debated (de Lapparent de Broin, 2002; Sereno *et al*., 2003; Carvalho *et al*., 2004; Jouve *et al*., 2006; Larsson & Sues, 2007; Turner & Buckley, 2008; Sereno & Larsson, 2009; Turner & Sertich, 2010; Pol & Powell, 2011; Bronzati *et al*., 2012; Pol *et al*., 2012, 2014; Adams, 2013; Kellner *et al*., 2014; Sertich & O'Connor, 2014; Leardi *et al*., 2015, Barrios *et al*., 2016; Fiorelli *et al*., 2016; Meunier & Larsson, 2017; Martinelli *et al*., 2018; Geroto & Bertini, 2019; Coria *et al*., 2019; Nicholl *et al*., 2021; Ruiz *et al*., 2021) are retrieved here, using mandibular characters, deeply nested within Peirosauridae and, furthermore, the topology presented in Fig. 2.13 does not change if we remove one or both taxa from the analysis. These results on mandibular characters reflect a methodological choice underlining the close relationships of *S. lapparenti*, *M. oblita* and peirosaurids but should be confronted to other lines of evidence.

Discussion

MNHN-SAM 136 as a peirosaurid

Cretaceous crocodylomorphs from Africa with a long mandibular symphysis in which the splenial contributes and laterally compressed teeth which are procumbent in the anterior part of the mandible are restricted to certain notosuchians (de Lapparent de Broin, 2002; Sereno & Larsson, 2009; Martin & de Lapparent de Broin, 2016; Meunier & Larsson, 2017; Ibrahim *et al.*, 2020). The morphology of MNHN-SAM 136 is very different from that of *Anatosuchus minor* and *Laganosuchus* Sereno & Larsson, 2009 because the mandible is overall not squared in the symphyseal region, as it is in those two taxa. The posterior alveoli are visible in lateral view, which allows to distinguish this specimen from *Araripesuchus wegeneri* (Sereno & Larsson, 2009). The medial part of the dentary symphysis does not bear an oval fenestra, so this specimen cannot be attributed to *Araripesuchus rattoides*. Among the remaining taxa, the peirosaurids are characterized by a heavily sculpted mandible and two waves of enlarged

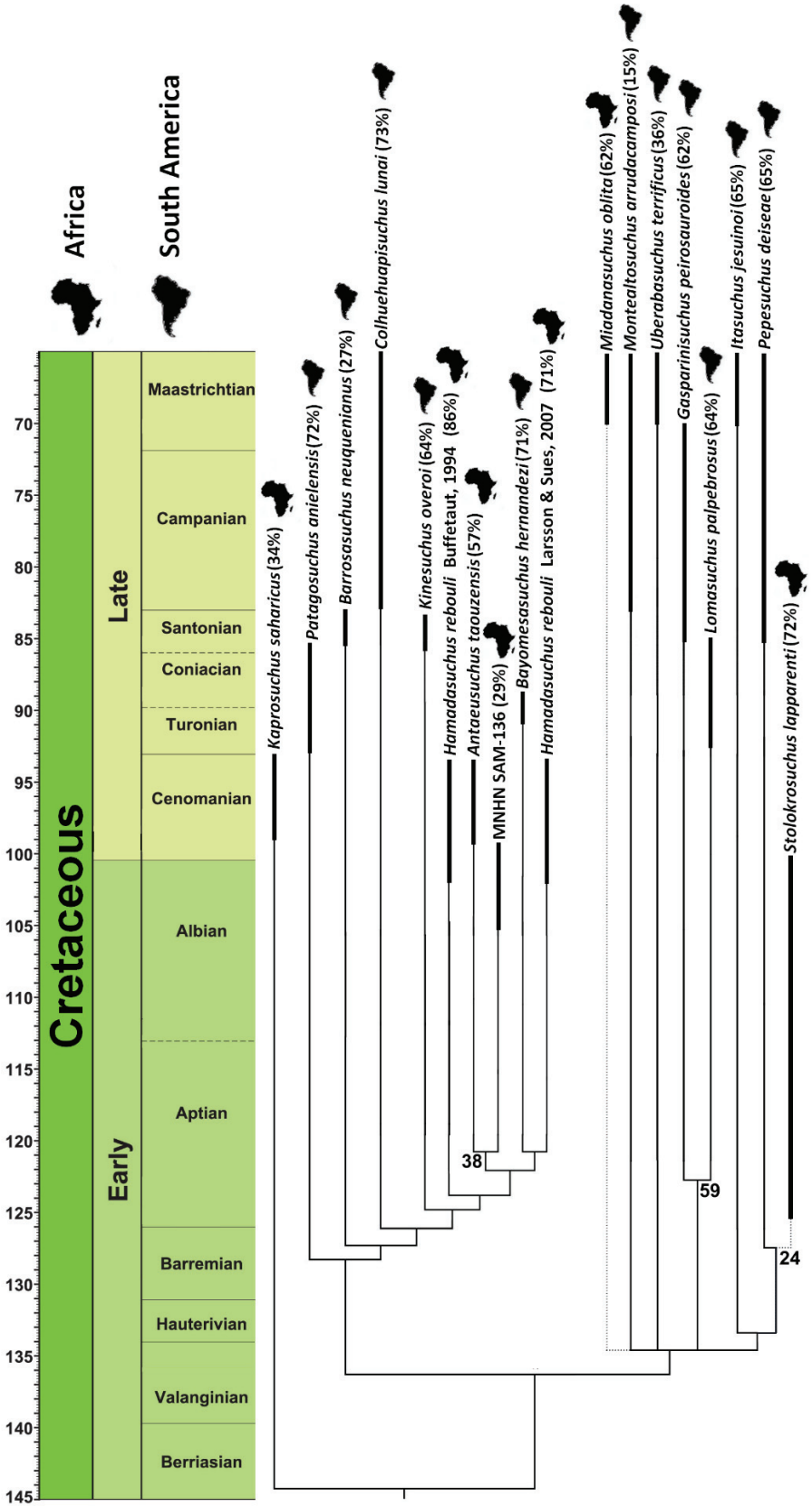

Figure 2.13: Time-calibrated phylogenetic tree on the Peirosauridae taxa (*sensu* Geroto & Bertini, 2019) sampled here, result obtained with mandibular characters only (branches in dashed lines indicate taxa that are often retrieved outside Peirosauridae). Bootstrap scores are indicated where superior to 25%. South America and Africa outlines correspond to the geographic occurrences of the taxon.

dentary teeth (Gasparini, 1982; Geroto & Bertini, 2019), as reported here in MNHN-SAM 136. Comparisons below will thus be made with peirosaurids of similar morphology that preserve comparable elements (for the full list of specimens, see Table 2); *Hamadasuchus rebouli* (Buffetaut, 1994; Larsson & Sues, 2007); *Montealtosuchus arrudacamposi* (Carvalho *et al*., 2007; *Uberabasuchus terrificus* (Carvalho *et al*., 2004), which will be treated here as such although it might be a junior synonym of *Peirosaurus tormini* Price, 1955; *Pepesuchus deiseae* (Campos *et al*., 2011; Geroto & Bertini, 2019); *Itasuchus jesuinoi* (Price, 1955); *Patagosuchus anielensis* (Lio *et al*., 2016); *Bayomesasuchus hernandezi* (Barrios *et al*., 2016); *Gasparinisuchus peirosauroides* (Martinelli *et al*., 2012); *Colhuehuapisuchus lunai* (Lamanna *et al*., 2019); *Barrosasuchus neuquenianus* (Coria *et al*., 2019); *Antaeusuchus taouzensis* (Nicholl *et al*., 2021) and *Kinesuchus overoi* (Filippi *et al*., 2018). In MNHN-SAM 136, the two dentaries separate dorsally at the level of the 7th dentary alveolus (as in *K. overoi, B. neuquenianus, G. peirosauroides, P. deiseae* and *I. jesuinoi*). The mandibular symphysis extends up to the 12th alveolus, as in *K. overoi* and *A. taouzensis*, whereas it only extends to the 11th alveolus in *H. rebouli,* the 10th alveolus in *B. hernandezi*, *M. arrudacamposi*, *C. lunai* and *P. deiseae*, the 9th alveolus in *P. anielensis* and to the 8th alveolus in *G. peirosauroides* and *B. neuquenianus.* In medial view, the symphyseal region is dorsoventrally shallow and, in dorsal view, it is narrow mediolaterally (as in *B. hernandezi*, *M. arrudacamposi*, *I. jesuinoi, H. rebouli* and *K. overoi*).

The first four alveoli are gradually directed anteriorly to anterolaterally and the dentary narrows significantly medially at the level of the 8th/9th alveoli (as in *P. deiseae* and *K. overoi*). In lateral view, the apex of the first wave of enlargement of the toothrow is the large 4th alveolus, whereas the second one is formed by the 12th/13th alveoli, which are also large (as in *B. neuquenianus, K. overoi, M. arrudacamposi, C. lunai, A. taouzensis* and *H. rebouli*). The fourth alveolus is not dorsally elevated markedly from the first one (as in *M. arrudacamposi, B. neuquenianus, K. overoi, I. jesuinoi, A. taouzensis* and *P. deiseae*). The dorsal and ventral dentary-splenial sutures are directed anteromedially to posterolaterally (V-shaped if both hemimandibles were assembled), as in *H. rebouli, B. hernandezi, K. overoi, A. taouzensis* and *P. deiseae*. In posterior view, the foramen *intermandibularis oralis* is displaced laterally, and it thus would have been paired. This is also seen in *A. taouzensis,* probably in *C. lunai* and *K. overoi,* although the foramen is still close to the splenial symphysis suture in the latter, almost touching it.

The surangular curves dorsally and forms the lateral margin of the articular fossa (as in *B. hernandezi*, *M. arrudacamposi* and *B. neuquenianus*). On the surangular, there is a tiny ridge

Table 2: Global mandibular measurements of peirosaurid taxa (in mm). * Distance between the extremities of the articular and the dentary. ** Distance between the extremities of the mandible at the posterior margin of the mandibular symphysis.

Taxon	Specimens	Mandibular length*	Mandibular fenestra heigth	Mandibular fenestra width	Mandibular symphysis width**	References
Hamadasuchus rebouli	ROM 49282	?	?	?	42	Larsson & Sues (2007)
Bayomesasuchus hernandezi	MCF PVPH-822	?	?	?	50	Barrios *et al.* (2016)
Pepesuchus deiseae	MN 7005-V, MCT 1723-R	?	?	?	36	Campos *et al.* (2011); Geroto & Bertini (2019)
Uberabasuchus terrificus	CPPLIP 630	280	60	20	68	Carvalho *et al.* (2004)
Montealtosuchus arrudacamposi	MPMA-16-0007-04	220	50	20	57	Carvalho *et al.* (2007)
Barrosasuchus neuquenianus	MCF-PVPH-413	383	36	9	100	Coria *et al.* (2019)
Kinesuchus overoi	MAUV-Pv-CO-583	?	?	?	50	Filippi *et al.* (2018)
Lomasuchus palpebrosus	MOZ 4084 PV	150	?	?	73	Gasparini *et al.* (1991)
Patagosuchus anielensis	MAÑE-PV 1	?	?	?	60	Lio *et al.* (2016)
Gasparinisuchus peirosauroides	MOZ 1750 PV	287	?	?	87	Martinelli *et al.* (2012)
Itasuchus jesuinoi	DGM-434-R	?	?	?	78	Price (1955)
Colhuehuapisuchus lunai	UNPSJB-PV 961	?	?	?	69	Lamanna *et al.* (2019)
Hamadasuchus rebouli	MNHN-SAM 136	460	100	45	90	This study
Antaeusuchus taouzensis	NHMUK PV R36829	?	?	?	87	Nicholl *et al.* (2021)

as in *M. arrudacamposi.* The lateral surface is not as well preserved as the other parts of the mandible, but it bears a prominent posterolateral ridge, as in *B. hernandezi*, *B. neuquenianus* and *U. terrificus* followed by a huge depression that is beneath the level of the articulation surface: this might be for the articulation with the quadratojugal condyle, indicating a double mandibular articulation,

Following this comparison and the phylogenetic analyses, MNHN-SAM 136 can be attributed confidently to Peirosauridae *sensu* Geroto & Bertini, 2019.

Taxonomic content of North African peirosaurids

In the Cretaceous of North Africa, a peirosaurid taxon of interest is *Hamadasuchus rebouli.* It was originally described by Buffetaut (1994) on the basis of a left anterior part of a dentary (MDE C001; Fig. 2.14C & 2.14D) from the upper Albian – Cenomanian of the Kem Kem group, Morocco, as a crocodylomorph with at least 15 closely separated alveoli in the dentary. The fourth alveolus is described as huge and the four alveoli posterior to it are small. The teeth posterior to the eighth one are tall, laterally compressed and with denticles on the mesiodistal carinae. Finally, the symphysis between the dentaries reaches the posterior margin of the 7th alveolus.

Other specimens were then described and attributed to *Hamadasuchus rebouli* by Larsson & Sues (2007) on the basis of a complete skull as well as several skull fragments and another left anterior part of a mandible that has more than 15 closely spaced alveoli in the dentary (ROM 49282; Fig. 2.14G & 2.14H). They also come from the Albian to Cenomanian Kem Kem Group of Morocco. Here, the fourth dentary alveolus is the biggest and the four alveoli behind it (at least) are small. Behind the 8th alveolus, only the 13th tooth is preserved, and it is laterally compressed. However, the symphysis between the dentaries only reaches the posterior margin of the 5th alveolus. Two other dentaries were mentioned (ROM 52045 and ROM 52047) but were not illustrated.

Of particular interest, another associated skull with a mandible in connection from the Kem Kem Group was briefly illustrated (BSPG 2005 I 83) and attributed to *Hamadasuchus* by Rauhut & Lopez-Arbarello (2005) but awaits a comprehensive description with most of the anatomy of the mandible remaining unknown.

Recently, in their review of the fauna from the Kem Kem Group of Morocco, Ibrahim *et al*. (2020) illustrated two other mandibular symphyses that they also assigned to *H. rebouli*

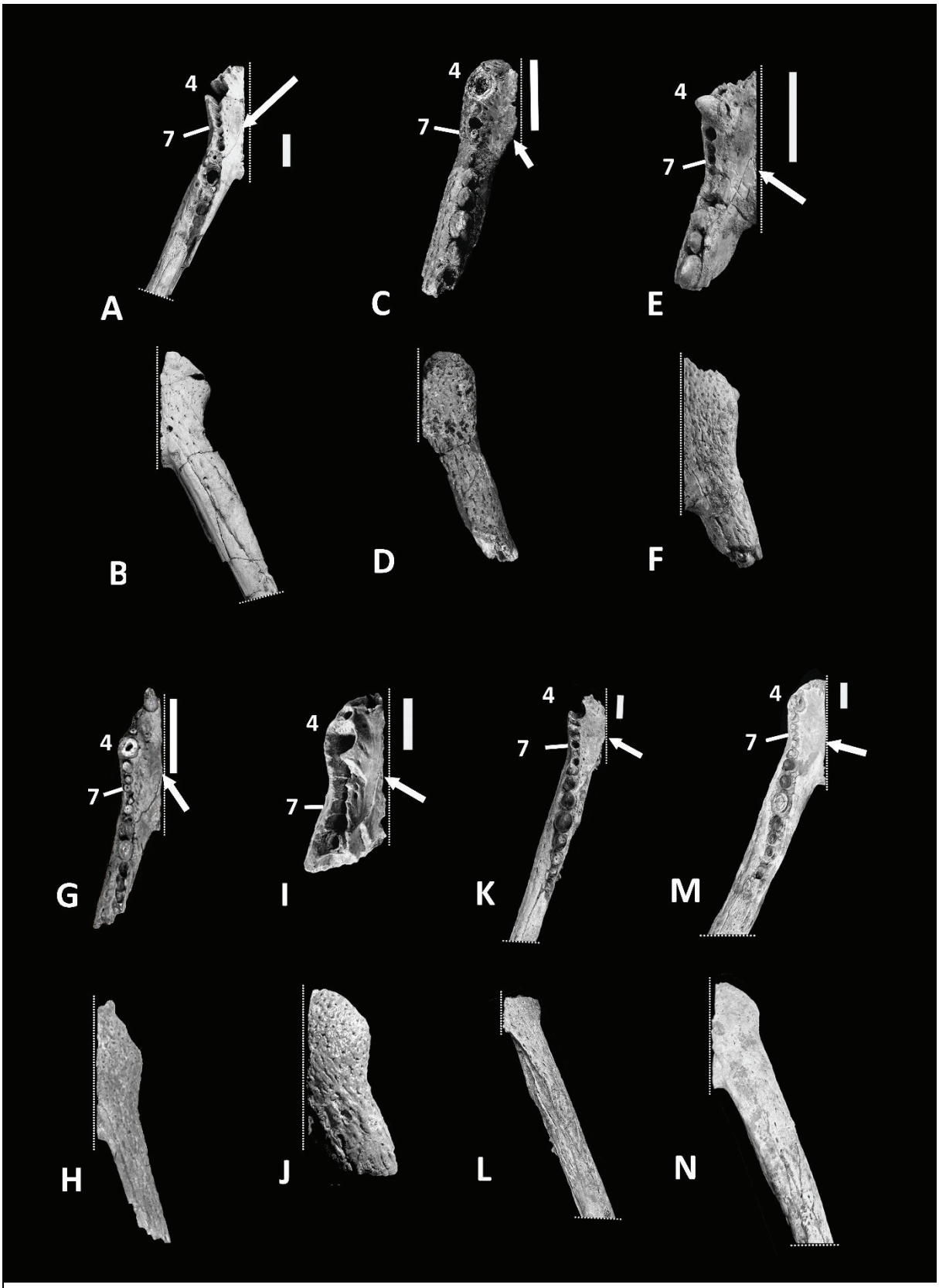

Figure 2.14: Comparisons of anterior parts of peirosaurid mandibles: MNHN-SAM 136 in dorsal (A) and ventral (B) view; MDE C001 in dorsal (C) and ventral (D) view; MNHN-MRS 3110 in dorsal (E) and ventral (F) view; ROM 49282 in dorsal (G) and ventral (H) view; NMC 41784 in dorsal (I) and ventral (J) view; NHMUK PV R36874 in dorsal (K) and ventral (L) view; NHMUK PV R36829 in dorsal (M) and ventral (N) view. 4: 4th alveolus, 7: 7th alveolus. Arrows indicate the suture between the dentary and the splenial in the symphysis. Scale bars are 3 cm.

(MNHN-MRS 3110; Fig. 2.14E & 2.14F and NMC 41784; Fig. 2.14I & 2.14J). However, these authors specify that the current *Hamadasuchus* diagnosis should be refined with the complete description of the skull (BSPG 2005 I 83) illustrated by Rauhut & Lopez-Arbarello (2005). In both cases, the dentaries are broken off before the 15th alveolus, but the alveoli are closely spaced. The 4th alveolus is the largest in each specimen, however the four alveoli behind it are small only in MNHN-MRS 3110, not in NMC 41784. In MNHN-MRS 3110, the teeth behind the 8th one are tall and laterally compressed. In MNHN-MRS 3110, the dentary symphysis reaches and completely includes the 7th - 8th alveolus (depending on the viewing angle), however it only reaches and completely includes the 5th to 6th alveolus in NMC 41784 (also depending on the viewing angle).

Finally, another peirosaurid taxon from the Cretaceous Kem Kem Group of Morocco, North Africa, was recently erected by Nicholl *et al*. (2021): *Antaeusuchus taouzensis*. This taxon closely resembles the *Hamadasuchus rebouli* holotype mandible and MNHN-SAM 136, but it also differs from them by the following traits: wide divergence angle of the mandibular rami (40-45°); relatively unornamented surface texture of dentary adorned with narrow, shallow ridges; rugose tooth enamel formed by anastomosing grooves and ridges. Two specimens were described: NHMUK PV R36829 (Fig. 2.14M & 2.14N) and NHMUK PV R36874 (Fig. 2.14K & 2.14L). Both have more than 15 alveoli in the dentary, as well as a large 4th alveolus with four small alveoli following posteriorly. In both specimens, the teeth posterior to the eighth one are tall, laterally compressed and possessing denticles. In NHMUK PV R36829, the dentary symphysis reaches the 7th to 8th alveolus, whereas it only reaches the 5th to 6th one in NHMUK PV R36874. Nicholl *et al*. (2021) also mention that the material described in Larsson & Sues (2007) differs from the type specimen (MDE C001; Buffetaut, 1994) and they would assign it to another taxon. However, they justifiably refrained from doing so pending complete description of BSPG 2005 I 83 (Rauhut & Lopez-Arbarello, 2005).

All those mandibular characters thus do vary and are summarized in Table 3. Can these anatomical traits concerning the mandible be considered as diagnostic of different taxa or could they just be due to different ontogenetic stages? To assess this, we used ontogenetic series of extant crocodylians, representing different morphotypes (*Alligator mississippiensis, Caiman crocodilus* Linnaeus, 1758*, Caiman latirostris, Gavialis gangeticus, Mecistops* Gray, 1844 sp.*, Osteolaemus tetraspis* Cope, 1860 and *Tomistoma schlegelii* Müller, 1846, see Supplementary file S6 to S9). The total number of alveoli completely involved in the mandibular symphysis as well as the number of alveoli completely involved in the dentary part of the mandibular

Table 3: Specific mandibular characters of specimens close to or assigned to *Hamadasuchus rebouli*.

Specimen	MNHN-SAM 136	*Hamadasuchus rebouli sensu* Buffetaut 1994 ; MDE C001	MNHN-MRS 3110	*Hamadasuchus rebouli sensu* Larsson & Sues 2007; ROM 49282	NMC 41784	*Antaeusuchus taouzensis* NHMUK PV R36829	*Antaeusuchus taouzensis* NHMUK PV R36874
Reference	This study	Buffetaut (1994)	Ibrahim *et al.* (2020)	Larsson & Sues (2007)	Ibrahim *et al.* (2020)	Nicholl *et al.* (2021)	Nicholl *et al.* (2021)
Number of alveoli completely involved in the mandibular symphysis	11	?	10/11?	11	?	11	?
Number of alveoli completely involved in the dentary part of the mandibular symphysis in dorsal view	7	7	7	5	5	8	5
Number of alveoli completely involved in the splenial part of the mandibular symphysis in ventral view	3	?	3 / 4?	4	2/3?	3	?
Number of mandibular alveoli	17	?	?	17	?	18	18
Lateral constriction of the dentary at the level of the 6^{th} to 10^{th} alveoli	Marked (but may be due to deformation)	Minor	Minor	Minor	Minor	Minor	Minor

Number of mandibular alveoli after which the alveoli become confluent	4	4	5	5	3	10	4
Angle of divergence of mandibular rami (in °)	40	26?		29		44	43
Largest alveolus after the 4th one	12	12	?	12/13	?	13	13

symphysis in dorsal view, do not vary throughout the different ontogenetic stages (apart from one specimen of *A. mississippiensis* and one specimen of *O. tetraspis*, showing a variation of only one alveolus). The number of alveoli involved in the ventral extension of the splenial part of the mandibular symphysis does not vary ontogenetically (apart from one alveolus in a specimen of *G. gangeticus*). Finally, the lateral constriction of the dentary at the level of the 6th to 10th dentary alveoli does not vary ontogenetically, but this is more subject to caution as a constriction was not observed in all the examined specimens of Crocodylia. On the other hand, the total number of mandibular alveoli, the number of mandibular alveoli after which the alveoli become confluent, the largest alveolus after the 4th one and the angle of divergence of the mandibular rami do vary significantly throughout ontogeny and we thus recommend against their use as systematic/phylogenetic characters. Moreover, it should be stressed that fossil species are represented by a handful of specimens and that ontogenetic series cannot be understood yet. These data thus bring important information that should be considered in future taxonomic studies looking at mandibular remains in the context of Crocodylomorpha.

As such, following the original diagnosis of Buffetaut (1994), the specimen ROM 49282 cannot be attributed to *H. rebouli* confidently because it only has five alveoli completely involved in the dentary part of the mandibular symphysis rather than seven +/- one. The other (mostly cranial) specimens described in Larsson & Sues (2007) also cannot be attributed to *H. rebouli* because no skull fragment is linked with a mandible. As suggested by Cavin *et al*. (2010), Ibrahim *et al*. (2020) and Nicholl *et al*. (2021), the specimens assigned to *H. rebouli* until now probably belong to at least two different taxa based on mandibular characters. One group would be composed of MDE C001, MNHN-SAM 136 and MNHN-MRS 3110 and another group of ROM 49282 (and probably subsequent material) and NMC 41784, the main point of divergence being the number of alveoli completely involved in the dentary part of the mandibular symphysis. However, we are aware that this hypothesis could be reinforced by diverging cranial or postcranial characters as well. That is why we refrain (for now) from creating a new taxon for the specimens that we here exclude from *H. rebouli*. This is pending a complete description and reassessment of BSPG 2005 I 83 which is the only fossil known where the mandible is linked to the skull and would thus allow to link cranial characters to the diagnosis of *H. rebouli* (or create a new species of *Hamadasuchus*). One must thus keep in mind that skull parts referred to *H. rebouli* (ROM 52620 for example) cannot be referred to this taxon for now, but they could be in the future.

Concerning the taxonomic status of the two specimens attributed to *Antaeusuchus*, we agree with Nicholl *et al*. (2021) in distinguishing NHMUK PV R36829 from all other specimens discussed above as another taxon, but solely based on the peculiar ornamentation of the dentary and the structure of the tooth enamel (though both characters may be subject to mechanical abrasion). The mandibular angle proposed as diagnostic is most probably of ontogenetic nature. However, the attribution to a new genus is open to debate, given all the other characteristics that make this taxon close to the holotype mandible and all the now referred specimens of *H. rebouli*. We would rather interpret this taxon composed solely of NHMUK PV R36829 for now as another species of *Hamadasuchus* and have adapted the emended diagnosis of the genus accordingly. Concerning the second specimen (NHMUK PV R36874), although it also has the peculiar ornamentation of the dentary and the structure of the tooth enamel seen in NHMUK PV R36829, the number of alveoli totally involved in the dentary part of the mandibular symphysis is significantly smaller (5 to 6 depending on the viewing angle) than in NHMUK PV R36829 (7 to 8 depending on the viewing angle). This is a crucial difference and makes NHMUK PV R36874 more closely related to some specimens referred to *Hamadasuchus* (ROM 49282 and NMC 41784). As a result, we are casting doubt on the current taxonomic attribution of this specimen which will hopefully be clarified in future studies.

As for MNHN-SAM 136, the combination of the following characters link this specimen with confidence to the genus *Hamadasuchus*: at least fifteen dentary alveoli; all alveoli are very close-set; four very small alveoli posterior to the large fourth alveolus; posterior dentary alveoli visible in lateral view; two waves of enlarged dentary teeth; eleven completely involved alveoli in the mandibular symphysis; symphyseal region shallow dorsoventrally and narrow mediolaterally; dorsal and ventral dentary-splenial sutures directed anteromedially to posterolaterally (V-shaped if both hemimandibles were assembled); ventrolateral dentary surface anterior to mandibular fenestra transversely compressed; dentary extends posteriorly beneath the mandibular fenestra; anterior alveoli of dentary procumbent; concavity for the reception of the enlarged maxillary tooth lateral to the 7th alveolus of the dentary; surangular overlaps dentary above the mandibular fenestra (see revised diagnosis, as well as support from the phylogenetic analyses). Certainly, we observe little morphological differences between the type specimen and the specimen from La Gara Samani. Nevertheless, the type specimen is of very limited completeness, so we decide to refer MNHN-SAM 136 to *Hamadasuchus* cf. *rebouli*.

Paleobiogeography and methodological implications

During the Cretaceous, the Gondwanan landmass separated, and the South Atlantic Ocean formed (Granot & Dyment, 2015). The two future continents (South America and Africa) were still connected at least until the late Aptian, as highlighted by studies on other crocodylomorphs genus: *Araripesuchus* and *Sarcosuchus* (Buffetaut & Taquet, 1977; Ortega *et al*., 2000) and then separated, effectively creating a vicariance effect (Turner, 2004). As seen in the phylogenetic results, the peirosaurid taxa studied here form two different groups (Fig. 2.13). However, these two groups do not represent a geographical separation, suggesting a Gondwanan distribution of peirosaurids during the Cretaceous (Sertich & O'Connor, 2014; Barrios *et al*., 2016), which will of course have to be confirmed by more detailed studies involving cranial remains as well.

Terrestrial taxa (probably like peirosaurids) are of particular interest when studying those hypotheses because they are constrained by land, and thus in theory cannot disperse in water, rendering biogeographic assumptions stronger. Another interesting question resulting from this is about the origin of peirosaurids: this clade would seem to have originated in Africa, as the oldest known fossils come from this continent (Larsson & Gado, 2000; this study). However, although there is a continental fossil record from the lower Cretaceous in South America (Gallina *et al*., 2014), absence of peirosaurid specimens in these strata does not mean that the clade did not originate in the continent (for example, *Amargasuchus minor* could very well be a South American peirosaurid from the Hauterivian). Furthermore, the repartition of notosuchian taxa has also been showed to be related to climate (Carvalho *et al*., 2010). This question must thus remain open and will hopefully be answered in future studies.

We have also demonstrated that, for Peirosauridae, mandibular characters bear a phylogenetic signal on their own and are important for better resolving phylogenetic relationships. Thus, they are of interest when studying the relationships of groups whose remains are fragmentary. As a result, we were able here to assess the phylogenetic relationships of some poorly known taxa, such as *K. overoi, P. anielensis* or *C. lunai*. However, as can be seen on the full Crocodylomorpha analysis, the results should be taken with caution, as some groups are retrieved in unexpected positions, and it is also probably linked to our character sampling: cranial characters remain important and must be included with the mandibular and postcranial characters when looking at such a large-scale taxonomic sample. Furthermore, the study of ontogenetic series of extant specimens has enabled us to validate some characters for use in

taxonomic/phylogenetic works while invalidating others (see Supplementary File S6 to S9). This is very important and should be widened whenever possible when dealing with fragmentary fossil remains that still have close extant representatives.

Taphonomy and paleoenvironmental implications

The external surface of MNHN-SAM 136 preserves at least seven instances of traces of bioerosion characterized by shallow gouges affecting the surface of the cortical bone (Fig. 2.11B-2.11H). These structures are straight to ovoid and centimetric in size. They can be attributed to dermestid traces and imply arid conditions with pupae developing on drying carcasses (Höpner & Bertling, 2017). As these structures only occur in fresh bone that was adjacent to dried tissues, they involve several weeks or months without water, which allows the development of such larvae (Martin & West, 1995). The subsequent erosion of the bone occurs after the infestation and removes the surface containing the pupation chamber, which explains those hollowed-out structures. These observations are consistent with a hot environment (Russell & Paesler, 2003; Holz, 2015), however with access to water (presence of aquatic taxa; de Lapparent de Broin *et al*., 1971; Busson & Cornée, 1991; de Lapparent de Broin, 2002; Meunier & Larsson, 2017).

Conclusion

A new peirosaurid mandibular ramus (MNHN-SAM 136) from the Albian - Cenomanian of North Africa is described and compared to other closely related taxa. It is referable to *Hamadasuchus* cf. *rebouli* of which an emended diagnosis is proposed, on the basis of the unique combination of several mandibular characters. The taxonomic content of this taxon is reviewed and, using ontogenetic series of extant crocodylians, we put forward some mandibular characters as suitable for taxonomic differentiation between specimens, whereas we argue against the use of others. As a result, several specimens currently attributed to *H. rebouli* are not congruent with the holotype mandible and probably represent a new peirosaurid taxon from the Cretaceous of North Africa. This will be confirmed by the future study of cranial remains attributable to *Hamadasuchus* and the erection of a new taxon if necessary. From these considerations, we studied the phylogenetic relationships of MNHN-SAM 136 using a mandibular character only matrix. The results show that those data bear a phylogenetic signal and are of particular interest in the case of a group mainly composed of taxa defined on fragmentary mandibular remains, clustering the fossil studied here with *Hamadasuchus rebouli sensu* Buffetaut, 1994.

Acknowledgements

This work was supported by the Agence Nationale de la Recherche (SEBEK project no. ANR-19-CE31-0006-01 to JEM). The authors would like to thank Diego Pol (Museo Paleontologico Egidio Feruglio, Trelew, Argentina) for providing a copy of Price (1955); Céline Salaviale (Univ Lyon 1) for technical support; Lawrence Witmer (Ohio University), Timothy Rowe (University of Texas), Blandine Bartschi (Univ Lyon 1), Cody Thompson (University of Michigan), David Blackburn (Florida Museum of Natural History), Didier Berthet (Musée des Confluences de Lyon), Marie Meister and Elisabeth Ludes-Fraulob (Université de Strasbourg), Irena Raselli (University of Fribourg), Thomas van de Kamp and Marcus Zuber (Staatliche Museum für Naturkunde Karlsruhe) for allowing access to the data for the extant specimens used in this study; Ronan Allain, Florent Goussard & Lilian Cazes (MNHN) for providing access and high quality pictures of MNHN-SAM 136 and MNHN-MRS 3110; Jean Leloeuff (Musée des Dinosaures d'Espéraza) for access and loan of the holotype of *Hamadasuchus rebouli* (MDE C001); France de Lapparent de Broin (MNHN) for valuable comments on a previous version of this manuscript; Philip Mannion (University College of London), Pedro Godoy (Stony Brook University), Patrick O'Connor (Ohio University) and Sally Thomas (Palaeontological Association) for insightful comments that greatly improved the quality of this manuscript.

Author contributions

Yohan Pochat-Cottilloux: Conceptualization, Data Curation, Formal Analysis, Investigation, Visualization, Methodology, Writing - original draft. **Vincent Perrier**: Supervision, Validation, Visualization, Writing - review & editing. **Romain Amiot:** Resources, Supervision, Validation, Project administration, Writing - review & editing. **Jeremy E. Martin:** Conceptualization, Resources, Supervision, Funding acquisition, Validation, Project administration, Writing - review & editing.

Data archiving statement

Data for this study are available in the article, the Supplementary Materials and the Morphobank project: http://dx.doi.org/10.7934/P4104.

Supplementary Materials

Supplementary Material S1, S2, S4 & S6 are available on this link: https://mycore.core-cloud.net/index.php/s/B4gZztOMzSFVGWK

Supplementary Material S3, S5 & S7-S9 are available in Appendix 3.

III- Scientific publication: 'New Cretaceous neosuchians (Crocodylomorpha) from Thailand bridge the evolutionary history of atoposaurids and paralligatorids'

This publication has been submitted for publication in *Zoological Journal of the Linnean Society* in June 2023.

New Cretaceous neosuchians (Crocodylomorpha) from Thailand bridge the evolutionary history of atoposaurids and paralligatorids

Yohan Pochat-Cottilloux [A], Komsorn Lauprasert [B], Phornphen Chantasit [C], Sita Manitkoon [B], Jérôme Adrien [D], Joël Lachambre [D], Romain Amiot [A], Jeremy E. Martin [A]

A: Univ Lyon, Univ Lyon 1, ENSL, CNRS, LGL-TPE, F-69622, Villeurbanne, France

B: Palaeontological Research and Education Centre, Mahasarakham University, Maha Sarakham, Thailand.

C: Sirindhorn Museum, Department of Mineral Resources, Kalasin, Thailand.

D: Laboratoire Matériaux, Ingénierie et Science, Institut National des Sciences Appliquées de Lyon, Villeurbanne, France.

Corresponding author: Yohan Pochat-Cottilloux, yohan.pochat-cottilloux@univ-lyon1.fr

Abstract

The origin of modern crocodylians is rooted in the Cretaceous but their evolutionary history is obscure because the relationships of outgroups and transitional forms are poorly resolved. Here, we describe a new form, *Varanosuchus sakonnakhonensis* gen. nov. sp. nov., from the Early Cretaceous of Thailand that fills an evolutionary gap between Paralligatoridae and Atoposauridae, two derived neosuchian lineages with previously unsettled phylogenetic relationships. Three individuals, including a complete skull and associated post-cranial remains allow for a detailed description and phylogenetic analysis. The new taxon is distinguished from all other crocodylomorphs by an association of features, including a narrow oreinostral morphology, a dorsal part of the postorbital with an anterolaterally facing edge, a depression on the posterolateral surface of the maxilla and fully pterygoid bound choanae. A phylogenetic analysis confirms the monophyly and taxonomic content of Atoposauridae and Paralligatoridae, and we underline the difficulty of reaching a robust definition of Eusuchia. Furthermore, we put forward further arguments related to the putative terrestrial ecology with semi-aquatic affinities of atoposaurids based on their oreinostral snout morphology and osteoderm ornamentation.

Keywords: Atoposauridae - CT scan – Neosuchia - Phu Sung - Sao Khua - Thailand

Introduction

Neosuchia is a crocodylomorph clade that appeared during the Jurassic and gave rise during the Cretaceous to modern forms (Salisbury *et al.,* 2006). While its major lineages, including Goniopholididae Cope, 1875, Pholidosauridae von Zittel & Eastman, 1902, Dyrosauridae, Atoposauridae, Paralligatoridae and Eusuchia are generally considered monophyletic (Jouve *et al.,* 2006; Turner, 2015; Martin *et al.,* 2016a; Tennant *et al.,* 2016; Meunier, 2017; Ristevski *et al.,* 2018), their interrelationships are still heavily debated. One major problem of this situation is the poor resolution over the origin and evolutionary processes at the neosuchian-eusuchian transition. For example, while Eusuchia is classically defined as possessing pterygoid-bound choanae, procoelous vertebral centra and a sagittal segmentation of the paravertebral shield (Benton & Clark, 1988; Clark, 1994), this can no longer be considered the norm and their evolutionary history is more complex than originally admitted (Salisbury *et al.,* 2006; Turner & Buckley, 2008; Pol *et al.,* 2009; Sweetman *et al.,* 2014; Turner, 2015; Turner & Pritchard, 2015; Tennant *et al.,* 2016; Leite & Fortier, 2018; Martin *et al.,* 2020a). Thus, those issues remain highly debated, particularly about the timing of the transition between 'basal' neosuchians and eusuchians, about which clade(s) are closer to Eusuchia, and which characters support those changes.

Among the fossils of particular interest to these issues are those belonging to the families Atoposauridae and Paralligatoridae, which have both been recently redefined (Turner, 2015; Tennant *et al.,* 2016; Adams, 2019; Kuzmin *et al*. 2019; Noto *et al.,* 2020; Rummy *et al.,* 2022). Atoposaurids *sensu* Tennant *et al*., 2016 only comprise five species from the Late Jurassic of France and Germany (Fig. 2.15; Tennant *et al.,* 2016 and references therein), and paralligatorids *sensu* Rummy *et al*., 2022 comprise at least eleven taxa from the Late Jurassic to the Cretaceous, distributed worldwide (Fig. 2.15; Turner, 2015; Tennant *et al.,* 2016; Adams, 2019; Kuzmin *et al.,* 2019; Noto *et al.,* 2020; Rummy *et al.,* 2022 and references therein). As those two families exhibit several variable morphological characters among those historically considered as autapomorphies of Eusuchia (see above), they are thus ideal candidates for illustrating the Neosuchia-Eusuchia transition. A better understanding of the relationships of those taxa is essential to understand the neosuchian diversification and paleobiogeographic evolution through time. Virtually nothing is known about their ecology, although Schwarz & Salisbury

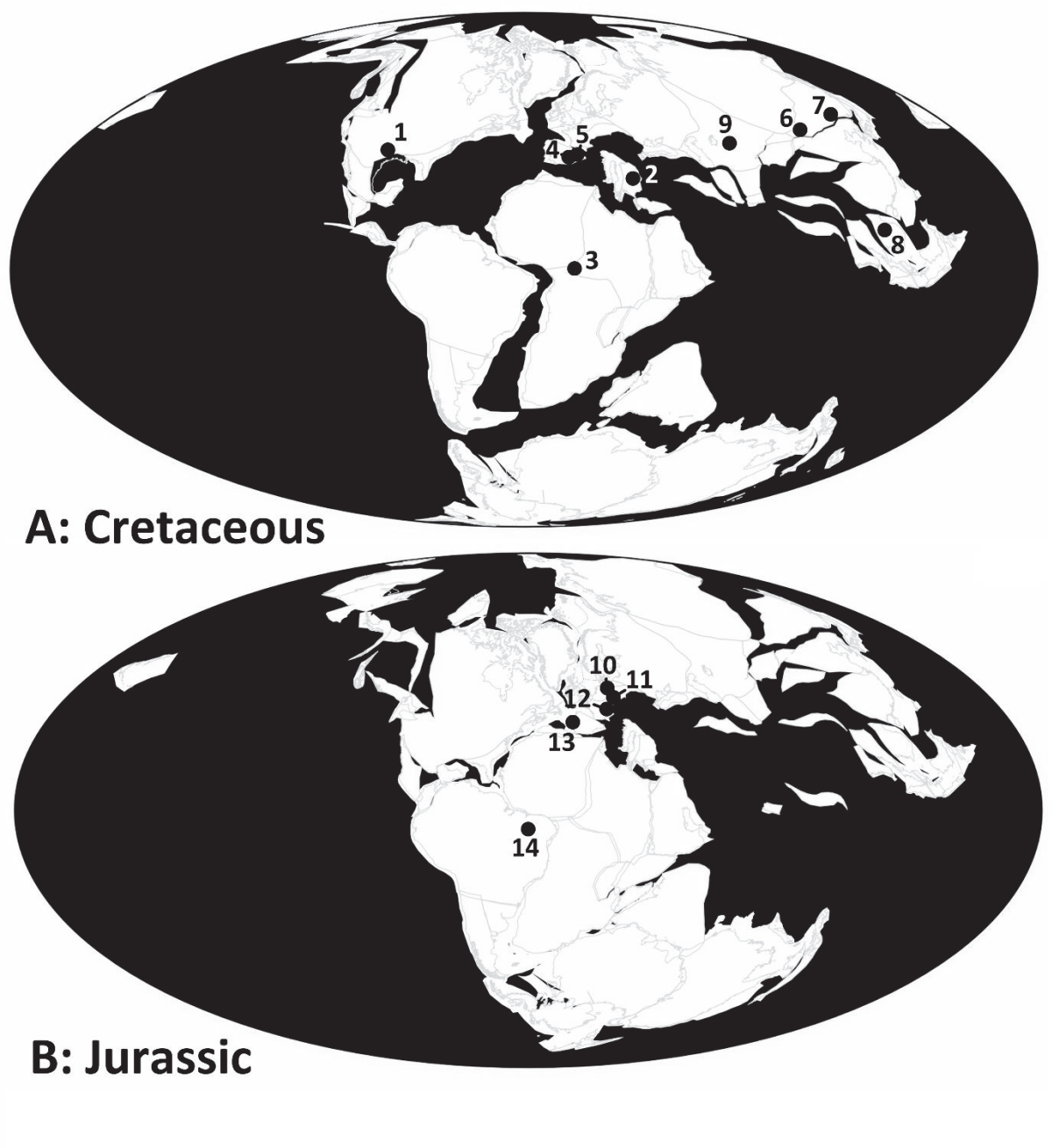

Figure 2.15: Paleogeographical distribution of putative atoposaurid and paralligatorid taxa. 1: *Wannchampsus kirpachi* Adams, 2014, *Tarsomordeo winkleri*, Glen Rose Form (Aptian, United States) and *Scolomastax sahlsteini* (Cenomanian, United States); 2: *Aprosuchus ghirai* Venczel & Codrea, 2019 and *Sabresuchus sympiestodon* Martin, Rabi & Csiki, 2010 (Maastrichtian, Romania); 3: *Brillanceausuchus babouriensis* (Barremian, Cameroon); 4: *Sabresuchus ibericus* (Barremian, Spain); 5: *Montsecosuchus deperiti* Vidal, 1915 (Barremian, Spain); 6: *Shamosuchus djadochtaensis* Mook, 1924 and *Paralligator gradilifrons* Konzhukova, 1954 (Cenomanian - Campanian, Mongolia); 7: *Rugosuchus nonganensis* Wu, Cheng & Russell, 2001 (Campanian, China) and *Yangjisuchus longshanensis* Rummy, Wu, Clark, Zhao, Jin, Shibata, Jin & Xu, 2022 (Albian - Cenomanian, China); 8: *Theriosuchus grandinaris* Lauprasert, Laojumpon, Saenphala, Cuny, Thirakhupt & Suteethorn, 2011 and Phu Sung specimens described here (Barremian, Thailand); 9: *Kansajsuchus extensus* Efimov, 1975 (Santonian - Campanian, Kazakhstan - Tadzhikistan); 10: *Knoetschkesuchus langenbergensis* Schwarz, Raddatz & Wings, 2017 (Kimmeridgian, Germany); 11: *Alligatorellus* Gervais, 1871 and *Atoposaurus oberndorferi* von Meyer, 1850 (Tithonian, Germany); 12: *Alligatorium* Gervais, 1871 and *Atoposaurus jourdani* von Meyer, 1850 (Kimmeridgian, Germany); 13: *Knoetschkesuchus guimarotae* (Kimmeridgian, Spain); 14: *Batrachomimus pastosbonensis* (Oxfordian – Kimmeridgian, Brazil). Maps are from Paleobiology Database.

(2005) hypothesized a terrestrial ecology for atoposaurids based on their very scarce fossil record, terrestrial environments being less prone to good conservation conditions.

Here, we describe three new specimens belonging to a new species of atoposaurid from the Early Cretaceous Sao Khua Formation of Thailand (early Valanginian – early Hauterivian; Tucker *et al.,* 2022). The specimens (Fig. 2.16-2.29; Supplementary Material S1 & S2; Supplementary Model S1-S6) come from the Phu Sung locality, a reddish micaceous silty mudstone continental deposit, and were found together within a faunal assemblage composed of sharks, bony fishes, and turtles (Chanthasit *et al.,* 2019; Ditbanjong *et al.,* 2019). They are of particular importance for proposing a new phylogenetic framework close to the Neosuchia - Eusuchia transition and highlight that Southeast Asia still holds an under-evaluated fossil record for understanding the evolution of neosuchians.

Material and methods

Character taxon matrix and coding

The character taxon matrix (CTM) used in this paper consists of 80 operational taxonomic units and 321 multistate characters (Supplementary Material S3 & S4); the outgroup is *Gracilisuchus stipanicicorum* Romer, 1972; all characters involved in the parsimony analysis are equally weighted and unordered. This CTM to which we added the scorable osteological characters of the specimens described here is taken from the complete dataset of Schwarz *et al*. (2017), modified from Turner (2015), with some adjustments made by Venczel & Codrea (2019). *Knoetschkesuchus guimarotae* scorings were updated following Eijkelboom (2020), *Shamosuchus ulanicus* Efimov, 1983 was removed as it is a junior synonym of *Shamosuchus djadochtaensis* (Turner, 2015) and *Pachycheilosuchus trinquei* Rogers, 2003 was removed as it is represented by a composite skeleton (Rogers, 2003). *Brillanceausuchus babouriensis* and *Montsecosuchus deperiti* were not included as well, pending future reassessment of those taxa (Tennant *et al.,* 2016).

Although previously recovered nested within neosuchians, we also chose to remove thalattosuchians because they most likely branch basally or sister to Mesoeucrocodylia (Wilberg *et al.,* 2022) and because the present study focuses on derived neosuchians. *Tarsomordeo winkleri*, *Scolomastax salhsteini* and *Yanjisuchus longshanensis* were not added in the matrix as they are too incomplete, however, we added *Kansajsuchus extensus* (Kuzmin *et al.,* 2019) and *Theriosuchus grandinaris*. Finally, some scorings were updated and those of

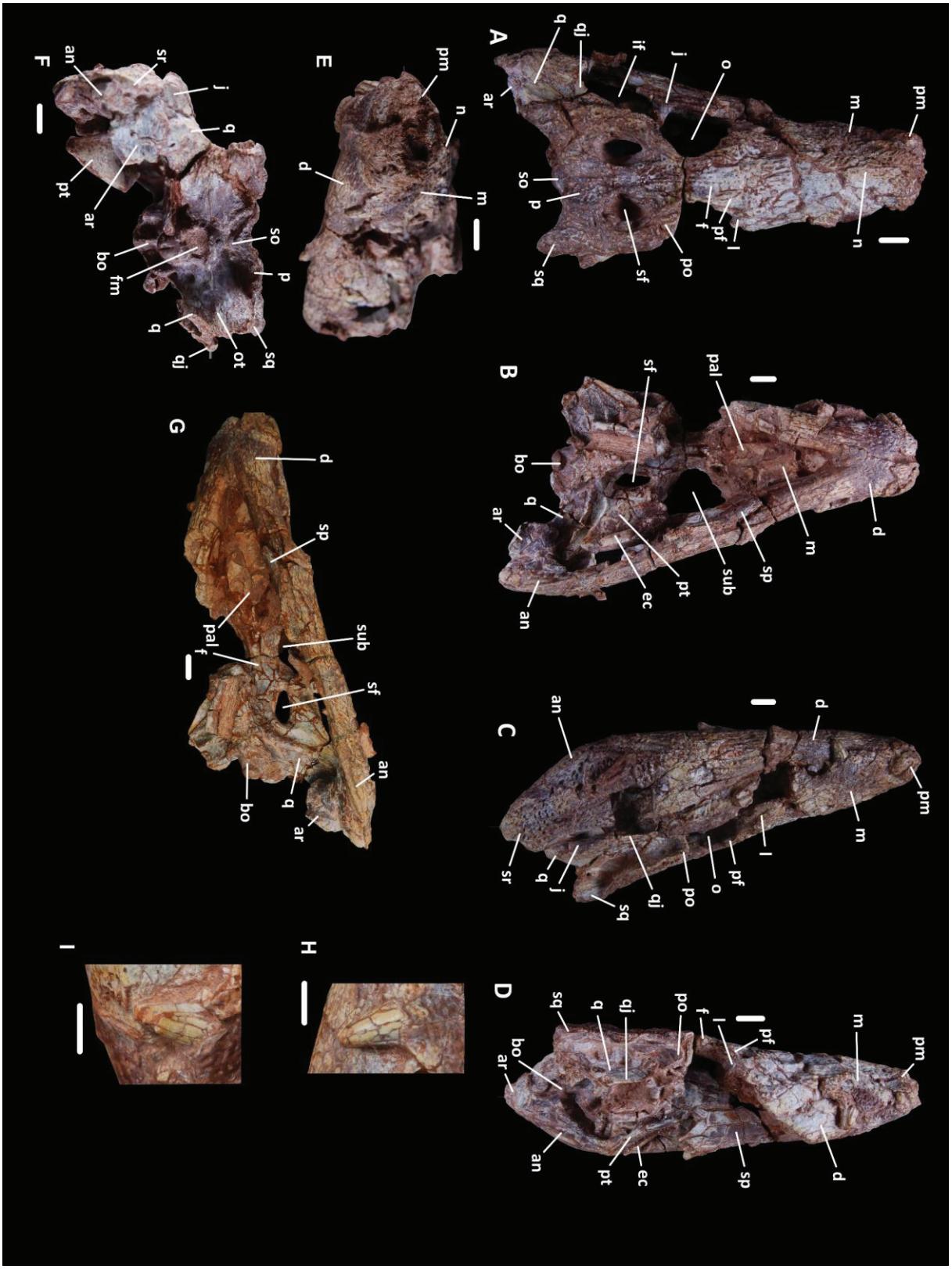

Figure 2.16: SM-2021-1-97: main part of the skull in dorsal (A), ventral (B), lateral (C & D), anterior (E), posterior (F) and lateroventral (G) views. H & I: two teeth visible in external view. an: angular, ar: articular, bo: basioccipital, d: dentary, ec: ectopterygoid, f: frontal, fm: foramen magnum, if: infratemporal fenestra, j: jugal, l: lacrimal, m: maxillary, n: nasal, o: orbit, ot: otoccipital, p: parietal, pal: palatine, pf: prefrontal, pm: premaxillary, po: postorbital, pt: pterygoid, q: quadrate, qj: quadratojugal, sf: supratemporal fenestra, so: supraoccipital, sp: splenial, sq: squamosal, sr: surangular, sub: suborbital fenestra. Scale bars are 1 cm.

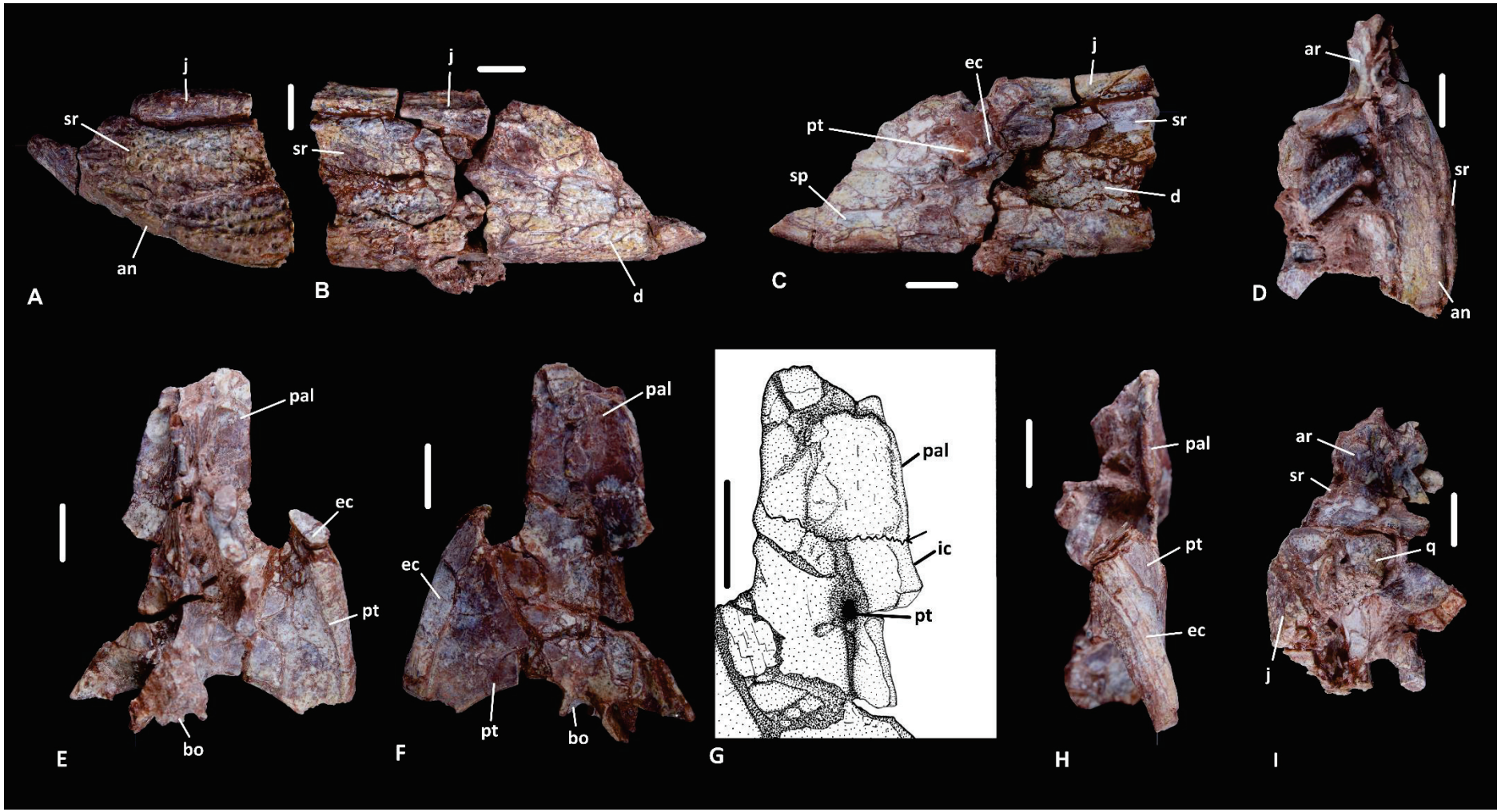

Figure 2.17: SM-2021-1-97: mandibular and pterygoid parts of the skull in lateral (A, B & H), medial (C), dorsal (E & I) and ventral (D, F & G) views. an: angular, ar: articular, bo: basioccipital, d: dentary, ec: ectopterygoid, ic: internal choana, j: jugal, pal: palatine, pt: pterygoid, q: quadrate, sp: splenial, sr: surangular. Arrow in G indicates palatine-pterygoid suture. Scale bars are 1 cm.

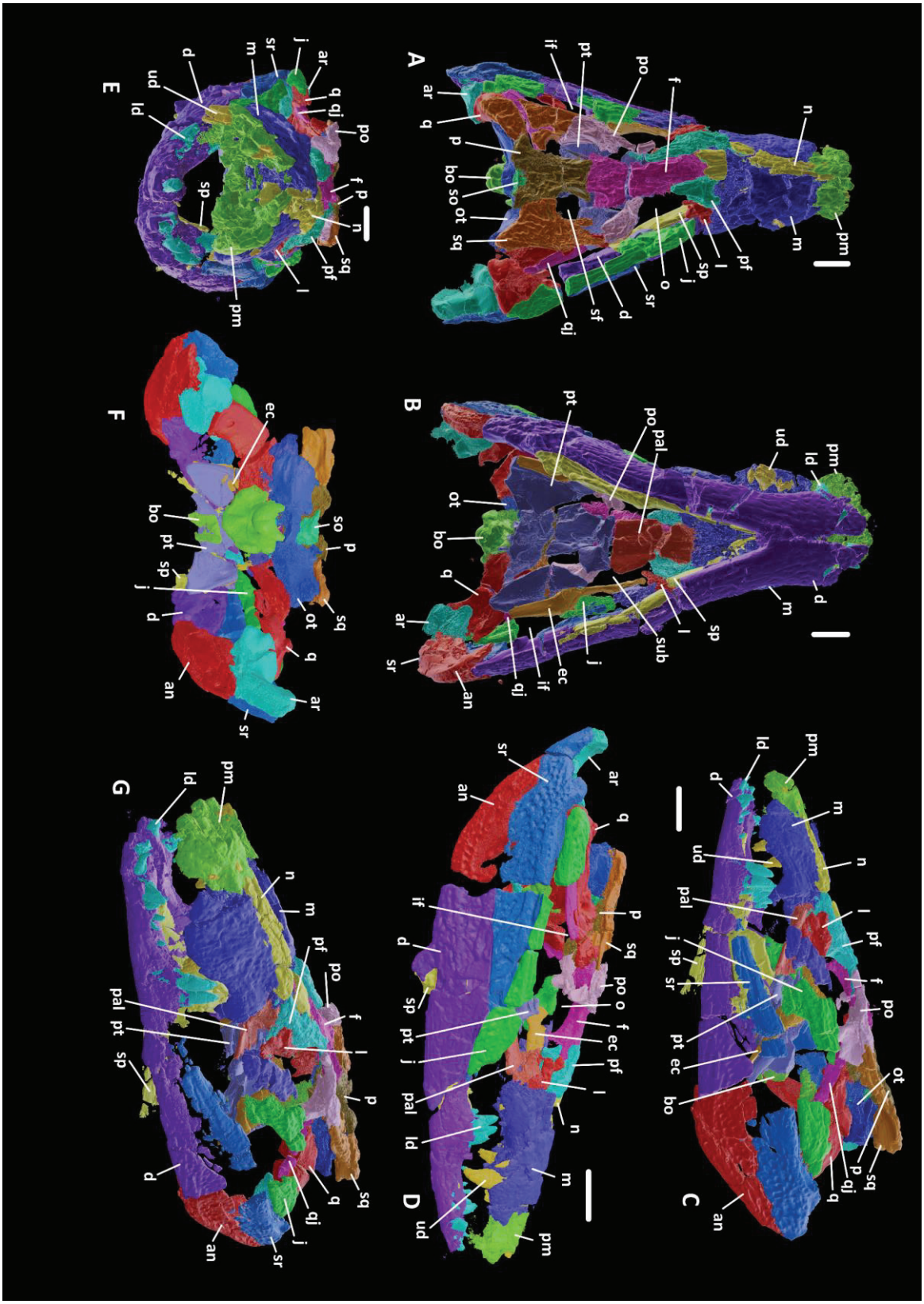

Figure 2.18: 3D reconstruction of SM-2021-1-97: full skull in dorsal (A), ventral (B), lateral (C & D), anterior (E), posterior (F) and anterior ¾ (G) views. an: angular, ar: articular, bo: basioccipital, d: dentary, ec: ectopterygoid, f: frontal, if: infratemporal fenestra, j: jugal, l: lacrimal, ld: lower dentition, m: maxillary, n: nasal, o: orbit, ot: otoccipital, p: parietal, pal: palatine, pf: prefrontal, pm: premaxillary, po: postorbital, pt: pterygoid, q: quadrate, qj: quadratojugal, sf: supratemporal fenestra, so: supraoccipital, sp: splenial, sq: squamosal, sr: surangular, sub: suborbital fenestra, ud: upper dentition. Scale bars are 2 cm.

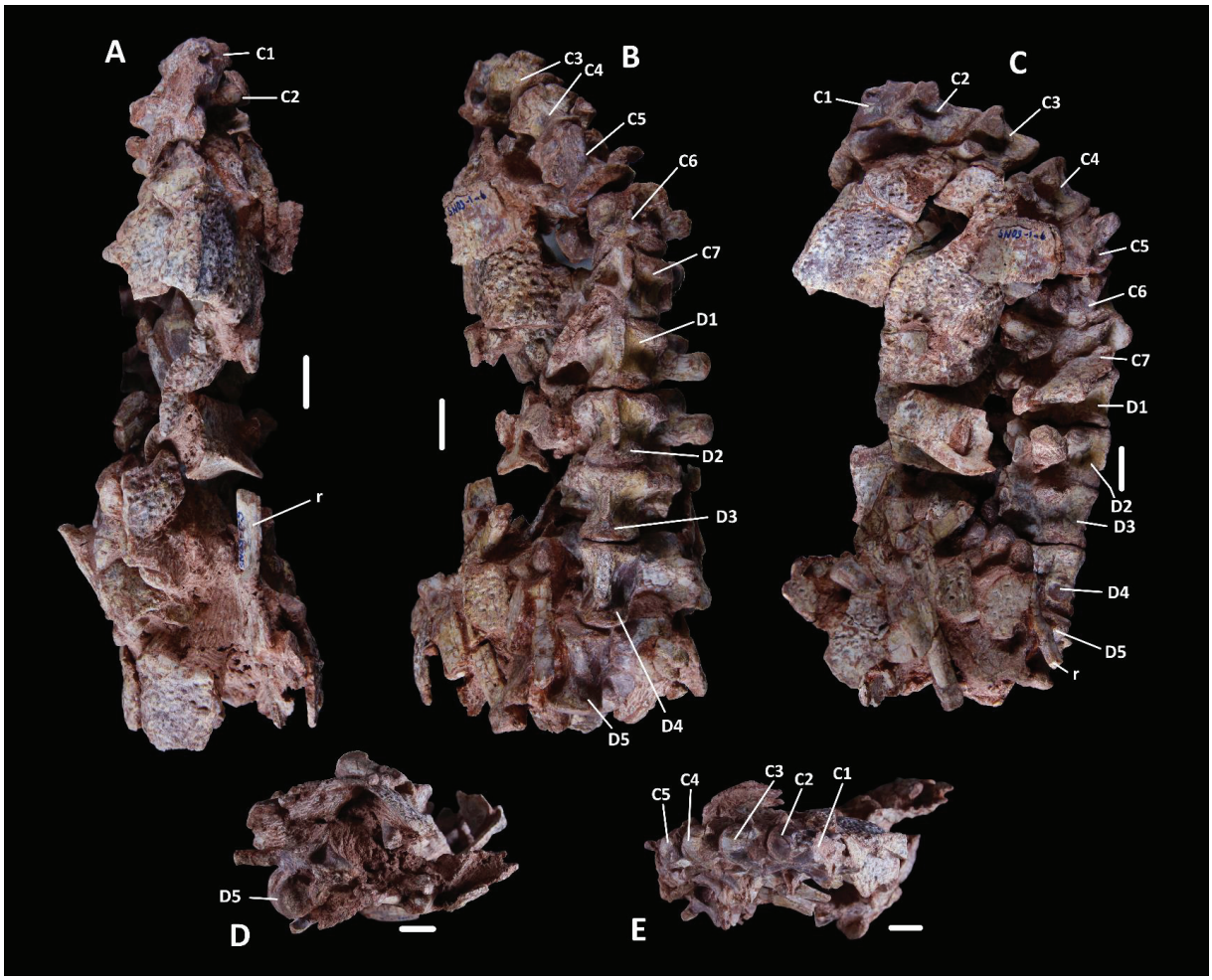

Figure 2.19: SM-2021-1-98: cervical vertebrae and osteoderms in dorsal (A), ventral (B), lateral (C), posterior (D) and anterior (E) views. C1-7: cervical vertebrae one to seven, D1-D5: dorsal vertebrae one to five, r: rib. Scale bars are 1 cm.

Bernissartia fagesii Dollo, 1883 were thoroughly revised on 80 characters, based on Martin *et al*. (2020a; see also Supplementary Material S5). Only the two most complete specimens from Phu Sung (SM-2021-1-97/101 and SM-2023-1-16) were scored because the third one is too incomplete to warrant a robust phylogenetic assessment.

Phylogenetic analyses

The analyses were made in parsimony, on TNT 1.5 (Goloboff & Catalano, 2016). New Technology Search was used enabling all search algorithms (Sectorial Search, Ratchet, Drift and Tree Fusing; Goloboff, 1999; Nixon, 1999). The default settings for these advanced search methods were only changed to increase the iterations of each method, it now features 100 sectorial search drifting cycles, 100 ratchet iterations, 100 drift cycles and 100 rounds of tree fusion per replicate. This tree-space search procedure was repeated for ten different random start seeds (following the procedure in Jouve, 2016) using driven search to find the minimum

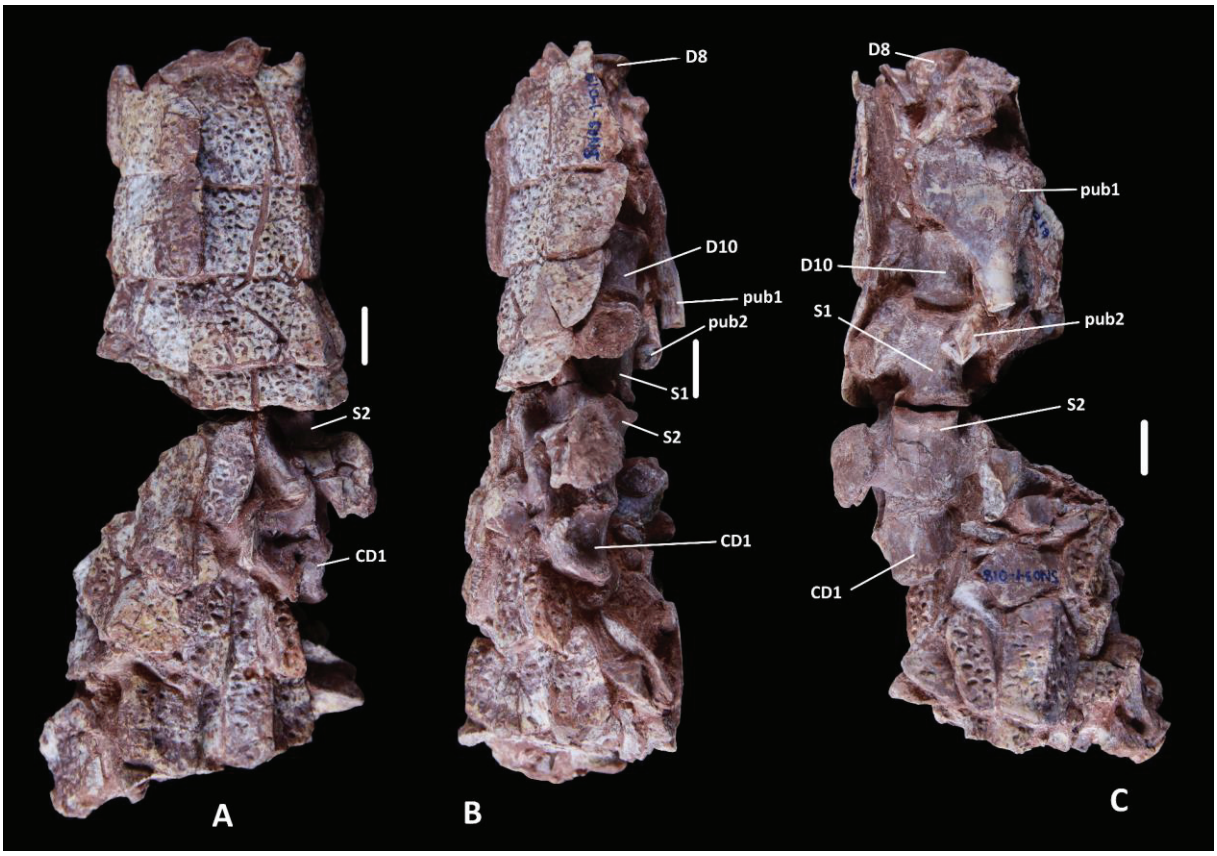

Figure 2.20: SM-2021-1-100: dorsal, sacrum and caudal vertebrae in dorsal (A), lateral (B) and ventral (C) views. CD1: caudal vertebra 1, D8 & D10: dorsal vertebrae eight and ten, pub1 & pub2: pubis one and two, S1 & S2: sacral vertebrae one and two. Scale bars are 1 cm.

length ten times. Otherwise, the default parameters were kept. Extended implied weighting (Goloboff, 2014) was not used as its utility remains controversial (Congreve & Lamsdell, 2016; Groh *et al.,* 2019). Bootstrap scores were then calculated. This procedure was further validated by a heuristic search of Wagner trees with 1,000 random addition sequences, followed by Tree Bisection Reconnection and saving 10 cladograms per rounds (Random seeds – 100). When necessary, the ACCTRAN optimization was used (Accelerated Transformation; Farris, 1970; Swofford & Maddison, 1987). FigTree 1.4.4 was used to visualize the phylogenetic trees obtained.

Computed tomography scan

The CT scan was performed in January 2021 at the Laboratoire Mateis (INSA Lyon, Villeurbanne, France) on a DTHE (Double Tomographe Haute Energie by RX Solutions). Detailed acquisition parameters are available in Supplementary Material S6.

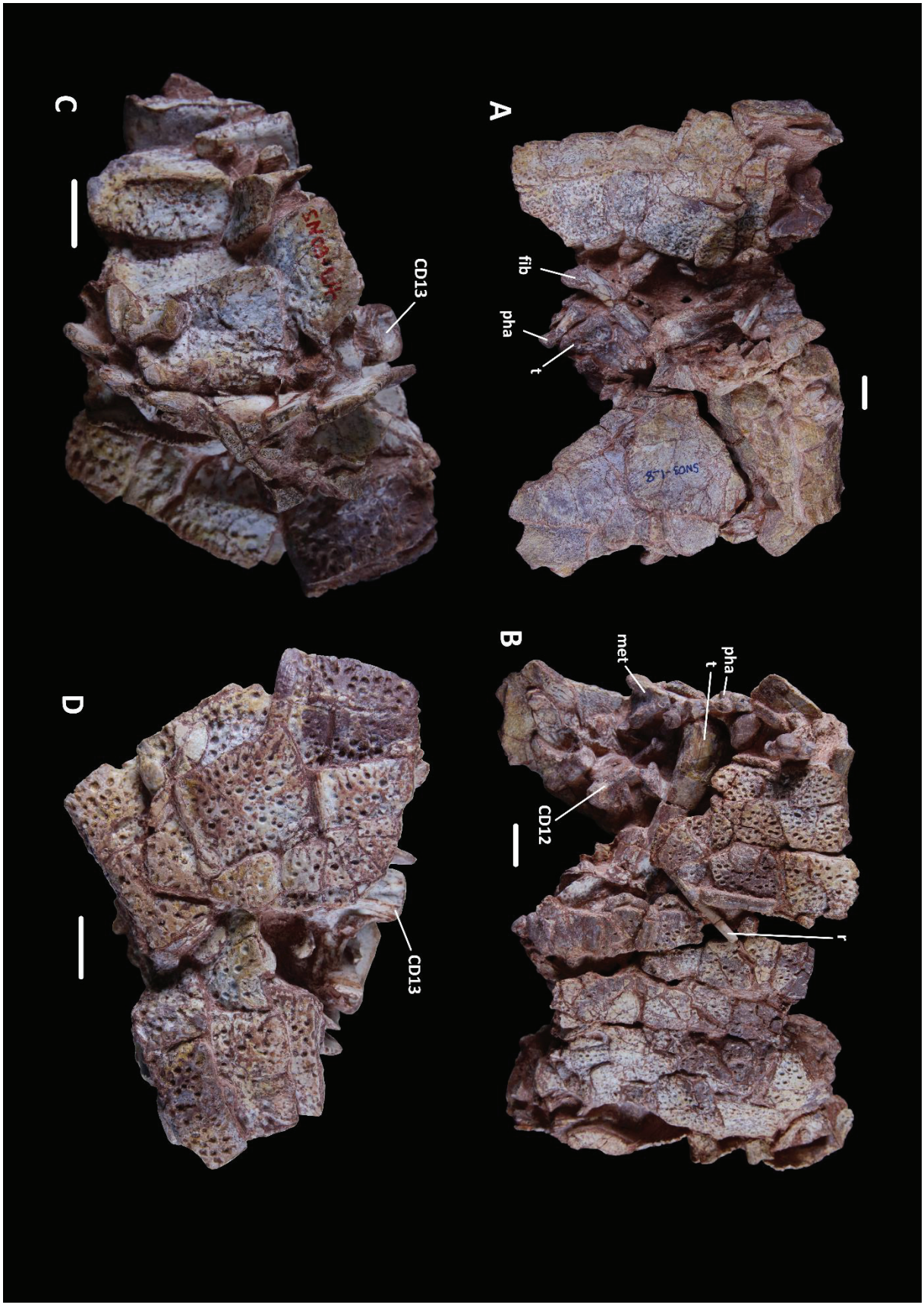

Figure 2.21: SM-2021-1-99 & SM-2021-1-101: caudal vertebrae and limb bones in dorsal (A & C) and ventral (B & D) views. CD12 & CD13: cervical vertebra twelve and thirteen, fib: fibula, met: turtle metatarsal, pha: phalanx, r: rib, t: tibia. Scale bars are 1 cm.

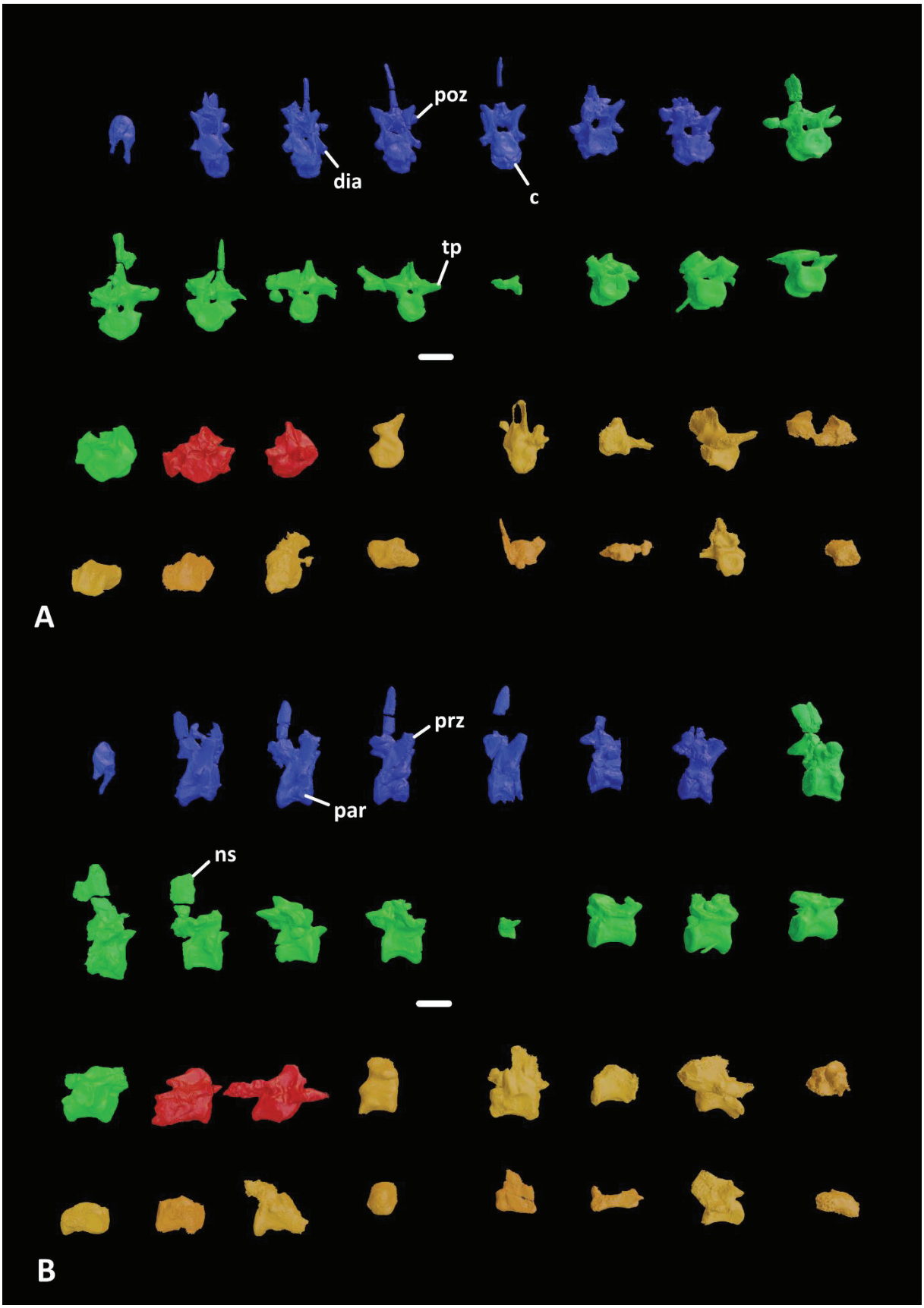

Figure 2.22: 3D reconstruction of SM-2021-1-97/101 vertebrae in anterior (A) and lateral (B) views. Blue vertebrae are cervical, green are dorsal, red are sacral and orange are caudal. c: centrum, dia: diapophysis, ns: neural spine, par: parapophyis, poz: postzygapophysis, prz: prezygapophysis, tp: transverse process. Scale bars are 3 cm.

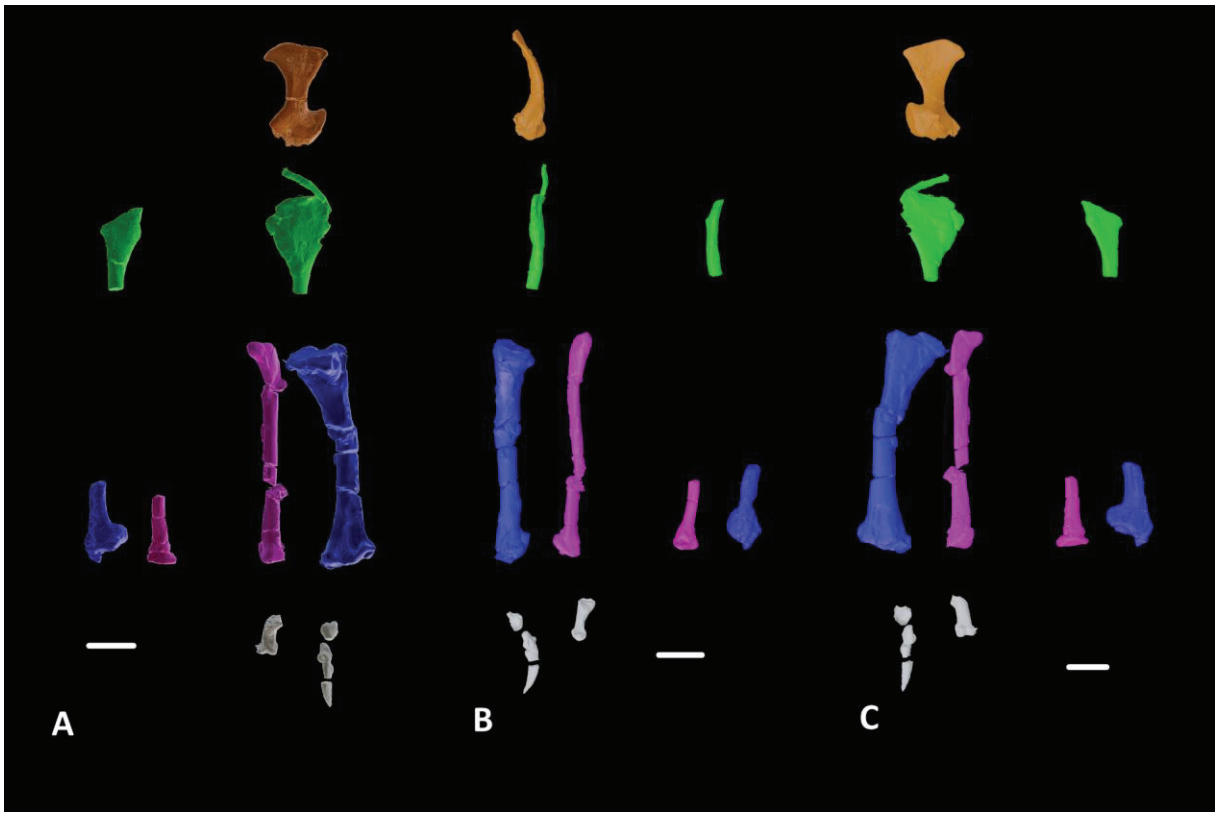

Figure 2.23: 3D reconstruction of SM-2021-1-97/101 limb bones and girdles in dorsal (A), lateral (B) and ventral (C) views. Orange: coracoid, green: pubis, purple: fibula, blue: tibia, white: digit and ungual. Scale bars are 2 cm.

Results

Systematic paleontology

Crocodylomorpha Hay, 1930

Crocodyliformes Hay, 1930 (*sensu* Benton & Clark, 1988)

Mesoeucrocodylia Whestone & Whybrow, 1983

Neosuchia Clark, 1986

Atoposauridae Gervais, 1871

Varanosuchus gen. nov.

Type species: *Varanosuchus sakonnakhonensis*

Derivation of name – due to its superficial resemblance with a monitor lizard.

Diagnosis – As for the type and only known species.

Varanosuchus sakonnakhonensis gen. nov. sp. nov.

Derivation of name – after the province of Sakon Nakhon, Thailand, where the holotype and referred specimens were found.

Holotype – SM-2021-1-97/101, a three-dimensionally preserved, almost complete skull lacking its anteriormost part (anterior part of premaxilla and nasal) with associated mostly

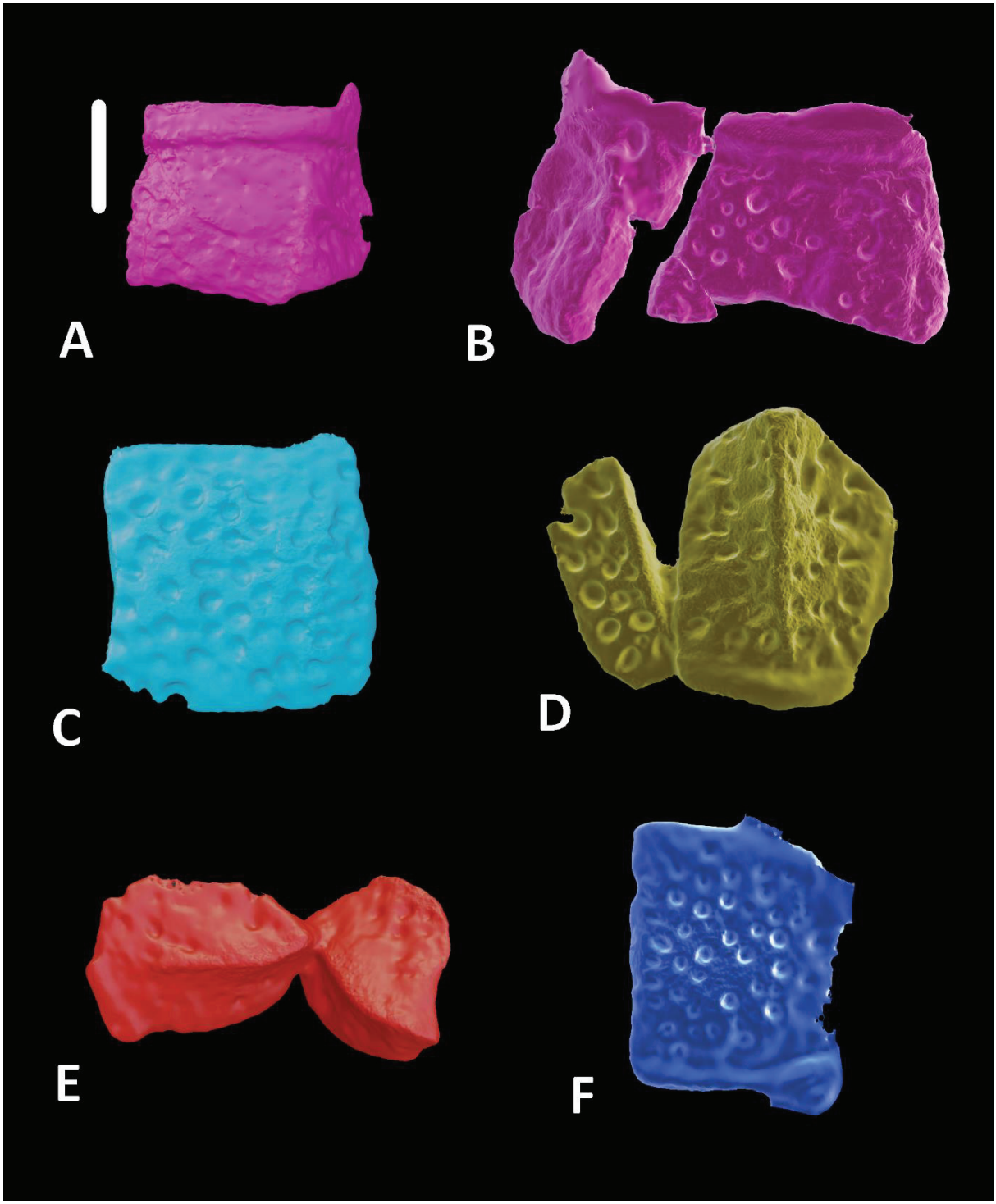

Figure 2.24: 3D reconstruction of SM-2021-1-97/101 osteoderms. Dorsal (A) and ventral (B) osteoderm of the cervical region. Dorsal (C) and ventral (D) osteoderm of the sacral region. Dorsal (E) and ventral (F) osteoderm of the caudal region. Scale bar is 2 cm.

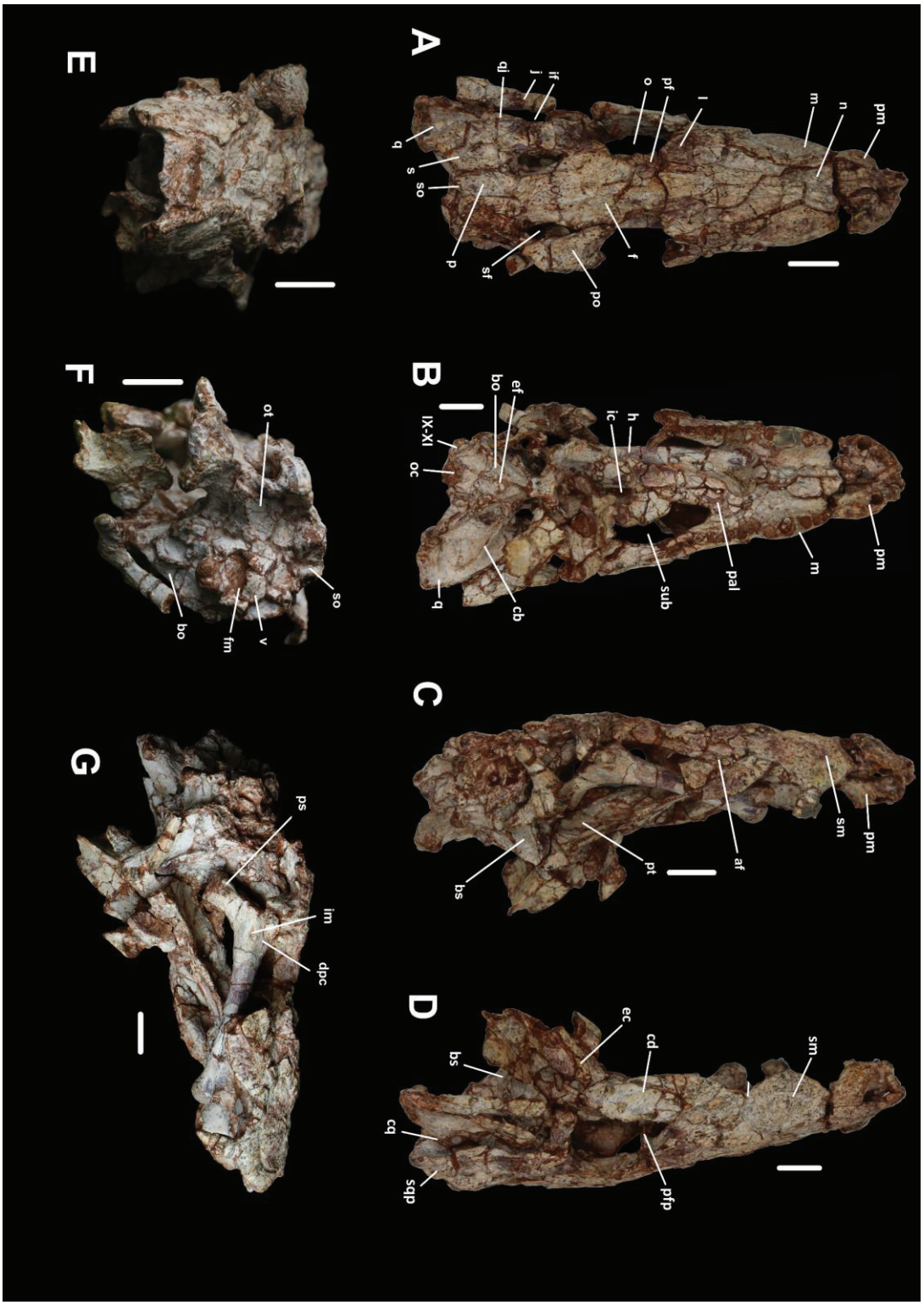

Figure 2.25: SM-2023-1-16 in dorsal (A), ventral (B), lateral (C & D), anterior (E), posterior (F) and ventrolateral (G) views. IX-XI: foramen for cranial nerve IX-XI, af: antorbital fenestra, bo: basioccipital, bs: basisphenoid, cb: crest B, cd: crest/depression on the jugal, cq: cranioquadrate groove, dpc: deltopectoral crest, ec: ectopterygoid, ef: eustachian foramen, f: frontal, fm: foramen magnum, h: humerus, ic: internal choana, if: infratemporal fenestra, im: insertion for the *M. teres major*, j: jugal, l: lacrimal, m: maxilla, n: nasal, o: orbit, oc: occipital condyle, ot: otoccipital, p: parietal, pal: palatine, pf: prefrontal, pfp: prefrontal pillar, pm: premaxillary, po: postorbital, ps: proximal extremity, pt: pterygoid, q: quadrate, qj: quadratojugal, s: squamosal, sf: supratemporal fenestra, so: supraoccipital, sqp: squamosal process, sm: sulcus on the maxilla, so: supraoccipital, sub: suborbital fenestra, v: vertebrae remains. Scale bars are 1 cm.

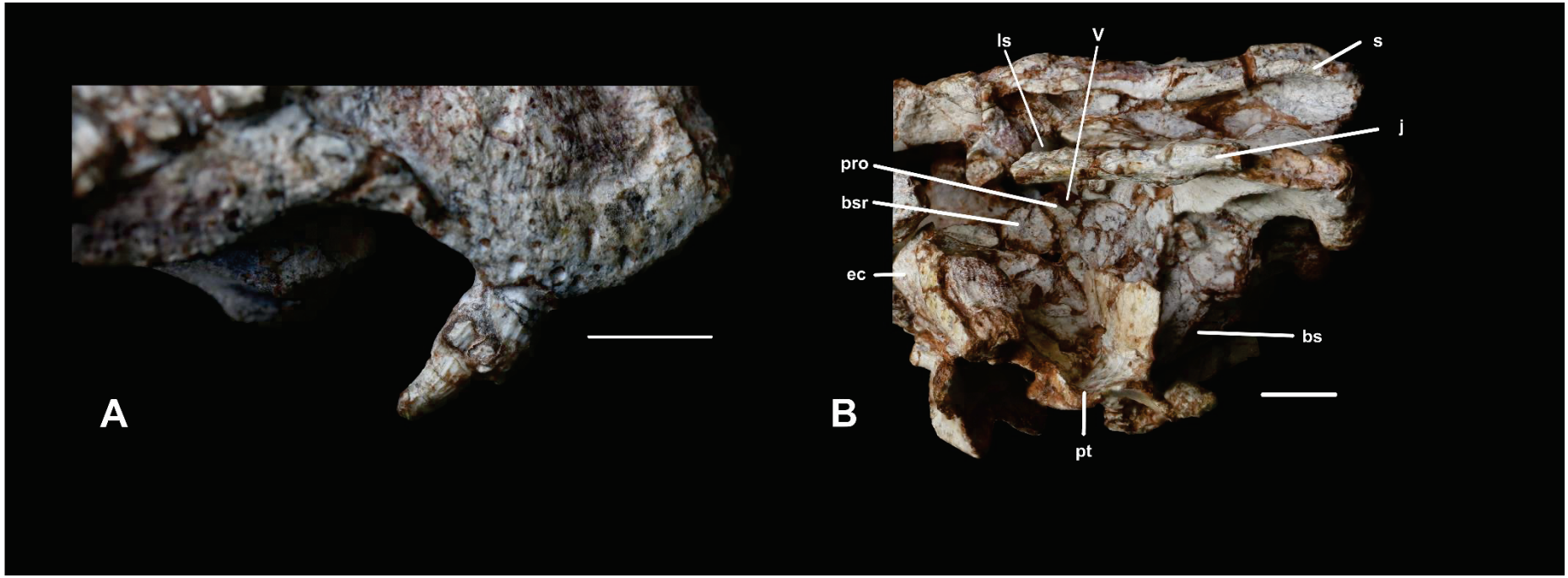

Figure 2.26: Details of SM-2023-1-16: tooth (A), braincase region (B). V: foramen for cranial nerve V, bs: basisphenoid, bsr: basisphenoid rostrum, ec: ectopterygoid, j: jugal, ls: laterosphenoid, pro: prootic, pt: pterygoid, s: squamosal. Scale bars are 1 cm.

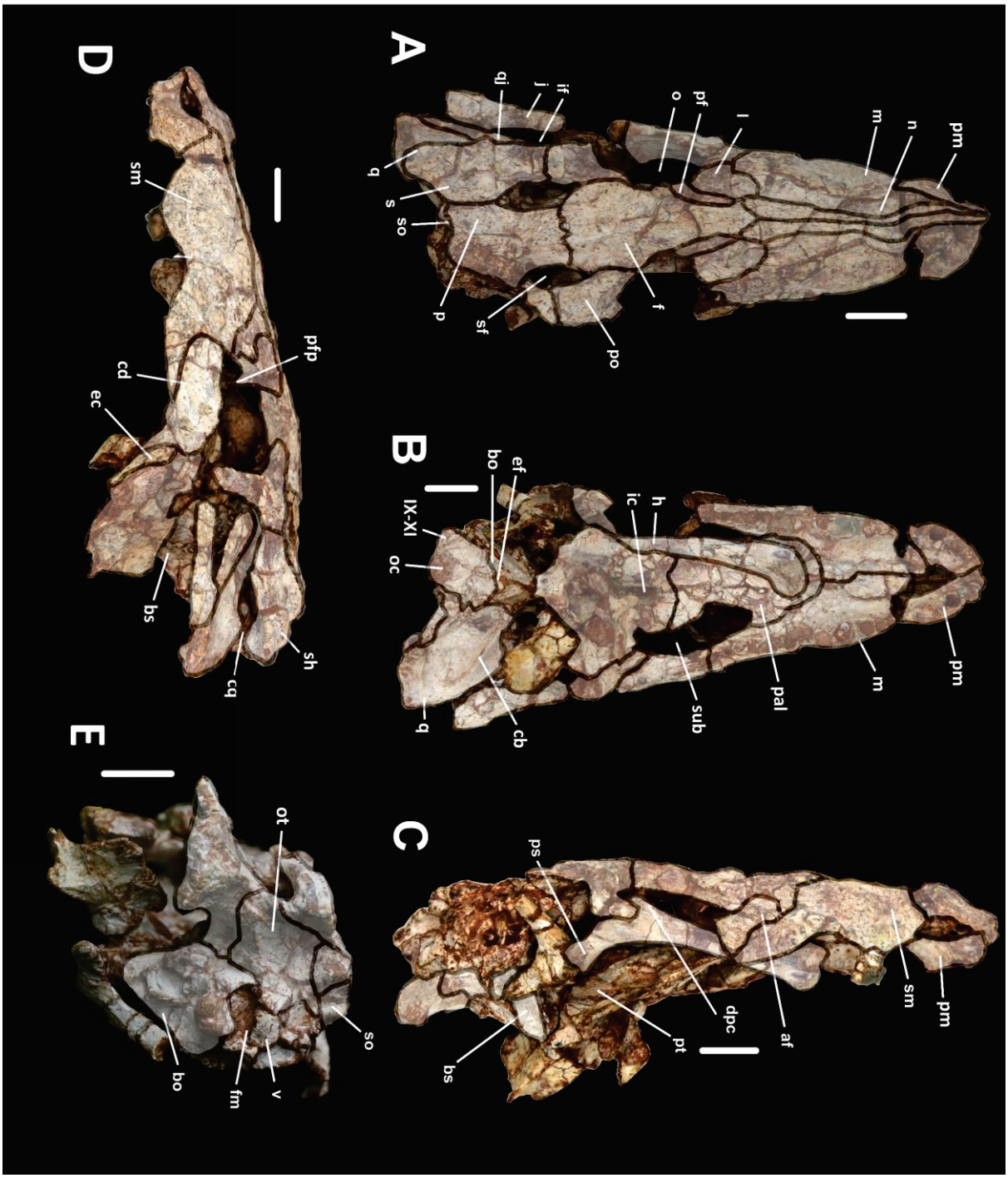

Figure 2.27: Outlines of the bones of SM-2023-1-16 in dorsal (A), ventral (B), lateral (C & D) and posterior (E) views. IX-XI: foramen for cranial nerve IX-XI, af: antorbital fenestra, bo: basioccipital, bs: basisphenoid, cb: crest B, cd: crest/depression on the jugal, cq: cranioquadrate passage, dpc: deltopectoral crest, ec: ectopterygoid, ef: eustachian foramen, f: frontal, fm: foramen magnum, h: humerus, ic: internal choanae, if: infratemporal fenestra, j: jugal, l: lacrimal, m: maxilla, n: nasal, o: orbit, oc: occipital condyle, ot: otoccipital, p: parietal, pal: palatine, pf: prefrontal, pfp: prefrontal pillar, pm: premaxillary, po: postorbital, ps: proximal surface, pt: pterygoid, q: quadrate, qj: quadratojugal, s: squamosal, sf: supratemporal fenestra, sh: squamosal 'horn', sm: maxillary sulcus, so: supraoccipital, sub: suborbital fenestra, v: vertebrae remains. Scale bars are 1 cm.

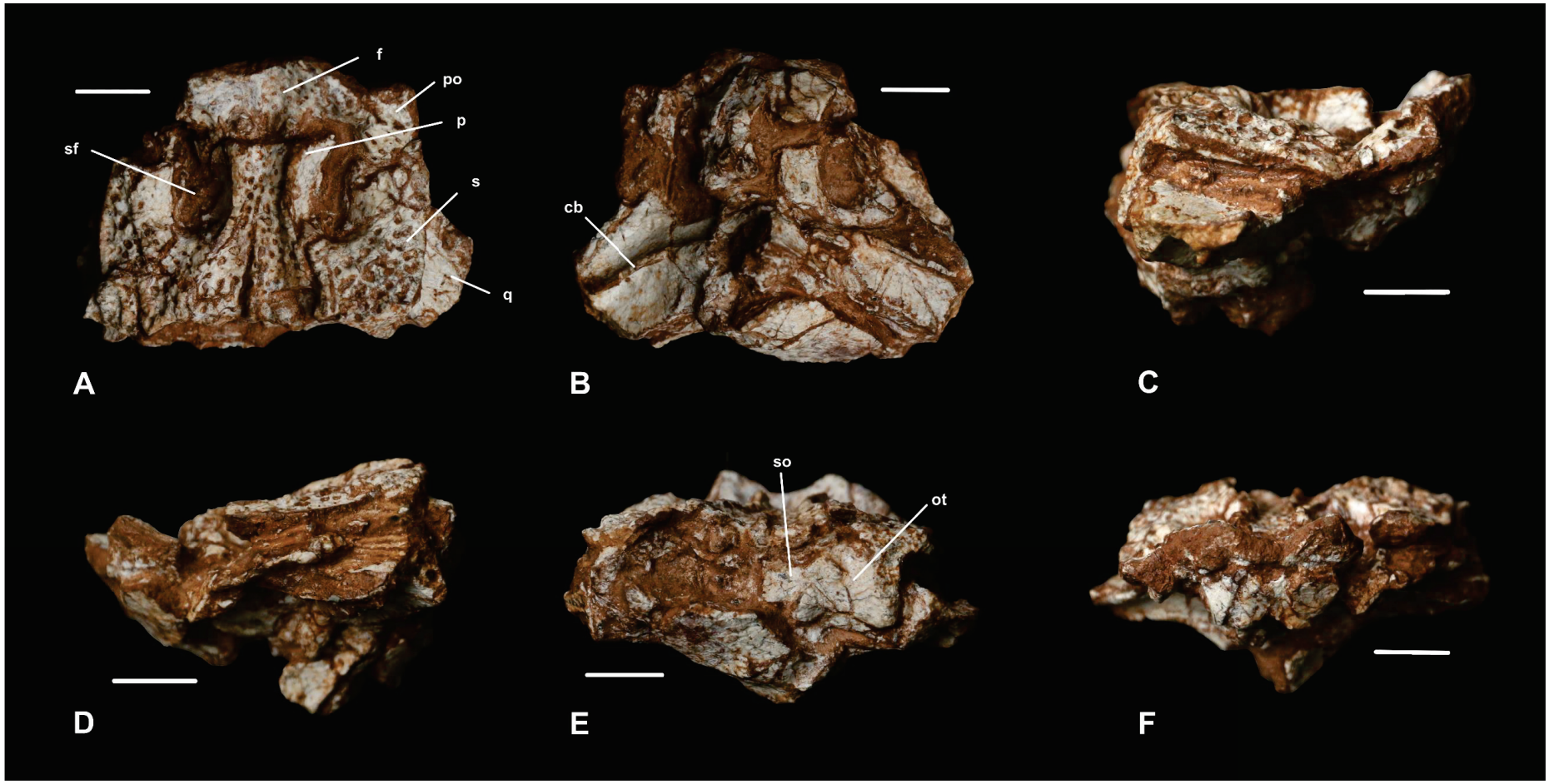

Figure 2.28: SM-2023-1-17 in dorsal (A), ventral (B), lateral (C & D), posterior (E) and anterior (F) views. cb: crest B, f: frontal, ot: otoccipital, p: parietal, po: postorbital, q: quadrate, s: squamosal, sf: supratemporal fenestra, so: supraoccipital. Scale bars are 1 cm.

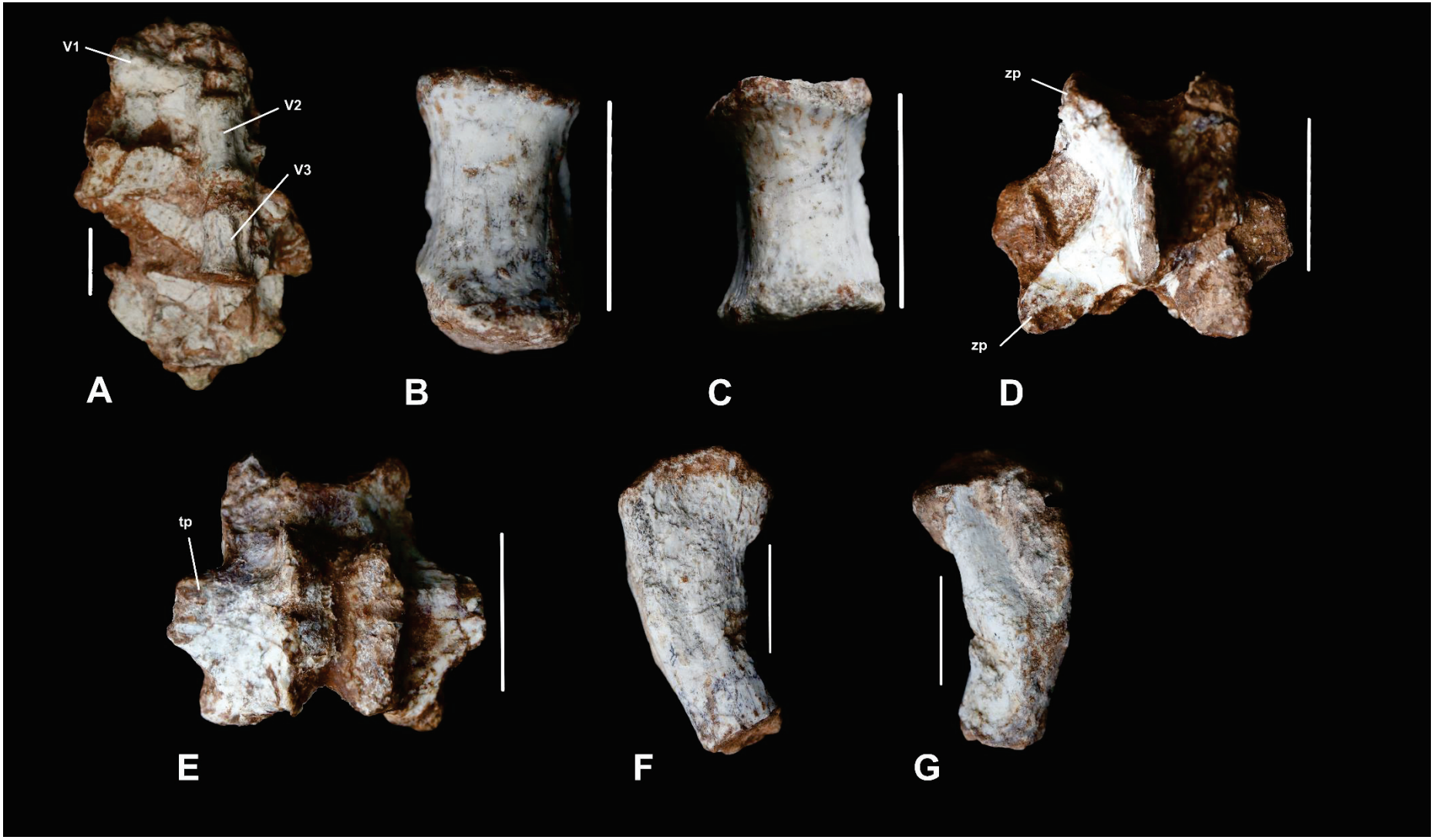

Figure 2.29: Different postcranial parts (SM-2023-1-17): three linked vertebrae centra (A), two vertebrae centra (B & C), upper part of a vertebra in dorsal (D) and ventral (E) views and proximal part of limb bone in anterior (F) and posterior (G) views. tp: tranverse process, V1: vertebra one, V2: vertebra two, V3: vertebra three, zp: zygapophysis. Scale bars are 1 cm.

complete post cranial skeleton, involving axial column and osteoderms. The specimen lacks most of the pectoral girdle (except for the coracoid) and all the forelimb elements. The pubis, tibia, fibula, and digit are the only elements known from the pubic girdle and the hindlimbs.

Type locality – Phu Sung locality, near Sakon Nakhon, Sakon Nakhon province, Thailand.

Stratigraphic horizon and range – The geological strata from where the new taxon originate belong to the Early Cretaceous Sao Khua Formation (Khorat Group) of Thailand (Chanthasit *et al.,* 2019; Ditbanjong *et al.,* 2019).

Referred specimens – SM-2023-1-16, a three-dimensionally preserved nearly complete skull. SM-2023-1-17, a three-dimensionally preserved partial skull table. Both specimens were found in the same strata as the holotype.

Diagnosis – a crocodylomorph characterized by the following unique combination of features: the dorsal part of the postorbital has an anterolaterally facing edge, fully pterygoid bound choanae, the quadrate has no fenestrae, the quadratojugal has no ornamentation, the outer surface of the squamosal is laterodorsally oriented, reduced and sculpted, there is a depression on the posterolateral surface of the maxilla, an altirostral rostrum, external nares facing anterolaterally or anteriorly, the posterodorsal corner of the squamosal has an unsculptured process, the premaxilla-maxilla suture in palatal view directed posteromedially, the ventral part of the lacrimal that does not (or only slightly) contact the jugal, the posterior end of the premaxilla is W-shaped with the anterior tip of the maxilla wedging between the premaxilla on the dorsal surface of the rostrum, lateral margins of the anterior half of the palatines (between suborbital fenestrae) are parallel to subparallel and a broad tabular-shaped frontal with the lateral sutures of the prefrontals parallel to each other, intertemporal width less than one third of the skull width, opened and ovoid supratemporal fenestrae, a supraoccipital exposed on the skull roof, a parietal width less than one third of the skull width, the posterior margin of the skull is not scalloped with a median process, the parietal-postorbital suture is not visible in dorsal view and the lateral margins of the squamosal and postorbital are not concave in dorsal view.

Description

Cranium (Fig. 2.16-2.18 & 2.25-2.28)

The specimens are rather short-snouted: as a result, the rostrum makes up for about half the size of the whole skull. The nasal is quite long, reaching the anterior limit of the skull. The braincase

occupies the posterior third of the skull. The cranial table is ornamented with circular ovoid pits dorsally.

Premaxilla (Fig. 2.16A, 2.16C-E, 2.18A-E, 2.18G, 2.25A-D & 2.27A-D):

The premaxilla, together with the anterior part of the nasal, forms the anterior part of the snout. It is straight posteriorly, forming an oblique suture with the maxilla in lateral view. In dorsal view, the opening for the nares is mostly composed of the premaxilla, with a participation of the nasal in its posterior part. On the ventral surface, the foramen *incisivum* is visible, it is unique and completely enclosed by the premaxillae. The contact between the two bones is straight anteroposteriorly. The contact between the maxilla and the premaxilla is straight lateromedially in ventral view, oblique in lateral view and straight lateromedially in dorsal view, with two posteriorly projecting processes of the premaxilla in SM-2021-1-97: one in the maxilla and one medially at the contact with the nasal. Medially in dorsal view, the two premaxillae do not contact, as they are separated by the nasals. At the contact with the maxilla, the posterior part of the premaxilla bears a pit to accommodate for the corresponding large dentary tooth: this is especially visible in right lateral view. Some pits are present in the lateral surface. Each premaxilla contains at least five teeth (although none are preserved). The preserved alveoli are quite large and separated, the third and fourth one being the largest ones in SM-2023-1-16.

Maxilla (Fig. 2.16A, 2.16C-E, 2.18A-E, 2.18G, 2.25A-E, 2.25G, 2.26A & 2.27A-D):

The two maxillae contact ventrally in an anteroposteriorly straight suture, whereas they are separated dorsally by the nasals, also in an anteroposteriorly straight suture. The triple junction between the maxilla, the premaxilla and the nasal is situated at the level of the first maxillary alveolus. The contact with the jugal is curved anteriorly to oblique in lateral view. Medially, there is a suture with the ectopterygoid which is also curved anteriorly. In lateral view, a depression for the insertion of a dentary tooth can be seen at the level of the sixth-seventh maxillary alveoli, where the maxilla curves medially. Dorsally, the maxilla has two planes, one directed dorsomedially to ventrolaterally, and one oriented anteroposteriorly and flat dorsoventrally: the specimens have an altirostral skull. The contact between these two planes is directed posteromedially until the most developed caniniform maxillary tooth (third alveolus in SM-2021-1-97) or the very marked lateral bulge of the maxilla (sixth alveolus on SM-2023-1-16), then it seems to widen again laterally. The lateral margin of the maxilla forms two convex waves, with the maximum curvature at the level of the fourth and penultimate maxillary alveoli.

Ventrally, the contact with the palatine is straight lateromedially and the maxilla constitutes the anterior and anterolateral margin of the suborbital fenestra. The ventral surface is smooth. From the preserved parts of this bone, it can be assessed that the maxilla contains at least twelve teeth. The largest alveoli, although separated, are the second and the third ones, then the next few alveoli are much smaller, before increasing in size again posteriorly. In ventral view, the alveolar rows globally diverge posterolaterally with a concavity at the level of the fifth alveolus. The largest tooth is preserved on each side, as well as some other fragments of other teeth. Those are caniniform teeth, with no particular carinae or ridges, and they are not compressed lateromedially.

Nasal (Fig. 2.16A, 2.16E, 2.18A, 2.18C, 2.18E, 2.18G, 2.25A, 2.25E, 2.27A & 2.27D):

The nasals are paired and elongated anteroposteriorly (no more than 1.5 - 2 cm). The sutures with the maxilla and the premaxilla are straight anteroposteriorly. The contact between the frontal and the nasals is V-shaped, with the frontal projecting anteriorly in the nasals. The anterior end of the nasal constitutes the posterior and medial margin of the internal nares. The posterior end of the nasals is squeezed between the contact with the frontal and the anterior projections of the prefrontals laterally in SM-2021-1-97 or the anterior projection of the lacrimal in SM-2023-1-16. The nasal does not contact the lacrimal in SM-2021-1-97, but it does in SM-2023-1-16. The bone is not visible in ventral view.

Lacrimal (Fig. 2.16A, 2.16C-D, 2.18A-E, 2.18G, 2.25A, 2.25D, 2.27A & 2.27C-D):

The lacrimal is triangular-shaped with one tip directed anteromedially. The posterior curved margin forms the anterior margin of the orbit. The medial side is bordered by the prefrontal (and the nasal in SM-2023-1-16), whereas the lateral side contacts the posterior part of the maxilla. The lacrimal is shorter anteroposteriorly than the prefrontal in SM-2021-1-97, whereas it is of the same size in SM-2023-1-16. The ventral surface is too damaged to be described.

Jugal (Fig. 2.16A, 2.16C, 2.16E-F, 2.17A-C, 2.17G, 2.18, 2.25A, 2.25C-E, 2.25G, 2.27A & 2.27C-D):

The jugal is elongate and plate-like (taller than wide). Anteriorly, it is directed straightly anteroposteriorly whereas posteriorly it curves mediolaterally (near the contact with the quadratojugal). The jugal sends a convex process to connect with the maxilla on the lateral side, at the same level as the lacrimal, extending to the penultimate alveolus in SM-2023-1-16. In this same specimen, a crest followed by a depression can be seen, both being directed

anteroposteriorly. Posteriorly, the bone connects medially with the quadratojugal almost all the way to the posterior extremity of the skull and almost participates in the articulation with the mandible. The jugal also forms most of the lateral edge of the orbit, however it does not form a dorsal bulge in this region. Behind the orbit, the jugal has a dorsomedially angled process which sutures with the postorbital in an anterolaterally curved suture. The posterior margin of this contact, together with the preserved posterior part of the jugal, forms the lateral and anterolateral margins of the infratemporal fenestra. The contact with the quadratojugal is straight and no foramina or special ornamentation can be seen.

Prefrontal (Fig. 2.16A, 2.16C-D, 2.18A-E, 2.18G, 2.25A, 2.25C-E, 2.25G, 2.27A & 2.27C-D):

The prefrontal is quite thin lateromedially in SM-2023-1-16. It is squeezed between the lacrimal laterally and the frontal (and the nasal in SM-2021-1-97) medially, both with straight sutures. Its anteromedialmost part connects with the posterolateralmost part of the nasal. It also connects anteriorly with the maxilla in a lateromedially straight suture, but only in SM-2021-1-97. It is wider anteriorly than posteriorly in SM-2021-1-97, whereas it is wider posteriorly than anteriorly in SM-2023-1-16. It makes most of the medial margin of the orbit. Ventrally, it is quite damaged, but connects with the palatine through a transversely expanded prefrontal pillar. Those pillars meet at the midline, although this might be due to taphonomic deformation.

Frontal (Fig. 2.16A, 2.16D, 2.18A, 2.18C-E, 2.18G, 2.25A, 2.25C-E, 2.27A, 2.27C-D, 2.28A & 2.28F):

The frontal forms a bridge between the rostrum and the postorbital region of the skull and makes for most of the posteromedial margin of both orbits. Those margins are dorsally raised. Anteriorly, it connects with the nasals in a V-shaped suture, with an anteriorly projected process of the frontal. Posteriorly, it sutures with the parietal and the postorbitals in zigzagged sutural surfaces that are overall straight. Laterally, it does not connect with the lacrimal but forms most of the medial margin of the prefrontal. It forms the anteromedial margin of the supratemporal fenestra. It is slightly concave, but more importantly, it bears a sagittal crest. It is not thick dorsoventrally and the ventral surface is smooth.

Postorbital (Fig. 2.16A, 2.16C-D, 2.18A-E, 2.18G, 2.25A, 2.25C-E, 2.27A, 2.27C-D, 2.28A, 2.28C-D & 2.28F):

The postorbital forms the posterior margin of the orbit, the anterolateral margin of the supratemporal fenestra and the anterior margin of the infratemporal fenestra. It has a T shape

with one branch directed medially, another one posteriorly and the final one ventrally. Medially it only contacts the frontal. Posteriorly, the suture with the squamosal is straight (curved posteriorly in SM-2023-1-17) and is situated rather anteriorly, at the level of the middle of the supratemporal fenestra. Laterally, the postorbital sends a long projection connecting with the jugal. As a result, it forms most of the anterior margin of the infratemporal fenestra.

Parietal (Fig. 2.16A, 2.16F, 2.18A, 2.18F-G, 2.25A, 2.25E, 2.27A, 2.27E, 2.28A, 2.28E):

This single bone is part of the skull roof. It has a rectangular shape with depressed sides, like an hourglass. It is less wide mediolaterally than the posterior part of the frontal in SM-2021-1-97 but as wide as in SM-2023-1-16. Its anterior edge is smaller than its posterior one in SM-2021-1-97 and SM-2023-1-17 as well because it widens abruptly posterior to the supratemporal fenestrae, but those edges are the same size in SM-2023-1-16. Laterally, the parietal forms the medial margin of both supratemporal fenestrae, expending ventrolaterally. Those margins are quite elevated dorsally. The parietal also bears a sagittal crest on its posterior part, aligned with the one of the frontal. On the posteromedial corner of the supratemporal fenestra, a foramen can be seen on each side in SM-2023-1-16. The parietal only contacts the frontal anteriorly, the supraoccipital posteriorly and the squamosal laterally. In SM-2023-1-17, the suture with the squamosal is raised, making a continuous ridge with the raised medial margin of the supratemporal fenestra.

Squamosal (Fig. 2.16A, 2.16C-D, 2.16F, 2.18A, 2.18C-D, 2.18G, 2.25A, 2.25D, 2.25F, 2.27A, 2.27D-E, 2.28A & 2.28C-E):

The squamosal is T-shaped and forms the posterolateral corner of the skull roof. It contacts the quadrate on the anterior side of the exit for the cranioquadrate tube and the otoccipital on the posterior side in SM-2021-1-97, whereas it contacts both sides of the quadrate in SM-2023-1-16. This suture is straight anteroposteriorly. The anterior process connecting with the postorbital is quite long and forms half of the lateral margin of the supratemporal fenestra. Posteriorly, the contact with the parietal is straight anteroposteriorly (curved laterally in SM-2023-1-17) and raised dorsally, forming a crest. In the posteriormost part, the squamosal contacts with the otoccipital ventrally: it forms the dorsolateral part of the skull. It also contacts the supraoccipital posteromedially in SM-2023-1-16 and SM-2023-1-17. Posterolaterally, the squamosal forms an elongated process that is directed posterolaterally and on the same plane as the one of the cranial table in SM-2021-1-97 or ventrally in SM-2023-1-16. On the lateral surface above the ear valve, the squamosal bears a groove directed anteroposteriorly.

Quadratojugal (Fig. 2.16A, 2.16C-D, 2.18A, 2.18C-E, 2.18G, 2.25A, 2.27A & 2.27D):

This bone extends posteriorly from the dorsomedial corner of the infratemporal fenestra. The posterior part is thin and squeezed between the quadrate medially and the jugal laterally. It extends almost all the way to the posterolateralmost part of the skull but does not participate in the articulation with the mandible. The suture with the jugal is straight in SM-2023-1-16 to curved medially in SM-2021-1-97/99, whereas the suture with the quadrate is curved laterally. The bone is smooth on all sides, thin and plate-like, and of the same width all the way, it is also higher mediodorsally than lateroventrally.

Quadrate (Fig. 2.16A-D, 2.16F-G, 2.17G, 2.18, 2.25A, 2.25D, 2.25F, 2.27 & 2.28B):

The quadrate has a complex shape. Anteriorly, it does not reach the infratemporal fenestra, but it reaches the ventral margin of the supratemporal fenestra and contacts the parietal. Dorsally, it contacts the squamosal anteriorly to the exit of the cranioquadrate tube in SM-2021-1-97/99 or on both sides in SM-2023-1-16. The suture with the quadratojugal is straight anteromedially to posterolaterally in SM-2021-1-97/99 whereas it is curved laterally in SM-2023-1-16. The quadrate should contact the pterygoid ventrally, but the area is too damaged on all specimens to describe. Posteriorly, the contact with the otoccipital is straight, situated posteriorly to the external ear valve, and posteroventrally the quadrate is also connected to the basioccipital. A preotic foramen, the oval opening leading into the cavity within the quadrate, can be observed at the anteromedial margin of the quadrate on SM-2021-1-97/99. The foramen aërum cannot be seen because the quadrate is too damaged posteriorly on all specimens. Crest B (Iordansky, 1973) is extremely developed ventrally, extending closely to the quadrate-quadratojugal suture posteriorly and curving anteromedially to medially. Posteriorly, the quadrate articulates with the mandible. Its surface is divided in two hemicondyles laterally and medially equal in size. The quadrate is bordered almost all the way by the squamosal and the otoccipital on the medial side and the quadratojugal on the lateral side. Medially, it sutures with the pterygoid and probably the other bones of the braincase, but the area is too damaged in all specimens to be described. This bone is 1-1.5 cm tall in cross-section and curved dorsally.

Supraoccipital (Fig. 2.16A, 2.16F, 2.18A, 2.18F, 2.25A, 2.25F, 2.27A, 2.27E & 2.28E):

This bone is triangular-shaped in posterior view. It is exposed in dorsal view. Laterally it connects with the otoccipital. It also does not participate in the formation of the foramen

magnum in SM-2021-1-97. It is more difficult to assess in SM-2023-1-16 and SM-2023-1-17 as those areas are covered by other fragments.

Otoccipital (Fig. 2.16F, 2.18A, 2.18C-D, 2.18F-G, 2.25F, 2.27E & 2.28E):

This bone connects laterally with the quadrate, medially with the supraoccipital and dorsally with the squamosal in a straight to curved contact. In posterior view, it extends laterally to the lateral edge of the skull (not in SM-2023-1-17). On SM-2021-1-97 there are three foramina: the lateralmost one is for the internal carotid artery and the two others are the two exits for cranial nerve XII. On SM-2023-1-16, a foramen can be seen dorsolaterally from the occipital condyle, it is the foramen for the cranial nerves IX to XI. The otoccipital also connects with the basioccipital ventrally. The whole bone is plate-like and gradually protrudes caudally with an angle of approximately 30 degrees to the vertical axis, showing a small ridge directed mediolaterally.

Basioccipital (Fig. 2.16B, 2.16D, 2.16F-G, 2.18A-B, 2.18F, 2.25B, 2.25F, 2.27B & 2.27E):

The basioccipital sutures laterally with the otoccipital (in posterior view), the quadrate (in lateral view) and the pterygoid posteroventrally (in SM-2021-1-97/99). It bears a median crest and two lateral tubera, and the median eustachian foramen is clearly visible ventrally to the central crest. The basioccipital is only preserved posteriorly, it has a plate-like shape directed anterolaterally to posteromedially. The occipital condyle is directed posteroventrally.

Palatine (Fig. 2.16B, 2.16G, 2.17D-E, 2.18B, 2.18G, 2.25B & 2.27B):

The palatine connects with the maxilla in an anteroposteriorly straight suture in SM-2021-1-97/99, whereas it is curved anteriorly in SM-2023-1-16. The posterior region is heavily damaged and remodelled but it does not include the choanae in SM-2021-1-97/99 (Fig. 2.17G). However, this could be the case in SM-2023-1-16, where the palatine would form its anterior margin, but, because of the poor state of preservation, it is difficult to assess. The suture with the pterygoid is also anteroposteriorly straight just anteriorly to the internal choanae. The paired palatines are flat when they meet at the midline. The ventral surface is smooth and raised dorsally in SM-2023-1-16. The vomer cannot be seen.

Pterygoid (Fig. 2.16B, 2.16D, 2.16F-G, 2.17C-F, 2.18B-D, 2.18F-G, 2.25C, 2.26B & 2.27B-C):

The pterygoid is sutured to the palatine anteriorly, the ectopterygoid laterally and the basioccipital posteriorly. Each pterygoid connects straightly with the corresponding ectopterygoid and tends to be more curved ventrally at that point. The internal choanae are ovoid, bordered by prominent anterior margins in ventral view and have no midline process. They are totally enclosed by the pterygoids in SM-2021-1-97/99 (their status is unknown in SM-2023-1-16) and are anterior to the posterior margin of the suborbital fenestra. Anteriorly, a median process of the pterygoid extends to contact the palatine and forms the ventral edge of the interorbital septum. The pterygoid is smooth on all surfaces except on the lateralmost sides.

Ectopterygoid (Fig. 2.16B, 2.16D, 2.17C, 2.17D-F, 2.18B-C, 2.18F-G, 2.25D, 2.26B, 2.27B & 2.27D):

This bone contacts the jugal and the maxilla laterally and the pterygoid medially (forming the pterygoid flange). The triple junction between the maxilla, the jugal and the ectopterygoid is situated at the middle of the anterior process of the ectopterygoid. The ectopterygoid could constitute the posterolateral margin of the suborbital fenestra, but it cannot be assessed with certainty due to the poor preservation of this area. This bone is curved ventrally and laterally.

Laterosphenoid (Fig. 2.26B):

The dorsoposterior ridge of the laterosphenoid connects with the parietal. The ventralmost part of the bone contacts the quadrate, forming the foramen for cranial nerve V.

Basisphenoid (Fig. 2.25C-D, 2.26B & 2.27C-D):

The basisphenoid is complex. Anteriorly, the basisphenoid rostrum is quite short and not dorsoventrally elevated. It does not contact the laterosphenoid, however it does contact the prootic and the pterygoid. Posteriorly, it has a plate-like shape directed anterolaterally to posteromedially. It contacts the pterygoid ventrally, the quadrate dorsally and the basioccipital posteriorly, encircling the eustachian foramen. This part also bears a crest directed anteroventrally to posterodorsally.

Prootic (Fig. 2.26B):

This small bone sutures with the laterosphenoid posteriorly on the posterior margin of the foramen and the basisphenoid rostrum anteriorly.

Dentition (Fig. 2.16C-E, 2.16H-I, 2.18C-E, 2.18G & 2.26A):

A large maxillary caniniform tooth is preserved on each side of the skull. It is conical and slightly curved lingually. The base of the tooth crown is ovoid in cross-section and the apex is pointed. There are no carinae or crenulations visible in SM-2021-1-97/99, whereas there are carinae but with no crenulations in SM-2023-1-16. The enamel, although quite damaged, shows thin and basoapically directed striations. This morphotype corresponds to the "pseudocaniniform" morphotype described in Schwarz & Salisbury (2005), Lauprasert *et al.* (2011) and Tennant *et al.* (2016). The upper dentition also preserves a smaller tooth, on the left side just anteriorly to the big caniniform tooth. On the mandible, a lot more teeth are present, throughout the toothrow, and they belong to both the "pseudocaniniform" and the "lanceolate-shaped" morphotypes (Schwarz & Salisbury, 2005; Lauprasert *et al.,* 2011; Tennant *et al.,* 2016). The anterior teeth are strongly procumbent and the fourth one is quite developed, as well as the twelfth and thirteenth one.

Cranial openings

There are no strict post temporal fenestrae: the sutures between the parietal, the supraoccipital and the otoccipital are quite thin anteroposteriorly but there is no clear opening in this region. The internal choanae are contained by the pterygoids (and maybe the palatines in SM-2023-1-16) and are situated just anteriorly to the contact with the palatine, quite anteriorly. No septum can be seen. The orbit is large, about half the length of the skull table. It is D-shaped in dorsal and lateral views. This opening is surrounded by the jugal, the maxilla, the lacrimal, the frontal, the prefrontal and the postorbital. The margins are not raised.

As in all diapsids, the skull possesses two pairs of temporal fenestrae: the supratemporal and infratemporal ones. The supratemporal fenestra is ovoid and flattened with its longest axis directed anteroposteriorly and almost the same length as the parietal. The supratemporal fossa is absent in SM-2021-1-97/99 and not very wide, whereas it quickly disappears ventrally in SM-2023-1-16 and SM-2023-1-17. The infratemporal fenestra is preserved on the left side in all specimens: it is not complete but appears triangular, it is bordered by the jugal laterally, the postorbital anteriorly and the quadratojugal medially. No spike-like projection inside the

fenestra can be seen. There is no antorbital fenestrae so to say, but a depression anterior to each orbit in dorsal view which probably corresponds to an antorbital foramen.

The cranioquadrate canal appears open as a groove in lateral view, just ventrally to the squamosal and posteriorly to the tympanic region. The foramen magnum is triangular-shaped, about one centimetre at its widest part.

Mandible (Fig. 2.16B-G, 2.17 & 2.18)

There is no external mandibular fenestra. Both coronoids are missing. Overall, the mandible is ornamented with circular to ovoid pits and grooves.

Dentary (Fig. 2.16B-E, 2.16G, 2.17B-C & 2.18B-G):

This bone is the only tooth-bearing element of the mandible, with at least fourteen alveoli. The two rami separate at the level of the sixth dentary tooth and are firmly sutured anteriorly. The symphyseal region remains quite wide anteriorly and is U-shaped at its anteriormost point. In medial view, the dentary is quite thin dorsoventrally and forms an acute angle anteriorly. Ventrally and dorsally, the medial suture with the splenial is oblique directed posterolaterally to anteromedially. The dentary remains uniform in width up to the point of divergence, where it begins to taper off. Posteriorly, the dentary connects dorsally with the surangular from the end of the toothrow, and ventrally with the angular at its posteriormost part. The ventral surface is smooth and curved dorsally anteriorly. The lateral side shows no groove ventral to the toothrow. In lateral view, the dorsal margin is sinusoidal, marked by two sets of waves, that culminate at the level of the fourth - fifth and twelfth - thirteenth dentary alveoli. There is also a medial depression to accommodate for the largest caniniform maxillary tooth at the level of the tenth dentary alveolus, especially visible on the left side. The ventral margin of the dentary is straight anteroposteriorly.

Splenial (Fig. 2.16B, 2.16G, 2.17C & 2.18):

The splenial is most exposed medially: it forms a vertical plate that sutures with the dentary and with the other splenial at the midline anteriorly. It reaches up to the sixth dentary tooth and is not exposed ventrally. Posteriorly, it becomes thin and plate-like along the medial surface of the dentary (even becoming the medial wall for the last posterior dentary alveoli, from the twelfth one) until it disappears posteriorly without meeting with the angular or the surangular. In posterior view, the circular foramen *intermandibularis oralis* is present at the point where

the two splenials diverge (not on the medial sides) and is quite small. The mandibular symphysis completely involves the first nine alveoli. The dorsal exposure of the splenial is strictly triangular-shaped and makes for more than one third of the mandibular symphysis. The dorsal surface bears rugosities whereas the medial surface is smooth and flat.

Angular (Fig. 2.16B-D, 2.16F-G, 2.17A-B, 2.17H, 2.18B-D & 2.18F-G):

The angular is the ventralmost mandible element (approximately one third of the total length of the mandible). In lateral view, it is elongated and curved dorsally posteriorly. Medially, the angular sutures with the dentary to form a huge medial depression (abductor chamber; Iordansky, 1973). Dorsally, and for all its length, it sutures with the surangular, finishing as a sharp process laterally to the retroarticular process and curving inwards and up. Only the lateral surface is ornamented, the others are smooth. The area of insertion of the *M. Pterygoideus* is not very developed and visible only in the posteroventral margin of the angular.

Surangular (Fig. 2.16C, 2.16F, 2.17A-C, 2.17G-H & 2.18):

This bone is robust and elongated. Anteriorly, its dorsal process might extend between the dentary and the splenial, but the preserved parts of the specimen only show a contact between the surangular and the dentary anteriorly, with the surangular dorsal to the dentary. Posteriorly, it tends to curve dorsally and sutures with the angular for the rest of its length. It also becomes more plate-like. This suture is linear anteriorly and curves dorsally posteriorly. The bone also curves medially and forms the lateral margin of the articular fossa. Laterally to this, there is a short ridge oriented anteroposteriorly, forming a depression. The dorsal surface is convex, not ornamented and flattens before the glenoid surface. On the lateral surface, there is a ridge directed posterodorsally to anteroventrally.

Articular (Fig. 2.16A-B, 2.16D, 2.16F-G, 2.17G-H, 2.18A-B & 2.18D-F):

The articular is the posteriormost element of the mandible. It has two dorsal surfaces separated by a ridge oriented lateromedially. The anterior surface articulates with the quadrate, the ridge helping to stabilize this articulation as its posterior wall is tall and dorsally edged. The articular fossa is divided into a lateral and a medial portion of equal sizes by a small ridge oriented anteroposteriorly. The posterior surface (retroarticular process) is overall concave and paddle-shaped. It seems to taper off posteriorly but the posteriormost part is broken on each side. Ventromedially, the articular forms the posteromedial wall of the abductor chamber. It sutures with the surangular at its lateral margin and with the angular at its ventral margin.

Axial skeleton (Fig. 2.19-2.22, 2.24, 2.29A-E)

There are at least 32 vertebrae consisting of at least seven cervicals, 10 dorsals, two sacrals and 14 caudals. The proatlas/atlas and axis are missing. All the preserved vertebrae seem to be amphicoelous. All processes are described based on the nomenclature of Gomes de Souza (2018).

Cervicals (Fig. 2.19A-C, 2.19E & 2.22):

The neural arches and spines are quite tall, narrow, and pointed dorsally. The diapophyseal processes are longer than the parapophyseal processes. The zygapophyses are quite large compared to the centra, with the prezygapophyses being larger than the postzygapophyses. These structures become horizontal posteriorly. All the centra are amphicoelous and the lateral sides of the centra (between the diapophyseal and parapophyseal processes) are notably depressed. The fourth and the fifth vertebrae have the taller neural spines (more than two times the height of the centrum). The hypapophyses are broken but their area of insertion on the centrum are still visible on all centra. On the fifth visible centrum, the proximal part of the hypapophysis is preserved, it is half the size of the centrum. The diapophyseal processes gradually increase in size posteriorly and they also migrate from the lateral side of the centrum to the lateral side of the neural arch. The parapophyseal processes do not seem to increase in size, however they also migrate dorsally, going from the lateroventral margin to the lateral side of the centrum posteriorly.

Dorsals (Fig. 2.19B-D, 2.20B-C & 2.22):

The neural spines are anteroposteriorly longer than those of the cervicals. The diapophyseal and parapophyseal processes are too damaged to be described. The ventral hypapophyses are either absent or too damaged to be seen from the second or third centra. The articular facets of the pre- and postzygapophyses are more horizontally oriented.

Sacrals (Fig. 2.20 & 2.22):

There are two sacral vertebrae of the same size. The base of their neural spine is quite long anteroposteriorly for both. On the second vertebra, the transverse processes and their articulation surface are more developed, probably because they are less damaged than on the second one. The costal caudalis is directed ventrally on the first sacral. The contact between the two centra is flat. The anterior articulation surface of the first sacral and the posterior articulation surface of the second sacral are both concave.

Caudals (Fig. 2.20, 2.21B-D & 2.22):

The first caudal vertebra is quite large, and its articulation surfaces are concave to flat. The other ones are quite damaged, the second has a neural spine that is preserved: it is quite high dorsoventrally and long anteroposteriorly. Some of them have two horizontal ridges on the centrum, maybe for the insertion of the chevron. A chevron is preserved: it is triangular-shaped and opened in the middle.

Ribs (Fig. 2.19A & 2.21B):

Some ribs are preserved, but it is difficult to identify to which vertebra they were attached. When those structures are preserved, the tuberculum is less developed than the capitulum. The ribs are slightly curved and are rod-like.

Pectoral girdle (Fig. 2.23)

Coracoid (Fig. 2.23):

The left coracoid is preserved. This bone is overall convex. The shaft is triangular, and both ends of the bone are extended. The coracoid foramen is visible in the proximalmost part. The articulation surface with the scapula is flat and the ventral part of the glenoid fossa is saddle-shaped and directed posteriorly. The distal end is more developed anteriorly than posteriorly.

Pelvic girdle (Fig. 2.20B-C & 2.23)

Pubis (Fig. 2.20B-C & 2.23):

The two bones are flat. The proximalmost part articulating with the rest of the pelvic girdle is missing in both. Overall, it has a round shape with a convex and narrow dorsal margin.

Forelimb (Fig. 2.25B-C, 2.25G & 2.27B-C)

Humerus (Fig. 2.25B-C, 2.25G & 2.27B-C):

The humerus is squeezed between the anterior margin of the suborbital fenestra and the right side of the basisphenoid rostrum. Its deltopectoral crest is slender and placed anteroproximally. On the proximomedial side, there is a ridge that connects the deltopectoral crest and the triangular-shaped humerus head. The humerus is quite straight and not very curved or twisted. The humerus head is very well-developed and unusual among crocodyliforms, extending posterolaterally. The articulation surface is flat and decreases anteromedially to articulate with the glenoid fossa. There is also a lateral projection when the humerus head reaches the shaft. The area of insertion for the *M. teres major* is visible on the posterior side. Distally, on the

bicondyle articulation with the zeugopod, the medial condyle for the ulna is larger than the lateral condyle for the radius.

Hindlimb (Fig. 2.21A-B & 2.23)

Tibia (Fig. 2.21A-B & 2.23):

The shaft of the left tibia, although deformed taphonomically, appears to be straight anteroposteriorly and curved laterally. However, both ends of the bone are on the same plane lateromedially. The proximal articulation surface is flat with a posterior concavity. The distal articulation surface is ovoid.

Fibula (Fig. 2.23):

The fibula is straight and very slender. The proximal end is compressed mediolaterally. The distal articulation surface bears two articulation surfaces that are flat to convex: one is posteromedial and would have articulated with the calcaneum and the other one is distal and would have articulated with the astragalus.

Digits (Fig. 2.23):

The preserved metatarsal is concave ventrally. The distal end is separated into two condyles with a depression on each side laterally and medially to the hemicondyles. The preserved ungual is curved ventrally and pike-shaped.

Osteoderms (Fig. 2.19-2.21 & 2.24)

The dermal armor consists of a dorsal shield composed of at least three rows of mediolaterally expanded osteoderms and a ventral shield composed of rectangular-shaped osteoderms sutured to each other. Some osteoderms bear a longitudinal keel that does not extend on the whole surface, but it is difficult to situate them on the body. Appendicular osteoderms could not be determined with certainty.

Dorsal shield (Fig. 2.19, 2.20A-B, 2.21A, 2.21C, 2.24A, 2.24C & 2.24E):

The osteoderms are more expanded mediolaterally anteriorly than posteriorly however their anteroposterior size remains the same. All osteoderms are flat or slightly arched dorsally and ornamented with circular pits, as is seen on the cranial table and the posterolateral side of the mandible. There is no particular process or spine. The articulation system is as follows: the anterior osteoderm overlaps the posterior osteoderm and the left osteoderm tends to overlap the right one. The margins are straight.

Ventral shield (Fig. 2.19, 2.20C, 2.21B, 2.21D, 2.24B, 2.24D & 2.24F):

The ventral shield is more damaged; however, it consists of square osteoderms. There are at least two rows of osteoderms. The ornamentation is the same as the dorsal shield, it consists of flat circular pits. The ventral shield is missing in the sacrum region.

Phylogenetic analyses

The analysis generated 41 most parsimonious trees and a consensus tree with a length of 1500 steps (Supplementary Material S5; consistency index = 0.26, retention index = 0.59). Although the support values are quite low (Supplementary Material S5), the main groups inside Neosuchia are retrieved and supported by numerous synapomorphies. Those results are also retrieved using the heuristic search procedure, although the consensus topology is less parsimonious (1513 steps, consistency index = 0.26, retention index = 0.59), hinting at the relative robustness of our analysis.

Based on ACCTRAN optimization, we retrieve Atoposauridae *sensu* Schwarz *et al*. (2017) as a monophyletic group (including *Varanosuchus sakonnakhonensis*; Fig. 2.30 node 4) based on the following combinations of characters: a broad oreinostral skull (char. 3), little participation of the premaxilla in the internarial bar (char. 4), the quadrate, squamosal and otoccipital do not meet to enclose the cranioquadrate passage (char. 49), one wave of enlarged maxillary teeth (char. 79), dorsal osteoderms with a well-developed process located anterolaterally in dorsal parasagittal osteoderms (char. 96), two parallel rows of dorsal osteoderms (char. 97), a symmetrically developed lateral compression on the maxillary teeth (char. 140) and a lacrimal that tapers ventroposteriorly and does not or only slightly contact the jugal (char. 229).

Furthermore, Paralligatoridae *sensu* Kuzmin *et al*. (2019) forms a monophyletic group (Fig. 2.30, node 5) defined by the following synapomorphies: no vascular opening on the dorsal surface of the postorbital bar (char. 27), the medial quadrate condyle expands ventrally, being separated from the lateral condyle by a deep intercondylar groove (char. 170), a sharp ridge along the lateral surface of the angular (char. 219), the ulna has a wide and rounded olecranon process (char. 260) and a foramen located the palatal premaxilla-maxilla suture near the alveolar border (char. 320).

Eusuchians (including *Bernissartia,* Atoposauridae, Paralligatoridae, Hylaeochampsidae Williston, 1925 and Crocodylia; Fig. 2.30, node 3) are also retrieved as a monophyletic group with the following synapomorphies: the choanal groove is undivided (char. 69), the cervical

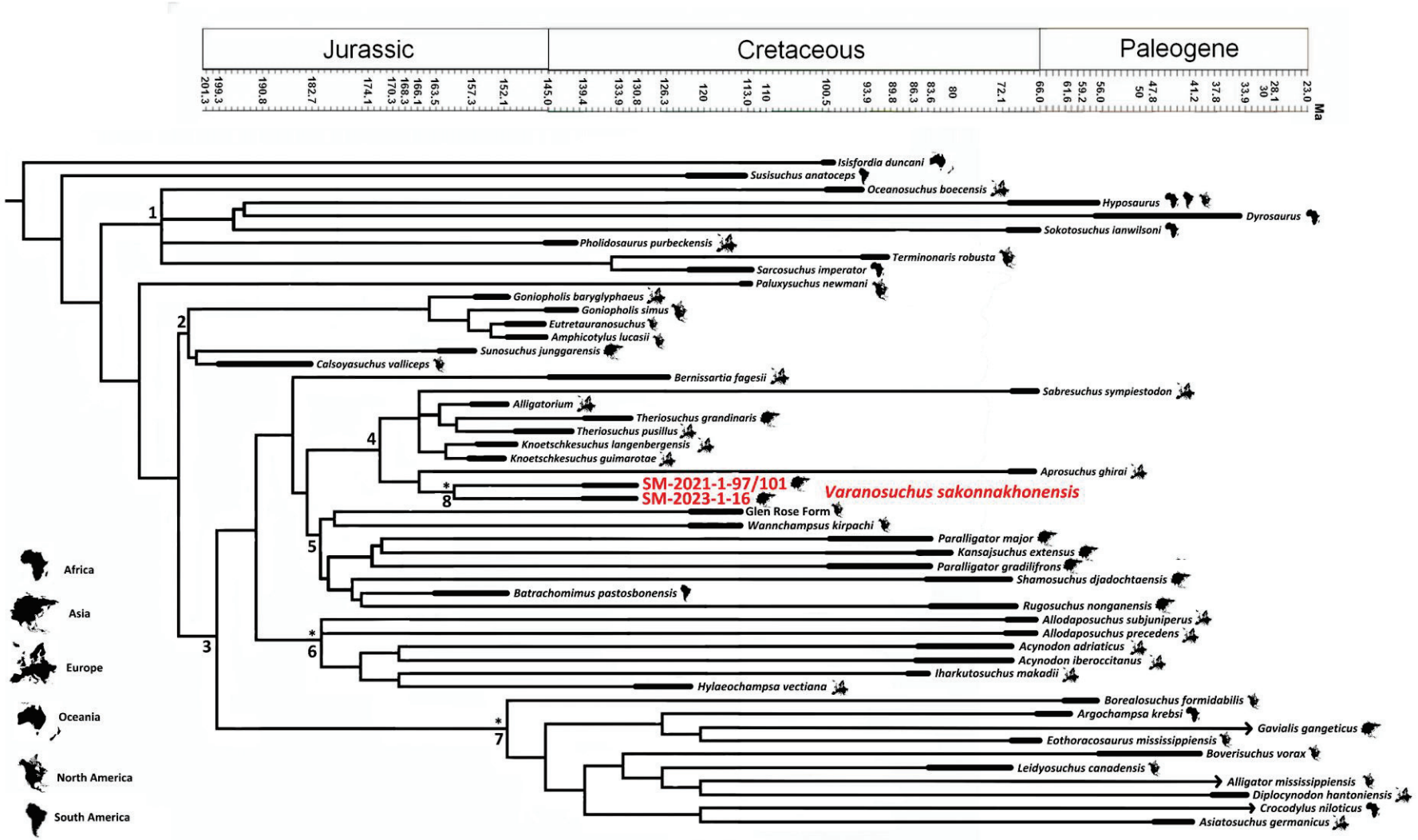

Figure 2.30: Time-calibrated phylogenetic tree. 1: Pholidosauridae + Dyrosauridae, 2: Goniopholididae, 3: Eusuchia, 4: Atoposauridae, 5: Paralligatoridae, 6: Hylaeochampsidae, 7: Crocodylia, 8: *Varanosuchus sakonnakhonensis*. Asterisks indicate clades displaying fully pterygoid bound choanae.

vertebrae are procoelous (char. 92), the dorsal osteoderms have a discrete convexity on the anterior margin (char. 96), there are more than two rows of dorsal primary osteoderms (char. 97) and the supraoccipital is exposed in the skull roof (char. 171).

Finally, the two specimens from Phu Sung are retrieved as a monophyletic group (Fig. 2.30, node 8) with the following synapomorphies: the dorsal part of the postorbital has an anterolaterally facing edge (char. 29), the quadrate has no fenestrae (char. 45), there are two waves of enlarged maxillary teeth (festooned; char. 79), a quadratojugal with no ornamentation (char. 145), the outer surface of the squamosal laterodorsally oriented is reduced and sculpted (char. 168) and there is a depression on the posterolateral surface of the maxilla (char. 207).

Discussion

Comparisons with other close crocodylomorphs from Thailand

Cretaceous crocodylomorphs reported from Thailand are restricted for now to certain neosuchians (Buffetaut & Ingavat, 1980, 1983, 1984; Lauprasert *et al.,* 2007, 2009, 2011; Martin *et al.,* 2014b). SM-2023-1-16 and SM-2021-1-97/101 are clearly not longirostrine, so they do not belong to *Chalawan thailandicus* Buffetaut & Ingavat, 1980 or the poorly known eusuchian from Ban Saphan Hin (Kubo *et al*., 2018). *Goniopholis phuwiangensis* Buffetaut & Ingavat, 1983 consists of an incomplete dentary and is considered by some as rather belonging to *Sunosuchus* Young, 1948 (de Andrade *et al.,* 2011). This fragment of dentary has the third and fourth alveoli as the largest one anteriorly and they are almost confluent, whereas it is the fourth and the fifth in SM-2021-1-97/101. *Siamosuchus phuphokensis* Lauprasert, Cuny, Buffetaut, Suteethorn & Thirakhupt, 2007 and *Khoratosuchus jintasakuli* Lauprasert, Cuny, Thirakhupt & Suteethorn, 2009 do not have an altirostral snout, so at least the two most complete specimens cannot be attributed to either of these taxa. However, Lauprasert *et al*. (2011) described an atoposaurid, *Theriosuchus grandinaris* from Phu Phok (Sao Khua Formation) which has an altirostral snout. This taxon is defined by the following unique combination of characters: nasal bone gradually wider posteriorly, weak notch at the suture between the premaxilla and the maxilla, combination of pseudocaniniform, lanceolate-shaped and labiolingually compressed with crenulated carinae teeth, mandibular symphysis not extending beyond the seventh dentary tooth and a slender prefrontal tapering anteriorly. The nasal of SM-2023-1-16 does not gradually widen posteriorly, it has a slender prefrontal rounded anteriorly and the only tooth preserved is a pseudocaniniform one. SM2021-1-97/101 has a nasal bone that is straight posteriorly, no particular notch at the premaxilla/maxilla suture,

lanceolate-shaped and pseudocaniniform teeth that do not seem to have carinae or denticles. Furthermore, the mandibular symphysis completely involves nine alveoli whereas it only involves seven in the holotype of *T. grandinaris,* and the dentary part of the mandibular symphysis completely involves six alveoli whereas it only involves four in *T. grandinaris* (Fig. 2.31). Those two last features do not vary ontogenetically and are diagnostic in crocodylomorphs (Pochat-Cottilloux *et al.,* 2023a). The prefrontal is not really tapered anteriorly but more rounded.

Comparisons with other close neosuchian taxa

SM-2023-1-16 and SM-2021-1-97/101 are distinguished from *Theriosuchus pusillus* Owen, 1878 because the nasal does not expand abruptly mediolaterally, the minimum infratemporal width is less than one-third of the total width of the cranial table and the choanae do not bear a septum (Tennant *et al.,* 2016). Furthermore, in SM-2021-1-97/101, the splenial is not inset posterodorsally from the ventral surface of the mandible, the specimen does not show low-crowned teeth, the first caudal vertebra is not biconvex, and the dorsal osteoderms are not squared which are further evidence that this specimen cannot be attributed to *T. pusillus* (Tennant *et al.,* 2016).

The three specimens do not belong to *Sabresuchus ibericus* because the palatal surface of the maxilla is unornamented and the tooth crowns do not have denticulate carinae (Brinkmann, 1989; 1992; Tennant *et al.,* 2016). Furthermore, SM-2021-1-97/101 has nine alveoli completely involved in the mandibular symphysis, its dentary teeth are separated, the occlusal dentary surface is not compressed, and the fifth maxillary tooth is not enlarged, which are further arguments to distinguish this specimen from *S. ibericus* (Tennant *et al.,* 2016).

Finally, the three specimens are distinct from *Sabresuchus sympiestodon* because the tooth enamel bears striations on the labial and lingual surfaces (Martin *et al.,* 2010; 2014a; Tennant *et al.,* 2016). Furthermore, SM-2021-1-97/101 does not have a diastema between the seventh and the eighth alveoli (Tennant *et al.,* 2016).

SM-2023-1-16 and SM-2021-1-97/101 are also not attributable to Atoposauridae *sensu* Tennant *et al.,* 2016, that is to say *Alligatorium*, *Alligatorellus* and *Atoposaurus* von Meyer, 1850). For example, *Alligatorium meyeri* Jourdan, 1862 has lateral margins of the nasals that are parallel and the lacrimal connects with the jugal (Tennant *et al.,* 2016), *Atoposaurus* has unsculpted

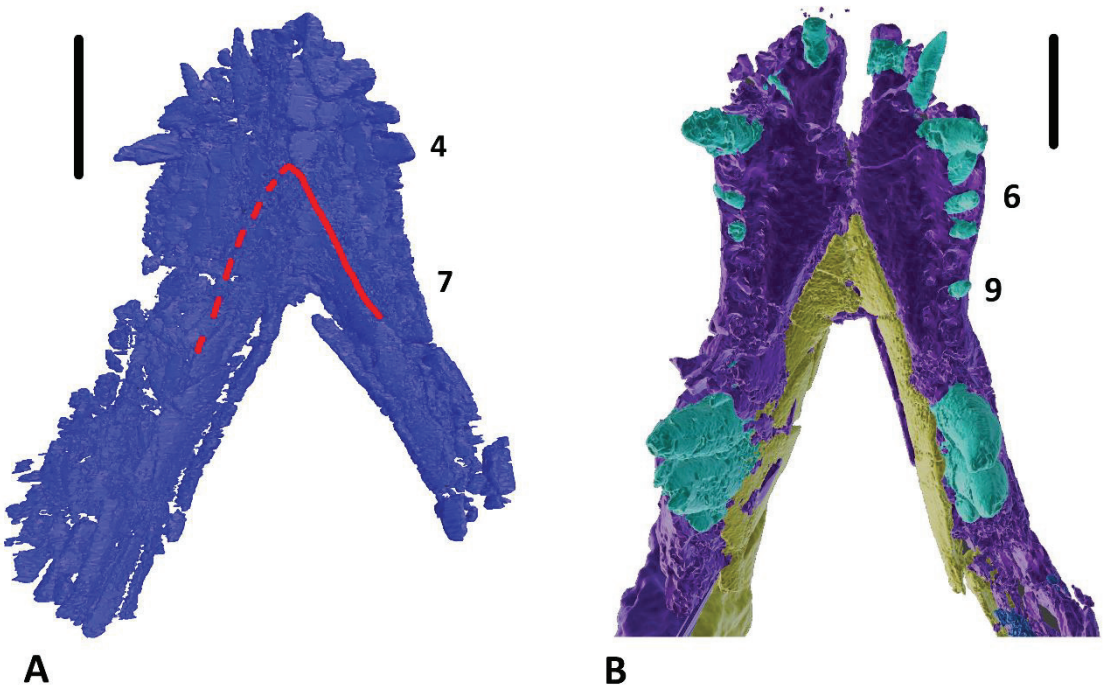

Figure 2.31: Comparison of the mandibular symphysis of *Theriosuchus grandinaris* (PRC-2; A) and *Varanosuchus sakonnakhonensis* (SM-2021-1-97/101; B) in dorsal view. Numbers indicate alveoli number. Scale bars are 1 cm for A and 2 cm for B.

dorsal bones of the cranial table and the snout (Tennant *et al.,* 2016) and *Alligatorellus* has an unopened supratemporal fenestra, a frontal thinner mediolaterally between the orbits than the nasals and with a broad anterior process, a squamosal extending to the posterior margin of the orbit and a supraoccipital excluded from the skull roof (Tennant & Mannion, 2014; Tennant *et al.,* 2016). Furthermore, in SM-2021-1-97/101, there is no contact between the jugal and the lacrimal, there is no external mandibular fenestra and the edges of the osteoderms are sculpted so it is distinct from *A. meyeri*. There are osteoderms so it cannot be attributed to *Atoposaurus*. Moreover, the external surface of the mandible is sculpted and the dorsal osteoderms do not have a lateral ridge, so it is different from *Alligatorellus.*

Montsecosuchus deperiti can also be excluded because this taxon has an intertemporal width greater than its interorbital width (which is also the case of *Alligatorium paintenense* Kuhn, 1961), a very mediolaterally narrow skull and a flat and ungrooved squamosal-parietal suture. SM-2021-1-97/101 has a paddle-shaped retroarticular process, only two sacral vertebrae and imbricated rectangular-shaped dorsal osteoderms which are further elements to distinguish it from *M. depereti* (Tennant *et al.,* 2016).

Brillanceausuchus babouriensis is also different because it has supratemporal fenestrae that are longer than the orbits, a fully pterygoidean choana, abruptly widening nasal with sinusoidal

lateral margins, a flat frontal dorsal surface, and a parietal-postorbital suture visible in dorsal view (Tennant *et al.,* 2016). In SM-2021-1-97/101, the base of the jugal postorbital process is directed posterodorsally, the posterolateral process of the squamosal is not depressed from the skull table, the retroarticular process is paddle-shaped and the dorsal osteoderms are rectangular which are further arguments to distinguish it from *B. babouriensis* (Tennant *et al.,* 2016).

Knoetschkesuchus Schwarz, Raddatz & Wings, 2017 is also different from these specimens because there are secondary pterygoidean choanae, the minimum intertemporal width is one third of the total width of the cranial table and there is an antorbital fenestra (Schwarz *et al.,* 2017). Furthermore, SM-2021-1-97/101 does not have an external mandibular fenestra.

Another recently described taxa is *Aprosuchus ghirai*. This taxon is defined by having a W-shaped frontal-nasal suture and a heterodont dentition of at least four tooth morphotypes (pseudocaniniforms, pseudoziphodont lanceolate, ziphodont lanceolate and "low-crowned'). SM-2023-1-16 and SM-2021-1-97/101 can be distinguished from this taxon because the frontal invades the nasals anteriorly and they do not show the four tooth morphotypes.

Some taxa included in Paralligatoridae also have this altirostral morphology, but the specimens described here do not belong to this family (*sensu* Turner, 2015) because they have at least two waves of enlargement of the maxilla and no orbitonasal sulcus on the maxilla. SM-2021-1-97/101 also has amphicoelous cervical and dorsal vertebrae and the largest maxillary tooth is the third one (*Shamosuchus djadochtaensis*; Turner, 2015); the squamosal does not extend to the orbit in lateral view and the maxilla does not extend posteriorly in the palatines (*Paralligator* Konzhukova, 1954; Turner, 2015).

SM-2021-1-97/101 and SM-2023-1-16 can be further distinguished from *Batrachomimus pastobonensis* because these specimens do not have scalloped lateral margins of the rostrum, do not have a long posterodorsal premaxilla process, have sculptured posterior parts of the maxilla, do not have laterally expanded posterior part of the nasals, do not have a jugal crest and do not have a constricted choanal septum that is hourglass-shaped and that extends anteriorly in the palatine (Montefeltro *et al.,* 2013). SM-2021-1-97/101 also does not have an angular that extends anteriorly to the orbit (Montefeltro *et al.,* 2013).

The three specimens from Phu Sung also differ from *Rugosuchus nonganensis* because the median ridge of the frontal continues towards the posterior end of the bone and the median ridge of the parietal extends to the anterior end of the bone in the Phu Sung specimens (Wu *et al.,*

2001). Furthermore, SM-2021-1-97/101 and SM-2023-1-16 do not have fossae on the dorsal surface of the maxilla (Wu *et al.,* 2001).

Wannchampsus kirpachi can also be excluded because the three specimens have the ventral rim of the earflap groove that is not laterally expanded into a sloping shelf (Adams, 2014). SM-2021-1-97/101 and SM-2023-1-16 do not have an enlarged third maxillary tooth and have internal choanae bordered exclusively by the pterygoids. SM-2021-1-97/101 does not have procoelous vertebrae.

The recently described *Tarsomordeo winkleri* (Adams, 2019) is different from SM-2021-1-97/101 because the dentary part of its mandibular symphysis completely includes only four alveoli whereas it includes six in the Phu Sung specimen. This character has been demonstrated to be diagnostic in crocodylomorphs because it does not vary ontogenetically (Pochat-Cottilloux *et al*., 2023a).

Scolomastax sahlsteini (Noto *et al.,* 2020) is also different from SM-2021-1-97/101 because this taxon has a dorsal expansion on the anterodorsal part of its surangular, while *Yanjisuchus longshanensis* (Rummy *et al.,* 2022) has a wedge-shaped elevation on the anterior part of the frontal, interorbital ridges with a groove in the interorbital region and an anteroposteriorly directed ridge on the jugal that distinguish this taxon from SM-2021-1-97/101 and SM-2023-1-16. SM-2021-1-97/101 is further distinguished from *Yanjisuchus* because it does not have a diastema posterior to the fourth dentary tooth.

Finally, *Kansajsuchus extensus* (Kuzmin *et al.,* 2019) is different from SM-2021-1-97/101 and SM-2023-1-16 because the premaxilla posterodorsal process is longer and this bone bears enlarged neurovascular foramina on its ventral surface; the nasals are separated from the external nares and ornamentation is absent on the alveolar margins; there are transverse crests with a dorsal groove in the interorbital region; there is a longitudinal ridge on the lateral surface of the jugal; and the supratemporal fenestrae are mediolaterally enlarged. In SM-2021-1-97/101, the enlarged maxillary alveoli are the second and third, whereas they are the fourth and fifth in *Kansajsuchus*, the prefrontal is longer than the lacrimal and the dentary part of the mandibular symphysis completely involves six alveoli, whereas it completely involves seven to eight in *Kansajsuchus*. In SM-2023-1-16, the lateral lamina of the squamosal does not cover most of the lateral surface of the postorbital, as it does in *Kansajsuchus*.

Comparisons with other small altirostral taxa

Other small altirostral forms also include *Araripesuchus* Price, 1959. However, those specimens do not belong to this genus because the dorsal surface of the postorbital does not have a vascular opening, the anteromedial margins of the palatine are not parallel and they do not have parachoanal fossae (*Araripesuchus buitreraensis*; Pol & Apesteguia, 2005; Dumont *et al.,* 2020a); the nasal contacts the lacrimal in SM-2023-1-16, the tenth dentary tooth is not hypertrophied in SM-2021-1-97/101 (*Araripesuchus tsangatsangana* Turner, 2006); the parietal width is less than one third of the skull width, and in SM-2021-1-97/101, the postorbital bar is not flush with the lateral surface of the jugal (*Araripesuchus patagonicus* Ortega, Gasparini, Buscalioni & Calvo, 2000) and the supratemporal fenestrae are not round, the posterior margin of the skull table is not scalloped with a median process, and in SM-2021-1-97/101, the supratemporal fossa is absent (*Araripesuchus wegeneri*; Buffetaut 1981; Sereno & Larsson, 2009). SM-2021-1-97/101 and SM-2023-1-16 also do not have antorbital fenestrae and SM-2021-1-97/101 does not have an external mandibular fenestra whereas the specimens assigned to *Araripesuchus* do (Ortega *et al.,* 2000; Turner, 2006; Dumont *et al.,* 2020a).

The three specimens from Phu Sung as belonging to the same taxon

The phylogenetic results highlight that SM-2021-1-97/101 and SM-2023-1-16 share six characters (see Results section 3). Among those, SM-2023-1-17 shares with SM-2021-1-97/101 and SM-2023-1-16 an outer surface of the squamosal laterodorsally oriented reduced and sculpted. Furthermore, SM-2023-1-17 also shares with SM-2021-1-97/101 and SM-2023-1-16 an intertemporal width less than one third of the skull width, opened and ovoid supratemporal fenestrae, a supraoccipital exposed on the skull roof, a parietal width less than one third of the skull width and the posterior margin of the skull that is not scalloped with a median process, a parietal-postorbital suture not visible in dorsal view and the lateral margins of the squamosal and postorbital that are not concave in dorsal view. SM-2021-1-97/101 and SM-2023-1-17 both have a parietal surface depressed compared with the one of the squamosals and the parietal-squamosal suture is raised and grooved. As a result, the three specimens from Phu Sung can be attributed with confidence to the same taxon.

Furthermore, all the differences observed in the description between the three specimens are part of ontogenetic variations, as highlighted in Supplementary Material S7 using extant brevirostrine ontogenetic series for comparison. The associated phylogenetic characters (i.e., characters 11, 12, 125, 243, 253, 265, 310) should thus be excluded from the CTM, as they

capture ontogenetic rather than phylogenetic variation. When we apply those settings, the topology obtained almost does not differ from the one in Figure 2.31, apart from Hylaeochampsidae that nests deeply in Crocodylia, *Alligatorium* that is less closely related to *Theriosuchus* and the position of *Boverisuchus* Kuhn, 1938 and *Asiatosuchus* Mook, 1940 (Supplementary Material S5), hinting at the relative robustness of our analyses.

The neosuchian-eusuchian transition and a redefinition of Atoposauridae and Eusuchia

We retrieve Atoposauridae *sensu* Schwarz *et al*. (2017) as a monophyletic group. This is contrary to what is found in Tennant *et al*. (2016) and would now include 'putative atoposaurids' such as *Theriosuchus*, *Knoetschkesuchus* and *Sabresuchus* Tennant, Mannion & Upchurch, 2016, as well as *Aprosuchus ghirai,* and *Varanosuchus sakonnakhonensis* the new taxon described here. However, the intrarelationships of atoposaurids remain difficult to interpret. The different genera would appear to be monophyletic (Fig. 2.31), however, they are retrieved in a polytomy once phylogenetic characters that capture ontogenetic variation are excluded (Supplementary Material S5), apart from *Knoetschkesuchus*, *Aprosuchus* Venczel & Codrea, 2019 and *Varanosuchus.*

On the other hand, Paralligatoridae *sensu* Kuzmin *et al*. (2019) is here retrieved in its entirety as a monophyletic group, and as a sister taxon to Atoposauridae (Fig. 2.30). This close relationship, which had already been highlighted in other studies (Turner, 2015; Turner & Pritchard, 2015; Schwarz *et al.,* 2017; Leite & Fortier, 2018; Kuzmin *et al.,* 2019; Venczel & Codrea, 2019; Noto *et al.,* 2020) is here strengthened with the addition of *Varanosuchus sakonnakhonensis*. The Glen Rose Form and *Wannchampsus* Adams, 2014 are retrieved as a sister clade to all other paralligatorids, as in Adams (2014), Kuzmin *et al*. (2019), Noto *et al*. (2020) and Rummy *et al*. (2022) which confirms the very close relationship of the two OTU and warrants a complete description and reassessment of USNM 22039. Furthermore, *Batrachomimus pastosbonensis* also warrants a complete reassessment, as it may instead be a notosuchian (Hester *et al.,* 2016). However, if it is truly a paralligatorid, then it implies a lack of fossil record of this clade of more than 20 million years.

Furthermore, we propose a topology where Eusuchia includes Crocodylia, Atoposauridae, Paralligatoridae and Hylaeochampsidae. Susisuchidae Salisbury, Frey, Martill & Buchy, 2003, on the other hand, is retrieved in a basal position in Neosuchia, as in Turner & Pritchard (2015) and Venczel & Codrea (2019). This is not that surprising, as the CTM we used here is mainly derived from this last study, however other studies have retrieved this clade as belonging to

Eusuchia (Leite & Fortier, 2018; Martin *et al.,* 2020a). Here, they are distinguished from Eusuchia partly because of characters that are still debated (choanal region and shape of centra; Salisbury *et al.,* 2006; Turner & Prichard, 2015; Leite & Fortier, 2018; Montefeltro *et al.,* 2019), so the input of CT scan techniques on those specimens would certainly shed some light on the relationships of this family.

Our phylogenetic hypothesis thus implies a new definition of Eusuchia, relying on characters from the choanal, cervical, dermal shield and supraoccipital region (see Results section 3). Unfortunately, those characters are either reversed in subsequent clades or absent in some fossil forms, which is why we would not qualify them as truly robust for defining Eusuchia. One thing is for certain though: we confirm here that some of the characters historically assigned to Eusuchia (pterygoid bound choanae and sagittal segmentation of the dorsal shield) are not valid anymore with the current knowledge on ontogenetic variations and fossil forms. A striking example is that *Varanosuchus sakonnakhonensis* (depending on the status of *Brillanceausuchus babouriensis*; Michard *et al.,* 1990; Tennant *et al.,* 2016) is now the only definitive known atoposaurid that has fully pterygoid bound choanae, which most parsimoniously becomes a convergence between this taxon, Hylaeochampsidae and Crocodylia and not an apomorphy of Eusuchia, occurring two to three times independently in Eusuchia (Fig. 2.30). Tennant *et al.* (2016) proposed that rather than the palatine and pterygoid bound choanae deriving in fully pterygoid bound choanae, the 'primitive' condition would be an anterior position of the choanae (retrieved in protosuchians for example; Wu *et al.,* 1996b) and the choanae migrating posteriorly in derived forms, reaching posteriorly to the posterior margin of the suborbital fenestrae in Hylaeochampsidae and Crocodylia (Clark & Norell, 1992; Martin, 2007; Delfino *et al.,* 2008a, b; Ösi, 2008; Martin *et al.,* 2016b). Although it is correct that posteriorly-placed choanae (i.e., posteriorly to the posterior margin of the suborbital fenestra) occur only in these two clades, they do not form a monophyletic group in our main analysis (Fig. 2.30). However, once characters depicting ontogenetic variations are removed (Supplementary Material S5), hylaeochampsids cluster with crocodylians, which makes their relationships unresolved and so a definite answer cannot be reached for now. A deeper sampling and knowledge of fossil forms around the Neosuchia-Eusuchia transition will probably allow to have a clearer view on this matter.

What about the paleoecology of atoposaurids?

Although not much is known about the ecology of atoposaurids, recent studies hint at a possible terrestrial lifestyle, partly because of their very poor stratigraphic occurrences (Schwarz & Salisbury, 2005) compatible with a terrestrial fossil record as well as their forward-facing nares (Martin *et al.,* 2014a). Here we put forward further conflicting arguments towards this hypothesis. It has been assessed that altirostral morphology and head posture are directly linked to a terrestrial rather than semi-aquatic lifestyle, because of the implied position of the nares and binocular vision (Stevens, 2006; Marinho *et al.,* 2013; Pochat-Cottilloux *et al.,* 2022b). *Varanosuchus sakonnakhonensis* has an altirostral snout (as other atoposaurids; Tennant *et al.,* 2016) and could exhibit those behaviours, making it suitable for a terrestrial lifestyle. This would of course be further reinforced when looking at the neuroanatomy of such specimens, which to our knowledge remains to be done.

Furthermore, Pochat-Cottilloux *et al*. (2023b) recently proposed, building on observations from Clarac *et al*. (2018) on thermoregulation mechanisms, that osteoderm ornamentation could be linked with lifestyle. Taxa exhibiting osteoderm ornamentation benefit of enhanced vascularization because this feature contributes to heat captation and is thus much more needed in aquatic environments where the physical properties are different than on land (Schmidt-Nielsen, 1997; Vogel, 2005). *Varanosuchus sakonnakhonensis*, as well as other atoposaurids (Tennant *et al.,* 2016), do have ornamented osteoderms, which, on the other hand, would point to semi-aquatic affinities.

The postcranial anatomy of *Varanosuchus* is remarkably well-preserved and allows estimations of its posture. Terrestriality is linked with a parasagittal posture (Parrish, 1987): here, *Varanosuchus* has elongated and relatively straight limb elements (Fig. 2.23, 2.25C & 2.27C) corresponding to an erect posture (Colbert & Mook, 1951; Pol *et al.,* 2012; Godoy *et al.,* 2016).

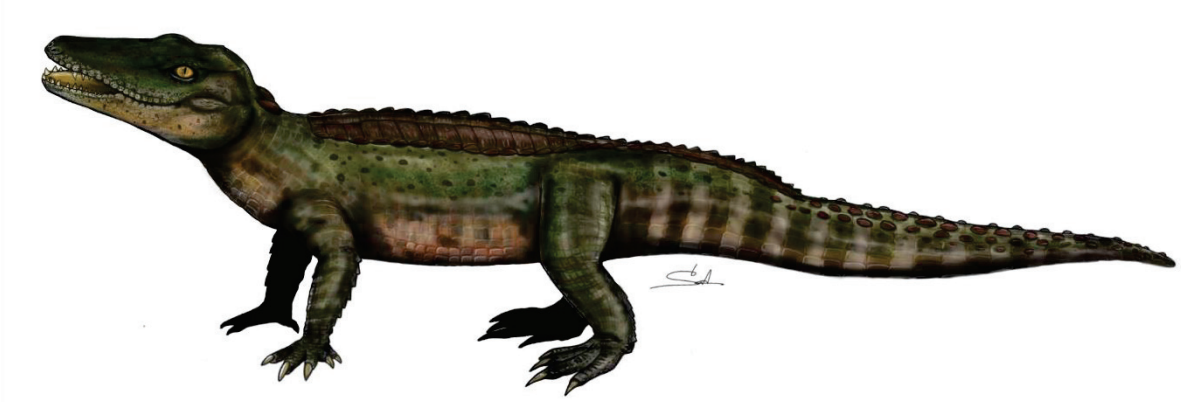

Figure 2.32: Reconstruction of *Varanosuchus sakonnakhonensis* in its living posture.

However, using the ratio between the humerus midshaft width and long-axis length (Turner, 2006; Adams, 2019), we obtain a value of 0.10, which is exactly the value separating morphologies considered as 'gracile' (i.e., linked with a terrestrial lifestyle) from those considered as 'robust' (i.e., linked with a semi-aquatic/aquatic lifestyle), so it is difficult to conclude on the posture of the organism by looking at the data brought by this bone. We thus infer a relatively erect posture for *Varanosuchus* (Fig. 2.32).

The various proxies on the paleoecology of *Varanosuchus sakonnakhonensis,* and atoposaurids in general, give conflicting results. However, it is also possible to hypothesize a terrestrial lifestyle but with semi-aquatic affinities for those forms, as is seen today in some extant species of lepidosaurs (Mebert, 2011; Chan *et al.,* 2020) and would be the most probable explanation for the observations we make here.

The paleobiogeography of paralligatorids compared to atoposaurids

Although they would seem to be very close phylogenetically, definite atoposaurid and paralligatorid occurrences have different paleogeographical and stratigraphic ranges (Fig. 2.30). Atoposaurids have a Laurasian distribution, whereas paralligatorids are only known in Asia and in North America (maybe also in South America but see above).

In terms of stratigraphic range, atoposaurids are present in Late Jurassic to Early Cretaceous strata, with *Sabresuchus sympiestodon* and *Aprosuchus ghirai* being the only representatives of this family in the Late Cretaceous, implying a lack of fossil record of more than 50 Myr. This huge stratigraphic gap could be filled when looking at specimens that may be attributed to Atoposauridae in the Cenomanian (Vullo & Néraudeau, 2008) and Campanian – Maastrichtian of France (Martin & Buffetaut, 2005; Martin *et al.,* 2014a), Middle Cretaceous of the United States (Winkler *et al.,* 1990; Cifelli *et al.,* 1999; Eaton *et al.,* 1999; Fiorillo, 1999; Garrison *et al.,* 2007; Oreska *et al.,* 2013; Foster, 2018) and Aptian – Albian of China (Wu *et al.,* 1996a; Mo *et al.,* 2016). Finally, the referral of some specimens from the Eocene of Yemen to Atoposauridae (Stevens *et al.,* 2013) is very surprising and warrants further investigation as well. On the other hand, except for *B. pastosbonensis* (of which a reassessment might be necessary; Hester *et al.,* 2016), paralligators are known from the Middle to Late Cretaceous (Fig. 2.30). One interesting thing to notice is that the two families have never been retrieved at the same time and the same place, which could be because the competition for resources between these two groups of very similar organisms would have been too important for them to cohabit, hinting at a similar ecology, or could also be a case of collection bias. However,

given how little evidence we currently have, the paleoecology of paralligatorids remains an open question.

Conclusion

We describe here three new specimens from the Early Cretaceous Phu Sung locality (Sao Khua Formation, Thailand) that we refer to *Varanosuchus sakonnakhonensis* gen. nov. sp. nov. Using CT scan data, we can provide an in-depth description, as well as a comparison with other close fossil forms. Although we notice some ontogenetic variations, *Varanosuchus sakonnakhonensis* is diagnosed by an altirostral morphology, a dorsal part of the postorbital with an anterolaterally facing edge, a depression on the posterolateral surface of the maxilla and a fully pterygoid bound choanae, among other traits.

A phylogenetic analysis confirms that this new taxon belongs to Atoposauridae *sensu* Schwarz *et al*. (2017), with a close relationship to *Aprosuchus ghirai* from the Maastrichtian of Romania (Venczel & Codrea, 2019). We also manage to distinguish this taxon from *Theriosuchus grandinaris* (Lauprasert *et al.,* 2011) from the same age also in Thailand. Paralligatoridae *sensu* Kuzmin *et al*. (2019) is retrieved as the sister clade to Atoposauridae, forming Eusuchia with Hylaeochampsidae and Crocodylia, while susisuchids are found as basal neosuchians: characters historically assigned to Eusuchia, such as fully pterygoid bound choanae for example, are not valid anymore. However, a robust definition of Eusuchia must still be provided.

Finally, the altirostral snout morphology and osteoderm ornamentation observed here in *Varanosuchus sakonnakhonensis* (and other atoposaurids) would match the hypothesis of a terrestrial lifestyle for those taxa but with semi-aquatic affinities. Further studies are needed to confirm this, for example using neuroanatomic or geochemical proxies.

Acknowledgments

This work was supported by the Agence Nationale de la Recherche (SEBEK project no. ANR-19-CE31-0006-01 to JEM) and the International Research Group PalBioDivASE (IRN) grant of CNRS. The authors would like to thank Céline Salaviale, Vincent Perrier and Jeanne Rolland (Univ Lyon 1) for technical support, as well as Didier Berthet (Musée des Confluences de Lyon), Lawrence Witmer (Ohio University), Thomas van der Kamp and Marcus Zuber (Staatliche Museum für Naturkunde Karlsruhe), Timothy Rowe (University of Texas),

Blandine Bartschi (Univ Lyon 1), Sébastien Bruaux (Royal Belgian Institute of Natural Sciences), Silke Schweiger and Viola Winkler (Natural History Museum Vienna), Medhi Mouana and Anne-Lise Charruault (University of Montpellier), Cody Thompson (University of Michigan), David Blackburn (Florida Museum of Natural History), Patrick Campbell and Susannah Maidment (Natural History Museum United Kingdom) and Christophe Borrely (Muséum d'Histoire Naturelle de Marseille) for access to extant specimens.

Authors contributions

Yohan Pochat-Cottilloux: Conceptualization, Methodology, Validation, Formal analysis, Investigation, Data Curation, Writing - Original draft, Writing - Review & Editing, Visualization; **Komsorn Lauprasert**: Conceptualization, Validation, Formal analysis, Investigation, Resources, Data Curation, Writing - Original draft, Writing - review and editing, Supervision, Project administration, Funding acquisition; **Phornphen Chantasit**: Conceptualization, Validation, Resources, Data Curation, Writing - review and editing, Supervision, Project administration, Funding acquisition; **Sita Manitkoon**: Writing - review and editing, Visualization; **Jérôme Adrien**: Methodology, Resources, Data Curation, Writing - review and editing; **Joël Lachambre**: Methodology, Resources, Data Curation, Writing - review and editing; **Romain Amiot**: Conceptualization, Validation, Resources, Writing - review and editing, Supervision, Project administration; **Jeremy E. Martin**: Conceptualization, Validation, Resources, Writing - review and editing, Supervision, Project administration, Funding acquisition.

Data availability statement

The data underlying this article are available in the article and in its supplementary material.

Supplementary Materials

Supplementary Material S1, S4 & S6-S7 and Supplementary Model S1-S6 are available on this link:

https://mycore.core-cloud.net/index.php/s/QKYU3NzcvSzxZIt

Supplementary Material S2, S3 & S5 are available in Appendix 4.

Chapter 3: The study of endocranial structures

Endocranial structures refer to the internal structures inside the skull of an organism, which in fossils is represented by the pneumatic cavities left in the bones by the organs they once housed. Their study is thus of the higher interest in fossil organisms, as the shape and morphology of those organs (brain, ear system, cranial nerves, arteries, sinuses…) is linked to their function and thus allows ecological inferences (Buchholtz & Seyfarth, 1999). Before the advent of computed tomography (CT) techniques in the 1990's, observations of the internal structures were based on fortuitous preservation conditions or destructive approaches (Cuvier, 1804; Eudes-Deslongchamps, 1863; Marsh, 1874, 1878; Morel de Glasville, 1876; Seeley, 1880; Lemoine, 1883-1884; Newton, 1888; Osborn, 1912; Edinger, 1921, 1925, 1926, 1927, 1928, 1938, 1939, 1940, 1941, 1942, 1948, 1951, 1975; Stensiö, 1963; Jerison, 1969; Galton, 1988, 1989, 2001). Historically, numerous internal structures were also studied via latex casts (Colbert, 1946a; Haight & Murray, 1981; Walker, 1990; Wharton, 2000; Paulina-Carabajal & Canale, 2010; Bona & Paulina-Carabajal, 2013), particularly in paleoanthropological studies (Radinsky, 1968, 1971; Holloway, 1981a, b, 2018; Falk *et al*., 1986) but this approach can lead to breaks or degradations of the original specimen. However, it is still comparable in terms of quality with modern CT techniques (Schoenemann *et al*., 2007).

X-rays are known since Röntgen (1896), but technologic advances did not allow to use them in paleontological studies until almost a century later (Rydberg *et al*., 2000; Beckmann, 2006). Briefly, the principles of a CT scan can be summarized as follows (Fig. 3.1; Wils, 2020): first, the X-rays are emitted from an X-ray source. Those X-rays go through the specimen depending on its thickness and density following the Beer-Lambert laws of absorption. Then, remaining X-rays hit a detector, opposite to the source, that converts them to digital signal. A CT-scan acquisition consists of numerous 2D radiographs of the specimen, under different angular positions, that are then stacked as a 3D reconstruction, after corrections for artifacts. The basic unit of the 2D images (pixels) are thus converted to 3D basic units (voxels). The output results in an image stack in greyscale mode, with black areas usually associated with non-absorbent materials (i.e., air) and white areas usually associated with most absorbent materials (i.e., sediment or fossilized bones). The degree of absorption of a material, and thus its recovered greyscale depends mostly on its structure and chemical composition: as fossils mainly have a different composition than their surrounding matrix, a greyscale contrast is expected between the two and allows separation using numerical tools. This step is known as segmentation: in each 2D image from the 3D image stack, the user selects, manually or through semi-automatic

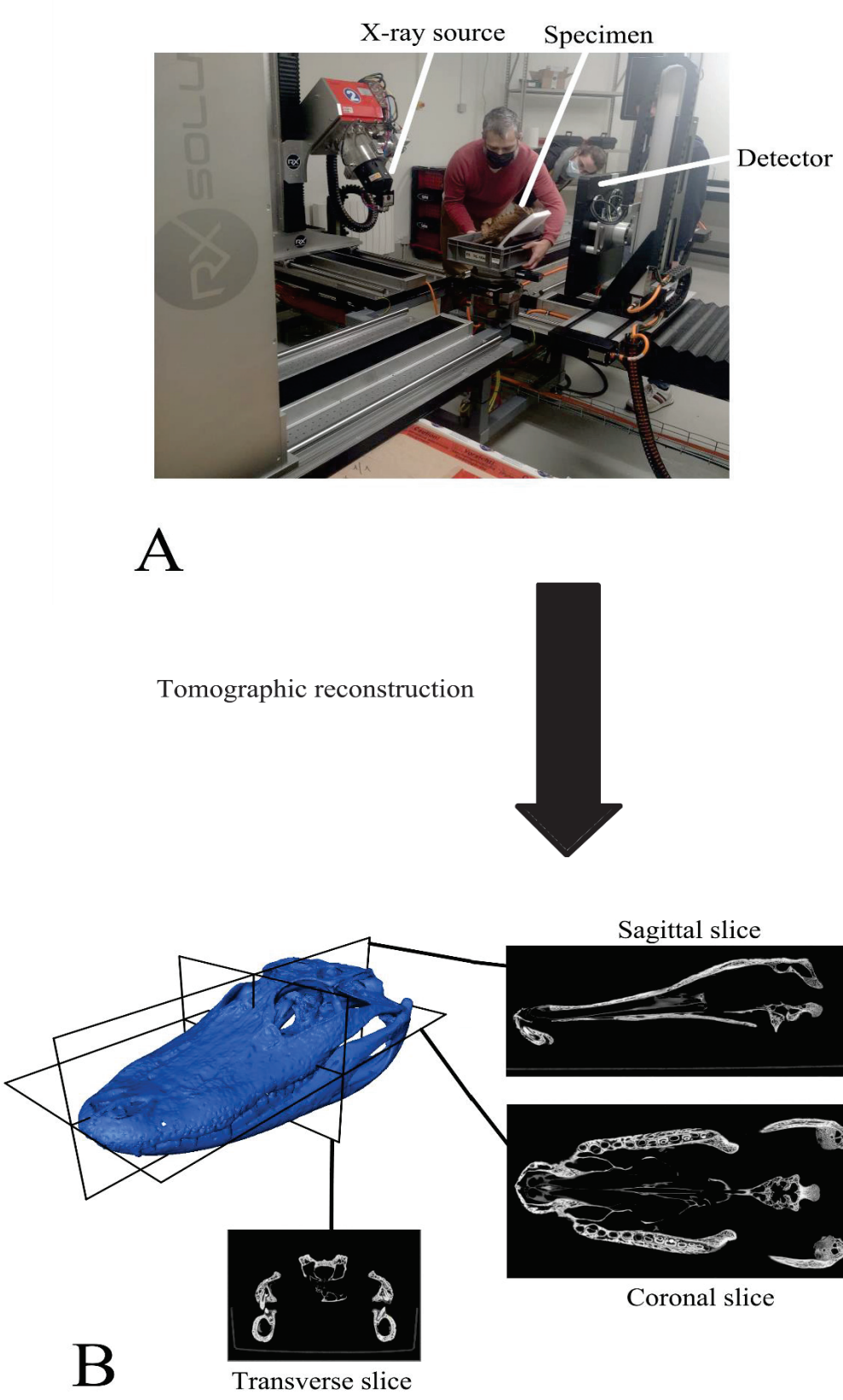

Figure 3.1: Schematic of a CT scan protocol. A: acquisition phase (illustrated CT scan is the Double Tomographe Haute Energie or DTHE by RX Solutions) housed at INSA Lyon. B: segmentation phase of an *Alligator mississippiensis* (MHNL 50002667).

algorithms, the areas of interest.

When all those selections are put together, 3D volumes are reconstructed, and can then be post-processed and visualized using various 3D manipulation softwares. In the framework of this thesis, the 3D image stacks were first pre-treated using ImageJ (version 1.53e; Schindelin *et al*., 2015), to correct contrast or resize the stack if needed. Then, the segmentation was performed using the software Avizo (version 7, 7.5, 8 and 9; Thermo Fisher Scientific). 3D post-processing softwares used include MeshLab (version 2020.07; Cignoni *et al*., 2008) and Blender (version 3.4; Mullen, 2011).

In crocodylomorphs, the study of the neuroanatomy and paleoneuroanatomy of extant and extinct specimens has been intense since the pioneering work of Colbert (1946a) on *Sebecus icaeorhinus* and is a field currently in full expansion with the advent of modern CT scan techniques (Holliday & Schachner, 2022). These studies have been recently reviewed in Barrios *et al*. (2023) and are summarized and updated in Table 4. The nomenclature that will be used to describe and compare the specimens in this thesis is issued from those studies.

The knowledge of the neuroanatomy of crocodylomorphs is thus very important and continues to be extended. However, it is still limited by several factors: first, some groups are poorly known or not at all (protosuchians, sphagesaurians, mahajangasuchids, peirosaurids, sebecosuchians, atoposaurids, paralligatorids, hylaeochampsids and fossil crocodylians for example). Second, the resolution of the scans is sometimes too limited or the CT scan not powerful enough to properly highlight certain structures (inner ears and cranial nerves particularly) or the fossil matrix too hard for the X-rays to go through; the matrix and fossil can also have the same density making their separation difficult. Third, the sharing of data and good scientific practices regarding open data are not always adopted by the community. Fourth, little is still known about ontogenetic variation of the endocranial structures of crocodylomorphs, apart from the most well-known extant species, and this is of the upmost importance while trying to understand their ecological or phylogenetical implications.

In this chapter, I will first assess current knowledge on the ontogenetic, ecological, and phylogenetical interpretations that can be made on the different endocranial structures. Then, a closer look will be taken at several specimens of altirostral crocodylomorphs for which the neuroanatomy is still unknown. Building on those results, I will finally assess the usefulness of the inner ear as an ontogenetic, ecological, and phylogenetical proxy in crocodylomorphs.

Table 4: Background of studies and specimens of crocodylomorphs neuroanatomy. Updated from Barrios *et al*. (2023; table 7.1).

Taxon	Specimen(s)	Provenance	Nature	Reference(s)
Sphenosuchus acutus Haughon, 1915	SAM PK 3014	Early Jurassic of South Africa	Natural endocast	Walker (1990)
Junggarsuchus sloani	IVPP14010	Middle-Late Jurassic of China	CT scan	Schwab *et al.* (2020); Ruebenstahl *et al*. (2022)
Almadasuchus figarii Pol, Rauhut, Lecuona, Leardi, Xu & Clark, 2013	MPEF-V 3838	Oxfordian of Argentina	CT scan	Leardi *et al*. (2020b)
Eopneumatosuchus colberti Bronzati, Montefeltro & Langer, 2012	MNA V2460	Early Jurassic of United States	CT scan	Dufeau (2011); Schwab *et al*. (2020); Melstrom *et al*. (2022)
Protosuchus haughtoni Busbey & Gow, 1984	BP/1/47700, 4746	Hettangian of United States	CT scan	Schwab *et al*. (2020); Bronzati *et al*. (2021); Cowgill *et al*. (2022)
Sebecus icaeorhinus	AMNH 3160	Eocene of Argentina	Latex cast	Colbert (1946a)
Zulmasuchus querejazus Buffetaut & Marshall, 1992	MHNC 6672	Paleocene of Bolivia	CT scan	David (2010)

Baurusuchus Price, 1945 sp.	IFSP-VTP/PALEO-0002, 0003; FEF-PV-R-1/9: FUP-Pv 000020, 000021	Campanian - Maastrichtian of Brazil	CT scan	Dumont *et al*. (2020b)
Campinasuchus dinizi	CPPLIP 1360	Turonian - Santonian of Brazil	CT scan	Fonseca *et al*. (2020)
Araripesuchus wegeneri	MNN GAD18	Aptian - Albian of Niger	CT scan	Sereno & Larsson (2009)
Araripesuchus buitreraensis	MPCA-PV-235	Cenomanian of Argentina	CT scan	Barrios (2021)
Araripesuchus patagonicus	MUCPv-267, 269	Cenomanian of Argentina	CT scan	Barrios (2021)
Anatosuchus minor	MNN GAD19	Aptian - Albian of Niger	CT scan	Sereno & Larsson (2009)
Notosuchus terrestris	MLP 64-IV-16-5, 16-31, 16-30, 16-8, 16-7; MACN-PV-RN-1037; MPCA-PV-237	Santonian of Argentina	CT scan	Barrios (2021)
Simosuchus clarki	UA 8679	Maastrichtian of Madagascar	CT scan	Kley *et al*. (2010)
Hamadasuchus sp.	ROM 52560	Aptian -	CT scan	Dufeau (2011);

		Cenomanian of Morocco		George & Holliday (2013)
Rukwasuchus yajabalijekundu Sertich & O'Connor, 2014	RRBP 08630	Aptian - Cenomanian of Tanzania	CT scan	Sertich & O'Connor (2014)
Lomasuchus palpebrosus	MOZ-Pv 4084	Turonian - Coniacian of Argentina	CT scan	Barrios (2021)
Gasparinisuchus peirosauroides	MOZ-Pv 1750	Santonian - Campanian of Argentina	CT scan	Barrios (2021)
Pelagosaurus typus Bronn, 1841	BRLSI M1413; NHMUK OR 32599	Toarcian of England	Sectioned braincase and CT scan	Eudes-Deslongchamps (1863); David (2010); Dufeau (2011); Pierce *et al*. (2017); Schwab *et al*. (2020)
Proexochokefalos heberti Morel de Glasville, 1876	MNHN.F unnumbered	Callovian of France	Natural endocast	Morel de Glasville (1876)
Charitomenosuchus leedsii Andrews, 1909	LPP.M 35	Callovian of France	Latex cast and CT scan	Wharton (2000); Schwab *et al*. (2020)
Plagiophthalmosuchus cf. *gracilirostris* Westphal, 1961	NHMUK PV OR 3395	Toarcian of England	CT scan	Brusatte *et al*. (2016); Schwab *et al*. (2020)

Plagiophthalmosuchus gracilirostris	NHMUK PV OR 15500	Toarcian of England	CT scan	Cowgill *et al*. (2022)
Macrospondylus bollensis Cuvier, 1824	SNSB-BSPG 1984 I258; MCZ VPRA-1063; NHMUK PV OR 14436	Toarcian of Germany	CT scan	Herrera *et al*. (2018); Schwab *et al*. (2020); Wilberg *et al*. (2021) ; Cowgill *et al*. (2022)
Eoneustes gaudryi Collot, 1905	NHMUK PV R 3263	Bathonian of England	CT scan	Cowgill *et al*. (2022)
Teleosaurus cadomensis Lamouroux, 1820	SMC J35177; MNHN AC 8746	Bathonian of France	Sectionned braincase	Eudes-Deslongchamps (1863); Seeley (1880); Jouve (2009)
Cricosaurus araucanensis Gasparini & Dellape, 1976	MLP 72-IV-7-1, 76-XI-19-1; MOZ PV 7201, 7261	Tithonian of Argentina	CT scan and natural endocast	Herrera *et al*. (2013b, 2018); Herrera (2015); Schwab *et al*. (2020)
Cricosaurus schroederi Kühn, 1936	MM unnumbered	Valanginian of Germany	CT scan	Schwab *et al*. (2020); Cowgill *et al*. (2022)
Torvoneustes coryphaeus Young, de Andrade, Etches & Beatty, 2013	MJML K1863	Kimmeridgian of England	CT scan	Schwab *et al*. (2020); Cowgill *et al*. (2023)
Thalattosuchus superciliosus de	MNHN 1870-133,. F RJN	Callovian - Oxfordian of	Sectionned braincase,	Wenz (1968); David (2010);

Blainville, 1853	256; NHMUK PV R 11999; AMNH 997	France and England	natural endocast and CT scan	Schwab *et al*. (2020); Cowgill *et al*. (2022)
'Metriorhynchus' cf. *'M.' brachyrhynchus* Eudes-Deslongchamps, 1868	NHMUK PV OR 32617, 32618	Callovian - Oxfordian of France	CT scan	Schwab *et al*. (2020, 2021a)
'Metriorhynchus' cf. *'M.' westermanni* Gasparini, 1980	MDA 2	Oxfordian of Chile	CT scan	Fernández *et al*. (2011); Herrera *et al*. (2018)
Dakosaurus cf. *andiniensis* Vignaud & Gasparini, 1996	MOZ-PV 058, 089	Late Tithonian - early Berriasian of Argentina	Natural endocast	Herrera & Vennari (2014); Herrera (2015); Fernández & Herrera (2022)
Pholidosaurus meyeri Dunker, 1843	Unnumbered	Berriasian of Germany	Natural endocast	Edinger (1938); Hopson (1979)
Pholidosaurus schaumburgensis von Meyer, 1841	Unnumbered	Berriasian of Germany	Natural endocast	Edinger (1938)
cf. *Rhabdognathus* Swinton, 1930	CNRST-SUNY-190	Maastrichtian - Paleocene of Mali	CT scan	George & Holliday (2013)
Rhabdognathus aslerensis Jouve, 2007	AMNH FARB 33354	Maastrichtian - Paleocene of Mali	CT scan	Erb & Turner (2021)
Dyrosaurus phosphaticus Thomas, 1893	MNHN.F.ALG 1	Eocene of Africa	CT scan	David (2010)

Goniopholis Owen, 1842 sp.	Unnumbered	Berriasian of England	Natural endocast	Edinger (1938)
Shamosuchus djadochtaensis	IGM 100-1195	Campanian of Mongolia	CT scan	Schwab *et al*. (2020)
Eutretauranosuchus delfsi Mook, 1967	CMNH 8028	Kimmeridgian of United States	CT scan	Smith *et al.* (2008); Dufeau (2011)
Aegisuchus witmeri Holliday & Gardner, 2012	ROM 54530	Cenomanian of Morocco	CT scan	Holliday & Gardner (2012)
Portugalosuchus azenhae Mateus, Puértolas-Pascual & Callapez, 2019	ML1818	Cenomanian of Portugal	CT scan	Puértolas-Pascual *et al*. (2023)
Allodaposuchus hulki Blanco, Fortuny, Vicente Luján, García-Marçà & Sellés, 2015	MCD 5139	Maastrichtian of Spain	CT scan	Blanco *et al*. (2015)
Lohuecosuchus megadontos Narváez, Brochu, Escaso, Pérez-García & Ortega, 2015	HUE-04498	Campanian - Maastrichtian of Spain	CT scan	Serrano-Martínez *et al*. (2019a)
Agaresuchus subjuniperus Puértolas-Pascual, Canudo & Moreno-Azanza, 2013	MPZ 2012/288	Campanian - Maastrichtian of Spain	CT scan	Puértolas-Pascual *et al*. (2022)

Agaresuchus fontisensis Narváez, Brochu, Escaso, Perez-García & Ortega, 2016	HUE-02502	Campanian - Maastrichtian of Spain	CT scan	Serrano-Martínez *et al*. (2020)
Arenysuchus gascabadiolorum Puértolas, Canudo & Cruzado-Caballero, 2011	MPZ 2011/184	Maastrichtian of Spain	CT scan	Puértolas-Pascual *et al*. (2022)
Thoracosaurus isorhynchus Pomel, 1847	Unnumbered	Maastrichtian of Spain	Natural endocast	Lemoine (1883-1884)
Gavialis gangeticus	TMM M5490; AMNH R81802; MLP 602; UF 118998; UMZC R5792; ZIN 7249; YPM HERR 008438; MNHN A-5312; MHNL 50001407; NHMUK 1873, 1846.1.7.3	Extant of India	Sectionned braincase, latex endocast and CT scan	Owen (1850); Wharton (2000); David (2010); Dufeau (2011); Gold *et al*. (2014); Pierce *et al*. (2017); Bona *et al*. (2017); Serrano-Martínez *et al*. (2019a, 2020); Schwab *et al*. (2020, 2021b); Barrios (2021); Kuzmin *et al*. (2021); Bourke *et al*. (2022); Cerio &

				Witmer (2022); Perrichon *et al*. (2023)
Gryposuchus neogaeus Rusconi, 1933	MLP 68-IX-5-1	Miocene of Argentina	CT scan	Bona *et al*. (2017)
Maomingosuchus petrolica Yeh, 1958	IVPP V2303	Eocene of China	Natural endocast	Yeh (1958)
Gunggamarandu maunala Ristevski, Price, Weisbecker & Salisbury, 2021	QMF14.547	Pliocene - Pleistocene of Australia	CT scan	Ristevski *et al*. (2021)
Tomistoma schlegelii	TMM M-6342; ZMMU MSU R-13859, 9296; USNM 211322; UCMP 81702; FMNH 11085, 98874; NHMUK 1893.3.6.14; MZS Cro094; UM1097	Extant of Southeastern Asia	Sectionned braincase and CT scan	Serrano-Martínez *et al*. (2019a, 2020); Schwab *et al*. (2020, 2021b); Kuzmin *et al*. (2021); Cerio & Witmer (2022); Cowgill *et al*. (2022); Perrichon *et al*. (2023)
Tomistoma downsoni Fourtau, 1918	NHMUK PV R 4769	Miocene of Egypt	CT scan	Burke & Mannion (2023)
Paludirex vincenti Ristevski, Yates, Price, Molnar,	CMC2019-010-5	Pliocene - Pleistocene of Australia	CT scan	Ristevski *et al*. (2020)

Weisbecker & Salisbury, 2020				
Trilophosuchus rackami	QMF16856	Miocene of Australia	CT scan	Ristevski (2022)
Crocodylus niloticus	Mostly unnumbered specimens	Extant of Africa	Sectionned braincase and CT scan	Eudes-Deslongchamps (1863); Edinger (1938); David (2010); George & Holliday (2013); Jirak & Janacek (2017); Serrano-Martínez *et al*. (2019a, 2020); Barrios (2021); Schwab *et al*. (2021b); Cerio & Witmer (2022); Perrichon *et al*. (2023)
Crocodylus acutus Cuvier, 1807	Mostly unnumbered specimens	Extant of Africa	Sectionned braincase, latex cast, CT scan	Owen (1850); Colbert (1946b); Gold *et al*. (2014); Jirak & Janacek (2017); Neenan *et al*. (2017); Schwab *et al*. (2020, 2021b); Bronzati *et al*.

				(2021); Cerio & Witmer (2022); Perrichon *et al*. (2023)
Crocodylus halli Murray, Russo, Zorrilla & McMahan, 2019	UF herp 145297	Extant of New Guinea	CT scan	Perrichon *et al*. (2023)
Crocodylus intermedius Graves, 1819	FMNH 75662	Extant of South America	CT scan	Bronzati *et al*. (2021)
Crocodylus johnstoni Krefft, 1873	OUVC 10425, 10426; FMNH 59071; TMM M-6807	Extant of Australia	CT scan	Witmer *et al*. (2008); George & Holliday (2013); Schwab *et al*. (2020, 2021b); Bronzati *et al*. (2021); Cerio & Witmer (2022)
Crocodylus moreletii Dumeril & Bibron, 1851	TMM M-4980; RVC-JRH-FMC3	Extant of Central America	CT scan	Franzosa (2004); David (2010); Schwab *et al*. (2020, 2021b); Bronzati *et al*. (2021); Cerio & Witmer (2022)

Crocodylus siamensis Schneider, 1801	UCBL WB41; MHNL 50001389	Extant of Southeastern Asia	CT scan	Kawabe *et al*. (2009); Perrichon *et al*. (2023)
Crocodylus palustris Lesson, 1831	NMS Z.1968.13.55; MHNL 50001398	Extant of Southeast Asia	CT scan	Schwab *et al*. (2021b); Perrichon *et al*. (2023)
Crocodylus porosus Schneider, 1801	Mostly unnumbered specimens	Extant of Australia	Sectionned braincase and CT scan	Kundrát *et al*. (2018); Bronzati *et al*. (2021); Schwab *et al*. (2021b); Cerio & Witmer (2022); Perrichon *et al*. (2023)
Crocodylus novaeguineae Schmidt, 1928	DVZ M9/13; OUVC 10609	Extant of New Guinea	Sectionned braincase	Kuzmin *et al*. (2021); Cerio & Witmer (2022)
Crocodylus rhombifer Cuvier, 1807	MNB AB50.0171; OUVC 10588 ; MHNL 42006506, 42006507	Extant of Cuba	CT scan	Schwab *et al*. (2020, 2021b); Cerio & Witmer (2022); Cowgill *et al*. (2022); Perrichon *et al*. (2023)
Voay robustus Grandidier & Vaillant,	MNHN.F.1908	Holocene of	CT scan	David (2010)

1872	-5	Madagascar		
Osteolaemus tetraspis	MZB 2006-0039; DVZ M7/13; RVC-JRH-FDC2, FDC3-Se2; FMNH 53632, 98936; UCBL 2019-1-236; MZS Cro040; NHMUK 1862.6.30.5; MHNM 9095.0	Extant of Africa	CT scan	David (2010); Serrano-Martínez *et al*. (2019a, 2020); Schwab *et al*. (2020, 2021b); Kuzmin *et al*. (2021); Cerio & Witmer (2022); Perrichon *et al*. (2023)
Mecistops cataphractus Cuvier, 1825	DVZ M6/13; TMM M-3529; MNHN 1913.0007	Extant of Africa	Sectionned braincase and CT scan	David (2010); Schwab *et al*. (2020, 2021b); Kuzmin *et al*. (2021)
Mecistops sp.	NMS Z.1859.13; UM N89; AMU Zoo-04721; MZS Cro083; MHNL 50001393; SVSTUA 022001	Extant of Africa	CT scan	Schwab *et al*. (2021b) ; Perrichon *et al*. (2023)
Diplocynodon tormis Buscalioni, Sanz & Casanovas, 1992	STUS-344	Eocene of Spain	CT scan	Serrano-Martínez *et al*. (2019b)

Diplocynodon ratelli Pomel, 1847	MNHN.F.SG 557	Miocene – Oligocene of Europe	CT scan	David (2010)
Leidyosuchus Lambe, 1907?	UNM B-401 A	Paleocene of United States	Natural endocast	Storrs *et al*. (1983)
Leidyosuchus canadensis Lambe, 1907	ROM 1903	Campanian of Canada	CT scan	George & Holliday (2013)
Alligator mississippiensis	Mostly unnumbered specimens	Extant of United States	Sectionned braincase, latex cast, and CT scan	Rabl-Rückhard (1878); Lemoine (1883-1884); Edinger (1938); Colbert (1946b); Brochu (1999); Klembara (2005); Witmer & Ridgely (2008); Sereno & Larsson (2009); George & Holliday (2013); Hurlburt *et al*. (2013); Dufeau & Witmer (2015); Porter *et al*. (2016); Fabbri *et al*. (2017); Kundrát *et al*.

				(2018); Serrano-Martínez *et al*. (2019a, 2020); Watanabe *et al*. (2019); Hu *et al*. (2020); Schwab *et al*. (2020, 2021b); Bronzati *et al*. (2021); Kuzmin *et al*. (2021); Cerio & Witmer (2022); Lessner & Holliday (2022); Tahara & Larsson (2022); Perrichon *et al*. (2023)
Alligator sinensis Fauvel, 1879	DVZ M 2/13, 3/13; TCWC 86174	Extant of China	Sectionned braincase	Iordansky (1973); Kuzmin *et al*. (2021); Cerio & Witmer (2022)
Paleosuchus palpebrosus Cuvier, 1807	FMNH 22817, 69867, 69869; OUVC 9602; CMN AR 35747	Extant of South America	Sectionned braincase and CT scan	Dufeau (2011); Bronzati *et al*. (2021); Cerio & Witmer (2022)

Paleosuchus trigonatus Schneider, 1801	AMNH 137175	Extant of South America	CT scan	Balanoff & Bever (2020)
Mourasuchus nativus Bocquentin Villanueva, 1984	MLP 73-IV-15-9	Miocene of South America	CT scan	Bona *et al*. (2013)
Caiman crocodilus	FMNH 73438, 73711; OUVC 9671, 11786; UCMP 42843, 42844, 123, 095; RVC-JRH-FCC1; UMMZ herps 128024, 46112, 155282	Extant of America	CT scan	David (2010); Brusatte *et al*. (2016); Jirak & Janacek (2017); Serrano-Martínez *et al*. (2019a, 2020); Schwab *et al*. (2020, 2021b); Bronzati *et al*. (2021); Kuzmin *et al*. (2021); Cerio & Witmer (2022); Perrichon *et al*. (2023)
Caiman gasparinae Bona & Paulina-Carabajal, 2013	MLP 73-IV-15-1	Miocene of South America	Latex cast	Bona & Paulina-Carabajal (2013)
Caiman latirostris	MACN 1420-7375; MLP 21; UMMZ herps 155283, 155284,	Extant of South America	CT scan	Barrios *et al*. (2023); Perrichon *et al*. (2023)

	155285, 155286, 155287, 155288,			
Caiman yacare Daudin, 1802	MLP 603; MACN-He 43694; ZMMU MSU R-6967; UMMZ herps 155289	Extant of South America	Sectionned braincase, latex cast, and CT scan	Bona & Paulina-Carabajal (2013); von Baczko *et al*. (2018); Barrios (2021); Kuzmin *et al*. (2021) ; Perrichon *et al*. (2023)
Melanosuchus niger Spix, 1825	UFRGS-PV 003-Z; RVC-JRH-FBC1; NMS Z.1859.13.804; MZS Cro073	Extant of South America	CT scan	George & Holliday (2013); Fonseca *et al*. (2020); Schwab *et al*. (2021b); Cerio & Witmer (2022); Perrichon *et al*. (2023)

As part of this thesis, 104 further specimens belonging to various groups of crocodylomorphs and representing different ontogenetic stages were CT scanned, to get as much data as possible on the neuroanatomy of this group and its variations. Those specimens, together with scan information, are detailed in Appendix 7. Those data were completed by the study of 40 specimens scanned in the framework of international collaborations or obtained through open data policies. Those specimens, together with provider information, are detailed in Appendix 8.

I- Nomenclature and links between structures and biological traits

Here, I will detail the different internal structures of the crocodylomorph skull, with corresponding ecological interpretations. Illustrations will mainly be based on an exquisitely preserved extant *Osteolaemus tetraspis* skull (UCBL 2019-1-236; Fig. 3.2-3.6), and 3D models concerning this specimen can be found here: https://mycore.core-cloud.net/index.php/s/SKr8x9TgPOX9qGx

a- Endocast

As in all amniotes (Romer, 1956; Hopson, 1979), the brain (and thus endocast) of crocodylomorphs is divided in three main parts: the forebrain (prosencephalon), the midbrain (mesencephalon) and the hindbrain (rhombencephalon; Fig. 3.2A, 3.3). Those three parts are organized with one another through two corresponding angles: the cephalic flexure angle (anteriorly) and the pontine flexure angle (posteriorly; Fig. 3.3).

The forebrain contains the olfactory bulb and the cerebral hemispheres, which are linked via the olfactory tract (Fig. 3.2A-C, E & F). The soft tissues cerebral hemispheres are separated by a deep groove, which houses the dorsal longitudinal venous sinus, that is integrated in the segmented endocast (and thus not separated or visible) and extends to the nasal cavity anteriorly and the midbrain posteriorly. This tract is compartmentalized dorsally by the internal surface of the frontal, but not ventrally, making its segmentation highly subjective. Its extension and shape are a direct reflection of the morphology of the individual orbital region. Posteriorly, in the posterior part of the forebrain (diencephalon in mature individuals) there is no differentiated organ linked with the parietal eye (photoreceptive pineal complex), contrary to several other reptiles (Gundy & Wurst, 1976; Engbretson, 1992; Tosini, 1997; Firth *et al*., 2010; Smith *et al*., 2018). Ventrally, the hypothalamus also bears a crest, incorporating cranial nerve II (optic), which is included in the endocast during segmentation. A ventral projection, called the pituitary or hypophyseal fossa (Fig. 3.2B, C, E & F), contains the pituitary gland and blood vessels (Porter *et al*., 2016).

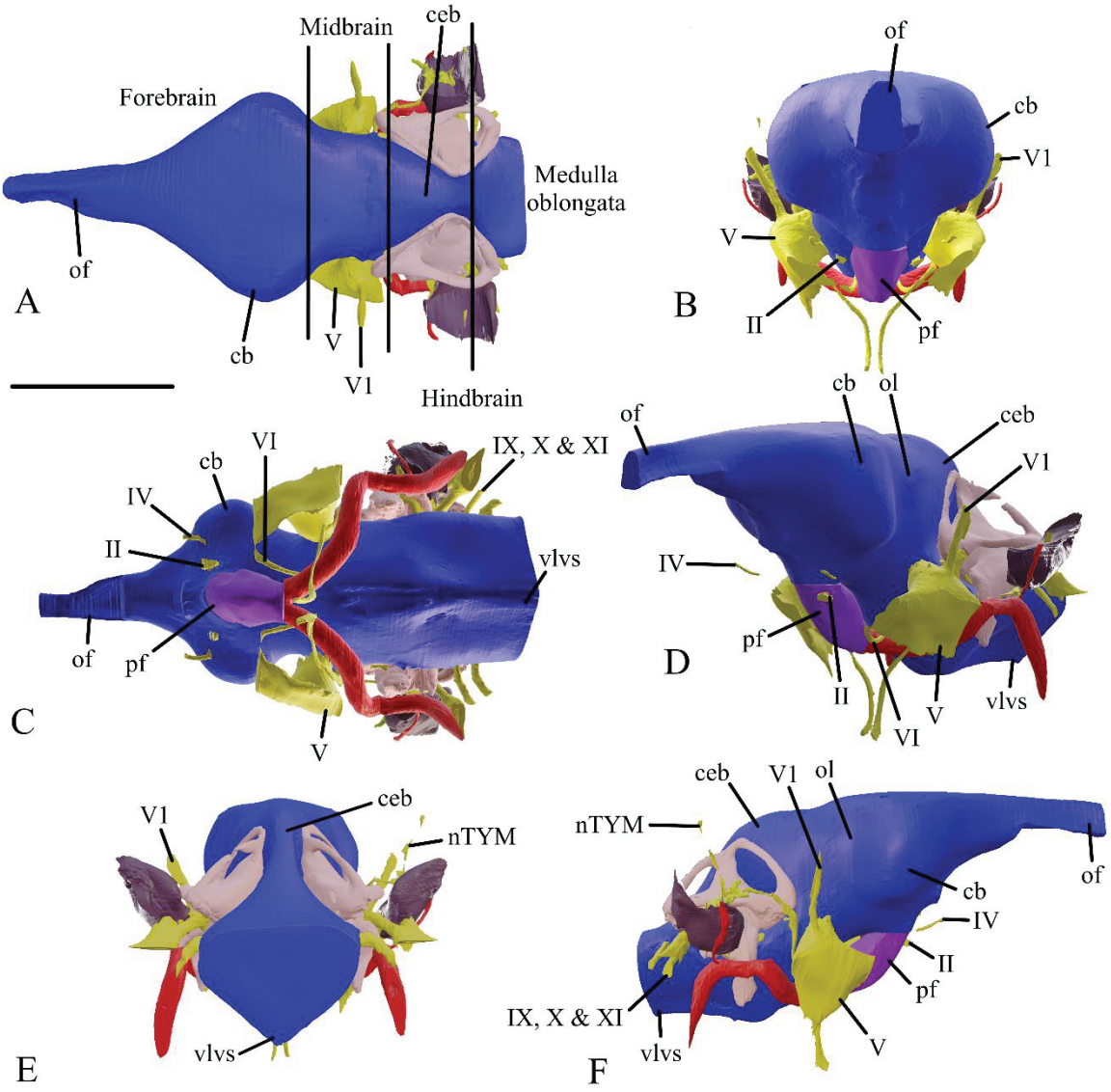

Figure 3.2: Endocast, endosseous labyrinths and cranial nerves and arteries of UCBL 2019-1-236 (*Osteolaemus tetraspis*) in dorsal (A), anterior (B), ventral (C), anterior 3/4 (D), posterior (E) and lateral (F) views. Blue: endocast, yellow: cranial nerves, pink: endosseous labyrinths, dark purple: *recessus scalae tympani*, red: internal carotid arteries, light purple: pituitary fossa. Roman numbers indicate the corresponding number of the cranial nerves. cb: cerebral hemisphere, ceb: cerebellum, nTYM: tympanic branch of the trigeminal ganglion, of: olfactory tract, ol: optic lobe, pf: pituitary fossa, vlvs: ventral longitudinal venous sinus. Scale bar is 2 cm.

The midbrain endocast incorporates the optic lobes associated with the optic tectum for the visual acuity and are usually situated at the ventral flexion of the endocast (Fig. 3.2C & E). The forebrain regroups the cerebellum (metencephalon) and associated otic capsule that houses the endosseous labyrinths and the medulla oblongata (myelencephalon; Fig. 3.2A & C-E). Ventrally, this area also encompasses the ventral longitudinal venous sinus, that is easily recognizable in most taxa (Fig. 3.2).

The endocast is used for several ecological interpretations. First, the olfactory acuity of an individual is measured via its olfactory bulb: indeed, it depends on the number and size of mitral

cells, odours receptors and olfactory receptor genes, which are correlated with the absolute and relative size of the olfactory bulbs (Bang & Cobb, 1968; Healy & Guilford, 1990; Buschhüter *et al*., 2008; Steiger *et al*., 2008; Zelenitsky *et al*., 2009, 2011). Those metrics are obtained by comparing the greatest diameter of the olfactory bulb to the greatest diameter of the cerebrum hemispheres, sometimes normalized by a log transformation, and scaled to body mass (Lautenschlager *et al*., 2012; Serrano-Martínez *et al*., 2020; Müller, 2022; Burke & Mannion, 2023). It is especially interesting in crocodylians, which have a developed sense of smell and use olfaction to navigate, locate food sources and communicate (Scott & Weldon, 1990; Weldon & Ferguson, 1993; Schwenk, 2008). Consequently, a higher ratio (i.e., larger olfactory bulbs), could be considered as an adaptation to greater olfactory acuity in terrestrial environments (Zelenitsky *et al*., 2009, 2011; Barrios *et al*., 2023).

Visual acuity is linked with the size of the eyeball: larger eyes house more photoreceptive and sensorial cells (Hall & Ross, 2006; Schmitz, 2009; Lautenschlager *et al*., 2012) and plays an important role in crocodylian lifestyle (Garrick & Lang, 1977; Nagloo *et al*., 2016). As that is often not preserved in the fossil record, the position of their optic lobes has been proposed as a proxy for visual acuity, in the form of a ratio between the volume of those optic lobes to the total volume of the endocast (Serrano-Martínez *et al*., 2019a, 2020; Puértolas-Pascual *et al*., 2022, 2023; Burke & Mannion, 2023). This proxy would benefit from further studies, as it does not consider body size, ontogeny, or the influence of soft tissues.

The total brain volume has been used as a proxy of cognitive capabilities (Jerison, 1973; Hopson, 1977) using the encephalization quotient: observed brain size is divided by expected brain size for a given body mass using regression equations established on extant representatives (Jerison, 1973; Hurlburt, 1996; Hurlburt *et al*., 2013). In crocodylians, as the regression used was calculated on extant reptiles, it is called the Reptile Encephalization Quotient (REQ). However, the usage of this ratio is problematic for two main reasons: the brain shape changes through ontogeny in extant crocodylians (Hurlburt *et al*., 2013; Jirak & Janacek, 2017; Watanabe *et al*., 2019; see also below) and its use on fossils specimens relies on brain volume and mass estimations, themselves based on body mass estimations (Webb *et al*., 1978; Farlow *et al*., 2005; Platt *et al*., 2011; Cotts *et al*., 2017; O'Brien *et al*., 2019; Serrano-Martínez *et al*., 2019a; Dumont *et al*., 2020b), thus making it highly uncertain.

The endocast could also be interesting to assess phylogenetic relationships, and some characters have been proposed, mainly on birds and dinosaurs (Holtz, 1998; Franzosa, 2004; Smith &

Clarke, 2012; Balanoff *et al*., 2018), mammals (Furusawa, 2004; Macrini, 2006; Macrini *et al*., 2006, 2007a; Pusch *et al*., 2019; Perini *et al*., 2021) and fishes (Poplin, 1984; Coates, 1999). However, the ontogenetic and intraspecific variations of this structure should first be assessed, before using it in a phylogenetic analysis (Macrini *et al*., 2007b; Macrini, 2009; Romick, 2013; Danilo *et al*., 2015; Jirak & Janacek, 2017; Ferreira *et al*., 2021; Kerber *et al*., 2021).

Finally, it is important to assess the relationship between the soft tissues and the structures they are housed in: do these organs completely fill the cavities? Can the remaining shape of the cavities be interpreted as equivalent to the shape of those organs? In the last few years, with the advent of iodine-contrast micro CT approaches that allow visualization of both soft tissues and bone structures (Gignac & Cley, 2014; Clement *et al*., 2015; Porter *et al*., 2016; Jirak & Janacek, 2017; Watanabe *et al*., 2019; Lessner & Holliday, 2022; Holliday *et al*., 2022; Fig. 3.4), those questions are beginning to be answered for several groups of vertebrates, and the results vary from one group to another (Balanoff & Bever, 2020). In some groups of vertebrates, a close endocast-brain relationship has been put forward, such as in mammals (Langston, 1975; Dumoncel *et al*., 2020), birds (Iwaniuk & Nelson, 2002; Early *et al*., 2020a, b) and dinosaurs (Osmólka, 2004; Evans, 2005), whereas it is not so evident in amphibians (Kim & Evans, 2014; Clement *et al*., 2021; Allemand *et al*., 2022) and lungfishes (Clement *et al*., 2015, 2021).

Jirak & Janacek (2017) showed that the endocast/brain volume relationship was not constant throughout ontogeny in crocodylians, with the brain representing only 30% of the endocast volume in larger individuals. However, this study was led on numerous taxa, each with a different ontogenetic stage, introducing an important taxonomic bias. In other studies (Hurlburt *et al*., 2013; Hu *et al*., 2020), this bias was corrected, and the results confirmed. However, in Watanabe *et al*., 2019, the same topic was assessed but a strong correlation between endocast and brain shape was found on different ontogenetic stages of the same taxon. Paleobiological interpretations on endocast shape in crocodylomorphs should thus be made with extreme caution (Fig. 3.3). Information on the relationships of other structures and the organs that are housed in them are also still needed, such as for the endosseous labyrinths, the pneumatic system of crocodylians or the cranial nerves and arteries.

b- <u>Cranial nerves</u>

Some cranial nerves in crocodylomorphs are easily identifiable because they are conservatively associated with external foramina. However, those structures are especially hard to segment in crocodylomorphs because most are not compartmentalized individually or at all. They are

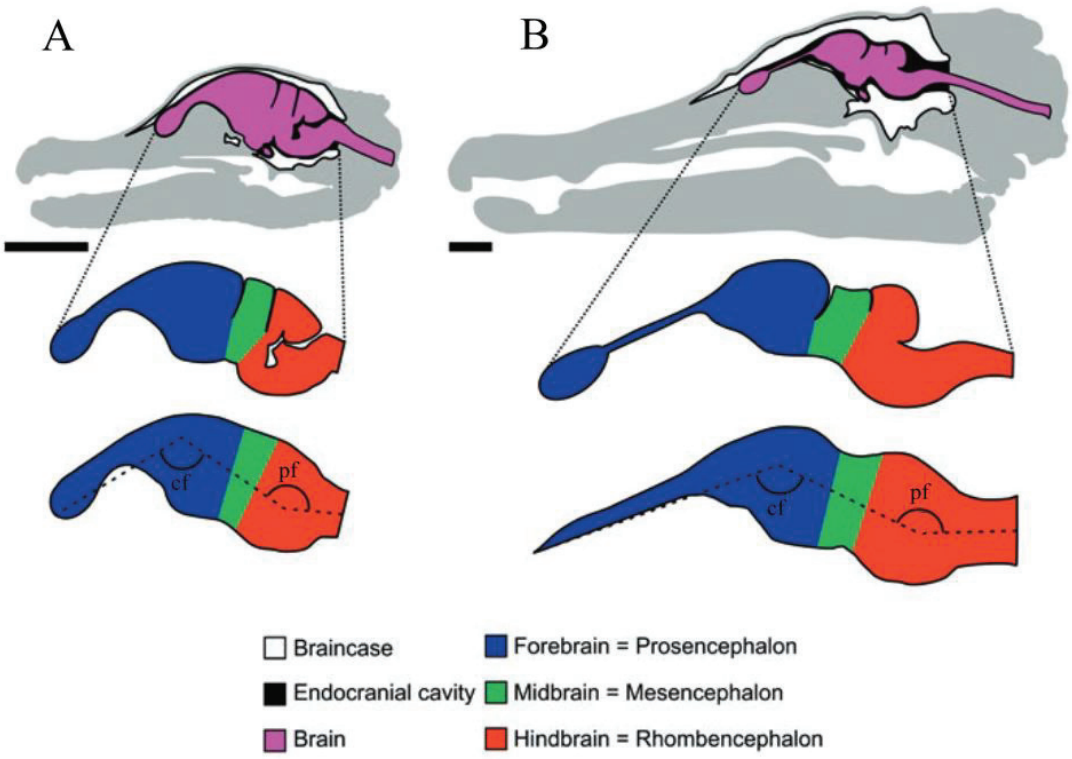

Figure 3.3: Sagittal slices through *Alligator mississippiensis* heads in perinatal (A) and juvenile (B) ontogenetic stages. cf: cephalic flexure angle, pf: pontine flexure angle. Scale bars are 1 cm. Modified from Barrios *et al*. (2023, fig. 7.3).

numerated with roman letters from I to XII (Fig. 3.5). A recent review of those structures in Crocodylia was recently published by Lessner & Holliday (2020) and will be summarized here.

Cranial nerve I (olfactory) transmits sensory signals via stimuli transmitted from the nasal cavity to the olfactory bulbs (Hansen, 2007; Fig. 3.5). Cranial nerve II (optic) transmits visual signals from the eye to the midline of the telencephalon (midbrain; Fig. 3.2B-D, F & 3.5). This nerve elongates during ontogeny because of the lengthening of the skull and the rostral displacement of the orbits. Cranial nerve III (oculomotor; Fig. 3.5) transmits motor signals from the ciliary ganglion, which controls the movement of the eye to the midbrain. Cranial nerve IV (trochlear) is also a motor nerve from the *m. obliquus dorsalis*, associated with the movement of the eye as well, to the midbrain (Fig. 3.2C, D, F & 3.5). Cranial nerve V (trigeminal) is the largest in the crocodylomorph skull and has been the most extensively surveyed (George & Holliday, 2013; Lessner & Holliday, 2020; Lessner *et al*., 2022, 2023; Fig. 3.2A-D, F & 3.5). It has several functions: from the common trigeminal fossa housing the trigeminal ganglion, the ophthalmic division (V_1; Fig. 3.2A, B & D-F) extends anteriorly to connect with the rostral integument (sensory receptors); while the maxillary (V_2) and mandibular (V_3) divisions extend

laterally and anteriorly to innervate sensory receptors in the maxillary alveoli, jugal, nasal and palatine, and the muscles responsible for the articulation of the mandible (*m. adductor mandibulae externus profondus & medialis*, *m. adductor mandibulae posterior*, *m. pseudotemporalis superficialis*, *m. pterygoideyus dorsalis & ventralis* and *m. intermandibularis*) respectively. This nerve has a high growth rate and follows an allometric trajectory during ontogeny (Lessner *et al*., 2022). Cranial nerve VI (abducens; Fig. 3.2C, D & 31) is a motor nerve involved in eye movement and closure of the associated nictitating membrane to protect and moisten this organ (Stibbe, 1928) that connects from the posterior limit of the pituitary fossa to the *m. lateral rectus* and the *m. quadratus.* This nerve also lengthens during ontogeny as the skull grows. Cranial nerve VII (facial; Fig. 3.5) transmits motor and sensory signals to the midbrain through two divisions: the palatine division that reaches the palatine, and the hyomandibular division that innervates muscles associated with the lower jaw and the neck (*m. depressor mandibulae* and *m. constrictor colli profundus*; Fig. 3.2E & F). Cranial nerve VIII (vestibulocochlear) is associated with the ampullae of the semicircular canals (see below) through sensory signals. It originates from the midbrain (Fig. 3.5). It decreases in size throughout ontogeny as the ear complex increases. Cranial nerve IX (glossopharyngeal) originates from the hindbrain and transmits both motor and sensory signals to muscles associated with hyal and branchial structures (*m. branchiohyodieus dorsalis & ventralis*; Li & Clarke, 2015; Fig. 3.2C, F & 3.5). The path of this nerve becomes increasingly tortuous throughout ontogeny. Cranial nerve X (vagus) transmits motor and sensory signals from the pharynx and the thorax musculature to the hindbrain (*m. constrictor larynges*, *m. cricoarytenoid*; Li & Clarke, 2015; Riede *et al*., 2015; Fig. 3.2C, F & 3.5). Like cranial nerve IX, this nerve becomes increasingly tortuous throughout ontogeny. Cranial nerve XI (accessory) is particular because it is involved in both cranial and cervical musculatures (Benninger & McNeill, 2010; Fig. 3.2C, F & 3.5). Finally, cranial nerve XII (hypoglossal) transmits motor signals from the hindbrain to the tongue and palate region (Fig. 3.2C, F & 3.5) via the *m. hyoglossus*, *m. genioglossus*, *m. geniohyoideus* and *m. episternobranchiotendineus* (Li & Clarke, 2015). Like cranial nerve IX and X, this nerve becomes increasingly tortuous throughout ontogeny.

The autonomic system is represented by two nerves, the sympathetic and the parasympathetic one. The sympathetic nerve innervates the same musculature as the maxillary and mandibular divisions of cranial nerve V and the parasympathetic nerve innervates the ciliary and sphincter

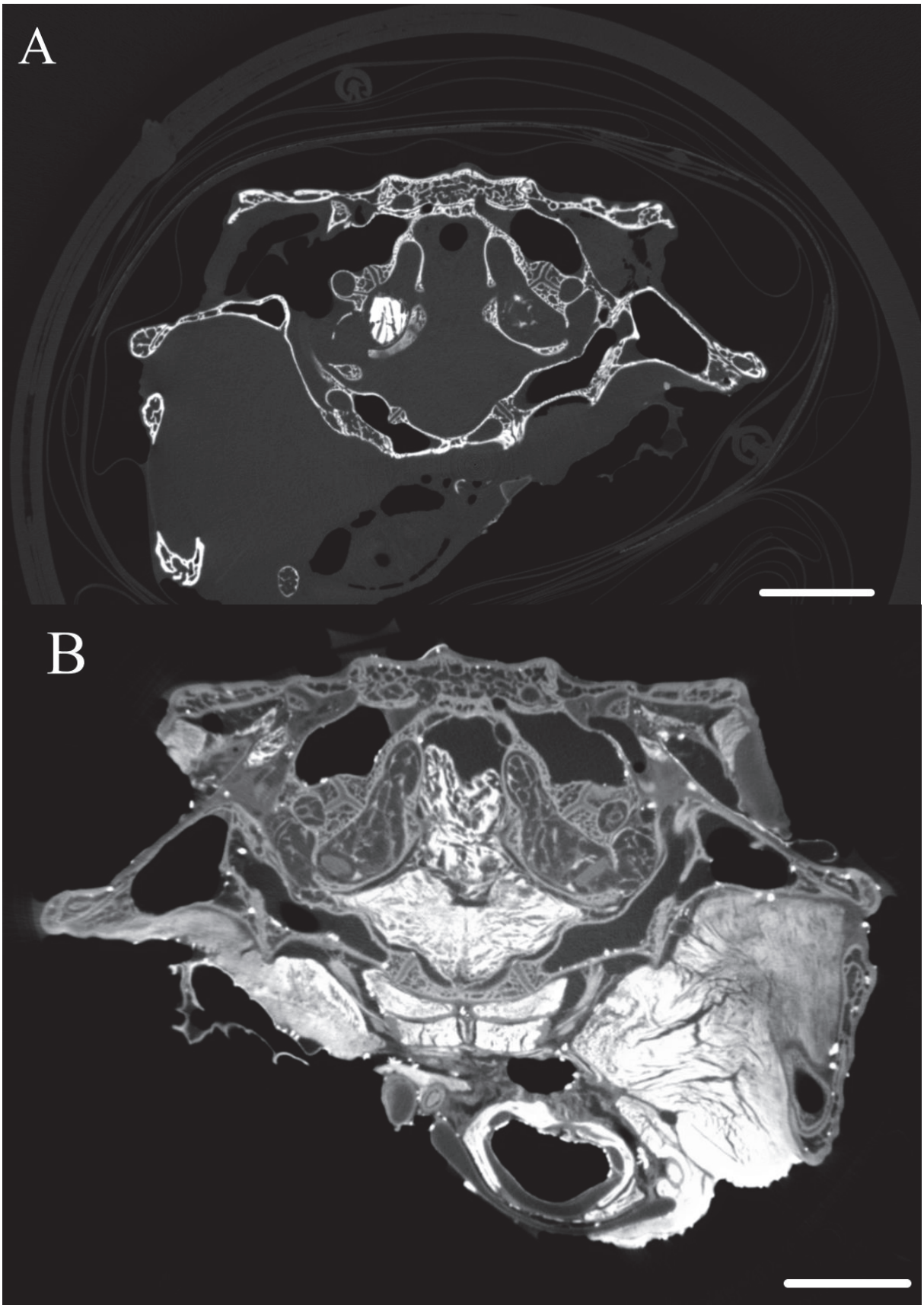

Figure 3.4: Transverse views of the same specimen (*Caiman crocodilus* UM unnumbered) using different CT scan techniques: traditional CT scan (A) and iodine-contrast CT scan (B). Scale bar are 1 cm.

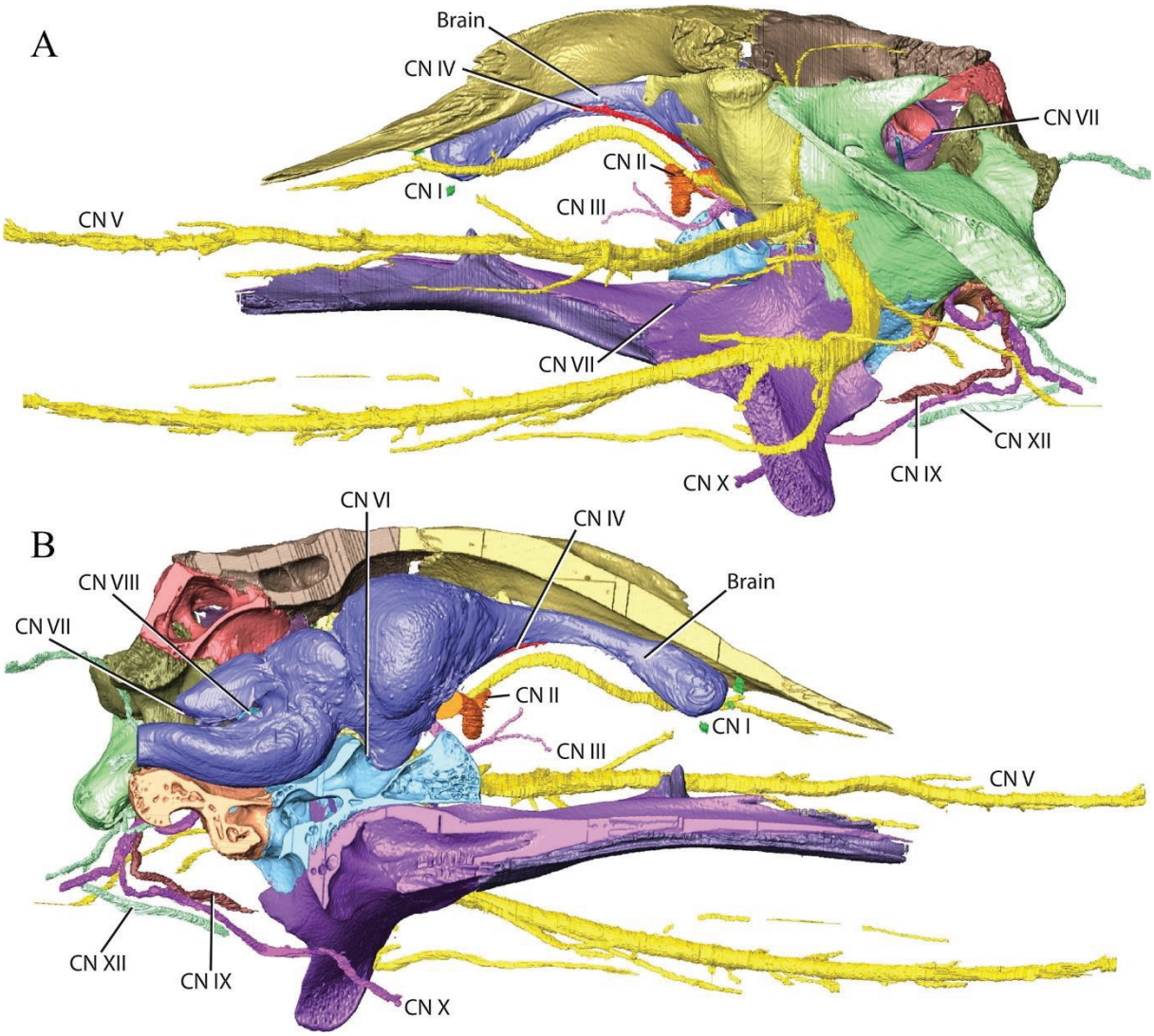

Figure 3.5: Cranial nerves, brain, and surrounding braincase bones of *Alligator mississippiensis* (MUVC AL623, 301) in lateral (A) and medial (B) views. Modified from Lessner & Holliday (2020, fig. 8).

muscles of the eyes, the orbital glands and the mucosa of the nasal cavity and palate (Bellairs & Shute, 1953). Those systems are unfortunately undistinguishable during segmentation.

In terms of ecological interpretations, only cranial nerve V has been used so far, to estimate the sensory abilities of the rostrum in extant and extinct crocodylomorphs. This could also be explained because the cranial nerves are one of the smallest internal structures and are thus difficult to segment or are often not preserved. The trigeminal fossa size was not found to be correlated with the skull length or endocast volume in a large sample of crocodylomorphs (George & Holliday, 2013), hinting at its possible ecological and/or phylogenetical signal. However, this was not the case in an ontogenetic series of *Alligator mississippiensis* (Lessner *et al*., 2022), which calls for caution when interpreting this structure. Nevertheless, as the development of integumentary sensory organs (ISO) is linked with adaptations to the aquatic

environment (Soares, 2002; Leitch & Catania, 2012; Di-Poï & Milinkovitch, 2013; Grap *et al*., 2020), it has been used recently for extinct crocodylomorphs as a proxy for lifestyle (Bowman *et al*., 2021; Lessner *et al*., 2023). Estimations can be obtained via the use of log transformed relations between the trigeminal fossa volume and the maxillomandibular foramen maximum diameter on one hand and the facial sensitivity and axon number on the other hand (George & Holliday, 2013) but are also subject to caution (Dumont *et al*., 2020b).

c- Inner ear

The inner ear (or endosseous labyrinth) consists of two main parts (Ekdale, 2016a; Fig. 3.6). The first one, the vestibular apparatus, is formed by three connected semicircular canals (anterior, posterior, and lateral; Highstein *et al*., 2004). The second one is the posteroventrally projected and tubular lagena (or cochlear duct; Manley, 2017). Those two structures are respectively innervated by the vestibular and cochlear divisions of cranial nerve VIII (Lessner & Holliday, 2020).

Those two structures are also linked with two different functions: the vestibular apparatus is linked with equilibrium, spatial position, and linear and angular acceleration, while the cochlear duct is linked with sound perception (Georgi, 2008). The sensory epithelia of those organs can be divided in two types: the maculae, which detect linear motions (including head orientation) and the cristae, which detect rotational motions. Those organs follow this principle: hair cells are deflected from the motion of the surrounding endolymphatic liquid (Ifediba *et al*., 2007; Georgi, 2008).

The soft tissues of the inner ear are only preserved through the endosseous labyrinths and, fortunately, their shape is very close (Curthoys & Oman, 1986, 1987) which makes their study in extinct organisms especially interesting. Furthermore, intraspecific variation seems to be limited (Welker *et al*., 2009; Schellhorn, 2017; Cerio & Witmer, 2019), but this need to be confirmed, as opposite results have also been found (Ekdale & Rowe, 2011; Perier *et al*., 2016; Gonzales *et al*., 2018). Likewise, ontogenetic variation has been observed in crocodylians (Schwab *et al*., 2021b), but not in mammals (Ekdale, 2009, 2010; Mennecart & Costeur, 2016 but see Alloing-Séguier *et al*., 2013).

As a result, estimations of the hearing capabilities of extinct organisms are possible, through regressed data on extant representatives (Gleich *et al*., 2005; Walsh *et al*., 2009). Coupled with the alignment of the maxillary toothrow (Marugán-Lobon *et al*., 2013) and the endocranial

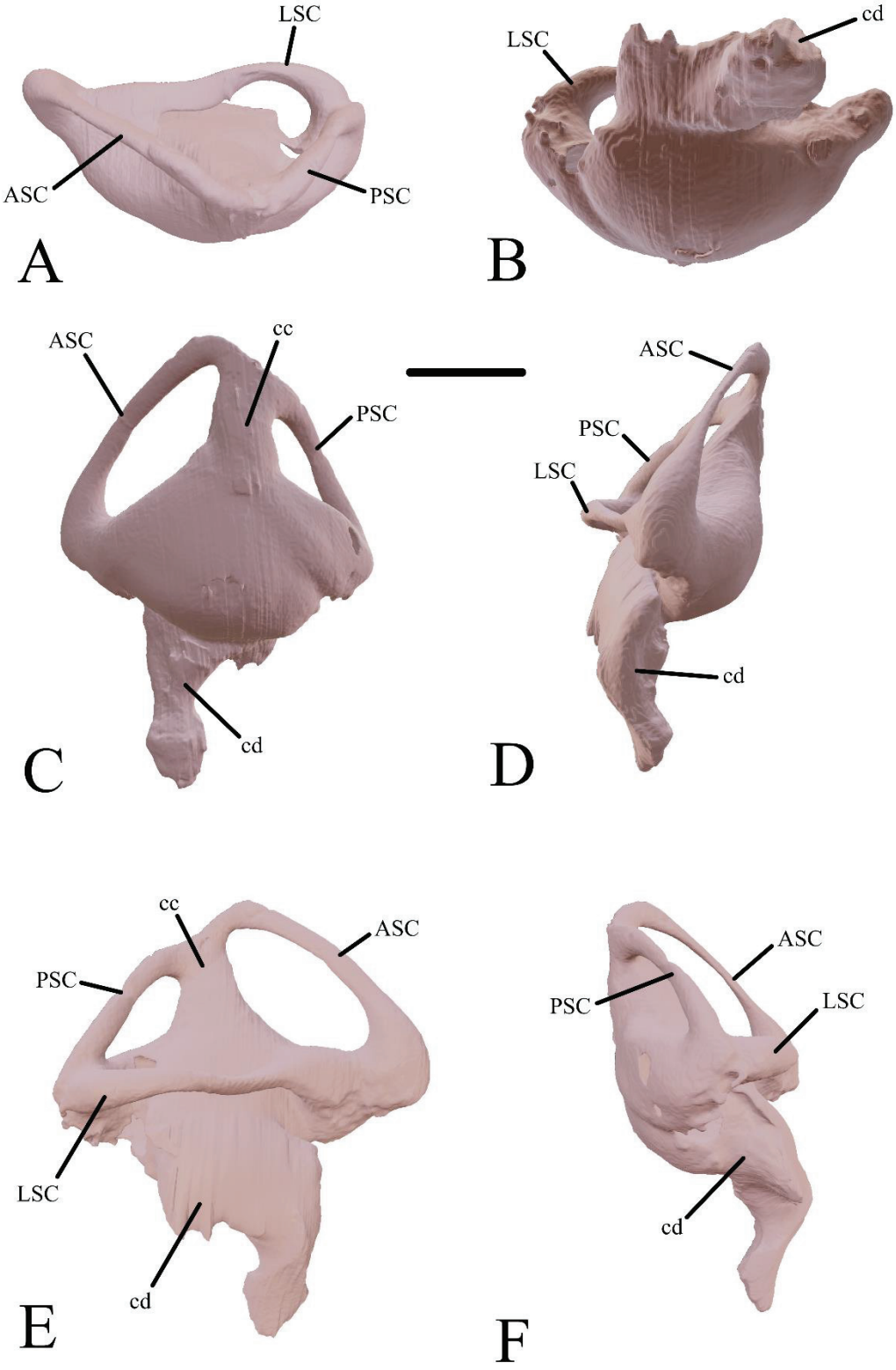

Figure 3.6: Right endosseous labyrinth of UCBL 2019-1-236 (*Osteolaemus tetraspis*) in dorsal (A), ventral (B), medial (C), anterior (D), lateral (E) and posterior (F) views. ASC: anterior semicircular canal, cc: common crus, cd: cochlear duct, LSC: lateral semicircular canal, PSC: posterior semicircular canal. Scale bar is 1 cm.

surface of the parietal (Kley *et al*., 2010; von Baczko *et al*., 2018) with the horizontal plane, the orientation of the lateral semicircular canal with the horizontal allows to estimate the alert head posture of an organism (Erichsen *et al*., 1989; Witmer *et al*., 2003, 2008; Hullar, 2006; Sampson & Witmer, 2007; Sereno *et al*., 2007; Witmer & Ridgely, 2008). The size of the anterior semicircular canal is also correlated with head mass (Georgi *et al*., 2013). Different morphologies of the inner ear have been found to be linked with different behaviours and locomotions (Hullar, 2006; Sipla, 2007; Grohé *et al*., 2015; Neenan *et al*., 2017; Palci *et al*., 2017; Costeur *et al*., 2018; Hanson *et al*., 2021, but see David *et al*., 2022 and Hanson *et al*., 2022) but also with phylogenetic relationships (Geisler & Luo, 1996; Fox & Meng, 1997; David, 2010; Maddin & Anderson, 2012; Alloing-Séguier *et al*., 2013; Billet *et al*., 2015; Ekdale, 2016b; Grohé *et al*., 2016; Palci *et al*., 2017; Costeur *et al*., 2018; Ladevèze *et al*., 2020; Tambusso *et al*., 2021). Recently, however this paradigm has begun to shift with independent studies finding no links between inner ears morphology and ecology or phylogeny (Foth *et al*., 2019; Evers *et al*., 2022; Latimer *et al*., 2023). In crocodylomorphs, Schwab *et al*. (2020) proposed that inner ear morphology is linked to lifestyle, with significant differences between aquatic and terrestrial forms. However, their analysis was contested by Bronzati *et al*. (2021), which rather argue that variations in inner ears morphology are explained by spatial constraints. A definitive answer must thus still be reached.

It has also been proposed that those difference in morphologies could be linked to body temperature, because this parameter has a direct effect on the viscosity of the endolymphatic liquid (Araújo *et al*., 2022), although this also needs to be confirmed.

Finally, a recent study (Schwab *et al*., 2022) showed that crocodylians possess otoliths that can sometimes be segmented (as in most other vertebrates; Carlström, 1963). This preliminary study highlights that those structures are strongly influenced by ontogeny but could also be interesting in terms of ecological and phylogenetic interpretations.

d- Cranial pneumaticity

The braincase sinuses of crocodylomorphs are very developed and unique to this clade (Kuzmin *et al*., 2021; Kuzmin, 2022b; Perrichon *et al*., 2023). They consist of diverticula (epithelial soft-tissue filled with air) which are preserved as recesses in the surrounding bones. The braincase pneumaticity can be subdivided into two main structures: the intertympanic sinus system, which occupies the dorsal part of the braincase, and the paratympanic sinus system, which is situated laterally and ventrally (Colbert, 1946b; Walker, 1990; Wu & Chatterjee, 1993; Dufeau &

Witmer, 2015; Brusatte *et al*., 2016; Pierce *et al*., 2017; Herrera *et al*., 2018; Leardi *et al*., 2020b; Kuzmin *et al*., 2021; Perrichon *et al*., 2023; Fig. 3.7). The intertympanic pneumatic recess carves the prootic and the supraoccipital and connects each pharyngotympanic cavity through the perilymphatic loop of the prootic. The intertympanic recess is also connected anterodorsally with the parietal pneumatic recess (absent in UCBL 2019-1-236; Fig. 3.8) and posteroventrally with the otoccipital pneumatic recess via two pairs of opening (Fig. 3.7A, 3.7E, 3.7F & 3.8). This last recess is connected ventrally to the rhomboidal recess, which is the ventral part of the paratympanic sinus system (Fig. 3.7B, 3.7D & 3.7F). The connections between the intertympanic pneumatic recess and the parietal pneumatic recess are situated at the level of the supraoccipital-parietal suture, and their number and size vary depending on the taxon (Perrichon *et al*., 2023; Fig. 3.8). On most of them, there is an anterolateral one and the parietal recess is connected with the intertympanic pneumatic recess through several foramina and posteromedial pair of openings (anterolateral and posteromedial pre-parietal processes respectively; Fig. 3.8). Throughout ontogeny, the intertympanic pneumatic recess inflates dorsoventrally, the communications between the intertympanic and the pharyngotympanic sinus systems diminish and the intertympanic recess becomes indiscernible from the otoccipital recess (Perrichon *et al*., 2023).

The pharyngotympanic sinus system comprises several structures and is connected to the pharynx via the pharyngotympanic tubes (Fig. 3.7B-F). The basioccipital recess (Fig. 3.7C & 3.7E) has two lateral cavities that connect with the main pharyngotympanic cavity (rhomboidal recess) and a central connection with its counterpart. The *recessus epitubaricus* is at the base of the main pharyngotympanic cavity, anteriorly to the rhomboidal recess (Fig. 3.7B-D & 3.7F). Anteriorly, there are the laterosphenoid and prootic recesses (Fig. 3.7A, 3.7B, 3.7D & 3.7F). The infundibular and quadrate recesses invade the quadrate (Fig. 3.7) and become separated during ontogeny (Kuzmin *et al*., 2021). From this region, the siphonium (Fig. 3.7B-F) extends posteriorly in the quadrate diverticulum (Brochu, 1999; Dufeau & Witmer, 2015) and even connects to the pneumatic recess within the articular when the mandible is in connection (Dufeau & Witmer, 2015). Ventrally, there is the median pharyngeal recess (Fig. 3.7B) which can be subdivided in a median canal, opening ventrally through the median pharyngeal (or Eustachian) foramen, and two lateral parabasisphenoid recesses (also named Eustachian tubes; Fig. 3.7B-F). This region becomes verticalized during ontogeny and is thus an important marker of ontogenetic status (Gold *et al*., 2014; Dufeau & Witmer, 2015). The pharyngotympanic sinus system and median pharyngeal sinus are interconnected to allow pressure equalization between

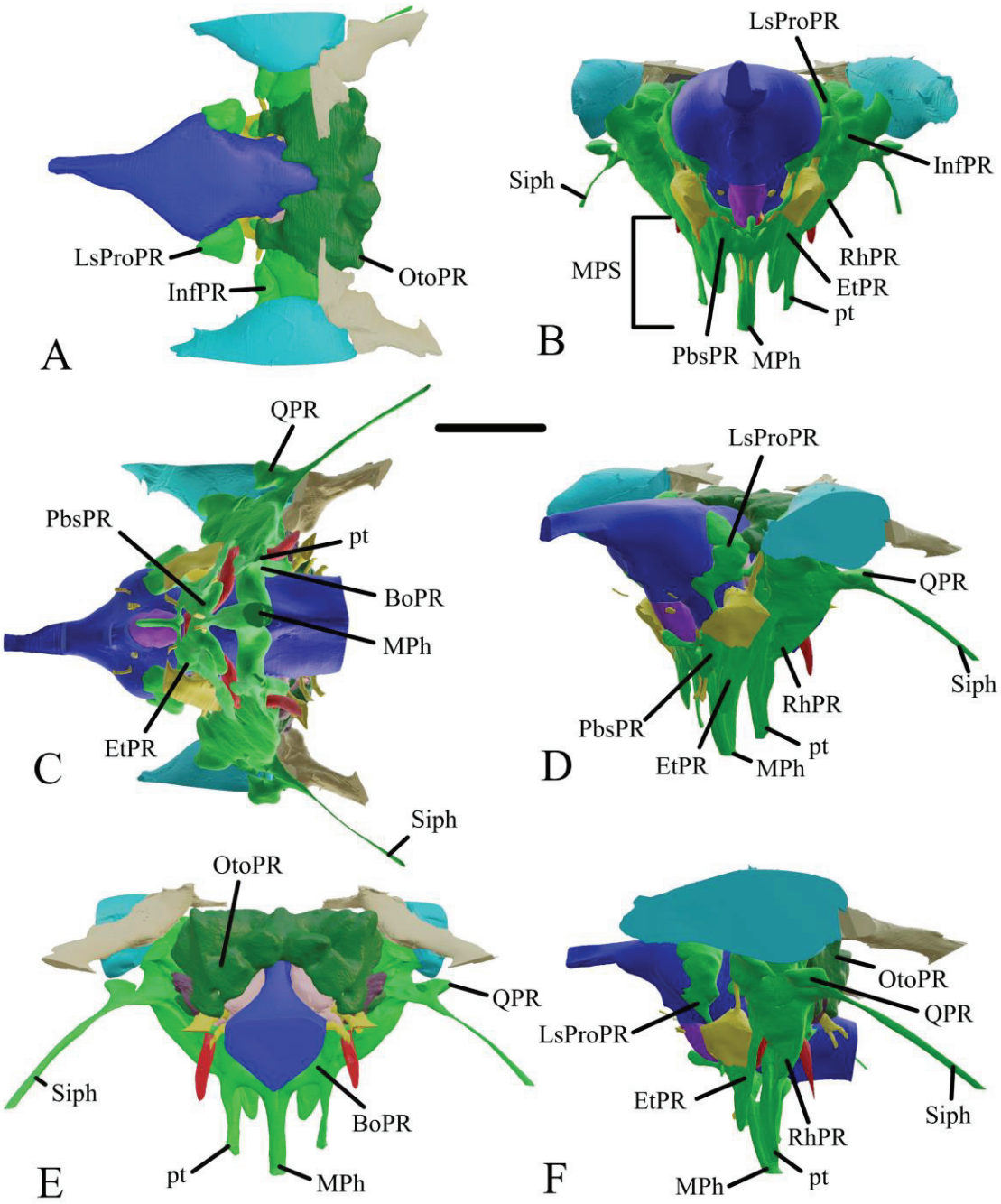

Figure 3.7: Endocast, endosseous labyrinths, cranial nerves and arteries and pneumatic cavities of UCBL 2019-1-236 (*Osteolaemus tetraspis*) in dorsal (A), anterior (B), ventral (C), anterior 3/4 (D), posterior (E) and lateral (F) views. Blue: endocast, yellow: cranial nerves, pink: endosseous labyrinths, dark purple: *recessus scalae tympani*, red: internal carotid arteries, light purple: pituitary fossa, light green: paratympanic sinus system, dark green: intertympanic sinus system, turquoise: meatal chamber, beige: cranioquadrate passages. BoPR: basioccipital pneumatic recess, EtPR: *recessus epitubaricus*, InfPR: infundibular pneumatic recess, LsProPR: laterosphenoid and prootic pneumatic recess, MPh: median pharyngeal canal, OtoPR: otoccipital pneumatic recess, PbsPR: parabasisphenoid pneumatic recess, pt: pharyngotympanic tubes, QPR: quadrate pneumatic recess, RhPR: rhomboidal pneumatic recess, Siph: siphonium. Scale bar is 2 cm.

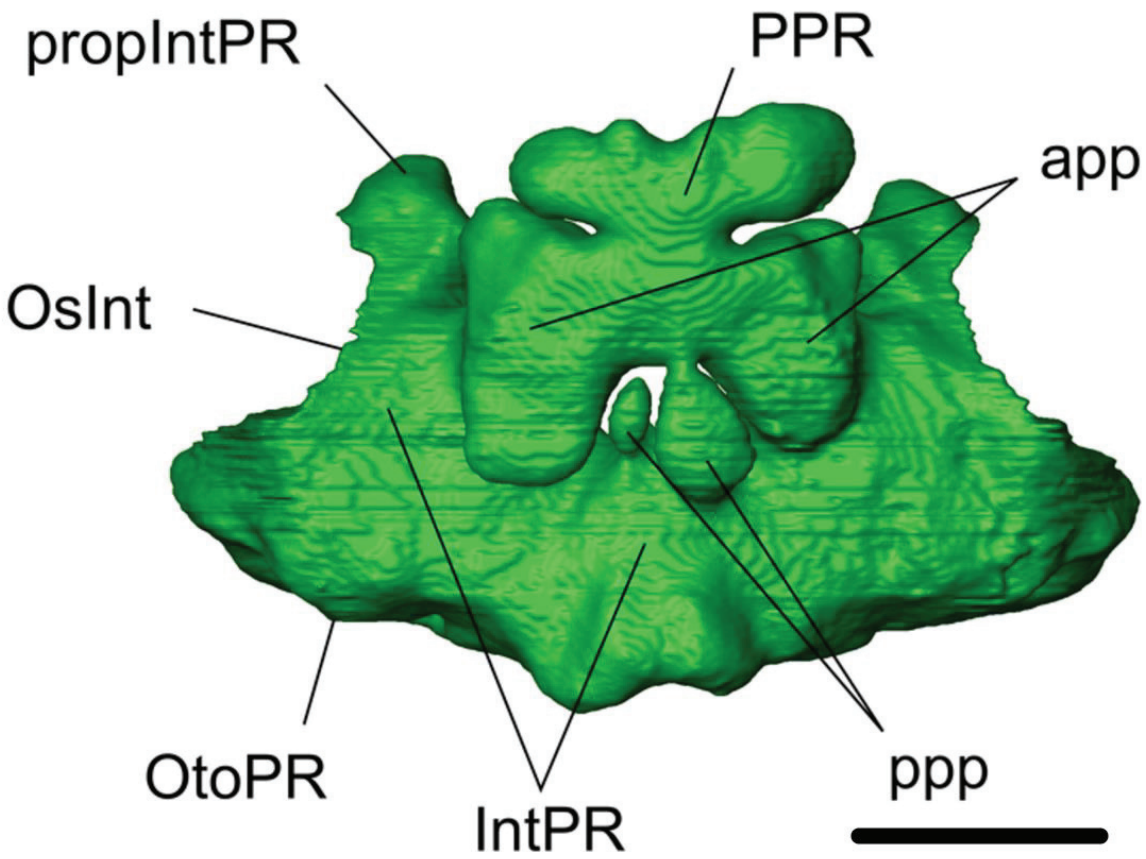

Figure 3.8: Intertympanic sinus system of *Osteolaemus tetraspis* (MHNM 9095.0) in dorsal view, homologous to the one of UCBL 2019-1-236 in Fig. 3.7 but with a parietal recess. app: anterolateral pre-parietal process, IntPR: intertympanic pneumatic recess, OsInt: ostium between the intertympanic recess and the middle ear, OtoPR: otoccipital pneumatic recess, ppp: posteromedial pre-parietal recess, PPR: parietal pneumatic recess, propIntPR: prootic part of the intertympanic pneumatic recess. Scale bar is 1 cm. Taken from Perrichon *et al.* (2023, fig. 1d).

the pharynx, the middle ear, and the environment (Colbert, 1946b; Dufeau & Witmer, 2015) through the median pharyngeal valve (Young & Bierman, 2019). Finally, the middle ear cavity (meatal chamber (Fig. 3.7) transmits the sound from the environment to the inner ear via the columella (soft tissue; Goldby, 1925) and could also allow improve resonance and sound pickup (Dufeau & Witmer, 2015). The cranioquadrate passages are part of the quadrate diverticulum (Fig. 3.7) and constitute an important character in crocodylomorph phylogenetic matrices (see Rio & Mannion, 2021 and Nicholl *et al*., 2021 for the latest versions).

Anteriorly, the rostrum houses the nasal cavity, which can be subdivided into three main parts (Fig. 3.9): the vestibule; the nasal cavity itself and the nasopharyngeal ducts (Parsons, 1970); as well as several paranasal sinuses (Witmer, 1995, 1997).

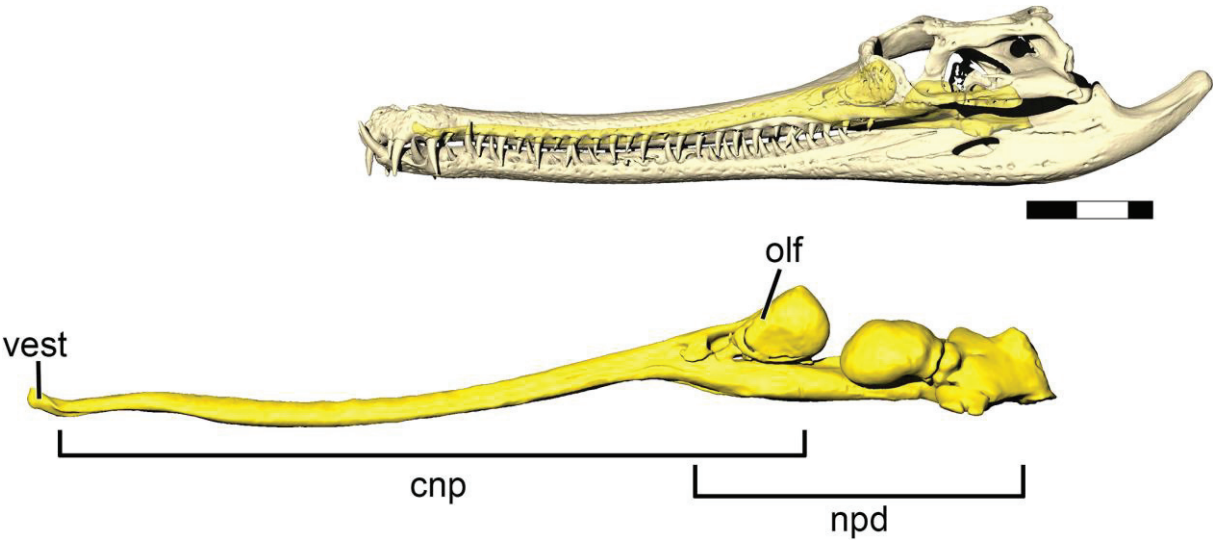

Figure 3.9: Nasal pneumaticity of *Gavialis gangeticus* (SA91285) in sagittal view. cnp: *cavum nasi proprium* (nasal cavity), npd: nasopharyngeal duct, olf: olfactory recess, vest: nasal vestibule. Scale bar is 10 cm. Modified from Bourke *et al*., (222, fig. 1).

It has been observed that the braincase pneumaticity is differently expanded between putative terrestrial crocodylomorphs (Fonseca *et al*., 2020), extant semi-aquatic crocodylians (Witmer *et al*., 2008; Bona *et al*., 2017; Serrano-Martinez *et al*., 2019b) and fully aquatic forms such as thalattosuchians (Brusatte *et al*., 2016; Pierce *et al*., 2017; Herrera *et al*., 2018; Schwab *et al*., 2021a; Wilberg *et al*., 2021). As such, those structures could be related to the living environment (Dufeau & Witmer, 2015) but this hypothesis must be further confirmed. Brusatte *et al*. (2016) proposed that the pneumaticity of the skull could be linked to buoyancy and density matters for semi-aquatic and aquatic forms, which can in fact be coupled with the lifestyle hypothesis. Finally, Dufeau & Witmer (2015) also proposed that the shape of the skull has an impact on the development of these structures, with less available space in longirostral forms compared with altirostral forms.

The nasal pneumaticity has been extensively studied, especially in thalattosuchians, because it houses the salt glands associated with a marine environment (Witmer, 1995, 1997; Fernández & Gasparini, 2000, 2008; Fernández & Herrera, 2009, 2022), which are also present in some extant crocodylians (Taplin & Griggs, 1981; Jackson *et al*., 1996). Furthermore, evidence of an active airflow in the paranasal sinuses of those aquatic fossil forms might be related to the salt glands, with pump actions of musculature draining them (Fernández & Herrera, 2022) or thermoregulation abilities (Cowgill *et al*., 2022; Young *et al*., 2023) although it could also be associated with acoustics, as in the extant gharial (Bourke *et al*., 2022).

Phylogenetically, the braincase pneumaticity could bear interesting characters, such as the presence or absence of the laterosphenoid, prootic and pterygoid recess throughout ontogeny,

the number of communications between the parietal and intertympanic recesses, the presence or absence of a connection between the infundibular and quadrate recesses throughout ontogeny, or the overall shape of those structures (Kuzmin *et al*., 2021; Kuzmin, 2022b; Perrichon *et al*., 2023) but those characters remain to be tested in a broad phylogenetic framework.

Throughout this chapter, the neuroanatomy of several specimens representatives of different clades of putative terrestrial altirostral crocodylomorphs will be studied to better infer their ecology and enrich current knowledge about crocodylomorph paleoneuroanatomy. Furthermore, I will propose an in-depth geometric morphometric study of the endosseous labyrinths using the extensive dataset presented in Appendices 7 & 8 to assess the ontogenetic, ecological, and phylogenetical signals of this structure in crocodylomorphs.

II- Scientific publication: 'The neuroanatomy of *Zulmasuchus querejazus* (Crocodylomorpha, Sebecidae) and its implications for the paleoecology of sebecosuchians'

This publication was first published in November 2021 in *The Anatomical Record*. Reference: Pochat-Cottilloux Y., Martin J. E., Jouve S., Perrichon G., Adrien J., Salaviale C., Muizon C. d., Cespedes R. & Amiot R. (2021). The neuroanatomy of *Zulmasuchus querejazus* (Crocodylomorpha, Sebecidae) and its implications for the paleoecology of sebecosuchians. *The Anatomical Record*, 305(10): 2708-2728. https://doi.org/10.1002/ar.24826

The neuroanatomy of *Zulmasuchus querejazus* (Crocodylomorpha, Sebecidae) and its implications for the paleoecology of sebecosuchians

Yohan Pochat-Cottilloux [A], Jeremy E. Martin [A], Stéphane Jouve [B], Gwendal Perrichon [A], Jérome Adrien [C], Céline Salaviale [A], Christian de Muizon[D], Ricardo Cespedes[E], Romain Amiot[A]

A: Univ Lyon, Univ Lyon 1, ENSL, CNRS, LGL-TPE, F-69622, Villeurbanne, France

B: Centre de Recherche en Paléontologie – Paris (CR2P), Sorbonne Université, 4 Place Jussieu, 75005, Paris, France.

C: Laboratoire Matériaux, Ingénierie et Science, Institut National des Sciences Appliquées de Lyon, 20 Avenue Albert Einstein, 69100 Villeurbanne, France.

D : Centre de Recherche en Paléontologie – Paris (CR2P), Muséum National d'Histoire Naturelle, CNRS/MNHN/Sorbonne Université, CP38, 57 rue Cuvier, F-75231 Paris cedex 05, France.

E: Museo de Historia Natural 'Alcide D'Orbigny', Cochabamba, Bolivia

Corresponding author: Yohan Pochat-Cottilloux, yohan.pochat-cottilloux@univ-lyon1.fr

Abstract

The endocranial structures of the sebecid crocodylomorph *Zulmasuchus querejazus* (MHNC 6672) from the Lower Paleocene of Bolivia are described in this manuscript. Using computed tomography scanning, the cranial endocast, associated nerves and arteries, endosseous labyrinths and cranial pneumatization are reconstructed and compared with those of extant and fossil crocodylomorphs, representative of different ecomorphological adaptations. *Zulmasuchus querejazus* exhibits an unusual flexure of the brain, pericerebral spines, semicircular canals with a narrow diameter, as well as enlarged pharyngotympanic sinuses. First, those structures allow to estimate the alert head posture and hearing capabilities of *Zulmasuchus.* Then, functional comparisons are proposed between this purportedly terrestrial taxon, semi-aquatic and aquatic forms (extant crocodylians, thalattosuchians and dyrosaurids). The narrow diameter of the semicircular canals but expanded morphology of the endosseous labyrinths and the enlarged pneumatization of the skull compared to other forms indeed tend to

indicate a terrestrial lifestyle for *Zulmasuchus*. Our results highlight the need to gather new data, especially from altirostral forms in order to further our understanding of the evolution of endocranial structures in crocodylomorphs with different ecomorphological adaptations.

Keywords: paleoneuroanatomy, Sebecidae, *Zulmasuchus*, Crocodylomorpha, Bolivia, Paleocene.

Introduction

Sebecidae is an extinct family of crocodylomorphs, known from the Paleocene to the Miocene (Langston, 1965; Paolillo & Linares, 2007; Pol & Powell, 2011). It is considered as the latest survivor of the highly diversified notosuchians, a group of terrestrial crocodylomorphs (Gasparini, 1971). Most of the phylogenetic analyses retrieve the sebecids as closely related to the baurusuchids, another group of large Cretaceous terrestrial predators, forming the sebecosuchians (Turner & Sertich, 2010; Pol *et al*., 2014; Leardi *et al*., 2015, 2018; Fiorelli *et al*., 2016; Godoy *et al*., 2016; Martinelli *et al*., 2018) but this monophyly has been extensively discussed and both groups have been sometimes considered as distantly related (Larsson & Sues, 2007; de Andrade *et al*., 2011; Young *et al*., 2017).

Sebecids were diverse and widely distributed in South America and were one of the major groups of terrestrial predators during the Early Cenozoic (Pol *et al*., 2012). This family has been intensively studied (Colbert, 1946a; Langston, 1965; Gasparini, 1984; Busbey, 1986; Buffetaut & Marshall, 1992; Gasparini *et al*., 1993; Paolillo & Linares, 2007; Molnar, 2010, 2012; Pol & Powell, 2011; Pol *et al*., 2012; Kellner *et al*., 2014) and is inferred to be terrestrial based on the similarity between the skulls of sebecids and those of other terrestrial archosaurian and reptilian carnivores (Busbey, 1986; Molnar, 2012) as well as their post-cranial anatomy (proportionately long limbs compared to neosuchians and inferred erect limb posture; Pol *et al*., 2012). Apart from an endocranial cast of *Sebecus icaeorhinus* (Colbert, 1946a), no data are available on the neuroanatomy of this group, although this is not the case of other sister taxa (see below).

Indeed, numerous Computed Tomography (CT) data have been published in the last years on the neuroanatomy of crocodylomorphs (apart from the pioneering study of Colbert, 1946a). Based on extant crocodylians for comparison (e.g., Witmer *et al*., 2008; George & Holliday, 2013; Dufeau & Witmer, 2015; Bona *et al*., 2017), the paleoneuroanatomy of extinct crocodylomorphs has received a lot of attention. These works have mostly been focused on eusuchians (Holliday & Gardner, 2012; Bona & Carabajal, 2013, Bona *et al*., 2013, 2017;

Blanco *et al*., 2015; Serrano-Martínez *et al*., 2019b) and thalattosuchians (Wenz, 1968; Wharton, 2000; Fernández *et al*., 2011; Brusatte *et al*., 2016; Pierce *et al*., 2017; Herrera *et al*., 2018; Schwab *et al*., 2021a; Wilberg *et al*., 2021). Descriptions of other groups remain scarce (Leardi *et al*., 2020b; Erb & Turner, 2021). There are a few studies on notosuchians (Sereno & Larsson, 2009; Kley *et al*., 2010; Sertich & O'Connor, 2014) and recently the neuroanatomy of two baurusuchids, *Baurusuchus* sp. and *Campinasuchus dinizi* was published (Dumont *et al*., 2020b; Fonseca *et al*., 2020). On the other hand, Sebecidae, its sister taxon, has not received any attention yet.

We describe here the internal anatomy of a braincase of *Zulmasuchus querejazus* (MHNC 6672) from the lower Paleocene of Bolivia, originally assigned to Sebecidae indet. by Buffetaut (1992). *Zulmasuchus querejazus* was originally described by Buffetaut & Marshall (1992) as a more primitive ziphodont form of sebecid than *Sebecus* Simpson, 1937, another genus of the same family first reported by Simpson (1937). The holotype (MHNC-P 3701) is an incomplete but well-preserved skull, lacking the premaxillae and the posterior portion. The skull studied here is from another specimen and consists mostly of the posterior part of the skull (encompassing the frontal dorsally and the pterygoids ventrally). Another complete skull of a juvenile specimen is known and is currently under description (MHNC-P 2706; Jouve *et al*., unpublished), which allows to link these two previous specimens as belonging to *Z. querejazus.*

All these three specimens were found in the Santa Lucia Formation, in the Tiupampa locality, near the Vila Vila village, about 90 km southeast of Cochabamba in the Mizque Province (southcentral Bolivia). In a recent review of the age of the Tiupampa beds, Muizon & Ladevèze (2020, fig. 4) have confirmed the early Paleocene age of the fauna, which is referred to the early Danian and corresponds to the paleomagnetic Chron 28r (ca. 65 Mya). The Tiupampa locality has provided a diverse fauna including diapsids (Muizon *et al*., 1983; Buffetaut & Marshall, 1992; Rage, 1991a; Jouve *et al*., 2020), fishes (Gayet, 1988, 1990; Gayet & Meunier, 1992), amphibians (Rage, 1991b), turtles (de Lapparent de Broin, 1992) and mammals, which alone constitute a large part of the relative abundance of the fossils remains (Marshall *et al*., 1983; Muizon, 1992, 1994, 1998; Muizon & Cifelli, 2000; Muizon *et al*., 1998, 2015, 2018; Muizon & Ladevèze, 2020).

Using Computed Tomography (CT), we have reconstructed and analysed the cranial endocast and associated nerves and arteries, endosseous labyrinths and braincase pneumaticity of *Z. querejazus*. This enabled us to discuss these structures in terms of alert head posture, hearing

and other ecomorphological traits, and put it into perspective with what is already known of baurusuchids, their probable closest relative (Pol *et al*., 2014), as well as thalattosuchians, dyrosaurids and extant crocodylians (the last three taxa being adapted to a semi-aquatic to aquatic environment), to further assess their paleobiology.

Material and methods

A well-preserved, uncrushed, and undeformed braincase of *Zulmasuchus querejazus* (MHNC 6672, Fig. 3.10) had its internal soft anatomy reconstructed. The Computed Tomography scan was performed in November 2020 at the Laboratoire Mateis (INSA, Lyon) with a Vtomex laboratory X-ray computed tomograph (GE Phoenix X-Ray GmbH). Scanning parameters were set to 150 kV tube voltage and 80 µA current; we also used a 0.5 mm copper filter at the source exit. Two acquisitions were made, with a voxel size of 75 µm and 30 µm, respectively. The exposure time was one second for each projection and there was a total of 1200 of them for the global acquisition and 1500 projections for the zoomed acquisition that served for the reconstruction of the endosseous labyrinths. Volume rendering and processing of scans of the endosseous labyrinths, sinuses and cranial endocasts were obtained using the software Avizo Lite (version 9.5.0), MeshLab (version 2020.02) and Blender (version 2.91). Processed volume files are available in MorphoMuseum (Pochat-Cottilloux *et al*., 2021). It is worth noting that the inner ear of this specimen has already been briefly illustrated in David (2010), although it was only identified as Sebecidae indet. at the time and is thus described for the first time in this manuscript.

Because the brain of nonavian reptiles does not entirely fill the endocranial cavity, the resulting endocast should be considered a cast of the dural envelope (including venous sinuses) rather than the brain itself (Witmer *et al*., 2008). We refer to these bone-bounded spaces that house soft-tissue structures as if they were the structures themselves. Furthermore, recent studies on extant taxa showed that the shape of the endocast and the brain of reptiles and birds is strongly correlated (Watanabe *et al*., 2019; Early *et al*., 2020a), which further validates this procedure.

The best mean hearing and hearing range of *Z. querejazus* were calculated following the correlation between these parameters and the minimum length of the cochlear duct (normalized to basicranial length), as described in Walsh *et al*. (2009). The best hearing frequency range is

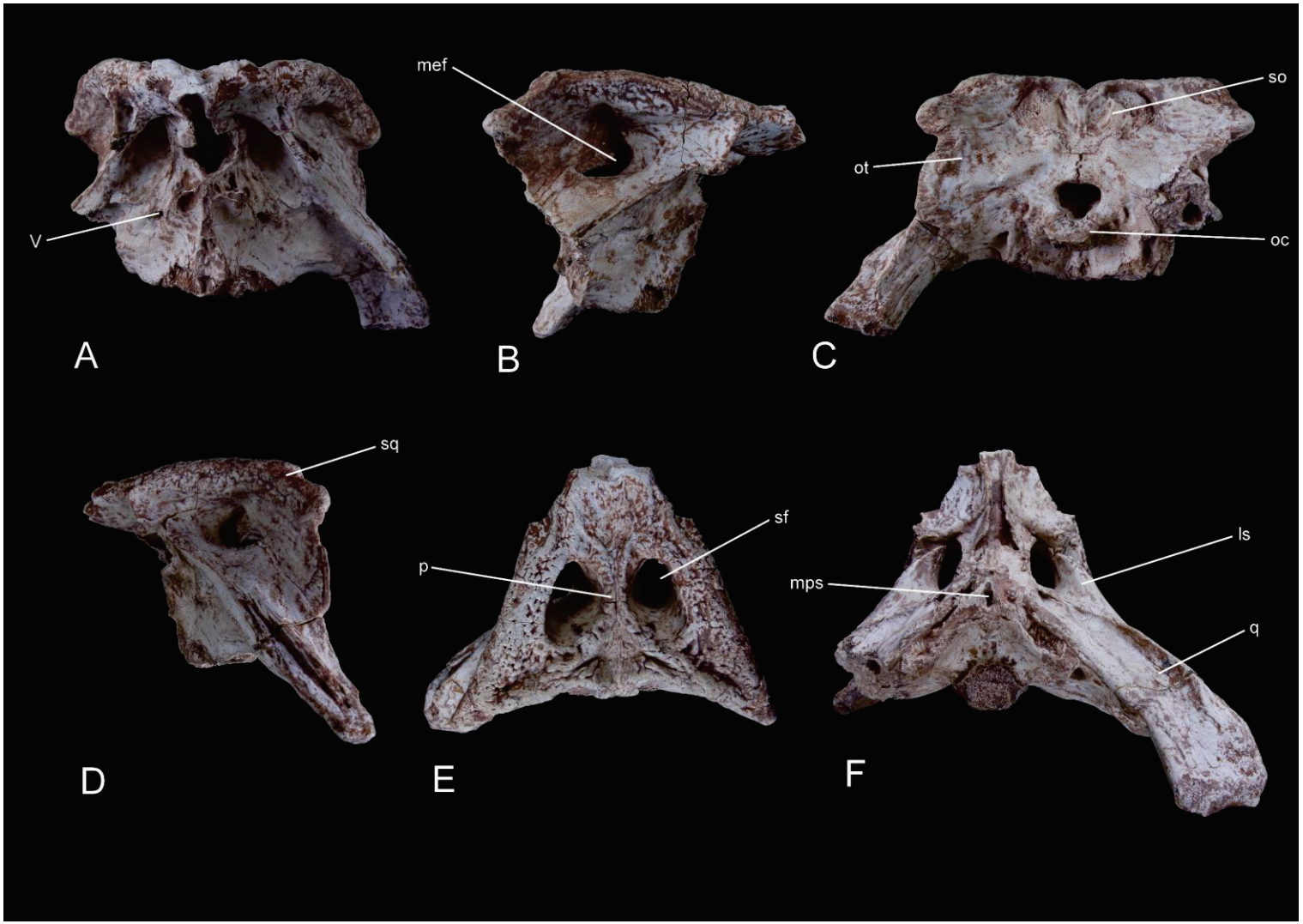

Figure 3.10: The skull of *Zulmasuchus querejazus* (MHNC 6672) in anterior (A), lateral (B & D), posterior (C), dorsal (E) and ventral (F) views. V: cranial nerve V, ls: laterosphenoid, mef: medial eustachian foramen, mps: median pharyngeal sinus, oc: occipital condyle, ot: otoccipital, p: parietal, q: quadrate, sf: supratemporal fossa, so: supraoccipital, sq: squamosal.

equal to $6104.3x + 6975.2$, where $x = \log \frac{length\ of\ the\ cochlear\ duct}{basicranial\ length}$. The best mean hearing frequency is equal to $3311.3x + 4000.8$, where $x = \log \frac{length\ of\ the\ cochlear\ duct}{basicranial\ length}$.

Comparative material

Descriptive data on extinct and extant crocodylomorph taxa used for comparison are summarized in Table 5 to avoid over-repetitions of references in the description. We follow the anatomical nomenclature published by Colbert (1946a); Kley *et al*. (2010); Sertich & O'Connor (2014); Brusatte *et al*. (2016); Bona *et al*. (2017); Pierce *et al*. (2017); Herrera *et al*. (2018); Serrano-Martínez *et al*. (2019b); Fonseca *et al*. (2020); Dumont *et al*. (2020b), Erb & Turner (2021) & Schwab *et al*. (2021a); Wilberg *et al*. (2021) concerning the endocranial structures (and references therein). The different measurements in Table 6 were obtained following the method of Pierce *et al*. (2017; fig. 2).

Results

Cranial endocast and associated nerves and vascular elements (Fig. 3.11-3.13):

MHNC 6672 lacks the anterior part of the frontal; therefore, the anterior part of the forebrain (i.e., optic chiasm and optic and olfactory tracts) could not be reconstructed. The cerebral hemispheres are not laterally expanded and do not show the typical round shape of extant and of some extinct crocodylians; they are more closely similar in shape to those of baurusuchids and to the thalattosuchians belonging to the genus *Macrospondylus* von Meyer, 1831 and *Plagiophthalmosuchus* Johnson, Young & Brusatte, 2020 (Table 6). They are symmetrically developed along the midline in dorsal view. The endocast shows a very well-marked pontine and cephalic flexure angle between the midbrain and the hindbrain (sigmoid shape in lateral view; Fig. 3.13D, Table 6). The midbrain produces a sharper angle to the hindbrain than in the extant species as well as in the baurusuchids and in the notosuchian *Simosuchus clarki*, even more than in thalattosuchians and dyrosaurids (as a result, the pontine flexure angle and the cephalic flexure angle are quite low, see Table 6 for comparative measurements). This condition is only observed to a lesser degree in *Rukwasuchus yajabalijekundu* and *Sebecus icaeorhinus*, which would make it a unique trait of *Zulmasuchus* among crocodylomorphs (although it does not differ statistically from the sample under a Wilcoxon test; p-value = 0.2 for the cephalic flexure angle and p-value = 0.12 for the pontine flexure angle). The dorsal part of the midbrain appears compressed mediolaterally where it accommodates for the labyrinths, as in other

Table 5: Comparative material used in this study is reported along with the published references of their associated studies.

Taxon	**Specimen**	**Publication or database**
Crocodylus porosus	OUVC 10899	Morphosource
Gavialis gangeticus	MLP 602; UF HERP 118998	Bona *et al*. (2017); Pierce *et al*. (2017); Morphosource
Caiman crocodilus	UMMZ HERPS 128024	Morphosource
Diplocynodon tormis	STUS-344	Serrano-Martínez *et al*. (2019b)
Pelagosaurus typus	BRLSI-M1413	Pierce *et al*. (2017)
Plagiophthalmosuchus cf. *gracilirostris*	NHMUK PV OR 33095	Brusatte *et al*. (2016)
Macrospondylus bollensis	SNSB-BSPG 1984 1258; MCZ VPRA-1063	Herrera *et al*. (2018); Wilberg *et al*. (2021)
Cricosaurus araucanensis	MLP 72-IV-7-1	Herrera *et al*. (2018)
'Metriorhynchus' cf. *brachyrhynchus*	NHMUK PV O 32617	Schwab *et al*. (2021a)
Rhabdognathus aslerensis	AMNH FARB 33354 formerly CNRST-SUNY 190	Brochu *et al*. (2002); Erb & Turner (2021)
Rukwasuchus yajabalijekundu	RRBP 08630	Sertich & O'Connor (2014)
Simosuchus clarki	UA 8679	Kley *et al*. (2010)
Campinasuchus dinizi	CPPLIP 1319, 1360	Fonseca *et al*. (2020)

Baurusuchus sp.	IFSP-VTP/PALEO-0002, 0003; FEF-PV-R-1/9; FUP-Pv 000020 and 000021	Dumont *et al*. (2020b)
Sebecus icaeorhinus	AMNH 3160	Colbert *et al*. (1946a)

crocodylomorphs but to a lesser degree than the extreme conformation seen in *Rhabdognathus aslerensis* (Fig. 3.13E). When compared with *Crocodylus porosus*, the dorsal margin of the endocast shows a much longer hindbrain in *Zulmasuchus querejazus* (about two centimetres in MHNC 6672). The hindbrain is well-preserved. The medulla oblongata is longer but thinner anteriorly compared to that in *C. porosus*.

The dorsal longitudinal venous sinus is well-developed anteroposteriorly, bearing a depression fully surrounded by pericerebral spines (named as such in this study for the first time) just anterior to the flexure between the midbrain and the forebrain (Fig. 3.13E). *Rukwasuchus* Sertich & O'Connor, 2014 and *Campinasuchus* Carvalho, Teixeira, Ferraz, Ribeiro, Martinelli, Neto, Sertich, Cunha, Cunha & Ferraz, 2011 are the only taxa where such a structure has been reported (only with lateral ridges in *Rukwasuchus* and a posterior one for *Campinasuchus*). Recently, it has also been reported in *Rhabdognathus*, linked with the caudal middle cerebral vein, but it differs from the specimen described here because it does not show a depression there. *Zulmasuchus* is thus unique among crocodylomorphs in possessing these structures on all the sides of this characteristic depression, accommodating for the internal face of the parietal.

Cranial nerve VI is developed anteroposteriorly, between the pituitary fossa ventrally and the ventral edge of the endocast dorsally. Posteriorly, it emerges from the hindbrain, at the level of the posterior edge of cranial nerve V (Fig. 3.13D and 3.13F).

The passage for cranial nerve V (Fig. 3.12B) is the largest in the neurocranium (as in other crocodylomorphs). It is laterally projected from the endocast and is located just anteriorly to the endosseous labyrinths (Fig. 3.13D). It was not possible to determine with certainty the position of the emerging nerve branches V_1, V_2 and V_3. Cranial nerve VII is not identified.

Laterally, the hindbrain bears two reliefs on each side: the posteriormost one is the starting point of cranial nerve XII (which has a small circumference and is directed posterolaterally); the anteriormost one could either be a second passage for cranial nerve XII (as in *G. gangeticus*) or the starting point of cranial nerve IX-XI, but it is difficult to identify because they could not

Table 6: Raw morphometric data of *Zulmasuchus* (MHNC 6672) and comparative material.

(Rounded to nearest mm or mm²)	*Pelagosaurus typus*	*Plagiophthalmosuchus* cf. *gracilirostris*	*Macrospondylus bollensis*	*Cricosaurus araucanensis*	*'Metriorhynchus'* cf. *brachyrhynchus*	*Rhabdognathus aslerensis*	*Gavialis gangeticus*	*Alligator mississippiensis*	*Crocodylus porosus*	*Diplocynodon tormis*	*Simosuchus clarki*	*Rukwasuchus yajabalijekundu*	*Campinasuchus dinizi*	*Baurusuchus* sp.	*Sebecus icaeorhinus*	*Zulmasuchus querejazus*
Skull width at cerebrum (SW)	52	?	33	40	74	89	168	73	39	25	58	37	32	?	147	42
Cephalic flexure angle (CF)	160	175	170	135	155	158	150	135	125	140	142	145	155	165	150	130
Pontine flexure angle (PF)	160	170	165	170	165	152	154	145	170	160	165	145	150	165	160	130
Endocast length (EL)	57	?	76	140	?	171	146	98	40	82	79	100	85	70	120	?
Olfactory tract length (+ bulbs) (OL)	21	?	26	69	?	49	55	48	18	36	25	45	39	32	46	?
Cerebrum width (CW)	15	28	19	25	40	26	32	21	18	23	25	28	13	14	30	35
Pituitary width (PW)	6	14	4	11	16	5	6	5	4	2	5	7	4	?	?	14
Pituitary height (PH)	7	12	6	9	12	10	9	8	3	6	9	10	4	?	9	17
Pituitary length (PL)	10	17	4.5	14	30	14	11	10	13	4	10	5	4	?	8	27
Labyrinth height (LH)	14	26	22	19	20	25	21	18	9	?	?	?	?	12	?	22
Labyrinth width (LW)	11	26	18	18	21	26	21	14	9	?	?	?	?	13	?	14
Endosseous cochlear duct length (ECL)	8	13	12	7	9	12	9	8	3	?	?	?	?	6	?	7
Anterior semi-circular canal area (AA)	9	38	18	?	?	19	36	35	11	?	?	?	?	2	?	7
Posterior semi-circular canal area (PA)	6	19	5	?	?	4	15	12	3	?	?	?	?	4	?	7
Lateral semi-circular canal area (LA)	4	14	7	?	?	8	22	13	3	?	?	?	?	1	?	6
Source	Pierce et al. (2017)	Brusatte et al. (2016)	Herrera et al. (2018); Erb and Turner (2021)	Herrera et al. (2018)	Schwab et al. (2021)	Erb and Turner (2021)	Pierce et al. (2017)	Witmer and Ridgely (2008)	This study	Serrano-Martínez et al. (2019)	Kley et al. (2010)	Sertich and O'Connor (2014)	Fonseca et al. (2020)	Dumont et al. (2020)	Colbert et al. (1946a)	This study

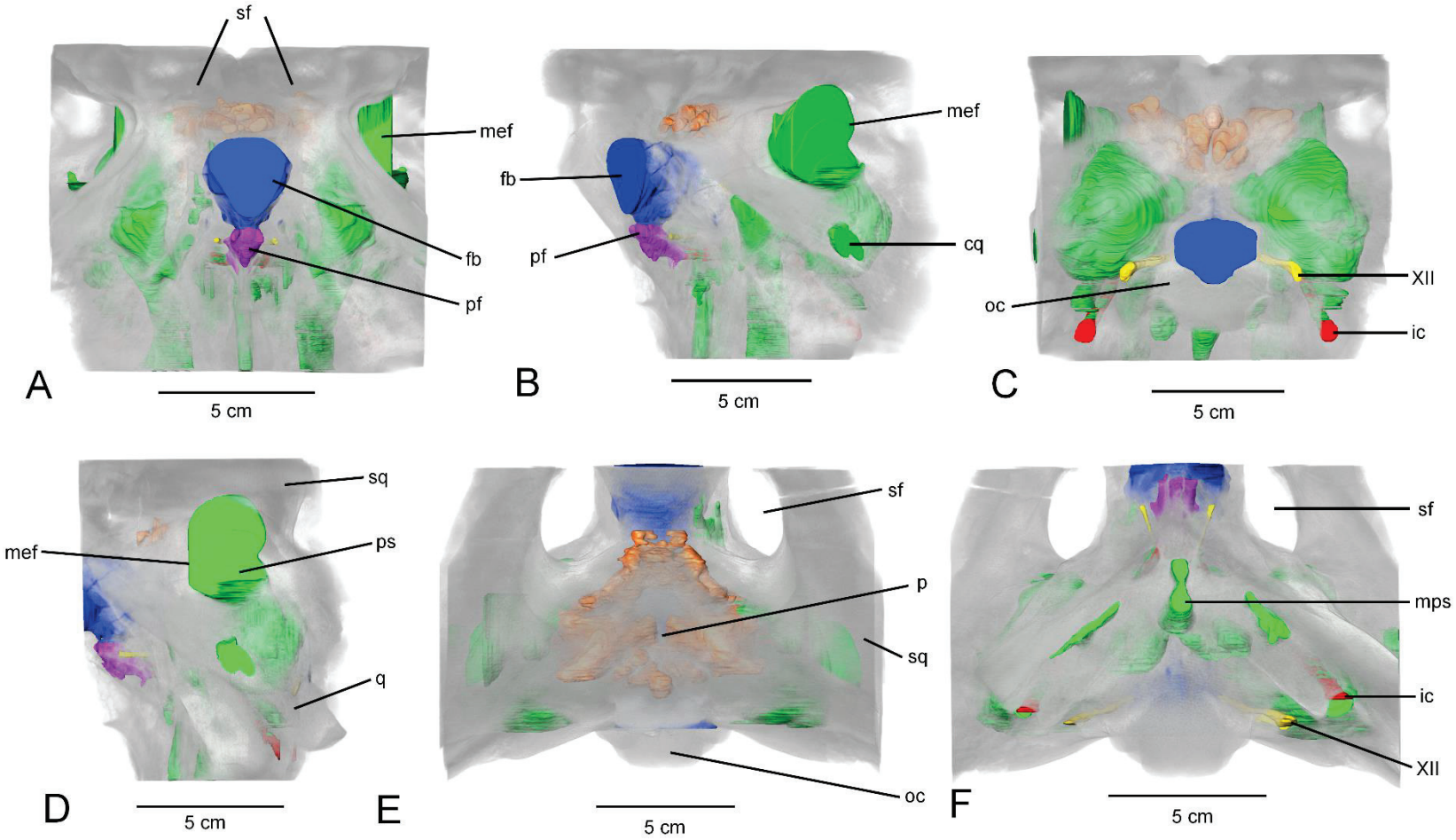

Figure 3.11: Three-dimensional reconstruction of the segmented part of the skull of *Zulmasuchus querejazus* (MHNC 6672) in anterior (A), anterior ¾ (B), posterior (C), lateral (D), dorsal (E) and ventral (F) views. Blue: endocast, green: pharyngotympanic sinus, orange: intertympanic diverticulum, red: internal carotid artery, yellow: cranial nerve, purple: pituitary fossa. XII: cranial nerve XII, cq: cranioquadrate passage, fb: forebrain, ic: internal carotid artery, mef: medial eustachian foramen, mps: median pharyngeal sinus, oc: occipital condyle, p: palate, pf: pituitary fossa, ps: pharyngotympanic sinus, q: quadrate, sf: supratemporal fossa, sq: squamosal.

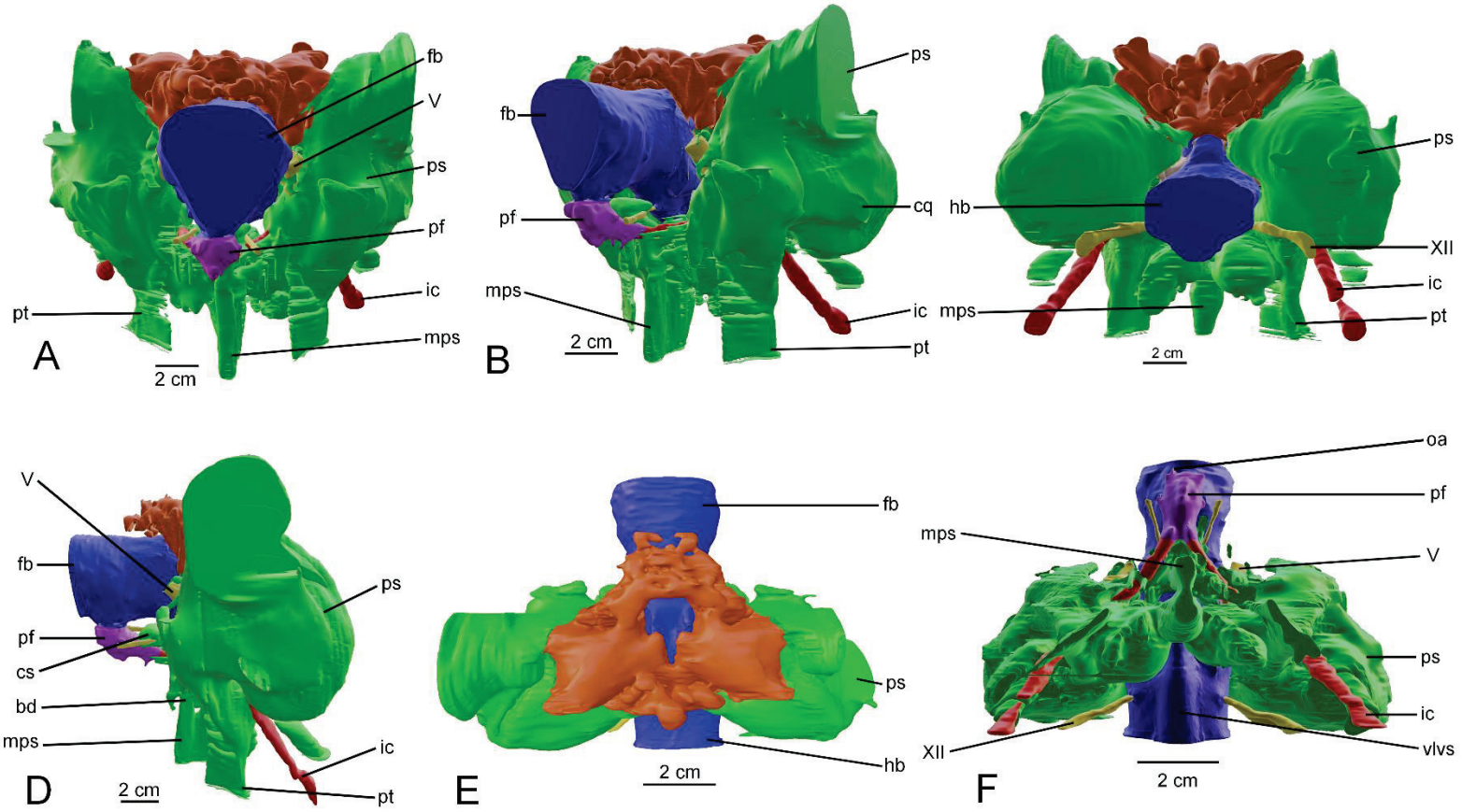

Figure 3.12: Three-dimensional reconstruction of the pneumatic cavities within the braincase of *Zulmasuchus querejazus* (MHNC 6672) in anterior (A), anterior 3/4 (B), posterior (C), lateral (D) dorsal (E) and ventral (F) views. Blue: endocast, light green: pharyngotympanic sinuses and eustachian system, orange: intertympanic diverticulum, red: internal carotid artery, yellow: cranial nerve, purple: pituitary fossa. V: cranial nerve V, XII: cranial nerve XII, bd: basisphenoid diverticulum, cq: cranioquadrate passage, cs: cavernous sinus, fb: forebrain, hb: hindbrain, ic: internal carotid artery, mps: median pharyngeal sinus, oa: orbital artery, pf: pituitary fossa, ps: pharyngotympanic sinus, pt: pharyngotympanic tube, vlvs: ventral longitudinal venous sinus.

be segmented in their entirety (Fig. 3.13D). Ventrally, the medulla oblongata bears a venous sinus, the ventral longitudinal venous sinus, that is clearly visible and well-developed, especially anteriorly (Fig. 3.13F). In *Zulmasuchus*, it is ridge-shaped, whereas it is much more rounded and shallower in extant crocodylians and dyrosaurids. The pituitary fossa is well-developed dorsoventrally when compared with that of *C. porosus*, but not as much as in gavialoids. It is also directed posteroventrally, in an intermediate manner between extant crocodylians, '*Metriorhynchus'*, *Cricosaurus* Wagner, 1858 and *Pelagosaurus* (where it is directed fully anteroposteriorly) and baurusuchids (where it is directed almost ventrally). Moreover, this condition is also seen in *Macrospondylus*, *Plagiophthalmosuchus*, *Rhabdognathus* and *Sebecus*. Anteriorly, two structures extending anteroposteriorly could be the starting points of the orbital arteries (Fig. 3.12F and 3.13F). In *Zulmasuchus*, the posterior part of the pituitary fossa reaches the level of the anterior margin of the trigeminal fossa, and it bears a ventral crest in its anterior portion (Fig. 3.12D and 3.13D). The internal carotid arteries enter the posterior end of the pituitary fossa separately at the level of the midline (Fig. 3.13F; as in other crocodylomorphs; Witmer *et al*., 2008). The canals for these arteries are large and the segmentation is missing a section at the ventral level of the endosseous labyrinths when they pass through the pharyngotympanic sinus and are thus not encased in bone (Fig. 3.13D). The posterior section of the carotid artery runs anterodorsally from the foramen for the internal carotid artery to below the endosseous labyrinths. On the posterior section, the bifurcation of the stapedial artery can be seen (Fig. 3.13). The anterior section of the internal carotid arteries extends anteroposteriorly and is curved medially entering the pituitary fossa (the limit between the internal carotid arteries and the pituitary fossa was established where the arteries are no longer separated and merge into a single structure).

Endosseous labyrinths (Fig. 3.13-3.15):

The endosseous labyrinths of *Z. querejazus* are well-preserved, including the cochlear duct and the vestibular system. The left labyrinth is better preserved than the right one, the latter lacking the distal part of the lateral semicircular canal. The ampullae are not clearly distinguishable from the canals, their shape is continuous with those of the semicircular canals. Both the anterior and posterior semicircular canals are circular in cross-section (Fig. 3.14) and are extremely narrow compared to those of extant crocodylians, and they all have the same maximum diameter, which is not the case in gavialoids for example (Fig. 3.15). The common crus have a rather narrow diameter, as the semicircular canals. The semicircular canals being

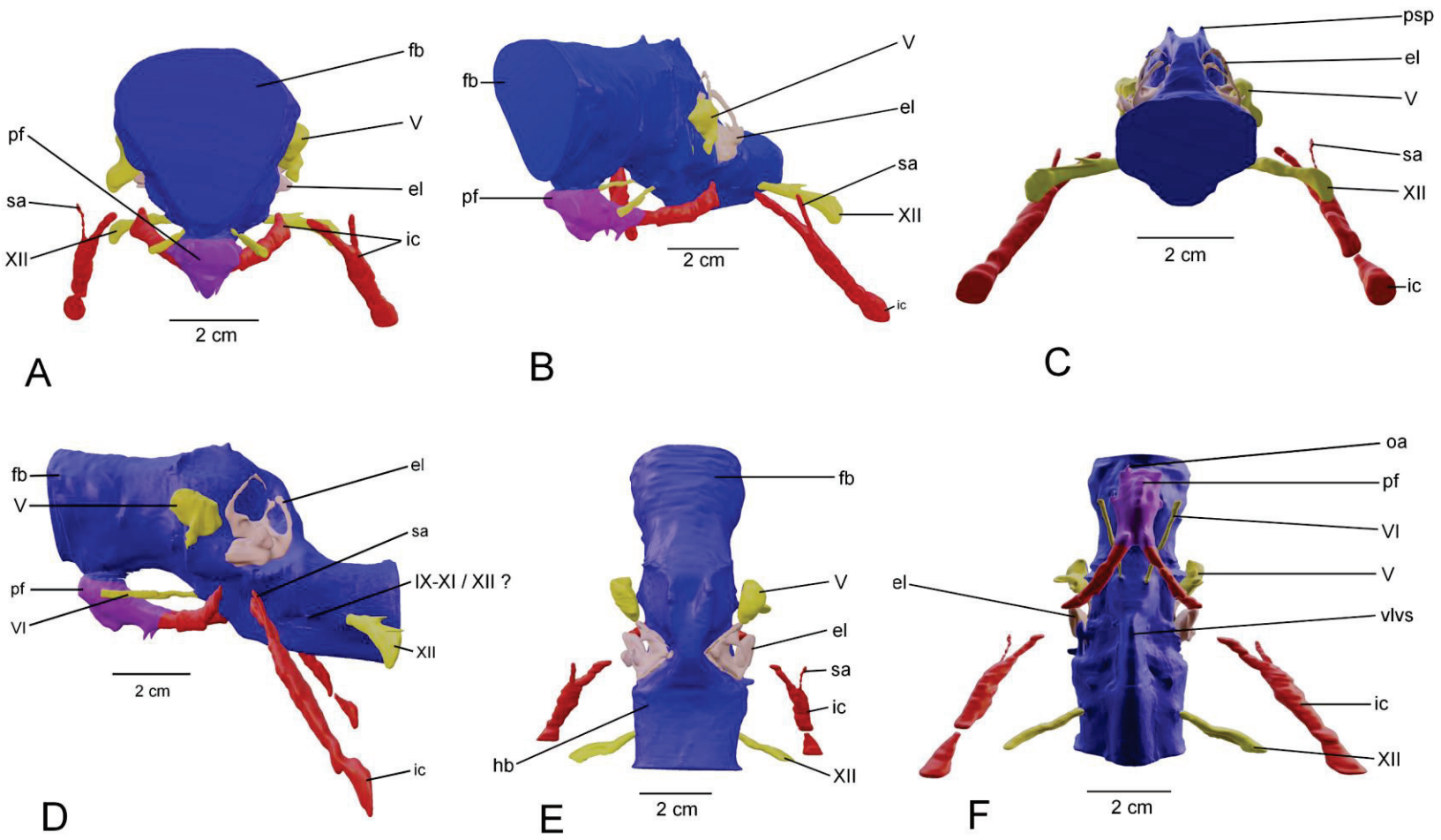

Figure 3.13: Three-dimensional reconstruction of the endocranial cavities of *Zulmasuchus querejazus* (MHNC 6672) in anterior (A), anterior 3/4 (B), posterior (C), lateral (D) dorsal (E) and ventral (F) views. Blue: endocast, red: internal carotid artery, yellow: cranial nerve, purple: pituitary fossa, V: cranial nerve V, VI: cranial nerve VI, IX-XI: cranial nerve IX-XI, XII: cranial nerve XII, el: endosseous labyrinth, fb: forebrain, hb: hindbrain, ic: internal carotid artery, oa: orbital artery, pf: pituitary fossa, psp: pericerebral spines, sa: stapedial artery, vlvs: ventral longitudinal venous sinus.

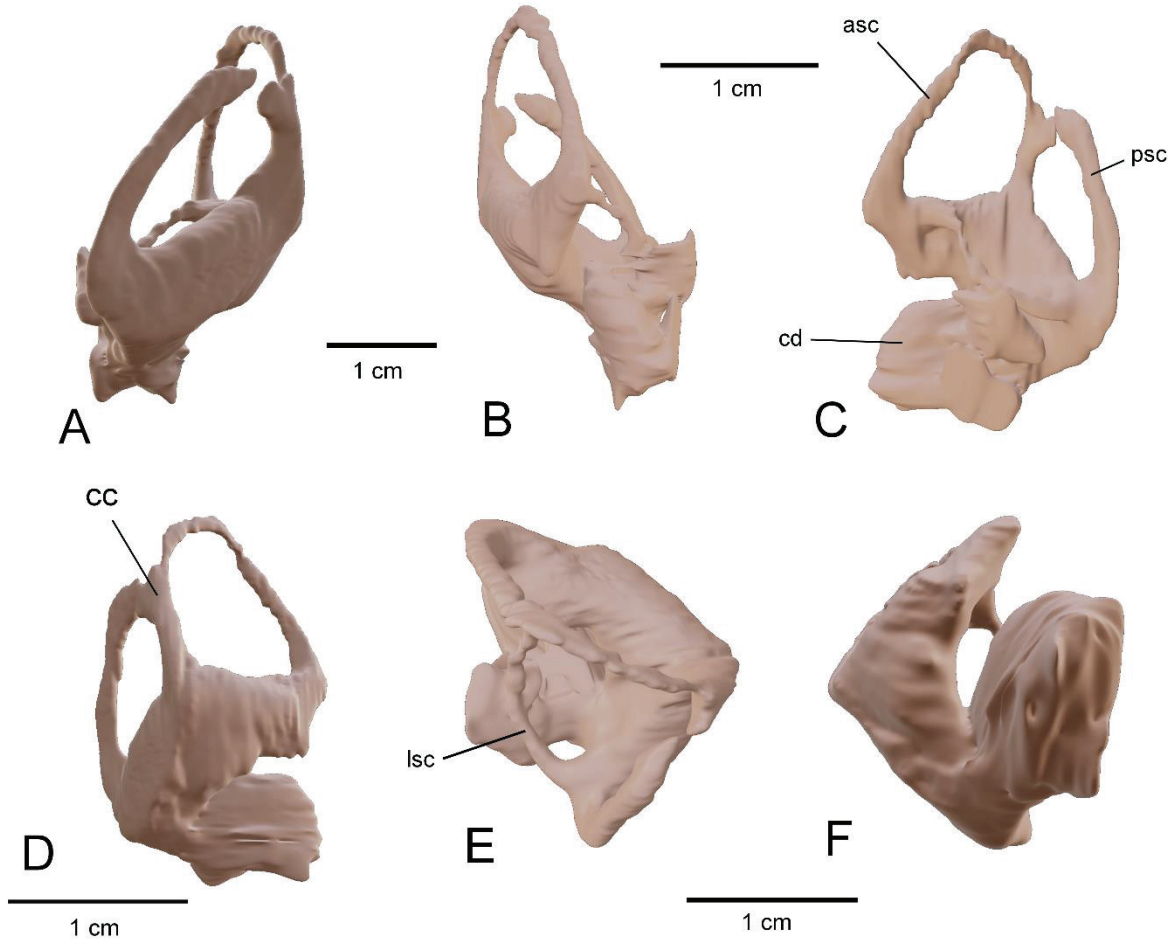

Figure 3.14: Three-dimensional reconstruction of the left endosseous labyrinth of *Zulmasuchus querejazus* (MHNC 6672) in posterior (A), anterior (B), lateral (C and D), dorsal (E) and ventral (F) views. asc: anterior semicircular canal, cc: common crus, cd: cochlear duct, lsc: lateral semicircular canal, psc: posterior semicircular canal.

narrower in diameter than those of extant crocodylians, the space between them is therefore much larger. The lateral semicircular canal is even narrower in diameter than the anterior and posterior ones (but this could be due to a preservation bias, as it appears to be filled and therefore difficult to distinguish from the bone during the segmentation process). It is curved ventrodorsally in lateral view, which is a peculiar characteristic regarding the comparison material. In dorsal view, the lateral semicircular canal is somewhat extended laterally (Fig. 3.14E). The anterior and posterior semicircular canals have a pyramidal shape rather than the typical ovoid shape exhibited by extant crocodylians. This shape is the result of the canals rising higher from the common crus and therefore also having to turn ventrally more sharply and run in a straighter, more direct course toward the anterior (or posterior) end. This morphology is consistent with what is found in other extinct crocodylomorphs. Therefore, the angle between the anterior and the lateral semicircular canals is higher than in extant crocodylians (70° for

Zulmasuchus vs 50° to 60° in modern crocodylians). The angle formed between the anterior and the posterior semicircular canals is approximately 90°, as it is in derived eusuchians (Bona & Paulina-Carabajal, 2013). The anterior canal is slightly more expanded dorsally than the posterior one, as it is in modern crocodylians (Witmer *et al*., 2008). As a result, the anterior semicircular canal area is slightly larger than the posterior one. On the other hand, both canals are similarly expanded anteroposteriorly. This condition is seen in thalattosuchians and *S. clarki* but not in extant crocodylians and *R. aslerensis* (Fig. 3.15). The lagenar section is quite developed and appears to be directed anteriorly, although this could be due to incomplete segmentation because this area is not enclosed by bone (Fig. 3.16). This part also bears a process directed laterally below the lateral semicircular canal, which could be one of the connections with cranial nerve VIII, as in extant crocodylians or the contact with the columella which is the auditory bone that connects the eardrum to the lateral part of the cochlea. It is difficult to assess because this part has never been described in other fossil crocodyliforms, apart from *Pelagosaurus*, where it is only briefly mentioned in Pierce *et al*. (2017; fig. 4). Therefore, comparisons are very scarce.

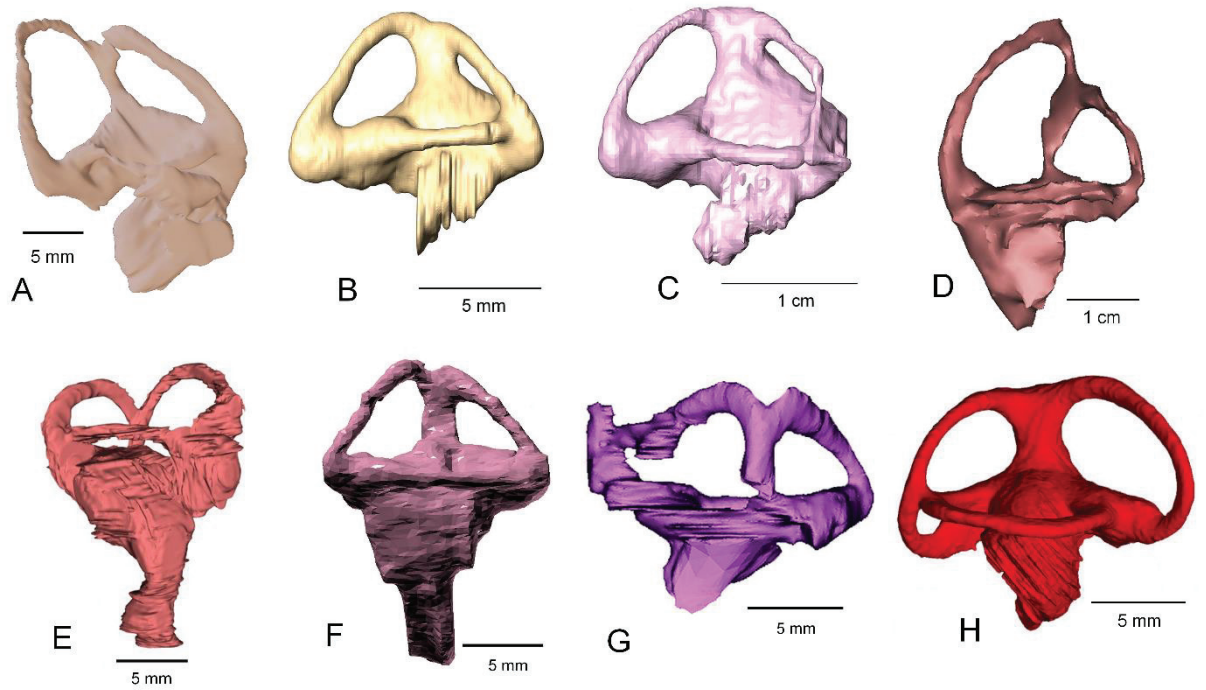

Figure 3.15*:* Three-dimensional reconstructions of the endosseous labyrinths of different reptiles in lateral view: A: *Zulmasuchus querejazus* (left, MHNC 6672); B: *Crocodylus porosus* (left, OUVC 10899); C: *Gavialis gangeticus* (left, UF herp 118998); D: *Viavenator exxoni* Filippi, Méndez, Juárez Valieri & Garrido, 2016 (left, MAU-Pv-Li-530 from Paulina-Carabajal & Filippi, 2018); E: *Baurusuchus* sp. (right, FUP-Pv 000021 from Dumont *et al*., 2020b, fig. 9b); F: *Pelagosaurus typus* (left, BRLSI M1413 from Pierce *et al*., 2017, fig. 6b); G: *Parringtonia gracilis* von Huene, 1939 (left NMT RB460, from Nesbitt *et al*., 2018, fig. 11K); H: *Platecarpus tympaniticus* Cope, 1869 (left, AMNH FRAB1645 from Yi & Norell, 2019). All structures are oriented with the lateral semicircular canal oriented horizontally.

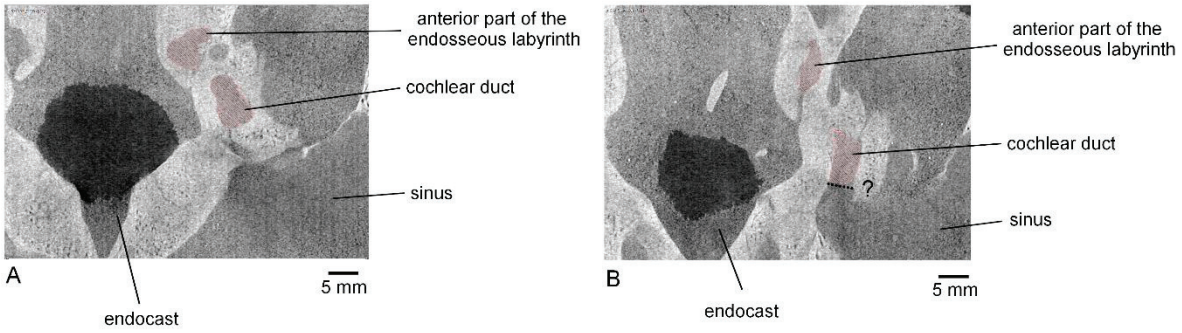

Figure 3.16: Illustration of one of the problems of segmentation: the limit between the cochlear duct and the pharyngotympanic sinus. A: posterior transverse slice where the limit is clear, B: anterior transverse slice where the limit is not clear.

Braincase pneumaticity (Fig. 3.12):

The pharyngotympanic system and the median pharyngeal system are part of the paratympanic sinus system, which serves to enhance acoustic capabilities of the middle ear (Dufeau & Witmer, 2015). They are described here following the nomenclature proposed by the same authors.

The intertympanic diverticulum is located along the dorsal margin of the cranial endocast, excavating the parietal and the supraoccipital internally (Fig. 3.12A, 3.12B, 3.12C, 3.12D and 3.12E). Laterally, it is continuous with the pharyngotympanic sinuses, which are located just dorsal to the endosseous labyrinths level. They can be separated in three parts: a central core and two lateral expansions (as in extant crocodyloids and gavialoids; Fig. 3.12E). In dorsal view, the connection between the two large lateral parts is situated more anteriorly than the lateral expansions, this part could also be the parietal diverticulum, but we were not able to really distinguish it from the intertympanic diverticulum. The whole structure shows a hole at the midline (Fig. 3.12E). In *C. porosus*, the intertympanic diverticulum is much more developed posteriorly, reaching the level of the posterior part of the medulla oblongata but it is less developed anteriorly. In fact, the condition of *Zulmasuchus* looks more like that of *Caiman* (Fig. 3.17). These structures are not observed in thalattosuchians.

The pharyngotympanic sinus is developed laterally to the inner ear region and merges dorsally with the intertympanic diverticulum (at the level of the supraoccipital-otoccipital suture; Fig. 3.12E; Dufeau & Witmer, 2015). It extends ventrally and laterally to the level of the endosseous labyrinths, surrounding the middle section of the internal carotid artery (Fig. 3.11B and 3.12B). The starting point of the large left cranioquadrate passage is segmented (Fig. 3.11D and 3.12D)

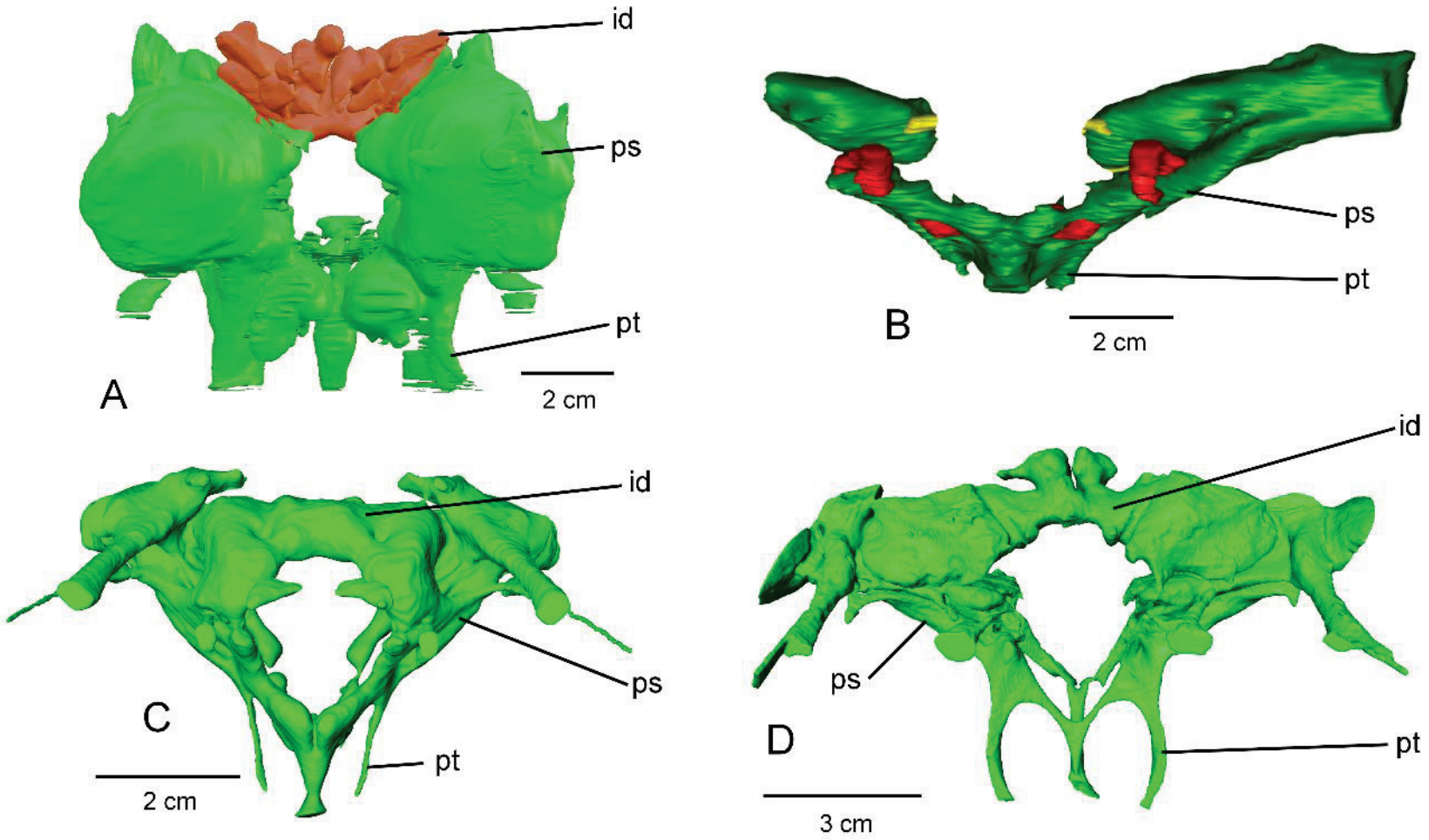

Figure 3.17: Three-dimensional reconstructions of the cranial pneumaticity of some crocodylomorphs in posterior view: A: *Zulmasuchus querejazus* (MHNC 6672); B: *Macrospondylus bollensis* (SNSB-BSPG 1984 I258, from Herrera *et al*., 2018, fig. 3G); C: *Caiman crocodilus* (UMMZ herps 128024); D: *Gavialis gangeticus* (UF herp 118998). id: intertympanic diverticulum, ps: pharyngotympanic sinus, pt: pharyngotympanic tube.

ventrally to the opening of the middle ear, but not the rest of it nor the siphonium. This is different from what is seen in *Cricosaurus* and other metriorhynchids where it is completely separated from the sinus by a thin bony lamina, but similar to what is known in extant crocodylians. The lateral expansions of the pharyngotympanic sinus are extremely developed and rounded, which is another peculiar characteristic of *Zulmasuchus* among other crocodylomorphs. The pharyngotympanic tubes, connected to the pharynx, are large, expanded lateromedially and ventrally directed. Ventrally, the pharyngotympanic sinuses merge posteriorly at the level of the basisphenoid diverticulum, bordering the hindbrain (Fig. 3.12F).

Ventral to this structure is the median pharyngeal sinus (Fig. 3.12A, 3.12B, 3.12C, 3.12D and 3.12F). It is directed anteroventrally, joins the ventral edge of the basisphenoid diverticulum and exits the skull through the median pharyngeal foramen. The ventralmost part could not be segmented (Fig. 3.11F). This part does not connect with the pharyngotympanic tubes directly, as they are linked through the pharyngotympanic sinus. Dorsally, the median pharyngeal sinus bifurcates into two branches: anterodorsally it joins a cavernous sinus located between the posterior part of the pituitary fossa and the ventral edge of the forebrain (Fig. 3.12D); posterodorsally, it meets with the pharyngotympanic sinus. This splitting suggests that the specimen is not a juvenile but rather a subadult, as this canal would then have been more horizontal (Fig. 3.12E; Serrano-Martínez *et al*., 2019b). The basisphenoid diverticulum is located between the anterior parts of the anterior section of the internal carotid arteries (where they meet at the midline, Fig. 3.12E and 3.13F). It is connected to the median pharyngeal sinus ventrally and extends posteriorly to meet with the pharyngotympanic sinuses.

Discussion

Comparison of the endocranial cavities of altirostral crocodylomorph taxa

Zulmasuchus exhibits several characteristics that are also observed in other altirostral taxa such as baurusuchids and peirosaurids. The endocast shows a very well-marked angle between the midbrain and the hindbrain, that is also seen to a lesser degree in *Sebecus icaeorhinus* (Colbert, 1946a) and *Rukwasuchus yajabalijekundu* (Sertich & O'Connor, 2014), as well as in baurusuchids (Dumont *et al*., 2020b; Fonseca *et al*., 2020). The dorsal part of the midbrain is compressed mediolaterally where it accommodates for the endosseous labyrinths, as in other altirostral taxa (and to various degrees in other crocodylomorphs). The cerebral hemispheres are not laterally expanded, as in baurusuchids (but also as in *Macrospondylus* and *Plagiophthalmosuchus*; Brusatte *et al*., 2016; Herrera *et al*., 2018; Wilberg *et al*., 2021).

Another peculiar characteristic of *Zulmasuchus* is the presence of a pair of pericerebral spines on the dorsal surface of the longitudinal sinus (Fig. 3.13), which have also been reported to a lesser degree in *Rukwasuchus* (Sertich & O'Connor, 2014, fig. 6). *Sebecus* and *Zulmasuchus* share the posteroventral orientation of the pituitary fossa (but it is also the case of some thalattosuchians and dyrosaurids; *Rhabdognathus, Macrospondylus* and *Plagiophthalmosuchus*, Brusatte *et al*., 2016; Herrera *et al*., 2018; Erb & Turner, 2021; Wilberg *et al*., 2021).

On the other hand, *Zulmasuchus* bears up to three apomorphic characters, such as a ventral crest on the pituitary fossa (Fig. 3.13), the narrow diameter of the semicircular canals with a lateral one curved both laterally and ventrally (Fig. 3.14), as well as an enlarged cranial pneumaticity (Fig. 3.12). However, those last two are subject to caution because those parts are not well documented yet in altirostral taxa.

Head posture

The orientation of the lateral semicircular canal is used in most studies as a proxy for the alert head posture where it is thought to be roughly horizontal in reptiles and birds (Erichsen *et al*., 1989; Witmer *et al*., 2003, 2008; Hullar, 2006; Sampson & Witmer, 2007; Sereno *et al*., 2007; Witmer & Ridgely, 2008). This method has been contested by other studies mainly focused on dinosaurs (Taylor *et al*., 2009; Marugán-Lobon *et al*., 2013), due to interspecific variation in orientations. Other proxies involve the alignment of either the maxillary toothrow (Marugán-Lobon *et al*., 2013) or the endocranial surface of the parietal (Kley *et al*., 2010; von Backo *et al*., 2018) with the horizontal plane.

Depending on the structure selected to align with the horizontal plane, we obtained a very different result on the head posture of *Zulmasuchus*. Considering a horizontal alignment of the lateral semicircular canal, the longitudinal axis of the skull makes an angle of 35° with the horizontal plane (Fig. 3.18A), whereas it is "only" of 10° if one relies on the orientation of the endocranial surface of the parietal (without considering the pericerebral spines; Fig. 3.18B). This difference could be explained because the lateral semicircular canal in MHNC 6672 has such a peculiar morphology (curved anteroposteriorly as well as mediolaterally), and consequently its orientation is more difficult to determine with precision. Although we do not have access to the maxillary toothrow of the specimen studied here, this data could be extrapolated by combining the holotype (MHNC-P 3701) and the specimen studied here (MHNC 6672), as they represent two parts of the skull that almost overlap. This can be seen in

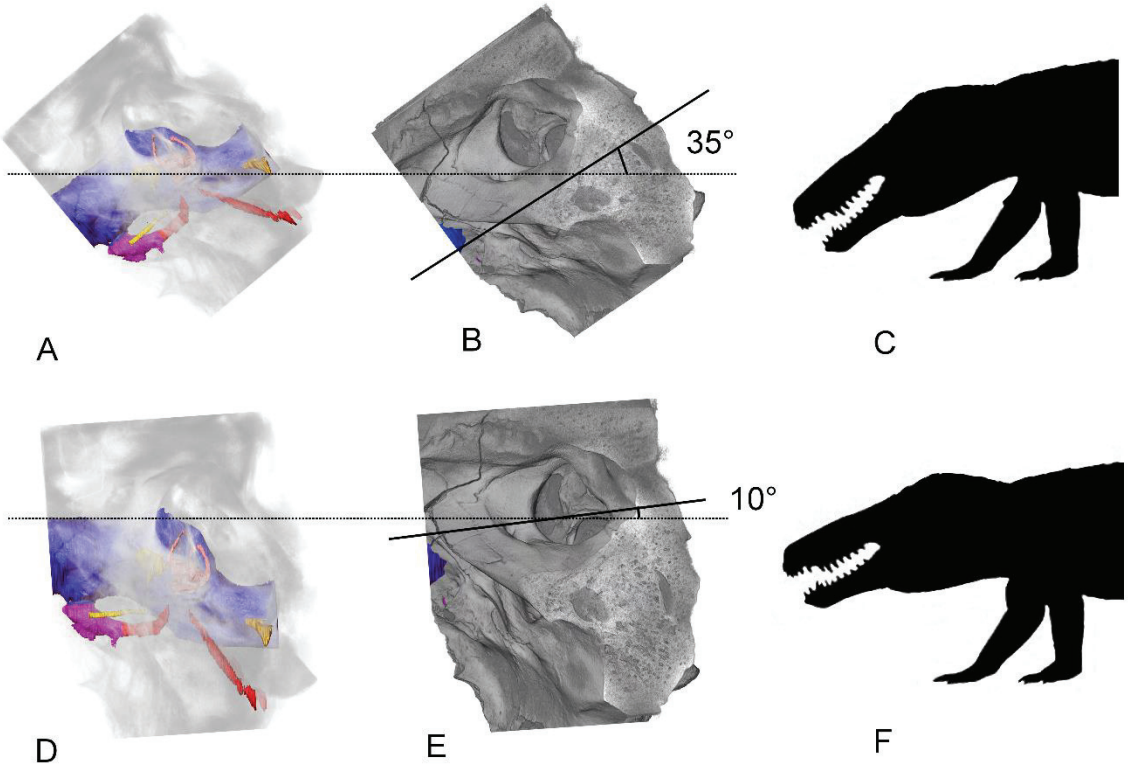

Figure 3.18: Inferred alert head posture aligning the lateral semicircular canal (A, B and C) and the endocranial surface of the parietal (D, E and F) with the horizontal plane of *Z. querejazus* (MHNC 6672). Drawings are taken from Fig. 3.20.

Fig. 3.19. This schematic allows to extrapolate the head posture of *Zulmasuchus*, but in no way it does represent an attempt to reconstruct the skull, as it is understood that these two specimens are distinct from each other. The value given by this proxy is approximately 7°, which is quite close to the alignment with the endocranial surface of the parietal. To avoid any morphological bias or individual variation, we have thus chosen to rely on the latter for our reconstruction (Fig. 3.20). It is also consistent with what is found in other notosuchians (Kley *et al*., 2010; Dumont *et al*., 2020b; Fonseca *et al*., 2020).

The head of *Zulmasuchus* would thus have been more inclined towards the ground than that of extant crocodylians (which are considered to have their longitudinal axis almost parallel to the horizontal plane; Witmer *et al*., 2008; Bona *et al*., 2017; Serrano-Martínez *et al*., 2019b, Fig. 3.20), thus allowing us to infer its ecology. This posture would have indeed allowed the nostrils to be closer to the ground and would have provided a better binocular vision over its high and narrow snout. These constitute further arguments in favour of terrestrial habits (Stevens, 2006; Marinho *et al*., 2013). Furthermore, this would also imply lower energy costs compared to keeping the head on the horizontal plane. It probably had effects on the musculature of the neck

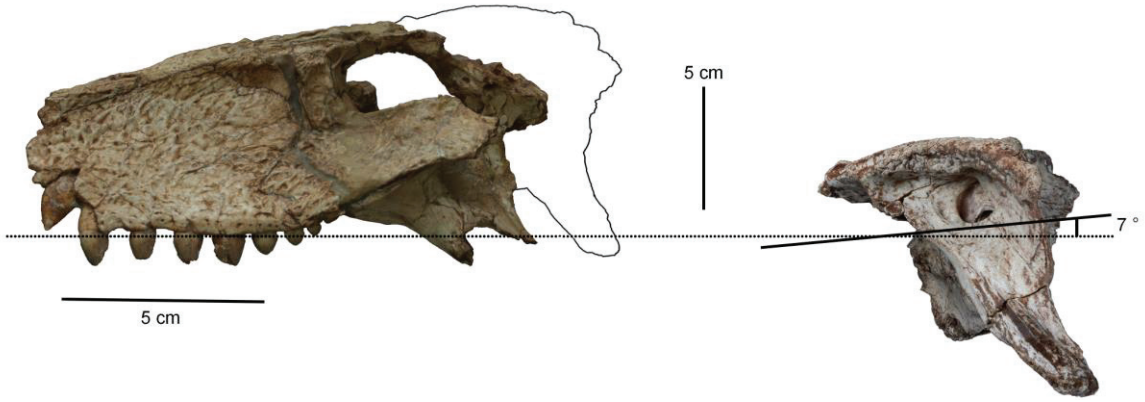

Figure 3.19: Attempted extrapolation of the head posture of *Zulmasuchus*, obtained by combining the holotype MHNC-P 3701 (left part) and MHNC 6672 (right part) and aligning the composite skull achieved with the maxillary toothrow, left lateral view.

of *Zulmasuchus* although it is difficult to assess because post-cranial elements have not been described yet (Buffetaut & Marshall, 1992; Paolillo & Linares, 2007). Such data would also enable studies on functional morphology linked to ecology, as it has already been done on theropods (Snively & Russell, 2007a, b). This altirostral skull morphology is particularly evident in baurusuchids as well (Marinho *et al*., 2013; Dumont *et al*., 2020b; Fonseca *et al*., 2020) and, to a lesser degree, in some theropods (Stevens, 2006; Schade *et al*., 2020), and

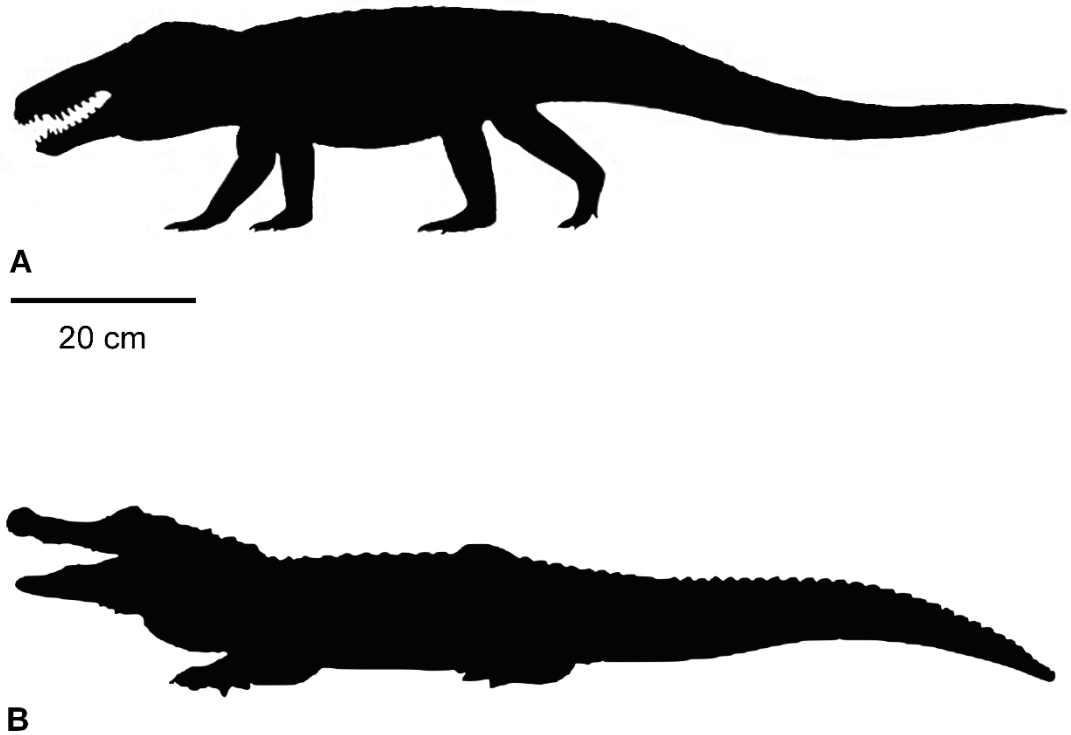

Figure 3.20: Interpretative drawings of the posture of *Zulmasuchus querejazus* (A; inspired by the work of Marco Auditore) and *Caiman crocodilus* (B; drawing by Mohamed Hassan).

suggests a similar ecology and predatory habits for *Zulmasuchus*. On the other hand, the body of modern crocodylians often floats completely submerged, just leaving their cranial sensory organs above the water line, which implies to keep the head in the horizontal plane (Witmer *et al*., 2008; Fig. 3.20). This would also imply a lower energy cost because the head is partially held horizontal by its buoyancy (Grigg & Kirshner, 2015). This does not appear to be the case in *Zulmasuchus*, as demonstrated above.

The anterior semicircular canal is slightly more dorsally elongate, which is in line with what is known from most other crocodylomorphs and is correlated with a moderate sensitivity to pitching (given its position, the endolymphatic liquid inside the canal moves when the head moves up and down in a 3D space, translating information collected by the cristae and allowing the brain to control the amount of acceleration of the head in one direction; Hudspeth, 1983; Rabbitt *et al*., 2004). Furthermore, although it has a very narrow cross-sectional diameter (David, 2010), the lateral semicircular canal is quite curved and expanded, which is a sign of increased sensitivity to yaw movements (again, the endolymphatic liquid inside this canal is subject to the movement of the head from side to side).

This suggests that *Zulmasuchus* could move its head to the full extent of its capabilities in the three axes in relation to its body, which further supports a terrestrial lifestyle. In fact, the inferred hunting strategies of sebecids and adaptation to their living environment (Pol *et al*., 2012) required *Zulmasuchus* to have a highly mobile head. On the other hand, semi-aquatic and aquatic crocodiles such as thalattosuchians, dyrosaurids or extant crocodylians have less expanded canals (Schwab *et al*., 2020), meaning a decreased sensitivity to pitching and yawing (as well as their head being more in line with their body movement; Schwab *et al*., 2020) which could confirm this hypothesis. In addition, although the semicircular canals of teleosaurids, dyrosaurids and extant crocodylians are expanded, linked to enhanced agility and aerobatic ability (Witmer *et al*., 2003; Sipla, 2007; Pierce *et al*., 2017), those of *Zulmasuchus* are even narrower in diameter and more expanded. Thus, it must have had a very agile and fast locomotion, which again makes sense if we consider a terrestrial ecology. This is also confirmed with what is observed in other large predatory reptiles: theropods and pseudosuchians have a strikingly close morphology of the endosseous labyrinths compared with *Z. querejazus* (Sanders & Smith, 2005; Witmer & Ridgely, 2009; Paulina-Carabajal & Succar, 2014; Xing *et al*., 2014; Nesbitt *et al*., 2018; Paulina-Carabajal & Filippi, 2018; Cerroni & Paulina-Carabajal, 2019; Paulina-Carabajal & Nieto, 2019), whereas marine reptiles such as metriorhynchids,

mosasaurs and plesiosaurs have a more rounded and less expanded morphology (Evans, 1999; Yi & Norell, 2019; see also Fig. 3.15).

Finally, the expanded anterior semicircular canal of *Z. querejazus* also means that it had an important head mass (Georgi *et al*., 2013): this taxon showing this characteristic high-snouted condition (Buffetaut & Marshall, 1992), a heavier head mass can indeed be inferred and would have also probably relied on developed neck musculature to hold this mass, in turn making the head movements mentioned above easier.

Hearing

Hearing in extant crocodylians is challenging to understand because these organisms interact with sound waves travelling in both the aquatic and in the aerial environment. Although their ear morphology and structures are very similar to those of birds (Gleich & Manley, 2000), and would therefore seem to be adapted to aerial hearing, crocodylians spend a lot of time submerged. It has been shown that they can hear in similar frequency ranges in both environments (Higgs *et al*., 2002). While they retain the classic scheme of hearing an airborne sound as in other reptiles, the way they can hear under water remains hypothetical and difficult to assess. The most logical explanation is that sound information underwater is conducted to the inner ear via the cranial bones, rather than through the tympanic membrane (Higgs *et al*., 2002). In terms of frequency, modern crocodylians globally emit and receive in the low to middle range (Wever, 1971). The sounds they emit are mostly used for inter-individual communication and social interactions (i.e., reproduction, parental care, and protection of juveniles; Beach, 1944; Herzog & Burghardt, 1977; Vliet, 1989; Wang *et al*., 2007; Vergne *et al*., 2012 and references therein). Recent studies also showed that the middle ear cavities are connected in Crocodylia, further enhancing their auditory capability (Bierman *et al*., 2014 and references therein).

The hearing range of *Z. querejazus* can be inferred because it is strongly correlated with cochlear duct measurements (derived from extant taxa; Walsh *et al*., 2009). This equation has already been applied on thalattosuchians (Brusatte *et al*., 2016), baurusuchids (Dumont *et al*., 2020b), maniraptorans (King *et al*., 2020) and basal dinosaurs (Ballel *et al*., 2020). Here, we complete this sampling with the addition of the presently described specimen of *Zulmasuchus* and other crocodylomorphs from which the data is available but has not been added yet (i.e., *P. typus*, Pierce *et al*., 2017; *M. bollensis* and *C. araucanensis*, Herrera *et al*., 2018 and Wilberg *et al*., 2021; *R. aslerensis*, Erb & Turner, 2021; '*M.*' *brachyrhynchus*, Schwab *et al*., 2021a; see

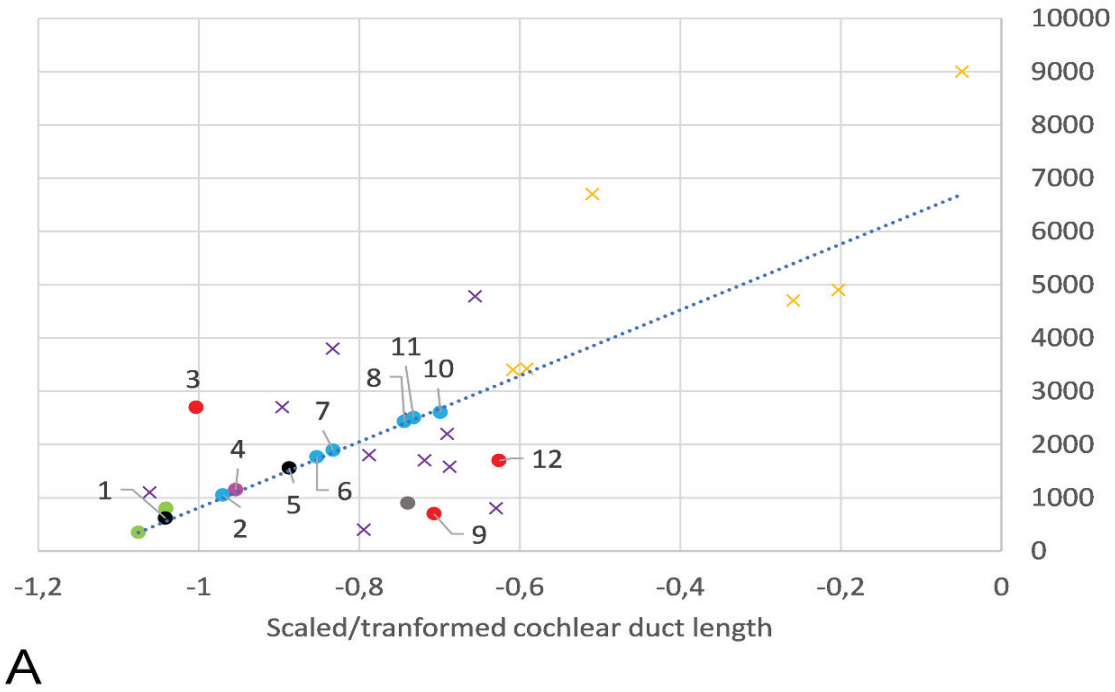

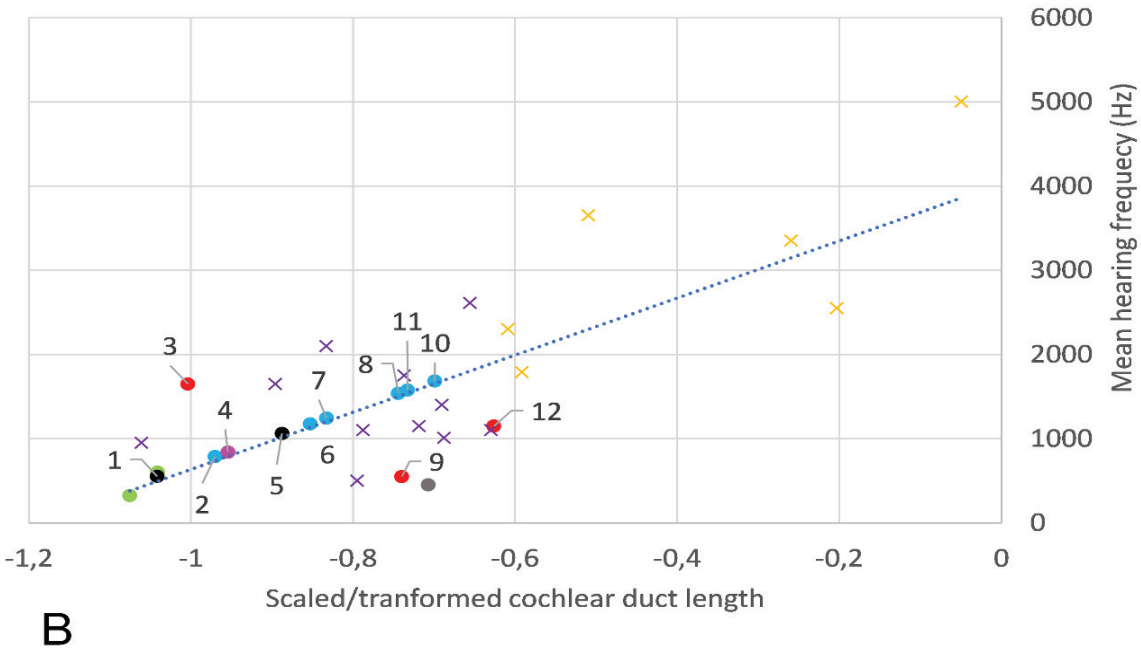

Figure 3.21: Mean hearing range (A, blue trend line: y = 6104.3x + 6975.2; ± 1483 Hz) and best hearing frequency (B, blue trend line: y = 3311.3x + 4000.8; ± 764 Hz) for *Z. querejazus* and other crocodylomorphs, using the methods of Walsh *et al*. (2009). Yellow crosses: Aves Linnaeus, 1758, purple crosses: Squamata Oppel, 1811; green circles: Testudines Batsch, 1788; grey circle: Rhynchocephalia Günther, 1867, red circles: extant crocodylians; blue circles: semi-aquatic and aquatic extinct crocodylomorphs; pink circle: *Zulmasuchus querejazus*; black circles: other terrestrial crocodylomorphs (see Supplementary Materia S1 for more information). 1: Juvenile *Baurusuchus* sp., 2: *Cricosaurus araucanensis*, 3: *Crocodylus acutus*, 4: *Zulmasuchus querejazus*, 5: Adult *Baurusuchus* sp., 6: *Pelagosaurus typus*, 7: '*Metriorhynchus'* cf. *brachyrhynchus*, 8: *Plagiophthalmosuchus* cf. *gracilirostris*, 9: *Alligator mississippiensis*, 10: *Rhabdognathus aslerensis*, 11: *Macrospondylus bollensis*, 12: *Caiman crocodilus.*

Fig. 3.21). *Zulmasuchus* displays a hearing range similar to the terrestrial baurusuchids with a best mean hearing frequency of 841 Hz and a hearing range of 1150 Hz. As mentioned by Dumont *et al*., (2020b), the juvenile specimen of *Baurusuchus* has lower values probably because the endosseous labyrinth was not segmented as precisely as that of the adult, therefore the calculation is potentially not reliable. However, obtained values for these specimens are in the range of the hearing capabilities of extant crocodylians (Walsh *et al*., 2009) and, more importantly, are lower than the ones of the semi-aquatic and aquatic extinct crocodylomorphs (mean of best hearing ranges: 2149.4 Hz and mean of best mean hearing frequency: 1393.8 Hz; Fig. 3.21). This is with the notable exception of the aquatic thalattosuchian *Cricosaurus araucanensis*, probably because the data on which its cochlear duct is reconstructed (Herrera *et al*., 2018) do not allow for a complete reconstruction of this part.

It also means that *Zulmasuchus* probably had vocalization frequencies in the same range as its hearing faculties, as it is the case in extant crocodylians (Vergne *et al*., 2009). As a result, terrestrial sebecosuchians would have been able to hear and vocalize in mid to low frequencies (< 2000 Hz; Dumont *et al*., 2020b), which is towards the known lower range of extant crocodylians.

Although not statistically significant (p-value = 0.8 for mean best hearing frequency and best mean hearing range), this result differs from sampled semi-aquatic and aquatic extinct crocodylomorphs which have a much larger hearing range and a higher mean hearing frequency, linked to a longer cochlear duct (Brusatte *et al*., 2016; Pierce *et al*., 2017; Herrera *et al*., 2018; Erb & Turner, 2021; Wilberg *et al*., 2021).

This difference could be explained by different needs in terms of communication. Lower frequencies travel further than higher frequencies, so organisms using those lower frequencies (such as *Zulmasuchus*) could have had the need to communicate in long ranges, as is the case nowadays with elephants (Garstang, 2004) or cetaceans (Tyack & Clark, 2000 and references therein). Other possibilities to be investigated over the processing of low frequencies could also be linked with prey acquisition or the phylogeny.

However, it remains difficult to assess the living environment of an organism based on its auditory capacities, as extant birds globally show high frequencies and aquatic turtles exhibit the lower values, whereas the semi-aquatic and aquatic thalattosuchians have higher values than the terrestrial sebecosuchians, so a specific trend does not emerge there. Furthermore, the segmentation of the cochlear duct can also be difficult, as the distinction between the sinus

system and the anterior part of this duct is not clearly delimited by bone (Fig. 3.16), so caution needs to be exercised when interpreting those values (see also Herrera *et al*., 2018, Schwab *et al*., 2020, 2021a; Erb & Turner, 2021).

Cranial pneumaticity

Zulmasuchus exhibits very developed pharyngotympanic sinuses (as in *Campinasuchus*; Fonseca *et al*., 2020), whereas these structures are less developed in extant crocodylians (Witmer *et al*., 2008; Bona *et al*., 2017; Serrano-Martínez *et al*., 2019b). The intertympanic diverticulum is also absent in thalattosuchians (Brusatte *et al*., 2016; Pierce *et al*., 2017; Herrera *et al*., 2018; Schwab *et al*., 2021a; Wilberg *et al*., 2021). It is difficult to assess the ancestral state of this trait, but it would seem to be related to the living environment (semi-aquatic and aquatic vs terrestrial; Brusatte *et al*., 2016). An enlargement of these structures allows improved resonance and sound pickup in aerial environments (Dufeau & Witmer, 2015). The selection of such structures then appears logical considering a terrestrial ecology for *Zulmasuchus* as the sound is more difficult to capture in the air than in the water (this is also the case or *C. dinizi*; Fonseca *et al*., 2020). On the other hand, thalattosuchians and dyrosaurids, and to a lesser degree extant crocodylians, would not necessarily rely on such developed structures, because the sound they capture does not come exclusively from the aerial environment but also from the aquatic one, where it travels more easily. Another hypothesis, which could be coupled with the first one, is the impact of such structures on the buoyancy and the density of the skull of semi-aquatic and aquatic forms (Brusatte *et al*., 2016). Finally, Dufeau & Witmer (2015) proposed a link between the extension of these structures and the shape of the rostrum: long-snouted specimens with a specialized diet (gharials, dyrosaurids or thalattosuchians for example, Brusatte *et al*., 2016; Erb & Turner, 2021) exhibit smaller structures than feeding generalists with smaller snouts such as *Hamadasuchus* (Dufeau, 2011). This last hypothesis appears controversial because on one hand it is reinforced by what is found in *Zulmasuchus*, which shows a combination of a snout of moderate length, with terrestrial habits (so probably a more generalist diet than semi-aquatic and aquatic forms), but on the other hand, if we compare the cranial pneumaticity between *Gavialis gangeticus* (longirostre taxon with specialized diet) and *Caiman crocodilus* (brevirostre taxon with generalist diet), they do not differ much when compared with other forms such as thalattosuchians or sebecosuchians (Fig. 3.17). Further studies are thus needed to assess whether cranial pneumaticity is linked with rostrum morphology and thus diet. As longirostrine taxa seem to be mostly semi-aquatic and aquatic, a possible explanation could also be linked in the difference in the point of equilibrium of the skull between floating in the

water and holding thanks to the neck musculature in an aerial environment. As the constraints exercised on a submerged skull are less important than on a non-submerged one, the development of "extreme" morphologies would then be facilitated.

The median pharyngeal sinus and the pharyngotympanic sinus are interconnected in extant crocodylians (Colbert, 1946b; Witmer *et al*.; 2008, Bona *et al*., 2017; Serrano-Martínez *et al*., 2019b), thalattosuchians (Wenz, 1968; Brusatte *et al*., 2016; Pierce *et al*., 2017; Herrera *et al*., 2018; Schwab *et al*., 2021a; Wilberg *et al*., 2021) and dyrosaurids (Erb & Turner, 2021), to allow pressure equalization between the middle ear, the pharynx and the external environment (Colbert, 1946b; Dufeau & Witmer, 2015). In *Alligator mississippiensis*, this phenomenon has been reported to be controlled by the median pharyngeal valve, which opens and closes regularly (Young & Bierman, 2019). This mechanism has only been observed in this taxon for now, so further studies are needed to assess if it is the rule inside Crocodylia, or even Crocodylomorpha. The only difference found so far in all sampled crocodylomorphs comes from *Pelagosaurus typus*, which does not possess a verticalized pharyngeal sinus, because of the ventral displacement of the basicranium (Pierce *et al*., 2017). *Zulmasuchus* and other sebecosuchians (Colbert, 1946a; Fonseca *et al*., 2020), although having a different ecology, do not differ from the general organisation of other crocodylomorphs, thus these structures seem to be of low interest when looking at behavioural or phylogenetic inferences. Caution must be exercised though, because it is difficult to reconstruct these structures in fossils, so the access to exquisitely preserved specimens or more precise work might contradict these observations in the future.

Implications

The endocranial cavities of crocodylomorphs are understudied and a lot of data are still missing to get a more complete view of the diversity and peculiarities of the group. This could prove important to better understand both their phylogenetic relationships and paleoecological characteristics.

First, the endocranial structures could bear phylogenetic information and would benefit from being incorporated into future phylogenetic studies. New characters would of course need to be diagnosed, and their relevance tested, especially regarding ontogeny, but it could bring new information in untangling the systematics of Crocodylomorpha, provided that new data are published concerning those structures in yet unsampled taxa. For example, it is difficult to tease

apart whether the observed short cochlear ducts in sebecosuchians is characteristic of the group (i.e., a synapomorphy) or if it is the ancestral condition of a larger taxonomic group that contains Sebecosuchia (for example, the middle Triassic suchian *Parringtonia gracilis* also has a rather short cochlear duct; Nesbitt *et al*., 2018). However, this does not seem to be the ancestral condition of the diapsids, as *Youngina capensis* Broom, 1914, a Permian basal diapsid reptile shows an elongated cochlear duct (Gardner *et al*., 2010). Other peculiar characteristics of *Z. querejazus* are the high flexure observed between the hindbrain and the forebrain, as well as the pericerebral spines associated with a depression described on the surface of the dorsal longitudinal venous sinus. Could these be considered synapomorphies of this taxon? It is of course too early to determine but these characteristics will need to be described with great consideration in future studies on other specimens.

The endocranial structures, by the very nature of the systems they house, are equally important when taking into consideration the paleoecology of these taxa. For example, the cochlear duct can be used as a proxy to the hearing capabilities of extant taxa (see above), which can already be of great use if we aim to know more about the behavior of such taxa. Other structures which are of particular interest are the pharyngotympanic sinuses and the intertympanic diverticulum: as mentioned above, their development could also be linked with the living environment, behavior, and diet. These assumptions again require more data to be collected on other terrestrial taxa, and if used in combination with the endosseous labyrinths data, could prove very useful to assess the living environment of a fossil taxon for which the data is available (as a supporting argument to more traditional inferences). This has allowed to better understand and strengthen the terrestrial habits of several sebecosuchians (Dumont *et al*., 2020b; Fonseca *et al*., 2020; this study), and this approach needs to be generalized to other taxa in this group, some of which are nicely preserved and would surely represent a source of high-definition reconstructions in future studies.

Finally, these features must be analysed with caution, to separate properly the ecological and phylogenetic signals, so as not to confuse them and thus reach erroneous conclusions (Losos, 2008). For example, if a given characteristic is thought to be the proof of a specific ecological trait, it could also be linked to a taxonomic sampling bias - that it could be a synapomorphy of this taxonomic group, rather than an ecological trait as a rule (one should note that it could very much be both as well). The same reasoning is valid the other way around (phylogenetic vs ecological information).

Conclusion

The endocranial cavities of *Zulmasuchus querejazus* are described. This taxon exhibits a highly curved endocast between the midbrain and the hindbrain, as well as pericerebral spines, the combination of both features being observed for the first time inside Crocodylomorpha. The endosseous labyrinths of MHNC 6672 are quite expanded but the semicircular canals are very narrow in cross-section. Finally, the intertympanic diverticulum and the pharyngotympanic sinus are well-developed compared to those of thalattosuchians, whereas the ventral part of the brain endocast shows no real difference from what is already known in other extinct and extant taxa.

The alert head posture of this specimen is inferred to be slightly inclined ~10° below horizontal based on the alignment of the endocranial surface of the parietal with the horizontal plane. This value is higher than that of extant crocodylians (which have a posture parallel to the horizontal plane for ecological reasons) and is coherent with what has been inferred in other notosuchians. This posture allowed *Zulmasuchus* to benefit from a binocular vision over his altirostral snout, a feature that can be associated with predatory and terrestrial habits.

Furthermore, the morphology of its endosseous labyrinth further supports a terrestrial lifestyle because its expanded canals allow for more mobility of the head, an essential trait in these motion methods. The length of the cochlear duct is linked with the hearing capabilities (which range among low frequencies in *Zulmasuchus*), inducing the ability to communicate at long distances between individuals. Caution still needs to be exercised because of segmentation biases.

Finally, the enlarged pharyngotympanic sinuses of this specimen, compared with thalattosuchians, allow to link these structures with the living environment of the organism they belong to. Semi-aquatic and aquatic forms (such as thalattosuchians) may not exploit the enhanced aerial perception given by the enlargement of these structures; hence they are more likely associated with terrestrial taxa. Other hypotheses are about the effect of the pneumatization on buoyancy or on the morphology of the snout (linked with diet). While it is difficult to favour one of those hypotheses for now, the differences observed are clearly linked to the living environment of the specimens.

All these observations could be tested and, if proven relevant, for example when considering ontogenetic changes, introduced as phylogenetic characters in future studies, to further

understand the systematics of this highly diverse group of archosaurs, but caution will need to be exercised regarding the conflict between ecological and phylogenetic signal in these structures. Further studies in the field of the neuroanatomy of Crocodylomorpha should help clarify those issues.

Acknowledgements

This work was supported by the Agence Nationale de la Recherche (SEBEK project N° ANR-19-CE31-0006-01 to JEM). The authors thank Marco Auditore (Museo Civico di Storia Naturale, Genoa, Italy) for permission to use the silhouette of the sebecosuchian (Fig. 3.18 and 3.20); David Blackburn (Florida Museum of Natural History) and Cody Thompson (University of Michigan) for allowing access respectively to the CT data of *Gavialis gangeticus* (UF herp 118998) and *Caiman crocodilus* (UMMZ herps 128024) via Morphosource and allowing us to use it in this study; Romain David (Max Planck Institute for Evolutionary Anthropology) for discussions about his previous segmentation of the specimen and the sharing of the data he used in his PhD thesis; Peggy Vincent (MNHN, UMR 7207) for transporting the specimen between Paris and Lyon. We are grateful to Logan King (University of Bristol), Yanina Herrera (Universidad Nacional de La Plata) and Timothy Smith (Slippery Rock University) for insightful comments that greatly improved the quality of this manuscript.

Authors contributions

Yohan Pochat-Cottilloux: Conceptualization, Methodology, Software, Validation, Formal analysis, Investigation, Data Curation, Writing - original draft, Writing - review and editing, Visualization, Project administration. **Jeremy E. Martin:** Conceptualization, Methodology, Validation, Resources, Data Curation, Writing - original draft, Writing - review and editing, Supervision, Project administration, Funding acquisition. **Stéphane Jouve:** Conceptualization, Validation, Resources, Writing - original draft, Writing - review and editing, Project administration, Funding acquisition. **Gwendal Perrichon:** Validation, Investigation, Writing - review and editing. **Jérôme Adrien:** Methodology, Software, Validation, Resources, Data Curation, Writing - review and editing. **Céline Salaviale:** Methodology, Software, Validation, Data Curation, Writing - review and editing. **Christian de Muizon:** Validation, Resources, Writing - review and editing, Project administration, Funding acquisition. **Ricardo Cespedes:** Validation, Resources, Data Curation, Writing - review and editing. **Romain Amiot:**

Conceptualization, Validation, Writing - review and editing, Supervision, Project administration.

Data archiving statement

Data for this study are available in the article, the Supplementary Material and the associated MorphoMuseum publication: Pochat-Cottilloux Y., Martin J. E., Jouve S., Perrichon G., Adrien J., Salaviale C., Muizon C. d., Cespedes R. & Amiot R. (2021). 3D models related to the publication: The neuroanatomy of *Zulmasuchus querejazus* (Crocodylomorpha, Sebecidae) and its implications for the paleoecology of sebecosuchians. *MorphoMuseum*, 7: e148. https://doi.org/10.18563/journal.m3.148

Supplementary Material

Supplementary Material S1 is available on this link: https://mycore.core-cloud.net/index.php/s/nMKvH0DymZFhukD

III- Scientific publication 'The neuroanatomy and pneumaticity of *Hamadasuchus* (Crocodylomorpha, Peirosauridae) from the Cretaceous of Morocco and its paleoecological significance for altirostral forms'

This publication was published in June 2023 in *Journal of Anatomy*. Reference: Pochat-Cottilloux Y., Rinder N., Perrichon G., Adrien J., Amiot R., Hua S. & Martin J. E. (2023). The neuroanatomy and pneumaticity of *Hamadasuchus* (Crocodylomorpha, Peirosauridae) from the Cretaceous of Morocco and its paleoecological significance for altirostral forms. *Journal of Anatomy*. https://doi.org/10.1111/joa.13887

The neuroanatomy and pneumaticity of *Hamadasuchus* (Crocodylomorpha, Peirosauridae) from the Cretaceous of Morocco and its paleoecological significance for altirostral forms

Yohan Pochat-Cottilloux[A], Nicolas Rinder[A], Gwendal Perrichon[A], Jérôme Adrien[B], Romain Amiot[A], Stéphane Hua[C], Jeremy E. Martin[A]

A: Univ Lyon, Univ Lyon 1, ENSL, CNRS, LGL-TPE, Villeurbanne, France.

B: Laboratoire Matériaux, Ingénierie et Science, Institut National des Sciences Appliquées de Lyon, Villeurbanne, France.

C: Paléospace, Villers-sur-Mer, France.

Corresponding author: Yohan Pochat-Cottilloux, yohan.pochat-cottilloux@univ-lyon1.fr

Abstract

We describe the endocranial structures of *Hamadasuchus*, a peirosaurid crocodylomorph from the late Albian - Cenomanian Kem Kem group of Morocco. The cranial endocast, associated nerves and arteries, endosseous labyrinths and cranial pneumatization, as well as the bones of the braincase of a new specimen are reconstructed and compared with extant and fossil crocodylomorphs, which represent different lifestyles. Cranial bones of this specimen are identified as belonging to *Hamadasuchus*, with close affinities with *Rukwasuchus yajabalijekundu*, another peirosaurid from the 'middle' Cretaceous of Tanzania. The endocranial structures are comparable to those of *R. yajabalijekundu*, but also to baurusuchids and sebecids (sebecosuchians). Paleobiological traits of *Hamadasuchus*, such as alert head posture, ecology and behaviour are explored for the first time, using quantitative metrics. The expanded but narrow semicircular canals and enlarged pneumatization of the skull of *Hamadasuchus* are linked to a terrestrial lifestyle. Continuing work on the neuroanatomy of supposedly terrestrial crocodylomorphs needs to be broadened to other groups and will allow to characterize whether some internal structures are affected by the lifestyle in these organisms.

Keywords: Morocco – Crocodylomorpha - Kem Kem – paleoneuroanatomy – Peirosauridae – *Hamadasuchus*

Introduction

Peirosaurids represent an extinct family of crocodylomorphs spanning from at least the Barremian to the Maastrichtian (Larsson & Gado, 2000; Lamanna *et al*., 2019). They were widely distributed in South America and Africa. However, not much is known about their ecology, as the cranial and postcranial elements are rare or remain undescribed. The group is diverse, comprising at least 16 different species (see Nicholl *et al*., 2021 for a complete review), but paradoxically, these taxa are mostly represented by mandibular fragments (Barrios *et al*., 2016; Lio *et al*., 2016; Filippi *et al*., 2018; Coria *et al*., 2019; Lamanna *et al*., 2019; Nicholl *et al*., 2021). Their phylogenetic relationships with other groups as well as within Peirosauridae are poorly known and subject to numerous debates. In most studies, Peirosauridae are placed close to uruguaysuchids and mahajangasuchids (Carvalho *et al*., 2004; Turner & Calvo, 2005; Turner, 2006; Turner & Sertich, 2010; Pol *et al*., 2012, 2014; Kellner *et al*., 2014; Sertich & O'Connor, 2014; Leardi *et al*., 2015, 2018; Barrios *et al*., 2016; Fiorelli *et al*., 2016; Godoy *et al*., 2016; Martinelli *et al*., 2018; Coria *et al*., 2019; Dumont *et al*., 2020b; Nicholl *et al*., 2021); other studies depict them as united with sebecids, forming the clade Sebecia (Larsson & Sues, 2007; Meunier & Larsson, 2017; Geroto & Bertini, 2019; Ruiz *et al*., 2021) or closely related to neosuchians (Sereno *et al*., 2003; Pol & Norell, 2004b; Company *et al*., 2005; Pol & Apesteguia, 2005; Zaher *et al*., 2006; Turner & Buckley, 2008; Leardi & Pol, 2009; Sereno & Larsson, 2009; Nascimento & Zaher, 2011; Pol & Powell, 2011).

Like notosuchians, peirosaurids are inferred to have had terrestrial habits by extrapolation with better known closely related groups (e.g., sebecids; Busbey, 1986; Molnar, 2012; Pol *et al*., 2012 and mahajangasuchids; Sereno & Larsson, 2009). However, evidence of a more aquatic lifestyle also exists in some specimens (Sena *et al*., 2018). The study of the neuroanatomy and the pneumaticity of the skull could hold relevant data about the neurosensorial capabilities of the specimen studied and thus opens the possibility to infer its lifestyle.

In the last decade, numerous studies using computed tomography (CT) data have been published (see Barrios *et al*., 2023 for a complete review) on eusuchians (Holliday & Gardner, 2012; Bona & Paulina-Carabajal, 2013; Bona *et al*., 2013, 2017; Blanco *et al*., 2015; Serrano-Martínez *et al*., 2019a, b, 2020; Erb & Turner, 2021; Puértolas-Pascual *et al*., 2022, 2023; Burke & Mannion, 2023), thalattosuchians (Fernández *et al*., 2011; Brusatte *et al*., 2016; Pierce *et al*., 2017; Herrera *et al*., 2018; Schwab *et al*., 2021a; Wilberg *et al*., 2021), early crocodylomorphs (Leardi *et al*., 2020; Melstrom *et al*., 2022; Ruebenstahl *et al*., 2022) and some notosuchians

(Sereno & Larsson, 2009; Kley *et al*., 2010; Dumont *et al*., 2020b; Fonseca *et al*., 2020; Pochat-Cottilloux *et al*., 2022b). Those studies are based on extant crocodylians databases for comparison (Witmer *et al*., 2008; Bona *et al*., 2017), as well as detailed studies focusing on certain parts of the braincase (Klembara, 2005; Dufeau, 2011; George & Holliday, 2013; Dufeau & Witmer, 2015; Montefeltro *et al*., 2016; Porter *et al*., 2016; Jirak & Janacek, 2017; Hu *et al*., 2020; Lessner & Holliday, 2020; Kuzmin *et al*., 2021; Lessner *et al*., 2022; Schwab *et al*., 2022; Perrichon *et al*., 2023). The neuroanatomy of Peirosauridae has been investigated in a few members of the group such as *Rukwasuchus yajabalijekundu* (Sertich & O'Connor, 2014) and *Hamadasuchus rebouli sensu* Larsson & Sues (2007; ROM 52620) by Dufeau (2011) and George & Holliday (2013). However, in both cases, those structures are not described in detail, especially the endosseous labyrinths and the cranial pneumaticity, and are not used for paleobiological inferences. Therefore, the endocranial structures of peirosaurids deserve an augmented treatment.

Since the recognition of *Hamadasuchus rebouli*, more complete peirosaurids specimens have been discovered, enhancing the diversity of this poorly known genus endemic to Africa (Rauhut & Lopez-Arbarello, 2005; Larsson & Sues, 2007; Ibrahim *et al*., 2020; Pochat-Cottilloux *et al*., 2023a). Here, we describe the internal and external anatomy of a new specimen of *Hamadasuchus* (UCBL-FSL 532408) from the late Albian - Cenomanian Kem Kem group of Morocco.

Using the reconstructed internal structures of this specimen (cranial endocast, endosseous labyrinths and braincase pneumaticity), we use several proxies to infer associated paleobiological traits of *Hamadasuchus*, putting them into perspective with comparative data on sebecosuchians, eusuchians and thalattosuchians. The data are also used to reconstruct the braincase osteology, allowing a robust taxonomic assessment of this specimen.

Material and methods

CT scan

The studied material consists of a complete skull of a crocodylomorph (UCBL-FSL 532408; Fig. 3.22), currently curated in the geological collections of Université Lyon 1. The specimen originates from an unknown location in the Kem Kem group of Morocco (late Albian - Cenomanian; Sereno *et al*., 1996; Martin & de Lapparent de Broin, 2016; Ibrahim *et al*., 2020). The skull was CT scanned in November 2020 at the Laboratoire Mateis (INSA Lyon,

Villeurbanne, France) to reconstruct its internal soft anatomy, as well as the bones constituting the braincase. We used a Vtomex laboratory X-ray computed tomograph (GE Phoenix X-Ray GmbH): scanning parameters were set to 140 kV tube voltage and 80 µA current and a 0.5 mm copper filter was used at the source exit. The scan has a voxel size of 86 µm and a one second exposure time for each of the 1,200 projections. Avizo Lite (version 9.5.0), MeshLab (version 2020.07) and Blender (version 2.91.2) were used for the volume rendering and calculations, as well as processing of scans of the endosseous labyrinths, sinuses and cranial endocast. Processed volumes are available in Pochat-Cottilloux *et al*. (2023c), see also Supplementary Material S1 & S2. Here, we describe the bone-bounded spaces that house soft tissue organs as such, given that numerous recent studies on extant taxa have showed that the shape of those structures is strongly correlated with their associated organs (Watanabe *et al*., 2019 on reptiles and Early *et al*., 2020b on birds).

Comparisons

To keep the description free of constant repetitions of references, we summarize the data on extinct and extant crocodylomorph taxa used for comparison in Table 7. In an effort to standardize descriptive studies in paleoneuroanatomy, we follow the anatomical nomenclature published by Colbert (1946a, 1946b), Kley *et al*. (2010), Sertich and O'Connor (2014), Dufeau & Witmer (2015), Brusatte *et al*. (2016), Bona *et al*. (2017), Pierce *et al*. (2017), Herrera *et al*. (2018), Serrano-Martínez *et al*. (2019a, b, 2020), Leardi *et al*. (2020), Lessner & Holliday (2020), Fonseca *et al*. (2020), Dumont *et al*. (2020), Erb & Turner (2021), Kuzmin *et al*. (2021), Schwab *et al*. (2021a), Wilberg *et al*. (2021), Melstrom *et al*. (2022), Pochat-Cottilloux *et al*. (2022b), Puértolas-Pascual *et al*. (2022, 2023), Ristevski (2022), Ruebenstahl *et al*. (2022), Burke & Mannion (2023) and Perrichon *et al*. (2023) concerning the endocranial structures (and references therein). Table 8 compiles several important measurements following Pierce *et al*. (2017; fig. 2).

Paleobiological inferences

Brain volume was estimated using the following relation: log BV = log EV * 0.7279 + 0.75624 where EV: endocranial volume and BV: brain volume (Dumont *et al*., 2020b and references therein; see also Supplementary Material S3). The volume of the sinus system was calculated using Blender v2.91 and skull width was measured as the largest skull width (including quadrates; see Supplementary Material S3). We chose to use the skull width rather than the skull length to prevent us from potential convergence problems related to the size of the

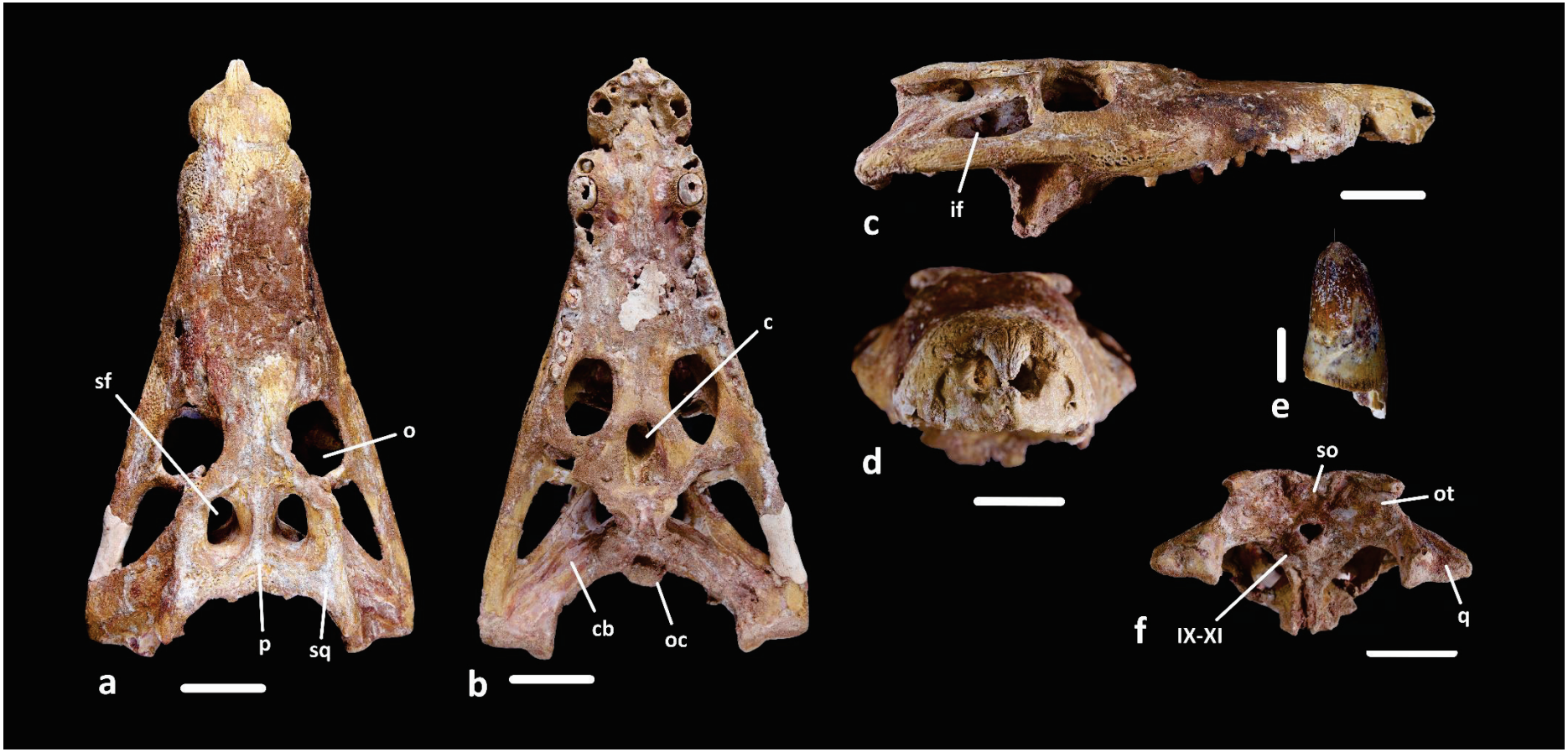

Figure 3.22: Skull of *Hamadasuchus* (UCBL-FSL 532408) in dorsal (a), ventral (b), lateral (c) anterior (d) and posterior (f) views, close up on a tooth (e). IX-XI: foramen for cranial nerve IX-XI, c: choana, cb: crest B, if: infratemporal fenestra, o: orbit, oc: occipital condyle, ot: otoccipital, p: parietal, q: quadrate, sf: supratemporal fenestra, so: supraoccipital, sq: squamosal. Scale bars for (a), (b), (c), (d) and (f) are 5 cm and 1 cm for (e).

Table 7: Comparative material used in this study. MHNC 6672 is here identified as *Zulmasuchus* mainly for consistency with previous studies, although there are conflicting views on the separation of this genus with *Sebecus* (Pol *et al*., 2012; Leardi *et al*., 2015, 2018; Fiorelli *et al*., 2016).

Taxon	**Specimen**	**Publication or database**
Alligator mississippiensis	UCBL WB35	This study
Caiman crocodilus	UMMZ HERPS 128024	Morphosource
Crocodylus acutus	MZS Cro 055	This study
Gavialis gangeticus	MLP 602; UF HERP 118998	Bona *et al*. (2017); Pierce *et al*. (2017); Morphosource
Mecistops sp.	MHNL 50001393	This study
Osteolaemus tetraspis	UCBL 2019-1-236	This study
Paleosuchus trigonatus	MHNL 50003939	This study
Tomistoma schlegelii	TMM M6342	Morphosource
Tomistoma downsoni	NHMUK PV R 4769	Burke & Mannion (2023)
Diplocynodon tormis	STUS-344	Serrano-Martínez *et al.* (2019b)
Arenysuchus gascabadiolorum	MPZ 2011/184	Puértolas-Pascual *et al.* (2022)
Agaresuchus fontisensis	HUE-02502; HUE-03713	Serrano-Martínez *et al*. (2020)
Agaresuchus subjuniperus	MPZ 2012/288	Puértolas-Pascual *et al*. (2022)
Trilophosuchus rackhami	QMF16856	Ristevski (2022)
Portugalosuchus azenhae	ML1818	Puértolas-Pascual *et al*. (2023)
Pelagosaurus typus	BRLSI-M1413	Pierce *et al*. (2017)
Plagiophthalmosuchus cf. *gracilirostris*	NHMUK PV OR 33095	Brusatte *et al*. (2016)
Macrospondylus bollensis	SNSB-BSPG 1984 1258; MCZ VPRA-1063	Herrera *et al*. (2018); Wilberg *et al.* (2021)
Cricosaurus araucanensis	MLP 72-IV-7-1	Herrera *et al*. (2018)

'Metriorhynchus' cf. *brachyrhynchus*	NHMUK PV O 32617	Schwab *et al*. (2021a)
Rhabdognathus aslerensis	AMNH FARB 33354 formerly CNRST-SUNY 190	Brochu *et al.* (2002); Erb & Turner (2021)
Rukwasuchus yajabalijekundu	RRBP 08630	Sertich & O'Connor (2014)
Simosuchus clarki	UA 8679	Kley *et al*. (2010)
Campinasuchus dinizi	CPPLIP 1319, 1360	Fonseca *et al*. (2020)
Baurusuchus sp.	IFSP-VTP/PALEO-0002, 0003; FEF-PV-R-1/9; FUP-Pv 000020, 000021	Dumont *et al*. (2020b)
Sebecus icaeorhinus	AMNH 3160	Colbert *et al*. (1946a)
Zulmasuchus querejazus	MHNC 6672	Pochat-Cottilloux *et al*. (2022b)
Sphenosuchus acutus	SAM 3014	Walker (1990)
Almadasuchus figarii	MPEF-PV 3838	Leardi *et al*. (2020)
Junggarsuchus sloani	IVPP14010	Ruebenstahl *et al*. (2022)
Eopneumatosuchus colberti	MNA V2460	Melstrom *et al*. (2022)

rostrum, as well as making it possible to include fossil specimens for which the skull length is unknown without having to estimate it.

Results

General preservation

The cranium is complete and well preserved. It is altirostral (short and elevated snout) and has heterodont ziphodont teeth. In some skull areas, however, the bone surface is not clear and is sometimes covered by sediment, which were probably glued to the bones during preparation. There are also two areas in which the surface is covered by white plaster, one ventrally in the palatal area, and one at the junction of the right jugal and quadratojugal. The braincase occupies the posterior third of the skull. For this paper, we will focus only on this part of the skull, while

Table 8: Raw morphometric data of UCBL-FSL 532408 (*Hamadasuchus*) and comparative material.

(Rounded to nearest mm or mm²)	*Pelagosaurus typus*	*Plagiophthalmosuchus* cf. *gracilirostris*	*Macrospondylus bollensis*	*Cricosaurus araucanensis*	*'Metriorhynchus'* cf. *brachyrhynchus*	*Rhabdognathus aslerensis*	*Gavialis gangeticus*	*Tomistoma downsoni*	*Alligator mississippiensis*	*Crocodylus porosus*	*Diplocynodon tormis*	*Arenysuchus gascabadiolorum*	*Agaresuch subjuniper*
Skull width at cerebrum (SW)	52	?	33	40	74	89	168	109	73	39	25	68	?
Cephalic flexure angle (CF)	160	175	170	135	155	158	150	143	135	125	140	159	154
Pontine flexure angle (PF)	160	170	165	170	165	152	154	149	145	170	160	160	156
Endocast length (EL)	57	?	76	140	?	171	146	146	98	40	82	32	88
Olfactory tract length (+ bulbs) (OL)	21	?	26	69	?	49	55	66	48	18	36	20	68
Cerebrum width (CW)	15	28	19	25	40	26	32	30	21	18	23	19	27
Pituitary width (PW)	6	14	4	11	16	5	6	9	5	4	2	6	7
Pituitary height (PH)	7	12	6	9	12	10	9	9	8	3	6	4	7
Pituitary length (PL)	10	17	4.5	14	30	14	11	17	10	13	4	6	14
Labyrinth height (LH)	14	26	22	19	20	25	21	19	18	9	?	?	?
Labyrinth width (LW)	11	26	18	18	21	26	21	15	14	9	?	?	?
Endosseous cochlear duct length (ECL)	8	13	12	7	9	12	9	11	8	3	?	?	?
Anterior semi-circular canal area (AA)	9	38	18	?	?	19	36	21	35	11	?	?	?
Posterior semi-circular canal area (PA)	6	19	5	?	?	4	15	10	12	3	?	?	?
Lateral semi-circular canal area (LA)	4	14	7	?	?	8	22	?	13	3	?	?	?
Source	Pierce et al. (2017)	Brusatte et al. (2016)	Herrera et al. (2018); Erb & Turner (2021)	Herrera et al. (2018)	Schwab et al. (2021)	Erb & Turner (2021)	Pierce et al. (2017)	Burke & Mannion (2023)	Witmer & Ridgely (2008)	Pochat-Cottilloux et al.	Serrano-Martínez et al. (2019)	Puértolas-Pascual et al. (2022)	Puértolas Pascual e al. (2022

(Rounded to nearest mm or	*Agaresuchus fontisensis*	*Trilophosuchus rackhami*	*Portugalosuchus azenhae*	*Simosuchus clarki*	*Rukwasuchus yajabalijekundu*	*Hamadasuchus*	*Campinasuchus dinizi*	*Baurusuchus* sp.	*Sebecus icaeorhinus*	*Zulmasuchus querejazus*	*Sphenosuchus acutus*	*Almadasuchus figarii*	*Eopneumatosuchus colberti*
Skull width at cerebrum (SW)	150	37	?	58	37	94	32	?	147	42	?	?	?
Cephalic flexure angle (CF)	155/160	136	159	142	145	165	155	165	150	130	152	161	170
Pontine flexure angle (PF)	155	142	159	165	145	150	150	165	160	130	146	170	160
Endocast length (EL)	107/133	56	112	79	100	70	85	70	120	?	?	58	?
Olfactory tract length (+ bulbs) (OL)	36/50	22	36	25	45	27	39	32	46	?	?	?	?
Cerebrum width (CW)	21/29	16	25	25	28	26	13	14	30	35	?	18	?
Pituitary width (PW)	4/6	3	5	5	7	6	4	?	?	14	?	?	?
Pituitary height (PH)	7/10	2	10	9	10	8	4	?	9	17	?	4	?
Pituitary length (PL)	4/10	4	24	10	5	14	4	?	8	27	?	7	?
Labyrinth height (LH)	?	13	19	?	?	10	?	12	?	22	?	?	?
Labyrinth width (LW)	?	10	17	?	?	14	?	13	?	14	?	?	?
Endosseous cochlear duct length (ECL)	?	6.5	6	?	?	?	?	6	?	7	?	?	?
Anterior semi-circular canal area (AA)	?	8	8	?	?	8	?	2	?	7	?	?	?
Posterior semi-circular canal area (PA)	?	4	5	?	?	5	?	4	?	7	?	?	?
Lateral semi-circular canal area (LA)	?	2	8	?	?	8	?	1	?	6	?	?	?
Source	Serrano-Martínez et al. (2021)	Ristevski (2022)	Puértolas-Pascual (2023)	Kley et al. (2010)	Sertich & O'Connor (2014)	This study	Fonseca et al. (2020)	Dumont et al. (2020)	Colbert et al. (1946)	Pochat-Cottilloux et al. (2022)	Walker (1990)	Leardi et al. (2020)	Melstrom et al. (2022)

a complete description of the skull and a reappraisal of *Hamadasuchus* will be the topic of a separate study. Overall, in the areas that are visible, the skull is ornamented with circular/ovoid pits dorsally.

Cranial openings:

There are no post temporal fenestrae to be seen, but the area is quite damaged and there seems to be an opening, so the absence of those structures is unsure (Fig. 3.22f & 3.23d).

The supratemporal fenestra is ovoid with its longest axis directed anteroposteriorly and extends posteriorly to more than half the length of the parietal. The supratemporal fossa is small and quickly disappears ventrally.

The foramen magnum is triangular-shaped, about 1.5 centimetres at its widest part and bordered by the otoccipital and the basioccipital.

The internal choanae are contained by the pterygoids and the palatines and are situated at the level of the contact between these bones, quite anteriorly relative to the whole skull.

Braincase

Frontal (Fig. 3.22a, 3.23a-c & 3.23e-f):

The frontal forms a bridge between the rostrum and the post-orbital region of the skull, it constitutes most of the medial margin of the orbit. Posteriorly, it contacts the postorbital obliquely, the parietal transversely and the laterosphenoid ventrally. The sutural surfaces are zigzagged. The frontal participates in the formation of the supratemporal fenestra, contributing to its anteromedial margin. It is dorsally concave and thick, with a slight depression anteriorly between the two orbits. On the midline dorsal surface, the frontal bears an anteroposteriorly directed crest (Fig. 3.23a). The ventral surface, although degraded, is smooth and convex ventrally to accommodate for the olfactory tract (Fig. 3.23b).

Postorbital (Fig. 3.22a, 3.22d-e, 3.23a-c & 3.23e-f):

The postorbital makes for the orbit's posterior margin, as well as the supratemporal fenestra anterolateral margin. The dorsal angle between the medial and posterior parts of the postorbital is not of 90°, as there is an anterolaterally facing edge. However, the ventral and posterior parts

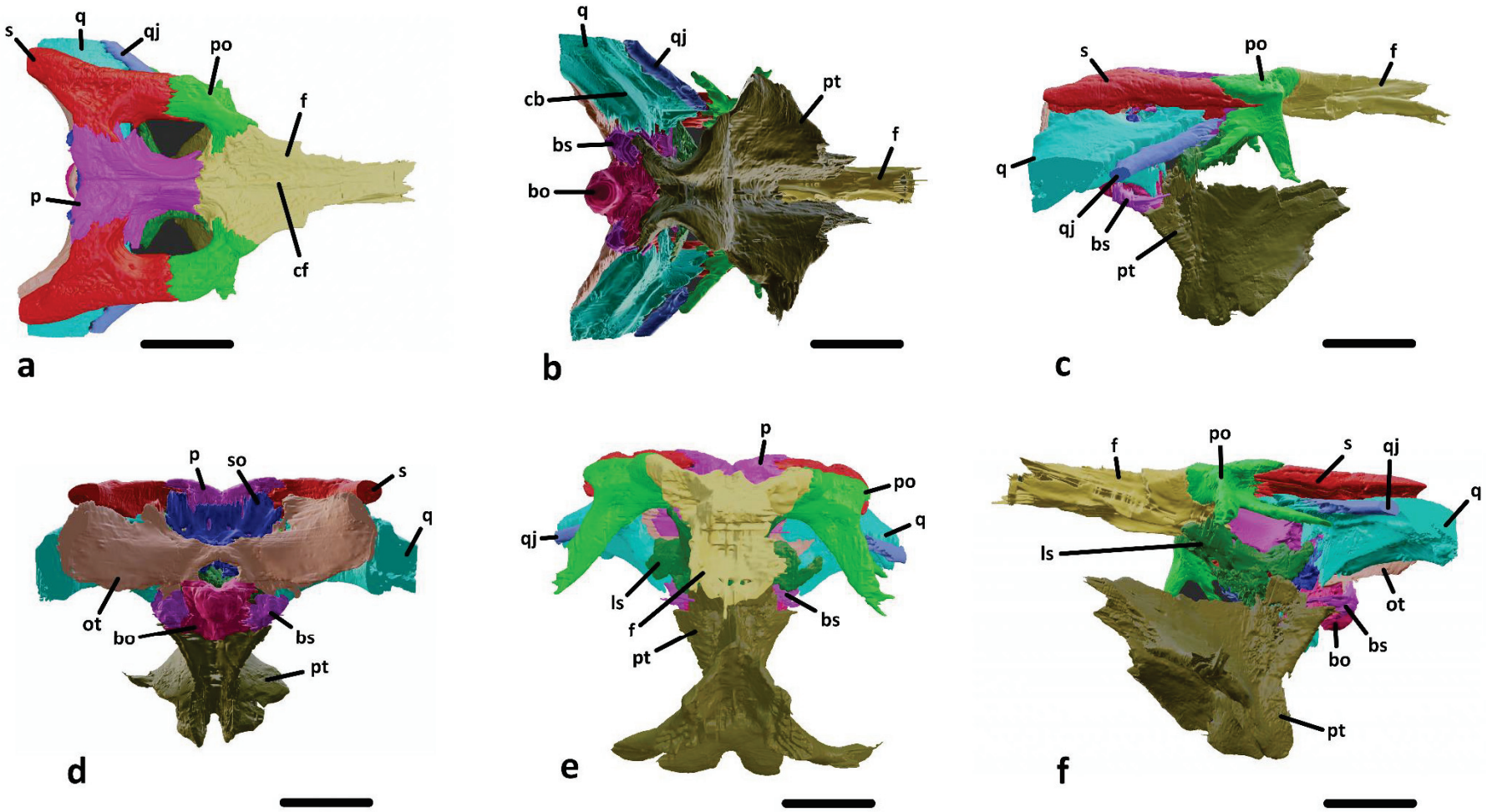

Figure 3.23: Three-dimensional reconstruction of the posterior part of the skull of UCBL-FSL 532408 (*Hamadasuchus*) based on segmented bones in dorsal (a), ventral (b), lateral (c), posterior (d), anterior (e) and ventrolateral (f) views. bo: basioccipital, bs: basisphenoid, cb: crest B, cf: crest on the frontal, f: frontal, ls: laterosphenoid, ot: otoccipital, p: parietal, po: postorbital, pt: pterygoid, q: quadrate, qj: quadratojugal, s: squamosal, so: supraoccipital. Scale bars are 5 cm.

do form a 90° angle in lateral view. Medially, it contacts the frontal but not the parietal. Posteriorly, it has a lateromedially oriented suture with the squamosal. The ventrolaterally descending process sutures with the dorsomedially ascending process of the jugal to form the postorbital bar. Posterolaterally, the postorbital extends along the anterior margin of the quadratojugal and forms the anteroventral margin of the anterior part of the squamosal (Fig. 3.22d-e, 3.23c & 3.23f).

Parietal (Fig. 3.22a, 3.23a & 3.23d-e):

The unpaired parietal is dorsally thin and elevated but tends to widen ventrally. In dorsal view, it is shaped like an hourglass with the posterior part being wider than the anterior one. Laterally, the parietal forms the medial margin of both supratemporal fenestrae and fossae. It contacts the frontal anteriorly and the squamosal laterally. The parietal is also exposed posteriorly, where it sutures with the dorsal margin of the supraoccipital (Fig. 3.22f & 3.23d).

Squamosal (Fig. 3.22a-b, 3.22d-e, 3.23a, 3.23c-d & 3.23f):

The squamosal is T-shaped and forms the posterolateral corner of the skull roof. It contacts the quadrate on both sides of the auditory meatus. This suture is anteroposteriorly straight. Anteriorly, a process connects with the postorbital to form the lateral margin of the supratemporal fenestra (Fig. 3.22a & 3.23a). This process is more extended ventrally than dorsally. Medially, the contact with the parietal is oblique dorsally and straight anteriorly within the supratemporal fossa. At its posteriormost part, the squamosal contacts with the otoccipital and the quadrate laterally and with the supraoccipital medially (Fig. 3.22f & 3.23d): the squamosal thus forms the posterodorsal part of the back of the skull.

Quadratojugal (Fig. 3.22a, 3.22c-e, 3.23a-c & 3.23e-f):

The quadratojugal extends posteriorly from the posterior margin of the infratemporal fenestra, connecting all the way with the quadrate on its medial side. The suture with the quadrate is straight ventrally and dorsally. This contact does not extend anteriorly beyond the level of the postorbital bar. The bone is smooth ventrally and pitted dorsally. It is thin and plate-like, wider mediodorsally than lateroventrally.

Quadrate (Fig. 3.22a-e & 3.23a-f):

The quadrate has a complex shape. Anteriorly, it goes all the way to the posterolateral margin of the supratemporal fenestra and contacts the parietal. Dorsally, it contacts the squamosal on

both sides of the auditory meatus and extends anteriorly to contact the postorbital (Fig. 3.23c & 3.23f). Laterally, the suture with the quadratojugal is straight all the way. The state of preservation of the specimen does not allow to state if the quadrate contacts the pterygoid ventrally. Posteriorly, it contacts the otoccipital straightly and the basisphenoid ventrally. Crest B (Iordansky, 1973; Fig. 3.22c & 3.23b) is clearly visible, extending in parallel to the quadrate-quadratojugal suture from the ventrolateral margin of the supratemporal fenestra to beyond the posterolateral most part of the quadrate. This bone is globally tall in cross-section (almost three centimetres maximum), it is flat on the dorsal surface and curved dorsally on the ventral surface.

Supraoccipital (Fig. 3.22b, 3.23a & 3.23d):

The supraoccipital has a rounded triangular shape in posterior view. It connects dorsolaterally with the squamosal and ventrolaterally with the otoccipital in an oblique suture. It does not participate in the formation of the foramen magnum. In dorsal view it does not invade the parietal anteriorly but forms two postoccipital processes that are situated on each side of the midline.

Otoccipital (Fig. 3.22b-c, 3.23b & 3.23d):

This bone forms most of the posterodorsal surface of the skull. It connects laterally with the quadrate and the squamosal and medially with the supraoccipital, in an obtuse angle directed medially (Fig. 3.22f & 3.23d). Dorsally, the contact with the squamosal is straight lateromedially. On the left bone, a foramen is visible corresponding to the exit for the cranial nerves IX to XI (Fig. 3.22f). Ventrally, the otoccipital forms the dorsal and lateral margins of the foramen magnum, and contacts ventrally with the basioccipital on both sides of the opening. Ventrolaterally, the otoccipital also connects with the basisphenoid. The otoccipital is plate-like and curved anteromedially.

Basioccipital (Fig. 3.22b-c, 3.23b, 3.23d & 3.23f):

The basioccipital sutures dorsally with the otoccipital, laterally with the basisphenoid and ventrally with the pterygoids. It forms the ventral margin of the foramen magnum (Fig. 3.22b & 3.23d). The occipital condyle is small and directed posteroventrally. Its dorsal surface is grooved to accommodate for the central nerve cord. The foramina for the lateral Eustachian tubes are not preserved and not visible on the CT slices.

Pterygoid (Fig. 3.22b-e & 3.23b-f):

The pterygoids are fused, they suture with the basisphenoid and the basioccipital posterodorsally. The posterior part is directed dorsoventrally, and the pterygoid wings are broken. In the otic region, the pterygoid connects with the laterosphenoid and the quadrate dorsally (Fig. 3.22f), although this part was quite damaged and could not be segmented very accurately. The internal choanae are ovoid with the largest axis directed anteroposteriorly and their margins are curved dorsally, which makes for a clear dorsal depression at the midline where the two pterygoids meet. There is no midline process, although the posteriormost part is damaged (Fig. 3.22c & 3.23b). It is also enclosed anteriorly by the palatines. Overall, it is located anteriorly in the bone, almost at the level of the pterygoid-palatine suture. The surface of the pterygoid is smooth, although most of it is covered by sediment.

Laterosphenoid (Fig. 3.22c & 3.23e-f):

This bone is shaped like an hourglass from a ventral point of view. It connects with the parietal to form the internal medial margin of the supratemporal fenestra. It also contacts with the pterygoid and the quadrate (Fig. 3.23f). Unfortunately, the prootic and the basisphenoid rostrum could not be distinguished because of the poor state of preservation of this part of the specimen (even on the CT data). Dorsally, it is also sutured with the postorbital and frontal via the capitate process (Fig. 3.23f).

Basisphenoid (Fig. 3.22b-c & 3.23b, 3.23d & 3.23f):

Only the posterior part of the basisphenoid could be observed. It contacts the posterior margin of the quadrate and the otoccipital but does not participate in the foramen magnum. Medially, it connects with the basioccipital along a sagittal suture (Fig. 3.22b & 3.23d).

Cranial endocast and associated nerves and vascular structures

The anterior part of the forebrain could be reconstructed up to the anterior part of the frontal. This includes the posterior part of the olfactory region (Fig. 3.24a-d, 3.24f, 3.25a-c & 3.25e-f). This part has a more tapered profile in this specimen of *Hamadasuchus* (as in *Rukwasuchus*) than it is in *Pelagosaurus*, *Rhabdognathus, Campinasuchus, Trilophosuchus* Willis, 1993, *Portugalosuchus* Mateus, Puértolas-Pascual & Callapez, 2019, *Tomistoma downsoni* or extant crocodylians where it is extremely thin dorsoventrally, although this could be a segmentation

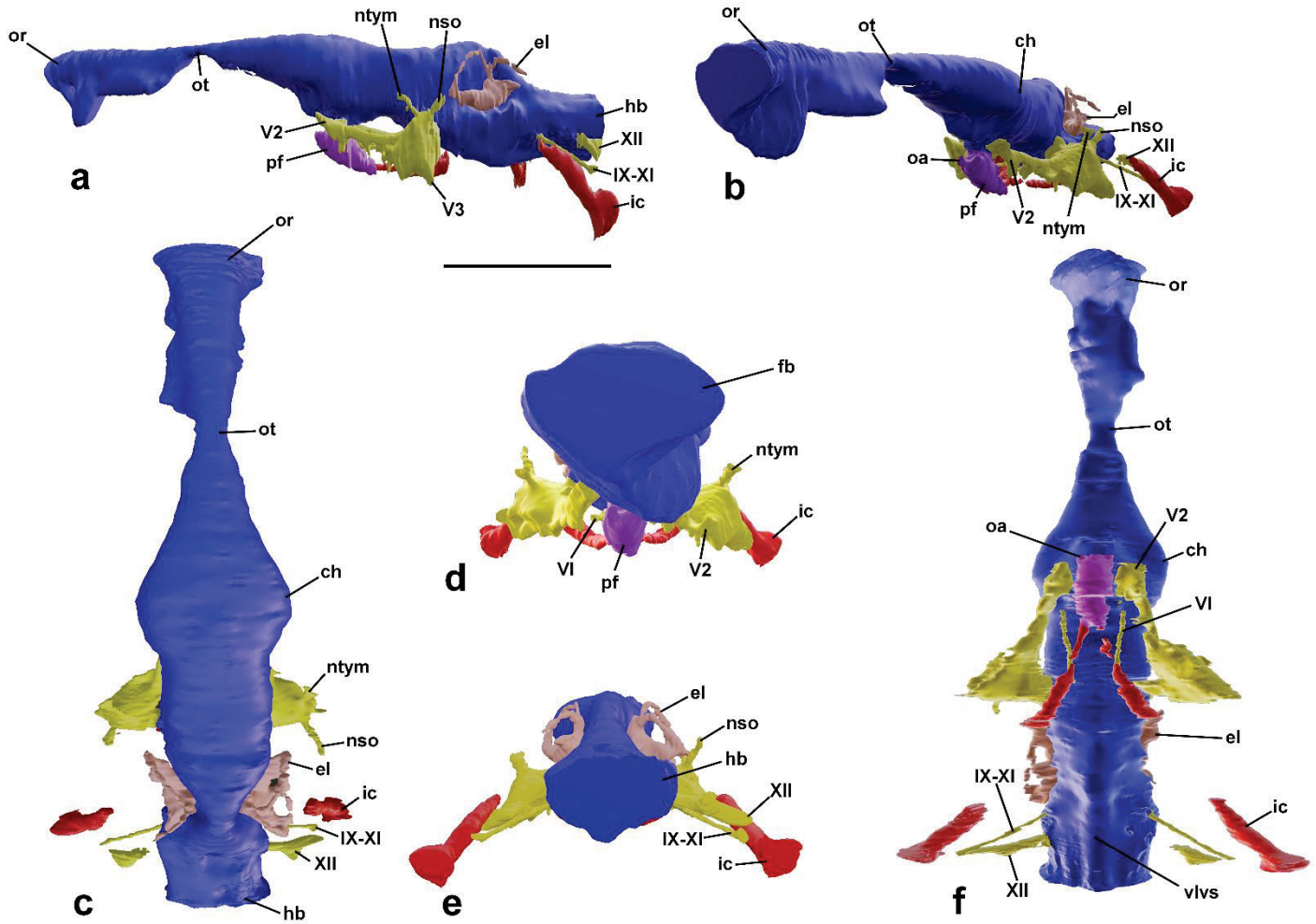

Figure 3.24: Three-dimensional reconstruction of the endocranial cavities within the braincase of UCBL-FSL 532408 (*Hamadasuchus*) in lateral (a), anterior ¾ (b), dorsal (c), anterior (d), posterior (e) and ventral (f) views. Blue: endocast, red: internal carotid artery, yellow: cranial nerve, purple: pituitary fossa. V2: maxillary division of cranial nerve V, V3: mandibular division of cranial nerve V, VI: cranial nerve VI, IX-XI: cranial nerve IX-XI, XII: cranial nerve XII, ch: cerebral hemisphere, el: endosseous labyrinth, fb: forebrain, hb: hindbrain, ic: internal carotid artery, nso: supraoccipital ramus of cranial nerve V, ntym: tympanic branch of cranial nerve V, oa: orbital artery, or: olfactory region, ot: olfactory tract, pf: pituitary fossa, vlvs: ventral longitudinal venous sinus. Scale bar is 3 cm.

bias. No grooves are visible, as in other extant and extinct crocodylomorphs, except for *Gavialis* where this structure creates a bulbous expansion and *Pelagosaurus* and *Eopneumatosuchus* Crompton & Smith, 1980 where it is paired. The olfactory tract (Fig. 3.24a-d, 3.24f, 3.25a-c & 3.25e-f) is long and flat along its dorsal margin, as is the dorsal margin of the skull bones of the interorbital area. This is different from *Rukwasuchus, Trilophosuchus*, *Tomistoma downsoni* and *Simosuchus* where it is bent ventrally and *Almadasuchus* Pol, Rauhut, Lecuona, Leardi, Xu & Clark, 2013 where it is bended dorsally. The cerebral hemispheres are laterally expanded in an intermediate manner, as in *Almadasuchus* and *Eopneumatosuchus* (Fig. 3.24a-d, 3.24f, 3.25a-c & 3.25e-f) between those of extant crocodylians, *Portugalosuchus* and *Tomistoma downsoni* (markedly expanded) and those of extinct crocodylomorphs where they are not laterally expanded (baurusuchids, *Macrospondylus*, *Plagiophthalmosuchus*, *Zulmasuchus, Sphenosuchus* Haughton, 1915; see also Table 8).

These structures exhibit a typical round shape and are symmetrically expanded along the midline in dorsal view. The endocast has a sigmoid shape in lateral view with a pontine and cephalic flexure angle that is similar to most extinct and extant crocodylomorphs (Fig. 3.24a-b), unlike *Rukwasuchus, Trilophosuchus* and *Zulmasuchus*, which have lower values, leading to more pronounced flexures (Table 8). On the other hand, *Almadasuchus, Eopneumatosuchus,* thalattosuchians (*Pelagosaurus*, *Plagiophthalmosuchus*, *Macrospondylus*, *Cricosaurus*, *'Metriorhynchus'*) and dyrosaurids (*Rhabdognathus*) have higher values, resulting in a "flatter" angle. The dorsal part of the hindbrain is compressed mediolaterally to accommodate for the endosseous labyrinths, as is seen in other crocodylomorphs with the notable exception of dyrosaurids, where this region is heavily compressed (*Rhabdognathus* for example). There are no signs of a depression linked with pericerebral spines (as in *Zulmasuchus*; Pochat-Cottilloux *et al*., 2022b), the caudal middle cerebral vein (as in *Rhabdognathus*) or an acute dorsal dural peak (as in *Trilophosuchus*; Ristevski, 2022) in dorsal view. However, this region has a blunt dorsal peak, as in allodaposuchids, *Almadasuchus* and *Baurusuchus.* The ventral longitudinal venous sinus is well expanded and is ridge-shaped, as in *Alligator* Daudin, 1809, *Crocodylus* Laurenti, 1768, *Portugalosuchus, Sphenosuchus* and *Zulmasuchus* (Fig. 3.24e-f). Apart from the significant dorsal post cerebral concavity noticed in *Rukwasuchus*, the overall shape and features of UCBL-FSL 532408 are remarkably close to those of this taxon.

Cranial nerve VI is expanded anteroposteriorly and is situated between the pituitary fossa ventrally and the ventral edge of the endocast dorsally. It comes out from the hindbrain just ventrally to the overly voluminous cranial nerve V (Fig. 3.24f).

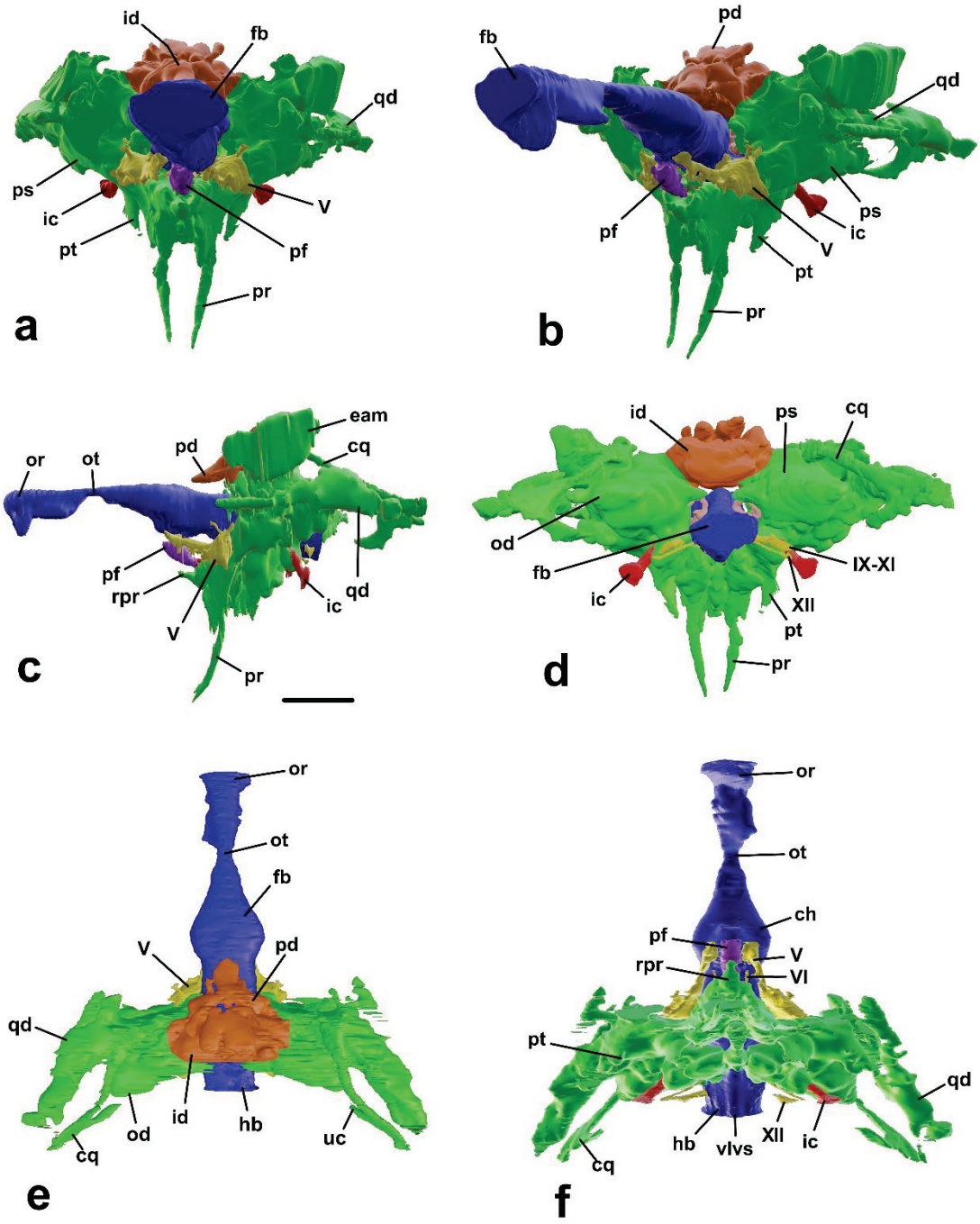

Figure 3.25: Three-dimensional reconstruction of the pneumatic cavities within the braincase of UCBL-FSL 532408 (*Hamadasuchus*) in anterior (a), anterior ¾ (b), lateral (c), posterior (d), dorsal (e) and ventral view (f). Blue: endocast, green: pharyngotympanic sinuses and eustachian system, orange: intertympanic diverticulum, red: internal carotid artery, yellow: cranial nerve, purple: pituitary fossa. V: cranial nerve V, VI: cranial nerve VI, IX-XI: cranial nerve IX-XI, XII: cranial nerve XII, ch: cerebral hemisphere, cq: cranioquadrate passage, eam: external auditory meatus, fb: forebrain, hb: hindbrain, ic: internal carotid artery, id: intertympanic diverticulum, od: otoccipital diverticulum, or: olfactory region, ot: olfactory tract, pd: parietal diverticulum, pf: pituitary fossa, pr: pterygoid recess, ps: pharyngotympanic sinus, pt: pharyngotympanic tube, qd: quadrate diverticulum, rpr: precarotid recess, uc: unidentified canal, vlvs: ventral longitudinal venous sinus. Scale bar is 2 cm.

Cranial nerve V is a large ganglion, laterally projecting from the endocast, anteroventrally to the endosseous labyrinths. The maxillary division (V_2) is the largest visible and extends anteriorly almost until the anterior end of the cerebral hemisphere (Fig. 3.24a-b). The beginning of the mandibular division (V_3) can be seen but could not be segmented further. Additionally, the two branches extending dorsally from the trigeminal ganglion are the tympanic branch (anteriorly) and the supraorbital ramus (posteriorly).

Cranial nerves IX-XI and XII are easily distinguishable (Fig. 3.24a, 3.24c & 3.24e-f). There are two canals linked with those nerves, the anteriormost one being for cranial nerve IX-XI and probably a part of cranial nerve XII, whereas the posteriormost one is probably for a part or the totality of cranial nerve XII (Fig. 3.24a-c & 3.24e-f).

The pituitary fossa is more extended anteroposteriorly than dorsoventrally. It is directed posteroventrally, as in *Zulmasuchus*, *Macrospondylus*, *Plagiophthalmosuchus*, *Rhabdognathus Arenysuchus* Puértolas, Canudo & Cruzado-Caballero, 2011*, Agaresuchus* Narváez, Brochu, Escaso, Perez-García & Ortega, 2016*, Sebecus, Trilophosuchus, Sphenosuchus, Portugalosuchus, Eopneumatosuchus*, *Tomistoma downsoni* and extant crocodylians whereas it is directed anteroposteriorly in '*Metriorhynchus'*, *Cricosaurus* and *Pelagosaurus* and ventrally in baurusuchids and *Rukwasuchus*. The starting point of the orbital arteries can be seen in the anteriormost part (Fig. 3.24a & 3.24f).

The internal carotid arteries have the typical shape found in all crocodylomorphs so far: they enter the posterior end of the pituitary fossa separately at the level of the midline, and the canals enclosing them (carotid pillars *sensu* Walker, 1990) are large. Those canals then pass through the pharyngotympanic sinus so they cannot be segmented. Finally, the posterior section runs anterodorsally from the foramen for the internal carotid artery to ventral to the endosseous labyrinths. As in Pochat-Cottilloux *et al*. (2022b), the limit between the internal carotid arteries and the pituitary fossa was established where the arteries are no longer separated and merge into a single structure.

Endosseous labyrinths

Those structures are partially preserved, the cochlear duct being missing. However, the main structures are still available, comprising the vestibular apparatus. The right one is the best-preserved one, so it is displayed here, whereas the left one is missing the lateral semicircular canal (Fig. 3.24a-c). The ampullae are not clearly distinguishable from the canals as their shape

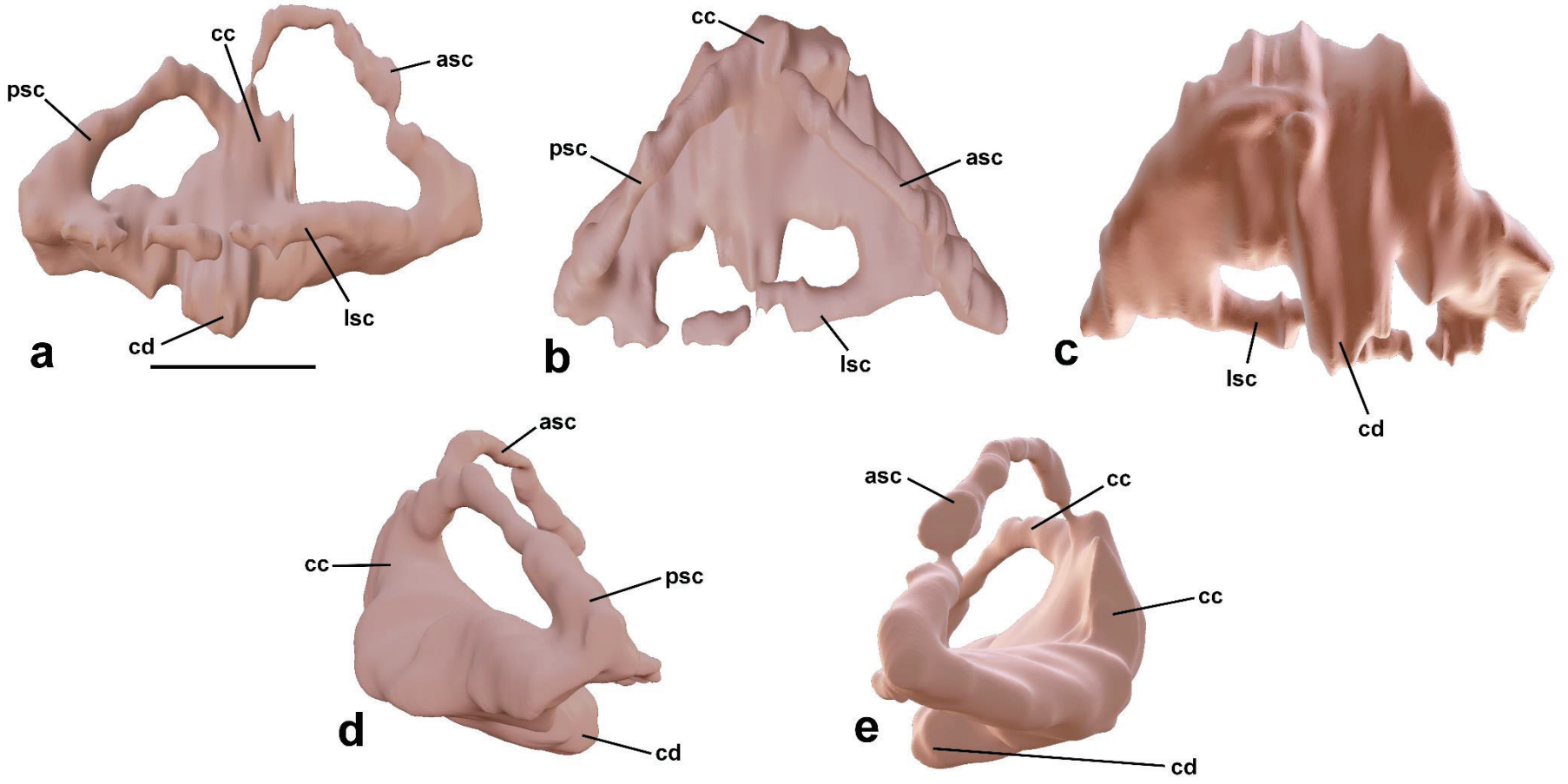

Figure 3.26: Three-dimensional reconstruction of the right endosseous labyrinth of UCBL-FSL 532408 (*Hamadasuchus*) in lateral (a), dorsal (b), ventral (c), posterior (d) and anterior (e) views. asc: anterior semicircular canal, cc: common crus, cd: cochlear duct, lsc: lateral semicircular canal, psc: posterior semicircular canal. Scale bar is 5 mm.

is continuous with those of the semicircular canals. All the canals are also circular in cross-section, and narrow compared to those of extant crocodylians and *Portugalosuchus*, but in a less extreme way than in *Zulmasuchus*, *Almadasuchus* and *Eopneumatosuchus*. However, the space between those canals is still important compared to other notosuchians (see comparative metrics in Table 8). The common crus is elongated dorsoventrally, in a comparable manner to what is seen in extant crocodylians and *Tomistoma downsoni* but less so than in *Trilophosuchus*, where it is especially high. The lateral semicircular canal is straight, whereas the anterior and posterior ones are much more bent (Fig. 3.26). As a result, the lateral canal does not extend laterally, and the anterior semicircular canal is more expanded dorsally than the posterior one, resulting in a larger area of the canal, as in modern crocodylians, *Portugalosuchus, Junggarsuchus, Eopneumatosuchus*, *Tomistoma downsoni* and *Trilophosuchus* (Table 8), whereas they are equally expanded anteroposteriorly, as in *Simosuchus clarki*, *Tomistoma downsoni* and thalattosuchians. In other words, the anterior semicircular canal has a pyramidal shape (as those of *Zulmasuchus, Simosuchus, Junggarsuchus, Eopneumatosuchus* and *Sphenosuchus*), whereas the posterior one is more rounded (like the ones of extant crocodylians, *Tomistoma downsoni* and *Portugalosuchus*). The angle between the anterior and the posterior semicircular canals is approximately 80° (Fig. 3.26a), which is less than *Caiman* Spix, 1825 and *Trilophosuchus* (100°; Bona & Paulina-Carabajal, 2013 and 98°; Ristevski, 2022) or *Zulmasuchus, Eopneumatosuchus* and *Simosuchus* (90°). However, the angle between the anterior and the lateral semicircular canal is the same as in all other extant crocodylians, thalattosuchians, *Trilophosuchus, Eopneumatosuchus* and *Portugalosuchus* (60°; Fig. 3.26a), while it is higher in *Almadasuchus, Zulmasuchus, Baurusuchus* and *Simosuchus* (70°). The lagenar section could not be segmented.

Braincase pneumaticity

The braincase of crocodylomorphs is heavily pneumatized with peculiar structures only found in this group (Kuzmin *et al*., 2021). The pharyngotympanic system and the median pharyngeal system form the paratympanic sinus system. Dorsally to these structures is the intertympanic diverticulum, which is located along the dorsal margin of the endocast. In UCBL-FSL 532408, this structure excavates the parietal, creating the parietal diverticulum (Fig. 3.25a-b, 3.25d-e) which has a peculiar shape. In dorsal view, it is anteriorly expanded along its midline showing two canals that emerge laterally to it (Fig. 3.25e). Those canals extend posterolaterally in the parietal, and the central expansion is bifurcated posteriorly. This arrangement is also present in *Zulmasuchus, Trilophosuchus* and extant crocodylians, however it is absent in thalattosuchians.

The structure also has a central opening, which is ovoid in shape. The intertympanic diverticulum itself is linked dorsally to the parietal diverticulum and links the two pharyngotympanic sinuses on each side of the endocast, as in all crocodyliforms (Clark, 1986; Leardi *et al*., 2020).

The pharyngotympanic sinuses are located just dorsolaterally to the level of the endosseous labyrinths (Fig. 3.25b-c). As in *Zulmasuchus,* they are rounded and expanded laterally, surrounding the endocast and the internal carotid arteries. These structures are also indistinguishable from the otoccipital diverticula, expanding posteriorly (Fig. 3.25d-e). Both quadrate diverticula are segmented, as well as the cranioquadrate passage on each side (Fig. 3.25b-c & 3.25e-f). These cranioquadrate passages are not separated from the sinus by a thin bony lamina, contrary to what is seen in metriorhynchids (Herrera *et al*., 2018). A canal separating from the cranioquadrate passage was also identified in the posterior part of the specimen, which has not been observed before in other crocodylomorphs (Fig. 3.25e-f) but could simply be vascularization or innervation. The expanded quadrate diverticulum exhibits an unidentified canal expanding anteriorly without contacting the rest of the paratympanic system or invading the postorbital or the squamosal, especially visible on the left side (Fig. 3.25b-c & 3.25e). This might be a peculiar structure of *Hamadasuchus* or due to the lack of sampling and reconstruction of this area in other studies. The basisphenoid diverticulum, which links the pharyngotympanic system with the median pharyngeal system is also very expanded (Fig. 3.25b-c) as in *Zulmasuchus*. The *recessus epitubaricus* and the rostral pneumatic recess are expanded and were reconstructed on the left side (Fig. 3.25c). The pharyngotympanic tubes are not reconstructed in their entirety, but they are ventrally directed and expanded mediolaterally. The pterygoid recesses are symmetrically expanded to those structures but have a more anterior origin (Fig. 3.25a-c & 3.25f). The median pharyngeal sinus is verticalized and connects with the basisphenoid diverticulum anteriorly and the pharyngotympanic system posteriorly (Fig. 3.25c & 3.25f), which suggests that the specimen is not a juvenile, otherwise it would have been more horizontal (Dufeau & Witmer, 2015; Serrano-Martínez *et al*., 2019a).

Discussion

Attribution to *Hamadasuchus* and detailed comparison with *Rukwasuchus yajabalijekundu*

This specimen can be attributed to Crocodylomorpha because it has no descending process of the squamosal (Parrish, 1993). It can be further attributed to Crocodyliformes because the

squamosals form most of the flat skull roof, the otoccipitals do not participate in the formation of the occipital condyle (Pol & Norell, 2004b), there is no incisive foramen on the palate (Pol & Powell, 2011), the frontal is sculpted with low ridges and furrows, the parietal has a subrectangular shape in dorsal view, there is a strongly concave anterior margin of the otic aperture, the quadrate contacts with the squamosal on the posteroventral border of the otic aperture, and there is a connection between the pharynx and the dorsal pneumatic system (Leardi *et al*., 2020).

Crocodylomorphs from the Cretaceous of Africa are numerous and diverse, but altirostral forms with a heterodont dentition are restricted to a handful of notosuchians. *Kaprosuchus saharicus* has posterodorsally projecting parietal-squamosal horns and a squared internal choana, which the specimen described here does not have. Uruguaysuchidae *sensu* Gasparini (1971; including *Araripesuchus wegeneri* and *Araripesuchus rattoides*) is diagnosed by having a vascular opening in the postorbital bar, a non-ornamented quadratojugal and a distinct development of the distal quadrate body ventral to the otoccipital-quadrate contact, traits that are absent in the specimen studied here. *Libycosuchus brevirostris* Stromer, 1914 has very small choanae and almost round supratemporal fenestrae, which our specimen does not have.

However, the specimen described here is remarkably similar to ROM 52620, ROM 52509 and ROM 54511 described as belonging to *Hamadasuchus rebouli* (Larsson & Sues, 2007) and RRBP 08360 described as the holotype of *Rukwasuchus yajabalijekundu* (Sertich & O'Connor 2014). Concerning the ROM specimens, they are in fact not directly referrable to *H. rebouli* for now because the overlapping part of the set of fossils does not correspond with the holotype of this taxon, which is a partial dentary (Buffetaut, 1994). However, given the close resemblance between the two, those specimens remain in an unresolved specific status, while still belonging to the genus *Hamadasuchus* (for more information, see discussion in Nicholl *et al*., 2021; Pochat-Cottilloux *et al*., 2023a). A future detailed comparison of UCBL FSL 532408 and other specimens attributable to *Hamadasuchus* will be beneficial on this topic (Rauhut & Lopez-Arbarello, 2005; Ibrahim *et al*., 2020).

Rukwasuchus is diagnosed by having a dorsally upturned tip of the posterior process of the squamosal and a ventrally descending process of the postorbital, which all ROM specimens assigned to *Hamadasuchus* and UCBL FSL 532408 lack. On the other hand, all ROM specimens are diagnosed by the combination of a thin intertemporal bar, oval rather than round supratemporal fenestrae with dorsomedial edges level with the skull table, tapered distal

squamosal prong, large posteroventral process on the postorbital that contacts the quadrate and quadratojugal, external auditory meatus fossa extending anteriorly over the entire length of the postorbital, prominent bilateral projections on the posterodorsal surface of the supraoccipital, no dorsal crest on the dorsal distal part of the quadrate and a supratemporal fossa covering most of the bony bar between the supratemporal fenestra and the orbit (Larsson & Sues, 2007). UCBL FSL 532408 also displays all those features, apart from the last one. We thus argue that this specimen can be attributed to *Hamadasuchus* rather than to *Rukwasuchus*. Nonetheless, those taxa remain remarkably close, as evidenced in Larsson & Sues (2007) and Sertich & O'Connor (2014): for example, they both share a depressed posterior parietal border and an anteroventrally projected process of the squamosal below the dorsal lamina of the postorbital.

In terms of neuroanatomy, *R. yajabalijekundu* exhibits a significant post cerebral concavity posteriorly to the cerebral hemispheres (Sertich & O'Connor, 2014; fig 6c) whereas it is not the case of the specimen studied here. The pituitary fossa is directed almost ventrally in *Rukwasuchus* whereas it is much more horizontal in UCBL FSL 532408. Furthermore, the ganglion of cranial nerve V is more expanded in this specimen than in *Rukwasuchus,* but this could also be due to a preservation or acquisition bias. Further work is needed to understand if those differences really highlight taxonomic differences or if they are more linked to ontogenetic and ecological differences.

Paleobiological inferences

Peirosaurids are almost exclusively known from cranial remains, which can be very fragmentary (Barrios *et al*., 2016; Lio *et al*., 2016; Lamanna *et al*., 2019). As such, inferences about their ecology and mobility are exceedingly difficult to make. Here we use for the first time the internal structures of a peirosaurid to infer several of their ecological and behavioural traits.

Head posture

Head posture can be inferred using the orientation of the lateral semicircular canal (Erichsen *et al*., 1989; Witmer *et al*., 2003, 2008; Hullar, 2006; Sampson & Witmer, 2007; Sereno *et al*., 2007; Witmer & Ridgely, 2008). However, this method could be subject to interspecific variation (Taylor *et al*., 2009; Marugán-Lobón *et al*., 2013), so we also estimated it with the alignment of the maxillary toothrow (Marugán-Lobón *et al*., 2013) or the endocranial surface of the parietal (Kley *et al*., 2010; von Baczko *et al*., 2018) with the horizontal plane. Those

three methods recover an angle between the longitudinal axis of the skull and the horizontal plane of 7 to 9° (Fig. 3.27), which is in line with other values inferred for other notosuchians (Kley *et al*., 2010; Dumont *et al*., 2020b; Fonseca *et al*., 2020; Pochat-Cottilloux *et al*., 2022b). This posture allows the nostrils to be closer to the ground and a better vision over the altirostral snout, which is in line with a terrestrial ecology (Stevens, 2006; Marinho *et al*., 2013) rather than a semi-aquatic or aquatic one where the longitudinal axis of the skull is considered parallel to the horizontal plane, especially for buoyancy purposes (Witmer *et al*., 2008; Bona *et al*., 2017; Serrano-Martinez *et al*., 2019a; Fig. 3.27d). This also implies lower energy costs compared to keeping the head on the horizontal plane, although this could only be confirmed by studying postcranial material. Apart from *Uberabasuchus* Carvalho, Ribeiro & Avilla, 2004 (de Vasconcellos & Carvalho, 2006) and osteoderms of *Montealtosuchus* Carvalho, de Vasconcellos & Tavares, 2007 (Tavares *et al*., 2015), postcranial anatomy is poorly known in Peirosauridae. This altirostral skull morphology is present in sebecosuchians as well (Marinho *et al*., 2013; Dumont *et al*., 2020b; Fonseca *et al*., 2020), which may be related to peirosaurids (Larsson & Sues, 2007; Pol *et al*., 2014). This morphology is also present in some theropods (Stevens, 2006; Schade *et al*., 2020), which suggests a similar terrestrial ecology and predatory habits for all those organisms.

Endosseous labyrinth

The anterior semicircular canal of *Hamadasuchus* is more expanded than the posterior one, as in most other crocodylomorphs and corresponds to a moderate sensitivity to pitching (the movement of the endolymphatic liquid inside the canal when the head moves up and down is transmitted to the brain via the cristae to control the acceleration; Hudspeth, 1983; Rabbitt *et al*., 2004). The same can be said for the lateral semicircular canal, which corresponds to the sensitivity of yaw (lateral acceleration) movements. As a result, *Hamadasuchus* would have been able to move its head to the full extent of its capabilities, especially up and down, which brings a further argument in favour of a terrestrial ecology. An especially interesting comparison to make here is with the internal structures of *Zulmasuchus querejazus* (Pochat-Cottilloux *et al*., 2022b): this crocodylomorph also has an extended anterior semicircular canal compared with the posterior one, however its lateral semicircular canal is much more expanded. It can thus be hypothesized that this could be the result of a slightly different adaptation of those two crocodylomorphs to hunting or moving, with *Zulmasuchus* also able to perform more pronounced lateral movement of the head, whereas it was less the case in *Hamadasuchus*. The

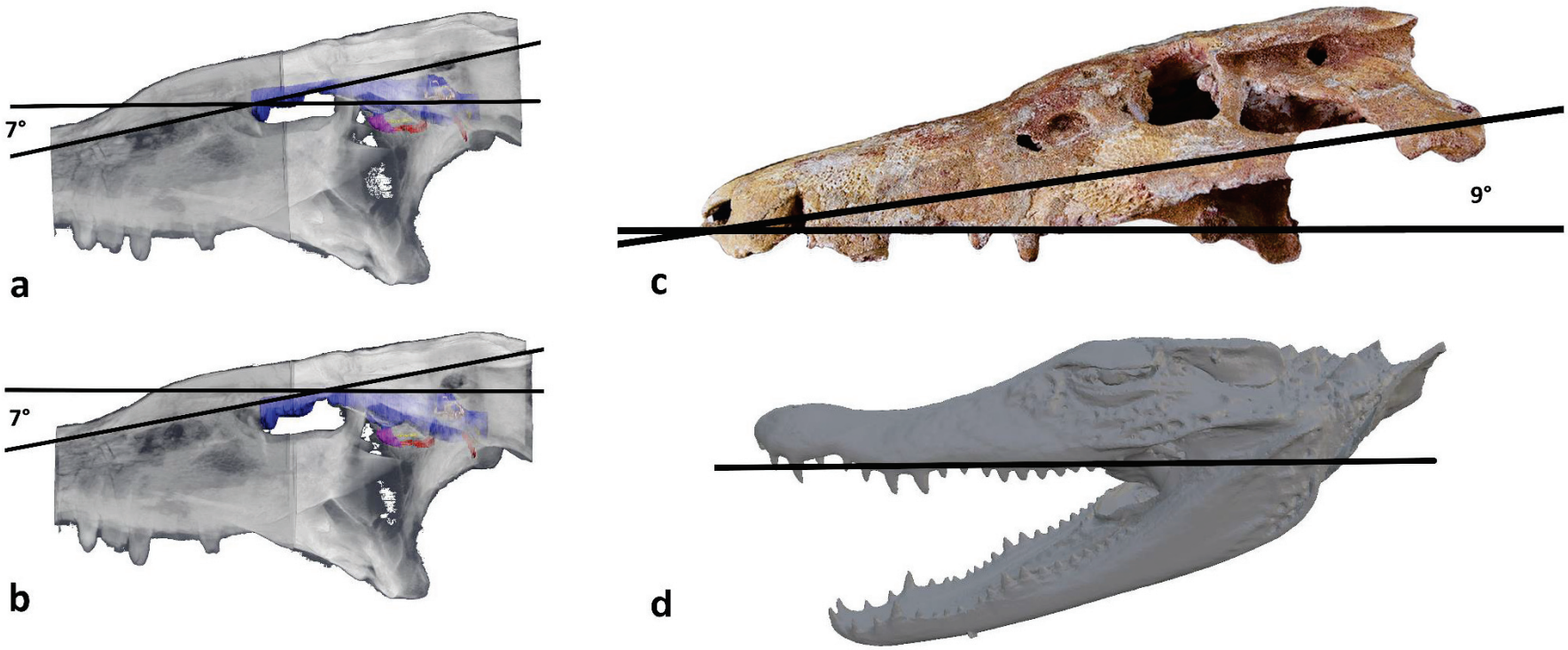

Figure 3.27: Inferred alert head posture of UCBL FSL 532408 aligning the lateral semicircular (a), the endocranial surface of the parietal (b) and the maxillary toothrow (c) with the horizontal plane. Extant representative (*Paleosuchus trigonatus* MHNL 50003939) for comparison (d).

endosseous labyrinth of *Hamadasuchus* is also close in shape to those of terrestrial predatory theropods, pseudosuchians and early crocodylomorphs (Fig. 3.28; Sanders & Smith, 2005; Witmer & Ridgely, 2009; Paulina-Carabajal & Succar, 2014; Xing *et al*., 2014; Paulina-Carabajal & Filippi, 2018; Nesbitt *et al*., 2018; Cerroni & Paulina-Carabajal, 2019; Paulina-Carabajal & Nieto, 2019). Those hypotheses are strengthened when looking at semi-aquatic and aquatic reptiles which have less expanded semicircular canals, linked with a head more in line with body movement (Fig. 3.28; Evans, 1999; Yi & Norell, 2019; Schwab *et al*., 2020). Furthermore, dyrosaurids (semi-aquatic to aquatic crocodylomorphs, mainly marine) have very expanded vestibules, which could be linked to an otolith-mediated inner ear for underwater vibration detection rather than tympanic driven impedance matching (Erb & Turner, 2021). This structure is absent in *Hamadasuchus* (as well as *Zulmasuchus*) which is a further argument for a terrestrial ecology in these taxa. Several studies have looked at the relationship between the shape of the endosseous labyrinth and the living environment: Schwab *et al*. (2020) retrieved a significant correlation between those variables using canonical variate analysis (CVA), sampling a variety of fossil and extant crocodylomorphs but Bronzati *et al*. (2021), after investigating on a broader archosauriform sample and including phylogenetic relationships *a priori*, concluded that those variations might be more related to constraints from the development of the skull. Furthermore, Schwab *et al*. (2021b) demonstrated that the shape of the endosseous labyrinth in extant crocodylians varies a lot throughout ontogeny, bringing more complexity to the debate, which thus remains open. As a result, no clear link between the shape of the endosseous labyrinth and ecology has been demonstrated so far.

Relative brain size

When looking at the endocast of any organism, an idea of its development can be obtained by comparing the metrics of the brain it represents to the metrics of the whole body of the organism, i.e., relative brain size. It is used to infer cognition and thermoregulation of extinct vertebrates, based on extant representatives (Jerison, 1973; Hopson, 1977). It is traditionally linked to the reptile encephalization quotient (REQ) in the case of crocodylomorphs, which consists of a linear regression between body mass and brain mass (Hurlburt, 1996). This approach has been widely used for paleobiological inferences on fossil crocodylomorphs (Serrano-Martínez *et al*., 2019a, b, 2020; Puértolas-Pascual *et al*., 2022) but, as rightly highlighted in Dumont *et al*. (2020b), this use is problematic because the REQ changes throughout ontogeny (corresponding with changes in brain morphology), even between different adult stages (Hurlburt *et al*., 2013). As a result, we completed the dataset of Dumont

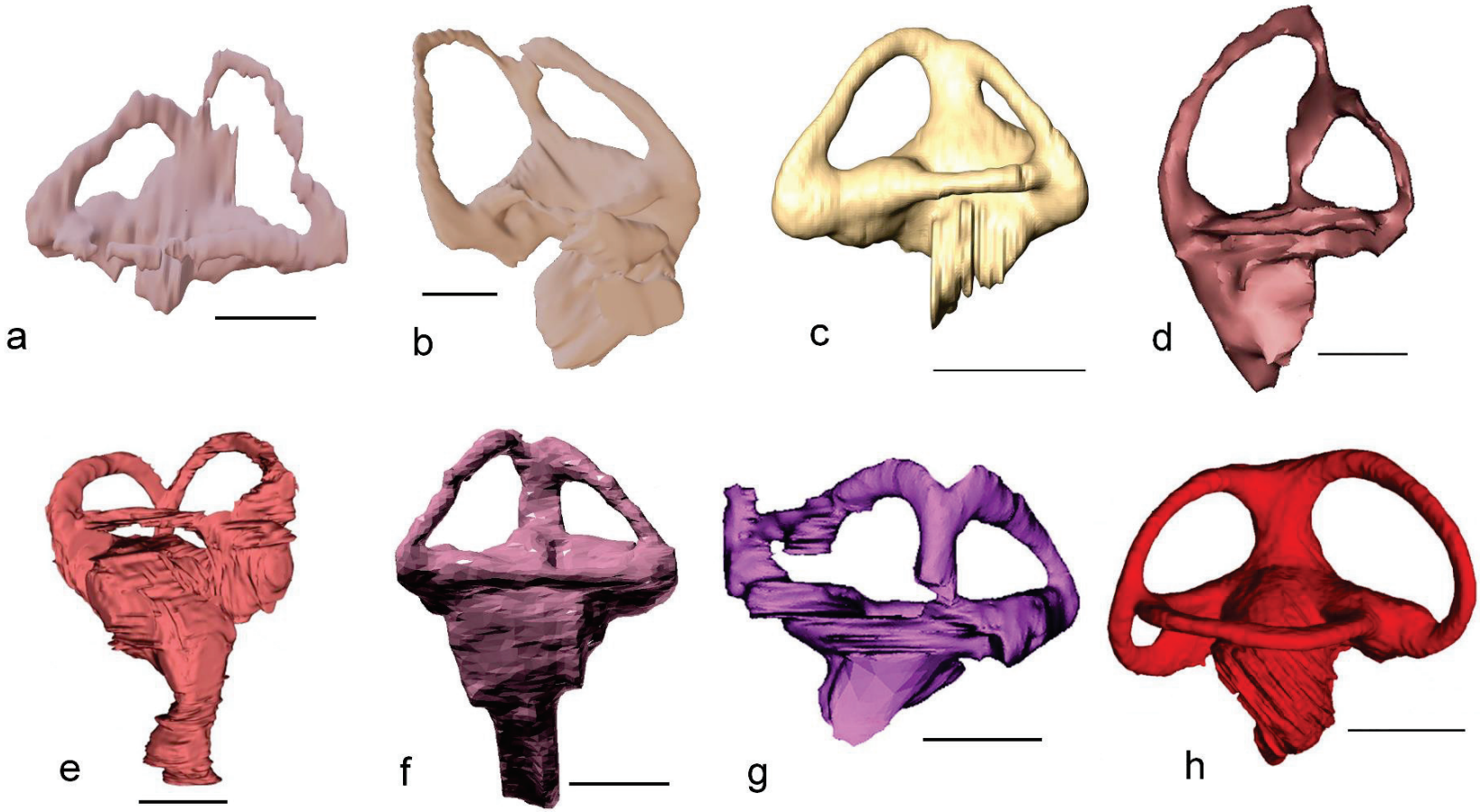

Figure 3.28: Three-dimensional reconstructions of the endosseous labyrinths of different reptiles in lateral view: (a) *Hamadasuchus* (right, UCBL FSL 532408); (b) *Zulmasuchus querejazus* (left, MHNC 6672 from Pochat-Cottilloux *et al*., 2022b); (c) *Crocodylus porosus* (left, OUVC 10899); (d) *Viavenator exxoni* (left, MAU-Pv-Li-530 from Paulina-Carabajal & Filippi, 2018); (e) *Baurusuchus* sp. (right, FUP-Pv 000021 from Dumont *et al*., 2020b, fig. 9b); (f) *Pelagosaurus typus* (left, BRLSI M1413 from Pierce *et al*., 2017, fig. 6b); (g) *Parringtonia gracilis* (left NMT RB460, from Nesbitt *et al*., 2018, fig. 11k); (h) *Platecarpus tympaniticus* (left, AMNH FRAB1645 from Yi & Norell, 2019). All structures are oriented with the lateral semicircular canal oriented horizontally. Scale bars are 5 mm.

et al. (2020b; fig. 8), which rather uses the raw log transformed measurements of body and brain mass (Fig. 3.29; see also Supplementary Material S3). Body mass is estimated from skull measurements in fossil specimens using linear regression between those metrics in extant crocodylians (Paiva *et al*., 2022). Brain mass can be derived from the endocranial volume (assuming a brain density of 1) from the following relation: $\log BV = \log EV * 0.7279 + 0.75624$ where EV: endocranial volume and BV: brain volume (Dumont *et al*., 2020b and references therein). Potential bias in those estimation methods exist and the results presented thereafter should thus be taken with the necessary precautions.

As can be seen in Fig. 3.29, across 148 extant and extinct specimens, *Hamadasuchus* (with the addition of the data available for ROM 52620 in George & Holliday, 2013) has an encephalization quotient in the range of modern crocodylians. With the addition of allodaposuchids (Serrano-Martínez *et al*., 2020; Puértolas-Pascual *et al*., 2022), the difference observed in baurusuchids originally proposed in Dumont *et al*. (2020b) now does not seem so important. The difference remains significant when looking at body mass (Wilcoxon test, p-value = 0.019) but not for brain mass (Wilcoxon test, p-value = 0.75). Furthermore, *Campinasuchus dinizi,* which is also a baurusuchid, has similar values as other baurusuchids (Fonseca *et al*., 2020). As a result, we argue that not much paleobiological inferences can be made using the relative brain size.

Cranial pneumaticity

The pneumaticity of the skull of *Hamadasuchus* seems to be very expanded, as in *Zulmasuchus* and *Campinasuchus* (Fonseca *et al*., 2020; Pochat-Cottilloux *et al*., 2022b). However, these structures are less expanded in extant crocodylians, allodaposuchids, *Portugalosuchus* and *Trilophosuchus* (Witmer *et al*., 2008; Bona *et al*., 2017; Serrano-Martínez *et al*., 2019a, b, 2020; Puértolas-Pascual *et al*., 2022, 2023; Ristevski, 2022). In fossils that show adaptations to the aquatic environment, some of those structures are even absent: for example, the intertympanic diverticulum and parietal diverticulum are missing in thalattosuchians (Brusatte *et al*., 2016; Pierce *et al*., 2017; Herrera *et al*., 2018; Schwab *et al*., 2021a; Wilberg *et al*., 2021). Multiple hypotheses have been formulated to explain these differences and are linked to one another: the enlargement of the sinuses could improve resonance and allow for better aerial sound pickup, whereas soundwaves travel more easily in the aquatic environment (Dufeau & Witmer, 2015; Herrera *et al*., 2018). The impact of those structures on the buoyancy and skull density in semi-aquatic to aquatic taxa could also be important (Brusatte *et al*., 2016). Finally, the development

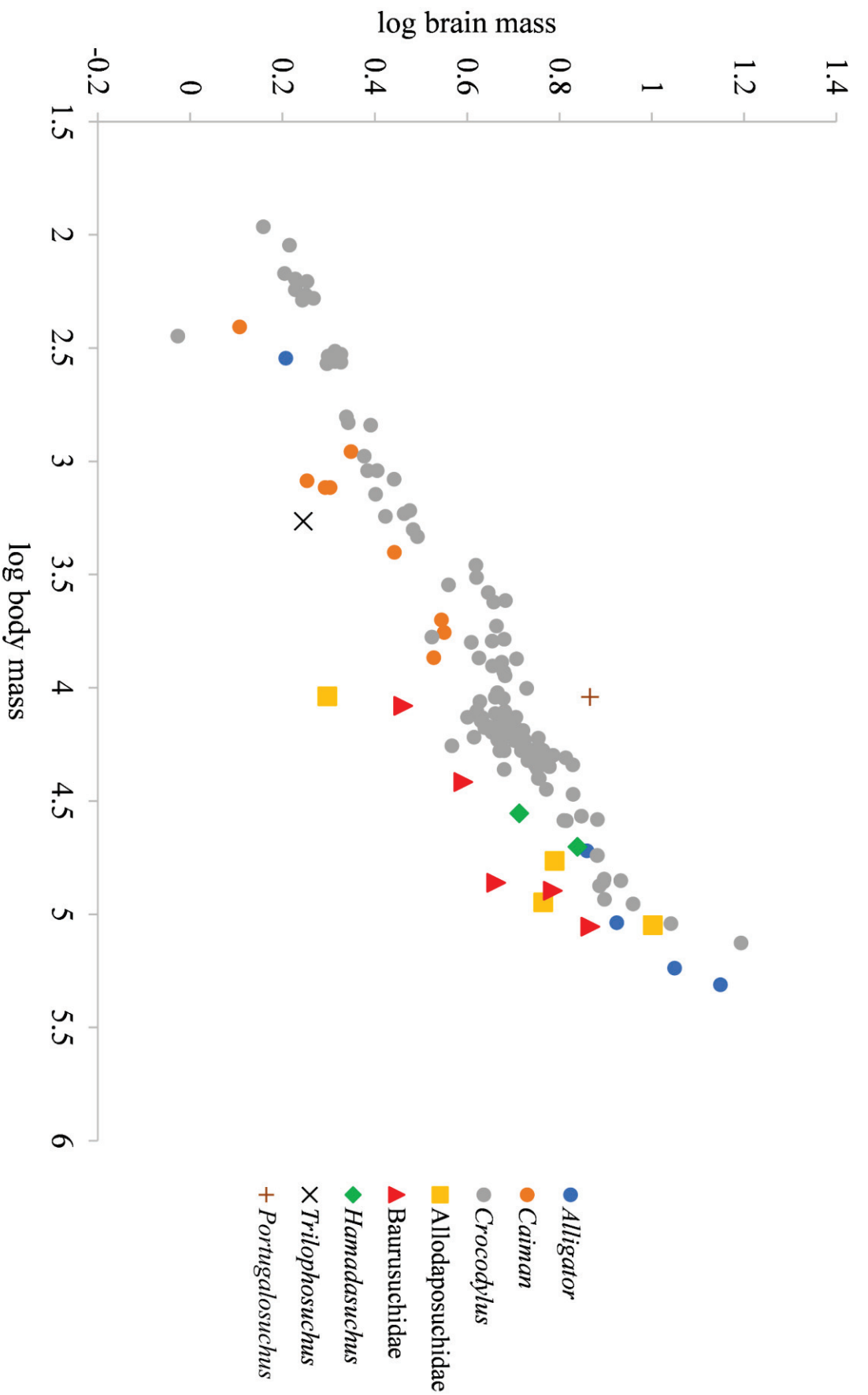

Figure 3.29: Body mass vs brain mass in different specimens of extant and extinct crocodylomorphs.

of the sinus system seems to also be linked to the shape of the rostrum (and thus the diet), which could have direct implications on the internal constraints of the skull and particularly the braincase (Dufeau & Witmer, 2015). As we previously stated, this hypothesis could be debatable because this pattern is not found in extant specimens (i.e., longirostrine *Gavialis* and brevirostrine *Caiman* have similar sinuses; Pochat-Cottilloux *et al*., 2022b, fig. 8). Finally, there seems to be a link between the development of the sinus system and the living environment in crocodylomorphs, as terrestrial forms, such as *Zulmasuchus*, have a very expanded cranial pneumaticity, whereas among forms showing adaptations to the aquatic environment, such as thalattosuchians, cranial pneumaticity is, as stated above, reduced.

To get a better view of the problem, we introduced the data obtained from the current study on *Hamadasuchus* in a dataset consisting of extant specimens of diverse ecologies, as well as fossil representatives such as *Diplocynodon* Pomel, 1847*, Trilophosuchus*, *Portugalosuchus* or *Zulmasuchus,* all adults (see Supplementary Material S3 for more information). To get an unbiased idea of the sinus volume of each specimen, we compared the log transformed sinus volume (without the cranioquadrate passages) to the log transformed skull width and skull length for each specimen (Fig. 3.30).

First, as can be seen on Fig. 3.30A, sinus volume is in fact strongly correlated with skull length (log skull length = 0.438 ± 0.106 * log sinus volume + 0.927 ± 0.126, 2 s.d.; $R^2 = 0.84$, p-value = $3.33.10^{-9}$), although their overall morphology seems quite similar. However, once sinus volume is normalized to skull length for each specimen, the different snout morphologies of extant crocodylians (i.e., brevirostrine for *Alligator, Caiman* and *Osteolaemus*, mesorostrine for *Crocodylus* and longirostrine for *Gavialis*, *Mecistops* and *Tomistoma*), which should be distinguished when considering the previous correlation, are undistinguishable under a Wilcoxon test (see Supplementary Material S3). As such, sinus volume is correlated to skull length but not to snout morphology.

Second, as can be seen on Fig. 3.30B, sinus volume is even better correlated to skull width (log skull width = 0.418 ± 0.064 * log sinus volume + 0.666 ± 0.078, 2 s.d.; $R^2 = 0.91$; p-value = $1.61.10^{-14}$). Finally, sinus volume could also be associated with lifestyle: when looking at a longirostrine extant specimen (*Gavialis*), *Crocodylus* and *Zulmasuchus* (black square), there is a difference in sinus volume between the three groups for specimens of the same size, which could be associated with their different lifestyle (respectively aquatic, semi-aquatic and terrestrial). *Trilophosuchus* (terrestrial) also has similarly expanded sinuses compared to

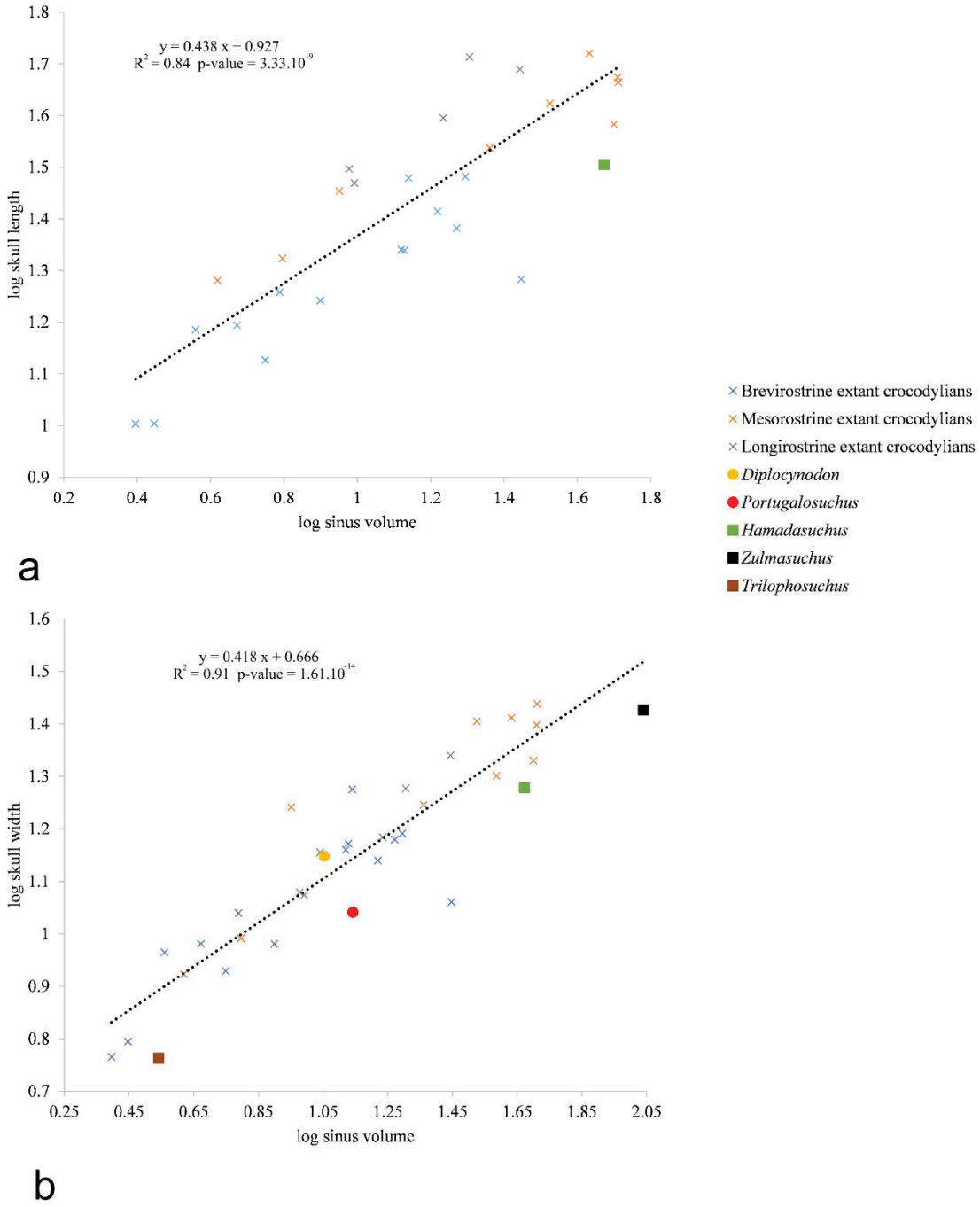

Figure 3.30: A: Sinus volume vs skull length in different specimens of extant crocodylians and *Hamadasuchus*, B: Sinus volume vs skull width in different specimens of extant and extinct crocodylomorphs.

caimans (semi-aquatic) of the same skull width. This would be linked with the hypotheses mentioned above, such as improved resonance and better aerial sound pickup or the impact on the buoyancy of such structures. As a result, *Hamadasuchus* displaying average values of sinus volume, would be associated with a terrestrial lifestyle, but with some semi-aquatic affinities, which was also recently highlighted using an independent histological approach (Pochat-Cottilloux *et al*., 2023b). However, these results come only by considering the sinus structure and volume which is still poorly understood and will have to be compared with other proxies

to reach a more robust answer. This method calls for a deeper sampling and remains limited in fully aquatic and fully terrestrial fossil forms, mainly because the sinuses as well as skull width must be completely preserved.

Conclusion

A detailed comparison of the cranial bones allows to identify the specimen described here as belonging to *Hamadasuchus*, pending a future reassessment of other specimens described as belonging to this genus. Close affinities with *Rukwasuchus yajabalijekundu* are also put forward.

The endocranial structures of *Hamadasuchus* are described here for the first time. The endocast has a sigmoidal shape, the endosseous labyrinths are expanded and the pneumaticity of the skull is very enlarged, with much higher volume of the sinuses compared to extant semi-aquatic representatives or aquatic fossil forms.

Using the endocranial structures, the alert head posture of the specimen is inferred to be about 7-9° with the horizontal plane, which is an important clue as to the terrestrial affinities of this taxon, linked with a binocular vision over the altirostral snout. Furthermore, the morphology of the endosseous labyrinth also brings information about the lifestyle of the organism: its expanded semicircular canals are related to enhanced mobility of the head, which is again in line with a terrestrial lifestyle. Finally, the enlarged sinus cavities are compared with those of some sebecosuchians: the hypotheses of sinus volume related to living environment and snout morphology are tested (scaled with skull size). The volume of the sinuses indeed seems to be correlated to both skull width and skull length. Although there is no significant link between sinus volume and snout morphology, cranial pneumaticity seems to be linked to the lifestyle, but these interpretations must be taken with caution, as lack of preservation in fossil forms and thus data, especially on terrestrial representatives, could be potential biases. These data indicate a more nuanced result concerning the ecology of *Hamadasuchus*, with semi-aquatic affinities more marked than in the sebecosuchians for example. In summary, this peirosaurid taxon is inferred to have had a terrestrial lifestyle, as for sebecosuchians, but with probable semi-aquatic affinities.

Another proxy which could be related to the lifestyle is tested: the relative brain size. However, it does not seem to bring out relevant information, as all sampled specimens are grouped, and, as a further limitation, is based on size estimates for extinct forms.

The study and interpretation of the internal structures of crocodylomorphs needs to be amplified and applied to other putatively terrestrial groups, such as atoposaurids or sphagesaurians, and may be coupled with other geochemical or histological proxies in order to further aid paleoecological and paleobiological inferences.

Acknowledgements

This work was supported by the Agence Nationale de la Recherche (SEBEK project no. ANR-19-CE31-0006-01 to Jeremy E. Martin). The authors would like to thank Céline Salaviale (Université Lyon 1, France) for help during the segmentation of the specimen; Emmanuel Robert and Nicolas Roumenoff (Université Lyon 1) for legal and conservative clarifications; Pedro Henrique Fonseca (Universidade Federal do Rio Grande do Sul) for pictures of *Campinasuchus dinizi*; David Blackburn (Florida Museum of Natural History, United States), Cody Thompson (University of Michigan, United States), Pedro Henrique Morais Fonseca (UFRGS, Brazil), Lawrence Witmer (Ohio University, United States), Blandine Bartschi (Université Lyon 1, France), Timothy Rowe (University of Texas, United States), Marie Meister and Elisabeth Ludes-Fraulob (Musée Zoologique de Strasbourg, France), Didier Berthet (Musée d'Histoire Naturelle de Lyon, France), Medhi Mouana and Anne-Lise Charrault (Université de Montpellier, France), Ronan Allain, Florent Goussard and Nour-Edine Jalil (Muséum National d'Histoire Naturelle, France), Margarethe Maillart (ENS Lyon, France) for access to diverse extant and extinct specimens as well as the sharing of CT data. They would also like to thank Jorgo Ristevski (University of Queensland) and an anonymous reviewer, as well as Philip Cox (University College London) for insightful comments that greatly improved the quality of this manuscript.

Authors contributions

Yohan Pochat-Cottilloux: Conceptualization, Methodology, Software, Validation, Formal analysis, Investigation, Data Curation, Writing - original draft, Writing - review and editing, Visualization. **Nicolas Rinder:** Methodology, Software, Investigation, Validation, Data Curation, Writing - review and editing. **Gwendal Perrichon:** Methodology, Software, Validation, Investigation, Writing - review and editing. **Jérôme Adrien:** Methodology, Software, Validation, Resources, Data Curation, Writing - review and editing, Project administration. **Romain Amiot:** Conceptualization, Validation, Writing - review and editing, Supervision, Project administration. **Stéphane Hua:** Validation, Writing - review and editing.

Jeremy E. Martin: Conceptualization, Validation, Resources, Data Curation, Writing - review and editing, Supervision, Project administration, Funding acquisition.

Data archiving statement

Data for this study are available in the article, the Supplementary Material and the associated MorphoMuseum publication: Pochat-Cottilloux Y., Rinder N., Perrichon G., Adrien J., Amiot R., Hua S. & Martin J. E. (2023). 3D models related to the publication: The neuroanatomy and pneumaticity of *Hamadasuchus* (Crocodylomorpha, Peirosauridae) from the Cretaceous of Morocco and its paleoecological significance for altirostral forms. *MorphoMuseum*, 9(2): e183. https://doi.org/10.18563/journal.m3.183

Supplementary Materials

Supplementary Material S1 & S2 are available in Appendix 9. Supplementary Material S3 is available on this link: https://mycore.core-cloud.net/index.php/s/37TOvxQy5TSDh3L

IV- Paleoneuroanatomy of *Varanosuchus sakonnakhonensis* from Thailand: paleobiological implications

This study is based on the most complete specimen of *Varanosuchus sakonnakhonensis* (SM-2021-1-97/101), a new taxon that was presented and described in detail in Chapter 2 (III). It is especially interesting to study as, to my knowledge, no data on the neuroanatomy of atoposaurids has ever been published, so it could bring further evidence to discuss the debated lifestyle of this clade. Although some studies hint towards a putative terrestrial lifestyle because of their fossil record (Schwarz & Salisbury, 2005) and their skull morphology (Martin *et al*., 2014a), in Chapter 2 (III) we proposed arguments in favour of a more contrasted lifestyle (semi-terrestrial), such as the ornamentation of the osteoderms (Pochat-Cottilloux *et al*., 2023b) or the inferred posture (Chapter 2, III).

Here, using the reconstructed endocranial structures and their paleobiological implications, I will infer several paleoecological traits of this atoposaurid, using the different proxies discussed previously in this Chapter and putting them in perspective with other clades representative of different lifestyles, described throughout this chapter or in the literature (Table 4, Appendices 7 & 8).

a- CT scan and comparisons

A complete skull (SM-2021-1-97/101) was found in the locality of Phu Sung (Sakon Nakhon, Thailand), in the Early Cretaceous of the Sao Khua Formation (Chanthasit *et al*., 2019; Ditbanjong *et al*., 2019). It was scanned in January 2022 at the Laboratoire Mateis (INSA Lyon, Villeurbanne, France), using the Double Tomographe à Haute Energie (DTHE, RX Solutions): scanning parameters were set to 220 kV tube voltage and 129 µA current. The scan has a voxel size of 30 µm. Processed volumes are available here: https://mycore.core-cloud.net/index.php/s/XqER2roioRkmz50. As stated previously, the description is focused on the spaces bounded by bones rather than the unpreserved soft tissues. In order not to weight down the description, comparisons will be made with the various specimens detailed in Table 4 and Appendices 7 & 8.

b- Description

Below are several important measurements following Pierce *et al*. (2017; fig. 2):

- Skull width at cerebrum: 4 cm
- Endocast length: 3.8 cm
- Cerebrum width: 0.8 cm
- Pituitary width: 0.5 cm
- Pituitary height: 0.7 cm
- Pituitary length: 1.1 cm

Cranial endocast and vascular structures

The endocast is badly preserved and probably does not exhibit its original shape due to deformation and taphonomic processes: for example, the pituitary fossa is detached from the endocast itself and the anteriormost part is shifted dorsally (Fig. 3.31). As a result, the real flexure angles of the endocast and its original volume cannot be estimated, the cranial nerves could not be segmented, and caution should be exercised when trying to make interpretations on the cranial endocast of this specimen. As such the olfactory tract and olfactory bulbs are unfortunately too damaged to be described. The cerebral hemispheres are not laterally expanded (Fig. 3.31A, 3.31C & 3.31F), as those of sebecosuchians, metriorhynchids and *Sphenosuchus*, but it is again likely due to a deformation bias. In lateral view (Fig. 3.31F), the endocast has a flat shape with high cephalic and pontine flexure values, as do early crocodylomorphs and

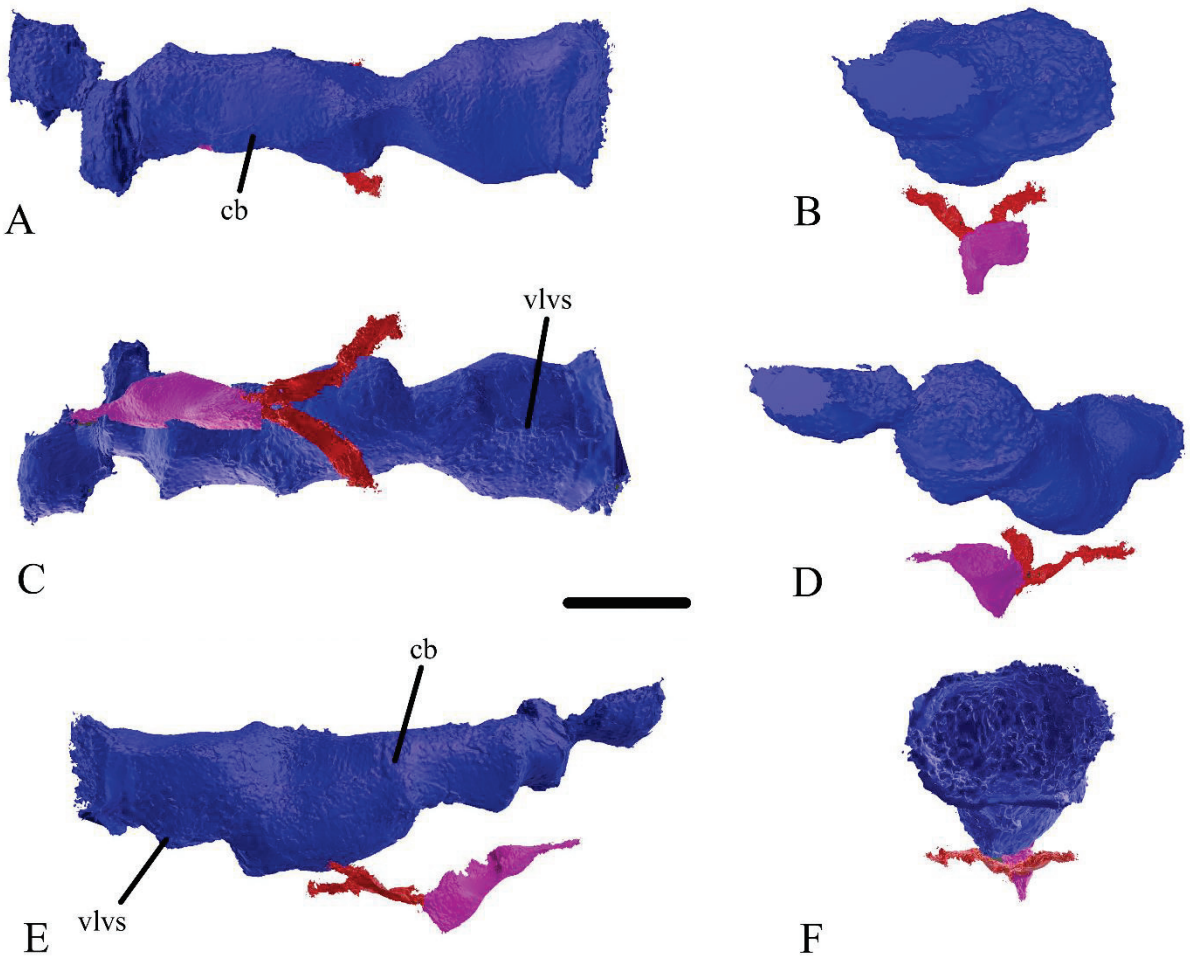

Figure 3.31: Three-dimensional reconstruction of the endocranial cavities within the braincase of SM-2021-1-97/101 (*Varanosuchus*) in dorsal (A), anterior (B), ventral (C), anterior ¾ (D), lateral (E) and posterior (F) views. Blue: endocast, red: internal carotid artery, purple: pituitary fossa. cb: cerebrum, vlvs: ventral longitudinal venous sinus. Scale bar is 2 cm.

thalattosuchians. The dorsal part of the hindbrain is compressed mediolaterally to accommodate for the endosseous labyrinths (which could unfortunately not be segmented), as in other crocodylomorphs. There are no special structures in the dorsal part of the cerebellum and the ventral longitudinal venous sinus is well expanded (Fig. 3.31C & F, as in *Alligator*, *Crocodylus*, *Portugalosuchus, Zulmasuchus*, *Hamadasuchus* and *Sphenosuchus*.

The pituitary fossa is more extended anteroposteriorly than dorsoventrally, and it is directed posteroventrally to anteroposteriorly, although it is difficult to assess its original orientation. Only the anterior part of the internal carotid arteries is preserved, which is the one connected to the posterior end of the pituitary fossa through the carotid pillars (*sensu* Walker, 1990).

Braincase pneumaticity

The intertympanic and pharyngotympanic sinus systems are better preserved (Fig. 3.32). In *Varanosuchus*, there does not seem to be a parietal diverticulum (Fig. 3.32A-B & 3.32D), as in thalattosuchians, although this might be linked to taphonomic processes. The intertympanic diverticulum itself links the two pharyngotympanic sinuses on each side of the endocast, as in all crocodyliforms (Clark, 1986; Leardi *et al*., 2020b). The otoccipital recesses are developed posteriorly (Fig. 3.32A & 3.32E) as in adult specimens of extant short-snouted crocodylians (Perrichon *et al*., 2023).

The rhomboidal pneumatic recess is moderately expanded, between what is observed in modern crocodylians, and *Zulmasuchus* and *Hamadasuchus* (Fig. 3.32B & 3.32D-E). The laterosphenoid and prootic pneumatic recesses are also expanded, in a similar manner to *Zulmasuchus* and *Hamadasuchus* (Fig. 3.32A & 3.32D). Ventrally, the median pharyngeal sinus is verticalized and very expanded, which makes identification of the different recesses and canals difficult (Fig. 3.32B-C). Nevertheless, it suggests that this specimen is mature, as it would otherwise have been more horizontal (Dufeau & Witmer, 2015; Serrano-Martínez *et al*., 2019b). However, on the left side, the parabasisphenoid and basioccipital pneumatic recesses are especially visible (Fig. 3.32D & 3.32F).

c- Paleobiological inferences

As described before in this chapter, the endocranial structures of *Varanosuchus* will now be used to assess key points of the lifestyle of atoposaurids. Unfortunately, as the CT scan data and the preservation of specimen are less exploitable than the two previous forms studied, inferences can only be made on its cranial pneumaticity.

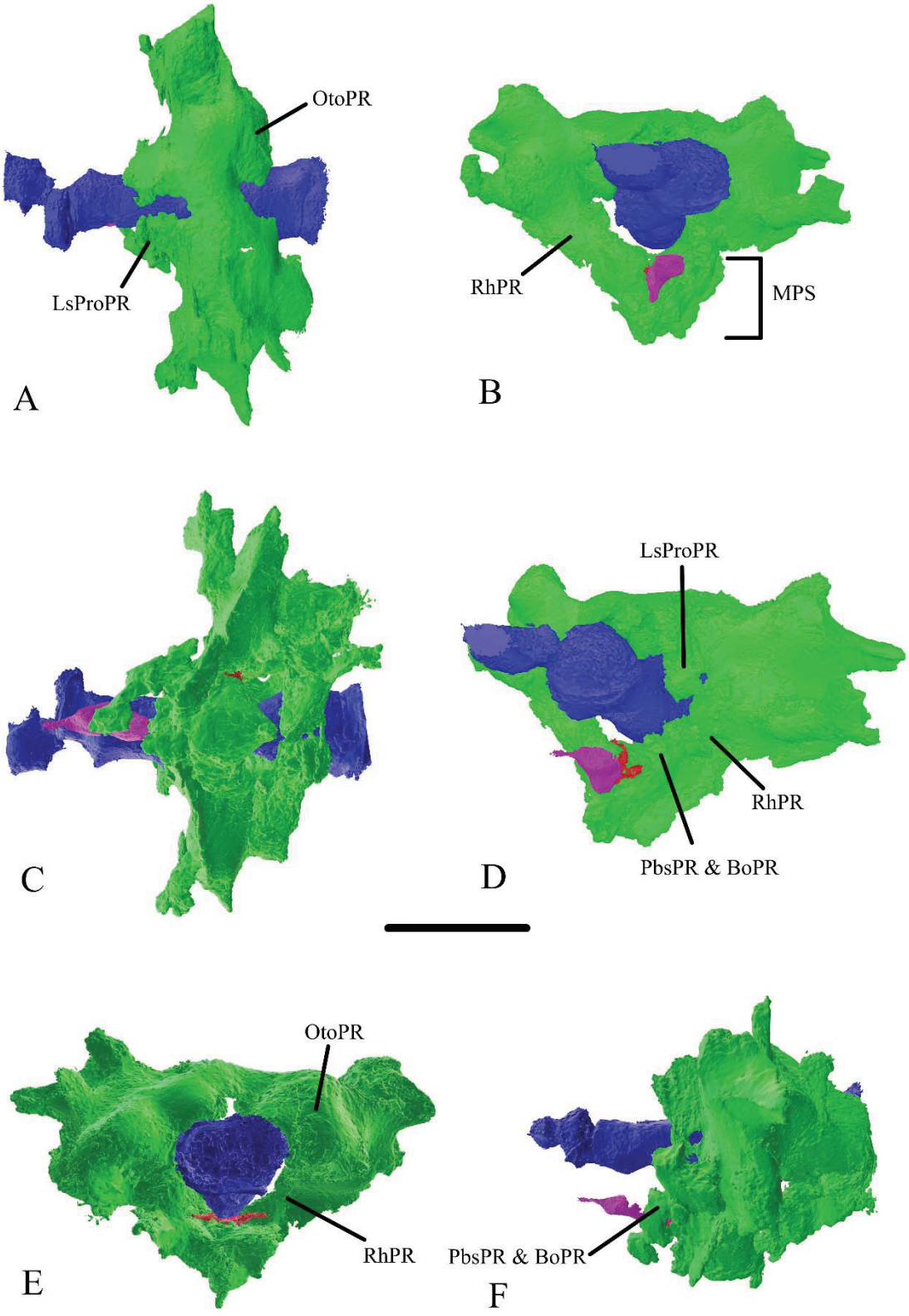

Figure 3.32: Three-dimensional reconstruction of the pneumatic cavities within the braincase of SM-2021-1 - 97/101(*Varanosuchus*) in dorsal (A), anterior (B), ventral (C), anterior ¾ (D), posterior (E) and lateral (F) views. Blue: endocast, green: cranial pneumaticity, red: internal carotid artery, purple: pituitary fossa. BoPR: basioccipital pneumatic recess, LsProPR: laterosphenoid and prootic pneumatic recesses, MPS: median pharyngeal sinus, OtoPR: otoccipital pneumatic recess, PbsPR: parabasisphenoid pneumatic recess, RhPR: rhomboidal pneumatic recess. Scale bar is 2 cm.

The pneumaticity of the skull of *Varanosuchus* seems to be expanded in an intermediate manner between those of *Zulmasuchus* (Pochat-Cottilloux *et al*., 2022b), *Campinasuchus* (Fonseca *et al*., 2020) and *Hamadasuchus* (Pochat-Cottilloux *et al*., 2023d), and those of extant crocodylians, allodaposuchids and *Portugalosuchus* (Witmer *et al*., 2008; Bona *et al*., 2017; Serrano-Martínez *et al*., 2019a, b; 2020; Puértolas-Pascual *et al*., 2022, 2023). In fact, the cranial pneumaticity of *Varanosuchus* is highly similar to the one of *Trilophosuchus rackhami* (Ristevski, 2022), a mekosuchine from the Miocene of Australia (Ristevski *et al*., 2023a). On the contrary, as stated previously, fossil forms that show adaptations to the aquatic environment, such as thalattosuchians, consistently have some of those structures missing (intertympanic and parietal pneumatic recesses; Brusatte *et al*., 2016; Pierce *et al*., 2017; Herrera *et al*., 2018; Schwab *et al*., 2021a; Wilberg *et al*., 2021).

As tested on *Hamadasuchus*, I have updated the dataset of the cranial pneumaticity presented in Pochat-Cottilloux *et al*. (2023d) to get an unbiased idea of the intertympanic and paratympanic sinus systems volume of *Varanosuchus*, compared with extant and extinct specimens of diverse ecologies. The log transformed sinus volume (without cranioquadrate passages) is compared to the log transformed skull width and skull length for each specimen (Fig. 3.33). In *Varanosuchus* (SM-2021-1-97/101), skull width is 12 centimetres, skull length is 17.1 centimetres and braincase pneumaticity volume is 5.4 cm^3.

The addition of *Varanosuchus* data does not change the correlation between sinus volume and skull length (Fig. 3.33A; log skull length = 0.439 ± 0.103 * log sinus volume + 0.925 ± 0.121, 2 s.d.; $R^2 = 0.85$, p-value = $2.00.10^{-9}$). *Varanosuchus* has similar values than extant brevirostrine specimens. Furthermore, sinus volume is also still correlated with skull width (log skull width = 0.410 ± 0.064 * log sinus volume + 0.677 ± 0.077, 2 s.d.; $R^2 = 0.91$, p-value = $1.54.10^{-14}$). Compared with specimens with a similar skull width, *Varanosuchus* has a small sinus volume (which is not the case for *Zulmasuchus* or *Hamadasuchus* for example). This could be evidence of a more aquatic lifestyle than previously thought, or a taphonomic artifact, as highlighted on the endocast. A hypothesis on the lifestyle of atoposaurids through the study of their internal structures can thus only be made with the addition of other specimens, and the cranial pneumaticity of crocodylomorphs needs to be better understood in terms of ontogeny, ecology and phylogeny (Kuzmin *et al*., 2021; Kuzmin, 2022b; Perrichon *et al*., 2023).

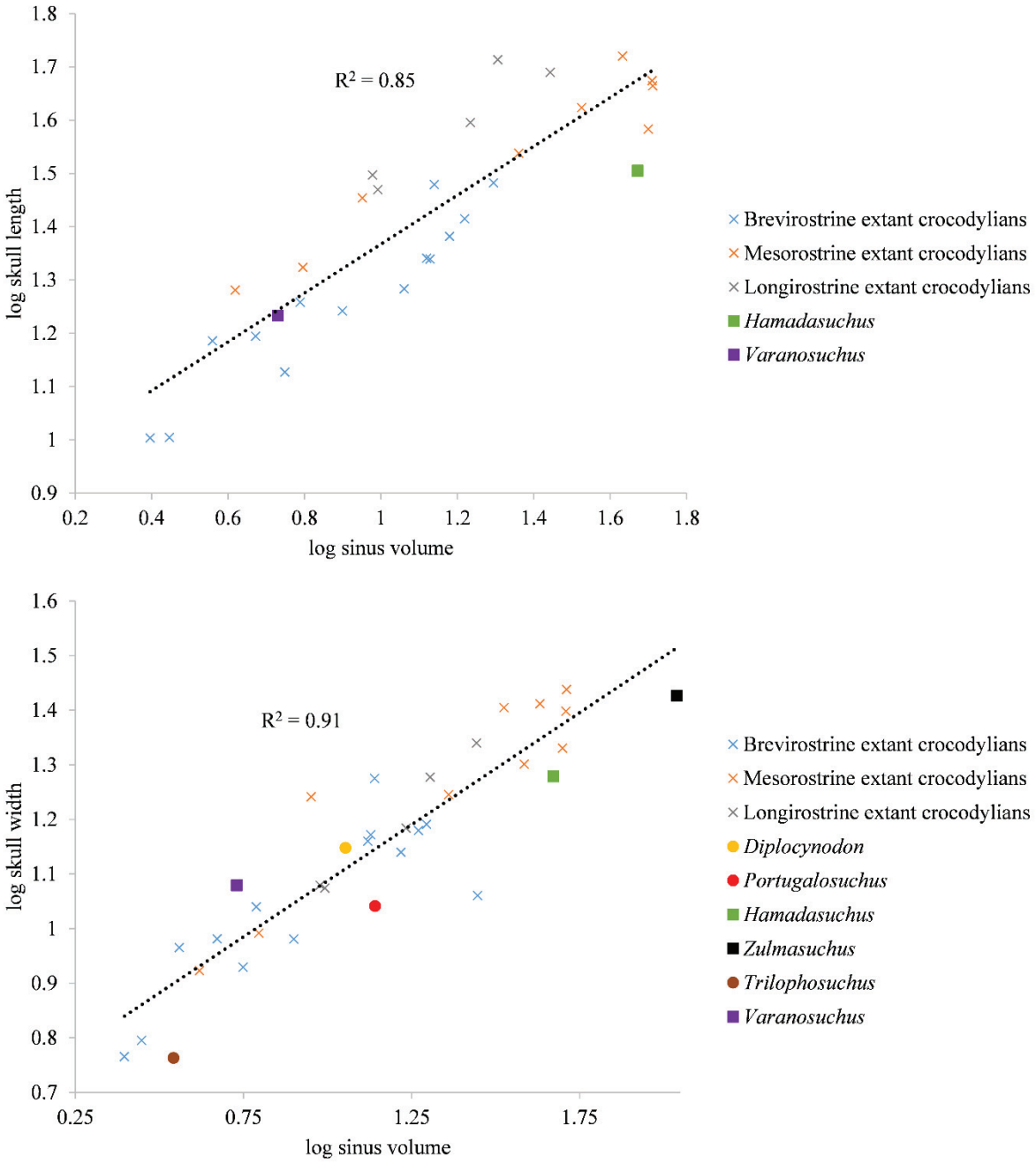

Figure 3.33: A: Sinus volume vs skull length in different specimens of extant crocodylians, *Hamadasuchus* and *Varanosuchus*, B: Sinus volume vs skull width in different specimens of extant and extinct crocodylomorphs.

V- Endosseous labyrinths and their links to ontogeny, phylogeny, and ecology in Crocodylomorpha

As previously stated (see I), the endosseous labyrinths of crocodylomorphs have been the subject of several recent studies, and their ontogenetic, ecological, and phylogenetic implications are currently under debate. Schwab *et al*. (2020) first detected an ecological signal on a sample of crocodylomorphs (n = 32) with a significant change in morphology between aquatic (thalattosuchians, n = 13), semi-aquatic (extant crocodylians, n = 14) and terrestrial

(sphenosuchians and *Protosuchus* Brown, 1934, n = 3) forms based on a 3D geometric morphometric approach. However, Bronzati *et al*. (2021) contested those results using a similar approach, but including phylogenetically informed statistical tests, on a much larger taxonomic sample (n = 82 including birds, turtles, and lizards, but only n = 14 crocodylomorphs and n = 3 terrestrial forms). Indeed, these authors found no support for an ecological signal in the endosseous labyrinths of their sample associated with the transition between habitats but rather recovered a link with the shape of the skull, dorsoventrally compressed skulls of thalattosuchians being associated with dorsoventrally low labyrinths. Finally, Schwab *et al*. (2021b) showed that ontogenetic variation also played a role, using an extant crocodylian dataset (n = 30) with several ontogenetic stages. Two major shifts occur: an increase in size throughout ontogeny, and a change in shape, with smaller semicircular canals in juveniles than in adults. As a result, they also concluded that the shape of the endosseous labyrinths was constrained by the skull, rather than linked to any ecological or phylogenetic signal.

Throughout this chapter, we have seen that the endosseous labyrinths of *Zulmasuchus* and *Hamadasuchus* differ in shape from those of extant semi-aquatic and extinct aquatic crocodylomorphs. With the addition of those data (and others), I aim to enlarge the taxonomic sample of terrestrial forms of crocodylomorphs, as previous studies could only incorporate three specimens, thus creating a significant bias. Based on an extensive dataset of extant specimens, representing almost all their taxonomic diversity, I will first try to reassess the link between endosseous labyrinth shape and ontogeny, before assessing its potential ecological and phylogenetic implications incorporating fossil forms.

Out of the 116 extant specimens studied in the framework of this thesis (see Appendices 7 & 8), the endosseous labyrinths of 101 of them could be segmented and used here. Those represent 21 species out of the 23 to 28 species that exist today, with ontogenetic series (at least four individuals of diverse size) for 11 of them. Out of the 37 extinct specimens studied in the framework of this thesis (see Appendices 7 & 8), the endosseous labyrinths of 22 of them could be segmented and used here. Those represent fossils with different inferred lifestyles, such as fully aquatic, semi-aquatic or terrestrial.

As it is especially difficult to identify clear limits between the different ontogenetic stages in crocodylians, due to their continuous growth and lack of data (Morris *et al*., 2019; Schwab *et al*., 2021b), I have decided to classify them in three different size classes. Extant specimens were classified as hatchlings, juveniles or adults depending on their skull length and genus

(following Perrichon *et al*., 2023, with subadults and adults regrouped). As ontogenetic variation in fossils is very difficult to assess, extinct specimens were defined as adults by default, unless proven otherwise.

In the dataset, some taxonomic uncertainties remain, such as the delimitation between *Crocodylus porosus* and *Crocodylus siamensis* (Perrichon *et al*., 2023), or the taxonomic content of *Crocodylus niloticus* and *Crocodylus suchus* Geoffroy Saint-Hilaire, 1807 (Hekkala *et al*., 2011; Meredith *et al*., 2011; Nicolaï & Matzke, 2019; Pan *et al*., 2021). On this last matter, here all specimens are assigned to *Crocodylus niloticus*, pending further morphological studies on their possible distinguishability. For now, there are no true morphological differences between *Mecistops cataphractus* and *Mecistops leptorhynchus* Bennett, 1835, so the specimens are designated as *Mecistops* sp. To detect the subtle morphological differences between *Mecistops cataphractus* and *Mecistops leptorhynchus* would indeed necessitate a separate geometric morphometric analysis of the skull of the specimens studied here (Carr *et al*., 2021), which is out of scope and finally not that useful here.

a- Geomorphometric analyses

To infer the shape variation of the dataset of endosseous labyrinths studied here, 3D geomorphometric analyses were used. Briefly, these consist in the statistical comparisons of the 3D coordinates of homologous points on the 3D volume of each endosseous labyrinth: these points are called landmarks. Here, I first used 26 of them, that were placed using the software MorphoDig 1.5.3 (Lebrun, 2018), and chosen to reflect the shape and extension of the structures, apart from the lagenar region which is a source of segmentation problem (see Pochat-Cottilloux *et al*., 2022b). The type I (clearly defined) and type II (maximum curvatures) landmarks (Bookstein, 1997) used are detailed in Fig. 3.34 and Table 9. Then, these 26 landmarks were used as the basis for building landmark curves corresponding to the outline of the semicircular canals and the vestibula. On the five landmark curves, 20 sliding semi-landmarks (Gunz & Mitteroecker, 2013; Bardua *et al*., 2019) were evenly distributed (i.e., 100 sliding semi-landmarks in total) to assess whether a different number of landmarks to characterize the same shapes had any influence on the statistical interpretations. Furthermore, the landmark placement protocol was also tested for any placement bias (i.e., significant error of landmark placement because of unclear definitions or difficult structures), by replotting the landmarks on the same set of three specimens ten times, each on different days, and comparing them statistically.

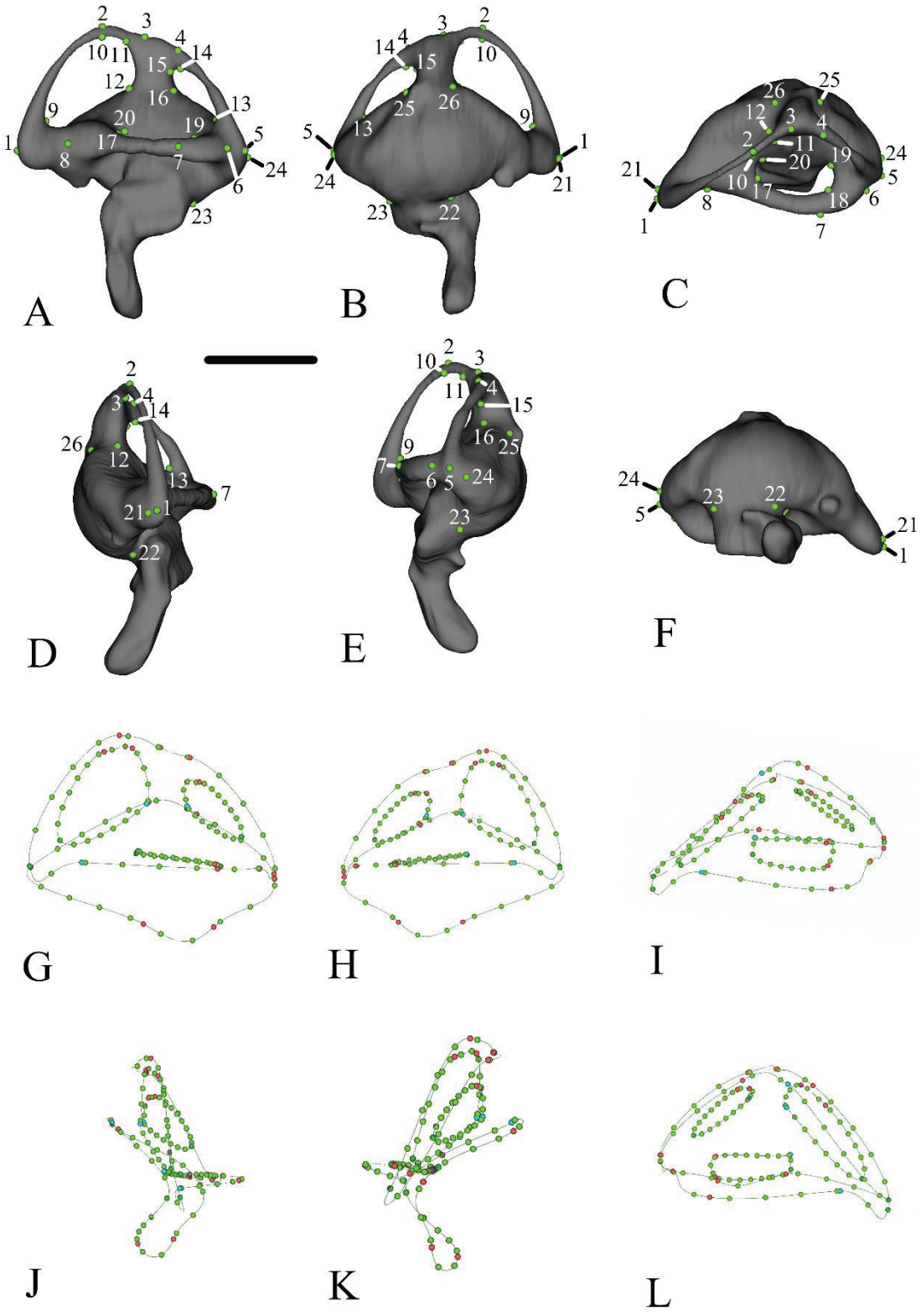

Figure 3.34: Location of the 3D landmarks captured on the specimens. First two rows: 26 type I and II numbered landmarks. Last two rows: 100 semi-sliding landmarks in green with landmarks of the first protocol in red for comparison. Left endosseous labyrinth from AMU Zoo-04721 (*Mecistops* sp.) in lateral (A & G), medial (B & H), dorsal (C & I), anterior (D & J), posterior (E & K) and ventral (F & L) views. Scale bar is 1 cm.

Table 9: Landmarks definition

Number	Definition
1	Anteriormost point in lateral view
2	Dorsalmost point of the anterior semicircular canal external surface in lateral view
3	Ventralmost point of the common crus in lateral view
4	Dorsalmost point of the posterior semicircular canal external surface in lateral view
5	Posteriormost point in lateral view
6	Posteriormost point of lateral semicircular canal external surface in dorsal view
7	Lateralmost point of lateral semicircular canal external surface in dorsal view
8	Anteriormost point of lateral semicircular canal external surface in dorsal view
9	Anteriormost point of anterior semicircular canal internal surface in lateral view
10	Dorsalmost point of anterior semicircular canal internal surface in lateral view
11	Posterodorsalmost point of anterior semicircular canal internal surface in lateral view
12	Posteroventralmost point of anterior semicircular canal internal surface in lateral view
13	Posteriormost point of posterior semicircular canal internal surface in lateral view
14	Dorsalmost point of posterior semicircular canal internal surface in lateral view
15	Anterodorsalmost point of anterior semicircular canal internal surface in lateral view
16	Anteroventralmost point of anterior semicircular canal internal surface in lateral view

17	Anterolateralmost point of lateral semicircular canal internal surface in dorsal view
18	Posterolateralmost point of lateral semicircular canal internal surface in dorsal view
19	Anteromedialmost point of lateral semicircular canal internal surface in dorsal view
20	Posteromedialmost point of lateral semicircular canal internal surface in dorsal view
21	Anteriormost point in medial view
22	Anteriormost point of cochlear duct in medial view
23	Posteriormost point of cochlear duct in medial view
24	Posteriormost point in medial view
25	Posterior intersection between common crus and vestibula in medial view
26	Anterior intersection between common crus and vestibula in medial view

All analyses were performed in R4.3.0 (R Core Team, 2023) using the packages geomorph 4.0.5 for geometric morphometric analyses (Adams & Otárola-Castillo, 2013), rgl 1.1.3 (R Core Team, 2023) and ggplot2 3.4.2 (Wickham, 2011) for visualization purposes and ape 5.7-1 (Paradis *et al*., 2004) and paleotree 3.4.5 (Bapst, 2012) for phylogenetic analyses.

On each sub-analyses run, the first step was to correct the differences in size and alignment of the different specimens through a generalized least-squares Procrustes Analysis (GPA) superimposition using the function *gpagen* (Rohlf & Slice, 1990; Baken *et al*., 2021). Then, principal component analyses (PCA) were used on the Procrustes shape coordinates (function *gm.prcomp*) to find the major axes of variation of each sub-datasets. To enhance the visualizations, 3D wireframes were created using the functions *PlotRefToTarget* and *shape.predictor*.

The effect of phylogeny on shape can be corrected or prioritized using phylogenetic PCA (Revell, 2009) or phylogenetically aligned component analysis (PACA; Collyer & Adams, 2021) respectively. Other factors, such as ecology (aquatic, terrestrial, semi-aquatic or

unknown), size (centroid size) or skull shape (brevirostre, mesorostre, longirostre), can be statistically correlated using Procrustes ANOVA for Procrustes shape variable (function *procD.lm)*, which corresponds to a non-parametric Permutational Multivariate Analysis of Variance (Anderson, 2001). Phylogenies were time-scaled using the function *timePaleoPhy*. The "mbl" method was used (Laurin, 2004), which dates internal nodes by the oldest species they include, with a minimum branch of one million years to avoid zero-length branches. Stratigraphic ranges of the different species used here were obtained from the Paleobiology Database (PBDB; https://www.paleobiodb.org).

To assess differences between the two landmarking protocols, a correlation test was run only on extant adults for each protocol (n = 65), to eliminate any ecological or ontogenetic bias. This correlation test was run through the function *integration.test*, which quantifies the degree of morphological integration between modules of Procrustes shape variables.

Then, the extant sample was studied to assess ontogenetic implications, using ontogenetic series of *Alligator*, *Caiman*, *Crocodylus*, *Gavialis*, *Mecistops*, *Osteolaemus*, *Paleosuchus* and *Tomistoma.* The ontogenetic trajectories were found using a linear regression between the Procrustes coordinates of the first axis of major variation and the log transformed centroid size of the specimens (function *lm*).

Finally, asymmetry between the left and right endosseous labyrinths has already been assessed in crocodylomorphs to be minimal (Schwab *et al*., 2020), so here the left endosseous labyrinth was used when available. If only the right endosseous labyrinth was available, it was mirrored using Blender v2.91 before landmark placement.

All necessary landmark files, the meshes used, and the R script are available here: https://mycore.core-cloud.net/index.php/s/QnSKKqRu39Tl5UO

b- Results and interpretations

First, the two landmarking protocols are found similar under an integration test (R^2 = 0.95, p-value = 0.001) on the extant adult specimens (Fig. 3.35). As a result, and for time saving, the first landmarking protocol was replicated on all specimens. The landmarking protocol is further validated as the different replications of the three different genera done on different days cluster on a PCA (Fig. 3.36) and are significantly separated (the Procrustes coordinated are significantly correlated with genus, R^2 = 0.76, p-value = 0.001).

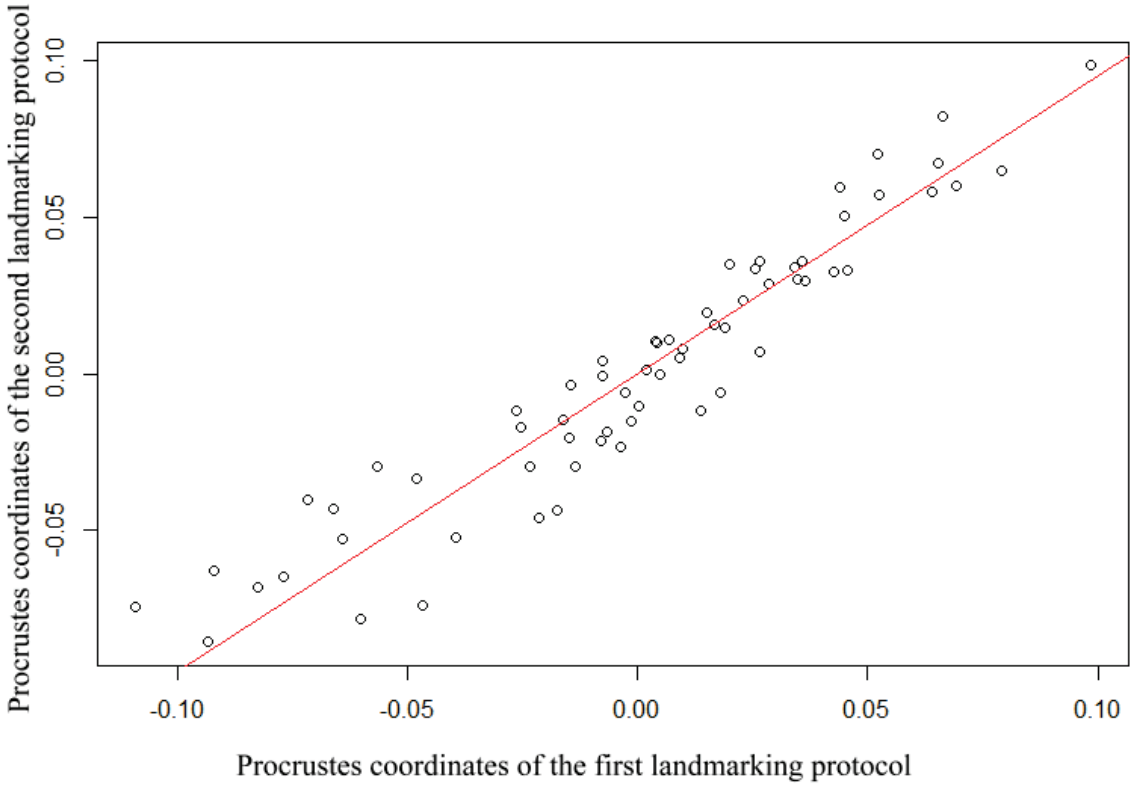

Figure 3.35: Correlation between the Procrustes coordinates of the two landmarking protocols.

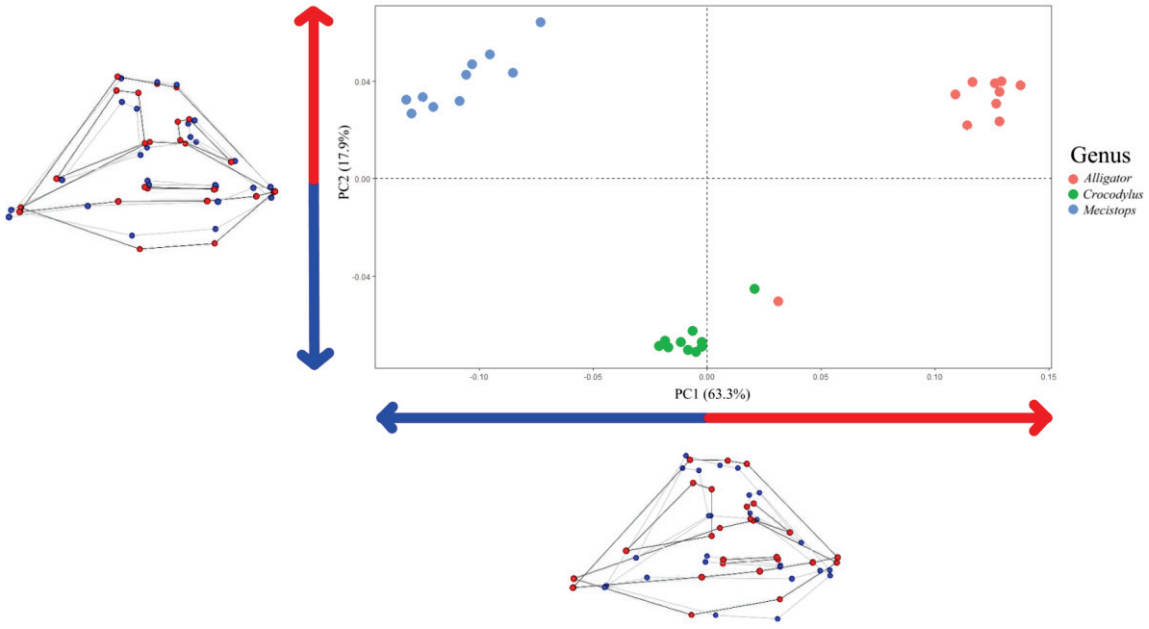

Figure 3.36: Morphospace occupation of endosseous labyrinth shape in the ten different replicates. Extreme shapes for each PC axes given with wireframes in lateral view.

In the extant sample (n = 103), the Procrustes ANOVA revealed a significant effect of size, genus, family, and skull shape (p = 0.001), at various percentages (Table 10). Furthermore, the first three principal components of the complete extant morphospace explain 41.8 % of the total

Table 10: Regression tests on the full extant sample (n = 103). Non-significant results highlighted in red.

Variable 1	**Variable 2**	**p-value**	**R^2**
Procrustes coordinates	Size	0.001	0.13
Procrustes coordinates	Genus	0.001	0.21
Procrustes coordinates	Family	0.001	0.10
Procrustes coordinates	Skull shape	0.001	0.07
PC1	Size	0.001	0.17
PC1	Genus	0.001	0.31
PC1	Family	0.001	0.22
PC1	Skull shape	0.006	0.11
PC2	Size	0.04	0.04
PC2	Genus	0.001	0.21
PC2	Family	0.003	0.12
PC2	Skull shape	0.05	0.05
PC3	Size	0.14	0.02
PC3	Genus	0.001	0.35
PC3	Family	0.45	0.03
PC3	Skull shape	0.005	0.09

variance, with changes throughout ontogeny (Fig. 3.37). The remaining components each accounted for less than 10% of the total variance and were thus not considered. PC1 is related to the anteroposterior compression of the endosseous labyrinth with positive values related to an anteroposterior elongation. PC2 characterizes the development of the semicircular canals, with positive values related to minimum development. PC3 is associated with the dorsoventral development of the endosseous labyrinth with negative values corresponding to a maximum dorsoventral development. PC1 and PC2 scores are significantly correlated with size, genus,

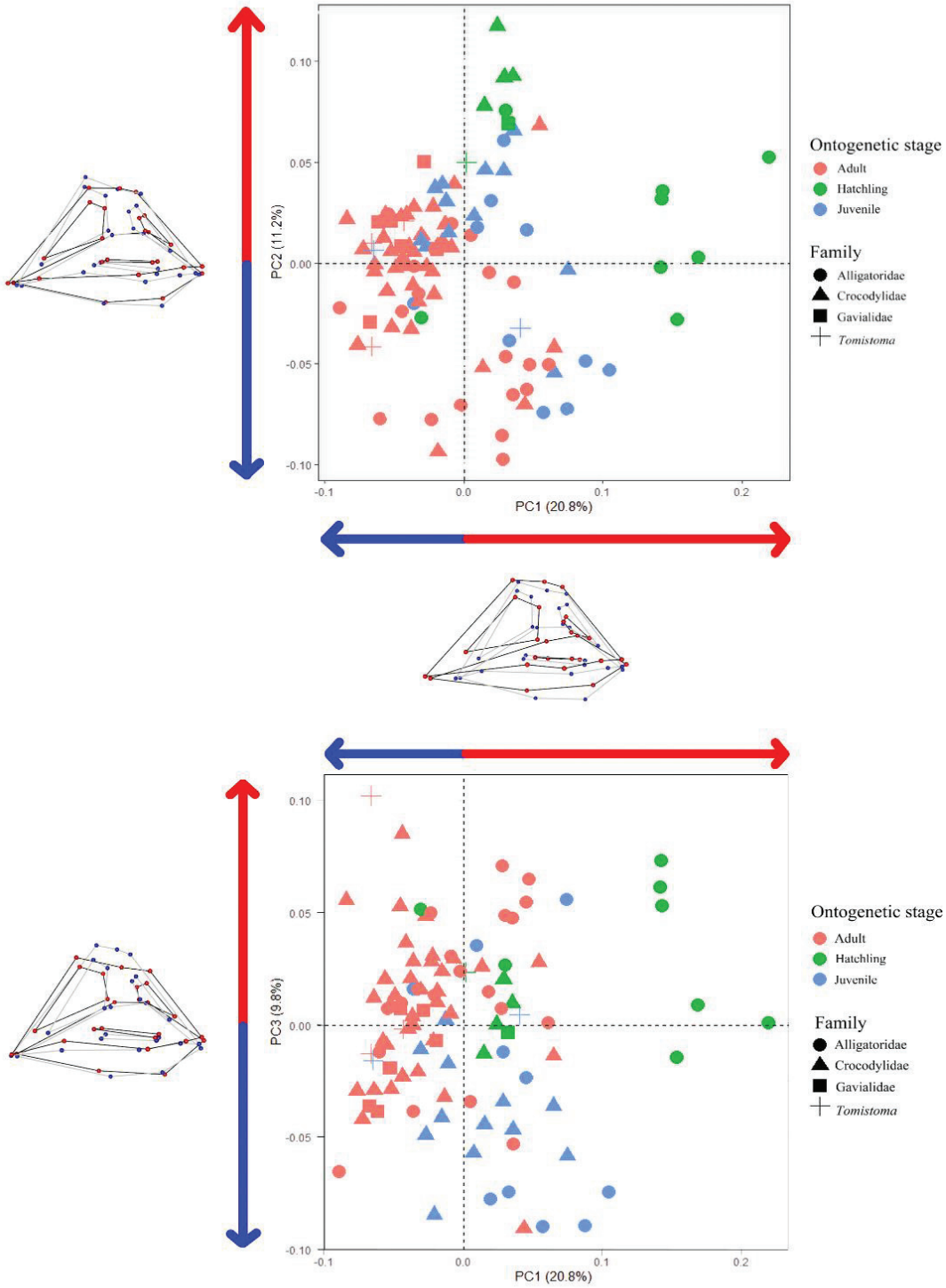

Figure 3.37: Morphospace occupation of endosseous labyrinth shape in the extant sample. Extreme shapes for each PC axes given with wireframes in lateral view.

family, and skull shape, while PC3 scores are only significantly correlated with genus and skull shape (Table 10).

As a result, adult specimens are located towards negative PC1 and PC2 values, juveniles towards null values and hatchlings specimens towards positive PC1 and PC2 values.

Alligatorids, *Tomistoma* and crocodylids are scattered in the extant morphospace, while gavialids are restricted to positive PC2 values.

As Schwab *et al*. (2021b) noticed, there is a strong ontogenetic signal in the endosseous labyrinth of extant crocodylians, with significant correlations in *Alligator*, *Caiman*, *Crocodylus*, *Gavialis, Mecistops*, *Osteolaemus* and *Tomistoma* (Fig. 3.38 & 3.39). The trend in *Paleosuchus* is not significant, but this might rather be due to the low number of specimens sampled (n = 4; Fig. 3.39C). During ontogeny, the endosseous labyrinth becomes anteroposteriorly compressed (PC1) with thinner semicircular canals (PC2). This agrees with the hypothesis put forward in Schwab *et al*. (2021b), that braincase dimensions, and how they change throughout ontogeny has a direct effect on the endosseous labyrinth size and shape. This is linked with the verticalization of the braincase in the first years of life of crocodylians (Tarsitano *et al*., 1989), resulting in a dorsoventral expansion of the braincase and a flattening of the skull roof (Witmer, 1995; Gold *et al*., 2014; Dufeau & Witmer, 2015; Morris *et al*., 2021). Negative allometries are retrieved in the ontogenetic series, meaning that the endosseous labyrinth development is slower than that of the skull. Thus, to assess the phylogenetic and ecological implications of the endosseous labyrinth, the dataset must consist only of adult specimens, to remove any ontogenetic bias (Schwab *et al*., 2021b). In the sample consisting only of adult specimens (extant and extinct, n = 91), the Procrustes ANOVA revealed a significant effect of size, genus, family, ecology, and skull shape ($p = 0.001$), at various percentages (Table 11). Furthermore, the first two principal components of the complete adult morphospace explain 26.1 % of the total variance, with changes throughout phylogeny and ecology (Fig. 3.40 & 3.41). The remaining components each accounted for less than 10% of the total variance and were thus not considered. PC1 is related to the anteroposterior compression of the endosseous labyrinth with positive values related to an anteroposterior elongation. PC2 is associated with the dorsoventral development of the endosseous labyrinth with negative values corresponding to a maximum dorsoventral development. PC1 and PC2 scores are significantly correlated with size, genus, family, and skull shape, while only PC1 is correlated with ecology.

Fully aquatic specimens are located towards PC1 negative values, but those specimens are also phylogenetically separated from extant crocodylians and terrestrial forms (Fig. 3.40). On the other hand, terrestrial and semi-aquatic forms are no separated. As a result, aquatic thalattosuchians (which are longirostrine) have an anteroposteriorly developed endosseous labyrinths, while semi-aquatic and terrestrial forms (mesorostrine and brevirostrine) have a more compressed endosseous labyrinth shape (Fig. 3.41).

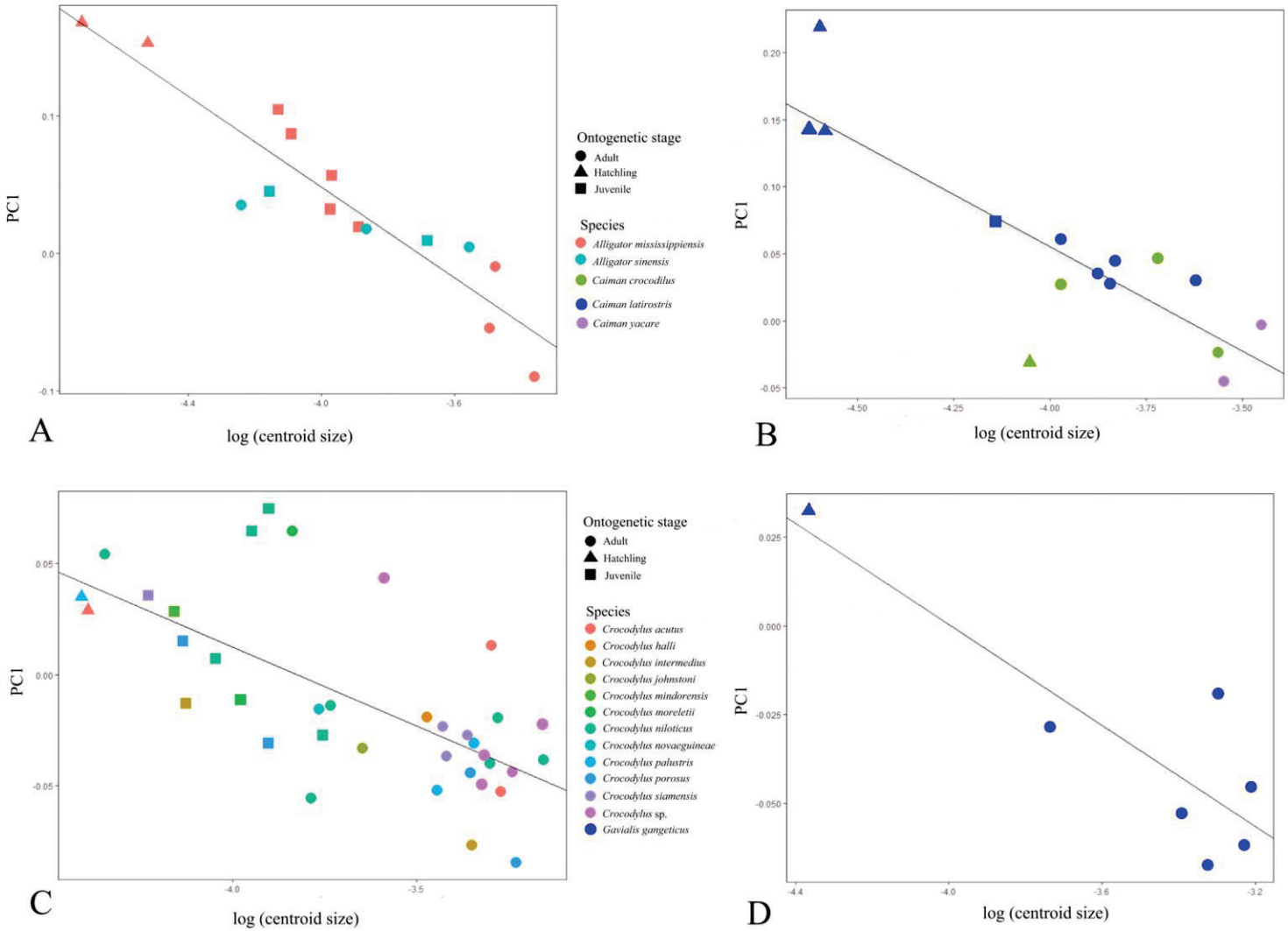

Figure 3.38: Plots of PC1 versus log-transformed centroid size, associated with the corresponding ontogenetic trend. A: *Alligator* ($R^2 = 0.85$, p-value = $7.06.10^{-7}$). B: *Caiman* ($R^2 = 0.74$, p-value = $1.10.10^{-5}$). C: *Crocodylus* ($R^2 = 0.45$, p-value = $3.91.10^{-6}$). D: *Gavialis* ($R^2 = 0.71$, p-value = 0.01).

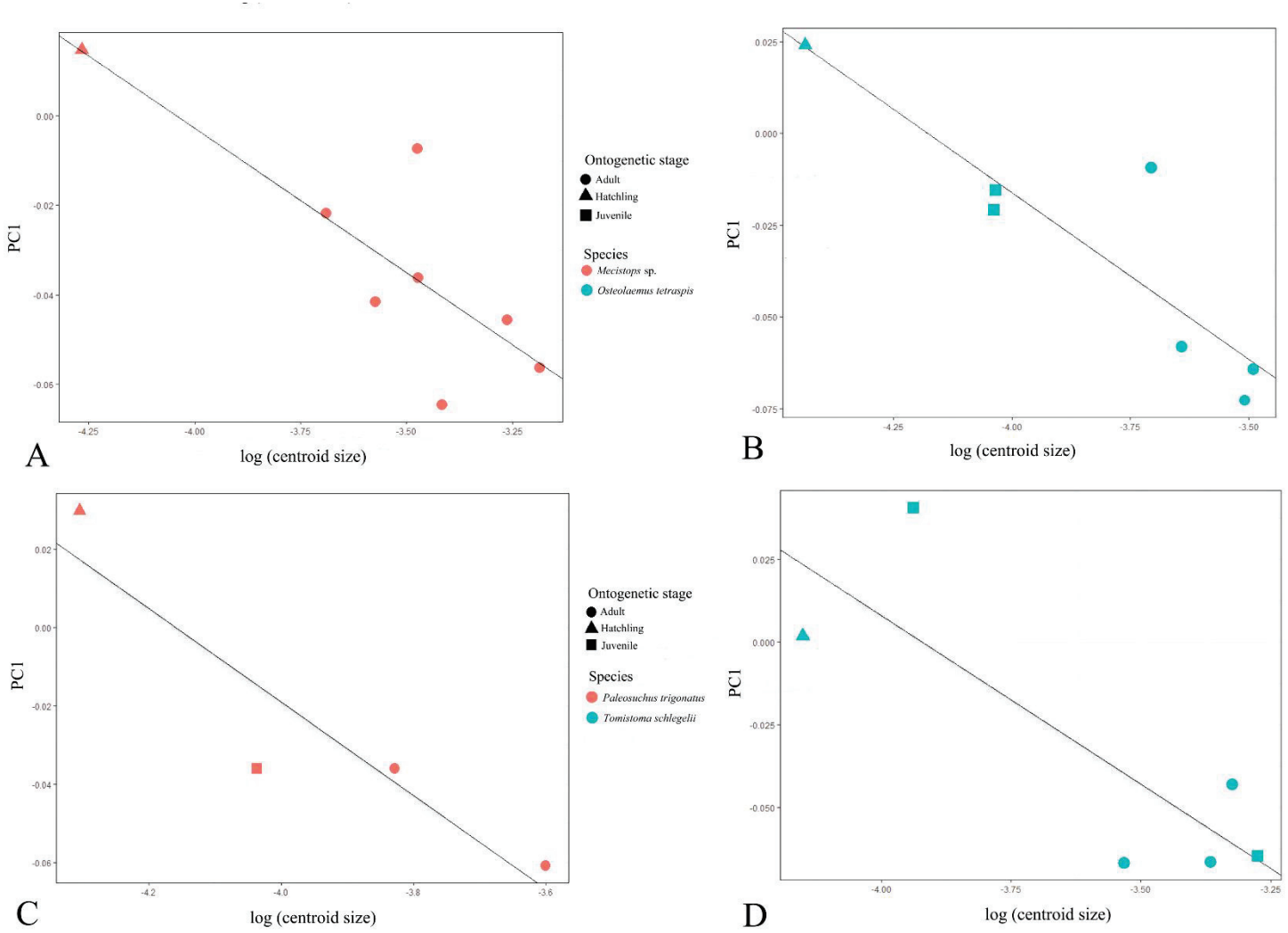

Figure 3.39: Plots of PC1 versus log-transformed centroid size, associated with the corresponding ontogenetic trend. A: *Mecistops* ($R^2 = 0.61$, p-value = 0.01). B: *Osteolaemus* ($R^2 = 0.77$, p-value = 0.006). C: *Paleosuchus* ($R^2 = 0.78$, p-value = 0.08). D: *Tomistoma* ($R^2 = 0.61$, p-value = 0.04).

Table 11: Regression tests on the full adult sample (n = 91). Non-significant results highlighted in red.

Variable 1	**Variable 2**	**p-value**	**R^2**
Procrustes coordinates	Size	0.001	0.04
Procrustes coordinates	Genus	0.001	0.56
Procrustes coordinates	Family	0.001	0.32
Procrustes coordinates	Skull shape	0.001	0.11
Procrustes coordinates	Ecology	0.001	0.15
PC1	Size	0.002	0.12
PC1	Genus	0.001	0.81
PC1	Family	0.001	0.69
PC1	Skull shape	0.01	0.21
PC1	Ecology	0.001	0.42
PC2	Size	0.002	0.12
PC2	Genus	0.001	0.71
PC2	Family	0.001	0.52
PC2	Skull shape	0.03	0.23
PC2	Ecology	0.08	0.08

However, the variations in shape, although they are studied only on adults, are still lightly influenced by size (Table 11). In order to remove this bias, the residual shape components (RSC) of a regression between the common allometric component (CAC; Mitteroecker *et al*., 2004) of the sample and the size was performed using the function *plotAllometry*. Then, another PCA was run on those residual components, which are effectively Procrustes coordinates corrected for the effect of allometry.

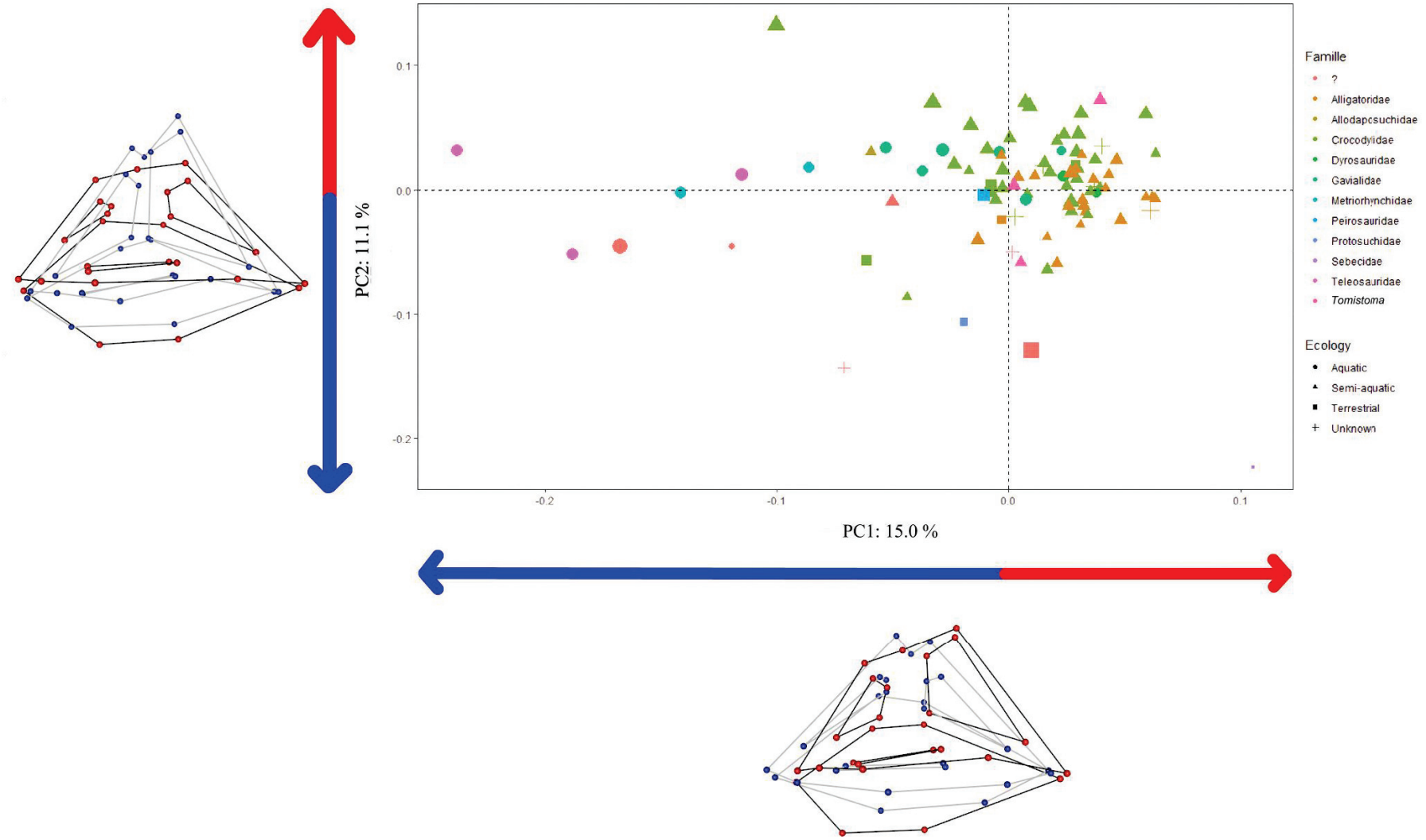

Figure 3.40: Morphospace occupation of endosseous labyrinth shape in the adult sample. Extreme shapes for each PC axes given with wireframes in lateral view. Point size is correlated with specimen size.

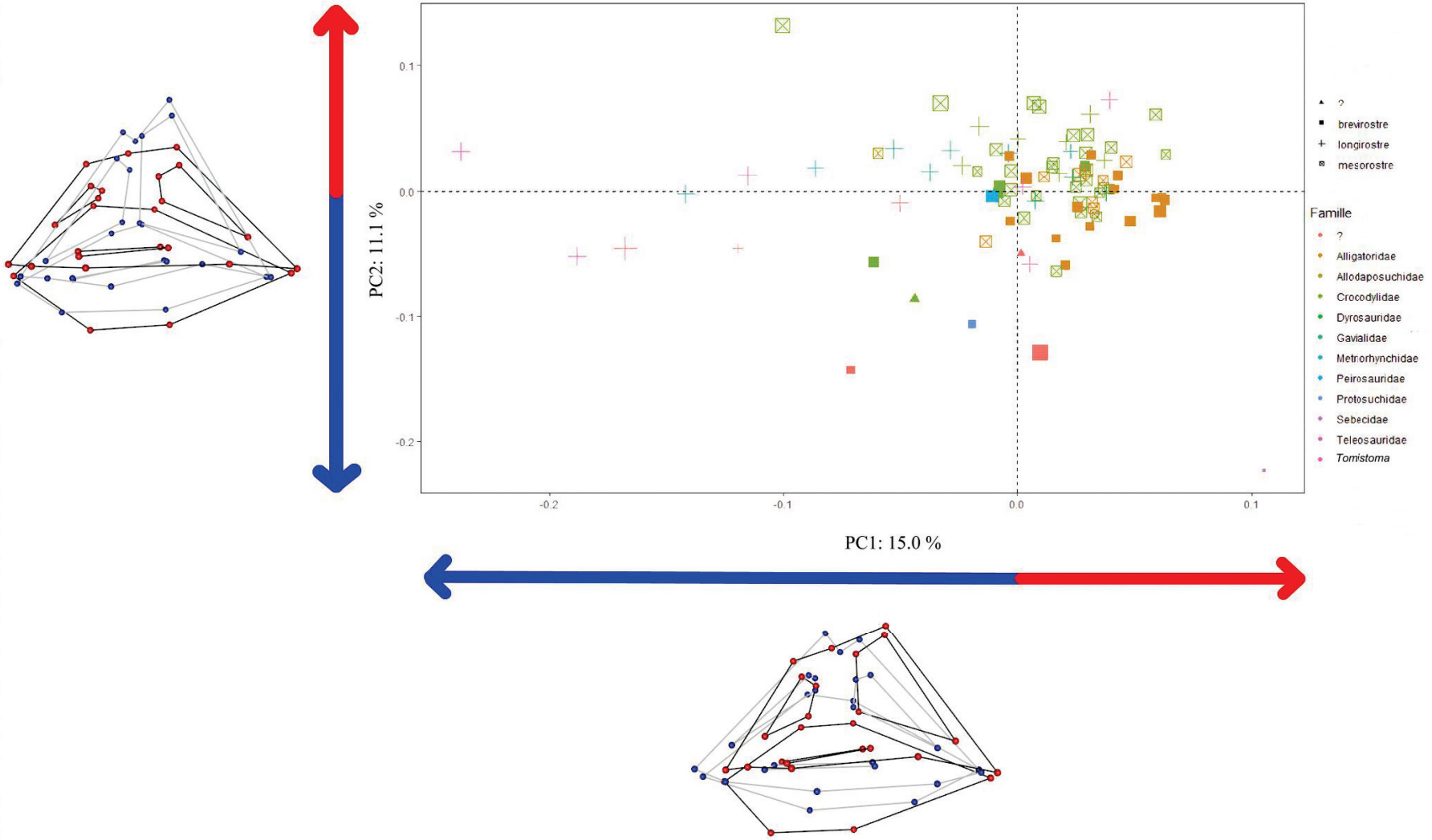

Figure 3.41: Morphospace occupation of endosseous labyrinth shape in the adult sample. Extreme shapes for each PC axes given with wireframes in lateral view. Point size is correlated with specimen size.

In the sample consisting only of adult specimens corrected for allometry (extant and extinct, n = 91), the Procrustes ANOVA revealed a significant effect of genus, family, ecology, and skull shape ($p \leqslant 0.005$), at various percentages (Table 12). Furthermore, the first two residual shape components of the complete adult morphospace corrected for allometry are linked with changes throughout phylogeny and ecology (Fig. 3.42 & 3.43). RSC1 is related to the shape of the lateral semicircular canal and the dorsal outline of the endosseous labyrinth with positive values related to smaller lateral semicircular canal and a straight dorsal outline of the endosseous labyrinth. RSC2 is associated with the size of the anterior and lateral semicircular canals, with RSC2 positive values related to smaller semicircular canals. RSC1 and RSC2 scores are significantly correlated with genus, family, and ecology, while only RSC1 is correlated with skull shape.

Fully aquatic specimens are located towards RSC1 negative values, but those specimens are also phylogenetically separated from extant crocodylians and terrestrial forms (Fig. 3.42). On the other hand, terrestrial and semi-aquatic forms are no separated. As a result, aquatic thalattosuchians (which are longirostrine) have a large semicircular canal and a small common crus (i.e., twisted dorsal outline of the endosseous labyrinth), while semi-aquatic and terrestrial forms (mesorostrine and brevirostrine) have smaller semicircular canals (Fig. 3.43).

In this same dataset of residual shape components coordinates, the phylogenetic signal can be assessed, using the multivariate version of the K-statistic (Kmult; Adams, 2014). This value varies between 0 and 1 and evaluates the degree of phylogenetic signal in a dataset compared to what is expected under a Brownian model of evolution: the higher the phylogenetic signal, the closest the value will be of 1. Here, Kmult = 0.13 (p-value = 0.001), which, although significant, implies a low impact of phylogeny on the total shape variation of the crocodylomorphs sampled here. Thus, I will not try to reconstruct ancestral states or evolutionary rates of the endosseous labyrinths in crocodylomorphs. As a result, when considering the effect of allometry, the variation of shape of the endosseous labyrinths of crocodylomorphs seems to be poorly related to phylogeny and ecology. Through phylogenetic-PCA, the dataset can also be corrected for the effect of phylogeny.

In the sample consisting only of adult specimens corrected for allometry and phylogeny (extant and extinct, n = 91), the first two residual shape components of the complete adult morphospace are linked with none of the remaining variables studied here (Fig. 3.44 & 3.45; Table 13), although Phy-RSC1 is significantly linked with ecology but most probably because of the three

Table 12: Regression tests on the full adult sample corrected for allometry (n = 91). Non-significant results highlighted in red.

Variable 1	**Variable 2**	**p-value**	**R^2**
Procrustes coordinates corrected for allometry	Size	1	< 0.01
Procrustes coordinates corrected for allometry	Genus	0.001	0.54
Procrustes coordinates corrected for allometry	Family	0.001	0.29
Procrustes coordinates corrected for allometry	Skull shape	0.005	0.08
Procrustes coordinates corrected for allometry	Ecology	0.001	0.10
RSC1	Genus	0.001	0.82
RSC1	Family	0.001	0.67
RSC1	Skull shape	0.01	0.16
RSC1	Ecology	0.001	0.30
RSC2	Genus	0.001	0.73
RSC2	Family	0.001	0.47
RSC2	Skull shape	0.72	0.02
RSC2	Ecology	0.003	0.15

outliers. Phy-RSC1 is related to the size of the endosseous labyrinths, with positive values related to smaller endosseous labyrinths. Phy-RSC2 is also associated with the size of the endosseous labyrinth, with Phy-RSC2 positive values related to largest endosseous labyrinths. It is surprising to see that these axes are linked with size, as the data is supposed to be corrected for allometry. This might be an artifact linked with a high loss of shape information due to the constraints applied here All the specimens are centered in the middle of the morphospace, except for three of them: two *Voay robustus* (NHMUK 36684 & 36685), which have the most positive Phy-RSC1 values and one *Paleosuchus trigonatus* (MHNL 42003939), which has the most positive Phy-RSC2 values. Thus, the endosseous labyrinths of those specimens are much larger than the rest of the sample, which is surprising because the effect of size has been

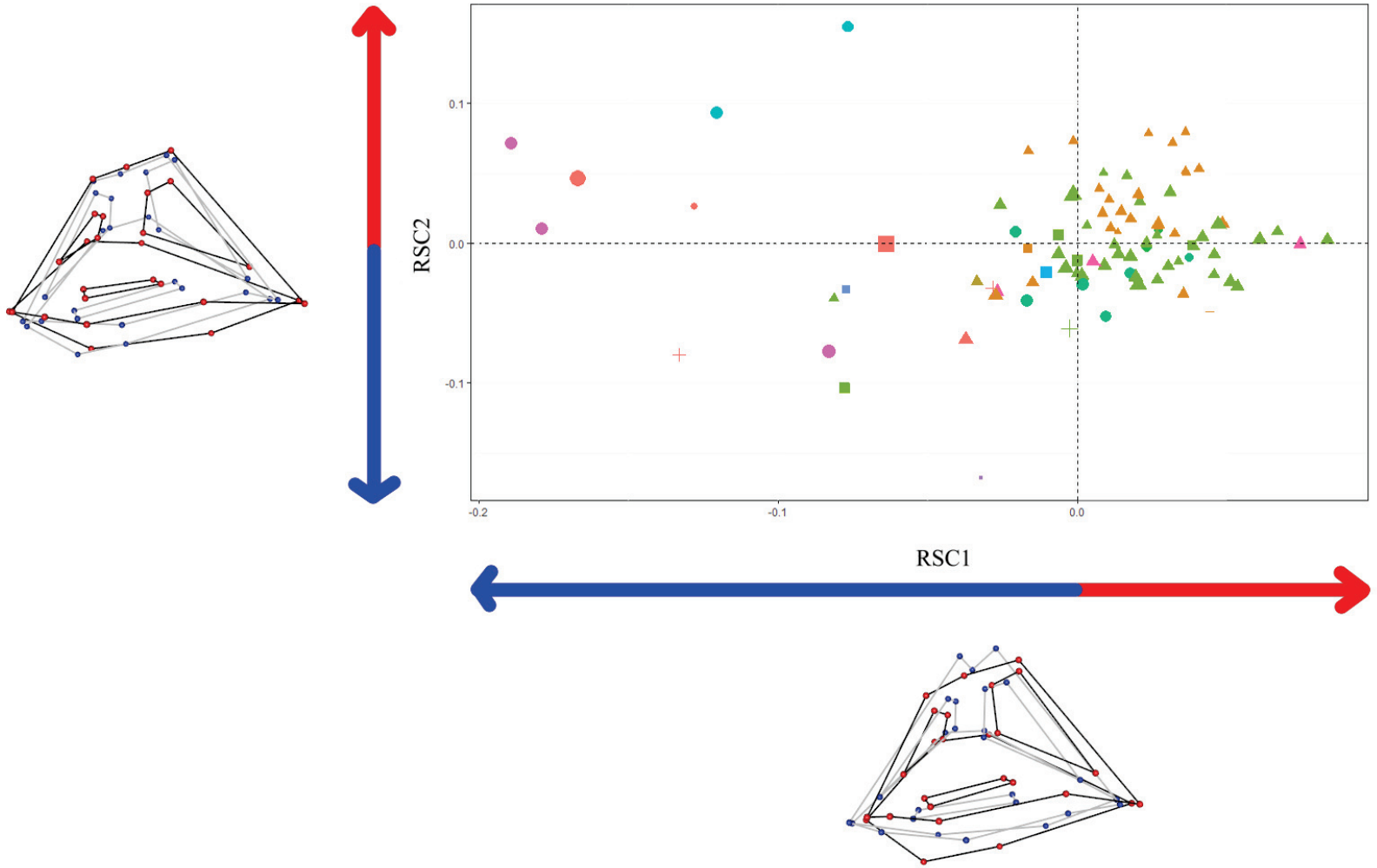

Figure 3.42: Morphospace occupation of endosseous labyrinth shape corrected for allometry in the adult sample. Extreme shapes for each PC axes given with wireframes in lateral view. Point size is correlated with specimen size.

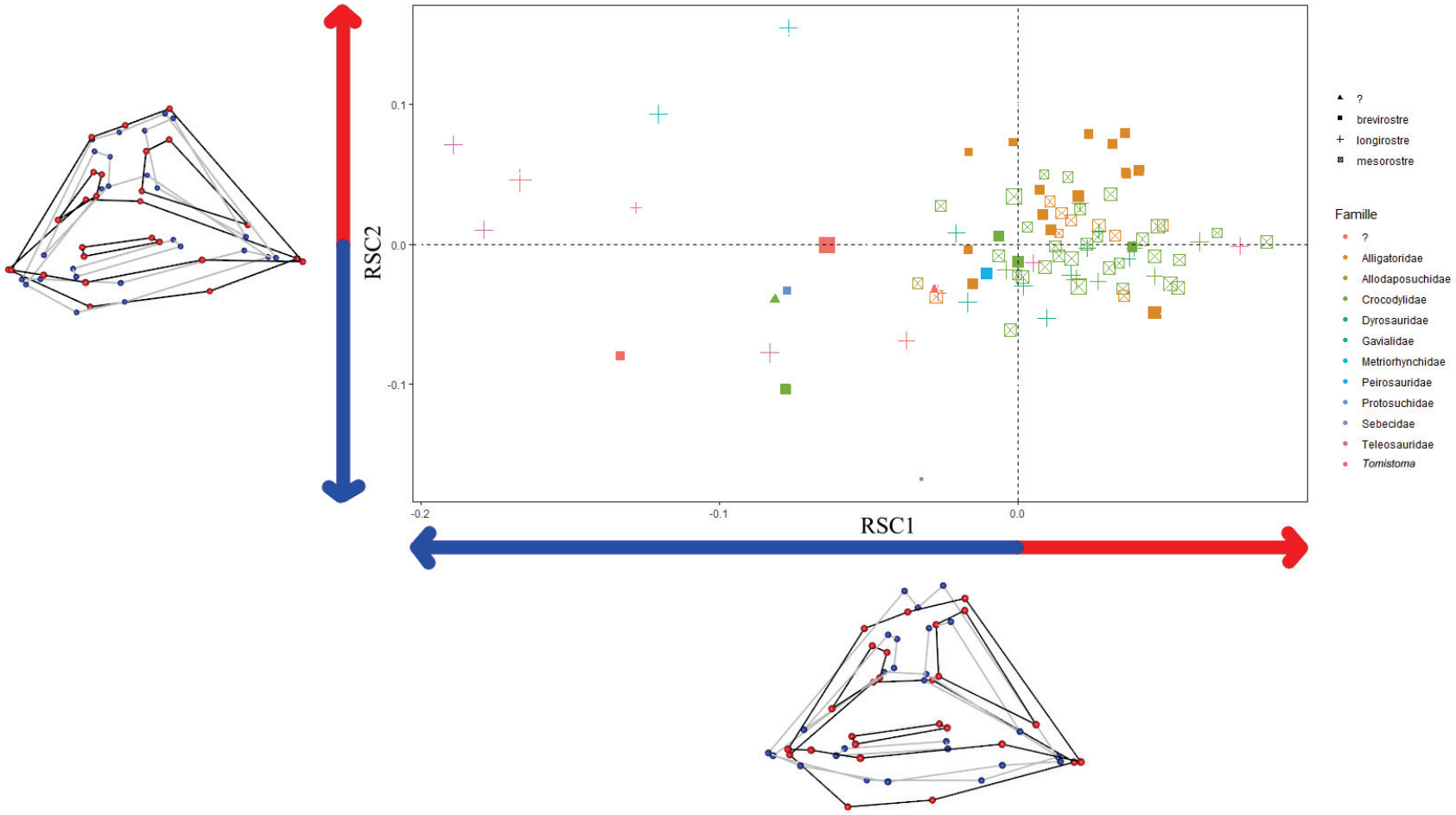

Figure 3.43: Morphospace occupation of endosseous labyrinth shape corrected for allometry in the adult sample. Extreme shapes for each PC axes given with wireframes in lateral view. Point size is correlated with specimen size.

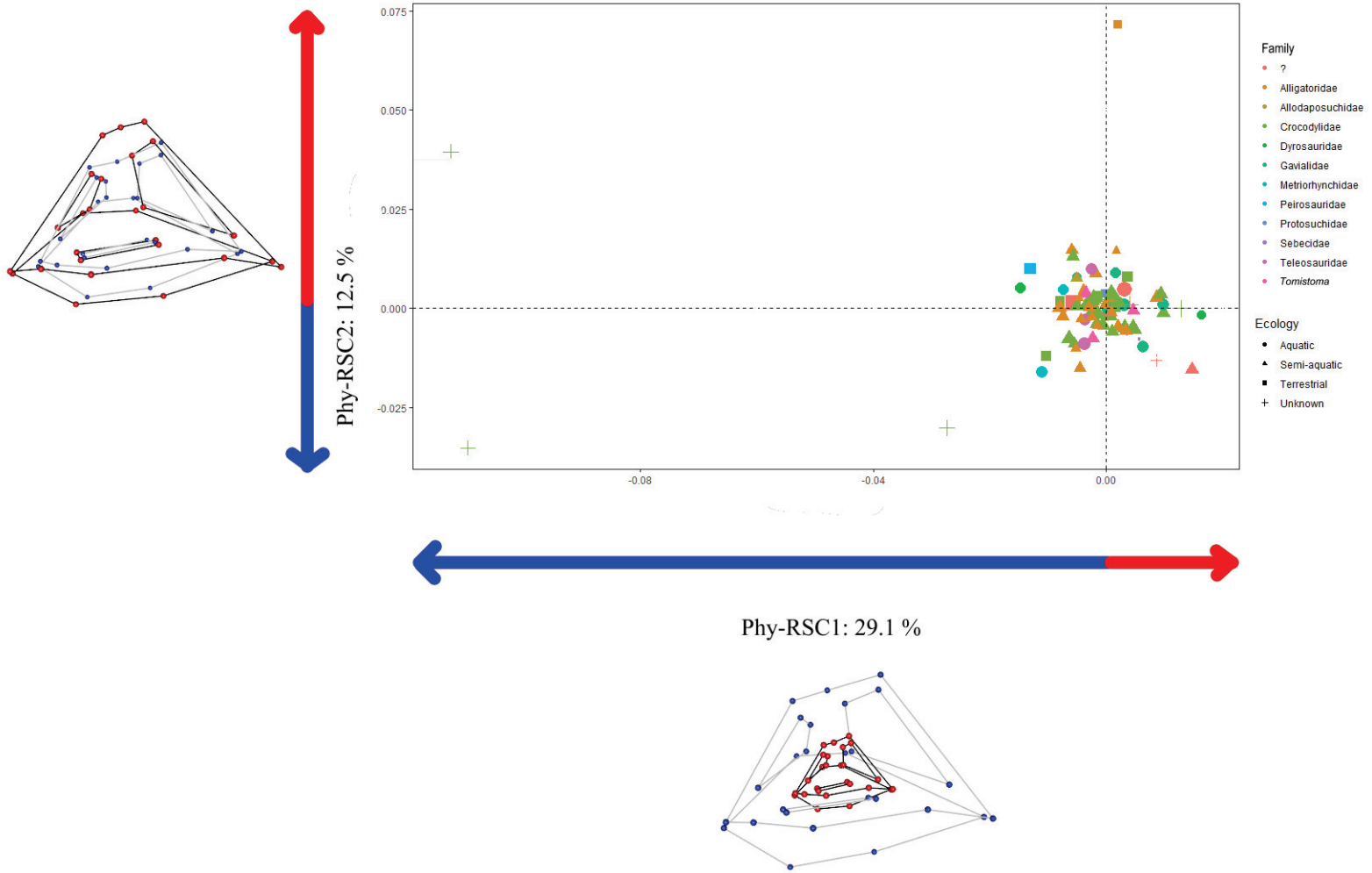

Figure 3.44: Morphospace occupation of endosseous labyrinth shape corrected for allometry and phylogeny in the adult sample. Extreme shapes for each PC axes given with wireframes in lateral view. Point size is correlated with specimen size.

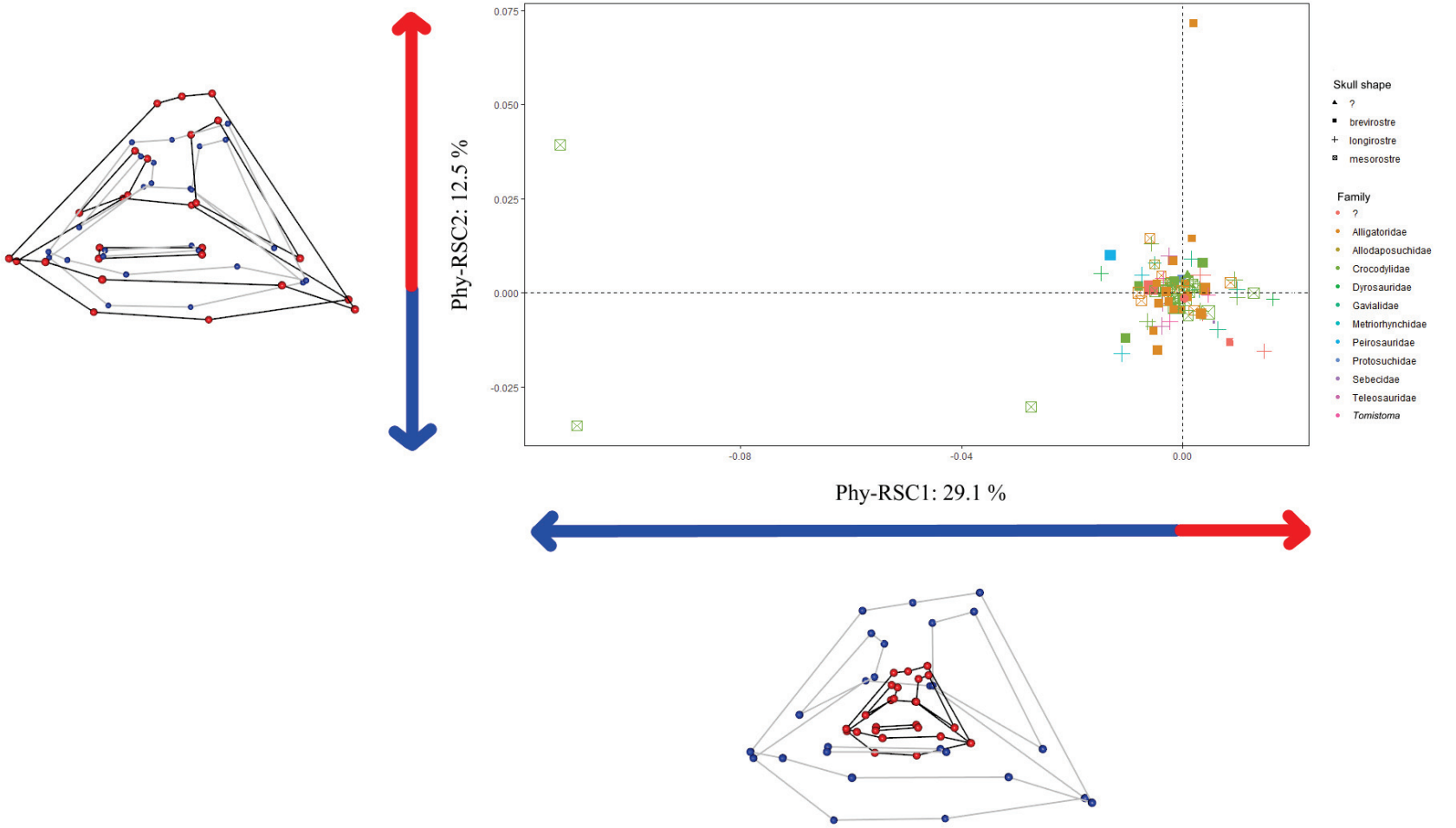

Figure 3.45: Morphospace occupation of endosseous labyrinth shape corrected for allometry and phylogeny in the adult sample. Extreme shapes for each PC axes given with wireframes in lateral view. Point size is correlated with specimen size.

Table 13: Regression tests on the full adult sample corrected for allometry and phylogeny (n = 91). Non-significant results highlighted in red.

Variable 1	**Variable 2**	**p-value**	**R^2**
Phy-RSC1	Size	0.87	< 0.01
Phy-RSC1	Genus	0.14	0.54
Phy-RSC1	Family	0.57	0.05
Phy-RSC1	Skull shape	0.22	0.04
Phy-RSC1	Ecology	0.004	0.23
Phy-RSC2	Size	0.47	< 0.01
Phy-RSC2	Genus	0.39	0.30
Phy-RSC2	Family	0.68	0.06
Phy-RSC2	Skull shape	0.77	0.01
Phy-RSC2	Ecology	0.10	0.08

previously corrected (Table 13). This could either be due to very subtle variations in shape, as most of the variance has already been considered in previous analyses (ontogeny and phylogeny), or because of a wrong taxonomic identification or phylogenetic placement, artificially correcting a phylogenetic bias that does not exist and thus displacing those specimens in the morphospace. Ecology and skull shape have no impact here on the shape variations of the endosseous labyrinths, and I can thus conclude that the endosseous labyrinths is not a good structural proxy for lifestyle in crocodylomorphs, as highlighted in Bronzati *et al*. (2021) and contrary to Schwab *et al*. (2020).

VI- Conclusions and perspectives

Recent advances in CT scan technologies have allowed to explore the internal structures of numerous crocodylomorphs, and we are beginning to get a more complete picture of the variations in extant and extinct forms. Here, the internal structures of *Zulmasuchus,*

Hamadasuchus and *Varanosuchus* are described. These taxa belong to several different clades with slightly different ecologies.

The internal structures of crocodylomorphs are of particular interest because they bear several paleoecological implications. The endocast and cranial nerves can be associated with different senses such as olfaction or vision. The endosseous labyrinths provide information about the alert head posture of the organism and the way it was able to move its skull, as well as its hearing capabilities. Finally, the peculiar cranial pneumaticity of crocodylomorphs is interesting because it could be linked to lifestyle, with enlarged sinuses corresponding to a terrestrial lifestyle, while aquatic forms have a reduced pneumaticity. This type of study still needs to be amplified in terrestrial forms, with fossil clades that are still poorly or not at all sampled, such as sphenosuchians, sebecosuchians, sphagesaurians, atoposaurids and paralligatorids.

The knowledge of the ecology of fossil forms comes from fundamental studies in extant forms, that need to be completed, especially on the function of cranial sinuses, and the relationship between the endosseous labyrinths and inner ears (hard versus soft tissues). Here, by taking a closer look at the shape variation of this structure on a large sample of crocodylomorphs both extant and extinct, I confirm the results of Schwab *et al*. (2021b): the endosseous labyrinths of crocodylomorphs are strongly linked with ontogeny, and follow a global negative allometric trend (i.e., inner ears grow continuously during ontogeny, but at a reduced rate compared to the skull). This structure also bears a phylogenetic signal, although it seems to be minimal and thus was not explored in further details. However, no significant ecological signal was found, agreeing with Bronzati *et al*. (2021) but not with Schwab *et al*. (2020).

Similar studies must be performed on the endocast and associated structures (Conedera, 2022), as well as cranial pneumaticity (Dufeau & Witmer, 2015; Kuzmin *et al*., 2021; Perrichon *et al*., 2023), to better understand their ontogenetic, ecological, and phylogenetic implications, and evaluate if they can help refine the phylogenetic relationships of some groups or better understand some fossil forms.

Chapter 4: Isotope systematics and the study of paleoecological trait and extinct environments

Another way of assessing the lifestyle of extinct organisms is through the study of their isotopic compositions in several chemical elements, that each rely on different mechanisms and can thus be linked with different paleoecological traits. In this chapter, those different proxies will first be explained, before being applied to case studies of fossil ecosystems representative of the clades studied in this work, as well as extant specimens.

I- Basics, notations, and formalism

The composition of an organism, and thus of its bones and teeth or scales which are often the only remains that will be fossilized, is dependent on the metabolism and physiology of this organism, as well as the impact its environment has on it, through biotic (related to living things and processes) and abiotic (related to non-living things and processes) factors, as well as the behaviour of this organism. Geochemistry is thus all about deciphering and understanding the impact of those different processes on the elemental and isotopic compositions of both living and fossils remains.

Bones of living organisms are mainly composed of a mineral matrix made of hydroxyapatite $Ca_{10}(PO_4)_6(OH)_2$ (main formula; Yoshimura & Suda, 1995), as well as an organic matrix made of collagen in fibrillar organisation (Viguet-Carrin *et al*., 2006) and non-collagenous proteins (Boskey, 1989), together with an extracellular matrix made of cells and water (Simkiss & Wilbur, 1989; Wilson *et al*., 2006). These last two components are mainly lost during fossilization processes after death. Bones are constantly remodelled through the life of an individual, through the loss of old bone and replacement by new bone (Frost, 1969; Manolagas, 2000; Parfitt, 2002, 2013; Hollinger, 2005; Glimcher, 2006; Hedges *et al*., 2007; Fig. 4.1).

Teeth are composed of enamel, itself mainly composed of hydroxyapatite (Deakins & Volker, 1941; Bartlett, 2013); dentin, which has a more heterogenous composition (Tjärderhane *et al*., 2009; Goldberg *et al*., 2011); and cementum which is even less mineralized, highly organic and remodelled and thus mostly not preserved in fossil specimens (Bosshardt & Selvig, 1997; Chen & Liu, 2014; Yamamoto *et al*., 2016). Although tooth development occurs in the first years of life in most mammals, in most other tooth-bearing vertebrates, tooth replacement occurs much more frequently and continuously through the life of an individual (Osborn, 1974; Richman & Handrigan, 2011; Whitlock & Richman, 2013; Tucker & Fraser, 2014).

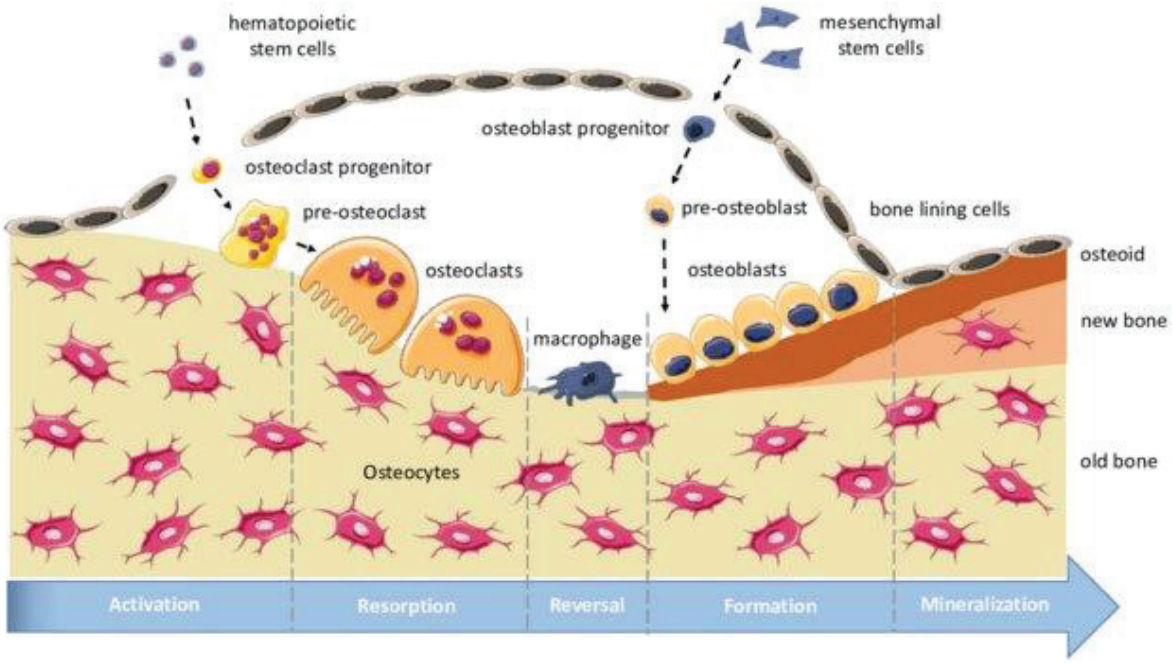

Figure 4.1: Phases of bone remodelling. Taken from Truesdell & Saunders (2020; fig. 1).

From its original formula (see above), hydroxyapatite can incorporate several elements through chemical substitutions (Cacciotti, 2016), such as minor (Na^+, Mg^{2+}) or trace (Sr^{2+}, K^+, Cl^-) elements. However, the main substitution is the replacement of either hydroxyl ions (type A) or phosphate groups (type B) by carbonate groups (Bonel, 1970). Thus, hydroxyapatite contains several elements of interest that will need to be isolated for further isotopic analyses.

Each element is characterized by an atomistic conformation, with the nucleus bearing a positive charge (association of protons or positively charged particles and neutrons or neutral particles), while electrons, charged negatively, orbit around it (Rutherford, 1911; Fig. 4.2). An element X can thus be defined as follows:

$$\frac{A}{Z}X$$

with Z: the number of protons and A: its number of nucleons (i.e., A = Z + number of neutrons). To maintain the neutrality of the element, there is thus also Z gravitating electrons. Two isotopes of a same element have the same number of protons (Z) but a different number of neutrons, and thus a different number of nucleons (A). Isotopes can either be stable (i.e., when the number of neutrons is not too different from the number of protons) or unstable (when the number of neutrons is too different from the number of protons) which will then undergo a

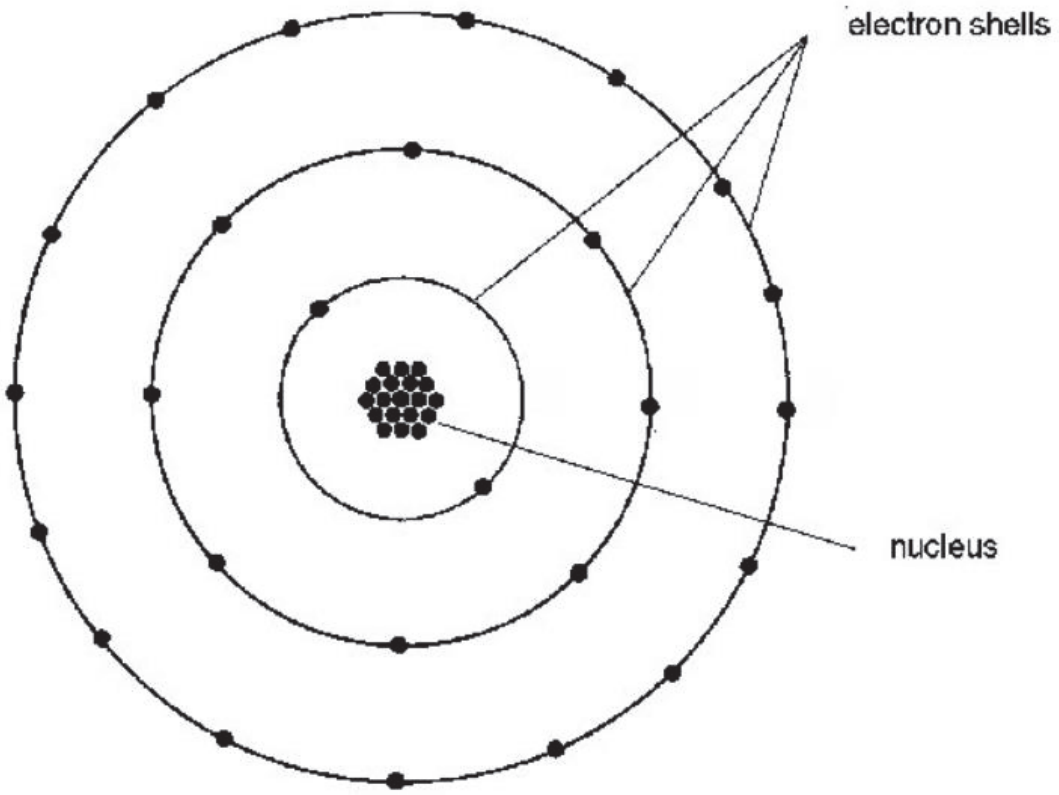

Figure 4.2: Schematic representation of an atom with the nucleus and the electrons. Modified from Mathys *et al*. (2002; fig. 4).

radioactive decay, through several processes that will not be explained here (Albarède, 2009). Isotopes of the same element have different natural abundances (Table 14), and thus the ratio of abundance between two isotopes of the same element (R, or isotopic ratio) can be defined as follows:

$$R = \frac{i_X}{j_X}$$

where i: heavy isotope (with more neutrons) and j: light isotope (with less neutrons) of the same element X. Natural abundance ratios of stable isotopes are modified through several processes, that are linked with the behaviour of the element studied, also called isotopic fractionation.

However, as precise measurements of natural abundance ratios of isotopes are often difficult to obtain, due to the precision threshold of detection instruments and numerous other measures bias that vary between analytical protocols, sample types and studied elements, the use of the delta notation (δ) has been implemented. This consists in the normalization of the ratio of abundance measured with that of a reference material, or isotopic standard to allow for reproducibility and comparison of measures between different laboratories (Hoefs, 1997;

Table 14: Natural abundances of stable isotopes studied in this thesis (Vocke, 1999; Coplen *et al*., 2002).

Element	Isotopes	Abundance (%)	Associated standard
Carbon	^{12}C	98.93	Vienna Pee-Dee-Bee Belemnite (V-PDB)
	^{13}C	1.07	
Nitrogen	^{14}N	99.63	Air (AIR)
	^{15}N	0.37	
Oxygen	^{16}O	99.76	Vienne Standard Mean Ocean Water (V-SMOW)
	^{17}O	0.04	
	^{18}O	0.20	
Calcium	^{40}Ca	96.94	Specpure Ca plasma standard solution (ICP Ca Lyon)
	^{42}Ca	0.65	
	^{43}Ca	0.14	
	^{44}Ca	2.09	
	^{46}Ca	<0.01	
Strontium	^{84}Sr	0.56	No standard as ratio of abundance is directly used
	^{86}Sr	9.86	
	^{87}Sr	7.00	
	^{88}Sr	82.58	

Albarède, 2009; Coplen, 2011) and can be defined as follows:

$$\delta^{i/j}X_{sample} = \left(\frac{R_{sample}}{R_{standard}} - 1\right) \times 10^3$$

where δ is expressed in ‰ (to avoid comparing very small values), R_{sample}: isotopic ratio measured in the sample and $R_{standard}$: isotopic ratio measured in the standard.

Isotopic compositions can be measured using mass spectrometers, which allow quantification of isotopic abundance ratios (Nier & Hanson, 1936; McKinney *et al*., 1950; Eiler, 2007). Although the processes differ slightly depending on the instrument and the element studied, the following general model always apply: first the samples are introduced (in gas phase, solid or acid solution), then they are ionized (charged with electricity) and accelerated through an electrical potential difference. The ions formed are then focalised using lenses and separated under a magnetic field, with their trajectory modified depending on their mass. Finally, the separated ions hit detectors and the measured intensity and the electric signal implied is converted to a numerical measure (Fig. 4.3).

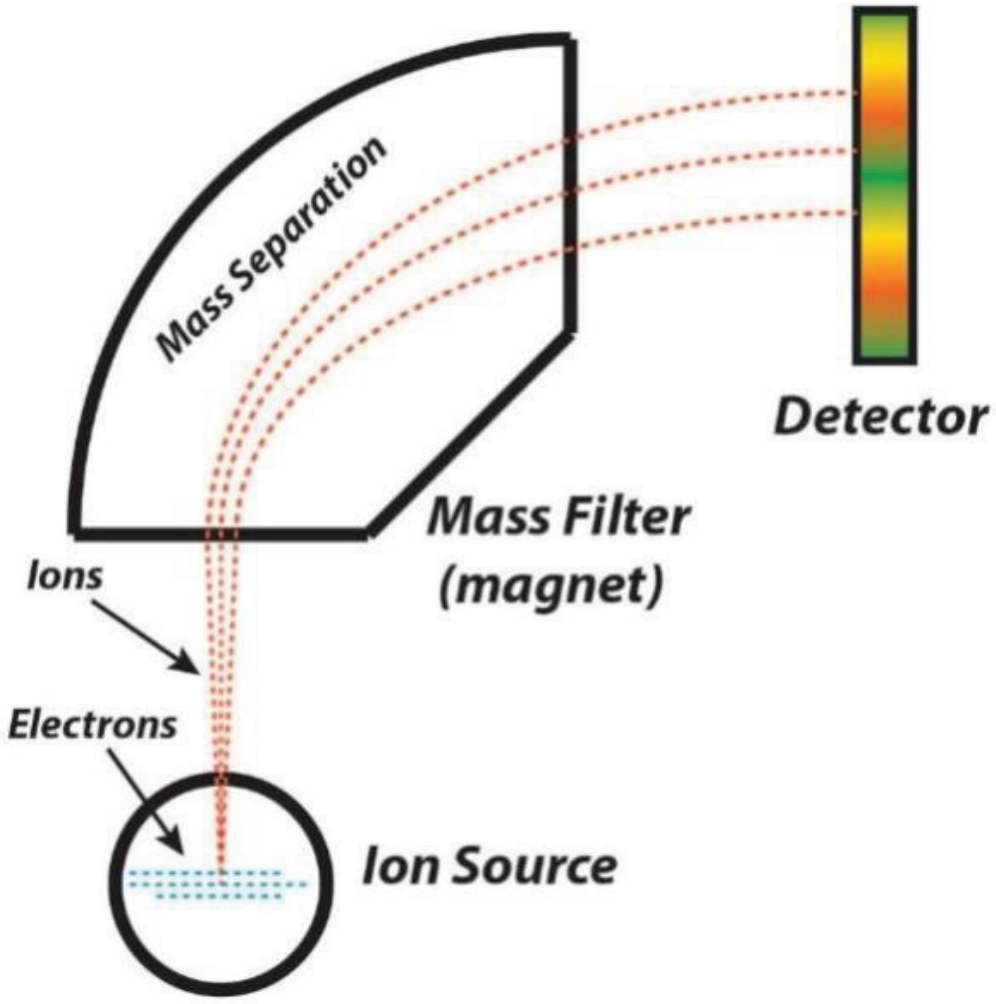

Figure 4.3: Schematic diagram of a mass spectrometer (taken from Radauscher, 2015; fig. 2.14).

II- Assessing the impact of diagenesis

During fossilization, numerous processes can alter the isotopic composition of an individual tissues. Those processes can occur during its life, between its death and its burying, or during the buried phase until its discovery, and are known as diagenetic processes, or diagenesis. They can either be abiotic or biotic and are regrouped as follows: absorption of allochthonous chemical elements from the surrounding matrix to the fossil, substitution of chemical elements between the surrounding matrix and the fossil, dissolution of a part or totality of the fossil or formation of new minerals from the elements already present (Kolodny *et al*., 1996; Blake *et al*., 1997; Kohn *et al*., 1999; Lécuyer *et al*., 2003; Trueman *et al*., 2003; Zazzo *et al*., 2004a, b; Reynard & Balter, 2014; Kendall *et al*., 2018). Those processes can also be combined, for example remineralisation happens when the organism tissues are dissolved and then replaced by new minerals, and their intensity depends on several factors, such as chemical stability, matrix and sample composition, pressure, temperature and duration of burying and structure of the tissue itself.

When undergoing a geochemical study, it is thus of the upmost importance to first infer the impact of diagenesis on the samples studied, as those can significantly modify the measured isotopic ratios, and thus alter interpretations. The first factor to take into consideration, when possible, is the choice of the tissue studied: as organic material tend to disappear or to be greatly altered during fossilization, we will prefer to analyse mineralized tissues (Cowie & Hedges, 1994; Kramer *et al*., 2003) and samples constituted of enamel rather than dentin or bone, because this tissue is less porous and therefore less likely to be affected by diagenetic processes (Nelson *et al*., 1986; Kohn *et al*., 1999; Budd *et al*., 2000; Hedges, 2002; Wopenka & Pasteris, 2005; Pasteris *et al*., 2008; Dodat *et al*., 2023). This enables the reliable study of ecosystems that have been extinct for several million years (Wang & Cerling, 1994; Sharp *et al*., 2000; Zazzo *et al*., 2004a; Goedert *et al*., 2016a, b; Martin *et al*., 2017a, b, 2022; Rey *et al*., 2017; Hassler *et al*., 2018). Secondly, minerals formed during diagenesis are mostly different than those formed during the life of the organism. Through elemental analysis and observation (microscopy, Raman spectroscopy, inductively coupled plasma spectrometer), those differences can be observed and quantified (Shemesh, 1990; Wright & Schwarcz, 1996; Reynard *et al*., 1999; Trueman, 1999, 2013; Metzger *et al*., 2004; Trueman *et al*., 2004, 2008; Kocsis *et al*., 2010; Reynard & Balter, 2014; Dal Sasso *et al*., 2016; Keenan, 2016). For example, the calcium/phosphorus ratio has been measured in modern vertebrate samples (2.15 ± 0.26, 2 s.d.; Balter *et al*., 2001), and so it is expected to find similar ratios in fossils that have

undergone moderate diagenetic processes (Hassler *et al*., 2018; Martin *et al*., 2022). Rare earth elements (REE) are also of interest because they are mostly absent from a living organism and are preferentially incorporated after its death, and thus are effectively a marker of early or late diagenetic conditions and burial conditions (Reynard *et al*., 1999; Kocsis *et al*., 2009; Hinz & Kohn, 2010; Suarez & Kohn, 2020). An efficient way of visualizing those processes is through an enrichment profile, where the concentration of each element for each sample is normalized to the concentration measured in a standard material, the North American Shale Composite (NASC; Haskin & Frey, 1966; Gromet *et al*., 1984; Fig. 4.4).

As the relative fractionation among the profile is characteristic of the REE incorporation process of a sample, several scenarios can occur (Reynard *et al*., 1999; Reynard & Balter, 2014): first, REE can be rapidly incorporated (within a few thousand years) into the fossils (Arrhenius *et al*., 1957; Bernat, 1975; Elderfield & Pagett, 1986) and will thus follow the patterns of compositions of either seawater in the marine environment (Shaw & Wasserburg, 1985; Elderfield & Pagett, 1986; Elderfield & Sholkovitz, 1987) or groundwater in continental environments (Henderson *et al*., 1983), and adsorption on, or diffusion /recrystallization near crystal surfaces is the major process, thus with low fractionation (curves Atlantic, Pacific SE, Pacific NW, NFS5 and PEH3 in Fig. 4.4). The second case corresponds to a moderate enrichment in ‘middle’ REE elements and may be associated with an incorporation through an inorganic adsorption pattern (Reynard *et al*., 1999), that are particularly relevant in continental environments with substantial variation of pH and water composition (Henderson *et al*., 1983; Trueman & Tuross, 2002; Kohn, 2008; Hinz & Kohn, 2010; Kocsis *et al*., 2010; Trueman *et al*., 2011). This pattern is also associated with low fractionation, although the result of different processes (curves Thelodont, *Panterodus* and P17a in Fig. 4.4). The third case is a large enrichment of ‘middle’ REE compared with others and is associated with fractionation patterns under strong crystal-chemical control (Reynard *et al*., 1999), i.e., low-grade metamorphism. It involves precipitation-solution mechanisms (curves P1, COU32A-C and COU34 in Fig. 4.4). This last pattern is the one most likely to affect isotopic compositions. Furthermore, the study of normalized lanthanum/ytterbium (La/Yb) and lanthanum/samarium (La/Sm) ratios can indicate the environmental origin and thus the constraints undergone by the samples (Reynard *et al*., 1999; Reynard & Balter, 2014; Fig. 4.5).

Then, they are also ways to estimate the impact of diagenesis on specific elements: for example, in the skeletal tissues of vertebrates (hydroxyapatite), carbonate and phosphate groups precipitate in equilibrium with body water, so the oxygen isotopic ratios measured on

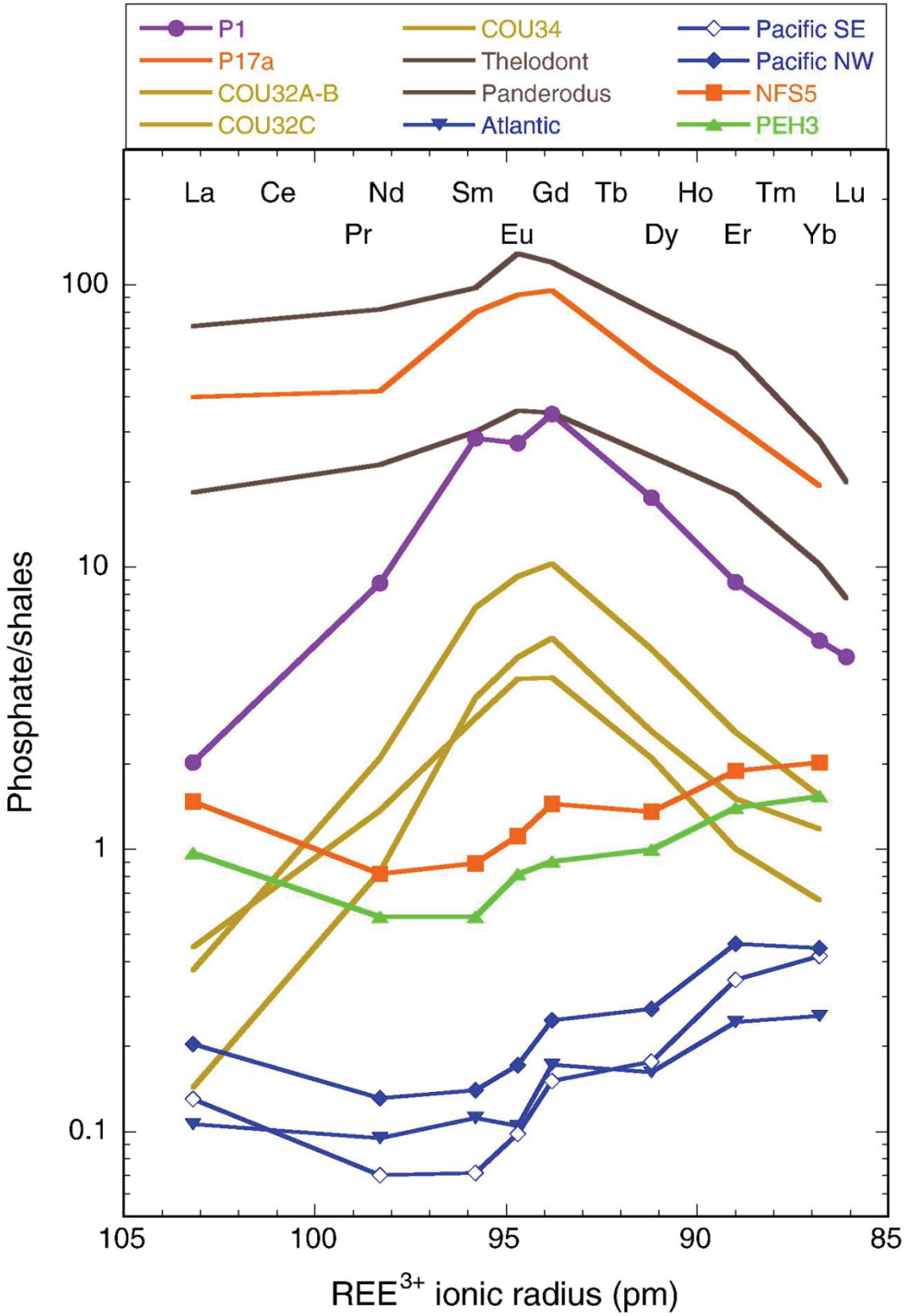

Figure 4.4: Patterns of REE enrichment profiles observed in the Atlantic and Pacific Ocean waters (data from Elderfield & Greaves, 1982; De Baar *et al*., 1983, 1985), Triassic and Tertiary fishes (respectively P1 and NFS5 & P17a, data from Grandjean *et al*., 1987, 1988; Grandjean, 1989; Grandjean & Albarède, 1989), Devonian conodonts (COU32A-C and COU34, data from Grandjean *et al*., 1993), Silurian thelodont fish and conodont *Panterodus* (data from Bertram *et al*., 1992) and Cretaceous marine reptiles (PEH3, data from Grandjean, 1989). Taken from Reynard & Balter (2014; fig. 10).

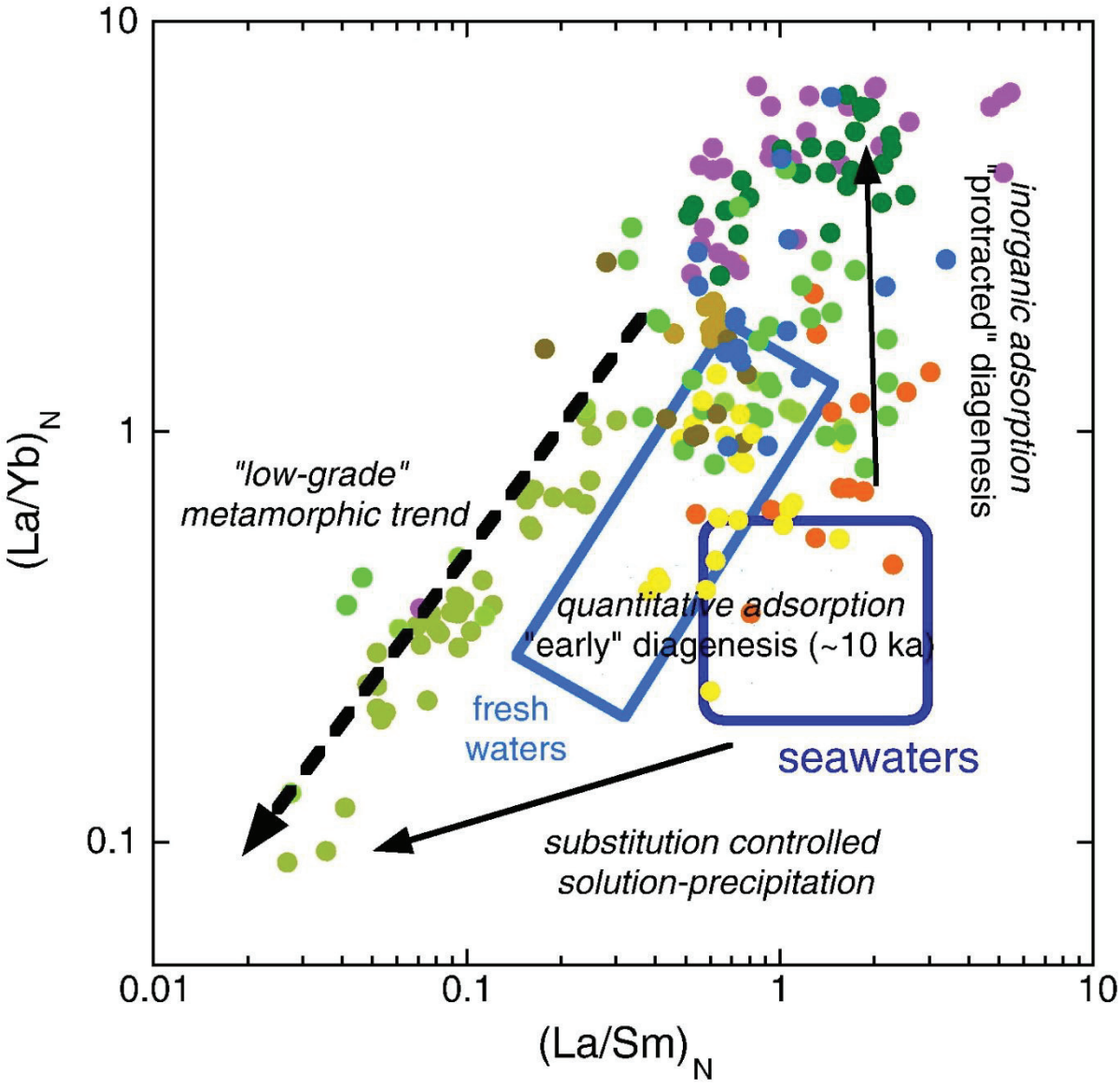

Figure 4.5: Normalized La/Yb vs La/Sm ratios observed in Devonian conodonts (khaki green circles, data from Grandjean *et al*., 1993), Silurian conodonts and fishes (brown circles, data from Bertram *et al*., 1992), Tertiary and Mesozoic fishes (green, blue and orange circles, data from Grandjean *et al*., 1988; Grandjean, 1989; Grandjean & Albarède, 1989), Quaternary fishes (yellow circles, data from Elderfield & Pagett, 1986), freshwaters (light blue rectangle, data from Elderfield *et al*., 1990; Giblin & Dickson, 1992; Johannesson & Lyons, 1995), seawaters (dark blue rectangle, data from Elderfield *et al*., 1990; German *et al*., 1995; Zhang & Nozaki, 1996). Modified from Reynard & Balter (2014; fig. 11).

hydroxyapatite with phosphate groups ($\delta^{18}O_p$) and the oxygen isotopic ratios measured on hydroxyapatite with carbonate groups ($\delta^{18}O_c$) should be correlated if the impact of diagenetic processes is moderate. On the other hand, as exchange rates between phosphate-water and carbonate-water are different, re-equilibration (and thus diagenetic alteration) of both systems should result in an isotopic shift from the expected correlation due to least one of the two complexes (Bryant *et al*., 1996; Iacumin *et al*., 1996; Zazzo *et al*., 2004a; Lécuyer *et al*., 2010; Chenery *et al*., 2012; Fig. 4.6). Concerning calcium isotopes concentrations, given the high quantity of calcium in vertebrate samples, it is unlikely that measured isotopic compositions

can be overprinted by diagenetic processes, even if those were to be important. Finally, particular caution has to be put on strontium isotope compositions interpretations, as this element is obtained in an organism either from the biopurification of calcium (replacement of calcium by sediment strontium or barium through physiological reactions; Comar *et al*., 1957; French, 1961; Balter *et al*., 2002a) or through diagenetic processes (Nelson *et al*., 1986; Brand, 1991; Sillen & Sealy, 1995; Budd *et al*., 2000; Copeland *et al*., 2010). An easy way to assess those processes is to compare the concentrations of strontium measured in the samples to those of other elements that are linked with diagenetic processes, such as lead, uranium, iron, manganese or REE: if they are linked, then the impact of diagenetic processes on the samples must be considered.

In the framework of this thesis, the elemental concentrations of major, minor, and rare earth elements were measured using a mass spectrometer coupled to an inductive plasma (ICP-MS) ICAP™ Q (Thermo Scientific™) and an inductively coupled plasma atomic emission spectrometer (ICP-AES) ICAP 7400 Series (Thermo Scientific™). The reliability of

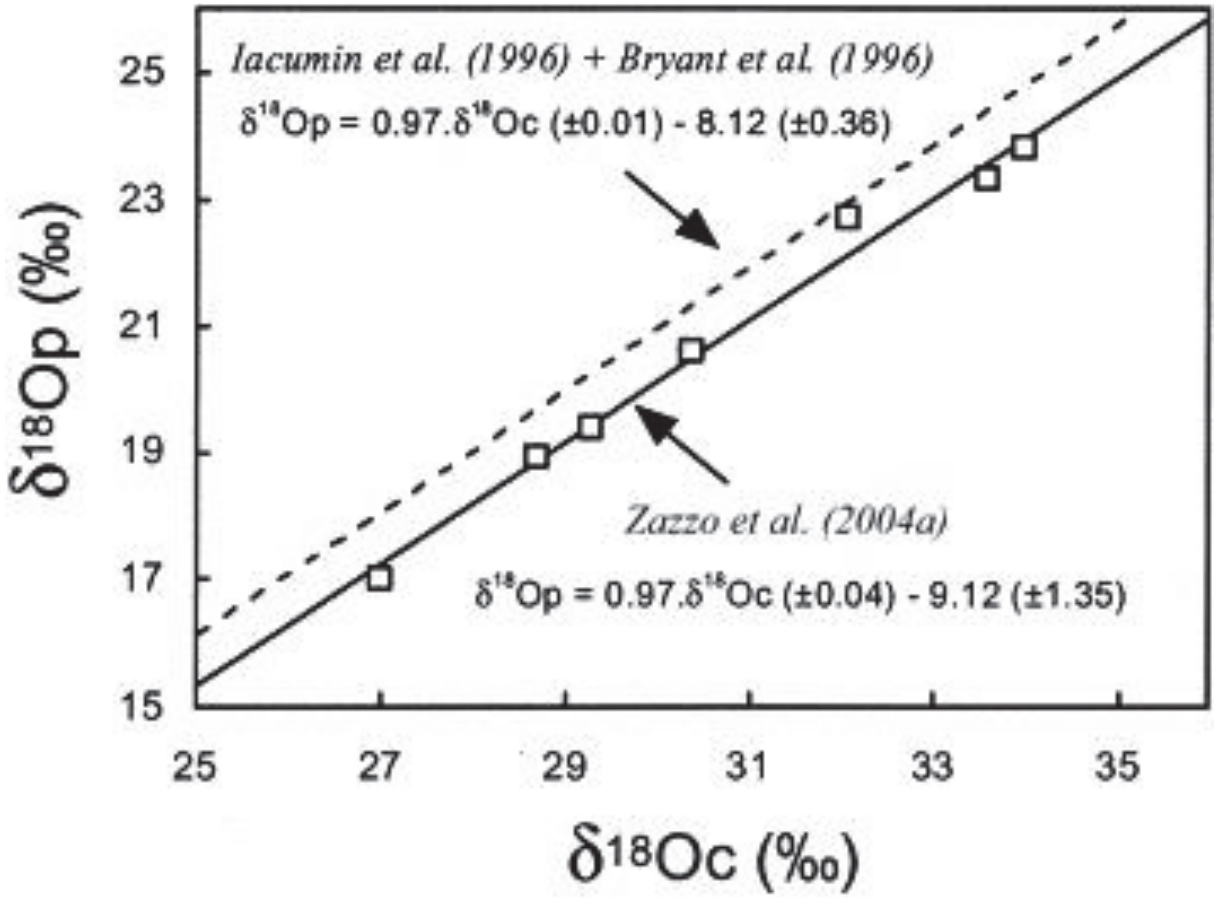

Figure 4.6: Oxygen isotope ratios measured on phosphate groups ($\delta^{18}O_p$) as a function of those measured on carbonate groups ($\delta^{18}O_c$) of modern hippopotamus tooth enamel, which have thus not undergone heavy diagenetic processes. Modified from Zazzo *et al*. (2004a; fig. 1).

measurements has been controlled through a set of blanks and the reference material NIST-SRM1400.

III- Oxygen isotope compositions: thermophysiology and lifestyle

Oxygen has three stable isotopes: ^{16}O, ^{17}O and ^{18}O (Table 14). In vertebrate teeth, bones, and scales, it is contained in hydroxyapatite inside either phosphate groups (PO_4^{3-}) or carbonate groups (CO_3^{2-}), as well as hydroxyl groups (OH^-). To quantify the relative abundance of oxygen isotopes with one another, the following notation is used:

$$\delta^{18}O\ (‰) = \left[\frac{\left({}^{18}O/_{16}O\right)_{sample}}{\left({}^{18}O/_{16}O\right)_{SMOW}} - 1\right] \times 10^3$$

Oxygen isotopic compositions vary because of several processes: first, as this element comes from the body fluids of the organism, there is a balanced thermodynamic fractionation process between the mineralized tissues and the body fluids, which is only linked to the temperature of the structure, i.e. body temperature (Longinelli & Nuti, 1973; Kolodny *et al*., 1983; Longinelli, 1984; Luz *et al*., 1984; Kohn, 1996; Lécuyer *et al*., 2013). In the case of homeothermic organisms (i.e., organisms that maintain the same temperature throughout the whole body), the oxygen isotopic compositions of mineralized tissues are thus fractionated with respect to the body fluids homogeneously throughout the whole body, but this strong hypothesis must be made, and it could not be the case in all organisms (Barrick *et al*., 1998; Stoskopf *et al*., 2001; Missell, 2004; Séon *et al*., 2022, but see Barrick & Showers, 1994, 1995; Barrick *et al*., 1996; Coulson *et al*., 2008; Clauzel *et al*., 2020). Second, the source of oxygen contained in body fluids is either atmospheric oxygen breathed (as well as atmospheric water vapour absorbed by the lungs) or water obtained from food and drink (Longinelli, 1984; Luz *et al*., 1984; Levinson *et al*., 1987; Fig. 4.7). As atmospheric oxygen has a constant and homogenous isotopic composition (23.5 ± 0.3 ‰; Dole *et al*., 1954; Kroopnick & Craig, 1972) and absorbed atmospheric water vapour can be considered as negligeable (Nagy & Costa, 1980; Bryant & Froelich, 1995), oxygen fluxes that influence oxygen isotopic compositions are thus those associated with food and drink. For non-marine organisms, drinking water corresponds to

meteoritic water (or rainwater), which is itself derived from the evaporation and precipitation of ocean and seawaters (Lécuyer, 2013) and is subject to several constraints, such as latitude, altitude, distance from the shore, season, and temperature (Dansgaard, 1964; Rozanski *et al*., 1992, 1993; Fricke & O'Neil, 1999), while isotopic fractionation between oxygen isotopic compositions of water from food and oxygen isotopic compositions of mineralized tissues depends on the diet of the organism (Barbour, 2007; Brettell *et al*., 2012; Cernusak *et al*., 2016; Pietsch & Tütken, 2016). Measurements of the $\delta^{18}O$ of the blood, body water, ambient water and mineralized tissues of wild and captive organisms have allowed to establish equations linking those parameters in several groups of organisms, which can then be applied to close fossil forms. For example, in extant crocodylians, the $\delta^{18}O$ of ambient water ($\delta^{18}O_{aw}$) is linked to the $\delta^{18}O$ of the phosphate groups of the mineralized tissues ($\delta^{18}O_p$) by the following equation (Amiot *et al*., 2007):

$$\delta^{18}O_{aw} = 0.82\ \delta^{18}O_p - 19.13$$

In mammals, the following equation applies (Amiot *et al*., 2004):

$$\delta^{18}O_{aw} = 1.11\ \delta^{18}O_p - 26.44$$

In birds, it is the following equation (Amiot *et al*., 2017):

$$\delta^{18}O_{aw} = 1.12\ \delta^{18}O_p - 24.22$$

In fishes, the following equation applies (Lécuyer *et al*., 2013):

$$\delta^{18}O_{aw} = T / 4.5 + \delta^{18}O_p - 26.09$$

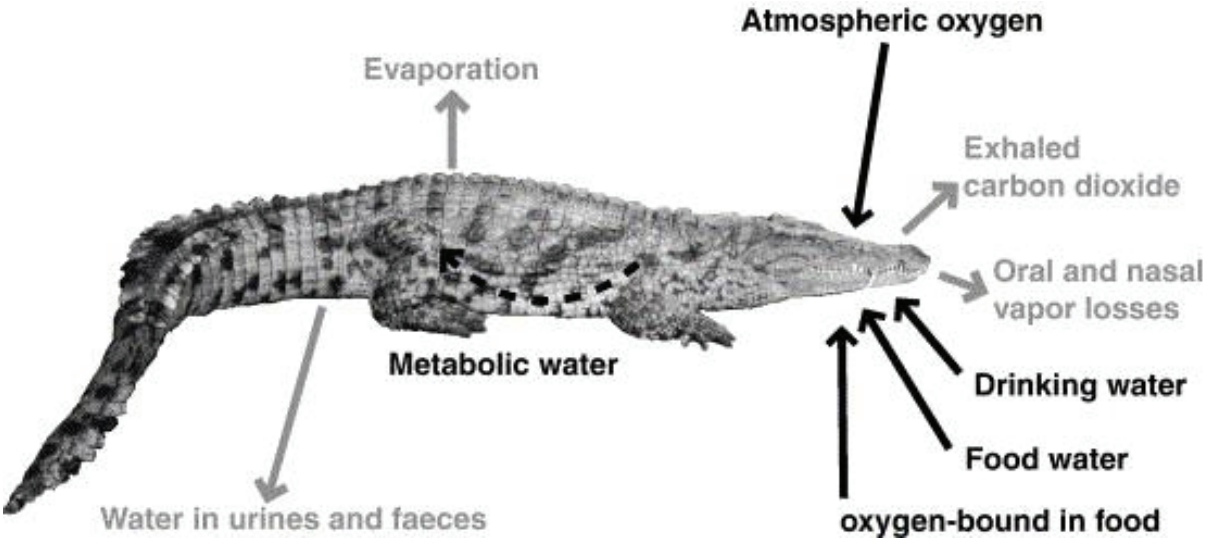

Figure 4.7: Oxygen fluxes undergone by a crocodilian individual. Taken from Amiot *et al*. (2007; fig. 4).

where T: temperature of mineralization of the tissues, which corresponds to both the body temperature and environmental temperature in fishes.

Furthermore, an additional fractionation is observed between the $\delta^{18}O_{aw}$ and the $\delta^{18}O$ of the body water ($\delta^{18}O_{bw}$) in terrestrial vertebrates, such that:

$$\delta^{18}O_{bw} = \delta^{18}O_{aw} + E$$

where E is an enrichment value dependant of the group of organisms studied. For example, it is ~ 2 ‰ in semi-aquatic crocodiles (Amiot *et al*., 2007), ~ 5.1 ‰ in terrestrial tortoises (Barrick *et al*., 1999), ~ 4.7 ‰ in terrestrial mammals (Longinelli, 1984; D'Angela & Longinelli, 1990) and ~ 7.1 ‰ in birds (Wolf *et al*., 2013).

Finally, the $\delta^{18}O_p$ and $\delta^{18}O_{bw}$ can be linked to the body temperature T_b through the following general equation adapted from the phosphate-water temperature scale (Lécuyer *et al*., 2013):

$$T_b = 117.4 - 4.5 (\delta^{18}O_p - \delta^{18}O_{bw})$$

Furthermore, higher water turnover and lower transcutaneous water evaporation in organisms having an aquatic lifestyle compared with those having a terrestrial lifestyle (at equivalent body temperatures), lead to lower $\delta^{18}O_p$ values for aquatic organisms compared with terrestrial ones (Fricke & Rogers, 2000; Clementz & Koch, 2001; Clementz *et al*., 2003, 2008; Amiot *et al*., 2006, 2010; Cerling *et al*., 2008; Rey *et al*., 2020a, b; Fig. 4.8). As a result, oxygen isotopic

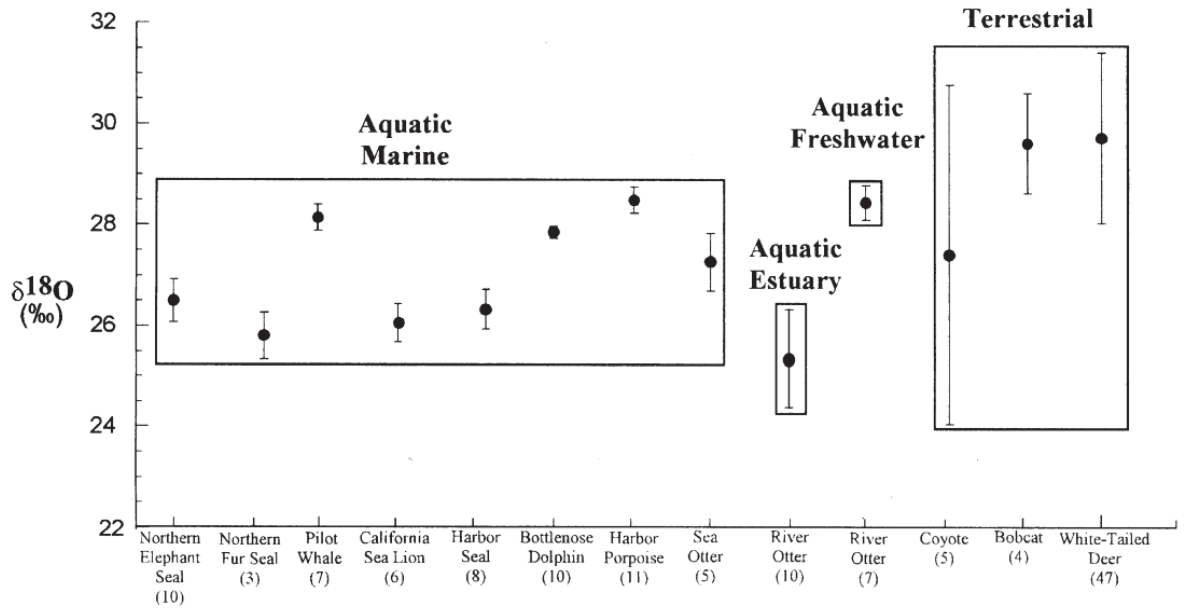

Figure 4.8: Mean $\delta^{18}O_p$ values for terrestrial and aquatic (marine, estuarine and freshwater) mammals. Taken from Clementz & Koch (2001; fig. 5).

compositions can be interpreted both in terms of living environment and thermoregulation strategy in fossil forms, building on the knowledge on extant organisms.

Analytically, after being sampled on the teeth or the bones via a Micro-Dremmel™ drill, either with an abrasive tip or a diamond head, or a micro-drill, the powders were treated before being analysed through different chemical protocols depending on the group of interest (phosphate or carbonate). The phosphate groups were extracted following the wet chemistry protocol of Crowson *et al*. (1991), modified in Lécuyer *et al*. (1993): briefly, it consists in a selective extraction of phosphate groups via the use of an ion exchange resin and precipitating them in the form of silver phosphate, with prior elimination of calcium (for more details, see Appendix 5: Supplementary Material S3). Acid pre-treatments were applied to carbonate groups, following Koch *et al*. (1997): briefly, organic matter was removed using NaClO (bleach) and secondary deposit of carbonate was removed using CH_3COOH (acetic acid; for more details, see Appendix 5: Supplementary Material S3). However, the effects of this treatment are controversial, and some studies have argued that it could also modify the isotopic signal of primary carbonates (Snoeck & Pellegrini, 2015; Pellegrini & Snoeck, 2016; Clauzel, 2022). $\delta^{18}O_c$ (and $\delta^{13}C$) values presented in this thesis must thus be interpreted with this in mind, and we will rely more on $\delta^{18}O_p$ values for oxygen and couple diet interpretations on $\delta^{13}C$ values with $\delta^{44/42}Ca$ values (see also IV and VI). It was unfortunately impossible to analyse samples both with and without carbonate pre-treatment to study its effect, as the mass of powder needed would be too important for most of the samples measured in this thesis.

$\delta^{18}O_p$ values were obtained with a continuous flow high temperature pyrolysis method (Lécuyer *et al*., 2007; Fourel *et al*., 2011). Whenever possible, five replicates (280-320 µg each) of each sample were mixed with pure graphite powder in excess and loaded in silver foil capsules. Pyrolysis was performed at 1450°C using a vario PYRO cube™ elemental analyser, where the carbon monoxide CO formed by pyrolysis was selectively trapped by a ‘Purge & Trap” system, before being analysed in the coupled Isoprime™ isotopic ratio mass spectrometer (Elementar UK). These measurements were made at the Plateforme d’Ecologie Isotopique du Laboratoire d’Ecologie des Hydrosystèmes Naturels et Anthropisés (LEHNA, UMR5023, Université Lyon 1). Oxygen isotopic compositions were then corrected for drift and subtraction of blanks to account for analytical variability. Measurements have finally been calibrated against both silver phosphates prepared from the NBS120c (internal standard for each chemistry; $\delta^{18}O_p$ = 21.7 ‰ V-SMOW; Lécuyer *et al*., 1993; Chenery *et al*., 2010; Halas *et al*., 2011), as well as NBS127 (9.3 ‰ V-SMOW; Hut, 1987; Halas & Szaran, 2001).

$\delta^{18}O_c$ values were measured using an iso-FLOW system connected on-line in continuous flow mode to a precisION mass spectrometer (Elementar UK). For each sample, three aliquots of one or two mg of pre-treated apatite powder were loaded in LABCO Exetainer 3.7 mL soda glass vials, round bottomed with Exetainer caps (LABCO UK), and reacted with anhydrous phosphoric acid at 90°C. The CO_2 gas generated during the acid digestion was then transferred to the mass spectrometer via the centrION interface. The materials used for calibration were Carrara marble ($\delta^{18}O_{c\ V\text{-}PDB}$ = - 1.95 ‰; Fourel *et al*., 2016), NBS18 ($\delta^{18}O_{c\ V\text{-}PDB}$ = -23 ‰) and NBS120c ($\delta^{18}O_{c\ V\text{-}PDB}$ = -1.13 ‰; Passey *et al*., 2007).

IV- Carbon isotope compositions: diet and food webs

To quantify the relative abundance of carbon isotopes with each other, the following notation is used:

$$\delta^{13}C(‰) = \left[\frac{\left({}^{13}C/{}_{12}C\right)_{sample}}{\left({}^{13}C/{}_{12}C\right)_{PDB}} - 1\right] \times 10^3$$

In terrestrial vertebrates, as carbonates are in isotopic equilibrium with body fluids, mineralized carbon mainly comes from the food and the metabolic activity of the intestinal microbiota (Lee-Thorp *et al*., 1989; Cerling & Harris, 1999; Passey *et al*., 2005). An individual will always have higher $\delta^{13}C$ values compared to its food and, although the isotopic fractionation induced from meat consumption is low (0 to 2 ‰; Bocherens & Drucker, 2003), it is higher between herbivores/omnivores and plants and will also be accounted in the total isotopic fractionation of carnivores: this mechanism is known as trophic enrichment (DeNiro & Epstein, 1978; Schwarcz & Schoeninger, 1991). Carbon isotopic fractionation between plants at the base of the food web and tissues of the organisms that feed on them is thus specific to each group of organisms: for example, it is approximately 9 ‰ in crocodiles (Lee-Thorp *et al*., 1989; Tieszen & Fagre, 1993; Stanton, 2006), whereas it is approximately 12 ‰ in mammals (Passey *et al*., 2005). In aquatic environments, this relationship is more complex, as the primary producers that constitute organism diet have $\delta^{13}C$ values that can vary because of differences in productivity, dissolved CO_2 concentration or bicarbonate utilization (Osmond *et al*., 1981; Fry

& Sherr, 1984; Rau *et al*., 1992; Hemminga & Mateo, 1996; MacLeod & Barton, 1998; Clementz & Koch, 2001).

The carbon isotopic fractionation between plants and their direct or indirect consumers is also different depending on their metabolism of organic matter synthesis (Bender, 1971; Smith & Epstein, 1971; O'Leary, 1988; Dawson *et al*., 2002). C_3 plants, in which the Calvin cycle during photosynthesis is initiated by the RubisCO enzyme, have $\delta^{13}C$ values between -37 and -20 ‰ (O'Leary, 1988; Kohn, 2010) whereas C_4 plants, in which the Calvin cycle is initiated by the PEP carboxylase and that appeared during the Oligocene (Pyankov *et al*., 2001a, b; Freitag & Stichler, 2002; Schütze *et al*., 2003; Sage, 2004; Niklaus & Kelly, 2019), have $\delta^{13}C$ values between -21 and -9 ‰ (O'Leary, 1988; Tieszen, 1991) and CAM (Crassulean Acid Metabolism) plants, adapted to the desert environment, have $\delta^{13}C$ values including both those of C_3 and C_4 plants (Messerschmid *et al*., 2021). Finally, the $\delta^{13}C$ value of atmospheric CO_2 must also be estimated in the period of interest, as it is the main source of the carbon isotopic composition of plants (Fricke, 2007).

Analytically, carbonate groups were pre-treated using the previously described protocol (see III) and $\delta^{13}C$ values were measured in the same way as $\delta^{18}O_c$ (see also III), with the same calibration materials: Carrara marble ($\delta^{13}C_{V\text{-}PDB}$ = 1.96 ‰; Fourel *et al*., 2016), NBS18 ($\delta^{13}C_{V\text{-}PDB}$ = -5.01 ‰) and NBS120c ($\delta^{13}C_{V\text{-}PDB}$ = -6.27 ‰; Passey *et al*., 2007).

V- Strontium isotope compositions: a proxy for lifestyle and environment

Strontium has four stable isotopes: ^{84}Sr, ^{86}Sr, ^{87}Sr and ^{88}Sr. Unlike other isotopic systems studied in this thesis, its isotopic composition is measured as the ratio $^{87}Sr/^{86}Sr$ as the quantity of ^{86}Sr does not vary in a closed system, while ^{87}Sr is radiogenic (from the radioactive disintegration of ^{87}Rb). As the β^- radioactive disintegration has a half-life of 49.10^9 years, ^{87}Sr has varying abundances throughout geological times and depends on the original concentration of ^{87}Rb before the closure of the system (Bentley, 2006). Furthermore, different behaviours during phase changes of rubidium and strontium induce variability in Rb/Sr and thus $^{87}Sr/^{86}Sr$ ratios, which is dependent on the geological substrate. Through subsequent leaching and erosion, strontium is transferred in the environment and will be available to be integrated in organisms, where it is not produced otherwise (Schulert *et al*., 1959; Price *et al*., 2002; Bentley, 2006; Pemmer *et al*., 2013; Lazzerini *et al*., 2021).

Strontium undergoes negligeable isotopic fractionation between systems (Graustein, 1989; Capo *et al*., 1998; Sillen *et al*., 1998; Price *et al*., 2002) or trophic levels (Flockhart *et al*., 2015;

Lewis *et al*., 2017) because this element is quite heavy. As a result, strontium isotopic compositions of the mineralized tissues of an organism are characteristic of its living environment. Although it has been widely used to trace the origin of individuals and their migration processes, for example in bioarcheological studies (Price *et al*., 1994a, b; Evans *et al*., 2006a, b; Knudson *et al*., 2009; Brettell *et al*., 2012; Linscott *et al*., 2023), here it will simply be used as a lifestyle proxy between different substrates belonging to aquatic or terrestrial environments.

Analytically, before the measurements, strontium needs to be purified through an acid digestion, using ultrapure, concentrated nitric acid (15 N) at 130°C for one hour, to get rid of any organic matter. Then, a wet chemistry protocol was applied to separate the element from the matrix, following protocols from Tacail *et al*. (2014; see also Appendix 5: Supplementary Material S3). The reliability of this process was controlled by also analysing NIST-SRM1486 (mean $^{87}Sr/^{86}Sr = 0.709292 \pm 3.98.10^{-5}$, 2 s.e.; Galler *et al*., 2007; De Muynck *et al*., 2009; Weber *et al*., 2017; Brazier *et al*., 2019; Guiserix *et al*., 2022) and column blanks. $^{87}Sr/^{86}Sr$ ratios were then measured using a Neptune Plus multi-collector ICP-MS (MC-ICP-MS) following previously described methods (Tacail *et al*., 2014, 2016), with monitoring of the standard NIST-SRM987 (mean $^{87}Sr/^{86}Sr = 0.710256 \pm 5.18.10^{-5}$; Clemens *et al*., 1993; McArthur *et al*., 2001; Faure & Mensing, 2005; Galler *et al*., 2007; De Muynck *et al*., 2009; Weber *et al*., 2017; Brazier *et al*., 2019; Guiserix *et al*., 2022).

VI- Calcium isotope compositions: diet and food webs

With the advent of new spectrometers technologies, calcium isotopes have received growing attention since the end of the 20th century (Gussone *et al*., 2016; Martin *et al*., 2017a; Tacail *et al*., 2020) especially in archeology (Chu *et al*., 2006; Reynard *et al*., 2010, 2013; Wright, 2014; Tacail *et al*., 2017, 2019, 2020; Martin *et al*., 2020b; Li *et al*., 2020; Dodat *et al*., 2021) and paleoecology (Clementz *et al*., 2003; Reynard *et al*., 2010; Clementz, 2012; Melin *et al*., 2014; Martin *et al*., 2015b, 2017b, 2018, 2020b, 2022; Hassler *et al*., 2018; Balter *et al*., 2019; Tacail *et al*., 2020).

Calcium has five stable isotopes: ^{40}Ca, ^{42}Ca, ^{43}Ca, ^{44}Ca, ^{46}Ca and the abundance of two of those different calcium isotopes is studied with the following equation:

$$\delta^{44/42}Ca\ (‰) = \left[\frac{\left({}^{44}Ca/_{42}Ca \right)_{sample}}{\left({}^{44}Ca/_{42}Ca \right)_{ICP\ Ca\ Lyon}} - 1 \right] \times 10^3$$

In the formation of bones and teeth, light calcium isotopes from blood are preferentially incorporated (Skulan & DePaolo, 1999; DePaolo, 2004; Chu *et al*., 2006; Reynard *et al*., 2010; Heuser *et al*., 2011, 2016). Furthermore, the kidneys reinject light calcium isotopes in the blood through the filtration of urine (Heuser & Eisenhauer, 2010; Morgan *et al*., 2012; Tacail *et al*., 2014, 2017, 2020; Channon *et al*., 2015; Heuser *et al*., 2016, 2019). Those two processes induce lower $\delta^{44/42}Ca$ values both in blood and further in mineralized tissues compared to food in an organism.

An isotopic fractionation between the $\delta^{44/42}Ca$ values of mineralized tissues and food of an organism has been consistently observed in a wide array of vertebrates (Skulan & DePaolo, 1999; Clementz *et al*., 2003; DePaolo, 2004; Chu *et al*., 2006; Reynard *et al*., 2010; Heuser *et al*., 2011; 2016; Clementz, 2012), with $\delta^{44/42}Ca$ values of an organism lower than its food (offset of 0.3 to 0.5 ‰; Martin *et al*., 2017b, 2018, 2022; Tacail *et al*., 2020; Fig. 4.9). This offset is slightly lower in marine ecosystems, as those organisms also incorporate calcium from the water (Blätter *et al*., 2011; Martin *et al*., 2015b).

Analytically, before the measurements, calcium needs to be purified through an acid digestion, using ultrapure, concentrated nitric acid (15 N) at 130°C for one hour, to get rid of any organic matter. Then, a wet chemistry protocol was applied to separate the element from the matrix, following protocols from Tacail *et al*. (2014; see also Appendix 5: Supplementary Material S3). The reliability of this process was controlled by also analysing NIST-SRM1486 (mean $\delta^{44/42}Ca_{\text{ICP Ca Lyon}}$ = -1.03 ± 0.04 ‰, 2 s.e.; Martin *et al*., 2015b; Hassler *et al*., 2018, 2021a, b) and column blanks. $\delta^{44/42}Ca$ values were then measured using a Neptune Plus multi-collector ICP-MS (MC-ICP-MS) following previously described methods (Tacail *et al*., 2014, 2016). The relationship: $\delta^{43/42}Ca = a\ \delta^{44/42}Ca + b$, where a is between 0.501 and 0.512 (Tacail, 2017) must be respected if there are no interferences. The whole protocol is summarized in Figure 4.10.

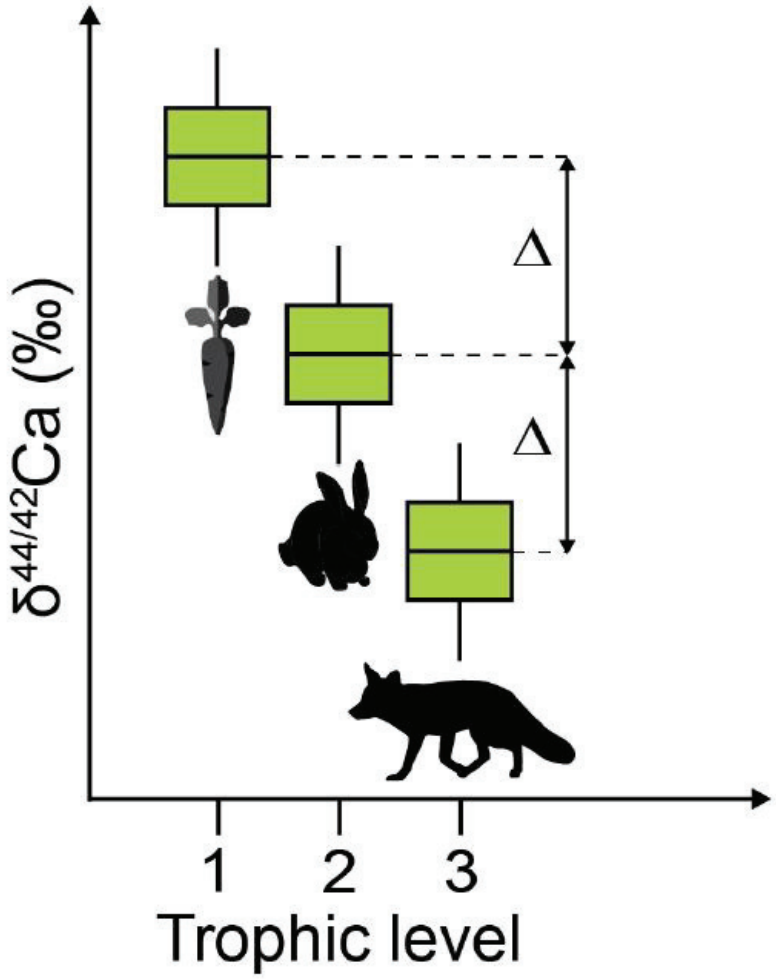

Figure 4.9: Simplified model of isotopic fractionation in a terrestrial food web. Modified from Hassler (2021; fig. I.6).

$\delta^{44/42}Ca$ and $\delta^{44/40}Ca$ measurements provide the same information as the isotopic fractionation are mass dependent (Gussone *et al*., 2016). However, as the mass difference is higher between ^{44}Ca and ^{40}Ca than between ^{44}Ca and ^{42}Ca, differences in $\delta^{44/40}Ca$ values will also be higher than differences in $\delta^{44/42}Ca$ values. As $\delta^{44/40}Ca$ values are generally measured with thermal ionization mass spectrometers (TIMS), they are also much more chronophageous to obtain and thus will not be used here (Russell *et al*., 1978; Skulan *et al*., 1997; Skulan & DePaolo, 1999) whereas $\delta^{44/42}Ca$ values measured on inductively coupled plasma mass spectrometers and multi-collector (MC-ICP-MS) are just as precise but less time consuming (Halicz *et al*., 1999; Wieser *et al*., 2004; Chu *et al*., 2006; Reynard *et al*., 2010; Morgan *et al*., 2011; Tacail *et al*., 2014; Channon *et al*., 2015; He *et al*., 2019). Furthermore, measurements of $\delta^{44/42}Ca$ values that involve inductively coupled plasma mass spectrometers and multi-collector (MC-ICP-MS) also induce an interference on the atomic mass 40 using argon (^{40}Ar) as vector and so make $\delta^{44/40}Ca$ values invalid. As a result, $\delta^{44}Ca$ values presented in this thesis will be those of $\delta^{44/42}Ca$.

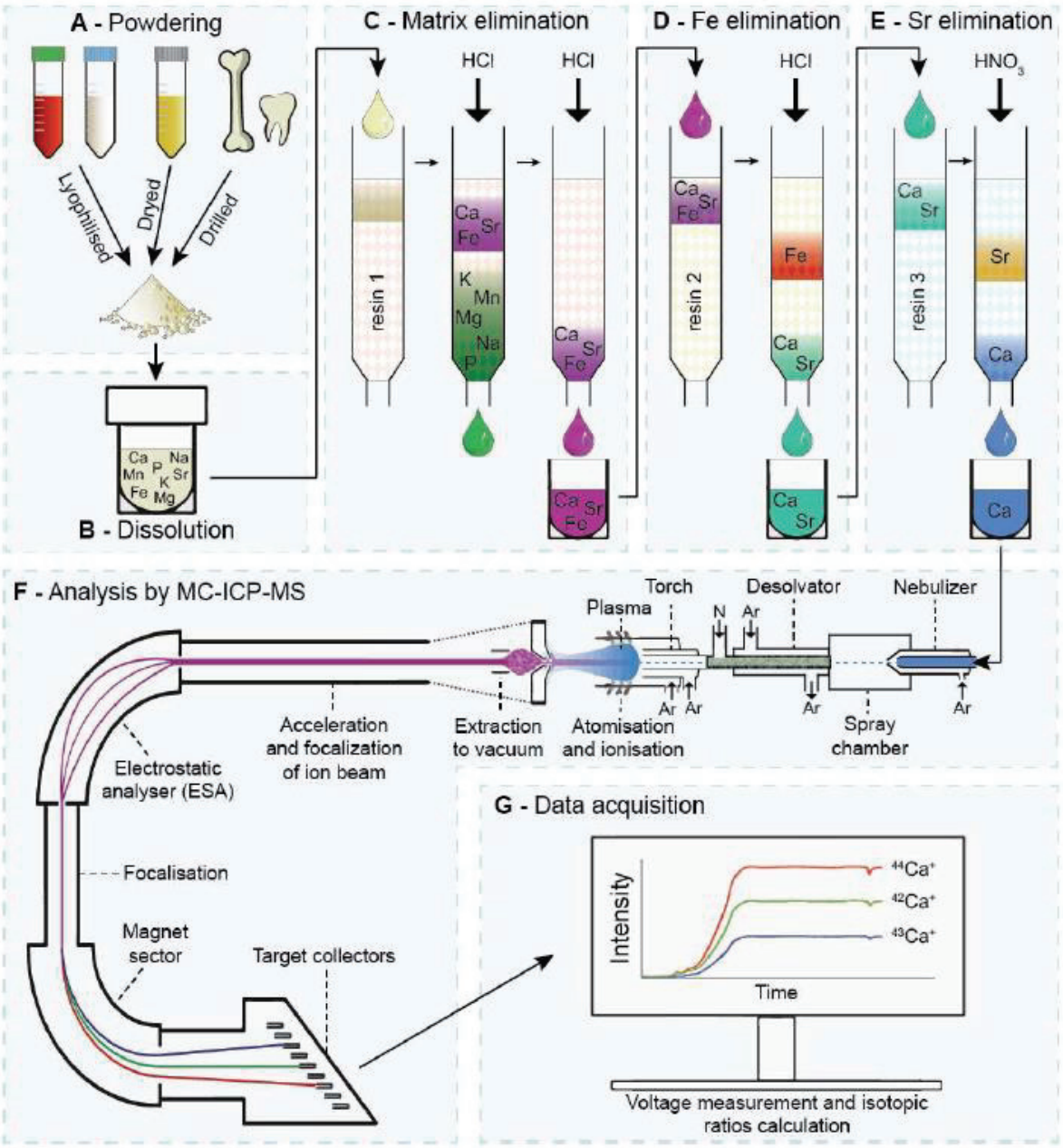

Figure 4.10: General steps for the processing of samples and the measurements of $\delta^{44/42}$Ca values. Taken from Hassler (2021, fig. II.1).

The isotopic fractionation of calcium between different tissues has been poorly studied so far, and would greatly benefit from further studies, especially in reptiles in which almost no data exist. Hassler *et al*. (2021b) measured no variation in $\delta^{44/42}$Ca values between cervid teeth and bone, while Heuser *et al*. (2011) measured a variation of + 0.50 ‰ in $\delta^{44/40}$Ca values (i.e., + 0.25 ‰ in $\delta^{44/42}$Ca values) between the enamel and bone of *Plateosaurus* von Meyer, 1837, but it is the only specimen on which the different tissues were sampled. In the framework of this thesis, when the same type of tissue could not be sampled for all organisms of the same fauna, both hypotheses concerning their $\delta^{44/42}Ca_{enamel}$ values will be made: no variation or a + 0.25 ‰ variation between the $\delta^{44/42}$Ca value of enamel and bone.

VII- Scientific publication ‘A multi-isotopic study reveals the paleoecology of a sebecid from the Paleocene of Bolivia’

This publication was published in June 2023 in *Palaeogeography, Palaeoclimatology, Palaeoecology*. Reference: Pochat-Cottilloux Y., Martin J. E., Faure-Brac M. G., Jouve S., Muizon C. d., Cubo J., Lécuyer C., Fourel F. & Amiot R. (2023). A multi-isotopic study reveals the paleoecology of a sebecid from the Paleocene of Bolivia. *Palaeogeography, Palaeoclimatology, Palaeoecology,* 625, 111667. https://doi.org/10.1016/j.palaeo.2023.111667

A multi-isotopic study reveals the paleoecology of a sebecid from the Paleocene of Bolivia

Yohan Pochat-Cottilloux[A], Jeremy E. Martin[A], Mathieu G. Faure-Brac[A, B] Stéphane Jouve[B], Christian de Muizon[C], Jorge Cubo[B], Christophe Lécuyer[A], François Fourel[D], Romain Amiot[A]

A: Univ Lyon, Univ Lyon 1, ENSL, CNRS, LGL-TPE, Villeurbanne, France

B: Sorbonne Université, Muséum National d'Histoire naturelle, CNRS, Centre de Recherche en Paléontologie – Paris (CR2P, UMR 7207), Paris, France

C: Centre de Recherche en Paléontologie – Paris (CR2P), Muséum National d'Histoire Naturelle, CNRS/MNHN/Sorbonne Université, Paris, France

D: Plateforme d'écologie isotopique, LEHNA, UMR CNRS 5023, Université Lyon 1, France

Corresponding author: Yohan Pochat-Cottilloux, yohan.pochat-cottilloux@univ-lyon1.fr

Abstract

Sebecids constitute a family of notosuchian crocodylomorphs of probable terrestrial habits. They are notable for having survived the Cretaceous-Paleogene mass extinction and are known until the Miocene in South America. However, ecological traits that favoured their resilience in continental ecosystems remain unknown. Here, using a multi-isotopic approach, we infer several paleoecological traits of a sebecid from the locality of Tiupampa (Bolivia), which contains a diverse vertebrate fauna of the Early Paleocene. After having constrained the effects of diagenesis, the study of the oxygen isotope compositions of apatite phosphate allows the identification of water resources for the various studied taxa and to infer an ectothermic thermoregulation strategy for the sebecids. A terrestrial lifestyle is also supported by different oxygen isotope compositions observed between sebecids and aquatic dyrosaurid crocodylomorphs. The radiogenic strontium isotope compositions confirm the continental affinities of this fauna, with no marine input in the paleoenvironment frequented by the different faunal elements. The calcium and carbon isotope compositions show that the sebecids from Tiupampa were at the top of a C_3-based food web. Finally, a local dry environment with tropical temperatures for those specimens is inferred both from oxygen and carbon isotope compositions of their hard tissues.

Keywords

Sebecidae; geochemistry; oxygen; carbon; calcium; strontium.

Introduction

Sebecidae is an extinct family of large supposedly terrestrial crocodylomorphs, known from the Maastrichtian to the Miocene (Langston, 1965; Paolillo & Linares, 2007; Pol & Powell, 2011; Sellés *et al*., 2020). They are the last survivors of the remarkably diverse group known as Notosuchia. Sebecids were distributed in South America and Europe and were one of the major groups of terrestrial predators during the Early Cenozoic (Pol *et al*., 2012; Martin, 2016; Martin *et al*., 2023). They are inferred to be terrestrial based on numerous traits: the skull of sebecids is similar to those of terrestrial sauropsid carnivores (Busbey, 1986; Molnar, 2012); their postcranial anatomy (proportionately long limbs) implies an erect posture compatible with a terrestrial lifestyle (Pol *et al*., 2012; Martin *et al*., 2023); and their neuroanatomy displays several terrestrial characteristics (inner ear and pneumaticity of the skull; Pochat-Cottilloux *et al*., 2022b). Through histological studies, they are further hypothesized to have been ectotherms (Cubo *et al*., 2020, 2022a).

While this ecology was inferred thanks to the study of morpho-anatomical characters, the use of stable isotope geochemistry could bring other evidence to assess their paleoecology and the numerous related issues. This has started to be applied recently, when Klock *et al*. (2022) assessed the diets of two South American notosuchians. The oxygen isotope compositions of apatite phosphate ($\delta^{18}O_p$) and carbonate ($\delta^{18}O_c$) from vertebrate bones, teeth and scales are linked to the animal body temperature and the oxygen isotope composition of body water, which is mainly derived from ingested ambient water (Kolodny *et al*., 1983; Longinelli, 1984; Luz *et al*., 1984; Faure-Brac *et al*., 2022). Physiological adaptations to a specific lifestyle (aquatic or terrestrial) affect the $\delta^{18}O$ of the body water by controlling the amount of input and output of oxygen, as well as the associated isotopic fractionations (Luz & Kolodny, 1985; Bryant & Froelich, 1995; Kohn, 1996). As a result, differences in $\delta^{18}O$ values between different vertebrate groups are linked to differences in either thermoregulation strategy, diet (e.g., herbivorous vs carnivorous) and/or living environment (Fricke & Rogers, 2000; Clementz & Koch, 2001; Clementz *et al*., 2003; Amiot *et al*., 2006, 2010).

The carbon isotope composition of vertebrate apatite constitutes a proxy of the animal diet. As the magnitude of ^{13}C-enrichments between vertebrate apatite and diet is known for several

extant groups, it allows the estimation of the carbon isotope composition of the base of the food web for fossil specimens. Furthermore, there is a trophic ^{13}C isotope enrichment between meat consumers and their food (i.e., lower $\delta^{13}C$ values) of 0 to 2 ‰ (Bocherens & Drucker, 2003). There are different expected values between C_3 and C_4-based food webs (Lee-Thorp *et al*., 1989; Tieszen & Fagre, 1993; Sillen & Lee-Thorp, 1994; Koch, 1998; Cerling & Harris, 1999; Passey *et al*., 2005; Stanton, 2006). This is done while keeping in mind that C_4 plants did not appear before the Oligocene (Niklaus & Kelly, 2019). In aquatic environments, the relationship is more complex, as the primary producers that constitute organism diets have $\delta^{13}C$ values that can vary because of differences in productivity, dissolved CO_2 concentration or bicarbonate utilization (Clementz & Koch, 2001 and references therein).

Calcium isotope compositions ($\delta^{44/42}Ca$) are also of interest because calcium is almost exclusively derived from food in terrestrial vertebrates (Skulan & DePaolo, 1999; Martin *et al*., 2018; Tacail *et al*., 2020). The observed change between the recorded isotopic value of their food relative to their mineralized tissues has allowed trophic levels to be inferred from continental food webs of the Cretaceous (Hassler *et al*., 2018; Martin *et al*., 2022).

Finally, the $^{87}Sr/^{86}Sr$ ratio of the mineralized tissues is a direct reflection of the geological substrate the animal lived on as it is not produced metabolically and is thus ingested through alimentation and water (Price *et al*., 2002; Lazzerini *et al*., 2021). It is hence possible to distinguish organisms living in different environments that are linked to different substrates (whether soils or waters).

Here, using a multi-isotopic approach involving those four isotopic systems, we discuss the impact of diagenetic processes on the preservation of the different geochemical proxies and infer several ecological traits of the sebecid from the locality of Tiupampa in terms of thermoregulation strategy, feeding habits and lifestyle, as well as a paleoenvironmental reconstruction of this Paleocene locality.

Material and methods

Sample collection

Seventeen samples of fossil tooth enamel (and dentine when not enough material was available) of crocodylomorphs, fish and mammals and two samples of fish scale enameloid were analysed for their oxygen isotope composition of apatite phosphate ($\delta^{18}O_p$), oxygen ($\delta^{18}O_c$) and carbon ($\delta^{13}C$) isotope composition of apatite carbonate, calcium isotope composition ($\delta^{44/42}Ca$),

radiogenic strontium isotope ratio ($^{87}Sr/^{86}Sr$) and elemental concentrations. Crocodylomorphs samples most probably come from adult individuals as the teeth are longer than one centimetre (Supplementary Material S1), compared with known fossil specimens (Buffetaut & Marshall, 1992; Paolillo & Linares, 2007; Jouve *et al*., 2020). Mammal samples belong to the taxon *Alcidedorbignya inopinata* Muizon & Marshall, 1987 which is inferred as agile, plantigrade, terrestrial and probably scansorial (Muizon *et al*., 2015). The sampled tooth type is unknown. The fish samples might either come from siluriforms (Gayet, 1988, 1990) or polypteriforms (Gayet & Meunier, 1992), but their referral is complex as the specimens described in previous studies from Tiupampa are not associated with teeth. Oxygen isotope compositions of phosphate ($\delta^{18}O_p$) of the samples have already been published in Faure-Brac *et al*. (2022), except for sebecid values. The details of the samples are given in Supplementary Material S1.

All the samples come from the locality of Tiupampa in the Santa Lucia Formation near the Vila Vila village about 90 km southeast of Cochabamba in the Mizque Province (southcentral Bolivia; Supplementary Material S2). This fauna dates back to the Early Paleocene (Early Danian, paleomagnetic Chron 28r, 65 Mya; Muizon & Ladevèze, 2020, fig. 4; Muizon & Billet, 2022) and has yielded a rich and diverse fauna including diapsids (Muizon *et al*., 1983; Rage, 1991a; Buffetaut & Marshall, 1992; Jouve *et al*., 2020; Pochat-Cottilloux *et al*., 2022b), fishes (Gayet, 1988, 1990; Gayet & Meunier, 1992), amphibians (Rage, 1991b), turtles (de Lapparent de Broin, 1992) and mammals, which constitute a large part of the relative abundance of the fossils (Marshall *et al*., 1983, 1995; Marshall & Muizon, 1988; Muizon & Marshall, 1991, 1992; Muizon, 1992, 1994, 1998; Muizon & Cifelli, 2000; Muizon *et al*., 1998, 2015, 2018, 2019; Muizon & Ladevèze, 2020, 2022; Muizon & Billet, 2022).

Analytical techniques

Oxygen isotope analysis of biogenic apatite phosphate

The vertebrate apatite powders were treated following the protocol described in Crowson *et al*. (1991) and Lécuyer *et al*. (1993) (see also Supplementary Material S3). Oxygen isotope compositions were measured using a vario PYRO cube™ elemental analyser coupled with an Isoprime™ isotopic ratio mass spectrometer (Elementar UK) in continuous flow mode at the Plateforme d'Ecologie Isotopique du Laboratoire d'Ecologie des Hydrosystèmes Naturels et Anthropisés (LEHNA, UMR5023, Université Lyon 1). For each sample (whenever possible), five replicates of 300 µg of Ag_3PO_4 were mixed with pure graphite powder in excess and loaded in silver foil capsules. Pyrolysis was performed at 1450°C. Measurements have been calibrated

against silver phosphate prepared from the NBS 120c ($\delta^{18}O_p$ = 21.7 ‰ V-SMOW; Lécuyer *et al*., 1993) and NBS 127 ($\delta^{18}O_p$ = 9.3 ‰ V-SMOW; Hut, 1987; Halas & Szaran, 2001). Isotopic compositions are reported in the δ notation relative to V-SMOW.

Oxygen and carbon isotope analysis of biogenic apatite carbonate

Potential organic contaminants as well as secondarily precipitated calcite were removed from the vertebrate apatite powder following the protocol of Koch *et al*. (1997; see also Supplementary Material S3 for more details). Stable isotope compositions were measured using an iso-FLOW system connected on-line in continuous flow mode to a precision mass spectrometer (Elementar UK). For each sample, three aliquots of 2 mg of pre-treated vertebrate apatite powder were loaded in LABCO Exetainer 3.7 mL soda glass vials, round bottomed with Exetainer caps (LABCO UK), and reacted with anhydrous phosphoric acid at 90°C. The CO_2 gas generated during the acid digestion was then transferred to the mass spectrometer via the centrION interface. The materials used for calibration were Carrara marble ($\delta^{18}O_{c\ V\text{-}PDB}$ = -1.95 ‰, $\delta^{13}C_{\ V\text{-}PDB}$ = 1.96 ‰; Fourel *et al*., 2016), NIST 8543 ($\delta^{18}O_{c\ V\text{-}PDB}$ = -23 ‰, $\delta^{13}C_{\ V\text{-}PDB}$ = -5.01 ‰) and NIST 120c ($\delta^{18}O_{c\ V\text{-}PDB}$ = -1.13 ‰, $\delta^{13}C_{\ V\text{-}PDB}$ = -6.27 ‰; Passey *et al*., 2007). Isotopic compositions are reported in the δ notation relative to V-SMOW for oxygen and V-PDB for carbon.

Calcium and strontium isotope analysis of vertebrate apatite

For these two elements, fifteen samples were duplicated and placed in Teflon beakers. The first duplicate was submitted to a leaching procedure following the protocol described in Balter *et al*. (2002b; see also Supplementary Material S3), to remove potential secondary calcite. The second one was left without leaching. All samples were then digested using ultrapure, concentrated nitric acid (15N) at 130°C for one hour, before being evaporated and re-dissolved in a dilute solution of ultrapure nitric acid (0.5N). Calcium and strontium from samples were chemically purified following previously described protocols (Tacail *et al*., 2014; see also Supplementary Material S3). The reliability of elutions has been controlled by also processing and analysing the standard material NIST-SRM1486 (mean $\delta^{44/42}Ca_{\ ICP\ Ca\ Lyon}$ = -1.03 ± 0.04 ‰, 2 s.e.; Martin *et al*., 2015b; Hassler *et al*., 2018, 2021a,b and references therein; Dodat *et al*., 2021; Martin *et al*., 2022; mean $^{87}Sr/^{86}Sr$ = 0.709292 ± $3.98.10^{-5}$, 2 s.e.; Galler *et al*., 2007; De Muynck *et al*., 2009; Weber *et al*., 2017; Brazier *et al*., 2019; Guiserix *et al*., 2022). Calcium and radiogenic strontium isotope abundance ratio ($^{44}Ca/^{42}Ca$ and $^{87}Sr/^{86}Sr$) were measured using a Neptune Plus multi-collector ICP-MS (MC-ICP-MS) following previously described

methods (Tacail *et al*., 2014, 2016). All calcium isotope compositions are expressed using the 'δ' notation defined as follows:

$$(1)\ \delta^{44/42}Ca = \left(\left(\frac{\left(\frac{^{44}Ca}{^{42}Ca}\right)sample}{\left(\frac{^{44}Ca}{^{42}Ca}\right)ICP\ Ca\ Lyon} \right) - 1 \right) * 1000$$

where $(^{44}Ca/^{42}Ca)_{sample}$ and $(^{44}Ca/^{42}Ca)_{ICP\ Ca\ Lyon}$ are the calcium isotope abundance ratios measured in sample and ICP Ca Lyon reference standard, respectively. The ICP Ca Lyon, which is used as a bracketing standard, is a Specpure calcium plasma standard solution (Alfa Aesar; Tacail *et al*., 2014, 2016, 2017; Martin *et al*., 2015b, 2017a). To assess the accuracy of the strontium isotope abundance ratios, the standard NIST-SRM987 was monitored (mean $^{87}Sr/^{86}Sr = 0.710256 \pm 5.18.10^{-5}$; Clemens *et al*., 1993; McArthur *et al*., 2001; Faure & Mensing, 2005; Galler *et al*., 2007; De Muynck *et al*., 2009; Weber *et al*., 2017; Brazier *et al*., 2019; Guiserix *et al*., 2022).

Elemental concentrations

Concentrations of major and trace elements were measured respectively on an inductively coupled plasma atomic emission spectrometer (ICP-AES; ICAP 7400 Series, Thermo Scientific) and on an inductively coupled plasma mass spectrometer (ICP-MS; ICAP-Q, Thermo Scientific). The reliability of measurements has been controlled through a set of blanks and the reference material NIST-SRM1400.

Thermophysiological inferences

The calculation of sebecid body temperatures was performed as follows:

The apatite phosphate $\delta^{18}O_p$ value is linked to the mineralization temperature (here body temperature T_b) and the $\delta^{18}O$ value of the body water ($\delta^{18}O_{bw}$) by the following equation adapted from the phosphate-water temperature scale (Lécuyer *et al*., 2013):

(1) $T_b = 117.4 - 4.5 * (\delta^{18}O_p - \delta^{18}O_{bw})$

Furthermore, the $\delta^{18}O$ of body water is linked to the $\delta^{18}O$ of ambient water and an enrichment value as follows:

(2) $\delta^{18}O_{bw} = \delta^{18}O_{aw} + E$

where $\delta^{18}O_{aw}$: $\delta^{18}O$ of ambient water and E: enrichment value.

In semi-aquatic to aquatic crocodylians, the $\delta^{18}O$ measured in the phosphate is linked to the $\delta^{18}O$ of ambient water by the following equation (Amiot *et al*., 2007):

(3) $\delta^{18}O_{aw} = 0.82 * \delta^{18}O_p - 19.13$

In mammals, it is the following equation (Amiot *et al*., 2004):

(4) $\delta^{18}O_{aw} = 1.11 * \delta^{18}O_p - 26.44$

The enrichment of sebecid body water relative to ambient water would be ~ 2 ‰ if this taxon was semi-aquatic to aquatic (as in extant crocodylians; Amiot *et al*., 2007) or ~ 5.1 ‰ if this taxon was terrestrial (value for terrestrial tortoises; Barrick *et al*., 1999).

Results

Oxygen isotope compositions of apatite phosphate

The phosphate oxygen isotope compositions of all samples are reported in Supplementary Material S4. Sebecid teeth have $\delta^{18}O_p$ values ranging from 20.1 to 21.5 ‰ (mean 2 s.d. = 0.3 ‰, n = 4), which are the highest values measured compared to dyrosaurids (17.5 to 20.4 ‰, mean 2 s.d. = 0.5 ‰, n = 4), fishes (15.0 to 20.0 ‰, mean 2 s.d. = 0.4 ‰, n = 3) and mammals (18.5 to 19.3 ‰, mean 2 s.d. = 0.3 ‰, n = 4; see also Fig. 4.11 & 4.12).

Oxygen and carbon isotope compositions of apatite carbonate

The isotopic compositions of all samples are reported in Supplementary Material S4. Analysed samples have $\delta^{18}O_c$ values ranging from 22.4 to 29 ‰ (mean 2 s.d. = 0.5 ‰, n = 13) and $\delta^{13}C$ values ranging from -12.6 to -9.5 ‰ (mean 2 s.d. = 0.1 ‰, n = 13). Sebecid teeth have $\delta^{18}O_c$ values that are significantly higher than those of the other sampled organisms (Wilcoxon test, p-value = 0.01; Fig. 4.11) and mammal teeth have $\delta^{13}C$ values that are significantly lower than those of other sampled organisms (Wilcoxon test, p-value = 0.02; Fig. 4.13).

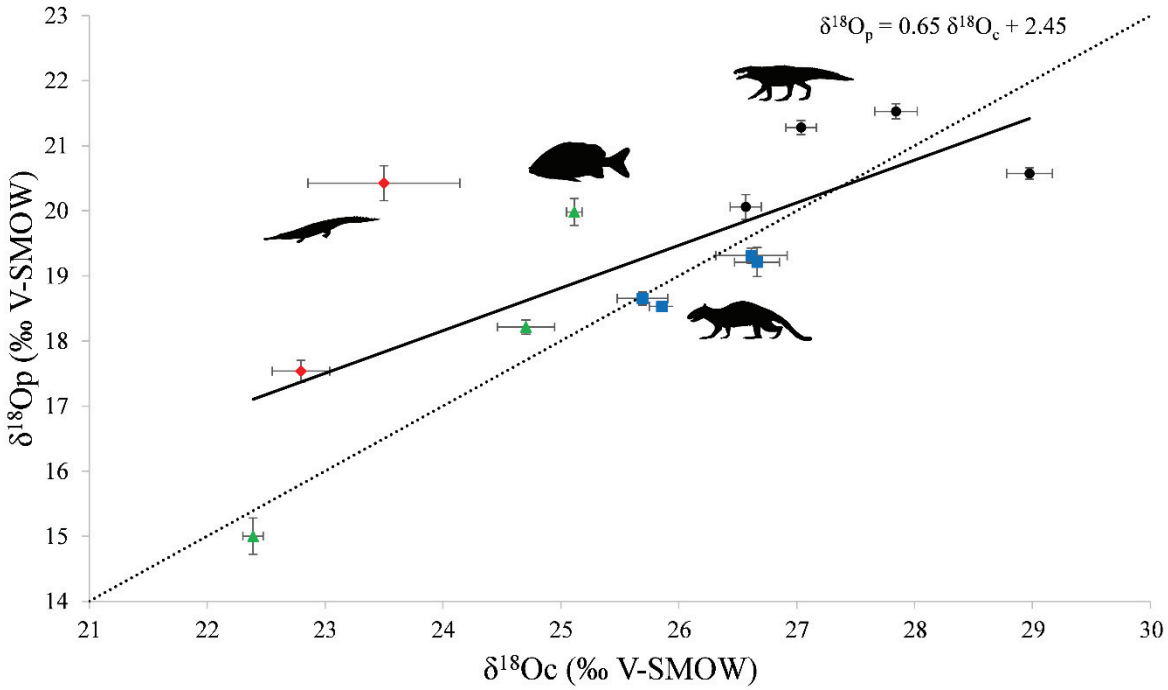

Figure 4.11: Oxygen isotope compositions of apatite phosphate reported against their corresponding oxygen isotope compositions of apatite carbonate. 2 s.d. for each sample are represented by bars. Black circles correspond to sebecids, blue squares to mammals, green triangles to fishes and red diamonds to dyrosaurids. Dashed line as a theoretical slope of 1. The shapes of the organisms are from phylopic.org.

Calcium isotope compositions of vertebrate apatite

Blanks realized during purification protocols have been analysed with the MC-ICP-MS Neptune Plus. All blanks contained less than 120 ng of calcium. Thus, considering our measurement precision, our isotopic measurements are not affected by this nano-pollution. The mass dependency curve of the isotopic measurements follows the expected relation for calcium (Fig. 4.14): the slope value is 0.504 ± 0.020 (2 s.e., n = 36), which agrees with the 0.5067 slope predicted by the linear approximation of exponential mass-dependent fractionation and is in line with previously published values (Tacail *et al.*, 2014, 2016, 2017; Martin *et al.*, 2015, 2017a, b, 2022; Hassler *et al.*, 2018, 2021a, b), supporting the accuracy of the measurements. The composition of all samples is reported in Supplementary Material S4. The standard NIST-SRM1486 has a $\delta^{44/42}$Ca mean value of -0.98 ± 0.05 ‰ (2 s.e., n = 26), which is also in line with previously published values (see Material & Methods). The $\delta^{44/42}$Ca values of the vertebrates sampled from Tiupampa range from -1.32 to -0.35 ‰ (mean 2 s.d. = 0.10 ‰, n = 31; Fig. 4.13). Mammal teeth have the highest values (mean value = -0.51 ± 0.24 ‰, 2 s.d., n = 9) and differ significantly from the other organisms (Wilcoxon test, p-value = $5.64.10^{-5}$) whereas sebecid teeth display the lower values (mean value = -1.24 ± 0.15 ‰, 2 s.e., n = 8) and also differ significantly from the other organisms (Wilcoxon test, p-value = $3.58.10^{-5}$).

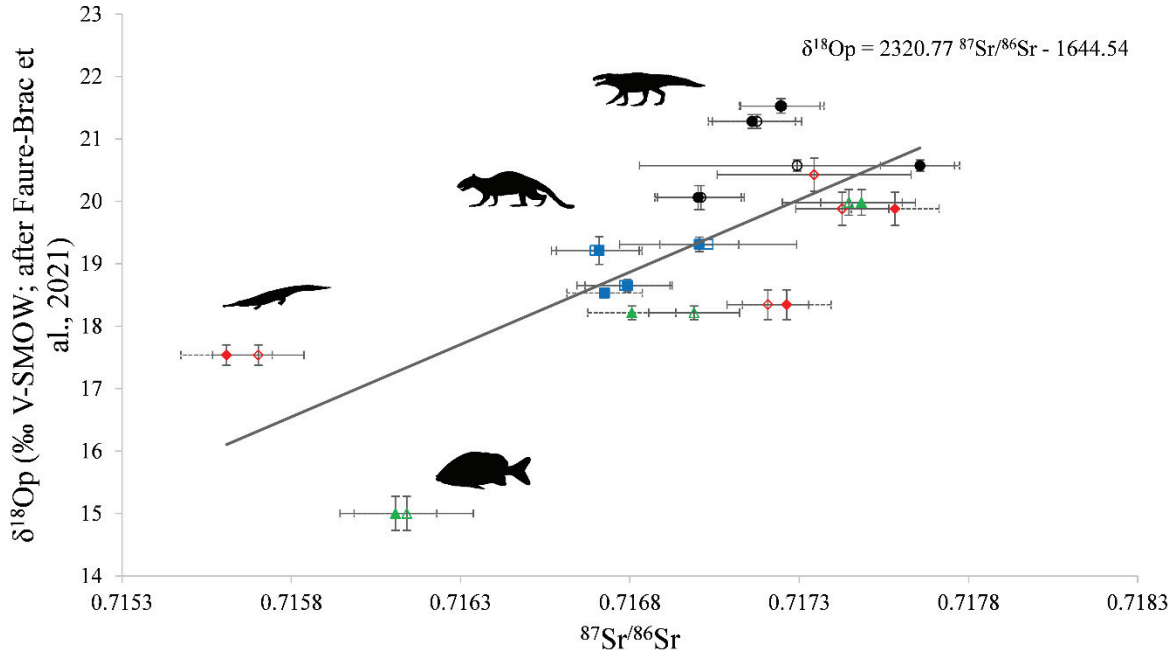

Figure 4.12: Oxygen isotope compositions of apatite phosphate reported against their corresponding strontium isotope compositions of vertebrate apatite. 2 s.d. for each sample are represented by bars. Black circles correspond to sebecids, blue squares to mammals, green triangles to fishes and red diamonds to dyrosaurids. Filled shapes and plain bars are leached samples, whereas empty shapes and dotted bars are unleached samples. The shapes of the organisms are from phylopic.org.

Strontium isotope compositions of vertebrate apatite

The composition of all samples is reported in Supplementary Material S4. The standard NIST-SRM1486 has a mean $^{87}Sr/^{86}Sr$ value of 0.709225 ± $3.34.10^{-4}$ (2 s.e., n = 6), and the standard NIST-SRM987 has a mean $^{87}Sr/^{86}Sr$ value of 0.710201 ± $2.68.10^{-4}$ (2 s.e., n = 37) which in line with previously published values (see Material & Methods). The $^{87}Sr/^{86}Sr$ values of the different organisms sampled range from 0.715554 to 0.717602 (mean 2 s.d. = $5.12.10^{-4}$, n = 29), and none of the groups of sampled organisms statistically differ from one another (Fig. 4.12).

Elemental concentrations

The full dataset compiling all the elemental and rare earth element concentrations measured in this study is reported in Supplementary Material S4 and Figure 4.14 & 4.15. An important result is that the mean ratio of calcium versus phosphorus is 2.12 ± 0.20, 2 s.d., n = 17 (molar ratio = 1.64 ± 0.14, 2 s.d., n = 17), suggesting that the stoichiometry of bioapatite is preserved.

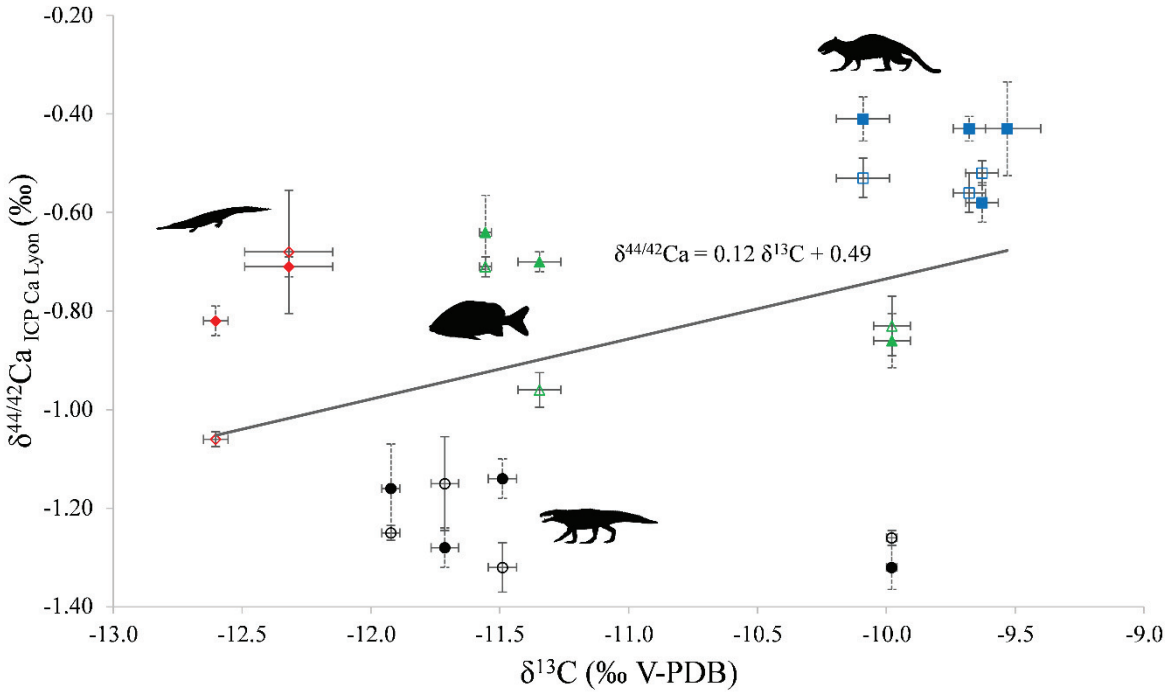

Figure 4.13: Calcium isotope compositions of vertebrate apatite reported against their corresponding carbon isotope compositions of apatite carbonate. 2 s.d. for each sample are represented by bars. Black circles correspond to sebecids, blue squares to mammals, green triangles to fishes and red diamonds to dyrosaurids. Filled shapes and plain bars are leached samples, whereas empty shapes and dotted bars are unleached samples. The shapes of the organisms are from phylopic.org.

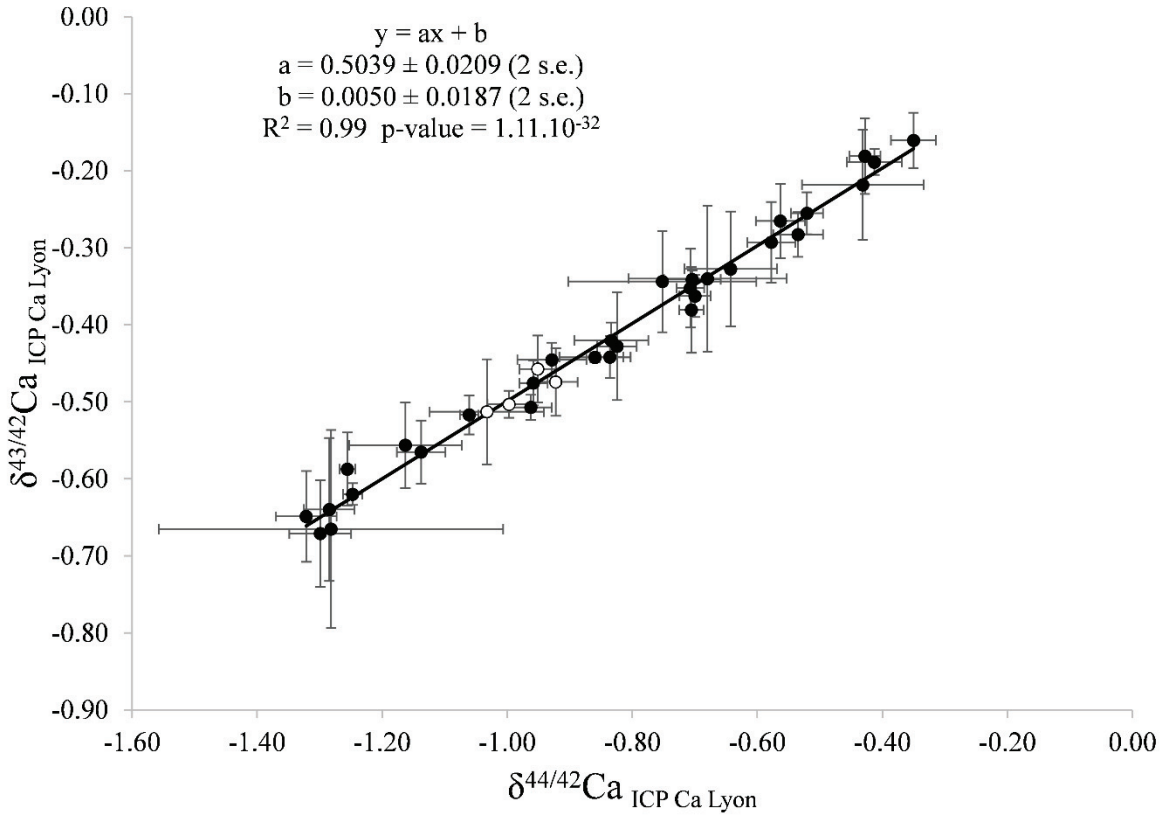

Figure 4.14: $\delta^{43/42}Ca$ values plotted against $\delta^{44/42}Ca$ values for all samples (black circles) and standards (white circles) studied.

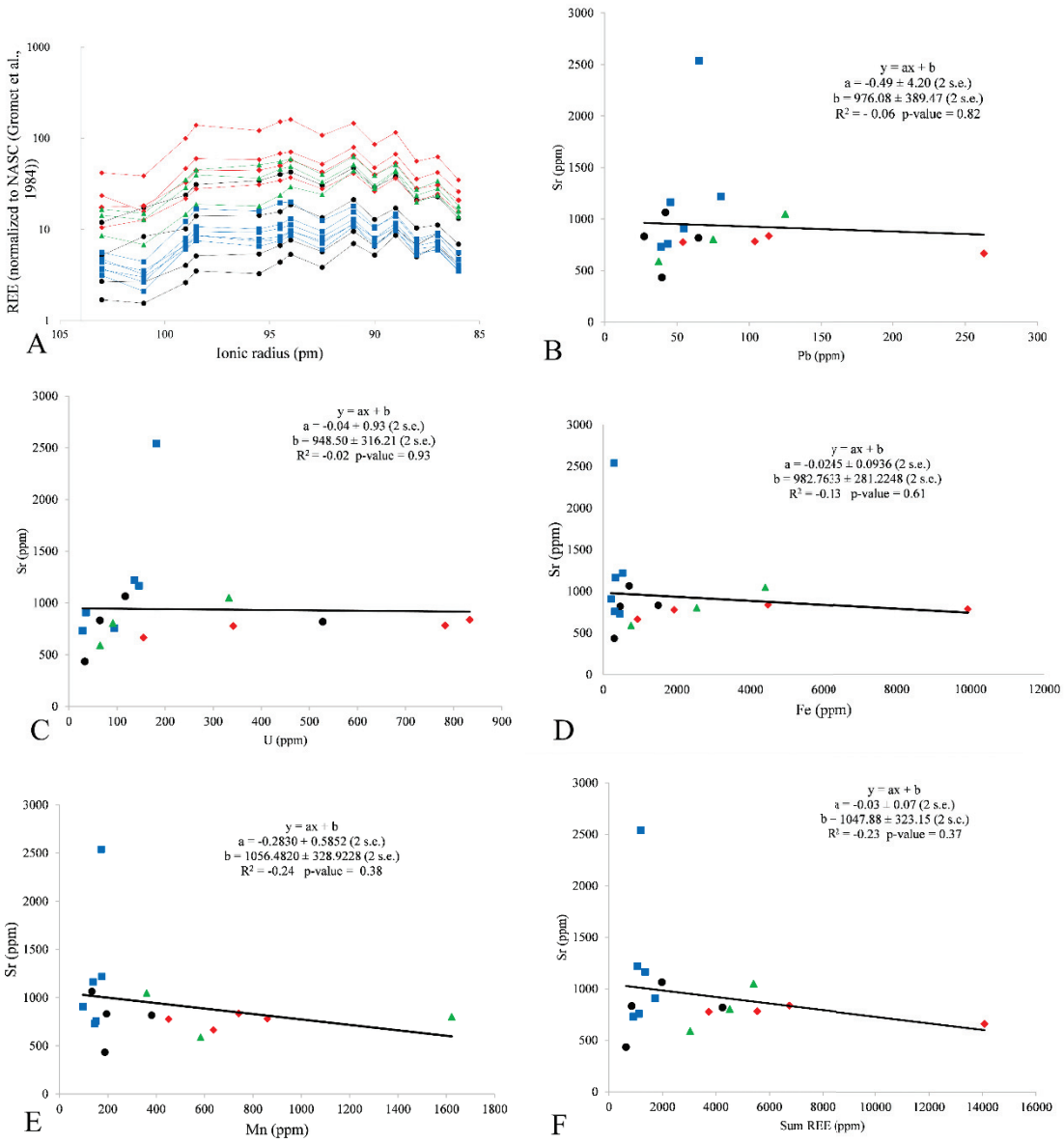

Figure 4.15: Diverse graphs highlighting the negligible impact of diagenesis on the samples. A: NASC normalized REE profiles of each sample from Tiupampa. Concentrations are plotted on a logarithmic scale. Black: sebecids, blue: mammals, green: fishes, red: dyrosaurids. Strontium concentration plotted against lead (B), uranium (C), iron (D), manganese (E) and sum of REE (F) concentrations. Black circles: sebecids, blue squares: mammals, green triangles: fishes, red diamonds: dyrosaurids.

Discussion

Assessing the impact of diagenesis on the isotope compositions

First, we must assess the state of isotopic preservation of the fossil samples studied as a prerequisite to interpret isotopic data in terms of paleoecological inferences. Although biotic and abiotic processes during taphonomy always have an impact on the measured compositions of fossil samples (secondary precipitation, ion adsorption, dissolution-recrystallization;

Kolodny *et al*., 1996; Blake *et al*., 1997; Lécuyer *et al*., 2003; Trueman *et al*., 2003; Zazzo *et al*., 2004a, b), there are several ways to assess their impact on the original preservation of the isotope compositions of the sample.

In the skeletal tissues of vertebrates, carbonates and phosphates precipitate in equilibrium with body water, such that $\delta^{18}O_p$ and $\delta^{18}O_c$ values are correlated. As exchanges rates between phosphate-water and carbonate-water are different, re-equilibration (and thus diagenetic alteration) of both systems is unexpected and altered samples should show an isotopic shift from the expected correlation in at least one of the two complexes. On the other hand, minimally altered samples should have $\delta^{18}O_p$ and $\delta^{18}O_c$ values that are correlated and display a slope close to unity, as established in other studies (Bryant *et al*., 1996; Iacumin *et al*., 1996; Zazzo *et al*., 2004b; Lécuyer *et al*., 2010; Chenery *et al*., 2012). Here, the correlation between the $\delta^{18}O_p$ and $\delta^{18}O_c$ values is significant ($R^2 = 0.73$, p-value = $4.79.10^{-3}$; Fig. 4.11) so the isotope compositions measured are preserved to a certain degree. One sample (GA1, fish scale enamel) greatly diverges from this slope. As it may have undergone some diagenetic processes modifying its oxygen and carbon isotope compositions, it will not be considered in the interpretations of these values.

Furthermore, using the elemental concentrations measured on each sample (Supplementary Material S4), we obtain a calcium/phosphorus ratio of 2.12 ± 0.2 (2 s.d., n = 17) which is in line with those measured in modern animals (2.15 ± 0.26, 2 s.d.; Balter *et al*., 2001) and other studies on fossil dinosaurs (2.3 ± 0.2, 2 s.d.; Hassler *et al*., 2018; 2.3 ± 0.12, 2 s.d.; Martin *et al*., 2022), bringing a further argument supporting the preservation of the fossils sampled here. Rare earth elements content (REE) can also indicate the state of preservation of our samples: as those elements are almost absent from a living organism, they can only be incorporated in reasonable quantity after its death, making it a marker of early or late diagenetic conditions as well as burial conditions (Reynard *et al*., 1999; Kocsis *et al*., 2009; Hinz & Kohn, 2010; Suarez & Kohn, 2020). Among fossils from Tiupampa, REE enrichment profiles (normalized to NASC, Haskin & Frey, 1966 and Gromet *et al*., 1984; Fig. 4.15A) are similar for each sample, meaning that those fossils can be considered as autochthonous (Trueman, 2013). Furthermore, none of those patterns are bell-shaped, indicating that the recrystallization processes were limited (Reynard *et al*., 1999; Lécuyer *et al*., 2004; Reynard & Balter, 2014). Strontium concentrations are not correlated with lead, uranium, iron, manganese, or the sum of REE (Fig. 4.15B-F), meaning that this element was not preferentially incorporated after the death of the organisms: the radiogenic strontium isotope compositions can thus be considered as reflecting

those of the substrates or waters where the organisms lived. Finally, lanthanum/ytterbium (La/Yb) and lanthanum/samarium (La/Sm) ratios for all samples fall within the range of modern freshwater samples (Fig. 4.16), indicating a moderate intensity of adsorption and substitutions processes (Reynard *et al*., 1999; Reynard & Balter, 2014).

Finally, the fact that we have mainly sampled enamel rather than dentine (whenever possible), hints to isotopic compositions less subject to diagenesis, because this tissue is highly mineralized and exhibit a lower porosity than dentine or bone (Wang & Cerling, 1994; Heuser *et al*., 2011; Martin *et al*., 2017a, b; Dodat *et al*., 2023). Furthermore, in the four isotopic systems studied here, there is no clear differences between enamel samples and enamel + dentine samples in the different groups of organisms, bringing further evidence to the low impact of diagenetic processes on the primary preservation of stable isotope compositions. Given the high quantity of calcium in vertebrates samples (at least 15% of mass here, see

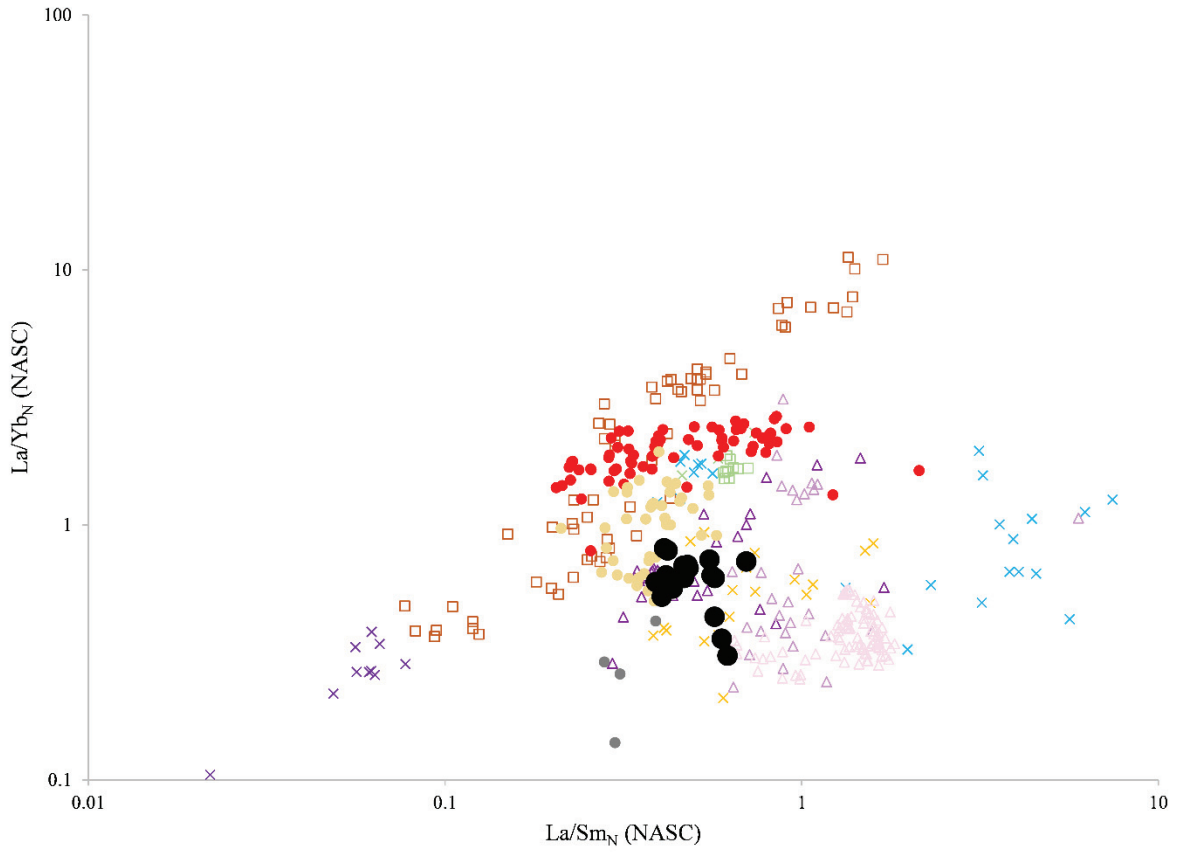

Figure 4.16: La/Sm$_N$ plotted against La/Yb$_N$ values (normalized to NASC; Haskin & Frey, 1966; Gromet *et al*., 1984) for multiple fossil and extant apatite samples, as well as modern waters (Reynard & Balter, 2014, and references therein). Squares: conodonts, crosses: fishes, triangles: waters, circles: fossil faunas. Brown: Devonian, light green: Silurian, blue: Mesozoic - Cenozoic, yellow: Quaternary, dark purple: freshwaters, purple: estuarine and coastal waters, pink: ocean waters, red: Gadoufaoua fauna (Niger, middle Cretaceous; Hassler *et al*., 2018), beige: Kem Kem fauna (Morocco, middle Cretaceous; Hassler *et al*., 2018), grey: dinosaur communities (USA, late Cretaceous; Martin *et al*., 2022), black: Tiupampa.

Supplementary Material S4), it is unlikely that the measured calcium isotopic compositions have been entirely overprinted by diagenetic processes, even if those were important. Also, leached and non-leached samples display the same values in calcium and radiogenic strontium isotope compositions (Wilcoxon test, p-value = 0.57, n = 14 and p-value = 0.98, n = 13 respectively), which is another argument for the weak impact of diagenesis on our samples.

In summary, there is no evidence for important diagenetic alteration of the elemental compositions of the samples analysed here, in all the different isotopic systems used (apart for GA1). As a result, associated isotope compositions reported here are interpreted in terms of paleotrophic networks, paleoenvironments and thermophysiological abilities.

Paleobiological inferences

Thermophysiology

Using equations (2) to (5), Faure-Brac *et al*. (2022) calculated that mammals have ingested ambient waters having an average $\delta^{18}O_{aw}$ value of -5.4 ± 0.9 ‰ (2 s.e.). In the present study, we add that dyrosaurids have ingested an ambient water having a $\delta^{18}O_{aw}$ value of -3.5 ± 2.2 ‰ (2 s.e., n = 4), which is in line with the other source of drinking water previously identified in Faure-Brac *et al*. (2022) (turtle sample: -2.1 ‰). As a result, it is a reasonable assumption that sebecids either consumed the same drinking water as dyrosaurids (and turtles and fishes) or as mammals, and that they either have a semi-aquatic (with an enrichment value of around 2 ‰) or terrestrial lifestyle (with an enrichment value of around 5.1 ‰). Those hypotheses are summarized in Figure 4.17. In the first case (Fig. 4.17A; semi-aquatic lifestyle), we obtain a mean body temperature ranging from 5 to 12°C with the $\delta^{18}O_{aw}$ value of mammals (Fig. 4.17A, green dot; mean value = 8 ± 6°C, 2 s.e., n = 4), or a mean body temperature ranging from 14 to 20°C with the $\delta^{18}O_{aw}$ value of dyrosaurids (Fig. 4.17A, red dot; mean value = 16 ± 6°C, 2 s.e., n = 4). Those values are both too low to be realistic. In the second case (Fig. 4.17B; terrestrial lifestyle), we obtain a mean body temperature ranging from 19 to 26°C with the $\delta^{18}O_{aw}$ value of mammals (Fig. 4.17B, green dot; mean value = 22 ± 6°C, 2 s.e., n = 4) or a mean body temperature ranging from 28 to 34°C with the $\delta^{18}O_{aw}$ value of dyrosaurids (Fig. 4.17B, red dot; mean value = 30 ± 6°C, 2 s.e., n = 4), which is in both cases much more realistic and implies an ectothermic thermoregulation strategy for the sebecids. Although, the source of drinking water for sebecids cannot be directly identified so far, we confirm here the interpretations obtained from an independent histological approach performed on notosuchians (Cubo *et al*.,

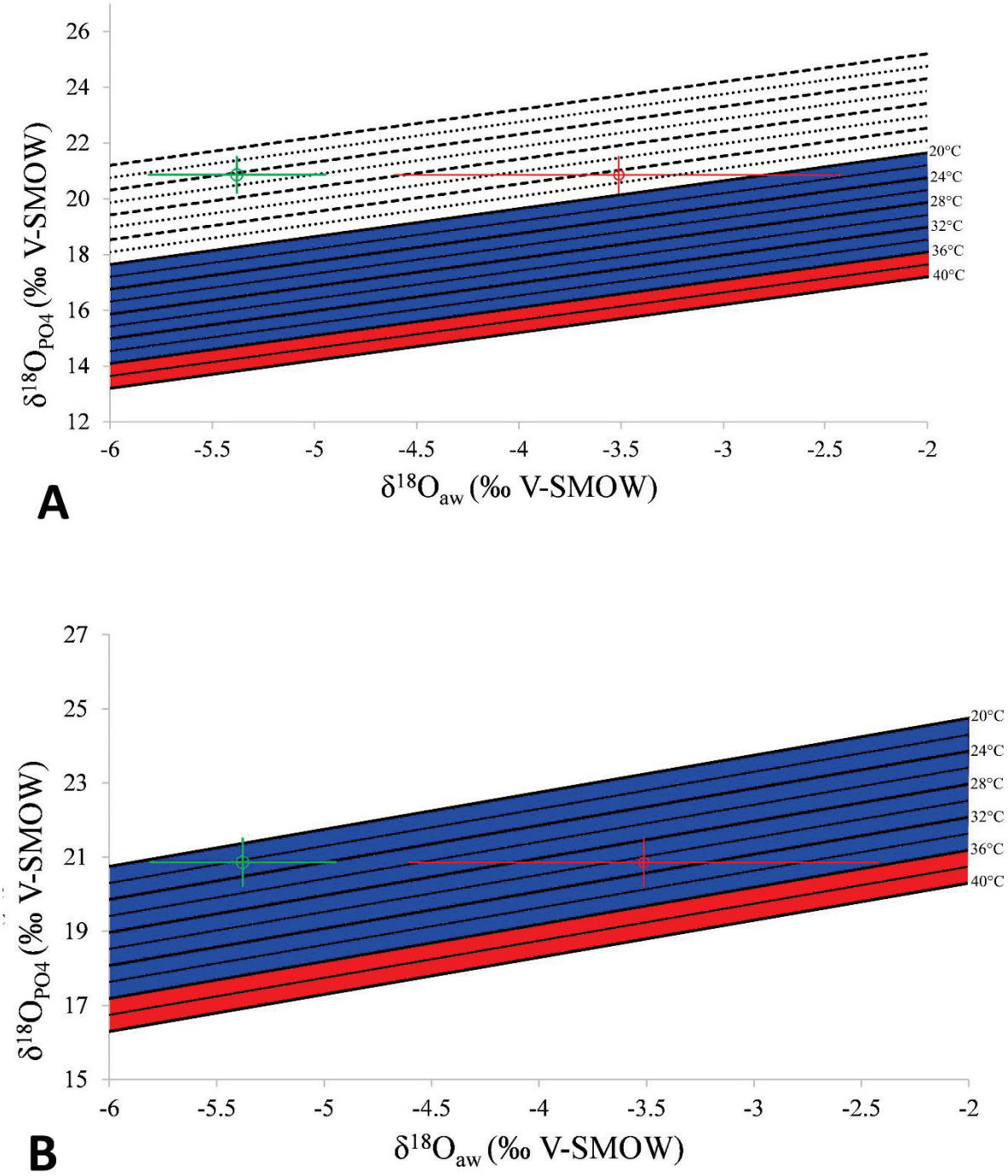

Figure 4.17: Sebecid oxygen isotope compositions of apatite phosphate are plotted against their possible ambient water values ($\delta^{18}O_{aw}$) within a frame showing expected vertebrates $\delta^{18}O_p$ - $\delta^{18}O_{aw}$ relationships for a range of body temperatures (black lines). The blue area represents the expected body temperatures range for ectotherm modern crocodylians, whereas the red area represents the expected body temperatures range for modern endotherms. Green dots: considering the $\delta^{18}O_{aw}$ value of mammals; red dots: considering the $\delta^{18}O_{aw}$ value of dyrosaurids. A: considering a semi-aquatic lifestyle, i.e., an enrichment value of 2 ‰, B: considering a terrestrial lifestyle, i.e., an enrichment value of 5.1 ‰.

2020, 2022a), which also estimated ectothermic thermoregulation strategies in representatives of this clade.

Lifestyle

The oxygen isotope composition of the samples studied here is mainly controlled by the body temperature and the drinking water. As we have assessed that the sebecids from Tiupampa were most probably ectotherms, which would put them in the same temperature range as the dyrosaurids sampled (25 - 38°C; Faure-Brac *et al*., 2022), the almost significant difference between the $\delta^{18}O_p$ of these two groups (mean $\delta^{18}O_p$ for dyrosaurids: 19 ± 2.7 ‰, 2 s.d., n = 4; mean $\delta^{18}O_p$ for sebecids: 20.9 ± 1.3 ‰, 2 s.d., n = 4; p-value = 0.06 under a Wilcoxon test) could be interpreted as a difference in lifestyle, especially if those two groups had the same drinking water, i.e., $\delta^{18}O_{aw}$ value of -3.5 ‰. Indeed, the difference between these two groups is due to higher water turnover and lower transcutaneous water evaporation in aquatic forms compared to terrestrial ones, which in turn translates to lower $\delta^{18}O_p$ values for aquatic forms compared to terrestrial ones with an equivalent body temperature. Furthermore, those differences are similar to those observed in Mesozoic and modern ecosystems (Cerling *et al*., 2008; Amiot *et al*., 2010). Unfortunately, this hypothesis cannot be confirmed by another independent proxy: strontium isotope compositions could have highlighted different substrates between the two groups, however the $^{87}Sr/^{86}Sr$ values are not significantly different from one another. Nonetheless, the strontium isotope compositions bring an interesting information about the global environment of Tiupampa: the $^{87}Sr/^{86}Sr$ value of seawater just after the end of the Cretaceous was $0.7079 \pm 4.83.10^{-5}$ (2 s.e., n = 10; Martin & Macdougall, 1991), which is much less than the values obtained for the Tiupampa fauna. Thus, as highlighted in Faure-Brac *et al*. (2022), Tiupampa can be considered as a strictly continental deposit and the dyrosaurids sampled here were not marine: they either belong to a yet unknown species or they represent marine individuals that had been living in the fluviatile system for at least a dental generation. The freshwater origin for the Tiupampa sediments was previously suggested (Gayet & Meunier, 1992; Muizon *et al*., 2015; Jouve *et al*., 2020) based on the sedimentology and fauna. The present work provides new arguments in this way, as well as evidence of a freshwater lifestyle for the dyrosaurids of Tiupampa.

Diet

Sebecids show depleted Ca isotope compositions in contrast to dyrosaurids, fishes and especially mammals which have the highest $\delta^{44/42}Ca$ values (Fig. 4.13). This is in line with the

fractionation that occurs within the body resulting in tissues being depleted in ^{44}Ca compared with the food source (Skulan & DePaolo, 1999; Chu *et al*., 2006; Tacail *et al*., 2014), indicating that sebecids were at the top of the food chain in this environment. The trophic pyramid would thus have been supported both by fishes and mammals, these last ones probably being herbivores given both their high $\delta^{44/42}Ca$ and $\delta^{13}C$ values. Those two groups would have thus represented two potential primary sources of calcium for predators. Considering a carnivore-herbivore offset of 0.3 to 0.5 ‰, as reported in other studies (Martin *et al*., 2018, 2022; Tacail *et al*., 2020), dyrosaurids ($\delta^{44/42}Ca$ values ranging from -0.68 to -1.06 ‰, mean 2 s.d. = 0.08 ‰, n = 8) would have preferentially fed on fishes ($\delta^{44/42}Ca$ values ranging from -0.64 to -0.96 ‰, mean 2 s.d. = 0.09 ‰, n = 6) or mammals ($\delta^{44/42}Ca$ values ranging from -0.35 to -0.75 ‰, mean 2 s.d. = 0.11 ‰, n = 9). However, given their long rostrum with sharp teeth, they were more likely adapted for piscivory (Jouve *et al*., 2020). Data obtained on sebecids are more difficult to interpret: applying a 0.3 to 0.5 ‰ offset corresponds to the values obtained for the dyrosaurids and fishes, however this does not necessarily fit with a terrestrial lifestyle, as inferred from other independent proxies (Pol *et al*., 2012; Pochat-Cottilloux *et al*., 2022b) and oxygen isotope compositions here. Thus, either sebecids did feed on dyrosaurids and fishes, possibly making them more semi-aquatic than previously thought and contradicting our results on oxygen isotope compositions, or there is another explanation for the observed distribution of $\delta^{44/42}Ca$ values. First, $\delta^{44/42}Ca$ values of prey mammals (-0.51 ± 0.24 ‰, 2 s.e., n = 9) could be modified by lactation and/or gestation processes with an offset of up to -0.3 ‰ (Hassler *et al*., 2021b), which would in turn make them suitable preys for sebecids. Though this is only applicable to female individuals, this could fit with the mortality profile observed in Tiupampa, which may indicate a breeding ground (Muizon & Billet, 2022) and be in line with a 0 to 2 ‰ trophic enrichment when looking at $\delta^{13}C$ values between sebecids and mammals (Bocherens & Drucker, 2003). Second, the preferred prey of sebecids could simply not have been sampled during our study, among the diverse fauna of the Tiupampa locality. Third, sebecids being at the top of the trophic network, could have possibly ingested a significant amount of bone material (Baquedano *et al*., 2012), modifying the measured calcium isotope compositions (Dodat *et al*., 2021). Interestingly, we notice an offset of ~ 0.1 ‰ between the $\delta^{44/42}Ca$ values of dyrosaurid samples composed exclusively of enamel (D1 & D3) and those composed of enamel and dentine (D2 & D4). This would seem to confirm the observation by Heuser *et al*. (2011) of an offset of ~ 0.14 - 0.18 ‰ in $\delta^{44/42}Ca$ values between samples made out exclusively of enamel and those made out exclusively of dentine. However, this trend is not retrieved in the

sebecid samples (S1, S3 & S4 vs S2 respectively), so the mechanisms at play here might be more complex.

Sebecids and dyrosaurids display respectively mean $\delta^{13}C$ values of -11.3 ± 1.8 ‰ (2 s.e., n = 4) and -12.5 ± 0.4 ‰ (2 s.e., n = 2), which, using an isotope fractionation of 9 ‰ between crocodile apatite and diet (Lee-Thorp *et al*., 1989; Tieszen & Fagre, 1993; Stanton, 2006), indicate a diet with a $\delta^{13}C$ value of -20.7 ± 1.8 ‰ (2 s.e., n = 6). Furthermore, using the data from Passey *et al*. (2005), we estimate a $\delta^{13}C$ apatite-diet offset of 12.3 ± 4.2 ‰ (2 s.e.) in mammals. Mammal samples thus display a $\delta^{13}C$ diet value of -22 ± 0.5 ‰ (2 s.e., n = 4). We then must estimate the $\delta^{13}C$ value of atmospheric CO_2 in the early Paleocene, as it has a direct effect on the stable carbon isotope composition of plants (Fricke, 2007). Through carbon and oxygen isotope compositions of benthic foraminifera in the literature (Cramer *et al*., 2009), we estimate the $\delta^{13}C_{CO2}$ during the Early Paleocene at -5.7 ± 0.8 ‰ (2 s.e., n = 83; see also Supplementary Material S5, equation 3 to 7), in contrast with modern $\delta^{13}C_{CO2}$ of -7 to -8 ‰ (Gröcke, 2002). Thus, C_3 plants $\delta^{13}C$ range during this period should shift towards values 1.8 ‰ higher, i.e., -35.5 to -18.5 ‰ (O'Leary, 1988; Kohn, 2010). The values calculated here for the Tiupampa fauna do match this expectation, although they belong to the higher part of the $\delta^{13}C$ range of plants, which would indicate an arid environment, as assessed in the Bauru Group (Upper Cretaceous of Brazil; Klock *et al*., 2022). The $\delta^{13}C$ values measured in Tiupampa vertebrates cluster in two groups: one with $\delta^{13}C$ values lower than -11.0 ‰ and one with $\delta^{13}C$ values higher than -10.5 ‰ (Fig. 4.13). Although this difference is significant (p-value = 0.005 under a Wilcoxon test), it is difficult to interpret as both clusters include samples belonging to the same taxonomic group (fishes and sebecids). More analyses would be needed to assess the potential ecological consequences of this clustering. Finally, it is interesting to observe that the $\delta^{44/42}Ca$ and $\delta^{13}C$ values of sebecids and dyrosaurids do not overlap (Fig. 4.13). This could either be due to a different source of alimentation (as hypothesized above) or a different digestive physiology leading to a different apatite-diet ^{13}C enrichment.

Paleoenvironmental reconstruction

$\delta^{18}O_{aw}$ values calculated from $\delta^{18}O_p$ values measured from different group of organisms using equations (4) and (5) range from -2.4 to -5.8 ‰ (mean value: -4.4 ± 2.5 ‰, 2 s.e., n = 8), which corresponds to continental surface water values measured today at tropical to equatorial latitudes (IAEA, 2022). As fish body water is not fractionated from the ambient water, their body temperature reflects the water temperature of their living environment. Using equation (2)

and the $\delta^{18}O_{aw}$ values calculated from turtles and crocodylians, those temperatures range from 12 to 22°C (mean value: 17 ± 10°C, 2 s.d., n = 2), which would be expected of a freshwater tropical environment and further indicates that those fish were also autochthonous. The measured $\delta^{18}O_p$ values in Tiupampa fauna are high and comparable to those measured in the terrestrial ecosystems of the Songliao basin (mean $\delta^{18}O$ = 22.20 ± 1.65 ‰, 2 s.d., n = 57; Huang *et al*., 2013; Gao *et al*., 2015; Zhang *et al*., 2018) and Nanxiong basin (mean $\delta^{18}O$ = 24.53± 1.92 ‰, 2 s.d., n = 6; Yin *et al*., 2023), but not as high as those measured in desertic environments (Lécuyer *et al*., 1999; Schoeninger *et al*., 2000), therefore being more in line with a dry environment. The $\delta^{18}O_{aw}$ values are also in accordance with climatic conditions measured nowadays in Pakistan or South China, with a mean annual temperature around 20°C and a mean precipitation of a few hundred millimetres per year (IAEA, 2022). Finally, this is also confirmed when looking at $\delta^{13}C$ values measured here: those correspond to C_3 plants with mean $\delta^{13}C$ values ranging from -20.5 to -21.7 ‰. These values indicate dry ecosystems today, with annual precipitation of less than 200 mm/year (Kohn, 2010, see also Supplementary Material S5). It would thus appear from two independent elements that the specimens sampled here were living in a dry environment, albeit with the presence of freshwater, contrary to what was hypothesized in other studies (Woodburne *et al*., 2014 and references therein). This is further confirmed by large scale studies that infer a global warming at the beginning of the Paleogene (Sewall & Sloan, 2001; Sewall, 2004; Quillévéré *et al*., 2008; Gilabert *et al*., 2022), and some regional scale studies in China (Gao *et al*., 2021) or France (Cojan & Moreau, 2006). In any case, those interpretations must thus be taken with caution as the data we use here is merely a local snapshot rather than a long-term interpretation.

Conclusion

Using a multi-isotopic proxy approach, we highlight several ecological traits of the sebecids from Tiupampa, as well as a paleoenvironmental reconstruction of this locality. After assessing the impact of diagenesis on our samples from numerous methods, we reconstruct a local dry environment with tropical temperatures for the specimens sampled here, inferred both from oxygen and carbon isotope compositions.

The calcium and carbon isotope compositions of vertebrate apatite indicate that the sebecids were at the top of the C_3-based food web, although their main source of alimentation remains elusive. The dominance of those terrestrial organisms in post-Cretaceous ecosystems is here ascertained, probably because of the disappearance of competitors, such as dinosaurs. Using

the oxygen isotope compositions of apatite phosphate, their inferred body temperature is consistent with those of extant ectotherms, such as crocodylians, as were also the dyrosaurids living in the same locality. We thus imply that the difference measured in $\delta^{18}O_p$ values between the two groups most probably reflects a difference in lifestyle, with aquatic dyrosaurids and terrestrial sebecids.

Those results would be especially interesting to compare to future multi-isotopic studies with a focus on similar communities living before the K/Pg crisis, as has already been done on dinosaurs using calcium isotope compositions (Martin *et al*., 2022) and to a lesser extent on other notosuchians using carbon and oxygen isotope compositions (Klock *et al*., 2022). Finally, the study of the strontium isotope compositions allows to clearly discard the marine influence from the environment sampled in this study, which is especially interesting due to the presence of dyrosaurids in the sampled organisms, which have until now mainly been inferred as a marine group.

Acknowledgements

This work was supported by the Agence Nationale de la Recherche (SEBEK project no. ANR-19-CE31-0006-01 to Jeremy E. Martin). The authors would like to thank Auguste Hassler (University of Aberdeen and University of Ottawa) for discussion about calcium isotopes; Pierre-Jean Dodat, Samuel Le Goff, Florent Arnaud-Godet, and Philippe Telouk (ENS Lyon) for technical expertise on the spectrometers; Erika Schumacher and Julián Bayona for helping us to illustrate our study by having transferred their work to the public domain or under a creative commons licence.

Authors contributions

Yohan Pochat-Cottilloux: Conceptualization, Validation, Formal analysis, Investigation, Data Curation, Writing - Original draft, Writing - Review & Editing, Visualization; **Jeremy E. Martin**: Conceptualization, Methodology, Validation, Formal analysis, Investigation, Resources, Data Curation, Writing - Review & Editing, Supervision, Project administration, Funding acquisition; **Mathieu G. Faure-Brac:** Conceptualization, Formal analysis, Investigation, Data Curation, Writing - Review & Editing; **Stéphane Jouve:** Resources, Writing - Review & Editing, Supervision; **Christian de Muizon:** Resources, Writing - Review & Editing; **Jorge Cubo**: Conceptualization, Writing - Review & Editing, Supervision, Project administration; **Christophe Lécuyer**: Conceptualization, Methodology, Writing - Review &

Editing, Supervision, Project administration; **François Fourel:** Methodology, Software, Resources, Writing - Review & Editing; **Romain Amiot:** Conceptualization, Methodology, Validation, Investigation, Resources, Data Curation, Writing - Review & Editing, Supervision, Project administration, Funding acquisition.

Data availability statement

The data underlying this article are available in the article and in its supplementary material.

Supplementary Materials

Supplementary Material S4 is available on this link: https://mycore.core-cloud.net/index.php/s/fbzve2jQPBKqwGn

Supplementary Material S1-S3 & S5 are available in Appendix 5.

VIII- A multi-isotopic landscape of Paleogene sebecosuchians from African and European localities

Following the results of Tiupampa (see VII), the same set of analyses was conducted on three other localities from the Eocene of France and Algeria. Those localities were chosen because of their younger ages and also their availability, to study if the same interpretations could be made on sebecids from younger strata, which are of the upmost importance to understand their resilience to the K/Pg biological crisis and their subsequent disappearance during the Paleogene. However, as will be regularly highlighted throughout the section, the results presented here need to be taken with caution, mainly because of the low number of samples studied, and must be taken more as preliminary interpretations. One of the reasons to explain that is that the successful analyses of complete fossil faunas require a thorough sampling of the fossil organisms, which mostly depends on the accessibility to those remains, as well as efficiency in pre-treatment chemical protocols. Furthermore, the samples analysed must not be diagenetically altered to be able to make paleoecological interpretations. Finally, it is also very time-costly: for example, the chemical preparation of silver phosphates associated with the measurements of $\delta^{18}O_p$ values lasts four days for eight to sixteen samples and the pre-treatment protocol of samples for the measurements of calcium and strontium isotope compositions also lasts four days for up to 24 samples. Finally, the measurement phase can also be time-consuming especially for calcium isotope compositions where the setting of the MC-ICP-MS (i.e., before any measurements can be made) often takes several days as well. The datasets with

all the values measured in the three localities are available here: https://mycore.core-cloud.net/index.php/s/7mCKw8rLbck2qh3 and all details for the samples are available in Appendix 6.

a- Presentation of the localities

The locality of Réalmont is in the Paleogene basin of the Castrais Area, along the eastern margin of the Castrais Area, in southwestern France (Fig. 4.18). This fauna dates back to the Bartonian (Mammal Paleogene or MP16; Escarguel *et al*., 1997; Martin, 2014, 2016; Remy, 2015) and has yielded mammals (Vasseur, 1894; Remy, 2015), turtles and diapsids (Vasseur, 1894; Martin *et al*., 2023).

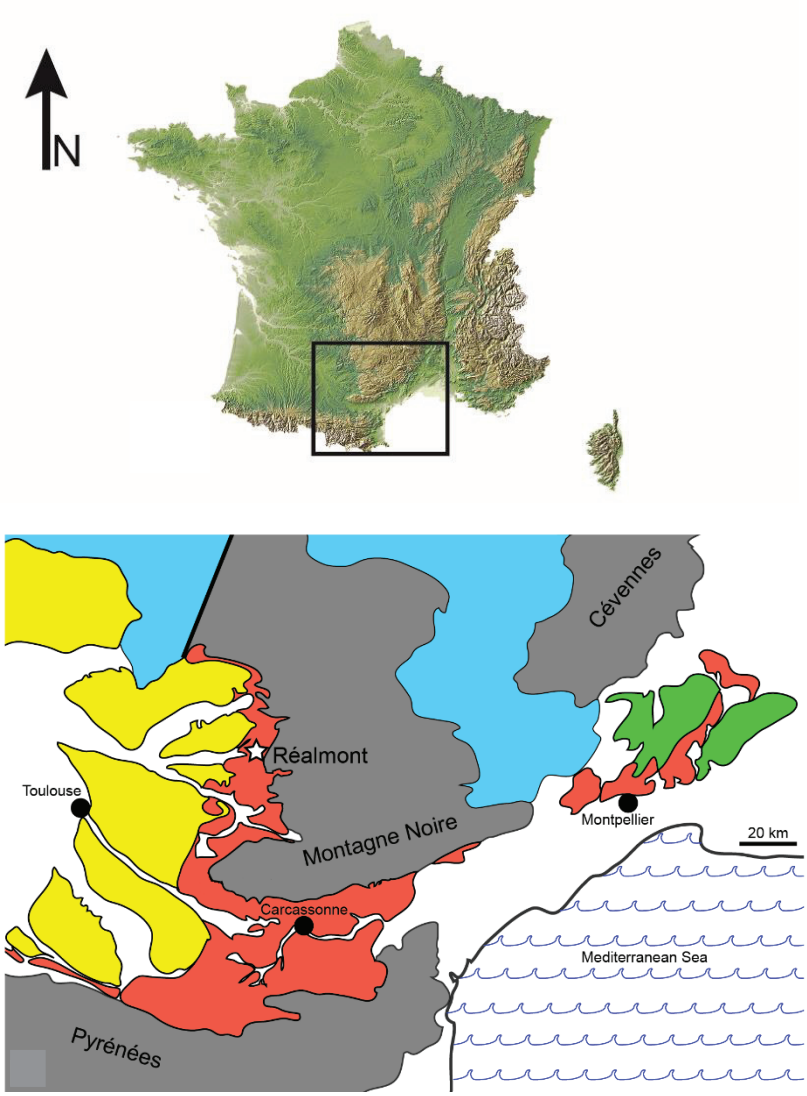

Figure 4.18: Geographical and geological context of the locality of Réalmont (France). Top: area of interest in southern France. Bottom: simplified geological map of the area. Plain gray: basement rock; blue dashes: marine Jurassic deposits; green points: continental Cretaceous deposits; orange crosses: Paleogene deposits; yellow oblique lines: Neogene deposits; white: Quaternary deposits. Modified from Martin *et al*. (2023; fig. 1).

The locality of Aumelas is in the lacustrine limestones of Montpellier, in southern France (Fig. 4.19). This fauna dates back to the Ypresian/Lutetian boundary (before MP13; Remy *et al*., 2019; Luccisano *et al*., 2020) and has yielded a diverse fauna of vertebrates (Hartenberger, 1963; Sudre, 1980; Remy *et al*., 2016, 2019; Luccisano *et al*., 2020).

The locality of El Kohol is in the Paleogene of Algeria, near the city of Brezina (Fig. 4.20). This fauna dates back to the Ypresian (between -52 and -51 Ma; Coster *et al*., 2012) and has yielded invertebrates (Mahboubi *et al*., 1984a), mammals (Mahboubi *et al*., 1984a, b, 1986, 2014; Court, 1994), turtles, fishes, amphibians, as well as a putative sebecid *Eremosuchus elkoholicus* Buffetaut, 1989 (Buffetaut, 1982a, 1989) and a diverse flora (Mahboubi *et al*., 1984a). Furthermore, some oxygen and carbon stable isotope compositions of carbonate apatite have already been measured on *Numidotherium koholense* Mahboubi, Ameur, Crochet & Jaeger, 1986 (Mahboubi *et al*., 2014).

b- Sample collections

In Réalmont, six samples of fossil tooth enamel of mammals and four samples of fossil bone of crocodylomorphs and turtles were analysed for their oxygen isotope composition of apatite phosphate ($\delta^{18}O_p$), oxygen ($\delta^{18}O_c$) and carbon ($\delta^{13}C$) isotope composition of apatite carbonate, calcium isotope composition ($\delta^{44/42}Ca$), radiogenic strontium isotope ratio ($^{87}Sr/^{86}Sr$) and elemental concentrations. One crocodylomorph sample comes from the splenial of a recently redescribed sebecid (*Dentaneosuchus crassiproratus*; Martin *et al*., 2023), while the other comes from a fragment of an unidentified crocodylomorph (possibly planocraniid). Mammal samples belong to the taxa *Palaeotherium* Cuvier, 1804 sp. and *Lophiodon* Cuvier, 1822 sp.

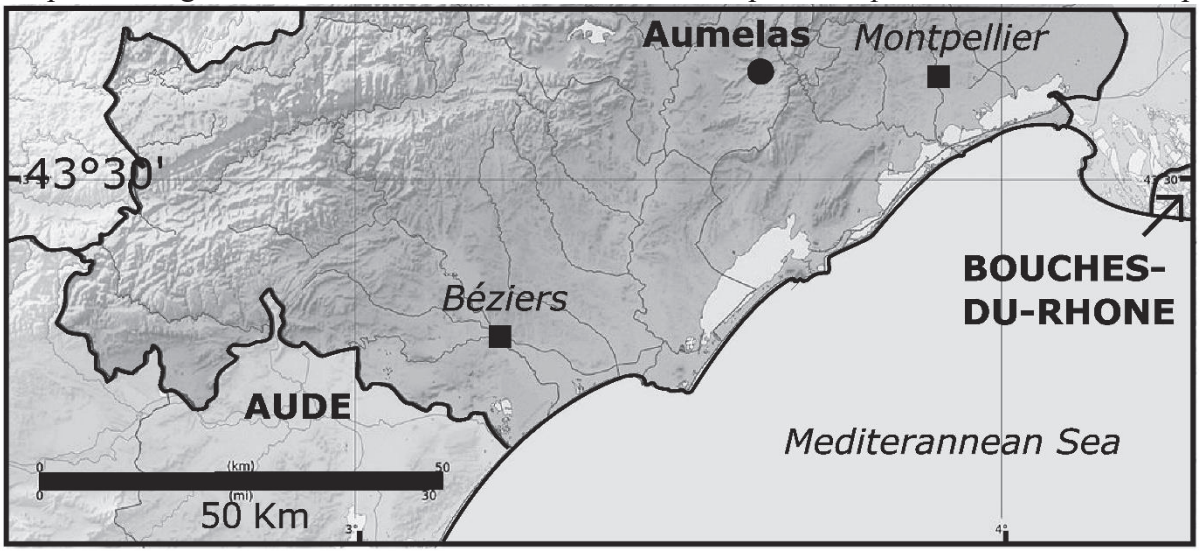

Figure 4.19: Map of Hérault (southern France) showing the location of the Aumelas locality. Modified from Luccisano *et al*. (2020; fig. 1).

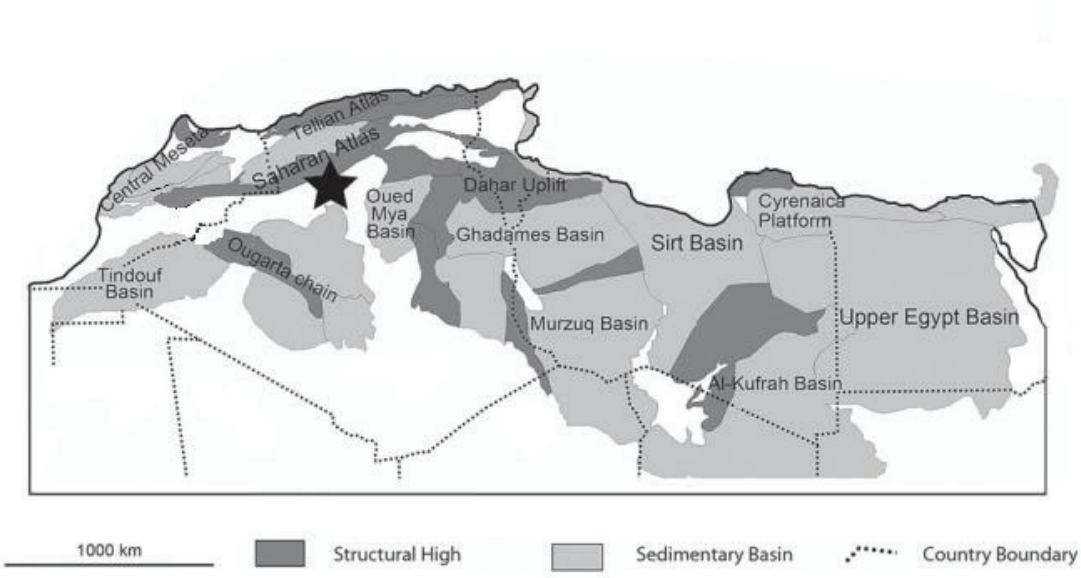

Figure 4.20: Location of the El Kohol locality indicated with a star among sedimentary basins and tectonic elements of North Africa. Modified from Coster *et al*. (2012; fig. 1).

which are inferred as browsers (Joomun *et al*., 2008). The tooth type sampled is unknown but most probably corresponds to molars. The taxonomic attribution of the turtle samples is also unknown.

In Aumelas, five samples of fossil tooth enamel (and dentine when not enough material was available) of mammals, three samples of fossil bone of crocodylomorphs and turtles and four samples of scale enamel and tooth enamel (and dentine when not enough material was available) of fishes were analysed for their oxygen isotope composition of apatite phosphate ($\delta^{18}O_p$), oxygen ($\delta^{18}O_c$) and carbon ($\delta^{13}C$) isotope composition of apatite carbonate, calcium isotope composition ($\delta^{44/42}Ca$), radiogenic strontium isotope ratio ($^{87}Sr/^{86}Sr$) and elemental concentrations. The crocodylomorph sample comes from the osteoderm of an unknown crocodylomorph (possibly planocraniid). Mammal samples belong to the taxa *Propalaeotherium* Gervais, 1849 sp. and *Pachynolophus* Pomel, 1847 sp. which are inferred as browsers (Hellmund, 2005; Joomun *et al*., 2008). The tooth type sampled is unknown. The taxonomic attribution of the fish samples is also unknown. The two samples of turtle bone belong to Podocnemididae Cope, 1868 and *Palaeoemys* Schleich, 1994 which are both living in aquatic environment (Mayerl *et al*., 2016).

In El Kohol, three samples of fossil tooth enamel of mammals and two samples of fossil bone of crocodylomorph and turtle were analysed for their oxygen isotope composition of apatite phosphate ($\delta^{18}O_p$), oxygen ($\delta^{18}O_c$) and carbon ($\delta^{13}C$) isotope composition of apatite carbonate,

calcium isotope composition ($\delta^{44/42}Ca$), radiogenic strontium isotope ratio ($^{87}Sr/^{86}Sr$) and elemental concentrations. The crocodylomorph sample comes from *Eremosuchus elkoholicus* which has been inferred to be terrestrial based mainly on its ziphodont dentition (Buffetaut, 1982a, 1989; see also Chapter 1, IIIe). Mammal samples belong to the taxa *Numidotherium koholense* which is reconstructed with a plantigrade, semi-sprawling gait (Court, 1994) and a terrestrial lifestyle (Mahboubi *et al*., 2014). The tooth type sampled is unknown. The taxonomic attribution of the turtle sample is also unknown.

c- Results

1- Oxygen isotope compositions of apatite phosphate

In Réalmont, *Dentaneosuchus* Astre, 1931 and mammals have significantly higher $\delta^{18}O_p$ values (ranging from 21.0 to 23.0 ‰, mean 2 s.d. = 0.4 ‰, n = 7) than the other unidentified crocodylomorph and turtles (ranging from 18.2 to 19.0 ‰, mean 2 s.d. = 0.3 ‰, n = 3) under a Wilcoxon test (p-value = 0.02; Fig. 4.21 & 4.22).

In Aumelas, $\delta^{18}O_p$ values measured on mammals and the unknown crocodylomorph range from 19.3 to 21.4 ‰ (mean 2 s.d. = 0.3 ‰, n = 6) and differ significantly from those of turtles and fishes (ranging from 17.8 to 19.9 ‰, mean 2 s.d. = 0.3 ‰, n = 6) under a Wilcoxon test (p-value = 0.009; Fig. 4.23 & 4.24).

In El Kohol, mammals have the higher $\delta^{18}O_p$ values measured, ranging from 21.5 to 25.7 ‰ (mean 2 s.d. = 0.3, n = 3) but do not differ significantly from measured values in *Eremosuchus* Buffetaut, 1989 and the turtle (ranging from 17.8 to 18.8 ‰, mean 2 s.d. = 0.3 ‰, n = 2) under a Wilcoxon test (p = 0.2; Fig. 4.25 & 4.26).

2- Oxygen and carbon isotope compositions of apatite carbonate

In Réalmont, analysed samples have significantly different $\delta^{18}O_c$ values between mammals (ranging from 28.0 to 30.8 ‰, mean 2 s.d. = 0.5 ‰, n = 6) and the other groups of organisms (ranging from 25.0 to 27.5 ‰, mean 2 s.d. = 0.8 ‰, n = 4) under a Wilcoxon test (p-value = 0.01). $\delta^{13}C$ values range between -10.4 and -8.4 ‰ (mean 2 s.d. = 0.3 ‰, n = 10; Fig. 4.27).

In Aumelas, analysed samples have significantly different $\delta^{18}O_c$ values between mammals and turtles (ranging from 27.7 to 29.0 ‰, mean 2 s.d. = 0.7 ‰, n = 6) and the unknown crocodylomorph and fishes (ranging from 24.9 to 26.4 ‰, mean 2 s.d. = 0.6 ‰, n = 3) under a Wilcoxon test (p-value = 0.02). $\delta^{13}C$ values between mammals and the unknown

crocodylomorph (ranging from -10.4 to -7.2 ‰, mean 2 s.d. = 0.3 ‰, n = 6) and turtles and fishes (ranging from -6.7 to -4.7 ‰, mean 2 s.d. = 0.2 ‰, n = 3; Fig. 4.29) are significantly different under a Wilcoxon test (p-value = 0.02).

In El Kohol, analysed samples have $\delta^{18}O_c$ values ranging from 23.6 to 31.4 ‰ (mean 2 s.d. = 0.4 ‰, n = 5) with none of the groups of organisms sampled differing significantly from the others (Fig. 4.25). It is interesting to note that the $\delta^{18}O_c$ values measured for *N. koholense* are similar to those measured on tooth enamel in Mahboubi *et al*. (2014; ranging from 28.7 to 32.8 ‰) Although $\delta^{13}C$ values of mammals are higher (ranging from -8.2 to -7.2 ‰, mean 2 s.d. = 0.6 ‰, n = 3) than those of the turtle and the crocodylomorph (ranging from -11 to -11.6 ‰, mean 2 s.d. = 0.2 ‰, n = 2; Fig. 4.31), the difference is not significant under a Wilcoxon test (p-value = 0.2). It is also interesting to note that the $\delta^{13}C$ values measured in *N. koholense* are higher than those measured on tooth enamel in Mahboubi *et al*. (2014; ranging from -10.6 to -8.2, n = 9), and differ significantly under a Wilcoxon test (p-value = 0.03).

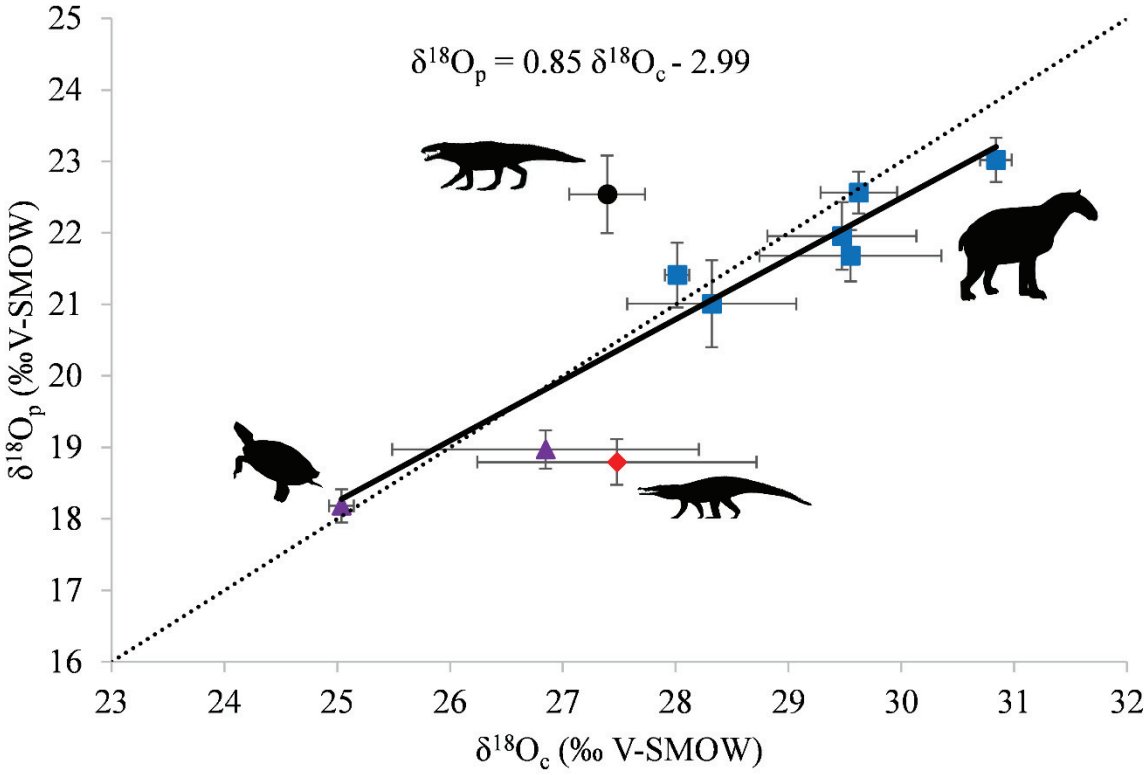

Figure 4.21: Oxygen isotope compositions of apatite phosphate reported against their corresponding oxygen isotope compositions of apatite carbonate in Réalmont. 2 s.d. for each sample are represented by bars. Black circle corresponds to *Dentaneosuchus crassiproratus*, blue squares to mammals, red diamond to the unknown crocodylomorph and purple triangles to turtles. Dashed line as a theoretical slope of 1. The shapes of the organisms are from phylopic.org.

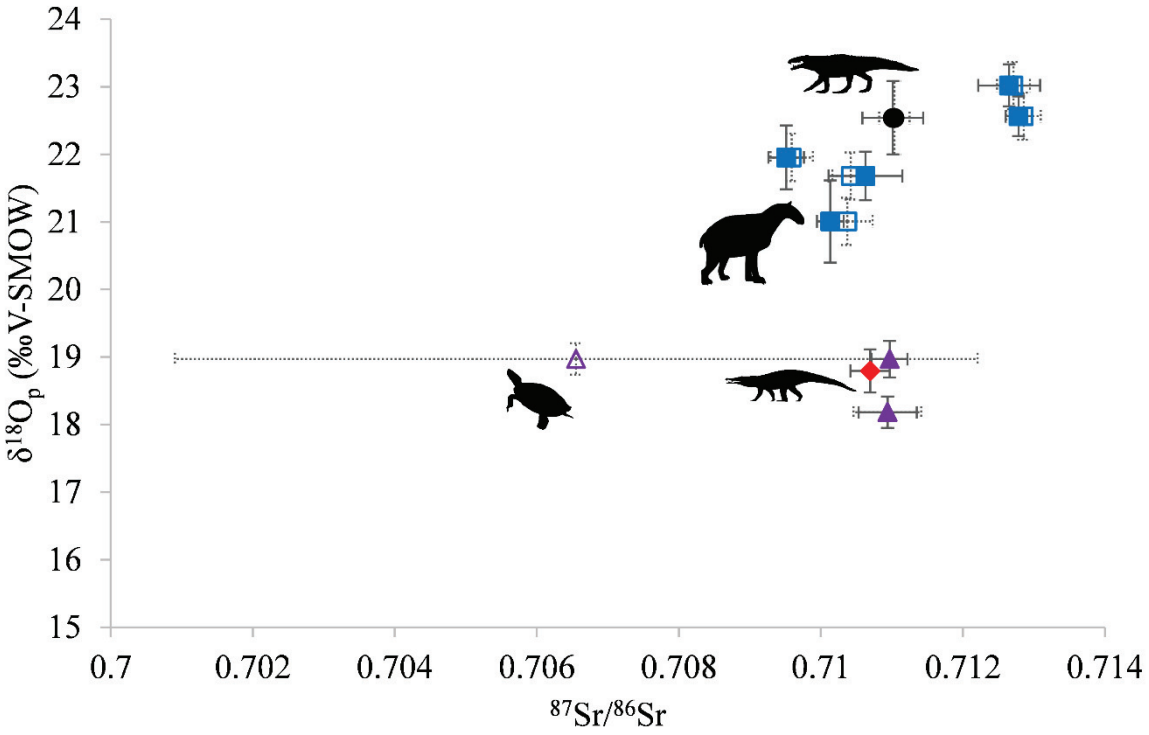

Figure 4.22: Oxygen isotope compositions of apatite phosphate reported against their corresponding strontium isotope compositions of vertebrate apatite in Réalmont. 2 s.d. for each sample are represented by bars. Black circle corresponds to *Dentaneosuchus crassiproratus*, blue squares to mammals, purple triangles to turtles and red diamond to the unknown crocodylomorph. Filled shapes and plain bars are leached samples, whereas empty shapes and dotted bars are unleached samples. The shapes of the organisms are from phylopic.org.

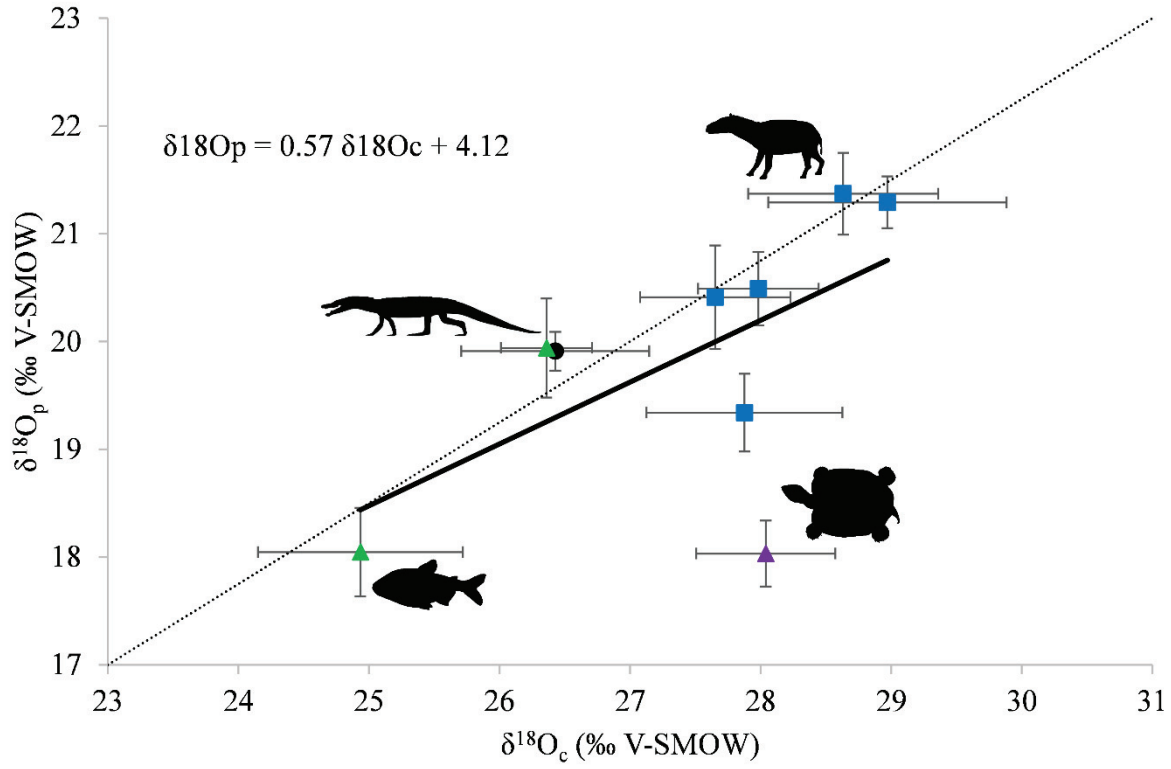

Figure 4.23: Oxygen isotope compositions of apatite phosphate reported against their corresponding oxygen isotope compositions of apatite carbonate in Aumelas. 2 s.d. for each sample are represented by bars. Black circle corresponds to the unknown crocodylomorph, blue squares to mammals, green triangles to fishes and purple triangle to the turtle. Dashed line as a theoretical slope of 1. The shapes of the organisms are from phylopic.org.

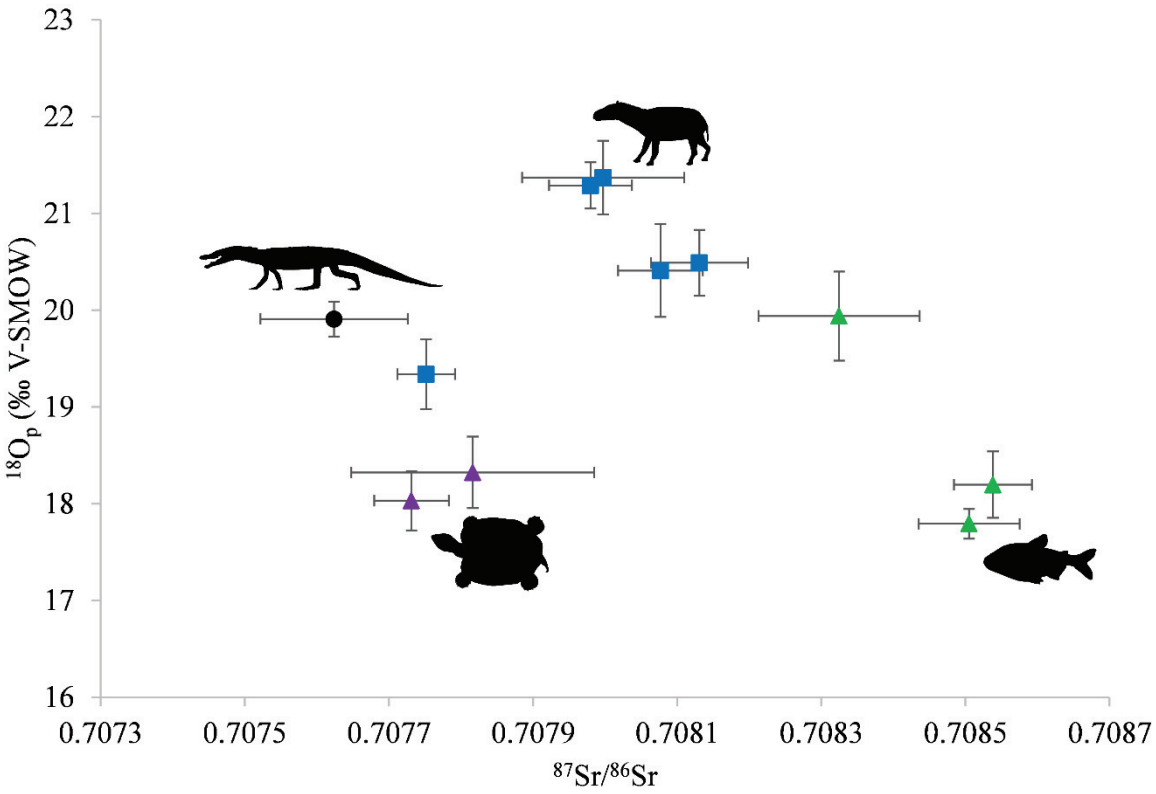

Figure 4.24: Oxygen isotope compositions of apatite phosphate reported against their corresponding strontium isotope compositions of vertebrate apatite in Aumelas. 2 s.d. for each sample are represented by bars. Black circle corresponds to the unknown crocodylomorph, blue squares to mammals, purple triangles to turtles and green triangles to the fishes. The shapes of the organisms are from phylopic.org.

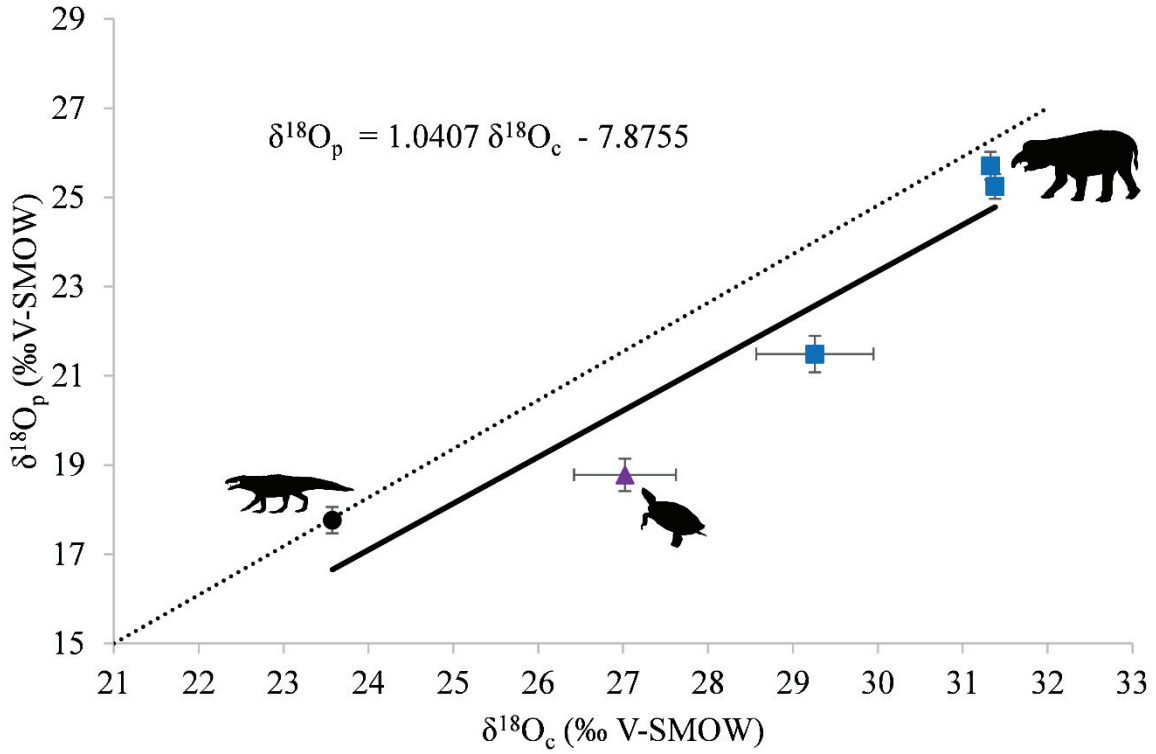

Figure 4.25: Oxygen isotope compositions of apatite phosphate reported against their corresponding oxygen isotope compositions of apatite carbonate in El Kohol. 2 s.d. for each sample are represented by bars. Black circle corresponds to *Eremosuchus*, blue squares to mammals, and purple triangle to the turtle. Dashed line as a theoretical slope of 1. The shapes of the organisms are from phylopic.org.

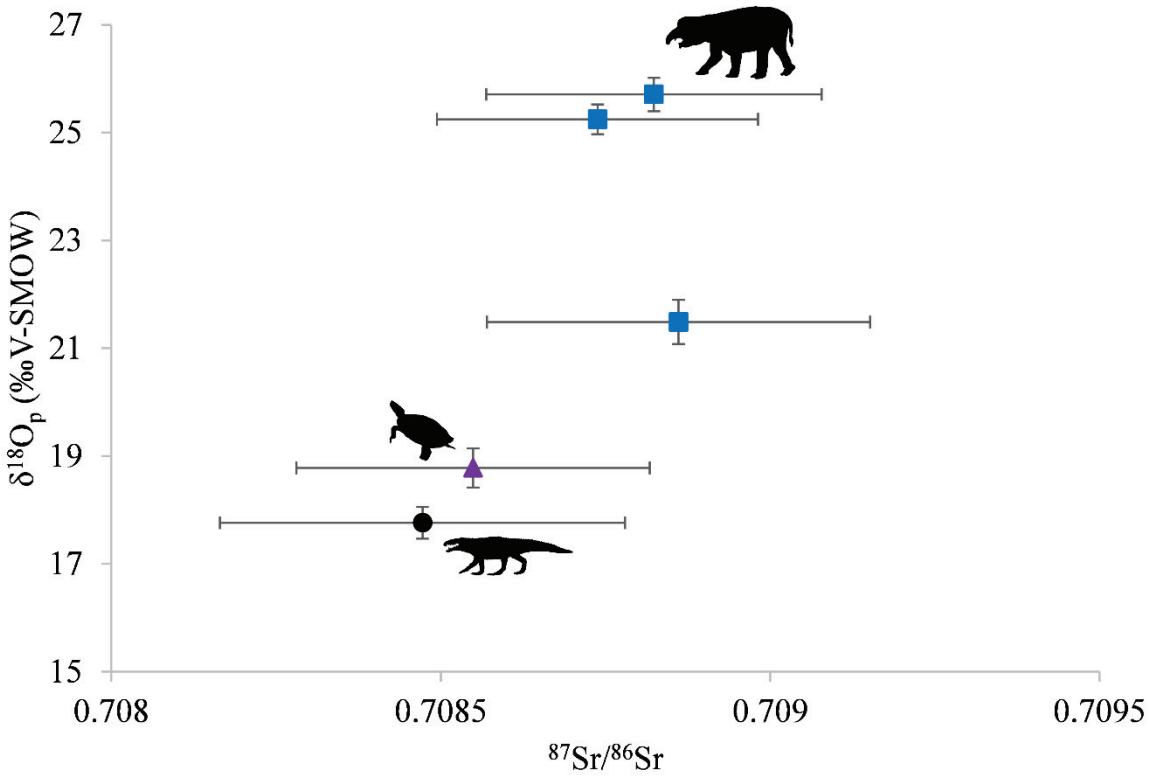

Figure 4.26: Oxygen isotope compositions of apatite phosphate reported against their corresponding strontium isotope compositions of vertebrate apatite in El Kohol. 2 s.d. for each sample are represented by bars. Black circle corresponds to *Eremosuchus*, blue squares to mammals and purple triangle to the turtle. The shapes of the organisms are from phylopic.org.

3- Calcium isotope compositions of vertebrate apatite

Blanks realized during purification protocols have been analysed with the MC-ICP-MS Neptune Plus. All blanks contained less than 150 ng of calcium. Thus, considering our measurement precision, our isotopic measurements are not affected by this nano-pollution. The mass dependency curve of the isotopic measurements follows the expected relation for calcium (Fig. 4.28, 4.30 & 4.32): in Réalmont, the slope value is 0.571 ± 0.06 (2 s.e., n = 20); in Aumelas, the slope value is 0.505 ± 0.05 (2 s.e., n = 12); and in Aumelas, the slope value is 0.471 ± 0.05 (2 s.e., n = 6). Those values agree with the 0.5067 slope predicted by the linear approximation of exponential mass-dependent fractionation and are in line with previously published values (Tacail *et al*., 2014, 2016, 2017; Martin *et al*., 2015, 2017a, b, 2022; Hassler *et al*., 2018, 2021a, b), supporting the accuracy of the measurements. The standard NIST-SRM1486 has a $\delta^{44/42}$Ca mean value of -0.95 ± 0.06 ‰ (2 s.e., n = 11) in Réalmont; -1.07 ± 0.01 ‰ (2 s.e., n = 3) in Aumelas; and -0.88 ± 0.10 ‰ (2 s.e., n = 3) in Aumelas. Those values are also in line with previously published values (Martin *et al*., 2015b; Hassler *et al*., 2018, 2021a, b; Dodat *et al*., 2021; Martin *et al*., 2022).

In Réalmont, mammal samples have $\delta^{44/42}$Ca values (ranging from -1.21 to -0.88 ‰, mean 2 s.d. = 0.10 ‰, n = 12) that are significantly lower than the others (ranging from -0.86 to -0.53 ‰, mean 2 s.d. = 0.11 ‰, n = 6; Fig. 4.27) under a Wilcoxon test (p-value = $8.7.10^{-4}$).

In Aumelas, the $\delta^{44/42}$Ca values of the samples range from -1.64 to -0.68 ‰ (mean 2 s.d. = 0.12 ‰, n = 11) with none of the sampled groups of organisms significantly differing from the others (Fig. 4.29).

In El Kohol, the $\delta^{44/42}$Ca values of the samples range from -1.26 to -0.61 ‰ (mean 2 s.d. = 0.06 ‰, n = 5) with mammals having lower values than the turtle and *Eremosuchus* (Fig. 4.31), although this difference is not significant under a Wilcoxon test (p-value = 0.2).

4- Radiogenic strontium isotope compositions of vertebrate apatite

The standard NIST-SRM1486 has a mean $^{87}Sr/^{86}Sr$ value of 0.709200 ± $3.13.10^{-5}$ (2 s.e., n = 2) in Réalmont; 0.708489 ± $1.47.10^{-3}$ (2 s.e., n = 1) in Aumelas; and 0.709344 ± $2.17.10^{-4}$ (2 s.e., n = 1) in El Kohol. The standard NIST-SRM987 has a mean $^{87}Sr/^{86}Sr$ value of 0.710256 ± $8.53.10^{-6}$ (2 s.e., n = 10) in Réalmont; 0.710256 ± $3.08.10^{-4}$ (2 s.e., n = 33) in Aumelas; and 0.710256 ± $3.91.10^{-5}$ (2 s.e., n = 27) in El Kohol. Those values are in line with previously published values (Clemens *et al*., 1993; McArthur *et al*., 2001; Faure & Mensing, 2005; Galler

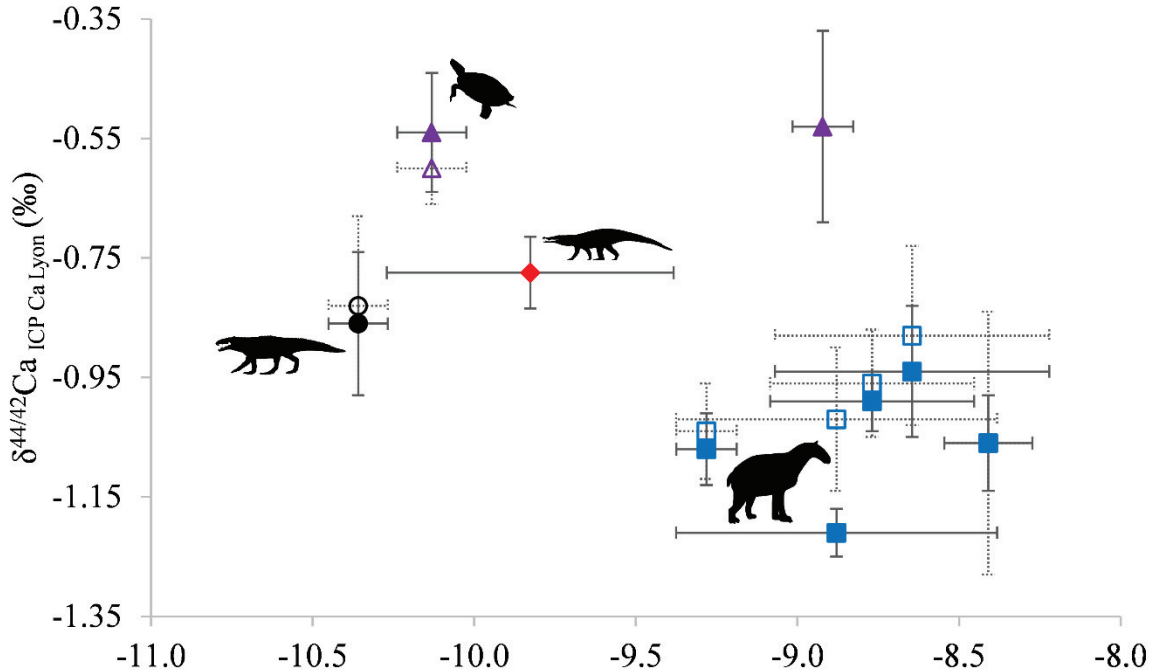

Figure 4.27: Calcium isotope compositions of vertebrate apatite reported against their corresponding carbon isotope compositions of apatite carbonate in Réalmont. 2 s.d. for each sample are represented by bars. Black circles correspond to *Dentaneosuchus crassiproratus*, blue squares to mammals, purple triangles to turtles and red diamond to the unknown crocodylomorph. Filled shapes and plain bars are leached samples, whereas empty shapes and dotted bars are unleached samples. The shapes of the organisms are from phylopic.org.

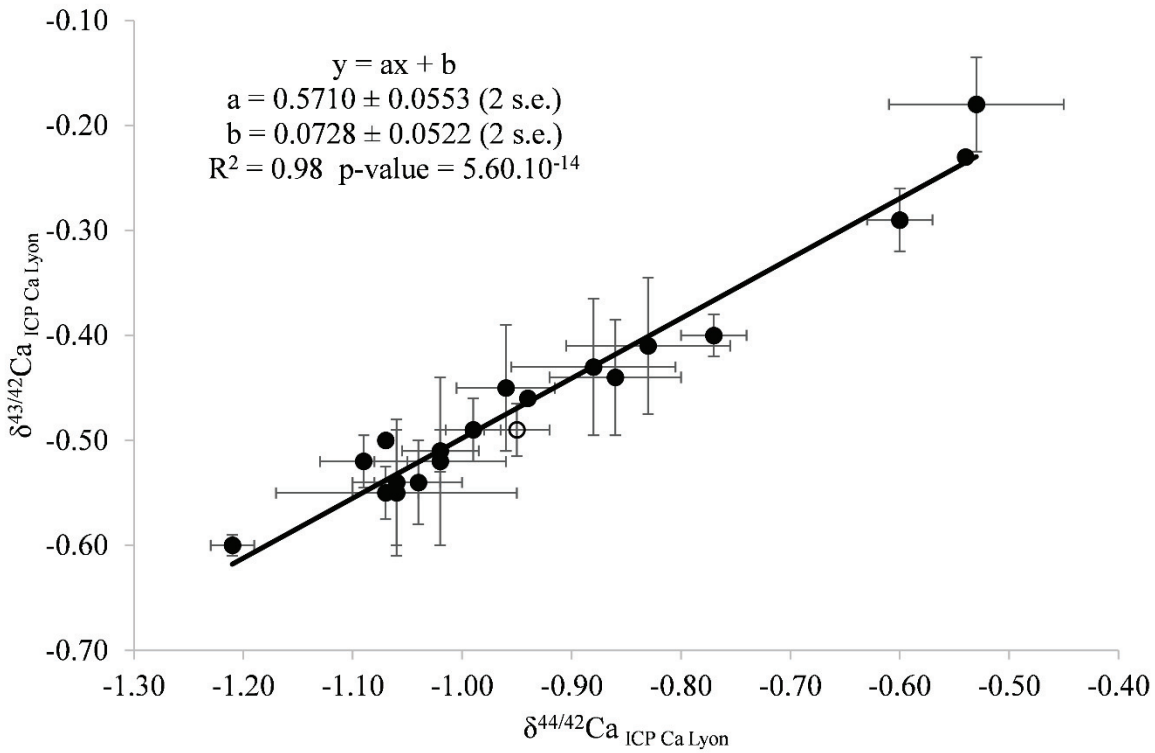

Figure 4.28: $\delta^{43/42}Ca$ values plotted against $\delta^{44/42}Ca$ values for all samples (black circles) and standards (white circles) studied in Réalmont.

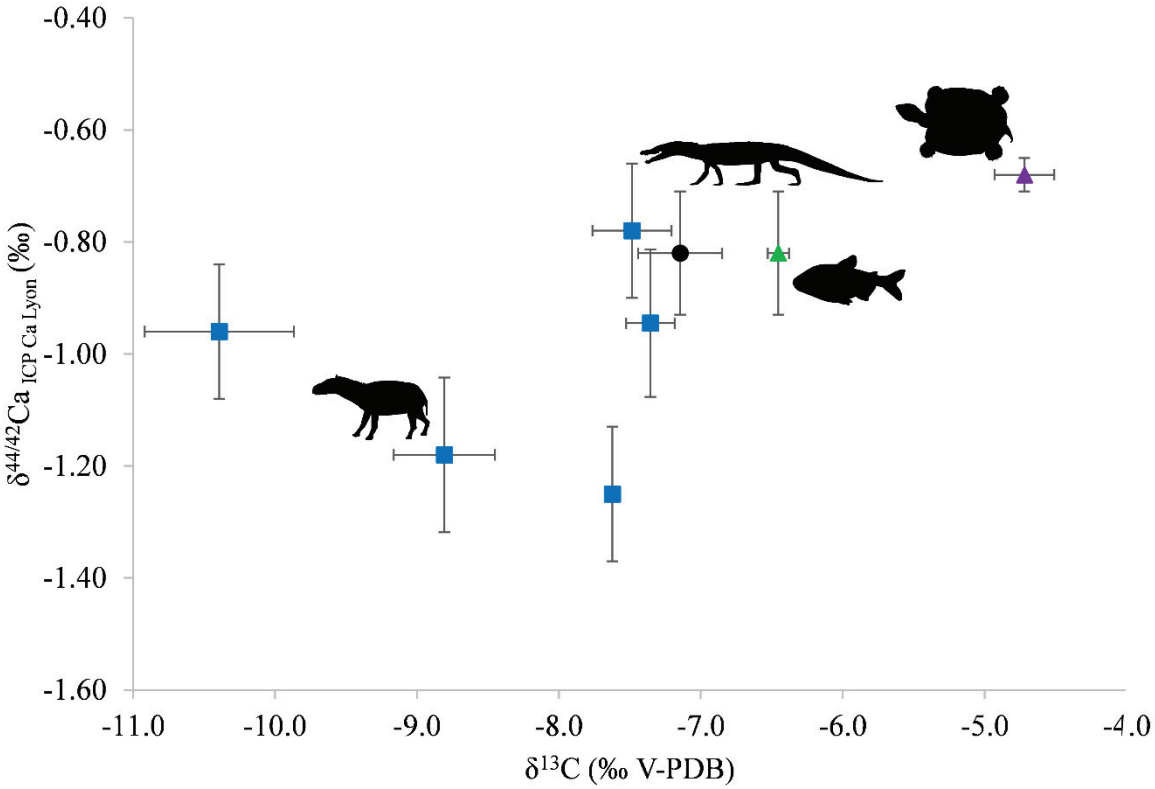

Figure 4.29: Calcium isotope compositions of vertebrate apatite reported against their corresponding carbon isotope compositions of apatite carbonate in Aumelas. 2 s.d. for each sample are represented by bars. Black circle corresponds to the unknown crocodylomorph, blue squares to mammals, purple triangle to the turtle and green triangle to the fish. The shapes of the organisms are from phylopic.org.

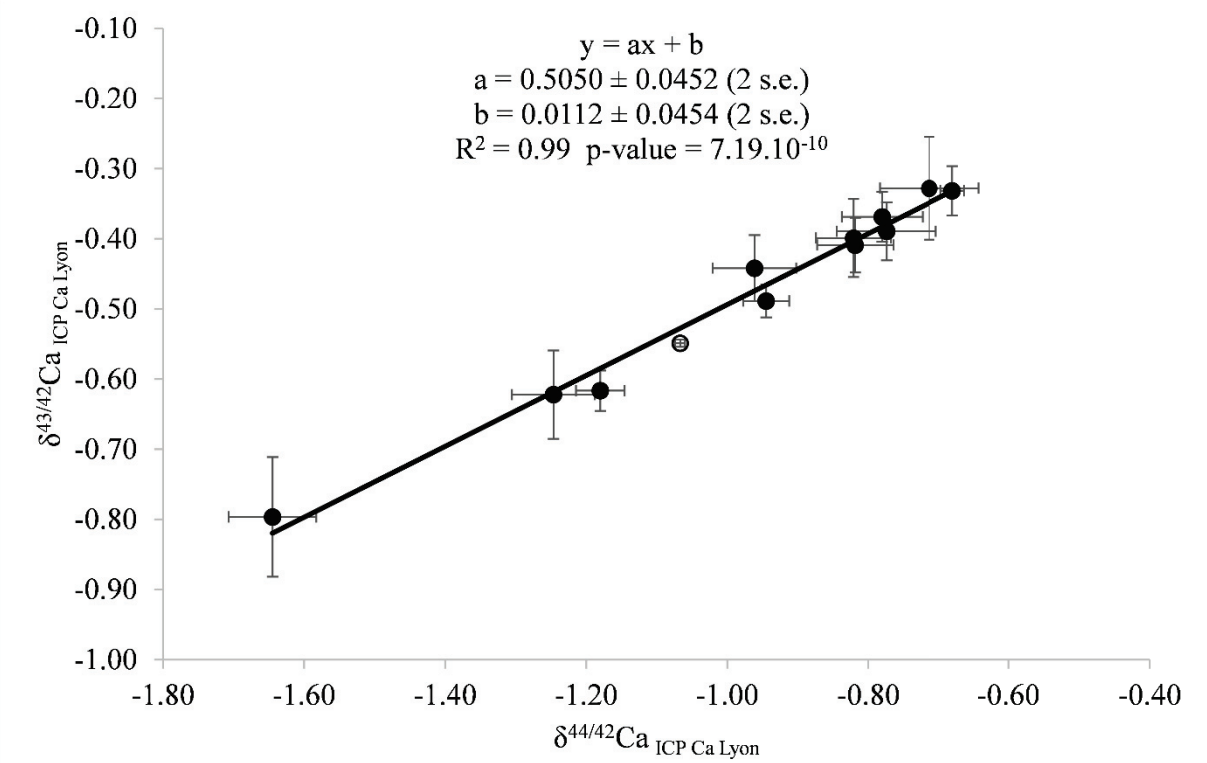

Figure 4.30: $\delta^{43/42}Ca$ values plotted against $\delta^{44/42}Ca$ values for all samples (black circles) and standards (white circles) studied in Aumelas.

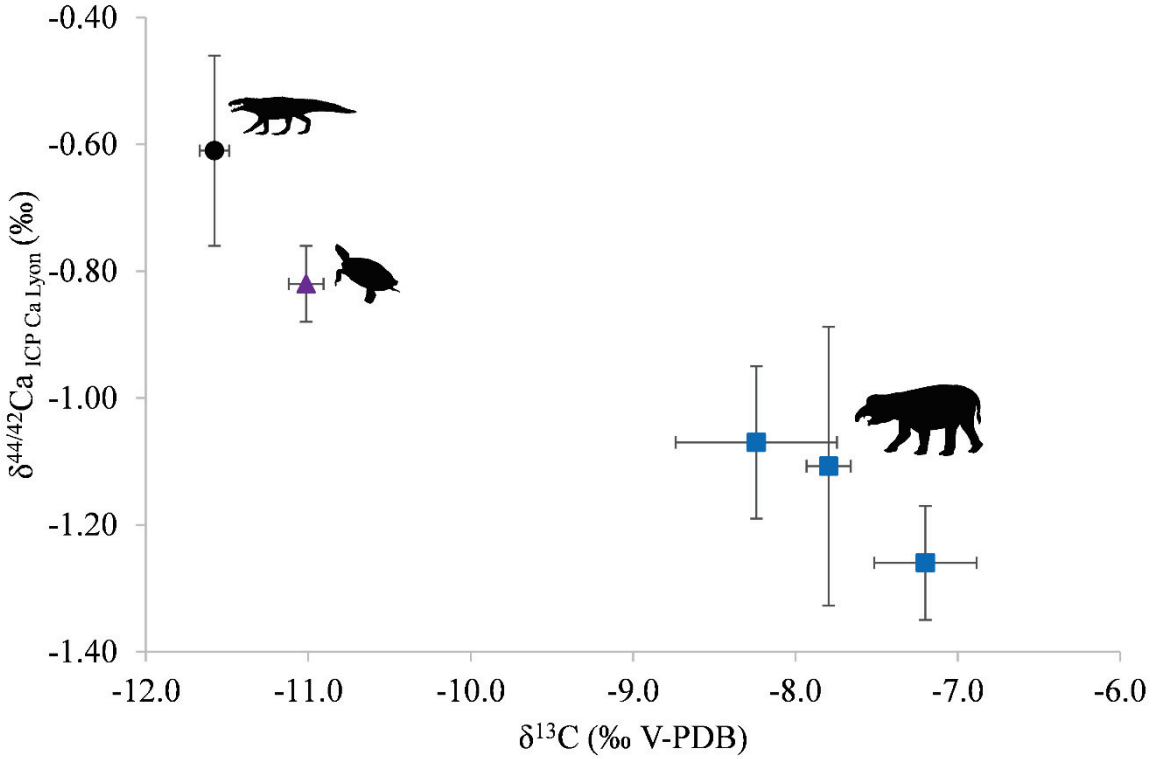

Figure 4.31: Calcium isotope compositions of vertebrate apatite reported against their corresponding carbon isotope compositions of apatite carbonate in El Kohol. 2 s.d. for each sample are represented by bars. Black circle corresponds to *Eremosuchus*, blue squares to mammals and purple triangle to the turtle. The shapes of the organisms are from phylopic.org.

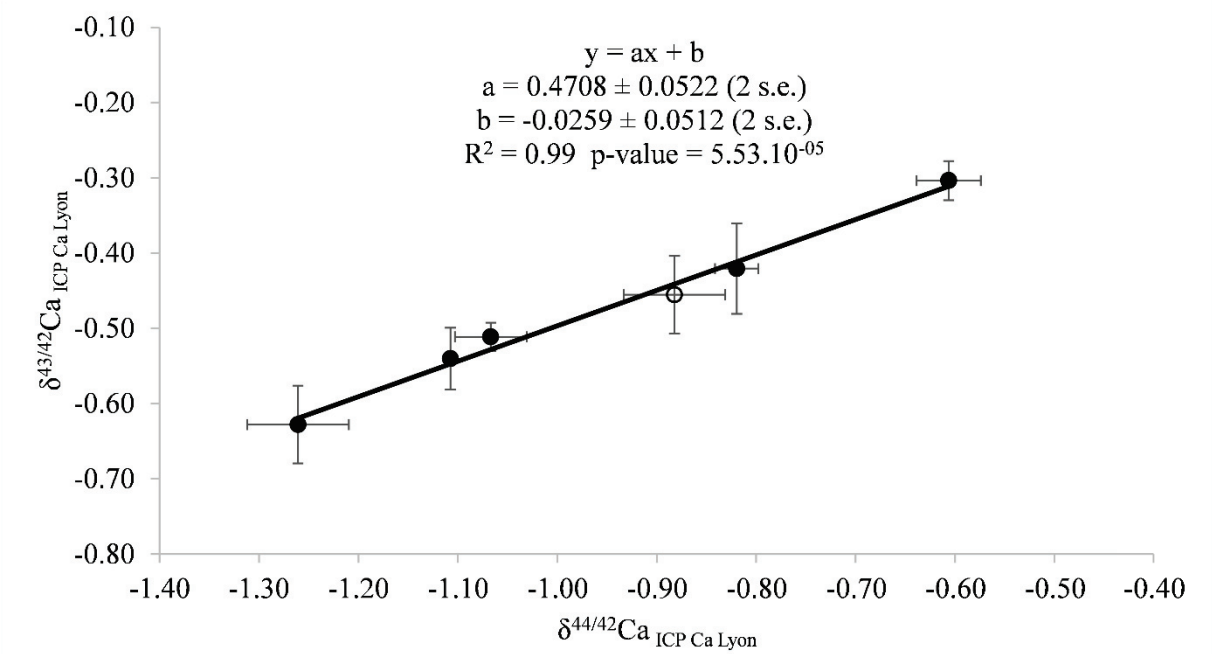

Figure 4.32: $\delta^{43/42}Ca$ values plotted against $\delta^{44/42}Ca$ values for all samples (black circles) and standards (white circles) studied in El Kohol.

et al., 2007; De Muynck *et al*., 2009; Weber *et al*., 2017; Brazier *et al*., 2019; Guiserix *et al*., 2022).

In Réalmont, the $^{87}Sr/^{86}Sr$ values of vertebrate apatites range from 0.709514 to 0.712857 (mean 2 s.d. = $5.98.10^{-4}$, n = 22) and a value measured on a turtle bone can be considered as an analytical outlier because it has a huge standard deviation. Statistically, there are two groups of mammals which have significantly different $^{87}Sr/^{86}Sr$ values under a Wilcoxon test (p-value = 0.004) but those are not taxonomical groups.

In Aumelas, the $^{87}Sr/^{86}Sr$ values of fishes (ranging from 0.708325 to 0.708535, mean 2 s.d. = $7.86.10^{-5}$, n = 3) are significantly different from those of the other groups of organisms (ranging from 0.707624 to 0.708131, mean 2 s.d. = $8.23.10^{-5}$, n = 8) under a Wilcoxon test (p-value = 0.01).

The $^{87}Sr/^{86}Sr$ values measured in El Kohol range from 0.708472 to 0.708861 (mean 2 s.d. = $2.73.10^{-4}$) and none of the groups of organisms sampled differ significantly from the others.

5- Elemental concentrations

An important result is that mean ratio of calcium versus phosphorus is 2.15 ± 0.32 2 s.d., n = 10 (molar ratio = 1.68 ± 0.25 2 s.d., n = 10) in Réalmont; 2.19 ± 1.00 2 s.d., n = 12 (molar ratio

= 1.69 ± 0.77 2 s.d., n = 12) in Aumelas; and 1.89 ± 0.59 2 s.d., n = 5 (molar ratio = 1.47 ± 0.46 2 s.d., n = 5) in El Kohol. This suggests that the stoichiometry of bioapatite is preserved.

d- Interpretations

1- Assessing the impact of diagenesis on the isotope compositions

As a prerequisite to interpret isotopic data, we first must assess the state of isotopic preservation of the fossil samples studied. In Réalmont, the correlation between the $\delta^{18}O_p$ and $\delta^{18}O_c$ values is significant ($R^2 = 0.82$, p-value = $1.31.10^{-6}$); in El Kohol, the correlation between the $\delta^{18}O_p$ and $\delta^{18}O_c$ values is also significant ($R^2 = 0.94$, p-value = $8.81.10^{-5}$). The slopes are close to unity, so the isotope compositions measured are preserved to a certain degree. In Aumelas, the correlation between the $\delta^{18}O_p$ and $\delta^{18}O_c$ values is significant ($R^2 = 0.86$, p-value = 0.003) if sample Aum1761 (podocnemidid bone) is removed. The isotope compositions of all the other samples are thus preserved to a certain degree, while Aum1761 will not be used in oxygen and carbon isotope interpretations.

Using the elemental concentrations measured on each sample, we obtain a calcium/phosphorus ratio of 2.15 ± 0.32 (2 s.d., n = 10) in Réalmont (except Rea 7 whose elemental concentrations could not be measured); 2.19 ± 1.00 (2 s.d., n = 12) in Aumelas; and 1.89 ± 0.59 (2 s.d., n = 5) in El Kohol. Those values are in line with those measured in modern animals (2.15 ± 0.26, 2 s.d.; Balter *et al*., 2001), fossil dinosaurs (2.3 ± 0.20, 2 s.d.; Hassler *et al*., 2018; 2.30 ± 0.12, 2 s.d.; Martin *et al*., 2022), Paleolithic remains (2.32 ± 0.19, 2 s.d.; Dodat *et al*., 2021) and samples from Tiupampa (2.12 ± 0.20, 2 s.d.; see II), bringing a further argument supporting the preservation of the fossils sampled here.

Among fossils from Réalmont, REE enrichment profiles (normalized to NASC, Haskin & Frey, 1966; Gromet *et al*., 1984; Fig. 4.33) are similar for each sample, except for Rea 4 and Rea 5 with anomalies in caesium and neodymium (Fig. 4.33A). Those samples are thus considered as allochthonous and not considered in all interpretations, while the others can be considered as autochthonous (Trueman, 2013). Among fossils from Aumelas and El Kohol, REE enrichment profiles (normalized to NASC, Haskin & Frey, 1966; Gromet *et al*., 1984; Fig. 4.34A & 4.35A) are similar for each sample. These can thus be considered as autochthonous (Trueman, 2013). Furthermore, none of those patterns are bell-shaped, indicating that the recrystallization processes were limited (Reynard *et al*., 1999; Lécuyer *et al*., 2004; Reynard & Balter, 2014).

In Réalmont, strontium concentrations are not correlated with lead, uranium, iron, manganese, or the sum of REE (Fig. 4.33B-F), and only with uranium in El Kohol (Fig. 4.35B-F), meaning that this element was not preferentially incorporated after the death of the organisms: the radiogenic strontium isotope compositions of those two faunas can thus be considered as reflecting those of the substrates or waters where the organisms lived. However, in Aumelas, although strontium concentrations are not correlated with lead, uranium, iron, they are correlated with manganese and the sum of REE (Fig. 4.34B-F), meaning that this element was also incorporated after the death of the organisms: the radiogenic strontium isotope compositions thus cannot be considered as reflecting entirely those of the substrates or waters where the organisms lived, and will thus not be interpreted in terms of living environments in

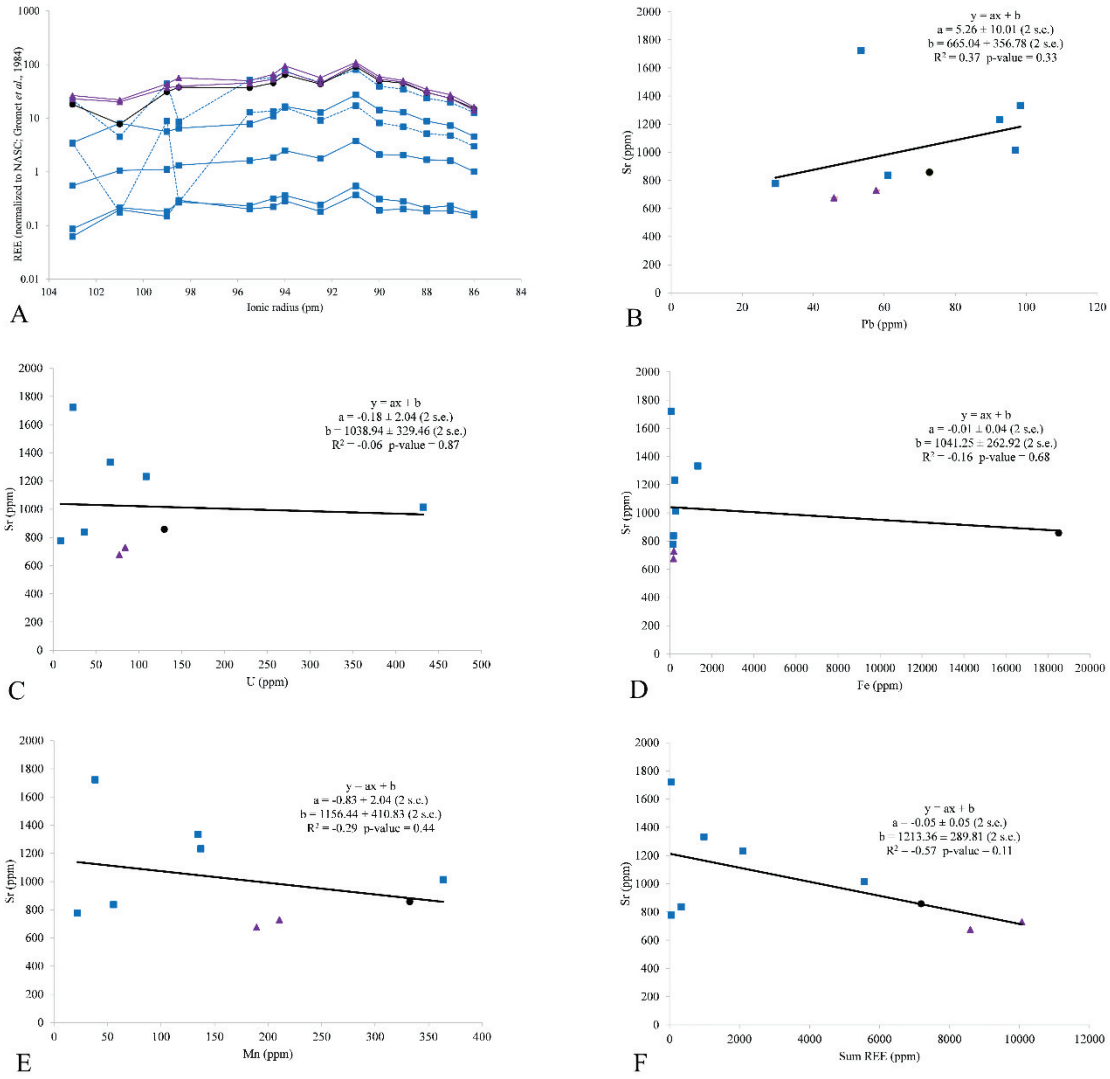

Figure 4.33: Diverse graphs highlighting the negligible impact of diagenesis on the samples in Réalmont. A: NASC normalized REE profiles of each sample from Réalmont. Concentrations are plotted on a logarithmic scale. Strontium concentration plotted against lead (B), uranium (C), iron (D), manganese (E) and sum of REE (F) concentrations. Black circles: *Dentaneosuchus crassiproratus*, blue squares: mammals, purple triangles: turtles.

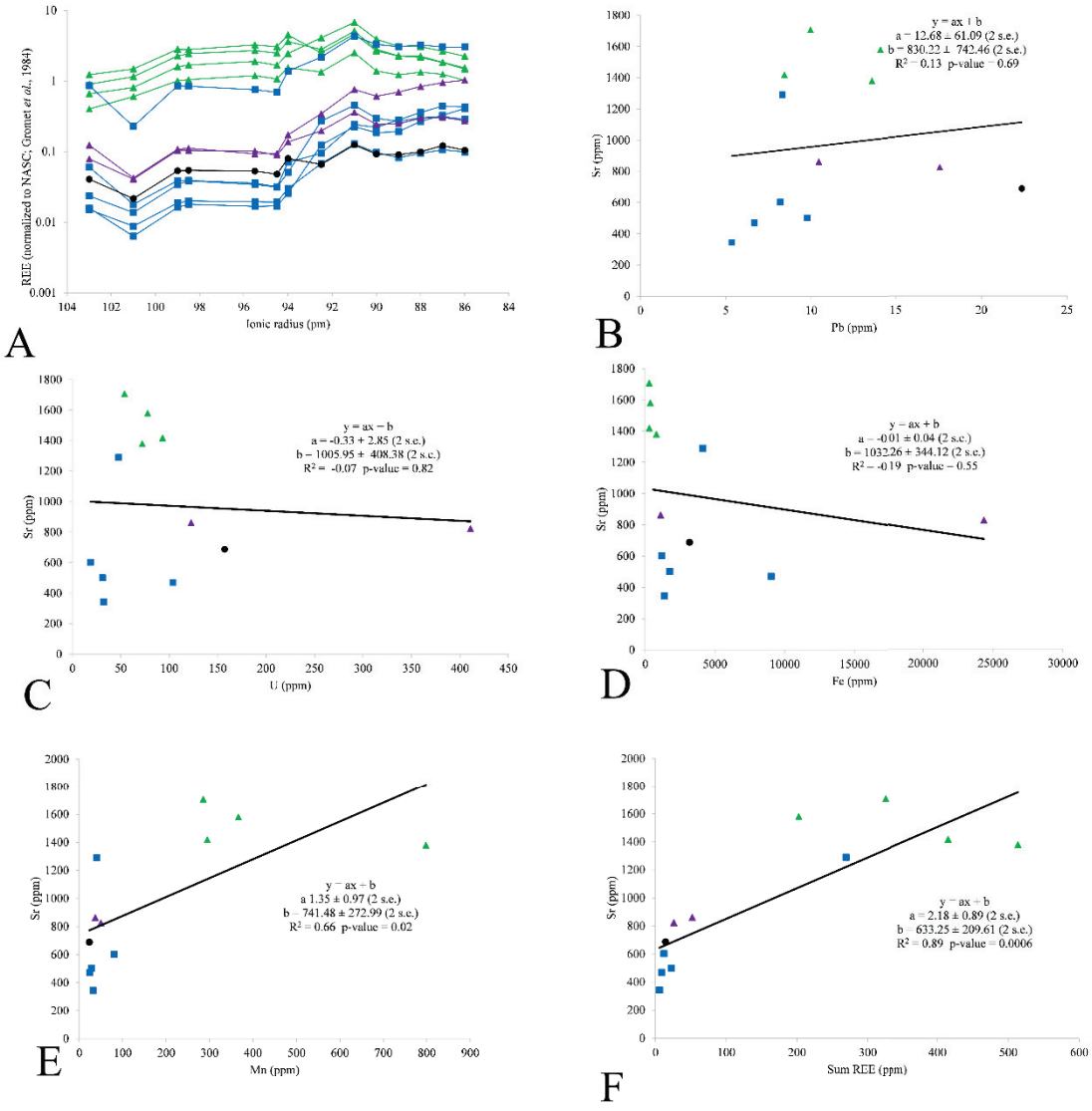

Figure 4.34: Diverse graphs highlighting the impact of diagenesis on the samples in Aumelas. A: NASC normalized REE profiles of each sample from Aumelas. Concentrations are plotted on a logarithmic scale. Strontium concentration plotted against lead (B), uranium (C), iron (D), manganese (E) and sum of REE (F) concentrations. Black circles: unknown crocodylomorph, blue squares: mammals, purple triangles: turtles, green triangles: fishes.

this fauna. Finally, lanthanum/ytterbium (La/Yb) and lanthanum/samarium (La/Sm) ratios for all samples fall within the range of modern freshwater samples (Fig. 4.36), indicating a moderate intensity of adsorption and substitutions processes (Reynard *et al.*, 1999; Reynard & Balter, 2014).

Given the high quantity of calcium in vertebrates samples (at least 15% of mass here), it is unlikely that the measured calcium isotopic compositions have been entirely overprinted by diagenetic processes, even if those were important. Also, in Réalmont, leached and non-leached samples display the same values in calcium and radiogenic strontium isotope compositions

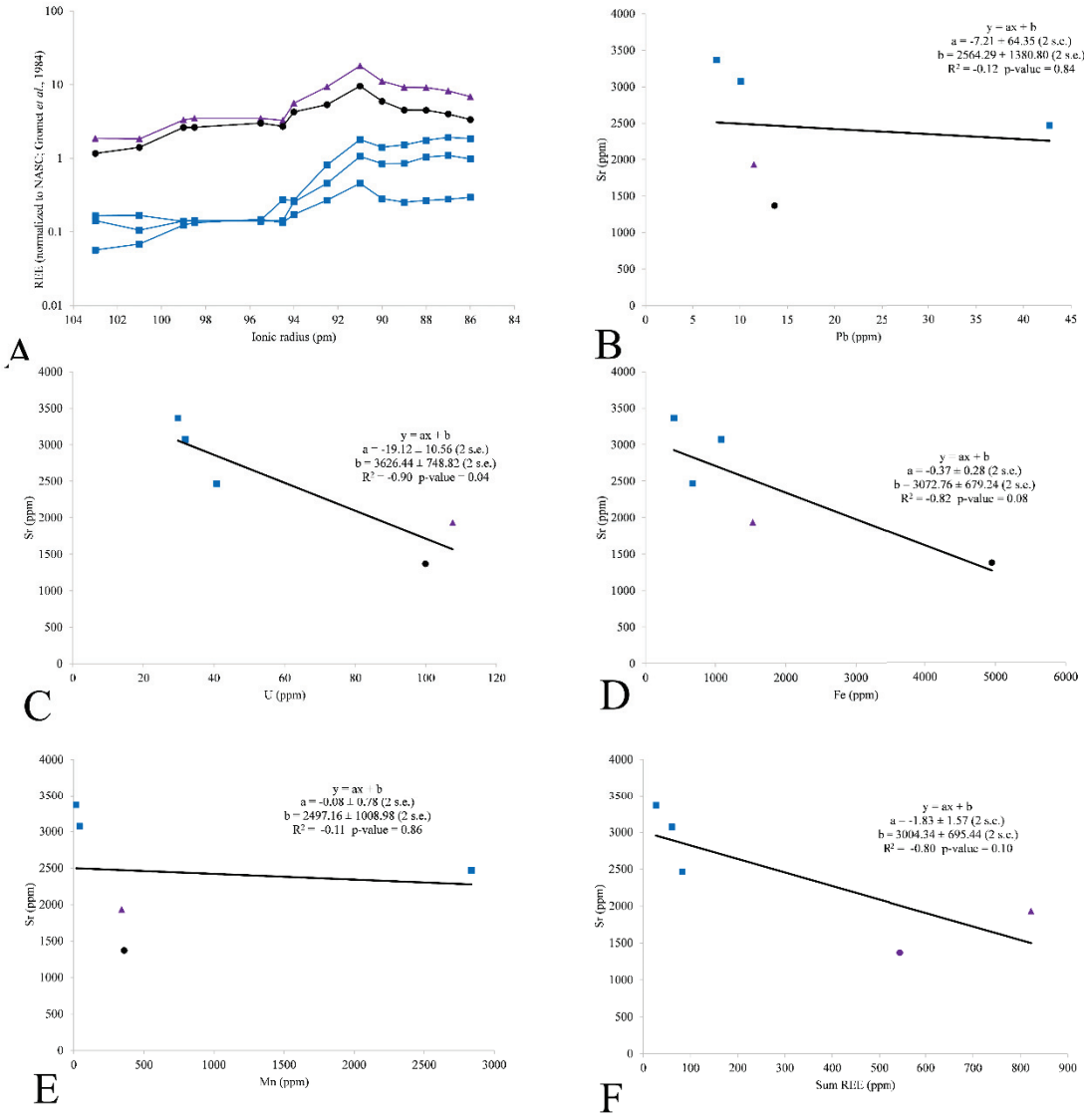

Figure 4.35: Diverse graphs highlighting the moderate impact of diagenesis on the samples in El Kohol. A: NASC normalized REE profiles of each sample from El Kohol. Concentrations are plotted on a logarithmic scale. Strontium concentration plotted against lead (B), uranium (C), iron (D), manganese (E) and sum of REE (F) concentrations. Black circles: *Eremosuchus elkoholicus*, blue squares: mammals, purple triangles: turtle.

(Wilcoxon test, p-value = 0.40, n = 8 and p-value = 0.86, n = 9 respectively), which is another argument for the weak impact of diagenesis on the samples from this fauna.

In summary, in Réalmont, there is no evidence for important diagenetic alteration of the elemental compositions of the samples analysed, in all the different isotopic systems used, except for Rea 4 and Rea 5. In Aumelas, while a single sample shows evidence of diagenetic alteration of its elemental compositions (Aum1761), the others do not. In El Kohol, there is no evidence for important diagenetic alteration of the elemental compositions of the samples analysed, in all the different isotopic systems used. As a result, associated isotope compositions

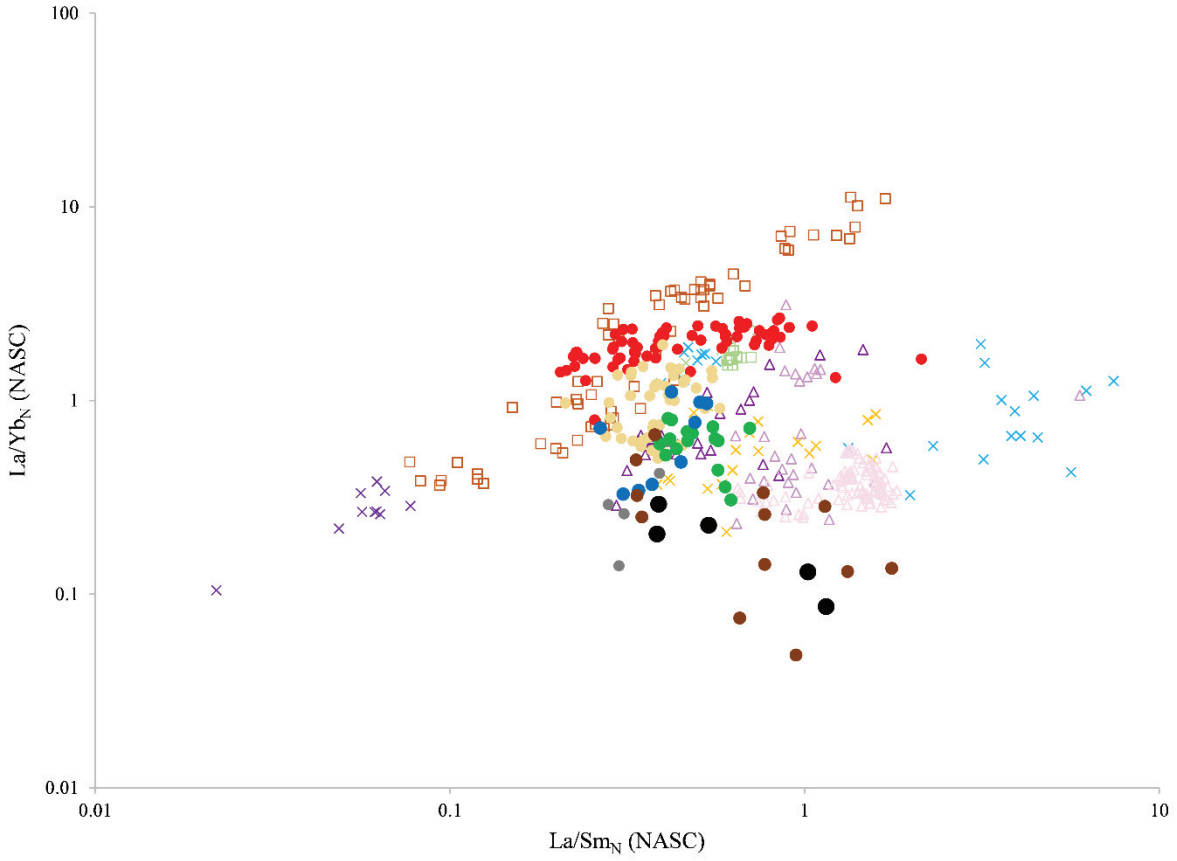

Figure 4.36: La/Sm$_N$ plotted against La/Yb$_N$ values (normalized to NASC; Haskin & Frey, 1966; Gromet *et al.*, 1984) for multiple fossil and extant apatite samples, as well as modern waters (Reynard & Balter, 2014, and references therein). Squares: conodonts, crosses: fishes, triangles: waters, circles: fossil faunas. Light brown: Devonian, light green: Silurian, light blue: Mesozoic - Cenozoic, yellow: Quaternary, dark purple: freshwaters, purple: estuarine and coastal waters, pink: ocean waters, red: Gadoufaoua fauna (Niger, middle Cretaceous; Hassler *et al.*, 2018), beige: Kem Kem fauna (Morocco, middle Cretaceous; Hassler *et al.*, 2018), grey: dinosaur communities (USA, late Cretaceous; Martin *et al.*, 2022), green: Tiupampa, dark blue: Réalmont, dark brown: Aumelas, black: El Kohol.

reported for those faunas are interpreted in terms of paleotrophic networks, paleoenvironments and thermophysiological abilities.

2- Thermophysiology

Using the equations presented in III, in Réalmont, I calculated that mammals and turtles have ingested the same ambient waters, with an average $\delta^{18}O_w$ value of -2.4 ± 1.3 ‰ (2 s.e., n = 6). As a result, when looking at the crocodylomorph samples studied here, it is a reasonable assumption that *Dentaneosuchus crassiproratus* and the unknown crocodylomorph either had a semi-aquatic (with an enrichment value between $\delta^{18}O$ values of ambient water and body water of 2 ‰) or a terrestrial lifestyle (with an enrichment value around 5.1 ‰). Those hypotheses are summarized in Figure 4.37. In the first case (Fig. 4.37A; semi-aquatic lifestyle), a mean body temperature ranging from 8 to 20°C (mean value = 14 ± 12°C, 2 s.d., n = 1) is inferred for

Dentaneosuchus crassiproratus, which is too low to be realistic, while a mean body temperature ranging from 23 to 37°C (mean value = 31 ± 12°C, 2 s.d., n = 1) is inferred for the unknown crocodylomorph and implies an ectothermic thermoregulation strategy for this specimen. In the second case (Fig. 4.37B; terrestrial lifestyle), a mean body temperature ranging from 22 to 34°C (mean value = 28 ± 12°C, 2 s.d., n = 1) is inferred for *Dentaneosuchus crassiproratus* and implies an ectothermic thermoregulation strategy for this specimen, while a mean body temperature ranging from 39 to 51°C (mean value = 45 ± 12°C, 2 s.d., n = 1) is inferred for the unknown crocodylomorph, which is too high to be realistic. Here, concerning *Dentaneosuchus*, the ectothermic regulations strategies inferred with independent histological approaches performed on notosuchians are once again confirmed (Cubo *et al*., 2020, 2022a), as well as the inferences made on the sebecids from the fauna of Tiupampa (see VII).

In Aumelas, I calculated that mammals and the turtle have ingested the same ambient water with an average $\delta^{18}O_w$ value of -3.2 ± 1.0 ‰ (2 s.e., n = 6). As a result, when looking at the crocodylomorph sample studied here, it is a reasonable assumption that it either had a semi-aquatic (with an enrichment value between $\delta^{18}O$ values of ambient water and body water of 2 ‰) or a terrestrial lifestyle (with an enrichment value around 5.1 ‰). Those hypotheses are summarized in Figure 4.38. In the first case (Fig. 4.38A; semi-aquatic lifestyle), a mean body temperature ranging from 18 to 27°C (mean value = 22 ± 10°C, 2 s.d., n = 1) is inferred for this crocodylomorph, implying an ectothermic thermoregulation strategy for this specimen. In the second case (Fig. 4.38B; terrestrial lifestyle), a mean body temperature ranging from 32 to 41°C (mean value = 37 ± 10°C, 2 s.d., n = 1) is inferred for the crocodylomorph and would rather imply an endothermic thermoregulation strategy for this specimen. Here, the thermoregulation strategy of the crocodylomorph from Aumelas would thus depend on its lifestyle, but those interpretations must be taken with extreme caution, given the very limited number of samples considered, and would benefit from further analyses.

In El Kohol, two sources of ambient water are identified: one involving two mammals with an average $\delta^{18}O_w$ value of 1.9 ± 0.7 ‰ (2 s.e., n = 2) and one involving a turtle and a mammal with an average $\delta^{18}O_w$ value of -2.5 ± 0.2 ‰ (2 s.e., n = 2). As a result, when looking at the sample from *Eremosuchus* studied here, it is a reasonable assumption that it either consumed one of the two sources of drinking water, and that it either had a semi-aquatic (with an enrichment value between $\delta^{18}O$ values of ambient water and body water of 2 ‰) or a terrestrial lifestyle (with an enrichment value around 5.1 ‰). Those hypotheses are summarized in Figure

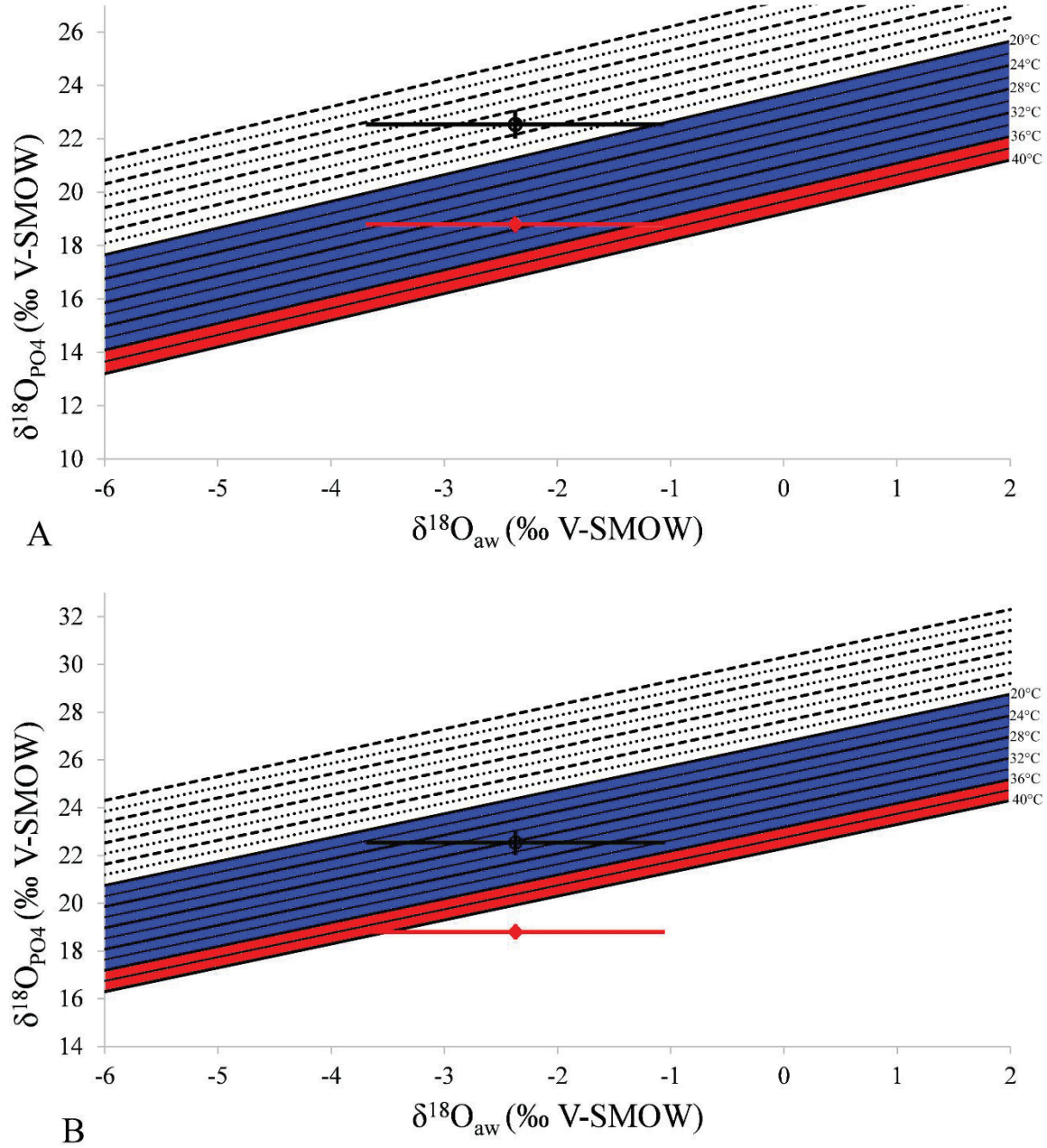

Figure 4.37: Crocodylomorph oxygen isotope compositions of apatite phosphate are plotted against their possible ambient water values ($\delta^{18}O_{aw}$) within a frame showing expected vertebrates $\delta^{18}O_p$ - $\delta^{18}O_{aw}$ relationships for a range of body temperatures (black lines) in Réalmont. The blue area represents the expected body temperature range for ectotherm modern crocodylians, whereas the red area represents the expected body temperatures range for modern endotherms. Black dot: *Dentaneosuchus crassiproratus*, red dot: unknown crocodylomorph. A: considering a semi-aquatic lifestyle, i.e., an enrichment value of 2 ‰, B: considering a terrestrial lifestyle, i.e., an enrichment value of 5.1 ‰.

4.39. In the first case (Fig. 4.39A; semi-aquatic lifestyle), a mean body temperature ranging from 34 to 36°C (mean value = 35 ± 2°C, 2 s.d., n = 1) is inferred for this crocodylomorph with the $\delta^{18}O_{aw}$ value of -2.5 ‰, implying a thermoregulation strategy at the limit between ectothermy and endothermy for this specimen, while a mean body temperature ranging from 52 to 58°C (mean value = 55 ± 6°C, 2 s.d., n = 1) is inferred with the $\delta^{18}O_{aw}$ value of 1.9 ‰, which

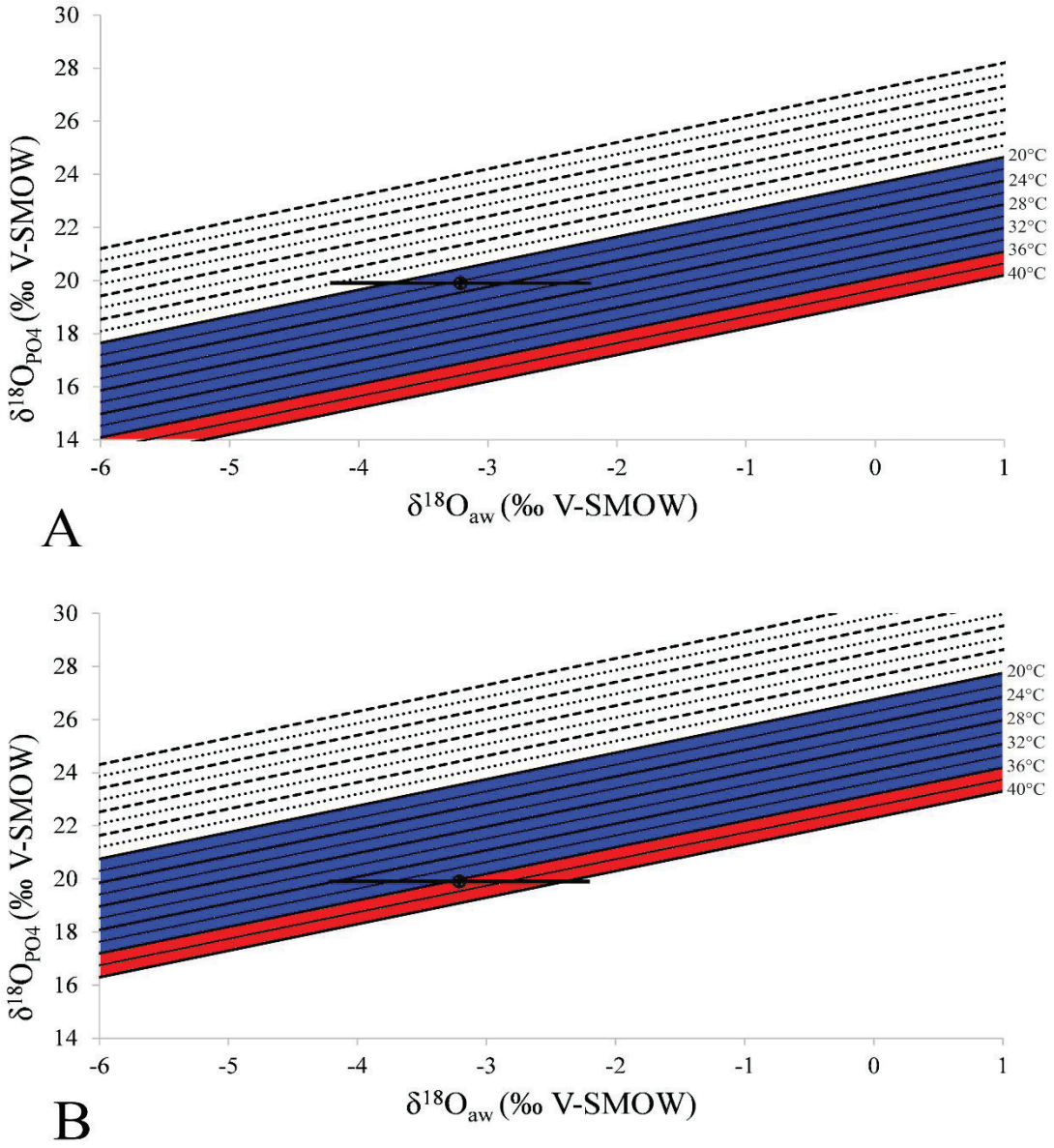

Figure 4.38: Crocodylomorph oxygen isotope compositions of apatite phosphate are plotted against their possible ambient water value ($\delta^{18}O_{aw}$) within a frame showing expected vertebrates $\delta^{18}O_p$ - $\delta^{18}O_{aw}$ relationships for a range of body temperatures (black lines) in Aumelas. The blue area represents the expected body temperature range for ectotherm modern crocodylians, whereas the red area represents the expected body temperatures range for modern endotherms. Black dot: unknown crocodylomorph from Aumelas. A: considering a semi-aquatic lifestyle, i.e., an enrichment value of 2 ‰, B: considering a terrestrial lifestyle, i.e., an enrichment value of 5.1 ‰.

is too high to be realistic. In the second case (Fig. 4.39B; terrestrial lifestyle), a mean body temperature ranging from 48 to 50°C (mean value = 49 ± 2°C, 2 s.d., n = 1) is inferred for the crocodylomorph with the $\delta^{18}O_{aw}$ value of -2.5 ‰, while a mean body temperature ranging from 66 to 72°C (mean value = 69 ± 6°C, 2 s.d., n = 1) is inferred with the $\delta^{18}O_{aw}$ value of 1.9 ‰. Those two ranges of values are also too high to be realistic. Here, the thermoregulation strategy of *Eremosuchus* is thus at the limit between ectothermy and endothermy, but, as in Aumelas,

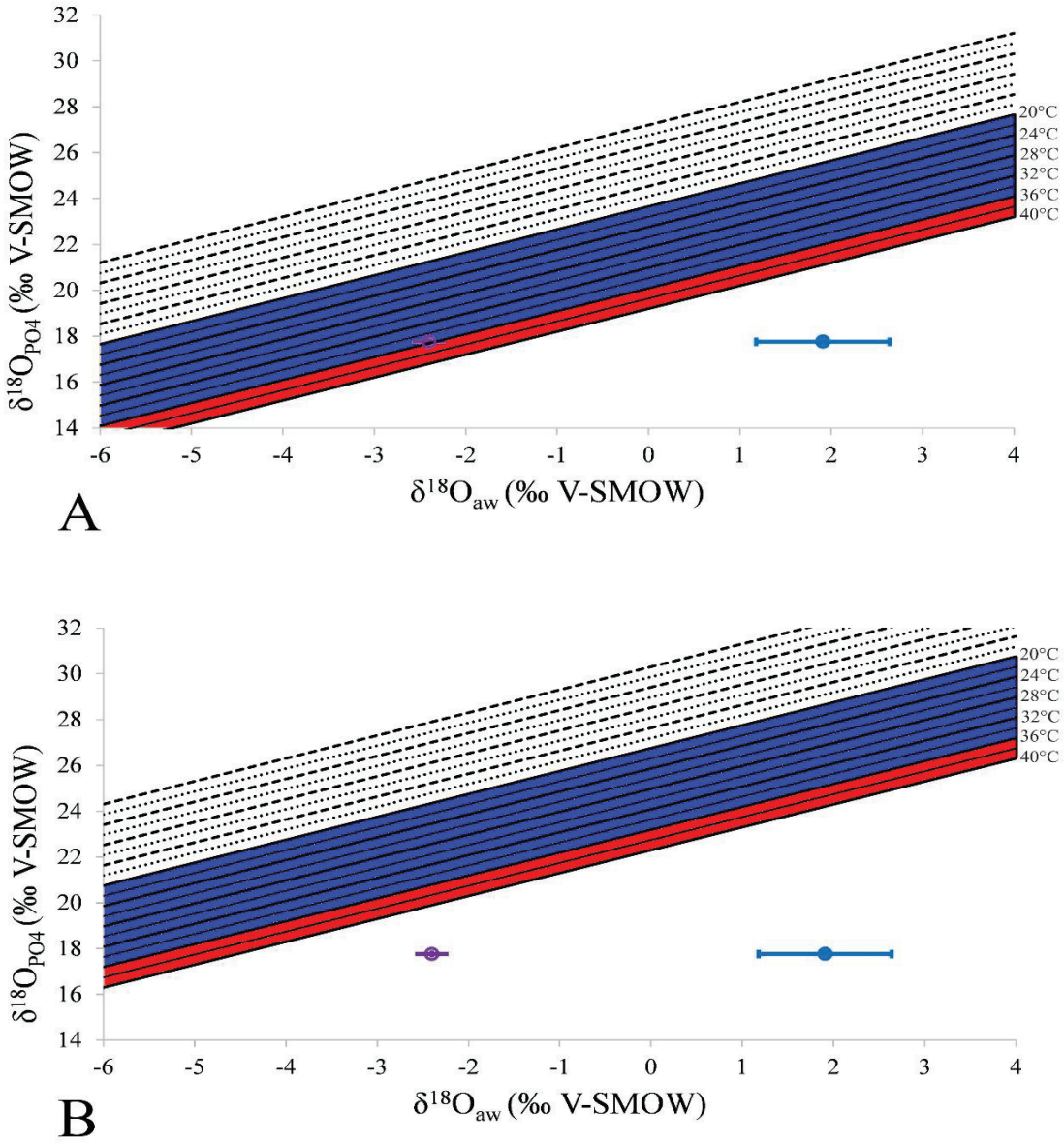

Figure 4.39: Crocodylomorph oxygen isotope compositions of apatite phosphate are plotted against their possible ambient water value ($\delta^{18}O_{aw}$) within a frame showing expected vertebrates $\delta^{18}O_p$ - $\delta^{18}O_{aw}$ relationships for a range of body temperatures (black lines) in El Kohol. The blue area represents the expected body temperature range for ectotherm modern crocodylians, whereas the red area represents the expected body temperatures range for modern endotherms. Purple dots: *Eremosuchus elkoholicus* with the $\delta^{18}O_{aw}$ value of -2.5 ‰, blue dots: *Eremosuchus elkoholicus* with the $\delta^{18}O_{aw}$ value of 1.9 ‰. A: considering a semi-aquatic lifestyle, i.e., an enrichment value of 2 ‰, B: considering a terrestrial lifestyle, i.e., an enrichment value of 5.1 ‰.

those interpretations must be taken with extreme caution, given the very limited number of samples considered, and would benefit from further analyses.

3- Lifestyle

As both crocodylomorphs from Réalmont are inferred to be ectotherms, their difference in $\delta^{18}O_p$ values could be interpreted as a difference in lifestyle, with *Dentaneosuchus crassiproratus*

having higher values in line with a terrestrial lifestyle and the unknown crocodylomorph having lower values in line with a semi-aquatic lifestyle. This is also seen in Mesozoic and modern ecosystems (Cerling *et al*., 2008; Amiot *et al*., 2010) and in the Tiupampa fauna (Pochat-Cottilloux *et al*., 2023e). This difference in lifestyle unfortunately cannot be confirmed with the strontium isotope compositions because the measured $^{87}Sr/^{86}Sr$ values of the two crocodylomorphs are not significantly different. However, the $^{87}Sr/^{86}Sr$ value of seawater during the Bartonian was $0.7077 \pm 1.01.10^{-4}$ (2 s.e., n = 20; Hess *et al*., 1986; Denison *et al*., 1993; Mead & Hodell, 1995), which is much less than the values obtained for the Réalmont fauna. Thus, there are no marine influences here. Finally, the significant difference in the $^{87}Sr/^{86}Sr$ values of mammals clustering them into two groups could be interpreted as a difference in living substrate (and thus environment), but this difference is unfortunately not reflected in $\delta^{18}O_p$ values.

The crocodylomorph from Aumelas either has an ectothermic or endothermic thermoregulation strategy depending on its lifestyle. If it has an ectothermic thermoregulation strategy, the difference in $\delta^{18}O_p$ values between this organism and the turtle sample (Fig. 4.23 & 4.24), which would be both ectotherm organisms, could be interpreted as a difference in lifestyle, with the crocodylomorph having a higher value in line with a terrestrial lifestyle and the turtle having a lower value in line with a semi-aquatic lifestyle. This is also seen in Mesozoic and modern ecosystems (Cerling *et al*., 2008; Amiot *et al*., 2010) and in the Tiupampa and Réalmont fauna. If the crocodylomorph has an endothermic thermoregulation strategy, then the similitude in $\delta^{18}O_p$ values between this organism and mammals (Fig. 4.23 & 4.24), which would both be endothermic organisms, could be interpreted as a similitude in lifestyle, compatible with a terrestrial lifestyle. As a result, while I am not able to conclude on the thermoregulation strategy of the crocodylomorph from Aumelas, it is inferred to be terrestrial. Unfortunately, the strontium isotope compositions cannot be interpreted in terms of lifestyle, as this element seems to have been affected by diagenetic processes.

Eremosuchus elkoholicus from El Kohol has a high ectothermic or low endothermic thermoregulation strategy. If it has a more ectothermic thermoregulation strategy, the similitude in $\delta^{18}O_p$ values between this organism and the turtle sample (Fig. 4.25 & 4.26), which would be both ectotherm organisms, could be interpreted as a similitude in lifestyle, compatible with a semi-aquatic environment. If *Eremosuchus* has a more endothermic thermoregulation strategy, then the difference in $\delta^{18}O_p$ values between this organism and mammals (Fig. 4.25 & 4.26), which would both be endothermic organisms, could be interpreted as a difference in

living environment. Mammals with higher values are in line with a terrestrial lifestyle while *Eremosuchus* has a lower value in line with a semi-aquatic lifestyle. As a result, while I am not able to conclude on the thermoregulation strategy of *Eremosuchus*, it is inferred to be semi-aquatic. Unfortunately, the strontium isotope compositions between the different groups of organisms have no significant differences, thus this interpretation cannot be supported with another independent proxy. However, the $^{87}Sr/^{86}Sr$ value of seawater during the Ypresian was $0.7076 \pm 1.00.10^{-5}$ (2 s.d., n = 1; Denison *et al*., 1993), which is much less than the values obtained for the El Kohol fauna. Thus, there are no marine influences here either.

4- Diet

As stated in VI, there could be an offset in an organism between the $\delta^{44/42}Ca$ values of bone and those of tooth enamel: to compare the different groups of organisms, we must thus account for this offset in the samples. In Réalmont, under the first hypothesis (no variation), the two crocodylomorphs do not have the lowest $\delta^{44/42}Ca_{enamel}$ values (ranging from -0.77 to -0.86 ‰, mean 2 s.d. = 0.11 ‰, n = 3) and probably fed on turtles ($\delta^{44/42}Ca$ values ranging from -0.53 to -0.60 ‰, mean 2 s.d. = 0.11 ‰, n = 3), although the difference is not significant. This result seems strange for *Dentaneosuchus,* given its large size (Martin *et al*., 2023) and terrestrial habits. Following the second hypothesis (variation of -0.25 ‰ between bone and enamel), the crocodylomorphs from Réalmont could have still preferentially fed on turtles if their calcium isotope compositions followed the same variation, but still not on mammals. Indeed, considering a carnivore - herbivore offset of 0.3 to 0.5 ‰, as reported in other studies (Martin *et al*., 2018, 2022; Tacail *et al*., 2020), crocodylomorphs (mean $\delta^{44/42}Ca_{enamel} = -1.07 \pm 0.09$ ‰, 2 s.e., n = 3) have similar values to those of mammals (mean $\delta^{44/42}Ca_{enamel} = -1.05 \pm 0.15$ ‰, 2 s.e., n = 8) that do not differ significantly. It would thus seem that *Dentaneosuchus* did not prey on the sampled mammals.

In Aumelas, under the first hypothesis (no variation), the crocodylomorph has one of the lowest $\delta^{44/42}Ca$ value and its prey would thus not have been sampled here. Following the second hypothesis (variation of -0.25 ‰ between bone and enamel), the crocodylomorph from Aumelas could have preferentially fed on mammals or fishes. Indeed, considering a carnivore-herbivore offset of 0.3 to 0.5 ‰, as reported in other studies (Martin *et al*., 2018, 2022; Tacail *et al*., 2020), the crocodylomorph ($\delta^{44/42}Ca_{enamel} = -1.07 \pm 0.11$ ‰, 2 s.d., n = 1) has a slightly higher value than fishes (ranging from -0.77 to -1.64 ‰, mean 2 s.d. = 0.12 ‰, n = 3) or mammals (ranging from -0.78 to -1.25 ‰, mean 2 s.d. = 0.13 ‰, n = 5).

In El Kohol, under the first hypothesis (no variation), *Eremosuchus* has the highest $\delta^{44/42}Ca$ value, and its prey would thus not have been sampled here. Following the second hypothesis (variation of -0.25 ‰ between bone and enamel), *Eremosuchus* still has the lowest $\delta^{44/42}Ca$ value, and its prey would thus not have been sampled here again. This result seems very strange and might be due either to diagenetic processes or specific calcium fluxes that have not been accounted for here. Further studies are needed to confirm those results and establish the trophic relationships in the three faunas with more certainty.

In Réalmont, crocodylomorphs display a mean $\delta^{13}C$ value of -10.1 ± 0.8 ‰ (2 s.e., n = 2), which, using an isotope fractionation of 9 ‰ between crocodile apatite and diet (Lee-Thorp *et al*., 1989; Tieszen & Fagre, 1993; Stanton, 2006) indicates a diet with a $\delta^{13}C$ value of -19.1 ± 0.8 ‰ (2 s.e., n = 2). Using the data from Passey *et al*. (2005), a $\delta^{13}C$ apatite - diet offset of 12.3 ± 4.2 ‰ (2 s.e.) was estimated for mammals. Mammal samples thus display a $\delta^{13}C$ diet value of -21.0 ± 0.4 ‰ (2 s.e., n = 4). Finally, carbon isotope fractionation between bone apatite and diet has been estimated between 9 and 12 ‰ in marine turtles, depending on their diet (Biasatti, 2004, and references therein). Therefore, turtles in Réalmont display a $\delta^{13}C$ diet value of -18.5 to -21.5 ± 1.7 ‰ (2 s.e., n = 2).

In Aumelas, the crocodylomorph displays a $\delta^{13}C$ value of -7.2 ± 0.3 ‰ (2 s.d., n = 1), which, using an isotope fractionation of 9 ‰ between crocodile apatite and diet (Lee-Thorp *et al*., 1989; Tieszen & Fagre, 1993; Stanton, 2006) indicates a diet with a $\delta^{13}C$ value of -16.2 ± 0.3 ‰ (2 s.d., n = 1). Using the data from Passey *et al*. (2005), a $\delta^{13}C$ apatite-diet offset of 12.3 ± 4.2 ‰ (2 s.e.) was estimated for mammals. Mammal samples thus display a $\delta^{13}C$ diet value of -21.2 ± 4.1 ‰ (2 s.e., n = 2). Finally, carbon isotope fractionation between bone apatite and diet has been estimated between 9 and 12 ‰ in marine turtles, depending on their diet (Biasatti, 2004, and references therein). Therefore, the turtle in Aumelas displays a $\delta^{13}C$ diet value of -13.7 to -16.7 ± 0.2 ‰ (2 s.d., n = 1).

In El Kohol, *Eremosuchus* displays a $\delta^{13}C$ value of -11.6 ± 0.2 ‰ (2 s.d., n = 1), which, using an isotope fractionation of 9 ‰ between crocodile apatite and diet (Lee-Thorp *et al*., 1989; Tieszen & Fagre, 1993; Stanton, 2006) indicate a diet with a $\delta^{13}C$ value of -20.6 ± 0.2 ‰ (2 s.d., n = 1). Using the data from Passey *et al*. (2005), a $\delta^{13}C$ apatite-diet offset of 12.3 ± 4.2 ‰ (2 s.e.) was estimated for mammals. Mammal samples thus display a $\delta^{13}C$ diet value of -20.0 ± 1.0 ‰ (2 s.e., n = 3). Finally, carbon isotope fractionation between bone apatite and diet has been estimated between 9 and 12 ‰ in marine turtles, depending on their diet (Biasatti, 2004

and references therein). Therefore, the turtle in El Kohol displays a $\delta^{13}C$ diet value of -20 to -23 ± 0.3 ‰ (2 s.d., n = 1).

As it has a direct effect on the stable carbon isotope compositions of plants (Fricke, 2007), the $\delta^{13}C$ value of atmospheric CO_2 was estimated through carbon and oxygen isotope compositions of benthic foraminifera in the literature (Cramer *et al*., 2009; see also Appendix 5; Supplementary Material S5) at -6.5 ± 0.7 ‰ (2 s.e., n = 797) during the Bartonian for Réalmont; -6.3 ± 0.5 ‰ (2 s.e., n = 77) during the Ypresian/Lutetian boundary for Aumelas; and -6.5 ± 0.6 ‰ (2 s.e., n = 148) during the middle Ypresian for El Kohol. Those values are in contrast with the modern $\delta^{13}C_{CO2}$ of -7 to -8 ‰ (Gröcke, 2002). Thus, C_3 plants $\delta^{13}C$ range during this period should shift towards values 1 ‰ higher, i.e., -36 to -19 ‰ in Réalmont and El Kohol; and 1.2 ‰ higher, i.e., - 35.8 to -18.8 ‰ in Aumelas (O'Leary, 1988; Kohn, 2010). The values calculated here for the Réalmont and El Kohol fauna, as well as the mammals from Aumelas correspond, although they belong to the higher part of the $\delta^{13}C$ range of plants, which would indicate an arid environment, as assessed in the Bauru Group (Upper Cretaceous of Brazil; Klock *et al*., 2022) or the Tiupampa fauna (see VII). However, in Aumelas, the crocodylomorph and turtle diet values do not correspond, which is surprising, and might be due to diagenetic processes altering their carbon isotope compositions or a diet based on unsampled more aquatic organisms.

5- Paleoenvironmental reconstructions

$\delta^{18}O_{aw}$ values calculated from $\delta^{18}O_p$ values measured from the different groups of organisms range from -1.34 to -3.1 ‰ (mean value: -2.6 ± 1.6 ‰, 2 s.e., n = 6) in Réalmont; -3.7 to -2.7 ‰ (mean value: -3.2 ± 1.0 ‰, 2 s.e., n = 6) in Aumelas; and -2.5 to 2.2 ‰ (mean value: -0.3 ± 5.1 ‰, 2 s.e., n = 4) in El Kohol. Those values correspond to continental surface water values measured today at tropical to equatorial latitudes (IAEA, 2022) and are in accordance with climatic conditions measured nowadays in Pakistan or South China, with a mean annual temperature around 20°C and a mean precipitation of a few hundred millimetres per year (IAEA, 2022).

The measured $\delta^{18}O_p$ values in Réalmont are high and comparable to those measured in the terrestrial ecosystem of Western Amazonia (mean $\delta^{18}O$ = 21.7 ± 1.7 ‰, 2 s.e., n = 3; Custódio *et al*., 2023) during the Bartonian, but not as high as those measured in desertic environments (Lécuyer *et al*., 1999; Schoeninger *et al*., 2000), therefore being more in line with a dry environment.

The measured $\delta^{18}O_p$ values in Aumelas are high and comparable to those measured in the terrestrial ecosystems of Germany (18.1 ± 1.0 ‰, 2 s.d., n = 1; Gehler *et al*., 2011) and Tunisia (mean $\delta^{18}O$ = 20.5 ± 0.9 ‰, 2 s.e., n = 22; Ounis *et al*., 2008) during the Ypresian/Lutetian, but not as high as those measured desertic environments (Lécuyer *et al*., 1999; Schoeninger *et al*., 2000), therefore being more in line with a dry environment.

The measured $\delta^{18}O_p$ values in El Kohol are high and comparable to those already measured in Mahboubi *et al*. (2014) in El Kohol, as well as those measured in the terrestrial ecosystem of Tunisia (mean $\delta^{18}O$ = 20.4 ± 0.8 ‰, 2 s.e., n = 21; Ounis *et al*., 2008) during the Ypresian, but not as high as those measured in desertic environments (Lécuyer *et al*., 1999; Schoeninger *et al*., 2000), therefore being more in line with a dry environment.

Finally, those reconstructions are also confirmed when looking at the $\delta^{13}C$ values measured here: those correspond to C_3 plants with mean $\delta^{13}C$ values ranging from -18.5 to -21 ‰ in Réalmont, -13.7 to -21.2 ‰ in Aumelas; and -20 to -23 ‰ in El Kohol. These values indicate dry ecosystems today, with annual precipitation of less than 100 to 200 mm/year (Kohn, 2010, see also Appendix 5, Supplementary Material S5). It would thus appear from two independent elements that the specimens sampled in the three faunas were living in a dry environment, albeit with the presence of freshwater. Although this is not seen in some large-scale studies (Payros *et al*., 2006; Less & Özcan, 2012), it is further confirmed in regional scale studies in Turkey (Akkiraz *et al*., 2006), Spain (Cavagnetto & Anadón, 1996), Namibia (Pickford, 2018), Tunisia (Karoui-Yaakoub *et al*., 2015) and Argentina (Fernicola *et al*., 2021). In any case, those interpretations must thus be taken with caution as the data we use here is merely a local snapshot rather than a long-term interpretation.

IX- The geochemical record of extant crocodylian teeth

Throughout this chapter, I presented results from fossil samples of diverse fauna using isotopic compositions of several elements to get a better idea of their paleoecology. Each specimen was represented by a single sample, and the samples values were compared with one another and their respective taxonomic group, to get a better idea of the trophic relationships of the fauna studied, as well as their living environment, two signals that could sometimes be difficult to differentiate. Here, I present a slightly different approach, studying several samples from the same individual (see also Klein *et al*., 2009). Four teeth were studied, belonging to three different extant species of crocodylians (Table 15), each representing a slightly different lifestyle. *Gavialis gangeticus* is nowadays critically endangered (Saikia, 2013; Lang *et al*.,

2019) and it is currently restricted to certain areas of the Gange river (India) which is linked with the South Asian monsoon and associated sedimentary discharge from the Himalayas (Goodbred, 2003). It is the most thoroughly aquatic of the extant crocodylians, and the only species without the ability to walk in a semi-upright stance (Bustard & Singh, 1978; Willis *et al*., 2007; Stevenson & Whitaker, 2010). Through its long rostrum and numerous small teeth, this species is particularly adapted for eating fish, although some large individuals have also been reported to feed on other preys (Lang *et al*., 2019). *Crocodylus siamensis* is more wildly spread in Southeast Asia (Cambodia, Indonesia, Laos, Thailand, Vietnam; Simpson & Bezuijen, 2010), thus also subject to environmental change during the monsoon, but more constrained. It is mostly a freshwater organism (Daltry *et al*., 2003; Bezuijen *et al*., 2006; Cox & Phothitay, 2008). Similarly to many other crocodylians, *C. siamensis* feeds on wide array of preys, such as invertebrates, frogs, reptiles, birds, and mammals (Daltry *et al*., 2003). *Osteolaemus tetraspis* is a small organism that can live seasonally in caves and has a generalist terrestrial diet (Pauwels *et al*., 2007; Shirley *et al*., 2017). It is known in western Africa, from Congo to Gambia (Eaton, 2010) and his specific behavior is associated with high variability of climates in the region (Shirley *et al*., 2017).

The objective of this study was to perform serial dentine micro-samplings to assess variations (if any) of the isotopic record of the different species. Ultimately, the goal is to implement a method that would be applicable to fossil samples, with the same interest as previously: reconstructing their paleoecology and paleoenvironment. To gain that information, several isotopic systems were chosen, with the idea to provide multi-isotopic data.

The oxygen isotope composition of the dentine was studied as a proxy of the oxygen isotope composition of the ambient water of each organism (see Chapter 4, III). Strontium isotope

Table 15: List of specimens sampled in this study.

Taxon	**Specimen**	**Ecology**
Gavialis gangeticus	MHNL 50001407	Mostly aquatic
Gavialis gangeticus	UCBL WB39	Mostly aquatic
Crocodylus siamensis	UCBL WB41	Semi-aquatic
Osteolaemus tetraspis	UCBL 2019-1-236	Terrestrial seasonally

compositions were also measured to gain insights into the living substrate of each organism, with variations linked to possible changes in environment (see Chapter 4, V). Calcium isotope compositions were measured as a proxy of the diet of each organism, again with variations linked to a possible change in diet (see Chapter 4, VI). Finally, nitrogen isotope compositions were measured as an independent proxy of diet.

Nitrogen has two stable isotopes: ^{14}N (major) and ^{15}N (minor). Contrary to the other elements studied in this thesis until now, nitrogen was measured on the organic part of the bone (collagen), and as such cannot be measured in most fossils (but see Leichliter *et al*., 2021, 2023). As other elements, the notation delta (δ) is used as following:

$$\delta^{15}N\ (‰) = \left[\frac{\left({}^{15N}/_{14N}\right)_{sample}}{\left({}^{15N}/_{14N}\right)_{AIR}} - 1\right] \times 10^3$$

The nitrogen of collagen comes from food (DeNiro & Epstein, 1981; Schwarcz & Schoeninger, 1991). Through the degradation of consumed animal proteins, the collagen is biosynthesized. As a result, the isotope compositions of collagen nitrogen and consumed proteins nitrogen are linked (Bocherens *et al*., 1991; Schwarcz, 1991). Nitrogen is first fixed by plants from the air through symbiosis with fixing bacteria or already metabolized nitrogen from the soil. Fractionation between air and plants is between -1 and 6.5 ‰ (Högberg, 1997; Hobbie *et al*., 2001; Marshall *et al*., 2007). As in carbon isotope compositions, there is a trophic enrichment between an organism and its food that varies between 3 and 6 ‰ (Schoeninger & DeNiro, 1984; Schwarcz & Schoeninger, 1991; Ambrose, 2002; Bocherens & Drucker, 2003; Caut *et al*., 2009; O'Connell *et al*., 2012). Herbivores are thus distinguishable from omnivores and carnivores. In some cases, one can even distinguish individuals that have the same general diet but that consume different quantities of meat, as it is more enriched in proteins than plants (Clauzel, 2022). Marine organisms can also be distinguished from terrestrial ones as they tend to have higher $\delta^{15}N$ values, as food webs are longer in marine ecosystems (Schoeninger & DeNiro, 1984; Schwarcz, 1991). Finally, nitrogen isotope compositions also depend on the climate, with arid conditions corresponding to an increase in $\delta^{15}N$ values (Ambrose & DeNiro, 1986; Schwarcz *et al*., 1999; Hedges *et al*., 2004).

a- Analytical procedures

The serial sampling was performed with the following two protocols: first, the teeth were included in resin and cut along the growth axis using a Buehler IsoMet Low Speed precision sectioning saw with a diamond-studded circular saw blade. The first protocol involved a computer-assisted micro drill device (MicroMill) allowing the sampling of around 200 µg of hydroxyapatite by drilling holes of 350-400 µm wide and 300 µm deep. The samples extracted using this protocol were used in calcium and strontium analyses. The second protocol involved a Dremel tool and allowed to pick up larger quantities of dentine, but following the lines of increment of the dentine, thus staying at the same time of dentine formation throughout each sample. The samples extracted using this protocol were used in oxygen and nitrogen analyses. Chemical preparations and measurements protocols were the same as those explained before for calcium, strontium, and oxygen isotope compositions.

Analytically, for nitrogen, dentine powders were measured at the LEHNA (combustion on a PYROcube™ with 'Purge & Trap' technology and connected in continuous flow to a IRMS IsoPrime100™). Some preliminary tests determined that 1 mg of dentine powder delivered enough signal to get reliable measures (Table 16). Isotope compositions were calibrated with international reference standards ammonium sulfates IAEA-N1 ($\delta^{15}N$ = 0.43 ‰ AIR; Böhlke *et al*., 1993; Gentile *et al*., 2013; Gillikin *et al*., 2017) and IAEA-N-2 ($\delta^{15}N$ = 20.41 ‰ AIR; Gonfiantini, 1978, 1984; Kendall & Grim, 1990; Böhlke *et al*., 1993; Böhlke & Coplen, 1995).

b- Samples

One of the difficulties encountered in this study is that although teeth of crocodylians are common, a precise provenance is often very hard to obtain. The teeth might either be isolated, wrongly labelled or fixed on the skull of another individual. The specimen might also be wrongly identified, and, in the case of widespread taxa, it might be difficult to identify its origin. As a result, the two *Gavialis* specimens (UCBL WB39 & MHNL 50001407) studied here are especially interesting, because the geographic area of the extant representatives of this taxon is extremely reduced (see above), and thus they clearly come from the Gange basin (India). The specimen of *Crocodylus siamensis* (UCBL WB41) is explicitly labelled from Vinh Long (Vietnam) and was historically collected in 1881. Finally, the specimen of *Osteolaemus tetraspis* (UCBL 2019-1-236) is also explicitly labelled to come from Gabon.

Table 16: Test measurements of $\delta^{15}N$ in the dentine of UCBL WB41 (*Crocodylus siamensis*). Signal above 2 nA is considered acceptable for measurements.

Sample	Signal (nA)	Weight (mg)	$\delta^{15}N$
Test 1	1.30	0.43	9.95
Test 2	1.34	0.48	10.33
Test 3	1.72	0.60	10.19
Test 4	4.87	1.69	7.78

c- Age model

To timescale the measured isotopic compositions, we could unfortunately not make thin sections of the sampled surfaces and count the number of incremental lines of dentine, as it is a destructive protocol, and those wild samples are rare, and thus important. The age model necessary to anchor the timing of our data was thus based on general observations made on tooth mineralization timings of *Alligator mississippiensis* (Erickson, 1996). In different individuals of different ontogenetic stages, between 83 and 122 incremental lines were measured. As those increments form daily (Schour & Steadman, 1935; Schour & Hoffman, 1939; Yilmaz *et al*., 1977; Bengston, 1988), the tooth replacement in this taxon lasts approximately between 83 and 122 days. The oldest specimen sampled in Erickson (1996) measured 1.40 m (young adult) and had 122 increments of dentine. Although Erickson (1996) observed that tooth replacement rates show a general slowing trend (maybe as teeth become larger), corroborating hypotheses that it diminishes with ontogeny (Poole, 1961), it cannot be confirmed until further histological studies are made, also on potential interspecific variations. Thus, I hypothesize for now that the dentine records of the specimens sampled here represent approximately 4 months (120 days), as they all represent adult individuals.

d- Results

Detailed results are available here: https://mycore.core-cloud.net/index.php/s/7mCKw8rLbck2qh3 . For the calcium analyses, blanks realized during the purification protocols have been analysed with the MC-ICP-MS Neptune Plus. All blanks contained less than 100 ng of calcium. Thus, considering our measurement precision, our isotopic measurements are not affected by this nano-pollution. The mass dependency curve of the isotopic measurements follows the expected relation for calcium (Fig. 4.40): the slope value

is 0.523 ± 0.025 (2 s.e., n = 40), which agrees with the 0.5067 slope predicted by the linear approximation of exponential mass-dependent fractionation and is in line with previously published values (Tacail *et al*., 2014, 2016, 2017; Martin *et al.,* 2015, 2017a, b, 2022; Hassler *et al*., 2018, 2021a, b) and other measured values in Chapter 4, supporting the accuracy of the measurements. The standard NIST-SRM1486 has a $\delta^{44/42}$Ca mean value of -0.97 ± 0.05 ‰ (2 s.e., n = 17) and a mean $^{87}Sr/^{86}Sr$ value of 0.709059 ± $6.33.10^{-4}$ (2 s.e., n = 4) which is also in line with previously published values (Clemens *et al*., 1993; McArthur *et al*., 2001; Faure & Mensing, 2005; Galler *et al*., 2007; De Muynck *et al*., 2009; ; Martin *et al*., 2015b; Weber *et al*., 2017; Hassler *et al*., 2018, 2021a, b; Brazier *et al*., 2019; Dodat *et al*., 2021; Guiserix *et al.,* 2022; Martin *et al*., 2022) and other measured values in Chapter 4. The standard NIST-SRM987 has a mean $^{87}Sr/^{86}Sr$ value of 0.710256 ± $2.57.10^{-4}$ (2 s.e., n = 10) which in line with previously published values (Clemens *et al.,* 1993; McArthur *et al*., 2001; Faure & Mensing, 2005; Galler *et al*., 2007; De Muynck *et al.,* 2009; Weber *et al.,* 2017; Brazier *et al*., 2019; Guiserix *et al*., 2022) and other measured values in Chapter 4.

In three out of the four teeth sampled, the nitrogen isotope compositions are anticorrelated to the calcium isotope compositions (Fig. 4.41, 4.43 & 4.44) and, when available, the oxygen isotope compositions are correlated with the strontium isotope compositions (Fig. 4.42-4.44).

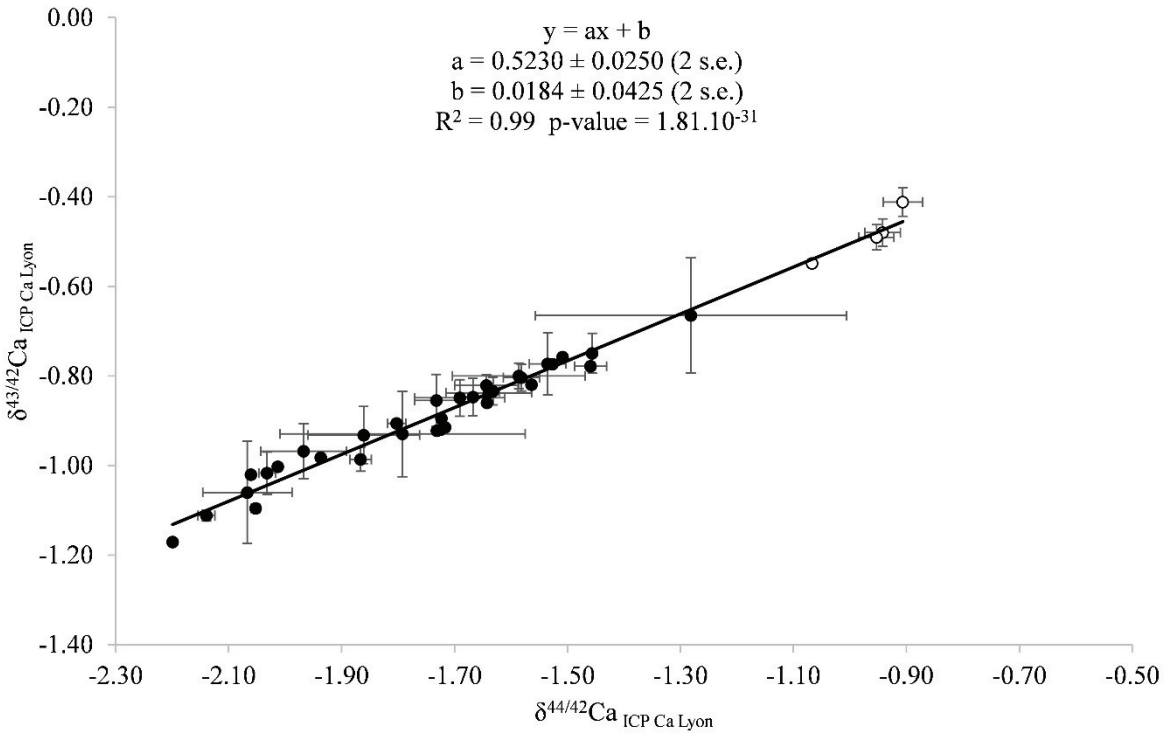

Figure 4.40: $\delta^{43/42}$Ca values plotted against $\delta^{44/42}$Ca values for all extant samples (black circles) and standards (white circles) studied.

Osteolaemus shows the most drastic change in calcium isotope compositions (Fig. 4.45A; ≈ 1 ‰), and variations in isotopic compositions are also important in the two teeth of *Gavialis* sampled (Fig. 4.41A & 4.42A).

e- Discussion

The anticorrelation of nitrogen and calcium isotope compositions (Fig. 4.41, 4.43 & 4.44) can be explained because nitrogen undergoes a trophic enrichment, while calcium undergoes a trophic depletion in ^{44}Ca. As a result, higher $\delta^{15}N$ values correspond to lower $\delta^{44/42}Ca$ values. Furthermore, the correlation of oxygen and strontium isotope compositions (Fig. 4.42-4.44), can be explained because those elements are both linked to the living environment, at least partially, with changes in the isotopic composition of available ambient water (for the oxygen isotope compositions) most likely associated with changes in the isotopic composition of the substrate (for the strontium isotope compositions).

The changes and intensities of changes in $\delta^{44/42}Ca$ values recorded in *Osteolaemus* (Fig. 4.45A) might be related to its lifestyle. Indeed, as stated above, this organism is known to estivate and change living environments seasonally, inducing a change in diet, probably reflected here in the calcium isotope compositions. This also reflected by a positive shift in $\delta^{15}N$ (≈ +1.5 ‰), as well as a negative shift in $\delta^{18}O$ and $^{87}Sr/^{86}Sr$ (≈ -0.002 and ≈ -1 ‰ respectively), confirming this change in living environment.

On the other hand, the variations in isotope compositions in the two teeth of *Gavialis* sampled (Fig. 4.41A & 4.42A) might rather be due to environmental constraints. Indeed, the Gange basin is highly impacted by sediment washing from the Himalayas, which might even modify calcium isotope compositions (Rea, 1992; English *et al*., 2000; Stewart *et al*., 2008; Tripathy *et al*., 2011). This is further evidenced by the similar variations in strontium isotope compositions, that record changes in living substrate of the organism (Fig. 4.41B & 4.42B).

Strontium isotope compositions provide evidence and confirm the provenance of the different organisms. For example, strontium isotope compositions of *Gavialis* were measured at 0.726851 ± 0.003080 (2 s.e., n = 9) and 0.720425 ± 0.003204 (2 s.e., n = 10) for UCBL WB39

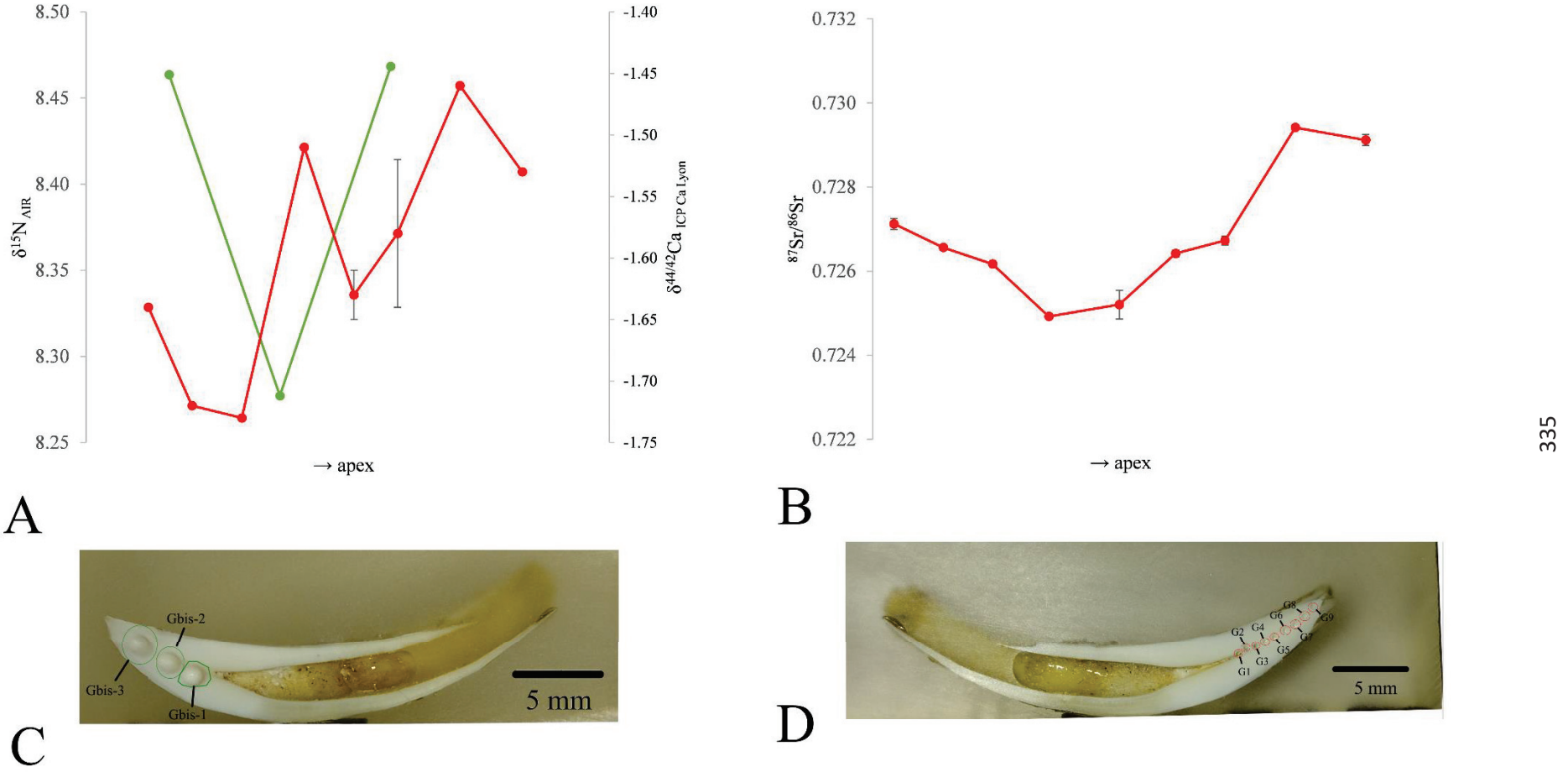

Figure 4.41: Serial isotope compositions of a tooth of *Gavialis gangeticus* (UCBL WB39). A: nitrogen (green) and calcium (red) isotope compositions. B: strontium isotope compositions. C: side of the tooth used for nitrogen sampling. D: side of the tooth used for calcium and strontium sampling. All graphs are scaled horizontally to the total size of the tooth.

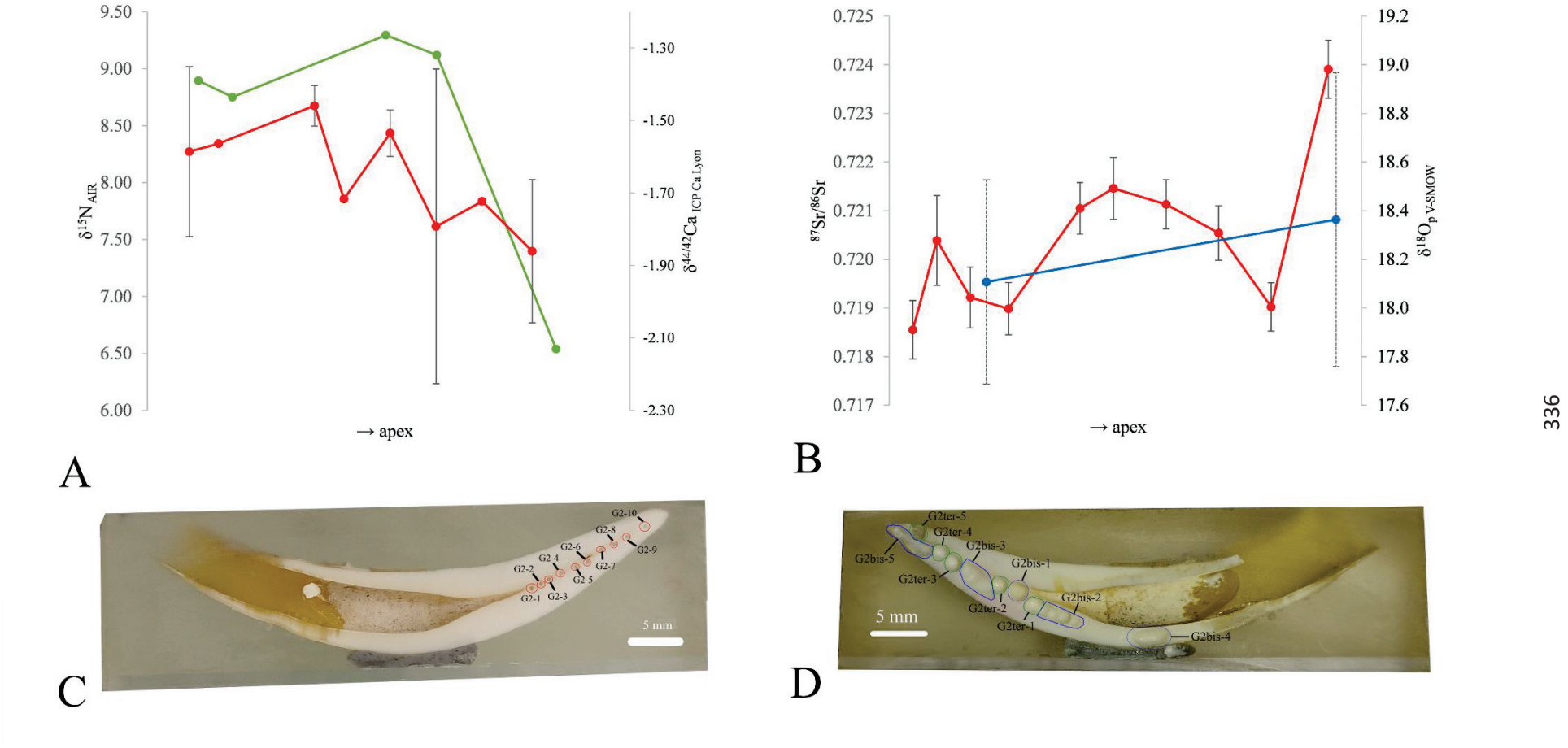

Figure 4.42: Serial isotope compositions of a tooth of *Gavialis gangeticus* (MHNL 50001407). A: nitrogen (green) and calcium (red) isotope compositions. B: strontium (red) and oxygen (blue) isotope compositions. C: side of the tooth used for calcium and strontium sampling. D: side of the tooth used for oxygen and nitrogen sampling. All graphs are scaled horizontally to the total size of the tooth.

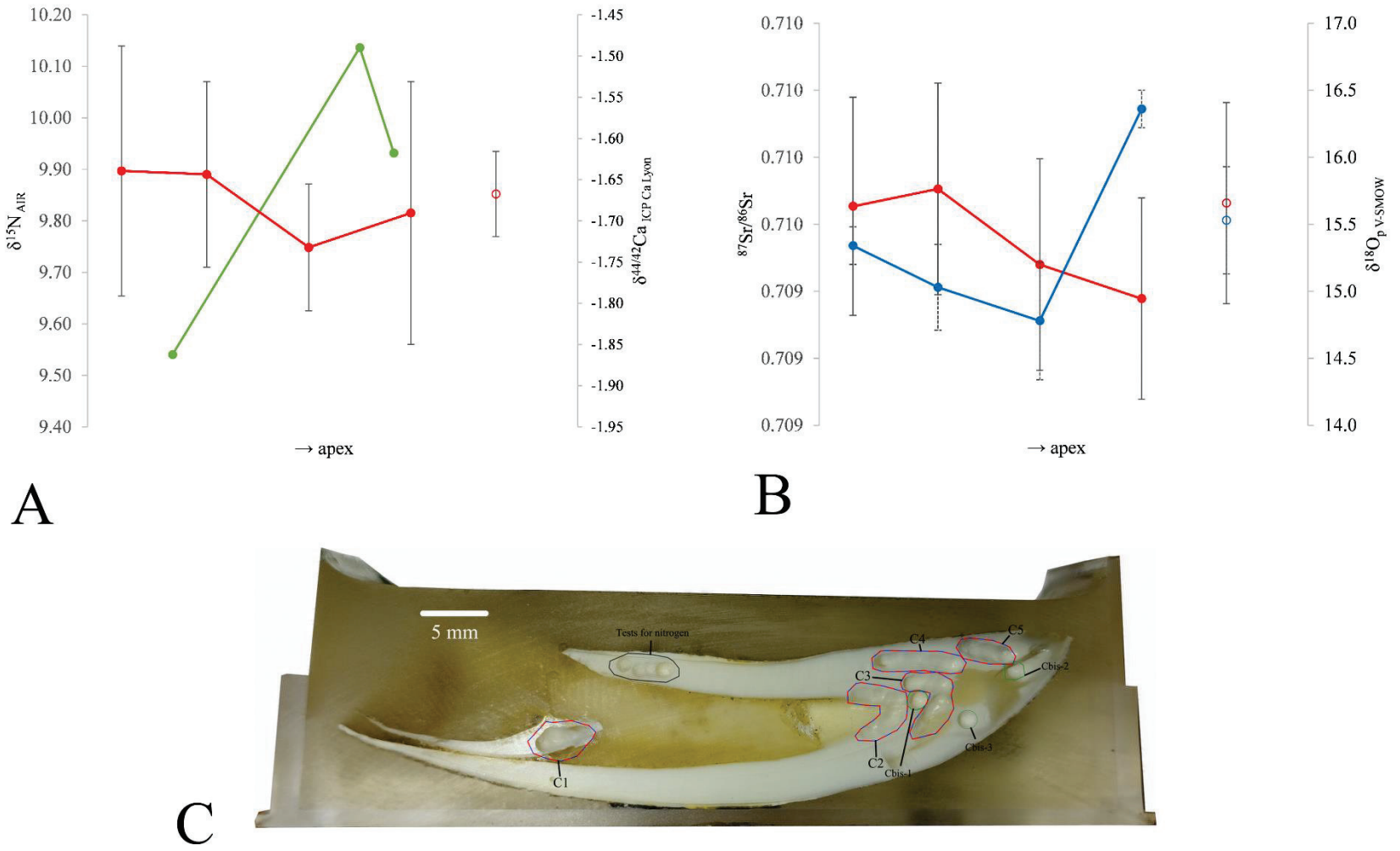

Figure 4.43: Serial isotope compositions of a tooth of *Crocodylus siamensis* (UCBL WB41). A: nitrogen (green) and calcium (red) isotope compositions. B: strontium (red) and oxygen (blue) isotope compositions. C: side of the tooth used for all samplings. Hollow points represent replacement tooth. All graphs are scaled horizontally to the total size of the tooth.

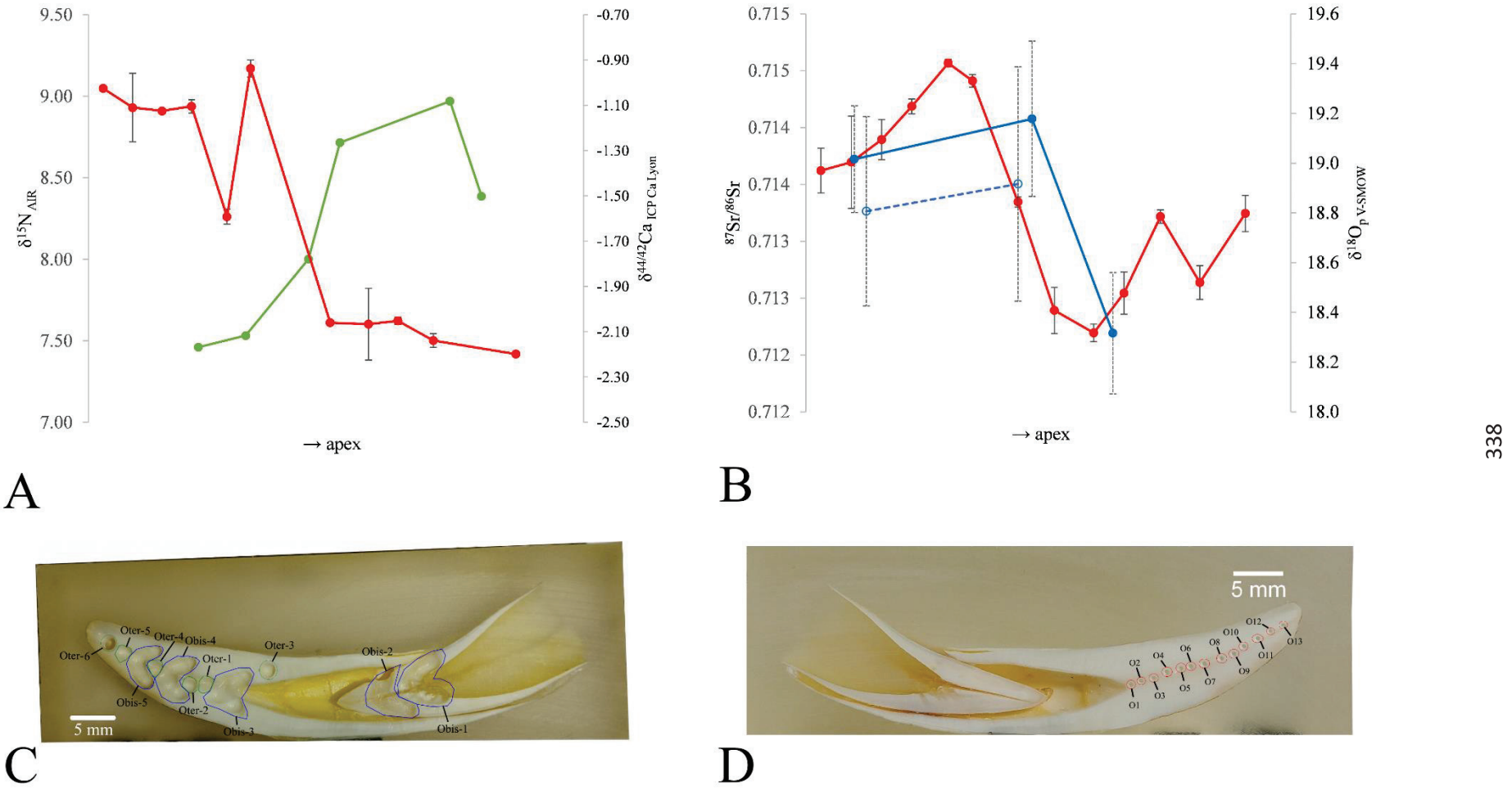

Figure 4.44: Serial isotope compositions of a tooth of *Osteolaemus tetraspis* (UCBL 2019-1-236). A: nitrogen (green) and calcium (red) isotope compositions. B: strontium (red) and oxygen (blue) isotope compositions. C: side of the tooth used for nitrogen and oxygen sampling. D: side of the tooth used for calcium and strontium sampling. Hollow points and doted curves represent replacement tooth. All graphs are scaled horizontally to the total size of the tooth.

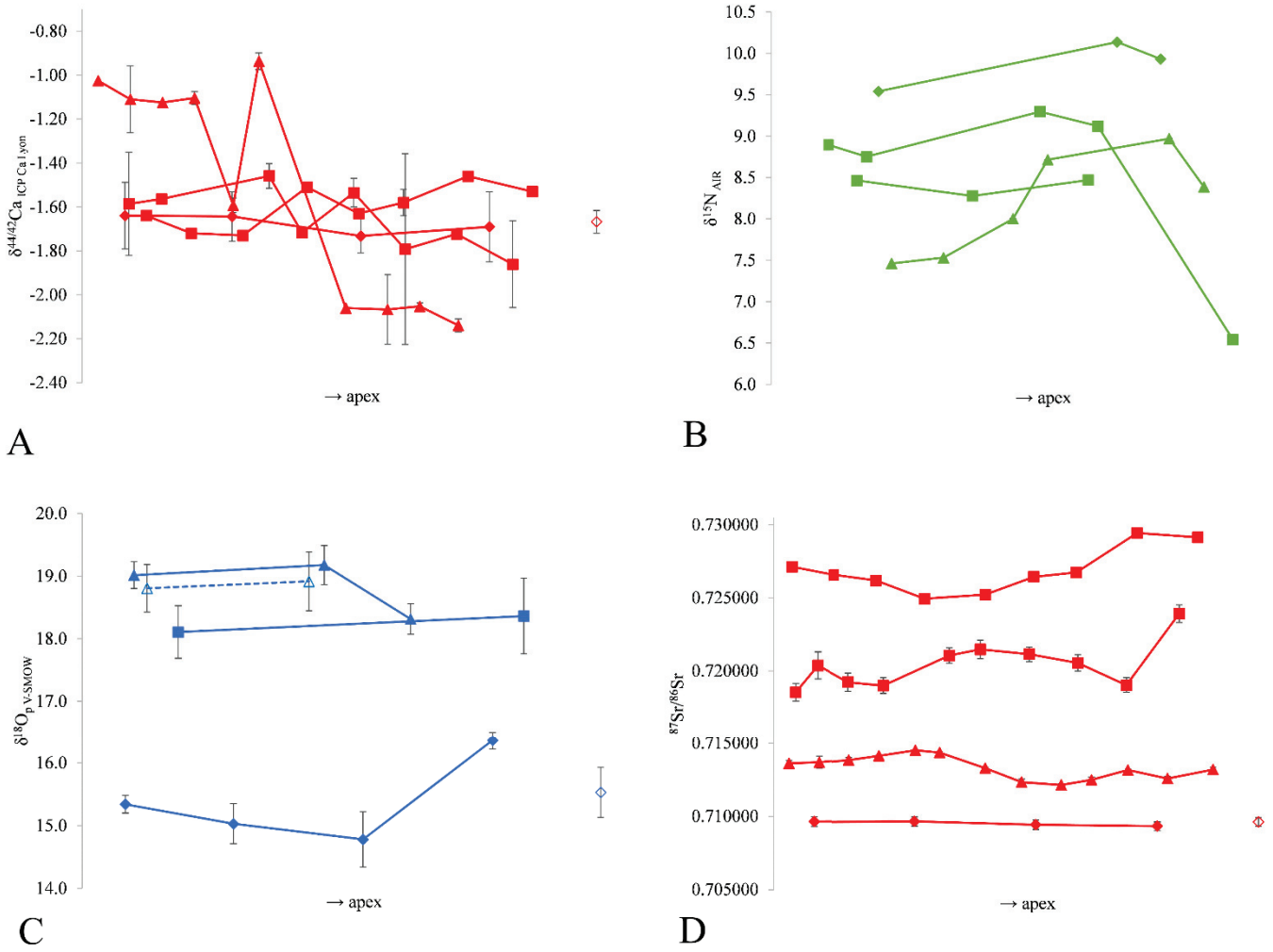

Figure 4.45: Serial isotope compositions of the four teeth sampled in this study. A: calcium, B: nitrogen, C: oxygen, D: strontium. Triangles: *Osteolaemus tetraspis* (UCBL 2019-1-236), squares: *Gavialis gangeticus* (MHNL 50001407 & UCBL WB39), circles: *Crocodylus siamensis* (UCBL WB41). Hollow points and dotted curves represent replacement teeth. All graphs are scaled horizontally to the total size of the teeth.

and MHNL 50001407 respectively, which correspond to those measured in the Gange basin in water (0.722037 ± 0.014586 2 s.e., n = 23; Krishnaswami *et al*., 1992; Yoshimura *et al*., 2021) and sediments (0.725428 ± 0.025631 2 s.e., n = 12; Yoshimura *et al*., 2021). Furthermore, using the equation of Amiot *et al*. (2007), *Gavialis* $\delta^{18}O_{aw}$ is -4.1 ± 0.3 ‰ (2 s.e., n = 2), and it is measured in the Gange water at -8.2 ± 4.6 ‰ (2 s.e., n = 7). Finally, it is also the case for *Osteolaemus* (mean $^{87}Sr/^{86}Sr$ = 0.713381 ± 0.001552 2 s.e., n = 13), as the mean value of the Ogooué and Mbei rivers (Gabon) is 0.717270 ± 0.005033 (2 s.e., n = 21; Moquet *et al*., 2021). The oxygen isotope compositions of the replacement tooth of *Osteolaemus* are similar to those of the 'main' tooth (Fig. 4.44B & 4.45C). Further studies are needed to understand if those preliminary results are also found in other species and elements.

f- Conclusion

The serial isotope composition records of extant crocodylians dentine are interesting prospects, which could potentially be extended to fossil forms. Relying on a multi-isotopic approach, the dietary and environmental habits of individual organisms can be assessed at a high precision (i.e., the one of the tooth replacement rate), with potential changes throughout the record. However, if made on fossil samples, such study should put a strong emphasis on the impact of diagenesis, as these processes are known to have more effect on this tissue, rather than on enamel for example (Nelson *et al*., 1986; Kohn *et al*., 1999; Budd *et al*., 2000; Hedges, 2002; Wopenka & Pasteris, 2005; Pasteris *et al*., 2008; Dodat *et al*., 2023).

Some analytical techniques will need to be improved. For example, one can notice that error bars (2 s.d. associated with each measure; Fig. 4.41-4.45) are quite high or missing, because the number of replicates during the measurement phase is quite low or restricted to one, respectively. This is because the sampling procedure is designed to be minimal, to allow for a precise time spatialization of each sample. This leads to the quantity of each element in a sample being low and reduces the number of times it can be measured independently. Promising techniques, such as LA-MC-ICP-MS (Sylvester, 2008; Lin *et al*., 2016) could help resolve those issues. The incorporation of carbonate measures could also prove interesting, to access $\delta^{18}O_c$ and $\delta^{13}C$ values, but those will need to be improved as well, as the current optimal threshold is 10 mg, which is not compatible with serial sampling.

Finally, apart from variations due to environmental or dietary variations, the isotope compositions of calcium, oxygen and strontium of the dentine sampled here do not vary much throughout the growth of the tooth, thus validating the use of a single sampling point as a proxy

for the overall value of the tooth of an organism, as done on fossil forms. This is especially important in rare and important specimens, where sampling must be limited.

X- Conclusions and perspectives

Shortly after the K/Pg biological crisis, it appears that sebecids were already at the top of the food-chain in terrestrial ecosystems, as is seen in Tiupampa, probably because the apex predator ecological niche was left vacant by the disappearance of non-avian theropod dinosaurs. European altirostral crocodylomorphs sampled here seem to have kept this ecology and feeding habits throughout the Eocene, with *Dentaneosuchus* and an unknown terrestrial crocodylomorph (probably a planocraniid) from Aumelas (France) also being predators in their respective environment. It is also interesting to note that all those crocodylomorphs are mostly inferred to be ectotherm terrestrial organisms, even in the aftermath of the K/Pg biological crisis. The results obtained on *Eremosuchus elkoholicus* from the Ypresian of Algeria are more nuanced and call for a reassessment of this enigmatic taxon, which might rather be semi-aquatic. In all studied cases, the paleoenvironmental reconstruction proposed is that of a dry and hot climate, which corresponds to the hyperthermal events of the Paleogene (Bowen *et al*., 2006; Lauretano *et al*., 2015; Li *et al*., 2022).

In Tiupampa and Réalmont, the interpretations made on the sebecid taxon are reinforced with the simultaneous sampling of at least one different semi-aquatic crocodylomorph. In all sampled faunas, the comparisons with other groups of organisms with known ecology strengthen the paleoecological inferences made. However, one must keep in mind that the interpretations made here rely only on a handful of samples, therefore relying also on non-parametrical statistics. The general trends observed here would need to be confirmed by other proxies, and higher sampling of each fauna, especially for Aumelas and El Kohol, where the taxonomic and intensity of sampling could be increased.

The combination of the different isotope systems proposed here is especially interesting, as it allows to confirm interpretations made on lifestyles and diets through independent elements, while enabling a detailed assessment of the impact of diagenetic processes on the samples studied, which is a prerequisite to the interpretations of isotope compositions data. To this regard, REE content and the combination of oxygen isotope compositions of phosphate and carbonate apatite are the most important to study the diagenetic processes underwent by the samples.

The oxygen isotope compositions of phosphate apatite that can be interpreted in terms of lifestyle and thermoregulation strategy. However, strontium isotope compositions reveal to be ineffective to decipher different living environments, while they are important to assess the influence of the marine environment on a fauna. On this matter, the addition of sulphur or lithium isotope compositions might be of interest (Burton & Vigier, 2011; Goedert *et al*., 2016b, 2018, 2020; Goedert, 2017; Thibon *et al*., 2022). The combination of calcium and carbon isotope compositions allows robust assessments of paleodiets and food webs in those paleoenvironments. The study of the trophic relationships between the different group of organisms sampled would benefit from input from other isotopic systems, such as zinc (Balter *et al*., 2010; Van Heghe *et al*., 2012; Jaouen *et al*., 2013, 2016a, b, 2020, 2022; Costas-Rodríguez *et al*., 2014), magnesium (Martin *et al*., 2014c, 2015c; Le Goff, 2021; Le Goff *et al*., 2021, 2022) or the promising nitrogen or hydrogen isotope compositions of vertebrate apatite (Polissar *et al*., 2009; Holobinko *et al*., 2011; Drewicz *et al*., 2020; Leichliter *et al*., 2021, 2023; Clauzel, 2022; Clauzel *et al*., 2022).

Further studies on the already sampled faunas would be interesting for several questions: what is the source of alimentation of the sebecids from Tiupampa? Can paleoecological differences between the various taxa of mammals from this Paleocene locality be assessed? What are the true taxonomic identities of the unknown crocodylomorphs from Réalmont and Aumelas? It would also be very interesting to apply this kind of procedures to faunas including sebecids, and more generally altirostral crocodylomorphs, dating before the K/Pg biological crisis, such as El Mirador (Spain; Sellés *et al*., 2020) for sebecids, the Adamantina formation for baurusuchids and sphagesaurians (see chapter 1), the Kem Kem beds, Morocco for peirosaurids (Ibrahim *et al*., 2020) or the Phu Sung fauna, Thailand (Chanthasit *et al*., 2019) for atoposaurids.

The serial isotopic compositions records of dentine have been assessed to be of interest in extant specimens and linked to variations in their environment and diet. This last study also supports the use of one sample on each organism in the fossil faunas. However, this method will need to be improved before being applied in fossil organisms, and potential effects of diagenetic alteration rigorously quantified. Finally, difficulties have been encountered when trying to establish an age model on the extant samples studied, because of the destructive nature of the histological sampling that would enable this. One way to resolve this would be with the use of high-resolution CT scans (i.e., synchrotron), that could enable to see the daily increments of dentine, as it is possible to see the line of arrested growth in long bones (Fig. 4.46).

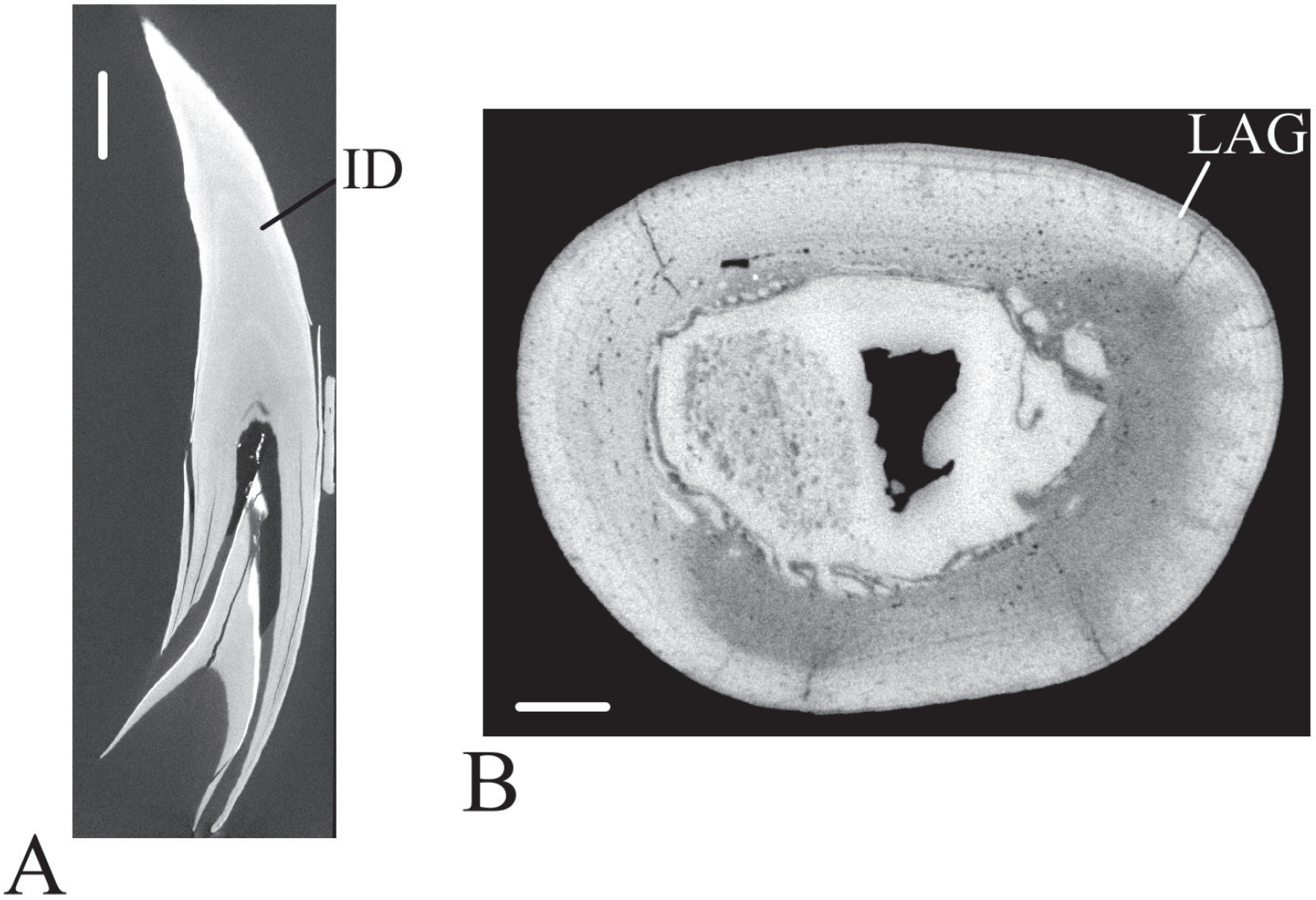

Figure 4.46: Examples of how CT scan can be used in histological studies. A: tooth of UCBL-2019-1-236 (*Osteolaemus tetraspis*) used for geochemical sampling in sagittal view. B: humerus of *Dentaneosuchus crassiproratus* (MHNT.PAL.2012.14.2) in transverse view. ID: main increment of dentine, LAG: line of arrested growth. Scale bars are 1 cm.

Chapter 5: Osteoderms histology and ornamentation

In previous chapters, the terrestrial lifestyle of several clades of crocodylomorphs was assessed using geochemical proxies and the study of their internal structures. In this chapter, I highlight a different proxy that might also be of interest to better understand those fossil organisms. Those results are to be taken as a preliminary study and would benefit from further sampling, however they could come as complementary to the previous data presented in Chapter 3 & 4. Osteohistology has been used since the beginning of the 21st century as a proxy to infer several paleoecological traits in extinct specimens (growth rate, size, lifestyle), comparing them with extant representatives (Wiffen *et al*., 1995; Horner *et al*., 1999, 2000, 2001; de Ricqlès *et al*., 2000, 2003a, b, 2016; Botha & Chinsamy, 2001; Padian *et al*., 2001, 2004; Horner & Padian, 2004; Sander *et al*., 2004; Scheyer & Sander, 2004, 2007; Steyer *et al*., 2004; Buffrénil *et al*., 2007; Scheyer & Sanchez-Villagra, 2007; Houssaye *et al*., 2009, 2010, 2011, 2013a, b, 2014a, b, 2015, 2016a, b, c, 2021a, b; Bourdon *et al*., 2009; Houssaye, 2009, 2012, 2013, 2014; Botha-Brink & Smith, 2011; Houssaye & Bardet, 2011; Laurin *et* al., 2011; Houssaye & Tafforeau, 2012; Hayashi *et al*., 2013; Legendre *et al*., 2013; Padian & Lamm, 2013; Straehl *et al*., 2013; Nakajima *et al*., 2014; Cubo *et al*. 2015, 2017; Klein *et al*., 2015, 2016; Kolb *et al*., 2015; Wintrich *et al*., 2017; Houssaye & Botton-Divet, 2018; Buffrénil *et al*., 2021; Spiekman, 2023 but see Houssaye *et al*., 2018a, b, 2019; Bader *et al*., 2022), sometimes quantitatively (Cubo *et al*., 2005, 2008, 2012, 2020, 2022a, b; Montes *et al*., 2007; Legendre, 2014; Legendre *et al*., 2016; Olivier *et al*., 2017 ; Faure-Brac & Cubo, 2020; Faure-Brac, 2021; Faure-Brac *et al*., 2022). Those studies are mostly focused on long bones and proportionally low in crocodylomorphs (see Buffrénil *et al*., 2021 for a review): here, the osteoderms of several crocodylomorphs are studied qualitatively using histological techniques.

I- Scientific publication: 'A survey of osteoderm histology and ornamentation among Crocodylomorpha: a new proxy to infer lifestyle?'

This publication was published in December 2022 in *Journal of Morphology*. Reference: Pochat-Cottilloux Y., Martin J. E., Amiot R., Cubo J. & Buffrénil V. d. (2022). A survey of osteoderm histology and ornamentation among Crocodylomorpha: A new proxy to infer lifestyle? *Journal of Morphology*, 284(1): e21542. https://doi.org/10.1002/jmor.21542.

Note: the specimen assigned here to *Iberosuchus* Antunes, 1975 is probably *Dentaneosuchus crassiproratus* (see Martin *et al*., 2023 for more details).

A survey of osteoderm histology and ornamentation among Crocodylomorpha: a new proxy to infer lifestyle?

Yohan Pochat-Cottilloux[A], Jeremy E. Martin[A], Romain Amiot[A], Jorge Cubo[B], Vivian de Buffrénil[B]

A: Univ Lyon, Univ Lyon 1, ENSL, CNRS, LGL-TPE, Villeurbanne, France.

B: Centre de Recherche en Paléontologie – Paris (CR2P), Sorbonne Université, 4 Place Jussieu, 75005, Paris, France.

Corresponding author: Yohan Pochat-Cottilloux, yohan.pochat-cottilloux@univ-lyon1.fr

Abstract

Osteoderms of eight extant and extinct species of crocodylomorphs are studied histologically and morphologically. Most osteoderms display the typical 'crocodylian' structure with a woven-fibered matrix surrounded by an upper and a lower parallel fibered matrix. The dorsal ornamentation of those specimens consists of a pit-and-ridge structure, with corresponding remodelling mechanisms. However, an osteoderm of *Iberosuchus* (Robiac, France), studied here for the first time, differs in being nearly devoid of ornamentation; moreover, it shows strong bundles of straight Sharpey's fibers perpendicular to the surface in its lateral and dorsal walls, along with a rough plywood-like structure in its basal plate. This suggests that this osteoderm was more deeply anchored within the dermis than the other osteoderms studied hitherto. This peculiar structure might have been linked to a terrestrial ecology and a specific thermoregulation strategy. Other notosuchians in our sample also do not exhibit ornamentation on their osteoderms, as opposed to neosuchians. Considering current interpretations of osteoderm function(s) in crocodylians, our observations are discussed in reference to possible eco-physiological peculiarities of Notosuchia in general, and *Iberosuchus* in particular.

Keywords paleohistology, osteoderm, Notosuchia, ornamentation.

Introduction

Osteoderms are part of the dermal armour of numerous sauropsids (lizards, Williams *et al*., 2022; dinosaurs, Curry Rogers *et al*., 2011; phytosaurs, Scheyer *et al*., 2014; aetosaurs, Cerda *et al*., 2018; placodonts, Scheyer, 2007). In most of these taxa, the ornamentation consists of hollow pits or grooves, separated by protruding ridges. The ontogenetic process responsible for this morphology has long remained controversial. It was first studied by Buffrénil (1982), who

concluded that in Crocodylomorpha, osteoderm ornamentation is mainly created by local bone resorption, with complex remodelling processes resulting in the adaptation of the depth and size of the pits to the size of the osteoderm during the growth of the individual. However, this interpretation was rejected by Vickaryous & Hall (2008) because they found no sign of osteoclasts (cells responsible for bone erosion) in these bony structures, arguing in favour of the formation of crests rather than the resorption of pits (as in temnospondyls, Witzmann & Soler-Gijon, 2010). Finally, Buffrénil *et al*. (2015) showed through an experimental approach (*in* vivo labelling of skeletal growth) and observations conducted on a wide taxonomic sample, including fossil forms, that although there is still no definite evidence of osteoclasts close to osteoderm surfaces, resorption is evidenced by both bone labelling technics and the occurrence of reversion lines. The formation of pits is thus mainly due to superficial bone resorption, followed by partial reconstruction, and to a lesser extent to the formation of ridges. The presence of osteoderm ornamentation is hypothesized to have been selected in semiaquatic crocodylomorphs because the presence of this feature contributes to heat captation, through enhanced vascularization (Clarac *et al*., 2018).

This process is plesiomorphic to Crocodylomorpha (absent in rauisuchians, Scheyer & Desojo, 2011): indeed, most taxa in this group show the classical ornamentation of hollow pits and grooves and protruding ridges. However, some taxa belonging to Notosuchia do not show this kind of ornamentation (baurusuchids, Cotts *et al*., 2017; *Malawisuchus mwakasyungutiensis,* Gomani, 1997; sebecids, Martin, 2016; *Simosuchus clarki*, Buckley *et al*., 2000; sphagesaurids, Martinelli *et al*., 2018). These taxa are also thought to have had more terrestrial habits than their neosuchian relatives (Pol *et al*., 2012; Klock *et al*., 2022). Given the apparent morphological differences in osteoderm ornamentation between putative terrestrial and semi-aquatic crocodylomorphs, the hypothesis of osteoderm morphology reflecting lifestyle is addressed.

To test this hypothesis, we compare the macroscopic structure of osteoderms belonging to 4 extinct notosuchians including the sebecid *Iberosuchus* described here for the first time, as well as those of semiaquatic neosuchians and a teleosaurid. Furthermore, we also aim to expand the histological taxonomic sample of previous studies, as well as gain insights on the paleoecology of those taxa using both histological (with a focus on *Iberosuchus*) and external features.

Material and methods

The sample used for histology consists of eight osteoderms belonging to eight extant and extinct crocodylomorph taxa (three are not identified at the species level). They represent at least five different families and genera (Table 17). All osteoderms were embedded under vacuum in a polyester resin (bones from extant specimens were dehydrated and defatted in ethanol and acetone before being embedded) and each was processed into at least one thin section, following the standard procedure for this kind of preparation (Lamm & Padian, 2013). The sections were then observed microscopically at low (x20) to medium (x40) power magnification, under natural or polarized transmitted light using three different devices: a Nikon Eclipse E600 POL photomicroscope, an Olympus CX-31P coupled with a Canon EOS6D, and a Zeiss Axioshop coupled with a Canon Power Shot A640. As the goal of this study is to include fossil taxa, soft tissue histology was not used. The terminology used to describe bone histology follows that of Francillon-Vieillot *et al*. (1990). Global compactness was measured and calculated manually.

Table 17: Specimens sampled in this study.

Family	Genus	Species	Age	Reference
Uruguaysuchidae	*Araripesuchus*	*tsangatsangana*	Campanian - Maastrichtian	MNHN-Histos 1685
Uruguaysuchidae	*Araripesuchus*	*wegeneri*	Aptian	MNHN-GDF 660
Sebecidae	*Iberosuchus*	indet.	Bartonian	UCBL-FSL 530948-90080
indet.	*Simosuchus*	*clarki*	Maastrichtian	MNHN-Histos 1759
Crocodylidae	*Crocodylus*	*acutus*	Extant	MNHN-Histos 1713
Crocodylidae	*Mecistops*	sp.	Extant	MNHN-Histos 1716
Teleosauridae	indet.	indet.	?	MNHN-Histos 1660
Dyrosauridae	indet.	indet.	?	MNHN-Histos 1724

The osteoderm belonging to *Iberosuchus* sp. (UCBL-FSL 530948-90080) was cut in four thin sections (see Supplementary Material S1). This specimen comes from the middle Eocene (upper Bartonian) Robiac locality (Gard, France), mostly known for its mammalian fauna (Sudre, 1969; Mathis, 1985; Remy, 2015; Martin, 2016). Remains of *Iberosuchus* in this locality were mentioned by Antunes, 1986 and Martin, 2016.

Results

The osteoderm of *Crocodylus acutus* (Fig. 5.1A) is triangular-shaped with a strongly differentiated dorsal keel. It is also highly cancellous: its global compactness (i.e., relative surface of the mineralized osseous tissue within the whole sectional surface) is quite low (83%). The thin section shows that inner remodelling was intense: there are almost no signs of primary bone left and secondary osteons are especially developed. A vascular canal outcrops at the top of the dorsal keel (Fig. 5.2D). The typical crocodylian dorsal ornamentation pattern can be observed in this osteoderm, with two huge pits that have undergone intense remodelling. One

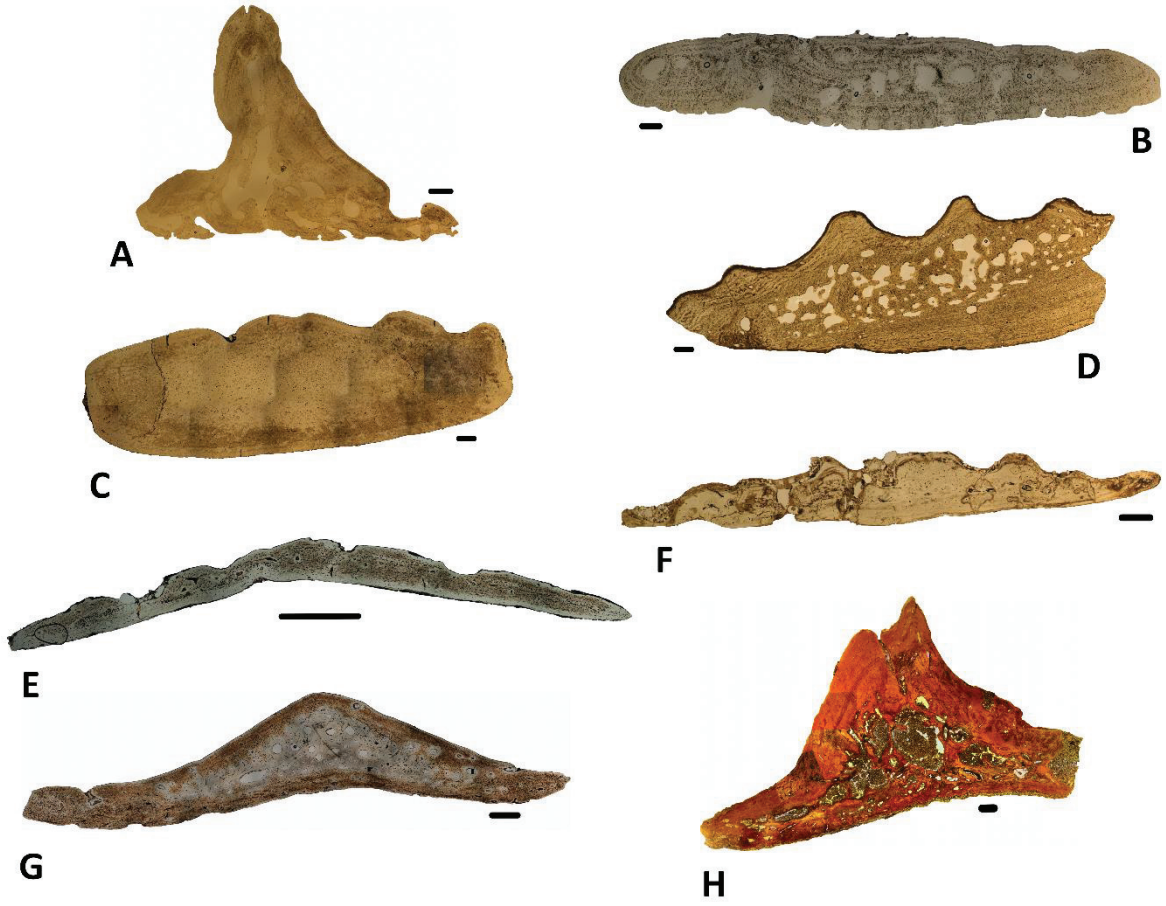

Figure 5.1: Thin sections of extant and extinct crocodylomorph osteoderms: (A) *Crocodylus acutus*; (B) *Mecistops* sp.; (C) Dyrosauridae indet.; (D) Teleosauridae indet.; (E) *Araripesuchus tsangatsangana*; (F) *Araripesuchus wegeneri*; (G) *Simosuchus clarki*; (H) *Iberosuchus*. Scale bars are 1 mm.

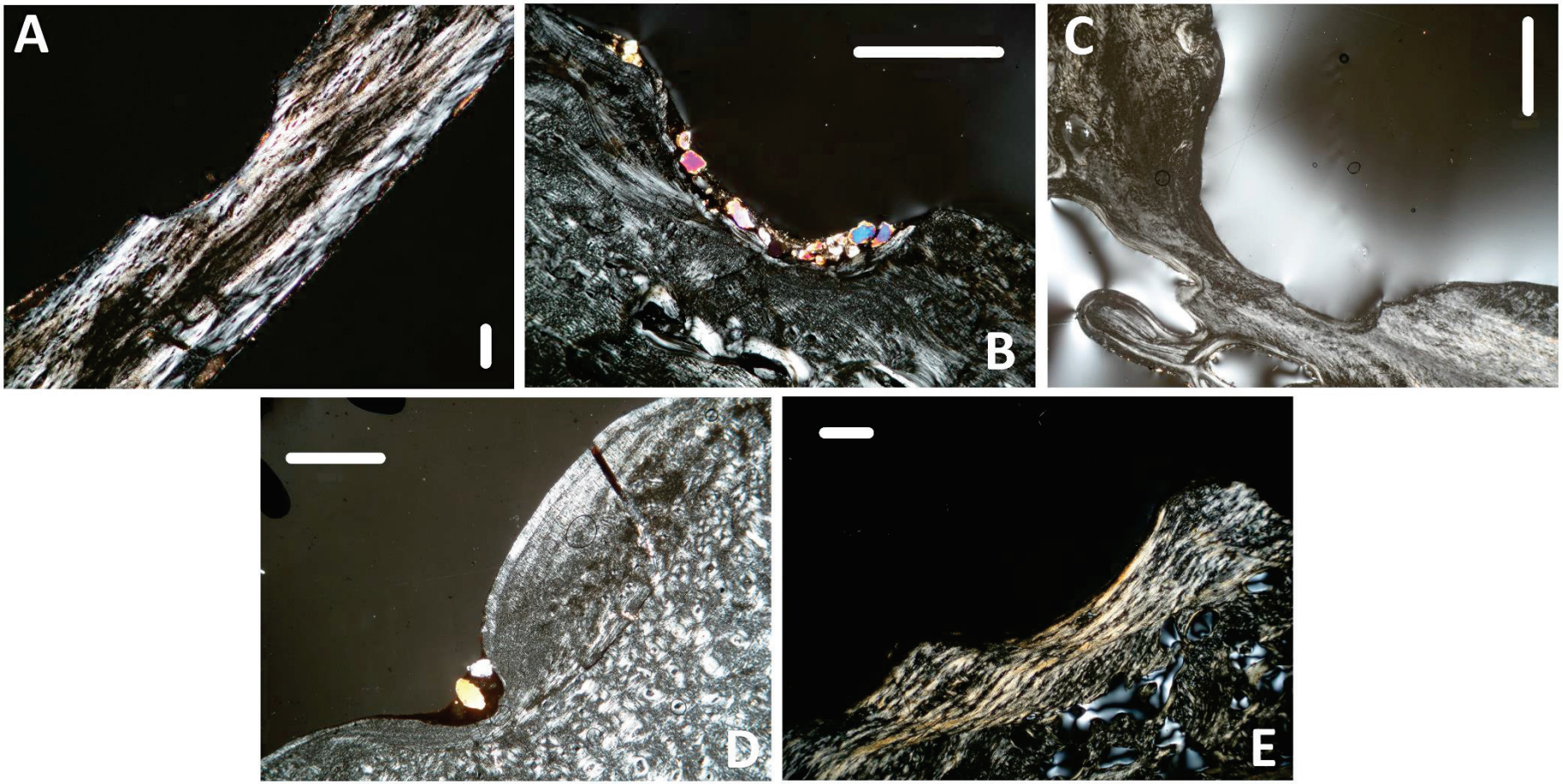

Figure 5.2: Pit-like structures on osteoderms of: (A) *Araripesuchus tsangatsangana*; (B*) Araripesuchus wegeneri*; (C) *Crocodylus acutus*; (D) Dyrosauridae indet.; (E) Teleosauridae indet. Scales are 0.1 mm for A and 1 mm for the rest.

of them is almost filled with secondary deposits of parallel fibers. The osteoderm of *Mecistops* sp. (Fig. 5.1B) is thin, elongate and almost rectangular-shaped in cross section. It has a medium level of global compactness (95%) and bone remodelling. The core part displays numerous secondary osteons developing centripetally and the superficial layers of parallel-fibered matrix are clearly visible. An interesting feature of this specimen is the presence of numerous vascular canals originating from the basal side. The dorsal ornamentation is reduced compared to other neosuchians specimens but is still present.

The osteoderm of the dyrosaurid (Fig. 5.1C) is extremely thick, compact (>99.9%), and almost devoid of cancellous bone. This specimen shows no signs of secondary deposits: even its core part is compact and does not show any resorption trace. However, ornamentation on the dorsal side involved secondary centrifugal deposits of parallel fibered tissues (Fig. 5.3D). This side also displays a few foramina through which inner vascular canals outcrop at the surface (Fig. 5.2E).

The osteoderm of the teleosaurid (Fig. 5.1D) is also quite thick, but less compact (91%): its core contains a formation of cancellous bone. The histological organisation described above for the other osteoderms also occurs in this osteoderm: the core consisting of woven-fibered bone is framed by two layers of parallel-fibered tissue. Some secondary osteons can also be found but they are rather sparce. The dorsal ornamentation is clearly visible and especially developed. It has the typical histological structure of crocodylian pit-and-ridge ornamentation, with secondary parallel-fibered matrix deposited at the bottom of the pits (Fig. 5.3E).

The osteoderm of *Araripesuchus tsangatsangana* (Fig. 5.1E) has an elongate and thin shape and a high global compactness (almost 100%). It has the typical histological structure of a crocodylomorph osteoderm (as described by Buffrénil *et al*., 2015): its core shows large globular osteocyte lacunae embedded within a woven-fibered matrix. This central formation is framed by two cortices made of parallel-fibered tissue (exhibiting thin annuli), forming the outer and inner walls. There are no secondary osteons, which would be clear signs of secondary ossification, however a lacuna of howship (bone resorption area; Francillon-Vieillot *et al*., 1990) can be seen in the parallel-fibered bone (Fig. 5.2B). The relative thinness of the parallel-fibered deposits suggests that the osteoderm was still in an early stage of development at the time of death. It also displays the typical crocodylian dorsal ornamentation (pits-and-ridges), which is also visible in thin section with local areas of bone resorption corresponding to pits. However, the osteoblastic reconstruction process that normally follows is not visible, which is

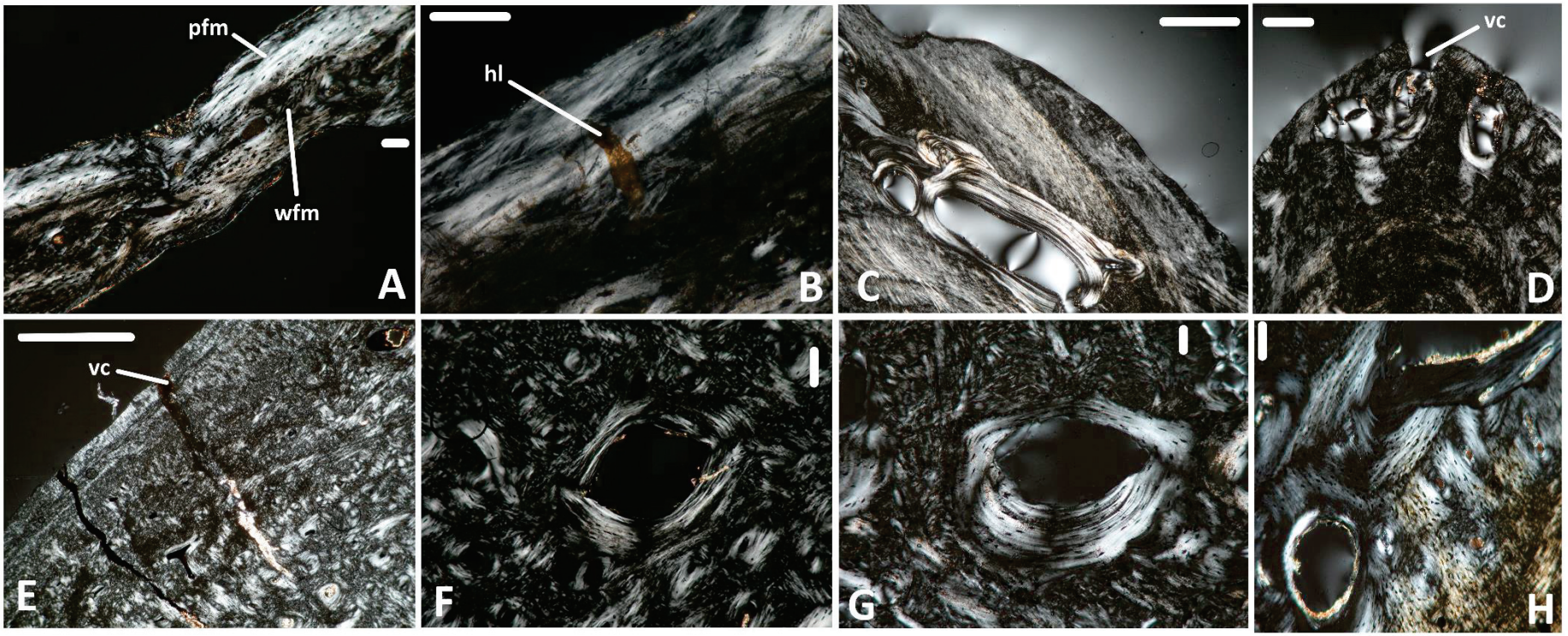

Figure 5.3: Histological structures of osteoderms: (A) typical osteoderm layout, with woven-fibered matrix (wfm) in between parallel-fibered matrix (pfm); (B) Howship lacuna (hl); (C, F, G & H) secondary osteon; (D & E) vascular canal (vc). (A & B) *Araripesuchus tsangatsangana*; (C & D) *Crocodylus acutus*; (E & F) Dyrosauridae indet.; (G) *Mecistops* sp.; (H) *Simosuchus clarki*. Scales are 0.1 mm for A, B, F, G & H and 1 mm for C, D & E.

possibly due to the early development stage of the individual.

The osteoderm of *Araripesuchus wegeneri* (Fig. 5.1F) has the same thin and elongate shape than *A. tsangatsangana* but a lower global compactness (98%). Secondary osteons are more visible in this specimen. The typical crocodylian dorsal ornamentation also occurs here, and, in relation with a more active remodelling, secondary centrifugal deposits can be seen in the bottom of the pits (Fig. 5.3B). Those are clearly separable from the subjacent bone tissues by a reversion line and a discordant orientation.

The osteoderm of *Simosuchus clarki* (Fig. 5.1G) is also elongate but bears a smooth dorsal keel, allowing its identification as a dorsal osteoderm (Hill, 2010). It has a medium global compactness (97%) with some cancellous bone in the core part. Together with numerous secondary osteons, those features reflect the remodelling activity that occurs in the central part of the osteoderm (but it is lesser than in the osteoderm studied by Hill, 2010). The main difference is the absence of pit-and-ridge patterns in the dorsal ornamentation of this specimen. Hill (2010) reported perpendicularly oriented fibers in the dorsal part of the osteoderm, but those structures were not observed here.

Finally, the osteoderm of *Iberosuchus* (Fig. 5.1H) has a triangular shape due to the strong differentiation of the keel. Global compactness (87%) is similar to that encountered in many neosuchians (see above). The sketch presented in Fig. 5.4 shows the local variation in the tissue composition of the osteoderm. It also gives the location of the photographic fields presented in Fig. 5.5. The core of the osteoderm is cancellous, with broad coalescent cavities separated by robust trabeculae (Fig. 5.4, green, Fig. 5.5A). The basal and lateral walls are thick, but their vascular supply is sparse. Some canals outcrop at the dorsal surface but the openings of the canals are not preferentially located in the middle of the pit floors. The core of the osteoderm consists of a small formation of woven-fibered bone tissue. In the dorsal three quarters of the osteoderm, the compact cortex consists of parallel-fibered bone with cyclical growth marks in the form of thin annuli, poorly characterized and unevenly spaced (Fig. 5.4, yellow, Fig. 5.5B-C). The lower, basal quarter of the osteoderm cortex (Fig. 5.4, blue) includes big interwoven fiber bundles with irregular orientations (Fig. 5.5D), within the parallel-fibered tissue. Most of the volume of the basal plate is an assemblage of extremely big fiber bundles (some 600 µm in diameter) displaying a clear geometrical structuration (Fig. 5.5E-F). They form a rough plywood-like structure where three bundle systems occur: two of them are horizontal (i.e., parallel to the surface of the basal cortex), but with diverging obliquities, to the right and to the

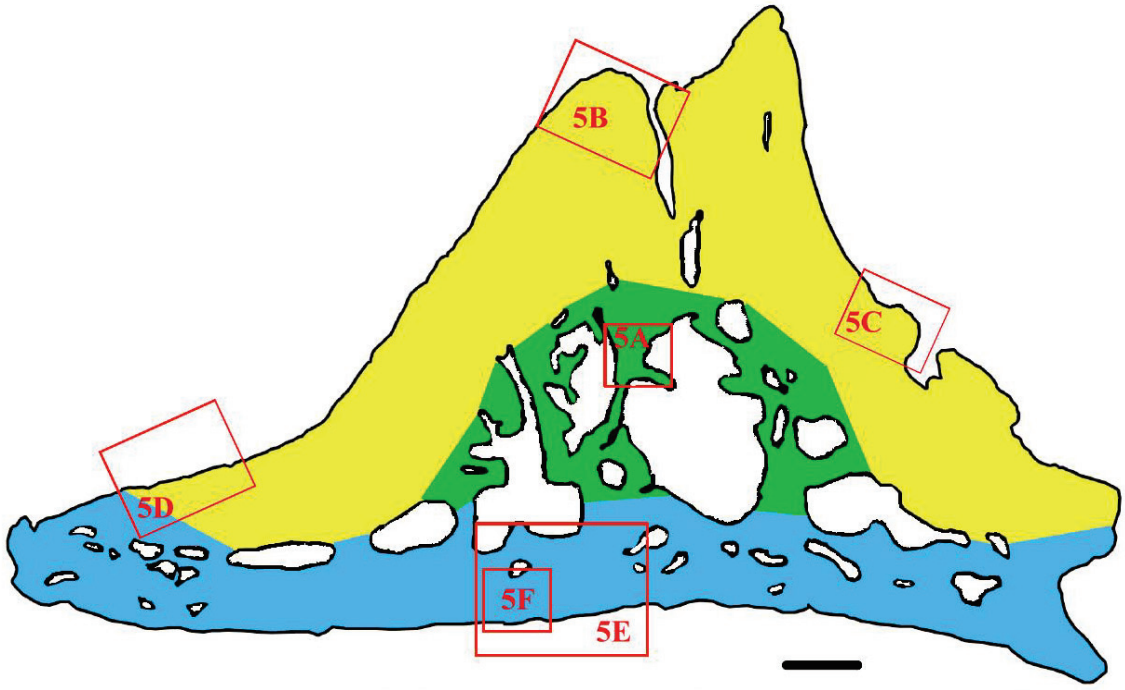

Figure 5.4: *Iberosuchus* osteoderm, schematic representation of the location of bone tissue types. Blue: incorporation and calcification of deep dermal fibers, green: remodeled woven-fibered bone, yellow: periosteal parallel-fibered tissue. The frames localize the pictures of Figure 5.5. Scale is 1 mm.

left (this results in distinct refringence patterns of these bundles in polarized light). The third system consists of vertically oriented fiber bundles. The surface of the basal plate lacks a tissue histologically recognizable as bone: the basal plate looks entirely made of diverse assemblages of calcified fibrillar material devoid of the basic characteristics of bone. Ornamentation on the dorsal surface of the osteoderm does not result from the succession of complete remodeling cycles, including osteoclastic resorption followed by osteoblastic reconstruction with lamellar secondary bone over the bottom of the pits. Some faint resorption traces can be observed on the floor of one pit only, but there is no evidence of a local reconstruction process. Moreover, the parallel-fibered tissue of the dorsal cortex, throughout its thickness and in every spot where it appears, is deeply penetrated by series of strong parallel bundles of fibers running perpendicularly or obliquely from the osteoderm surface (Fig. 5.5B-D). These bundles are sparser, but their diameter is much bigger and their orientation less even towards the base of the osteoderm.

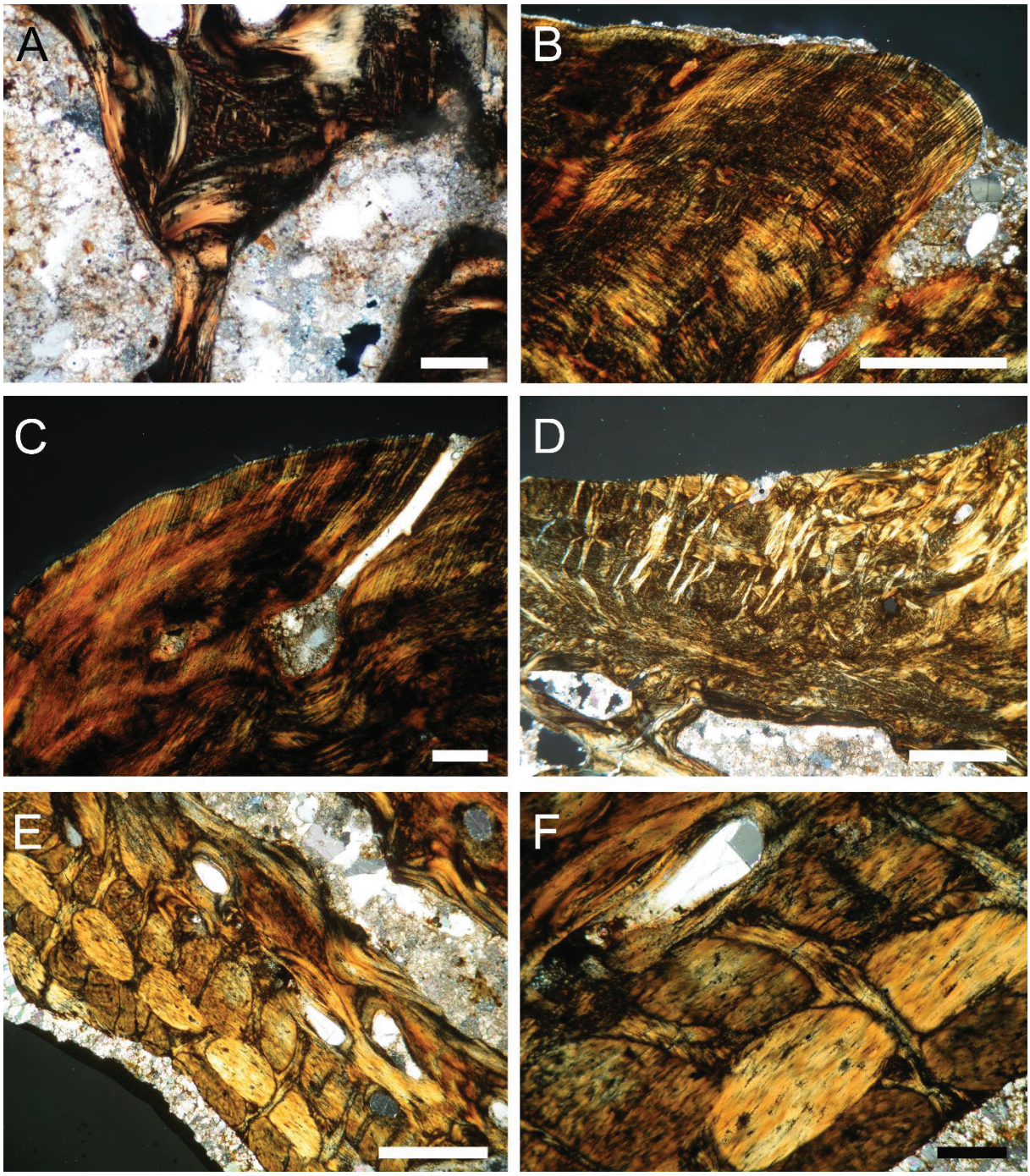

Figure 5.5: *Iberosuchus* osteoderm, histological tissue types forming the osteoderm (see also Figure 5.4). All pictures are seen in polarized light. (A) Remodeled woven-fibered bone in the core of the osteoderm. (B & C) Parallel-fibered bone on the apex and walls of the osteoderm. This tissue contains long and straight fiber bundles from the loose dermis (*stratum superficiale*). (D) Parallel-fibered tissue with extremely thick fiber bundles from the neighboring dermis. (E & F) Rough plywood-like formation representing the incorporation into the osteoderm and the calcification of a part of the dense dermis (*stratum compactum*). Scales are 0.2 mm for A, C and F and 1 mm for B, D and E.

Discussion

Peculiar characteristics of the osteoderm of *Iberosuchus*

The microanatomical characteristics of *Iberosuchus* osteoderm do not differ from those of most crocodylomorph osteoderms in terms of gross geometry and global compactness (Vickaryous & Hall, 2008, Burns *et al*., 2013, Buffrénil *et al*., 2015). However, the peculiar histological structure of this specimen shows two unique features: (1) there is no typical remodelling involved in the differentiation and growth of superficial ornamentation (Fig. 5.5B-C) and (2) the occurrence of strong fiber bundles, either interwoven or forming a plywood-like structure within the lower cortex (Fig. 5.5E-F) is unknown in other crocodylomorphs, at least in adults (the situation could occur during early ontogenetic stages: Vickaryous & Hall 2008). These histological peculiarities, and especially the abundance and distribution of extrinsic, non-osseous fiber bundles, suggest a special mode of growth.

The osteoderms of *Iberosuchus* were strongly anchored into the dermis. In other crocodylians, however, the permanent superficial remodelling of ornamented surfaces prevents a strong and stable anchoring of the upper side of the osteoderms (as well as the thinness of the *stratum superficiale*, or superficial dermis; Vickaryous & Hall, 2008; Burns *et al*., 2013; Clarac *et al*., 2018). Most anchoring fibers are then limited to thin Sharpey's fibers in the parallel-fibered tissue of the basal plate, or in deep cortical strata elsewhere.

Histologically, *Iberosuchus* osteoderm may be compared with those of *Simosuchus clarki* described by Hill (2010), which also show perpendicularly oriented fibers relative to the external surface. However, those structures are not encountered in the specimen described here (MNHN-Histos 1759). It may also be compared with those recently described of *Mariliasuchus amarali, Armadillosuchus arrudai, Itasuchus jesuinoi, Uberabasuchus terrificus, Aplestosuchus sordidus* and another baurusuchid (Sena *et al*., 2023). Indeed, these also exhibit Sharpey fibers on the external surface, indicating that the deep implantation of osteoderms could be a general feature of notosuchians. Furthermore, the carapace plates of some fully aquatic turtles, especially the Trionychidae Gray, 1825, are covered with thick dermal tissue which, along with the cambial and cornified layers of the epidermis, constitutes a tough, though flexible, protection (Cherepanov, 1995; Alibardi & Toni, 2006; Scheyer *et al*., 2007; Scheyer & Cerda, 2021). The basal cortex of *Trionyx triunguis* Forskal, 1775 or *Tryonyx spiniferus* LeSueur, 1827 plates typically consists of an orthogonal plywood-like system with regularly arranged horizontal and vertical fiber bundles (a geometric pattern much more regular than in

Iberosuchus). Moreover, the dorsal cortex shows the same kind of strong pattern consisting of parallel bundles of fibers penetrating the cortex vertically throughout its whole thickness as observed in *Iberosuchus* (Buffrénil *et al*., 2015).

The histological characteristics of the osteoderm of *Iberosuchus,* compared to those of its integument, suggest that its formation mode was different from that of most neosuchians (for a complete review, see Vickaryous & Hall, 2008; Buffrénil *et al*., 2015). The thick, roughly orthogonal plywood formation that exclusively composes the basal part of the osteoderm may have formed through a local incorporation and calcification of the fibrillar apparatus of the dense *stratum compactum*, in the depth of the dermis. The osteoderm cortex at this level, being essentially composed of extrinsic fibrillar material, did not result from osteoblastic osteogenesis, but from a process akin to metaplasia (at least for the extra-cellular matrix). Conversely, the cortex located in a more superficial position grew through the typical osteoblastic osteogenesis of parallel-fibered bone. Moreover, as in soft-shelled tortoises (Cherepanov, 1995, Alibardi & Toni 2006; Scheyer *et al*., 2007; Scheyer & Cerda, 2021), a thick and relatively dense dermal layer, from which the strong perforating parallel fibers originated, covered the external side of the osteoderm. According to this interpretation, osteoderm formation and position within the skin were deeper in *Iberosuchus* than in other crocodylomorphs: by incorporating the fibers of the *stratum compactum*, the osteoderm tends to sink into the dense dermis, and their development is unlikely to have occurred mainly in the *stratum superficiale*, as it does in neosuchians. The distribution of extrinsic fibers within the osteoderm shows that it was firmly attached to both the superficial and deep dermal layers through its upper (ornamented) and basal surfaces respectively.

The histological data presented here show that the peculiar morphology of osteoderm ornamentation in *Iberosuchus* was not due to a total filling of former ornamental pits (as it may occur, at least locally, in many crocodylomorphs; see Buffrénil *et al*. 2015); it was due to a disappearance (or de-differentiation) of the basic morphogenetic mechanisms that create ornamental reliefs (iterative remodelling of the ornamental surface).

The functional meaning of the histological peculiarities of the *Iberosuchus* osteoderm remains enigmatic, as are more generally the lifestyle and ecological adaptations of this taxon. Its overall morphology suggests a terrestrial animal adapted to active predation and possibly relying on a high metabolic activity, as compared with other close taxa (Pol *et al*., 2012). However, the histological characteristics of *Iberosuchus* limb bones (Cubo *et al*., 2017), and the basal

metabolic rate inferred using these features (Cubo *et al*., 2020), are closer to those of bradymetabolic lizards than to those of dinosauromorphs or mammals (Buffrénil *et al*., 2021). The histological peculiarities of *Iberosuchus* osteoderm might be related to muscular insertion. Crocodylian osteoderms are indeed considered to improve the insertion of the epaxial muscles into the skin and increase their efficiency for thrust production during swimming (Seidel, 1979, Schwarz-Wings *et al*., 2009). In the context of the terrestrial and cursorial locomotion commonly attributed to sebecosuchians, a tougher integration of the osteoderms within the dermis would not have been involved in improving propulsion but might have been beneficial to the control of an erect posture in forms like *Iberosuchus*. This hypothesis, although also put forward recently in Sena *et al*. (2023), currently remains conjectural and calls for further substantiation.

A possible involvement of intradermal blood vessels in thermoregulation also remains a possibility. In extant forms, an important role is attributed to dermal vascularization in the regulation of thermal exchanges in crocodiles (Seidel, 1979; Clarac *et al*., 2018 but see Veenstra & Broeckhoven, 2022). Dermal thickening and superficial vascular proliferation might then have, in some taxa, restored a capacity to accelerate blood warming. However, no positive anatomical data about skin vascularization in extinct crocodiles is available in support of this conjecture. Moreover, this would constitute a hazardous solution, likely to produce important haemorrhage in the case of skin injuries.

Osteoderm ornamentation as a paleoecological proxy?

More generally, osteoderm ornamentation is absent in most notosuchians (Fig. 5.6) apart from uruguaysuchids, peirosaurids and *Candidodon* Carvalho & Campos, 1988. Those taxa are inferred to have been terrestrial (Dumont *et al*., 2021), however some bear pits on their osteoderms (Price, 1955; Ortega *et al*., 2000; Leardi & Pol, 2009; Sereno & Larsson, 2009; Tavares *et al*., 2015; Lio *et al*., 2016; Coria *et al*., 2019).

These observations could be linked to both the living environment and thermoregulation. The presence of osteoderm ornamentation may have been selected in semiaquatic crocodylomorphs because the presence of this feature contributes to heat captation, through enhanced vascularization (Clarac *et al* 2018). Indeed, all the species studied here are inferred to be ectotherms (from histological and geochemical proxies; Cubo *et al*., 2020; Faure-Brac *et al*., 2022). Because thermal conductivity, heat capacity and density in water are higher than those

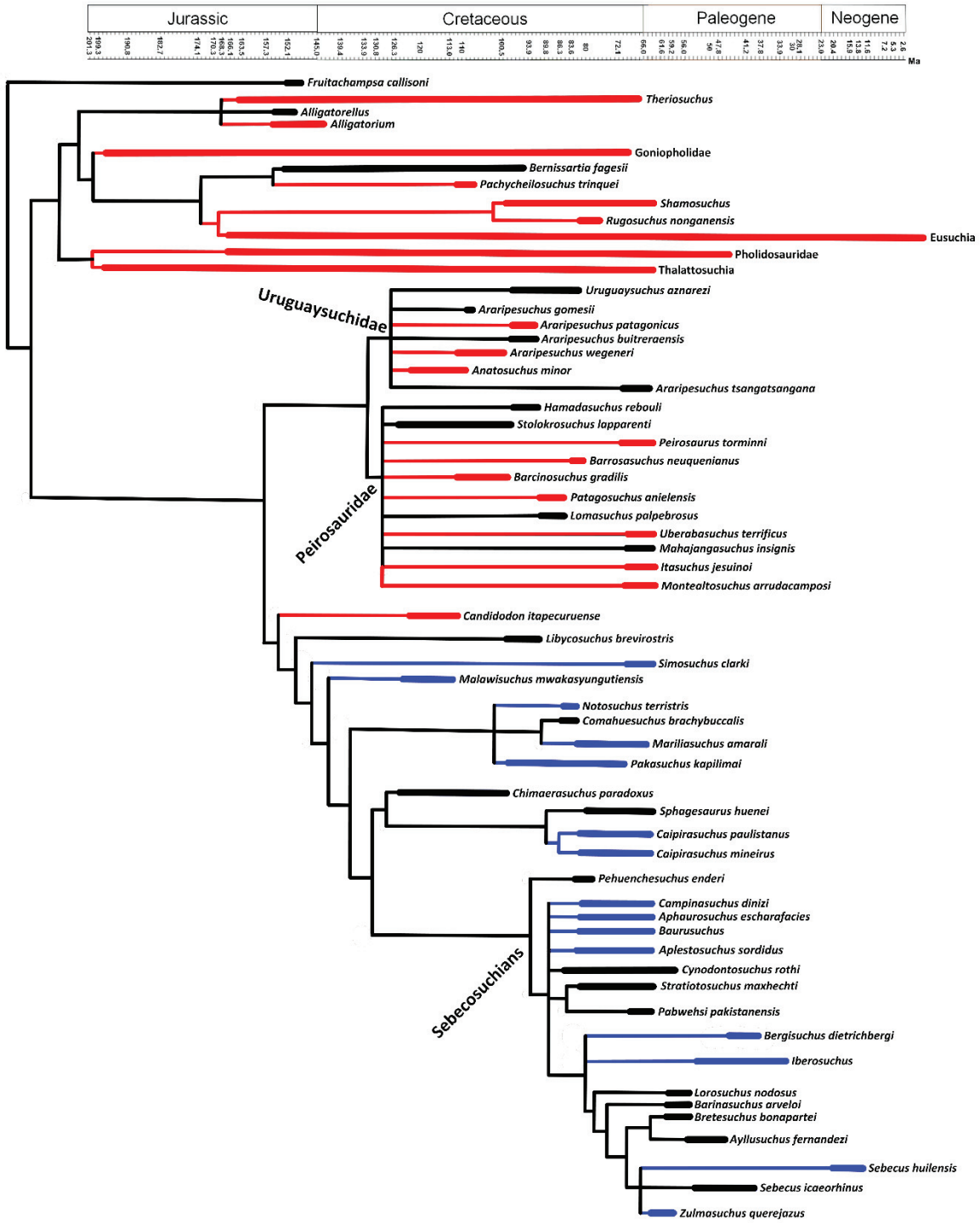

Figure 5.6: Phylogenetic relationships of some crocodylomorphs highlighting the morphology of osteoderms. Red branches represent the presence of ornamentation whereas the absence of ornamentation is in blue. Black is the unknown condition. Occurrences and phylogenetic relationships are from Gomani, 1997; Ortega *et al*., 2000; Pol, 2005; Marinho *et al*., 2006; Sereno & Larsson, 2009; Hill, 2010; Nascimento & Zaher, 2010; O'Connor *et al*., 2010; Nobre & Carvalho, 2013; Godoy *et al*., 2014; Leardi *et al*., 2015; Tavares *et al*., 2015; Martin, 2016; Iori *et al*., 2016; Cotts *et al*., 2017; Martinelli *et al*., 2018; Montefeltro, 2019; Darlim *et al*., 2021a; *Marchetti et al*., 2022; Sena *et al*., 2023, as well as data from Fossil Work. *Iberosuchus* osteoderm is hypothetically placed at the base of Sebecidae.

in air, body heat loss is higher in water than in air and maintaining a high body temperature is

more costly (Schmidt-Nielsen, 1997; Vogel 2005). Selective pressure for osteoderm ornamentation may thus be lower in terrestrial taxa, so this feature could become vestigial or completely disappear. This could then support a terrestrial ecology but with semi-aquatic affinities for uruguaysuchids, peirosaurids and *Candidodon*, as seen today for example in extant dwarf crocodiles belonging to the genus *Osteolaemus* (Shirley *et al*., 2017). This idea has been put forward in a histological study of *Pepesuchus deiseae* (Peirosauridae), where Sena *et al*. (2018) observed osteosclerosis in metacarpals and fibro-lamellar tissue in advanced ontogeny, linking it with a more aquatic lifestyle. However, as for the impact of dermal vascularization, the debate on the ecological impact of osteoderm ornamentation remains open (Seidel, 1979; Clarac *et al*., 2018; Veenstra & Broeckhoven, 2022).

Furthermore, as seen in Fig. 5.6, the loss of osteoderm ornamentation is restricted to a group including *Simosuchus clarki* and sebecosuchians, becoming the derived condition in notosuchians. As a result, another possibility could be that notosuchians illustrate a case of phylogenetic time lag (Harvey & Pagel, 1991): the osteoderm ornamentation representing the ancestral condition in crocodylomorphs having been ultimately lost (derived condition) in derived notosuchians. Ornamentation is identified in some of them, such as uruguaysuchids, peirosaurids and *Candidon*, even though it would not have the hypothesized thermoregulative function because those taxa would not need it.

Conclusion

For the first time, an osteoderm of *Iberosuchus* from France (Robiac) is described. Histologically, we notice some peculiar characteristics such as a dorsal surface penetrated by a series of strong parallel bundles of fibers running perpendicularly from the osteoderm surface, which does not bear any trace of bone remodelling, as other crocodylomorph osteoderms do. The organisation of the basal part of the specimen is also different from what is known in other crocodylomorphs and suggests a deeper osteoderm implantation within the integument in this taxon. Up to now, the interpretation of this special and puzzling characteristic in functional terms remains uncertain and conjectural. Further data on notosuchian ecology, based on different lines of evidence than histology, remains obviously needed.

More generally, we observe that the ornamentation of osteoderms is lost in derived notosuchians. As those taxa are inferred to be terrestrial, we hypothesize that the osteoderm ornamentation might be linked to lifestyle: it would allow a greater surface of exchange in aquatic to semi aquatic environments, to account for a greater temperature loss in those

environments. Conversely, this morphological trait would have been ultimately lost in terrestrial notosuchians.

However, this issue remains open, and further studies are needed to better understand the impact and function of osteoderm ornamentation in crocodylomorphs. A better sampling of extinct forms would also be of interest, to better tackle the evolution of this trait throughout Crocodylomorpha history.

Acknowledgements

We thank Ronan Allain (MNHN) for access to the *A. wegeneri* material, Damien Germain (MNHN) for access to the histological collections of the MNHN, Séverin Morel (MNHN) for preparing the thin sections of the osteoderm of *Iberosuchus*, as well as Matthias Starck (University of Munich) and an anonymous reviewer for insightful comments that greatly improved the quality of this manuscript. This work was supported by the Agence Nationale de la Recherche (SEBEK project no. ANR-19-CE31-0006-01 to JEM) and by Sorbonne Université (project Emergences 2019 n° 243374 to JC).

Authors contributions

Yohan Pochat-Cottilloux: Conceptualization, Methodology, Software, Validation, Formal Analysis, Investigation, Data Curation, Writing - Original Draft, Writing - Review & Editing, Visualization. **Jeremy E. Martin**: Conceptualization, Validation, Resources, Data Curation, Writing - Review & Editing, Supervision, Project administration, Funding acquisition. **Romain Amiot**: Conceptualization, Validation, Writing - Review & Editing, Supervision, Project administration. **Jorge Cubo**: Conceptualization, Methodology, Software, Validation, Formal analysis, Investigation, Resources, Data Curation, Writing - Review & Editing, Visualization, Supervision, Project administration, Funding acquisition. **Vivian de Buffrénil**: Methodology, Validation, Formal analysis, Investigation, Writing - Original Draft.

Data archiving statement

Data for this study are available in the article and the Supplementary Material.

Supplementary Material

Supplementary Material S1 is available in Appendix 10.

General conclusions and perspectives

Throughout this PhD thesis, the main objectives were to study and assess the adaptations to terrestriality of diverse clades of altirostral (i.e., with a rostrum length equal to or less than three times its height) crocodylomorphs and understand the evolutionary timing of those adaptations. Further research objectives included the assessment of additional proxies to infer their paleoecology with more robustness.

This began in Chapter 1, with a review of the different non-semi-aquatic adaptations in the fossil record of crocodylomorphs. 'Early' crocodylomorphs (sphenosuchians and protosuchians) were ancestrally terrestrial, with an erect posture. Most notosuchians (uruguaysuchids, peirosaurids, mahajangasuchids, sphagesaurians, sebecids and baurusuchids) are also inferred to be terrestrial, with diverse adaptations, to omnivory and herbivory, or to a burrowing behavior. Adaptations to terrestriality are also found in neosuchians (the clade that include extant crocodylians), with clades such as atoposaurids, paralligatorids, mekosuchins and planocraniids exhibiting an altirostral morphology linked with this lifestyle. On the other hand, throughout its evolutionary history, Crocodylomorpha also included fully aquatic forms, such as thalattosuchians or dyrosaurids, with some specimens even exhibiting adaptations to a fully pelagic lifestyle. The inference of the living environment of those organisms has mainly been based on their skull morphology (orientation of the orbits and the external nares), their limb and girdle morphology (linked with posture) and their dentition (linked with possible diets).

Although those observations are valid, there lies the need to better understand the phylogenetic relationships of all those organisms, which is a prerequisite to any large-scale comparisons and evolutionary trend studies. This matter was addressed in Chapter 2, where I first noticed that the relationships of peirosaurids, sebecids and baurusuchids are complex to assess. From a literature review of phylogenetic analyses conducted on the subject, I conclude that neither the grouping of sebecids and peirosaurids (Sebecia) or sebecids with baurusuchids (Sebecosuchia) as sister taxa are supported by unambiguous synapomorphies, and, as those are equally supported in the literature by a complete combination of characters, it is difficult to favour one or the other. Then, a published study focused on the taxonomic status and content of *Hamadasuchus*, a peirosaurid taxon from the Cretaceous of Morocco. A new mandibular ramus and ontogenetic series of extant crocodylians allowed to amend the diagnosis of *H. rebouli* (the

only valid species of the genus), as well as to reduce its taxonomic content. Finally, a complete study and phylogenetic assessment of new specimens of atoposaurids from the Cretaceous of Thailand allowed to create a new taxon, *Varanosuchus sakonnakhonensis*. It is the second occurrence of atoposaurids from Thailand, adding to the huge diversity of Cretaceous crocodylomorphs in Southeast Asia and allows a reassessment of the phylogenetic relationships of some neosuchians clades. A focus was also put on the paleoecological adaptations of those specimens, with numerous characteristics hinting for a terrestrial lifestyle but with semi-aquatic affinities (or semi-terrestrial).

Chapter 3 then focused on a powerful proxy when trying to assess the paleoecology of extinct organisms: the reconstruction of internal structures. Starting from a review of the advances of CT scan techniques, that have enabled so much data to be obtained since the beginning of the 21st century, the internal structures of three taxa representative of three different putatively terrestrial clades were studied: sebecids (*Zulmasuchus*), peirosaurids (*Hamadasuchus*) and atoposaurids (*Varanosuchus*). In crocodylomorphs, the endocast and cranial nerves are associated with several senses such as olfaction or vision; the endosseous labyrinths bring information about the alert head posture and its head movement abilities, as well as hearing capabilities; the size of the peculiar cranial pneumaticity of those organisms may be linked to lifestyle. As a result, *Zulmasuchus* is inferred to be a fully terrestrial notosuchian, while *Hamadasuchus* could also have had some semi-aquatic affinities and *Varanosuchus* was probably semi-terrestrial. A closer look was then taken at the inner ear of crocodylomorphs, using a 3D geometric morphometric approach on an extensive dataset of both extant and extinct specimens, including most main known lifestyles of this group. As highlighted in recent studies, a strong link between shape and ontogeny was found, as well as a minimal phylogenetic signal. However, the shape of those structures does not seem to correlate with ecology.

Another independent proxy was then used in Chapter 4, the geochemical approach, with a special focus on sebecids. The combination of the isotope compositions of oxygen, carbon, calcium, and strontium was studied in several faunas from the Paleogene, with the objective of understanding and assessing several of their paleoecological traits. Oxygen and strontium isotope compositions bring information about the living environment of an organism, while carbon and calcium isotope compositions are related to its diet. Sebecids were already at the top of the terrestrial food-chain shortly after the beginning of the Paleogene, as evidenced in the fauna of Tiupampa (Bolivia) and maintained this position throughout the Paleogene, as

evidenced in the Fauna of Aumelas and Réalmont (France). However, the mysterious putative sebecid *Eremosuchus elkoholicus* from the fauna of El Kohol (Algeria) is found as semi-aquatic, warranting a reassessment of this taxon. While I confirm that sebecids filled the apex predator ecological niche that was left vacant by the disappearance of non-avian theropod dinosaurs, their survival to the Cretaceous/Paleogene transition remains mysterious. Furthermore, the geochemical record of dentine through serial sampling across the growth axis could also be of interest, notably to detect changes in ecology throughout a short period (i.e., the timing of development of the tooth, or tooth replacement rate). Measuring the oxygen and strontium (living environment proxy) and calcium and nitrogen (dietary proxy) isotope compositions of four teeth belonging to three different extant species of crocodylians, I observed that those variations are anticorrelated between calcium and nitrogen and correlated between oxygen and strontium. The specimen of *Osteolaemus* shows the most drastic changes in isotope compositions, which is in line with its seasonal changes of lifestyle. Although several limitations need to be addressed, this protocol could bring interesting results in fossil forms.

Finally, in Chapter 5, I presented a preliminary study of another proxy that might be of interest when trying to assess the paleoecology of an extinct organism. A published histological study of osteoderms of a selection of crocodylomorphs with different lifestyles was conducted, with a sebecid exhibiting peculiar structures, corresponding to a deeper implantation of the osteoderm within the dermis in this taxon, that could be linked with its posture and terrestrial lifestyle. Furthermore, we observed that osteoderm ornamentation was lost in derived notosuchians, and therefore that it might be linked to a terrestrial lifestyle, with associated thermoregulatory issues.

Considering all those findings, the main results that come as answers to the problematics given in the introduction are as follows:

- In addition to morphological observations, the lifestyle can be assessed independently in an extinct organism through the study of its internal structures, the isotopic compositions of its skeletal elements, and the histology and ornamentation of its osteoderms;
- Terrestriality is the ancestral condition of crocodylomorphs, with several subsequent convergent adaptations to the semi-aquatic and aquatic environments (such as extant crocodylians, which are thus not ‘living fossils’) throughout their evolutionary history;

- I can confirm that sebecids had already attained the ecological niche of apex predator (replacing non-avian theropod dinosaurs) in the aftermath of this transition, and have retained it throughout most of the Paleogene;
- The altirostral morphology is not necessarily associated with a fully terrestrial lifestyle, with clades exhibiting an ecology with semi-aquatic affinities, that could be qualified as semi-terrestrial;

This thesis also highlighted several interesting perspectives, which will hopefully be addressed in future studies:

- In addition to the description of new specimens and the reassessment of key taxa, alternative hypotheses based on postcranial or internal data could help tackle remaining phylogenetic and taxonomic conflicts. Ontogenetic variations must also be considered and should rely on the study of extant representatives (especially in crocodylomorphs);
- The function and ontogenetic, phylogenetic, and ecological implications of the cranial pneumaticity and endocast in crocodylomorphs must be better understood and could potentially bring further evidence to paleoecological interpretations in fossil forms. Likewise, the relationship between endosseous labyrinths and inner ears (i.e., hard versus soft tissues) must also be studied;
- Multi-isotopic studies would benefit from the inclusion of even more independent elements, such as zinc, magnesium, nitrogen, or hydrogen. Such studies should be led on terrestrial fauna of the Cretaceous (Adamantina Formation of Brazil, Kem Kem Group of Morocco or Phu Sung fauna of Thailand, for example), to understand how notosuchians fitted in with dinosaurs, see whether their interfaunal relationships were the same as during the Paleogene or not and understand how some lineages, such as Sebecidae, survived the end Cretaceous extinction event;
- Improvements of analytical techniques and better understanding of calcium fluxes between the different tissues of reptiles will hopefully allow detailed and precise studies of extinct organisms during a very short period, corresponding to their tooth replacement rate.

References

Abler W. L. (1992). The serrated teeth of tyrannosaurid dinosaurs, and biting structures in other animals. *Paleobiology*, 18(2): 161-183. https://doi.org/10.1017/S0094837300013956

Adams D. C. (2014). A generalized K statistic for estimating phylogenetic signal from shape and other high-dimensional multivariate data. *Systematic biology*, 63(5): 685-697. https://doi.org/10.1093/sysbio/syu030

Adams D. C. & Otárola-Castillo E. (2013). geomorph: an R package for the collection and analysis of geometric morphometric shape data. *Methods in Ecology and Evolution*, 4(4): 393-399. https://doi.org/10.1111/2041-210X.12035

Adams T. L. (2013). A new neosuchian crocodyliform from the Lower Cretaceous (Late Aptian) Twin Mountains Formation of north-central Texas. *Journal of Vertebrate Paleontology*, 33(1): 85-101. https://doi.org/10.1080/02724634.2012.713277

Adams T. L. (2014). Small crocodyliform from the Lower Cretaceous (Late Aptian) of Central Texas and its systematic relationship to the evolution of Eusuchia. *Journal of Paleontology*, 88(5): 1031-1049. https://doi.org/10.1666/12-089

Adams T. L. (2019). Small terrestrial crocodyliform from the Lower Cretaceous (late Aptian) of central Texas and its implications on the paleoecology of the Proctor Lake Dinosaur locality. *Journal of Vertebrate Paleontology*, 39(3): e1623226. https://doi.org/10.1080/02724634.2019.1623226

Akkiraz M. S., Akguen F., Oercen S., Bruch A. & Mosbrugger V. (2006). Stratigraphic and Palaeoenvironmental Significance of Bartonian–Priabonian (Middle–Late Eocene) Microfossils from the Başçeşme Formation, Denizli Province, Western Anatolia. *Turkish Journal of Earth Sciences*, 15(2): 155-180.

Albarède F. (2009). *Geochemistry An Introduction.* Cambridge University Press, New York.

Alibardi L. & Toni M. (2006). Skin structure and cornification proteins in the soft-shelled turtle *Trionyx spiniferus*. *Zoology*, 109(3): 182-195. https://doi.org/10.1016/j.zool.2005.11.005

Allain R., Vullo R., Rozada L., Anquetin J., Bourgeais R., Goedert J., Lasseron M., Martin J. E., Pérez-García A., Peyre de Fabrègues C., Royo-Torres R., Augier D., Bailly G., Cazes L., Despres Y., Gailliègue A., Gomez B., Goussard F., Lenglet T., Vacant R., Mazan & Tournepiche J. F. (2022). Vertebrate paleobiodiversity of the Early Cretaceous (Berriasian) Angeac-Charente Lagerstätte (southwestern France): implications for continental faunal turnover at the J/K boundary. *Geodiversitas*, 44(25): 683-752. https://doi.org/10.5252/geodiversitas2022v44a25

Allemand R., Abdul-Sater J., Macrì S., Di-Poï N., Daghfous G. & Silcox M. T. (2022). Endocast, brain, and bones: Correspondences and spatial relationships in squamates. *The Anatomical Record*: https://doi.org/10.1002/ar.25142

Alloing-Séguier L., Sánchez-Villagra M. R., Lee M. S. & Lebrun R. (2013). The bony labyrinth in diprotodontian marsupial mammals: diversity in extant and extinct forms and relationships with size and phylogeny. *Journal of Mammalian Evolution*, 20: 191-198. https://doi.org/10.1007/s10914-013-9228-3

Ambrose S. H. (2002). Controlled diet and climate experiments on nitrogen isotope ratios of rats. In Ambrose S. H. & Katzenberg M. A. (eds.) *Biogeochemical Approaches to Paleodietary Analysis*, Springer: 243-259. https://doi.org/10.1007/0-306-47194-9_12

Ambrose S. H. & DeNiro M. J. (1986). The isotopic ecology of East African mammals. *Oecologia*, 69: 395-406. https://doi.org/10.1007/BF00377062

Amiot R., Lécuyer C., Buffetaut E., Fluteau F., Legendre S. & Martineau F. (2004). Latitudinal temperature gradient during the Cretaceous Upper Campanian–Middle Maastrichtian: δ18O record of continental vertebrates. *Earth and Planetary Science Letters*, 226(1-2): 255-272. https://doi.org/10.1016/j.epsl.2004.07.015

Amiot R., Lécuyer C., Buffetaut E., Escarguel G., Fluteau F. & Martineau F. (2006). Oxygen isotopes from biogenic apatites suggest widespread endothermy in Cretaceous dinosaurs. *Earth and Planetary Science Letters*, 246(1-2): 41-54. https://doi.org/10.1016/j.epsl.2006.04.018

Amiot R., Lécuyer C., Escarguel G., Billon-Bruyat J. P., Buffetaut E., Langlois C., Martin S., Martineau F. & Mazin J. M. (2007). Oxygen isotope fractionation between crocodylian phosphate and water. *Palaeogeography, Palaeoclimatology, Palaeoecology*, 243(3-4): 412-420. https://doi.org/10.1016/j.palaeo.2006.08.013

Amiot R., Buffetaut E., Lécuyer C., Wang X., Boudad L., Ding Z., Fourel F., Hutt S., Martineau F., Medeiros M. A., Mo J., Simon L., Suteethorn V., Sweetman S., Tong H., Zhang F. & Zhou Z. (2010). Oxygen isotope evidence for semi-aquatic habits among spinosaurid theropods. *Geology*, 38(2): 139-142. https://doi.org/10.1130/G30402.1

Amiot R., Angst D., Legendre S., Buffetaut E., Fourel F., Adolfssen J., André A., Voica-Bojar A., Canoville A., Barral A., Goedert J., Halas S., Kusuhashi N., Pestchevitskaya E., Rey K., Royer A., Saraiva A. F. S., Savary-Sismondini B., Siméon J. L., Touzeau A., Zhou Z. & Lécuyer C. (2017). Oxygen isotope fractionation between bird bone phosphate and drinking water. *The Science of Nature*, 104: 1-13. https://doi.org/10.1007/s00114-017-1468-2

Amoudji Y. Z., Guinot G., Hautier L., Kassegne K. E., Chabrol N., Charruault A. L., Johnson A. K C., Sarr R., Da Costa P. W. D. & Martin J. E. (2021). New data on the Dyrosauridae (Crocodylomorpha) from the Paleocene of Togo. *Annales de Paléontologie*, 107(2): 102472. https://doi.org/10.1016/j.annpal.2021.102472

Anderson M. J. (2001). A new method for non-parametric multivariate analysis of variance. *Austral Ecology*, 26(1): 32-46. https://doi.org/10.1111/j.1442-9993.2001.01070.pp.x

Antunes M. T. (1975). *Iberosuchus,* crocodile Sebecosuchien nouveau, l'Eocène ibérique au Nord de la Chaîne Centrale, et l'origine du canyon de Nazaré. *Comunicaçoes dos Serviços Geologicos de Portugal*, 59: 285-330.

Antunes M. T. (1986). *Iberosuchus* et *Pristichampsu*s, crocodiliens de l'éocène données complémentaires, discussion, distribution stratigraphique. *Ciências da Terra/Earth Sciences Journal,* 8: 111–121.

Araújo Júnior H. I. & Marinho T. d. S. (2013). Taphonomy of a *Baurusuchus* (Crocodyliformes, Baurusuchidae) from the Adamantina Formation (Upper Cretaceous, Bauru Basin), Brazil: implications for preservational modes, time resolution and paleoecology. *Journal of South American Earth Sciences*, 47: 90-99. https://doi.org/10.1016/j.jsames.2013.07.006

Araújo R., David R., Benoit J., Lungmus J. K., Stoessel A., Barrett P. M., Maisano J. A., Ekdale E., Orliac M., Luo Z. X., Martinelli A. G., Hoffman E. A., Sidor C. A., Martins R. M. S., Spoor F. & Angielczyk K. D. (2022). Inner ear biomechanics reveals a Late Triassic origin for mammalian endothermy. *Nature*, 607(7920): 726-731. https://doi.org/10.1038/s41586-022-04963-z

Arcucci A. B., Marsicano C. A. & Caselli A. T. (2004). Tetrapod association and palaeoenvironment of the Los Colorados Formation (Argentina): a significant sample from Western Gondwana at the end of the Triassic. *Geobios*, 37(5): 557-568. https://doi.org/10.1016/j.geobios.2003.04.008

Arrhenius G., Bramlette M. N. & Picciotto E. (1957). Localization of radioactive and stable heavy nuclides in ocean sediments. *Nature*, 180: 85-86.

Astre G. (1931). Les crocodiliens fossiles des terrains tertiaires sous-pyrénéens. *Bulletin de la Société d'Histoire Naturelle de Toulouse*, 61: 25-71.

Aubier P., Jouve S., Schnyder J. & Cubo J. (2023). Phylogenetic structure of the extinction and biotic factors explaining differential survival of terrestrial notosuchians at the Cretaceous–Palaeogene crisis. *Palaeontology*, 66(1): e12638. https://doi.org/10.1111/pala.12638

Augusta B. G. & Zaher H. (2019). Enamel dentition microstructure of *Mariliasuchus amarali* (Crocodyliformes, Notosuchia), from the Upper Cretaceous (Turonian–Santonian) of the Bauru Basin, Brazil. *Cretaceous Research*, 99: 255-268. https://doi.org/10.1016/j.cretres.2019.03.013

Bader C., Böhmer C., Abou M. & Houssaye A. (2022). How does bone microanatomy and musculature covary? An investigation in the forelimb of two species of martens (*Martes foina*, *Martes martes*). *Journal of Anatomy*, 241(1): 145-167. https://doi.org/10.1111/joa.13645

Baken E. K., Collyer M. L., Kaliontzopoulou A. & Adams D. C. (2021). geomorph v4. 0 and gmShiny: Enhanced analytics and a new graphical interface for a comprehensive morphometric experience. *Methods in Ecology and Evolution*, 12(12): 2355-2363. https://doi.org/10.1111/2041-210X.13723

Balanoff A. M., Norell M. A., Hogan A. V. & Bever G. S. (2018). The endocranial cavity of oviraptorosaur dinosaurs and the increasingly complex, deep history of the avian brain. *Brain, Behavior and Evolution*, 91: 125-135. https://doi.org/10.1159/000488890

Balanoff A. M. & Bever G. S. (2020). The role of endocasts in the study of brain evolution. In Kaas J. H. (eds.) *Evolutionary Neuroscience*, Academic Press: 29-49. https://doi.org/10.1016/B978-0-12-820584-6.00003-9

Ballell A., Moon B. C., Porro L. B., Benton M. J. & Rayfield E. J. (2019). Convergence and functional evolution of longirostry in crocodylomorphs. *Palaeontology*, 62(6): 867-887. https://doi.org/10.1111/pala.12432

Ballell A., King J. L., Neenan J. M., Rayfield E. J. & Benton M. J. (2020). The braincase, brain and palaeobiology of the basal sauropodomorph dinosaur *Thecodontosaurus antiquus*. *Zoological Journal of the Linnean Society*, 20: 1-22. https://doi.org/10.1093/zoolinnean/zlaa157

Balouet J. C. & Buffetaut E. (1987). *Mekosuchus inexpectatus*, n. g., n. sp., Crocodilien nouveau de l'Holocène de Nouvelle Calédonie. *Comptes Rendus de l'Académie des Sciences de Paris*, 304(14): 853-857.

Balter V., Person A., Labourdette N., Drucker D. Renard M. & Vandermeersch B. (2001). Were Neandertalians essentially carnivores? Sr and Ba preliminary results of the mammalian palaeobiocoenosis of Saint-Césaire. *Comptes Rendus de l'Académie des Sciences Série I*, 332: 59-65.

Balter V., Bocherens H., Person A., Labourdette N., Renard M. & Vandermeersch B. (2002a). Ecological and physiological variability of Sr/Ca and Ba/Ca in mammals of West European mid-Würmian food webs. *Palaeogeography, Palaeoclimatology, Palaeoecology*, 186(1-2): 127-143. https://doi.org/10.1016/S0031-0182(02)00448-0

Balter V., Saliège J. F., Bocherens H. & Person A. (2002b). Evidence of physico–chemical and isotopic modifications in archaeological bones during controlled acid etching. *Archaeometry,* 44(3): 329-336. https://doi.org/10.1111/1475-4754.t01-1-00065

Balter V., Zazzo A., Moloney A. P., Moynier F., Schmidt O., Monahan F. J. & Albarède F. (2010). Bodily variability of zinc natural isotope abundances in sheep. *Rapid Communications in Mass Spectrometry*, 24(5): 605-612. https://doi.org/10.1002/rcm.4425

Bandeira K. L., Brum A. S., Pêgas R. V., Cidade G. M., Holgado B., Cidade A. & de Souza R. G. (2018). The Baurusuchidae vs Theropoda record in the Bauru Group (Upper Cretaceous, Brazil): a taphonomic perspective. *Journal of Iberian Geology*, 44: 25-54. https://doi.org/10.1007/s41513-018-0048-4

Bang B. G. & Cobb S. (1968). The Size of the Olfactory Bulb in 108 Species of Birds. The Auk, 85(1): 55-61. https://doi.org/10.2307/4083624

Bapst D. W. (2012). paleotree: an R package for paleontological and phylogenetic analyses of evolution. *Methods in Ecology and Evolution*, 3(5): 803-807. https://doi.org/10.1111/j.2041-210X.2012.00223.x

Baquedano E., Domínguez-Rodrigo M. & Musiba C. (2012). An experimental study of large mammal bone modification by crocodiles and its bearing on the interpretation of crocodile predation at FLK Zinj and FLK NN3. *J. of Archaeol. Sci.*, 39(6): 1728-1737. https://doi.org/10.1016/j.jas.2012.01.010

Barbosa J. A., Kellner A. W. A. & Viana M. S. S. (2008). New dyrosaurid crocodylomorph and evidences for faunal turnover at the K–P transition in Brazil. *Proceedings of the Royal Society B: Biological Sciences*, 275(1641): 1385-1391. https://doi.org/10.1098/rspb.2008.0110

Barbour M. M. (2007). Stable oxygen isotope composition of plant tissue: a review. *Functional Plant Biology*, 34(2): 83-94. https://doi.org/10.1071/FP06228

Bardua C., Felice R. N., Watanabe A., Fabre A. C. & Goswami A. (2019). A practical guide to sliding and surface semilandmarks in morphometric analyses. *Integrative Organismal Biology*, 1(1): obz016. https://doi.org/10.1093/iob/obz016

Barrick R. E. & Showers W. J. (1994). Thermophysiology of *Tyrannosaurus rex*: evidence from oxygen isotopes. *Science*, 265(5169): 222-224. https://doi.org/10.1126/science.265.5169.222

Barrick R. E. & Showers W. J. (1995). Oxygen isotope variability in juvenile dinosaurs (*Hypacrosaurus*): evidence for thermoregulation. *Paleobiology*, 21(4): 552-560. https://doi.org/10.1017/S0094837300013531

Barrick R. E., Showers W. J. & Fischer A. G. (1996). Comparison of thermoregulation of four ornithischian dinosaurs and a varanid lizard from the Cretaceous Two Medicine Formation: evidence from oxygen isotopes. *Palaios*, 11(4): 295-305. https://doi.org/10.2307/3515240

Barrick R. E., Stoskopf M. K., Marcot J. D., Russell D. A. & Showers W. J. (1998). The thermoregulatory functions of the *Triceratops* frill and horns: heat flow measured with oxygen isotopes. *Journal of Vertebrate Paleontology*, 18(4): 746-750. https://doi.org/10.1080/02724634.1998.10011103

Barrick R. E., Fischer A. G. & Showers W. J. (1999). Oxygen isotopes from turtle bone: applications for terrestrial paleoclimates?. *Palaios*, 14(2): 186-191. https://doi.org/10.2307/3515374

Barrientos-Lara J. I., Herrera L. Y., Fernández M. S. & Alvarado Ortega J. (2016). Occurrence of *Torvoneustes* (Crocodylomorpha, Metriorhynchidae) in marine Jurassic deposits of Oaxaca, Mexico. *Revista Brasileira de Paleontologia*, 19(3): 415-424. https://doi.org/10.4072/rbp.2016.3.07

Barrios F. (2021). *El neurocráneo de los notosúquios (Crocodyliformes) del Cretácico Superior de la Cuenca Neuquina (Patagonia, Argentina): morfologia endocraneana y sus inferencias paleoneurológicas.* Unpublished PhD thesis, Universidad Nacional de La Plata, 427 p.

Barrios F., Paulina-Carabajal A. & Bona P. (2016). A new peirosaurid (Crocodyliformes, Mesoeucrocodylia) from the Upper Cretaceous of Patagonia, Argentina. *Ameghiniana*, 53(1): 14-25. https://doi.org/10.5710/AMGH.03.09.2015.2903

Barrios F., Bona P., Paulina-Carabajal A. & Gasparini Z. (2018). Re-description of the cranio-mandibular anatomy of *Notosuchus terrestris* (Crocodyliformes, Mesoeucrocodylia) from the Upper Cretaceous of Patagonia. *Cretaceous Research*, 83: 3-39. https://doi.org/10.1016/j.cretres.2017.08.016

Barrios F., Bona P., Paulina-Carabajal A., Leardi J. M., Holliday C. M. & Lessner E. J. (2023). An Overview on the Crocodylomorpha Cranial Neuroanatomy: Variability, Morphological Patterns and Paleobiological Implications. In Dozo M. T., Paulina-Carabajal A., Macrini T. E. & Walsh S. (eds.) *Paleoneurology of Amniotes: New Directions in the Study of Fossil Endocasts*, Springer: 213-266. https://doi.org/10.1007/978-3-031-13983-3_7

Bartlett J. D. (2013). Dental enamel development: proteinases and their enamel matrix substrates. *International Scholarly Research Notices*, 2013: 1-24.

Batsch A. J. G. C. (1788). *Versuch einer Anleitung, zur Kenntniß und Geschichte der Thiere und Mineralien, für akademische Vorlesungen entworfen, und mit den nöthigsten Abbildungen versehen. Erster Theil, Allgemeine Geschichte der Natur; besondre der Säugthiere, Vögel, Amphibien und Fische.* Akademische Buchhandlung, Jena.

Beach F. A. (1944). Responses of captive alligators to auditory stimulation. *The American Naturalist*, 78(779): 481-505.

Beckmann E. C. (2006). CT scanning the early days. *The British Journal of Radiology*, 79(937): 5-8. https://doi.org/10.1259/bjr/29444122

Bellairs A. A. & Shute C. C. D. (1953). Observations on the narial musculature of Crocodilia and its innervation from the sympathetic system. *Journal of Anatomy*, 87(4): 367-378.

Bender M. M. (1971). Variations in the $^{13}C/^{12}C$ ratios of plants in relation to the pathway of photosynthetic carbon dioxide fixation. *Phytochemistry*, 10(6): 1239-1244. https://doi.org/10.1016/S0031-9422(00)84324-1

Bengston J. L. (1988). Long-term trends in the foraging patterns of female Antarctic fur seals at South Georgia. In Sahrhage D. (ed.) *Antarctic Ocean and resources variability*, Springer: 286-291. https://doi.org/10.1007/978-3-642-73724-4_24

Bennett E. T. (1835). *Crocodilus leptorhynchus*. *Proceedings of the zoological society of London*, 3: 128-132.

Benninger B. & McNeil J. (2010). Transitional nerve: a new and original classification of a peripheral nerve supported by the nature of the accessory nerve (CN XI). *Neurology research international*, 2010: 476018. https://doi.org/10.1155/2010/476018

Benson R. B., Godoy P., Bronzati M., Butler R. J. & Gearty W. (2022). Reconstructed evolutionary patterns for crocodile-line archosaurs demonstrate impact of failure to log-transform body size data. *Communications Biology*, 5(171): 1-4. https://doi.org/10.1038/s42003-022-03071-y

Bentley A. R. (2006). Strontium isotopes from the earth to the archaeological skeleton: a review. *Journal of Archaeological Method and Theory*, 13(3): 135-187. https://doi.org/10.1007/s10816-006-9009-x

Benton M. J. & Clark J. M. (1988). Archosaur phylogeny and the relationships of the Crocodylia. In *The phylogeny and Classification of the Tetrapods, Volume I: Amphibians, Reptiles, Birds*. The Systematics Association: 295-338.

Benyoucef M., Pérez-García A., Bendella M., Ortega F., Vullo R., Bouchemla I. & Ferré B. (2022). The "mid"-Cretaceous (Lower Cenomanian) Continental Vertebrates of Gara Samani, Algeria. Sedimentological Framework and Palaeodiversity. *Frontiers in Earth Science*, 10: 9270659. https://doi.org/10.3389/feart.2022.927059

Berckhemer F. (1929). Beitrag zur Kenntnis der Krokodilier des schwäbischen oberen Lias. *Neues Jahrbuch für Mineralogie, Geologie und Paläontologie, Abteilung B*, 64: 1-60.

Bernat M. (1975). Les isotopes de l'uranium et du thorium et les terres rares dans l'environnement marin. *Cahiers ORSTOM Série Géologie*, 7: 65-83.

Bertram C. J., Elderfield H., Aldridge R. J. & Morris S. C. (1992). $^{87}Sr/^{86}Sr$, $^{143}Nd/^{144}Nd$ and REEs in Silurian phosphatic fossils. *Earth and Planetary Science Letters*, 113(1-2): 239-249. https://doi.org/10.1016/0012-821X(92)90222-H

Bezuijen M. R., Phothitay C., Hedemark M. & Chanrya S. (2006). Preliminary status review of the Siamese Crocodile (*Crocodylus siamensis* (Crocodylia, Reptilia) in the Lao People's Democratic republic. Government of Lao PDR & Wildlife Conservation Society: Vientiane.

Biasatti D. M. (2004). Stable carbon isotopic profiles of sea turtle humeri: implications for ecology and physiology. *Palaeogeography, Palaeoclimatology, Palaeoecology*, 206(3-4): 203-216. https://doi.org/10.1016/j.palaeo.2004.01.004

Bickelmann C. & Klein N. (2009). The late Pleistocene horned crocodile *Voay robustus* (Grandidier & Vaillant, 1872) from Madagascar in the Museum für Naturkunde Berlin. *Fossil Record*, 12(1): 13-21. https://doi.org/10.1002/mmng.200800007

Bierman H. S., Thornton J. L., Jones H. G., Koka K., Young B. A., Brandt C., Christensen-Dalsgaard J., Carr, C. E. & Tollin, D. J. (2014). Biophysics of directional hearing in the American alligator (*Alligator mississippiensis*). *Journal of Experimental Biology*, 217(7): 1094-1107. https://doi.org/10.1242/jeb.092866

Billet G., Hautier L. & Lebrun R. (2015). Morphological diversity of the bony labyrinth (inner ear) in extant xenarthrans and its relation to phylogeny. *Journal of Mammalogy*, 96(4): 658-672. https://doi.org/10.1093/jmammal/gyv074

Blake R. E., O'neil J. R. & Garcia G. A. (1997). Oxygen isotope systematics of biologically mediated reactions of phosphate: I. Microbial degradation of organophosphorus compounds. *Geochim. et Cosmochim. acta*, 61(20): 4411-4422. https://doi.org/10.1016/S0016-7037(97)00272-X

Blanco A. (2021). Importance of the postcranial skeleton in eusuchian phylogeny: Reassessing the systematics of allodaposuchid crocodylians. *Plos One*, 16(6): e0251900. https://doi.org/10.1371/journal.pone.0251900

Blanco A., Fortuny J., Vicente A., Lujan A. H., García-Marçà J. A. & Sellés A. G. (2015). A new species of *Allodaposuchus* (Eusuchia, Crocodylia) from the Maastrichtian (Late Cretaceous) of Spain: phylogenetic and paleobiological implications. *PeerJ*, 3: e1171. https://doi.org/10.7717/peerj.1171

Blas X. P. I., Loyal R. S., Schleich H. H., Agrasar E. L. & Llinas E. (2004). Pristichampsine cranial remains from the basal redbed facies of the Subathu Formation (Himachal Pradesh, India) and some palaeobiographical remarks. *PalArch's Journal of Vertebrate Palaeontology*, 3(1): 1-8.

Blättler C. L., Jenkyns H. C., Reynard L. M. & Henderson G. M. (2011). Significant increases in global weathering during Oceanic Anoxic Events 1a and 2 indicated by calcium isotopes. *Earth and Planetary Science Letters*, 309(1-2): 77-88. https://doi.org/10.1016/j.epsl.2011.06.029

Bocherens H., Fizet M., Mariotti A., Lange-Badre B., Vandermeersch B., Borel J. P. & Bellon G. (1991). Isotopic biogeochemistry (^{13}C, ^{15}N) of fossil vertebrate collagen: application to the study of a past food web including Neandertal man. *Journal of Human Evolution*, 20(6): 481-492. https://doi.org/10.1016/0047-2484(91)90021-M

Bocherens H. & Drucker D. (2003). Trophic level isotopic enrichment of carbon and nitrogen in bone collagen: case studies from recent and ancient terrestrial ecosystems. *International Journal of Osteoarchaeology*, 13(1-2): 46-53. https://doi.org/10.1002/oa.662

Böhlke J. K. & Coplen T. B. (1995). Interlaboratory comparison of reference materials for nitrogen-isotope-ratio measurements. *Consultants meeting on stable isotope standards and intercomparison materials*, Vienna: 51-66.

Böhlke J. K., Gwinn C. J. & Coplen T. B. (1993). New reference materials for nitrogen-isotope-ratio measurements. *Geostandards Newsletter*, 17(1): 159-164. https://doi.org/10.1111/j.1751-908X.1993.tb00131.x

Bona P. & Paulina Carabajal A. (2013). *Caiman gasparinae* sp. nov., a huge alligatorid (Caimaninae) from the late Miocene of Paraná, Argentina. *Alcheringa: An Australasian Journal of Palaeontology*, 37(4): 462-473. https://doi.org/10.1080/03115518.2013.785335

Bona P., Degrange F. J. & Fernández M. S. (2013). Skull anatomy of the bizarre crocodylian *Mourasuchus nativus* (Alligatoridae, Caimaninae). *The Anatomical Record*, 296(2): 227-239. https://doi.org/10.1002/ar.22625

Bona P., Paulina-Carabajal A. & Gasparini Z. (2017). Neuroanatomy of *Gryposuchus neogaeus* (Crocodylia, Gavialoidea): a first integral description of the braincase and endocranial morphological variation in extinct and extant gavialoids. *Earth and Environmental Science Transactions of the Royal Society of Edinburgh*, 106(4): 235-246. https://doi.org/10.1017/S1755691016000189

Bonaparte J. F. (1969). Dos nuevos "faunas" de reptiles triásicos de Argentina. *Gondwana Stratigraphy*, 283-306.

Bonaparte J. F. (1991). Los vertebrados fósiles de la Formación Rio Colorado, de la Ciudad de Neuquén y Cercanías, Cretácico Superior, Argentina. *Revista del Museo Argentino de Ciencias Naturales 'Bernardino Rivadavia' e Instituto Nacional de Investigación de las Ciencias Naturales : Paleontologia*, 4(3): 17-123.

Bonel G. (1970). *Contribution à l'étude de la carbonatation des apatites*. Unpublished PhD thesis, Université Paul Sabatier.

Bookstein F. L. (1997). Landmark methods for forms without landmarks: morphometrics of group differences in outline shape. *Medical Image Analysis*, 1(3): 225-243. https://doi.org/10.1016/S1361-8415(97)85012-8

Bordy E. M., Hancox P. J. & Rubidge B. S. (2004a). A description of the sedimentology and palaeontology of the Late Triassic–Early Jurassic Elliot Formation in Lesotho. *Palaeontologia africana*, 40: 43-58.

Bordy E. M., Hancox P. J. & Rubidge B. S. (2004b). Fluvial style variations in the Late Triassic–Early Jurassic Elliot Formation, main Karoo Basin, South Africa. *Journal of African Earth Sciences*, 38(4): 383-400. https://doi.org/10.1016/j.jafrearsci.2004.02.004

Boskey A. L. (1989). Noncollagenous matrix proteins and their role in mineralization. *Bone and mineral*, 6(2): 111-123. https://doi.org/10.1016/0169-6009(89)90044-5

Bosshardt D. D. & Selvig K. A. (1997). Dental cementum: the dynamic tissue covering of the root. *Periodontology*, 13: 41-75.

Botha J. & Chinsamy A. (2001). Growth patterns deduced from the bone histology of the cynodonts *Diademodon* and *Cynognathus*. *Journal of Vertebrate Paleontology*, 20(4): 705-711. https://doi.org/10.1671/0272-4634(2000)020[0705:GPDFTB]2.0.CO;2

Botha-Brink J. & Smith R. M. (2011). Osteohistology of the Triassic archosauromorphs *Prolacerta, Proterosuchus*, *Euparkeria*, and *Erythrosuchus* from the Karoo Basin of South Africa. *Journal of Vertebrate Paleontology*, 31(6): 1238-1254. https://doi.org/10.1080/02724634.2011.621797

Bourdon E., Castanet J., de Ricqlès A., Scofield P., Tennyson A., Lamrous H. & Cubo J. (2009). Bone growth marks reveal protracted growth in New Zealand kiwi (Aves, Apterygidae). *Biology Letters*, 5(5): 639-642. https://doi.org/10.1098/rsbl.2009.0310

Bourke J. M., Fontenot N. & Holliday C. (2022). Septal deviation in the nose of the longest faced crocodylian: A description of nasal anatomy and airflow in the Indian gharial (*Gavialis gangeticus*) with comments on acoustics. *The Anatomical Record*, 305(10): 2883-2903. https://doi.org/10.1002/ar.24831

Bowen G. J., Bralower T. J., Delaney M. L., Dickens G. R., Kelly D. C., Koch P. L., Kump L. R., Meng J., Sloan L. C., Thomas E., Wing S. L. & Zachos J. C. (2006). Eocene hyperthermal event offers insight into greenhouse warming. *Eos, Transactions American Geophysical Union*, 87(17): 165-169. https://doi.org/10.1029/2006EO170002

Bowman C. I., Young M. T., Schwab J. A., Walsh S., Witmer L. M., Herrera Y., Choiniere J., Dollman K. N. & Brusatte S. L. (2021). Rostral neurovasculature indicates sensory trade-offs in Mesozoic pelagic crocodylomorphs. *The Anatomical Record*, 305(10): 2654-2669. https://doi.org/10.1002/ar.24733

Brand U. (1991). Strontium isotope diagenesis of biogenic aragonite and low-Mg calcite. *Geochimica et Cosmochimica Acta*, 55(2): 505-513. https://doi.org/10.1016/0016-7037(91)90008-S

Bravo G. G., Pol D. & García-López D. A. (2021). A new sebecid mesoeucrocodylian from the Paleocene of northwestern Argentina. *Journal of Vertebrate Paleontology*, 41(3): e1979020. https://doi.org/10.1080/02724634.2021.1979020

Bravo G. G., Pol D., Armella M. A. & Gómez K. (2022). The choanal anatomy of the *Sebecus icaeorhinus* Simpson, 1937 and the variation of the palatine shape in notosuchians (Crocodyliformes, Mesoeucrocodylia). *Journal of Paleontology*, 96(6): 1400-1412. https://doi.org/10.1017/jpa.2022.48

Brazier J. M., Schmitt A. D., Pelt E., Lemarchand D., Gangloff S., Tacail T. & Balter V. (2019). Determination of Radiogenic $^{87}Sr/^{86}Sr$ and Stable $\delta^{88/86}Sr_{SRM987}$ Isotope Values of Thirteen Mineral, Vegetal and Animal Reference Materials by DS-TIMS. *Geostandards and Geoanalytical Research*, 44(2): 331-348. https://doi.org/10.1111/ggr.12308

Brettell R., Montgomery J. & Evans J. (2012). Brewing and stewing: the effect of culturally mediated behaviour on the oxygen isotope composition of ingested fluids and the implications for human provenance studies. *Journal of Analytical Atomic Spectrometry*, 27(5): 778-785. https://doi.org/10.1039/C2JA10335D

Brinkmann W. (1989). Vorläufige Mitteilung über die Krokodilier-Faunen aus dem Ober-Jura (Kimmeridgium) der Kohlegrube Guimarota, bei Leiria (Portugal) und der Unter-Kreide (Barremium) von Una (Provinz Cuenca, Spanien). *Documenta Naturae,* 56: 1–28.

Brinkmann W. (1992). Die Krokodilier-Fauna aus der Unter-Kreide (Ober-Barremium) von Una (Provinz Cuenca, Spanien). *Berliner Geowissenschaftliche Abhandlungen*, 5: 1-117.

Brochu C. A. (1997). Morphology, fossils, divergence timing, and the phylogenetic relationships of *Gavialis*. *Systematic Biology*, 46(3): 479-522. https://doi.org/10.1093/sysbio/46.3.479

Brochu C. A. (1999). Phylogenetics, taxonomy, and historical biogeography of Alligatoroidea. *Journal of Vertebrate Paleontology,* 19(S2): 9-100. https://doi.org/10.1080/02724634.1999.10011201

Brochu C. A. (2000). Phylogenetic relationships and divergence timing of *Crocodylus* based on morphology and the fossil record. *Copeia*, 2000(3): 657-673. https://doi.org/10.1643/0045-8511(2000)000[0657:PRADTO]2.0.CO;2

Brochu C. A. (2001). Crocodylian snouts in space and time: phylogenetic approaches toward adaptive radiation. *American Zoologist*, 41(3:, 564-585. https://doi.org/10.1093/icb/41.3.564

Brochu C. A. (2003). Phylogenetic approaches toward crocodylian history. *Annual Review of Earth and Planetary Sciences*, 31(1): 357-397. https://doi.org/10.1146/annurev.earth.31.100901.141308

Brochu C. A. (2004). Alligatorine phylogeny and the status of *Allognathosuchus* Mook, 1921. *Journal of Vertebrate Paleontology*, 24(4): 857-873. https://doi.org/10.1671/0272-4634(2004)024[0857:APATSO]2.0.CO;2

Brochu C. A. (2007). Morphology, relationships, and biogeographical significance of an extinct horned crocodile (Crocodylia, Crocodylidae) from the Quaternary of Madagascar. *Zoological Journal of the Linnean Society*, 150(4): 835-863. https://doi.org/10.1111/j.1096-3642.2007.00315.x

Brochu C. A. (2012). Phylogenetic relationships of Palaeogene ziphodont eusuchians and the status of *Pristichampsus* Gervais, 1853. *Earth and Environmental Science Transactions of the Royal Society of Edinburgh,* 103(3-4): 521-550. https://doi.org/10.1017/S1755691013000200

Brochu C. A., Bouaré M. L., Sissoko F., Roberts E. M. & O'Leary M. A. (2002). A dyrosaurid crocodyliform braincase from Mali. *Journal of Paleontology*, 76(6): 1060-1071. https://doi.org/10.1666/0022-3360(2002)076<1060:ADCBFM>2.0.CO;2

Bronn H. G. (1841). Über die fossilen Gaviale der Lias-Formation und der Oolithe. *Archiv für Naturgeschichte*, 8: 77-82.

Bronzati M., Montefeltro F. C. & Langer M. C. (2012). A species-level supertree of Crocodyliformes. *Historical Biology*, 24(6): 598-606. https://doi.org/10.1080/08912963.2012.662680

Bronzati M., Montefeltro F. C. & Langer M. C. (2015). Diversification events and the effects of mass extinctions on Crocodyliformes evolutionary history. *Royal Society open science*, 2(5): 140385. https://doi.org/10.1098/rsos.140385

Bronzati M., Benson R. B., Evers S. W., Ezcurra M. D., Cabreira S. F., Choiniere J., Dollman K. N., Paulina-Carabajal A., Radermacher V. J., Roberto-da-Silva L., Sobral G., Stocker M. R., Witmer L. M., Langer M. X. & Nesbitt S. J. (2021). Deep evolutionary diversification of semicircular canals in archosaurs. *Current Biology*, 31(12): 2520-2529. https://doi.org/10.1016/j.cub.2021.03.086

Broom R. (1914). A new Thecodont Reptile. *Proceedings of the Zoological Society of London*, 1914: 1072-1077.

Brown B. (1933). An ancestral crocodile. *American Museum Novitates*, 638: 1-4.

Brown B. (1934). A change of names. *Science*, 79(2039): 80.

Brusatte S. L., Muir A., Young M. T., Walsh S., Steel L. & Witmer L. M. (2016). The braincase and neurosensory anatomy of an Early Jurassic marine crocodylomorph: implications for crocodylian sinus evolution and sensory transitions. *The Anatomical Record*, 299(11): 1511-1530. https://doi.org/10.1002/ar.23462

Bryant J. D. & Froelich P. N. (1995). A model of oxygen isotope fractionation in body water of large mammals. *Geochimica et Cosmochimica Acta*, 59(21): 4523-4537. https://doi.org/10.1016/0016-7037(95)00250-4

Bryant J. D., Koch P. L., Froelich P. N., Showers W. J. & Genna B. J. (1996). Oxygen isotope partitioning between phosphate and carbonate in mammalian apatite. *Geochim. et Cosmochim. Acta*, 60(24): 5145-5148. https://doi.org/10.1016/S0016-7037(96)00308-0

Buchanan L. A. (2008). The Systematics, Palaeobiology and Palaeoecology of *Kambara taraina* sp. nov. from the Eocene Rundle Formation, Queensland. Unpublished PhD thesis, Monash University, 340 p.

Buchanan L. A. (2009). *Kambara taraina* sp. nov. (Crocodylia, Crocodyloidea), a new Eocene mekosuchine from Queensland, Australia, and a revision of the genus. *Journal of Vertebrate Paleontology*, 29(2): 473-486. https://doi.org/10.1671/039.029.0220

Buchholtz E. A. & Seyfarth E. A. (1999). The gospel of the fossil brain: Tilly Edinger and the science of paleoneurology. *Brain Research Bulletin*, 48(4): 351-361. https://doi.org/10.1016/S0361-9230(98)00174-9

Buchy M. C. (2008). New occurrence of the genus *Dakosaurus* (Reptilia, Thalattosuchia) in the Upper Jurassic of north-eastern Mexico, with comments upon skull architecture of *Dakosaurus* and *Geosaurus*. *Neues Jahrbuch für Geologie und Paläontologie-Abhandlungen*, 249(1): 1-8. https://doi.org/10.1127/0077-7749/2008/0249-0001

Buchy M. C., Stinnesbeck W., Frey E. & Gonzalez Gonzalez A. H. (2007). First occurrence of the genus *Dakosaurus* (Crocodyliformes, Thalattosuchia) in the Late Jurassic of Mexico. *Bulletin de la Société Géologique de France*, 178(5): 391-397. https://doi.org/10.2113/gssgfbull.178.5.391

Buchy M. C., Young M. T. & de Andrade M. B. (2013). A new specimen of *Cricosaurus saltillensis* (Crocodylomorpha: Metriorhynchidae) from the Upper Jurassic of Mexico: evidence for craniofacial convergence within Metriorhynchidae. *Oryctos*, 10: 9-21.

Buckley G. A. & Brochu C. A. (1999). An enigmatic new crocodile from the Upper Cretaceous of Madagascar. *Special papers in palaeontology*, 60(60): 149-175.

Buckley G. A., Brochu C. A., Krause D. W. & Pol D. (2000). A pug-nosed crocodyliform from the Late Cretaceous of Madagascar. *Nature*, 405(6789): 941-944. https://doi.org/10.1038/35016061

Budd P., Montgomery J., Barreiro B. & Thomas R. G. (2000). Differential diagenesis of strontium in archaeological human dental tissues. *Applied Geochemistry*, 15(5): 687-694. https://doi.org/10.1016/S0883-2927(99)00069-4

Buffetaut E. (1974a). *Les Crocodiliens du Sénonien Inférieur d'In Beceten (République du Niger).* Unpublished PhD thesis, Université Paris VI, 146 p.

Buffetaut E. (1974b). *Trematochampsa taqueti,* un crocodilien nouveau du Sénonien inférieur du Niger. *Comptes Rendus de l'Académie des Sciences Paris, Séries D*, 279: 1749-1752.

Buffetaut E. (1976a). Ostéologie et affinités de *Trematochampsa taqueti* (Crocodylia, Mesosuchia) du Sénonien inférieur d'in Beceten (République du Niger). *Geobios*, 9(2): 143-198. https://doi.org/10.1016/S0016-6995(76)80013-7

Buffetaut E. (1976b). Une nouvelle définition de la famille des Dyrosauridae de Stefano, 1930 (Crocodylia, Mesosuchia) et ses conséquences : inclusion des genres *Hyposaurus* et *Sokotosuchus* dans les Dyrosauridae. *Geobios*, 9(3): 333-336.

Buffetaut E. (1979). Présence du crocodilien *Phosphatosaurus* (Mesosuchia, Dyrosauridae) dans le Paléocène du Niger et du Mali. *Paläontologische Zeitschrift*, 53(3/4): 323-333.

Buffetaut E. (1981). Die biogeographische Geschichte der Krokodilier, mit Beschreibung einer neuen Art, *Araripesuchus wegeneri*. *Geologische Rundschau*, 70: 611-624. https://doi.org/10.1007/BF01822139

Buffetaut E. (1982a). A ziphodont mesosuchian crocodile from the Eocene of Algeria and its implications for vertebrate dispersal. *Nature*, 300(5888): 176-178. https://doi.org/10.1038/300176a0

Buffetaut E. (1982b). Un problème de paléobiogéographie continentale: les Crocodiliens mésosuchiens ziphodontes de l'Eocène européen. *Bulletin de la Société Géologique de France,* 24(5-6): 1101-1107.

Buffetaut E. (1983). The crocodylian *Theriosuchus* Owen, 1879 in the Wealden of England. *Bulletin of the British Museum of natural History*, 37(3): 93.97.

Buffetaut E. (1985a). Présence de Trematochampsidae (Crocodylia, Mesosuchia) dans le Crétacé supérieur du Brésil. Implications paléobiogéographiques. *Comptes Rendus de l'Académie des Sciences de Paris*, 301(16): 1221-1224.

Buffetaut E. (1985b). Les crocodiliens de l'Eocène inférieur de Dormaal (Brabant, Belgique). *Bulletin de la Société belge de Géologie*, 94(1): 51-59.

Buffetaut E. (1986). Un mésosuchien ziphodonte dans l'Eocène supérieur de La Livinière (Hérault, France). *Geobios,* 19(1): 101-108.

Buffetaut E. (1989). A new ziphodont mesosuchian crocodile from the Eocene of Algeria. *Palaeontographica*, 208(1-3): 1-10.

Buffetaut E. (1992). Fossil crocodylians from Tiupampa, (Santa Lucia Formation, Early Paleocene) Bolivia: a preliminary report. *Revista Técnica de YPFB, Fosiles y Facies da Bolivia, I, Vertebrados*, 12: 541-544, December 1991 (but printed in March 1992).

Buffetaut E. (1994). A new crocodylian from the Cretaceous of southern Morocco. *Comptes rendus de l'Académie des sciences. Série 2. Sciences de la terre et des planètes*, 319(12): 1563-1568.

Buffetaut E. & Hoffstetter R. (1977). Découverte du Crocodilien *Sebecus* dans le Miocène du Pérou oriental. *Comptes Rendus de l'Académie des Sciences de Paris,* 284(17): 1663-1666.

Buffetaut E. & Taquet P. (1977). The giant crocodylian *Sarcosuchus* in the Early Cretaceous of Brazil and Niger. *Palaeontology*, 20(1): 203-208.

Buffetaut E. & Thierry J. (1977). Les crocodiliens fossiles du Jurassique Moyen et Supérieur de Bourgogne. *Geobios*, 10(2): 151-194. https://doi.org/10.1016/S0016-6995(77)80091-0

Buffetaut E. & Taquet P. (1979). An early Cretaceous terrestrial crocodylian and the opening of the South Atlantic. *Nature*, 280(5722): 486-487. https://doi.org/10.1038/280486a0

Buffetaut E. & Ingavat R. (1980). A new crocodilian from the Jurassic of Thailand, *Sunosuchus thailandicus* n. sp. (Mesosuchia, Goniopholididae)), and the palaeogeographical history of South-East Asia in the Mesozoic. *Geobios*, 13(6): 879-889. https://doi.org/10.1016/S0016-6995(80)80042-8

Buffetaut E. & Ingavat R. (1983). *Goniopholis phuwiangensis* nov. sp., a new mesosuchian crocodile from the Mesozoic of north-eastern Thailand. *Geobios*, 16(1): 79-91. https://doi.org/10.1016/S0016-6995(83)80048-5

Buffetaut E & Ingavat R. (1984). The lower jaw of *Sunosuchus thailandicus*, a mesosuchian crocodylian from the Jurassic of Thailand. *Palaeontology*, 27(1): 199-206.

Buffetaut E. & Marshall L. G. (1992). A new crocodylian, *Sebecus querejazus*, nov. sp. (Mesosuchia, Sebecidae) from the Santa Lucia formation (Early Paleocene) at Vila Vila, southcentral Bolivia. *Fósiles y Facies de Bolivia*, 1: 545-557.

Buffrénil V. de (1982). Morphogenesis of bone ornamentation in extant and extinct crocodylians. *Zoomorphology*, 99(2): 155-166. https://doi.org/10.1007/BF00310307

Buffrénil V., Houssaye A. & Böhme W. (2007). Bone vascular supply in monitor lizards (Squamata: Varanidae): influence of size, growth, and phylogeny. *Journal of Morphology*, 269(5): 533-543. https://doi.org/10.1002/jmor.10604

Buffrénil V. de, Clarac F., Fau M., Martin S., Martin B., Pellé E. & Laurin M. (2015). Differentiation and growth of bone ornamentation in vertebrates: a comparative histological study among the Crocodylomorpha. *Journal of Morphology*, 276(4): 425-445. https://doi.org/10.1002/jmor.20351

Buffrénil V. de, Laurin M. & Jouve S. (2021). The Crocodylomorpha. In *Vertebrate Skeletal histology and paleohistology*. CRC Press: 486-510.

Bunzel E. (1871). *Die Reptilfauna der Gosau-Formation in der Neuen Welt bei Wiener-Neustadt.* Braumüller, 42 p.

Burke P. M. & Mannion P. D. (2023). Neuroanatomy of the crocodylian *Tomistoma dowsoni* from the Miocene of North Africa provides insights into the evolutionary history of gavialoids. *Journal of Anatomy*: https://doi.org/10.1111/joa.13846

Burns M. E., Vickaryous M. K. & Currie P. J. (2013). Histological variability in fossil and recent alligatoroid osteoderms: systematic and functional implications. *Journal of Morphology*, 274(6): a 676-686. https://doi.org/10.1002/jmor.20125

Burton K. W. & Vigier N. (2011). Lithium isotopes as tracers in marine and terrestrial environments. In Baskaran M. (eds), *Handbook of Environmental Isotope Geochemistry*, *Vol I*, Springer: 41-59. https://doi.org/10.1007/978-3-642-10637-8_4

Busbey A. B. (1986). New material of *Sebecus* cf. *huilensis* (Crocodilia: Sebecosuchidae) from the Miocene La Venta formation of Colombia. *Journal of Vertebrate Paleontology*, 6(1): 20-27. https://doi.org/10.1080/02724634.1986.10011595

Busbey A. B. (1997). The structural consequences of skull flattening in crocodylians. In Thomason J. J. (ed.) *Functional Morphology in Vertebrate Paleontology*, Cambridge University Press: 172-191.

Busbey A. B. & Gow C. (1984). A new protosuchian crocodile from the Upper Triassic Elliot Formation of South Africa. *Palaeontologia africana*, 25: 127-149.

Buscalioni Á. D. (2017). The Gobiosuchidae in the early evolution of Crocodyliformes. *Journal of Vertebrate Paleontology*, 37(3): e1324459. https://doi.org/10.1080/02724634.2017.1324459

Buscalioni A. D. & Sanz J. L. (1990). *Montsecosuchus depereti* (Crocodylomorpha, Atoposauridae), new denomination for *Alligatorium depereti* Vidal, 1915 (Early Cretaceous, Spain): redescription and phylogenetic relationships. *Journal of Vertebrate Paleontology*, 10(2): 244-254. https://doi.org/10.1080/02724634.1990.10011810

Buschhüter D., Smitka M., Puschmann S., Gerber J. C., Witt M., Abolmaali N. D. & Hummel T. (2008). Correlation between olfactory bulb volume and olfactory function. *NeuroImage*, 42(2): 498-502. https://doi.org/10.1016/j.neuroimage.2008.05.004

Busson G. & Cornée A. (1991). The Sahara from the Middle Jurassic to the Middle Cretaceous: data on environments and climates based on outcrops in the Algerian Sahara. *Journal of African Earth Sciences (and the Middle East)*, 12(1-2): 85-105. https://doi.org/10.1016/0899-5362(91)90060-C

Bustard H. R. & Singh L. A. K. (1978). Studies on the Indian gharial *Gavialis gangeticus* (Gmelin) (Reptilia, Crocodilia). Change in terrestrial locomotory pattern with age. *Journal of Bombay Natural History Society*, 74: 534-536.

Cacciotti I. (2016). Cationic and anionic substitutions in hydroxyapatite. In Antoniac I. V. (eds.) *Handbook of bioceramics and biocomposites*, Springer: 145-211. https://doi.org/10.1007/978-3-319-12460-5_7

Caldwell M. W. (2002). From fins to limbs to fins: limb evolution in fossil marine reptiles. *American Journal of Medical Genetics*, 112(3): 236-249. https://doi.org/10.1002/ajmg.10773

Carlström D. (1963). A crystallographic study of vertebrate otoliths. *The Biological Bulletin*, 125(3): 441-463. https://doi.org/10.2307/1539358

Calvo J. O. & Porfiri J. D. (2010). New material of peirosaurids from Neuquén, Patagonia: its age. *Brazilian Geographical Journal: Geosciences and Humanities research medium*, 1: 50-64.

Campos Z. & Magnusson W. E. (2013). Thermal relations of dwarf caiman, *Paleosuchus palpebrosus*, in a hillside stream: evidence for an unusual thermal niche among crocodylians. *Journal of Thermal Biology*, 38(1): 20-23. https://doi.org/10.1016/j.jtherbio.2012.09.004

Campos D. d. A., Suarez J. M., Riff D. & Kellner A. W. A. (2001). Short note on a new Baurusuchidae (Crocodyliformes, Metasuchia) from the Upper Cretaceous of Brazil. *Boletim do Museu Nacional Nova Série Rio de Janeiro*, 57: 1-7.

Campos D. d. A., Oliveira G. R., Figueiredo R. G., Riff D., Azevedo S. A., Carvalho L. B. & Kellner A. W. (2011). On a new peirosaurid crocodyliform from the Upper Cretaceous, Bauru Group, southeastern Brazil. *Anais da Academia Brasileira de Ciências*, 83: 317-327. https://doi.org/10.1590/S0001-37652011000100020

Capo R. C., Stewart B. W. & Chadwick O. A. (1998). Strontium isotopes as tracers of ecosystem processes: theory and methods. *Geoderma*, 82(1-3): 197-225. https://doi.org/10.1016/S0016-7061(97)00102-X

Carr A. N., Nestler J. H., Vliet K. A., Brochu C. A., Murray C. M. & Shirley M. H. (2021). Use of continuous cranial shape variation in the identification of divergent crocodile species of the genus *Mecistops*. *Journal of Morphology*, 282(8): 1219-1232. https://doi.org/10.1002/jmor.21365

Carvalho I. d. S. (1994). *Candidodon*: um crocodilo com heterodontia (Notosuchia, Cretáceo Inferior-Brasil). *Anais da Academia Brasileira de Ciências*, 66(3): 331-346.

Carvalho I. d. S. & Campos D. d. a. (1988). Um mamifero triconodonte do Cretáceo Inferior do Maranhão, Brasil. *Anais de Academia Brasileira de Ciências*, 60(4): 437-446.

Carvalho I. d. S. & Bertini R. J. (1999). *Mariliasuchus*: um novo Crocodylomorpha (Notosuchia) do Cretáceo da Bacia Bauru, Brasil. *Geologia Colombiana*, 24: 83-105.

Carvalho I. d. S., Ribeiro L. C. B. & Avilla L. d. S. (2004). *Uberabasuchus terrificus* sp. nov., a new Crocodylomorpha from the Bauru Basin (Upper Cretaceous), Brazil. *Gondwana Research*, 7(4): 975-1002. https://doi.org/10.1016/S1342-937X(05)71079-0

Carvalho I. d. S., Campos A. D. C. A. & Nobre P. H. (2005). *Baurusuchus salgadoensis*, a new crocodylomorpha from the Bauru Basin (Cretaceous), Brazil. *Gondwana Research*, 8(1): 11-30. https://doi.org/10.1016/S1342-937X(05)70259-8

Carvalho I. d. S., de Vasconcellos F. M., Tavares S. A. S. (2007). *Montealtosuchus arrudacamposi*, a new peirosaurid crocodile (Mesoeucrocodylia) from the Late Cretaceous Adamantina Formation of Brazil. *Zootaxa*, 1607: 35-46. https://doi.org/10.11646/zootaxa.1607.1.3

Carvalho I. d. S., Gasparini Z. B., Salgado L., de Vasconcellos F. M. & Marinho T. d. S. (2010). Climate's role in the distribution of the Cretaceous terrestrial Crocodyliformes throughout Gondwana. *Palaeogeography, Palaeoclimatology, Palaeoecology*, 297(2): 252-262.

Carvalho I. d. S., Teixeira V. d. P. A., Ferraz M. L. d. F., Ribeiro L. C. B., Martinelli A. G., Neto F. M., Sertich J. J. Cunha G. C., Cunha I. C. & Ferraz P. F. (2011a). *Campinasuchus dinizi* gen. et sp. nov., a new Late Cretaceous baurusuchid (Crocodyliformes) from the Bauru Basin, Brazil. *Zootaxa*, 2871(1): 19-42. https://doi.org/10.11646/zootaxa.2871.1.2

Carvalho I. d. S., Teixeira V. d. P. A., Ferraz M. L. d. F., Ribeiro L. C. B., Martinelli A. G., Neto F. M., Sertich J. J., Cunha G. C., Cunha I. C. & Ferraz P. F. (2011b). O sítio paleontológico Fazenda Três Antas, uma nova localidade fossilífera do Cretáceo Superior (grupo Bauru) no município de Campina Verde, Triângulo Mineiro (Brasil): considerações gerais. *XXII Congresso Brasileiro de Paleontologia*, 708-709.

Caselli A. T., Marsicano C. A. & Arcucci A. B. (2001). Sedimentología y paleontología de la Formación Los Colorados, Triásico superior (provincias de La Rioja y San Juan, Argentina). *Revista de la Asociación Geológica Argentina*, 56: 173-188.

Cau A. (2014). The affinities of '*Steneosaurus barettoni*' (Crocodylomorpha, Thalattosuchia), from the Jurassic of Northern Italy, and implications for cranial evolution among geosaurine metriorhynchids. *Historical Biology*, 26(4): 433-440. https://doi.org/10.1080/08912963.2013.784906

Cau A. (2019). A revision of the diagnosis and affinities of the metriorhynchoids (Crocodylomorpha, Thalattosuchia) from the Rosso Ammonitico Veronese Formation (Jurassic of Italy) using specimen-level analyses. *PeerJ*, 7: e7364. https://doi.org/10.7717/peerj.7364

Cau A. & Fanti F. (2011). The oldest known metriorhynchid crocodylian from the Middle Jurassic of North-eastern Italy: *Neptunidraco ammoniticus* gen. et sp. nov. *Gondwana Research*, 19(2): 550-565. https://doi.org/10.1016/j.gr.2010.07.007

Caut S., Angulo E. & Courchamp F. (2009). Variation in discrimination factors ($\Delta^{15}N$ and $\Delta^{13}C$): the effect of diet isotopic values and applications for diet reconstruction. *Journal of Applied Ecology*, 46(2): 443-453. https://doi.org/10.1111/j.1365-2664.2009.01620.x

Cavagnetto C. & Anadón P. (1996). Preliminary palynological data on floristic and climatic changes during the Middle Eocene-Early Oligocene of the eastern Ebro Basin, northeast Spain. *Review of Palaeobotany and Palynology*, 92(3-4): 281-305. https://doi.org/10.1016/0034-6667(95)00096-8

Cavin L., Tong H., Boudad L., Meister C., Piuz A., Tabouelle J., Aarab M., Amiot R., Buffetaut E., Dyke G., Hua S. & Le Loeuff J. (2010). Vertebrate assemblages from the early Late Cretaceous of southeastern Morocco: an overview. *Journal of African Earth Sciences*, 57(5): 391-412. https://doi.org/10.1016/j.jafrearsci.2009.12.007

Cerda I. A., Desojo J. B. & Scheyer T. M. (2018). Novel data on aetosaur (Archosauria, Pseudosuchia) osteoderm microanatomy and histology: palaeobiological implications. *Palaeontology*, 61(5): 721-745. https://doi.org/10.1111/pala.12363

Cerio D. G. & Witmer L. M. (2019). Intraspecific variation and symmetry of the inner-ear labyrinth in a population of wild turkeys: Implications for paleontological reconstructions. *PeerJ*, 7: e7355. https://doi.org/10.7717/peerj.7355

Cerio D. G. & Witmer L. M. (2022). Orbital soft tissues, bones, and allometry: Implications for the size and position of crocodylian eyes. *The Anatomical Record*: https://doi.org/10.1002/ar.25133

Cerling T. E. & Harris J. M. (1999). Carbon isotope fractionation between diet and bioapatite in ungulate mammals and implications for ecological and paleoecological studies. *Oecologia*, 120: 347-363. https://doi.org/10.1007/s004420050868

Cerling T. E., Harris J. M., Hart J. A., Kaleme P., Klingel H., Leakey M. G., Levin N. E., Lewison R. L. & Passey B. H. (2008). Stable isotope ecology of the common hippopotamus. *Journal of Zoology*, 276(2): 204-212. https://doi.org/10.1111/j.1469-7998.2008.00450.x

Cernusak L. A., Barbour M. M., Arndt S. K., Cheesman A. W., English N. B., Feild T. S., Helliker B. R., Holloway-Phillips M. M., Holtum J. A. M., Kahmen A., McInerney F. A., Munksgaard N. C., Simonin K. A., Song X., Stuart-Williams H., West J. B. & Farquhar G. D. (2016). Stable isotopes in leaf water of terrestrial plants. *Plant, Cell & Environment*, 39(5): 1087-1102. https://doi.org/10.1111/pce.12703

Cerroni M. A. & Paulina-Carabajal A. (2019). Novel information on the endocranial morphology of the abelisaurid theropod *Carnotaurus sastrei*. *Comptes Rendus Palevol*, 18(8): 985-995. https://doi.org/10.1016/j.crpv.2019.09.005

Chan W. H., Lau A., Martelli P., Tsang D., Lee W. H. & Sung Y. H. (2020). Spatial ecology of the introduced Chinese water dragon *Physignathus cocincinus* in Hong Kong. *Current Herpetology*, 39(1): 55-65. https://doi.org/10.5358/hsj.39.55

Channon M. B., Gordon G. W., Morgan J. L., Skulan J. L., Smith S. M. & Anbar A. D. (2015). Using natural, stable calcium isotopes of human blood to detect and monitor changes in bone mineral balance. *Bone*, 77: 69-74. https://doi.org/10.1016/j.bone.2015.04.023

Chanthasit P., Suteethorn S., Naksri W., Tong H., Wongko K. & Sonoda T. (2019). New Vertebrate Fossil Site from the Early Cretaceous Sao Khua Formation, Sakon Nakhon Province, Northeastern Thailand. *Open Journal of Geology*, 9(10): 619-623. https://doi.org/10.4236/ojg.2019.910057

Chen H. & Liu Y. (2014). Teeth. In Shen J. Z. & Kosmač T. (eds.) *Advanced Ceramics for Dentistry*, Butterworth-Heinemann: 5-21. https://doi.org/10.1016/B978-0-12-394619-5.00002-X

Chenery C. A., Müldner G., Evans J., Eckardt H. & Lewis M. (2010). Strontium and stable isotope evidence for diet and mobility in Roman Gloucester, UK. *Journal of Archaeological Science*, 37(1): 150-163. https://doi.org/10.1016/j.jas.2009.09.025

Chenery C. A., Pashley V., Lamb A. L., Sloane H. J. & Evans J. A. (2012). The oxygen isotope relationship between the phosphate and structural carbonate fractions of human bioapatite. *Rapid Communications in Mass Spectrometry*, 26(3): 309-319. https://doi.org/10.1002/rcm.5331

Cherepanov G. O. (1995). Ontogenetic development of the shell in *Trionyx sinensis* (Trionychidae, Testudinata) and some questions on the nomenclature of bony plates. *Russian Journal of Herpetology*, 2(2): 129-133.

Chiappe L. M. (1988). A new trematochampsid crocodile from the Early Cretaceous of north-western Patagonia, Argentina and its palaeobiogeographical and phylogenetic implications. *Cretaceous Research*, 9(4): 379-389. https://doi.org/10.1016/0195-6671(88)90009-2

Choubert G., Faure-Muret A. & Chanteux P. (1976). *Geological World Atlas*. Commission de la carte géologique du Monde, Paris, 22 p.

Chu N. C., Henderson G. M., Belshaw N. S. & Hedges R. E. (2006). Establishing the potential of Ca isotopes as proxy for consumption of dairy products. *Applied Geochemistry*, 21(10): 1656-1667. https://doi.org/10.1016/j.apgeochem.2006.07.003

Cifelli R. L., Nydam R. L., Gardner J. D., Weil A., Eaton J. G., Kirkland J. I. & Madsen S. K. (1999). Medial Cretaceous vertebrates from the Cedar Mountain Formation, Emery County, Utah: the Mussentuchit local fauna. *Vertebrate paleontology in Utah*, 99(1): 219-242.

Cignoni P., Callieri M., Corsini M., Dellepiane M., Ganovelli F. & Ranzuglia G. (2008). MeshLab: an Open-source Mesh Processing Tool. In Scarano V., De Chiara R. & Erra U. (eds.) *Eurographics Italian Chapter Conference*, The Eurographics Association: 129-136.

Clarac F., Buffrénil V. d., Cubo J. & Quilhac A. (2018). Vascularization in ornamented osteoderms: physiological implications in ectothermy and amphibious lifestyle in the crocodylomorphs?. *The Anatomical Record*, 301(1): 175-183. https://doi.org/10.1002/ar.23695

Clark J. M. (1986). Phylogenetic relationships of the crocodylomorph archosaurs. Unpublished D. Phil. Thesis, University of Chicago.

Clark J. M. (1994). Patterns of evolution in Mesozoic Crocodyliformes. In Fraser N. C., Sues H. D. (eds.) *In the shadows of dinosaurs: early Mesozoic tetrapods*. Cambridge University Press, 84-97.

Clark J. M. (2011). A new shartegosuchid crocodyliform from the Upper Jurassic Morrison Formation of western Colorado. *Zoological Journal of the Linnean Society*, 163(suppl_1): S152-S172. https://doi.org/10.1111/j.1096-3642.2011.00719.x

Clark J. M. & Norell M. (1992). The Early Cretaceous crocodylomorph *Hylaeochampsa vectiana* from the wealden of the Isle of Wight. *American Museum Novitates*, 3032: 1-19.

Clark J. M. & Sues H. D. (2002). Two new basal crocodylomorph archosaurs from the Lower Jurassic and the monophyly of the Sphenosuchia. *Zoological Journal of the Linnean Society*, 136(1): 77-95. https://doi.org/10.1046/j.1096-3642.2002.00026.x

Clark J. M., Jacobs L. L. & Downs W. R. (1989). Mammal-Like Dentition in a Mesozoic Crocodylian. *Science*, 244: 1064-1066. https://doi.org/10.1126/science.244.4908.1064

Clark J. M., Sues H. D. & Berman D. S. (2001). A new specimen of *Hesperosuchus agilis* from the Upper Triassic of New Mexico and the interrelationships of basal crocodylomorph archosaurs. *Journal of Vertebrate Paleontology*, 20(4): 683-704. https://doi.org/10.1671/0272-4634(2000)020[0683:ANSOHA]2.0.CO;2

Clark J. M., Xu X., Forster C. A. & Wang Y. (2004). A Middle Jurassic 'sphenosuchian' from China and the origin of the crocodylian skull. *Nature*, 430(7003): 1021-1024. https://doi.org/10.1038/nature02802

Clauzel T. (2022). *Etude isotopique de peuples de Gaule du Nord durant le Second Âge du Fer : climat, alimentation, migrations*. Unpublished PhD thesis, Université Claude Bernard Lyon 1, 469 p.

Clauzel T., Richardin P., Ricard J., Le Béchennec Y., Amiot R., Fourel F., Phouybanhdyt B., Vinçon-Laugier A., Flandrois J. P. & Lécuyer C. (2020). The Gauls experienced the Roman Warm Period: Oxygen isotope study of the Gallic site of Thézy-Glimont, Picardie, France. *Journal of Archaeological Science: Reports*, 34: 102595. https://doi.org/10.1016/j.jasrep.2020.102595

Clauzel T., Richardin P., Ricard J., Le Béchennec Y., Amiot R., Fourel F., .Joseph D., Vinçon-Laugier A., Flandrois J. P. & Lécuyer C. (2022). Hydrogen isotope measurements of bone and dental tissues from archaeological human and animal samples and their use as climatic and diet proxies. *Journal of Archaeological Science*, 147: 105676. https://doi.org/10.1016/j.jas.2022.105676

Clemens S. C., Farrell J. W. & Gromet L. P. (1993). Synchronous changes in seawater strontium isotope composition and global climate. *Nature*, 363(6430): 607-610. https://doi.org/10.1038/363607a0

Clement A. M., Nysjö J., Strand R. & Ahlberg P. E. (2015). Brain–endocast relationship in the Australian lungfish, *Neoceratodus forsteri*, elucidated from tomographic data (Sarcopterygii: Dipnoi). *PLoS One*, 10(10): e0141277. https://doi.org/10.1371/journal.pone.0141277

Clement A. M., Mensforth C. L., Challands T. J., Collin S. P. & Long J. A. (2021). Brain reconstruction across the fish-tetrapod transition; Insights from modern amphibians. *Frontiers in Ecology and Evolution*, 9: 640345. https://doi.org/10.3389/fevo.2021.640345

Clementz M. T. (2012). New insight from old bones: stable isotope analysis of fossil mammals. *Journal of Mammalogy*, 93(2): 368-380. https://doi.org/10.1644/11-MAMM-S-179.1

Clementz M. T. & Koch P. L. (2001). Differentiating aquatic mammal habitat and foraging ecology with stable isotopes in tooth enamel. *Oecologia*, 129: 461-472. https://doi.org/10.1007/s004420100745

Clementz M. T., Hoppe K. A. & Koch P. L. (2003). A paleoecological paradox: the habitat and dietary preferences of the extinct tethythere Desmostylus, inferred from stable isotope analysis. *Paleobiology*, 29(4): 506-519. https://doi.org/10.1666/0094-8373(2003)029<0506:APPTHA>2.0.CO;2

Clementz M. T., Holroyd P. A. & Koch P. L. (2008). Identifying aquatic habits of herbivorous mammals through stable isotope analysis. *Palaios*, 23(9): 574-585. https://doi.org/10.2110/palo.2007.p07-054r

Coates M. I. (1999). Endocranial preservation of a Carboniferous actinopterygian from Lancashire, UK, and the interrelationships of primitive actinopterygians. *Philosophical Transactions of the Royal Society of London. Series B: Biological Sciences*, 354(1382): 435-462. https://doi.org/10.1098/rstb.1999.0396

Cojan I. & Moreau M. G. (2006). Correlation of terrestrial climatic fluctuations with global signals during the Upper Cretaceous–Danian in a compressive setting (Provence, France). *Journal of Sedimentary Research*, 76(3): 589-604. https://doi.org/10.2110/jsr.2006.045

Colbert E. H. (1946a). *Sebecus*, representative of a peculiar suborder of fossil Crocodylia from Patagonia. *Bulletin of the American Museum of Natural History*, 87(4): 223-270.

Colbert E. H. (1946b). The Eustachian Tubes in the Crocodilia. *Copeia*, 1946(1): 12-14. https://doi.org/10.2307/1438813

Colbert E. H. (1952). A pseudosuchian reptile from Arizona. *Bulletin of the American Museum of Natural History*, 99(10): 565-592.

Colbert E. H. & Mook C. C. (1951). The ancestral crocodylian *Protosuchus*. *Bulletin of the American Museum of Natural History*, 97(3): 143-182.

Collyer M. L. & Adams D. C. (2021). Phylogenetically aligned component analysis. *Methods in Ecology and Evolution*, 12(2): 359-372. https://doi.org/10.1111/2041-210X.13515

Comar C. L., Russell R. S. & Wasserman R. H. (1957). Strontium-calcium movement from soil to man. *Science*, 126(3272): 485-492. https://doi.org/10.1126/science.126.3272.485

Company J., Suberbiola X. P., Ruiz-Omeñaca J. I. & Buscalioni A. D. (2005). A new species of *Doratodon* (Crocodyliformes: Ziphosuchia) from the Late Cretaceous of Spain. *Journal of Vertebrate Paleontology*, 25(2): 343-353. https://doi.org/10.1671/0272-4634(2005)025[0343:ANSODC]2.0.CO;2

Congreve C. R. & Lamsdell J. C. (2016). Implied weighting and its utility in palaeontological datasets: a study using modelled phylogenetic matrices. *Palaeontology*, 59(3): 447-462. https://doi.org/10.1111/pala.12236

Conedera D. (2022). *Morphometric variability of crocodylians endocast: taxonomic and ecological implications*. Unpublished master thesis, Université Lyon 1, 5 p.

Cope E. D. (1860). *Osteolaemus tetraspis*. *Proceedings of the Academy of Natural Science of Philadelphia*: 549-550.

Cope E. D. (1868). On the origin of genera. *Proceedings of the National Academy of Sciences*, 20: 242-300.

Cope E. D. (1869). On the reptilian orders Pythonomorpha and Streptosauria. *Proceedings of the Boston Society of Natural History*, 12: 250-266.

Cope E. D. (1875). Check-list of North American Batrachia and Reptilia. *Bulletin of the United States National Museum, Washington D. C.*, 1: 1-104.

Coplen T. B. (2011). Guidelines and recommended terms for expression of stable-isotope-ratio and gas-ratio measurement results. *Rapid Communications in Mass Spectrometry*, 25(17): 2538-2560. https://doi.org/10.1002/rcm.5129

Coplen T. B., Böhlke J. K., De Bievre P., Ding T., Holden N. E., Hopple J. A., Krouse H. R., Lamberty A., Peiser H. S., Revesz K., Rieder S. E., Rosman K. J. R., Roth E., Taylor P. D. P., Vocke R. D. & Xiao Y. (2002). Isotope-abundance variations of selected elements (IUPAC Technical Report). *Pure and Applied Chemistry*, 74(10): 1987-2017. https://doi.org/10.1351/pac200274101987

Coria R. A., Ortega F., Arcucci A. B. & Currie P. J. (2019). A new and complete peirosaurid (Crocodyliformes, Notosuchia) from Sierra Barrosa (Santonian, Upper Cretaceous) of the Neuquén Basin, Argentina. *Cretaceous Research*, 95: 89-105. https://doi.org/10.1016/j.cretres.2018.11.008

Costas-Rodríguez, M., Van Heghe L. & Vanhaecke F. (2014). Evidence for a possible dietary effect on the isotopic composition of Zn in blood via isotopic analysis of food products by multi-collector ICP-mass spectrometry. *Metallomics*, 6(1): 139-146. https://doi.org/10.1039/c3mt00244f

Coster P., Benammi M., Mahboubi M., Tabuce R., Adaci M., Marivaux L., Bensalah M., Mahboubi S., Mahboubi A., Mebrouk F., Maameri C. & Jaeger J. J. (2012). Chronology of the Eocene continental deposits of Africa: Magnetostratigraphy and biostratigraphy of the El Kohol and Glib Zegdou Formations, Algeria. *Geological Society of America Bulletin*, 124(9-10): 1590-1606. https://doi.org/10.1130/B30565.1

Costeur L., Grohé C., Aguirre-Fernández G., Ekdale E., Schulz G., Müller B. & Mennecart B. (2018). The bony labyrinth of toothed whales reflects both phylogeny and habitat preferences. *Scientific Reports*, 8(1): 1-6. https://doi.org/10.1038/s41598-018-26094-0

Cotts L., Pinheiro A. E. P., Marinho T. S., Carvalho I. d. S. & Di Dario F. (2017). Postcranial skeleton of *Campinasuchus dinizi* (Crocodyliformes, Baurusuchidae) from the Upper Cretaceous of Brazil, with comments on the ontogeny and ecomorphology of the species. *Cretaceous Research*, 70: 163-188. https://doi.org/10.1016/j.cretres.2016.11.003

Coulson A. B., Kohn M. J., Shirley M. H., Joyce W. G. & Barrick R. E. (2008). Phosphate–oxygen isotopes from marine turtle bones: Ecologic and paleoclimatic applications. *Palaeogeography, Palaeoclimatology, Palaeoecology*, 264(1-2): 78-84. https://doi.org/10.1016/j.palaeo.2008.04.008

Court N. (1994). Limb posture and gait in *Numidotherium koholense*, a primitive proboscidean from the Eocene of Algeria. *Zoological Journal of the Linnean Society*, 111(4): 297-338. https://doi.org/10.1111/j.1096-3642.1994.tb01487.x

Cowgill T., Young M. T., Schwab J. A., Walsh S., Witmer L. M., Herrera Y., Dollman K. N., Choiniere J. N. & Brusatte S. L. (2022). Paranasal sinus system and upper respiratory tract evolution in Mesozoic pelagic crocodylomorphs. *The Anatomical Record*, 305(10): 2583-2603. https://doi.org/10.1002/ar.24727

Cowgill T., Young M. T., Schwab J. A., Walsh S., Witmer L. M., Herrera Y., Dollman K. N., Turner A. H. & Brusatte S. L. (2023). Cephalic salt gland evolution in Mesozoic pelagic crocodylomorphs. *Zoological Journal of the Linnean Society*, 197(3): 812-835. https://doi.org/10.1093/zoolinnean/zlac027

Cowie G. L. & Hedges J. I. (1994). Biochemical indicators of diagenetic alteration in natural organic matter mixtures. *Nature*, 369(6478): 304-307. https://doi.org/10.1038/369304a0

Crowson R. A., Showers W. J., Wright E. K. & Hoering T. C. (1991). Preparation of phosphate samples for oxygen isotope analysis. *Analytical Chemistry*, 63(20): 2397-2400.

Cox J. H. & Phothitay C. (2008). Surveys of the Siamese crocodile *Crocodylus siamensis* in Vavannakhet Province, Lao PDR, 6 May-4 June 2008. *OZ Minerals Ltd. & Wildlife Conservation Society: Vientiane*.

Cramer B. S., Toggweiler J. R., Wright J. D., Katz M. E. & Miller K. G. (2009). Ocean overturning since the Late Cretaceous: Inferences from a new benthic foraminiferal isotope compilation. *Paleoceanography*, 24(4). https://doi.org/10.1029/2008PA001683

Crompton A. W. & Smith K. K. (1980). A new genus and species of crocodilian from the Kayenta Formation (Late Triassic?) of Northern Arizona. In Jacobs L. L. (ed.) *Aspects of vertebrate history: Essays in honor of Edwin Harris Colbert*: 193-217.

Crowson R. A., Showers W. J., Wright E. K. & Hoering T. C. (1991). Preparation of phosphate samples for oxygen isotope analysis. *Analytical Chemistry*, 63(20): 2397-2400.

Crush P. J. (1984). A late Upper Triassic sphenosuchid crocodylian from Wales. *Palaeontology*, 27(1): 131-157.

Csiki-Sava Z., Buffetaut E., Ősi A., Pereda-Suberbiola X. & Brusatte S. L. (2015). Island life in the Cretaceous-faunal composition, biogeography, evolution, and extinction of land-living vertebrates on the Late Cretaceous European archipelago. *ZooKeys*, (469): 1-161. https://doi.org/10.3897/zookeys.469.8439

Cubo J., Ponton F., Laurin M., De Margerie E. D. & Castanet J. (2005). Phylogenetic signal in bone microstructure of sauropsids. *Systematic Biology*, 54(4): 562-574. https://doi.org/10.1080/10635150591003461

Cubo J., Legendre P., de Ricqlès A., Montes L., De Margerie E., Castanet J. & Desdevises Y. (2008). Phylogenetic, functional, and structural components of variation in bone growth rate of amniotes. *Evolution & Development*, 10(2): 217-227. https://doi.org/10.1111/j.1525-142X.2008.00229.x

Cubo J., Le Roy N., Martinez-Maza C. & Montes L. (2012). Paleohistological estimation of bone growth rate in extinct archosaurs. *Paleobiology*, 38(2): 335-349. https://doi.org/10.1666/08093.1

Cubo J., Woodward H., Wolff E. & Horner J. R. (2015). First reported cases of biomechanically adaptive bone modeling in non-avian dinosaurs. *PloS One*, 10(7): e0131131. https://doi.org/10.1371/journal.pone.0131131

Cubo J., Köhler M. & Buffrénil V. de (2017). Bone histology of *Iberosuchus macrodon* (Sebecosuchia, Crocodylomorpha). *Lethaia*, 50(4): 495-503. https://doi.org/10.1111/let.12203

Cubo J., Sena M. V., Aubier P., Houee G., Claisse P., Faure-Brac M. G., Allain R., Andrade R. C. L. P., Sayão J. M. & Oliveira G. R. (2020). Were Notosuchia (Pseudosuchia: Crocodylomorpha) warm-blooded? A palaeohistological analysis suggests ectothermy. *Biological Journal of the Linnean Society*, 131(1): 154-162. https://doi.org/10.1093/biolinnean/blaa081

Cubo J., Aubier P., Faure-Brac M. G., Martet G., Pellarin R., Pelletan I. & Sena M. V. (2022a). Paleohistological inferences of thermometabolic regimes in Notosuchia (Pseudosuchia: Crocodylomorpha) revisited. *Paleobiology*, 1-11. https://doi.org/10.1017/pab.2022.28

Cubo J., Buscalioni A. D., Legendre L. J., Bourdon E., Sanz J. L. & de Ricqlès A. (2022b). Palaeohistological inferences of resting metabolic rates in *Concornis* and *Iberomesornis* (Enantiornithes, Ornithothoraces) from the Lower Cretaceous of Las Hoyas (Spain). *Palaeontology*, 65(1): e12583. https://doi.org/10.1111/pala.12583

Cunha G. O., Santucci R. M., de Andrade M. B. & de Oliveira C. E. M. (2020). Description and phylogenetic relationships of a large-bodied sphagesaurid notosuchian from the Upper Cretaceous Adamantina Formation, Bauru Group, São Paulo, southeastern Brazil. *Cretaceous Research*, 106: 104259. https://doi.org/10.1016/j.cretres.2019.104259

Cuny G., Buffetaut E., Cappetta H., Martin M., Mazin J. M. & Rose J. M. (1991). Nouveaux restes de Vertébrés du Jurassique terminal du Boulonnais (Nord de la France). *Neues Jahrbuch für Geologie und Paläontologie-Abhandlungen*, 180(3): 323-347. https://doi.org/10.1127/njgpa/180/1991/323

Cuny G., Laojumpon C. & Lauprasert K. (2010). Fossil vertebrate remains from Kut Island (Gulf of Thailand, Early Cretaceous). *Cretaceous Research*, 31(4): 415-423. https://doi.org/10.1016/j.cretres.2010.05.007

Currie B. S., Colombi C. E., Tabor N. J., Shipman T. C. & Montañez I. P. (2009). Stratigraphy and architecture of the Upper Triassic Ischigualasto Formation, Ischigualasto Provincial Park, San Juan, Argentina. *Journal of South American Earth Sciences*, 27(1): 74-87. https://doi.org/10.1016/j.jsames.2008.10.004

Curry Rogers K., D'emic M., Rogers R., Vickaryous M. & Cagan A. (2011). Sauropod dinosaur osteoderms from the Late Cretaceous of Madagascar. *Nature communications*, 2(1): 1-5. https://doi.org/10.1038/ncomms1578

Curthoys I. S. & Oman C. M. (1986). Dimensions of the horizontal semicircular duct, ampulla and utricle in rat and guinea pig. *Acta Oto-Laryngologica*, 101(1-2): 1-10. https://doi.org/10.3109/00016488609108601

Curthoys I. S. & Oman C. M. (1987). Dimensions of the horizontal semicircular duct, ampulla and utricle in the human. *Acta Oto-Laryngologica*, 103(3-4): 254-261. https://doi.org/10.3109/00016488709107280

Custódio M. A., Roddaz M., Santos R. V., Antoine P. O., Marivaux L., Stutz N. S., Dantas E. L., Jaramillo C., Louterbach M., Hurtado C. & Gonçalves G. O. (2023). New stratigraphic and paleoenvironmental constraints on the Paleogene paleogeography of Western Amazonia. *Journal of South American Earth Sciences*, 124: 104256. https://doi.org/10.1016/j.jsames.2023.104256

Cuvier G. (1800). Sur une nouvelle espèce de crocodile fossile. *Bulletin de la Société Philomathique de Paris*, 2: 159.

Cuvier G. (1804). Sur les espèces d'animaux dont proviennent les os fossiles répandus dans la pierre à plâtre des environs de Paris. *Annales du Muséum d'Histoire Naturelle, Paris*, 3(1804) : 275-303, 364-387, 442-472.

Cuvier G. (1808). Sur les ossemens fossiles de crocodiles, et particulièrement sur ceux des environs du Havre et de Honfleur, avec des remarques sur les squelettes des sauriens de la Thuringe. *Annales du Muséum d'Histoire Naturelle*, 12: 73-110.

Cuvier G. (1822). *Recherches sur les Ossemens Fossiles*. Dufour & d'Ocagne, Paris, 548 p.

Cuvier G. (1824). *Recherches sur les ossements fossiles*. Dufour & d'Ocagne, Paris, 548 p.

D'Amore D. C. & Blumensehine R. J. (2009). Komodo monitor (*Varanus komodoensis*) feeding behavior and dental function reflected through tooth marks on bone surfaces, and the application to ziphodont paleobiology. *Paleobiology*, 35(4): 525-552. https://doi.org/10.1666/0094-8373-35.4.525

D'Angela D. & Longinelli A. (1990). Oxygen isotopes in living mammal's bone phosphate: further results. *Chemical Geology: Isotope Geoscience Section*, 86(1): 75-82. https://doi.org/10.1016/0168-9622(90)90007-Y

D'Emic M. D., Whitlock J. A., Smith K. M., Fisher D. C. & Wilson J. A. (2013). Evolution of high tooth replacement rates in sauropod dinosaurs. *PLoS One*, 8(7): e69235. https://doi.org/10.1371/journal.pone.0069235

Da Costa Pereira P. V. L. G., Pedro Bogado J., Baptista Ribeiro T., Paiva Belfort L., de Valais S. & Roberto dos Anjos Candeiro C. (2022). Dino on the menu: tooth traces in a sauropod epiphysis from the Presidente Prudente Formation (Campanian-Maastrichtian), Bauru Group, Brazil-palaeobiological and palaeoecological implications. *Historical Biology*, 34(11): 2079-2088. https://doi.org/10.1080/08912963.2021.2000603

de Andrade M. B. & Bertini R. J. (2008). A new *Sphagesaurus* (Mesoeucrocodylia: Notosuchia) from the Upper Cretaceous of Monte Alto City (Bauru Group, Brazil), and a revision of the Sphagesauridae. *Historical Biology*, 20(2): 101-136. https://doi.org/10.1080/08912960701642949

de Andrade M. B., Young M. T., Desojo J. B. & Brusatte S. L. (2010). The evolution of extreme hypercarnivory in Metriorhynchidae (Mesoeucrocodylia: Thalattosuchia) based on evidence from microscopic denticle morphology. *Journal of Vertebrate Paleontology*, 30(5): 1451-1465. https://doi.org/10.1080/02724634.2010.501442

de Andrade M. B., Edmonds R., Benton M. J. & Schouten R. (2011). A new Berriasian species of *Goniopholis* (Mesoeucrocodylia, Neosuchia) from England, and a review of the genus. *Zoological Journal of the Linnean Society*, 163(suppl_1): S66-S108. https://doi.org/10.1111/j.1096-3642.2011.00709.x

de Andrade R. C. L. P., & Sayão J. M. (2014). Paleohistology and lifestyle inferences of a dyrosaurid (Archosauria: Crocodylomorpha) from Paraíba Basin (Northeastern Brazil). *PloS one*, 9(7): e102189. https://doi.org/10.1371/journal.pone.0102189

de Andrade R. C. L. P., Sena M. V. A, Brum A. S., Campos D. A., Kellner A. W. A., Bantim R. A. M. B. & Sayão J. M. (2023). Osteohistology of the big-sized cretaceous crocodylomorph *Stratiotosuchus maxhechti* (Notosuchia, Baurusuchidae) indicates fast growth and niche partitioning with medium-sized theropods. *Journal of South American Earth Sciences,* 104363. https://doi.org/10.1016/j.jsames.2023.104363

De Baar H. J. W., Bacon M. P. & Brewer P. G. (1983). Rare-earth distributions with a positive Ce anomaly in the Western North Atlantic Ocean. *Nature*, 301(5898): 324-327. https://doi.org/10.1038/301324a0

De Baar H. J., Bacon M. P., Brewer P. G. & Bruland K. W. (1985). Rare earth elements in the Pacific and Atlantic Oceans. *Geochimica et Cosmochimica Acta*, 49(9): 1943-1959. https://doi.org/10.1016/0016-7037(85)90089-4

de Celis A., Narváez I., Arcucci A. & Ortega F. (2021). Lagerstätte effect drives notosuchian palaeodiversity (Crocodyliformes, Notosuchia). *Historical Biology*, 33(11): 3031-3040. https://doi.org/10.1080/08912963.2020.1844682

de Lapparent de Broin F. (1992). Fossil turtles from Bolivia. *Fósiles y facies de Bolivia*, 12: 509-527.

de Lapparent de Broin F. (2002). *Elosuchus*, a new genus of crocodile from the Cretaceous of the North of Africa. *Comptes Rendus Palevol*, 1(5): 275-285. https://doi.org/10.1016/S1631-0683(02)00049-0

de Lapparent de Broin F., Grenot C. & Vernet R. (1971). Sur la découverte d'un nouveau gisement de Vertébrés dans le Continental Intercalaire saharien: la Gara Samani (Algérie). *Comptes Rendus de l'Académie des Sciences de Paris*, 272: 1219-1221.

De Muynck D., Huelga-Suarez G., Van Heghe L., Degryse P. & Vanhaecke F. (2009). Systematic evaluation of a strontium-specific extraction chromatographic resin for obtaining a purified Sr fraction with quantitative recovery from complex and Ca-rich matrices. *Journal of Analytical Atomic Spectrometry*, 24(11): 1498-1510. https://doi.org/10.1039/B908645E

de Oliveira F. A., Santucci R. M., de Oliveira C. E. M. & de Andrade M. B. (2021). Morphological and compositional analyses of coprolites from the Upper Cretaceous Bauru Group reveal dietary habits of notosuchian fauna. *Lethaia*, 54(5): 664-686. https://doi.org/10.1111/let.12431

de Ricqlès A. J., Padian K., Horner J. R. & Francillon-Vieillot H. (2000). Palaeohistology of the bones of pterosaurs (Reptilia: Archosauria): anatomy, ontogeny, and biomechanical implications. *Zoological Journal of the Linnean Society*, 129(3): 349-385. https://doi.org/10.1111/j.1096-3642.2000.tb00016.x

de Ricqlès A. J., Padian K. & Horner J. R. (2003a). On the bone histology of some Triassic pseudosuchian archosaurs and related taxa. *Annales de Paléontologie*, 89, (2): 67-101. https://doi.org/10.1016/S0753-3969(03)00005-3

de Ricqlès A. J., Padian K., Horner J. R., Lamm E. T. & Myhrvold N. (2003b). Osteohistology of *Confuciusornis sanctus* (theropoda: Aves). *Journal of Vertebrate Paleontology*, 23(2): 373-386. https://doi.org/10.1671/0272-4634(2003)023[0373:OOCSTA]2.0.CO;2

de Ricqlès A., Bourdon E., Legendre L. J. & Cubo J. (2016). Preliminary assessment of bone histology in the extinct elephant bird *Aepyornis* (Aves, Palaeognathae) from Madagascar. *Comptes Rendus Palevol*, 15(1-2): 197-208. https://doi.org/10.1016/j.crpv.2015.01.003

de Stefano G. (1903). Nuovi rettili degli strati a fosfato della Tunisia. *Bollettino delle Societa Geologica Italiana*, 22 : 51-80.

de Stefano G. (1905). Appunti sui batraci et sui reptili del Quercy appartenenti alla collezione Rossignol. *Bollettino della Societa geologica italiana*, 24: 1-67.

de Vasconcellos F. M. (2006). Descrição do pós-crânio de *Uberabasuchus terrificus* Carvalho, Ribeiro e á 2004 (Crocodyliformes, Peirosauridae) do Cretáceo Superior da bacia Bauru: inferências morfofuncionais e paleoautoecológicas. *Anuário do Instituto de Geociências*, 29(2): 270-270.

de Vasconcellos F. M. & Cávalho I. d. S. (2005). Ontogeny stages of *Mariliasuchus amarali*, Crocodyliformes Mesoeucrocodylia from Adamantina formation, upper cretaceous of Bauru Basin, Brazil. *Anuário do Instituto de Geociências*, 28(1): 49-69.

de Vasconcellos F. M. & Carvalho I. d. S. (2006). Condicionante etológico na tafônomia de *Uberabasuchus terrificus* (Crocodyliformes, Peirosauridae) da Bacia Bauru (Cretáceo Superior). *Geociências*, 25(2): 225-230.

de Vasconcellos F. M. & Carvalho I. d. S. (2010). Paleoichnological assemblage associated with *Baurusuchus salgadoensis* remains, a Baurusuchidae Mesoeucrocodylia from the Bauru Basin, Brazil (Late Cretaceous). *Bulletin of the New Mexico Museum of Natural History and Science*, 51: 227-237.

de Vasconcellos F. M., Arruda J. T., Rocha-Barbosa O. & Carvalho I. d. S. (2004). Falanges ungueais de crocodilomorfos da Bacia Bauru (Cretáceo Superior, Brasil). *Anuário do Instituto de Geociências*, 27: 53-63.

de Vasconcellos F. M., Marinho T. S. & Carvalho I. d. S. (2007). The locomotion pattern of *Baurusuchus salgadoensis* Carvalho, Nobre & Campos, 2005 and the distribution of Baurusuchidae in Gondwanaland. *Nature Precedings*. https://doi.org/10.1038/npre.2007.808.1

de Vasconcellos F. M., Morato L., Marinho T. S. & Carvalho I. d. S. (2008). Occurrence of gastroliths in *Baurusuchus* (Baurusuchidae, Mesoeucrocodylia) from Adamantina Formation, Bauru Basin. *Nature Precedings.* https://doi.org/10.1038/npre.2008.1950.1

Dal Sasso G., Lebon M., Angelini I., Maritan L., Usai D. & Artioli G. (2016). Bone diagenesis variability among multiple burial phases at Al Khiday (Sudan) investigated by ATR-FTIR spectroscopy. *Palaeogeography, Palaeoclimatology, Palaeoecology*, 463: 168-179. https://doi.org/10.1016/j.palaeo.2016.10.005

Dal Sasso C., Pasini G., Fleury G. & Maganuco S. (2017). *Razanandrongobe sakalavae*, a gigantic mesoeucrocodylian from the Middle Jurassic of Madagascar, is the oldest known notosuchian. *PeerJ*, 5: e3481. https://doi.org/10.7717/peerj.3481

dos Santos M. D., Santucci M. R., de Oliveira M. C. E. & de Andrade M. B. (2022). A baurusuchid yearling (Mesoeucrocodylia, Crocodyliformes), from the Adamantina Formation, Bauru Group, Upper Cretaceous of Brazil. *Historical Biology*, 34(11): 2137-2151. https://doi.org/10.1080/08912963.2021.2001807

Daltry J. C., Chheang D., Em P., Poeung M., Sam H., Tan T. & Simpson B. K. (2003). Status of the Siamese Crocodile in the Central Cardamom Mountains, Cambodia. *Fauna & Flora International: Cambodia Programe, and Department of Forestry and Wildlife: Phnom Penh.*

Danilo L., Remy J., Vianey-Liaud M., Mérigeaud S. & Lihoreau F. (2015). Intraspecific Variation of Endocranial Structures in Extant *Equus*: A Prelude to Endocranial Studies in Fossil Equoids: Endocranial

Intraspecific Variation in *Equus*. *Journal of Mammalian Evolution*, 22: 561-582. https://doi.org/10.1007/s10914-015-9293-x

Dansgaard W. (1964). Stable isotopes in precipitation. *Tellus*, 16(4): 436-468. https://doi.org/10.3402/tellusa.v16i4.8993

Darlim G., Carvalho I. d. S., Tavares S. A. S. & Langer M. C. (2021a). A new Pissarrachampsinae specimen from the Bauru Basin, Brazil, adds data to the understanding of the Baurusuchidae (Mesoeucrocodylia, Notosuchia) distribution in the Late Cretaceous of South America. *Cretaceous Research*, 128: 104969. https://doi.org/10.1016/j.cretres.2021.104969

Darlim G., Montefeltro F. C. & Langer M. C. (2021b). 3D skull modelling and description of a new baurusuchid (Crocodyliformes, Mesoeucrocodylia) from the Late Cretaceous (Bauru Basin) of Brazil. *Journal of Anatomy*, 239(3): 622-662. https://doi.org/10.1111/joa.13442

Daudin F. M. (1801). *Histoire Naturelle, Générale et Particuliere des Reptiles*. Dufart, France.

David R. (2010). *Le système des canaux semi-circulaires des archosaures: anatomie, morphométrie, morphologie fonctionnelle, évolution*. Unpublished PhD thesis, Muséum National d'Histoire Naturelle, 317 p.

David R., Bronzati M. & Benson R. B. (2022). Comment on "The early origin of a birdlike inner ear and the evolution of dinosaurian movement and vocalization". *Science*, 376(6600): eabl6710. https://doi.org/10.1126/science.abl6710

Dawson J. J. C., Billett M. F., Neal C. & Hill S. (2002). A comparison of particulate dissolved and gaseous carbon in two contrasting upland streams in the UK. *Journal of Hydrology*, 257(1-4): 226-246. https://doi.org/10.1016/S0022-1694(01)00545-5

Deakins M. & Volker J. F. (1941). Amount of organic matter in enamel from several types of human teeth. *Journal of Dental Research*, 20(2): 117-121. https://doi.org/10.1177/00220345410200020201

Delfino M., Codrea V., Folie A., Dica P., Godefroit P. & Smith T. (2008a). A complete skull of *Allodaposuchus precedens* Nopcsa, 1928 (Eusuchia) and a reassessment of the morphology of the taxon based on the Romanian remains. *Journal of Vertebrate Paleontology*, 28(1): 111-122. https://doi.org/10.1671/0272-4634(2008)28[111:ACSOAP]2.0.CO;2

Delfino M., Martin J. E. & Buffetaut E. (2008b). A new species of *Acynodon* (Crocodylia) from the upper cretaceous (Santonian–Campanian) of Villaggio del Pescatore, Italy. *Palaeontology*, 51(5): 1091-1106. https://doi.org/10.1111/j.1475-4983.2008.00800.x

DeNiro M. J. & Epstein S. (1978). Influence of diet on the distribution of carbon isotopes in animals. *Geochimica et Cosmochimica Acta*, 42(5): 495-506. https://doi.org/10.1016/0016-7037(78)90199-0

DeNiro M. J. & Epstein S. (1981). Influence of diet on the distribution of nitrogen isotopes in animals. *Geochimica et Cosmochimica Acta*, 45(3): 341-351. https://doi.org/10.1016/0016-7037(81)90244-1

Denison R. E., Koepnick R. B., Fletcher A., Dahl D. A. & Baker M. C. (1993). Reevaluation of early Oligocene, Eocene, and Paleocene seawater strontium isotope ratios using outcrop samples from the US Gulf Coast. *Paleoceanography*, 8(1): 101-126. https://doi.org/10.1029/92PA02338

Denton Jr R. K., Dobie J. L. & Parris D. C. (1997). The marine crocodylian *Hyposaurus* in North America. In Callaway J. M. & Nicholls E. L, *Ancient Marine Reptiles,* Academic Press: 375-397. https://doi.org/10.1016/B978-012155210-7/50020-X

DePaolo D. J. (2004). Calcium isotopic variations produced by biological, kinetic, radiogenic and nucleosynthetic processes. *Reviews in Mineralogy and Geochemistry*, 55(1): 255-288. https://doi.org/10.2138/gsrmg.55.1.255

Dias W. A., Iori F. V., Ghilardi A. M. & Fernandes M. A. (2020). The pterygoid region and cranial airways of *Caipirasuchus paulistanus* and *Caipirasuchus montealtensis* (Crocodyliformes, Sphagesauridae), from the Upper Cretaceous Adamantina Formation, Bauru Basin, Brazil. *Cretaceous Research*, 106: 104192. https://doi.org/10.1016/j.cretres.2019.104192

Di-Poï N. & Milinkovitch M. C. (2013). Crocodylians evolved scattered multi-sensory micro-organs. *EvoDevo*, 4(1): 1-16. https://doi.org/10.1186/2041-9139-4-19

Ditbanjong P., Chanthasit P. & Wongko K. (2019). Sedimentology and Stratigraphy of Phu Sung Fossil Site of the Lower Cretaceous Sao Khua Formation, Sakon Nakhon Province, Northeastern Thailand. *Open Journal of Geology*, 9(10): 684-688. https://doi.org/10.4236/ojg.2019.910075

Dodat P. J., Tacail T., Albalat E., Gómez-Olivencia A., Couture-Veschambre C., Holliday T., Madelaine S., Martin J. E., Rmoutilova R., Maureille B. & Balter V. (2021). Isotopic calcium biogeochemistry of MIS 5 fossil vertebrate bones: application to the study of the dietary reconstruction of Regourdou 1 Neandertal fossil. *Journal of Human Evolution*, 151: 102925. https://doi.org/10.1016/j.jhevol.2020.102925

Dodat P. J., Martin J. E., Olive S., Hassler A., Albalat E., Boisserie J. R., Merceron G., Souron A., Maureille B. & Balter V. (2023). Limits of calcium isotopes diagenesis in fossil bone and enamel. *Geochimica et Cosmochimica Acta*. https://doi.org/10.1016/j.gca.2023.04.012

Dole M., Lane G. A., Rudd D. P. & Zaukelies D. A. (1954). Isotopic composition of atmospheric oxygen and nitrogen. *Geochimica et Cosmochimica Acta*, 6(2-3): 65-78. https://doi.org/10.1016/0016-7037(54)90016-2

Dollman K. N., Clark J. M., Norell M. A., Xing X. & Choiniere J. N. (2018). Convergent evolution of a eusuchian-type secondary palate within Shartegosuchidae. *American Museum Novitates*, 2018(3901): 1-23. https://doi.org/10.1206/3901.1

Dollman K. N., Viglietti P. A. & Choiniere J. N. (2019). A new specimen of *Orthosuchus stormbergi* (Nash 1968) and a review of the distribution of Southern African Lower Jurassic crocodylomorphs. *Historical Biology*, 31(5): 653-664. https://doi.org/10.1080/08912963.2017.1387110

Dollman K. N., Clark J. M., Viglietti P. A., Browning C. & Choiniere J. N. (2021). Revised anatomy, taxonomy and biostratigraphy of *Notochampsa istedana* Broom, 1904, a Lower Jurassic crocodyliform from the Clarens

Formation (Stormberg Group), and its implications for early crocodyliform phylogeny. *Journal of Systematic Palaeontology*, 19(9): 651-675. https://doi.org/10.1080/14772019.2021.1948926

Dollo L. (1883). Première note sur les crocodiliens de Bernissart. *Bulletin du Musée Royal d'Histoire Naturelle de Belgique*, 2: 309-338.

Dollo L. (1914). Sur la découverte de Téléosauriens tertiaires au Congo. *Bulletin de l'Académie royale de Belgique*, 7: 288-298.

Drewicz A. E., Trayler R. B., Holloway M. E., Harrigan C. O. & Kohn M. J. (2020). The interpretability of stable hydrogen isotopes in modern herbivore tooth enamel. *Geochimica et Cosmochimica Acta*, 270: 84-94. https://doi.org/10.1016/j.gca.2019.11.013

Dubiel R. F., Ridgley J. L. & Armstrong A. K. (1989). Depositional environments of the Upper Triassic Chinle Formation in the eastern San Juan basin and vicinity, New Mexico. *US Geological Survey Bulletin*, 1808-B: 1-22.

Dufeau D. L. (2011). *The evolution of cranial pneumaticity in Archosauria: patterns of paratympanic sinus development.* Unpublished PhD thesis, Ohio University, p. 174.

Dufeau D. L. & Witmer L. M. (2015). Ontogeny of the middle-ear air-sinus system in *Alligator mississippiensis* (Archosauria: Crocodylia). *PLoS One*, 10(9): e0137060. https://doi.org/10.1371/journal.pone.0137060

Dumoncel J., Subsol G., Durrleman S., Bertrand A., de Jager E., Oettlé A. C., Lockhat Z., Suleman F. E. & Beaudet A. (2020). Are endocasts reliable proxies for brains? A 3D quantitative comparison of the extant human brain and endocast. *Journal of Anatomy*, 238(2): 480-488. https://doi.org/10.1111/joa.13318

Dumont M. F., Bona P., Pol D. & Apesteguía S. (2020a). New anatomical information on *Araripesuchus buitreraensis* with implications for the systematics of Uruguaysuchidae (Crocodyliforms, Notosuchia). *Cretaceous Research*, 113: 104494. https://doi.org/10.1016/j.cretres.2020.104494

Dumont M. V., Santucci R. M., de Andrade M. B. & de Oliveira C. E. M. (2020b). Paleoneurology of *Baurusuchus* (Crocodyliformes: Baurusuchidae), ontogenetic variation, brain size, and sensorial implications. *The Anatomical Record*, 305(10): 2670-2694. https://doi.org/10.1002/ar.24567

Dumont M. F., Pereyra M. E., Bona P. & Apesteguía S. (2021). New data on the palaeosteohistology and growth dynamic of the notosuchian *Araripesuchus* Price, 1959. *Lethaia*, 54(4): 578-590. https://doi.org/10.1111/let.12423

Early C. M., Iwaniuk A. N., Ridgely R. C. & Witmer L. M. (2020a). Endocast structures are reliable proxies for the sizes of corresponding regions of the brain in extant birds. *Journal of Anatomy*, 237(6): 1162-1176. https://doi.org/10.1111/joa.13285

Early C. M., Ridgely R. C. & Witmer L. M. (2020b). Beyond endocasts: using predicted brain-structure volumes of extinct birds to assess neuroanatomical and behavioral inferences. *Diversity*, 12(1): 1-23. https://doi.org/10.3390/d12010034

Eaton M. J. (2010). Dwarf crocodile *Osteolaemus tetraspis*. In Manolis S. C. & Stevenson C. (eds.) *Crocodiles. Status Survey and Conservation Action Plan*, Crocodile Specialist Group: 127-132.

Eaton J. G., Cifelli R. L., Hutchison J. H., Kirkland J. I. & Parrish J. M. (1999). Cretaceous vertebrate faunas from the Kaiparowits Plateau, south-central Utah. *Vertebrate paleontology in Utah*, 99(1), 345-354.

Eberth D. A., Brinkman D. B., Chen P. J., Yuan F. T., Wu S. Z., Li G. & Cheng X. S. (2001). Sequence stratigraphy, paleoclimate patterns, and vertebrate fossil preservation in Jurassic Cretaceous strata of the Junggar Basin, Xinjiang Autonomous Region, People's Republic of China. *Canadian Journal of Earth Sciences*, 38(12): 1627-1644. https://doi.org/10.1139/e01-067

Edinger T. (1921). Über *Nothosaurus*. I. Ein Steinkern der Schädelhöhle. *Senckenbergiana*, 3: 121-129.

Edinger T. (1925). Das Zentralnervensystem von *Placodus gigas* Ag. *Abhandlungen der Senckenbergischen Naturforschenden Gesselschaft*, 88: 311-318.

Edinger T. (1926). The brain of *Archaeopteryx*. *Annals and Magazine of Natural History, Series 9*. 18: 151-156.

Edinger T. (1927). Das Gehirn der Pterosaurier. *Zeitschrift für Anatomie und Entwicklungsgeschichte*, 83: 105-112.

Edinger T. (1928). Über einige fossile Gehirne. *Paläontologische Zeitschrift*, 9: 379-402.

Edinger T. (1938). Über Steinkerne von Hirn-und Ohr-Höhlen der Mesosuchier *Goniopholis* und *Pholidosaurus* uas dem Bückeburger Wealden. *Acta Zoologica*, 19(3): 467-505. https://doi.org/10.1111/j.1463-6395.1938.tb00693.x

Edinger T. (1939). Two notes on the central nervous system of fossil Sirenia. *Bulletin of the Faculty of Science Fouad I University of Cairo*, 19: 43-57.

Edinger T. (1940). The brains of three Pontian ovibovinae from China. *Bulletin of the Geological Institute of Uppsala*, 28: 133-140.

Edinger T. (1941). The brain of *Pterodactylus*. *American Journal of Science*, 239: 665-682.

Edinger T. (1942). The pituitary body in giant animals fossil and living: a survey and a suggestion. *The Quarterly Review of Biology*, 17: 31-45.

Edinger T. (1948). Evolution of the horse brain. *Geological Society of America Memoir*, 25: 1-277.

Edinger T. (1951). The brains of the Odontognathae. *Evolution*, 5: 6-24.

Edinger T. (1975). Paleoneurology 1804-1966. An annotated bibliography. *Advances in Anatomy, Embryology, and Cell Biology*, 49: 1-258.

Efimov M. B. (1975). ПОЗДНЕМЕЛОВЫЕ КРОКОДИЛЫ СРЕДНЕЙ АЗИИ И КАЗАХСТАНА [Late Cretaceous crocodiles of Central Asia and Kazakhstan]. *Paleontologicheskii Zhurnal*, 9: 417-420.

Efimov M. B. (1983). Review of fossil crocodiles of Mongolia. *Trudy Sovmestnoi Sovetsko-Mongol'skoi Paleontologischeskoi Ekspeditsii*, 24: 76–96.

Efimov M. B. (1988). [The fossil crocodiles and champsosaurides of Mongolia and the USSR]. *Trudy Somestnaya Sovetsko-Mongolskya Paleontologicheskaya Expeditsiya*, 36: 1–108. [In Russian.]

Efimov M. B. (1993). The Eocene crocodiles of the GUS – a history of development. *Kaupia,* 3: 23–25.

Engbretson G. A. (1992). Neurobiology of the lacertilian parietal eye system. *Ethology Ecology & Evolution*, 4(1): 89-107. https://doi.org/10.1080/08927014.1992.9525353

Eijkelboom I. (2020). *Postcranial remains of* Knoetschkesuchus guimarotae *(Atoposauridae, Crocodylomorpha) from the Late Jurassic of Portugal and its locomotor behaviour.* Unpublished master thesis, Utrecht University, 34 p.

Eiler J. M. (2007). "Clumped-isotope" geochemistry—The study of naturally-occurring, multiply-substituted isotopologues. *Earth and Planetary Science Letters*, 262(3-4): 309-327. https://doi.org/10.1016/j.epsl.2007.08.020

Ekdale E. G. (2009). *Variation within the bony labyrinth of mammals.* Unpublished PhD thesis, The university of Texas, 439 p.

Ekdale E. G. (2010). Ontogenetic variation in the bony labyrinth of *Monodelphis domestica* (Mammalia: Marsupialia) following ossification of the inner ear cavities. *The Anatomical Record*293(11): 1896-1912. https://doi.org/10.1002/ar.21234

Ekdale E. G. (2016a). Form and function of the mammalian inner ear. *Journal of Anatomy*, 228(2): 324-337. https://doi.org/10.1111/joa.12308

Ekdale E. G. & Rowe T. (2011). Morphology and variation within the bony labyrinth of zhelestids (Mammalia, Eutheria) and other therian mammals. *Journal of Vertebrate Paleontology*, 31(3): 658-675. https://doi.org/10.1080/02724634.2011.557284

Elderfield H. & Greaves M. J. (1982). The rare earth elements in seawater. *Nature*, 296(5854): 214-219. https://doi.org/10.1038/296214a0

Elderfield H. & Pagett R. (1986). Rare earth elements in ichthyoliths: variations with redox conditions and depositional environment. *Science of the Total Environment*, 49: 175-197. https://doi.org/10.1016/0048-9697(86)90239-1

Elderfield H. & Sholkovitz E. T. (1987). Rare earth elements in the pore waters of reducing nearshore sediments. *Earth and Planetary Science Letters*, 82(3-4): 280-288. https://doi.org/10.1016/0012-821X(87)90202-0

Elderfield H., Upstill-Goddard R. & Sholkovitz E. R. (1990). The rare earth elements in rivers, estuaries, and coastal seas and their significance to the composition of ocean waters. *Geochimica et Cosmochimica Acta*, 54(4): 971-991. https://doi.org/10.1016/0016-7037(90)90432-K

English N. B., Quade J., DeCelles P. G. & Garzione C. N. (2000). Geologic control of Sr and major element chemistry in Himalayan Rivers, Nepal. *Geochimica et Cosmochimica Acta*, 64(15): 2549-2566. https://doi.org/10.1016/S0016-7037(00)00379-3

Erb A. & Turner A. H. (2021). Braincase anatomy of the Paleocene crocodyliform *Rhabdognathus* revealed through high resolution computed tomography. *PeerJ*, 9: e11253. https://doi.org/10.7717/peerj.11253

Erichsen J. T., Hodos W., Evinger C., Bessette B. B. & Phillips S. J. (1989). Head orientation in pigeons: postural, locomotor and visual determinants. *Brain, Behavior and Evolution*, 33(5): 268-278. https://doi.org/10.1159/000115935

Erickson G. M. (1996). Daily deposition of dentine in juvenile *Alligator* and assessment of tooth replacement rates using incremental line counts. *Journal of Morphology*, 228(2): 189-194. https://doi.org/10.1002/(SICI)1097-4687(199605)228:2<189::AID-JMOR7>3.0.CO;2-0

Escarguel G., Marandat B. & Legendre S. (1997). Sur l'âge numérique des faunes de mammifères du Paléogène d'Europe occidentale, en particulier celles de l'Eocène inférieur et moyen. In Aguilar J. P., Legendre S. & Michaux J. (eds.) *Actes du congrès BiochroM'97*, Mémoires et travaux de l'E.P.H.E., Montpellier: 769-805.

Eudes-Deslongchamps E. (1867-1869). Prodrôme des téléosauriens du Calvados. Notes paléontologiques : 95-354.

Eudes-Deslongchamps E. (1868a). Note sur le squelette et la restauration de *Teleosaurus cadomensis*. *Bulletin de la Société Linéenne de Normandie*, 10: 80-85.

Eudes-Deslongchamps E. (1869). Mémoire sur les Téléosauriens de la Normandie. *Bulletin de la Société Linéenne de Normandie*, 2(3): 124-221.

Eudes-Deslongchamps E. (1870). Note sur les reptiles fossiles appartenant à la famille des Téléosauriens dont les débris ont été recueillis dans les assises jurassiques de Normandie. *Bulletin de la Société Géologique de France*, 2/27: 299-348.

Eudes-Deslongchamps J. A. (1849). Procès-verbal de la course linéenne aux Vaches Noires. *Mémoires de la Société Linéenne de Normandie*, 8: 72-88.

Eudes-Deslongchamps J. A. (1863). Mémoires sur les Téléosauriens de l'Epoque Jurassique du Département du Calvados. Premier Mémoire contenant l'exposé des caractères généraux des Téléosauriens comparés à ceux des crocodiliens et la description particulière des espèces du Lias Supérieur. *Mémoires de la Société Linéenne de Normandie*, 13(3): 1-138.

Eudes-Deslongchamps J. A. (1866). Sur la découverte d'une mâchoire inférieure entière de *Steneosaurus megistorhynchus* (GEOFF.), trouvée à Allemagne et comparaison de cette espèce avec le *Teleosaurus larteti* (DESL.). *Bulletin de la Société Linéenne de Normandie*, 10: 80-85.

Eudes-Deslongchamps J. A. (1868b). Note sur un tronçon de mâchoire supérieure d'une espèce nouvelle de Téléosaure. *Bulletin de la Société Linéenne de Normandie*, 1: 222-225.

Eudes-Deslongchamps J. A. (1868c). Remarques sur l'os de la mâchoire inférieure des Téléosauriens, désigné sous le nom de complémentaire. *Bulletin de la Société Linéenne de Normandie*, 2: 381-473.

Eudes-Deslongchamps J. A. (1896). Histoire d'une vocation. Découverte du premier individu du *Teleosaurus cadomensis*. *Bulletin de la Société Linéenne de Normandie*, 4: 26-49.

Eudes-Deslongchamps J. A. & Blainville H. D. (1853). Lettres sur les Crocodiles vivants et fossiles. *Mémoires de la Société Linéenne de Normandie*, 9: 103-138.

Evans M. (1999). A new reconstruction of the skull of the Callovian elasmosaurid plesiosaur *Muraenosaurus leedsii* Seeley. *Mercian Geologist*, 14(4): 191-198.

Evans D. C. (2005). New evidence on brain-endocranial cavity relationships in ornithischian dinosaurs. *Acta Palaeontologica Polonica*, 50(3): 617-622.

Evans J. A., Chenery C. A. & Fitzpatrick A. P. (2006a). Bronze Age childhood migration of individuals near Stonehenge, revealed by strontium and oxygen isotope tooth enamel analysis. *Archaeometry*, 48(2): 309-321. https://doi.org/10.1111/j.1475-4754.2006.00258.x

Evans J., Stoodley N. & Chenery C. (2006b). A strontium and oxygen isotope assessment of a possible fourth century immigrant population in a Hampshire cemetery, southern England. *Journal of Archaeological Science*, 33(2): 265-272. https://doi.org/10.1016/j.jas.2005.07.011

Evers S. W., Joyce W. G., Choiniere J. N., Ferreira G. S., Foth C., Hermanson G., Yi H., Johnson C. M., Werneburg I. & Benson R. B. (2022). Independent origin of large labyrinth size in turtles. *Nature Communications*, 13(1): 5807. https://doi.org/10.1038/s41467-022-33091-5

Ezcurra M. D. & Agnolín F. L. (2012). A new global palaeobiogeographical model for the late Mesozoic and early Tertiary. *Systematic Biology*, 61(4): 553-566. https://doi.org/10.1093/sysbio/syr115

Fabbri M., Mongiardino Koch N., Pritchard A. C., Hanson M., Hoffman E., Bever G. S., Balanoff A. M., Morris Z. S., Field D. J., Camacho J., Rowe T. B., Norell M. A., Smith R. M. & Bhullar B. A. S. (2017). The skull roof tracks the brain during the evolution and development of reptiles including birds. *Nature Ecology & Evolution*, 1(10): 1543-1550. https://doi.org/10.1038/s41559-017-0288-2

Falk D., Cheverud J., Vannier M. W. & Conroy G. C. (1986). Advanced computer graphics technology reveals cortical asymmetry in endocasts of rhesus monkeys. *Folia Primatologica*, 46(2): 98-103. https://doi.org/10.1159/000156242

Farlow J. O., Hurlburt G. R., Elsey R. M., Britton A. R. & Langston W. (2005). Femoral dimensions and body size of *Alligator mississippiensis*: estimating the size of extinct mesoeucrocodylians. *Journal of Vertebrate Paleontology*, 25(2): 354-369. https://doi.org/10.1671/0272-4634(2005)025[0354:FDABSO]2.0.CO;2

Farris J. S. (1970). Methods for computing Wagner trees. *Systematic Biology*, 19(1): 83-92. https://doi.org/10.1093/sysbio/19.1.83

Faure G. & Mensing T. M. (2005). *Isotopes, Principles and applications.* John Wiley & Sons, Inc., 897 p.

Faure-Brac M. G. (2021). *Effects of thermophysiology on the evolution of Pseudosuchia (Archosauria): contributions of paleohistology and isotopic geochemistry using phylogenetic comparative methods*. Unpublished PhD thesis, Sorbonne Universités, 274 p.

Faure-Brac M. G. & Cubo J. (2020). Were the synapsids primitively endotherms? A palaeohistological approach using phylogenetic eigenvector maps. *Philosophical Transactions of the Royal Society B*, 375(1793): 20190138. https://doi.org/10.1098/rstb.2019.0138

Faure-Brac M. G., Amiot R., Muizon C. de, Cubo J. & Lécuyer C. (2022). Combined paleohistological and isotopic inferences of thermometabolism in extinct Neosuchia, using *Goniopholis* and *Dyrosaurus* (Pseudosuchia: Crocodylomorpha) as case studies. *Paleobiology*, 48(2): 302-323. https://doi.org/10.1017/pab.2021.34

Ferreira J. D., Dozo M. T., de Moura Bubadué J. & Kerber L. (2021). Morphology and postnatal ontogeny of the cranial endocast and paranasal sinuses of capybara (*Hydrochoerus hydrochaeris*), the largest living rodent. *Journal of Morphology*, 283(1): 66-90. https://doi.org/10.1002/jmor.21428

Fernández M. & Gasparini Z. (2000). Salt glands in a Tithonian metriorhynchid crocodyliform and their physiological significance. *Lethaia*, 33(4): 269-276. https://doi.org/10.1080/002411600750053835

Fernández M. & Gasparini Z. (2008). Salt glands in the Jurassic metriorhynchid *Geosaurus*: implications for the evolution of osmoregulation in Mesozoic marine crocodyliforms. *Naturwissenschaften*, 95: 79-84. https://doi.org/10.1007/s00114-007-0296-1

Fernández M. S. & Herrera Y. (2009). Paranasal sinus system of *Geosaurus araucanensis* and the homology of the antorbital fenestra of metriorhynchids (Thalattosuchia: Crocodylomorpha). *Journal of Vertebrate Paleontology*, 29(3): 702-714. https://doi.org/10.1671/039.029.0323

Fernández M. S. & Herrera Y. (2022). Active airflow of the paranasal sinuses in extinct crocodyliforms: Evidence from a natural cast of the thalattosuchian *Dakosaurus andiniensis*. *The Anatomical Record*, 305(10): 2604-2619. https://doi.org/10.1002/ar.24678

Fernández M. S., Paulina-Carabajal A., Gasparini Z. & Chong Diaz G. (2011). A metriorhynchid crocodyliform braincase from northern Chile. *Journal of Vertebrate Paleontology*, 31(2): 369-377. https://doi.org/10.1080/02724634.2011.550361

Fernicola J. C., Zimicz A. N., Chornogubsky L., Ducea M., Cruz L. E., Bond M., Arnal M., Cárdenas M. & Fernández M. (2021). The early Eocene climatic optimum at the lower section of the Lumbrera Formation (Ypresian, Salta Province, Northwestern Argentina): origin and early diversification of the Cingulata. *Journal of Mammalian Evolution*, 28(3): 621-633. https://doi.org/10.1007/s10914-021-09545-w

Figueiredo R. G. & Kellner A. W. (2021). Morphological variation in the dentition of Uruguaysuchidae (Crocodyliformes: Notosuchia). *Anais da Academia Brasileira de Ciências*, 93 : 1-17. https://doi.org/10.1590/0001-3765202120201594

Filippi L. S., Méndez A. H., Juárez Valieri R. D. & Garrido A. C. (2016). A new brachyrostran with hypertrophied axial structures reveals an unexpected radiation of latest Cretaceous abelisaurids. *Cretaceous Research*, 60: 209-219. https://doi.org/10.1016/j.cretres.2015.12.018

Filippi L. S., Barrios F. & Garrido A. C. (2018). A new peirosaurid from the Bajo de la Carpa Formation (Upper Cretaceous, Santonian) of Cerro Overo, Neuquén, Argentina. *Cretaceous Research*, 83: 75-83. https://doi.org/10.1016/j.cretres.2017.10.021

Filippi L. S., Valieri R. D. J. & Barrios F. (2021). The prefrontal of *Rinconsaurus caudamirus* (Sauropoda, Titanosauria) as a crocodyliform ilium. *Cretaceous Research*, 125: 104852. https://doi.org/10.1016/j.cretres.2021.104852

Fiorelli L. E. & Calvo J. O. (2007). The first "protosuchian" (Archosauria: Crocodyliformes) from the Cretaceous (Santonian) of Gondwana. *Arquivos do Museu Nacional, Rio de Janeiro,* 65(4): 417-459.

Fiorelli L. E. & Calvo J. (2008). New remains of *Notosuchus terrestris* Woodward, 1896 (Crocodyliformes: Mesoeucrocodylia) from Late Cretaceous of Neuquén, Patagonia, Argentina. *Arquivos do Museu Nacional, Rio de Janeiro*, 66(1): 83-124.

Fiorelli L. E., Leardi J. M., Hechenleitner E. M., Pol D., Basilici G. & Grellet-Tinner G. (2016). A new Late Cretaceous crocodyliform from the western margin of Gondwana (La Rioja Province, Argentina). *Cretaceous Research*, 60: 194-209. https://doi.org/10.1016/j.cretres.2015.12.003

Fiorillo A. R. (1999). Non-mammalian microvertebrate remains from the Robison Eggshell site, Cedar Mountain Formation (Lower Cretaceous), Emery County, Utah. In Gillette D. D., *Vertebrate paleontology in Utah*, 99(1): 259-268.

Firth B. T., Christian K. A., Belan I. & Kennaway D. J. (2010). Melatonin rhythms in the Australian freshwater crocodile (*Crocodylus johnstoni*): a reptile lacking a pineal complex?. *Journal of Comparative Physiology B*, 180: 67-72. https://doi.org/10.1007/s00360-009-0387-8

Fitzinger L. J. (1826). *Neue classification der reptilien nach ihren natürlichen verwandtschaften: nebst einer verwandtschafts-tafel und einem verzeichnisse der reptilien-sammlung des K. K. zoologischen museum's zu Wien*. Heubner J. G., Vienna, 66 p.

Fitzinger L. J. (1843). *Systema Reptilium*. Braumüller & Seidel, Vienna, 106 p.

Flockhart D. T., Kyser T. K., Chipley D., Miller N. G. & Norris D. R. (2015). Experimental evidence shows no fractionation of strontium isotopes ($^{87}Sr/^{86}Sr$) among soil, plants, and herbivores: implications for tracking wildlife and forensic science. *Isotopes in Environmental and Health Studies*, 51(3): 372-381. https://doi.org/10.1080/10256016.2015.1021345

Foffa D. & Young M. T. (2014). The cranial osteology of *Tyrannoneustes lythrodectikos* (Crocodylomorpha: Metriorhynchidae) from the Middle Jurassic of Europe. *PeerJ*, 2: e608. https://doi.org/10.7717/peerj.608

Foffa D., Young M. T., Stubbs T. L., Dexter K. G. & Brusatte S. L. (2018a). The long-term ecology and evolution of marine reptiles in a Jurassic seaway. *Nature Ecology & Evolution*, 2(10): 1548-1555. https://doi.org/10.1038/s41559-018-0656-6

Foffa D., Young M. T., Brusatte S. L., Graham M. R. & Steel L. (2018b). A new metriorhynchid crocodylomorph from the Oxford Clay Formation (Middle Jurassic) of England, with implications for the origin and diversification of Geosaurini. *Journal of Systematic Palaeontology*, 16(13): 1123-1143. https://doi.org/10.1080/14772019.2017.1367730

Foffa D., Johnson M. M., Young M. T., Steel L. & Brusatte S. L. (2019). Revision of the Late Jurassic deep-water teleosauroid crocodylomorph *Teleosaurus megarhinus* Hulke, 1871 and evidence of pelagic adaptations in Teleosauroidea. *PeerJ*, 7: e6646. https://doi.org/10.7717/peerj.6646

Fonseca P. H. M., Martinelli A. G., Marinho T. d. S., Ribeiro L. C. B., Schultz C. L. & Soares M. B. (2020). Morphology of the endocranial cavities of *Campinasuchus dinizi* (Crocodyliformes: Baurusuchidae) from the Upper Cretaceous of Brazil. *Geobios*, 58: 1-16. https://doi.org/10.1016/j.geobios.2019.11.001

Forrest R. (2003). Evidence for scavenging by the marine crocodile Metriorhynchus on the carcass of a plesiosaur. *Proceedings of the Geologists' Association*, 114: 363-366.

Forskal P. (1775). *Descriptiones animalium, avium, amphibiorum, piscium, insectorum, vermium; quae in itinere Orientali observavit petrus Forskal.* Mölleri, Hauniae, 164 p.

Foster J. (2018). A new atoposaurid crocodylomorph from the Morrison Formation (Upper Jurassic) of Wyoming, USA. *Geology of the intermountain West*, 5: 287-295. https://doi.org/10.31711/giw.v5.pp287-295

Foth C., Evers S. W., Joyce W. G., Volpato V. S. & Benson R. B. (2019). Comparative analysis of the shape and size of the middle ear cavity of turtles reveals no correlation with habitat ecology. *Journal of Anatomy*, 235(6): 1078-1097. https://doi.org/10.1111/joa.13071

Fourel F., Martineau F., Lécuyer C., Kupka H. J., Lange L., Ojeimi C. & Seed M. (2011). $^{18}O/^{16}O$ ratio measurements of inorganic and organic materials by elemental analysis–pyrolysis–isotope ratio mass spectrometry continuous-flow techniques. *Rapid Communications in Mass Spectrometry*, 25(19): 2691-2696. https://doi.org/10.1002/rcm.5056

Fourel F., Martineau F., Tóth E. E., Görög A., Escarguel G. & Lécuyer C. (2016). Carbon and oxygen isotope variability among foraminifera and ostracod carbonated shells. *Ann. Univ. Mariae Curie-Sklodowska, sect. AAA–Phys.*, 70, 133.

Fox R. C. & Meng J. (1997). An X-radiographic and SEM study of the osseous inner ear of multituberculates and monotremes (Mammalia): implications for mammalian phylogeny and evolution of hearing. *Zoological Journal of the Linnean Society*, 121(3): 249-291. https://doi.org/10.1111/j.1096-3642.1997.tb00339.x

Fraas E. (1901). Die Meerkrokodile (Thalattosuchia n. g.) eine neue sauriergruppe der Juraformation. *Jahreshefte des Vereins fur vaterlandische Naturkunde, Wurttemberg*, 57: 409-418.

Francillon-Vieillot H., Buffrénil V. de, Castanet J., Géraudie J., Meunier F. J., Sire J. Y., Zylberberg L. & de Ricqlès A. (1990). Microstructure and mineralization of vertebrate skeletal tissues. *Skeletal biomineralization: patterns, processes and evolutionary trends*, 1: 471-530.

Franzosa J. W. (2004). *Evolution of the brain in Theropoda (Dinosauria).* Unpublished PhD thesis, The University of Texas, 357 p.

Fraser N. C. & Sues H. D. (1994). Assemblages of small tetrapods from British Late Triassic fissure deposits. *In the Shadow of the Dinosaurs*: 214-226.

Freitag H. & Stichler W. (2002). *Bienertia cycloptera* Bunge ex Boiss., Chenopodiaceae, another C4 plant without Kranz tissues. *Plant Biology*, 4(01): 121-132. https://doi.org/10.1055/s-2002-20444

French N. R. (1961). Review and discussion of barium. In Schultz V. & Klement A. W. (eds.) *Radioecology*. Reinhold, New York: 557-560.

Frey E. (1988). Das Tragsystem der Krokodile – eine biomechanische und phylogenetische Analyse. *Stuttgarter Beiträge für Naturkunde*, 426: 1-60.

Fricke H. C. (2007). Stable isotope geochemistry of bonebed fossils: reconstructing paleoenvironments, paleoecology, and paleobiology, in *Bonebeds: Genesis, Analysis, and Paleobiological Significance*. University of Chicago Press, Chicago: 437-490. https://doi.org/10.7208/chicago/9780226723730.003.0008

Fricke H. C. & O'Neil J. R. (1999). The correlation between 18O/16O ratios of meteoric water and surface temperature: its use in investigating terrestrial climate change over geologic time. *Earth and Planetary Science Letters*, 170(3): 181-196. https://doi.org/10.1016/S0012-821X(99)00105-3

Fricke H. C. & Rogers R. R. (2000). Multiple taxon–multiple locality approach to providing oxygen isotope evidence for warm-blooded theropod dinosaurs. *Geology*, 28(9): 799-802. https://doi.org/10.1130/0091-7613(2000)28<799:MTLATP>2.0.CO;2

Frost H. M. (1969). Tetracycline-based histological analysis of bone remodeling. *Calcified tissue research*, 3: 211-237. https://doi.org/10.1007/BF02058664

Fry B. & Sherr E. B. (1989). $\delta^{13}C$ measurements as indicators of carbon flow in marine and freshwater ecosystems. In Rundel P. W., Ehleringer J. R. & Nagy K. A. (eds.) *Stable isotopes in ecological research,* Springer, New York: 196-229. https://doi.org/10.1007/978-1-4612-3498-2_12

Furusawa H. (2004). A phylogeny of the North Pacific Sirenia (Dugongidae: Hydrodamalinae) based on a comparative study of endocranial casts. *Paleontological Research*, 8(2): 91-98. https://doi.org/10.2517/prpsj.8.91

Galler P., Limbeck A., Boulyga S. F., Stingeder G., Hirata T. & Prohaska T. (2007). Development of an on-line flow injection Sr/matrix separation method for accurate, high-throughput determination of Sr isotope ratios

by multiple collector-inductively coupled plasma-mass spectrometry. *Analytical Chemistry*, 79(13): 5023-5029. https://doi.org/10.1021/ac070307h

Gallina P. A., Apesteguia S., Haluza A. & Canale J. I. (2014). A diplodocid sauropod survivor from the Early Cretaceous of South America. *PLoS One*, 9(5): e97128. https://doi.org/10.1371/journal.pone.0097128

Galton P. M. (1971). The prosauropod dinosaur *Ammosaurus*, the crocodile *Protosuchus*, and their bearing on the age of the Navajo Sandstone of northeastern Arizona. *Journal of Paleontology*, 45(5): 781-795.

Galton P. M. (1988). Skull bones and endocranial casts of stegosaurian dinosaur *Kentrosaurus* Hennig, 1915 from Upper Jurassic of Tanzania, East Africa. *Geologica et Palaeontologica*, 22: 123-143.

Galton P. M. (1989). Crania and endocranial casts from ornithopod dinosaurs of the families Dryosauridae and Hypsilophodentidae (Reptilia: Ornithischia). *Geologica et Palaeontologica*, 23: 217-239.

Galton P. M. (2001). Endocranial casts of the plated dinosaur *Stegosaurus* (Upper Jurassic, western USA): a complete undistorted cast and the original specimens of Othniel Charles Marsh. In: K Carpenter (eds.) *The armored dinosaurs*, Indiana University Press, Bloomington: 103–129.

Gandola R., Buffetaut E., Monaghan N. & Dyke G. (2006). Salt glands in the fossil crocodile Metriorhynchus. *Journal of Vertebrate Paleontology*, 26(4): 1009-1010. https://doi.org/10.1671/0272-4634(2006)26[1009:SGITFC]2.0.CO;2

Gao Y. (2001). A new species of *Hsisosuchus* from Dashanpu, Zigong, Sichuan. *Vertebrata PalAsiatica*, 39: 177-184.

Gao Y., Ibarra D. E., Wang C., Caves J. K., Chamberlain C. P., Graham S. A. & Wu H. (2015). Mid-latitude terrestrial climate of East Asia linked to global climate in the Late Cretaceous. *Geology*, 43(4): 287-290. https://doi.org/10.1130/G36427.1

Gao Y., Ibarra D. E., Rugenstein J. K. C., Chen J., Kukla T., Methner K., Gao Y., Huang H., Lin Z., Zhang L., Xi D., Wu H., Carroll A. R., Graham S. A., Chamberlain C. P. & Wang C. (2021). Terrestrial climate in mid-latitude East Asia from the latest Cretaceous to the earliest Paleogene: A multiproxy record from the Songliao Basin in northeastern China. *Earth-Sciences Reviews*, 216: 103572. https://doi.org/10.1016/j.earscirev.2021.103572

Gardner N. M., Holliday C. M. & O'Keefe F. R. (2010). The braincase of *Youngina capensis* (Reptilia, Diapsida): new insights from high-resolution CT scanning of the holotype. *Palaeontologia electronica*, 13(3).

Garrick L. D. & Lang J. W. (1977). Social signals and behaviors of adult alligators and crocodiles. *American Zoologist*, 17(1): 225-239. https://doi.org/10.1093/icb/17.1.225

Garrison J. R., Brinkman D., Nichols D. J., Layer P., Burge D. & Thayn D. (2007). A multidisciplinary study of the Lower Cretaceous Cedar Mountain Formation, Mussentuchit Wash, Utah: a determination of the

paleoenvironment and paleoecology of the Eolambia caroljonesa dinosaur quarry. *Cretaceous Research*, 28(3): 461-494. https://doi.org/10.1016/j.cretres.2006.07.007

Garstang M. (2004). Long-distance, low-frequency elephant communication. *Journal of Comparative Physiology A*, 190(10): 791-805. https://doi.org/10.1007/s00359-004-0553-0

Gasparini Z. (1971). Los Notosuchia del Cretácico de América del Sur como un nuevo infraorden de los Mesosuchia (Crocodilia). *Ameghiniana*, 8(2): 83-103.

Gasparini Z. (1982). Una nueva familia de cocodrilos zifodontes cretácicos de América del Sur. *Actas V Congreso Latinoamericano de Geologia, Buenos Aires*, 1981(4): 317-329.

Gasparini Z. (1984). New Tertiary Sebecosuchia (Crocodylia: Mesosuchia) from Argentina. *Journal of Vertebrate Paleontology*, 4(1): 85-95. https://doi.org/10.1080/02724634.1984.10011988

Gasparini Z., Chiappe L. M. & Fernandez M. (1991). A new Senonian peirosaurid (Crocodylomorpha) from Argentina and a synopsis of the South American Cretaceous crocodylians. *Journal of Vertebrate Paleontology*, 11(3): 316-333. https://doi.org/10.1080/02724634.1991.10011401

Gasparini Z., Fernandez M. & Powell J. (1993). New tertiary sebecosuchians (Crocodylomorpha) from South America: phylogenetic implications. *Historical Biology*, 7(1): 1-19. https://doi.org/10.1080/10292389309380440

Gasparini Z., Vignaud P. & Chong G. (2000). The Jurassic Thalattosuchia (Crocodyliformes) of Chile; a paleobiogeographic approach. *Bulletin de la Société géologique de France*, 171(6): 657-664. https://doi.org/10.2113/171.6.657

Gasparini Z., Paulina-Carabajal A. & Chong G. (2008). Un nuevo espécimen de cocodrilo marino del Jurásico Medio del norte de Chile: revalidación de *Metriorhynchus westermanni* (Crocodyliformes: Metriorhynchidae). *Revista geológica de Chile*, 35(2): 335-346. http://doi.org/10.4067/S0716-02082008000200008

Gatesy J., Amato G., Norell M., DeSalle R. & Hayashi C. (2003). Combined support for wholesale taxic atavism in gavialine crocodylians. *Systematic Biology*, 52(3): 403-422. https://doi.org/10.1080/10635150390197037

Gatesy J., Geisler J. H., Chang J., Buell C., Berta A., Meredith R. W., Springer M. S. & McGowen M. R. (2013). A phylogenetic blueprint for a modern whale. *Molecular Phylogenetics and Evolution*, 66(2): 479-506. https://doi.org/10.1016/j.ympev.2012.10.012

Gayet M. (1988). Le plus ancien crâne de Siluriforme: *Andinichthys bolivianensis* nov. gen., nov. sp.(Andinichthyidae nov. fam.) du Maastrichtien de Tiupampa (Bolivie). *Comptes rendus de l'Académie des sciences Série 2*, 307(7): 833-836.

Gayet M. (1990). Nouveaux Siluriformes du Maastrichtien de Tiupampa (Bolivie). *Comptes rendus de l'Académie des sciences Série 2,* 310(6): 867-872.

Gayet M. & Meunier F. J. (1992). Polyptériformes (pisces, cladistia) du maastrichtien et du paléocène de bolivie. *Geobios*, 25: 159-168. https://doi.org/10.1016/S0016-6995(06)80325-6

Gehler A., Tütken T. & Pack A. (2011). Triple oxygen isotope analysis of bioapatite as tracer for diagenetic alteration of bones and teeth. *Palaeogeography, Palaeoclimatology, Palaeoecology*, 310(1-2): 84-91. https://doi.org/10.1016/j.palaeo.2011.04.014

Geisler J. H. & Luo Z. (1996). The petrosal and inner ear of *Herpetocetus* sp. (Mammalia: Cetacea) and their implications for the phylogeny and hearing of archaic mysticetes. *Journal of Paleontology*, 70(6): 1045-1066. https://doi.org/10.1017/S0022336000038749

Gentile N., Rossi M. J., Delémont O. & Siegwolf R. T. (2013). δ ^{15}N measurement of organic and inorganic substances by EA-IRMS: a speciation-dependent procedure. *Analytical and Bioanalytical Chemistry*, 405: 159-176. https://doi.org/10.1007/s00216-012-6471-z

Geoffroy Saint-Hilaire E. (1807). *Description de deux crocodiles qui existent dans le Nil, comparés au crocodile de Saint-Domingue*. Muséum National d'Histoire Naturelle.

Geoffroy Saint-Hilaire E. (1825). Recherches sur l'organisation des Gavials, sur leurs affinités naturelles desquelles résulte la nécessité d'une autre distribution générique : *Gavialis, Teleosaurus, Steneosaurus*. *Mémoire du Muséum National d'Histoire naturelle*, 12: 97-155.

Geoffroy Saint-Hilaire (1831). Recherches sur les grands sauriens trouvés à l'état fossile aux confins maritimes de la Basse Normandie, attribués d'abord au Crocodile, puis déterminés sous les noms de *Teleosaurus* et *Steneosaurus*. *Mémoire de l'académie des sciences de Paris*, 12: 1-138.

George I. D. & Holliday C. M. (2013). Trigeminal nerve morphology in *Alligator mississippiensis* and its significance for crocodyliform facial sensation and evolution. *The Anatomical Record*, 296(4): 670-680. https://doi.org/10.1002/ar.22666

Georgi J. A. (2008). *Semicircular Canal Morphology as Evidence of Locomotor Environment in Amniotes*. Unpublished PhD thesis, Stony Brook University, 223 p.

Georgi J. A., Sipla J. S. & Forster C. A. (2013). Turning semicircular canal function on its head: dinosaurs and a novel vestibular analysis. *PLoS One*, 8(3): e58517. https://doi.org/10.1371/journal.pone.0058517

German C. R., Masuzawa T., Greaves M. J., Elderfield H. & Edmond J. M. (1995). Dissolved rare earth elements in the Southern Ocean: Cerium oxidation and the influence of hydrography. *Geochimica et Cosmochimica Acta*, 59(8): 1551-1558. https://doi.org/10.1016/0016-7037(95)00061-4

Geroto C. F. C. & Bertini R. J. (2012). Descriçao de um espécime juvenil de Baurusuchidae (Crocodyliformes: Mesoeucrocodylia) do Grupo Bauru (Neocretáceo): Consideraçoes preliminares sobre ontogenia. *Revista do Instituto Geológico*, 33(2): 13-29. https://doi.org/10.5935/0100-929X.20120007

Geroto C. F. C. & Bertini R. J. (2019). New material of *Pepesuchus* (Crocodyliformes; Mesoeucrocodylia) from the Bauru Group: implications about its phylogeny and the age of the Adamantina Formation. *Zoological Journal of the Linnean Society*, 185(2): 312-334. https://doi.org/10.1093/zoolinnean/zly037

Gervais P. (1849). Recherches sur les mammifères fossiles des genres *Palaeotherium* et *Lophiodon*, et sur les autres animaux de la même classe que l'on a trouvés avec eux dans le midi de la France. *Comptes Rendus des séances de l'Académie des Sciences, Paris*, 29: 381-384.

Gervais P. (1871). Remarques au sujet des Reptiles provenant des calcaires lithographiques de Cirin, dans le Bugey, qui sont conservés au Musée de Lyon. *Comptes Rendus Sommaire des Séances de la Société géologique de France,* 73: 603–607.

Giblin A. M. & Dickson B. L. (1992). Source, distribution and economic significance of trace elements in groundwaters from Lake Tyrrell, Victoria, Australia. *Chemical Geology*, 96(1-2): 133-149. https://doi.org/10.1016/0009-2541(92)90125-O

Gierliński G. & Potemska A. (1985). *Protosuchus* sp. z dolnej jury północnego obrzeżenia Gór Świętokrzyskich. *Przegląd Geologiczny*, 33(10): 567-570.

Gignac P. M. & Kley N. J. (2014). Iodine-enhanced micro-CT imaging: Methodological refinements for the study of the soft-tissue anatomy of post-embryonic vertebrates. *Journal of Experimental Zoology Part B: Molecular and Developmental Evolution*, 322(3): 166-176. https://doi.org/10.1002/jez.b.22561

Gilabert V., Batenburg S. J., Arenillas I. & Arz J. A. (2022). Contribution of orbital forcing and Deccan volcanism to global climatic and biotic changes across the Cretaceous-Paleogene boundary at Zumaia, Spain. *Geology*, 50(1): 21-25. https://doi.org/10.1130/G49214.1

Gillikin D. P., Lorrain A., Jolivet A., Kelemen Z., Chauvaud L. & Bouillon S. (2017). High-resolution nitrogen stable isotope sclerochronology of bivalve shell carbonate-bound organics. *Geochimica et Cosmochimica Acta*, 200: 55-66. https://doi.org/10.1016/j.gca.2016.12.008

Gleich O. & Manley G. A. (2000). The hearing organ of birds and crocodilia. In Dooling R. J., Fay R. R. & Popper A. N. (eds.) *Comparative hearing: Birds and Reptiles*, Springer: 70-138. https://doi.org/10.1007/978-1-4612-1182-2_3

Gleich O., Dooling R. J. & Manley G. A. (2005). Audiogram, body mass, and basilar papilla length: correlations in birds and predictions for extinct archosaurs. *Naturwissenschaften*, 92: 595-598. https://doi.org/10.1007/s00114-005-0050-5

Glimcher M. J. (2006). Bone: nature of the calcium phosphate crystals and cellular, structural, and physical chemical mechanisms in their formation. Reviews in Mineralogy and Geochemistry, 64(1): 223-282. https://doi.org/10.2138/rmg.2006.64.8

Gmelin J. F. (1789). Caroli a Linné : Systema Naturae. In Beer G. E. (ed.) *Tomus I, Lipsiae*: 1057-1058.

Godoy P. L. (2014). *Osteologia e filogenia de dois Crocodyliformes fósseis:* Aplestosuchus sordidus *do Cretáceo do Brasil e* Eocaiman cavernensis *do Eoceno da Argentina.* Unpublished PhD thesis, Universidade de São Paulo, 94 p.

Godoy P. L., Montefeltro F. C., Norell M. A. & Langer M. C. (2014). An additional baurusuchid from the Cretaceous of Brazil with evidence of interspecific predation among Crocodyliformes. *PLoS One*, 9(5): e97138. https://doi.org/10.1371/journal.pone.0097138

Godoy P. L., Bronzati M., Eltink E., Júlio C. D. A., Cidade G. M., Langer M. C. & Montefeltro F. C. (2016). Postcranial anatomy of *Pissarrachampsa sera* (Crocodyliformes, Baurusuchidae) from the Late Cretaceous of Brazil: insights on lifestyle and phylogenetic significance. *PeerJ*, 4: e2075. https://doi.org/10.7717/peerj.2075

Goedert J. (2017). *Ecologie des premiers tétrapodes dévoilée par la composition isotopique du soufre ($^{34}S/^{32}S$) de leurs squelettes*. Unpublished PhD thesis, Université Lyon 1, 239 p.

Goedert J., Amiot R., Boudad L., Buffetaut E., Fourel F., Godefroit P., Kusuhashi N., Suteethorn V., Tong H., Watabe M. & Lécuyer C. (2016a). Preliminary investigation of seasonal patterns recorded in the oxygen isotope compositions of theropod dinosaur tooth enamel oxygen isotope seasonality in theropod teeth. *Palaios*, 31(1): 10-19. https://doi.org/10.2110/palo.2015.018

Goedert J., Fourel F., Amiot R., Simon L. & Lécuyer C. (2016b). High-precision 34S/32S measurements in vertebrate bioapatites using purge-and-trap elemental analyser/isotope ratio mass spectrometry technology. *Rapid Communications in Mass Spectrometry*, 30(18): 2002-2008. https://doi.org/10.1002/rcm.7690

Goedert J., Lécuyer C., Amiot R., Arnaud-Godet F., Wang X., Cui L., Cuny G., Douay G., Fourel F., Panczer G., Simon L., Steyer J. B. & Zhu M. (2018). Euryhaline ecology of early tetrapods revealed by stable isotopes. *Nature*, 558(7708): 68-72. https://doi.org/10.1038/s41586-018-0159-2

Goedert J., Amiot R., Berthet D., Fourel F., Simon L. & Lécuyer C. (2020). Combined oxygen and sulphur isotope analysis—a new tool to unravel vertebrate (paleo)-ecology. *The Science of Nature*, 107: 1-9. https://doi.org/10.1007/s00114-019-1664-3

Göhlich U. B., Chiappe L. M., Clark J. M. & Sues H. D. (2005). The systematic position of the Late Jurassic alleged dinosaur *Macelognathus* (Crocodylomorpha: Sphenosuchia). *Canadian Journal of Earth Sciences*, 42(3): 307-321. https://doi.org/10.1139/e05-005

Gold M. E. L., Brochu C. A. & Norell M. A. (2014). An expanded combined evidence approach to the *Gavialis* problem using geometric morphometric data from crocodylian braincases and Eustachian systems. *PloS One*, 9(9): e105793. https://doi.org/10.1371/journal.pone.0105793

Goldberg M., Kulkarni A. B., Young M. & Boskey A. (2011). Dentin: Structure, Composition and Mineralization: The role of dentin ECM in dentin formation and mineralization. *Frontiers in Bioscience (Elite Edition)*, 3, 711-735. https://doi.org/10.2741/e281

Goldby F. (1925). The development of the columella auris in the Crocodilia. *Journal of Anatomy*, 59(3): 301-325.

Goloboff P. A. (1999). Analyzing large data sets in reasonable times: solutions for composite optima. *Cladistics*, 15(4): 415-428. https://doi.org/10.1006/clad.1999.0122

Goloboff P. A. (2014). Extended implied weighting. *Cladistics*, 30(3): 260-272. https://doi.org/10.1111/cla.12047

Goloboff P. A. & Catalano S. A. (2016). TNT version 1.5, including a full implementation of phylogenetic morphometrics. *Cladistics*, 32(3): 221-238. https://doi.org/10.1111/cla.12160

Gomani E. M. (1997). A crocodyliform from the Early Cretaceous dinosaur beds, northern Malawi. *Journal of Vertebrate Paleontology*, 17(2): 280-294. https://doi.org/10.1080/02724634.1997.10010975

Gomes de Souza L. (2018). Comments on the serial homology and homologues of vertebral lateral projections in Crocodylia (Eusuchia). *The Anatomical Record*, 301(7): 1203-1215. https://doi.org/10.1002/ar.23802

Gonfiantini R. (1978). Standards for stable isotope measurements in natural compounds. *Nature*, 271(5645): 534-536. https://doi.org/10.1038/271534a0

Gonfiantini R. (1984). Stable isotope reference samples for geochemical and hydrological investigations. *The International Journal of Applied Radiation and* Isotopes, 35(5): 426. https://doi.org/10.1016/0020-708X(84)90059-0

Gonzales L. A., Malinzak M. D. & Kay R. F. (2018). Intraspecific variation in semicircular canal morphology—A missing element in adaptive scenarios?. *American Journal of Physical Anthropology*, 168(1): 10-24. https://doi.org/10.1002/ajpa.23692

Goodbred S. L. (2003). Response of the Ganges dispersal system to climate change: a source-to-sink view since the last interstade. *Sedimentary Geology*, 162(1-2): 83-104. https://doi.org/10.1016/S0037-0738(03)00217-3

Grandjean P. (1989). *Les terres rares et la composition isotopique du néodyme dans les phosphates biogènes: traceurs des processus paléo-océanographiques et sédimentaires*. Unpublished PhD thesis, Institut National Polytechnique de Lorraine Nancy, 319 p.

Grandjean P. & Albarède F. (1989). Ion probe measurement of rare earth elements in biogenic phosphates. *Geochimica et Cosmochimica Acta*, 53(12): 3179-3183. https://doi.org/10.1016/0016-7037(89)90097-5

Grandjean P., Cappetta H., Michard A. & Albarède F. (1987). The assessment of REE patterns and $^{143}Nd/^{144}Nd$ ratios in fish remains. *Earth and Planetary Science Letters*, 84(2-3): 181-196. https://doi.org/10.1016/0012-821X(87)90084-7

Grandjean P., Cappetta H. & Albarède F. (1988). The Ree and ε_{Nd} of 40–70 Ma old fish debris from the west-African platform. *Geophysical Research Letters*, 15(4): 389-392. https://doi.org/10.1029/GL015i004p00389

Grandjean P., Feist R. & Albarède F. (1993). Rare earth elements in old biogenic apatites. *Geochimica et Cosmochimica Acta*, 57(11): 2507-2514. https://doi.org/10.1016/0016-7037(93)90413-Q

Granot R. & Dyment J. (2015). The cretaceous opening of the South Atlantic Ocean. *Earth and Planetary Science Letters*, 414: 156-163. https://doi.org/10.1016/j.epsl.2015.01.015

Grap N. J., Machts T., Essert S. & Bleckmann H. (2020). Stimulus discrimination and surface wave source localization in Crocodylians. *Zoology*, 139: 125743. https://doi.org/10.1016/j.zool.2020.125743

Graustein W. C. (1989). $^{87}Sr/^{86}Sr$ ratios measure the sources and flow of strontium in terrestrial ecosystems. In Rundel P. W., Ehleringer J. R. & Nagy K. A. (eds.) *Stable Isotopes in Ecological Research*, Springer, New York: 491-512. https://doi.org/10.1007/978-1-4612-3498-2_28

Gray J. E. (1825). A synopsis of the genera of reptiles and amphibia, with a description of some new species. *Annals of Philosophy*, 10: 193-217.

Gray J. E. (1844). *Catalogue of tortoises, crocodylians and amphisbaenians in the collection of the British Museum*. Edward Newman, London, 80 p.

Gray J. E. (1862). A Synopsis of the Species of Alligators. *Annals and Magazine of Natural History*, 10(35): 327-331.

Grigg G. & Kirshner D. (2015). *Biology and Evolution of Crocodylians*. Cornell University Press, 671 p.

Gröcke D. R. (2002). The carbon isotope composition of ancient CO2 based on higher-plant organic matter. *Philosophical Transactions of the Royal Society of London. Series A: Mathematical, Physical and Engineering Sciences*, 360(1793): 633-658. https://doi.org/10.1098/rsta.2001.0965

Groh S. S., Upchurch P., Barrett P. M. & Day J. J. (2019). The phylogenetic relationships of neosuchian crocodiles and their implications for the convergent evolution of the longirostrine condition. *Zoological Journal of the Linnean Society*, 188(2): 473-506. https://doi.org/10.1093/zoolinnean/zlz117

Grohé C., Tseng Z. J., Lebrun R., Boistel R. & Flynn J. J. (2016). Bony labyrinth shape variation in extant Carnivora: a case study of Musteloidea. *Journal of Anatomy*, 228(3): 366-383. https://doi.org/10.1111/joa.12421

Gromet L. P., Haskin L. A., Korotev R. L. & Dymek R. F. (1984). The "North American shale composite": Its compilation, major and trace element characteristics. *Geochim. et cosmochim. acta*, 48(12): 2469-2482. https://doi.org/10.1016/0016-7037(84)90298-9

Guiserix D., Albalat E., Ueckermann H., Davechand P., Iaccheri L. M., Bybee G., Badenhorst S. & Balter V. (2022). Simultaneous analysis of stable and radiogenic strontium isotopes in reference materials, plants and modern tooth enamel. *Chemical Geology*, 606: 121000. https://doi.org/10.1016/j.chemgeo.2022.121000

Gundy G. C. & Wurst G. Z. (1976). Parietal eye-pineal morphology in lizards and its physiological implications. *The Anatomical Record*, 185(4): 419-431. https://doi.org/10.1002/ar.1091850404

Günther A. (1867). Contribution to the anatomy of *Hatteria* (*Rhynchocephalus*, Owen). *Philosophical Transactions of the Royal Society of London*, 157(1867): 595-629.

Gunz P. & Mitteroecker P. (2013). Semilandmarks: a method for quantifying curves and surfaces. *Hystrix, the Italian Journal of Mammalogy*, 24(1): 103-109. https://doi.org/10.4404/hystrix-24.1-6292

Gussone N., Schmitt A. D., Heuser A., Wombacher F., Dietzel M., Tipper E. & Schiller M. (2016). *Calcium stable isotope geochemistry*, Springer, Berlin, 260 p.

Haddoumi H., Allain R., Meslouh S., Metais G., Monbaron M., Pons D., Rage J. C., Vullo R., Zouhri S. & Gheerbrant E. (2016). Guelb el Ahmar (Bathonian, Anoual Syncline, eastern Morocco): first continental flora and fauna including mammals from the Middle Jurassic of Africa. *Gondwana Research*, 29(1): 290-319. https://doi.org/10.1016/j.gr.2014.12.004

Haight J. R. & Murray P. F. (1981). The cranial endocast of the early Miocene marsupial, *Wynyardia bassiana*: an assessment of taxonomic relationships based upon comparisons with recent forms. *Brain, Behavior and Evolution*, 19(1-2): 17-36. https://doi.org/10.1159/000121632

Halas S. & Szaran J. (2001). Improved thermal decomposition of sulfates to SO_2 and mass spectrometric determination of $\delta^{34}S$ of IAEA SO-5, IAEA SO-6 and NBS-127 sulfate standards. *Rapid Comm. in Mass Spectrometry*, 15(17): 1618-1620. https://doi.org/10.1002/rcm.416

Halas S., Skrzypek G., Meier-Augenstein W., Pelc A. & Kemp H. F. (2011). Inter-laboratory calibration of new silver orthophosphate comparison materials for the stable oxygen isotope analysis of phosphates. *Rapid Communications in Mass Spectrometry*, 25(5): 579-584. https://doi.org/10.1002/rcm.4892

Halicz L., Galy A., Belshaw N. S. & O'Nions R. K. (1999). High-Precision Calcium-Isotopic Ratio Measurement by Multiple Collector Inductively Coupled Mass Spectrometry (Multiple Collector Inductively Coupled Plasma Mass Spectrometry): Preliminary Data of Calcium-Isotopic Ratios in Carbonates. *Ninth Annual VM Goldschmidt Conference*, Cambridge, United States.

Hall M. I. & Ross C. F. (2006). Eye shape and activity pattern in birds. *Journal of Zoology*, 271(4): 437-444. https://doi.org/10.1111/j.1469-7998.2006.00227.x

Hallgren L. (1987). Infrared spectroscopic analysis of fossil coprolites. *Scientific Publications of the Science Museum of Minnesota*, 6: 1–31.

Halliday T. J., De Andrade M. B., Benton M. J. & Efimov M. B. (2013). A re-evaluation of goniopholidid crocodylomorph material from Central Asia: Biogeographic and phylogenetic implications. *Acta Palaeontologica Polonica*, 60(2): 291-312. https://doi.org/10.4202/app.2013.0018

Hangjae Y., Yungnam Y. & Hyesu Y. (2005). A new protosuchian (Archosauria: Crocodyliformes) skull from the Hasandong Formation (Lower Cretaceous) of Hadong, Korea. *Korean Journal of Paleontology*, 21(1): 146-150.

Hansen A. (2007). Olfactory and solitary chemosensory cells: two different chemosensory systems in the nasal cavity of the American alligator, *Alligator mississippiensis*. *BMC Neuroscience*, 8: 1-10. https://doi.org/10.1186/1471-2202-8-64

Hanson M., Hoffman E. A., Norell M. A. & Bhullar B. A. S. (2021). The early origin of a birdlike inner ear and the evolution of dinosaurian movement and vocalization. *Science*, 372(6542): 601-609. https://doi.org/10.1126/science.abb4305

Hanson M., Hoffman E. A., Norell M. A. & Bhullar B. A. S. (2022). Response to Comment on "The early origin of a birdlike inner ear and the evolution of dinosaurian movement and vocalization". *Science*, 376(6600), eabl8181. https://doi.org/10.1126/science.abl8181

Harris J. D., Lucas S. G., Estep J. W. & Li J. (2000). A new and unusual sphenosuchian (Archosauria: Crocodylomorpha) from the lower Jurassic Lufeng formation, People's Republic of China. *Neues Jahrbuch für Geologie und Paläontologie-Abhandlungen*, 215(1): 47-68. https://doi.org/10.1127/njgpa/215/2000/47

Hartenberger J. L. (1963). Un gisement de la zone de Mammifères d'Issel (Eocène moyen) dans les calcaires lacustres d'Aumelas (Hérault). *Comptes-rendus sommaires de la Société géologique de France*, 9: 321-322.

Harvey P. H. & Pagel M. D. (1991). *The comparative method in evolutionary biology*. Oxford: Oxford university press.

Haskin L. A. & Frey F. A. (1966). Dispersed and Not-So-Rare Earths: The relative abundances of these elements reflect the earth's geochemical evolution from primordial matter. *Science*, 152(3720): 299-314. https://doi.org/10.1126/science.152.3720.299

Hassler A. (2021). *Stratégies de reproduction mammaliennes et isotopie du calcium : témoins actuels et perspectives fossiles*. Unpublished PhD thesis, Ecole Normale Supérieure de Lyon, 257 p.

Hassler A., Martin J. E., Amiot R., Tacail T., Godet F. A., Allain R. & Balter V. (2018). Calcium isotopes offer clues on resource partitioning among Cretaceous predatory dinosaurs. *Proceedings of the Royal Society B: Biological Sciences*, 285(1876): 20180197. https://doi.org/10.1098/rspb.2018.0197

Hassler A., Martin J. E., Ferchaud S., Grivault D., Le Goff S., Albalat E., Hernandez J. A., Tacail T. & Balter V. (2021a). Lactation and gestation controls on calcium isotopic compositions in a mammalian model. *Metallomics*, 13(6): mfab019. https://doi.org/10.1093/mtomcs/mfab019

Hassler A., Martin J. E., Merceron G., Garel M. & Balter V. (2021b). Calcium isotopic variability of cervid bioapatite and implications for mammalian physiology and diet. *Palaeogeography, Palaeoclimatology, Palaeoecology*, 573: 110418. https://doi.org/10.1016/j.palaeo.2021.110418

Hastings A. K., Bloch J. I., Cadena E. A. & Jaramillo C. A. (2010). A new small short-snouted dyrosaurid (Crocodylomorpha, Mesoeucrocodylia) from the Paleocene of Northeastern Colombia. *Journal of Vertebrate Paleontology*, 30(1): 139-162. https://doi.org/10.1080/02724630903409204

Hastings A. K., Bloch J. I. & Jaramillo C. A. (2011). A new longirostrine dyrosaurid (Crocodylomorpha, Mesoeucrocodylia) from the Paleocene of north-eastern Colombia: biogeographic and behavioural implications for New-World Dyrosauridae. *Palaeontology*, 54(5): 1095-1116. https://doi.org/10.1111/j.1475-4983.2011.01092.x

Hastings A. K., Bloch J. I., Jaramillo C. A., Rincon A. F. & MacFadden B. J. (2013). Systematics and biogeography of crocodylians from the Miocene of Panama. *Journal of Vertebrate Paleontology*, 33(2): 239-263. https://doi.org/10.1080/02724634.2012.713814

Hastings A. K., Bloch J. I. & Jaramillo C. A. (2015). A new blunt-snouted dyrosaurid, *Anthracosuchus balrogus* gen. et sp. nov. (Crocodylomorpha, Mesoeucrocodylia), from the Palaeocene of Colombia. *Historical Biology*, 27(8): 998-1020. https://doi.org/10.1080/08912963.2014.918968

Haughton S. H. (1915). A new thecodont from the Stormberg beds. *Annals of the South African Museum*, 12: 98-105.

Hay O. P. (1930). *Second Bibliography and Catalogue of the Fossil Vertebrata of North America*, 390 (II): 1-1074.

Hay W. W., DeConto R. M., Wold C. N., Wilson K. M., Voigt S., Schulz M., Wold A. R., Dullo W. C., Ronov A. B., Balukhovsky A. N. & Söding E. (1999). Alternative global Cretaceous paleogeography. *Geological Society of America, Special Paper*, 332: 1-47. https://doi.org/10.1130/0-8137-2332-9.1

Hayashi S., Houssaye A., Nakajima Y., Chiba K., Ando T., Sawamura H., Inuzuka N., Kaneko N. & Osaki T. (2013). Bone inner structure suggests increasing aquatic adaptations in Desmostylia (Mammalia, Afrotheria). *PLoS One*, 8(4): e59146. https://doi.org/10.1371/journal.pone.0059146

He D., Zhu Z., Zhao L., Belshaw N. S., Zheng H., Li X. & Hu S. (2019). A practical method for measuring high precision calcium isotope ratios without chemical purification for calcium carbonate samples by multiple collector inductively coupled plasma mass spectrometry. *Chemical Geology*, 514: 105-111. https://doi.org/10.1016/j.chemgeo.2019.03.020

Healy S. & Guilford T. (1990). Olfactory-bulb size and nocturnality in birds. *Evolution*, 44(2): 339-346. https://doi.org/10.1111/j.1558-5646.1990.tb05203.x

Hecht M. K. (1991). *Araripesuchus Price*, 1959. In *Santana Fossils, An Illustrated Atlas,* TFH Publications, New Jersey: 342-347.

Hedges R. E. (2002). Bone diagenesis: an overview of processes. *Archaeometry*, 44(3): 319-328. https://doi.org/10.1111/1475-4754.00064

Hedges R. E., Stevens R. E. & Richards M. P. (2004). Bone as a stable isotope archive for local climatic information. *Quaternary Science Reviews*, 23(7-8): 959-965. https://doi.org/10.1016/j.quascirev.2003.06.022

Hedges R. E., Clement J. G., Thomas C. D. L. & O'Connell T. C. (2007). Collagen turnover in the adult femoral mid-shaft: Modeled from anthropogenic radiocarbon tracer measurements. *American Journal of Physical Anthropology*, 133(2): 808-816. https://doi.org/10.1002/ajpa.20598

Hekkala E. (2004). *Conservation Genetics at the Species Boundary: Case studies from African and Caribbean Crocodiles (genus:* Crocodylus*).* Unpublished PhD thesis, Columbia University, 138 p.

Hekkala E., Amato G., DeSalle R. & Blum M. J. (2010). Molecular assessment of population differentiation and individual assignment potential of Nile crocodile (*Crocodylus niloticus*) populations. *Conservation Genetics*, 11: 1435-1443. https://doi.org/10.1007/s10592-009-9970-5

Hekkala E., Shirley M. H., Amato G., Austin J. D., Charter S., Thorbjarnarson J., Vliet K. A., Houck M. L., Desalle R. & Blum M. J. (2011). An ancient icon reveals new mysteries: mummy DNA resurrects a cryptic species within the Nile crocodile. *Molecular Ecology*, 20(20): 4199-4215. https://doi.org/10.1111/j.1365-294X.2011.05245.x

Hekkala E., Platt S. G., Thorbjarnarson J. B., Rainwater T. R., Tessler M., Cunningham S. W., Twomey C. & Amato G. (2015). Integrating molecular, phenotypic and environmental data to elucidate patterns of crocodile hybridization in Belize. *Royal Society Open Science*, 2(9): 150409. https://doi.org/10.1098/rsos.150409

Hekkala E., Gatesy J., Narechania A., Meredith R., Russello M., Aardema M. L., Jensen E., Montanari S., Brochu C., Norell M. & Amato G. (2021). Paleogenomics illuminates the evolutionary history of the extinct Holocene "horned" crocodile of Madagascar, *Voay robustus*. *Communications Biology*, 4(1): 1-11. https://doi.org/10.1038/s42003-021-02017-0

Hemminga M. A. & Mateo M. A. (1996). Stable carbon isotopes in seagrasses: variability in ratios and use in ecological studies. *Marine Ecology Progress Series*, 140: 285-298. https://doi.org/10.3354/meps140285

Henderson P., Marlow C. A., Molleson T. I. & Williams C. T. (1983). Patterns of chemical change during bone fossilization. *Nature*, 306(5941): 358-360. https://doi.org/10.1038/306358a0

Herrera Y. (2015). Metriorhynchidae (Crocodylomorpha: Thalattosuchia) from Upper Jurassic-Lower Cretaceous of Neuquén Basin (Argentina), with comments on the natural casts of the brain. In Fernández M. & Herrera Y (eds.) *Reptiles Extintos – Volumen en Homenaje a Zulma Gasparini*, PE-APA, 15(1): 159-171. https://doi.org/10.5710/PEAPA.09.06.2015.104

Herrera Y. & Vennari V. V. (2014). Cranial anatomy and neuroanatomical features of a new specimen of Geosaurini (Crocodylomorpha: Metriorhynchidae) from west-central Argentina. *Historical Biology*, 27(1): 33-41. https://doi.org/10.1080/08912963.2013.861831

Herrera Y., Fernández M. S. & Gasparini Z. (2013a). Postcranial skeleton of *Cricosaurus araucanensis* (Crocodyliformes: Thalattosuchia): morphology and palaeobiological insights. *Alcheringa: An Australasian Journal of Palaeontology*, 37(3): 285-298. https://doi.org/10.1080/03115518.2013.743709

Herrera Y., Fernández M. S. & Gasparini Z. (2013b). The snout of *Cricosaurus araucanensis*: a case study in novel anatomy of the nasal region of metriorhynchids. *Lethaia*, 46(3): 331-340. https://doi.org/10.1111/let.12011

Herrera Y., Gasparini Z. & Fernández M. S. (2015). *Purranisaurus potens* Rusconi, an enigmatic metriorhynchid from the Late Jurassic–Early Cretaceous of the Neuquén Basin. *Journal of Vertebrate Paleontology*, 35(2): e904790. https://doi.org/10.1080/02724634.2014.904790

Herrera Y., Fernandez M. S., Lamas S. G., Campos L., Talevi M. & Gasparini Z. (2017). Morphology of the sacral region and reproductive strategies of Metriorhynchidae: a counter-inductive approach. *Earth and Environmental Science Transactions of the Royal Society of Edinburgh*, 106(4): 247-255. https://doi.org/10.1017/S1755691016000165

Herrera Y., Leardi J. M. & Fernández M. S. (2018). Braincase and endocranial anatomy of two thalattosuchian crocodylomorphs and their relevance in understanding their adaptations to the marine environment. *PeerJ*, 6: e5686. https://doi.org/10.7717/peerj.5686

Herzog H. A. & Burghardt G. M. (1977). Vocalization in juvenile crocodylians. *Zeitschrift für Tierpsychologie*, 44(3): 294-304. https://doi.org/10.1111/j.1439-0310.1977.tb00997.x

Hess J., Bender M. L. & Schilling J. G. (1986). Evolution of the ratio of strontium-87 to strontium-86 in seawater from Cretaceous to present. *Science*, 231(4741): 979-984. https://doi.org/10.1126/science.231.4741.979

Hester P. M., Lucas S. G. & Ulmer-Scholle D. (2001). Lacustrine depositional environments of the Upper Triassic Redonda Formation, east-central New Mexico. *New Mexico Geological Society Guidebook*, 52: 153-168. *76th annual meeting of the Society of Vertebrate Paleontology*, Salt Lake City.

Hester D. A., Brochu C. A. & Turner A. H. (2016). A re-evaluation of the crocodyliform *Batrachomimus pastosbonensis* from the Late Jurassic of Brazil: implications for neosuchian phylogeny, biogeography, and divergence timing.

Heuser A. & Eisenhauer A. (2010). A pilot study on the use of natural calcium isotope ($^{44}Ca/^{40}Ca$) fractionation in urine as a proxy for the human body calcium balance. *Bone*, 46(4): 889-896. https://doi.org/10.1016/j.bone.2009.11.037

Heuser A., Tütken T., Gussone N. & Galer S. J. (2011). Calcium isotopes in fossil bones and teeth—Diagenetic versus biogenic origin. *Geochimica et Cosmochimica Acta*, 75(12): 3419-3433. https://doi.org/10.1016/j.gca.2011.03.032

Heuser A., Eisenhauer A., Scholz-Ahrens K. E. & Schrezenmeir J. (2016). Biological fractionation of stable Ca isotopes in Göttingen minipigs as a physiological model for Ca homeostasis in humans. *Isotopes in Environmental and Health Studies*, 52(6): 633-648. https://doi.org/10.1080/10256016.2016.1151017

Heuser A., Frings-Meuthen P., Rittweger J. & Galer S. J. (2019). Calcium isotopes in human urine as a diagnostic tool for bone loss: additional evidence for time delays in bone response to experimental bed rest. *Frontiers in Physiology*, 10(12): 1-11. https://doi.org/10.3389/fphys.2019.00012

Higgs D., Brittan-Powell E., Soares D., Souza M., Carr C., Dooling R. & Popper A. (2002). Amphibious auditory responses of the American alligator (*Alligator mississipiensis*). *Journal of Comparative Physiology A*, 188(3): 217-223. https://doi.org/10.1007/s00359-002-0296-8

Highstein S.M., Fay R.R. & Popper A.N. (2004). *The Vestibular System*. Springer-Verlag, New York, 576 p.

Hill R. V. (2010). Osteoderms of *Simosuchus clarki* (Crocodyliformes: Notosuchia) from the late cretaceous of Madagascar. *Journal of Vertebrate Paleontology*, 30(sup1): 154-176. https://doi.org/10.1080/02724634.2010.518110

Hill R. V., Mccartney J. A., Roberts E., Bouaré M., Sissoko F. & O'leary M. A. (2008). Dyrosaurid (Crocodyliformes: Mesoeucrocodylia) fossils from the Upper Cretaceous and Paleogene of Mali: implications for phylogeny and survivorship across the K/T boundary. *American Museum Novitates*, 2008(3631): 1-19. https://doi.org/10.1206/598.1

Hinz E. A. & Kohn M. J. (2010). The effect of tissue structure and soil chemistry on trace element uptake in fossils. *Geochimica et Cosmochimica Acta*, 74(11): 3213-3231. https://doi.org/10.1016/j.gca.2010.03.011

Hobbie E. A., Olszyk D. M., Rygiewicz P. T., Tingey D. T. & Johnson M. G. (2001). Foliar nitrogen concentrations and natural abundance of ^{15}N suggest nitrogen allocation patterns of Douglas-fir and mycorrhizal fungi during development in elevated carbon dioxide concentration and temperature. *Tree Physiology*, 21(15): 1113-1122. https://doi.org/10.1093/treephys/21.15.1113

Hoefs J. (1997). *Stable Isotope Geochemistry.* Springer, 504 p. https://doi.org/10.1007/978-3-030-77692-3

Högberg P. (1997). Tansley review no. 95 ^{15}N natural abundance in soil–plant systems. *The New Phytologist*, 137(2): 179-203. https://doi.org/10.1046/j.1469-8137.1997.00808.x

Holliday C. M. & Gardner N. M. (2012). A new eusuchian crocodyliform with novel cranial integument and its significance for the origin and evolution of Crocodylia. *PLoS One*, 7(1): e30471. https://doi.org/10.1371/journal.pone.0030471

Holliday C. M. & Schachner E. R. (2022). Dispatches from the age of crocodiles: New discoveries from ancient lineages. *The Anatomical Record*, 305(10): 2343-2352. https://doi.org/10.1002/ar.25043

Holliday C. M., Sellers K. C., Lessner E. J., Middleton K. M., Cranor C., Verhulst C. D., Lautenschlager S., Bader K., Brown M. A. & Colbert M. W. (2022). New frontiers in imaging, anatomy, and mechanics of crocodylian jaw muscles. *The Anatomical Record*, 305(10): 3016-3030. https://doi.org/10.1002/ar.25011

Hollinger J. O. (2005). Bone dynamics: morphogenesis, growth, modeling, and remodeling. In Lieberman J. R. & Friedlaender G. E. (eds.) *Bone Regeneration and Repair*, Humana Totowa: 1-19. https://doi.org/10.1385/1-59259-863-3:001

Holloway R. L. (1981a). The endocast of the Omo L338y-6 Juvenile Hominid: gracile or robust *Australopithecus*?. *American Journal of Physical Anthropology*, 54(1): 109-118. https://doi.org/10.1002/ajpa.1330540113

Holloway R. L. (1981b). Volumetric and asymmetry determinations on recent hominid endocasts: Spy I and II, Djebel Ihroud I, and the Salé Homo erectus specimens, with some notes on neandertal brain size. *American Journal of Physical Anthropology*, 55(3): 385-393. https://doi.org/10.1002/ajpa.1330550312

Holloway R. L. (2018). On the making of endocasts: the new and the old in paleoneurology. In Bruner E., Ogihara N. & Tanabe H. C. (eds.) *Digital endocasts: From skulls to brains*, Springer: 1-8. https://doi.org/10.1007/978-4-431-56582-6_1

Holobinko A., Meier-Augenstein W., Kemp H. F., Prowse T. & Ford S. M. (2011). ^{2}H stable isotope analysis of human tooth enamel: a new tool for forensic human provenancing?. *Rapid communications in mass spectrometry*, 25(7): 910-916. https://doi.org/10.1002/rcm.4942

Holt T. R., Salisbury S. W. & Willis P. (2005). A new species of mekosuchine crocodylian from the middle Palaeogene Rundle Formation, central Queensland. *Memoirs of the Queensland Museum*, 50(2): 207-218.

Holtz T. R. (1998). A new phylogeny of the carnivorous dinosaurs. *GAIA: Revista de geociências*, 15(5): 5-61.

Holz M. (2015). Mesozoic paleogeography and paleoclimates–a discussion of the diverse greenhouse and hothouse conditions of an alien world. *Journal of South American Earth Sciences*, 61: 91-107. https://doi.org/10.1016/j.jsames.2015.01.001

Höpner S. & Bertling M. (2017). Holes in bones: ichnotaxonomy of bone borings. *Ichnos*, 24(4): 259-282. https://doi.org/10.1080/10420940.2017.1289937

Hopson J. A. (1977). Relative brain size and behavior in archosaurian reptiles. *Annual Review of Ecology and Systematics*, 8(1): 429-448. https://doi.org/10.1146/annurev.es.08.110177.002241

Hopson J. A. (1979). Paleoneurology. In Gans C., Northcutt R. G. & Ulinski P. (eds.) *Biology of the Reptilia (Neurology A) vol 9*. Academic Press, New York: 211-236.

Horner J. R. & Padian K. (2004). Age and growth dynamics of *Tyrannosaurus rex*. *Proceedings of the Royal Society of London. Series B: Biological Sciences*, 271(1551): 1875-1880. https://doi.org/10.1098/rspb.2004.2829

Horner J. R., de Ricqlès A. & Padian K. (1999). Variation in dinosaur skeletochronology indicators: implications for age assessment and physiology. *Paleobiology*, 25(3): 295-304. https://doi.org/10.1017/S0094837300021308

Horner J. R., de Ricqlès A. & Padian K. (2000). Long bone histology of the hadrosaurid dinosaur *Maiasaura peeblesorum*: growth dynamics and physiology based on an ontogenetic series of skeletal elements. *Journal of Vertebrate Paleontology*, 20(1): 115-129. https://doi.org/10.1671/0272-4634(2000)020[0115:LBHOTH]2.0.CO;2

Horner J. R., Padian K. & de Ricqlès A. (2001). Comparative osteohistology of some embryonic and perinatal archosaurs: developmental and behavioral implications for dinosaurs. *Paleobiology*, 27(1): 39-58. https://doi.org/10.1666/0094-8373(2001)027<0039:COOSEA>2.0.CO;2

Houssaye A. (2009). *La "pachyostose" chez les squamates du Crétacé supérieur : implications phylogénétiques, morphofonctionnelles et paléoécologiques*. Unpublished PhD thesis, Muséum National d'Histoire Naturelle.

Houssaye A. (2012). Palaeoecological and morphofunctional interpretation of bone mass increase: an example in Late Cretaceous shallow marine squamates. *Biological Reviews*, 88(1): 117-139. https://doi.org/10.1111/j.1469-185X.2012.00243.x

Houssaye A. (2013). Bone histology of aquatic reptiles: what does it tell us about secondary adaptation to an aquatic life?. *Biological Journal of the Linnean Society*, 108(1): 3-21. https://doi.org/10.1111/j.1095-8312.2012.02002.x

Houssaye A. (2014). Advances in vertebrate palaeohistology: recent progress, discoveries, and new approaches. *Biological Journal of the Linnean Society*, 112(4): 645-648. https://doi.org/10.1111/bij.12346

Houssaye A. & Bardet N. (2011). Rib and vertebral micro-anatomical characteristics of hydropelvic mosasauroids. *Lethaia*, 45(2): 200-209. https://doi.org/10.1111/j.1502-3931.2011.00273.x

Houssaye A. & Tafforeau P. (2012). What vertebral microanatomy reveals about the ecology of juvenile mosasaurs (Reptilia, Squamata). *Journal of Vertebrate Paleontology*, 32(5): 1042-1048. https://doi.org/10.1080/02724634.2012.680999

Houssaye A. & Botton-Divet L. (2018). From land to water: evolutionary changes in long bone microanatomy of otters (Mammalia: Mustelidae). *Biological Journal of the Linnean Society*, 125(2): 240-249. https://doi.org/10.1093/biolinnean/bly118

Houssaye A., Buffrenil d. V., Rage J. C. & Bardet N. (2008). An analysis of vertebral 'pachyostosis' in *Carentonosaurus mineaui* (Mosasauroidea, Squamata) from the Cenomanian (early Late Cretaceous) of France, with comments on its phylogenetic and functional significance. *Journal of Vertebrate Paleontology*, 28(3): 685-691. https://doi.org/10.1671/0272-4634(2008)28[685:AAOVPI]2.0.CO;2

Houssaye A., Mazurier A., Herrel A., Volpato V., Tafforeau P., Boistel R. & Buffrénil d. V. (2010). Vertebral microanatomy in squamates: structure, growth and ecological correlates. *Journal of Anatomy*, 217(6): 715-727. https://doi.org/10.1111/j.1469-7580.2010.01307.x

Houssaye A., Bardet N., Rage J. C., Suberbiola X. P., Bouya B., Amaghzaz M. & Amalik M. (2011). A review of *Pachyvaranus crassispondylus* Arambourg, 1952, a pachyostotic marine squamate from the latest Cretaceous phosphates of Morocco and Syria. *Geological Magazine*, 148(2): 237-249. https://doi.org/10.1017/S0016756810000580

Houssaye A., Lindgren J., Pellegrini R., Lee A. H., Germain D. & Polcyn M. J. (2013a). Microanatomical and histological features in the long bones of mosasaurine mosasaurs (Reptilia, Squamata)–implications for aquatic adaptation and growth rates. *PLoS One*, 8(10): e76741. https://doi.org/10.1371/journal.pone.0076741

Houssaye A., Boistel R., Böhme W. & Herrel A. (2013b). Jack-of-all-trades master of all? Snake vertebrae have a generalist inner organization. *Naturwissenschaften*, 100: 997-1006. https://doi.org/10.1007/s00114-013-1102-x

Houssaye A., Scheyer T. M., Kolb C., Fischer V. & Sander P. M. (2014a). A new look at ichthyosaur long bone microanatomy and histology: implications for their adaptation to an aquatic life. *PLoS One*, 9(4): e95637. https://doi.org/10.1371/journal.pone.0095637

Houssaye A., Tafforeau P. & Herrel A. (2014b). Amniote vertebral microanatomy–what are the major trends?. *Biological Journal of the Linnean Society*, 112(4): 735-746. https://doi.org/10.1111/bij.12311

Houssaye A., Tafforeau P., Muizon d. C. & Gingerich P. D. (2015). Transition of Eocene whales from land to sea: evidence from bone microstructure. *PLoS One*, 10(2): e0118409. https://doi.org/10.1371/journal.pone.0118409

Houssaye A., Sander M. P. & Klein N. (2016a). Adaptive patterns in aquatic amniote bone microanatomy—more complex than previously thought. *Integrative and Comparative Biology*, 56(6): 1349-1369. https://doi.org/10.1093/icb/icw120

Houssaye A., Fernandez V. & Billet G. (2016b). Hyperspecialization in some South American endemic ungulates revealed by long bone microstructure. *Journal of Mammalian Evolution*, 23: 221-235. https://doi.org/10.1007/s10914-015-9312-y

Houssaye A., Waskow K., Hayashi S., Cornette R., Lee A. H. & Hutchinson J. R. (2016c). Biomechanical evolution of solid bones in large animals: a microanatomical investigation. *Biological Journal of the Linnean Society*, 117(2): 350-371. https://doi.org/10.1111/bij.12660

Houssaye A., Taverne M. & Cornette R. (2018a). 3D quantitative comparative analysis of long bone diaphysis variations in microanatomy and cross-sectional geometry. *Journal of Anatomy*, 232(5): 836-849. https://doi.org/10.1111/joa.12783

Houssaye A., Nakajima Y. & Sander P. M. (2018b). Structural, functional, and physiological signals in ichthyosaur vertebral centrum microanatomy and histology. *Geodiversitas*, 40(2): 161-170. https://doi.org/10.5252/geodiversitas2018v40a7

Houssaye A., Herrel A., Boistel R. & Rage J. C. (2019). Adaptation of the vertebral inner structure to an aquatic life in snakes: Pachyophiid peculiarities in comparison to extant and extinct forms. *Comptes Rendus Palevol*, 18(7): 783-799. https://doi.org/10.1016/j.crpv.2019.05.004

Houssaye A., de Perthuis A. & Houée G. (2021a). Sesamoid bones also show functional adaptation in their microanatomy—The example of the patella in Perissodactyla. *Journal of Anatomy*, 240(1): 50-65. https://doi.org/10.1111/joa.13530

Houssaye A., Martin F., Boisserie J. R. & Lihoreau F. (2021b). Paleoecological inferences from long bone microanatomical specializations in Hippopotamoidea (Mammalia, Artiodactyla). *Journal of Mammalian Evolution*, 28(3): 847-870. https://doi.org/10.1007/s10914-021-09536-x

Hu K., King J. L., Romick C. A., Dufeau D. L., Witmer L. M., Stubbs T. L., Rayfield E. J. & Benton M. J. (2020). Ontogenetic endocranial shape change in alligators and ostriches and implications for the development of

the non-avian dinosaur endocranium. *The Anatomical Record*, 304(8): 1759-1775. https://doi.org/10.1002/ar.24579

Hua S. (1997). *Adaptations des crocodiliens mésosuchiens au milieu marin*. Unpublished PhD thesis, Université Paris 6, 211 p.

Hua S. (2020). A new specimen of *Teleidosaurus calvadosii* (Eudes-Deslongchamps, 1866) (Crocodylia, Thalattosuchia) from the middle Jurassic of France. *Annales de Paléontologie* , 106(4): 102423. https://doi.org/10.1016/j.annpal.2020.102423

Hua S. & Buffrénil V. d. (1996). Bone histology as a clue in the interpretation of functional adaptations in the Thalattosuchia (Reptilia, Crocodylia). *Journal of Vertebrate Paleontology*, 16(4): 703-717. https://doi.org/10.1080/02724634.1996.10011359

Hua S. & Buffetaut E. (1997). Crocodylia. In Callaway J. M., *Ancient Marine Reptiles*: 357-374.

Hua S., Vignaud P., Atrops F. & Clément A. (2000). *Enaliosuchus macrospondylus* (Crocodylia, Metriorhynchidae) du Valanginien de Barret-le-Bas (Hautes Alpes, France): Un cas unique de remontée des narines externes parmi les crocodiliens. *Géobios*, 33(4): 467-474. https://doi.org/10.1016/S0016-6995(00)80080-7

Hua S., Pennetier G. & Pennetier E. (2021). A juvenile *Steneosaurus* in the Callovian of Normandy (France); a genus too hastily consigned to the wastebasket?. *Carnets Natures*, 8: 1-8.

Huang C., Retallack G. J., Wang C. & Huang Q. (2013). Paleoatmospheric pCO2 fluctuations across the Cretaceous–Tertiary boundary recorded from paleosol carbonates in NE China. *Palaeogeography., Palaeoclimatology, Palaeoecology*, 385: 95-105. https://doi.org/10.1016/j.palaeo.2013.01.005

Hudspeth A. J. (1983). The hair cells of the inner ear. *Scientific American*, 248(1): 54-65.

Hullar T. E. (2006). Semicircular canal geometry, afferent sensitivity, and animal behavior. *The Anatomical Record*, 288(4): 466-472. https://doi.org/10.1002/ar.a.20304

Hunt A. P. (1989). Late Triassic vertebrate localities in New Mexico. In Lucas S. G. & Hunt A. P. (eds.) *The dawn of the Age of Dinosaurs in the American Southwest: Albuquerque*, New Mexico Museum of Natural History and Science: 72-101.

Hunt A. P. & Lockley M. G. (1995). A nonmarine tetrapod from the Middle Jurassic of the United States: A primitive crocodyliform from the Entrada Sandstone of eastern Utah. *Journal of Vertebrate Paleontology*, 15(3): 554-560. https://doi.org/10.1080/02724634.1995.10011248

Hunt A. P., Lucas S. G. & Spielmann J. A. (2006). Sexual dimorphism in a large brachyrostral phytosaur (Archosauria: Crurotarsi) from the Late Triassic of western North America. *New Mexico Museum of Natural History and Science Bulletin*, 37: 563-567.

Hurlburt G. R. (1996). *Relative brain size in recent and fossil amniotes: determination and interpretation.* Unpublished PhD thesis, University of Toronto, 253 p.

Hurlburt G. R., Ridgely R. C. & Witmer L. M. (2013). Relative size of brain and cerebrum in tyrannosaurid dinosaurs: an analysis using brain-endocast quantitative relationships in extant alligators. In Parrish J. M., Molnar R. E., Currie P. J. & Koppelhus E. B. (eds.) *Tyrannosaurid Paleobiology*, Indiana University Press: 135-156.

Hut G. (1987). *Consultants' group meeting on stable isotope reference samples for geochemical and hydrological investigations.* International Atomic Energy Agency, Vienna, Austria, 42 p.

Huxley T. H. (1875). On *Stagonolepis robertsoni*, and on the evolution of the Crocodilia. *Quarterly Journal of the Geological Society*, 31(1-4): 423-438.

Hwang S. H. (2005). Phylogenetic patterns of enamel microstructure in dinosaur teeth. *Journal of Morphology*, 266(2): 208-240. https://doi.org/10.1002/jmor.10372

Iacumin P., Bocherens H., Mariotti A. & Longinelli A. (1996). Oxygen isotope analyses of co-existing carbonate and phosphate in biogenic apatite: a way to monitor diagenetic alteration of bone phosphate?. *Earth and Planet. Sci. Lett.*, 142(1-2): 1-6. https://doi.org/10.1016/0012-821X(96)00093-3

IAEA (2022). Global Network of Isotopes in Precipitation. The GNIP Database. https://nucleus.iaea.org/wiser/index.aspx

Ibrahim N., Sereno P. C., Varricchio D. J., Martill D. M., Dutheil D. B., Unwin D. M., Baidder L., Larsson H. C. E., Zouhri S. & Kaoukaya A. (2020). Geology and paleontology of the upper cretaceous Kem Kem group of eastern Morocco. *ZooKeys*, 928: 1-216. https://doi.org/10.3897/zookeys.928.47517

Ifediba M. A., Rajguru S. M., Hullar T. E. & Rabbitt R. D. (2007). The role of 3-canal biomechanics in angular motion transduction by the human vestibular labyrinth. *Annals of Biomedical Engineering*, 35: 1247-1263. https://doi.org/10.1007/s10439-007-9277-y

Iordansky N. N. (1973). The skull of the Crocodilia. *Biology of the Reptilia*, 4: 201-262.

Iori F. V. & Carvalho I. d. S. (2009). *Morrinhosuchus luziae*, um novo Crocodylomorpha Notosuchia da Bacia Bauru, Brasil. *Brazilian Journal of Geology*, 39(4): 717-725.

Iori F. V. & Carvalho I. d. S. (2011). *Caipirasuchus paulistanus*, a new sphagesaurid (Crocodylomorpha, Mesoeucrocodylia) from the Adamantina Formation (Upper Cretaceous, Turonian–Santonian), Bauru Basin, Brazil. *Journal of Vertebrate Paleontology*, 31(6): 1255-1264. https://doi.org/10.1080/02724634.2011.602777

Iori F. V. & Garcia K. L. (2012). *Barreirosuchus franciscoi*, um novo Crocodylomorpha Trematochampsidae da Bacia Bauru, Brasil. *Brazilian Journal of Geology*, 42(2): 397-410. https://doi.org/10.5327/Z0375-75362012000200013

Iori F. V., Carvalho I. S., Santos E. F., Doro L. F. & Campos A. C. A. (2011). Ocorrência de *Pepesuchus deiseae* (Crocodyliforme) no município de Catanduva, estado de São Paulo (Bacia Bauru, Cretáceo Superior). *XXII Congresso Brasileiro de Paleontologia, Natal*: 728-730.

Iori F. V., Marinho T. S., Carvalho I. S. & Campos A. C. A. (2013). Taxonomic reappraisal of the sphagesaurid crocodyliform *Sphagesaurus montealtensis* from the late Cretaceous Adamantina Formation of São Paulo State, Brazil. *Zootaxa*, 3686(2): 183-200. https://doi.org/10.11646/zootaxa.3686.2.4

Iori F. V., Carvalho I. d. S. & Marinho T. S. (2016). Postcranial skeletons of *Caipirasuchus* (Crocodyliformes, Notosuchia, Sphagesauridae) from the Upper Cretaceous (Turonian–Santonian) of the Bauru Basin, Brazil. *Cretaceous Research*, 60: 109-120. https://doi.org/10.1016/j.cretres.2015.11.017

Iori F. V., Marinho T. S., Carvalho I. d. S. & dos Santos Frare L. A. (2018). Cranial morphology of *Morrinhosuchus luziae* (Crocodyliformes, Notosuchia) from the Upper Cretaceous of the Bauru Basin, Brazil. *Cretaceous Research*, 86: 41-52. https://doi.org/10.1016/j.cretres.2018.02.010

Irmis R. B., Nesbitt S. J. & Sues H. D. (2013). Early Crocodylomorpha. *Geological Society, London, Special Publications*, 379(1): 275-302. https://doi.org/10.1144/SP379.24

Iwaniuk A. N. & Nelson J. E. (2002). Can endocranial volume be used as an estimate of brain size in birds?. *Canadian Journal of Zoology*, 80(1): 16-23. https://doi.org/10.1139/z01-204

Jackson K., Butler D. G. & Brooks D. R. (1996). Habitat and phylogeny influence salinity discrimination in crocodylians: implications for osmoregulatory physiology and historical biogeography. *Biological Journal of the Linnean Society*, 58(4): 371-383. https://doi.org/10.1111/j.1095-8312.1996.tb01441.x

Janke A., Gullberg A., Hughes S., Aggarwal R. K. & Arnason U. (2005). Mitogenomic analyses place the gharial (*Gavialis gangeticus*) on the crocodile tree and provide pre-K/T divergence times for most crocodylians. *Journal of Molecular Evolution*, 61: 620-626. https://doi.org/10.1007/s00239-004-0336-9

Jaouen K., Pons M. L. & Balter V. (2013). Iron, copper and zinc isotopic fractionation up mammal trophic chains. *Earth and Planetary Science Letters*, 374: 164-172. https://doi.org/10.1016/j.epsl.2013.05.037

Jaouen K., Szpak P. & Richards M. P. (2016a). Zinc isotope ratios as indicators of diet and trophic level in arctic marine mammals. *PLoS One*, 11(3): e0152299. https://doi.org/10.1371/journal.pone.0152299

Jaouen K., Beasley M., Schoeninger M., Hublin J. J. & Richards M. P. (2016b). Zinc isotope ratios of bones and teeth as new dietary indicators: results from a modern food web (Koobi Fora, Kenya). *Scientific Reports*, 6(1): 26281. https://doi.org/10.1038/srep26281

Jaouen K., Trost M., Bourgon N., Colleter R., Le Cabec A., Tütken T., Oliveira R. E., Pons M. L., Méjean P., Steinbrenner S., Chmeleff J. & Strauss A. (2020). Zinc isotope variations in archeological human teeth (Lapa do Santo, Brazil) reveal dietary transitions in childhood and no contamination from gloves. *PLoS One*, 15(5): e0232379. https://doi.org/10.1371/journal.pone.0232379

Jaouen K., Villalba-Mouco V., Smith G. M., Trost M., Leichliter J., Lüdecke T., Méjean P., Mandrou S., Chmeleff J., Guiserix D., Bourgon N., Blasco F., Cardoso J. M., Duquenoy C., Moubtahij Z., Garcia D. C. S., Richards M., Tütken T., Hublin J. J., Utrilla P. & Montes L. (2022). A Neandertal dietary conundrum: Insights provided by tooth enamel Zn isotopes from Gabasa, Spain. *Proceedings of the National Academy of Sciences of the United States of America*, 119(43): e2109315119. https://doi.org/10.1073/pnas.2109315119

Jerison H. J. (1969). Brain evolution and dinosaur brains. *The American Naturalist*, 103: 575-588. https://doi.org/10.1086/282627

Jerison H. J. (1973). *Evolution of the brain and intelligence*. New York, NY: Academic Press, 482 p.

Jirak D. & Janacek J. (2017). Volume of the crocodylian brain and endocast during ontogeny. *PLoS One*, 12(6): e0178491. https://doi.org/10.1371/journal.pone.0178491

Johannesson K. H. & Lyons W. B. (1995). Rare-earth element geochemistry of Colour Lake, an acidic freshwater lake on Axel Heiberg Island, Northwest Territories, Canada. *Chemical Geology*, 119(1-4): 209-223. https://doi.org/10.1016/0009-2541(94)00099-T

Johnson M. M. (2019). *The taxonomy, systematics and ecomorphological diversity of Teleosauroidea (Crocodylomorpha, Thalattosuchia), and the evaluation of the genus* 'Steneosaurus'. Unpublished PhD thesis, University of Edinburgh, 1062 p.

Johnson M. M., Young M. T., Steel L. & Lepage Y. (2015). *Steneosaurus edwardsi* (Thalattosuchia: Teleosauridae), the largest known crocodylomorph of the Middle Jurassic. *Biological Journal of the Linnean Society*, 115(4): 911-918. https://doi.org/10.1111/bij.12525

Johnson M. M., Young M. T., Steel L., Foffa D., Smith A. S., Hua S., Havlik P., Howlett E. A. & Dyke G. (2018). Re-description of '*Steneosaurus*' *obtusidens* Andrews, 1909, an unusual macrophagous teleosaurid crocodylomorph from the Middle Jurassic of England. *Zoological Journal of the Linnean Society*, 182(2): 385-418. https://doi.org/10.1093/zoolinnean/zlx035

Johnson M. M., Young M. T., Brusatte S. L., Thuy B. & Weis R. (2019). A catalogue of teleosauroids (Crocodylomorpha: Thalattosuchia) from the Toarcian and Bajocian (Jurassic) of southern Luxembourg. *Historical Biology*, 31(9): 1179-1194. https://doi.org/10.1080/08912963.2018.1427090

Johnson M. M., Young M. T. & Brusatte S. L. (2020a). Emptying the wastebasket: a historical and taxonomic revision of the Jurassic crocodylomorph *Steneosaurus*. *Zoological Journal of the Linnean Society*, 189(2): 428-448. https://doi.org/10.1093/zoolinnean/zlaa027

Johnson M. M., Young M. T. & Brusatte S. L. (2020b). Re-description of two contemporaneous mesorostrine teleosauroids (Crocodylomorpha: Thalattosuchia) from the Bathonian of England and insights into the early evolution of Machimosaurini. *Zoological Journal of the Linnean Society*, 189(2), 449-482.

Johnson M. M., Young M. T., Brignon A. & Brusatte S. L. (2022a). Addition to "the phylogenetics of Teleosauroidea (Crocodylomorpha; Thalattosuchia) and Implications for their ecology and evolution". *Bulletin of Phylogenetic Nomenclature*, 1(1): 1-7. https://doi.org/10.11646/BPN.1.1.1

Johnson M. M., Foffa D., Young M. T. & Brusatte S. L. (2022b). The ecological diversification and evolution of Teleosauroidea (Crocodylomorpha, Thalattosuchia), with insights into their mandibular biomechanics. *Ecology and Evolution*, 12(11): e9484. https://doi.org/10.1002/ece3.9484

Joomun S. C., Hooker J. J. & Collinson M. E. (2008). Dental wear variation and implications for diet: an example from Eocene perissodactyls (Mammalia). *Palaeogeography, Palaeoclimatology, Palaeoecology*, 263(3-4): 92-106. https://doi.org/10.1016/j.palaeo.2008.03.001

Jourdan C. (1862). Une communication relative à deux nouveaux fossiles trouvés dans le calcaire lithographique de Cirin. *Annales des Sciences Physiques et Naturelles de la Société d'Agriculture et d' Industrie de Lyon 3rd series,* 6: 32–33.

Jouve S. (2005). A new description of the skull of *Dyrosaurus phosphaticus* (Thomas, 1893) (Mesoeucrocodylia: Dyrosauridae) from the Lower Eocene of North Africa. *Canadian Journal of Earth Sciences*, 42(3): 323-337. https://doi.org/10.1139/e05-008

Jouve S. (2007). Taxonomic revision of the dyrosaurid assemblage (Crocodyliformes: Mesoeucrocodylia) from the Paleocene of the Iullemmeden Basin, West Africa. *Journal of Paleontology*, 81(1): 163-175. https://doi.org/10.1666/0022-3360(2007)81[163:TROTDA]2.0.CO;2

Jouve S. (2009). The skull of *Teleosaurus cadomensis* (Crocodylomorpha; Thalattosuchia), and phylogenetic analysis of Thalattosuchia. *Journal of Vertebrate Paleontology*, 29(1): 88-102. https://doi.org/10.1080/02724634.2009.10010364

Jouve S. (2016). A new basal tomistomine (Crocodylia, Crocodyloidea) from Issel (Middle Eocene; France): palaeobiogeography of basal tomistomines and palaeogeographic consequences. *Zoological Journal of the Linnean Society*, 177(1): 165-182. https://doi.org/10.1111/zoj.12357

Jouve S. (2021). Differential diversification through the K-Pg boundary, and post-crisis opportunism in longirostrine crocodyliforms. *Gondwana Research*, 99: 110-130. https://doi.org/10.1016/j.gr.2021.06.020

Jouve S. & Schwarz D. (2004). *Congosaurus bequaerti*, a Paleocene Dyrosaurid (Crocodyliformes; Mesoeucrocodylia) from Landana (Angola). *Bulletin de l'Institut Royal des Sciences Naturelles de Belgique*, 74: 129-146.

Jouve S., Iarochene M., Bouya B. & Amaghzaz M. (2005). A new dyrosaurid crocodyliform from the Paleocene of Morocco and a phylogenetic analysis of Dyrosauridae. *Acta Palaeontologica Polonica*, 50(3): 581-594.

Jouve S., Iarochene M., Bouya B. & Amaghzaz M. (2006). A new species of *Dyrosaurus* (Crocodylomorpha, Dyrosauridae) from the early Eocene of Morocco: phylogenetic implications. *Zoological Journal of the Linnean Society*, 148(4): 603-656. https://doi.org/10.1111/j.1096-3642.2006.00241.x

Jouve S., Bouya B. & Amaghzaz M. (2008). A long-snouted dyrosaurid (Crocodyliformes, Mesoeucrocodylia) from the Paleocene of Morocco: phylogenetic and palaeobiogeographic implications. *Palaeontology*, 51(2): 281-294. https://doi.org/10.1111/j.1475-4983.2007.00747.x

Jouve S., Muizon C. d., Cespedes-Paz R., Sossa-Soruco V. & Knoll S. (2020). The longirostrine crocodyliforms from Bolivia and their evolution through the Cretaceous–Palaeogene boundary. *Zoological Journal of the Linnean Society*, 192(2): 475-509. https://doi.org/10.1093/zoolinnean/zlaa081

Kälin J. A. (1939). Ein extrem kurzschnauziger Crocodilide aus den Phosphoriten des Quercy *Arambourgia* (nov. gen.) *gaudryi* de Stefano. *Abhandlungen der Schweizerischen Palaeontologischen Gesellschaft*, 62: 1-18.

Karl H. V., Grönig E., Brauckmann C. & Knötschke N. (2006). Revision of the genus *Enaliosuchus* Koken, 1883 (Archosauromorpha: Metriorhynchidae) from the Early Cretaceous of Northwestern Germany. *Studia Geologica Salmanticensia*, 42: 49-59.

Karoui-Yaakoub N., M'Barek-Jemaï M. B. Mtimet M. S. & Molina E. (2015). Integrated stratigraphy of the Ypresian–Lutetian transition in northern Tunisia: Correlation and paleoenvironmental reconstruction. *Journal of African Earth Sciences*, 110: 176-187. https://doi.org/10.1016/j.jafrearsci.2015.07.001

Kawabe S., Shimokawa T., Miki H., Okamoto T. & Matsuda S. (2009). A simple and accurate method for estimating the brain volume of birds: possible application in paleoneurology. *Brain, Behavior and Evolution*, 74(4): 295-301. https://doi.org/10.1159/000270906

Keenan S. W. (2016). From bone to fossil: A review of the diagenesis of bioapatite. *American Mineralogist*, 101(9): 1943-1951. https://doi.org/10.2138/am-2016-5737

Kellner A. W., Campos D. A., Riff D. & de Andrade M. B. (2011a). A new crocodylomorph (Sphagesauridae, Notosuchia) with horn-like tubercles from Brazil. *Zoological Journal of the Linnean Society*, 163(suppl_1): S57-S65. https://doi.org/10.1111/j.1096-3642.2011.00712.x

Kellner A. W., Figueiredo R. G., Azevedo S. A. & Campos D. A. (2011b). A new cretaceous notosuchian (Mesoeucrocodylia) with bizarre dentition from Brazil. *Zoological Journal of the Linnean Society*, 163(suppl_1): S109-S115. https://doi.org/10.1111/j.1096-3642.2011.00711.x

Kellner A. W., Pinheiro A. E. & Campos D. A. (2014). A new sebecid from the Paleogene of Brazil and the crocodyliform radiation after the K–Pg boundary. *PLoS One*, 9(1): e81386. https://doi.org/10.1371/journal.pone.0081386

Kendall C. & Grim E. (1990). Combustion tube method for measurement of nitrogen isotope ratios using calcium oxide for total removal of carbon dioxide and water. *Analytical Chemistry*, 62(5): 526-529.

Kendall C., Eriksen A. M. H., Kontopoulos I., Collins M. J. & Turner-Walker G. (2018). Diagenesis of archaeological bone and tooth. *Palaeogeography, Palaeoclimatology, Palaeoecology*, 491: 21-37. https://doi.org/10.1016/j.palaeo.2017.11.041

Kent D. V. & Tauxe L. (2005). Corrected Late Triassic latitudes for continents adjacent to the North Atlantic. *Science*, 307(5707): 240-244. https://doi.org/10.1126/science.1105826

Kerber L., Ferreira J. D., Fonseca P. H. M., Franco A., Martinelli A. G., Soares M. B. & Ribeiro A. (2021). An additional brain endocast of the ictidosaur *Riograndia guaibensis* (Eucynodontia: Probainognathia): intraspecific variation of endocranial traits. *Anais da Academia Brasileira de Ciências*, 93(S2): 1-8. https://doi.org/10.1590/0001-3765202120200084

Khosla A., Sertich J. J., Prasad G. V. & Verma O. (2009). Dyrosaurid remains from the intertrappean beds of India and the Late Cretaceous distribution of Dyrosauridae. *Journal of Vertebrate Paleontology*, 29(4): 1321-1326. https://doi.org/10.1671/039.029.0416

Kim R. & Evans D. (2014). Relationships among brain, endocranial cavity, and body sizes in reptiles. *Society of Vertebrate Paleontology 74th annual meeting*, Berlin, Germany.

King J. L., Sipla J. S., Georgi J. A., Balanoff A. M. & Neenan J. M. (2020). The endocranium and trophic ecology of *Velociraptor mongoliensis*. *Journal of Anatomy*, 237(5), 861-869. https://doi.org/10.1111/joa.13253

Klein N., Scheyer T. & Tütken T. (2009). Skeletochronology and isotopic analysis of a captive individual of *Alligator mississippiensis* Daudin, 1802. *Fossil Record*, 12(2): 121-131. https://doi.org/10.1002/mmng.200900002

Klein N., Houssaye A., Neenan J. M. & Scheyer T. M. (2015). Long bone histology and microanatomy of Placodontia (Diapsida: Sauropterygia). *Contributions to Zoology*, 84(1): 59-S15.

Klein N., Sander P. M., Krahl A., Scheyer T. M. & Houssaye A. (2016). Diverse aquatic adaptations in *Nothosaurus* spp.(Sauropterygia)—inferences from humeral histology and microanatomy. *PloS One*, 11(7): e0158448. https://doi.org/10.1371/journal.pone.0158448

Klembara J. (2005). Ontogeny of the partial secondary wall of the otoccipital region of the endocranium in prehatching *Alligator mississippiensis* (Archosauria, Crocodylia). *Journal of Morphology*, 266(3): 319-330. https://doi.org/10.1002/jmor.10380

Kley N. J., Sertich J. J., Turner A. H., Krause D. W., O'Connor P. M. & Georgi J. A. (2010). Craniofacial morphology of *Simosuchus clarki* (Crocodyliformes: Notosuchia) from the late Cretaceous of Madagascar. *Journal of Vertebrate Paleontology*, 30(sup1): 13-98. https://doi.org/10.1080/02724634.2010.532674

Klock C., Leuzinger L., Santucci R. M., Martinelli A. G., Marconato A., Marinho T. S., Luz Z. & Vennemann T. (2022). A bone to pick: stable isotope compositions as tracers of food sources and paleoecology for notosuchians in the Brazilian Upper Cretaceous Bauru Group. *Cretaceous Research*, 131, 105113. https://doi.org/10.1016/j.cretres.2021.105113

Knoll F. & Rohrberg K. (2012). CT scanning, rapid prototyping and re-examination of a partial skull of a basal crocodylomorph from the Late Triassic of Germany. *Swiss Journal of Geosciences*, 105(1): 109-115. https://doir.org/10.1007/s00015-012-0094-4

Knoll F., Cuny G., Mojon P. O., López-Antoñanzas R. & Huguet D. (2013). A new vertebrate-, ostracod-, and charophyte-bearing locality in the Middle Jurassic of the Grands Causses (southern France). *Proceedings of the Geologists' Association*, 124(3): 525-529. https://doi.org/10.1016/j.pgeola.2012.09.001

Knudson K. J., Williams S. R., Osborn R., Forgey K. & Williams P. R. (2009). The geographic origins of Nasca trophy heads using strontium, oxygen, and carbon isotope data. *Journal of Anthropological Archaeology*, 28(2): 244-257. https://doi.org/10.1016/j.jaa.2008.10.006

Koch P. L. (1998). Isotopic reconstruction of past continental environments. *Annual Review of Earth and Planetary Sciences*, 26(1): 573-613.

Koch P. L., Tuross N. & Fogel M. L. (1997). The effects of sample treatment and diagenesis on the isotopic integrity of carbonate in biogenic hydroxylapatite. *Journal of Archaeological Science*, 24(5): 417-429. https://doi.org/10.1006/jasc.1996.0126

Kocsis L., Ősi A., Vennemann T., Trueman C. N. & Palmer M. R. (2009). Geochemical study of vertebrate fossils from the Upper Cretaceous (Santonian) Csehbánya Formation (Hungary): Evidence for a freshwater habitat of mosasaurs and pycnodont fish. *Palaeogeography, Palaeoclimatology, Palaeoecology*, 280(3-4): 532-542. https://doi.org/10.1016/j.palaeo.2009.07.009

Kocsis L., Trueman C. N. & Palmer M. R. (2010). Protracted diagenetic alteration of REE contents in fossil bioapatites: direct evidence from Lu–Hf isotope systematics. *Geochimica et Cosmochimica Acta*, 74(21): 6077-6092. https://doi.org/10.1016/j.gca.2010.08.007

Kohn M. J. (1996). Predicting animal δ18O: accounting for diet and physiological adaptation. *Geochimica et Cosmochimica Acta*, 60(23): 4811-4829. https://doi.org/10.1016/S0016-7037(96)00240-2

Kohn M. J. (2008). Models of diffusion-limited uptake of trace elements in fossils and rates of fossilization. *Geochimica et Cosmochimica Acta*, 72(15): 3758-3770. https://doi.org/10.1016/j.gca.2008.05.045

Kohn M. J. (2010). Carbon isotope compositions of terrestrial C3 plants as indicators of (paleo) ecology and (paleo) climate. *Proceedings of the National Academy of Sciences*, 107(46), 19691-19695. https://doi.org/10.1073/pnas.1004933107

Kohn M. J., Schoeninger M. J. & Barker W. W. (1999). Altered states: effects of diagenesis on fossil tooth chemistry. *Geochimica et Cosmochimica Acta*, 63(18): 2737-2747. https://doi.org/10.1016/S0016-7037(99)00208-2

Kolb C., Scheyer T. M., Veitschegger K., Forasiepi A. M., Amson E., Van der Geer A. A. E., Van den Hoek Ostende L. W., Hayashi S., Sanchez-Villagra M. R. (2015). Mammalian bone palaeohistology: a survey and new data with emphasis on island forms. *PeerJ*, 3: e1358. https://doi.org/10.7717/peerj.1358

Kolodny Y., Luz B. & Navon O. (1983). Oxygen isotope variations in phosphate of biogenic apatites, I. Fish bone apatite—rechecking the rules of the game. *Earth and Planetary Science Letters*, 64(3): 398-404. https://doi.org/10.1016/0012-821X(83)90100-0

Kolodny Y., Luz B., Sander M. & Clemens W. A. (1996). Dinosaur bones: fossils or pseudomorphs? The pitfalls of physiology reconstruction from apatitic fossils. *Palaeogeograph., Palaeoclim., Palaeoecol.*, 126(1-2): 161-171. https://doi.org/10.1016/S0031-0182(96)00112-5

Konzhukova E. D. (1954). New fossil crocodylian from Mongolia. *Trudy Paleontologicheskogo Instituta ANSSSR,* 48: 171–194.

Kotsakis T., Delfino M. & Piras P. (2004). Italian Cenozoic crocodylians: taxa, timing and palaeobiogeographic implications. *Palaeogeography, Palaeoclimatology, Palaeoecology*, 210(1): 67-87. https://doi.org/10.1016/j.palaeo.2004.03.013

Kramer M. G., Sollins P., Sletten R. S. & Swart P. K. (2003). N isotope fractionation and measures of organic matter alteration during decomposition. *Ecology*, 84(8): 2021-2025. https://doi.org/10.1890/02-3097

Krishnaswami S., Trivedi J. R., Sarin M. M., Ramesh R. & Sharma K. K. (1992). Strontium isotopes and rubidium in the Ganga-Brahmaputra river system: Weathering in the Himalaya, fluxes to the Bay of Bengal and contributions to the evolution of oceanic $^{87}Sr/^{86}Sr$. *Earth and Planetary Science Letters*, 109(1-2): 243-253. https://doi.org/10.1016/0012-821X(92)90087-C

Kriwet J., Rauhut O. W. M. & Gloy U. (1997). Microvertebrate remains (Pisces, Archosauria) from the Middle Jurassic (Bathonian) of southern France. *Neues Jahrbuch für Geologie und Paläontologie-Abhandlungen*, 206(1): 1-28.

Kroopnick P. & Craig H. (1972). Atmospheric oxygen: isotopic composition and solubility fractionation. *Science*, 175(4017): 54-55. https://doi.org/10.1126/science.175.4017.54

Kubo T., Shibata M., Naksri W., Jintasakul P. & Azuma Y. (2018). The earliest record of Asian Eusuchia from the Lower Cretaceous Khok Kruat formation of northeastern Thailand. *Cretaceous Research*, 82: 21-28. https://doi.org/10.1016/j.cretres.2017.05.021

Kuhn O. (1938). Die Crocodilier aus dem mittleren Eozän des Geiseltales bei Halle. *Nova Acta Leopoldina*, 39: 313–28

Kuhn O. (1961). Die Tier-und pflanzenweit des Solnhofener Schiefers. *Geologica Bavarica*, 48.

Kuhn O. (1968). *Die vorzeitlichten Krokodile*, Munich, 124 p.

Kundrát M., Xu X., Hančová M., Gajdoš A., Guo Y. & Chen D. (2018). Evolutionary disparity in the endoneurocranial configuration between small and gigantic tyrannosauroids. *Historical Biology*, 32(5): 620-634. https://doi.org/10.1080/08912963.2018.1518442

Kurzanov S. M., Efimov M. B. & Gubin Y. M. (2003). New Archosaurs from the Jurassic of Siberia and Mongolia. *Paleontological Journal*, 37(1): 53-57.

Kuzmin I. T. (2022a). Crocodyliform remains from the Upper Cretaceous of Central Asia–evidence for one of the oldest Crocodylia?. *Cretaceous Research*, 138: 105266. https://doi.org/10.1016/j.cretres.2022.105266

Kuzmin I. T. (2022b). *Anatomy, development and evolution of braincase in Crocodylomorpha (Diapsida: Archosauria)*. Unpublished PhD thesis, Saint Petersburg State University, 176 p.

Kuzmin I. T., Skutschas P. P., Boitsova E. A. & Sues H. D. (2019). Revision of the large crocodyliform *Kansajsuchus* (Neosuchia) from the Late Cretaceous of Central Asia. *Zoological Journal of the Linnean Society*, 185(2): 335-387. https://doi.org/10.1093/zoolinnean/zly027

Kuzmin I. T., Boitsova E. A., Gombolevskiy V. A., Mazur E. V., Morozov S. P., Sennikov A. G., Skutschas P. P. & Sues H. D. (2021). Braincase anatomy of extant Crocodylia, with new insights into the development and evolution of the neurocranium in crocodylomorphs. *Journal of Anatomy*, 239(5): 983-1038. https://doi.org/10.1111/joa.13490

Ladevèze S., Selva C. & Muizon C. d. (2020). What are "opossum-like" fossils? The phylogeny of herpetotheriid and peradectid metatherians, based on new features from the petrosal anatomy. *Journal of Systematic Palaeontology*, 18(17): 1463-1479. https://doi.org/10.1080/14772019.2020.1772387

Lamm E. T. & Padian K. (2013). Preparation and sectioning of specimens. *Bone histology of fossil tetrapods: advancing methods, analysis, and interpretation*, 55-160.

Lamanna M. C., Smith J. B., Attia Y. S. & Dodson P. (2004). From dinosaurs to dyrosaurids (Crocodyliformes): removal of the post-Cenomanian (Late Cretaceous) record of Ornithischia from Africa. *Journal of Vertebrate Paleontology*, 24(3): 764-768. https://doi.org/10.1671/0272-4634(2004)024[0764:FDTDCR]2.0.CO;2

Lamanna M. C., Casal G. A., Ibiricu L. M. & Martínez R. D. (2019). A new peirosaurid crocodyliform from the Upper Cretaceous Lago Colhué Huapi Formation of Central Patagonia, Argentina. *Annals of Carnegie Museum*, 85(3): 193-211. https://doi.org/10.2992/007.085.0301

Lang J. W. (2015). Behavorial Ecology of the Gharial (*Gavialis gangeticus*). *Society for Integrative and Comparative Biology Annual Meeting*.

Lang J. W., Chowfin S. & Ross J. P. (2019). *Gavialis gangeticus*. *The IUCN Red List of Threatened Species*, 2019: e.T8966A3148543. http://doi.org/10.2305/IUCN.UK.2019-1.RLTS.T8966A3148543.en

Langston W. (1965). Fossil crocodylians from Colombia and the Cenozoic history of the Crocodilia in South America. *University of California Publications in Geological Sciences*, 52: 1-157.

Langston W. (1975). Ziphodont crocodiles: *Pristichampsus vorax* (Troxell), new combination, from the Eocene of North America. *Fieldiana: Geology*, 33: 291–314.

Langston W. (1995). Dyrosaurs (Crocodilia: Mesosuchia) from the Paleocene Umm Himar Formation, Kingdom of Saudi Arabia. *Us Geological Survey, Bulletin,* 2093-F: 1-36.

Larsson H. C. E. & Sidor C. A. (1999). Unusual crocodyliform teeth from the Late Cretaceous (Cenomanian) of southeastern Morocco. *Journal of Vertebrate Paleontology*, 19(2): 398-401. https://doi.org/10.1080/02724634.1999.10011152

Larsson H. C. & Gado B. (2000). A new Early Cretaceous crocodyliform from Niger. *Neues Jahrbuch für Geologie und Paläontologie-Abhandlungen*, 217(1): 131-141. https://doi.org/10.1127/njgpa/217/2000/131

Larsson H. C. & Sues H. D. (2007). Cranial osteology and phylogenetic relationships of *Hamadasuchus rebouli* (Crocodyliformes: Mesoeucrocodylia) from the Cretaceous of Morocco. *Zoological Journal of the Linnean Society*, 149(4): 533-567. https://doi.org/10.1111/j.1096-3642.2007.00271.x

Lasseron M., Allain R., Gheerbrant E., Haddoumi H., Jalil N. E., Métais G., Rage J. C., Vullo R. & Zouhri S. (2020). New data on the microvertebrate fauna from the Upper Jurassic or lowest Cretaceous of Ksar Metlili (Anoual Syncline, eastern Morocco). *Geological Magazine*, 157(3): 367-392. https://doi.org/10.1017/S0016756819000761

Latimer A. E., Sherratt E., Bonnet T. & Scheyer T. M. (2023). Semicircular canal shape diversity among modern lepidosaurs: life habit, size, allometry. *BMC Ecology and Evolution*, 23(1): 10. https://doi.org/10.1186/s12862-023-02113-1

Lauprasert K., Cuny G., Buffetaut E., Suteethorn V. & Thirakhupt K. (2007). *Siamosuchus phuphokensis*, a new goniopholidid from the Early Cretaceous (ante-Aptian) of northeastern Thailand. *Bulletin de la Société géologique de France*, 178(3): 201-216. https://doi.org/10.2113/gssgfbull.178.3.201

Lauprasert K., Cuny G., Thirakhupt K. & Suteethorn V. (2009). *Khoratosuchus jintasakuli* gen. et sp. nov., an advanced neosuchian crocodyliform from the Early Cretaceous (Aptian-Albian) of NE Thailand. *Geological Society, London, Special Publications*, 315(1): 175-187. https://doi.org/10.1144/SP315.13

Lauprasert K., Laojumpon C., Saenphala W., Cuny G., Thirakhupt K. & Suteethorn V. (2011). Atoposaurid crocodyliforms from the Khorat Group of Thailand: first record of Theriosuchus from Southeast Asia. *Paläontologische Zeitschrift*, 85: 37-47. https://doi.org/10.1007/s12542-010-0071-z

Laurenti J. N. (1768). *Specimen Medicum, Exhibens Synopsin Reptilium Emendatum cum Experimentis circa Venena et Antidota Reptilium Austriacorum, quod Authoritate et Consensu.* Joan Thomae Nob de Trattnern, Caes Reg Aulae Typographi, et Bibliop, Vienna, Austria.

Lauretano V., Littler K., Polling M., Zachos J. C. & Lourens L. J. (2015). Frequency, magnitude and character of hyperthermal events at the onset of the Early Eocene Climatic Optimum. *Climate of the Past*, 11(10): 1313-1324. https://doi.org/10.5194/cp-11-1313-2015

Laurin M. (2004). The evolution of body size, Cope's rule and the origin of amniotes. *Systematic Biology*, 53(4): 594-622. https://doi.org/10.1080/10635150490445706

Laurin M., Canoville A. & Germain D. (2011). Bone microanatomy and lifestyle: a descriptive approach. *Comptes Rendus Palevol*, 10(5-6): 381-402. https://doi.org/10.1016/j.crpv.2011.02.003

Lautenschlager S., Rayfield E. J., Altangerel P., Zanno L. E. & Witmer L. M. (2012). The endocranial anatomy of Therizinosauria and its implications for sensory and cognitive function. *PLoS One*, 7(12): e52289. https://doi.org/10.1371/journal.pone.0052289

Lazzerini N., Balter V., Coulon A., Tacail T., Marchina C., Lemoine M., Bayarkhuu N., Turbat T., Lepetz S. & Zazzo A. (2021). Monthly mobility inferred from isoscapes and laser ablation strontium isotope ratios in caprine tooth enamel. *Sci. Rep.*, 11(1): 1-11. https://doi.org/10.1038/s41598-021-81923-z

Le Goff S. (2021). *Evaluation de la balance minérale osseuse ç l'aide des isotopes stables et naturels du calcium et du magnésium dans les biofluides humains*. Unpublished PhD thesis, Université de Lyon, 244 p.

Le Goff S., Albalat E., Dosseto A., Godin J. P. & Balter V. (2021). Determination of magnesium isotopic ratios of biological reference materials via multi-collector inductively coupled plasma mass spectrometry. *Rapid Communications in Mass Spectrometry*, 35(10): e9074. https://doi.org/10.1002/rcm.9074

Le Goff S., Godin J. P., Albalat E., Nieves J. M. R. & Balter V. (2022). Magnesium stable isotope composition, but not concentration, responds to obesity and early insulin-resistant conditions in minipig. *Scientific Reports*, 12(1): 10941. https://doi.org/10.1038/s41598-022-14825-3

Le Mort J. (2019). *Etude d'un* Metriorhynchus brachyrhynchus *(Thalattosuchia; Metriorhynchidae) des Falaises des Vaches Noires (Normandie, Calvados).* Unpublished master thesis, Université de Rennes 1, 21 p.

Le Mort J., Martin J. E., Picot L. & Hua S. (2022). First description of the most complete *Metriorhynchus* aff. *Superciliosus* (Thalattosuchia) specimen from the Callovian of the Vaches-Noires cliffs (Normandy, France) and limitations in the classification of Metriorhynchidae. *Annales de Paléontologie*, 108(3): 102539. https://doi.org/10.1016/j.annpal.2022.102539

Leardi J. M. & Pol D. (2009). The first crocodyliform from the Chubut Group (Chubut Province, Argentina) and its phylogenetic position within basal Mesoeucrocodylia. *Cretaceous Research*, 30(6): 1376-1386. https://doi.org/10.1016/j.cretres.2009.08.002

Leardi J. M., Pol D., Novas F. E. & Suárez Riglos M. (2015). The postcranial anatomy of *Yacarerani boliviensis* and the phylogenetic significance of the notosuchian postcranial skeleton. *Journal of Vertebrate Paleontology*, 35(6): e995187. https://doi.org/10.1080/02724634.2014.995187

Leardi J. M., Pol D. & Gasparini Z. (2018). New Patagonian baurusuchids (Crocodylomorpha; Notosuchia) from the Bajo de la Carpa Formation (Upper Cretaceous; Neuquén, Argentina): new evidences of the early sebecosuchian diversification in Gondwana. *Comptes Rendus Palevol*, 17(8): 504-521. https://doi.org/10.1016/j.crpv.2018.02.002

Leardi J. M., Yáñez I. & Pol D. (2020a). South American Crocodylomorphs (Archosauria; Crocodylomorpha): A review of the early fossil record in the continent and its relevance on understanding the origins of the clade. *Journal of South American Earth Sciences*, 104: 102780. https://doi.org/10.1016/j.jsames.2020.102780

Leardi J. M., Pol D. & Clark J. M. (2020b). Braincase anatomy of *Almadasuchus figarii* (Archosauria, Crocodylomorpha) and a review of the cranial pneumaticity in the origins of Crocodylomorpha. *Journal of Anatomy*, 237(1): 48-73. https://doi.org/10.1111/joa.13171

Lebrun R. (2018). MorphoDig, an open-source 3d freeware dedicated to biology. *IPC5: the 5th International Palaeontological Congress,* Paris.

Lecuona A., Ezcurra M. D. & Irmis R. B. (2016). Revision of the early crocodylomorph *Trialestes romeri* (Archosauria, Suchia) from the lower Upper Triassic Ischigualasto Formation of Argentina: one of the oldest-known crocodylomorphs. *Papers in Palaeontology*, 2(4): 585-622. https://doi.org/10.1002/spp2.1056

Lécuyer C. (2013). *Water on Earth: Physicochemical and Biological Properties*. Wiley, 260 p. https://doi.org/10.1002/9781118574928

Lécuyer C., Grandjean P., O'Neil J. R., Cappetta H. & Martineau F. (1993). Thermal excursions in the ocean at the Cretaceous—Tertiary boundary (northern Morocco): δ18O record of phosphatic fish debris. *Palaeogeography, Palaeoclimatology, Palaeoecology*, 105(3-4): 235-243. https://doi.org/10.1016/0031-0182(93)90085-W

Lécuyer C., Grandjean P., Mazin J. & Buffrénil V.D. (1999). Oxygen isotope compositions of reptile bones and teeth: a potential record of terrestrial and marine paleo-environments. In: Hoch E., Brantsen A.K. (Eds.), *Secondary Adaptation to Life in Wate*r, Copenhagen University, Geologisk Museum, Denmark, p. 33.

Lécuyer C., Bogey C., Garcia J. P., Grandjean P., Barrat J. A., Floquet M., Bardet N. & Pereda-Superbiola X. (2003). Stable isotope composition and rare earth element content of vertebrate remains from the Late Cretaceous of northern Spain (Laño): did the environmental record survive?. *Palaeogeography, Palaeoclimatology, Palaeoecology*, 193(3-4): 457-471. https://doi.org/10.1016/S0031-0182(03)00261-X

Lécuyer C., Reynard B. & Grandjean P. (2004). Rare earth element evolution of Phanerozoic seawater recorded in biogenic apatites. *Chemical Geology*, 204(1-2): 63-102. https://doi.org/10.1016/j.chemgeo.2003.11.003

Lécuyer C., Fourel F., Martineau F., Amiot R., Bernard A., Daux V., Escarguel G. & Morrison J. (2007). High-precision determination of $^{18}O/^{16}O$ ratios of silver phosphate by EA-pyrolysis-IRMS continuous flow technique. *Journal of Mass Spectrometry*, 42(1): 36-41. https://doi.org/10.1002/jms.1130

Lécuyer C., Balter V., Martineau F., Fourel F., Bernard A., Amiot R., Gardien V., Otero O., Legendre S., Panczer G. Simon L. & Martini R. (2010). Oxygen isotope fractionation between apatite-bound carbonate and water determined from controlled experiments with synthetic apatites precipitated at 10–37 C. *Geochim. et Cosmochim. Acta*, 74(7): 2072-2081. https://doi.org/10.1016/j.gca.2009.12.024

Lécuyer C., Amiot R., Touzeau A. & Trotter J. (2013). Calibration of the phosphate δ18O thermometer with carbonate–water oxygen isotope fractionation equations. *Chemical Geology*, 347: 217-226. https://doi.org/10.1016/j.chemgeo.2013.03.008

Lee M. S. & Yates A. M. (2018). Tip-dating and homoplasy: reconciling the shallow molecular divergences of modern gharials with their long fossil record. *Proceedings of the Royal Society B*, 285(1881): 20181071. https://doi.org/10.1098/rspb.2018.1071

Lee-Thorp J. A., Sealy J. C. & Van Der Merwe N. J. (1989). Stable carbon isotope ratio differences between bone collagen and bone apatite, and their relationship to diet. *J. of Archaeol. Sci.*, 16(6): 585-599. https://doi.org/10.1016/0305-4403(89)90024-1

Lefranc J. P. & Toutin N. (1971). Un gisement de *Desertella foureaui* (Lamellibranche préhétérodonte) dans le soubassement albien du Tademait Ouest (Sahara algérien). *Bulletin de la Société d'Histoire naturelle d'Afrique du Nord*, 62(1-2): 103-110.

Lefranc J. P. & Guiraud R. (1990). The Continental Intercalaire of northwestern Sahara and its equivalents in the neighbouring regions. *Journal of African Earth Sciences (and the Middle East)*, 10(1-2): 27-77. https://doi.org/10.1016/0899-5362(90)90047-I

Legendre L. J. (2014). *Les crocodiles sont-ils devenus secondairement ectothermes ? Etude paléohistologique*. Unpublished PhD thesis, Sorbonne Universités, 174 p.

Legendre L. J., Segalen L. & Cubo J. (2013). Evidence for high bone growth rate in *Euparkeria* obtained using a new paleohistological inference model for the humerus. *Journal of Vertebrate Paleontology*, 33(6): 1343-1350. https://doi.org/10.1080/02724634.2013.780060

Legendre L. J., Guénard G., Botha-Brink J. & Cubo J. (2016). Palaeohistological evidence for ancestral high metabolic rate in archosaurs. *Systematic Biology*, 65(6): 989-996. https://doi.org/10.1093/sysbio/syw033

Legendre S., Sigé B., Astruc J. G., De Bonis L., Crochet J. Y., Denys C., Godinot M., Hartenberger J. L., Lévêque F., Marandat B., Mourer-Chauviré C., Rage J. C., Remy J. A., Sudre J. & Vianey-Liaud M. (1997). Les phosphorites du Quercy: 30 ans de recherche. Bilan et perspectives. *Geobios*, 30: 331-345. https://doi.org/10.1016/S0016-6995(97)80038-1

Leichliter J. N., Lüdecke T., Foreman A. D., Duprey N. N., Winkler D. E., Kast E. R., Vonhof H., Sigman D. M., Haug G. H., Clauss M., Tütken T. & Martínez-García A. (2021). Nitrogen isotopes in tooth enamel record diet and trophic level enrichment: Results from a controlled feeding experiment. *Chemical Geology*, 563: 120047. https://doi.org/10.1016/j.chemgeo.2020.120047

Leichliter J. N., Lüdecke T., Foreman A. D., Bourgon N., Duprey N. N., Vonhof H., Souksavatdy V., Bacon A. M., Sigman D. M., Tütken T. & Martínez-García A. (2023). Tooth enamel nitrogen isotope composition records trophic position: a tool for reconstructing food webs. *Communications Biology*, 6(373): 1-13. https://doi.org/10.1038/s42003-023-04744-y

Leitch D. B. & Catania K. C. (2012). Structure, innervation and response properties of integumentary sensory organs in crocodylians. *Journal of Experimental Biology*, 215(23): 4217-4230. https://doi.org/10.1242/jeb.076836

Leite K. J. & Fortier D. C. (2018). The palate and choanae structure of the *Susisuchus anatoceps* (Crocodyliformes, Eusuchia): phylogenetic implications. *PeerJ*, 6: e5372. https://doi.org/10.7717/peerj.5372

Lemoine V. (1883-1884). Note sur l'encéphale du gavial du Mont-Aime, étudié sur trois moulages naturels. *Bulletin de la Société Géologique de France*, 12(3): 158-162.

Less G. & Özcan E. (2012). Bartonian-Priabonian larger benthic foraminiferal events in the Western Tethys. *Austrian Journal of Earth Sciences*, 105(1): 129-140.

Lessner E. J. & Holliday C. M. (2020). A 3D ontogenetic atlas of *Alligator mississippiensis* cranial nerves and their significance for comparative neurology of reptiles. *The Anatomical Record*, 305(10): 2854-2882. https://doi.org/10.1002/ar.24550

Lessner E. J., Elsey R. M. & Holliday C. M. (2022). Ontogeny of the trigeminal system and associated structures in *Alligator mississippiensis*. *Journal of Morphology*, 283(9): 1210-1230. https://doi.org/10.1002/jmor.21498

Lessner E. J., Dollman K. N., Clark J. M., Xu X. & Holliday C. M. (2023). Ecomorphological patterns in trigeminal canal branching among sauropsids reveal sensory shift in suchians. *Journal of Anatomy*, 242(5): 927-952. https://doi.org/10.1111/joa.13826

LeSueur C. A. (1827). Note sur deux espèces de tortues du genere *Trionyx*. *Mémoires du Muséum d'Histoire Naturelle de Paris*, 15: 257-268.

Levinson A. A., Luz B. & Kolodny Y. (1987). Variations in oxygen isotopic compositions of human teeth and urinary stones. *Applied Geochemistry*, 2(4): 367-371. https://doi.org/10.1016/0883-2927(87)90021-7

Lewis J., Pike A. W., Coath C. D. & Evershed R. P. (2017). Strontium concentration, radiogenic ($^{87}Sr/^{86}Sr$) and stable ($\delta^{88}Sr$) strontium isotope systematics in a controlled feeding study. *STAR: Science & Technology of Archaeological Research*, 3(1): 45-57. https://doi.org/10.1080/20548923.2017.1303124

Li J. (1976). Fossil of Sebecosuchia discovered from Nanxiong, Guangdong. *Vertebrata PalAsiatica,* 14:169–74.

Li J. (1984). A new species of *Planocrania* from Hengdong, Hunan. *Vertebrata PalAsiatica*, 22: 123–33.

Li Z. & Clarke J. A. (2015). New insight into the anatomy of the hyolingual apparatus of *Alligator mississippiensis* and implications for reconstructing feeding in extinct archosaurs. *Journal of Anatomy*, 227(1): 45-61. https://doi.org/10.1111/joa.12320

Li J., Wu X. C. & Li X. (1994). New material of *Hsisosuchus chungkingensis* from Sichuan, China. *Vertebrata palasiatica*, 32(2): 107-126.

Li Q., Nava A., Reynard L. M., Thirlwall M., Bondioli L. & Müller W. (2020). Spatially-resolved Ca isotopic and trace element variations in human deciduous teeth record diet and physiological change. *Environmental Archaeology*, 27(5): 474-483. https://doi.org/10.1080/14614103.2020.1758988

Li Y., Sun P., Liu Z., Bai Y., Xu Y., Ma L. & Liu R. (2022). Eocene hyperthermal events in the terrestrial system: Geochronological and astrochronological constraints in the Fushun Basin, NE China. *Marine and Petroleum Geology*, 139: 105604. https://doi.org/10.1016/j.marpetgeo.2022.105604

Lin J., Liu Y., Yang Y. & Hu Z. (2016). Calibration and correction of LA-ICP-MS and LA-MC-ICP-MS analyses for element contents and isotopic ratios. *Solid Earth Sciences*, 1(1): 5-27. https://doi.org/10.1016/j.sesci.2016.04.002

Linnaeus C. (1758). *Systema Naturae per Regna Tria Naturae, Secundum Classes, Ordines, Genera, Species, cum Characteribus, Differentiis, Synonymis, Locis. Editio Decima*, 1: 1-824.

Linscott B., Pike A. W., Angelucci D. E., Cooper M. J., Milton J. S., Matias H. & Zilhão J. (2023). Reconstructing Middle and Upper Paleolithic human mobility in Portuguese Estremadura through laser ablation strontium isotope analysis. *Proceedings of the National Academy of Sciences*, 120(20): e2204501120. https://doi.org/10.1073/pnas.2204501120

Lio G., Agnolín F. L., Valieri R. J., Filippi L. & Rosales D. (2016). A new peirosaurid (Crocodilyformes) from the Late Cretaceous (Turonian–Coniacian) of Patagonia, Argentina. *Historical Biology*, 28(6): 835-841. https://doi.org/10.1080/08912963.2015.1043999

Lio G., Agnolin F. L., Martinelli A. G., Ezcurra M. D. & Novas F. E. (2018). New specimen of the enigmatic, late Cretaceous crocodyliform *Neuquensuchus universitas* sheds light on the anatomy of the species. *Cretaceous Research*, 83: 62-74. https://doi.org/10.1016/j.cretres.2017.09.014

Longinelli A. (1984). Oxygen isotopes in mammal bone phosphate: a new tool for paleohydrological and paleoclimatological research?. *Geochimica et Cosmochimica Acta*, 48(2): 385-390. https://doi.org/10.1016/0016-7037(84)90259-X

Longinelli A. & Nuti S. (1973). Revised phosphate-water isotopic temperature scale. *Earth and Planetary Science Letters*, 19(3): 373-376. https://doi.org/10.1016/0012-821X(73)90088-5

Losos J. B. (2008). Phylogenetic niche conservatism, phylogenetic signal and the relationship between phylogenetic relatedness and ecological similarity among species. *Ecology letters*, 11(10): 995-1003. https://doi.org/10.1111/j.1461-0248.2008.01229.x

Luccisano V., Sudre J. & Lihoreau F. (2020). Revision of the Eocene artiodactyls (Mammalia, Placentalia) from Aumelas and Saint-Martin-de-Londres (Montpellier limestones, Hérault, France) questions the early European artiodactyl radiation. *Journal of Systematic Palaeontology*, 18(19): 1631-1656. https://doi.org/10.1080/14772019.2020.1799253

Luz B. & Kolodny Y. (1985). Oxygen isotope variations in phosphate of biogenic apatites, IV. Mammal teeth and bones. *Earth and Planetary Science Letters*, 75(1): 29-36. https://doi.org/10.1016/0012-821X(85)90047-0

Luz B., Kolodny Y. & Horowitz M. (1984). Fractionation of oxygen isotopes between mammalian bone-phosphate and environmental drinking water. *Geochimica et Cosmochimica Acta*, 48(8): 1689-1693. https://doi.org/10.1016/0016-7037(84)90338-7

MacLeod N. A. & Barton D. R. (1998). Effects of light intensity, water velocity, and species composition on carbon and nitrogen stable isotope ratios in periphyton. *Canadian Journal of Fisheries and Aquatic Sciences*, 55(8): 1919-1925. https://doi.org/10.1139/f98-075

Macrini T. E. (2006). *The Evolution of Endocranial Space in Mammals and Non-mammalian Cynodonts*. Unpublished PhD thesis, The University of Texas, 277 p.

Macrini T. E. (2009). Description of a digital cranial endocast of *Bathygenys reevesi* (Merycoidodontidae; Oreodontoidea) and implications for apomorphy-based diagnosis of isolated, natural endocasts. *Journal of Vertebrate Paleontology*, 29(4): 1199-1211. https://doi.org/10.1671/039.029.0413

Macrini T. E., Rowe T. & Archer M. (2006). Description of a cranial endocast from a fossil platypus, *Obdurodon dicksoni* (Monotremata, Ornithorhynchidae), and the relevance of endocranial characters to monotreme monophyly. *Journal of Morphology*, 267(8): 1000-1015. https://doi.org/10.1002/jmor.10452

Macrini T. E., Rougier G. W. & Rowe T. (2007a). Description of a cranial endocast from the fossil mammal *Vincelestes neuquenianus* (Theriiformes) and its relevance to the evolution of endocranial characters in therians. *The Anatomical Record*, 290(7): 875-892. https://doi.org/10.1002/ar.20551

Macrini T. E., Rowe T. & VandeBerg J. L. (2007b). Cranial endocasts from a growth series of *Monodelphis domestica* (Didelphidae, Marsupialia): a study of individual and ontogenetic variation. *Journal of Morphology*, 268(10): 844-865. https://doi.org/10.1002/jmor.10556

Madzia D., Sachs S., Young M. T., Lukeneder A. & Skupien P. (2021). Evidence of two lineages of metriorhynchid crocodylomorphs in the Lower Cretaceous of the Czech Republic. *Acta Palaeontologica Polonica*, 66(2): 357-367. https://doir.org/10.4202/app.00801.2020

Maganuco S., Dal Sasso C. & Pasini G. (2006). A new large predatory archosaur from the Middle Jurassic of Madagascar. *Atti della Società Italiana di Scienze Naturali e del Museo Civico di Storia Naturale in Milano*, 147(1): 19-51.

Magnusson W. E. & Lima A. P. (1991). The ecology of a cryptic predator, *Paleosuchus trigonatus*, in a tropical rainforest. *Journal of Herpetology*, 25:41-48. https://doi.org/10.2307/1564793

Mahboubi M., Ameur R., Crochet J. Y. & Jaeger J. J. (1984a). Implications paléobiogéographiques de la découverte d'une nouvelle localité éocène à vertébrés continentaux en Afrique nord-occidentale: El Kohol (Sud-Oranais, Algérie). *Geobios*, 17(5): 625-629. https://doi.org/10.1016/S0016-6995(84)80033-9

Mahboubi M., Ameur R., Crochet J. Y. & Jaeger J. J. (1984b). The earliest known Proboscidean from the Lower Eocene of North-West Africa (Algeria). *Nature*, 308: 543-544.

Mahboubi M., Ameur R., Crochet J. Y. & Jaeger J. J. (1986). El Kohol (Saharan atlas, Algeria): a new Eocene mammal locality in northwestern Africa. *Palaeontographica Abteilung A*, 192: 15-49.

Mahboubi S., Bocherens H., Scheffler M., Benammi M. & Jaeger J. J. (2014). Was the Early Eocene proboscidean *Numidotherium koholense* semi-aquatic or terrestrial? Evidence from stable isotopes and bone histology. *Comptes Rendus Palevol*, 13(6): 501-509. https://doi.org/10.1016/j.crpv.2014.01.002

Mamani C. A., Leardi J. M. & Desojo J. B. (2022). Nuevos restos postcraneanos de Crocodylomorpha (Archosauria, Pseudosuchia) de la Formación Los Colorados (Triásico Tardío), provincia de La Rioja, Argentina. *Revista del Museo Argentino de Ciencias Naturales*, 24(1): 47-76.

Manley G. A. (2017). Comparative auditory neuroscience: understanding the evolution and function of ears. *Journal of the Association for Research in Otolaryngology*, 18: 1-24. https://doi.org/10.1007/s10162-016-0579-3

Mannion P. D., Chiarenza A. A., Godoy P. L. & Cheah Y. N. (2019). Spatiotemporal sampling patterns in the 230 million year fossil record of terrestrial crocodylomorphs and their impact on diversity. *Palaeontology*, 62(4): 615-637. https://doi.org/10.1111/pala.12419

Manolagas S. C. (2000). Birth and death of bone cells: basic regulatory mechanisms and implications for the pathogenesis and treatment of osteoporosis. *Endocrine Reviews*, 21(2), 115-137. https://doi.org/10.1210/edrv.21.2.0395

Manzini F. F., Brandt Neto M. & Vizotto L. D. (1996). Cintura pélvica de *Baurusuchus pachecoi* Price, 1945 em sedimentos da Formação Adamantina (Grupo Bauru, Cretáceo Superior). *Boletim do 4º Simpósio Sobre o Cretáceo do Brasil*: 273-276.

Marchetti I., Delcourt R., Tavares S. A., Canalli J., Nascimento P. M. & Ricardi-Branco F. (2022). Morphological and paleohistological description of a new Baurusuchidae specimen from the Adamantina Formation, Upper Cretaceous of Brazil. *Journal of South American Earth Sciences*, 114: 103693. https://doi.org/10.1016/j.jsames.2021.103693

Marinho T. S. & Carvalho I. d. S. (2009). An armadillo-like sphagesaurid crocodyliform from the Late Cretaceous of Brazil. *Journal of South American Earth Sciences*, 27(1): 36-41. https://doi.org/10.1016/j.jsames.2008.11.005

Marinho T. S., Ribeiro L. C. B. & Carvalho I. d. S. (2006). Morfologia de osteodermos de crocodilomorfos do sítio Paleontológico de Peirópolis (Bacia Bauru, Cretáceo Superior). *Anuário do Instituto de Geociências*, 29(2): 44-53.

Marinho T. S., Iori F. V., Carvalho I. d. S. & de Vasconcellos F. M. (2013). *Gondwanasuchus scabrosus* gen. et sp. nov., a new terrestrial predatory crocodyliform (Mesoeucrocodylia: Baurusuchidae) from the Late Cretaceous Bauru Basin of Brazil. *Cretaceous Research*, 44: 104-111. https://doi.org/10.1016/j.cretres.2013.03.010

Marinho T. S., Martinelli A. G., Basilici G., Soares M. V. T., Marconato A., Ribeiro L. C. & Iori F. V. (2022). First Upper Cretaceous notosuchians (Crocodyliformes) from the Uberaba Formation (Bauru Group), southeastern Brazil: enhancing crocodyliform diversity. *Cretaceous Research*, 129: 105000. https://doi.org/10.1016/j.cretres.2021.105000

Marsh O. C. (1874). Small size of the brain in Tertiary mammals. *American Journal of Science and Arts, Series 3*, 8: 66–67. https://doi.org/10.1080/00222937408680947

Marsh O. C. (1877). Notice on some new vertebrate fossils. *American Journal of Arts and Sciences*, 14: 249-256.

Marsh O. C. (1878). Brain of a Fossil Mammal. *Nature*, 17: 340-340. https://doi.org/10.1038/017340a0

Marsh O.C. (1884). A new order of extinct Jurassic reptiles (Macelognatha). *American Journal of Sciences*, 27(3): 341.

Marshall L. G. & Muizon C. de (1988). The dawn of the age of mammals in South-America. *National Geographic Research*, 4(1): 23-55.

Marshall L. G., Muizon C. de & Sigé B. (1983). Late Cretaceous mammals (Marsupialia) from Bolivia. *Geobios*, 16(6): 739-745. https://doi.org/10.1016/S0016-6995(83)80090-4

Marshall L. G. & Muizon C de & Sigogneau-Russell D. (1995). *Pucadelphys andinus* (Marsupialia, Mammalia) from the Early Paleocene of Bolivia. *Mémoires du Muséum national d'Histoire naturelle*, 165:1-164.

Marshall J. D., Brooks J. R. & Lajtha K. (2007). Sources of variation in the stable isotopic composition of plants. In Michener R. & Lajtha K. (eds.) *Stables Isotopes in Ecology and Environmental Science*, Blackwell Publishing: 22-61.

Martin B.G.H. & Bellairs A.D.A. (1977). The narial excrescence and pterygoid bulla of the gharial, *Gavialis gangeticus* (Crocodylia). *Journal of Zoology,* 184: 541-558. https://doi.org/10.1111/j.1469-7998.1977.tb04169.x

Martin E. E. & Macdougall J. D. (1991). Seawater Sr isotopes at the Cretaceous/Tertiary boundary. *Earth and Planetary Science Letters*, 104(2-4): 166-180. https://doi.org/10.1016/0012-821X(91)90202-S

Martin J. E. (2007). New material of the Late Cretaceous globidontan *Acynodon iberoccitanus* (Crocodylia) from southern France. *Journal of Vertebrate Paleontology*, 27(2): 362-372. https://doi.org/10.1671/0272-4634(2007)27[362:NMOTLC]2.0.CO;2

Martin J. E. (2013). Surviving a potentially lethal injury? Bite mark and associated trauma in the vertebra of a dyrosaurid crocodylian. *Palaios*, 28(1): 6-8. https://doi.org/10.2110/palo.2012.p12-068r

Martin J. E. (2014). A sebecosuchian in a middle Eocene karst with comments on the dorsal shield in Crocodylomorpha. *Acta Palaeontologica Polonica*, 60(3): 673-680. https://doi.org/10.4202/app.00072.2014

Martin J. E. (2016). New material of the ziphodont mesoeucrocodylian *Iberosuchus* from the Eocene of Languedoc, southern France. *Annales de Paléontologie,* 102(2): 135-144. https://doi.org/10.1016/j.annpal.2016.05.002

Martin J. E. & Buffetaut E. (2005). An overview of the Late Cretaceous crocodylian assemblage from Cruzy, southern France. *Kaupia*, 14: 33-40.

Martin J. E. & Vincent P. (2013). New remains of *Machimosaurus hugii* von Meyer, 1837 (Crocodilia, Thalattosuchia) from the Kimmeridgian of Germany. *Fossil Record*, 16(2): 179-196. https://doi.org/10.1002/mmng.201300009

Martin J. E. & de Lapparent de Broin F. (2016). A miniature notosuchian with multicuspid teeth from the Cretaceous of Morocco. *Journal of Vertebrate Paleontology*, 36(6): e1211534. https://doi.org/10.1080/02724634.2016.1211534

Martin J. E., Rabi M. & Csiki Z. (2010). Survival of *Theriosuchus* (Mesoeucrocodylia: Atoposauridae) in a Late Cretaceous archipelago: a new species from the Maastrichtian of Romania. *Naturwissenschaften*, 97: 845-854. https://doi.org/10.1007/s00114-010-0702-y

Martin J. E., Rabi M., Csiki-Sava Z. & Vasile Ş. (2014a). Cranial morphology of *Theriosuchus sympiestodon* (Mesoeucrocodylia, Atoposauridae) and the widespread occurrence of Theriosuchus in the Late Cretaceous of Europe. *Journal of Paleontology*, 88(3): 444-456. https://doi.org/10.1666/13-106

Martin J. E., Lauprasert K., Buffetaut E., Liard R. & Suteethorn V. (2014b). A large pholidosaurid in the Phu Kradung Formation of north-eastern Thailand. *Palaeontology*, 57(4): 757-769. https://doi.org/10.1111/pala.12086

Martin J. E., Vance D. & Balter V. (2014c). Natural variation of magnesium isotopes in mammal bones and teeth from two South African trophic chains. *Geochimica et Cosmochimica Acta*, 130: 12-20. https://doi.org/10.1016/j.gca.2013.12.029

Martin J. E., Vincent P. & Falconnet J. (2015a). The taxonomic content of *Machimosaurus* (Crocodylomorpha, Thalattosuchia). *Comptes Rendus Palevol*, 14(4): 305-310. https://doi.org/10.1016/j.crpv.2015.03.006

Martin J. E., Tacail T., Adnet S., Girard C. & Balter V. (2015b). Calcium isotopes reveal the trophic position of extant and fossil elasmobranchs. *Chemical Geology*, 415: 118-125. https://doi.org/10.1016/j.chemgeo.2015.09.011

Martin J. E., Vance D. & Balter V. (2015c). Magnesium stable isotope ecology using mammal tooth enamel. *Proceedings of the National Academy of Sciences*, 112(2): 430-435. https://doi.org/10.1073/pnas.1417792112

Martin J. E., Raslan-Loubatié J. & Mazin J. M. (2016a). Cranial anatomy of *Pholidosaurus purbeckensis* from the Lower Cretaceous of France and its bearing on pholidosaurid affinities. *Cretaceous Research*, 66: 43-59. https://doi.org/10.1016/j.cretres.2016.05.008

Martin J. E., Delfino M., Garcia G., Godefroit P., Berton S. & Valentin X. (2016b). New specimens of *Allodaposuchus precedens* from France: intraspecific variability and the diversity of European Late Cretaceous eusuchians. *Zoological Journal of the Linnean Society*, 176(3): 607-631. https://doi.org/10.1111/zoj.12331

Martin J. E., Tacail T. & Balter V. (2017a). Non-traditional isotope perspectives in vertebrate palaeobiology. *Palaeontology*, 60(4): 485-502. https://doi.org/10.1111/pala.12300

Martin J. E., Vincent P., Tacail T., Khaldoune F., Jourani E., Bardet N. & Balter V. (2017b). Calcium isotopic evidence for vulnerable marine ecosystem structure prior to the K/Pg extinction. *Current Biology*, 27(11): 1641-1644. https://doi.org/10.1016/j.cub.2017.04.043

Martin J. E., Tacail T., Cerling T. E. & Balter V. (2018). Calcium isotopes in enamel of modern and Plio-Pleistocene East African mammals. *Earth and Planetary Science Letters*, 503: 227-235. https://doi.org/10.1016/j.epsl.2018.09.026

Martin J. E., Sarr R. & Hautier L. (2019). A dyrosaurid from the Paleocene of Senegal. *Journal of Paleontology*, 93(2): 343-358. https://doi.org/10.1017/jpa.2018.77

Martin J. E., Smith T., Salaviale C., Adrien J. & Delfino M. (2020a). Virtual reconstruction of the skull of *Bernissartia fagesii* and current understanding of the neosuchian–eusuchian transition. *Journal of Systematic Palaeontology*, 18(13): 1079-1101. https://doi.org/10.1080/14772019.2020.1731722

Martin J. E., Tacail T., Braga J., Cerling T. E. & Balter V. (2020b). Calcium isotopic ecology of Turkana Basin hominins. *Nature Communications*, 11(1): 3587. https://doi.org/10.1038/s41467-020-17427-7

Martin J. E., Hassler A., Montagnac G., Therrien F. & Balter V. (2022). The stability of dinosaur communities before the K− Pg boundary: A perspective from southern Alberta using calcium isotopes as a dietary proxy. *GSA Bulletin*, 134(9-10): 2548-2560. https://doi.org/10.1130/B36222.1

Martin J. E., Pochat-Cottilloux Y., Laurent Y., Perrier V., Robert E. & Antoine P. O. (2023). Anatomy and phylogeny of an exceptionally large sebecid (Crocodylomorpha) from the middle Eocene of southern France. *Journal of Vertebrate Paleontology*, 42(4): e2193828. https://doi.org/10.1080/02724634.2023.2193828

Martin L. D. & West D. L. (1995). The recognition and use of dermestid (Insecta, Coleoptera) pupation chambers in paleoecology. *Palaeogeography, Palaeoclimatology, Palaeoecology*, 113(2-4): 303-310. https://doi.org/10.1016/0031-0182(95)00058-T

Martinelli A. G. & Pais D. F. (2008). A new baurusuchid crocodyliform (Archosauria) from the Late Cretaceous of Patagonia (Argentina). *Comptes Rendus Palevol*, 7(6): 371-381. https://doi.org/10.1016/j.crpv.2008.05.002

Martinelli A. G., Sertich J. J., Garrido A. C. & Praderio Á. M. (2012). A new peirosaurid from the Upper Cretaceous of Argentina: Implications for specimens referred to *Peirosaurus torminni* Price (Crocodyliformes: Peirosauridae). *Cretaceous Research*, 37: 191-200. https://doi.org/10.1016/j.cretres.2012.03.017

Martinelli A. G., Marinho T. S., Iori F. V. & Ribeiro L. C. B. (2018). The first *Caipirasuchus* (Mesoeucrocodylia, Notosuchia) from the Late Cretaceous of Minas Gerais, Brazil: new insights on sphagesaurid anatomy and taxonomy. *PeerJ*, 6: e5594. https://doi.org/10.7717/peerj.5594

Martinelli A. G., Basilici G., Fiorelli L. E., Klock C., Karfunkel J., Diniz A. C., Soares M. V. T., Marconato A., da Silva J. I., Ribeiro L. C. B. & Marinho T. S. (2019). Palaeoecological implications of an Upper Cretaceous tetrapod burrow (Bauru Basin; Peirópolis, Minas Gerais, Brazil). *Palaeogeography, Palaeoclimatology, Palaeoecology*, 528: 147-159. https://doi.org/10.1016/j.palaeo.2019.05.015

Martínez R. N., Apaldetti C., Correa G., Colombi C. E., Fernandez E., Malnis P. S., Praderio A., Abelin D., Benegas L. G., Aguilar-Cameo A. & Alcober O. A. (2015). A new Late Triassic vertebrate assemblage from northwestern Argentina. *Ameghiniana*, 52(4): 379-390. https://doi.org/10.5710/AMGH.27.04.2015.2889

Martínez R. N., Alcober O. A. & Pol D. (2018). A new protosuchid crocodyliform (Pseudosuchia, Crocodylomorpha) from the Norian Los Colorados formation, northwestern Argentina. *Journal of Vertebrate Paleontology*, 38(4): 1-12. https://doi.org/10.1080/02724634.2018.1491047

Martins K. C. (2021). *A new baurusuchid (Crocodyliformes Notosuchia) from the Adamantina Formation (Bauru Group, Late Cretaceous), and a new phylogenetic analysis of notosuchians*. Unpublished master thesis, Universidade Estadual Paulista "Júlio de Mesquita Filho", 130 p.

Marugán-Lobón J., Chiappe L. M. & Farke A. A. (2013). The variability of inner ear orientation in saurischian dinosaurs: testing the use of semicircular canals as a reference system for comparative anatomy. *PeerJ*, 1: e124. https://doi.org/10.7717/peerj.124

Mateus O., Puértolas-Pascual E. & Callapez P. M. (2019). A new eusuchian crocodylomorph from the Cenomanian (Late Cretaceous) of Portugal reveals novel implications on the origin of Crocodylia. *Zoological Journal of the Linnean Society*, 186(2): 501-528.

Mathis C. (1985). Contribution à la connaissance des Mammifères de Robiac (Éocène supérieur): Creodonta et Carnivora. *Bulletin du Muséum national d'histoire naturelle. Section C, Sciences de la terre, paléontologie, géologie, minéralogie*, 7(4): 305-326.

Mathys P., Oetterli C., Stern W. B., Oglesby L., Arx M. H. & Künzli N. (2002). *Elemental Analysis of $PM_{2.5}$ samples collected in the framework of the ECRHS II study*, 55 p.

Mayerl C. J., Brainerd E. L. & Blob R. W. (2016). Pelvic girdle mobility of cryptodire and pleurodire turtles during walking and swimming. *Journal of Experimental Biology*, 219(17): 2650-2658. https://doi.org/10.1242/jeb.141622

McAliley L. R., Willis R. E., Ray D. A., White P. S., Brochu C. A. & Densmore III L. D. (2006). Are crocodiles really monophyletic? —Evidence for subdivisions from sequence and morphological data. *Molecular Phylogenetics and Evolution*, 39(1): 16-32. https://doi.org/10.1016/j.ympev.2006.01.012

McArthur J. M., Howarth R. J. & Bailey T. R. (2001). Strontium isotope stratigraphy: LOWESS version 3: best fit to the marine Sr-isotope curve for 0–509 Ma and accompanying look-up table for deriving numerical age. *The Journal of Geology*, 109(2): 155-170. https://doi.org/10.1086/319243

McKinney C. R., McCrea J. M., Epstein S., Allen H. A. & Urey H. C. (1950). Improvements in mass spectrometers for the measurement of small differences in isotope abundance ratios. *Review of Scientific Instruments*, 21(8): 724-730. https://doi.org/10.1063/1.1745698

Mead G. A. & Hodell D. A. (1995). Controls on the $^{87}Sr/^{86}Sr$ composition of seawater from the middle Eocene to Oligocene: Hole 689B, Maud Rise, Antarctica. *Paleoceanography*, 10(2): 327-346. https://doi.org/10.1029/94PA03069

Mead J. I., Steadman D. W., Bedford S. H., Bell C. J. & Spriggs M. (2002). New extinct mekosuchine crocodile from Vanuatu, South Pacific. *Copeia*, 2002(3): 632-641. https://doi.org/10.1643/0045-8511(2002)002[0632:NEMCFV]2.0.CO;2

Mebert K. (2011). The dice snake, *Natrix tessellata*: biology, distribution and conservation of a Palaearctic species. *Mertensiella*, 18: 1-456.

Megirian D. (1994). A new species of *Quinkana molnar* (Eusuchia: Crocodylidae) from the Miocene Camfield beds of Northern Australia. *The Beagle: Records of the Museums and Art Galleries of the Northern Territory*, 11: 145-166.

Megirian D., Murray P. F. & Willis P. (1991). A new crocodile of the gavial ecomorph morphology from the Miocene of northern Australia. *The Beagle: Records of the Museums and Art Galleries of the Northern Territory*, 8: 135-157.

Melin A. D., Crowley B. E., Brown S. T., Wheatley P. V., Moritz G. L., Yit Yu F. T., Bernard H., DePaolo D. J., Jacobson A. D. & Dominy N. J. (2014). Calcium and carbon stable isotope ratios as paleodietary indicators. American Journal of Physical Anthropology, 154(4): 633-643. https://doi.org/10.1002/ajpa.22530

Melstrom K. M., Turner A. H. & Irmis R. B. (2022). Reevaluation of the cranial osteology and phylogenetic position of the early crocodyliform *Eopneumatosuchus colberti*, with an emphasis on its endocranial anatomy. *The Anatomical Record*, 305(10): 2557-2582. https://doi.org/10.1002/ar.24777

Mennecart B. & Costeur L. (2016). Shape variation and ontogeny of the ruminant bony labyrinth, an example in Tragulidae. *Journal of Anatomy*, 229(3): 422-435. https://doi.org/10.1111/joa.12487

Meredith R. W., Hekkala E. R., Amato G. & Gatesy J. (2011). A phylogenetic hypothesis for *Crocodylus* (Crocodylia) based on mitochondrial DNA: evidence for a trans-Atlantic voyage from Africa to the New World. *Molecular Phylogenetics and Evolution*, 60(1): 183-191. https://doi.org/10.1016/j.ympev.2011.03.026

Messerschmid T. F., Wehling J., Bobon N., Kahmen A., Klak C., Los J. A., Nelson D. B., Santos P. d., de Vos J. M. & Kadereit G. (2021). Carbon isotope composition of plant photosynthetic tissues reflects a Crassulacean Acid Metabolism (CAM) continuum in the majority of CAM lineages. *Perspectives in Plant Ecology, Evolution and Systematics*, 51: 125619. https://doi.org/10.1016/j.ppees.2021.125619

Metzger C. A., Terry D. O. & Grandstaff D. E. (2004). Effect of paleosol formation on rare earth element signatures in fossil bone. *Geology*, 32(6): 497-500. https://doi.org/10.1130/G20376.1

Meunier L. M. (2017). *Phylogeny of Pholidosauridae*. Unpublished PhD thesis, McGill University, 280 p.

Meunier L. M. & Larsson H. C. (2017). Revision and phylogenetic affinities of *Elosuchus* (Crocodyliformes). *Zoological Journal of the Linnean Society*, 179(1): 169-200. https://doi.org/10.1111/zoj.12448

Meunier L. M. & Larsson H. C. (2018). *Trematochampsa taqueti* as a nomen dubium and the crocodyliform diversity of the Upper Cretaceous In Beceten Formation of Niger. *Zoological Journal of the Linnean Society*, 182(3): 659-680. https://doi.org/10.1093/zoolinnean/zlx061

Michard J. G., de Lapparent de Broin F., Brunet M. & Hell J. (1990). Le plus ancien crocodilien néosuchien spécialisé à caractères « eusuchiens » du continent africain (Crétacé inférieur, Cameroun). *Comptes Rendus de l'Académie des Sciences de Paris*, 311: 365-371.

Milián-García Y., Ramos-Targarona R., Pérez-Fleitas E., Sosa-Rodríguez G., Guerra-Manchena L., Alonso-Tabet M., Espinosa-López G. & Russello M. A. (2015). Genetic evidence of hybridization between the critically endangered Cuban crocodile and the American crocodile: implications for population history and in situ/ex situ conservation. *Heredity*, 114(3): 272-280. https://doi.org/10.1038/hdy.2014.96

Milián-García Y., Amato G., Gatesy J., Hekkala E., Rossi N. & Russello M. (2020). Phylogenomics reveals novel relationships among Neotropical crocodiles (*Crocodylus* spp.). *Molecular Phylogenetics and Evolution*, 152: 106924. https://doi.org/10.1016/j.ympev.2020.106924

Missell C. A. (2004). *Thermoregulatory adaptations of* Acrocanthosaurus atokensis *– evidence from oxygen isotopes.* Unpublished master thesis, North Carolina State University, 82 p.

Mitteroecker P., Gunz P., Bernhard M., Schaefer K. & Bookstein F. L. (2004). Comparison of cranial ontogenetic trajectories among great apes and humans. *Journal of Human Evolution*, 46(6): 679-698. https://doi.org/10.1016/j.jhevol.2004.03.006

Mo J., Buffetaut E., Tong H., Amiot R., Cavin L., Cuny G., Suteethorn V. & Jiang S. (2016). Early Cretaceous vertebrates from the Xinlong Formation of Guangxi (southern China): a review. *Geological Magazine*, 153(1): 143-159. https://doi.org/10.1017/S0016756815000394

Molnar R. E. (1981). Pleistocene ziphodont crocodylians of Queensland. *Records of the Australian Museum*, 33(19): 803-834. https://doi.org/10.3853/j.0067-1915.33.1981.198

Molnar R. E. (1982). *Pallimnarchus* and other Cenozoic crocodiles in Queensland. *Memoirs of the Queensland Museum*, 20(3): 657-673.

Molnar R. E. (2010). A new reconstruction of the skull of *Sebecus icaeorhinus* (Crocodyliformes: Sebecosuchia) from the Eocene of Argentina. *Brazilian Geographical Journal: Geosciences and Humanities Research Medium*, 1(2).

Molnar R. E. (2012). Jaw musculature and jaw mechanics of *Sebecus icaeorhinus* Simpson, 1937 (Mesoeucrocodylia, Sebecosuchia). *Earth and Environmental Science Transactions of the Royal Society of Edinburgh*, 103(3-4): 501-519. https://doi.org/10.1017/S1755691013000285

Molnar R. E., Worthy T. & Willis P. M. A. (2002). An extinct Pleistocene endemic mekosuchine crocodylian from Fiji. *Journal of Vertebrate Paleontology*, 22(3): 612-628. https://doi.org/10.1671/0272-4634(2002)022[0612:AEPEMC]2.0.CO;2

Montefeltro F. C. (2019). The osteoderms of baurusuchid crocodyliforms (Mesoeucrocodylia, Notosuchia). *Journal of Vertebrate Paleontology*, 39(2): e1594242. https://doi.org/10.1080/02724634.2019.1594242

Montefeltro F. C., Larsson H. C. & Langer M. C. (2011). A new baurusuchid (Crocodyliformes, Mesoeucrocodylia) from the Late Cretaceous of Brazil and the phylogeny of Baurusuchidae. *PLoS One*, 6(7): e21916. https://doi.org/10.1371/journal.pone.0021916

Montefeltro F. C., Larsson H. C., de França M. A. & Langer M. C. (2013). A new neosuchian with Asian affinities from the Jurassic of northeastern Brazil. *Naturwissenschaften*, 100: 835-841. https://doi.org/10.1007/s00114-013-1083-9

Montefeltro F. C., Andrade D. V. & Larsson H. C. (2016). The evolution of the meatal chamber in crocodyliforms. *Journal of Anatomy*, 228(5): 838-863. https://doi.org/10.1111/joa.12439

Montefeltro F. C., Bronzati M., Langer M. C. & Anelli L. E. (2019). A new specimen of *Susisuchus anatoceps* (Crocodyliformes, Neosuchia) with a non-eusuchian-type palate. *Journal of Vertebrate Paleontology*, 39(5): e1716240. https://doi.org/10.1080/02724634.2019.1716240

Montefeltro F. C., Lautenschlager S., Godoy P. L., Ferreira G. S. & Butler R. J. (2020). A unique predator in a unique ecosystem: modelling the apex predator within a Late Cretaceous crocodyliform-dominated fauna from Brazil. *Journal of Anatomy*, 237(2): 323-333. https://doi.org/10.1111/joa.13192

Montes L., Le Roy N., Perret M., Buffrenil d. V., Castanet J. & Cubo J. (2007). Relationships between bone growth rate, body mass and resting metabolic rate in growing amniotes: a phylogenetic approach. *Biological Journal of the Linnean Society*, 92(1): 63-76. https://doi.org/10.1111/j.1095-8312.2007.00881.x

Mook C. C. (1924). A new crocodylian from Mongolia. *American Museum Novitates,* 117: 1–5.

Mook C. C. (1940). A new fossil crocodilian from Colombia. *Proceedings of the United States National Museum*, 91(3122): 55-61.

Moquet J. S., Bouchez J., Braun J. J., Bogning S., Mbonda A. P., Carretier S., Regard V., Bricquet J. P., Paiz M. C., Mambela E. & Gaillardet J. (2021). Contrasted chemical weathering rates in cratonic basins: the Ogooue and Mbei rivers, Western Central Africa. *Frontiers in Water*, 2: 589070. https://doi.org/10.3389/frwa.2020.589070

Moreau J. D., Fara E., Néraudeau D. & Gand G. (2019). New Hettangian tracks from the Causses Basin (Lozère, southern France) complement the poor fossil record of earliest Jurassic crocodylomorphs in Europe. *Historical Biology*, 31(3): 341-352. https://doi.org/10.1080/08912963.2017.1370587

Morel de Glasville M. (1876). Sur la cavité crânienne et la position du trou optique dans le *Steneosaurus heberti*. *Bulletin de la Société Géologique de France,* 3(4): 342-348.

Morgan J. L., Gordon G. W., Arrua R. C., Skulan J. L., Anbar A. D. & Bullen T. D. (2011). High-precision measurement of variations in calcium isotope ratios in urine by multiple collector inductively coupled plasma mass spectrometry. *Analytical Chemistry*, 83(18): 6956-6962. https://doi.org/10.1021/ac200361t

Morgan J. L., Skulan J. L., Gordon G. W., Romaniello S. J., Smith S. M. & Anbar A. D. (2012). Rapidly assessing changes in bone mineral balance using natural stable calcium isotopes. *Proceedings of the National Academy of Sciences*, 109(25): 9989-9994. https://doi.org/10.1073/pnas.1119587109

Morris Z. S., Vliet K. A., Abzhanov A. & Pierce S. E. (2019). Heterochronic shifts and conserved embryonic shape underlie crocodylian craniofacial disparity and convergence. *Proceedings of the Royal Society B*, 286(1897): 20182389. https://doi.org/10.1098/rspb.2018.2389

Morris Z. S., Vliet K. A., Abzhanov A. & Pierce S. E. (2021). Developmental origins of the crocodylian skull table and platyrostral face. *The Anatomical Record*, 305(10): 2838-2853. https://doi.org/10.1002/ar.24802

Mueller-Töwe I. J. (2005). Phylogenetic relationships of the Thalattosuchia. *Zitteliana A*,45: 211-213.

Mueller-Töwe I. J. (2006a). *Anatomy, phylogeny, and palaeoecology of the basal thalattosuchians (Mesoeucrocodylia) from the Liassic of Central Europe.* Unpublished PhD thesis, Universität Mainz, 369 p.

Mueller-Töwe I. J. (2006b). Feeding options in *Steneosaurus bollensis* (Mesoeucrocodylia, Thalattosuchia). *Hantkeniana,* 5: 46-48.

Muizon C. de (1992). La fauna de mamíferos de Tiupampa (Paleoceno inferior, Formación Santa Lucía), Bolivia. *Fosiles y facies de Bolivia*, 12(3–4): 575-624.

Muizon C. de (1994). A new carnivorous marsupial from the Palaeocene of Bolivia and the problem of marsupial monophyly. *Nature*, 370(6486): 208-211. https://doi.org/10.1038/370208a0

Muizon C. de (1998). *Mayulestes ferox*, a borhyaenoid (Metatheria, Mammalia) from the early Palaeocene of Bolivia. Phylogenetic and paleobiologic implications. *Geodiversitas*, 20(1): 19–142.

Muizon C. de & Marshall L. G. (1987). Le plus ancien Pantodonte (Mammalia) du Crétacé supérieur de Bolivie. *Comptes rendus hebdomadaires des Séances de l'Académie des Sciences*, 304: 205-208.

Muizon C. de & Marshall L. G. (1991). Nouveaux Condylarthres du paléocene inférieur de Tiupampa (Bolivie). *Bulletin du Muséum national d'histoire naturelle. Section C, Sciences de la terre, paléontologie, géologie, minéralogie*, 13(3-4): 201-227.

Muizon C. de & Marshall L. G. (1992). *Alcidedorbignya inopinata* (Mammalia: Pantodonta) from the early Paleocene of Bolivia: phylogenetic and paleobiogeographic implications. *Journal of Paleontology*, 66(3): 499-520. https://doi.org/10.1017/S002233600003403X

Muizon C. de & Cifelli R. L. (2000). The "condylarths" (archaic Ungulata, Mammalia) from the early Palaeocene of Tiupampa (Bolivia): implications on the origin of the South American ungulates. *Geodiversitas*, 22(1): 47-150.

Muizon C. de & Ladevèze S. (2020). Cranial anatomy of *Andinodelphys cochabambensis*, a stem metatherian from the early Palaeocene of Bolivia. *Geodiversitas*, 42(30): 597-739. https://doi.org/10.5252/geodiversitas2020v42a30

Muizon C. de & Billet G. (2022). Dental ontogeny in the early Paleocene placental mammal *Alcidedorbignya inopinata* (Pantodonta) from Tiupampa (Bolivia). *Geodiversitas*, 44(32): 989-1050. https://doi.org/10.5252/geodiversitas2022v44a32

Muizon C. de & Ladevèze S. (2022). New material of *Incadelphys antiquus* (Pucadelphyda, Metatheria, Mammalia) from the early Palaeocene of Bolivia reveals phylogenetic affinities with enigmatic North and South American metatherians. *Geodiversitas*, 44(22): 609-643. https://doi.org/10.5252/geodiversitas2022v44a22

Muizon C. de, Gayet M., Lavenu A., Marshall L. G., Sigé B. & Villaroel C. (1983). Late Cretaceous vertebrates, including mammals, from Tiupampa, southcentral Bolivia. *Geobios*, 16(6): 747-753. https://doi.org/10.1016/S0016-6995(83)80091-6

Muizon C. de, Cifelli R. L. & Bergqvist L. P. (1998). Eutherian tarsals from the early Paleocene of Bolivia. *Journal of Vertebrate Paleontology*, 18(3): 655-663. https://doi.org/10.1080/02724634.1998.10011092

Muizon C. de, Billet G., Argot C., Ladevèze S. & Goussard F. (2015). *Alcidedorbignya inopinata*, a basal pantodont (Placentalia, Mammalia) from the early Palaeocene of Bolivia: anatomy, phylogeny and palaeobiology. *Geodiversitas*, 37(4): 397-634. https://doi.org/10.5252/g2015n4a1

Muizon C. de, Ladevèze S., Selva C., Vignaud R. & Goussard F. (2018). *Allqokirus australis* (Sparassodonta, Metatheria) from the early Palaeocene of Tiupampa (Bolivia) and the rise of the metatherian carnivorous radiation in South America. *Geodiversitas*, 40(3): 363-459. https://doi.org/10.5252/geodiversitas2018v40a16

Muizon C. de, Billet G. & Ladevèze S. (2019). New remains of kollpaniine "condylarths" (Panameriungulata) from the early Palaeocene of Bolivia shed light on hypocone origins and molar proportions among ungulate-like placentals. *Geodiversitas*, 41(1): 841-874. https://doi.org/10.5252/geodiversitas2019v41a25

Mullen T. (2011). *Mastering Blender*. John Wiley & Sons, 704 p.

Müller S. (1846). Ueber den Charakter der Thierwelt auf den lnseln des indischen Archipels, ein Beitrag zur zoologischen Geographie. *Weigmann's Archiv für Naturgeschichte*, 12: 109-128.

Müller R. T. (2022). Olfactory acuity in early sauropodomorph dinosaurs. *Historical Biology*, 34(2): 346-351. https://doi.org/10.1080/08912963.2021.1914600

Murray C. M., Russo P., Zorrilla A. & McMahan C. D. (2019). Divergent morphology among populations of the New Guinea crocodile, *Crocodylus novaeguineae* (Schmidt, 1928): diagnosis of an independent lineage and description of a new species. *Copeia*, 107(3): 517-523. https://doi.org/10.1643/CG-19-240

Nagloo N., Collin S. P., Hemmi J. M. & Hart N. S. (2016). Spatial resolving power and spectral sensitivity of the saltwater crocodile, *Crocodylus porosus*, and the freshwater crocodile, *Crocodylus johnstoni*. *Journal of Experimental Biology*, 219(9): 1394-1404. https://doi.org/10.1242/jeb.135673

Nagy K. A. & Costa D. P. (1980). Water flux in animals: analysis of potential errors in the tritiated water method. *American Journal of Physiology-Regulatory, Integrative and Comparative Physiology*, 238(5): 454-465. https://doi.org/10.1152/ajpregu.1980.238.5.R454

Nakajima Y., Houssaye A. & Endo H. (2014). Osteohistology of the Early Triassic ichthyopterygian reptile *Utatsusaurus hataii*: Implications for early ichthyosaur biology. *Acta Palaeontologica Polonica*, 59(2): 343-352. https://doi.org/10.4202/app.2012.0045

Narváez I., Brochu C. A., Escaso F., Pérez-García A. & Ortega F. (2016). New Spanish Late Cretaceous eusuchian reveals the synchronic and sympatric presence of two allodaposuchids. *Cretaceous Research*, 65: 112-125. https://doi.org/10.1016/j.cretres.2016.04.018

Narváez I., Celis A. D., Escaso F., De Jesús S. M., Pérez-García A., Rodríguez A. & Ortega F. (2021). Redescription and phylogenetic placement of the Spanish middle Eocene eusuchian *Duerosuchus piscator* (Crocodylia, Planocraniidae). *Journal of Vertebrate Paleontology*, 41(3): e1974868. https://doi.org/10.1080/02724634.2021.1974868

Nash D. (1968). A crocodile from the Upper Triassic of Lesotho. *Journal of Zoology*, 156(2): 163-179. https://doi.org/10.1111/j.1469-7998.1968.tb05927.x

Nascimento P. M. & Zaher H. (2010). A new species of *Baurusuchus* (Crocodyliformes, Mesoeucrocodylia) from the Upper Cretaceous of Brazil, with the first complete postcranial skeleton described for the family Baurusuchidae. *Papéis avulsos de Zoologia*, 50: 323-361. https://doi.org/10.1590/S0031-10492010002100001

Nascimento P. M. & Zaher H. (2011). The skull of the Upper Cretaceous baurusuchid crocodile *Baurusuchus albertoi* Nascimento & Zaher 2010, and its phylogenetic affinities. *Zoological Journal of the Linnean Society*, 163(suppl_1): S116-S131. https://doi.org/10.1111/j.1096-3642.2011.00708.x

Navarro T. G., Cerda I. A. & Diego P. (2023). Microstructural characterization and growth dynamics in *Notosuchus terrestris*, a Mesoeucrocodylia crocodyliform from the Upper Cretaceous of Northem Patagonia, Argentina. *Cretaceous Research*, 105607. https://doi.org/10.1016/j.cretres.2023.105607

Neenan J. M., Reich T., Evers S. W., Druckenmiller P. S., Voeten D. F., Choiniere J. N., Barrett P. M., Pierce S. E. & Benson R. B. (2017). Evolution of the sauropterygian labyrinth with increasingly pelagic lifestyles. *Current Biology*, 27(24): 3852-3858. https://doi.org/10.1016/j.cub.2017.10.069

Nelson B. K., DeNiro M. J., Schoeninger M. J., De Paolo D. J. & Hare P. E. (1986). Effects of diagenesis on strontium, carbon, nitrogen and oxygen concentration and isotopic composition of bone. *Geochimica et Cosmochimica Acta*, 50(9): 1941-1949. https://doi.org/10.1016/0016-7037(86)90250-4

Néraudeau D., Allain R., Ballevre M., Batten D. J., Buffetaut E., Colin J. P., Dabard M. P., Daviero-Gomez V., El Albani A., Gomez B., Grosheny D., Le Loeuff J., Leprince A., Martín-Closas C., Masure E., Mazin J. M., Philippe M., Pouech J., Tong H., Tournepiche J. F. & Vullo R. (2012). The Hauterivian–Barremian lignitic bone bed of Angeac (Charente, south-west France): stratigraphical, palaeobiological and palaeogeographical implications. *Cretaceous Research*, 37: 1-14. https://doi.org/10.1016/j.cretres.2012.01.006

Nesbitt S. J. (2009). The early evolution of archosaurs: relationships and the origin of major clades. Unpublished PhD thesis, Columbia University, 656 p.

Nesbitt S. J. (2011). The early evolution of archosaurs: relationships and the origin of major clades. *Bulletin of the American Museum of Natural History*, 352: 1-292.

Nesbitt S. J., Irmis R. B., Lucas S. G. & Hunt A. P. (2005). A giant crocodylomorph from the Upper Triassic of New Mexico. *Paläontologische Zeitschrift*, 79: 471-478. https://doi.org/10.1007/BF02988373

Nesbitt S. J., Turner A. H., Erickson G. M. & Norell M. A. (2006). Prey choice and cannibalistic behaviour in the theropod *Coelophysis*. *Biology Letters*, 2(4): 611-614. https://doi.org/10.1098/rsbl.2006.0524

Nesbitt S. J., Brusatte S. L., Desojo J. B., Liparini A., De França M. A., Weinbaum J. C. & Gower D. J. (2013). Rauisuchia. *Geological Society, London, Special Publications*, 379(1): 241-274. https://doi.org/10.1144/SP379.1

Nesbitt S. J., Stocker M. R., Parker W. G., Wood T. A., Sidor C. A. & Angielczyk K. D. (2018). The braincase and endocast of *Parringtonia gracilis*, a Middle Triassic suchian (Archosaur: Pseudosuchia). *Journal of Vertebrate Paleontology*, 37(1), 122-141. https://doi.org/10.1080/02724634.2017.1393431

Neupane B., Singh B. K., Poudel P., Panthi S. & Khatri N. D. (2020). Habitat occupancy and threat assessment of gharial (*Gavialis gangeticus*) in the Rapti River, Nepal. *Global Ecology and Conservation*, 24: e01270. https://doi.org/10.1016/j.gecco.2020.e01270

Newton E. T. (1888). I. On the skull, brain, and auditory organ of a new species of Pterosaurian (*Scaphognathus purdoni*) from the upper Lias, near Whitby, Yorkshire. *Proceedings of the Royal Society of London*, 43(258-265): 436-440. https://doi.org/10.1098/rspl.1887.0166

Nicholl C. S., Hunt E. S., Ouarhache D. & Mannion P. D. (2021). A second peirosaurid crocodyliform from the Mid-Cretaceous Kem Kem Group of Morocco and the diversity of Gondwanan notosuchians outside South America. *Royal Society Open Science*, 8(10): 211254. https://doi.org/10.1098/rsos.211254

Nicolaï M. P. & Matzke N. J. (2019). Trait-based range expansion aided in the global radiation of Crocodylidae. *Global Ecology and Biogeography*, 28(9): 1244-1258. https://doi.org/10.1111/geb.12929

Niedźwiedzki G., Szrek P., Narkiewicz K., Narkiewicz M. & Ahlberg P. E. (2010). Tetrapod trackways from the early Middle Devonian period of Poland. *Nature*, 463(7277): 43-48. https://doi.org/10.1038/nature08623

Nier A. O. & Hanson E. E. (1936). A mass-spectrographic analysis of the ions produced in HCl under electron impact. *Physical Review*, 50(8): 722-726. https://doi.org/10.1103/PhysRev.50.722

Nieto M. N., Degrange F. J., Sellers K. C., Pol D. & Holliday C. M. (2022). Biomechanical performance of the cranio-mandibular complex of the small notosuchian *Araripesuchus gomesii* (Notosuchia, Uruguaysuchidae). *The Anatomical Record*, 305(10): 2695-2707. https://doi.org/10.1002/ar.24697

Niklaus M. & Kelly S. (2019). The molecular evolution of C4 photosynthesis: opportunities for understanding and improving the world's most productive plants. *Journal of Experimental Botany*, 70(3): 795-804. https://doi.org/10.1093/jxb/ery416

Nixon K. C. (1999). The parsimony ratchet, a new method for rapid parsimony analysis. *Cladistics*, 15(4): 407-414. https://doi.org/10.1006/clad.1999.0121

Nobre P. H. (2004). Morfologia pós-craniana de *Candidodon itapecuruense* (Crocodylomorpha, Mesoeucrocodylia), do Cretáceo do Brasil. *Revista Brasileira de Paleontologia,* 7(1): 87-92.

Nobre P. H. & Carvalho I. d. S. (2006). *Adamantinasuchus navae*: a new gondwanan Crocodylomorpha (Mesoeucrocodylia) from the Late Cretaceous of Brazil. *Gondwana Research*, 10(3-4): 370-378. https://doi.org/10.1016/j.gr.2006.05.008

Nobre P. H. & Carvalho I. d. S. (2013). Postcranial skeleton of *Mariliasuchus amarali* Carvalho and Bertini, 1999 (Mesoeucrocodylia) from the Bauru Basin, Upper Cretaceous of Brazil. *Ameghiniana*, 50(1): 98-113. https://doi.org/10.5710/AMGH.15.8.2012.500

Nobre P. H., Carvalho I. d. S., de Vasconcellos F. M. & Nava W. R. (2007). *Mariliasuchus robustus*, a new Crocodylomorpha (Mesoeucrocodylia) from the Bauru Basin, Brazil. *Anuário do Instituto de Geociências*, 30(1): 38-49.

Nobre P. H., Carvalho I. d. S., de Vasconcellos F. M. & Souto P. R. (2008). Feeding behavior of the Gondwanic Crocodylomorpha *Mariliasuchus amarali* from the Upper Cretaceous Bauru Basin, Brazil. *Gondwana Research*, 13(1): 139-145. https://doi.org/10.1016/j.gr.2007.08.002

Noto C. R. (2022). Specialized Feeding Morphology in the Small Crocodyliform *Scolomastax* and Implications for Woodbine Paleoecology. *The FASEB Journal*, 36(S1). https://doi.org/10.1096/fasebj.2022.36.S1.R4336

Noto C. R., Drumheller S. K., Adams T. L. & Turner A. H. (2020). An enigmatic small neosuchian crocodyliform from the Woodbine Formation of Texas. *The Anatomical Record*, 303(4): 801-812. https://doi.org/10.1002/ar.24174

Novas F. E., Pais D. F., Pol D., Carvalho I. D. S., Scanferla A., Mones A. & Riglos M. S. (2009). Bizarre notosuchian crocodyliform with associated eggs from the Upper Cretaceous of Bolivia. *Journal of Vertebrate Paleontology*, 29(4): 1316-1320. https://doi.org/10.1671/039.029.0409

O'Brien H. D., Lynch L. M., Vliet K. A., Brueggen J., Erickson G. M. & Gignac P. M. (2019). Crocodylian head width allometry and phylogenetic prediction of body size in extinct crocodyliforms. *Integrative Organismal Biology*, 1(1): obz006. https://doi.org/10.1093/iob/obz006

O'Connell T. C., Kneale C. J., Tasevska N. & Kuhnle G. G. (2012). The diet-body offset in human nitrogen isotopic values: A controlled dietary study. *American Journal of Physical Anthropology*, 149(3): 426-434. https://doi.org/10.1002/ajpa.22140

O'Connor P. M., Sertich J. J., Stevens N. J., Roberts E. M., Gottfried M. D., Hieronymus T. L., Jinnah Z. A., Ridgely R., Ngasala S. E. & Temba J. (2010). The evolution of mammal-like crocodyliforms in the Cretaceous Period of Gondwana. *Nature*, 466(7307): 748-751. https://doi.org/10.1038/nature09061

O'Leary M. H. (1988). Carbon isotopes in photosynthesis. *Bioscience*, 38(5): 328-336. https://doi.org/10.2307/1310735

Oaks J. R. (2011). A time-calibrated species tree of Crocodylia reveals a recent radiation of the true crocodiles. *Evolution*, 65(11): 3285-3297. https://doi.org/10.1111/j.1558-5646.2011.01373.x

Olivier C., Houssaye A., Jalil N. E. & Cubo J. (2017). First palaeohistological inference of resting metabolic rate in an extinct synapsid, *Moghreberia nmachouensis* (Therapsida: Anomodontia). *Biological Journal of the Linnean Society*, 121(2): 409-419. https://doi.org/10.1093/biolinnean/blw044

Oppel M. (1811). *Die Ordnungen, Familien und Gattungen der Reptilien als Prodom einer Naturgeschichte Derselben*. Joseph Lindauer, Munich: 12-86.

Oreska M. P., Carrano M. T. & Dzikiewicz K. M. (2013). Vertebrate paleontology of the Cloverly Formation (Lower Cretaceous), I: faunal composition, biogeographic relationships, and sampling. *Journal of Vertebrate Paleontology*, 33(2): 264-292. https://doi.org/10.1080/02724634.2012.717567

Ortega F. (2004). *Historia evolutiva de los cocodrilos mesoeucrocodylia*. Unpublished PhD thesis, Universidad Autonoma de Madrid, 350 p.

Ortega F., Buscalioni A. D. & Gasparini Z. (1996). Reinterpretation and new denomination of *Atacisaurus crassiproratus* (middle Eocene; Issel, France) as cf. *Iberosuchus* (Crocodylomorpha, Metasuchia). *Geobios*, 29(3): 353-364. https://doi.org/10.1016/S0016-6995(96)80037-4

Ortega F., Gasparini Z., Buscalioni A. D. & Calvo J. O. (2000). A new species of *Araripesuchus* (Crocodylomorpha, Mesoeucrocodylia) from the lower Cretaceous of Patagonia (Argentina). *Journal of Vertebrate Paleontology*, 20(1): 57-76. https://doi.org/10.1671/0272-4634(2000)020[0057:ANSOAC]2.0.CO;2

Osborn H. F. (1912). Crania of *Tyrannosaurus* and *Allosaurus*. *Memoirs of the American Museum of Natural History*, 1: 1-30.

Osborn J. W. (1974). On the control of tooth replacement in reptiles and its relationship to growth. *Journal of Theoretical Biology*, 46(2): 509-527. https://doi.org/10.1016/0022-5193(74)90012-5

Ősi A. (2008). Cranial osteology of *Iharkutosuchus makadii*, a Late Cretaceous basal eusuchian crocodyliform from Hungary. *Neues Jahrbuch für Geologie und Paläontologie-Abhandlungen*, 248(3): 279-299. https://doi.org/10.1127/0077-7749/2008/0248-0279

Ősi A. (2014). The evolution of jaw mechanism and dental function in heterodont crocodyliforms. *Historical Biology*, 26(3): 279-414. https://doi.org/10.1080/08912963.2013.777533

Ősi A., Young M. T., Galácz A. & Rabi M. (2018). A new large-bodied thalattosuchian crocodyliform from the Lower Jurassic (Toarcian) of Hungary, with further evidence of the mosaic acquisition of marine adaptations in Metriorhynchoidea. *PeerJ*, 6: e4668. https://doi.org/10.7717/peerj.4668

Osmólska H. (1972). Preliminary note on a crocodylian from the Upper Cretaceous of Mongolia. *Palaeontologica Polonica*, 27: 43-47.

Osmólska H. (2004). Evidence on relation of brain to endocranial cavity in oviraptorid dinosaurs. *Acta Palaeontologica Polonica*, 49(2): 321-324.

Osmólska H., Hua S. & Buffetaut E. (1997). *Gobiosuchus kielanae* [Protosuchia] from the Late Cretaceous of Mongolia: anatomy and relationships. *Acta Palaeontologica Polonica*, 42(2): 257-289.

Osmond C. B., Valaane N., Haslam S. M., Uotila P. & Roksandic Z. (1981). Comparisons of $\delta^{13}C$ values in leaves of aquatic macrophytes from different habitats in Britain and Finland; some implications for photosynthetic processes in aquatic plants. *Oecologia*, 50: 117-124. https://doi.org/10.1007/BF00378804

Ounis A., Kocsis L., Chaabani F. & Pfeifer H. R. (2008). Rare earth elements and stable isotope geochemistry ($\delta^{13}C$ and $\delta^{18}O$) of phosphorite deposits in the Gafsa Basin, Tunisia. *Palaeogeography, Palaeoclimatology, Palaeoecology*, 268(1-2): 1-18. https://doi.org/10.1016/j.palaeo.2008.07.005

Ouwens P. A. (1912). On a large *Varanus* species from the Island of Komodo. *Bulletin du Jardin Botanique de Buitenzorg, Series*, 2(1-6): 1-3.

Owen R. (1842). Report on British fossil reptiles. In Taylor R. & Taylor J. E. (eds.) *British Association for the Advancement of science for 1841.* London.

Owen R. (1850). On the communications between the cavity of the tympanum and the palate in the crocodilia (gavials, alligators and crocodiles). *Philosophical Transactions of the Royal Society of London*, 140: 521-527. https://doi.org/10.1098/rstl.1850.0028

Owen R. (1878). On the fossils called 'granicones': being a contribution to the histology of the exo- skeleton in 'Reptilia'. *Journal of the Royal Microscopical Society,* 1: 222–236.

Padian K. & Lamm E. T. (2013). *Bone histology of fossil tetrapods: advancing methods, analysis, and interpretation*. University of California Press, 285 p.

Padian K., de Ricqlès A. J. & Horner J. R. (2001). Dinosaurian growth rates and bird origins. *Nature*, 412(6845): 405-408. https://doi.org/10.1038/35086500

Padian K., Horner J. R. & de Ricqlès A. (2004). Growth in small dinosaurs and pterosaurs: the evolution of archosaurian growth strategies. *Journal of Vertebrate Paleontology*, 24(3): 555-571. https://doi.org/10.1671/0272-4634(2004)024[0555:GISDAP]2.0.CO;2

Paiva A. L. S., Godoy P. L., Souza R. B., Klein W. & Hsiou A. S. (2022). Body size estimation of Caimaninae specimens from the Miocene of South America. *Journal of South American Earth Sciences*, 118, 103970. https://doi.org/10.1016/j.jsames.2022.103970

Palci A., Hutchinson M. N., Caldwell M. W. & Lee M. S. (2017). The morphology of the inner ear of squamate reptiles and its bearing on the origin of snakes. *Royal Society Open Science*, 4(8): 170685. https://doi.org/10.1098/rsos.170685

Pan T., Miao J. S., Zhang H. B., Yan P., Lee P. S., Jiang X. Y., Ouyang J. H., Deng Y. P., Zhang B. W. & Wu X. B. (2021). Near-complete phylogeny of extant Crocodylia (Reptilia) using mitogenome-based data. *Zoological Journal of the Linnean Society*, 191(4): 1075-1089. https://doi.org/10.1093/zoolinnean/zlaa074

Paolillo A. & Linares O. J. (2007). Nuevos cocodrilos Sebecosuchia del Cenozoico Suramericano (Mesosuchia: Crocodylia). *Contribuciones ocasionales editada por el Laboratorio de Paleobiología*, 3: 1-25.

Paradis E., Claude J. & Strimmer K. (2004). APE: analyses of phylogenetics and evolution in R language. *Bioinformatics*, 20(2): 289-290. https://doi.org/10.1093/bioinformatics/btg412

Parfitt A. M. (2002). Targeted and nontargeted bone remodeling: relationship to basic multicellular unit origination and progression. *Bone*, 30(1): 5-7. https://doi.org/10.1016/S8756-3282(01)00642-1

Parfitt A. M. (2013). Skeletal Heterogeneity and the Purposes of Bone Remodeling: Implications for the Understanding of Osteoporosis. In Marcus R., Feldman D., Dempster D. W., Luckey M. & Cauley J. A. (eds.) *Osteoporosis*, Academic Press: 855-872. https://doi.org/10.1016/B978-0-12-415853-5.00036-4

Parrish J. M. (1987). The origin of crocodylian locomotion. *Paleobiology*, 13(4): 396-414. https://doi.org/10.1017/S0094837300009003

Parrish J. M. (1991). A new specimen of an early crocodylomorph (cf. *Sphenosuchus* sp.) from the Upper Triassic Chinle Formation of Petrified Forest National Park, Arizona. *Journal of Vertebrate Paleontology*, 11(2): 198-212.

Parrish J. M. (1993). Phylogeny of the Crocodylotarsi, with reference to archosaurian and crurotarsan monophyly. *Journal of Vertebrate Paleontology*, 13(3): 287-308. https://doi.org/10.1080/02724634.1993.10011511

Parsons T. S. (1970). The nose and Jacobson's organ, in Gans C. & Parsons T. S.(eds.) *Biology of the Reptilia*, Academic Press, New York: 99-191.

Passey B. H., Robinson T. F., Ayliffe L. K., Cerling T. E., Sponheimer M., Dearing M. D., Roeder B. L. & Ehleringer J. R. (2005). Carbon isotope fractionation between diet, breath CO2, and bioapatite in different mammals. *J. of Archaeol. Sci.*, 32(10): 1459-1470. https://doi.org/10.1016/j.jas.2005.03.015

Passey B. H., Cerling T. E. & Levin N. E. (2007). Temperature dependence of oxygen isotope acid fractionation for modern and fossil tooth enamels. *Rapid Comm. in Mass Spectrometry*, 21(17): 2853-2859. https://doi.org/10.1002/rcm.3149

Pasteris J. D., Wopenka B. & Valsami-Jones E. (2008). Bone and tooth mineralization: why apatite?. *Elements*, 4(2): 97-104. https://doi.org/10.2113/GSELEMENTS.4.2.97

Paulina-Carabajal A. & Canale J. I. (2010). Cranial endocast of the carcharodontosaurid theropod *Giganotosaurus carolinii* Coria & Salgado, 1995. *Neues Jahrbuch fur Geologie und Palaontologie–Abhandlungen,* 258: 249-256. https://doi.org/10.1127/0077-7749/2010/0104

Paulina-Carabajal A. & Succar C. (2014). The endocranial morphology and inner ear of the abelisaurid theropod *Aucasaurus garridoi*. *Acta Palaeontologica Polonica*, 60(1): 141-144. https://doi.org/10.4202/app.2013.0037

Paulina-Carabajal A. & Filippi L. (2018). Neuroanatomy of the abelisaurid theropod *Viavenator*: The most complete reconstruction of a cranial endocast and inner ear for a South American representative of the clade. *Cretaceous Research*, 83: 84-94. https://doi.org/10.1016/j.cretres.2017.06.013

Paulina-Carabajal A. & Nieto M. N. (2019). Brief Comment on the Brain and Inner Ear of *Giganotosaurus carolinii* (Dinosauria: Theropoda) Based on CT scans. *Ameghiniana*, 57(1): 58-62. https://doi.org/10.5710/AMGH.25.10.2019.3237

Pauwels O. S. G., Barr B., Sanchez M. L. & Burger M. (2007). Diet records for the dwarf crocodile, *Osteolaemus tetraspis tetraspis* in Rabi oil fields and Loango National Park, southwestern Gabon. *Hamadryad*, 31(2): 258-264.

Payros A., Orue-Etxebarria X. & Pujalte V. (2006). Covarying sedimentary and biotic fluctuations in Lower–Middle Eocene Pyrenean deep-sea deposits: Palaeoenvironmental implications. *Palaeogeography, Palaeoclimatology, Palaeoecology*, 234(2-4): 258-276. https://doi.org/10.1016/j.palaeo.2005.10.013

Pellegrini M. & Snoeck C. (2016). Comparing bioapatite carbonate pre-treatments for isotopic measurements: Part 2—Impact on carbon and oxygen isotope compositions. *Chemical Geology*, 420: 88-96. https://doi.org/10.1016/j.chemgeo.2015.10.038

Pellegrini R. A., Callahan W. R., Hastings A. K., Parris D. C. & McCauley J. D. (2021). Skeletochronology and paleohistology of *Hyposaurus rogersii* (Crocodyliformes, Dyrosauridae) from the early Paleogene of New Jersey, USA. *Animals*, 11(3067): 1-28. https://doi.org/10.3390/ani11113067https://www.mdpi.com/journal/animals

Pemmer B., Roschger A., Wastl A., Hofstaetter J. G., Wobrauschek P., Simon R., Thaler H. W., Roschger P., Klaushofer K. & Streli C. (2013). Spatial distribution of the trace elements zinc, strontium and lead in human bone tissue. *Bone*, 57(1): 184-193. https://doi.org/10.1016/j.bone.2013.07.038

Peng G. (1995). Late Jurassic protosuchian *Sichuanosuchus huidongensis* (Archosauria: Crocodyliformes) from Zigong, Sichuan, China. *Vertebrata PalAsiatica*, 34: 269-278.

Peng G. & Shu S. (2005). A new species of *Hsisosuchus* from the Late Jurassic of Zigong, Sichuan, China. *Vertebrata palasiatica*, 43(4), 312-324.

Perier A., Lebrun R & Marivaux L. (2016). Different level of intraspecific variation of the bony labyrinth morphology in slow-versus fast-moving primates. *Journal of Mammalian Evolution*, 23(4): 353-368. https://doi.org/10.1007/s10914-016-9323-3

Perini F. A., Macrini T. E., Flynn J. J., Bamba K., Ni X., Croft D. A. & Wyss A. R. (2021). Comparative endocranial anatomy, encephalization, and phylogeny of Notoungulata (Placentalia, Mammalia). *Journal of Mammalian Evolution*, 29: 369-394. https://doi.org/10.1007/s10914-021-09583-4

Perrichon G., Hautier L., Pochat-Cottilloux Y., Raselli I., Salaviale C., Dailh B., Rinder N., Fernandez V., Adrien J., Lachambre J. & Martin J. E. (2023). Ontogenetic variability of the intertympanic sinus distinguishes lineages within Crocodylia. *Journal of Anatomy*: https://doi.org/10.1111/joa.13830

Pickford M. (2018). Freshwater aquatic and aquaphile vertebrates from Black Crow (Ypresian/Lutetian, Namibia) and their palaeoenvironmental significance. *Communications of the Geological Survey of Namibia*, 18: 26-37.

Pierce S. E. & Benton M. J. (2006). *Pelagosaurus typus* Bronn, 1841 (Mesoeucrocodylia: Thalattosuchia) from the Upper Lias (Toarcian, Lower Jurassic) of Somerset, England. *Journal of Vertebrate Paleontology*, 26(3): 621-635. https://doi.org/10.1671/0272-4634(2006)26[621:PTBMTF]2.0.CO;2

Pierce S. E., Angielczyk K. D. & Rayfield E. J. (2009). Morphospace occupation in thalattosuchian crocodylomorphs: skull shape variation, species delineation and temporal patterns. *Palaeontology*, 52(5): 1057-1097. https://doi.org/10.1111/j.1475-4983.2009.00904.x

Pierce S. E., Williams M. & Benson R. B. (2017). Virtual reconstruction of the endocranial anatomy of the early Jurassic marine crocodylomorph *Pelagosaurus typus* (Thalattosuchia). *PeerJ*, 5: e3225. https://doi.org/10.7717/peerj.3225

Pietsch S. J. & Tütken T. (2016). Oxygen isotope composition of North American bobcat (*Lynx rufus*) and puma (*Puma concolor*) bone phosphate: implications for provenance and climate reconstruction. *Isotopes in environmental and health studies*, 52(1-2): 164-184. https://doi.org/10.1080/10256016.2015.1113957

Pinheiro A. E. P., Bertini R. J., Andrade M. D. & Neto R. M. (2008). A new specimen of *Stratiotosuchus maxhechti* (Baurusuchidae, Crocodyliformes) from the Adamantina Formation (Upper Cretaceous), Southeastern Brazil. *Revista Brasileira de Paleontologia*, 11(1): 37-50.

Pinheiro A. E. P., da Costa Pereira P. V. L. G., de Souza R. G., Brum A. S., Lopes R. T., Machado A. S., Bergqvist L. P. & Simbras F. M. (2018). Reassessment of the enigmatic crocodyliform "*Goniopholis*" *paulistanus* Roxo, 1936: Historical approach, systematic, and description by new materials. *Plos One,* 13(8): e0199984. https://doi.org/10.1371/journal.pone.0199984

Pinheiro A. E. P., Souza L. G., Bandeira K. L., Brum A. S., Pereira P. V. L. G., Castro L. O. R., Ramos R. R. C. & Simbras F. M. (2021). The first notosuchian crocodyliform from the Araçatuba Formation (Bauru Group, Paraná Basin), and diversification of sphagesaurians. *Anais da Academia Brasileira de Ciências*, 93(S2): e20201591. https://doi.org/10.1590/0001-3765202120201591

Pinheiro A. E. P., Costa Pereira P. V. L. G., de Vasconcellos F. M., Brum A. S., de Souza L. G., Costa F. R., Castro L. O. R., da Silva K. F. & Bandeira K. L. N. (2023). New Itasuchidae (Sebecia, Ziphosuchia) remains and the radiation of an elusive Mesoeucrocodylia clade. *Historical Biology*, 2023: 1-26. https://doi.org/10.1080/08912963.2022.2139179

Platt S. G., Rainwater T. R., Thorbjarnarson J. B. & Martin D. (2011). Size estimation, morphometrics, sex ratio, sexual size dimorphism, and biomass of *Crocodylus acutus* in the coastal zone of Belize. *Salamandra*, 47(4): 179-192.

Pletsch T., Erbacher J., Holbourn A. E., Kuhnt W., Moullade M., Oboh-Ikuenobede F. E., Söding E. & Wagner T. (2001). Cretaceous separation of Africa and South America: the view from the West African margin (ODP Leg 159). *Journal of South American Earth Sciences*, 14(2): 147-174. https://doi.org/10.1016/S0895-9811(01)00020-7

Plieninger T. (1846). Prof. Dr Th. Plieninger hielt nachstehenden vortrag über ein neues Sauriergenus und die Einreihung der Saurier mit flachen, schneidenden Zähnen in eine Familie. *Württembergische Naturwissenschaftliche Jahreshefte*, 2: 129-183.

Pochat-Cottilloux Y., Martin J. E., Jouve S., Amiot R., Perrichon G., Adrien J., Salaviale C., Muizon C. de & Cespedes R. (2021). 3D models related to the publication: The neuroanatomy of *Zulmasuchus querejazus* (Crocodylomorpha, Sebecidae) and its implications for the paleoecology of sebecosuchians. *MorphoMuseum*, 7: e148. https://doi.org/10.18563/journal.m3.148

Pochat-Cottilloux Y., Allain R. & Lasseron M. (2022a). Microvertebrate fauna from Gadoufaoua (Niger, Aptian, Early Cretaceous). *Comptes Rendus Palevol*, 21(41): 901-926. https://doi.org/10.5852/cr-palevol2022v21a41

Pochat-Cottilloux Y., Martin J. E., Jouve S., Perrichon G., Adrien J., Salaviale C., Muizon C. d., Cespedes R. & Amiot R. (2022b). The neuroanatomy of *Zulmasuchus querejazus* (Crocodylomorpha, Sebecidae) and its implications for the paleoecology of sebecosuchians. *The Anatomical Record*, 305(10): 2708-2728. https://doi.org/10.1002/ar.24826

Pochat-Cottilloux Y., Perrier V., Amiot R. & Martin J. E. (2023a). A peirosaurid mandible from the Albian/Cenomanian (Lower Cretaceous) of Algeria and the taxonomic content of *Hamadasuchus* (Crocodylomorpha, Peirosauridae). *Papers in Palaeontology*, 9(2): e1485. https://doi.org/10.1002/spp2.1485

Pochat-Cottilloux Y., Martin J. E., Amiot R., Cubo J. & de Buffrénil V. d. (2023b). A survey of osteoderm histology and ornamentation among Crocodylomorpha: A new proxy to infer lifestyle?. *Journal of Morphology*, 284(1): e21542. https://doi.org/10.1002/jmor.21542

Pochat-Cottilloux Y., Rinder N., Perrichon G., Adrien J., Amiot R., Hua S. & Martin J. E. (2023c). 3D models related to the publication: The neuroanatomy and pneumaticity of *Hamadasuchus* from the Cretaceous of Morocco and its significance for the paleoecology of Peirosauridae and other altirostral crocodylomorphs. *MorphoMuseum*. https://doi.org/10.18563/journal.m3.183

Pochat-Cottilloux Y., Rinder N., Perrichon G., Adrien J., Amiot R., Hua S. & Martin J. E. (2023d). The neuroanatomy and pneumaticity of *Hamadasuchus* (Crocodylomorpha, Peirosauridae) from the Cretaceous of Morocco and its paleoecological significance for altirostral forms. *Journal of Anatomy*. https://doi.org/10.1111/joa.13887

Pochat-Cottilloux Y., Martin J. E., Faure-Brac M. G., Jouve S., Muizon C. d., Cubo J., Lécuyer C., Fourel F. & Amiot R. (2023e). A multi-isotopic study reveals the palaeoecology of a sebecid from the Paleocene of Bolivia. *Palaeogeography, Palaeoclimatology, Palaeoecology*, 625: 111667. https://doi.org/10.1016/j.palaeo.2023.111667

Poe S. (1996). Data set incongruence and the phylogeny of crocodylians. *Systematic Biology*, 45(4): 393-414. https://doi.org/10.1093/sysbio/45.4.393

Pol D. (2003). New remains of *Sphagesaurus huenei* (Crocodylomorpha: Mesoeucrocodylia) from the late Cretaceous of Brazil. *Journal of Vertebrate Paleontology*, 23(4): 817-831. https://doi.org/10.1671/A1015-7

Pol D. (2005). Postcranial remains of *Notosuchus terrestris* Woodward (Archosauria: Crocodyliformes) from the Upper Cretaceous of Patagonia, Argentina. *Ameghiniana*, 42(1): 21-38.

Pol D. & Norell M. A. (2004a). A new gobiosuchid crocodyliform taxon from the Cretaceous of Mongolia. *American Museum Novitates*, 2004(3458): 1-31. https://doi.org/10.1206/0003-0082(2004)458<0001:ANGCTF>2.0.CO;2

Pol D. & Norell M. A. (2004b). A new crocodyliform from Zos Canyon, Mongolia. *American Museum Novitates*, 2004(3445): 1-36. https://doi.org/10.1206/0003-0082(2004)445<0001:ANCFCM>2.0.CO;2

Pol D. & Apesteguía S. (2005). New *Araripesuchus* remains from the early late cretaceous (Cenomanian–Turonian) of Patagonia. *American Museum Novitates*, 2005(3490): 1-38. https://doi.org/10.1206/0003-0082(2005)490[0001:NARFTE]2.0.CO;2

Pol D. & Gasparini Z. (2009). Skull anatomy of *Dakosaurus andiniensis* (Thalattosuchia: Crocodylomorpha) and the phylogenetic position of Thalattosuchia. *Journal of Systematic Palaeontology,* 7(2): 163-197. https://doi.org/10.1017/S1477201908002605

Pol D. & Powell J. E. (2011). A new sebecid mesoeucrocodylian from the Rio Loro Formation (Palaeocene) of north-western Argentina. *Zoological Journal of the Linnean Society*, 163(suppl_1): S7-S36. https://doi.org/10.1111/j.1096-3642.2011.00714.x

Pol D. & Leardi J. M. (2015). Diversity patterns of Notosuchia (Crocodyliformes, mesoeucrocodylia) during the cretaceous of Gondwana. *Publicación Electrónica de la Asociación Paleontológica Argentina*, 15: 172-186.

Pol D., Ji S. A., Clark J. M. & Chiappe L. M. (2004). Basal crocodyliforms from the Lower Cretaceous Tugulu Group (Xinjiang, China), and the phylogenetic position of *Edentosuchus*. *Cretaceous Research*, 25(4): 603-622. https://doi.org/10.1016/j.cretres.2004.05.002

Pol D., Turner A. H. & Norell M. A. (2009). Morphology of the Late Cretaceous crocodylomorph *Shamosuchus djadochtaensis* and a discussion of neosuchian phylogeny as related to the origin of Eusuchia. *Bulletin of the American Museum of Natural History*, 2009(324): 1-103. https://doi.org/10.1206/0003-0090-324.1.1

Pol D., Leardi J. M., Lecuona A. & Krause M. (2012). Postcranial anatomy of *Sebecus icaeorhinus* (Crocodyliformes, Sebecidae) from the Eocene of Patagonia. *Journal of Vertebrate Paleontology*, 32(2): 328-354. https://doi.org/10.1080/02724634.2012.646833

Pol D., Rauhut O. W., Lecuona A., Leardi J. M., Xu X. & Clark J. M. (2013). A new fossil from the Jurassic of Patagonia reveals the early basicranial evolution and the origins of Crocodyliformes. *Biological Reviews*, 88(4): 862-872. https://doi.org/10.1111/brv.12030

Pol D., Nascimento P. M., Carvalho A. B., Riccomini C., Pires-Domingues R. A. & Zaher H. (2014). A new notosuchian from the Late Cretaceous of Brazil and the phylogeny of advanced notosuchians. *PLoS One*, 9(4): e93105. https://doi.org/10.1371/journal.pone.0093105

Polissar P. J., Fulton J. M., Junium C. K., Turich C. C. & Freeman K. H. (2009). Measurement of ^{13}C and ^{15}N isotopic composition on nanomolar quantities of C and N. *Analytical Chemistry*, 81(2): 755-763. https://doi.org/10.1021/ac801370c

Pomel A. (1847). Notes sur les mammifères et reptiles fossiles des terrains éocènes de Paris, inférieurs au dépôt gypseux. *Archives des Sciences Physiques et Naturelles de Genève*, 4: 326-330.

Poole D. F. G. (1961). Notes on tooth replacement in the Nile crocodile *Crocodilus niloticus*. *Proceedings of the Zoological Society of London*, 136 (1): 131-140. https://doi.org/10.1111/j.1469-7998.1961.tb06083.x

Poplin C. M. (1984). *Lawrenciella schaefferi* ng, n. sp. (Pisces: Actinopterygii) and the use of endocranial characters in the classification of the Palaeonisciformes. *Journal of Vertebrate Paleontology*, 4(3): 413-421. https://doi.org/10.1080/02724634.1984.10012019

Porter W. R., Sedlmayr J. C. & Witmer L. M. (2016). Vascular patterns in the heads of crocodylians: blood vessels and sites of thermal exchange. *Journal of Anatomy*, 229(6): 800-824. https://doi.org/10.1111/joa.12539

Pouech J., Mazin J. M. & Billon-Bruyat J. P. (2006). Microvertebrate biodiversity from Cherves-de-Cognac (Lower Cretaceous, Berriasian: Charente, France). *Mesozoic Terrestrial Ecosystems*, 2006: 96-100.

Pouech J., Amiot R., Lécuyer C., Mazin J. M., Martineau F. & Fourel F. (2014). Oxygen isotope composition of vertebrate phosphates from Cherves-de-Cognac (Berriasian, France): environmental and ecological significance. *Palaeogeography, Palaeoclimatology, Palaeoecology*, 410: 290-299. https://doi.org/10.1016/j.palaeo.2014.05.036

Prasad G. V. & de Lapparent de Broin F. (2002). Late Cretaceous crocodile remains from Naskal (India): comparisons and biogeographic affinities. *Annales de Paléontologie*, 88(1) : 19-71). https://doi.org/10.1016/S0753-3969(02)01036-4

Price L. I. (1945). A new reptile from the Upper Cretaceous of Brazil. *Notas Preliminares e Estudos – Ministério da Agricultura, Divisão de Geologia e Mineralogia*, 25: 1-9.

Price L. I. (1950). On a new crocodylian, *Sphagesaurus*, from the Cretaceous of the State of São Paulo, Brazil. *Anais da Academia Brasileira de Ciências*, 22(1): 77-83.

Price L. I. (1955). Novos crocodilídeos dos arenitos da Série Bauru. Cretáceo do Estado de Minas Gerais. *Anais da Academia brasileira de Ciências*, 27(4): 487-498.

Price L. I. (1959). Sôbre um crocodilídeo Notossúquio do Cretácico Brasileiro. *Boletim do Departamento Nacional da Produçao Mineral, Divisao de Geologia e Mineralogia, Rio de Janeiro*, 188: 7-55.

Price T. D., Johnson C. M., Ezzo J. A., Ericson J. & Burton J. H. (1994a). Residential mobility in the prehistoric southwest United States: a preliminary study using strontium isotope analysis. *Journal of Archaeological Science*, 21(3): 315-330. https://doi.org/10.1006/jasc.1994.1031

Price T. D., Grupe G. & Schröter P. (1994b). Reconstruction of migration patterns in the Bell Beaker period by stable strontium isotope analysis. *Applied Geochemistry*, 9(4): 413-417. https://doi.org/10.1016/0883-2927(94)90063-9

Price T. D., Burton J. H. & Bentley R. A. (2002). The characterization of biologically available strontium isotope ratios for the study of prehistoric migration. *Archaeom.*, 44(1): 117-135. https://doi.org/10.1016/j.jas.2005.03.015

Puértolas E., Canudo J. I. & Cruzado-Caballero P. (2011). A new crocodylian from the Late Maastrichtian of Spain: implications for the initial radiation of crocodyloids. *PLoS One*, 6(6): e20011. https://doi.org/10.1371/journal.pone.0020011

Puértolas-E., Blanco A., Brochu C. A. & Canudo J. I. (2016). Review of the Late Cretaceous-early Paleogene crocodylomorphs of Europe: extinction patterns across the K-PG boundary. *Cretaceous Research*, 57: 565-590. https://doi.org/10.1016/j.cretres.2015.08.002

Puértolas-Pascual E., Serrano-Martínez A., Pérez-Pueyo M., Bádenas B. & Canudo J. I. (2022). New data on the neuroanatomy of basal eusuchian crocodylomorphs (Allodaposuchidae) from the Upper Cretaceous of Spain. *Cretaceous Research*, 135: 105170. https://doi.org/10.1016/j.cretres.2022.105170

Puértolas-Pascual E., Kuzmin I. T., Serrano-Martínez A. & Mateus O. (2023). Neuroanatomy of the crocodylomorph *Portugalosuchus azenhae* from the late cretaceous of Portugal. *Journal of Anatomy*: https://doi.org/10.1111/joa.13836

Pusch L. C., Kammerer C. F. & Fröbisch J. (2019). Cranial anatomy of the early cynodont *Galesaurus planiceps* and the origin of mammalian endocranial characters. *Journal of Anatomy*, 234(5): 592-621. https://doi.org/10.1111/joa.12958

Pyankov V. I., Artyusheva E. G., Edwards G. E., Black C. C. & Soltis P. S. (2001a). Phylogenetic analysis of tribe Salsoleae (Chenopodiaceae) based on ribosomal ITS sequences: implications for the evolution of photosynthesis types. *American Journal of Botany*, 88(7): 1189-1198. https://doi.org/10.2307/3558329

Pyankov V., Ziegler H., Kuz'min A. & Edwards G. (2001b). Origin and evolution of C4 photosynthesis in the tribe Salsoleae (Chenopodiaceae) based on anatomical and biochemical types in leaves and cotyledons. *Plant Systematics and Evolution*, 230: 43-74. https://doi.org/10.1007/s006060170004

Queiroz M. V. L. (2022). *A new Peirosauridae (Crocodyliformes Notosuchia) from the Adamantina Formation (Bauru Group, Late Cretaceous), and a new phylogenetic analysis of notosuchians.* Unpublished master thesis, Universidade Estadual Paulista "Júlio de Mesquita Filho", 118 p.

Quillévéré F., Norris R. D., Kroon D. & Wilson P. A. (2008). Transient ocean warming and shifts in carbon reservoirs during the early Danian. *Earth and Planetary Science Letters*, 265(3-4): 600-615. https://doi.org/10.1016/j.epsl.2007.10.040

R Core Team (2023). *R: A Language and Environment for Statistical Computing. Vienna: R Foundation for Statistical Computing*. Available from: https://www.R-project.org/

Raath M. A. (1981). A protosuchid crocodylian from the Forest Sandstone Formation (upper Karoo) of Zimbabwe. *Palaeontologia africana*, 24: 169-74.

Rabbitt R., Damiano E. & Grant J. W. (2004). Biomechanics of the Semicircular Canals and Otolith Organs, in Highstein S. M., Fay R. R. & Popper A. N. (eds.) *The Vestibular System*, Springer: 153-201. https://doi.org/10.1007/0-387-21567-0_4

Rabi M. & Sebők N. (2015). A revised Eurogondwana model: Late Cretaceous notosuchian crocodyliforms and other vertebrate taxa suggest the retention of episodic faunal links between Europe and Gondwana during most of the Cretaceous. *Gondwana Research*, 28(3): 1197-1211. https://doi.org/10.1016/j.gr.2014.09.015

Rabl-Rückhard H. (1878). Das centralnervensystem des alligators. *Zeitschrift für Wissenschaftliche Zoologie*, 30: 336-375.

Radauscher E. (2015). *Design, Fabrication, and Characterization of Carbon Nanotube Field Emission Device for Advanced Applications*. Unpublished PhD thesis, Duke University, 227 p.

Radinsky L. B. (1968). A new approach to mammalian cranial analysis, illustrated by examples of prosimian primates. *Journal of Morphology*, 124(2): 167-179. https://doi.org/10.1002/jmor.1051240204

Radinsky L. B. (1971). An example of parallelism in carnivore brain evolution. *Evolution*, 25(3): 518-522. https://doi.org/10.2307/2407350

Rage J. C. (1991a). Squamate reptiles from the early Paleocene of the Tiupampa area (Santa Lucia Formation), Bolivia. *Fósiles y facies de Bolivia*, 1: 503-508.

Rage J. C. (1991b). Gymnophionan Amphibia from the Early Paleocene (Santa Lucia Formation) of Tiupampa (Bolivia): the oldest known Gymnophiona. *Revista Técnica de YPFB*, 12: 3-4.

Rana R. S. & Sati K. K. (2000). Late Cretaceous-Palaeocene crocodylians from the Deccan trap-associated sedimentary sequences of peninsular India. *Journal of the Palaeontological Society of India*, 45: 123-136.

Rasmusson Simons E. L. & Buckley G. A. (2009). New material of "*Trematochampsa*" *oblita* (Crocodyliformes, Trematochampsidae) from the Late Cretaceous of Madagascar. *Journal of Vertebrate Paleontology*, 29(2): 599-604. https://doi.org/10.1671/039.029.0224

Rau G. H., Takahashi T., Des Marais D. J., Repeta D. J. & Martin J. H. (1992). The relationship between $\delta^{13}C$ of organic matter and [CO2 (aq)] in ocean surface water: data from a JGOFS site in the northeast Atlantic Ocean and a model. *Geochimica et Cosmochimica Acta*, 56(3): 1413-1419. https://doi.org/10.1016/0016-7037(92)90073-R

Rauhe M. (1990). Habit-habitus-Wechselbeziehung von *Allognathosuchus gaudryi* Stefano 1905 (= *Allognathosuchus haupti* Weitzel 1935). *Geologisches Jahrbuch Hessen*, 118: 53-61.

Rauhe M. & Rossmann T. (1995). News about fossil crocodiles from the middle Eocene of Messel and Geiseltal, Germany. *Hallesches Jahrbuch für Geowissenschaften*, 17: 81–92.

Rauhut O. W. M. & Lopez-Arbarello A. (2005). Wirbeltierreste aus der "mittleren" Kreide des Kem Kem, Marokko. *Freunde der Bayerischen Staatssamlung für Paläontologie und Geologie, Jahresbericht und Mitteilungen,* 34: 41-45.

Rea D. K. (1992). Delivery of Himalayan sediment to the northern Indian Ocean and its relation to global climate, sea level, uplift, and seawater strontium. In Duncan R. A., Rea D. K., Kidd R. B., von Rad U. & Weissel J. K. (eds.) *Synthesis of Results from Scientific Drilling in the Indian Ocean*, American Geophysical Union: 387-402. https://doi.org/10.1029/GM070p0387

Remy J. A. (2015). Les Périssodactyles (Mammalia) du gisement Bartonien supérieur de Robiac (Éocène moyen du Gard, Sud de la France). *Palaeovertebrata*, 39(1): e31-98.

Remy J. A., Krasovec G. & Marandat B. (2016). A new species of *Propalaeotherium* (Palaeotheriidae, Perissodactyla, Mammalia) from the Middle Eocene locality of Aumelas (Hérault, France). *Palaeovertebrata*, 40(2): 1-8. https://doi.org/10.18563/pv.40.2.e1

Remy J. A., Krasovec G., Lopez É., Marandat B. & Lihoreau F. (2019). The Palaeotheriidae (Equoidea, Perissodactyla, Mammalia) from the Eocene fauna of Aumelas (Hérault department, France). *Geodiversitas*, 41(1): 525-585. https://doi.org/10.5252/geodiversitas2019v41a13

Revell L. J. (2009). Size-correction and principal components for interspecific comparative studies. *Evolution*, 63(12): 3258-3268. https://doi.org/10.1111/j.1558-5646.2009.00804.x

Rey K., Amiot R., Fourel F., Abdala F., Fluteau F., Jalil N. E., Liu J., Rubidge B. S., Steyer J. S., Viglietti P. A., Wang X. & Lécuyer C. (2017). Oxygen isotopes suggest elevated thermometabolism within multiple Permo-Triassic therapsid clades. *Elife*, 6: e28589. https://doi.org/10.7554/eLife.28589.001

Rey K., Day M. O., Amiot R., Fourel F., Luyt J., Lécuyer C. & Rubidge B. S. (2020a). Stable isotopes ($\delta^{18}O$ and $\delta^{13}C$) give new perspective on the ecology and diet of *Endothiodon bathystoma* (Therapsida, Dicynodontia)

from the late Permian of the South African Karoo Basin. *Palaeogeography, Palaeoclimatology, Palaeoecology*, 556: 109882. https://doi.org/10.1016/j.palaeo.2020.109882

Rey K., Day M. O., Amiot R., Fourel F., Luyt J., Van den Brandt M. J., Lécuyer C. & Rubidge B. S. (2020b). Oxygen isotopes and ecological inferences of Permian (Guadalupian) tetrapods from the main Karoo Basin of South Africa. *Palaeogeography, Palaeoclimatology, Palaeoecology*, 538: 109485. https://doi.org/10.1016/j.palaeo.2019.109485

Reynard B. & Balter V. (2014). Trace elements and their isotopes in bones and teeth: Diet, environments, diagenesis, and dating of archeological and paleontological samples. *Palaeogeography, Palaeoclimatology, Palaeoecology*, 416: 4-16. https://doi.org/10.1016/j.palaeo.2014.07.038

Reynard B., Lécuyer C. & Grandjean P. (1999). Crystal-chemical controls on rare-earth element concentrations in fossil biogenic apatites and implications for paleoenvironmental reconstructions. *Chemical Geology*, 155(3-4): 233-241. https://doi.org/10.1016/S0009-2541(98)00169-7

Reynard L. M., Henderson G. M. & Hedges R. E. (2010). Calcium isotope ratios in animal and human bone. *Geochimica et Cosmochimica Acta*, 74(13): 3735-3750. https://doi.org/10.1016/j.gca.2010.04.002

Reynard L. M., Pearson J. A., Henderson G. M. & Hedges R. E. (2013). Calcium isotopes in juvenile milk-consumers. *Archaeometry*, 55(5): 946-957. https://doi.org/10.1111/j.1475-4754.2012.00715.x

Ricart R. S. D., Santucci R. M., de Andrade M. B., Oliveira C. E. M., Nava W. R. & Degrazia G. F. (2021). Dental histology of three notosuchians (Crocodylomorpha) from the Bauru Group, Upper Cretaceous, South-eastern Brazil. *Historical Biology*, 33(7): 1012-1023. https://doi.org/10.1080/08912963.2019.1675057

Richman J. M. & Handrigan G. R. (2011). Reptilian tooth development. *Genesis*, 49(4): 247-260. https://doi.org/10.1002/dvg.20721

Riede T., Li Z., Tokuda I. T. & Farmer C. G. (2015). Functional morphology of the *Alligator mississippiensis* larynx with implications for vocal production. *The Journal of Experimental Biology*, 218(7): 991-998. https://doi.org/10.1242/jeb.117101

Riff D. (2003). *Descrição morfológica do crânio e mandíbula de* Stratiotosuchus maxhechti *(Crocodylomorpha, Cretáceo Superior do Brasil) e seu posicion amento filogenético.* Unpublished master thesis, Universidade Federal do Rio de Janeiro, 187 p.

Riff D. & Kellner A. W. A. (2011). Baurusuchid crocodyliforms as theropod mimics: clues from the skull and appendicular morphology of *Stratiotosuchus maxhechti* (Upper Cretaceous of Brazil). *Zoological Journal of the Linnean Society*, 163(suppl_1): S37-S56. https://doi.org/10.1111/j.1096-3642.2011.00713.x

Rio J. P. & Mannion P. D. (2021). Phylogenetic analysis of a new morphological dataset elucidates the evolutionary history of Crocodylia and resolves the long-standing gharial problem. *PeerJ*, 9: e12094. https://doi.org/10.7717/peerj.12094

Ristevski J. (2022). Neuroanatomy of the mekosuchine crocodylian *Trilophosuchus rackhami* Willis, 1993. *Journal of Anatomy*, 241(4): 981-1013. https://doi.org/10.1111/joa.13732

Ristevski J., Young M. T., de Andrade M. B. & Hastings A. K. (2018). A new species of *Anteophthalmosuchus* (Crocodylomorpha, Goniopholididae) from the Lower Cretaceous of the Isle of Wight, United Kingdom, and a review of the genus. *Cretaceous Research*, 84: 340-383. https://doi.org/10.1016/j.cretres.2017.11.008

Ristevski J., Yates A. M., Price G. J., Molnar R. E., Weisbecker V. & Salisbury S. W. (2020). Australia's prehistoric 'swamp king': revision of the Plio-Pleistocene crocodylian genus Pallimnarchus de Vis, 1886. *PeerJ*, 8: e10466. https://doi.org/10.7717/peerj.10466

Ristevski J., Price G. J., Weisbecker V. & Salisbury S. W. (2021). First record of a tomistomine crocodylian from Australia. *Scientific Reports*, 11(1): 12158. https://doi.org/10.1038/s41598-021-91717-y

Ristevski J., Weisbecker V., Scanlon J. D., Price G. J. & Salisbury S. W. (2023a). Cranial anatomy of the mekosuchine crocodylian *Trilophosuchus rackhami* Willis, 1993. *The Anatomical Record*, 306(2): 239-297. https://doi.org/10.1002/ar.25050

Ristevski J., Willis P. M., Yates A. M., White M. A., Hart L. J., Stein M. D., Price G. J. & Salisbury S. W. (2023b). Migrations, diversifications and extinctions: the evolutionary history of crocodyliforms in Australasia. *Alcheringa*: 1-46. https://doi.org/10.1080/03115518.2023.2201319

Rodriguez de La Rosa R.A., Cevallos-Ferriz S.R.S., Silva-Pineda A. (1998). Paleobiological implications of Campanian coprolites. *Palaeogeography, Palaeoclimatology, Palaeoecology,* 142: 231–254. https://doi.org/10.1016/S0031-0182(98)00052-2

Rogers J. V. (2003). *Pachycheilosuchus trinquei*, a new procoelous crocodyliform from the Lower Cretaceous (Albian) Glen Rose Formation of Texas. *Journal of Vertebrate Paleontology*, 23(1): 128-145. https://doi.org/10.1671/0272-4634(2003)23[128:PTANPC]2.0.CO;2

Rohlf F. J. & Slice D. (1990). Extensions of the Procrustes method for the optimal superimposition of landmarks. *Systematic Biology*, 39(1): 40-59. https://doi.org/10.2307/2992207

Romer A. S. (1956). The early evolution of land vertebrates. *Proceedings of the American Philosophical Society*, 100(3): 157-167.

Romer A. S. (1972). The Chañares (Argentina) Triassic reptile fauna. XIII. An early ornithosuchid pseudosuchian, *Gracilisuchus stipanicicorum*, gen. et sp. nov. *Breviora*, 389: 1-24.

Romick C. A. (2013). *Ontogeny of the brain endocasts of ostriches (Aves:* Struthio camelus*) with implications for interpreting extinct dinosaur endocasts*. Unpublished master thesis, Ohio University, 47 p.

Röntgen W. K. (1896). A New Form of Radiation. *Science*, 3: 726-729.

Rooney L. (2018). *Postcranial Morphology and The Locomotor Adaptations of Extant and Extinct Crocodylomorphs and Lepidosaurs*. Unpublished master thesis, East Tennessee State University, 57 p.

Roos J., Aggarwal R. K. & Janke A. (2007). Extended mitogenomic phylogenetic analyses yield new insight into crocodylian evolution and their survival of the Cretaceous–Tertiary boundary. *Molecular Phylogenetics and Evolution*, 45(2): 663-673. https://doi.org/10.1016/j.ympev.2007.06.018

Rossmann T. (1998). Studien an känozoischen Krokodilen: 2. Taxonomische Revision der Familie Pristichampsidae Efimov (Crocodilia: Eusuchia). *Neues Jahrbuch für Geologie und Paläontologie Abhandlungen*, 210: 85–128.

Rossmann T., Rauhe M. & Ortega F. (2000). Studies on Cenozoic crocodiles: 8. *Bergisuchus dietrichbergi* Kuhn (Sebecosuchia: Bergisuchidae n. fam.) from the Middle Eocene of Germany, some new systematic and biological conclusions. *PalZ*, 74: 379-392. https://doi.org/10.1007/BF02988108

Roxo M. G. O. (1936). On a new species of fossil Crocodilia from Brazil, *Goniopholis paulistanus* sp. n. *Anais da Academia Brasileira de Ciências*, 8(1): 33-34.

Rozanski K., Araguas-Araguas L. & Gonfiantini R. (1992). Relation between long-term trends of oxygen-18 isotope composition of precipitation and climate. *Science*, 258(5084): 981-985. https://doi.org/10.1126/science.258.5084.981

Rozanski K., Araguas-Araguas L. & Gonfiantini R. (1993). Isotopic patterns in modern global precipitation. *Climate change in continental isotopic records*, 78: 1-36.

Ruebenstahl A. A., Klein M. D., Yi H., Xu X. & Clark J. M. (2022). Anatomy and relationships of the early diverging Crocodylomorphs *Junggarsuchus sloani* and *Dibothrosuchus elaphros*. *The Anatomical Record*, 305(10): 2463-2556. https://doi.org/10.1002/ar.24949

Ruiz J. V., Bronzati M., Ferreira G. S., Martins K. C., Queiroz M. V., Langer M. C. & Montefeltro F. C. (2021). A new species of *Caipirasuchus* (Notosuchia, Sphagesauridae) from the Late Cretaceous of Brazil and the evolutionary history of Sphagesauria. *Journal of Systematic Palaeontology*, 19(4): 265-287. https://doi.org/10.1080/14772019.2021.1888815

Rummy P., Wu X. C., Clark J. M., Zhao Q., Jin C. Z., Shibata M., Jin F. & Xu X. (2022). A new paralligatorid (Crocodyliformes, Neosuchia) from the mid-Cretaceous of Jilin Province, northeastern China. *Cretaceous Research*, 129: 105018. https://doi.org/10.1016/j.cretres.2021.105018

Rusconi C. (1946). Ave y reptil oligocenos de Mendoza. *Boletin Paleontológico de Buenos Aires*, 21: 1-3.

Russell W. A., Papanastassiou D. A. & Tombrello T. A. (1978). Ca isotope fractionation on the Earth and other solar system materials. *Geochimica et Cosmochimica Acta*, 42(8): 1075-1090. https://doi.org/10.1016/0016-7037(78)90105-9

Russell D. A. & Paesler M. A. (2003). Environments of mid-Cretaceous Saharan dinosaurs. *Cretaceous Research*, 24(5): 569-588. https://doi.org/10.1016/S0195-6671(03)00072-7

Rutherford E. (1911). LXXIX. The scattering of α and β particles by matter and the structure of the atom. *The London, Edinburgh, and Dublin Philosophical Magazine and Journal of Science*, 21(125): 669-688. https://doi.org/10.1080/14786440508637080

Rydberg J., Buckwalter K. A., Caldemeyer K. S., Phillips M. D., Conces Jr D. J., Aisen A. M., Persohn S. A. & Kopecky K. K. (2000). Multisection CT: scanning techniques and clinical applications. *Radiographics*, 20(6): 1787-1806. https://doi.org/10.1148/radiographics.20.6.g00nv071787

Sacco F. (1896). Il coccodrilli del Monte Bolca. *Memorie della Reale Accademia delle Scienze de Torino*, 245: 75–87.

Sachs S., Johnson M. M., Young M. T. & Abel P. (2019). The mystery of *Mystriosaurus*: Redescribing the poorly known Early Jurassic teleosauroid thalattosuchians *Mystriosaurus laurillardi* and *Steneosaurus brevior*. *Acta Palaeontologica Polonica*, 64(3): 565-579. https://doi.org/10.4202/app.00557.2018

Sachs S., Young M. T. & Hornung J. J. (2020). The enigma of *Enaliosuchus*, and a reassessment of the Lower Cretaceous fossil record of Metriorhynchidae. *Cretaceous Research*, 114: 104479. https://doi.org/10.1016/j.cretres.2020.104479

Sachs S., Young M. T., Abel P. & Mallison H. (2021). A new species of *Cricosaurus* (Thalattosuchia, Metriorhynchidae) based upon a remarkably well-preserved skeleton from the Upper Jurassic of Germany. *Palaeontologia Electronica*, 24(2): 1-28. https://doi.org/10.26879/928

Sage R. F. (2004). The evolution of C_4 photosynthesis. *New Phytologist*, 161: 341-370.

Saikia P. K. (2013). Indian Gharial (*Gavialis gangeticus*): Status, Ecology and Conservation. *Rare Animals of India*, 2013: 76-100.

Salih K. O., Evans D. C., Bussert R., Klein N. & Müller J. (2022). *Brachiosuchus kababishensis*, a new long-snouted dyrosaurid (Mesoeucrocodylia) from the Late Cretaceous of north central Sudan. Historical Biology, 34(5), 821-840. https://doi.org/10.1080/08912963.2021.1947513

Salisbury S. W. & Willis P. M. A. (1996). A new crocodylian from the early Eocene of south-eastern Queensland and a preliminary investigation of the phylogenetic relationships of crocodyloids. *Alcheringa*, 20(3): 179-226. https://doi.org/10.1080/03115519608619189

Salisbury S. W., Frey E., Martill D. M. & Buchy M. C. (2003). A new crocodilian from the Lower Cretaceous Crato of north-eastern Brazil. *Palaeontographica. Abteilung A, Palaozoologie – Stratigraphie*, 270(1-3): 3-47. https://doi.org/10.1127/pala/270/2003/3

Salisbury S. W., Molnar R. E., Frey E. & Willis P. M. (2006). The origin of modern crocodyliforms: new evidence from the Cretaceous of Australia. *Proceedings of the Royal Society B: Biological Sciences*, 273(1600): 2439-2448. https://doi.org/10.1098/rspb.2006.3613

Sampson S. D. & Witmer L. M. (2007). Craniofacial anatomy of *Majungasaurus crenatissimus* (Theropoda: Abelisauridae) from the late Cretaceous of Madagascar. *Journal of Vertebrate Paleontology*, 27(S2): 32-104. https://doi.org/10.1671/0272-4634(2007)27[32:CAOMCT]2.0.CO;2

Sander P. M., Klein N., Buffetaut E., Cuny G., Suteethorn V. & Le Loeuff J. (2004). Adaptive radiation in sauropod dinosaurs: bone histology indicates rapid evolution of giant body size through acceleration. *Organisms Diversity & Evolution*, 4(3): 165-173. https://doi.org/10.1016/j.ode.2003.12.002

Sanders R. K. & Smith D. K. (2005). The endocranium of the theropod dinosaur *Ceratosaurus* studied with computer tomography. *Acta Palaeontologica Polonica*, 50(3): 601-616.

Santiago L. A. & Andrés L. A. (2009). Nuevo género de Crocodylia del Eoceno medio de la Península Ibérica (Zamora, España): *Duerosuchus piscator* nov. gen., nov. Sp. *Studia Geologica Salmanticensia*, 45(2): 149-173.

Santos B. R. C. (2014). *Análise dos pós-crânio de* Candidodon itapecuruense *(Crocodyliformes) da Formação Itapecuru, Bacia do Parnaíba.* Unpublished master thesis, Universidade Federale do Rio de Janeiro, 67 p.

Santos B. R. C., Carvalho I. d. S., Medeiros M. A. & Santos R. B. (2011). Dentes de *Candidodon itapecuruense* da Ilha do Cajual (Formação Alcântara), Cretáceo do Maranhão. *Congresso Brasileiro de Paleontologia*, 22: 379-383.

Savage D. E. (1951). Report on Fossil Vertebrates from the Upper Magdalena Valley, Colombia. *Science*, 114(2955): 186-187.

Scavezzoni I. & Fischer V. (2021). The postcranial skeleton of *Cerrejonisuchus improcerus* (Crocodyliformes: Dyrosauridae) and the unusual anatomy of dyrosaurids. *PeerJ*, 9: e11222. https://doi.org/10.7717/peerj.11222

Schade M., Rauhut O. W. & Evers S. W. (2020). Neuroanatomy of the spinosaurid *Irritator challengeri* (Dinosauria: Theropoda) indicates potential adaptations for piscivory. *Scientific Reports*, 10(1): 1-9. https://doi.org/10.1038/s41598-020-66261-w

Schellhorn R. (2017). Intraspecific variation in the domestic cat bony labyrinth revealed by different measurement techniques. *Journal of Morphology*, 279(3): 409-417. https://doi.org/10.1002/jmor.20781

Scheyer T. M. (2007). Skeletal histology of the dermal armor of Placodontia: the occurrence of 'postcranial fibro-cartilaginous bone' and its developmental implications. *Journal of Anatomy*, 211(6): 737-753. https://doi.org/10.1111/j.1469-7580.2007.00815.x

Scheyer T. M. & Sander P. M. (2004). Histology of ankylosaur osteoderms: implications for systematics and function. *Journal of Vertebrate Paleontology*, 24(4): 874-893. https://doi.org/10.1671/0272-4634(2004)024[0874:HOAOIF]2.0.CO;2

Scheyer T. M. & Sanchez-Villagra M. R. (2007). Carapace bone histology in the giant pleurodiran turtle *Stupendemys geographicus*: phylogeny and function. *Acta Palaeontologica Polonica*, 52(1): 137-154.

Scheyer T. M. & Sander P. M. (2007). Shell bone histology indicates terrestrial palaeoecology of basal turtles. *Proceedings of the Royal Society B: Biological Sciences*, 274(1620): 1885-1893. https://doi.org/10.1098/rspb.2007.0499

Scheyer T. M. & Desojo J. B. (2011). Palaeohistology and external microanatomy of rauisuchian osteoderms (Archosauria: Pseudosuchia). *Palaeontology*, 54(6): 1289-1302. https://doi.org/10.1111/j.1475-4983.2011.01098.x

Scheyer T. M. & Cerda I. A. (2021). Testudines. In *Vertebrate Skeletal Histology and Paleohistology*, CRC Press: 385-398.

Scheyer T. M., Sander P. M., Joyce W. G., Böhme W. & Witzel U. (2007). A plywood structure in the shell of fossil and living soft-shelled turtles (Trionychidae) and its evolutionary implications. *Organisms Diversity & Evolution*, 7(2): 136-144. https://doi.org/10.1016/j.ode.2006.03.002

Scheyer T. M., Desojo J. B. & Cerda I. A. (2014). Bone histology of phytosaur, aetosaur, and other archosauriform osteoderms (Eureptilia, Archosauromorpha). *The Anatomical Record*, 297(2): 240-260. https://doi.org/10.1002/ar.22849

Schindelin J., Rueden C. T., Hiner M. C. & Eliceiri K. W. (2015). The ImageJ ecosystem: An open platform for biomedical image analysis. *Molecular Reproduction and Development*, 82(7-8): 518-529. https://doi.org/10.1002/mrd.22489

Schleich H. H. (1994). Neue Reptilienfunde aus dem Tertiär Deutschlands. 13. Schildkröten-une Krokodilreste aus der eozänen Braunkohle des Untertagebaues bei Borken (Hessen) (Reptilia: Crocodylia, Testudines). *Courier Forschung Institut Senckenberg,* 173: 79-101.

Schmidt-Nielsen K. (1997). *Animal physiology: adaptation and environment.* Cambridge.

Schmitz L. (2009). Quantitative estimates of visual performance features in fossil birds. *Journal of Morphology*, 270(6): 759-773. https://doi.org/10.1002/jmor.10720

Schoenemann P. T., Gee J., Avants B., Holloway R. L., Monge J. & Lewis J. (2007). Validation of plaster endocast morphology through 3D CT image analysis. *American Journal of Physical Anthropology*, 132(2): 183-192. https://doi.org/10.1002/ajpa.20499

Schoeninger M. J. & DeNiro M. J. (1984). Nitrogen and carbon isotopic composition of bone collagen from marine and terrestrial animals. *Geochimica et Cosmochimica Acta*, 48(4): 625-639. https://doi.org/10.1016/0016-7037(84)90091-7

Schoeninger M. J., Kohn M. J. & Valley J. W. (2000). Tooth oxygen isotope ratios as paleoclimate monitors in arid ecosystems. In: Ambrose, S.H., Katzenberg, M.A.(Eds.), *Biogeochemical Approaches to Paleodietary Analysis, Advances in Archaeological and Museum Science*. Plenum, New York, pp. 117–140.

Schour I. & Steadman S. R. (1935). The growth and daily rhythm of the incisor of the rat. *Anatomical Record*, 63: 325-333.

Schour I. & Hoffman M. M. (1939). Studies in tooth development II. The rate of apposition of enamel and dentin in man and other mammals. *Journal of Dental Research*, 18(2): 161-175. https://doi.org/10.1177/00220345390180020601

Schulert A. R., Peets E. A., Laszlo D., Spencer H., Charles M. & Samachson J. (1959). Comparative metabolism of strontium and calcium in man. *The International Journal of Applied Radiation and Isotopes*, 4(3-4): 144-153. https://doi.org/10.1016/0020-708X(59)90186-3

Schumacher G. H. (1973). The head muscles and hyolaryngeal skeleton of turtles and crocodylians. *Biology of the Reptilia*, 4: 101-199.

Schütze P., Freitag H. & Weising K. (2003). An integrated molecular and morphological study of the subfamily Suaedoideae Ulbr. (Chenopodiaceae). *Plant Systematics and Evolution*, 239: 257-286. https://doi.org/10.1007/s00606-003-0013-2

Schwab J. A., Young M. T., Neenan J. M., Walsh S. A., Witmer L. M., Herrera Y., Allain R., Brochu C. A., Choiniere J. N., Clark J. M., Dollman K. N., Etches S., Fritsch G., Gignac P. M., Ruebenstahl A., Sachs S., Turner A. H., Vignaud P., Wilberg E. W., Xu X., Zanno L. E. & Brusatte S. L. (2020). Inner ear sensory system changes as extinct crocodylomorphs transitioned from land to water. *Proceedings of the National Academy of Sciences*, 117(19): 10422-10428. https://doi.org/10.1073/pnas.2002146117

Schwab J. A., Young M. T., Herrera Y., Witmer L. M., Walsh S. A., Katsamenis O. L. & Brusatte S. L. (2021a). The braincase and inner ear of '*Metriorhynchus*' cf. '*M.*'*brachyrhynchus*–implications for aquatic sensory adaptations in crocodylomorphs. *Journal of Vertebrate Paleontology*, 41(1): e1912062. https://doi.org/10.1080/02724634.2021.1912062

Schwab J. A., Young M. T., Walsh S. A., Witmer L. M., Herrera Y., Brochu C. A., Butler I. B. & Brusatte S. L. (2021b). Ontogenetic variation in the crocodylian vestibular system. *Journal of Anatomy*, 240(5): 821-832. https://doi.org/10.1111/joa.13601

Schwab J. A., Young M. T., Walsh S. A., Witmer L. M., Herrera Y., Timmons Z. L., Butler I. B. & Brusatte S. L. (2022). 'Ear stones' in crocodylians: a cross-species comparative and ontogenetic survey of otolith structures. *Royal Society Open Science*, 9(3): 211633. https://doi.org/10.1098/rsos.211633

Schwarcz H. P. (1991). Some theoretical aspects of isotope paleodiet studies. *Journal of Archaeological Science*, 18(3): 261-275. https://doi.org/10.1016/0305-4403(91)90065-W

Schwarcz H. P. & Schoeninger M. J. (1991). Stable isotope analyses in human nutritional ecology. *American Journal of Physical Anthropology*, 34(S13): 283-321. https://doi.org/10.1002/ajpa.1330340613

Schwarcz H. P., Dupras T. L. & Fairgrieve S. I. (1999). ^{15}N Enrichment in the Sahara: In Search of a Global Relationship. *Journal of Archaeological Science*, 26(6): 629-636. https://doi.org/10.1006/jasc.1998.0380

Schwartz H. L. & Gillette D. D. (1994). Geology and taphonomy of the Coelophysis quarry, upper Triassic Chinle formation, ghost ranch, New Mexico. *Journal of Paleontology*, 68(5): 1118-1130. https://doi.org/10.1017/S0022336000026718

Schwarz D. (2003). *Konstruktionsmorphologische und evolutionsbiologische Analyse der Dyrosauridae (Crocodilia).* Unpublished PhD thesis, Freie Universität Berlin, 426 p.

Schwarz D. (2014). The feeding apparatus of dyrosaurids (Crocodyliformes). *Geological Magazine*, 151(1): 144-166. https://doi.org/10.1017/S0016756813000460

Schwarz D. & Salisbury S. W. (2005). A new species of *Theriosuchus* (Atoposauridae, Crocodylomorpha) from the late Jurassic (Kimmeridgian) of Guimarota, Portugal. *Geobios,* 38(6): 779-802. https://doi.org/10.1016/j.geobios.2004.04.005

Schwarz D., Frey E. & Martin T. (2006). The postcranial skeleton of the Hyposaurinae (Dyrosauridae; Crocodyliformes). *Palaeontology*, 49(4): 695-718. https://doi.org/10.1111/j.1475-4983.2006.00563.x

Schwarz D., Rees J & Lindgren J. (2009). Lower cretaceous mesoeucrocodylians from Scandinavia (Denmark and Sweden). *Cretaceous Research*, 30(5): 1345-1355. https://doi.org/10.1016/j.cretres.2009.07.011

Schwarz D., Raddatz M. & Wings O. (2017). *Knoetschkesuchus langenbergensis* gen. nov. sp. nov., a new atoposaurid crocodyliform from the Upper Jurassic Langenberg Quarry (Lower Saxony, northwestern Germany), and its relationships to *Theriosuchus. PLoS One*, 12(2): e0160617. https://doi.org/10.1371/journal.pone.0160617

Schwarz-Wings D., Frey E. & Martin T. (2009). Reconstruction of the bracing system of the trunk and tail in hyposaurine dyrosaurids (Crocodylomorpha; Mesoeucrocodylia). Journal of Vertebrate Paleontology, 29(2), 453-472. https://doi.org/10.1671/039.029.0228

Schwenk K. (2008). Comparative anatomy and physiology of chemical senses in nonavian aquatic reptiles. In Thewissen J. G. M. & Nummela S. (eds.) *Sensory evolution on the threshold: adaptations in secondarily aquatic vertebrates*, University of California Press: 65-81.

Scott T. P. & Weldon P. J. (1990). Chemoreception in the feeding behaviour of adult American alligators, *Alligator mississippiensis*. *Animal Behaviour*, 39(2): 398-400. https://doi.org/10.1016/S0003-3472(05)80887-5

Seeley H. G. (1880). Note on the cranial characters of a large teleosaur from the Whitby Lias preserved in the Woodwardian Museum of the University of Cambridge, indicating a new species, *Teleosaurus eucephalus*. *Quarterly Journal of the Geological Society*, 36(1-4): 627-634. https://doi.org/10.1144/GSL.JGS.1880.036.01-04.46

Seeley H. G. (1881). The reptile fauna of the Gosau Formation preserved in the geological museum of the University of Vienna. *Quaternary Journal of the Geological Society of London*, 37: 620-702.

Seidel M. R. (1979). The osteoderms of the American alligator and their functional significance. *Herpetologica*, 35, 4: 375-380.

Sellés A. G., Blanco A., Vila B., Marmi J., López-Soriano F. J., Llácer S., Frigola J., Canals M. & Galobart À. (2020). A small Cretaceous crocodyliform in a dinosaur nesting ground and the origin of sebecids. *Scientific Reports*, 10(1): 15293. https://doi.org/10.1038/s41598-020-71975-y

Sellwood B. W. & Valdes P. J. (2006). Mesozoic climates: General circulation models and the rock record. *Sedimentary geology*, 190(1-4): 269-287. https://doi.org/10.1016/j.sedgeo.2006.05.013

Sena M. V. (2017). Uso de Osteohistologia como um proxy para avaliação de taxas de crescimentos e ontogenia em fósseis de *Pepesuchus deiseae* e *Mariliasuchus amarali* (Mesoeucrocodylia, Notosuchia). Unpublished PhD thesis, Universidade Federal de Pernambuco, 115 p.

Sena M. A., de Andrade R. C. L. P., Bantim R. A. M., Sayão J. M., Barbosa J. A. & Oliveira G. R. (2017). New dyrosaurid remains (crocodyliformes, mesoeucrocodylia) from the Paleocene of the Paraíba basin, ne Brazil. *Revista Brasileira de Paleontologia*, 20(3): 345-354. https://doi.org/10.4072/rbp.2017.3.06

Sena M. V., Andrade R. C., Sayao J. M. & Oliveira G. R. (2018). Bone microanatomy of *Pepesuchus deiseae* (Mesoeucrocodylia, Peirosauridae) reveals a mature individual from the Upper Cretaceous of Brazil. *Cretaceous Research*, 90: 335-348. https://doi.org/10.1016/j.cretres.2018.06.008

Sena M. V., de Andrade R. C. L. P., Carvalho L. B., Azevedo S. A. K., Sayão J. M. & Oliveira G. R. (2022). Paleohistology of the crocodyliform *Mariliasuchus amarali* Carvalho & Bertini, 1999 (Mesoeucrocodylia, Notosuchia) based on a new specimen from the Upper Cretaceous of Brazil. *Comptes Rendus Palevol*, 21(17): 349-361. https://doi.org/10.5852/cr-palevol2022v21a17

Sena M. V., Marinho T. D. S., Montefeltro F. C., Langer M. C., Fachini T. S., Nava W. R., Pinheiro A. E. P., Araújo E. V. d., Aubier P., de Andrade R. C. L. P., Sayão J. M., de Oliveira G. R. & Cubo J. (2023). Osteohistological characterization of notosuchian osteoderms: Evidence for an overlying thick leathery layer of skin. *Journal of Morphology*, 284(1): e21536. https://doi.org/10.1002/jmor.21536

Séon N., Amiot R., Martin J. E., Young M. T., Middleton H., Fourel F., Picot L., Valentin X. & Lécuyer C. (2020). Thermophysiologies of Jurassic marine crocodylomorphs inferred from the oxygen isotope composition of their tooth apatite. *Philosophical Transactions of the Royal Society B*, 375(1793: 20190139. https://doi.org/10.1098/rstb.2019.0139

Séon N., Amiot R., Suan G., Lécuyer C., Fourel F., Demaret F., Vinçon-Laugier A., Charbonnier S. & Vincent P. (2022). Intra-skeletal variability in phosphate oxygen isotope composition reveals regional heterothermies in marine vertebrates. *Biogeosciences*, 19(10): 2671-2681.

Sereno P. C. & Wild R. (1992). *Procompsognathus*: theropod, "thecodont" or both?. *Journal of Vertebrate Paleontology*, 12(4): 435-458. https://doi.org/10.1080/02724634.1992.10011473

Sereno P. & Larsson H. (2009). Cretaceous crocodyliforms from the Sahara. *ZooKeys*, 28: 1-143. https://doi.org/10.3897/zookeys.28.325

Sereno P. C., Dutheil D. B., Iarochene M., Larsson H. C., Lyon G. H., Magwene P. M., Sidor C. A., Varrichio D. J. & Wilson J. A. (1996). Predatory dinosaurs from the Sahara and Late Cretaceous faunal differentiation. *Science*, 272(5264): 986-991. https://doi.org/10.1126/science.272.5264.986

Sereno P. C., Sidor C. A., Larsson H. C. E. & Gado B. (2003). A new notosuchian from the Early Cretaceous of Niger. *Journal of Vertebrate Paleontology*, 23(2): 477-482. https://doi.org/10.1671/0272-4634(2003)023[0477:ANNFTE]2.0.CO;2

Sereno P. C., Wilson J. A., Witmer L. M., Whitlock J. A., Maga A., Ide O. & Rowe T. A. (2007). Structural extremes in a Cretaceous dinosaur. *PloS One*, 2(11): e1230. https://doi.org/10.1371/journal.pone.0001230

Serrano-Martínez A., Knoll F., Narváez I., Lautenschlager S. & Ortega F. (2019a). Inner skull cavities of the basal eusuchian *Lohuecosuchus megadontos* (Upper Cretaceous, Spain) and neurosensorial implications. *Cretaceous Research*, 93: 66-77. https://doi.org/10.1016/j.cretres.2018.08.016

Serrano-Martínez A., Knoll F., Narváez I. & Ortega F. (2019b). Brain and pneumatic cavities of the braincase of the basal alligatoroid *Diplocynodon tormis* (Eocene, Spain). *Journal of Vertebrate Paleontology*, 39(1): e1572612. https://doi.org/10.1080/02724634.2019.1572612

Serrano-Martínez A., Knoll F., Narváez I., Lautenschlager S. & Ortega F. (2020). Neuroanatomical and neurosensorial analysis of the Late Cretaceous basal eusuchian *Agaresuchus fontisensis* (Cuenca, Spain). *Papers in Palaeontology*, 7(1): 641-656. https://doi.org/10.1002/spp2.1296

Sertich J. J. & O'Connor P. M. (2014). A new crocodyliform from the middle Cretaceous Galula Formation, southwestern Tanzania. *Journal of Vertebrate Paleontology*, 34(3): 576-596. https://doi.org/10.1080/02724634.2013.819808

Sewall J. O. (2004). *Early Paleogene climate: causes and consequences.* Unpublished PhD thesis, University of California, 79 p.

Sewall J. O. & Sloan L. C. (2001). Equable Paleogene climates: the result of a stable, positive Arctic oscillation?. *Geophysical Research Letters*, 28(19): 3693-3695. https://doi.org/10.1029/2001GL013776

Sharp Z. D., Atudorei V. & Furrer H. (2000). The effect of diagenesis on oxygen isotope ratios of biogenic phosphates. *American Journal of Science*, 300(3): 222-237. https://doi.org/10.2475/ajs.300.3.222

Shaw H. F. & Wasserburg G. J. (1985). Sm-Nd in marine carbonates and phosphates: Implications for Nd isotopes in seawater and crustal ages. *Geochimica et Cosmochimica Acta*, 49(2): 503-518. https://doi.org/10.1016/0016-7037(85)90042-0

Shemesh A. (1990). Crystallinity and diagenesis of sedimentary apatites. *Geochimica et Cosmochimica Acta*, 54(9): 2433-2438. https://doi.org/10.1016/0016-7037(90)90230-I

Shiller T. A., Porras-Muzquiz H. G. & Lehman T. M. (2016). *Sabinosuchus coahuilensis*, a new dyrosaurid crocodyliform from the Escondido Formation (Maastrichtian) of Coahuila, Mexico. *Journal of Vertebrate Paleontology*, 36(6): e1222586. https://doi.org/10.1080/02724634.2016.1222586

Shirley M. H. & Austin J. D. (2017). Did Late Pleistocene climate change result in parallel genetic structure and demographic bottlenecks in sympatric Central African crocodiles, *Mecistops* and *Osteolaemus*?. *Molecular ecology*, 26(22): 6463-6477. https://doi.org/10.1111/mec.14378

Shirley M. H., Vliet K. A., Carr A. N. & Austin J. D. (2014). Rigorous approaches to species delimitation have significant implications for African crocodylian systematics and conservation. *Proceedings of the Royal Society B: Biological Sciences*, 281(1776): 20132483. https://doi.org/10.1098/rspb.2013.2483

Shirley M. H., Burtner B., Oslisly R., Sebag D. & Testa O. (2017). Diet and body condition of cave-dwelling dwarf crocodiles (*Osteolaemus tetraspis*, Cope 1861) in Gabon. *African Journal of Ecology*, 55(4): 411-422. https://doi.org/10.1111/aje.12365

Shirley M. H., Carr A. N., Nestler J. H., Vliet K. A. & Brochu C. A. (2018). Systematic revision of the living African slender-snouted crocodiles (*Mecistops* Gray, 1844). *Zootaxa*, 4504(2): 151-193. https://doi.org/10.11646/ZOOTAXA.4504.2.1

Sillen A. & Lee-Thorp J. A. (1994). Trace element and isotopic aspects of predator-prey relationships in terrestrial foodwebs. *Palaeogeography, Palaeoclimatology, Palaeoecology*, 107(3-4): 243-255. https://doi.org/10.1016/0031-0182(94)90097-3

Sillen A. & Sealy J. C. (1995). Diagenesis of strontium in fossil bone: a reconsideration of Nelson *et al*. (1986). *Journal of Archaeological Science*, 22(2): 313-320. https://doi.org/10.1006/jasc.1995.0033

Sillen A., Hall G., Richardson S. & Armstrong R. (1998). $^{87}Sr/^{86}Sr$ ratios in modern and fossil food-webs of the Sterkfontein Valley: implications for early hominid habitat preference. *Geochimica et Cosmochimica Acta*, 62(14): 2463-2473. https://doi.org/10.1016/S0016-7037(98)00182-3

Simkiss K. & Wilbur K. M. (1989). *Biomineralization Cell Biology and Mineral Deposition*. Academic Press, San Diego, 337 p.

Simmons D. J. (1965). The non-therapsid reptiles of the Lufeng Basin, Yunnan, China. *Fieldiana: Geology,* 15(1): 1-93.

Simpson G. G. (1937). New reptiles from the Eocene of South America. *American Museum Novitates*, 927: 1-3.

Simpson B. K. & Bezuijen M. R. (2010). Siamese Crocodile *Crocodylus siamensis*. In Manolis S. C. & Stevenson C. (eds.) *Crocodiles. Status Survey and Conservation Action Plan*, Crocodile Specialist Group: 120-126.

Sipla J. S. (2007). *The Semicircular Canals of Birds and Non-Avian Theropod Dinosaurs*. Unpublished PhD thesis, Stony Brook University, 241 p.

Skulan J., DePaolo D. J. & Owens T. L. (1997). Biological control of calcium isotopic abundances in the global calcium cycle. *Geochimica et Cosmochimica Acta*, 61(12): 2505-2510. https://doi.org/10.1016/S0016-7037(97)00047-1

Skulan J. & DePaolo D. J. (1999). Calcium isotope fractionation between soft and mineralized tissues as a monitor of calcium use in vertebrates. *Proceedings of the National Academy of Sciences*, 96(24): 13709-13713. https://doi.org/10.1073/pnas.96.24.13709

Smith B. N. & Epstein S. (1971). Two categories of $^{13}C/^{12}C$ ratios for higher plants. *Plant Physiology*, 47(3): 380-384. https://doi.org/10.1104/pp.47.3.380

Smith R. & Kitching J. (1997). Sedimentology and vertebrate taphonomy of the *Tritylodon* acme zone: a reworked palaeosol in the Lower Jurassic Elliot Formation, Karoo Supergroup, South Africa. *Palaeogeography, Palaeoclimatology, Palaeoecology*, 131(1-2): 29-50. https://doi.org/10.1016/S0031-0182(96)00143-5

Smith N. A. & Clarke J. A. (2012). Endocranial anatomy of the Charadriiformes: sensory system variation and the evolution of wing-propelled diving. *PLoS One*, 7(11): e49584. https://doi.org/10.1371/journal.pone.0049584

Smith D. K., Dufeau D., Sanders K. R., Ridgley R. & Witmer L. (2008). The cranial endocast of *Eutretauranosuchus delfsi* (Crocodyliformes, Goniopholididae) and its relationship to other cephalic spaces. *68th Annual Meeting Society of Vertebrate Paleontology*, Cleveland.

Smith R. M., Marsicano C. A. & Wilson J. A. (2009). Sedimentology and paleoecology of a diverse Early Jurassic tetrapod tracksite in Lesotho, southern Africa. *Palaios*, 24(10): 672-684. https://doi.org/10.2110/palo.2008.p08-115r

Smith T., Kumar K., Rana R. S., Folie A., Solé F., Noiret C., Steeman T., Sahni A. & Rose K. D. (2016). New early Eocene vertebrate assemblage from western India reveals a mixed fauna of European and Gondwana affinities. *Geoscience Frontiers*, 7(6): 969-1001. https://doi.org/10.1016/j.gsf.2016.05.001

Smith K. T., Bhullar B. A. S., Köhler G. & Habersetzer J. (2018). The only known jawed vertebrate with four eyes and the bauplan of the pineal complex. *Current Biology*, 28(7): 1101-1107. https://doi.org/10.1016/j.cub.2018.02.021

Snively E. & Russell A. P. (2007a). Functional morphology of neck musculature in the Tyrannosauridae (Dinosauria, Theropoda) as determined via a hierarchical inferential approach. *Zoological Journal of the Linnean Society*, 151(4): 759-808. https://doi.org/10.1111/j.1096-3642.2007.00334.x

Snively E. & Russell A. P. (2007b). Functional variation of neck muscles and their relation to feeding style in Tyrannosauridae and other large theropod dinosaurs. *The Anatomical Record:* 290(8): 934-957. https://doi.org/10.1002/ar.20563

Snoeck C. & Pellegrini M. (2015). Comparing bioapatite carbonate pre-treatments for isotopic measurements: Part 1—Impact on structure and chemical composition. *Chemical Geology*, 417: 394-403. https://doi.org/10.1016/j.chemgeo.2015.10.004

Soares D. (2002). An ancient sensory organ in crocodylians. *Nature*, 417(6886): 241-242. https://doi.org/10.1038/417241a

Soto M., Pol D. & Perea D. (2011). A new specimen of *Uruguaysuchus aznarezi* (Crocodyliformes: Notosuchia) from the middle Cretaceous of Uruguay and its phylogenetic relationships. *Zoological Journal of the Linnean Society*, 163(suppl_1): S173-S198. https://doi.org/10.1111/j.1096-3642.2011.00717.x

Souza R. G. D., Figueiredo R. G., Azevedo S. A., Riff D. & Kellner A. W. (2020a). Systematic revision of *Sarcosuchus hartti* (Crocodyliformes) from the Recôncavo Basin (Early Cretaceous) of Bahia, north-eastern Brazil. *Zoological Journal of the Linnean Society*, 188(2): 552-578. https://doi.org/10.1093/zoolinnean/zlz057

Souza R. G. D., Hörmanseder B. M., Figueiredo R. G. & Campos D. D. A. (2020b). Description of new dyrosaurid specimens from the Late Cretaceous–Early Paleogene of New Jersey, United States, and comments on *Hyposaurus* systematics. *Historical Biology*, 32(10): 1377-1393. https://doi.org/10.1080/08912963.2019.1593403

Spiekman S. N. F. (2023). A revision and histological investigation of *Saltoposuchus connectens* (Archosauria: Crocodylomorpha) from the Norian (Late Triassic) of south-western Germany. *Zoological Journal of the Linnean Society*. https://doi.org/10.1093/zoolinnean/zlad035

Spindler F., Lauer R., Tischlinger H. & Mäuser M. (2021). The integument of pelagic crocodylomorphs (Thalattosuchia: Metriorhynchidae). *Palaeontologia Electronica*, 24(2): 1-41. https://doi.org/10.26879/1099

Spix J. B. v. (1825). *Animalia nova sive Species novae Lacertarum, quas in Intinere per Brasiliam Annis 1817-1820 jussu et auspiciis Maximiliani Josephi I. Bavariae regis suscepto collegit et descripsit Dr. J. B. de Spix*. Munich, Germany.

Stanton K. J. (2006). *Stable oxygen and carbon isotope analyses of extinct archosaurs (Dinosauria) and their closest extant relatives, ratite birds and crocodylians.* PhD thesis. University of California, Davis. 164 pp.

Stefanic C. M., Nestler J. H., Seiffert E. R. & Turner A. H. (2019). New crocodylomorph material from the Fayum depression, Egypt, including the first occurrence of a sebecosuchian in African late Eocene deposits. *Journal of Vertebrate Paleontology*, 39(6): e1729781. https://doi.org/10.1080/02724634.2019.1729781

Steiger S. S., Fidler A. E., Valcu M. & Kempenaers B. (2008). Avian olfactory receptor gene repertoires: evidence for a well-developed sense of smell in birds?. *Proceedings of the Royal Society B: Biological Sciences*, 275(1649): 2309-2317. https://doi.org/10.1098/rspb.2008.0607

Stein M., Salisbury S. W., Hand S. J. Archer M. & Godthelp H. (2012). Humeral morphology of the early Eocene mekosuchine crocodylian *Kambara* from the Tingamarra Local Fauna southeastern Queensland, Australia. *Alcheringa*, 36(4): 473-486. https://doi.org/10.1080/03115518.2012.671697

Stein M., Archer M. & Hand S. J. (2015). Dwarfism and feeding behaviours in Oligo-Miocene crocodiles from Riversleigh, northwestern Queensland, Australia. *Acta Palaeontologica Polonica*, 61(1): 135-142. https://doi.org/10.4202/app.00134.2014

Stein M., Hand S. J. & Archer M. (2016). A new crocodile displaying extreme constriction of the mandible, from the late Oligocene of Riversleigh, Australia. *Journal of Vertebrate Paleontology*, 36(5): e1179041. https://doi.org/10.1080/02724634.2016.1179041

Stein M., Yates A., Hand S. J. & Archer M. (2017). Variation in the pelvic and pectoral girdles of Australian Oligo–Miocene mekosuchine crocodiles with implications for locomotion and habitus. *PeerJ*, 5: e3501. https://doi.org/10.7717/peerj.3501

Stein M. D., Hand S. J., Archer M., Wroe S. & Wilson L. A. (2020). Quantitatively assessing mekosuchine crocodile locomotion by geometric morphometric and finite element analysis of the forelimb. *PeerJ*, 8: e9349. https://doi.org/10.7717/peerj.9349

Stensiö E.A. (1963). The brain and cranial nerves in fossil lower craniate vertebrates. *Skrifter utgitt av Det Norske Videnskaps-Akademi i Oslo. I. Matematisk-naturvidenskapelig klasse Ny*, 13: 1–120.

Stevens K. A. (2006). Binocular vision in theropod dinosaurs. *Journal of Vertebrate Paleontology*, 26(2): 321-330. https://doi.org/10.1671/0272-4634(2006)26[321:BVITD]2.0.CO;2

Stevens N. J., Hill R. V., Al-Wosabi M., Schulp A., As-Saruri M., Al-Nimey F., Jolley L. A., Schulp-Stuip Y. & O'Connor P. (2013). A middle Eocene mesoeucrocodylian (Crocodyliformes) from the Kaninah Formation, Republic of Yemen. *Geologos*, 19(3): 175-183.

Stevenson C. & Whitaker R. (2010). Indian Gharial *Gavialis gangeticus*. In Manolis S. C. & Stevenson C. (eds.) *Crocodiles. Status Survey and Conservation Action Plan*. Crocodile Specialist Group: 139-143.

Stewart R. J., Hallet B., Zeitler P. K., Malloy M. A., Allen C. M. & Trippett D. (2008). Brahmaputra sediment flux dominated by highly localized rapid erosion from the easternmost Himalaya. *Geology*, 36(9): 711-714. https://doi.org/10.1130/G24890A.1

Steyer J. S., Laurin M., Castanet J. & de Ricqlès A. (2004). First histological and skeletochronological data on temnospondyl growth: palaeoecological and palaeoclimatological implications. *Palaeogeography, Palaeoclimatology, Palaeoecology*, 206(3-4): 193-201. https://doi.org/10.1016/j.palaeo.2004.01.003

Stibbe E. P. (1928). A comparative study of the nictitating membrane of birds and mammals. *Journal of Anatomy*, 62(2): 159-176.

Stockdale M. T. & Benton M. J. (2021). Environmental drivers of body size evolution in crocodile-line archosaurs. *Communications biology*, 4(38): 1-11. https://doi.org/10.1038/s42003-020-01561-5

Stockdale M. T. & Benton M. J. (2022). Reply to: 'Reconstructed evolutionary patterns from crocodile-line archosaurs demonstrate the impact of failure to log-transform body size data'. *Communications biology*, 5(170): 1-4. https://doi.org/10.1038/s42003-022-03072-x

Storrs G. W., Lucas S. G. & Schoch R. M. (1983). Endocranial cast of an early Paleocene crocodylian from the San Juan basin, New Mexico. *Copeia*, 1983(3): 842-845. https://doi.org/10.2307/1444362

Storrs G. W. (1986). A Dyrosaurid Crocodile (Crocodylia: Mesosuchia) from the Paleocene of Pakistan. *Postilla*, 197: 1-16.

Stoskopf M. K., Barrick R. E. & Showers W. J. (2001). Oxygen isotope variability in bones of wild caught and constant temperature reared sub-adult American alligators. *Journal of Thermal Biology*, 26(3): 183-191. https://doi.org/10.1016/S0306-4565(00)00041-3

Straehl F. R., Scheyer T. M., Forasiepi A. M., MacPhee R. D. & Sanchez-Villagra M. R. (2013). Evolutionary patterns of bone histology and bone compactness in xenarthran mammal long bones. *PLoS One*, 8(7): e69275. https://doi.org/10.1371/journal.pone.0069275

Stromer E. V. (1914). Ergebnisse der Forschungreisen Prof. E. Stromers in den Wusten Agyptens: II. Wirbeltier-Reste der Baharije-Stufe (unterstes Cenoman). 1. Einleitung und 2. *Libycosuchus*. *Abhandlungen der Koniglichen Bayerischen Akademie der Wissenschaften, Mathematisch-Physikalischen Klasse* 27(3):1-15.

Stubbs T. L., Pierce S. E., Rayfield E. J. & Anderson P. S. (2013). Morphological and biomechanical disparity of crocodile-line archosaurs following the end-Triassic extinction. *Proceedings of the Royal Society B: Biological Sciences*, 280(1770): 20131940. https://doi.org/10.1098/rspb.2013.1940

Suarez C. A. & Kohn M. J. (2020). Caught in the act: A case study on microscopic scale physicochemical effects of fossilization on stable isotopic composition of bone. *Geochimica et Cosmochimica Acta*, 268: 277-295. https://doi.org/10.1016/j.gca.2019.10.008

Sudre J. (1969). Les gisements de Robiac (Eocène supérieur) et leurs faunes de Mammifères. *Palaeovertebrata,* 2: 95-156.

Sudre J. (1980). *Aumelasia gabineaudi* n g. n sp. nouveau Dichobunidae (Artiodactyla, Mammalia) du gisement d'Aumelas (Hérault) d'âge Lutétien terminal. *Palaeovertebrata*, 9: 197–211.

Sues H. D., Shubin N. H., Olsen P. E. & Amaral W. W. (1996). On the cranial structure of a new protosuchid (Archosauria: Crocodyliformes) from the McCoy Brook Formation (Lower Jurassic) of Nova Scotia, Canada. *Journal of Vertebrate Paleontology*, 16(1): 34-41. https://doi.org/10.1080/02724634.1996.10011281

Sues H. D., Olsen P. E., Carter J. G. & Scott D. M. (2003). A new crocodylomorph archosaur from the Upper Triassic of North Carolina. *Journal of Vertebrate Paleontology*, 23(2): 329-343. https://doi.org/10.1671/0272-4634(2003)023[0329:ANCAFT]2.0.CO;2

Sweetman S. C., Pedreira-Segade U. & Vidovic S. U. (2014). A new bernissartiid crocodyliform from the Lower Cretaceous Wessex Formation (Wealden Group, Barremian) of the Isle of Wight, southern England. *Acta Palaeontologica Polonica*, 60(2): 257-268. https://doi.org/10.4202/app.00038.2013

Swinton W. E. (1930). On the fossil Reptilia from Sokoto Province. *Geological Survey of Nigeria*, 13: 1-62.

Swofford D. L. & Maddison W. P. (1987). Reconstructing ancestral character states under Wagner parsimony. *Mathematical biosciences*, 87(2): 199-229. https://doi.org/10.1016/0025-5564(87)90074-5

Sylvester P. J. (2008). LA-(MC)-ICP-MS trends in 2006 and 2007 with particular emphasis on measurement uncertainties. *Geostandards and Geoanalytical Research*, 32(4): 469-488. https://doi.org/10.1111/j.1751-908X.2008.00924.x

Tacail T. (2017). *Physiologie isotopique du Calcium chez les mammifères*. Unpublished PhD thesis, Ecole Normale Supérieure de Lyon, 220 p.

Tacail T., Albalat E., Télouk P. & Balter V. (2014). A simplified protocol for measurement of Ca isotopes in biological samples. *Journal of Analytical Atomic Spectrometry*, 29(3): 529-535. https://doi.org/10.1039/C3JA50337B

Tacail T., Télouk P. & Balter V. (2016). Precise analysis of calcium stable isotope variations in biological apatites using laser ablation MC-ICPMS. *Journal of Analytical Atomic Spectrometry*, 31(1): 152-162. https://doi.org/10.1039/C5JA00239G

Tacail T., Thivichon-Prince B., Martin J. E., Charles C., Viriot L. & Balter V. (2017). Assessing human weaning practices with calcium isotopes in tooth enamel. *Proceedings of the National Academy of Sciences*, 114(24): 6268-6273. https://doi.org/10.1073/pnas.1704412114

Tacail T., Martin J. E., Arnaud-Godet F., Thackeray J. F., Cerling T. E., Braga J. & Balter V. (2019). Calcium isotopic patterns in enamel reflect different nursing behaviors among South African early hominins. *Science Advances*, 5(8): eaax3250. https://doi.org/10.1126/sciadv.aax3250

Tacail T., Le Houedec S. & Skulan J. L. (2020). New frontiers in calcium stable isotope geochemistry: perspectives in present and past vertebrate biology. *Chemical Geology*, 537: 119471. https://doi.org/10.1016/j.chemgeo.2020.119471

Tahara R. & Larsson H. C. (2022). Paratympanic sinuses in juvenile *Alligator*. *The Anatomical Record*, 305(10): 2926-2979. https://doi.org/10.1002/ar.24932

Talevi M., Herrera Y. & Fernández M. S. (2016). A microanatomical and histological study of a femur of *Cricosaurus araucanensis* (Crocodylomorpha: Thalattosuchia). *VI Simposio Argentino de Jurásico.*

Tambusso P. S., Varela L., Góis F., Moura J. F., Villa C. & Fariña R. A. (2021). The inner ear anatomy of glyptodonts and pampatheres (Xenarthra, Cingulata): Functional and phylogenetic implications. *Journal of South American Earth Sciences*, 108: 103189. https://doi.org/10.1016/j.jsames.2021.103189

Taplin L. E. & Grigg G. C. (1981). Salt glands in the tongue of the estuarine crocodile *Crocodylus porosus*. *Science*, 212(4498): 1045-1047. https://doi.org/10.1126/science.212.4498.1045

Taquet P. & Russell D. A. (1998). New data on spinosaurid dinosaurs from the Early Cretaceous of the Sahara. *Comptes Rendus de l'Académie des Sciences*, 327(5): 347-353. https://doi.org/10.1016/S1251-8050(98)80054-2

Tarsitano S. F., Frey E. & Riess J. (1989). The evolution of the Crocodilia: a conflict between morphological and biochemical data. *American Zoologist*, 29(3): 843-856. https://doi.org/10.1093/icb/29.3.843

Tavares S. A. S., Ricardi-Branco F. & Carvalho I. d. S. (2015). Osteoderms of *Montealtosuchus arrudacamposi* (Crocodyliformes, Peirosauridae) from the Turonian-Santonian (Upper Cretaceous) of Bauru Basin, Brazil. *Cretaceous Research*, 56: 651-661. https://doi.org/10.1016/j.cretres.2015.07.002

Tavares S. A. S., Branco F. R., Carvalho I. d. S. & Maldanis L. (2017). The morphofunctional design of *Montealtosuchus arrudacamposi* (Crocodyliformes, Upper Cretaceous) of the Bauru Basin, Brazil. *Cretaceous Research*, 79: 64-76. https://doi.org/10.1016/j.cretres.2017.07.003

Taylor M. P., Wedel M. J. & Naish D. (2009). Head and neck posture in sauropod dinosaurs inferred from extant animals. *Acta Palaeontologica Polonica*, 54(2): 213-220. https://doi.org/10.4202/app.2009.0007

Tennant J. P. & Mannion P. D. (2014). Revision of the Late Jurassic crocodyliform *Alligatorellus*, and evidence for allopatric speciation driving high diversity in western European atoposaurids. *PeerJ*, 2: e599. https://doi.org/10.7717/peerj.599

Tennant J. P., Mannion P. D. & Upchurch P. (2016). Evolutionary relationships and systematics of Atoposauridae (Crocodylomorpha: Neosuchia): implications for the rise of Eusuchia. *Zoological Journal of the Linnean Society*, 177(4): 854-936. https://doi.org/10.1111/zoj.12400

Thibon F., Goedert J., Séon N., Weppe L., Martin J. E., Amiot R., Adnet S., Lambert O., Bustamente P., Lécuyer C. & Vigier N. (2022). The ecology of modern and fossil vertebrates revisited by lithium isotopes. *Earth and Planetary Science Letters*, 599: 117840. https://doi.org/10.1016/j.epsl.2022.117840

Thies D., Windolf R. & Mudroch A. (1997). First record of Atoposauridae (Crocodylia: Metamesosuchia) in the Upper Jurassic (Kimmeridgian) of Northwest Germany. *Neues Jahrbuch fur Geologie und Palaontologie Abhandlungen*, 205: 393-411.

Tieszen L. L. (1991). Natural variations in the carbon isotope values of plants: implications for archaeology, ecology, and paleoecology. *Journal of Archaeological Science*, 18(3): 227-248. https://doi.org/10.1016/0305-4403(91)90063-U

Tieszen L. L. & Fagre T. (1993). Effect of diet quality and composition on the isotopic composition of respiratory CO2, bone collagen, bioapatite, and soft tissues. In *Prehistoric human bone,* Springer, Berlin, Heidelberg, 121-155. https://doi.org/10.1007/978-3-662-02894-0_5

Tjäderhane L., Carrilho M. R., Breschi L., Tay F. R. & Pashley D. H. (2009). Dentin basic structure and composition—an overview. *Endodontic Topics*, 20(1): 3-29. https://doi.org/10.1111/j.1601-1546.2012.00269.x

To K. H., Nesbitt S. & Stocker M. R. (2022). An early-diverging crocodylomorph from the early Norian (Late Triassic) of Texas demonstrates a wide distribution of early members across low-latitude Pangea. *Journal of Vertebrate Paleontology*, 41(6): e2075752. https://doi.org/10.1080/02724634.2021.2075752

Tosini G. (1997). The pineal complex of reptiles: physiological and behavioral roles. *Ethology Ecology & Evolution*, 9(4): 313-333. https://doi.org/10.1080/08927014.1997.9522875

Tripathy G. R., Singh S. K., Bhushan R. & Ramaswamy V. (2011). Sr–Nd isotope composition of the Bay of Bengal sediments: impact of climate on erosion in the Himalaya. *Geochemical Journal*, 45(3): 175-186. https://doi.org/10.2343/geochemj.1.0112

Troxell E. L. (1925). The Bridger crocodiles. *American Journal of Science*, 5(9): 29–72.

Trueman C. N. (1999). Rare earth element geochemistry and taphonomy of terrestrial vertebrate assemblages. *Palaios*, 14(6): 555-568. https://doi.org/10.2307/3515313

Trueman C. N. (2013). Chemical taphonomy of biomineralized tissues. *Palaeontology*, 56(3): 475-486. https://doi.org/10.1111/pala.12041

Trueman C. N. & Tuross N. (2002). Trace elements in recent and fossil bone apatite. *Reviews in Mineralogy and Geochemistry*, 48(1): 489-521. https://doi.org/10.2138/rmg.2002.48.13

Trueman C. N., Chenery C., Eberth D. A. & Spiro B. (2003). Diagenetic effects on the oxygen isotope composition of bones of dinosaurs and other vertebrates recovered from terrestrial and marine sediments. *J. of the Geol. Soc.*, 160(6): 895-901. https://doi.org/10.1144/0016-764903-019

Trueman C. N., Behrensmeyer A. K., Tuross N. & Weiner S. (2004). Mineralogical and compositional changes in bones exposed on soil surfaces in Amboseli National Park, Kenya: diagenetic mechanisms and the role of sediment pore fluids. *Journal of Archaeological Science*, 31(6): 721-739. https://doi.org/10.1016/j.jas.2003.11.003

Trueman C. N., Privat K. & Field J. (2008). Why do crystallinity values fail to predict the extent of diagenetic alteration of bone mineral?. *Palaeogeography, Palaeoclimatology, Palaeoecology*, 266(3-4): 160-167. https://doi.org/10.1016/j.palaeo.2008.03.038

Trueman C. N., Kocsis L., Palmer M. R. & Dewdney C. (2011). Fractionation of rare earth elements within bone mineral: a natural cation exchange system. *Palaeogeography, Palaeoclimatology, Palaeoecology*, 310(1-2): 124-132. https://doi.org/10.1016/j.palaeo.2011.01.002

Truesdell S. L & Saunders M. M. (2020). Bone remodeling platforms: Understanding the need for multicellular lab-on-a-chip systems and predictive agent-based models. *Mathematical Biosciences and Engineering*, 17(2): 1233-1252. https://doi.org/10.3934/mbe.2020063

Tucker A. S. & Fraser G. J. (2014). Evolution and developmental diversity of tooth regeneration. *Seminars in Cell & Developmental Biology*, 25-26: 71-80. https://doi.org/10.1016/j.semcdb.2013.12.013

Tucker R. T., Hyland E. G., Gates T. A., King M. R., Roberts E. M., Foley E. K., Berndt D., Hanta R., Khansubha S., Aswasereelert W. & Zanno L. E. (2022). Age, depositional history, and paleoclimatic setting of Early Cretaceous dinosaur assemblages from the Sao Khua Formation (Khorat Group), Thailand. *Palaeogeography, Palaeoclimatology, Palaeoecology*, 601: 111107. https://doi.org/10.1016/j.palaeo.2022.111107

Turner A. H. (2004). Crocodyliform biogeography during the Cretaceous: evidence of Gondwanan vicariance from biogeographical analysis. *Proceedings of the Royal Society of London. Series B: Biological Sciences*, 271(1552): 2003-2009. https://doi.org/10.1098/rspb.2004.2840

Turner A. H. (2006). Osteology and phylogeny of a new species of *Araripesuchus* (Crocodyliformes: Mesoeucrocodylia) from the Late Cretaceous of Madagascar. *Historical Biology*, 18(3): 255-369. https://doi.org/10.1080/08912960500516112

Turner A. H. (2015). A review of *Shamosuchus* and *Paralligator* (Crocodyliformes, Neosuchia) from the Cretaceous of Asia. *PLoS One*, 10(2): e0118116. https://doi.org/10.1371/journal.pone.0118116

Turner A. H. & Calvo J. O. (2005). A new sebecosuchian crocodyliform from the Late Cretaceous of Patagonia. *Journal of Vertebrate Paleontology*, 25(1): 87-98. https://doi.org/10.1671/0272-4634(2005)025[0087:ANSCFT]2.0.CO;2

Turner A. H. & Buckley G. A. (2008). *Mahajangasuchus insignis* (Crocodyliformes: Mesoeucrocodylia) cranial anatomy and new data on the origin of the eusuchian-style palate. *Journal of Vertebrate Paleontology*, 28(2): 382-408. https://doi.org/10.1671/0272-4634(2008)28[382:MICMCA]2.0.CO;2

Turner A. H. & Sertich J. J. (2010). Phylogenetic history of *Simosuchus clarki* (Crocodyliformes: Notosuchia) from the late cretaceous of Madagascar. *Journal of Vertebrate Paleontology*, 30(sup1): 177-236. https://doi.org/10.1080/02724634.2010.532348

Turner A. H. & Pritchard A. C. (2015). The monophyly of Susisuchidae (Crocodyliformes) and its phylogenetic placement in Neosuchia. *PeerJ*, 3: e759. https://doi.org/10.7717/peerj.759

Tyack P. L. & Clark C. W. (2000). Communication and acoustic behavior of dolphins and whales. In Au W. W. L., Fay R. R. & Popper A. N. (eds.) *Hearing by whales and dolphins*, Springer: 156-224. https://doi.org/10.1007/978-1-4612-1150-1_4

Tykoski R. S., Rowe T. B., Ketcham R. A. & Colbert M. W. (2002). *Calsoyasuchus valliceps*, a new crocodyliform from the Early Jurassic Kayenta Formation of Arizona. *Journal of Vertebrate Paleontology*, 22(3): 593-611. https://doi.org/10.1671/0272-4634(2002)022[0593:CVANCF]2.0.CO;2

Uriona T. J., Lyon M. & Farmer C. G. (2019). Lithophagy prolongs voluntary dives in american alligators (*Alligator mississippiensis*). *Integrative Organismal Biology*, 1(1): oby008. https://doi.org/10.1093/iob/oby008

Van Heghe L., Engström E., Rodushkin I., Cloquet C. & Vanhaecke F. (2012). Isotopic analysis of the metabolically relevant transition metals Cu, Fe and Zn in human blood from vegetarians and omnivores using multi-collector ICP-mass spectrometry. *Journal of Analytical Atomic Spectrometry*, 27(8): 1327-1334. https://doi.org/10.1039/C2JA30070B

van Hoepen E. C. N. (1915). Contributions to the knowledge of the reptiles of the Karroo formation. 4. A new pseudosuchian from the Orange Free State. *Annals of the Transvaal Museum*, 5: 83–87.

von Baczko M. B., Taborda J. R. & Desojo J. B. (2018). Paleoneuroanatomy of the aetosaur *Neoaetosauroides engaeus* (Archosauria: Pseudosuchia) and its paleobiological implications among archosauriforms. *PeerJ*, 6: e5456. https://doi.org/10.7717/peerj.5456

von Meyer H. (1830). Achte Versammlung der Naturforscher und Aerzte zu Heidelberg im September 1829. *Isis von Oken,* 1830: 517-519.

von Meyer H. (1831). Neue fossile Reptilien aus der Ordung der Saurier. *Nova Acta Academiae Leopoldino-Carolinae, Curios*, 15: 173-184.

von Meyer H. (1837). Mittheilungen, an Professor Bronn gerichtet. *Neues Jahrbuch für Mineralogie, Geognosie, Geologie und Petrefaktenkunde*, 1837: 314-317.

von Meyer H. (1850). Mittheilungen an Professor Bronn gerichtet. *Neues Jahrbuch für Mineralogie, Geognosie, Geologie und Petrefaktenkunde* : 195–204.

von Huene F. (1939). Ein Kleiner Pseudosuchier und ein Saurischier aus den ostafrikanischen Mandaschichten. *Neues Jahrbuch für Mineralogie, Geologie und Paläontologie, Beilage-Band, Abteilung B*, 81(1): 61-69.

von Zittel K. A. & Eastman C. R. (1902). *Text-Book of Palaeontology. Volume II.* Macmillan and Company, Limited, London, 283 p.

Vasseur M. G. (1894). Note préliminaire sur les terrains tertiaires de l'Albigeois. *Bulletin des services de la carte géologique de France*, 37: 75-80.

Veenstra L. L. I. & Broeckhoven C. (2022). Revisiting the thermoregulation hypothesis of osteoderms: a study of the crocodylian *Paleosuchus palpebrosus* (Crocodilia: Alligatoridae). *Biological Journal of the Linnean Society,* 2022, 1-13. https://doi.org/10.1093/biolinnean/blac001

Venczel M. & Codrea V. A. (2019). A new *Theriosuchus*-like crocodyliform from the Maastrichtian of Romania. *Cretaceous Research*, 100: 24-38. https://doi.org/10.1016/j.cretres.2019.03.018

Venczel M., Sabau I. & Codrea V. A. (2021). Crocodylian remains from the late Paleocene of Jibou, Romania. *Folia naturae Bihariae Oradea*, 48: 77-108.

Vergne A. L., Pritz M. B. & Mathevon N. (2009). Acoustic communication in crocodylians: from behaviour to brain. *Biological Reviews*, 84(3): 391-411. https://doi.org/10.1111/j.1469-185X.2009.00079.x

Vergne A. L., Aubin T., Martin S. & Mathevon N. (2012). Acoustic communication in crocodylians: information encoding and species specificity of juvenile calls. *Animal Cognition*, 15(6): 1095-1109. https://doi.org/10.1007/s10071-012-0533-7

Vickaryous M. K. & Hall B. K. (2008). Development of the dermal skeleton in *Alligator mississippiensis* (Archosauria, Crocodylia) with comments on the homology of osteoderms. *Journal of Morphology*, 269(4): 398-422. https://doi.org/10.1002/jmor.10575

Vidal L. M. (1915). Nota geologica y paleontologica sobre el Jurasico superior de la provincia de Lerida. *Boletin del Instituto Geologico de Espana,* 16: 17-55.

Viguet-Carrin S., Garnero P. & Delmas P. D. (2006). The role of collagen in bone strength. *Osteoporosis international*, 17: 319-336. https://doi.org/10.1007/s00198-005-2035-9

Vliet K. A. (1989). Social displays of the American alligator (*Alligator mississippiensis*). *American Zoologist*, 29(3): 1019-1031. https://doi.org/10.1093/icb/29.3.1019

Vocke R. D. (1999). Atomic weights of the elements 1997. *Pure and Applied Chemistry*, 71(8): 1593-1607. https://doi.org/10.1351/pac199971081593

Vogel S. (2005). Living in a physical world V. Maintaining temperature. *Journal of Biosciences*, 30(5): 581-590.

Vullo R. & Néraudeau D. (2008). Cenomanian vertebrate assemblages from southwestern France: a new insight into the European mid-Cretaceous continental fauna. *Cretaceous Research*, 29(5-6): 930-935. https://doi.org/10.1016/j.cretres.2008.05.010

Vullo R., Abit D., Ballèvre M., Billon-Bruyat J. P., Bourgeais R., Buffetaut E., Daviero-Gomez V., Garcia G., Gomez B., Mazin J. M., Morel S., Néraudeau D., Pouech J., Rage J. C., Schnyder J. & Tong H. (2014). Palaeontology of the Purbeck-type (Tithonian, Late Jurassic) bonebeds of Chassiron (Oléron Island, western France). *Comptes Rendus Palevol*, 13(5): 421-441. https://doi.org/10.1016/j.crpv.2014.03.003

Wagner A. (1858). Zur Kenntniss der Sauier aus den lithographischen Schiefen. *Abhandlungen der Mathemat.-Physikalischen Classe der Königlich Bayerischen Akademie der Wissenschaften*, 8: 415-528.

Waitkuwait W. E. (1989). Present knowledge on the west African slender-snouted crocodile, *Crocodylus cataphractus* Cuvier 1824 and the west African dwarf crocodile *Osteolaemus tetraspis*, Cope 1861. In IUCN Publication New Series (eds.), *Crocodiles their Ecology, Management, and Conservation*: 259-275.

Walker A. D. (1970). A revision of the Jurassic reptile *Hallopus victor* (Marsh), with remarks on the classification of crocodiles. *Philosophical Transactions of the Royal Society of London. B, Biological Sciences*, 257(816): 323-372.

Walker A. D. (1990). A revision of *Sphenosuchus acutus* Haughton, a crocodylomorph reptile from the Elliot Formation (late Triassic or early Jurassic) of South Africa. *Philosophical Transactions: Biological Sciences*, 330: 1-120.

Walker S. E. & Brett C. E. (2002). Post-Paleozoic patterns in marine predation: was there a Mesozoic and Cenozoic marine predatory revolution?. *The Paleontological Society Papers*, 8: 119-194. https://doi.org/10.1017/S108933260000108X

Walsh S. A., Barrett P. M., Milner A. C., Manley G. & Witmer L. M. (2009). Inner ear anatomy is a proxy for deducing auditory capability and behaviour in reptiles and birds. *Proceedings of the Royal Society B: Biological Sciences*, 276(1660): 1355-1360. https://doi.org/10.1098/rspb.2008.1390

Wang Y. & Cerling T. E. (1994). A model of fossil tooth and bone diagenesis: implications for paleodiet reconstruction from stable isotopes. *Palaeogeography, Palaeoclimatology, Palaeoecology*, 107(3-4): 281-289. https://doi.org/10.1016/0031-0182(94)90100-7

Wang X., Wang D., Wu X., Wang R. & Wang C. (2007). Acoustic signals of Chinese alligators (*Alligator sinensis*): social communication. *The Journal of the Acoustical Society of America*, 121(5): 2984-2989. https://doi.org/10.1121/1.2714910

Waskow K., Grzegorczyk D. & Sander P. M. (2018). The first record of *Tyrannoneustes* (Thalattosuchia: Metriorhynchidae): a complete skull from the Callovian (late Middle Jurassic) of Germany. *PalZ*, 92: 457-480. https://doi.org/10.1007/s12542-017-0395-z

Watanabe A., Gignac P. M., Balanoff A. M., Green T. L., Kley N. J. & Norell M. A. (2019). Are endocasts good proxies for brain size and shape in archosaurs throughout ontogeny?. *Journal of Anatomy*, 234(3): 291-305. https://doi.org/10.1111/joa.12918

Webb G. J. W., Messel H., Crawford J. & Yerbury M. J. (1978). Growth rates of *Crocodylus porosus* (Reptilia: Crocodilia) from Arnhem Land, northern Australia. *Wildlife Research*, 5(3): 385-399. https://doi.org/10.1071/WR9780385

Weber M., Lugli F., Jochum K. P., Cipriani A. & Scholz D. (2017). Calcium carbonate and phosphate reference materials for monitoring bulk and microanalytical determination of Sr isotopes. *Geostandards and Geoanalytical Research*, 42(1): 77-89. https://doi.org/10.1111/ggr.12191

Weldon P. J. & Ferguson M. W. (1993). Chemoreception in crocodylians: anatomy, natural history, and empirical results. *Brain, Behavior and Evolution*, 41(3-5): 239-245. https://doi.org/10.1159/000113845

Welker K. L., Orkin J. D. & Ryan T. M. (2009). Analysis of intraindividual and intraspecific variation in semicircular canal dimensions using high-resolution x-ray computed tomography. *Journal of Anatomy*, 215(4): 444-451. https://doi.org/10.1111/j.1469-7580.2009.01124.x

Wenz S. (1968). Contribution à l'étude du genre *Metriorhynchus* : crâne et moulage endocranien de *Metriorhynchus superciliosus*. *Annales de Paléontologie*, 54(2): 149-183.

Westphal Z. (1961). Zu Systematik der deutschen und englischen Lias-Krokodilier. *Neues Jahrbuch für geologie un Paläontologie, Abhandlungen*, 113(2): 207-218.

Wever E. G. (1971). Hearing in the Crocodilia. *Proceedings of the National Academy of Sciences*, 68(7): 1498-1500. https://doi.org/10.1073/pnas.68.7.1498

Wharton D. S. (2000). An enlarged endocranial venous system in *Steneosaurus pictaviensis* (Crocodylia: Thalattosuchia) from the Upper Jurassic of Les Lourdines, France. *Comptes Rendus de l'Académie des Sciences-Series IIA-Earth and Planetary Science*, 331(3): 221-226. https://doi.org/10.1016/S1251-8050(00)01397-5

Whetstone K. N. & Whybrow P. J. (1983). A 'cursorial' crocodylian from the Triassic of Lesotho (Basutoland), southern Africa. *Occasional Papers of the Museum of National History, University of Kansas*, 106: 1-37.

Whiteside D. I. & Marshall J. E. (2008). The age, fauna and palaeoenvironment of the Late Triassic fissure deposits of Tytherington, South Gloucestershire, UK. *Geological Magazine*, 145(1): 105-147. https://doi.org/10.1017/S0016756807003925

Whiteside J. H., Grogan D. S., Olsen P. E. & Kent D. V. (2011). Climatically driven biogeographic provinces of Late Triassic tropical Pangea. *Proceedings of the National Academy of Sciences*, 108(22): 8972-8977. https://doi.org/10.1073/pnas.1102473108

Whitlock J. A. & Richman J. M. (2013). Biology of tooth replacement in amniotes. *International Journal of Oral Science*, 5(2): 66-70. https://doi.org/10.1038/ijos.2013.36

Wickham H. (2011). ggplot2. *Wiley interdisciplinary reviews: computational statistics*, 3(2): 180-185. https://doi.org/10.1002/wics.147

Wieser M. E., Buhl D., Bouman C. & Schwieters J. (2004). High precision calcium isotope ratio measurements using a magnetic sector multiple collector inductively coupled plasma mass spectrometer. *Journal of Analytical Atomic Spectrometry*, 19(7): 844-851. https://doi.org/10.1039/B403339F

Wiffen J., Buffrénil d. V., de Ricqlès A. & Mazin J. M. (1995). Ontogenetic evolution of bone structure in Late Cretaceous Plesiosauria from New Zealand. *Geobios*, 28(5): 625-640. https://doi.org/10.1016/S0016-6995(95)80216-9

Wilberg E. W. (2015a). What's in an outgroup? The impact of outgroup choice on the phylogenetic position of Thalattosuchia (Crocodylomorpha) and the origin of Crocodyliformes. *Systematic Biology*, 64(4): 621-637. https://doi.org/10.1093/sysbio/syv020

Wilberg E. W. (2015b). A new metriorhynchoid (Crocodylomorpha, Thalattosuchia) from the Middle Jurassic of Oregon and the evolutionary timing of marine adaptations in thalattosuchian crocodylomorphs. *Journal of Vertebrate Paleontology*, 35(2): e902846. https://doi.org/10.1080/02724634.2014.902846

Wilberg E. W. (2017). Investigating patterns of crocodyliform cranial disparity through the Mesozoic and Cenozoic. *Zoological Journal of the Linnean Society*, 181(1): 189-208. https://doi.org/10.1093/zoolinnean/zlw027

Wilberg E. W., Turner A. H. & Brochu C. A. (2019). Evolutionary structure and timing of major habitat shifts in Crocodylomorpha. *Scientific reports*, 9(1): 514. https://doi.org/10.1038/s41598-018-36795-1

Wilberg E. W., Beyl A. R., Pierce S. E. & Turner A. H. (2021). Cranial and endocranial anatomy of a three-dimensionally preserved teleosauroid thalattosuchian skull. *The Anatomical Record*, 305(10): 2620-2653. https://doi.org/10.1002/ar.24704

Wilberg E. W., Godoy P. L., Griffiths E. F., Turner A. H. & Benson R. B. (2022). A new early diverging thalattosuchian (Crocodylomorpha) from the Early Jurassic (Pliensbachian) of Dorset, UK and implications for

the origin and evolution of the group. *Journal of Vertebrate Paleontology*: e2161909. https://doi.org/10.1080/02724634.2022.2161909

Wilkinson L. E., Young M. T. & Benton M. J. (2008). A new metriorhynchid crocodylian (Mesoeucrocodylia: Thalattosuchia) from the Kimmeridgian (Upper Jurassic) of Wiltshire, UK. *Palaeontology*, 51(6): 1307-1333. https://doi.org/10.1111/j.1475-4983.2008.00818.x

Williston S. W. (1925). *The osteology of the Reptiles*. Gregory W. K., 300 p.

Wils P. (2020). Analyses non destructives par tomographie à rayons X. *Les nouvelles de l'archéologie*, 159: 13-19. https://doi.org/10.4000/nda.9047

Williams C., Kirby A., Marghoub A., Kéver L., Ostashevskaya-Gohstand S., Bertazzo S., Moazen M., Abzhanov A., Herrel A., Evans S. E. & Vickaryous M. (2022). A review of the osteoderms of lizards (Reptilia: Squamata). *Biological Reviews*, 97(1): 1-19. https://doi.org/10.1111/brv.12788

Willis P. M. A. (1993). *Trilophosuchus rackhami* gen. et sp. nov., a new crocodylian from the early Miocene limestones of Riversleigh, northwestern Queensland. *Journal of Vertebrate Paleontology*, 13(1): 90-98. https://doi.org/10.1080/02724634.1993.10011489

Willis P. M. A. (1997). Review of fossil crocodylians from Australasia. *Australian Zoologist*, 30(3): 287-298. https://doi.org/10.7882/AZ.1997.004

Willis P. M. A. & Molnar R. E. (1991). A new middle Tertiary crocodile from Lake Palankarinna, South Australia. *Records of the South Australian Museum*, 25(1): 39-55.

Willis P. M. A. & Mackness B. S. (1996). *Quinkana babarra*, a New Species of Ziphodont Mekosuchine from the Early Pliocene Bluff Downs Local Fauna, Northern Australia with a Revision of the Genus. *Proceedings of the Linnean Society of New South Wales*, 116: 143-151.

Willis P. M. A., Murray P. & Megirian D. (1990). *Baru darrowi* gen. et sp. nov., a large, broad-snouted crocodyline (Eusuchia: Crocodylidae) from mid-Tertiary freshwater limestones in Northern Australia. *Memoirs of the Queensland Museum*, 29: 521-540.

Willis P. M. A., Molnar R. E. & Scanlon J. D. (1993). An Early Eocene Crocodylian from Murgon, Southeastern Queensland. *Kaupia*, 3: 27-33.

Willis R. E., McAliley L. R., Neeley E. D. & Densmore III L. D. (2007). Evidence for placing the false gharial (*Tomistoma schlegelii*) into the family Gavialidae: inferences from nuclear gene sequences. *Molecular Phylogenetics and Evolution*, 43(3): 787-794. https://doi.org/10.1016/j.ympev.2007.02.005

Wilson J. A., Malkani M. S. & Gingerich P. D. (2001). New crocodyliform (Reptilia, Mesoeucrocodylia) from the Upper Cretaceous Pab Formation of Vitakri, Balochistan (Pakistan). *Contributions from the Museum of Paleontology, The University of Michigan*, 30(12): 231-336.

Wilson E. E., Awonusi A., Morris M. D., Kohn D. H., Tecklenburg M. M. & Beck L. W. (2006). Three structural roles for water in bone observed by solid-state NMR. *Biophysical Journal*, 90(10): 3722-3731. https://doi.org/10.1529/biophysj.105.070243

Winkler D. A., Murry P. A. & Jacobs L. L. (1990). Early Cretaceous (Comanchean) vertebrates of central Texas. *Journal of Vertebrate Paleontology*, 10(1): 95-116. https://doi.org/10.1080/02724634.1990.10011794

Wintrich T., Hayashi S., Houssaye A., Nakajima Y. & Sander P. M. (2017). A Triassic plesiosaurian skeleton and bone histology inform on evolution of a unique body plan. *Science Advances*, 3(12): e1701144. https://doi.org/10.1126/sciadv.1701144

Witmer L. M. (1995). Homology of facial structures in extant archosaurs (birds and crocodylians), with special reference to paranasal pneumaticity and nasal conchae. *Journal of Morphology*, 225(3): 269-327. https://doi.org/10.1002/jmor.1052250304

Witmer L. M. (1997). The evolution of the antorbital cavity of archosaurs: a study in soft-tissue reconstruction in the fossil record with an analysis of the function of pneumaticity. *Journal of Vertebrate Paleontology*, 17(S1): 1-76. https://doi.org/10.1080/02724634.1997.10011027

Witmer L. M. (2009a). Feathered dinosaurs in a tangle. *Nature*, 461(7264): 601-602. https://doi.org/10.1038/461601a

Witmer L. M. (2009b). Fuzzy origins for feathers. *Nature*, 458(7236): 294-295. https://doi.org/10.1038/458293a

Witmer L. M. & Ridgely R. C. (2008). The paranasal air sinuses of predatory and armored dinosaurs (Archosauria: Theropoda and Ankylosauria) and their contribution to cephalic structure. *The Anatomical Record*, 291(11): 1362-1388. https://doi.org/10.1002/ar.20794

Witmer L. M. & Ridgely R. C. (2009). New insights into the brain, braincase, and ear region of tyrannosaurs (Dinosauria, Theropoda), with implications for sensory organization and behavior. *The Anatomical Record*, 292(9): 1266-1296. https://doi.org/10.1002/ar.20983

Witmer L. M., Chatterjee S., Franzosa J. & Rowe T. (2003). Neuroanatomy of flying reptiles and implications for flight, posture and behaviour. *Nature*, 425(6961): 950-953. https://doi.org/10.1038/nature02048

Witmer L. M., Ridgely R. C., Dufeau D. L. & Semones M. C. (2008). Using CT to peer into the past: 3D visualization of the brain and ear regions of birds, crocodiles, and nonavian dinosaurs. In Endo H. & Frey R. (eds.) *Anatomical imaging: towards a new morphology*, Springer: 67-87. https://doi.org/10.1007/978-4-431-76933-0_6

Witzmann F. & Soler-Gijón R. (2010). The bone histology of osteoderms in temnospondyl amphibians and in the chroniosuchian *Bystrowiella*. *Acta Zoologica*, 91(1): 96-114. https://doi.org/10.1111/j.1463-6395.2008.00385.x

Wolf N., Newsome S. D., Fogel M. L. & Del Rio C. M. (2013). The relationship between drinking water and the hydrogen and oxygen stable isotope values of tissues in Japanese Quail (*Cortunix japonica*). *The Auk*, 130(2): 323-330. https://doi.org/10.1525/auk.2013.12075

Woodburne M. O., Goin F. J., Bond M., Carlini A. A., Gelfo J. N., López G. M., Iglesias A. & Zimicz A. N. (2014). Paleogene land mammal faunas of South America; a response to global climatic changes and indigenous floral diversity. *Journal of Mammalian Evolution*, 21(1): 1-73. https://doi.org/10.1007/s10914-012-9222-1

Woodward A. S. (1896). On two Mesozoic crocodylians *Notosuchus* (genus novum) and *Cynodontosuchus* (genus novum) from the Red Sandstones of the Territory of Neuquén (Argentina Republic). *Anales del Museo de La Plata,* 4: 1-20.

Wopenka B. & Pasteris J. D. (2005). A mineralogical perspective on the apatite in bone. *Materials Science and Engineering: C*, 25(2): 131-143. https://doi.org/10.1016/j.msec.2005.01.008 .

Wright C. (2014). *Calcium isotopes in sheep dental enamel: a new approach to studying weaning and dairying in the archaeological record*. Unpublished PhD thesis, University of Oxford, 377 p.

Wright L. E. & Schwarcz H. P. (1996). Infrared and isotopic evidence for diagenesis of bone apatite at Dos Pilas, Guatemala: palaeodietary implications. *Journal of Archaeological Science*, 23(6): 933-944. https://doi.org/10.1006/jasc.1996.0087

Wroe S. (2002). A review of terrestrial mammalian and reptilian carnivore ecology in Australian fossil faunas, and factors influencing their diversity: the myth of reptilian domination and its broader ramifications. *Australian Journal of Zoology*, 50(1): 1-24. https://doi.org/10.1071/ZO01053

Wu X. C. & Chatterjee S. (1993). *Dibothrosuchus elaphros*, a crocodylomorph from the Lower Jurassic of China and the phylogeny of the Sphenosuchia. *Journal of Vertebrate Paleontology*, 13(1): 58-89. https://doi.org/10.1080/02724634.1993.10011488

Wu X. C. & Li J. (1994). Phylogenetic relationship of *Hsisosuchus*. *Vertebrata Palasiatica*, 32(03): 166-180.

Wu X. C. & Sues H. D. (1996a). Reassessment of *Platyognathus hsui* Young, 1944 (Archosauria: Crocodyliformes) from the Lower Lufeng Formation (Lower Jurassic) of Yunnan, China. *Journal of Vertebrate Paleontology*, 16(1): 42-48. https://doi.org/10.1080/02724634.1996.10011282

Wu X. C. & Sues H. D. (1996b). Anatomy and phylogenetic relationships of *Chimaerasuchus paradoxus*, an unusual crocodyliform reptile from the Lower Cretaceous of Hubei, China. *Journal of Vertebrate Paleontology*, 16(4): 688-702. https://doi.org/10.1080/02724634.1996.10011358

Wu X. C., Brinkman D. B. & Lu J. C. (1994a). A new species of *Shantungosuchus* from the Lower Cretaceous of Inner Mongolia (China), with comments on *S. chuhsienensis* Young, 1961 and the phylogenetic position of the genus. *Journal of Vertebrate Paleontology*, 14(2): 210-229. https://doi.org/10.1080/02724634.1994.10011553

Wu X. C., Li J. & Li X. (1994b). Phylogenetic relationship of *Hsisosuchus*. *Vertebrata PalAsiatica*, 32:166-180.

Wu X. C., Sues H. D. & Sun A. (1995). A plant-eating crocodyliform reptile from the Cretaceous of China. *Nature*, 376(6542): 678-680. https://doi.org/10.1038/376678a0

Wu X. C., Sues H. D. & Brinkman D. B. (1996a). An atoposaurid neosuchian (Archosauria: Crocodyliformes) from the Lower Cretaceous of Inner Mongolia (People's Republic of China). *Canadian Journal of Earth Sciences*, 33(4): 599-605. https://doi.org/10.1139/e96-044 .

Wu X. C., Sues H. D. & Dong Z. M. (1996b). *Sichuanosuchus shuhanensis*, a new? Early Cretaceous protosuchian (Archosauria: Crocodyliformes) from Sichuan (China), and the monophyly of Protosuchia. *Journal of Vertebrate Paleontology*, 17(1): 89-103. https://doi.org/10.1080/02724634.1997.10010956

Wu X. C., Sues H. D. & Dong Z. M. (1997). *Sichuanosuchus shuhanensis*, a new? Early Cretaceous protosuchian (Archosauria: Crocodyliformes) from Sichuan (China), and the monophyly of Protosuchia. *Journal of Vertebrate Paleontology*, 17(1): 89-103. https://doi.org/10.1080/02724634.1997.10010956

Wu X. C., Cheng Z. W. & Russell A. P. (2001). Cranial anatomy of a new crocodyliform (Archosauria: Crocodylomorpha) from the Lower Cretaceous of Song-Liao Plain, northeastern China. *Canadian Journal of Earth Sciences*, 38(12): 1653-1663. https://doi.org/10.1139/e01-055

Wu L., Wu X. C., You H. L., Zhang Y., Zhao J., Yuan Y., Zhang H. & Li S. (2023). A new specimen of *Hsisosuchus* (Mesoeucrocodylia, Crocodyliformes) from the Upper Jurassic of Yunnan, China with implications for the diversity of the ventral trunk shield of osteoderms in the genus. *Historical Biology*, 1-12. https://doi.org/10.1080/08912963.2023.2170796

Xing L., Paulina-Carabajal A., Currie P. J., Xu X., Zhang J., Wang T., Burns M. E. & Dong Z. (2014). Braincase anatomy of the basal theropod *Sinosaurus* from the Early Jurassic of China. *Acta Geologica Sinica-English Edition*, 88(6): 1653-1664. https://doi.org/10.1111/1755-6724.12335

Yamamoto T., Hasegawa T., Yamamoto T., Hongo H. & Amizuka N. (2016). Histology of human cementum: Its structure, function, and development. *Japanese Dental Science Review*, 52(3): 63-74. https://doi.org/10.1016/j.jdsr.2016.04.002

Yates A. M. (2017). The biochronology and palaeobiogeography of *Baru* (Crocodylia: Mekosuchinae) based on new specimens from the Northern Territory and Queensland, Australia. *PeerJ*, 5: e3458. https://doi.org/10.7717/peerj.3458

Yates A. M. & Pledge N. S. (2017). A Pliocene mekosuchine (Eusuchia: Crocodilia) from the Lake Eyre Basin of South Australia. *Journal of Vertebrate Paleontology*, 37(1): e1244540. https://doi.org/10.1080/02724634.2017.1244540

Yeh H. K. (1958). A new crocodile from Maoming, Kwangtung. *Vertebrata PalAsiatica*, 2(4): 237-242.

Yi H. & Norell M. (2019). The bony labyrinth of *Platecarpus* (Squamata: Mosasauria) and aquatic adaptations in squamate reptiles. *Palaeoworld*, 28(4): 550-561. https://doi.org/10.1016/j.palwor.2018.12.001

Yilmaz S., Newman H. N. & Poole D. F. G. (1977). Diurnal periodicity of von Ebner growth lines in pig dentine. *Archives of Oral Biology*, 22(8-9): 511-513. https://doi.org/10.1016/0003-9969(77)90046-2

Yin Y., Zhang L., Gu X., Yin R., Wen Y., Jin T. & Wang C. (2023). High terrestrial temperature in the low-latitude Nanxiong Basin during the Cretaceous-Paleogene boundary interval. *Palaeogeography, Palaeoclimatology, Palaeoecology*, 617: 111489. https://doi.org/10.1016/j.palaeo.2023.111489

Yoshimura M. & Suda H. (1995). Hydrothermal Processing of Hydroxyapatite: Past, Present, and Future. In CRC Press (eds.) *Hydroxyapatite and Related Materials*, Boca Raton, 28 p.

Yoshimura T., Wakaki S., Kawahata H., Hossain H. Z., Manaka T., Suzuki A., Ishikawa T. & Ohkouchi N. (2021). Stable strontium isotopic compositions of river water, groundwater and sediments from the Ganges–Brahmaputra–Meghna River system in Bangladesh. *Frontiers in Earth Science*, 9: 592062. https://doi.org/10.3389/feart.2021.592062

Young C. C. (1948). Fossil crocodiles in China, with notes on dinosaurian remains associated with the Kansu crocodiles. *Bulletin of the Geological Society of China*, 28(3-4): 255-288.

Young C. C. (1961). On a new crocodile from Chuhsien, E. Shantung. *Vertebrata palasiatica*, 5(1): 6-10.

Young C. C. & Chow M. Z. (1953). New discoveries of the Mesozoic reptiles from Sichuan. *Palaeontologica Sinica*, 1:87-109.

Young M. T. (2014). Filling the 'Corallian Gap': re-description of a metriorhynchid crocodylomorph from the Oxfordian (Late Jurassic) of Headington, England. *Historical Biology*, 26(1): 80-90. https://doi.org/10.1080/08912963.2012.760559

Young M. T. & de Andrade M. B. (2009). What is *Geosaurus*? Redescription of *Geosaurus giganteus* (Thalattosuchia: Metriorhynchidae) from the Upper Jurassic of Bayern, Germany. *Zoological Journal of the Linnean Society*, 157(3): 551-585. https://doi.org/10.1111/j.1096-3642.2009.00536.x

Young B. A. & Bierman H. S. (2019). On the median pharyngeal valve of the American alligator (*Alligator mississippiensis*). *Journal of Morphology*, 280(1): 58-67. https://doi.org/10.1002/jmor.20914

Young M. T., Brusatte S. L., Ruta M. & de Andrade M. B. (2010). The evolution of Metriorhynchoidea (Mesoeucrocodylia, Thalattosuchia): an integrated approach using geometric morphometrics, analysis of disparity, and biomechanics. *Zoological Journal of the Linnean Society*, 158(4): 801-859. https://doi.org/10.1111/j.1096-3642.2009.00571.x

Young M. T., Bell M. A. & Brusatte S. L. (2011a). Craniofacial form and function in Metriorhynchidae (Crocodylomorpha: Thalattosuchia): modelling phenotypic evolution with maximum-likelihood methods. *Biology letters*, 7(6): 913-916. https://doi.org/10.1098/rsbl.2011.0357

Young M. T., Bell M. A., de Andrade M. B. & Brusatte S. L. (2011b). Body size estimation and evolution in metriorhynchid crocodylomorphs: implications for species diversification and niche partitioning. *Zoological Journal of the Linnean Society*, 163(4): 1199-1216. https://doi.org/10.1111/j.1096-3642.2011.00734.x

Young M. T., Brusatte S. L., de Andrade M. B., Desojo J. B., Beatty B. L., Steel L., Fernández M. S., Sakamoto M., Ruiz-Omeñaca J. I. & Schoch R. R. (2012a). The cranial osteology and feeding ecology of the metriorhynchid crocodylomorph genera *Dakosaurus* and *Plesiosuchus* from the Late Jurassic of Europe. *PlosOne*, 7(9): e44985. https://doi.org/10.1371/journal.pone.0044985

Young M. T., Brusatte S. L., Beatty B. L., de Andrade M. B. & Desojo J. B. (2012b). Tooth-on-tooth interlocking occlusion suggests macrophagy in the Mesozoic marine crocodylomorph Dakosaurus. *The Anatomical Record*, 295(7): 1147-1158. https://doi.org/10.1002/ar.22491

Young M. T., de Andrade M. B., Etches S. & Beatty B. L. (2013a). A new metriorhynchid crocodylomorph from the Lower Kimmeridge Clay Formation (Late Jurassic) of England, with implications for the evolution of dermatocranium ornamentation in Geosaurini. *Zoological Journal of the Linnean Society*, 169(4): 820-848. https://doi.org/10.1111/zoj.12082

Young M. T., Beatty B. L., Brusatte S. L. & Steel L. (2013b). First evidence of denticulated dentition in teleosaurid crocodylomorphs. *Acta Palaeontologica Polonica*, 60(3): 661-671. https://doi.org/10.4202/app.00002.2013

Young M. T., de Andrade M. B., Cornée J. J., Steel L. & Foffa D. (2014a). Re-description of a putative Early Cretaceous "teleosaurid" from France, with implications for the survival of metriorhynchids and teleosaurids across the Jurassic-Cretaceous Boundary. *Annales de Paléontologie*, 100(2): 165-174. https://doi.org/10.1016/j.annpal.2014.01.002

Young M. T., Hua S., Steel L., Foffa D., Brusatte S. L., Thüring S., Mateus O., Ruiz-Omeñaca J. I., Havlik P., Lepage Y. & de Andrade M. B. (2014b). Revision of the late Jurassic teleosaurid genus *Machimosaurus* (Crocodylomorpha, Thalattosuchia). *Royal Society Open Science*, 1(2): 140222. https://doi.org/10.1098/rsos.140222

Young M. T., Steel L., Brusatte S. L., Foffa D. & Lepage Y. (2014c). Tooth serration morphologies in the genus *Machimosaurus* (Crocodylomorpha, Thalattosuchia) from the Late Jurassic of Europe. *Royal Society Open Science*, 1(3): 140269. https://doi.org/10.1098/rsos.140269

Young M. T., Steel L. & Middleton H. (2014d). Evidence of the metriorhynchid crocodylomorph genus *Geosaurus* in the Lower Kimmeridge Clay Formation (Late Jurassic) of England. *Historical Biology*, 26(5): 551-555. https://doi.org/10.1080/08912963.2013.801468

Young M. T., Hua S., Steel L., Foffa D., Brusatte S. L., Thüring S., Mateus O., Ruiz-Omeñaca J. I., Havlik P., Lepage Y. & de Andrade M. B. (2015a). Addendum to 'Revision of the Late Jurassic teleosaurid genus *Machimosaurus* (Crocodylomorpha, Thalattosuchia)'. *Royal Society Open Science*, 2(2): 150024. https://doi.org/10.1098/rsos.150024

Young M. T., Steel L., Rigby M. P., Howlett E. A. & Humphrey S. (2015b). Largest known specimen of the genus *Dakosaurus* (Metriorhynchidae: Geosaurini) from the Kimmeridge Clay Formation (Late Jurassic) of England, and an overview of *Dakosaurus* specimens discovered from this formation (including reworked specimens from the Woburn Sands Formation). *Historical Biology*, 27(7): 947-953. https://doi.org/10.1080/08912963.2014.915822

Young M. T., Rabi M., Bell M. A., Foffa D., Steel L., Sachs S. & Peyer K. (2016a). Big-headed marine crocodyliforms and why we must be cautious when using extant species as body length proxies for long-extinct relatives. *Palaeontologia Electronica*, 19(3): 1-14.

Young M. T., Tennant J. P., Brusatte S. L., Challands T. J., Fraser N. C., Clark N. D. & Ross D. A. (2016b). The first definitive Middle Jurassic atoposaurid (Crocodylomorpha, Neosuchia), and a discussion on the genus *Theriosuchus*. *Zoological journal of the Linnean Society*, 176(2): 443-462. https://doi.org/10.1111/zoj.12315

Young M. T., Hastings A. K., Allain R. & Smith T. J. (2017). Revision of the enigmatic crocodyliform *Elosuchus felixi* de Lapparent de Broin, 2002 from the Lower–Upper Cretaceous boundary of Niger: potential evidence for an early origin of the clade Dyrosauridae. *Zoological Journal of the Linnean Society*, 179(2): 377-403. https://doi.org/10.1111/zoj.12452

Young M. T., Sachs S., Abel P., Foffa D., Herrera Y. & Kitson J. J. (2020a). Convergent evolution and possible constraint in the posterodorsal retraction of the external nares in pelagic crocodylomorphs. *Zoological Journal of the Linnean Society*, 189(2): 494-520. https://doi.org/10.1093/zoolinnean/zlaa021

Young M. T., Foffa D., Steel L. & Etches S. (2020b). Macroevolutionary trends in the genus *Torvoneustes* (Crocodylomorpha: Metriorhynchidae) and discovery of a giant specimen from the Late Jurassic of Kimmeridge, UK. *Zoological Journal of the Linnean Society*, 189(2): 483-493. https://doi.org/10.1093/zoolinnean/zlz101

Young M. T., Brignon A., Sachs S., Hornung J. J., Foffa D., Kitson J. J., Johnson M. M. & Steel L. (2021). Cutting the Gordian knot: a historical and taxonomic revision of the Jurassic crocodylomorph *Metriorhynchus*. *Zoological Journal of the Linnean Society*, 192(2): 510-553. https://doi.org/10.1093/zoolinnean/zlaa092

Young M. T., Bowman C. I. W., Erb A., Schwab J. A., Witmer L. M., Herrera Y. & Brusatte S. L. (2023). Evidence for a novel cranial thermoregulatory pathway in thalattosuchian crocodylomorphs. *PeerJ*, 11: e15353. https://doi.org/10.7717/peerj.15353

Zaher H., Pol D., Carvalho A. B., Riccomini C., Campos D. & Nava W. (2006). Redescription of the cranial morphology of *Mariliasuchus amarali*, and its phylogenetic affinities (Crocodyliformes, Notosuchia). *American Museum Novitates*, 2006(3512): 1-40. https://doi.org/10.1206/0003-0082(2006)3512[1:ROTCMO]2.0.CO;2

Zazzo A., Lécuyer C., Sheppard S. M., Grandjean P. & Mariotti A. (2004a). Diagenesis and the reconstruction of paleoenvironments: a method to restore original δ18O values of carbonate and phosphate from fossil tooth enamel. *Geochimica et Cosmochimica Acta*, 68(10): 2245-2258. https://doi.org/10.1016/j.gca.2003.11.009

Zazzo A., Lécuyer C. & Mariotti A. (2004b). Experimentally-controlled carbon and oxygen isotope exchange between bioapatites and water under inorganic and microbially-mediated conditions. *Geochim. et Cosmochim. Acta*, 68(1): 1-12. https://doi.org/10.1016/S0016-7037(03)00278-3

Zelenitsky D. K., Therrien F. & Kobayashi Y. (2009). Olfactory acuity in theropods: palaeobiological and evolutionary implications. *Proceedings of the Royal Society B: Biological Sciences*, 276(1657): 667-673. https://doi.org/10.1098/rspb.2008.1075

Zelenitsky D. K., Therrien F., Ridgely R. C., McGee A. R. & Witmer L. M. (2011). Evolution of olfaction in non-avian theropod dinosaurs and birds. *Proceedings of the Royal Society B: Biological Sciences*, 278(1725): 3625-3634. https://doi.org/10.1098/rspb.2011.0238

Zhang F. (1981). [A fossil crocodile from Anhui province]. V*ertebrataPalasiatica*, 19: 206–207 [Chinese].

Zhang J. & Nozaki Y. (1996). Rare earth elements and yttrium in seawater: ICP-MS determinations in the East Caroline, Coral Sea, and South Fiji basins of the western South Pacific Ocean. *Geochimica et Cosmochimica Acta*, 60(23): 4631-4644. https://doi.org/10.1016/S0016-7037(96)00276-1

Zhang L., Wang C., Wignall P. B., Kluge T., Wan X., Wang Q. & Gao Y. (2018). Deccan volcanism caused coupled pCO2 and terrestrial temperature rises, and pre-impact extinctions in northern China. *Geology*, 46(3): 271-274. https://doi.org/10.1130/G39992.1

Zonneveld J. P., Gunnell G. F. & Bartels W. S. (2000). Early Eocene fossil vertebrates from the southwestern Green River Basin, Lincoln and Uinta Counties, Wyoming. *Journal of Vertebrate Paleontology*, 20(2): 369-386. https://doi.org/10.1671/0272-4634(2000)020[0369:EEFVFT]2.0.CO;2

Appendix 1: List of publications involved in the Sebecia/Sebecosuchia debate with corresponding phylogenetic datasets and synapomorphies

Blue: associated with the Sebecosuchia hypothesis

Red: associated with the Sebecia hypothesis

Bold: identified conflict within the same phylogenetic definitions

Underlined: identified conflict within both phylogenetic definitions

Sebecia:

Larsson & Sues (2007):

Matrix built using: Benton & Clark (1988); Norell (1988); Norell & Clark (1990); Sereno (1991); Buscalioni *et al*. (1992); Parrish (1993); Wu & Chatterjee (1993); Clark (1994); Wu *et al.* (1994, 1997); Wu & Sues (1996); Brochu (1997); Larsson (2000); Sereno *et al.* (2001, 2003). **Introducing nine new characters.**

Characters diagnostic of Sebecia: Large nutrient foramen on palatal surface of premaxilla-maxilla contact; premaxilla palatal shelves.

Phylogenetic search procedure: heuristic searches in PAUP*: 200 repetitions.

Sereno & Larsson (2009):

Matrix built using: Benton & Clark (1988); Norell (1988, 1989); Norell & Clark (1990); Sereno (1991); Buscalioni *et al*. (1992); Parrish (1993); Gasparini *et al*. (1993, 2005, 2006); Wu & Chatterjee (1993); Clark (1994); Wu & Sues (1996); Brochu (1997); Gomani (1997); Wu *et al*. (1994, 1997); Pol (1999a); Larsson (2000); Ortega *et al.* (2000); Sereno *et al.* (2001, 2003); Pol *et al*. (2004); Pol & Apesteguia (2005); Zaher *et al*. (2006); Larsson & Sues (2007); Turner & Buckley (2008). **Introducing five new characters.**

Characters diagnostic of Sebecia: Frontoparietal suture does not enter supratemporal fenestra: broad postorbital-parietal contact; quadratojugal posteroventral extension forms lateral extension to the quadrate condyles and participates in mandibular joint; depression on anterodorsal surface of postorbital for a palpebral element; premaxilla midline extension into anterior margin of external nares present and less than fifty percent; circumnarial fossa; premaxilla - maxilla lateral fossa excavates alveolus of last premaxillary tooth; serrated carinae of maxillary and opposing dentary teeth; constricted cheek teeth crown base; mandibular symphysis deep and tapering anteriorly in lateral view; splenial robust dorsally posterior to symphysis; retroarticular process projects posterodorsally.

Phylogenetic search procedure: heuristic searches: 50 repetitions.

Young & de Andrade (2009):

Matrix built using: data not available.

Characters diagnostic of Sebecia: data not available.

Phylogenetic search procedure: heuristic searches in PAUP*: 200 repetitions. Characters unordered, equal weighting.

de Andrade *et al.* (2011):

Matrix built using: Clark (1994); Ortega *et al*. (2000); Sereno *et al*. (2001, 2003); Pol (2003); Pol & Apesteguia (2005); Gasparini *et al*. (2006); Jouve *et al*. (2006); de Andrade & Bertini (2008a, b); Turner & Buckley (2008); Young & de Andrade (2009); de Andrade (2010). **Introducing 165 new characters.**

Characters diagnostic of Sebecia: mandible projects dorsally at premaxilla-maxilla suture; mandible is curved posteroventrally, with maximum curvature at posterior section of angular; dorsal border at dentary-surangular contact strongly arched dorsally; symphysis longer than wide and V or Y-shaped; symphysis clearly constricted at fifth-sixth alveoli; retroarticular posterodorsally oriented; retroarticular process surface poorly concave and facing dorsally; fourth dentary alveolus larger than third.

Phylogenetic search procedure: heuristic searches in PAUP*: 1000 repetitions. 24 characters ordered, equal weighting.

Riff & Kellner (2011):

Matrix built using: Clark (1994); Wu & Sues (1996); Buscalioni & Sanz (1988); Gomani (1997); Ortega *et al*. (1996, 2000); Wu *et al*. (1997); Brochu (1999); Buckley & Brochu (1999); Pol (1999a); Sereno *et al*. (2001); Pol & Norell (2004a, b); Pol & Apesteguia (2005); Gasparini *et al*. (2006); Larsson & Sues (2007). **Introducing ten new characters.**

Characters diagnostic of Sebecia: data not available.

Phylogenetic search procedure: heuristic searches in PAUP*: 100 repetitions. Characters unordered, equal weighting.

Pinheiro *et al*. (2018):

Matrix built using: Buscalioni & Sanz (1988); Norell (1988); Gasparini *et al*. (1993); Clark (1994); Ortega *et al*. (1996, 2000); Wu & Sues (1996); Brochu (1997, 1999); Gomani (1997); Wu *et al*. (1997); Buckley & Brochu (1999); Pol (1999a, b); Buckley *et al*. (2000); Sereno *et al*. (2001); Martinelli (2003); Pol & Norell (2004a, b); Pol *et al*. (2004); Turner (2004, 2006); Pol & Apesteguia (2005); Zaher *et al*. (2006); Larsson & Sues (2007); de Andrade & Bertini (2008a); Turner & Buckley (2008); Novas *et al*. (2009); Pol & Gasparini (2009); Pol *et al*. (2009); Sereno & Larsson (2009); O'Connor *et al*. (2010); Turner & Sertich (2010); de Andrade *et al*. (2011); Montefeltro *et al*. (2011); Nascimento & Zaher (2011); Pol & Powell (2011) ; Riff & Kellner (2011); Pol *et al*. (2012, 2014). **Introducing one new character.**

Characters diagnostic of Sebecia: Primary pterygoidean palate forms posterior, lateral and part of the anterior margin of the choana; lateral surface of the anterior region of the surangular and the posterior section of the dentary with a deep, well-defined longitudinal groove; surangular forms one-third of the glenoid fossa and quadratojugal bears an articular condyle; dentary with lateral concavity for reception of the enlarged maxillary tooth; dorsal edge of dentary sinusoidal, with two concave waves; splenial robust posterior to symphysis; **jugal portion of postorbital bar anteriorly continuous but posteriorly inset from lateral surface of jugal**;

snout sinusoidal in dorsal view; anterior half of palatines between suborbital fenestrae flared anteriorly; first and second premaxillary teeth nearly confluent; premaxilla-maxilla lateral fossa excavating alveolus of last premaxillary tooth.

Phylogenetic search procedure: heuristic searches in TNT: 3000 repetitions.

Geroto & Bertini (2019):

Matrix built using: Buscalioni & Sanz (1990); Sereno (1991); Gasparini *et al*. (1991, 2006); Clark (1994); Ortega *et al*. (1996, 2000); Wu & Sues (1996); Brochu (1997); Gomani (1997); Wu *et al*. (1997); Buckley & Brochu (1999); Buscalioni *et al*. (1999); Buckley *et al*. (2000); Pol (2003); Sereno *et al*. (2003); Jouve (2004, 2009); Pol & Norell (2004a); de Andrade (2005); Pol & Apesteguia (2005); Turner (2006); Zaher *et* al. (2006); Larsson & Sues (2007); Pinheiro (2007); de Andrade & Bertini (2008a, b); Turner & Buckley (2008); Novas *et al*. (2009) ; Sereno & Larsson (2009); Turner & Sertich (2010); de Andrade *et al*. (2011); Montefeltro *et al*. (2011, 2013); Nascimento & Zaher (2011); Young *et al*. (2011); Pol *et al*. (2012, 2014); Godoy *et al*. (2014). **Introducing 38 new characters.**

Characters diagnostic of Sebecia: Parietal plane and narrow (width) between supratemporal fenestrae; symphysis clearly constricted at fifth-sixth alveoli; dentary smoothly curving anteriorly at mandibular symphysis; fourth dentary tooth is hypertrophied caniniform; infratemporal fenestra equal in size to orbit; neural spine in cervical vertebrae with only posterior/all rod-like.

Phylogenetic search procedure: heuristic searches in TNT: 10000 repetitions. Multistate characters ordered when possible.

Martins (2021):

Matrix built using: Norell (1988); Buscalioni & Sanz (1988); Buscalioni *et al*. (1992); Gasparini *et al*. (1991, 1993); Wu & Chatterjee (1993); Clark (1994); Ortega *et al*. (1996, 2000); Wu & Sues (1996); Gomani (1997); Wu *et al*. (1997); Brochu (1999); Buckley & Brochu (1999); Pol (1999); Buckley *et al*. (2000); Larsson & Gado (2000); Sereno *et al*. (2001); Clark & Sues (2002); Martinelli (2003); Jouve (2004, 2009); Pol & Norell (2004a, b); Pol & Apesteguia (2005); Gasparini *et al*. (2006); Jouve *et al*. (2006); Turner (2006); Zaher *et al*. (2006); Larsson & Sues (2007); Ösi *et al*. (2007); Pinheiro (2007); de Andrade & Bertini (2008a, b); Turner &

Buckley (2008); Wilkinson *et al*. (2008); Pol *et al*. (2009, 2012, 2014); Sereno & Larsson (2009); Young & de Andrade (2009); Nascimento & Zaher (2010); Turner & Sertich (2010); de Andrade *et al*. (2011); Montefeltro *et al*. (2011, 2013, 2016); Pol & Powell (2011); Riff & Kellner (2011); Godoy *et al*. (2014); Geroto & Bertini (2019); Darlim *et al*. (2021) ; Ruiz *et al*. (2021). **Introducing three new characters.**

Characters diagnostic of Sebecia: **Jugal portion of postorbital bar flush with lateral surface of jugal**; maxillae sagittal contact bearing a longitudinal series of foramina; pterygoid flanges relatively short, and do not reach laterally the level of the quadrate medial condyle; cheek teeth base constricted.

Phylogenetic search procedure: heuristic searches in TNT: 10000 repetitions. Equal weighting.

Pinheiro *et al*. (2021):

Matrix built using: Pol *et al*. (2012, 2014); Leardi *et al*. (2015a); Fiorelli *et al*. (2016); Martinelli *et al*. (2018); Pinheiro *et al*. (2018); Cunha *et al*. (2020). **Introducing five new characters.**

Characters diagnostic of Sebecia: Data not available.

Phylogenetic search procedure: New Technology Search (Sectorial, Ratchet, Tree fusing) in TNT: find minimum length 50 times followed by heuristic searches in TNT with trees found previously. Unordered characters.

Ruiz *et al*. (2021):

Matrix built using: Buscalioni & Sanz (1988); Norell (1988); Buscalioni *et al*. (1992); Gasparini *et al*. (1993, 2006); Wu & Chatterjee (1993); Clark (1994); Ortega *et al*. (1996, 2000); Wu & Sues (1996); Gomani (1997); Wu *et al*. (1997); Brochu (1999); Buckley & Brochu (1999); Pol (1999a ,b); Buckley *et al*. (2000); Larsson & Gado (2000); Sereno *et al*. (2001); Clark & Sues (2002); Martinelli (2003); Jouve (2004, 2009); Pol & Norell (2004a, b); Pol *et al*. (2004, 2009, 2012, 2014); Pol & Apesteguia (2005); Jouve *et al*. (2006); Turner (2006); Zaher *et al*. (2006); Larsson & Sues (2007); Ösi *et al*. (2007); de Andrade & Bertini (2008); Turner & Buckley (2008); Wilkinson *et al*. (2008); Sereno & Larsson (2009); Young & de Andrade (2009); Nascimento & Zaher (2010); Turner & Sertich (2010); de Andrade & Bertini (2011);

Montefeltro *et al*. (2011, 2013, 2016); Pol & Powell (2011); Riff & Kellner (2011). **Introducing eleven new characters.**

Characters diagnostic of Sebecia: **Jugal portion of postorbital bar flush with lateral surface of jugal**; maxillae sagittal contact bearing a series of longitudinal foramina; pterygoid flanges relatively short, and do not reach laterally the level of the quadrate medial condyle; tooth with transitional morphology at premaxillary-maxillary contact.

Phylogenetic search procedure: Heuristic searches in TNT: 10000 repetitions.

Queiroz (2022):

Matrix built using: Buscalioni & Sanz (1988); Norell (1988); Buscalioni *et al*. (1992); Gasparini *et al*. (1993, 2006); Wu & Chatterjee (1993); Clark (1994); Ortega *et al*. (1996, 2000); Wu & Sues (1996); Gomani (1997); Wu *et al*. (1997); Brochu (1999); Buckley & Brochu (1999); Pol (1999a, b); Larsson & Gado (2000); Sereno *et al*. (2001); Clark & Sues (2002); Martinelli (2003); Jouve (2004, 2009); Pol & Norell (2004a, b); Pol *et al*. (2004, 2009, 2012, 2014); de Andrade (2005); Jouve *et al*. (2006); Pol & Apesteguia (2005); Turner (2006); Zaher *et al*. (2006); Larsson & Sues (2007); Ösi *et al*. (2007); de Andrade & Bertini (2008); Turner & Buckley (2008); Wilkinson *et al*. (2008); Sereno & Larsson (2009); Young & de Andrade (2009); Nascimento & Zaher (2010); Turner & Sertich (2010); de Andrade *et al*. (2011); Montefeltro *et al*. (2011, 2013, 2016); Pol & Powell (2011) ; Riff & Kellner (2011); Pinheiro *et al*. (2018); Geroto & Bertini (2019); Ruiz *et al*. (2021). **Introducing four new characters.**

Characters diagnostic of Sebecia: posterior extent of maxilla anterior to anterior margin of orbit; unsculpted region in the dentary below the toothrow absent; dorsal edge of dentary sinusoidal, with two concave waves; splenial robust dorsally; anterior dentary teeth opposite premaxilla-maxilla contact more than twice the length of other dentary teeth; dentary alveoli five to nine converging to the main axis of the symphysis and dentary alveoli ten to twelve diverging.

Phylogenetic search procedure: Heuristic searches in TNT: 10000 repetitions.

Pinheiro *et al.* (2023):

Matrix built using: Buscalioni & Sanz (1988); Norell (1988); Gasparini *et al.* (1993); Clark (1994); Ortega *et al.* (1996, 2000); Wu & Sues (1996); Brochu (1997, 1999, 2011); Gomani (1997); Wu *et al.* (1997); Buckley & Brochu (1999); Pol (1999a, b); Buckley *et al.* (2000); Sereno *et al.* (2001); Martinelli (2003); Pol & Norell (2004a, b); Pol *et al.* (2004, 2012, 2014); Turner (2004, 2006); Pol & Apesteguia (2005); Zaher *et al.* (2006); Larsson & Sues (2007); Riff (2007); de Andrade & Bertini (2008a ,b); Turner & Buckley (2008); Novas *et al.* (2009); Pol & Gasparini (2009); Sereno & Larsson (2009); O'Connor *et al.* (2010); Turner & Sertich (2010); de Andrade *et al.* (2011); Montefeltro *et al.* (2011); Pol & Powell (2011); Riff & Kellner (2011); Pinheiro *et al.* (2018, 2021). **Introducing four new characters.**

Characters diagnostic of Sebecia: Primary pterygoidean palate forms posterior, lateral and part of the anterior margin of the choana; lateral surface of the anterior region of the surangular and the posterior region of the dentary with a deep, well-defined longitudinal groove; dentary with lateral concavity for the reception of the enlarged maxillary tooth; dorsal edge of dentary sinusoidal with two concave waves; splenial robust posterior to symphysis; **jugal portion of postorbital bar anteriorly continuous but posteriorly inset from lateral surface of jugal**; lateral contour of snout sinusoidal; premaxillary palate circular paramedian depressions located anteriorly on the premaxilla; anterior half of palatines between suborbital fenestrae flared anteriorly; first and second premaxillary teeth nearly confluent; premaxilla - maxilla lateral fossa excavating alveolus of last premaxillary tooth.

Phylogenetic search procedure: New Technology Search (Sectorial, Ratchet, Tree fusing) in TNT: find minimum length 60 times followed by heuristic searches in TNT with trees found previously. Unordered characters.

Sebecosuchia:

Gasparini *et al.* (1991):

Matrix built using: none. **Introducing 19 new characters.**

Characters diagnostic of Sebecosuchia: laterally compressed rostrum; absence of antorbital fenestra; internal nares very large; strongly concave palate; vertical pterygoids.

Phylogenetic search procedure: implicit enumeration in Hennig86.

Gasparini *et al.* (1993):

Matrix built using: no data available.

Characters diagnostic of Sebecosuchia: mesorostry; rostrum strongly compressed; absence of antorbital fenestra; anterior palate concave; very large choanae; vertical pterygoids; serrations of the teeth.

Phylogenetic search procedure: implicit enumeration in Hennig86. All characters except one ordered.

Ortega *et al.* (1996):

Matrix built using: Legasa *et al*. (1994). **Introducing 14 new characters.**

Characters diagnostic of Sebecosuchia: longitudinal depression of the dentary that forms a deep fossa around the mandibular fenestra.

Phylogenetic search procedure: implicit enumeration in Hennig86.

Gomani (1997):

Matrix built using: Benton & Clark (1988); Clark (1994); Gasparini *et al*. (1991). **Introducing eight new characters.**

Characters diagnostic of Sebecosuchia: narrow rostrum anterior to orbits and broadening abruptly at the orbits; strongly concave palate; squamosal position not bent; extremely large choanae.

Phylogenetic search procedure: branch-and-bound in PAUP.

Buckley & Brochu (1999):

Matrix built using: Clark (1994); Ortega *et al*. (1996). **Introducing five new characters.**

Characters diagnostic of Sebecosuchia: narrow rostrum anterior to orbits and broadening abruptly at the orbits; dorsal surface of frontal and parietal with narrow midline ridge; posterolateral edge of squamosal extends posteriorly as a long process; choanae extremely large, nearly half of skull width; antorbital fenestra absent; lateral surface of dentary with longitudinal groove.

Phylogenetic search procedure: heuristic search in PAUP.

Buckley *et al*. (2000):

Matrix built using: Clark (1994); Buckley & Brochu (1999); Ortega *et al*. (1996); Gomani (1997). **Introducing three new characters.**

Characters diagnostic of Sebecosuchia: Data not available.

Phylogenetic search procedure: Data not available.

Ortega *et al*. (2000):

Matrix built using: Molnar (1981); Clark (1986, 1994); Benton & Clark (1988); Clark *et al*. (1989); Buscalioni & Sanz (1990); Parrish (1991); Gasparini *et al*. (1991, 1993); Sereno & Wild (1992); Wu & Chatterjee (1993); Legasa *et al*. (1994); Wu *et al*. (1994, 1995); Busbey (1995); Ortega & Buscalioni (1995); Ortega *et al*. (1996); Wu & Sues (1996).

Characters diagnostic of Sebecosuchia: distance from anterior orbital edge to anterior contour of rostrum equal or longer than distance from anterior orbital edge to posterior parietal contour; premaxillary - maxillary notch; teeth set in isolated alveoli; infratemporal fenestra much longer than deep; big slot-like *intramandibularis* foramen; lateral surface of anterior branch of jugal with a pronounced triangular depression; second or third maxillary alveoli enlarged; lateral surface of jugal not visible in ventral view, jugal is straight.

Phylogenetic search procedure: Data not available.

Sereno *et al*. (2001):

Matrix built using: Clark (1994); Ortega *et al*. (1996); Wu & Sues (1996); Wu *et al*. (1997, 2001); Buckley *et al*. (2000); Larsson (2000); Larsson & Gado (2000). **Introducing ten new characters.**

Characters diagnostic of Sebecosuchia: Data not available.

Phylogenetic search procedure: Three characters ordered.

Tykosky *et al*. (2002):

Matrix built using: Buckley *et al*. (2000). **Introducing two new characters.**

Characters diagnostic of Sebecosuchia: Data not available.

Phylogenetic search procedure: Heuristic searches in PAUP. Different runs with all characters unordered, two characters ordered, and five characters ordered.

Pol (2003):

Matrix built using: Buscalioni & Sanz (1988); Clark (1994); Ortega *et al*. (1996, 2000); Wu & Sues (1996); Wu *et al*. (1996); Brochu (1997); Gomani (1997); Pol (1999a ,b); Buckley *et al*. (2000).

Characters diagnostic of Sebecosuchia: Rostrum much higher than wide; notch at premaxilla - maxilla contact ventrally opened as a large fenestra; anterior dentary teeth opposite premaxillary - maxillary contact more than twice the length of other dentary teeth; unsculpted region along alveolar margin on lateral surface of maxilla absent; lateral surface of the dentary with a longitudinal depression; tooth margins with denticulate carinae; infratemporal fenestra very anteroposteriorly elongated.

Phylogenetic search procedure: Heuristic searches in NONA: 10000 repetitions. Equal weighting.

Sereno *et al*. (2003):

Matrix built using: Clark (1994); Ortega *et al*. (1996); Wu & Sues (1996); Wu *et al*. (1997); Buckley *et al*. (2000); Larsson (2000); Larsson & Gado (2000); Sereno *et al*. (2001); Wu *et al*. (2001). **Introducing three new characters.**

Characters diagnostic of Sebecosuchia: Data not available.

Phylogenetic search procedure: Four ordered characters.

Carvalho *et al*. (2004):

Matrix built using: Ortega *et al*. (2000). **Introducing one new character.**

Characters diagnostic of Sebecosuchia: Distance from anterior orbital edge to anterior contour of rostrum at least twice longer than distance from anterior orbital edge to posterior parietal contour; premaxillary - maxillary suture zigzag-shaped in lateral view; premaxillary - maxillary notch; nasals caudally separated by an anterior sagittal projection of the frontal; quadratojugal not exposed in lateral view; outer surface of squamosal dorsally oriented; antorbital fenestra absent; splenial robust posterior to symphysis; mesial and distal margin of tooth crowns with denticulate carinae; glenoid fossa of articular craniocaudally similar to articular surface of quadrate; tip of maxillary and dentary tooth crowns caudally curved; postmaxillary internal nares absent; lacrimal descending lateral process laminar; cranial jugal branch much deeper than caudal one; lateral surface of jugal not visible in ventral view, jugal straight.

Phylogenetic search procedure: Heuristic searches in PAUP: 100 repetitions. Reweighted characters after a first run.

Pol & Norell (2004a):

Matrix built using: Buscalioni & Sanz (1988); Gasparini *et al*. (1993); Clark (1994); Ortega *et al*. (1996, 2000); Wu & Sues (1996); Brochu (1997); Gomani (1997); Wu *et al*. (1997); Buckley & Brochu (1999); Pol (1999a, b); Buckley *et al*. (2000). **Introducing seven new characters.**

Characters diagnostic of Sebecosuchia: Data not available.

Phylogenetic search procedure: Heuristic searches in NONA: 1000 repetitions. Equal weighting.

Pol & Norell (2004b):

Matrix built using: Buscalioni & Sanz (1988); Gasparini *et al*. (1993); Clark (1994); Ortega *et al*. (1996, 2000); Wu & Sues (1996); Brochu (1997); Gomani (1997); Wu *et al*. (1997); Buckley & Brochu (1999); Pol (1999a, b); Buckley *et al*. (2000); Pol & Norell (2004a). **Introducing ten new characters.**

Characters diagnostic of Sebecosuchia: Data not available.

Phylogenetic search procedure: Heuristic searches in NONA: 1000 repetitions. Equal weighting.

Pol *et al*. (2004):

Matrix built using: Buscalioni & Sanz (1988); Gasparini *et al*. (1991); Clark (1994); Ortega *et al*. (1996, 2000); Wu & Sues (1996); Brochu (1997); Gomani (1997); Wu *et al*. (1997); Buckley & Brochu (1999); Pol (1999a, b); Buckley *et al*. (2000); Pol & Norell (2004a). **Introducing three new characters.**

Characters diagnostic of Sebecosuchia: Data not available.

Phylogenetic search procedure: Heuristic searches in NONA: 1000 repetitions. Equal weighting.

Company *et al*. (2005):

Matrix built using: Ortega *et al*. (1996, 2000); Tykosky *et al*. (2002).

Characters diagnostic of Sebecosuchia: presence of premaxillary-maxillary notch; enlargement of second or third maxillary tooth; big, slot-like foramen *intramandibularis oralis*.

Phylogenetic search procedure: Branch-and-bound in PAUP.

Pol & Apesteguia (2005):

Matrix built using: Buscalioni & Sanz (1988); Gasparini *et al*. (1993); Clark (1994); Ortega *et al*. (1996, 2000); Wu & Sues (1996); Brochu (1997); Gomani (1997); Wu *et al*. (1997); Buckley & Brochu (1999); Pol (1999a, b); Buckley *et al*. (2000); Sereno *et al*. (2001); Martinelli (2003); Pol & Norell (2004a, b); Pol *et al*. (2004); Zaher *et al*. (2006). **Introducing eleven new characters.**

Characters diagnostic of Sebecosuchia: Data not available.

Phylogenetic search procedure: Heuristic searches in TNT: 1000 repetitions. Equal weighting.

Turner & Calvo (2005):

Matrix built using: Clark (1994); Ortega *et al*. (1996); Gomani (1997); Wu *et al*. (1997); Buckley & Brochu (1999); Buckley *et al*. (2000); Pol (2003); Sereno *et al*. (2003). **Introducing five new characters.**

Characters diagnostic of Sebecosuchia: lateral surface of dentary with longitudinal groove; sigmoidal toothrow in dorsal view.

Phylogenetic search procedure: Unordered characters and equal weighting.

Turner (2006):

Matrix built using: Clark (1994); Ortega *et al*. (1996); Gomani (1997); Wu *et al*. (1997); Buckley & Brochu (1999); Buckley *et al*. (2000); Pol (2003); Sereno *et al*. (2003); Turner (2004); Turner & Calvo (2005). **Introducing two new characters.**

Characters diagnostic of Sebecosuchia: rostrum narrow anterior to orbits, broadening abruptly at orbits; rostrum higher than wide; antorbital fenestra absent; lateral surface of dentary with longitudinal groove; splenial robust posterodorsal to symphysis; toothrow sigmoidal in dorsal view; anteriorly, palatines are narrow and "arrow"-shaped, sharply dividing the maxillae.

Phylogenetic search procedure: Heuristic searches in PAUP: 1000 repetitions. Unordered characters, equal weighting.

Zaher *et al*. (2006):

Matrix built using: Buscalioni & Sanz (1988); Gasparini *et al*. (1991); Clark (1994); Ortega *et al*. (1996, 2000); Wu & Sues (1996); Brochu (1997); Gomani (1997); Wu *et al*. (1997); Buckley & Brochu (1999); Pol (1999a, b); Buckley *et al*. (2000); Pol & Norell (2004a, b). **Introducing six new characters.**

Characters diagnostic of Sebecosuchia: narrow oreinirostral rostrum; ventrally opened notch at premaxilla - maxilla contact present as a large fenestra; one wave of enlarged maxillary teeth; anterior dentary teeth opposite premaxilla - maxilla contact more than twice the length of other dentary teeth; unsculpted region along alveolar margin on lateral surface of maxilla absent; lateral surface of the dentary with a longitudinal depression; tooth margin with denticulate carinae; nasal lateral edges nearly parallel; unsculpted region in the dentary below the toothrow absent; infratemporal fenestra very anteroposteriorly elongated.

Phylogenetic search procedure: Heuristic searches in PAUP: 100 repetitions.

Fiorelli & Calvo (2007):

Matrix built using: Buscalioni & Sanz (1988); Sereno (1991); Clark (1994); Ortega *et al*. (1996, 2000); Wu & Sues (1996); Brochu (1997); Gomani (1997); Wu *et al*. (1997); Buckley & Brochu (1999); Pol (1999a); Buckley *et al*. (2000); Martinelli (2003); Pol & Norell (2004a, b); Pol *et al*. (2004); Fiorelli (2005). **Introducing 20 new characters.**

Characters diagnostic of Sebecosuchia: external surface of dorsal cranial bones slightly grooved; narrow oreinirostral rostrum; jugal participating in margin of antorbital fossa; lateral surface of the dentary with a longitudinal depression; tooth margin with denticulate carinae; nasal lateral edges nearly parallel; antorbital region of jugal more dorsoventrally expanded than infraorbital region; cheek teeth constricted at base of crown; foramen *intramandibularis oralis* big and slot-like; ectopterygoid medial process forked.

Phylogenetic search procedure: Heuristic searches in NONA: 1000 repetitions. 25 characters ordered, equal weighting.

Fiorelli & Calvo (2008):

Matrix built using: Sereno (1991); Clark (1994); Wu & Sues (1996); Pol (1999a, b); Sereno *et al*. (2001); Martinelli (2003); Pol & Norell (2004b); Pol *et al*. (2004); Fiorelli (2005); Pol & Apesteguia (2005); Zaher *et al*. (2006); Fiorelli & Calvo (2007).

Characters diagnostic of Sebecosuchia: data not available.

Phylogenetic search procedure: Heuristic searches in TNT: 1000 replications. Equal weighting.

Turner & Buckley (2008):

Matrix built using: Buscalioni & Sanz (1988); Norell (1988); Gasparini *et al*. (1993, 2006); Clark (1994); Ortega *et al*. (1996, 2000); Wu & Sues (1996); Brochu (1997, 1999); Gomani (1997); Wu *et al*. (1997); Buckley & Brochu (1999); Pol (1999a, b); Buckley *et al*. (2000); Sereno *et al*. (2001); Martinelli (2003); Pol & Norell (2004a, b); Pol *et al*. (2004); Turner (2004); Pol & Apesteguia (2005); Turner (2006); Zaher *et al*. (2006). **Introducing six new characters.**

Characters diagnostic of Sebecosuchia: Data not available.

Phylogenetic search procedure: Heuristic searches in TNT: 1000 replications. Equal weighting.

Novas *et al*. (2009):

Matrix built using: Data not available.

Characters diagnostic of Sebecosuchia: Data not available.

Phylogenetic search procedure: Data not available.

Pol *et al*. (2009):

Matrix built using: Buscalioni & Sanz (1988); Norell (1988); Gasparini *et al*. (1993); Clark (1994); Ortega *et al*. (1996, 2000); Wu & Sues (1996); Brochu (1997, 1999); Gomani (1997); Wu *et al*. (1997); Buckley & Brochu (1999); Pol (1999a, b); Buckley *et al*. (2000); Sereno *et*

al. (2001); Pol & Norell (2004a, b); Pol *et al*. (2004); Pol & Apesteguia (2005); Turner (2006); Zaher *et al*. (2006); Pol & Gasparini (2009). **Introducing nine new characters.**

Characters diagnostic of Sebecosuchia: Data not available.

Phylogenetic search procedure: Heuristic searches in TNT: 1000 replications. Equal weighting.

Turner & Sertich (2010):

Matrix built using: Buscalioni & Sanz (1988); Norell (1988); Clark (1994); Ortega *et al*. (1996, 2000); Wu & Sues (1996); Brochu (1997, 1999); Gomani (1997); Wu *et al*. (1997); Buckley & Brochu (1999); Pol (1999a, b); Buckley *et al*. (2000); Sereno *et al*. (2001); Jouve (2004, 2009); Pol & Norell (2004a, b); Pol *et al*. (2004, 2009); Pol & Apesteguia (2005); Gasparini *et al*. (2006); Turner (2006); de Andrade & Bertini (2008a, b); Turner & Buckley (2008); Sereno & Larsson (2009). **Introducing seven new characters.**

Characters diagnostic of Sebecosuchia: Data not available.

Phylogenetic search procedure: Heuristic searches in TNT: 1000 replications. 34 ordered characters, equal weighting.

Iori & Carvalho (2011):

Matrix built using: Novas *et al*. (2009).

Characters diagnostic of Sebecosuchia: Data not available.

Phylogenetic search procedure: Data not available.

Nascimento & Zaher (2011):

Matrix built using: Buscalioni & Sanz (1988); Gasparini *et al*. (1991); Clark (1994); Ortega *et al*. (1996, 2000); Wu & Sues (1996); Brochu (1997); Gomani (1997); Wu *et al*. (1997); Brochu (1999); Buckley & Brochu (1999); Pol (1999a, b); Buckley *et al*. (2000); Sereno *et al*. (2001);

Martinelli (2003); Pol & Norell (2004a, b); Pol *et al*. (2004); Gasparini *et al*. (2005); Pol & Apesteguia (2005); Riff (2007). **Introducing five new characters.**

Characters diagnostic of Sebecosuchia: Ventrally opened notch on ventral edge of rostrum at premaxilla - maxilla contact present as a large fenestra, closed or almost closed by the premaxilla - maxilla external contact; one wave of enlarged maxillary teeth; anterior dentary teeth opposite premaxilla - maxilla contact more than twice the length of other dentary teeth; **mandibular symphysis shallow and anteriorly convex in lateral view**; no unsculpted region along alveolar margin on lateral surface of maxillary; tooth margins with denticulate carinae; nasal lateral edges nearly parallel; no unsculpted region in the dentary below the toothrow; dentary with lateral concavity for the reception of the enlarged maxillary tooth; dorsal edge of dentary with a single dorsal expansion and concave posterior to this; **lateral surface of dentaries below alveolar margin, at mid to posterior region of toothrow vertically oriented, continuous with rest of lateral surface of the dentaries**; evaginated maxillary alveolar edges present as a continuous sheet.

Phylogenetic search procedure: Heuristic searches in PAUP: 100 replications.

Pol & Powell (2011):

Matrix built using: Buscalioni & Sanz (1988); Norell (1988); Gasparini *et al*. (1993); Clark (1994); Ortega *et al*. (1996, 2000); Wu & Sues (1996); Brochu (1997, 1999); Gomani (1997); Wu *et al*. (1997); Buckley & Brochu (1999); Pol (1999a, b); Buckley *et al*. (2000); Larsson & Gado (2000); Sereno *et al*. (2001); Martinelli (2003); Pol & Norell (2004a, b); Pol *et al*. (2004, 2009); Turner (2004, 2006); Pol & Apesteguia (2005); Zaher *et al*. (2006); Larsson & Sues (2007); Riff (2007); de Andrade & Bertini (2008a); Turner & Buckley (2008); Pol & Gasparini (2009). **Introducing sixteen new characters.**

Characters diagnostic of Sebecosuchia: Data not available.

Phylogenetic search procedure: Heuristic searches in TNT: 1000 replications. 35 ordered characters, equal weighting.

Soto *et al.* (2011):

Matrix built using: Buscalioni & Sanz (1988); Gasparini *et al*. (1993); Clark (1994); Ortega *et al*. (1996, 2000); Wu & Sues (1996); Brochu (1997, 1999); Gomani (1997); Wu *et al*. (1997, 2001); Buckley & Brochu (1999); Pol (1999a, b); Buckley *et al*. (2000); Sereno *et al*. (2001); Martinelli (2003); Pol (2003); Pol & Norell (2004a, b); Pol *et al*. (2004); Pol & Apesteguia (2005); Gasparini *et al*. (2006); Zaher *et al*. (2006); Pol & Gasparini (2009). **Introducing seventeen new characters.**

Characters diagnostic of Sebecosuchia: Narrow oreinirostral rostrum; ventrally opened notch on ventral edge of rostrum at premaxilla - maxilla contact present as a large fenestra; one wave of enlarged maxillary teeth; anterior dentary teeth opposite premaxilla - maxilla contact more than twice the length of other dentary teeth; **mandibular symphysis deep and anteriorly convex in lateral view**; unsculpted region along alveolar margin on lateral surface of maxilla absent; lateral surface of the anterior region of surangular and posterior region of the dentary with a longitudinal depression; tooth margins with denticulate carinae; nasal lateral edges nearly parallel; unsculpted region in the dentary below the toothrow absent; dorsal edge of dentary with a single dorsal expansion and concave posterior to this**; lateral surface of dentaries below alveolar margin, at mid to posterior region of toothrow vertically oriented, continuous with rest of lateral surface of the dentaries**; evaginated maxillary alveolar edges present as a continuous sheet.

Phylogenetic search procedure: Heuristic searches in TNT: 1000 replications. 31 ordered characters, equal weighting.

Pol *et al.* (2012):

Matrix built using: Buscalioni & Sanz (1988); Norell (1988); Gasparini *et al*. (1993); Clark (1994); Ortega *et al*. (1996, 2000); Wu & Sues (1996); Gomani (1997); Wu *et al.* (1997); Brochu (1997, 1999); Buckley & Brochu (1999); Pol (1999a, b); Buckley *et al*. (2000); Larsson & Gado (2000); Sereno *et al*. (2001); Martinelli (2003); Pol & Norell (2004a, b); Pol *et al.* (2004, 2009); Pol & Apesteguia (2005); Turner (2006); Zaher *et al*. (2006) ; Larsson & Sues (2007); Riff (2007); de Andrade & Bertini (2008); Turner & Buckley (2008); Novas *et* al. (2009); Pol & Gasparini (2009); Pol & Powell (2011). **Introducing fifty-two new characters.**

Characters diagnostic of Sebecosuchia: **Mandibular symphysis deep and anteriorly convex in lateral view**; unsculpted region in the dentary below the toothrow absent; dorsal edge of dentary with a single dorsal expansion and concave posterior to this; **lateral surface of dentaries below alveolar margin, at mid to posterior region of toothrow vertically oriented, continuous with rest of lateral surface of the dentaries**.

Phylogenetic search procedure: Heuristic searches in TNT: 1000 replications. 37 ordered characters, equal weighting.

Adams (2013):

Matrix built using: Pol *et al*. (2009); Turner & Sertich (2010).

Characters diagnostic of Sebecosuchia: Data not available.

Phylogenetic search procedure: Heuristic searches in TNT: 1000 replications. Equal weighting.

Iori *et al*. (2013):

Matrix built using: Novas *et al*. (2009).

Characters diagnostic of Sebecosuchia: Data not available.

Phylogenetic search procedure: Data not available.

Adams (2014):

Matrix built using: Buscalioni & Sanz (1988); Norell (1988); Clark (1994); Ortega *et al*. (1996, 2000); Wu & Sues (1996); Brochu (1997, 1999); Gomani (1997); Wu *et al*. (1997); Buckley & Brochu (1999); Pol (1999a, b); Buckley *et al*. (2000); Sereno *et al*. (2001); Martinelli (2003); Jouve (2004, 2009); Pol & Norell (2004a, b); Pol *et al*. (2004, 2009); Turner (2004, 2006); Pol & Apesteguia (2005); Gasparini *et al*. (2006); Zaher *et al*. (2006); de Andrade & Bertini (2008a, b); Turner & Buckley (2008); Sereno & Larsson (2009); Turner & Sertich (2010); Adams (2013); Pritchard *et al*. (2013); Turner (2015).

Characters diagnostic of Sebecosuchia: Data not available.

Phylogenetic search procedure: Heuristic searches in TNT: 1000 replications. Equal weighting.

Kellner *et al.* (2014):

Matrix built using: Buscalioni & Sanz (1988); Norell (1988); Gasparini *et al.* (1993); Clark (1994); Ortega *et al.* (1996, 2000); Wu & Sues (1996); Gomani (1997); Wu *et al.* (1997); Brochu (1997, 1999); Buckley & Brochu (1999); Pol (1999a, b); Buckley *et al.* (2000); Larsson & Gado (2000); Sereno *et al.* (2001); Martinelli (2003); Pol & Norell (2004a, b); Pol *et al.* (2004, 2009); Pol & Apesteguia (2005); Turner (2006); Zaher *et al.* (2006) ; Larsson & Sues (2007); Riff (2007); de Andrade & Bertini (2008a, b); Turner & Buckley (2008); Novas *et* al. (2009); Pol & Gasparini (2009); Pol & Powell (2011); Pol *et al.* (2012).

Characters diagnostic of Sebecosuchia: **Mandibular symphysis deep and anteriorly convex in lateral view**; unsculpted region in the dentary below the toothrow absent; dorsal edge of dentary with a single dorsal expansion and concave posterior to this; **lateral surface of dentaries below alveolar margin, at mid to posterior of toothrow vertically oriented, continuous with rest of lateral surface of dentaries**.

Phylogenetic search procedure: Characters unordered and ordered.

Pol *et al.* (2014):

Matrix built using: Buscalioni & Sanz (1988); Norell (1988); Gasparini *et al.* (1993); Clark (1994); Ortega *et al.* (1996, 2000); Wu & Sues (1996); Brochu (1997, 1999); Gomani (1997); Wu *et al.* (1997); Buckley & Brochu (1999); Pol (1999a, b); Buckley *et al.* (2000); Sereno *et al.* (2001); Martinelli (2003); Pol & Norell (2004a, b); Pol *et al.* (2004, 2009, 2012); Turner (2004, 2006); Pol & Apesteguia (2005); Zaher *et al.* (2006); Larsson & Sues (2007); Riff (2007); de Andrade & Bertini (2008a); Turner & Buckley (2008); Pol & Gasparini (2009); Sereno & Larsson (2009); O'Connor *et al.* (2010); Turner & Sertich (2010); de Andrade *et al.* (2011); Montefeltro *et al.* (2011); Nascimento & Zaher (2011); Pol & Powell (2011); Riff & Kellner (2011). **Introducing thirty-four new characters.**

Characters diagnostic of Sebecosuchia: Ventrally opened notch on ventral edge of rostrum at premaxilla - maxilla contact present as a large notch; anterior dentary teeth opposite premaxilla - maxilla contact more than twice the length of other dentary teeth; unsculpted region along alveolar margin on lateral surface of maxilla absent; lateral surface of the anterior region of the surangular and posterior region of the dentary with a deep, well-defined longitudinal groove; dorsoventral height of antorbital region of jugal more expanded than infraorbital region; large and aligned neurovascular foramina on lateral maxillary surface absent; no unsculpted region in the dentary below the toothrow; outer surface of squamosal along the site of attachment of the ear valve groove reduced and vertically oriented; skull roof trapezoidal shape in dorsal view; **lateral surface of dentaries below alveolar margin, at mid to posterior region of toothrow vertically oriented, continuous with rest of lateral surface of the dentaries**; paraoccipital process development lateral to cranioquadrate opening long; ventral margin of jugal at posterior end of ectopterygoid contact separated by a notch from infratemporal bar of jugal.

Phylogenetic search procedure: Heuristic searches in TNT: 10000 replications. 42 ordered characters, equal weighting.

Sertich & O'Connor (2014):

Matrix built using: Buscalioni & Sanz (1988); Norell (1988); Clark (1994); Ortega *et al*. (1996, 2000); Wu & Sues (1996); Brochu (1997, 1999); Gomani (1997); Wu *et al*. (1997); Buckley & Brochu (1999); Pol (1999a, b); Buckley *et al*. (2000); Sereno *et al*. (2001); Jouve (2004, 2009); Pol & Norell (2004a, b); Pol *et al*. (2004, 2009); Pol & Apesteguia (2005); Gasparini *et al*. (2006); Turner (2006); de Andrade & Bertini (2008a, b); Turner & Buckley (2008); Sereno & Larsson (2009); Turner & Sertich (2010). **Introducing three new characters.**

Characters diagnostic of Sebecosuchia: Data not available.

Phylogenetic search procedure: Heuristic searches in TNT: 1000 replications. Equal weighting.

Leardi *et al.* (2015a):

Matrix built using: Buscalioni & Sanz (1988); Norell (1988); Gasparini *et al*. (1993); Clark (1994); Ortega *et al*. (1996, 2000); Wu & Sues (1996); Brochu (1997, 1999); Gomani (1997);

Wu *et al*. (1997); Buckley & Brochu (1999); Pol (1999a, b); Buckley *et al*. (2000); Sereno *et al*. (2001); Martinelli (2003); Pol & Norell (2004a, b); Pol *et al*. (2004, 2009, 2012, 2014); Turner (2004, 2006); Pol & Apesteguia (2005); Zaher *et al*. (2006); Larsson & Sues (2007); Riff (2007); de Andrade & Bertini (2008); Turner & Buckley (2008); Pol & Gasparini (2009); Sereno & Larsson (2009); O'Connor *et al*. (2010); Turner & Sertich (2010); de Andrade *et al*. (2011); Montefeltro *et al*. (2011); Nascimento & Zaher (2011); Pol & Powell (2011); Riff & Kellner (2011). **Introducing twenty-five new characters.**

Characters diagnostic of Sebecosuchia: narrow oreinirostral rostrum; large ventrally opened notch on ventral edge of rostrum at premaxilla - maxilla contact; anterior dentary teeth opposite premaxilla - maxilla contact more than twice the length of other dentary teeth; unsculpted region along alveolar margin on lateral surface of maxilla absent; lateral surface of the anterior region of the surangular and posterior region of the dentary with a deep, well-defined longitudinal groove; dorsoventral height of antorbital region of jugal more expanded than infraorbital region; large and aligned neurovascular foramina on lateral maxillary surface absent; no unsculpted region in the dentary below the toothrow; outer surface of squamosal along the site of attachment of the ear valve groove reduced and vertically oriented; skull roof trapezoidal shape in dorsal view; **lateral surface of dentaries below alveolar margin, at mid to posterior region of toothrow vertically oriented, continuous with rest of lateral surface of the dentaries**; paraoccipital process development lateral to cranioquadrate opening long; ventral margin of jugal at posterior end of ectopterygoid contact separated by a notch from infratemporal bar of jugal.

Phylogenetic search procedure: Heuristic searches in TNT: 10000 replications. 43 ordered characters, equal weighting.

Leardi *et al.* (2015b):

Matrix built using: Buscalioni & Sanz (1988); Norell (1988); Gasparini *et al*. (1993); Clark (1994); Ortega *et al*. (1996, 2000); Wu & Sues (1996); Brochu (1997, 1999); Gomani (1997); Wu *et al*. (1997); Buckley & Brochu (1999); Pol (1999a, b); Buckley *et al*. (2000); Sereno *et al*. (2001); Martinelli (2003); Pol & Norell (2004a, b); Pol *et al*. (2004, 2009, 2012, 2014); Turner (2004, 2006); Pol & Apesteguia (2005); Zaher *et al*. (2006); Larsson & Sues (2007); Riff (2007); de Andrade & Bertini (2008); Turner & Buckley (2008); Pol & Gasparini (2009);

Sereno & Larsson (2009); O'Connor *et al*. (2010); Turner & Sertich (2010); de Andrade *et al*. (2011); Montefeltro *et al*. (2011); Nascimento & Zaher (2011); Pol & Powell (2011); Riff & Kellner (2011); Leardi *et al*. (2015a). **Introducing two new characters.**

Characters diagnostic of Sebecosuchia: Suture between the postorbital and the squamosal convex anteriorly in lateral view.

Phylogenetic search procedure: Heuristic searches in TNT: 1000 or 10000 replications. 43 ordered characters, equal weighting.

Fiorelli *et al*. (2016):

Matrix built using: Buscalioni & Sanz (1988); Norell (1988); Sereno (1991); Gasparini *et al*. (1993); Clark (1994); Ortega *et al*. (1996, 2000); Wu & Sues (1996); Gomani (1997); Brochu (1997, 1999); Wu *et al*. (1997); Buckley & Brochu (1999); Pol (1999a, b); Buckley *et al*. (2000); Sereno *et al*. (2001); Martinelli (2003); Pol & Norell (2004a, b); Pol *et al*. (2004, 2009, 2012, 2014); Turner (2004, 2006); Pol & Apesteguia (2005); Zaher *et al*. (2006); Fiorelli & Calvo (2007); Larsson & Sues (2007); Riff (2007); de Andrade & Bertini (2008b); Turner & Buckley (2008); Novas *et al*. (2009); Pol & Gasparini (2009); Sereno & Larsson (2009); O'Connor *et al*. (2010); Turner & Sertich (2010); de Andrade *et al*. (2011); Montefeltro *et al*. (2011); Nascimento & Zaher (2011); Pol & Powell (2011); Riff & Kellner (2011); Pritchard *et al*. (2013); Leardi *et al*. (2015a, b). **Introducing one new character.**

Characters diagnostic of Sebecosuchia: narrow oreinirostral rostrum; large ventrally opened notch at premaxilla-maxilla contact; anterior dentary teeth opposite premaxilla - maxilla contact twice the length of other dentary teeth; no unsculpted region along alveolar margin on lateral surface of maxilla; lateral surface of the anterior region of the dentary and posterior region of the surangular with a deep, well-defined longitudinal groove; antorbital region of jugal more expanded dorsoventrally than infraorbital region; no large and aligned neurovascular foramina on lateral maxillary surface; no unsculpted region in the dentary below the toothrow; outer surface of squamosal along the site of the attachment of ear valve groove reduced and vertically oriented; skull roof trapezoidal-shaped in dorsal view; **lateral surface of dentaries below alveolar margin, at mid to posterior of toothrow vertically oriented, continuous with rest of lateral surface of dentaries**; long paraoccipital process development lateral to

cranioquadrate opening; ventral margin of jugal at posterior end of ectopterygoid contact separated by a notch from infratemporal bar of jugal.

Phylogenetic search procedure: Heuristic searches in TNT: 1000 or 10000 replications. 43 ordered characters, equal weighting.

Godoy *et al*. (2016):

Matrix built using: Buscalioni & Sanz (1988); Norell (1988); Gasparini *et al*. (1993); Clark (1994); Ortega *et al*. (1996, 2000); Wu & Sues (1996); Brochu (1997, 1999); Gomani (1997); Wu *et al*. (1997); Buckley & Brochu (1999); Pol (1999a, b); Buckley *et al*. (2000); Sereno *et al*. (2001); Martinelli (2003); Pol & Norell (2004a, b); Pol *et al*. (2004, 2009, 2012, 2014); Turner (2004, 2006); Pol & Apesteguia (2005); Zaher *et al*. (2006); Larsson & Sues (2007); Riff (2007); de Andrade & Bertini (2008a); Turner & Buckley (2008); Pol & Gasparini (2009); Sereno & Larsson (2009); O'Connor *et al*. (2010); Turner & Sertich (2010); de Andrade *et al*. (2011); Montefeltro *et al*. (2011); Nascimento & Zaher (2011); Pol & Powell (2011); Riff & Kellner (2011); Leardi *et al*. (2015a, b).

Characters diagnostic of Sebecosuchia: Suture between the postorbital and the squamosal convex anteriorly in lateral view.

Phylogenetic search procedure: Heuristic searches in TNT: 10000 replications.

Martin & de Lapparent de Broin (2016):

Matrix built using: Buscalioni & Sanz (1988); Norell (1988); Gasparini *et al*. (1993); Clark (1994); Ortega *et al*. (1996, 2000); Wu & Sues (1996); Brochu (1997, 1999); Gomani (1997); Wu *et al*. (1997); Buckley & Brochu (1999); Pol (1999a, b); Buckley *et al*. (2000); Sereno *et al*. (2001); Martinelli (2003); Pol & Norell (2004a, b); Pol *et al*. (2004, 2009, 2012, 2014); Turner (2004, 2006); Pol & Apesteguia (2005); Zaher *et al*. (2006); Larsson & Sues (2007); Riff (2007); de Andrade & Bertini (2008a, b); Turner & Buckley (2008); Pol & Gasparini (2009); Sereno & Larsson (2009); O'Connor *et al*. (2010); Turner & Sertich (2010); de Andrade *et al*. (2011); Montefeltro *et al*. (2011); Nascimento & Zaher (2011); Pol & Powell (2011); Riff & Kellner (2011).

Characters diagnostic of Sebecosuchia: Data not available.

Phylogenetic search procedure: Heuristic searches in TNT: 1000 replications.

Dal Sasso *et al.* (2017):

Matrix built using: Buscalioni & Sanz (1988); Norell (1988); Sereno (1991); Gasparini *et al.* (1993); Clark (1994); Ortega *et al.* (1996, 2000); Wu & Sues (1996); Gomani (1997); Brochu (1997, 1999); Wu *et al.* (1997); Buckley & Brochu (1999); Pol (1999a, b); Buckley *et al.* (2000); Sereno *et al.* (2001); Martinelli (2003); Pol & Norell (2004a, b); Pol *et al.* (2004, 2009, 2012, 2014); Turner (2004, 2006); Pol & Apesteguia (2005); Zaher *et al.* (2006); Fiorelli & Calvo (2007); Larsson & Sues (2007); Riff (2007); de Andrade & Bertini (2008a, b); Turner & Buckley (2008); Novas *et al.* (2009); Pol & Gasparini (2009); Sereno & Larsson (2009); O'Connor *et al.* (2010); Turner & Sertich (2010); de Andrade *et al.* (2011); Montefeltro *et al.* (2011); Nascimento & Zaher (2011); Pol & Powell (2011); Riff & Kellner (2011); Pritchard *et al.* (2013); Leardi *et al.* (2015a, b); Fiorelli *et al.* (2016).

Characters diagnostic of Sebecosuchia: **mandibular symphysis deep and anteriorly concave in lateral view**; denticulate carinae; dorsal edge of the dentary with a single dorsal expansion and concave posterior to this; **lateral surface of dentaries below alveolar margin, at mid to posterior region of toothrow vertically oriented, continuous with rest of lateral surface of the dentaries**.

Phylogenetic search procedure: Heuristic searches in PAUP: 50000 replications. 43 ordered characters.

Leardi *et al.* (2018):

Matrix built using: Buscalioni & Sanz (1988); Norell (1988); Gasparini *et al.* (1993); Clark (1994); Ortega *et al.* (1996, 2000); Wu & Sues (1996); Brochu (1997, 1999); Gomani (1997); Wu *et al.* (1997); Buckley & Brochu (1999); Pol (1999a, b); Buckley *et al.* (2000); Sereno *et al.* (2001); Martinelli (2003); Pol & Norell (2004a, b); Pol *et al.* (2004, 2009, 2012, 2014); Turner (2004, 2006); Pol & Apesteguia (2005); Zaher *et al.* (2006); Larsson & Sues (2007); Riff (2007); de Andrade & Bertini (2008a, b); Turner & Buckley (2008); Pol & Gasparini (2009); Sereno & Larsson (2009); O'Connor *et al.* (2010); Turner & Sertich (2010); de Andrade *et al.* (2011); Montefeltro *et al.* (2011); Nascimento & Zaher (2011); Pol & Powell (2011); Riff

& Kellner (2011); Leardi *et al*. (2015a, b); Fiorelli *et al*. (2016). **Introducing one new character.**

Characters diagnostic of Sebecosuchia: Maxilla with six teeth; nasal - premaxilla suture laterally concave; anterior region of dentary symphysis in ventral view has a distinct anterior process with parallel lateral margins; transitional tooth located at the contact between the premaxilla and the maxilla, both of which contribute to the alveolar walls.

Phylogenetic search procedure: New Technology Search in TNT: minimum length hit 100 times. 43 ordered characters.

Martinelli *et al*. (2018):

Matrix built using: Buscalioni & Sanz (1988); Norell (1988); Sereno (1991); Gasparini *et al*. (1993); Clark (1994); Ortega *et al*. (1996, 2000); Wu & Sues (1996); Gomani (1997); Brochu (1997, 1999); Wu *et al*. (1997); Buckley & Brochu (1999); Pol (1999a, b); Buckley *et al*. (2000); Sereno *et al*. (2001); Martinelli (2003); Pol & Norell (2004a, b); Pol *et al*. (2004, 2009, 2012, 2014); Turner (2004, 2006); Pol & Apesteguia (2005); Zaher *et al*. (2006); Fiorelli & Calvo (2007); Larsson & Sues (2007); Riff (2007); de Andrade & Bertini (2008a, b); Turner & Buckley (2008); Novas *et al*. (2009); Pol & Gasparini (2009); Sereno & Larsson (2009); O'Connor *et al*. (2010); Turner & Sertich (2010); de Andrade *et al*. (2011); Montefeltro *et al*. (2011); Nascimento & Zaher (2011); Pol & Powell (2011); Riff & Kellner (2011); Pritchard *et al*. (2013); Leardi *et al*. (2015a, b); Fiorelli *et al*. (2016).

Characters diagnostic of Sebecosuchia: narrow oreinirostral rostrum; large ventrally opened notch at premaxilla-maxilla contact; anterior dentary teeth opposite premaxilla-maxilla contact twice the length of other dentary teeth; no unsculpted region along alveolar margin on lateral surface of maxilla; lateral surface of the anterior region of the dentary and posterior region of the surangular with a deep, well-defined longitudinal groove; antorbital region of jugal more expanded dorsoventrally than infraorbital region; no large and aligned neurovascular foramina on lateral maxillary surface; no unsculpted region in the dentary below the toothrow; outer surface of squamosal along the site of the attachment of ear valve groove reduced and vertically oriented; skull roof trapezoidal-shaped in dorsal view; cross section of distal end of quadrate mediolaterally wide and anteroposteriorly thin, being approximately three times as wide as long; **lateral surface of dentaries below alveolar margin, at mid to posterior of toothrow**

vertically oriented, continuous with rest of lateral surface of dentaries; long paraoccipital process development lateral to cranioquadrate opening; quadrate body distal to otoccipital-quadrate contact in posterior view oriented ventrolaterally; posterolateral region of nasals with well-developed posterolateral processes that deflect ventrally, forming part of the lateral surface of the snout; ventral margin of jugal at posterior end of ectopterygoid contact separated by a notch from infratemporal bar of jugal.

Phylogenetic search procedure: Heuristic searches in TNT: 10000 replications. 43 ordered characters, equal weighting.

Coria *et al.* (2019):

Matrix built using: Buscalioni & Sanz (1988); Norell (1988); Gasparini *et al.* (1993); Clark (1994); Ortega *et al.* (1996, 2000); Wu & Sues (1996); Brochu (1997, 1999); Gomani (1997); Wu *et al.* (1997); Buckley & Brochu (1999); Pol (1999a, b); Buckley *et al.* (2000); Sereno *et al.* (2001); Martinelli (2003); Pol & Norell (2004a, b); Pol *et al.* (2004, 2009, 2012, 2014); Turner (2004, 2006); Pol & Apesteguia (2005); Zaher *et al.* (2006); Larsson & Sues (2007); Riff (2007); de Andrade & Bertini (2008a, b); Turner & Buckley (2008); Pol & Gasparini (2009); Sereno & Larsson (2009); O'Connor *et al.* (2010); Turner & Sertich (2010); de Andrade *et al.* (2011); Montefeltro *et al.* (2011); Nascimento & Zaher (2011); Pol & Powell (2011); Riff & Kellner (2011); Barrios *et al.* (2016).

Characters diagnostic of Sebecosuchia: data not available.

Phylogenetic search procedure: Heuristic searches in TNT: 10000 replications. 42 ordered characters, equal weighting.

Cunha *et al.* (2020):

Matrix built using: Buscalioni & Sanz (1988); Norell (1988); Sereno (1991); Gasparini *et al.* (1993); Clark (1994); Ortega *et al.* (1996, 2000); Wu & Sues (1996); Gomani (1997); Brochu (1997, 1999); Wu *et al.* (1997); Buckley & Brochu (1999); Pol (1999a, b); Buckley *et al.* (2000); Sereno *et al.* (2001); Martinelli (2003); Pol & Norell (2004a, b); Pol *et al.* (2004, 2009, 2012, 2014); Turner (2004, 2006); Pol & Apesteguia (2005); Zaher *et al.* (2006); Fiorelli &

Calvo (2007); Larsson & Sues (2007); Riff (2007); de Andrade & Bertini (2008a); Turner & Buckley (2008); Novas *et al*. (2009); Pol & Gasparini (2009); Sereno & Larsson (2009); O'Connor *et al*. (2010); Turner & Sertich (2010); de Andrade *et al*. (2011); Montefeltro *et al*. (2011); Nascimento & Zaher (2011); Pol & Powell (2011); Riff & Kellner (2011); Pritchard *et al*. (2013); Leardi *et al*. (2015a, b); Fiorelli *et al*. (2016).

Characters diagnostic of Sebecosuchia: Data not available.

Phylogenetic search procedure: Heuristic searches: 10000 replications. Unordered characters, equal weighting.

Dumont *et al*. (2020):

Matrix built using: Buscalioni & Sanz (1988); Norell (1988); Sereno (1991); Gasparini *et al*. (1993); Clark (1994); Ortega *et al*. (1996, 2000); Wu & Sues (1996); Gomani (1997); Brochu (1997, 1999); Wu *et al*. (1997); Buckley & Brochu (1999); Pol (1999a, b); Buckley *et al*. (2000); Sereno *et al*. (2001); Martinelli (2003); Pol & Norell (2004a, b); Pol *et al*. (2004, 2009, 2012, 2014); Turner (2004, 2006); Pol & Apesteguia (2005); Zaher *et al*. (2006); Fiorelli & Calvo (2007); Larsson & Sues (2007); Riff (2007); de Andrade & Bertini (2008a, b); Turner & Buckley (2008); Novas *et al*. (2009); Pol & Gasparini (2009); Sereno & Larsson (2009); O'Connor *et al*. (2010); Turner & Sertich (2010); de Andrade *et al*. (2011); Montefeltro *et al*. (2011); Nascimento & Zaher (2011); Pol & Powell (2011); Riff & Kellner (2011); Pritchard *et al*. (2013); Leardi *et al*. (2015a, b); Fiorelli *et al*. (2016).

Characters diagnostic of Sebecosuchia: narrow oreinirostral rostrum; large ventrally opened notch at premaxilla-maxilla contact; anterior dentary teeth opposite premaxilla - maxilla contact twice the length of other dentary teeth; no unsculpted region along alveolar margin on lateral surface of maxilla; lateral surface of the anterior region of the dentary and posterior region of the surangular with a deep, well-defined longitudinal groove; antorbital region of jugal more expanded dorsoventrally than infraorbital region; no large and aligned neurovascular foramina on lateral maxillary surface; no unsculpted region in the dentary below the toothrow; outer surface of squamosal along the site of the attachment of ear valve groove reduced and vertically oriented; skull roof trapezoidal-shaped in dorsal view; **lateral surface of dentaries below alveolar margin, at mid to posterior of toothrow vertically oriented, continuous with rest of lateral surface of dentaries**; long paraoccipital process development lateral to

cranioquadrate opening; ventral margin of jugal at posterior end of ectopterygoid contact separated by a notch from infratemporal bar of jugal.

Phylogenetic search procedure: New Technology Search (sectorial search and tree fusing) in TNT: minimum length hit 50 times. 43 ordered characters, equal weighting.

Sellés *et al.* (2020):

Matrix built using: Buscalioni & Sanz (1988); Norell (1988); Gasparini *et al.* (1993); Clark (1994); Ortega *et al.* (1996, 2000); Wu & Sues (1996); Brochu (1997, 1999); Gomani (1997); Wu *et al.* (1997); Buckley & Brochu (1999); Pol (1999a, b); Buckley *et al.* (2000); Sereno *et al.* (2001); Martinelli (2003); Pol & Norell (2004a, b); Pol *et al.* (2004, 2009, 2012, 2014); Turner (2004, 2006); Pol & Apesteguia (2005); Zaher *et al.* (2006); Larsson & Sues (2007); Riff (2007); de Andrade & Bertini (2008a, b); Turner & Buckley (2008); Pol & Gasparini (2009); Sereno & Larsson (2009); O'Connor *et al.* (2010); Turner & Sertich (2010); de Andrade *et al.* (2011); Montefeltro *et al.* (2011); Nascimento & Zaher (2011); Pol & Powell (2011); Riff & Kellner (2011).

Characters diagnostic of Sebecosuchia: Data not available.

Phylogenetic search procedure: Heuristic searches in TNT: 10000 replications. 42 ordered characters, equal weighting.

Bravo *et al.* (2021):

Matrix built using: Buscalioni & Sanz (1988); Norell (1988); Sereno (1991); Gasparini *et al.* (1993); Clark (1994); Ortega *et al.* (1996, 2000); Wu & Sues (1996); Gomani (1997); Brochu (1997, 1999); Wu *et al.* (1997); Buckley & Brochu (1999); Pol (1999a, b); Buckley *et al.* (2000); Sereno *et al.* (2001); Martinelli (2003); Pol & Norell (2004a, b); Pol *et al.* (2004, 2009, 2012, 2014); Turner (2004, 2006); Pol & Apesteguia (2005); Zaher *et al.* (2006); Fiorelli & Calvo (2007); Larsson & Sues (2007); Riff (2007); de Andrade & Bertini (2008a, b); Turner & Buckley (2008); Novas *et al.* (2009); Pol & Gasparini (2009); Sereno & Larsson (2009); O'Connor *et al.* (2010); Turner & Sertich (2010); de Andrade *et al.* (2011); Montefeltro *et al.*

(2011); Nascimento & Zaher (2011); Pol & Powell (2011); Riff & Kellner (2011); Pritchard *et al*. (2013); Leardi *et al*. (2015a, b); Fiorelli *et al*. (2016); Martínez *et al*. (2018).

Characters diagnostic of Sebecosuchia: palatal parts of premaxillae do not meet posterior to incisive foramen; dorsal surface of mandibular symphysis strongly concave and narrow, trough-shaped; premaxillary palate circular paramedian depressions located anteriorly on the premaxilla.

Phylogenetic search procedure: New Technology Search in TNT: minimum length hit 30 times. 43 ordered characters, equal and extended implied weighting (3<K<15).

Nicholl *et al*. (2021):

Matrix built using: Buscalioni & Sanz (1988); Norell (1988); Gasparini *et al*. (1993); Clark (1994); Ortega *et al*. (1996, 2000); Wu & Sues (1996); Brochu (1997, 1999); Gomani (1997); Wu *et al*. (1997); Buckley & Brochu (1999); Pol (1999a, b); Buckley *et al*. (2000); Sereno *et al*. (2001); Martinelli (2003); Pol & Norell (2004a, b); Pol *et al*. (2004, 2009, 2012, 2014); Turner (2004, 2006); Pol & Apesteguia (2005); Zaher *et al*. (2006); Larsson & Sues (2007); Riff (2007); de Andrade & Bertini (2008a, b); Turner & Buckley (2008); Pol & Gasparini (2009); Sereno & Larsson (2009); O'Connor *et al*. (2010); Turner & Sertich (2010); de Andrade *et al*. (2011); Montefeltro *et al*. (2011); Nascimento & Zaher (2011); Pol & Powell (2011); Riff & Kellner (2011); Leardi *et al*. (2015a, 2018); Fiorelli *et al*. (2016); Martínez *et al*. (2018).

Characters diagnostic of Sebecosuchia: Data not available.

Phylogenetic search procedure: New Technology Search (sectorial search, drift and tree fusing) in TNT: stabilize consensus five times. 43 ordered characters, equal and extended implied weighting (K=8 & K=12).

Marinho *et al*. (2022):

Matrix built using: Buscalioni & Sanz (1988); Norell (1988); Sereno (1991); Gasparini *et al*. (1993); Clark (1994); Ortega *et al*. (1996, 2000); Wu & Sues (1996); Gomani (1997); Brochu (1997, 1999); Wu *et al*. (1997); Buckley & Brochu (1999); Pol (1999a, b); Buckley *et al*. (2000); Sereno *et al*. (2001); Martinelli (2003); Pol & Norell (2004a, b); Pol *et al*. (2004, 2009,

2012, 2014); Turner (2004, 2006); Pol & Apesteguia (2005); Zaher *et al*. (2006); Fiorelli & Calvo (2007); Larsson & Sues (2007); Riff (2007); de Andrade & Bertini (2008a); Turner & Buckley (2008); Novas *et al*. (2009); Pol & Gasparini (2009); Sereno & Larsson (2009); O'Connor *et al*. (2010); Turner & Sertich (2010); de Andrade *et al*. (2011); Montefeltro *et al*. (2011); Nascimento & Zaher (2011); Pol & Powell (2011); Riff & Kellner (2011); Pritchard *et al*. (2013); Leardi *et al*. (2015a); Fiorelli *et al*. (2016).

Characters diagnostic of Sebecosuchia: Data not available.

Phylogenetic search procedure: Heuristic searches in TNT: 10000 replications. 43 ordered characters, equal weighting.

Martin *et al*. (2023):

Matrix built using: Buscalioni & Sanz (1988); Norell (1988); Gasparini *et al*. (1993); Clark (1994); Ortega *et al*. (1996, 2000); Wu & Sues (1996); Brochu (1997, 1999); Gomani (1997); Wu *et al*. (1997); Buckley & Brochu (1999); Pol (1999a, b); Buckley *et al*. (2000); Sereno *et al*. (2001); Martinelli (2003); Pol & Norell (2004a, b); Pol *et al*. (2004, 2009, 2012, 2014); Turner (2004, 2006); Pol & Apesteguia (2005); Zaher *et al*. (2006); Larsson & Sues (2007); Riff (2007); de Andrade & Bertini (2008a, b); Turner & Buckley (2008); Pol & Gasparini (2009); Sereno & Larsson (2009); O'Connor *et al*. (2010); Turner & Sertich (2010); de Andrade *et al*. (2011); Montefeltro *et al*. (2011); Nascimento & Zaher (2011); Pol & Powell (2011); Riff & Kellner (2011); Leardi *et al*. (2015a, 2018); Fiorelli *et al*. (2016); Martínez *et al*. (2018); Nicholl *et al*. (2021).

Characters diagnostic of Sebecosuchia: Articular facet for quadrate condyle wider than broad, dentary symphysis U-shaped in ventral view, smoothly curving anteriorly, maxillary teeth in isolated alveoli, **flat lateral surface of dentaries facing laterally or laterodorsally but divided by a ridge from the rest of the lateral surface of the dentary**, perinarial fossa is a large concave surface facing anteriorly, projecting anteroventrally from the external nares opening toward the alveolar margin.

Phylogenetic search procedure: New Technology Search (sectorial search, ratchet, drift, and tree fusing) in TNT: minimum length hit 10 times. 43 ordered characters, equal weighting.

References:

Adams T. L. (2013). A new neosuchian crocodyliform from the Lower Cretaceous (Late Aptian) Twin Mountains Formation of north-central Texas. *Journal of Vertebrate Paleontology*, 33(1): 85-101. https://doi.org/10.1080/02724634.2012.713277

Adams T. L. (2014). Small crocodyliform from the Lower Cretaceous (Late Aptian) of Central Texas and its systematic relationship to the evolution of Eusuchia. *Journal of Paleontology*, 88(5): 1031-1049. https://doi.org/10.1666/12-089

Barrios F., Paulina-Carabajal A. & Bona P. (2016). A new peirosaurid (Crocodyliformes, Mesoeucrocodylia) from the Upper Cretaceous of Patagonia, Argentina. *Ameghiniana*, 53(1): 14-25. https://doi.org/10.5710/AMGH.03.09.2015.2903

Benton M. J. & Clark J. M. (1988). Archosaur phylogeny and the relationships of the Crocodylia. In *The phylogeny and Classification of the Tetrapods, Volume I: Amphibians, Reptiles, Birds*. The Systematics Association: 295-338.

Bravo G. G., Pol D. & García-López D. A. (2021). A new sebecid mesoeucrocodylian from the Paleocene of northwestern Argentina. *Journal of Vertebrate Paleontology*, 41(3): e1979020. https://doi.org/10.1080/02724634.2021.1979020

Brochu C. A. (1997). Morphology, fossils, divergence timing, and the phylogenetic relationships of *Gavialis*. *Systematic Biology*, 46(3): 479-522. https://doi.org/10.1093/sysbio/46.3.479

Brochu C. A. (1999). Phylogenetics, taxonomy, and historical biogeography of Alligatoroidea. *Journal of Vertebrate Paleontology*, 19(S2): 9-100. https://doi.org/10.1080/02724634.1999.10011201

Brochu C. A. (2011). Phylogenetic relationships of *Necrosuchus ionensis* Simpson, 1937 and the early history of caimanines. *Zoological Journal of the Linnean Society*, 163(suppl 1): S228-S256. https://doi.org/10.1111/j.1096-3642.2011.00716.x

Buckley G. A. & Brochu C. A. (1999). An enigmatic new crocodile from the Upper Cretaceous of Madagascar. *Special papers in palaeontology*, 60(60): 149-175.

Buckley G. A., Brochu C. A., Krause D. W. & Pol D. (2000). A pug-nosed crocodyliform from the Late Cretaceous of Madagascar. *Nature*, 405(6789): 941-944. https://doi.org/10.1038/35016061

Busbey A. B. (1995). The structural consequences of skull flattening in crocodylians. In Thomason J. J. (eds.) *Functional Morphology in Vertebrate Paleontology*: 173-192.

Buscalioni A. D. & Sanz J. L. (1988). Phylogenetic relationships of the Atoposauridae (Archosauria, Crocodylomorpha). *Historical Biology*, 1(3): 233-250. https://doi.org/10.1080/08912968809386477

Buscalioni A. D. & Sanz J. L. (1990). La Familia Atoposauridae: una aproximación a la historia de los cocodrylos enaños. *Trabajos Museo Geologia,* 1: 77- 89.

Buscalioni A. D., Sanz J. L. & Casanovas M. L. (1992). A new species of the eusuchian crocodile *Diplocynodon* from the Eocene of Spain. *Neues Jahrbuch für Geologie und Paläontologie, Abhandlungen,* 187: 1–29.

Buscalioni A. D., Ortega F. & Vasse S. (1999). The Upper Cretaceous crocodylian assemblage from Laño (North-Central Spain): implications in the knowledge of the Cretaceous European faunas. *Estudios Museo Ciencias Naturales Alava*, 14: 213-233.

Carvalho I. d. S., Ribeiro L. C. B. & dos Santos Avilla L. (2004). *Uberabasuchus terrificus* sp. nov., a new Crocodylomorpha from the Bauru Basin (Upper Cretaceous), Brazil. *Gondwana Research*, 7(4): 975-1002. https://doi.org/10.1016/S1342-937X(05)71079-0

Clark J. M. (1986). *Phylogenetic relationships of the crocodylomorphs archosaurs*. Unpublished PhD thesis, University of Chicago, 525 p.

Clark J. M. (1994). Patterns of evolution in Mesozoic Crocodyliformes. In Sues H. D. (eds.) *The Shadow of the Dinosaurs: Early Mesozoic Tetrapods*. New York: Cambridge University Press: 84–97.

Clark J. M. & Sues H. D. (2002). Two new basal crocodylomorph archosaurs from the Lower Jurassic and the monophyly of the Sphenosuchia. *Zoological Journal of the Linnean Society*, 136(1): 77-95. https://doi.org/10.1046/j.1096-3642.2002.00026.x

Clark J. M., Jacobs L. L. & Downs W. R. (1989). Mammal-like dentition in a Mesozoic crocodylian. *Science*, 244(4908): 1064-1066. https://doi.org/10.1126/science.244.4908.1064

Company J., Suberbiola X. P., Ruiz-Omeñaca J. I. & Buscalioni A. D. (2005). A new species of *Doratodon* (Crocodyliformes: Ziphosuchia) from the Late Cretaceous of Spain. *Journal of Vertebrate Paleontology*, 25(2): 343-353. https://doi.org/10.1671/0272-4634(2005)025[0343:ANSODC]2.0.CO;2

Coria R. A., Ortega F., Arcucci A. B. & Currie P. J. (2019). A new and complete peirosaurid (Crocodyliformes, Notosuchia) from Sierra Barrosa (Santonian, Upper Cretaceous) of the Neuquén Basin, Argentina. *Cretaceous Research*, 95: 89-105. https://doi.org/10.1016/j.cretres.2018.11.008

Cunha G. O., Santucci R. M., de Andrade M. B. & de Oliveira C. E. M. (2020). Description and phylogenetic relationships of a large-bodied sphagesaurid notosuchian from the Upper Cretaceous Adamantina Formation, Bauru Group, São Paulo, southeastern Brazil. *Cretaceous Research*, 106: 104259. https://doi.org/10.1016/j.cretres.2019.104259

de Andrade M. B. (2005). *Revisões sistemática e taxonômica dos Notosuchia (Metasuchia, Crocodylomorpha)*. Unpublished Msc thesis, Universidade Estadual Paulista, 239 p.

de Andrade M. B. (2010). *The evolution of Gondwanan Mesoeucrocodylia (Crutotarsi, Crocodylomorpha) from Jurassic to Cretaceous*. Unpublished PhD thesis, University of Bristol, 256 p.

de Andrade M. B. & Bertini R. J. (2008a). A new *Sphagesaurus* (Mesoeucrocodylia: Notosuchia) from the Upper Cretaceous of Monte Alto City (Bauru Group, Brazil), and a revision of the Sphagesauridae. *Historical Biology*, 20(2): 101-136. https://doi.org/10.1080/08912960701642949

de Andrade M. B. & Bertini R. J. (2008b). Morphology of the dental carinae in *Mariliasuchus amarali* (Crocodylomorpha, Notosuchia) and the pattern of tooth serration among basal Mesoeucrocodylia. *Arquivos do Museu Nacional*, 66(1): 63-82.

de Andrade M. B., Edmonds R., Benton M. J. & Schouten R. (2011). A new Berriasian species of *Goniopholis* (Mesoeucrocodylia, Neosuchia) from England, and a review of the genus. *Zoological Journal of the Linnean Society*, 163(suppl 1): S66-S108. https://doi.org/10.1111/j.1096-3642.2011.00709.x

Dal Sasso C., Pasini G., Fleury G. & Maganuco S. (2017). *Razanandrongobe sakalavae*, a gigantic mesoeucrocodylian from the Middle Jurassic of Madagascar, is the oldest known notosuchian. *PeerJ*, 5: e3481. https://doi.org/10.7717/peerj.3481

Darlim G., Montefeltro F. C. & Langer M. C. (2021). 3D skull modelling and description of a new baurusuchid (Crocodyliformes, Mesoeucrocodylia) from the Late Cretaceous (Bauru Basin) of Brazil. *Journal of Anatomy*, 239(3): 622-662. https://doi.org/10.1111/joa.13442

Dumont M. F., Bona P., Pol D. & Apesteguía S. (2020). New anatomical information on *Araripesuchus buitreraensis* with implications for the systematics of Uruguaysuchidae (Crocodyliforms, Notosuchia). *Cretaceous Research*, 113: 104494. https://doi.org/10.1016/j.cretres.2020.104494

Fiorelli L. E. (2005). *Nuevos restos de Notosuchus terrestris Woodward, 1896 (Crocodyliformes: Mesoeucrocodylia) del Cretácico Superior (Santoniano) de la Provincia de Neuquén, Patagonia, Argentina*. Unpublished Msc thesis, Universidad Nacional de Córdoba, 79 p.

Fiorelli L. E. & Calvo J. O. (2007). The first "protosuchian" (Archosauria: Crocodyliformes) from the Cretaceous (Santonian) of Gondwana. *Arquivos do Museu Nacional, Rio de Janeiro,* 65(4): 417-459.

Fiorelli L. E. & Calvo J. (2008). New remains of *Notosuchus terrestris* Woodward, 1896 (Crocodyliformes: Mesoeucrocodylia) from Late Cretaceous of Neuquén, Patagonia, Argentina. *Arquivos do Museu Nacional, Rio de Janeiro*, 66(1): 83-124.

Fiorelli L. E., Leardi J. M., Hechenleitner E. M., Pol D., Basilici G. & Grellet-Tinner G. (2016). A new Late Cretaceous crocodyliform from the western margin of Gondwana (La Rioja Province, Argentina). *Cretaceous Research*, 60: 194-209. https://doi.org/10.1016/j.cretres.2015.12.003

Gasparini Z., Chiappe L. M. & Fernandez M. (1991). A new Senonian peirosaurid (Crocodylomorpha) from Argentina and a synopsis of the South American Cretaceous crocodylians. *Journal of Vertebrate Paleontology*, 11(3): 316-333. https://doi.org/10.1080/02724634.1991.10011401

Gasparini Z., Fernandez M. & Powell J. (1993). New tertiary sebecosuchians (Crocodylomorpha) from South America: phylogenetic implications. *Historical Biology*, 7(1): 1-19. https://doi.org/10.1080/10292389309380440

Gasparini Z., Cichowolski M. & Lazo D. G. (2005). First record of *Metriorhynchus* (Reptilia: Crocodyliformes) in the Bathonian (Middle Jurassic) of the Eastern Pacific. *Journal of Paleontology*, 79(4): 801-805. https://doi.org/10.1666/0022-3360(2005)079[0801:FROMRC]2.0.CO;2

Gasparini Z., Pol D. & Spalletti L. A. (2006). An unusual marine crocodyliform from the Jurassic-Cretaceous boundary of Patagonia. *Science*, 311(5757): 70-73. https://doi.org/10.1126/science.1120803

Geroto C. F. C. & Bertini R. J. (2019). New material of *Pepesuchus* (Crocodyliformes; Mesoeucrocodylia) from the Bauru Group: implications about its phylogeny and the age of the Adamantina Formation. *Zoological Journal of the Linnean Society*, 185(2): 312-334. https://doi.org/10.1093/zoolinnean/zly037

Godoy P. L., Montefeltro F. C., Norell M. A. & Langer M. C. (2014). An additional baurusuchid from the Cretaceous of Brazil with evidence of interspecific predation among Crocodyliformes. *PLoS One*, 9(5): e97138. https://doi.org/10.1371/journal.pone.0097138

Godoy P. L., Bronzati M., Eltink E., Júlio C. D. A., Cidade G. M., Langer M. C. & Montefeltro F. C. (2016). Postcranial anatomy of *Pissarrachampsa sera* (Crocodyliformes, Baurusuchidae) from the Late Cretaceous of Brazil: insights on lifestyle and phylogenetic significance. *PeerJ*, 4: e2075. https://doi.org/10.7717/peerj.2075

Gomani E. M. (1997). A crocodyliform from the Early Cretaceous dinosaur beds, northern Malawi. *Journal of Vertebrate Paleontology*, 17(2): 280-294. https://doi.org/10.1080/02724634.1997.10010975

Iori F. V. & Carvalho I. d. S. (2011). *Caipirasuchus paulistanus*, a new sphagesaurid (Crocodylomorpha, Mesoeucrocodylia) from the Adamantina Formation (Upper Cretaceous, Turonian–Santonian), Bauru Basin, Brazil. *Journal of Vertebrate Paleontology*, 31(6): 1255-1264. https://doi.org/10.1080/02724634.2011.602777

Iori F. V., Marinho T. S., Carvalho I. S. & Campos A. C. A. (2013). Taxonomic reappraisal of the sphagesaurid crocodyliform *Sphagesaurus montealtensis* from the late Cretaceous Adamantina Formation of São Paulo State, Brazil. *Zootaxa*, 3686(2): 183-200. https://doi.org/10.11646/zootaxa.3686.2.4

Jouve S. (2004). *Etude des Crocodyliformes fini Crétacé-Paléogène du Bassin des Oulad Abdoun (Maroc), et comparaison avec les faunes africaines contemporaines: Systématique, Phylogénie et Paléobiogéographie.* Unpublished PhD thesis, Muséum National d'Histoire Naturelle.

Jouve S. (2009). The skull of *Teleosaurus cadomensis* (Crocodylomorpha; Thalattosuchia), and phylogenetic analysis of Thalattosuchia. *Journal of Vertebrate Paleontology*, 29(1): 88-102. https://doi.org/10.1080/02724634.2009.10010364

Jouve S., Iarochene M., Bouya B. & Amaghzaz M. (2006). A new species of *Dyrosaurus* (Crocodylomorpha, Dyrosauridae) from the early Eocene of Morocco: phylogenetic implications. *Zoological Journal of the Linnean Society*, 148(4): 603-656. https://doi.org/10.1111/j.1096-3642.2006.00241.x

Kellner A. W., Pinheiro A. E. & Campos D. A. (2014). A new sebecid from the Paleogene of Brazil and the crocodyliform radiation after the K–Pg boundary. *PLoS One*, 9(1): e81386. https://doi.org/10.1371/journal.pone.0081386

Larsson (2000). *Ontogeny and Phylogeny of the Archosauriform Skeleton*. Unpublished PhD thesis, The University of Chicago.

Larsson H. C. & Gado B. (2000). A new Early Cretaceous crocodyliform from Niger. *Neues Jahrbuch für Geologie und Paläontologie-Abhandlungen*, 1: 131-141. https://doi.org/10.1127/njgpa/217/2000/131

Larsson H. C. & Sues H. D. (2007). Cranial osteology and phylogenetic relationships of *Hamadasuchus rebouli* (Crocodyliformes: Mesoeucrocodylia) from the Cretaceous of Morocco. *Zoological Journal of the Linnean Society*, 149(4): 533-567. https://doi.org/10.1111/j.1096-3642.2007.00271.x

Leardi J. M., Pol D., Novas F. E. & Suárez Riglos M. (2015a). The postcranial anatomy of *Yacarerani boliviensis* and the phylogenetic significance of the notosuchian postcranial skeleton. *Journal of Vertebrate Paleontology*, 35(6): e995187. https://doi.org/10.1080/02724634.2014.995187

Leardi J. M., Fiorelli L. E. & Gasparini Z. (2015b). Redescription and reevaluation of the taxonomical status of *Microsuchus schilleri* (Crocodyliformes: Mesoeucrocodylia) from the Upper Cretaceous of Neuquén, Argentina. *Cretaceous Research*, 52: 153-166. https://doi.org/10.1016/j.cretres.2014.09.007

Leardi J. M., Pol D. & Gasparini Z. (2018). New Patagonian baurusuchids (Crocodylomorpha; Notosuchia) from the Bajo de la Carpa Formation (Upper Cretaceous; Neuquén, Argentina): new evidences of the early sebecosuchian diversification in Gondwana. *Comptes Rendus Palevol*, 17(8): 504-521. https://doi.org/10.1016/j.crpv.2018.02.002

Legasa O., Buscalioni Á. D. & Gasparini Z. (1994). The serrated teeth of *Sebecus* and the iberoccitanian crocodile. A morphological and ultrastructural comparison. *Studia Geologica. Salmanticensia*, 29: 127-144.

Marinho T. S., Martinelli A. G., Basilici G., Soares M. V. T., Marconato A., Ribeiro L. C. & Iori F. V. (2022). First Upper Cretaceous notosuchians (Crocodyliformes) from the Uberaba Formation (Bauru Group), southeastern Brazil: enhancing crocodyliform diversity. *Cretaceous Research*, 129: 105000. https://doi.org/10.1016/j.cretres.2021.105000

Martin J. E. & de Lapparent de Broin F. (2016). A miniature notosuchian with multicuspid teeth from the Cretaceous of Morocco. *Journal of Vertebrate Paleontology*, 36(6): e1211534. https://doi.org/10.1080/02724634.2016.1211534

Martin J. E., Pochat-Cottilloux Y., Laurent Y., Perrier V., Robert E. & Antoine P. O. (2023). Anatomy and phylogeny of an exceptionally large sebecid (Crocodylomorpha) from the middle Eocene of southern France. *Journal of Vertebrate Paleontology*, 42(4): e2193828. https://doi.org/10.1080/02724634.2023.2193828

Martinelli A. G. (2003). *Comahuesuchus brachybuccalis* (Archosauria, Crocodyliformes) from the Late Cretaceous of Río Negro Province (Argentina). *Ameghiniana*, 40(4): 559-572.

Martinelli A. G., Marinho T. S., Iori F. V. & Ribeiro L. C. B. (2018). The first *Caipirasuchus* (Mesoeucrocodylia, Notosuchia) from the Late Cretaceous of Minas Gerais, Brazil: new insights on sphagesaurid anatomy and taxonomy. *PeerJ*, 6: e5594. https://doi.org/10.7717/peerj.5594

Martínez R. N., Alcober O. A. & Pol D. (2018). A new protosuchid crocodyliform (Pseudosuchia, Crocodylomorpha) from the Norian Los Colorados formation, northwestern Argentina. *Journal of Vertebrate Paleontology*, 38(4): 1-12. https://doi.org/10.1080/02724634.2018.1491047

Martins K. C. (2021). *A new baurusuchid (Crocodyliformes Notosuchia) from the Adamantina Formation (Bauru Group, Late Cretaceous), and a new phylogenetic analysis of notosuchians.* Unpublished Msc thesis, Universidade Estadual Paulista, 130 p.

Molnar R. E. (1981). Pleistocene ziphodont crocodylians of Queensland. *Records of the Australian Museum*, 33(19): 803-834. https://doi.org/10.3853/j.0067-1915.33.1981.198

Montefeltro F. C., Larsson H. C. & Langer M. C. (2011). A new baurusuchid (Crocodyliformes, Mesoeucrocodylia) from the Late Cretaceous of Brazil and the phylogeny of Baurusuchidae. *PLoS One*, 6(7): e21916. https://doi.org/10.1371/journal.pone.0021916

Montefeltro F. C., Larsson H. C., de França M. A. & Langer M. C. (2013). A new neosuchian with Asian affinities from the Jurassic of northeastern Brazil. *Naturwissenschaften*, 100: 835-841. https://doi.org/10.1007/s00114-013-1083-9

Montefeltro F. C., Andrade D. V. & Larsson H. C. (2016). The evolution of the meatal chamber in crocodyliforms. *Journal of Anatomy*, 228(5): 838-863. https://doi.org/10.1111/joa.12439

Nascimento P. M. & Zaher H. (2010). A new species of *Baurusuchus* (Crocodyliformes, Mesoeucrocodylia) from the Upper Cretaceous of Brazil, with the first complete postcranial skeleton described for the family Baurusuchidae. *Papéis avulsos de Zoologia*, 50: 323-361. https://doi.org/10.1590/S0031-10492010002100001

Nascimento P. M. & Zaher H. (2011). The skull of the Upper Cretaceous baurusuchid crocodile *Baurusuchus albertoi* Nascimento & Zaher 2010, and its phylogenetic affinities. *Zoological Journal of the Linnean Society*, 163(suppl_1): S116-S131. https://doi.org/10.1111/j.1096-3642.2011.00708.x

Nicholl C. S., Hunt E. S., Ouarhache D. & Mannion P. D. (2021). A second peirosaurid crocodyliform from the Mid-Cretaceous Kem Kem Group of Morocco and the diversity of Gondwanan notosuchians outside South America. *Royal Society Open Science*, 8(10): 211254. https://doi.org/10.1098/rsos.211254

Norell M. A. (1988). *Cladistic Approaches to Paleobiology as Applied to the Phylogeny of Alligatorids.* Unpublished PhD thesis, Yale University, 264 p.

Norell M. A. (1989). The higher level relationships of the extant Crocodylia. *Journal of Herpetology*,23(4): 325-335. https://doi.org/10.2307/1564042

Norell M. A. & Clark J. M. (1990). A reanalysis of *Bernissartia fagesii*, with comments on its phylogenetic position and its bearing on the origin and diagnosis of the Eusuchia. *Bulletin de l'Institut Royal des Sciences Naturelles de Belgique*, 60: 115-128.

Novas F. E., Pais D. F., Pol D., Carvalho I. D. S., Scanferla A., Mones A. & Riglos M. S. (2009). Bizarre notosuchian crocodyliform with associated eggs from the Upper Cretaceous of Bolivia. *Journal of Vertebrate Paleontology*, 29(4): 1316-1320. https://doi.org/10.1671/039.029.0409

O'Connor P. M., Sertich J. J., Stevens N. J., Roberts E. M., Gottfried M. D., Hieronymus T. L., Jinnah Z. A., Ridgely R., Ngasala S. E. & Temba J. (2010). The evolution of mammal-like crocodyliforms in the Cretaceous Period of Gondwana. *Nature*, 466(7307): 748-751. https://doi.org/10.1038/nature09061

Ortega F. & Buscalioni A. D. (1995). Las Hoyas Crocodiles, an Evidence of the Transition Model of the Eusuchian dorsal Armor Construction. *Extended Abstract of the second International Symposium on Lithographic Limestones*, Spain: 107-110.

Ortega F., Buscalioni A. D. & Gasparini Z. (1996). Reinterpretation and new denomination of *Atacisaurus crassiproratus* (middle Eocene; Issel, France) as cf. *Iberosuchus* (Crocodylomorpha, Metasuchia). *Geobios*, 29(3): 353-364. https://doi.org/10.1016/S0016-6995(96)80037-4

Ortega F., Gasparini Z., Buscalioni A. D. & Calvo J. O. (2000). A new species of *Araripesuchus* (Crocodylomorpha, Mesoeucrocodylia) from the lower Cretaceous of Patagonia (Argentina). *Journal of Vertebrate Paleontology*, 20(1): 57-76. https://doi.org/10.1671/0272-4634(2000)020[0057:ANSOAC]2.0.CO;2

Ősi A., Clark J. M. & Weishampel D. B. (2007). First report on a new basal eusuchian crocodyliform with multicusped teeth from the Upper Cretaceous (Santonian) of Hungary. *Neues Jahrbuch für Geologie und Paläontologie Abhandlung*en, 243(2): 169-177. https://doi.org/10.1127/0077-7749/2007/0243-0169

Parrish J. M. (1991). A new specimen of an early crocodylomorph (cf. *Sphenosuchus* sp.) from the Upper Triassic Chinle Formation of Petrified Forest National Park, Arizona. *Journal of Vertebrate Paleontology*, 11(2): 198-212.

Parrish J. M. (1993). Phylogeny of the Crocodylotarsi, with reference to archosaurian and crurotarsan monophyly. *Journal of Vertebrate Paleontology*, 13(3): 287-308. https://doi.org/10.1080/02724634.1993.10011511

Pinheiro A. E. P. (2007). *Revisões cladística-filogenética e considerações paleobiogeográficas sobre Sebecosuchia (Metasuchia, Crocodylomorpha), do Cretáceo Superior ao Mioceno*. Unpublished Msc thesis, Universidade Estadual Paulista, 267 p.

Pinheiro A. E. P., da Costa Pereira P. V. L. G., de Souza R. G., Brum A. S., Lopes R. T., Machado A. S., Bergqvist L. P. & Simbras F. M. (2018). Reassessment of the enigmatic crocodyliform "*Goniopholis*" *paulistanus* Roxo, 1936: Historical approach, systematic, and description by new materials. *Plos One,* 13(8): e0199984. https://doi.org/10.1371/journal.pone.0199984

Pinheiro A. E. P., Souza L. G., Bandeira K. L., Brum A. S., Pereira P. V. L. G., Castro L. O. R., Ramos R. R. C. & Simbras F. M. (2021). The first notosuchian crocodyliform from the Araçatuba Formation (Bauru Group, Paraná Basin), and diversification of sphagesaurians. *Anais da Academia Brasileira de Ciências*, 93(S2): e20201591. https://doi.org/10.1590/0001-3765202120201591

Pinheiro A. E. P., Costa Pereira P. V. L. G., de Vasconcellos F. M., Brum A. S., de Souza L. G., Costa F. R., Castro L. O. R., da Silva K. F. & Bandeira K. L. N. (2023). New Itasuchidae (Sebecia, Ziphosuchia) remains and the radiation of an elusive Mesoeucrocodylia clade. *Historical Biology*, 2023: 1-26. https://doi.org/10.1080/08912963.2022.2139179

Pol D. (1999a). *El esqueleto postcraneano de Notosuchus terrestris (Archosauria: Crocodyliformes) del Cretácico Superior de la Cuenca Neuquina y su información filogenética*. Unpublished MSc thesis, Universidad de Buenos Aires, 158 p.

Pol D. (1999b). Basal mesoeucrocodylian relationships: new clues to old conflicts. *Journal of Vertebrate Paleontology*, 19(3): 69A.

Pol D. (2003). New remains of *Sphagesaurus huenei* (Crocodylomorpha: Mesoeucrocodylia) from the late Cretaceous of Brazil. *Journal of Vertebrate Paleontology*, 23(4): 817-831. https://doi.org/10.1671/A1015-7

Pol D. & Norell M. A. (2004a). A new gobiosuchid crocodyliform taxon from the Cretaceous of Mongolia. *American Museum Novitates*, 2004(3458): 1-31. https://doi.org/10.1206/0003-0082(2004)458<0001:ANGCTF>2.0.CO;2

Pol D. & Norell M. A. (2004b). A new crocodyliform from Zos Canyon, Mongolia. *American Museum Novitates*, 2004(3445): 1-36. https://doi.org/10.1206/0003-0082(2004)445<0001:ANCFCM>2.0.CO;2

Pol D. & Apesteguía S. (2005). New *Araripesuchus* remains from the early late cretaceous (Cenomanian–Turonian) of Patagonia. *American Museum Novitates*, 2005(3490): 1-38. https://doi.org/10.1206/0003-0082(2005)490[0001:NARFTE]2.0.CO;2

Pol D. & Gasparini Z. (2009). Skull anatomy of *Dakosaurus andiniensis* (Thalattosuchia: Crocodylomorpha) and the phylogenetic position of Thalattosuchia. *Journal of Systematic Palaeontology,* 7(2): 163-197. https://doi.org/10.1017/S1477201908002605

Pol D. & Powell J. E. (2011). A new sebecid mesoeucrocodylian from the Rio Loro Formation (Palaeocene) of north-western Argentina. *Zoological Journal of the Linnean Society*, 163(suppl_1): S7-S36. https://doi.org/10.1111/j.1096-3642.2011.00714.x

Pol D., Ji S. A., Clark J. M. & Chiappe L. M. (2004). Basal crocodyliforms from the Lower Cretaceous Tugulu Group (Xinjiang, China), and the phylogenetic position of *Edentosuchus*. *Cretaceous Research*, 25(4): 603-622. https://doi.org/10.1016/j.cretres.2004.05.002

Pol D., Turner A. H. & Norell M. A. (2009). Morphology of the Late Cretaceous crocodylomorph *Shamosuchus djadochtaensis* and a discussion of neosuchian phylogeny as related to the origin of Eusuchia. *Bulletin of the American Museum of Natural History*, 2009(324): 1-103. https://doi.org/10.1206/0003-0090-324.1.1

Pol D., Leardi J. M., Lecuona A. & Krause M. (2012). Postcranial anatomy of *Sebecus icaeorhinus* (Crocodyliformes, Sebecidae) from the Eocene of Patagonia. *Journal of Vertebrate Paleontology*, 32(2): 328-354. https://doi.org/10.1080/02724634.2012.646833

Pol D., Nascimento P. M., Carvalho A. B., Riccomini C., Pires-Domingues R. A. & Zaher H. (2014). A new notosuchian from the Late Cretaceous of Brazil and the phylogeny of advanced notosuchians. *PLoS One*, 9(4): e93105. https://doi.org/10.1371/journal.pone.0093105

Pritchard A. C., Turner A. H., Allen E. R. & Norell M. A. (2013). Osteology of a North American goniopholidid (*Eutretauranosuchus delfsi*) and palate evolution in Neosuchia. *American Museum Novitates*, 2013(3783): 1-56. https://doi.org/10.1206/3783.2

Queiroz M. V. L. (2022). *A new Peirosauridae (Crocodyliformes Notosuchia) from the Adamantina Formation (Bauru Group, Late Cretaceous), and a new phylogenetic analysis of notosuchians.* Unpublished master thesis, Universidade Estadual Paulista "Júlio de Mesquita Filho", 118 p.

Riff D. (2007). *Anatomia appendicular de* Stratiotosuchus maxhechti *(Baurusuchidae, Cretáceo Superior do Brasil) e análise filogenética dos Mesoeucrocodylia.* Unpublished PhD thesis, Museu Nacional da Universidade Federal do Rio de Janeiro, 395 p.

Riff D. & Kellner A. W. A. (2011). Baurusuchid crocodyliforms as theropod mimics: clues from the skull and appendicular morphology of *Stratiotosuchus maxhechti* (Upper Cretaceous of Brazil). *Zoological Journal of the Linnean Society*, 163(suppl_1): S37-S56. https://doi.org/10.1111/j.1096-3642.2011.00713.x

Ruiz J. V., Bronzati M., Ferreira G. S., Martins K. C., Queiroz M. V., Langer M. C. & Montefeltro F. C. (2021). A new species of *Caipirasuchus* (Notosuchia, Sphagesauridae) from the Late Cretaceous of Brazil and the evolutionary history of Sphagesauria. *Journal of Systematic Palaeontology*, 19(4): 265-287. https://doi.org/10.1080/14772019.2021.1888815

Sellés A. G., Blanco A., Vila B., Marmi J., López-Soriano F. J., Llácer S., Frigola J., Canals M. & Galobart À. (2020). A small Cretaceous crocodyliform in a dinosaur nesting ground and the origin of sebecids. *Scientific Reports*, 10(1): 15293. https://doi.org/10.1038/s41598-020-71975-y

Sereno P. C. (1991). Basal archosaurs: phylogenetic relationships and functional implications. *Journal of Vertebrate Paleontology*, 11(S4): 1-53. https://doi.org/10.1080/02724634.1991.10011426

Sereno P. C. & Wild R. (1992). *Procompsognathus*: theropod, "thecodont" or both?. *Journal of Vertebrate Paleontology*, 12(4): 435-458. https://doi.org/10.1080/02724634.1992.10011473

Sereno P. & Larsson H. (2009). Cretaceous crocodyliforms from the Sahara. *ZooKeys*, 28: 1-143. https://doi.org/10.3897/zookeys.28.325

Sereno P. C., Larsson H. C., Sidor C. A. & Gado B. (2001). The giant crocodyliform Sarcosuchus from the Cretaceous of Africa. *Science*, 294(5546): 1516-1519. https://doi.org/10.1126/science.1066521

Sereno P. C., Sidor C. A., Larsson H. C. E. & Gado B. (2003). A new notosuchian from the Early Cretaceous of Niger. *Journal of Vertebrate Paleontology*, 23(2): 477-482. https://doi.org/10.1671/0272-4634(2003)023[0477:ANNFTE]2.0.CO;2

Sertich J. J. & O'Connor P. M. (2014). A new crocodyliform from the middle Cretaceous Galula Formation, southwestern Tanzania. *Journal of Vertebrate Paleontology*, 34(3): 576-596. https://doi.org/10.1080/02724634.2013.819808

Soto M., Pol D. & Perea D. (2011). A new specimen of *Uruguaysuchus aznarezi* (Crocodyliformes: Notosuchia) from the middle Cretaceous of Uruguay and its phylogenetic relationships. *Zoological Journal of the Linnean Society*, 163(suppl_1): S173-S198. https://doi.org/10.1111/j.1096-3642.2011.00717.x

Turner A. H. (2004). Crocodyliform biogeography during the Cretaceous: evidence of Gondwanan vicariance from biogeographical analysis. *Proceedings of the Royal Society of London. Series B: Biological Sciences*, 271(1552): 2003-2009. https://doi.org/10.1098/rspb.2004.2840

Turner A. H. (2006). Osteology and phylogeny of a new species of *Araripesuchus* (Crocodyliformes: Mesoeucrocodylia) from the Late Cretaceous of Madagascar. *Historical Biology*, 18(3): 255-369. https://doi.org/10.1080/08912960500516112

Turner A. H. (2015). A review of *Shamosuchus* and *Paralligator* (Crocodyliformes, Neosuchia) from the Cretaceous of Asia. *PLoS One*, 10(2): e0118116. https://doi.org/10.1371/journal.pone.0118116

Turner A. H. & Calvo J. O. (2005). A new sebecosuchian crocodyliform from the Late Cretaceous of Patagonia. *Journal of Vertebrate Paleontology*, 25(1): 87-98. https://doi.org/10.1671/0272-4634(2005)025[0087:ANSCFT]2.0.CO;2

Turner A. H. & Buckley G. A. (2008). *Mahajangasuchus insignis* (Crocodyliformes: Mesoeucrocodylia) cranial anatomy and new data on the origin of the eusuchian-style palate. *Journal of Vertebrate Paleontology*, 28(2): 382-408. https://doi.org/10.1671/0272-4634(2008)28[382:MICMCA]2.0.CO;2

Turner A. H. & Sertich J. J. (2010). Phylogenetic history of *Simosuchus clarki* (Crocodyliformes: Notosuchia) from the late cretaceous of Madagascar. *Journal of Vertebrate Paleontology*, 30(sup1): 177-236. https://doi.org/10.1080/02724634.2010.532348

Tykoski R. S., Rowe T. B., Ketcham R. A. & Colbert M. W. (2002). *Calsoyasuchus valliceps*, a new crocodyliform from the Early Jurassic Kayenta Formation of Arizona. *Journal of Vertebrate Paleontology*, 22(3): 593-611. https://doi.org/10.1671/0272-4634(2002)022[0593:CVANCF]2.0.CO;2

Wilkinson L. E., Young M. T. & Benton M. J. (2008). A new metriorhynchid crocodylian (Mesoeucrocodylia: Thalattosuchia) from the Kimmeridgian (Upper Jurassic) of Wiltshire, UK. *Palaeontology*, 51(6): 1307-1333. https://doi.org/10.1111/j.1475-4983.2008.00818.x

Wu X. C. & Chatterjee S. (1993). *Dibothrosuchus elaphros*, a crocodylomorph from the Lower Jurassic of China and the phylogeny of the Sphenosuchia. *Journal of Vertebrate Paleontology*, 13(1): 58-89. https://doi.org/10.1080/02724634.1993.10011488

Wu X. C. & Sues H. D. (1996). Anatomy and phylogenetic relationships of *Chimaerasuchus paradoxus*, an unusual crocodyliform reptile from the Lower Cretaceous of Hubei, China. *Journal of Vertebrate Paleontology*, 16(4): 688-702. https://doi.org/10.1080/02724634.1996.10011358

Wu X. C., Brinkman D. B. & Lu J. C. (1994). A new species of *Shantungosuchus* from the Lower Cretaceous of Inner Mongolia (China), with comments on *S. chuhsienensis* Young, 1961 and the phylogenetic position of the genus. *Journal of Vertebrate Paleontology*, 14(2): 210-229. https://doi.org/10.1080/02724634.1994.10011553

Wu X. C., Brinkman D. B., Lu J. C. & Sues H. D. (1995). Protosuchians (Archosauria: Crocodyliformes) from China. In Sun A. & Wang Y. (eds.) *Short Papers of the Sixth Symposium on Mesozoic Terrestrial Ecosystems and Biota*.

Wu X. C., Sues H. D. & Brinkman D. B. (1996). An atoposaurid neosuchian (Archosauria: Crocodyliformes) from the Lower Cretaceous of Inner Mongolia (People's Republic of China). *Canadian Journal of Earth Sciences*, 33(4): 599-605. https://doi.org/10.1139/e96-044

Wu X. C., Sues H. D. & Dong Z. M. (1997). *Sichuanosuchus shuhanensis*, a new? Early Cretaceous protosuchian (Archosauria: Crocodyliformes) from Sichuan (China), and the monophyly of Protosuchia. *Journal of Vertebrate Paleontology*, 17(1): 89-103. https://doi.org/10.1080/02724634.1997.10010956

Wu X. C., Cheng Z. W. & Russell A. P. (2001). Cranial anatomy of a new crocodyliform (Archosauria: Crocodylomorpha) from the Lower Cretaceous of Song-Liao Plain, northeastern China. *Canadian Journal of Earth Sciences*, 38(12): 1653-1663. https://doi.org/10.1139/e01-055

Young M. T. & de Andrade M. B. (2009). What is *Geosaurus*? Redescription of *Geosaurus giganteus* (Thalattosuchia: Metriorhynchidae) from the Upper Jurassic of Bayern, Germany. *Zoological Journal of the Linnean Society*, 157(3): 551-585. https://doi.org/10.1111/j.1096-3642.2009.00536.x

Young M. T., Bell M. A., de Andrade M. B. & Brusatte S. L. (2011). Body size estimation and evolution in metriorhynchid crocodylomorphs: implications for species diversification and niche partitioning. *Zoological Journal of the Linnean Society*, 163(4): 1199-1216. https://doi.org/10.1111/j.1096-3642.2011.00734.x

Zaher H., Pol D., Carvalho A. B., Riccomini C., Campos D. & Nava W. (2006). Redescription of the cranial morphology of *Mariliasuchus amarali*, and its phylogenetic affinities (Crocodyliformes, Notosuchia). *American Museum Novitates*, 2006(3512): 1-40. https://doi.org/10.1206/0003-0082(2006)3512[1:ROTCMO]2.0.CO;2

Appendix 2: List of publications related to Figure 2.3

1: **Bravo G. G., Pol D. & García-López D. A. (2021).** A new sebecid mesoeucrocodylian from the Paleocene of northwestern Argentina. *Journal of Vertebrate Paleontology*, 41(3): e1979020. https://doi.org/10.1080/02724634.2021.1979020

2: **Nicholl C. S., Hunt E. S., Ouarhache D. & Mannion P. D. (2021).** A second peirosaurid crocodyliform from the Mid-Cretaceous Kem Kem Group of Morocco and the diversity of Gondwanan notosuchians outside South America. *Royal Society Open Science*, 8(10): 211254. https://doi.org/10.1098/rsos.211254

3: **Marinho T. S., Martinelli A. G., Basilici G., Soares M. V. T., Marconato A., Ribeiro L. C. & Iori F. V. (2022).** First Upper Cretaceous notosuchians (Crocodyliformes) from the Uberaba Formation (Bauru Group), southeastern Brazil: enhancing crocodyliform diversity. *Cretaceous Research*, 129: 105000. https://doi.org/10.1016/j.cretres.2021.105000

4: **Ruiz J. V., Bronzati M., Ferreira G. S., Martins K. C., Queiroz M. V., Langer M. C. & Montefeltro F. C. (2021).** A new species of *Caipirasuchus* (Notosuchia, Sphagesauridae) from the Late Cretaceous of Brazil and the evolutionary history of Sphagesauria. *Journal of Systematic Palaeontology*, 19(4): 265-287. https://doi.org/10.1080/14772019.2021.1888815

5: **Dumont M. F., Bona P., Pol D. & Apesteguía S. (2020).** New anatomical information on *Araripesuchus buitreraensis* with implications for the systematics of Uruguaysuchidae (Crocodyliforms, Notosuchia). *Cretaceous Research*, 113: 104494. https://doi.org/10.1016/j.cretres.2020.104494

6: **Sellés A. G., Blanco A., Vila B., Marmi J., López-Soriano F. J., Llácer S., Frigola J., Canals M. & Galobart À. (2020).** A small Cretaceous crocodyliform in a dinosaur nesting ground and the origin of sebecids. *Scientific Reports*, 10(1): 15293. https://doi.org/10.1038/s41598-020-71975-y

7: **Pinheiro A. E. P., Souza L. G., Bandeira K. L., Brum A. S., Pereira P. V. L. G., Castro L. O. R., Ramos R. R. C. & Simbras F. M. (2021).** The first notosuchian crocodyliform from the Araçatuba Formation (Bauru Group, Paraná Basin), and diversification of sphagesaurians. *Anais da Academia Brasileira de Ciências*, 93(S2): e20201591. https://doi.org/10.1590/0001-3765202120201591

8: **Cunha G. O., Santucci R. M., de Andrade M. B. & de Oliveira C. E. M. (2020).** Description and phylogenetic relationships of a large-bodied sphagesaurid notosuchian from the Upper Cretaceous Adamantina Formation, Bauru Group, São Paulo, southeastern Brazil. *Cretaceous Research*, 106: 104259. https://doi.org/10.1016/j.cretres.2019.104259

9: **Darlim G., Montefeltro F. C. & Langer M. C. (2021).** 3D skull modelling and description of a new baurusuchid (Crocodyliformes, Mesoeucrocodylia) from the Late Cretaceous (Bauru Basin) of Brazil. *Journal of Anatomy*, 239(3): 622-662. https://doi.org/10.1111/joa.13442

10: **Geroto C. F. C. & Bertini R. J. (2019).** New material of *Pepesuchus* (Crocodyliformes; Mesoeucrocodylia) from the Bauru Group: implications about its phylogeny and the age of the Adamantina Formation. *Zoological Journal of the Linnean Society*, 185(2): 312-334. https://doi.org/10.1093/zoolinnean/zly037

11: **Leardi J. M., Pol D. & Gasparini Z. (2018).** New Patagonian baurusuchids (Crocodylomorpha; Notosuchia) from the Bajo de la Carpa Formation (Upper Cretaceous; Neuquén, Argentina): new evidences of the early sebecosuchian diversification in Gondwana. *Comptes Rendus Palevol*, 17(8): 504-521. https://doi.org/10.1016/j.crpv.2018.02.002

12: **Dal Sasso C., Pasini G., Fleury G. & Maganuco S. (2017).** *Razanandrongobe sakalavae*, a gigantic mesoeucrocodylian from the Middle Jurassic of Madagascar, is the oldest known notosuchian. *PeerJ*, 5: e3481. https://doi.org/10.7717/peerj.3481

13: **Barrios F., Paulina-Carabajal A. & Bona P. (2016).** A new peirosaurid (Crocodyliformes, Mesoeucrocodylia) from the Upper Cretaceous of Patagonia, Argentina. *Ameghiniana*, 53(1): 14-25. https://doi.org/10.5710/AMGH.03.09.2015.2903

14: **Pinheiro A. E. P., da Costa Pereira P. V. L. G., de Souza R. G., Brum A. S., Lopes R. T., Machado A. S., Bergqvist L. P. & Simbras F. M. (2018).** Reassessment of the enigmatic crocodyliform "*Goniopholis*" *paulistanus* Roxo, 1936: Historical approach, systematic, and description by new materials. *Plos One,* 13(8): e0199984. https://doi.org/10.1371/journal.pone.0199984

15: **Turner A. H. (2015).** A review of *Shamosuchus* and *Paralligator* (Crocodyliformes, Neosuchia) from the Cretaceous of Asia. *PLoS One*, 10(2): e0118116. https://doi.org/10.1371/journal.pone.0118116

16: **Godoy P. L., Bronzati M., Eltink E., Júlio C. D. A., Cidade G. M., Langer M. C. & Montefeltro F. C. (2016).** Postcranial anatomy of *Pissarrachampsa sera* (Crocodyliformes, Baurusuchidae) from the Late Cretaceous of Brazil: insights on lifestyle and phylogenetic significance. *PeerJ*, 4: e2075. https://doi.org/10.7717/peerj.2075

17: **Fiorelli L. E., Leardi J. M., Hechenleitner E. M., Pol D., Basilici G. & Grellet-Tinner G. (2016).** A new Late Cretaceous crocodyliform from the western margin of Gondwana (La Rioja Province, Argentina). *Cretaceous Research*, 60: 194-209. https://doi.org/10.1016/j.cretres.2015.12.003

18: **Montefeltro F. C., Andrade D. V. & Larsson H. C. (2016).** The evolution of the meatal chamber in crocodyliforms. *Journal of Anatomy*, 228(5): 838-863. https://doi.org/10.1111/joa.12439

19: **Leardi J. M., Pol D., Novas F. E. & Suárez Riglos M. (2015a).** The postcranial anatomy of *Yacarerani boliviensis* and the phylogenetic significance of the notosuchian postcranial skeleton. *Journal of Vertebrate Paleontology*, 35(6): e995187. https://doi.org/10.1080/02724634.2014.995187

20: **Martin J. E. & de Lapparent de Broin F. (2016).** A miniature notosuchian with multicuspid teeth from the Cretaceous of Morocco. *Journal of Vertebrate Paleontology*, 36(6): e1211534. https://doi.org/10.1080/02724634.2016.1211534

21: **Meunier L. M. & Larsson H. C. (2018).** *Trematochampsa taqueti* as a nomen dubium and the crocodyliform diversity of the Upper Cretaceous In Beceten Formation of Niger. *Zoological Journal of the Linnean Society*, 182(3): 659-680. https://doi.org/10.1093/zoolinnean/zlx061

22: **Martinelli A. G., Marinho T. S., Iori F. V. & Ribeiro L. C. B. (2018).** The first *Caipirasuchus* (Mesoeucrocodylia, Notosuchia) from the Late Cretaceous of Minas Gerais, Brazil: new insights on sphagesaurid anatomy and taxonomy. *PeerJ*, 6: e5594. https://doi.org/10.7717/peerj.5594

23: **Coria R. A., Ortega F., Arcucci A. B. & Currie P. J. (2019).** A new and complete peirosaurid (Crocodyliformes, Notosuchia) from Sierra Barrosa (Santonian, Upper Cretaceous) of the Neuquén Basin, Argentina. *Cretaceous Research*, 95: 89-105. https://doi.org/10.1016/j.cretres.2018.11.008

24: **Barrios F., Bona P., Paulina-Carabajal A. & Gasparini Z. (2018).** Re-description of the cranio-mandibular anatomy of *Notosuchus terrestris* (Crocodyliformes, Mesoeucrocodylia) from the Upper Cretaceous of Patagonia. *Cretaceous Research*, 83: 3-39. https://doi.org/10.1016/j.cretres.2017.08.016

25: **Soto M., Pol D. & Perea D. (2011).** A new specimen of *Uruguaysuchus aznarezi* (Crocodyliformes: Notosuchia) from the middle Cretaceous of Uruguay and its phylogenetic relationships. *Zoological Journal of the Linnean Society*, 163(suppl_1): S173-S198. https://doi.org/10.1111/j.1096-3642.2011.00717.x

26: **Leardi J. M., Fiorelli L. E. & Gasparini Z. (2015b).** Redescription and reevaluation of the taxonomical status of *Microsuchus schilleri* (Crocodyliformes: Mesoeucrocodylia) from the Upper Cretaceous of Neuquén, Argentina. *Cretaceous Research*, 52: 153-166. https://doi.org/10.1016/j.cretres.2014.09.007

27: **Turner A. H. & Sertich J. J. (2010).** Phylogenetic history of *Simosuchus clarki* (Crocodyliformes: Notosuchia) from the late cretaceous of Madagascar. *Journal of Vertebrate Paleontology*, 30(sup1): 177-236. https://doi.org/10.1080/02724634.2010.532348

28: **Iori F. V., Marinho T. S., Carvalho I. S. & Campos A. C. A. (2013).** Taxonomic reappraisal of the sphagesaurid crocodyliform *Sphagesaurus montealtensis* from the late Cretaceous Adamantina Formation of São Paulo State, Brazil. *Zootaxa*, 3686(2): 183-200. https://doi.org/10.11646/zootaxa.3686.2.4

29: **O'Connor P. M., Sertich J. J., Stevens N. J., Roberts E. M., Gottfried M. D., Hieronymus T. L., Jinnah Z. A., Ridgely R., Ngasala S. E. & Temba J. (2010).** The evolution of mammal-like crocodyliforms in the Cretaceous Period of Gondwana. *Nature*, 466(7307): 748-751. https://doi.org/10.1038/nature09061

30: **Brochu C. A. (2011).** Phylogenetic relationships of *Necrosuchus ionensis* Simpson, 1937 and the early history of caimanines. *Zoological journal of the linnean society*, 163(suppl 1): S228-S256. https://doi.org/10.1111/j.1096-3642.2011.00716.x

31: **Young M. T., Bell M. A., de Andrade M. B. & Brusatte S. L. (2011).** Body size estimation and evolution in metriorhynchid crocodylomorphs: implications for species diversification and niche partitioning. *Zoological Journal of the Linnean Society*, 163(4): 1199-1216. https://doi.org/10.1111/j.1096-3642.2011.00734.x

32: **de Andrade M. B., Edmonds R., Benton M. J. & Schouten R. (2011).** A new Berriasian species of *Goniopholis* (Mesoeucrocodylia, Neosuchia) from England, and a review of the genus. *Zoological Journal of the Linnean Society*, 163(suppl 1): S66-S108. https://doi.org/10.1111/j.1096-3642.2011.00709.x

33: **Iori F. V. & Carvalho I. d. S. (2011).** *Caipirasuchus paulistanus*, a new sphagesaurid (Crocodylomorpha, Mesoeucrocodylia) from the Adamantina Formation (Upper Cretaceous, Turonian–Santonian), Bauru Basin, Brazil. *Journal of Vertebrate Paleontology*, 31(6): 1255-1264. https://doi.org/10.1080/02724634.2011.602777

34: **Riff D. & Kellner A. W. A. (2011).** Baurusuchid crocodyliforms as theropod mimics: clues from the skull and appendicular morphology of *Stratiotosuchus maxhechti* (Upper Cretaceous of Brazil). *Zoological Journal of the Linnean Society*, 163(suppl_1): S37-S56. https://doi.org/10.1111/j.1096-3642.2011.00713.x

35: **Montefeltro F. C., Larsson H. C. & Langer M. C. (2011).** A new baurusuchid (Crocodyliformes, Mesoeucrocodylia) from the Late Cretaceous of Brazil and the phylogeny of Baurusuchidae. *PLoS One*, 6(7): e21916. https://doi.org/10.1371/journal.pone.0021916

36: **Godoy P. L., Montefeltro F. C., Norell M. A. & Langer M. C. (2014).** An additional baurusuchid from the Cretaceous of Brazil with evidence of interspecific predation among Crocodyliformes. *PLoS One*, 9(5): e97138. https://doi.org/10.1371/journal.pone.0097138

37: **Pol D., Leardi J. M., Lecuona A. & Krause M. (2012).** Postcranial anatomy of *Sebecus icaeorhinus* (Crocodyliformes, Sebecidae) from the Eocene of Patagonia. *Journal of Vertebrate Paleontology*, 32(2): 328-354. https://doi.org/10.1080/02724634.2012.646833

38: **Nascimento P. M. & Zaher H. (2010).** A new species of *Baurusuchus* (Crocodyliformes, Mesoeucrocodylia) from the Upper Cretaceous of Brazil, with the first complete postcranial skeleton described for the family Baurusuchidae. *Papéis avulsos de Zoologia*, 50: 323-361. https://doi.org/10.1590/S0031-10492010002100001

39: **Kellner A. W., Pinheiro A. E. & Campos D. A. (2014).** A new sebecid from the Paleogene of Brazil and the crocodyliform radiation after the K–Pg boundary. *PLoS One*, 9(1): e81386. https://doi.org/10.1371/journal.pone.0081386

40: **Pol D., Turner A. H. & Norell M. A. (2009).** Morphology of the Late Cretaceous crocodylomorph *Shamosuchus djadochtaensis* and a discussion of neosuchian phylogeny as

related to the origin of Eusuchia. *Bulletin of the American Museum of Natural History*, 2009(324): 1-103. https://doi.org/10.1206/0003-0090-324.1.1

41: **Pol D., Nascimento P. M., Carvalho A. B., Riccomini C., Pires-Domingues R. A. & Zaher H. (2014).** A new notosuchian from the Late Cretaceous of Brazil and the phylogeny of advanced notosuchians. *PLoS One*, 9(4): e93105. https://doi.org/10.1371/journal.pone.0093105

42: **Pol D. & Gasparini Z. (2009).** Skull anatomy of *Dakosaurus andiniensis* (Thalattosuchia: Crocodylomorpha) and the phylogenetic position of Thalattosuchia. *Journal of Systematic Palaeontology,* 7(2): 163-197. https://doi.org/10.1017/S1477201908002605

43: **Pritchard A. C., Turner A. H., Allen E. R. & Norell M. A. (2013).** Osteology of a North American goniopholidid (*Eutretauranosuchus delfsi*) and palate evolution in Neosuchia. *American Museum Novitates*, 2013(3783): 1-56. https://doi.org/10.1206/3783.2

44: **Pol D. & Powell J. E. (2011).** A new sebecid mesoeucrocodylian from the Rio Loro Formation (Palaeocene) of north-western Argentina. *Zoological Journal of the Linnean Society*, 163(suppl_1): S7-S36. https://doi.org/10.1111/j.1096-3642.2011.00714.x

45: **Nascimento P. M. & Zaher H. (2011).** The skull of the Upper Cretaceous baurusuchid crocodile *Baurusuchus albertoi* Nascimento & Zaher 2010, and its phylogenetic affinities. *Zoological Journal of the Linnean Society*, 163(suppl_1): S116-S131. https://doi.org/10.1111/j.1096-3642.2011.00708.x

46: **Sertich J. J. & O'Connor P. M. (2014).** A new crocodyliform from the middle Cretaceous Galula Formation, southwestern Tanzania. *Journal of Vertebrate Paleontology*, 34(3): 576-596. https://doi.org/10.1080/02724634.2013.819808

47: **Adams T. L. (2013).** A new neosuchian crocodyliform from the Lower Cretaceous (Late Aptian) Twin Mountains Formation of north-central Texas. *Journal of Vertebrate Paleontology*, 33(1): 85-101. https://doi.org/10.1080/02724634.2012.713277

48: **Sereno P. & Larsson H. (2009).** Cretaceous crocodyliforms from the Sahara. *ZooKeys*, 28: 1-143. https://doi.org/10.3897/zookeys.28.325

49: **Young M. T. & de Andrade M. B. (2009).** What is *Geosaurus*? Redescription of *Geosaurus giganteus* (Thalattosuchia: Metriorhynchidae) from the Upper Jurassic of Bayern,

Germany. *Zoological Journal of the Linnean Society*, 157(3): 551-585. https://doi.org/10.1111/j.1096-3642.2009.00536.x

50: **Adams T. L. (2014).** Small crocodyliform from the Lower Cretaceous (Late Aptian) of Central Texas and its systematic relationship to the evolution of Eusuchia. *Journal of Paleontology*, 88(5): 1031-1049. https://doi.org/10.1666/12-089

51: **Montefeltro F. C., Larsson H. C., de França M. A. & Langer M. C. (2013).** A new neosuchian with Asian affinities from the Jurassic of northeastern Brazil. *Naturwissenschaften*, 100: 835-841. https://doi.org/10.1007/s00114-013-1083-9

52: **Novas F. E., Pais D. F., Pol D., Carvalho I. D. S., Scanferla A., Mones A. & Riglos M. S. (2009).** Bizarre notosuchian crocodyliform with associated eggs from the Upper Cretaceous of Bolivia. *Journal of Vertebrate Paleontology*, 29(4): 1316-1320. https://doi.org/10.1671/039.029.0409

53: **Gasparini Z., Pol D. & Spalletti L. A. (2006).** An unusual marine crocodyliform from the Jurassic-Cretaceous boundary of Patagonia. *Science*, 311(5757): 70-73. https://doi.org/10.1126/science.1120803

54: **Zaher H., Pol D., Carvalho A. B., Riccomini C., Campos D. & Nava W. (2006).** Redescription of the cranial morphology of *Mariliasuchus amarali*, and its phylogenetic affinities (Crocodyliformes, Notosuchia). *American Museum Novitates*, 2006(3512): 1-40. https://doi.org/10.1206/0003-0082(2006)3512[1:ROTCMO]2.0.CO;2

55: **Turner A. H. & Buckley G. A. (2008).** *Mahajangasuchus insignis* (Crocodyliformes: Mesoeucrocodylia) cranial anatomy and new data on the origin of the eusuchian-style palate. *Journal of Vertebrate Paleontology*, 28(2): 382-408. https://doi.org/10.1671/0272-4634(2008)28[382:MICMCA]2.0.CO;2

56: **Pol D. & Apesteguía S. (2005).** New *Araripesuchus* remains from the early late cretaceous (Cenomanian–Turonian) of Patagonia. *American Museum Novitates*, 2005(3490): 1-38. https://doi.org/10.1206/0003-0082(2005)490[0001:NARFTE]2.0.CO;2

57: **Company J., Suberbiola X. P., Ruiz-Omeñaca J. I. & Buscalioni A. D. (2005).** A new species of *Doratodon* (Crocodyliformes: Ziphosuchia) from the Late Cretaceous of Spain. *Journal of Vertebrate Paleontology*, 25(2): 343-353. https://doi.org/10.1671/0272-4634(2005)025[0343:ANSODC]2.0.CO;2

58: **Ősi A., Clark J. M. & Weishampel D. B. (2007).** First report on a new basal eusuchian crocodyliform with multicusped teeth from the Upper Cretaceous (Santonian) of Hungary. *Neues Jahrbuch für Geologie und Paläontologie Abhandlung*en, 243(2): 169-177. https://doi.org/10.1127/0077-7749/2007/0243-0169

59: **Turner A. H. & Calvo J. O. (2005).** A new sebecosuchian crocodyliform from the Late Cretaceous of Patagonia. *Journal of Vertebrate Paleontology*, 25(1): 87-98. https://doi.org/10.1671/0272-4634(2005)025[0087:ANSCFT]2.0.CO;2

60: **Jouve S., Iarochene M., Bouya B. & Amaghzaz M. (2006).** A new species of *Dyrosaurus* (Crocodylomorpha, Dyrosauridae) from the early Eocene of Morocco: phylogenetic implications. *Zoological Journal of the Linnean Society*, 148(4): 603-656. https://doi.org/10.1111/j.1096-3642.2006.00241.x

61: **Pol D. & Norell M. A. (2004a).** A new gobiosuchid crocodyliform taxon from the Cretaceous of Mongolia. *American Museum Novitates*, 2004(3458): 1-31. https://doi.org/10.1206/0003-0082(2004)458<0001:ANGCTF>2.0.CO;2

62: **Turner A. H. (2004).** Crocodyliform biogeography during the Cretaceous: evidence of Gondwanan vicariance from biogeographical analysis. *Proceedings of the Royal Society of London. Series B: Biological Sciences*, 271(1552): 2003-2009. https://doi.org/10.1098/rspb.2004.2840

63: **Turner A. H. (2006).** Osteology and phylogeny of a new species of *Araripesuchus* (Crocodyliformes: Mesoeucrocodylia) from the Late Cretaceous of Madagascar. *Historical Biology*, 18(3): 255-369. https://doi.org/10.1080/08912960500516112

64: **Jouve S. (2009).** The skull of *Teleosaurus cadomensis* (Crocodylomorpha; Thalattosuchia), and phylogenetic analysis of Thalattosuchia. *Journal of Vertebrate Paleontology*, 29(1): 88-102. https://doi.org/10.1080/02724634.2009.10010364

65: **de Andrade M. B. & Bertini R. J. (2008a).** A new *Sphagesaurus* (Mesoeucrocodylia: Notosuchia) from the Upper Cretaceous of Monte Alto City (Bauru Group, Brazil), and a revision of the Sphagesauridae. *Historical Biology*, 20(2): 101-136. https://doi.org/10.1080/08912960701642949

66: **Larsson H. C. & Sues H. D. (2007).** Cranial osteology and phylogenetic relationships of *Hamadasuchus rebouli* (Crocodyliformes: Mesoeucrocodylia) from the Cretaceous of

Morocco. *Zoological Journal of the Linnean Society*, 149(4): 533-567. https://doi.org/10.1111/j.1096-3642.2007.00271.x

67: **Wilkinson L. E., Young M. T. & Benton M. J. (2008).** A new metriorhynchid crocodylian (Mesoeucrocodylia: Thalattosuchia) from the Kimmeridgian (Upper Jurassic) of Wiltshire, UK. *Palaeontology*, 51(6): 1307-1333. https://doi.org/10.1111/j.1475-4983.2008.00818.x

68: **Sereno P. C., Larsson H. C., Sidor C. A. & Gado B. (2001).** The giant crocodyliform Sarcosuchus from the Cretaceous of Africa. *Science*, 294(5546): 1516-1519. https://doi.org/10.1126/science.1066521

69: **Wu X. C., Cheng Z. W. & Russell A. P. (2001).** Cranial anatomy of a new crocodyliform (Archosauria: Crocodylomorpha) from the Lower Cretaceous of Song-Liao Plain, northeastern China. *Canadian Journal of Earth Sciences*, 38(12): 1653-1663. https://doi.org/10.1139/e01-055

70: **Ortega F., Buscalioni A. D. & Gasparini Z. (1996).** Reinterpretation and new denomination of *Atacisaurus crassiproratus* (middle Eocene; Issel, France) as cf. *Iberosuchus* (Crocodylomorpha, Metasuchia). *Geobios*, 29(3): 353-364. https://doi.org/10.1016/S0016-6995(96)80037-4

71: **Brochu C. A. (1997).** Morphology, fossils, divergence timing, and the phylogenetic relationships of *Gavialis*. *Systematic Biology*, 46(3): 479-522. https://doi.org/10.1093/sysbio/46.3.479

72: **Parrish J. M. (1993).** Phylogeny of the Crocodylotarsi, with reference to archosaurian and crurotarsan monophyly. *Journal of Vertebrate Paleontology*, 13(3): 287-308. https://doi.org/10.1080/02724634.1993.10011511

73: **Sereno P. C. (1991).** Basal archosaurs: phylogenetic relationships and functional implications. *Journal of Vertebrate Paleontology*, 11(S4): 1-53. https://doi.org/10.1080/02724634.1991.10011426

74: **Gasparini Z., Fernandez M. & Powell J. (1993).** New tertiary sebecosuchians (Crocodylomorpha) from South America: phylogenetic implications. *Historical Biology*, 7(1): 1-19. https://doi.org/10.1080/10292389309380440

75: **Wu X. C., Sues H. D. & Brinkman D. B. (1996).** An atoposaurid neosuchian (Archosauria: Crocodyliformes) from the Lower Cretaceous of Inner Mongolia (People's Republic of China). *Canadian Journal of Earth Sciences*, 33(4): 599-605. https://doi.org/10.1139/e96-044

76: **Buscalioni A. D. & Sanz J. L. (1988).** Phylogenetic relationships of the Atoposauridae (Archosauria, Crocodylomorpha). *Historical Biology*, 1(3): 233-250. https://doi.org/10.1080/08912968809386477

77: **Norell M. A. (1989).** The higher level relationships of the extant Crocodylia. *Journal of Herpetology*,23(4): 325-335. https://doi.org/10.2307/1564042

78: **Wu X. C., Sues H. D. & Dong Z. M. (1997).** *Sichuanosuchus shuhanensis*, a new? Early Cretaceous protosuchian (Archosauria: Crocodyliformes) from Sichuan (China), and the monophyly of Protosuchia. *Journal of Vertebrate Paleontology*, 17(1): 89-103. https://doi.org/10.1080/02724634.1997.10010956

79: **Buckley G. A. & Brochu C. A. (1999).** An enigmatic new crocodile from the Upper Cretaceous of Madagascar. *Special papers in palaeontology*, 60(60): 149-175.

80: **Gomani E. M. (1997).** A crocodyliform from the Early Cretaceous dinosaur beds, northern Malawi. *Journal of Vertebrate Paleontology*, 17(2): 280-294. https://doi.org/10.1080/02724634.1997.10010975

81: **Pol D. & Norell M. A. (2004b).** A new crocodyliform from Zos Canyon, Mongolia. *American Museum Novitates*, 2004(3445): 1-36. https://doi.org/10.1206/0003-0082(2004)445<0001:ANCFCM>2.0.CO;2

82: **Pol D. (2003).** New remains of *Sphagesaurus huenei* (Crocodylomorpha: Mesoeucrocodylia) from the late Cretaceous of Brazil. *Journal of Vertebrate Paleontology*, 23(4): 817-831. https://doi.org/10.1671/A1015-7

83: **Buckley G. A., Brochu C. A., Krause D. W. & Pol D. (2000).** A pug-nosed crocodyliform from the Late Cretaceous of Madagascar. *Nature*, 405(6789): 941-944. https://doi.org/10.1038/35016061

84: **Sereno P. C. & Wild R. (1992).** *Procompsognathus*: theropod, "thecodont" or both?. *Journal of Vertebrate Paleontology*, 12(4): 435-458. https://doi.org/10.1080/02724634.1992.10011473

85: **Sereno P. C., Sidor C. A., Larsson H. C. E. & Gado B. (2003).** A new notosuchian from the Early Cretaceous of Niger. *Journal of Vertebrate Paleontology*, 23(2): 477-482. https://doi.org/10.1671/0272-4634(2003)023[0477:ANNFTE]2.0.CO;2

86: **Tykoski R. S., Rowe T. B., Ketcham R. A. & Colbert M. W. (2002).** *Calsoyasuchus valliceps*, a new crocodyliform from the Early Jurassic Kayenta Formation of Arizona. *Journal of Vertebrate Paleontology*, 22(3): 593-611. https://doi.org/10.1671/0272-4634(2002)022[0593:CVANCF]2.0.CO;2

87: **Carvalho I. d. S., Ribeiro L. C. B. & dos Santos Avilla L. (2004).** *Uberabasuchus terrificus* sp. nov., a new Crocodylomorpha from the Bauru Basin (Upper Cretaceous), Brazil. *Gondwana Research*, 7(4): 975-1002. https://doi.org/10.1016/S1342-937X(05)71079-0

88: **Pol D., Ji S. A., Clark J. M. & Chiappe L. M. (2004).** Basal crocodyliforms from the Lower Cretaceous Tugulu Group (Xinjiang, China), and the phylogenetic position of *Edentosuchus*. *Cretaceous Research*, 25(4): 603-622. https://doi.org/10.1016/j.cretres.2004.05.002

89: **Brochu C. A. (1999).** Phylogenetics, taxonomy, and historical biogeography of Alligatoroidea. *Journal of Vertebrate Paleontology*, 19(S2): 9-100. https://doi.org/10.1080/02724634.1999.10011201

90: **Wu X. C. & Sues H. D. (1996).** Anatomy and phylogenetic relationships of *Chimaerasuchus paradoxus*, an unusual crocodyliform reptile from the Lower Cretaceous of Hubei, China. *Journal of Vertebrate Paleontology*, 16(4): 688-702. https://doi.org/10.1080/02724634.1996.10011358

91: **Clark J. M. & Sues H. D. (2002).** Two new basal crocodylomorph archosaurs from the Lower Jurassic and the monophyly of the Sphenosuchia. *Zoological Journal of the Linnean Society*, 136(1): 77-95. https://doi.org/10.1046/j.1096-3642.2002.00026.x

92: **Wu X. C., Brinkman D. B. & Lu J. C. (1994).** A new species of *Shantungosuchus* from the Lower Cretaceous of Inner Mongolia (China), with comments on *S. chuhsienensis* Young, 1961 and the phylogenetic position of the genus. *Journal of Vertebrate Paleontology*, 14(2): 210-229. https://doi.org/10.1080/02724634.1994.10011553

93: **Ortega F., Gasparini Z., Buscalioni A. D. & Calvo J. O. (2000).** A new species of *Araripesuchus* (Crocodylomorpha, Mesoeucrocodylia) from the lower Cretaceous of Patagonia

(Argentina). *Journal of Vertebrate Paleontology*, 20(1): 57-76. https://doi.org/10.1671/0272-4634(2000)020[0057:ANSOAC]2.0.CO;2

94: **Clark J. M., Jacobs L. L. & Downs W. R. (1989).** Mammal-like dentition in a Mesozoic crocodylian. *Science*, 244(4908): 1064-1066. https://doi.org/10.1126/science.244.4908.1064

95: **Gasparini Z., Chiappe L. M. & Fernandez M. (1991).** A new Senonian peirosaurid (Crocodylomorpha) from Argentina and a synopsis of the South American Cretaceous crocodylians. *Journal of Vertebrate Paleontology*, 11(3): 316-333. https://doi.org/10.1080/02724634.1991.10011401

96: **Wu X. C. & Chatterjee S. (1993).** *Dibothrosuchus elaphros*, a crocodylomorph from the Lower Jurassic of China and the phylogeny of the Sphenosuchia. *Journal of Vertebrate Paleontology*, 13(1): 58-89. https://doi.org/10.1080/02724634.1993.10011488

Appendix 3: Supplementary Material concerning the publication 'A peirosaurid mandible from the Albian/Cenomanian (Lower Cretaceous) of Algeria and the taxonomic content of *Hamadasuchus* (Crocodylomorpha, Peirosauridae)'

Supplementary Material S3: Characters list and taxonomic sample

Characters underlined have been modified or created by the authors.

Continuous characters:

Character 1 [CONTINUOUS]: Mandibular symphysis, posterior extent, number of full alveoli involved (in Rio & Mannion, 2021 character 221, modified from Brochu, 2004, character 166).

Character 2 [CONTINUOUS]: Number of alveoli completely involved in the dentary part of the mandibular symphysis in dorsal view (from personal observations).

Mandibular openings:

Character 3: External mandibular fenestra: absent (0), rounded (1), ellipsoid or subrectangular, anteroposteriorly elongated (2), dorsally rounded and anteriorly tapered (3), almost a parallelogram (4), boomerang-shaped (5) (modified from Clark, 1994, character 75 and Nascimento & Zaher, 2011, character 261).

Character 4: Foramen *intermandibularis oralis*: small or absent (0), or big and slot like, with its anteroposterior length being approximately or more than 50% of the depth of the splenial (1) (in Pol *et al*., 2014, character 174, modified from Ortega *et al*., 2000, character 90).

Character 5 [ORDERED]: Location of the anterior opening for the mandibular nerve (V3): located at or close to the rostral margin of the splenial (0), or enclosed in the splenial and located on the anterior region of splenial (i.e., anterior foramen *intermandibularis oralis sensu* Brochu, 1999) (1), or enclosed in the splenial but located at the anteroposterior midpoint of the splenial (2) (in Pol *et al*., 2014, character 368, modified from Brochu, 1999, character 41).

Character 6: Foramen *intermandibularis caudalis*: present and enclosed between the angular and splenial below the mandibular adductor fossa (0), or absent with imperforated splenial-angular suture (1) (in Pol *et al*., 2014, character 369).

Character 7: Posterior portion of external mandibular fenestra: sculpted (0), smooth (1) (in Geroto & Bertini, 2019, character 213).

Character 8: Foramen *intermandibularis medius* (FIM) anteroposterior length relative to foramen *intermandibularis caudalis* (FIC): short, less than 25% FIC length (0), long, equal or greater than 25% FIC length (1) (in Rio & Mannion, 2021 character 259).

Character 9: Position of foramen *intermandibularis medius*: on coronoid-splenial suture (0), entirely within coronoid (1) (from Norell, 1988 character 12).

Dentary:

Character 10 [ORDERED]: Dentary: extends posteriorly beneath external mandibular fenestra (0), extends posteriorly further than the last tooth of the mandibular toothrow but closer than the external mandibular fenestra (1), extends posteriorly closer than the last tooth of the mandibular toothrow and reaches the external mandibular fenestra (modified from Clark, 1994, character 70 and Pinheiro, 2007, character 188).

Character 11: Unsculpted region in the dentary below the toothrow: absent (0), or present (1) (in Pol, 1999, character 213).

Character 12: Dentary compression and lateroventral surface anterior to external mandibular fenestra: compressed and vertical (0), or not compressed and convex (1) (in Pol *et al*., 2014, character 160, modified from Ortega *et al*., 1995, character 2).

Character 13 [ORDERED]: Lateral surface of dentaries below alveolar margin, at mid to posterior region of toothrow: vertically oriented, continuous with rest of lateral surface of the dentaries (0), or flat surface facing laterally or laterodorsally but divided by a ridge from rest of the lateral surface of the dentaries (1), or posterior region of alveolar facing dorsally, forming

a broad alveolar shelf that is strongly inset medially from the lateral surface of the dentaries (2) (in Pol *et al*., 2014, character 193, modified from Pol & Apesteguía, 2005, character 188).

Character 14: Orientation of the anterior dentary teeth: vertical or subvertical (0), strongly procumbent, anteriorly inclined, the first pair of teeth almost horizontal (1) (modified from de Andrade, 2005, character 134).

Character 15: Size of neurovascular foramina on mid to posterior region of alveolar edge of the dentary: small (0), or extremely large, being approximately as anteroposteriorly long as half an alveolus (1) (in Pol *et al*., 2014, character 365).

Character 16: Sutural contact between dentary and surangular above the external mandibular fenestra: dentary overlaps surangular (0), or surangular overlaps dentary (1), or interdigitated and vertically oriented suture (2) (in Pol *et al*., 2014, character 366).

Character 17 [ORDERED]: Dentary shape in lateral view: with anterior and middle portions as high as the posterior (0), posterior section in a higher plane than anterior, showing a gradual enlargement (1), posterior section higher than anterior, showing an abrupt ascension (2) (in de Andrade, 2005, character 104).

Character 18: Dentary alveoli 7º and 8º: same size (0), 7º smaller than 8º (1) (in Montefeltro *et al*., 2011, character 484).

Character 19 [ORDERED]: First and third teeth of dentary in mandibular symphysis: not aligned anteroposteriorly or mediolaterally (0), aligned anteroposteriorly (1), aligned mediolaterally (2) (modified from de Andrade, 2005, character 135).

Character 20 [ORDERED]: Dentary symphyseal teeth forming pairs: symphyseal teeth pairs absent (0), symphysial teeth pairs present (1), complete symphysial battery (2) (in Geroto & Bertini, 2019, character 241, modified from de Andrade & Bertini, 2008, character 141).

Character 21: Hypertrophied mandibular caniniform: absent (0), present, being the fourth dentary teeth (1), present, not being the fourth dentary teeth (2) (in Clark, 1994, character 80).

Character 22 [ORDERED]: Pattern of mandibular dentition after the fourth dentary teeth: isodont caniniform (0), predominantly caniniform, followed by molariforms (1), 3-4 caniniforms, followed by molariforms (2), enlarged molariform, followed by small molariforms (3), isodont molariform (4) (in Geroto & Bertini, 2019, character 243).

Character 23: Implantation of middle dentary teeth: tooth set disposed in a groove, the roots originally isolated from each other only by soft tissue (0), tooth set in isolated alveoli (1) (in de Andrade, 2005, character 139).

Character 24: Transverse section of medially and posteriorly dentary teeth: with strong lateral compression (0), transverse section circular to subcircular, without significant lateral compression (1), partially losangular, showing asymmetric lateral compression, only evident on anterior margin of teeth, results in a teardrop-like transverse section (2) (in Geroto & Bertini, 2019, character 245, modified from Brochu, 1997, character 116).

Character 25: Dentary, alveoli 3 and 4: confluent (0), separate (1) (from Brochu, 1997, character 52).

Character 26: Orientation of posteriormost alveoli: in a straight line (0), in a laterally curved line (1) (from Rio & Mannion, 2021, character 227).

Character 27: Dentary, acute posterior process in the angular, ventral to the external mandibular fenestra: present (0), absent (1) (from Jouve, 2016, character 240).

Character 28: Diastema: absent or regularly arranged teeth (0), present, clearly separating the fourth and fifth alveoli (1), present, clearly separating the fifth and sixth alveoli (2) (modified from Ruiz *et al*., 2021, character 506 and personal observations).

Splenial:

Character 29 [ORDERED]: Splenial involvement in symphysis in ventral view: not involved (0), involved slightly in symphysis forming up to 20% symphyseal length (1), or forming close to 30% of the symphyseal length (2), or extensively involved forming up to 50% of the

symphyseal length and occupying more than the length of five alveoli (3) (in Pol *et al*., 2014, character 77, modified from Clark, 1994, character 77 and Brochu, 1999, character 43).

Character 30: Ventral exposure of splenials along mandibular rami, posterior to the symphysis: absent (0), or present (1) (in Pol *et al*., 2014, character 119, modified from Ortega *et al*., 1996, character 9).

Character 31: Splenial: thin posterior to symphysis (0), or splenial robust dorsally posterior to symphysis, being much broader than the lateral alveolar margin of the dentary at the same region (1) (in Pol *et al*., 2014, character 161, modified from Ortega *et al*., 1995, character 7 and Buckley & Brochu, 1999, character 110).

Character 32: Medial surface of splenials posterior to symphysis: flat or slightly convex (0), or markedly concave (1) (in Pol & Apesteguía, 2005, character 185).

Character 33: Splenial, position of anteriormost tip relative to Meckelian fossa: splenial involved in mandibular symphysis (0), ventral (1), dorsal (2) (modified from Clark, 1994, character 77).

Character 34: Acute posterior process separating angular and coronoid: present (0), absent (1) (from Brochu, 1997, character 59).

Character 35: Splenials: not fused (0), fused (1) (from personal observations).

Mandibular symphysis:

Character 36: Shape of dentary symphysis in ventral view: tapering anteriorly forming an angle (V-shaped) (0), U-shaped, smoothly curving anteriorly (1), or lateral edges longitudinally oriented, convex anterolateral corner, and extensive transversely oriented anterior edge (2) (modified from Pol, 1999, character 212).

Character 37: Mandibular symphysis in lateral view: shallow and tapering anteriorly (0), deep and tapering anteriorly (1), deep and anteriorly convex (2), or shallow and anteriorly convex (3) (in Pol *et al*., 2014, character 103, modified from Wu & Sues, 1996, character 17).

Character 38: Splenial - dentary suture at symphysis on ventral surface: splenial not involved in symphysis (0), v-shaped (1), or transversal (2) (modified from Pol & Apesteguía, 2005, character 180).

Character 39: Shape of splenial - dentary suture adjacent to dentary toothrow (in dorsal view): constricted, laterally concave (narrow 'V'-shape) (0), straight (wide 'V'-shape) (1) (from Rio & Mannion, 2021, character 225, modified from Brochu, 1997, character 43).

Character 40: Posterior peg at the posterior edge of the mandibular symphysis: absent (0), or present, located on the ventral surface of symphysis (1), present, located on the posterior surface of the symphysis (2) (modified from Pol & Apesteguía, 2005, character 181 and Geroto & Bertini, 2019, character 370).

Character 41: Left and right toothrow along mandibular symphysis: well separated from each other by a broad dorsal surface of the symphysis (0), or closely located to each other (forming a symphyseal tooth battery in most taxa) (1) (in Pol *et al*., 2014, character 384, modified from de Andrade *et al*., 2011, character 399).

Character 42: Posteroventral symphyseal depressions: absent (0), present (1) (in Montefeltro *et al*., 2011, character 64).

Character 43: Structure of anterior portion of the mandibular symphysis: shallow, anteriorly spatulate, angle less than 45º (0), anteriorly verticalized, angle more than 45º (1) (in Geroto & Bertini, 2019, character 181, modified from Wu & Sues, 1996, character 17).

Coronoid:

Character 44: Coronoid size: short and located below the dorsal edge of the mandibular ramus (0), or anteriorly extended with posterior region elevated at the dorsal margin of the mandibular ramus (1) (in Pol *et al*., 2014, character 175, modified from Ortega *et al*., 2000, character 98).

Character 45: Coronoid tuberosities on the medial surface of anterior region of surangular: absent or poorly developed (0), well developed, forming prominent elongated crests divided by a deep longitudinal sulcus (1) (in Pol *et al*., 2014, character 372).

Character 46: Anterior extent relative to level of anterior margin of foramen *intermandibularis caudalis*: anterior (0), at the same level or posterior (1) (from Jouve *et al*., 2015, character 228).

Character 47: Orientation of posterior dorsal process: inclined anteriorly across entire length (0), horizontal towards posterior end (1) (from Brochu, 1997, character 54).

Character 48: Prominent medioventral lamina extending over inner (medial) surface of Meckelian fossa: present (0), absent (1) (from Brochu, 1997, character 55).

Surangular:

Character 49: Dorsal edge of surangular: flat (0) or arched dorsally (1) (in Clark, 1994, character 74).

Character 50: Surangular participating in quadrate articulation: does not participate in quadrate articulation (0), participates in quadrate articulation, but forms only the lateral wall of glenoid fossa and quadratojugal lacks an articular condyle (1), participates in quadrate articulation, forms approximately one-third of the glenoid fossa and quadratojugal bears an articular condyle (2) (in Geroto & Bertini, 2019, character 208, modified from Buckley & Brochu, 1999, character 102).

Character 51: Longitudinal ridge along the dorsolateral surface of surangular: absent (0), or present (1) (in Pol & Norell, 2004, character 187).

Character 52: Enlarged foramen at anterior end of surangular groove: absent (0), or present (1) (in Pol & Gasparini, 2009, character 245).

Character 53 [ORDERED]: Arrangement of the anterior and middle portions of mandibular rami in dorsal view: very near, almost parallel (0), confluent in "V" (1), distant from each, other forming an arch in “U” shape (2) (modified from Pol, 2003, character 155).

Character 54: Surangular anterior border: single or lightly furcated, directed to the lateral surface of the mandible (0), clearly furcated and divergent, the medial ramus directed toward splenial, and lateral ramus directed toward dentary (1) (in de Andrade & Bertini, 2008, character 113).

Character 55: Surangular medial shelf above the coronoid process: absent (0), present (1) (modified from Geroto & Bertini, 2019, character 203).

Character 56: Surangular posterior border: posterior edge bend upward, forming a concavity (0), posterior edge bend downward, forming a convexity (1), straight (2) (in Geroto & Bertini, 2019, character 206).

Character 57: Presence of a surangular extension to the retroarticular process: present in all extension of retroarticular process (0), excluded of distal portion of retroarticular process (1) (in Geroto & Bertini, 2019, character 207, modified from Brochu, 1997, character 51).

Character 58: Surangular - dentary suture, intersection with external mandibula fenestra: anterior to posterodorsal corner (0), at posterodorsal corner (1) (from Brochu, 1997, character 65).

Character 59: Surangular - angular suture, intersection with external mandibular fenestra: at posterodorsal angle (0), at posterior margin (1), passes broadly along ventral margin (2) (from Norell, 1988, character 40).

Character 60: Relative length of the anterior processes of surangular: unequal, ventral process <75% anteroposterior length of dorsal process (measured from surangular foramen) (0), sub-equal, ventral process ≥75% length of dorsal process (1) (from Brochu, 1997, character 48).

Character 61 [ORDERED]: Anterodorsal process (spur) lingual to posteriormost dentary alveoli, between splenial and dentary: absent (0), not reaching one full alveolus (1), reaching one to two alveoli (2), reaching three or more alveoli (3) (modified from Brochu, 1997, character 61 and Rio & Mannion, 2021, character 242 and 243).

Character 62: Sulcus on dorsal margin lateral to glenoid fossa: absent (0), present (1) (from Lee & Yates, 2018, character 204).

Character 63: Surangular - articular suture, shape in glenoid fossa: straight, oriented anteroposteriorly (0), bowed laterally (1) (from Brochu, 1997, character 162).

Character 64: Strong pitted pattern on angular and posterior surangular: absent (0), present (1) (from de Andrade *et al*., 2011, character 17).

Character 65: Lateral surface of the anterior region of surangular and posterior region of dentary: without longitudinal depression (0), or with longitudinal depression (1) (from Ortega *et al*., 1996, character 5).

Angular:

Character 66: Insertion area for *M. pterygoideous* posterior: does not extend onto lateral surface of angular (0) or extends onto lateral surface of angular (1) (in Clark, 1994, character 76).

Character 67: Angular posterior to external mandibular fenestra: widely exposed on lateral surface of mandible (0) or shifted to the ventral surface of mandible (1) (in Wu *et al*., 1997, character 110).

Character 68: Posteroventral edge of mandibular ramus: straight or convex (0), or markedly deflected (1) (in Wu *et al*., 1997, character 112).

Character 69: Posteroventral margin of the angular: straight or gently arched dorsally (0) or strongly arched dorsally (1) (in Pol *et al*., 2009, character 280).

Character 70: Smooth elongated fossa extending along ventral margin of external mandibular fenestra on the angular: absent, lateral surface of the angular reaching the ventral edge of the fenestra (0), or present, separated from the lateral surface of the angular by a sharp ridge (1) (in Pol *et al*., 2014, character 371).

Character 71: Morphology of mandible ventral margin, in lateral view: mandible is curved ventrally, with maximum curvature at anterior section of angular, below the external mandibular fenestra (when present), or not curved at all (0), mandible is curved posteroventrally, with maximum curvature at posterior section of angular, below (or almost below) the mandibular glenoid fossa, usually posterior to external mandibular fenestra (when present) (1) (in de Andrade *et al*., 2011, character 323).

Character 72 [ORDERED]: Length of the angular anterior ramus (in lateral view): short, not surpassing the anterior border of the external mandibular fenestra (0), moderately elongated, slightly surpassing the external mandibular fenestra (1), very long, reaching far beyond the fenestra (2) (in de Andrade, 2005, character 114).

Character 73: Sharp ridge on the surface of the angular: absent (0), or present on the ventral-most margin (1), or present along the lateral surface (2) (in Pol *et al*., 2014, character 219, modified from Pol & Norell, 2004, character 186).

Character 74: Angular and surangular: margins flush with lateral surface of mandible (0), margins everted forming flange (1) (from Lee & Yates, 2018, character 199).

Character 75: Surangular, angular suture, lingual intersection with articular in the floor of the adductor chamber: at ventral tip (0), dorsal to ventral tip (1) (from Brochu, 1997, character 67).

Articular:

Character 76: Prearticular: present (0), or absent (1) (in Pol *et al*., 2014, character 72).

Character 77: Articular facet for quadrate condyle: wider than broad (0), or elongated, equal to or more than twice the length of the quadrate condyles (1) (in Pol *et al*., 2014, character 104, modified from Wu & Sues, 1996, character 23).

Character 78: Posterior border of articular glenoid fossa: incipient or continuous with glenoid surface (0), well developed, with a ridge limiting the posterior mandibular moves (1) (in Wu & Sues, 1996, character 23).

Character 79: Position of foramen aërum: at medial margin of retroarticular process (0), inset from medial margin of retroarticular process (1) (from Brochu, 1997, character 49).

Character 80: Lamina extending from posterior edge of foramen aërum: absent (0), present (1) (from Rio & Mannion, 2021, character 249).

Character 81: Lingual foramen for articular and alveolar nerve: perforates surangular only (0), perforates surangular-articular suture (1) (from Brochu, 2007, character 69).

Character 82: Anterior process on posterior wall of adductor chamber: absent (0), present, dorsal to lingual foramen (1), present, ventral to lingual foramen (2) (modified from Brochu, 1997, character 44 and Rio & Mannion, 2021, character 254 and 255).

Character 83: Posterior end of the glenoid facet of articular: located above the surangular-angular suture (0), or ventrally recessed, located at or below the dorsoventral midpoint of the posterior mandibular ramus (i.e., surangular forming a high lateral wall that covers the posterior end of the glenoid facet) (1) (from Pol *et al*., 2014, character 348).

Retroarticular process:

Character 84: Retroarticular process: absent or extremely reduced (0), very short, wider than long and thick (1), with a rounded surface, longer than wide and flat, posteroventrally oriented and facing dorsomedially (2), elongated posteriorly, in triangular shape and facing dorsally (3), projecting dorsally in a paddle shape (4) (modified from Clark, 1994, character 71).

Character 85: Length of the lateral flange of the retroarticular process relative to the lateromedial width of the glenoid facets of the articular: shorter (0), or approximately the same length or longer (1) (in Pol *et al*., 2014, character 374).

Character 86: Rounded bulge at the posterior end of the lateral flange of the retroarticular process: absent (0), or present (1) (in Pol *et al*., 2014, character 375).

Character 87: Orientation of the ridge on the dorsal surface of retroarticular process that divides the lateral and medial flanges of the retroarticular process: directed posteriorly, parallel

to the longitudinal axis of the mandibular ramus (0), or directed posterolaterally, approximately at 45 degrees with the longitudinal axis of the mandibular ramus (1) (in Pol *et al*., 2014, character 376).

Character 88: Small bulge located proximally on the medial flange of the retroarticular process, posteriorly to the medial glenoid facet of the articular and associated with the foramen aërum in some taxa: absent (0), or present (1) (in Pol *et al*., 2014, character 377).

Character 89: Anteromedial end of medial flange of the retroarticular process: connected to the posteromedial corner of the medial glenoid facet of the articular through a dorsally directed crest (0) or extending anteriorly as a distinct anterior process up to the level of the anteroposterior midpoint of the medial glenoid of the articular (1) or projecting anteroventrally as deep pendant process (2) (in Pol *et al*., 2014, character 378).

Character 90: Orientation of medial flange of the retroarticular process: facing dorsally or slightly dorsomedially, having a similar orientation to the lateral flange to the medial flange of the retroarticular process (0), or facing medially, strongly deflected, and forming an angle of approximately 90 degrees with the dorsal surface of the lateral flange (1) (in Pol *et al*., 2014, character 379).

Character 91: Medial edge of the medial flange of the retroarticular process: straight or slightly convex (0), or strongly convex forming a paddle-shaped medial flange; its margin forms an extensive arch of approximately half circumference when viewed in dorsal view (1) (in Pol *et al*., 2014, character 380).

Character 92: Presence of a longitudinal crest in retroarticular surface: absent (0), present (1) (in de Andrade *et al*., 2011 character 364).

Taxonomic sample

Adamantinasuchus navae Nobre & Carvalho, 2006. UFRJ DG 107-R

Anatosuchus minor Sereno, Sidor, Larsson & Gado, 2003. MNN GDF603 (Sereno & Larsson, 2009)

Antaeusuchus taouzensis Nicholl, Hunt, Ouarhache & Mannion, 2021. NHMUK PV R36829

Aphaurosuchus escharafacies Darlim, Montefeltro & Langer, 2021. LPRP 0697

Aplestosuchus sordidus Godoy, Montefeltro, Norell & Langer, 2014. LPRP/USP 0229a

Araripesuchus buitreraensis Pol & Apesteguia, 2005. MPCA-PV 235

Araripesuchus gomesii Price, 1959. DGM 423-R

Araripesuchus patagonicus Ortega, Gasparini, Buscalioni & Calvo, 2000. MN 6093-V

Araripesuchus wegeneri Buffetaut, 1981. MNN GAD14, MNN GAD20, MNN GAD26 (Sereno & Larsson, 2009)

Armadillosuchus arrudai Marinho & Carvalho, 2009. UFRJ DG 303-R, MPMA-64-0001-04

Barcinosuchus gradilis Leardi & Pol, 2009. MPEF PV 3095

Barinasuchus arveloi Paolillo & Linares, 2007. MAAT-0260, MCN-USB: 01-94 PB

Barrosasuchus neuquenianus Coria, Ortega, Arcucci & Currie, 2019. MCF-PVPH-413

Baurusuchus albertoi Nascimento & Zaher, 2010. MZSP-PV 140 (Nascimento & Zaher, 2011)

Baurusuchus pachecoi Price, 1945. DGM 229-R

Baurusuchus salgadoensis Carvalho, Campos & Nobre, 2005. MPMA 62-0001-02

Bayomesasuchus hernandezi Barrios, Paulina-Carabajal & Bona, 2016. MCF PVPH-822

Bergisuchus dietrichberg Kuhn, 1968. HLMD-Me 7003, GM XVIII-49 (Rossmann *et al*., 2000)

Bretesuchus bonapartei Gasparini, Fernandez & Powell, 1993. PVL 4735

Caipirasuchus attenboroughi Ruiz, Bronzati, Ferreira, Martins, Queiroz, Langer & Montefeltro, 2021. LAPEISA-0001

Caipirasuchus montealtensis de Andrade & Bertini, 2008. MPMA 15-0001/90, MPMA 68-0003/12 (Iori *et al.*, 2013)

Caipirasuchus paulistanus Iori & Carvalho, 2011. MPMA 67-0001/00

Campinasuchus dinizi Carvalho, Teixeira, Ferraz, Ribeiro, Martinelli, Neto, Sertich, Cunha, Cunha, Ferraz, 2011. CPP 1234, CPP 1235, CPP 1237

Candidodon itapecuruense Carvalho & Campos, 1988. MN 4154-V

Chimaerasuchus paradoxus Wu, Sues & Sun, 1995. IVPP V8274 (Wu & Sues, 1996)

Comahuesuchus brachybuccalis Bonaparte, 1991. MUCPv 202, MACN-N 30, MACN-N 31, P 6131 MOZ (Martinelli, 2003).

Colhuehuapisuchus lunai Lamanna, Casal, Ibiricu & Martínez, 2019. UNPSJB-PV 961

Cynodontosuchus rothi Woodward, 1896. MLP 64-IV-16-2 (Gasparini, 1972).

Dibothrosuchus elaphros Simmons, 1965. FMNH CUP 2081, IVPP V 7907 (Wu & Chatterjee, 1993)

Doratodon carcharidens Bunzel, 1871. IPUW 2349/57 (Company *et al*., 2005).

Eremosuchus elkoholicus Buffetaut, 1989. KB-301, KA-401

Gasparinisuchus peirosauroides Martinelli, Sertich, Garrido & Praderio, 2012. MOZ 1750 PV

Gondwanasuchus scabrosus Marinho, Iori, Carvalho & de Vasconcellos, 2013. UFRJ DG 408-R

Hamadasuchus rebouli Buffetaut, 1994. MDE C001

Hamadasuchus rebouli Larsson & Sues, 2007. ROM 52620

Iberosuchus Antunes, 1975. Specimen from Muséum d'Histoire Naturelle, Toulouse, France (Ortega *et al*., 1996)

Itasuchus jesuinoi Price, 1955. DGM 434-R

Kaprosuchus saharicus Sereno & Larsson, 2009. MNN IGU12

Kinesuchus overoi Filippi, Barrios & Garrido, 2018. MAU-Pv-CO-583

Labidiosuchus amicum Kellner, Figueiredo, Azevedo & Campos, 2011. DGM 1480-R

Lavocatchampsa sigogneaurussellae Martin & de Lapparent de Broin, 2016. MNHN F MRS 2097

Libycosuchus brevirostris Stromer, 1914. BSP 1912 VIIL 574-578 (Ibrahim *et al*., 2020).

Lomasuchus palpebrosus Gasparini, Chiappe & Fernandez, 1991. MOZ 4084 PV

Lorosuchus nodosus Pol & Powell, 2011. PVL 6219

Mahajangasuchus insignis Buckley & Brochu, 1999. UA 8654, FMNH PR 2450, UA 9737 (Turner & Buckley, 2008)

Mariliasuchus amarali Carvalho & Bertini, 1999. UFRJ DG 50-R, MZSP-PV-50, MZSP-PV-51 (Zaher *et al*., 2006)

Miadanasuchus oblita Buffetaut & Taquet, 1979. FMNH PR 2343 (Rasmusson Simons & Buckley, 2009)

MHNN SAM-136. This study

Montealtosuchus arrudacamposi Carvalho, de Vasconcellos & Tavares, 2007. MPMA 16-0007-04

Morrinhosuchus luziae Iori & Carvalho, 2009. MPMA 07-0009/01, MPMA 12-0050/07, MPMA 04-0019/15

Notosuchus terrestris Woodward, 1986. MACN-PV-RN-1037, MACN-PV-sn, MCF-PVPH 710, MLP 64-IV-16-5, MPCA-Pv-237, MPCA-Pv-528, MPCA-Pv-791, MUCPv-35, MUCPv-147 (Fiorelli & Calvo, 2008; Barrios *et al*., 2018).

Pabweshi pakistanensis Wilson, Malkani & Gingerich, 2001. GSP UM 2000-2001

Pakasuchus kapilimai O´Connor, Sertich, Stevens, Roberts, Gottfried, Hieronymus, Jinnah, Ridgely, Ngasala & Temba, 2010. RRBP 08631, RRBP 05103

Patagosuchus anielensis Lio, Agnolin, Juarez Valieri, Filippi & Rosales, 2016. MAÑE-PV 1

Pehuenchesuchus enderi Turner & Calvo, 2005. MAU PV-CRS-440

Pepesuchus deiseae Campos, Oliveira, Figueiredo, Riff, Azevedo, Carvalho & Kellner, 2011. MN 7005-V, MCT 1723-R, MCT 1788-R (Geroto & Bertini, 2018)

Pissarrachampsa sera Montefeltro, Larsson & Langer, 2011. LPRP/USP 0018

Sebecus ayrampu Bravo, Pol & García-López, 2021. PVL 2606

Sebecus icaeorhinus Simpson, 1937. AMNH 3160, MPEF-PV 1776 (Colbert, 1946; Pol *et al*., 2012)

Simosuchus clarki Buckley, Brochu, Krause & Pol, 2000. FMNH PR 2596-2598, UA 8679 (Kley *et al*., 2010; Krause *et al*., 2010).

Stolokrosuchus lapparenti Larsson & Gado, 2000. MNN GDF600

Stratiotosuchus maxhechti Campos, Suarez, Riff & Kellner, 2001. URC RC•73 (Pinheiro *et al.*, 2008)

Uberabasuchus terrificus Carvalho, Ribeiro & Avilla, 2004. CPPLIP 630

Uruguaysuchus aznarezi Rusconi, 1933. FC DPV 2320 (*S*oto *et al.*, 2011).

Yacarerani boliviensis Novas, Pais, Pol, Carvalho, Scanferia, Mones & Riglos, 2009. MNK PAL5063, MNK-PAL5064-A, MNK-PAL-5064-D

Supplementary Material S5: Phylogenetic analyses

Uninformative characters:

6, 8, 9, 34, 35, 44, 46, 47, 48, 52, 67, 69, 74, 75, 76, 79, 80, 81, 82, 90, 92.

Taxa excluded from the analyses:

Araripesuchus wegeneri => 80% missing data

Armadillosuchus arrudai => 91% missing data

Barcinosuchus gradilis => 80% missing data

Barinasuchus arveloi => 80% missing data

Bergisuchus dietrichberg => 80% missing data

Chimaerasuchus paradoxus => 83% missing data

Cynodontosuchus rothi => 83% missing data

Pabweshi pakistanensis => 82% missing data

Previous analyses on Notosuchia:

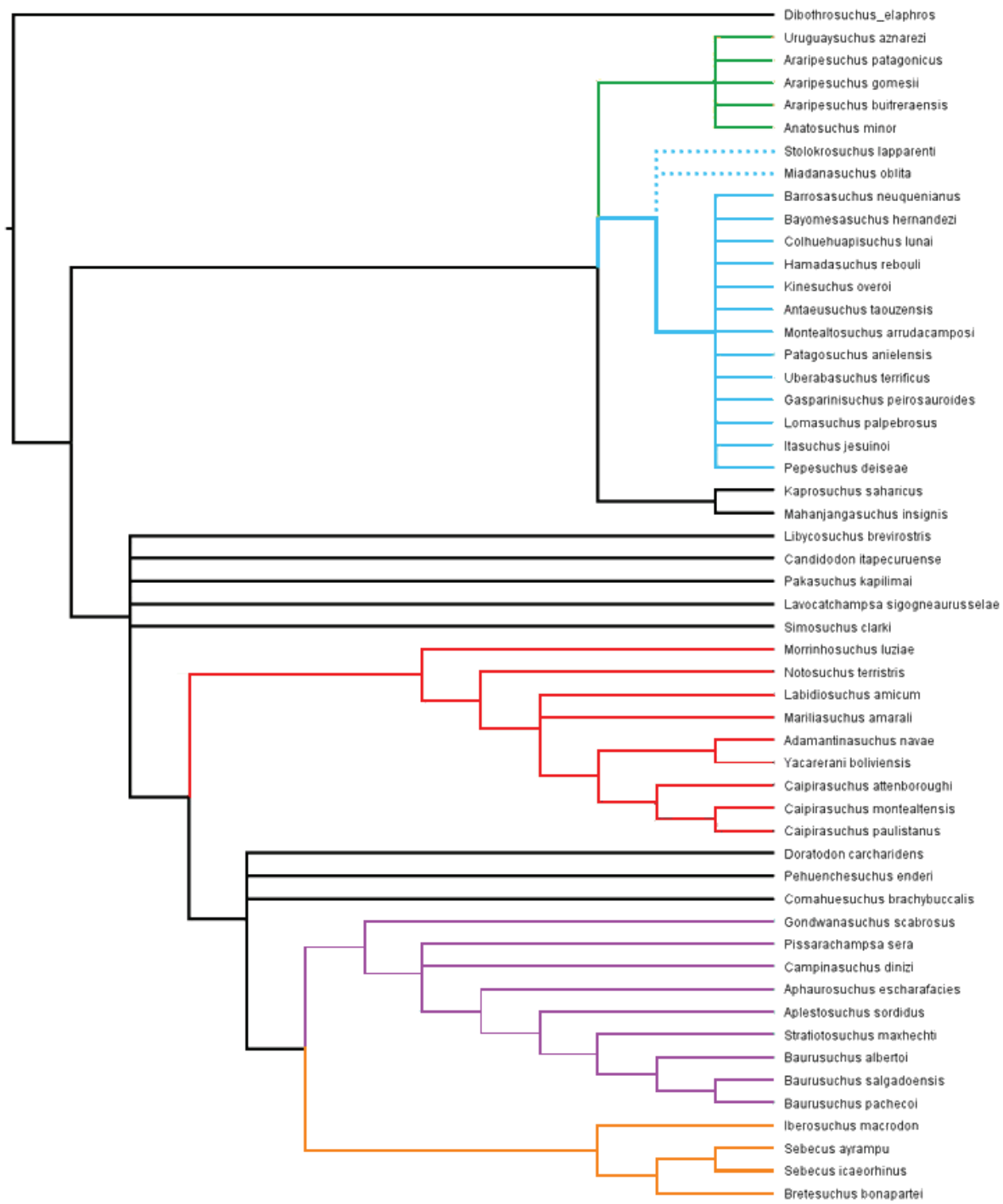

Green: Uruguaysuchidae, blue: Peirosauridae, red: “advanced” notosuchians, purple: Baurusuchidae, orange: Sebecidae. Consensus from Company *et al*. 2005; Kellner *et al*. 2014; Pol *et al*. 2014; Martin & de Lapparent de Broin 2016; Geroto & Bertini 2019; Bravo *et al*. 2021; Darlim *et al*. 2021; Nicholl *et al*. 2021; Ruiz *et al*. 2021.

Notosuchia analysis

94 trees of 377 steps generated, consensus is 437 steps.

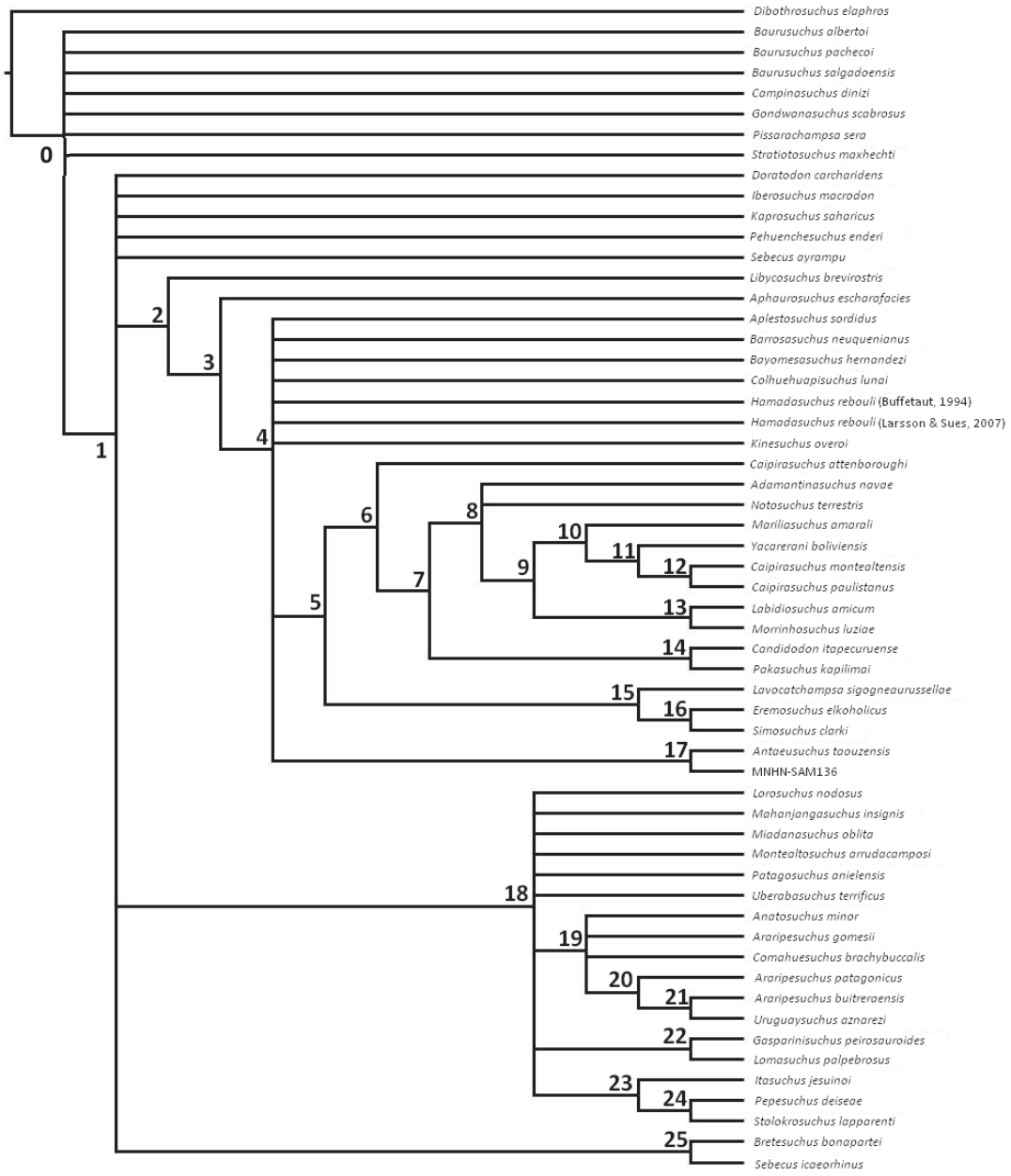

List of synapomorphies

Node 0: 3(2), 4(1), 17(1), 29(1), 30(1), 33(0), 37(2), 58(0), 65(1), 76(1), 78(0), 84(2), 90(1), 91(1)

Node 1: 42(0), 43(0), 50(1), 54(0), 85(1), 88(1), 89(0)

Node 2: 13(1), 19(0), 37(1), 39(1), 65(0), 85(0)

Node 3: 26(1), 49(1), 73(1), 78(1), 87(1)

Node 4: 16(1), 23(0), 50(2), 66(0)

Node 5: 21(0), 77(1)

Node 6: 1(6), 13(2), 24(1), 36(0), 45(1)

Node 7: 11(1), 72(0)

Node 8: 5(2), 20(2), 29(1), 70(1)

Node 9: 16(0), 40(2), 72(1)

Node 10: 30(0)

Node 11: 15(1), 23(1), 24(2), 41(1)

Node 12: 55(1), 56(0)

Node 13: 1(7)

Node 14: 22(4)

Node 15: 22(4), 53(2)

Node 16: 11(1), 23(1), 37(2)

Node 17: 65(1)

Node 18: 1(8), 4(0), 7(0), 22(2), 37(0), 38(2), 56(1), 64(1), 66(0), 78(1), 84(3), 91(0)

Node 19: 1(9), 2(7), 11(1), 16(0), 24(1), 29(2), 39(1), 66(1), 84(2)

Node 20: 10(0), 13(1), 40(1)

Node 21: 24(0), 64(0)

Node 22: 1(7), 22(3)

Node 23: 20(1), 24(1)

Node 24: 11(1), 31(1)

Node 25: 11(1), 17(2), 26(1), 51(1), 66(0), 71(1), 73(1)

Peirosauridae analysis

3 trees of 112 steps generated, consensus is 114 steps.

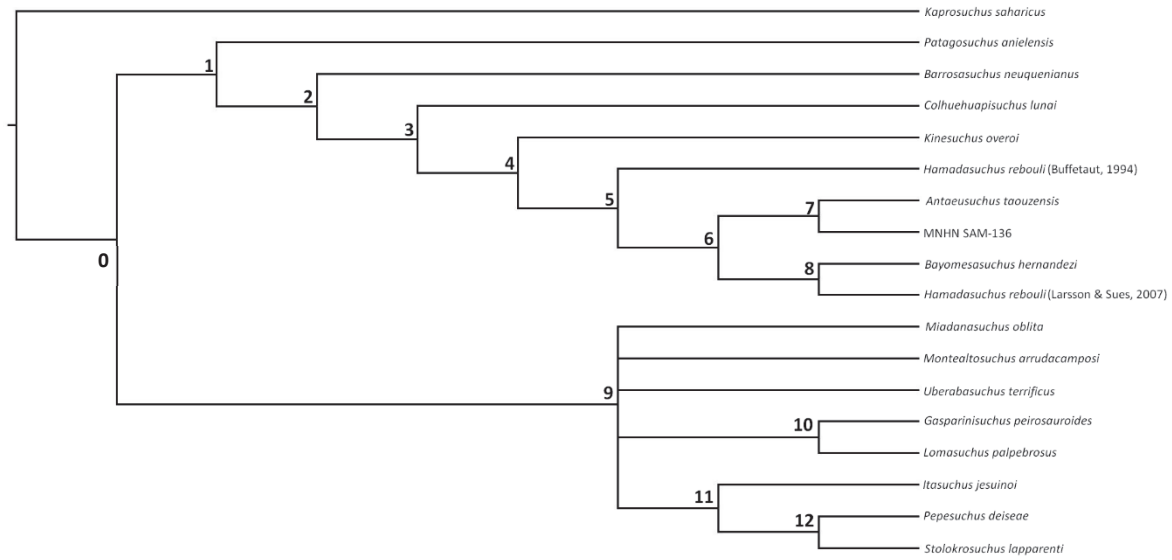

List of synapomorphies:

Node 0: 11(0), 16(1), 18(0), 21(1), 56(1), 78(1)

Node 1: 11(0), 22(0)

Node 2: 2(6), 14(1)

Node 3: 1(10)

Node 4: 1(11), 2(7)

Node 5: 26(0)

Node 6: 12(1)

Node 7: 13(1)

Node 8: 2(5)

Node 9: 7(0), 22(2), 37(0), 59(1), 72(1)

Node 10: 1(7), 22(3)

Node 11: 20(1), 24(1), 72(2)

Node 12: 11(1), 31(1)

Supplementary Material S7: An example of the variation (or not) of mandibular characters in an ontogenetic series of *Caiman latirostris*

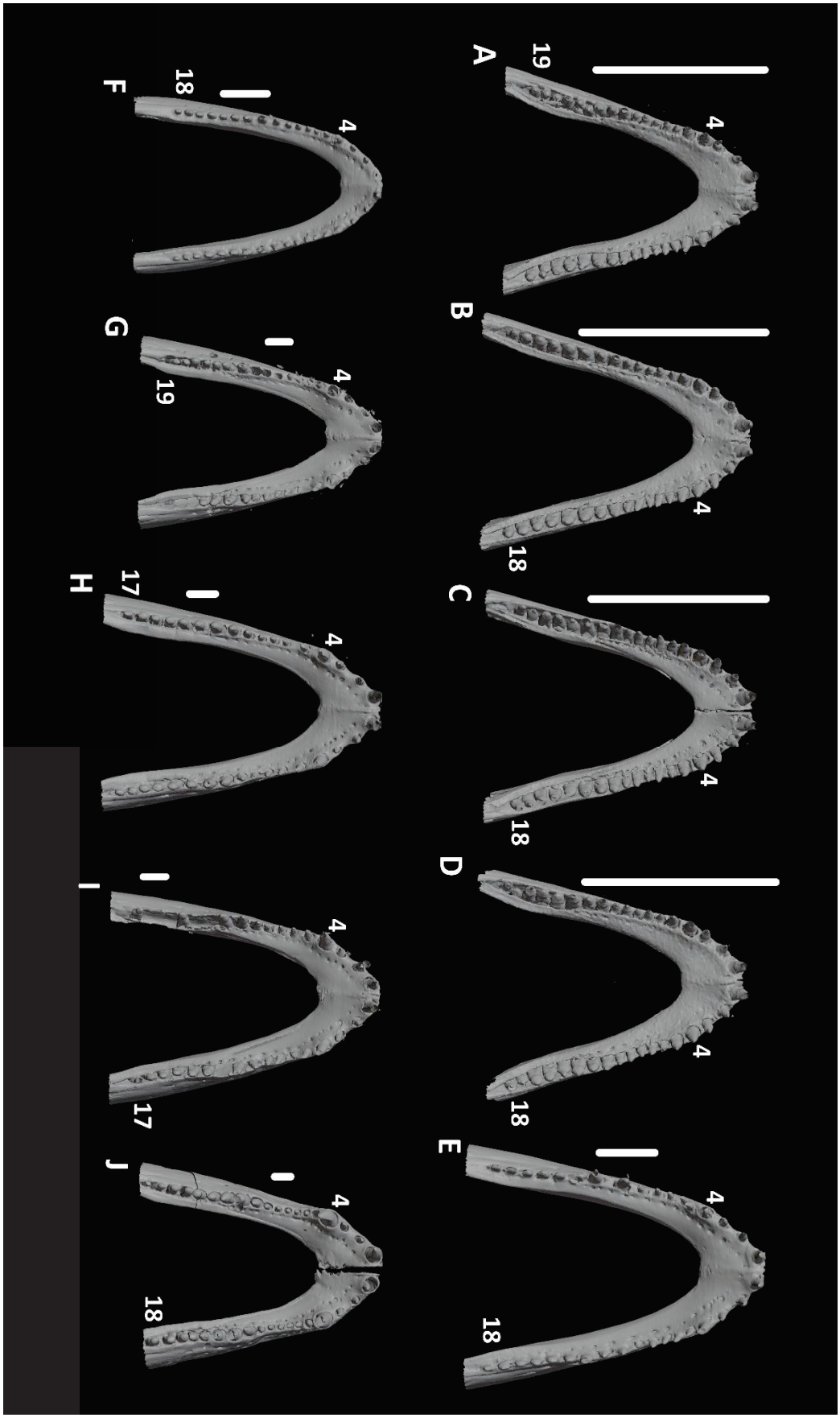

A: SMNK-REP 314; B: SMNK-REP 315; C: SMNK-REP 316; D: SMNK-REP 317; E: UMMZ herps 155287; F: UMMZ herps 155284; G: UMMZ herps 155286; H: UMMZ herps 155288; I: UMMZ herps 155283; J: UMMZ herps 155285. Numbers indicate alveoli numbers. Scale bars represent 1 cm.

Supplementary Material S8: An example of the variation (or not) of mandibular characters in an ontogenetic series of *Alligator mississippiensis*

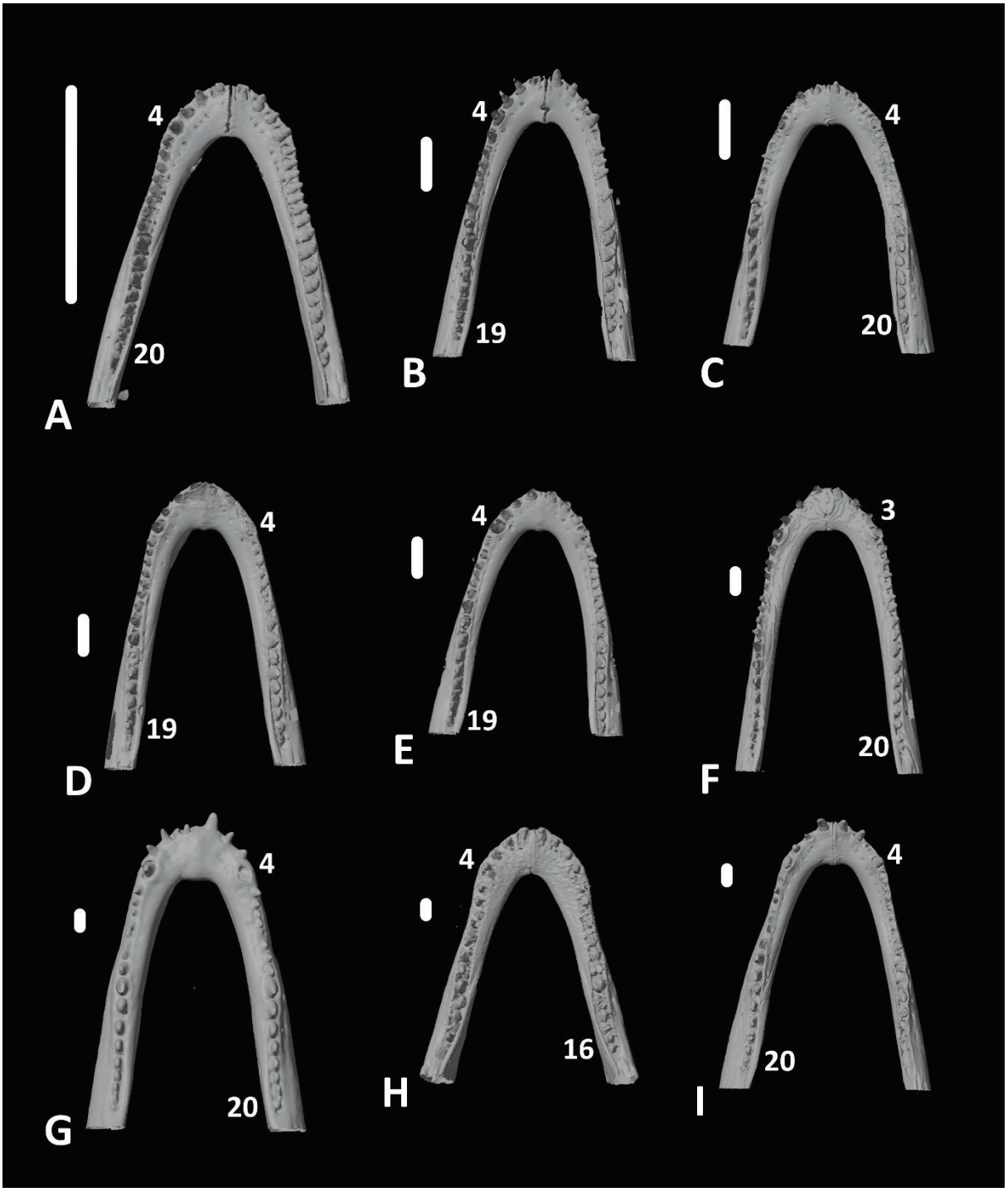

A: SMNK-REP 164; B: OUVC 11415; C: SMNK-REP 311; D: SMNK-REP 308; E: SMNK-REP 309; F: TMM M-983; G: OUVC 9761; H: OUVC 10606; I: UCBL WB35. Numbers indicate alveoli numbers. Scale bars represent 1 cm.

Supplementary Material S9: An example of the variation (or not) of mandibular characters in an ontogenetic series of *Mecistops*

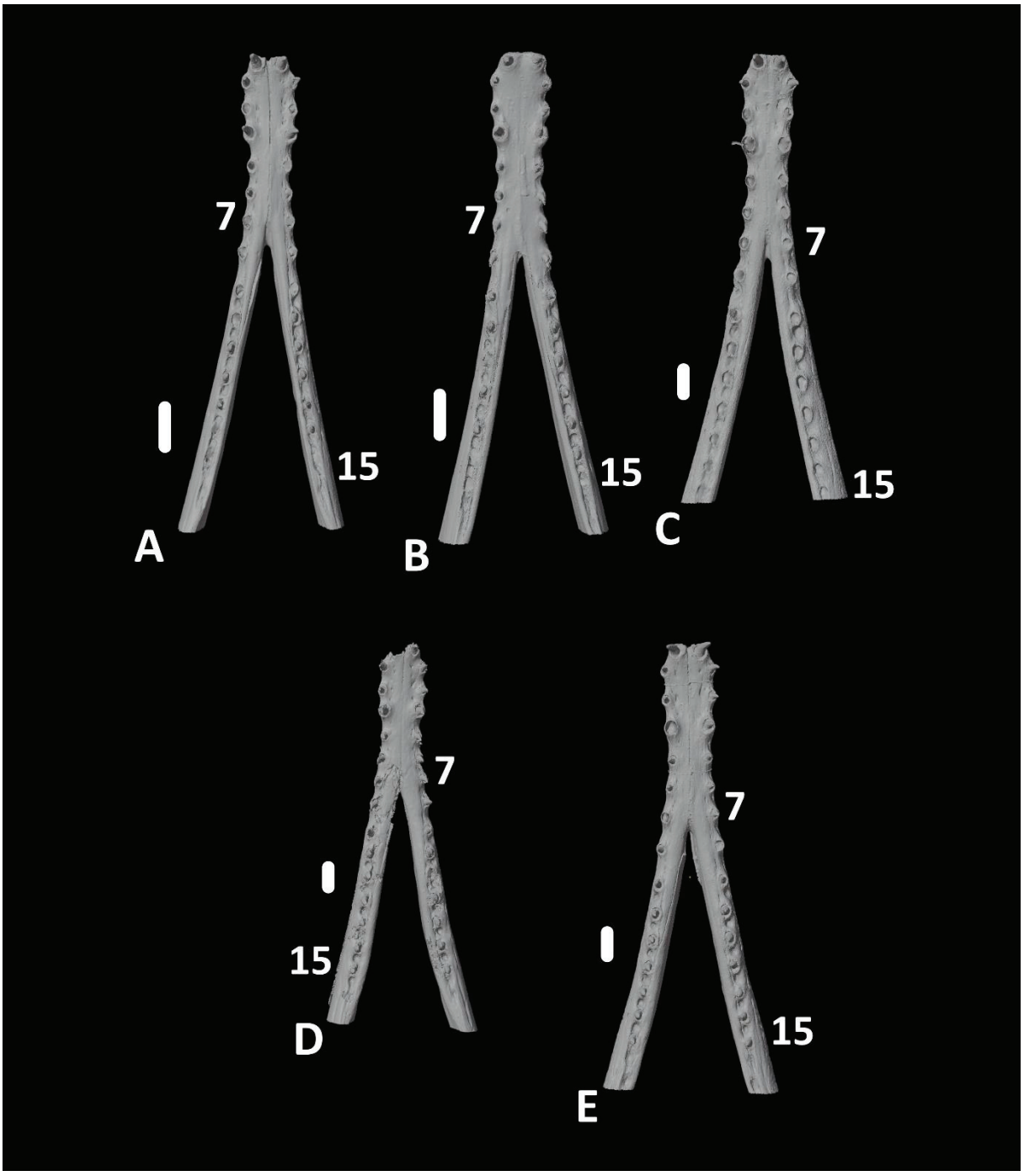

A: SVSTUA 022001; B: MHNL 50001393; C: AMU Zoo-04721; D: MZS Cro083; E: UM N89. Numbers indicate alveoli numbers. Scale bars are 2 cm.

References

Antunes M. T. (1975). *Iberosuchus,* crocodile Sebecosuchien nouveau, l'Eocène ibérique au Nord de la Chaîne Centrale, et l'origine du canyon de Nazaré. *Comunicaçoes dos Serviços Geologicos de Portugal*, 59: 285-330.

Barrios F., Paulina-Carabajal A. & Bona P. (2016). A new peirosaurid (Crocodyliformes, Mesoeucrocodylia) from the Upper Cretaceous of Patagonia, Argentina. *Ameghiniana*, 53(1): 14-25. https://doi.org/10.5710/AMGH.03.09.2015.2903

Barrios F., Bona P., Paulina-Carabajal A. & Gasparini Z. (2018). Re-description of the cranio-mandibular anatomy of *Notosuchus terrestris* (Crocodyliformes, Mesoeucrocodylia) from the Upper Cretaceous of Patagonia. *Cretaceous Research*, 83: 3-39. https://doi.org/10.1016/j.cretres.2017.08.016

Bonaparte J. F. (1991). Los vertebrados fósiles de la Formación Rio Colorado, de la Ciudad de Neuquén y Cercanías, Cretácico Superior, Argentina. *Revista del Museo Argentino de Ciencias Naturales 'Bernardino Rivadavia' e Instituto Nacional de Investigación de las Ciencias Naturales : Paleontologia*, 4(3): 17-123.

Brochu C. A. (1997). Morphology, fossils, divergence timing, and the phylogenetic relationships of *Gavialis*. *Systematic Biology*, 46(3): 479-522. https://doi.org/10.1093/sysbio/46.3.479

Brochu C. A. (1999). Phylogenetics, taxonomy, and historical biogeography of Alligatoroidea. *Journal of Vertebrate Paleontology*, 19(S2): 9-100. https://doi.org/10.1080/02724634.1999.10011201

Brochu C. A. (2004). Alligatorine phylogeny and the status of *Allognathosuchus* Mook, 1921. *Journal of Vertebrate Paleontology*, 24(4): 857-873. https://doi.org/10.1671/0272-4634(2004)024[0857:APATSO]2.0.CO;2

Bravo G. G., Pol D. & García-López D. A. (2021). A new sebecid mesoeucrocodylian from the Paleocene of northwestern Argentina. *Journal of Vertebrate Paleontology*, 41(3): e1979020. https://doi.org/10.1080/02724634.2021.1979020

Buckley G. A. & Brochu C. A. (1999). An enigmatic new crocodile from the Upper Cretaceous of Madagascar. *Special papers in palaeontology*, 60(60): 149-175.

Buckley G. A., Brochu C. A., Krause D. W. & Pol D. (2000). A pug-nosed crocodyliform from the Late Cretaceous of Madagascar. *Nature*, 405(6789): 941-944. https://doi.org/10.1038/35016061

Buffetaut E. (1981). Die biogeographische Geschichte der Krokodilier, mit Beschreibung einer neuen Art, *Araripesuchus wegeneri*. *Geologische Rundschau*, 70: 611-624. https://doi.org/10.1007/BF01822139

Buffetaut E. (1989). A new ziphodont mesosuchian crocodile from the Eocene of Algeria. *Palaeontographica*, 208(1-3): 1-10.

Buffetaut E. (1994). A new crocodylian from the Cretaceous of southern Morocco. *Comptes rendus de l'Académie des sciences. Série 2. Sciences de la terre et des planètes*, 319(12): 1563-1568.

Buffetaut E. & Taquet P. (1979). An early Cretaceous terrestrial crocodylian and the opening of the South Atlantic. *Nature*, 280(5722): 486-487. https://doi.org/10.1038/280486a0

Bunzel E. (1871). *Die Reptilfauna der Gosau-Formation in der Neuen Welt bei Wiener-Neustadt.* Braumüller, 42 p.

Campos D. d. A., Suarez J. M., Riff D. & Kellner A. W. A. (2001). Short note on a new Baurusuchidae (Crocodyliformes, Metasuchia) from the Upper Cretaceous of Brazil. *Boletim do Museu Nacional Nova Série Rio de Janeiro*, 57: 1-7.

Campos D. d. A., Oliveira G. R., Figueiredo R. G., Riff D., Azevedo S. A., Carvalho L. B. & Kellner A. W. (2011). On a new peirosaurid crocodyliform from the Upper Cretaceous, Bauru Group, southeastern Brazil. *Anais da Academia Brasileira de Ciências*, 83: 317-327. https://doi.org/10.1590/S0001-37652011000100020

Carvalho I. d. S. & Campos A. D. C. A. (1988). Um mamifero triconodonte do Cretáceo da Bacia Bauru, Brasil. *Anais da Academia Brasileira de Ciências*, 60(4): 437-446.

Carvalho I. d. S. & Bertini R. J. (1999). *Mariliasuchus*: um novo Crocodylomorpha (Notosuchia) do Cretáceo da Bacia Bauru, Brasil. *Geologia Colombiana*, 24: 83-105.

Carvalho I. d. S., Ribeiro L. C. B. & dos Santos Avilla L. (2004). *Uberabasuchus terrificus* sp. nov., a new Crocodylomorpha from the Bauru Basin (Upper Cretaceous), Brazil. *Gondwana Research*, 7(4): 975-1002. https://doi.org/10.1016/S1342-937X(05)71079-0

Carvalho I. d. S., Campos A. D. C. A. & Nobre P. H. (2005). *Baurusuchus salgadoensis*, a new crocodylomorpha from the Bauru Basin (Cretaceous), Brazil. *Gondwana Research*, 8(1): 11-30. https://doi.org/10.1016/S1342-937X(05)70259-8

Carvalho I. d. S., de Vasconcellos F. M., Tavares S. A. S. (2007). *Montealtosuchus arrudacamposi*, a new peirosaurid crocodile (Mesoeucrocodylia) from the Late Cretaceous Adamantina Formation of Brazil. *Zootaxa*, 1607: 35-46. https://doi.org/10.11646/zootaxa.1607.1.3

Carvalho, I. d. S., Teixeira V. D. P. A., Ferraz M. L. D. F., Ribeiro L. C. B., Martinelli A. G., Neto F. M., Sertich J. J. W., Cunha G. C., Cunha I. C. & Ferraz P. F. (2011*).* *Campinasuchus dinizi* gen. et sp. nov., a new Late Cretaceous baurusuchid (Crocodyliformes) from the Bauru Basin, Brazil. *Zootaxa*, 2871(1): 19-42. https://doi.org/10.11646/zootaxa.2871.1.2

Clark J. M. (1994). Patterns of evolution in Mesozoic Crocodyliformes. In Sues H. D. (eds.) *The Shadow of the Dinosaurs: Early Mesozoic Tetrapods*. New York: Cambridge University Press: 84–97.

Colbert E. H. (1946). *Sebecus*, representative of a peculiar suborder of fossil Crocodylia from Patagonia. *Bulletin of the American Museum of Natural History*, 87(4): 223-270.

Company J., Suberbiola X. P., Ruiz-Omeñaca J. I. & Buscalioni A. D. (2005). A new species of *Doratodon* (Crocodyliformes: Ziphosuchia) from the Late Cretaceous of Spain. *Journal of Vertebrate Paleontology*, 25(2): 343-353. https://doi.org/10.1671/0272-4634(2005)025[0343:ANSODC]2.0.CO;2

Coria R. A., Ortega F., Arcucci A. B. & Currie P. J. (2019). A new and complete peirosaurid (Crocodyliformes, Notosuchia) from Sierra Barrosa (Santonian, Upper Cretaceous) of the Neuquén Basin, Argentina. *Cretaceous Research*, 95: 89-105. https://doi.org/10.1016/j.cretres.2018.11.008

de Andrade M. B. (2005). *Revisões sistemática e taxonômica dos Notosuchia (Metasuchia, Crocodylomorpha)*. Unpublished Msc thesis, Universidade Estadual Paulista, 239 p.

de Andrade M. B. & Bertini R. J. (2008). A new *Sphagesaurus* (Mesoeucrocodylia: Notosuchia) from the Upper Cretaceous of Monte Alto City (Bauru Group, Brazil), and a revision of the Sphagesauridae. *Historical Biology*, 20(2): 101-136. https://doi.org/10.1080/08912960701642949

de Andrade M. B., Edmonds R., Benton M. J. & Schouten R. (2011). A new Berriasian species of *Goniopholis* (Mesoeucrocodylia, Neosuchia) from England, and a review of the genus. *Zoological Journal of the Linnean Society*, 163(suppl 1): S66-S108. https://doi.org/10.1111/j.1096-3642.2011.00709.x

Darlim G., Montefeltro F. C. & Langer M. C. (2021). 3D skull modelling and description of a new baurusuchid (Crocodyliformes, Mesoeucrocodylia) from the Late Cretaceous (Bauru Basin) of Brazil. *Journal of Anatomy*, 239(3): 622-662. https://doi.org/10.1111/joa.13442

Filippi L. S., Barrios F. & Garrido A. C. (2018). A new peirosaurid from the Bajo de la Carpa Formation (Upper Cretaceous, Santonian) of Cerro Overo, Neuquén, Argentina. *Cretaceous Research*, 83: 75-83. https://doi.org/10.1016/j.cretres.2017.10.021

Fiorelli L. E. & Calvo J. (2008). New remains of *Notosuchus terrestris* Woodward, 1896 (Crocodyliformes: Mesoeucrocodylia) from Late Cretaceous of Neuquén, Patagonia, Argentina. *Arquivos do Museu Nacional, Rio de Janeiro*, 66(1): 83-124.

Gasparini Z. (1972). Los Sebecosuchia (Crocodilia) del territorio Argentino: consideraciones sobre su 'status' taxonomico. *Ameghiniana*, 9(1): 23-34.

Gasparini Z., Chiappe L. M. & Fernandez M. (1991). A new Senonian peirosaurid (Crocodylomorpha) from Argentina and a synopsis of the South American Cretaceous crocodylians. *Journal of Vertebrate Paleontology*, 11(3): 316-333. https://doi.org/10.1080/02724634.1991.10011401

Gasparini Z., Fernandez M. & Powell J. (1993). New tertiary sebecosuchians (Crocodylomorpha) from South America: phylogenetic implications. *Historical Biology*, 7(1): 1-19. https://doi.org/10.1080/10292389309380440

Geroto C. F. C. & Bertini R. J. (2019). New material of *Pepesuchus* (Crocodyliformes; Mesoeucrocodylia) from the Bauru Group: implications about its phylogeny and the age of the Adamantina Formation. *Zoological Journal of the Linnean Society*, 185(2): 312-334. https://doi.org/10.1093/zoolinnean/zly037

Godoy P. L., Montefeltro F. C., Norell M. A. & Langer M. C. (2014). An additional baurusuchid from the Cretaceous of Brazil with evidence of interspecific predation among Crocodyliformes. *PLoS One*, 9(5): e97138. https://doi.org/10.1371/journal.pone.0097138

Ibrahim N., Sereno P. C., Varricchio D. J., Martill D. M., Dutheil D. B., Unwin D. M., Baidder L., Larsson H. C. E., Zouhri S. & Kaoukaya A. (2020). Geology and paleontology of the upper cretaceous Kem Kem group of eastern Morocco. *ZooKeys*, 928: 1-216. https://doi.org/10.3897/zookeys.928.47517

Iori F. V. & Carvalho I. d. S. (2009). *Morrinhosuchus luziae*, um novo Crocodylomorpha Notosuchia da Bacia Bauru, Brasil. *Brazilian Journal of Geology*, 39(4): 717-725.

Iori F. V. & Carvalho I. d. S. (2011). *Caipirasuchus paulistanus*, a new sphagesaurid (Crocodylomorpha, Mesoeucrocodylia) from the Adamantina Formation (Upper Cretaceous, Turonian–Santonian), Bauru Basin, Brazil. *Journal of Vertebrate Paleontology*, 31(6): 1255-1264. https://doi.org/10.1080/02724634.2011.602777

Iori F. V., Marinho T. S., Carvalho I. S. & Campos A. C. A. (2013). Taxonomic reappraisal of the sphagesaurid crocodyliform *Sphagesaurus montealtensis* from the late Cretaceous Adamantina Formation of São Paulo State, Brazil. *Zootaxa*, 3686(2): 183-200. https://doi.org/10.11646/zootaxa.3686.2.4

Jouve S. (2016). A new basal tomistomine (Crocodylia, Crocodyloidea) from Issel (Middle Eocene; France): palaeobiogeography of basal tomistomines and palaeogeographic consequences. *Zoological Journal of the Linnean Society*, 177(1): 165-182. https://doi.org/10.1111/zoj.12357

Jouve S., Bouya B., Amaghzaz M. & Meslouh S. (2015). *Maroccosuchus zennaroi* (Crocodylia: Tomistominae) from the Eocene of Morocco: phylogenetic and palaeobiogeographical implications of the basalmost tomistomine. *Journal of Systematic Palaeontology*, 13(5): 421-445. https://doi.org/10.1080/14772019.2014.913078

Kellner A. W., Figueiredo R. G., Azevedo S. A. & Campos D. A. (2011). A new cretaceous notosuchian (Mesoeucrocodylia) with bizarre dentition from Brazil. *Zoological Journal of the Linnean Society*, 163(suppl_1): S109-S115. https://doi.org/10.1111/j.1096-3642.2011.00711.x

Kley N. J., Sertich J. J., Turner A. H., Krause D. W., O'Connor P. M. & Georgi J. A. (2010). Craniofacial morphology of *Simosuchus clarki* (Crocodyliformes: Notosuchia) from the late Cretaceous of Madagascar. *Journal of Vertebrate Paleontology*, 30(sup1): 13-98. https://doi.org/10.1080/02724634.2010.532674

Krause D. W., Sertich J. J., Rogers R. R. Kast S. C., Rasoamiaramanana A. H. & Buckley G. A. (2010). Overview of the discovery, distribution, and geological context of *Simosuchus clarki* (Crocodyliformes: Notosuchia) from the Late Cretaceous of Madagascar. *Journal of Vertebrate Paleontology*, 30(sup1): 4-12. https://doi.org/10.1080/02724634.2010.516784

Kuhn O. (1968). *Die vorzeitlichten Krokodile*, Munich, 124 p.

Lamanna M. C., Casal G. A., Ibiricu L. M. & Martínez R. D. (2019). A new peirosaurid crocodyliform from the Upper Cretaceous Lago Colhué Huapi Formation of Central Patagonia, Argentina. *Annals of Carnegie Museum*, 85(3): 193-211. https://doi.org/10.2992/007.085.0301

Larsson H. C. & Gado B. (2000). A new Early Cretaceous crocodyliform from Niger. *Neues Jahrbuch für Geologie und Paläontologie-Abhandlungen*, 217(1): 131-141. https://doi.org/10.1127/njgpa/217/2000/131

Larsson H. C. & Sues H. D. (2007). Cranial osteology and phylogenetic relationships of *Hamadasuchus rebouli* (Crocodyliformes: Mesoeucrocodylia) from the Cretaceous of Morocco. *Zoological Journal of the Linnean Society*, 149(4): 533-567. https://doi.org/10.1111/j.1096-3642.2007.00271.x

Leardi J. M. & Pol D. (2009). The first crocodyliform from the Chubut Group (Chubut Province, Argentina) and its phylogenetic position within basal Mesoeucrocodylia. *Cretaceous Research*, 30(6): 1376-1386. https://doi.org/10.1016/j.cretres.2009.08.002

Lee M. S. & Yates A. M. (2018). Tip-dating and homoplasy: reconciling the shallow molecular divergences of modern gharials with their long fossil record. *Proceedings of the Royal Society B*, 285(1881): 20181071. https://doi.org/10.1098/rspb.2018.1071

Lio G., Agnolín F. L., Valieri R. J., Filippi L. & Rosales D. (2016). A new peirosaurid (Crocodilyformes) from the Late Cretaceous (Turonian–Coniacian) of Patagonia, Argentina. *Historical Biology*, 28(6): 835-841. https://doi.org/10.1080/08912963.2015.1043999

Marinho T. S. & Carvalho I. d. S. (2009). An armadillo-like sphagesaurid crocodyliform from the Late Cretaceous of Brazil. *Journal of South American Earth Sciences*, 27(1): 36-41. https://doi.org/10.1016/j.jsames.2008.11.005

Marinho T. S., Iori F. V., Carvalho I. d. S. & de Vasconcellos F. M. (2013). *Gondwanasuchus scabrosus* gen. et sp. nov., a new terrestrial predatory crocodyliform (Mesoeucrocodylia: Baurusuchidae) from the Late Cretaceous Bauru Basin of Brazil. *Cretaceous Research*, 44: 104-111. https://doi.org/10.1016/j.cretres.2013.03.010

Martin J. E. & de Lapparent de Broin F. (2016). A miniature notosuchian with multicuspid teeth from the Cretaceous of Morocco. *Journal of Vertebrate Paleontology*, 36(6): e1211534. https://doi.org/10.1080/02724634.2016.1211534

Martinelli A. G. (2003). *Comahuesuchus brachybuccalis* (Archosauria, Crocodyliformes) from the Late Cretaceous of Río Negro Province (Argentina). *Ameghiniana*, 40(4): 559-572.

Martinelli A. G., Sertich J. J., Garrido A. C. & Praderio Á. M. (2012). A new peirosaurid from the Upper Cretaceous of Argentina: Implications for specimens referred to *Peirosaurus torminni* Price (Crocodyliformes: Peirosauridae). *Cretaceous Research*, 37: 191-200. https://doi.org/10.1016/j.cretres.2012.03.017

Montefeltro F. C., Larsson H. C. & Langer M. C. (2011). A new baurusuchid (Crocodyliformes, Mesoeucrocodylia) from the Late Cretaceous of Brazil and the phylogeny of Baurusuchidae. *PLoS One*, 6(7): e21916. https://doi.org/10.1371/journal.pone.0021916

Nascimento P. M. & Zaher H. (2010). A new species of *Baurusuchus* (Crocodyliformes, Mesoeucrocodylia) from the Upper Cretaceous of Brazil, with the first complete postcranial skeleton described for the family Baurusuchidae. *Papéis avulsos de Zoologia*, 50: 323-361. https://doi.org/10.1590/S0031-10492010002100001

Nascimento P. M. & Zaher H. (2011). The skull of the Upper Cretaceous baurusuchid crocodile *Baurusuchus albertoi* Nascimento & Zaher 2010, and its phylogenetic affinities. *Zoological Journal of the Linnean Society*, 163(suppl_1): S116-S131. https://doi.org/10.1111/j.1096-3642.2011.00708.x

Nicholl C. S., Hunt E. S., Ouarhache D. & Mannion P. D. (2021). A second peirosaurid crocodyliform from the Mid-Cretaceous Kem Kem Group of Morocco and the diversity of Gondwanan notosuchians outside South America. *Royal Society Open Science*, 8(10): 211254. https://doi.org/10.1098/rsos.211254

Nobre P. H. & Carvalho I. d. S. (2006). *Adamantinasuchus navae*: a new gondwanan Crocodylomorpha (Mesoeucrocodylia) from the Late Cretaceous of Brazil. *Gondwana Research*, 10(3-4): 370-378. https://doi.org/10.1016/j.gr.2006.05.008

Norell M. A. (1988). *Cladistic Approaches to Paleobiology as Applied to the Phylogeny of Alligatorids.* Unpublished PhD thesis, Yale University, 264 p.

Novas F. E., Pais D. F., Pol D., Carvalho I. D. S., Scanferla A., Mones A. & Riglos M. S. (2009). Bizarre notosuchian crocodyliform with associated eggs from the Upper Cretaceous of Bolivia. *Journal of Vertebrate Paleontology*, 29(4): 1316-1320. https://doi.org/10.1671/039.029.0409

O'Connor P. M., Sertich J. J., Stevens N. J., Roberts E. M., Gottfried M. D., Hieronymus T. L., Jinnah Z. A., Ridgely R., Ngasala S. E. & Temba J. (2010). The evolution of mammal-like crocodyliforms in the Cretaceous Period of Gondwana. *Nature*, 466(7307): 748-751. https://doi.org/10.1038/nature09061

Ortega F. & Buscalioni A. D. (1995). Las Hoyas Crocodiles, an Evidence of the Transition Model of the Eusuchian dorsal Armor Construction. *Extended Abstract of the second International Symposium on Lithographic Limestones*, Spain: 107-110.

Ortega F., Buscalioni A. D. & Gasparini Z. (1996). Reinterpretation and new denomination of *Atacisaurus crassiproratus* (middle Eocene; Issel, France) as cf. *Iberosuchus* (Crocodylomorpha, Metasuchia). *Geobios*, 29(3): 353-364. https://doi.org/10.1016/S0016-6995(96)80037-4

Ortega F., Gasparini Z., Buscalioni A. D. & Calvo J. O. (2000). A new species of *Araripesuchus* (Crocodylomorpha, Mesoeucrocodylia) from the lower Cretaceous of Patagonia (Argentina). *Journal of Vertebrate Paleontology*, 20(1): 57-76. https://doi.org/10.1671/0272-4634(2000)020[0057:ANSOAC]2.0.CO;2

Paolillo A. & Linares O. J. (2007). Nuevos cocodrilos Sebecosuchia del Cenozoico Suramericano (Mesosuchia: Crocodylia). *Contribuciones ocasionales editada por el Laboratorio de Paleobiología*, 3: 1-25.

Pinheiro A. E. P. (2007). *Revisões cladística-filogenética e considerações paleobiogeográficas sobre Sebecosuchia (Metasuchia, Crocodylomorpha), do Cretáceo Superior ao Mioceno*. Unpublished Msc thesis, Universidade Estadual Paulista, 267 p.

Pinheiro A. E. P., Bertini R. J., Andrade M. D. & Neto R. M. (2008). A new specimen of *Stratiotosuchus maxhechti* (Baurusuchidae, Crocodyliformes) from the Adamantina Formation (Upper Cretaceous), Southeastern Brazil. *Revista Brasileira de Paleontologia*, 11(1): 37-50.

Pol D. (1999). *El esqueleto postcraneano de Notosuchus terrestris (Archosauria: Crocodyliformes) del Cretácico Superior de la Cuenca Neuquina y su información filogenética*. Unpublished MSc thesis, Universidad de Buenos Aires, 158 p.

Pol D. (2003). New remains of *Sphagesaurus huenei* (Crocodylomorpha: Mesoeucrocodylia) from the late Cretaceous of Brazil. *Journal of Vertebrate Paleontology*, 23(4): 817-831. https://doi.org/10.1671/A1015-7

Pol D. & Norell M. A. (2004). A new gobiosuchid crocodyliform taxon from the Cretaceous of Mongolia. *American Museum Novitates*, 2004(3458): 1-31. https://doi.org/10.1206/0003-0082(2004)458<0001:ANGCTF>2.0.CO;2

Pol D. & Apesteguía S. (2005). New *Araripesuchus* remains from the early late cretaceous (Cenomanian–Turonian) of Patagonia. *American Museum Novitates*, 2005(3490): 1-38. https://doi.org/10.1206/0003-0082(2005)490[0001:NARFTE]2.0.CO;2

Pol D. & Gasparini Z. (2009). Skull anatomy of *Dakosaurus andiniensis* (Thalattosuchia: Crocodylomorpha) and the phylogenetic position of Thalattosuchia. *Journal of Systematic Palaeontology,* 7(2): 163-197. https://doi.org/10.1017/S1477201908002605

Pol D. & Powell J. E. (2011). A new sebecid mesoeucrocodylian from the Rio Loro Formation (Palaeocene) of north-western Argentina. *Zoological Journal of the Linnean Society*, 163(suppl_1): S7-S36. https://doi.org/10.1111/j.1096-3642.2011.00714.x

Pol D., Turner A. H. & Norell M. A. (2009). Morphology of the Late Cretaceous crocodylomorph *Shamosuchus djadochtaensis* and a discussion of neosuchian phylogeny as related to the origin of Eusuchia. *Bulletin of the American Museum of Natural History*, 2009(324): 1-103. https://doi.org/10.1206/0003-0090-324.1.1

Pol D., Leardi J. M., Lecuona A. & Krause M. (2012). Postcranial anatomy of *Sebecus icaeorhinus* (Crocodyliformes, Sebecidae) from the Eocene of Patagonia. *Journal of Vertebrate Paleontology*, 32(2): 328-354. https://doi.org/10.1080/02724634.2012.646833

Pol D., Nascimento P. M., Carvalho A. B., Riccomini C., Pires-Domingues R. A. & Zaher H. (2014). A new notosuchian from the Late Cretaceous of Brazil and the phylogeny of advanced notosuchians. *PLoS One*, 9(4): e93105. https://doi.org/10.1371/journal.pone.0093105

Price L. I. (1945). A new reptile from the Upper Cretaceous of Brazil. *Notas Preliminares e Estudos – Ministério da Agricultura, Divisão de Geologia e Mineralogia*, 25: 1-9.

Price L. I. (1955). Novos crocodilídeos dos arenitos da Série Bauru. Cretáceo do Estado de Minas Gerais. *Anais da Academia brasileira de Ciências*, 27(4): 487-498.

Price L. I. (1959). Sôbre um crocodilídeo Notossúquio do Cretácico Brasileiro. *Boletim do Departamento Nacional da Produçao Mineral, Divisao de Geologia e Mineralogia, Rio de Janeiro*, 188: 7-55.

Rasmusson Simons E. L. & Buckley G. A. (2009). New material of "*Trematochampsa*" *oblita* (Crocodyliformes, Trematochampsidae) from the Late Cretaceous of Madagascar. *Journal of Vertebrate Paleontology*, 29(2): 599-604. https://doi.org/10.1671/039.029.0224

Rio J. P. & Mannion P. D. (2021). Phylogenetic analysis of a new morphological dataset elucidates the evolutionary history of Crocodylia and resolves the long-standing gharial problem. *PeerJ*, 9: e12094. https://doi.org/10.7717/peerj.12094

Rossmann T., Rauhe M. & Ortega F. (2000). Studies on Cenozoic crocodiles: 8. *Bergisuchus dietrichbergi* Kuhn (Sebecosuchia: Bergisuchidae n. fam.) from the Middle Eocene of Germany, some new systematic and biological conclusions. *PalZ*, 74: 379-392. https://doi.org/10.1007/BF02988108

Ruiz J. V., Bronzati M., Ferreira G. S., Martins K. C., Queiroz M. V., Langer M. C. & Montefeltro F. C. (2021). A new species of *Caipirasuchus* (Notosuchia, Sphagesauridae) from the Late Cretaceous of Brazil and the evolutionary history of Sphagesauria. *Journal of Systematic Palaeontology*, 19(4): 265-287. https://doi.org/10.1080/14772019.2021.1888815

Rusconi C. (1933). Sobre reptiles cretáceos del Uruguay (*Uruguaysuchus aznarezi* n. g. n. sp.) y sus relaciones con los notosúquidos de Patagonia. *Boletín del Instituto Geológico del Uruguay*, 19: 1-64.

Sereno P. & Larsson H. (2009). Cretaceous crocodyliforms from the Sahara. *ZooKeys*, 28: 1-143. https://doi.org/10.3897/zookeys.28.325

Sereno P. C., Sidor C. A., Larsson H. C. E. & Gado B. (2003). A new notosuchian from the Early Cretaceous of Niger. *Journal of Vertebrate Paleontology*, 23(2): 477-482. https://doi.org/10.1671/0272-4634(2003)023[0477:ANNFTE]2.0.CO;2

Simmons D. J. (1965). The non-therapsid reptiles of the Lufeng Basin, Yunnan, China. *Fieldiana: Geology,* 15(1): 1-93.

Simpson G. G. (1937). New reptiles from the Eocene of South America. *American Museum Novitates*, 927: 1-3.

Soto M., Pol D. & Perea D. (2011). A new specimen of *Uruguaysuchus aznarezi* (Crocodyliformes: Notosuchia) from the middle Cretaceous of Uruguay and its phylogenetic relationships. *Zoological Journal of the Linnean Society*, 163(suppl_1): S173-S198. https://doi.org/10.1111/j.1096-3642.2011.00717.x

Stromer E. V. (1914). Ergebnisse der Forschungreisen Prof. E. Stromers in den Wusten Agyptens: II. Wirbeltier-Reste der Baharije-Stufe (unterstes Cenoman). 1. Einleitung und 2. *Libycosuchus*. *Abhandlungen der Koniglichen Bayerischen Akademie der Wissenschaften, Mathematisch-Physikalischen Klasse* 27(3):1-15.

Turner A. H. & Calvo J. O. (2005). A new sebecosuchian crocodyliform from the Late Cretaceous of Patagonia. *Journal of Vertebrate Paleontology*, 25(1): 87-98. https://doi.org/10.1671/0272-4634(2005)025[0087:ANSCFT]2.0.CO;2

Turner A. H. & Buckley G. A. (2008). *Mahajangasuchus insignis* (Crocodyliformes: Mesoeucrocodylia) cranial anatomy and new data on the origin of the eusuchian-style palate. *Journal of Vertebrate Paleontology*, 28(2): 382-408. https://doi.org/10.1671/0272-4634(2008)28[382:MICMCA]2.0.CO;2

Wilson J. A., Malkani M. S. & Gingerich P. D. (2001). New crocodyliform (Reptilia, Mesoeucrocodylia) from the Upper Cretaceous Pab Formation of Vitakri, Balochistan (Pakistan). *Contributions from the Museum of Paleontology, The University of Michigan*, 30(12): 231-336.

Woodward A. S. (1896). On two Mesozoic crocodylians *Notosuchus* (genus novum) and *Cynodontosuchus* (genus novum) from the Red Sandstones of the Territory of Neuquén (Argentina Republic). *Anales del Museo de La Plata,* 4: 1-20.

Wu X. C. & Chatterjee S. (1993). *Dibothrosuchus elaphros*, a crocodylomorph from the Lower Jurassic of China and the phylogeny of the Sphenosuchia. *Journal of Vertebrate Paleontology*, 13(1): 58-89. https://doi.org/10.1080/02724634.1993.10011488

Wu X. C. & Sues H. D. (1996). Reassessment of *Platyognathus hsui* Young, 1944 (Archosauria: Crocodyliformes) from the Lower Lufeng Formation (Lower Jurassic) of Yunnan, China. *Journal of Vertebrate Paleontology*, 16(1): 42-48. https://doi.org/10.1080/02724634.1996.10011282

Wu X. C., Sues H. D. & Sun A. (1995). A plant-eating crocodyliform reptile from the Cretaceous of China. *Nature*, 376(6542): 678-680. https://doi.org/10.1038/376678a0

Wu X. C., Sues H. D. & Dong Z. M. (1997). *Sichuanosuchus shuhanensis*, a new? Early Cretaceous protosuchian (Archosauria: Crocodyliformes) from Sichuan (China), and the monophyly of Protosuchia. *Journal of Vertebrate Paleontology*, 17(1): 89-103. https://doi.org/10.1080/02724634.1997.10010956

Zaher H., Pol D., Carvalho A. B., Riccomini C., Campos D. & Nava W. (2006). Redescription of the cranial morphology of *Mariliasuchus amarali*, and its phylogenetic affinities (Crocodyliformes, Notosuchia). *American Museum Novitates*, 2006(3512): 1-40. https://doi.org/10.1206/0003-0082(2006)3512[1:ROTCMO]2.0.CO;2

Appendix 4: Supplementary Material concerning the publication 'New Cretaceous neosuchians (Crocodylomorpha) from Thailand bridge the evolutionary history of atoposaurids and paralligatorids'

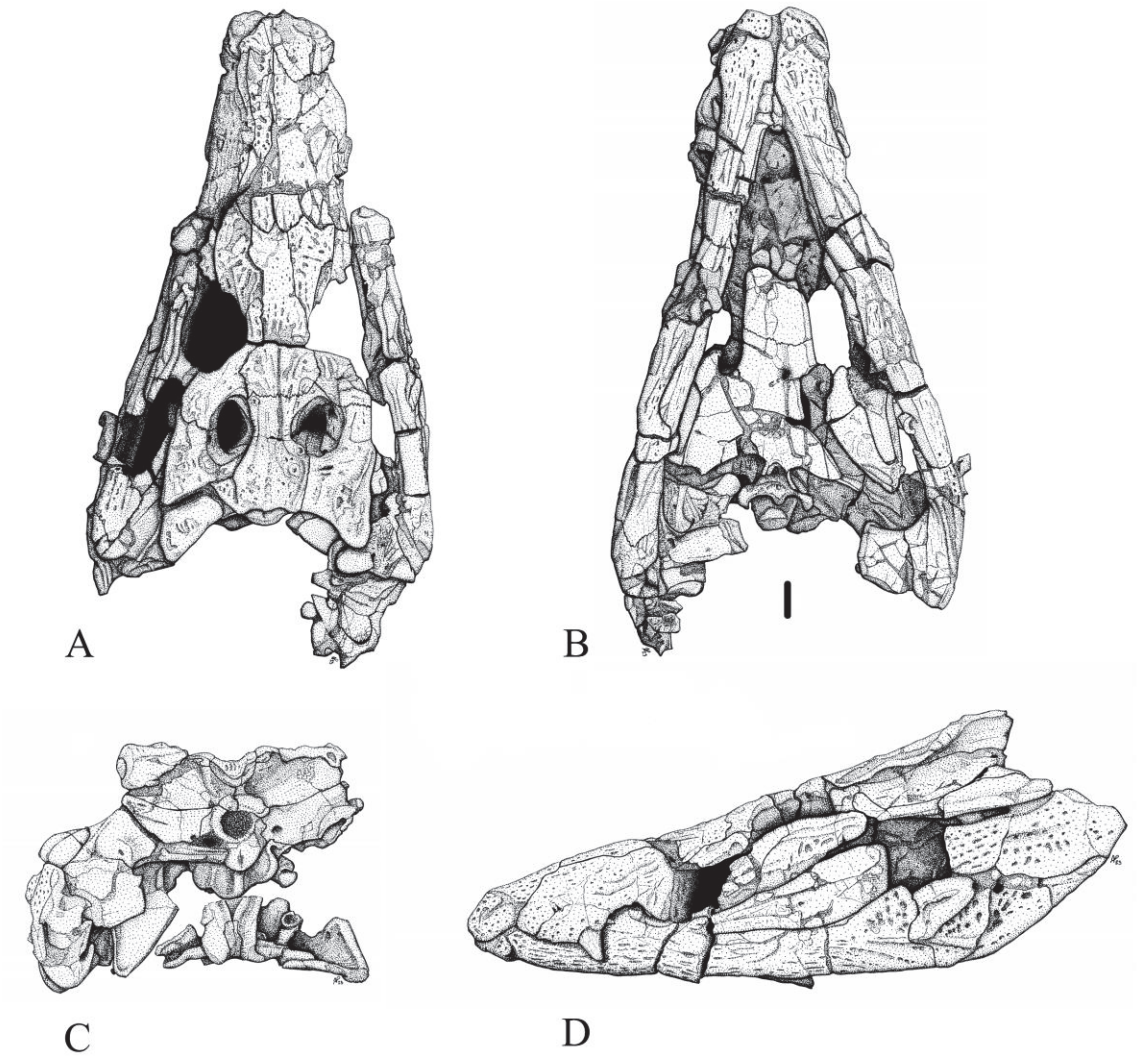

Supplementary Material S2: Drawings of the skull of *Varanosuchus sakonnakhonensis* (SM-2021-1-97/99) in dorsal (A), ventral (B), posterior (C) and lateral (D) views. Scale bar is 1 cm.

Supplementary Material S3: List of characters:

Character 1 (Turner, 2015: char. 1, modified from Clark, 1994: char. 1): External surface of dorsal cranial bones: smooth (0), slightly grooved (1), heavily ornamented with deep pits and grooves (2)

Character 2 (Turner, 2015: char. 2, modified from Clark, 1994: char. 2): Skull expansion at orbits: gradual (0), abrupt (1).

Character 3 (Turner, 2015: char. 3, modified from Clark, 1994: char. 3): Rostrum proportions: narrow oreinirostral (0), broad oreinirostral (1), nearly tubular (2), platyrostral (3).

Character 4 (Clark, 1994: char. 4): Premaxilla participation in internarial bar: forming at least ventral half (0), little participation (1).

Character 5 (Clark, 1994: char. 5): Premaxilla anterior to nares: narrow (0), broad (1).

Character 6 (Turner, 2015: char. 6, modified from Clark, 1994: char. 6): External nares facing anterolaterally or anteriorly (0); dorsally, not separated by premaxillary bar from anterior edge of rostrum (1); dorsally, separated by premaxillary bar (2)

Character 7 (Clark, 1994: char. 7): Palatal parts of premaxillae: do not meet posterior to incisive foramen (0), meet posteriorly along contact with maxillae (1).

Character 8 (Clark, 1994: char. 8): Premaxilla-maxilla contact: premaxilla loosely overlies maxilla (i.e., posterodorsal process of premaxilla overlaps anterodorsal surface of maxilla) (0) or sutured together along butt joint (1).

Character 9 (Turner, 2015: char. 9, modified from Clark, 1994: char. 9): Ventrally opened notch on ventral edge of rostrum at premaxilla-maxilla contact: absent (0), present as notch (1), present as large fenestra (2)

Character 10 (Pol *et al.*, 2009: char. 10, modified from Clark, 1994: char. 10): Posterior palatal branches of maxillae anterior to palatines: do not meet (0), meet extensively but posteriormost parts fail to meet (1), meet entirely (2)

Character 11 (Clark, 1994: char. 11): Nasal contacts lacrimal (0), does not contact lacrimal (1).

Character 12 (Clark, 1994: char. 12): Lacrimal contacts nasal along medial edge only (0), or along medial and anterior edges (1).

Character 13 (Clark, 1994: char. 13): Nasal contribution to narial border: present (0), absent (1).

Character 14 (Clark, 1994: char. 14): Nasal-premaxilla contact: present (0), absent (1).

Character 15 (Turner, 2015: char. 15, modified from Clark, 1994: char. 15): Descending process of prefrontal: does not contact palate (0), contacts palate (1).

Character 16 (Clark, 1994: char. 16): Postorbital-jugal contact: postorbital anterior to jugal (0), postorbital medial to jugal (1), or postorbital lateral to jugal (2).

Character 17 (Clark, 1994: char. 17): Anterior part of jugal with respect to posterior part: as broad (0), twice as broad (1).

Character 18 (Clark, 1994: char. 18): Jugal bar beneath infratemporal fenestra: dorsolaterally flattened (0), rod-shaped (1).

Character 19 (Clark, 1994: char. 19): Quadratojugal dorsal process: narrow, contacting only small part of postorbital (0); broad, extensively contacting postorbital (1).

Character 20 (Clark, 1994: char. 20): Frontal width between orbits: narrow, as broad as nasals (0); broad, twice as broad as nasals (1).

Character 21 (Clark, 1994: char. 21): Frontals in mature specimens: paired (0), unpaired (1).

Character 22 (Clark, 1994: char. 22): Dorsal surface of frontal and parietal: flat (0), with midline ridge (1).

Character 23 (Buckley & Brochu, 1999: char. 81, modified from Clark, 1994: char. 23): Parieto-postorbital suture: absent from dorsal surface of skull roof and supratemporal fossa (0), absent from dorsal surface of skull roof but broadly present within supratemporal fossa (1), present within supratemporal fossa and on dorsal surface of skull roof (2).

Character 24 (Clark, 1994: char. 24): Dorsal surface of supratemporal roof: complex (0); dorsally flat ‘skull table’ developed, with postorbital and squamosal bearing flat shelves extending laterally beyond quadrate contact (1).

Character 25 (Turner, 2015: char. 25, modified from Clark, 1994: char. 25): Postorbital bar: sculpted (if skull sculpted) (0), unsculpted (1).

Character 26 (Turner, 2015: char. 26, modified from Clark, 1994: char. 26): Postorbital bar: transversely flattened (0), cylindrical (1).

Character 27 (Clark, 1994: char. 27): Vascular opening on dorsal surface of postorbital bar: absent (0), present (1).

Character 28 (Turner, 2015: char. 28, modified from Clark, 1994: char. 28): Postorbital anterolateral process: absent or poorly developed (0); well developed, long, and acute (1).

Character 29 (Clark, 1994: char. 29): Dorsal part of postorbital: with anterior and lateral edges only (0), with anterolaterally facing edge (1).

Character 30 (Clark, 1994: char. 30): Dorsal end of postorbital bar broadens dorsally, continuous with dorsal part of postorbital (0); dorsal part of postorbital bar constricted, distinct from dorsal part of postorbital (1).

Character 31 (Clark, 1994: char. 31): Bar between orbit and supratemporal fossa in mature specimens: broad and solid, with broadly sculpted dorsal surface if sculpture present (0); bar narrow, sculpting restricted to anterior surface (1).

Character 32 (Turner, 2015: char. 32, modified from Clark, 1994: char. 32): Parietal: with broad occipital portion (0), without broad occipital portion (1).

Character 33 (Clark, 1994: char. 33): Parietal: with broad sculpted region separating supratemporal fossae (0), with sagittal crest between supratemporal fossae (1).

Character 34 (Clark, 1994: char. 34): Postparietal (dermosupraoccipital): a distinct element (0), not distinct (fused with parietal?) (1).

Character 35 (Clark, 1994: char. 35): Posterodorsal corner of squamosal: squared off, lacking extra ‘lobe’ (0); with unsculptured ‘lobe’ (1).

Character 36 (Turner, 2015: char. 36, modified from Clark, 1994: char. 36): Posterolateral process of squamosal: poorly developed and projecting horizontally at same level of skull (0); elongate, thin, and posteriorly directed, not ventrally deflected (1); elongate, posterolaterally directed, and ventrally deflected (2).

Character 37 (Clark, 1994: char. 37): Palatines: do not meet on palate below narial passage (0); form palatal shelves that do not meet (1); meet ventral to narial passage, forming part of secondary palate (2).

Character 38 (Clark, 1994: char. 38): Pterygoid: restricted to palate and suspensorium, joints with quadrate and basisphenoid overlapping (0); extends dorsally to contact laterosphenoid and form ventrolateral edge of trigeminal foramen, strongly sutured to quadrate and laterosphenoid (1).

Character 39 (Turner, 2015: char. 39, modified from Clark, 1994: char. 39): Choanal opening: continuous with pterygoid ventral surface except for anterior and anterolateral borders (0), opens into palate through deep midline depression (choanal groove) (1).

Character 40 (Clark, 1994: char. 40): Palatal surface of pterygoids: smooth (0), sculpted (1).

Character 41 (Clark, 1994: char. 41): Pterygoids posterior to choanae: separated (0), fused (1).

Character 42 (Ortega *et al.*, 2000: char. 139, modified from Clark, 1994: char. 38): Depression on primary pterygoidean palate posterior to choana: absent or moderate in size, being narrower than palatine bar (0), wider than palatine bar (1).

Character 43 (Clark, 1994: char. 43): Primary pterygoidean palate, role in forming choanal opening: does not enclose choana (0), completely encloses choana (1).

Character 44 (Pol *et al.*, 2009: char. 44, modified from Clark, 1994: char. 44): Anterior edge of choanae situated between suborbital fenestra (or anteriorly) (0), situated near the posterior edge of suborbital fenestra (1), situated near the posterior edge of pterygoid flange (2)

Character 45 (Clark, 1994: char. 45): Quadrate: without fenestrae (0), with single fenestra (1), with three or more fenestrae on dorsal and posteromedial surfaces (2)

Character 46 (Clark, 1994: char. 46): Posterior edge of quadrate: broad medial to tympanum, gently concave (0); or posterior edge narrow dorsal to otoccipital contact, strongly concave (1).

Character 47 (Clark, 1994: char. 47): Dorsal, primary head of quadrate articulates with: squamosal, otoccipital, and prootic (0); prootic and laterosphenoid (1).

Character 48 (Clark, 1994: char. 48): Ventrolateral contact of otoccipital with quadrate: very narrow (0), broad (1).

Character 49 (Clark, 1994: char. 49): Quadrate, squamosal, and otoccipital: do not meet to enclose cranioquadrate passage (0), enclose passage near lateral edge of skull (1), meet broadly lateral to passage (2).

Character 50 (Clark, 1994: char. 50): Pterygoid ramus of quadrate: with flat ventral edge (0), with deep groove along ventral edge (1).

Character 51 (Clark, 1994: char. 51): Ventromedial part of quadrate: does not contact

otoccipital (0), contacts otoccipital to enclose carotid artery and form passage for cranial nerves IX–XI (1).

Character 52 (Clark, 1994: char. 52): Eustachian tubes: not enclosed between basioccipital and basisphenoid (0); entirely enclosed (1).

Character 53 (Clark, 1994: char. 53): Basisphenoid rostrum (cultriform process): slender (0); dorsoventrally expanded (1).

Character 54 (Clark, 1994: char. 54): Basipterygoid process: prominent, forming movable joint with pterygoid (0); small or absent, with basisphenoid joint suturally closed (1).

Character 55 (Ortega *et al.*, 2000: char. 68, modified from Clark, 1994: char. 55): Basisphenoid ventral surface: shorter than basioccipital (0); wide and similar to, or longer, in length than basioccipital (1).

Character 56 (Clark, 1994: char. 56): Basisphenoid: exposed on ventral surface of braincase (0), virtually excluded from ventral surface by pterygoid and basioccipital (1).

Character 57 (Clark, 1994: char. 57): Basioccipital: without well-developed bilateral tuberosities (0), with large pendulous tubera (1).

Character 58 (Clark, 1994: char. 58): Otoccipital: without laterally concave descending flange ventral to subcapsular process (0); with flange (1).

Character 59 (Clark, 1994: char. 59): Cranial nerves IX–XI: all pass through common large foramen vagi in otoccipital (0); cranial nerve IX passes medial to nerves X and XI in separate passage (1).

Character 60 (Clark, 1994: char. 60): Otoccipital: without large ventrolateral part ventral to paroccipital process (0); with large ventrolateral part (1).

Character 61 (Clark, 1994: char. 61): Crista interfenestralis between fenestrae pseudorotunda and ovalis: nearly vertical (0); horizontal (1).

Character 62 (Clark, 1994: char. 62): Supraoccipital: forms dorsal edge of foramen magnum (0); exoccipitals broadly meet dorsal to foramen magnum, separating supraoccipital from foramen magnum (1).

Character 63 (Clark, 1994: char. 63): Mastoid antrum: does not extend into supraoccipital

(0); extends through transverse canal in supraoccipital to connect middle ear regions (1).

Character 64 (Clark, 1994: char. 64): Posterior surface of supraoccipital: nearly flat (0); with bilateral posterior prominences (1).

Character 65 (Turner, 2015: char. 65, modified from Clark, 1994: char. 65): Palpebrals: absent (0); one small palpebral present in orbit (1); one large palpebral (2); two large palpebrals (3)

Character 66 (Clark, 1994: char. 66): External nares: divided by septum (0); confluent (1).

Character 67 (Clark, 1994: char. 67): Antorbital fenestra: as large as orbit (0); about half the diameter of orbit (1); much smaller than the orbit (2); absent (3)

Character 68 (Ortega *et al.*, 2000: char. 41, modified from Clark, 1994: char. 68): Supratemporal fenestrae extension: relatively large, covering most of surface of skull roof (0); relatively short, fenestrae surrounded by flat and extended skull roof (1).

Character 69 (Turner, 2015: char. 69, modified from Clark, 1994: char. 69): Choanal groove: undivided (0); partially septated (1); completely septated (2)

Character 70 (Clark, 1994: char. 70): Dentary: extends posteriorly beneath mandibular fenestra (0); does not extend beneath fenestra (1).

Character 71 (Turner, 2015: char. 71, modified from Clark, 1994: char. 71): Retroarticular process: absent or extremely reduced (0); very short, broad, and robust (1); with extensive, rounded, wide, and flat (or slightly concave) surface projecting posteroventrally and facing dorsomedially (2); posteriorly elongate, triangular, and facing dorsally (3); posteroventrally projecting and paddle-shaped (4).

Character 72 (Clark, 1994: char. 72): Prearticular: present (0); absent (1).

Character 73 (Turner, 2015: char. 73, modified from Clark, 1994: char. 73): Articular: without medial process (0); with short process not contacting braincase (1); with process articulating with otoccipital and basisphenoid (2)

Character 74 (Clark, 1994: char. 74): Dorsal edge of surangular: flat (0); arched dorsally (1).

Character 75 (Clark, 1994: char. 75): Mandibular fenestra: present (0); absent (1).

Character 76 (Clark, 1994: char. 76): Insertion area for M. pterygoideous posterior: does not extend onto lateral surface of angular (0); extends onto lateral surface of angular (1).

Character 77 (Turner, 2015: char. 77, modified from Clark, 1994: char. 77): Splenial involvement in mandibular symphysis in ventral view: not involved (0); involved slightly in symphysis (1); extensively involved (2)

Character 78 (Turner & Sertich, 2010: char. 78, modified from Clark, 1994: char. 78): Posterior premaxillary teeth: similar in size to anterior teeth (0); longer but does not form an enlarged caniniform tooth (1); much longer forming one large premaxillary caniniform tooth (2); much longer forming two large premaxillary caniniform teeth (3)

Character 79 (Turner, 2015: char. 79, modified from Clark, 1994: char. 79): Maxillary tooth waves: absent, no tooth size variation (0); one wave of teeth enlarged (1); enlarged maxillary teeth occur in two waves (festooned) (2)

Character 80 (Clark, 1994: char. 80): Anterior dentary teeth opposite premaxilla-maxilla contact: no more than twice the length of other dentary teeth (0); more than twice the length (1).

Character 81 (Turner, 2015: char. 81, modified from Clark, 1994: char. 81): Dentary teeth posterior to tooth opposite premaxilla-maxilla contact: equal in size (0); enlarged dentary teeth opposite to smaller teeth in maxillary toothrow (1).

Character 82 (Ortega *et al.*, 2000: char. 120, modified from Clark, 1994: char. 82): Anterior and posterior scapular edges: symmetrical in lateral view (0); anterior edge more strongly concave than posterior edge (1); dorsally narrow with straight edges (2).

Character 83 (Ortega *et al.*, 2000: char. 121, modified from Clark, 1994: char. 83): Coracoid length: up to two-thirds of scapular length (0); subequal in length to scapula (1).

Character 84 (Clark, 1994: char. 84): Anterior process of ilium: similar in length to posterior process (0); one-quarter or less length of posterior process (1).

Character 85 (Clark, 1994: char. 85): Pubis: rod-like without expanded distal end (0); with expanded distal end (1).

Character 86 (Clark, 1994: char. 86): Pubis: forms anterior half of ventral edge of acetabulum (0); contacting ilium but partially excluded from acetabulum by anterior process of

ischium (1); completely excluded from acetabulum by anterior process of ischium (2)

Character 87 (Clark, 1994: char. 87): Distal end of femur: with large lateral facet for fibula (0); with very small facet (1).

Character 88 (Clark, 1994: char. 88): Fifth pedal digit: with phalanges (0); without phalanges (1).

Character 89 (Clark, 1994: char. 89): Atlas intercentrum: broader than long (0); as long as broad (1).

Character 90 (Turner, 2015: char. 90, modified from Clark, 1994: char. 90): Cervical neural spines: all anteroposteriorly large (0); only posterior ones rod-like (1); all spines rod-like (2)

Character 91 (Buscalioni & Sanz, 1988: char. 37 and Brochu, 1997: char. 7, modified from Clark, 1994: char. 91): Hypapophyses in cervicodorsal vertebrae: absent (0); present only in cervical vertebrae (1); present in cervical and first two dorsal vertebrae (2); present up to the third dorsal vertebra (3); present up to the fourth dorsal vertebrae (4)

Character 92 (Clark, 1994: char. 92): Cervical vertebrae: amphicoelous or amphyplatyan (0); procoelous (1).

Character 93 (Clark, 1994: char. 93): Trunk vertebrae: amphicoelous or amphyplatyan (0); procoelous (1).

Character 94 (Clark, 1994: char. 94): All caudal vertebrae: amphicoelous or amphyplatyan (0); first caudal vertebra biconvex with other procoelous (1); procoelous (2).

Character 95 (Turner, 2015: char. 95, modified from Clark, 1994: char. 95): Dorsal osteoderms, shape: rounded or ovate (0); rectangular, broader than long (1); square (2); rectangular, longer than broad (3).

Character 96 (Turner, 2015: char. 96, modified from Clark, 1994: char. 96 and Brochu, 1997: char. 40): Dorsal osteoderms: without articular anterior process (0); with a discrete convexity on anterior margin (1); with a well-developed process located anterolaterally in dorsal parasagittal osteoderms (2)

Character 97 (Ortega *et al.*, 2000: char. 107 & 108, modified from Clark, 1994: char. 97):

Rows of dorsal primary osteoderms (sensu Frey, 1988): two parallel rows (0); more than two rows (1); more than four rows (2)

Character 98 (Clark, 1994: char. 98): Osteoderms: some or all imbricated (0); sutured to one another (1).

Character 99 (Clark, 1994: char. 99): Tail osteoderms: dorsal only (0); surrounding tail (1).

Character 100 (Clark, 1994: char. 100): Trunk osteoderms: absent from ventral part of the trunk (0); present on ventral part (1).

Character 101 (Clark, 1994: char. 101): Osteoderms: with longitudinal keels on dorsal surfaces (0); without longitudinal keels (1).

Character 102 (Wu & Sues, 1996: char. 14): Jugal: participating in margin of antorbital fossa (0); separated from it (1).

Character 103 (Turner, 2015: char. 103, modified from Wu & Sues, 1996: char. 17): Mandibular symphysis in lateral view: shallow and tapering anteriorly (0); deep and tapering anteriorly (1); deep and anteriorly convex (2); shallow and anteriorly convex (3).

Character 104 (Turner, 2015: char. 104, modified from Wu & Sues, 1996: char. 23): Articular facet for quadrate condyle: equal in length to quadrate condyles (0); slightly longer (1); close to three times length of quadrate condyles (2)

Character 105 (Turner, 2015: char. 105, modified from Wu & Sues, 1996: char. 24 and Wu *et al.*, 1997: char. 124): Jaw joint: placed level with occipital condyle (0); below occipital condyle but above level of lower toothrow (1); below level of toothrow (2)

Character 106 (Turner, 2015: char. 106, modified from Wu & Sues, 1996: char. 27 and Ortega *et al.*, 2000: char. 133): Premaxillary tooth number: six (0); five (1); four (2); three (3); two (4)

Character 107 (Turner, 2015: char. 107, modified from Wu & Sues, 1996: char. 29): Unsculptured region along alveolar margin on lateral surface of maxilla: absent (0); present (1).

Character 108 (Wu & Sues, 1996: char. 30): Maxillary tooth number: eight or more (0); seven (1); six (2); five (3); four (4)

Character 109 (Wu & Sues, 1996: char. 33): Coracoid, posteromedial or ventromedial

process absent (0); elongate posteromedial process present (1); distally expanded ventromedial process present (2).

Character 110 (Wu & Sues, 1996: char. 40): Radiale and ulnare, size: short and massive (0); elongate (1).

Character 111 (Turner, 2015: char. 111, modified from Gomani, 1997: char. 4): Prefrontals anterior to orbits: elongate, oriented parallel to anteroposterior axis of skull (0); short and broad, oriented posteromedially-anterolaterally (1).

Character 112 (Turner, 2015: char. 112, modified from Gomani, 1997: char. 32): Basioccipital and ventral part of otoccipital, orientation: facing posteriorly (0); posteroventrally (1).

Character 113 (Buscalioni & Sanz, 1988: char. 35): Vertebral centra, shape: cylindrical (0); spool-shaped (1).

Character 114 (Turner, 2015: char. 114, modified from Buscalioni & Sanz, 1988: char. 39): Transverse process of posterior dorsal vertebrae, shape: dorsoventrally low and laminar (0); dorsoventrally high (1).

Character 115 (Buscalioni & Sanz, 1988: char. 44): Number of sacral vertebrae: two (0); more than two (1).

Character 116 (Buscalioni & Sanz, 1988: char. 49): Supraacetabular crest: present (0); absent (1).

Character 117 (Buscalioni & Sanz, 1988: char. 54): Proximal end of radiale, shape: expanded symmetrically, similarly to distal end (0); more expanded proximolaterally than proximomedially (1).

Character 118 (Ortega *et al.*, 1996: char. 5): Lateral surface of anterior region of surangular and posterior region of dentary: without longitudinal depression (0); with longitudinal depression (1).

Character 119 (Ortega *et al.*, 1996: char. 9): Ventral exposure of splenials: absent (0); present (1).

Character 120 (Turner, 2015: char. 120, modified from de Andrade & Bertini, 2008: char.

120; Ortega *et al.*, 1996: char. 11 and Ortega *et al.*, 2000: char. 100): Tooth margin carinae: without carinae or with smooth or crenulated carinae (0); with homogeneous denticulate carinae (denticles are small and symmetrical in form as in ziphodont teeth) (1); with heterogeneous carinae possessing rounded tubercle-like denticles, developed preferentially along posterior margin (2).

Character 121 (Turner, 2015: char. 121, modified from Pol, 1999a: char. 133 and Ortega *et al.*, 2000: char. 145): Lateral surface of anterior process of jugal: flat or convex (0); with broad shelf below the orbit with triangular depression underneath it (1).

Character 122 (Pol, 1999a: char. 134): Jugal, extension below the orbit: does not exceed the anterior margin of orbit (0); exceeds margin of orbit (1).

Character 123 (Pol, 1999a: char. 135): Notch in premaxilla on lateral edge of external nares: absent (0); present on the dorsal half of the external nares lateral margin (1).

Character 124 (Pol, 1999a: char. 136): Dorsal border of external nares: formed mostly by the nasals (0); formed by both the nasals and premaxilla (1).

Character 125 (Pol, 1999a: char. 138): Posterodorsal process of premaxilla: absent (0); present extending posteriorly and wedging between maxilla and nasal (1).

Character 126 (Pol, 1999a: char. 139 and Ortega *et al.*, 2000: char. 9): Premaxilla-maxilla suture in palatal view, medial to alveolar region, orientation of suture: anteromedially directed (0); sinusoidal, posteromedially directed on its lateral half and anteromedially directed along its medial region (1); posteromedially directed (2); straight (3); posteromedially curved (U-shaped) (4).

Character 127 (Pol, 1999a: char. 140): Nasal lateral border posterior to external nares: laterally concave (0); straight (1).

Character 128 (Pol, 1999a: char. 141): Nasal lateral edges: nearly parallel (0); oblique to each other, converging anteriorly (1); oblique to each other, diverging anteriorly (2).

Character 129 (Pol, 1999a: char. 143): Palatine anteromedial margin: exceeding anterior margin of suborbital fenestrae: extending anteriorly between maxillae (0); not exceeding anterior margin of suborbital fenestrae (1).

Character 130 (Pol, 1999a: char. 144): Dorsoventral height of jugal antorbital region with

respect to infraorbital region equal or lower (0); antorbital region more expanded than infraorbital region (1).

Character 131 (Pol, 1999a: char. 145): Maxilla-lacrimal contact in antorbital fossa: partially included (0); completely included (1).

Character 132 (Pol, 1999a: char. 146): Lateral eustachian tube openings, location: located posteriorly to medial opening (0); aligned anteroposteriorly and dorsoventrally (1).

Character 133 (Pol, 1999a: char. 147): Anterior process of ectopterygoid: developed (0); reduced or absent (1).

Character 134 (Pol, 1999a: char. 148): Posterior process of ectopterygoid: developed (0); reduced or absent (1).

Character 135 (Pol, 1999a: char. 149 and Ortega *et al.*, 2000: char. 13): Small foramen located in the lateral surface of premaxilla-maxilla suture in lateral surface (not for big mandibular teeth): absent (0); present (1).

Character 136 (Pol, 1999a: char. 150): Jugal posterior process, extent of process: exceeding posteriorly the infratemporal fenestrae (0); does not exceed infratemporal fenestrae (1).

Character 137 (Pol, 1999a: char. 151): Compressed crown of maxillary teeth, orientation: oriented parallel to the longitudinal axis of skull (0); obliquely disposed (1).

Character 138 (Pol, 1999a: char. 152): Large and aligned neurovascular foramina on lateral maxillary surface: absent (0); present (1).

Character 139 (Turner, 2015: char. 139, modified from Pol, 1999a: char. 153): External surface of maxilla and premaxilla, general shape: with single plane facing laterally (0); with ventral region facing laterally and dorsal region facing dorsolaterally (1).

Character 140 (Turner, 2015: char. 140, modified from Pol, 1999a: char. 154; Ortega *et al.*, 2000: char. 104 and de Andrade & Bertini, 2008: char. 135): Maxillary teeth, lateral compression: absent (0); present, compression asymmetrically occurring only along distal margin giving teeth a teardrop shape (1); present, lateral compression symmetrically developed (2).

Character 141 (Pol, 1999a: char. 155): Posteroventral corner of quadratojugal: reaching

quadrate condyles (0); does not reach quadrate condyles (1).

Character 142 (Turner, 2015: char. 142, modified from Pol, 1999a: char. 156): Base of postorbital process of jugal, orientation: directed posterodorsally (0); directed dorsally (1); directed anterodorsally (2)

Character 143 (Pol, 1999a: char. 157): Postorbital process of jugal, location on jugal: anteriorly placed (0); in middle (1); posteriorly positioned (2)

Character 144 (Pol, 1999a: char. 158 and Ortega *et al.*, 2000: char. 36): Postorbital-ectopterygoid contact: present (0); absent (1).

Character 145 (Pol, 1999a: char. 161): Quadratojugal, ornamentation: absent (0); ornamented at the base (1).

Character 146 (Pol, 1999a: char. 162): Prefrontal-maxilla contact in the inner anteromedial region of orbit absent (0); present (1).

Character 147 (Pol, 1999a: char. 163): Basisphenoid, exposure on braincase: without lateral exposure (0); with lateral exposure (1).

Character 148 (Pol, 1999a: char. 165): Quadrate process of pterygoids: well developed (0); poorly developed (1).

Character 149 (Turner, 2015: char. 149, modified from Pol, 1999a: char. 166 and Ortega *et al.*, 2000: char. 44): Quadrate major axis, direction of orientation: posteroventrally (0); ventrally (1); anteroventrally (2)

Character 150 (Pol, 1999a: char. 167): Quadrate distal end: with only one plane facing posteriorly (0); with two distinct faces in posterior view, a posterior one and a medial one bearing foramen aërum (1).

Character 151 (Pol, 1999a: char. 168): Anteroposterior development of neural spine in axis: well developed, covering all of neural arch length (0); poorly developed, located over posterior half of neural arch (1).

Character 152 (Pol, 1999a: char. 169): Prezygapophyses of axis, development relative to neural arch: not exceeding edge of neural arch (0); exceeding the anterior margin of neural arch (1).

Character 153 (Pol, 1999a: char. 170): Postzygapophyses of axis: well developed, curved laterally (0); poorly developed (1).

Character 154 (Turner, 2015: char. 154, modified from Pol, 1999b: char. 212): Shape of dentary symphysis in ventral view: tapering anteriorly forming an angle (0); U-shaped, smoothly curving anteriorly (1); lateral edges longitudinally oriented, convex anterolateral corner and extensive transversally oriented anterior edge (2)

Character 155 (Pol, 1999b: char. 213): Unsculpted region in the dentary below the toothrow absent (0); present (1).

Character 156 (Buckley & Brochu, 1999: char. 102): Surangular, contribution to the glenoid fossa: forms only the lateral wall of glenoid (0); forms approximately one-third of the glenoid (1).

Character 157 (Turner, 2015: char. 157, modified from Buckley & Brochu, 1999: char. 102): Femur, anterior margin: linear (0); bears flange for PIFI 1 musculature (1).

Character 158 (Turner, 2015: char. 158, modified from Buckley & Brochu, 1999: char. 105): Dentary, lateral surface: smooth lateral to seventh alveolus (0); with lateral concavity for the reception of the enlarged maxillary tooth (1).

Character 159 (Turner, 2015: char. 159, modified from Ortega *et al.*, 1996: char. 1 and Buckley & Brochu, 1999: char. 107): Dorsal edge of dentary: slightly concave or straight and subparallel to the longitudinal axis of skull (0); straight with an abrupt dorsal expansion, being straight posteriorly (1); with a single dorsal expansion and concave posterior to this (2); sinusoidal, with two concave waves (3)

Character 160 (Turner, 2015: char. 160, modified from Ortega *et al.*, 1996: char. 2 and Buckley & Brochu, 1999: char. 108): Dentary compression and ventrolateral surface anterior to mandibular fenestra: compressed and vertical (0); not compressed and convex (1).

Character 161 (Ortega *et al.*, 1996: char. 7 and Buckley & Brochu, 1999: char. 110): Splenial posterior to symphysis: thin (0); robust dorsally (1).

Character 162 (Ortega *et al.*, 1996: char. 13 and Buckley *et al.*, 2000: char. 117): Cheek teeth: not constricted at base of crown (0); constricted (1).

Character 163 (Ortega *et al.*, 2000: char. 10): Ventral edge of premaxilla, location relative to

maxilla: at the same height as the ventral edge of maxilla (0); located deeper, with the dorsal contour of anterior part of dentary strongly concave (1).

Character 164 (Turner, 2015: char. 164, modified from Ortega *et al.*, 2000: char. 19): Maxillary dental implantation: teeth in isolated alveoli (0); located in dental groove (1).

Character 165 (Ortega *et al.*, 2000: char. 24): Caudal tip of nasals: converge at sagittal plane (0); separated by anterior sagittal projection of frontals (1).

Character 166 (Ortega *et al.*, 2000: char. 33): Relative length between squamosal and postorbital: squamosal is longer (0); postorbital longer (1).

Character 167 (Turner, 2015: char. 167, modified from Ortega *et al.*, 2000: char. 34): Jugal portion of postorbital bar, relative to lateral surface of jugal: flush with lateral surface (0); anteriorly continuous but posteriorly inset (1); medially displaced and a ridge separate postorbital bar from lateral surface of jugal (2)

Character 168 (Ortega *et al.*, 2000: char. 42): Outer surface of squamosal laterodorsally oriented: extensive (0); reduced and sculpted (1); reduced and unsculpted (2).

Character 169 (Ortega *et al.*, 2000: char. 47): Quadratojugal spine at posterior margin of infratemporal fenestra: absent (0); present (1).

Character 170 (Turner, 2015: char. 170, modified from Ortega *et al.*, 2000: char. 53): Quadrate condyles: poorly developed intercondylar groove (0); medial condyle expands ventrally, being separated from lateral condyle by a deep intercondylar groove (1).

Character 171 (Ortega *et al.*, 2000: char. 62): Exposure of supraoccipital in skull roof: absent (0); present (1).

Character 172 (Ortega *et al.*, 2000: char. 70): Nasal participation in antorbital fenestra: present (0); absent (1).

Character 173 (Ortega *et al.*, 2000: char. 75): Anterior opening of temporo-orbital canal in dorsal view: exposed (0); hidden and overlapped by squamosal rim of supratemporal fossa (1).

Character 174 (Ortega *et al.*, 2000: char. 90): Foramen *intramandibularis oralis*: small or absent (0); big and slotlike (1).

Character 175 (Turner, 2015: char. 175, modified from Ortega *et al.*, 2000: char. 98):

Coronoid size: short and located below the dorsal edge of the mandibular ramus (0); anteriorly extended with posterior region elevated at dorsal margin of mandibular ramus (1).

Character 176 (Ortega *et al.*, 2000: char. 101): Width of root of teeth with respect to crown: narrower or equal (0); wider (1).

Character 177 (Ortega *et al.*, 2000: char. 109): Gap in cervico-thoracic dorsal armor: absent (0); present (1).

Character 178 (Ortega *et al.*, 2000: char. 130): Lateral contour of snout in dorsal view: straight (0); sinusoidal (1).

Character 179 (Ortega *et al.*, 2000: char. 138): Pterygoidean flanges: laminar and expanded (0); bar-like and elongate (1); bar-like and poorly developed (2).

Character 180 (Ortega *et al.*, 2000: char. 146): Ectopterygoid medial process, shape: single (0); forked (1).

Character 181 (Turner, 2015: char. 181, modified from Ortega *et al.*, 2000: char. 157): Skull roof, shape in dorsal view: rectangular (0); trapezoidal (1).

Character 182 (Ortega *et al.*, 2000: char. 30): Prefrontal pillars when integrated in palate: pillars transversely expanded (0); transversely expanded in their dorsal part and columnar ventrally (1); longitudinally expanded in their dorsal part and columnar ventrally (2).

Character 183 (Ortega *et al.*, 2000: char. 21): Ventral edge of maxilla in lateral view: straight or convex (0); sinusoidal (1).

Character 184 (Turner, 2015: char. 184, modified from Ortega *et al.*, 2000: char. 156): Position of first enlarged maxillary teeth: second or third alveolus (0); fourth or fifth (1).

Character 185 (Pol & Apesteguía, 2005: char. 180): Splenial-dentary suture at symphysis on ventral surface: v-shaped (0); transversal (1).

Character 186 (Pol & Apesteguía, 2005: char. 181): Posterior peg at symphysis: absent (0); present (1).

Character 187 (Pol & Apesteguía, 2005: char. 182): Posterior ridge on glenoid fossa of articular: present (0); absent (1).

Character 188 (Turner, 2015: char. 188, modified from Pol *et al.*, 2009: char. 188; Gomani, 1997: char. 46; Buckley *et al.*, 2000: char. 113 & de Andrade & Bertini, 2008: char. 149): Cusps of teeth, number and conformation: one unique cusp (0); one main cusp with smaller cusps arranged in one row (1); one main cusp with smaller cusps arranged in more than one row (2); several cusps of equal size arranged in more than one row (3)

Character 189 (Pol & Apesteguía, 2005: char. 184): Dorsal surface of mandibular symphysis: flat or slightly concave (0); strongly concave and narrow, trough-shaped (1).

Character 190 (Pol & Apesteguía, 2005: char. 185): Medial surface of splenials posterior to symphysis: flat or slightly convex (0); markedly concave (1).

Character 191 (Pol & Apesteguía, 2005: char. 186): Choanal septum shape: narrow vertical bony sheet (0); T-shaped bar expanded ventrally (1); massive and blocky (2).

Character 192 (Pol & Norell, 2004a: char. 164): Cross-section of distal end of quadrate: mediolaterally wide and anteroposteriorly thin (0); subquadrangular (1).

Character 193 (Pol & Apesteguía, 2005: char. 188): Lateral surface of dentaries below alveolar margin, at mid to posterior region of toothrow: vertically oriented, continuous with rest of lateral surface of dentaries (0); flat surface exposed dorsolaterally, divided by ridge from rest of lateral surface of dentaries (1).

Character 194 (Pol & Norell, 2004a: char. 165): Palatine-pterygoid contact on palate: palatines overlie pterygoids (0); palatines firmly sutured to pterygoids (1).

Character 195 (Pol *et al.*, 2004: char. 164): Ectopterygoid main axis orientation: laterally or slightly anterolaterally (0); anteriorly, subparallel to the skull longitudinal axis (1).

Character 196 (Wu *et al.*, 1997: char. 103): Squamosal descending process: absent (0); present (1).

Character 197 (Turner, 2015: char. 197, modified from Wu *et al.*, 1997: char. 105): Development of distal quadrate body ventral to otoccipital-quadrate contact: distinct (0); incipiently distinct (1); indistinct (2)

Character 198 (Wu *et al.*, 1997: char. 106): Pterygoid flanges: thin and laminar (0); dorsoventrally thick, with pneumatic spaces (1).

Character 199 (Wu *et al.*, 1997: char. 108): Postorbital participation in infratemporal fenestra: almost or entirely excluded (0); bordering infratemporal fenestra (1).

Character 200 (Wu *et al.*, 1997: char. 109): Palatines, contribution to suborbital fenestra: form margin of suborbital fenestra (0); excluded from margin of suborbital fenestra (1).

Character 201 (Wu *et al.*, 1997: char. 110): Angular posterior to mandibular fenestra, location on mandible: widely exposed on lateral surface of mandible (0); shifted to ventral surface of mandible (1).

Character 202 (Wu *et al.*, 1997: char. 112): Posteroventral edge of mandibular ramus, shape: straight or convex (0); markedly deflected (1).

Character 203 (Pol *et al.*, 2009: char. 203, modified from Wu *et al.*, 1997: char. 128): Quadrate ramus of pterygoid, width in ventral view: narrow (0); broad (1).

Character 204 (Wu *et al.*, 1997: char. 121): Pterygoids, contact on palate: not in contact anterior to basisphenoid on palate (0); pterygoids in contact (1).

Character 205 (Turner, 2015: char. 205, modified from Wu *et al.*, 1997: char. 122): Olecranon: well developed (0); absent (1).

Character 206 (Wu *et al.*, 1997: char. 123): Cranial table width with respect to ventral portion of skull: as wide as ventral portion (0); narrower than the ventral portion of the skull (1).

Character 207 (Wu *et al.*, 1997: char. 127): Depression on posterolateral surface of maxilla: absent (0); present (1).

Character 208 (Pol *et al.*, 2009: char. 208, modified from Wu *et al.*, 1997: char. 128): Paired anterior palatal fenestrae: absent (0); present (1).

Character 209 (Pol & Norell, 2004a: char. 179): Paired ridges located medially on ventral surface of basisphenoid: absent (0); present (1).

Character 210 (Pol *et al.*, 2004: char. 179): Ventral margin of infratemporal bar of jugal: straight (0); dorsally arched (1).

Character 211 (Pol & Norell, 2004a: char. 180): Posterolateral end of quadratojugal, shape and relationship with quadrate: acute or rounded, tightly overlapping the quadrate (0); with sinusoidal ventral edge and wide and rounded posterior edge slightly overhanging the lateral

surface of the quadrate (1).

Character 212 (Pol & Norell, 2004a: char. 181): Quadrate body distal to otoccipital-quadrate, orientation of contact in posterior view: ventrally oriented (0); ventrolaterally oriented (1).

Character 213 (Gasparini *et al.*, 1993: char. 3): Wedge-like process of maxilla in lateral surface of premaxilla-maxilla suture: absent (0); present (1).

Character 214 (Pol & Norell, 2004b: char. 181): Palpebrals: separated from (or weakly sutured to) lateral edge of frontals (0); extensively sutured to each other and to lateral margin of frontals (1).

Character 215 (Pol & Norell, 2004b: char. 182): External surface of ascending process of jugal: exposed laterally (0); exposed posterolaterally (1).

Character 216 (Turner & Sertich, 2010: char. 216, modified from Pol & Norell, 2004b: char. 183): Longitudinal ridge on lateral surface of jugal below infratemporal fenestra: absent (0); present, running entire length of posterior process of jugal (1); present, running entire length of jugal (2)

Character 217 (Pol & Norell, 2004b: char. 184): Dorsal surface of posterolateral region of squamosal: without ridges (0); with three curved ridges oriented longitudinally (1).

Character 218 (Pol & Norell, 2004b: char. 185): Ridge along dorsal section of quadrate-quadratojugal contact: absent (0); present (1).

Character 219 (Pol *et al.*, 2009: char. 219, modified from Pol & Norell, 2004b: char. 186): Sharp ridge on the surface of the angular: absent (0); present on the ventral-most margin (1); present along the lateral surface (2).

Character 220 (Pol & Norell, 2004b: char. 187): Longitudinal ridge along the dorsolateral surface of surangular: absent (0); present (1).

Character 221 (Pol & Norell, 2004b: char. 188): Dorsal surface of osteoderms ornamented with anterolaterally and anteromedially directed ridges (fleur de lys pattern of Osmólska *et al.*, 1997): absent (0); or present (1).

Character 222 (Pol & Norell, 2004b: char. 189): Cervical region surrounded by lateral and ventral osteoderms sutured to dorsal elements: absent (0); present (1).

Character 223 (Pol & Norell, 2004b: char. 190): Appendicular osteoderms: absent (0); present (1).

Character 224 (Ortega *et al.*, 2000: char. 72): Supratemporal fenestra: present (0); absent (1).

Character 225 (Pol *et al.*, 2009: char. 225, modified from Pol & Apesteguía, 2005: char. 221): Flat ventral surface of internal nares septum: parallel sided (0); tapering anteriorly (1); expanding anteriorly (2).

Character 226 (Turner, 2015: char. 226, modified from Pol & Apesteguía, 2005: char. 221): Perinarial fossa: restricted extension (0); extensive, with distinctly concave surface facing anteriorly (1); large concave surface facing anteriorly, projecting anteroventrally from external nares and opening toward alveolar margin (2); extremely large and well-developed, occupying nearly entire surface of premaxilla ventral to external naris (3)

Character 227 (Turner, 2015: char. 227, modified from Sereno *et al.*, 2001: char. 67): Premaxillary palate, circular paramedian depressions: absent (0); present, located anteriorly on premaxilla (1); present, located at premaxilla-maxilla suture (2).

Character 228 (Pol & Apesteguía, 2005: char. 223): Nasals, shape of posterolateral region: flat surface facing dorsally (0); lateral region deflected ventrally, forming part of the lateral surface of snout (1).

Character 229 (Zaher *et al.*, 2006: char. 193): Lacrimal, posterior extent and relationship with jugal: lacrimal: extending posteroventrally, widely contacting the jugal (0); tapers ventroposteriorly, does not contact or contacts jugal only slightly (1).

Character 230 (Zaher *et al.*, 2006: char. 194): Jugal, large foramen on the lateral surface, near its anterior margin: absent (0); present (1).

Character 231 (Turner, 2015: char. 231, modified from Zaher *et al.*, 2006: char. 195): Procumbent premaxillary alveoli: absent (0); present (1).

Character 232 (Zaher *et al.*, 2006: char. 196 & Turner, 2004: char. 119, modified from Martinelli, 2003: char. 36): Palatines, orientation: run parasagittally along midline (0); diverge laterally becoming rod-like caudally forming palatine bars (1).

Character 233 (Zaher *et al.*, 2006: char. 197): Ectopterygoid, participation in the palatine bar: absent (0); present (1).

Character 234 (Pol & Norell, 2004a: char. 183): Choanal opening: opened posteriorly and continuous with pterygoid surface (0); closed posteriorly by an elevated wall formed by the pterygoids (1).

Character 235 (Zaher *et al.*, 2006: char. 198): Ectopterygoid, extent of medial projection on the ventral surface of pterygoid flanges: barely extended (0); widely extended, covering approximately the lateral half of the ventral surface of the pterygoid flanges (1).

Character 236 (Gasparini *et al.*, 2006: char. 236): Evaginated maxillary alveolar edges: absent (0), present as continuous sheet (1); present as discrete evaginations at each alveolus (2).

Character 237 (Gasparini *et al.*, 2006: char. 237): Premaxilla, foramen in perinarial depression: absent (0); present (1).

Character 238 (Sereno *et al.*, 2001: char. 27): Frontal, anterior ramus with respect to anterior tip of the prefrontal: ending posteriorly (0); ending anteriorly (1).

Character 239 (Turner, 2015: char. 239, modified from Sereno *et al.*, 2001: char. 68): Premaxilla, anterior alveolar margin orientation: vertical (0); inturned (1).

Character 240 (Turner, 2015: char. 240, modified from Sereno *et al.*, 2001: char. 69): Premaxillary toothrow orientation: arched posteriorly from midline (0); angled posterolaterally, at 120◦ angle (1); transverse (2)

Character 241 (Sereno *et al.*, 2001: char. 70): Last premaxillary tooth position relative to toothrow: anterior (0); anterolateral (1).

Character 242 (Gasparini *et al.*, 2006: char. 242): Posterior teeth with rings of undulated enamel: absent (0); present (1).

Character 243 (Gasparini *et al.*, 2006: char. 243, modified from Brochu, 1999: char. 108): Maxilla-palatine suture, shape of palatines: palatine anteriorly rounded (0); palatine anteriorly pointed (1); palatine invaginated (2).

Character 244 (Gasparini *et al.*, 2006: char. 244): Postorbital bar, lateral surface formed by: postorbital and jugal (0); only by postorbital (1).

Character 245 (Gasparini *et al.*, 2006: char. 245): Surangular groove, enlarged foramen at anterior end: absent (0); present (1).

Character 246 (Gasparini *et al.*, 2006: char. 246): Shape of antorbital fossa: subcircular or subtriangular (0); elongate, low, and oriented obliquely (1).

Character 247 (Gasparini *et al.*, 2006: char. 247): Prefrontal lateral development: reduced (0); enlarged, extending laterally over the orbit (1).

Character 248 (Gasparini *et al.*, 2006: char. 248): Foramen for the internal carotid artery: reduced, similar in size to openings for cranial nerves IX–XI (0); extremely enlarged (1).

Character 249 (Gasparini *et al.*, 2006: char. 249): Squamosal posterolateral region, lateral to paroccipital process: narrow (0); bearing subrounded flat surface (1).

Character 250 (Gasparini *et al.*, 2006: char. 250): Posteromedial branch of squamosal, orientation: transversely oriented (0); posterolaterally oriented (1).

Character 251 (Gasparini *et al.*, 2006: char. 251): Squamosal, dorsal margin of occipital flange: straight (0); dorsally concave (1).

Character 252 (Gasparini *et al.*, 2006: char. 252): Sculpture in external surface of rostrum: absent (0); present (1).

Character 253 (Gasparini *et al.*, 2006: char. 253): Longitudinal depressions on palatal surface of maxillae and palatines: absent (0); present (1).

Character 254 (Gasparini *et al.*, 2006: char. 254): Angle between medial and anterior margins of supratemporal fossa: approximately 90 degrees (0); approximately 45 degrees (1).

Character 255 (Gasparini *et al.*, 2006: char. 255): Sacral vertebrate, direction of transverse process: laterally (0); markedly deflected ventrally (1).

Character 256 (Gasparini *et al.*, 2006: char. 256): Prefrontal and lacrimal around orbits: forming flat rims (0); evaginated, forming elevated rims (1).

Character 257 (Gasparini *et al.*, 2006: char. 257): Nasal bones: paired (0); partially or completely fused (1).

Character 258 (Brochu, 1997: char. 3): Axial neural spines, width of posterior half: wide (0); narrow (1).

Character 259 (Brochu, 1997: char. 19): Axis hypapophysis, deep fork: present (0); absent

(1).

Character 260 (Brochu, 1997: char. 27): Ulna, width of olecranon process: narrow and subangular (0); wide and rounded (1).

Character 261 (Brochu, 1997: char. 29): M. teres major and M. dorsalis scapulae: insert separately on humerus, scars can be distinguished dorsal to deltopectoral crest (0); insert with common tendon, single insertion scar (1).

Character 262 (Turner, 2015: char. 262, modified from Brochu, 1997: char. 53): Dentary, projection of anterior alveoli: project anterodorsally (0); weakly procumbent (1); strongly procumbent (2)

Character 263 (Brochu, 1997: char. 84): Squamosal, dorsal and ventral rims of squamosal groove for external ear valve musculature: parallel (0); squamosal groove flares anteriorly (1).

Character 264 (Brochu, 1997: char. 91): Ectopterygoid, contact with maxilla near toothrow: ectopterygoid abuts maxillary toothrow (0); maxilla broadly separates ectopterygoid from maxillary toothrow (1).

Character 265 (Brochu, 1997: char. 92): Shallow fossa at anteromedial corner of supratemporal fenestra: present (0); absent, anteromedial corner of supratemporal fenestra smooth (1).

Character 266 (Pol *et al.*, 2009 : char. 266, modified from Brochu, 1997: char. 103): Lateral margins of frontal, relative to the skull surface: flush with skull surface (0); elevated, forming ridged orbital margins (1).

Character 267 (Brochu, 1997: char. 130): Laterosphenoid, orientation of capitate process: laterally oriented (0); anteroposteriorly oriented toward midline (1).

Character 268 (Pol *et al.*, 2009 : char. 268, modified from Brochu, 1997: char. 141): Exoccipital, development of boss and paroccipital process: process lateral to cranioquadrate opening short (0); boss small or absent on paroccipital process, process lateral to cranioquadrate opening long (1).

Character 269 (Brochu, 1997: char. 149, modified from Norell, 1988: char. 32): Ectopterygoid, extent along lateral pterygoid flange, at maturity: extends to posterior tip of lateral pterygoid flange (0); does not extend to posterior tip of lateral pterygoid (1).

Character 270 (Turner, 2015: char. 270, modified from Brochu, 1997: char. 153): Incisive foramen, location relative to premaxillary toothrow: foramen situated far from premaxillary toothrow, at the level of the second or third alveolus (0); abuts premaxillary toothrow (1); projects between first premaxillary teeth (2).

Character 271 (Pritchard *et al.*, 2013: char. 271, modified from Turner, 2006: char. 126): Ventral surface of choanal septum: smooth to slightly depressed (0); marked by an acute groove (1); vomeral septum divided into bilateral laminae (2).

Character 272 (Pol *et al.*, 2009: char. 272, modified from Turner, 2006: char. 128): Proximal-most portion of fibular head: straight sided to weakly developed posteriorly (0); very sharply projecting posteriorly, forming distinct extension (1).

Character 273 (Turner, 2015: char. 273, modified from Turner, 2006: char. 129): Cervical rib shaft, posterior process, posterodorsally projecting spine at the junction with tubercular process: absent (0); present (1).

Character 274 (Turner, 2015: char. 274, modified from Pol *et al.*, 2009: char. 274): Longitudinal keels on dorsal surfaces of osteoderms: restricted to the posterior edge of osteoderm (0); not restricted to the posterior edge (1).

Character 275 (Pol *et al.*, 2009: char. 275): Jugal, anteriorly on lateral surface below orbits: lacks a depression (0); possesses a depression (1).

Character 276 (Schwarz *et al.*, 2017: char. 276, modified from Pol *et al.*, 2009: char. 276): Transverse ridge crossing the frontal anteromedial to the orbits: absent (0); present as a ridge (1); present as prominent anteriorly curved shelf (transverse interorbital crest sensu Andrade and Hornung 2011) (2)

Character 277 (Pol *et al.*, 2009: char. 277): Shallow hemispherical depression on the lacrimal and/or prefrontal anterior to orbital margin (not articulation facet for palpebral): absent (0); present (1).

Character 278 (Pol *et al.*, 2009: char. 278): Anterior half of interfenestral bar between suborbital fenestrae: lateral margins are parallel to subparallel (0); flared anteriorly (1).

Character 279 (Pol *et al.*, 2009: char. 279): Posterior half of interfenestral bar between suborbital fenestrae: lateral margins are parallel to subparallel (0); flared posteriorly (1).

Character 280 (Pol *et al.*, 2009: char. 280): Angular, shape of posteroventral margin: straight or gently arched dorsally (0); strongly arched dorsally (1).

Character 281 (Pol *et al.*, 2009: char. 281): Squamosal, lateral margin of dorsal surface: squared off with continuous ear valve groove (0); bears a prominent depressed area just anterior to posterior lobe of squamosal, groove for ear valve discontinuous (1).

Character 282 (Pol *et al.*, 2009: char. 282): Fibula, shaft distal to iliofibularis trochanter: straight (0); bowed posteriorly (1).

Character 283 (Buckley & Brochu, 1999: char. 106): Scapular blade width: no more than twice the length of the scapulocoracoid articulation (0); scapular blade very broad and greater than twice the length of scapulocoracoid articulation (1).

Character 284 (Pritchard *et al.*, 2013: char. 284, modified from Buckley *et al.*, 2000: char. 115): Vomer, exposure on palate: vomer contributes flattened plate to secondary palate (0); vomer forms no part of secondary palate (1).

Character 285 (Turner & Buckley, 2008: char. 285): Supraoccipital, when present on dorsal skull roof: with narrow exposure, parietal forms portion of occipital surface (0); with broad exposure, parietal does not form portion of occipital surface (1).

Character 286 (Turner & Buckley, 2008: char. 286): Jugal, anterior and posterior processes: inline dorsoventrally (0); anterior and posterior processes at a sharp angle to one another, both processes slope ventrally to form a strongly arched jugal (1).

Character 287 (Turner & Buckley, 2008: char. 287): Lateral expansion of posterodorsal edge of surangular anterior to glenoid fossa: absent (0); present (1).

Character 288 (Turner & Buckley, 2008: char. 288): In lateral view, anterior process of the squamosal extending to the orbital margin, overlapping the postorbital: absent (0); present (1).

Character 289 (Turner & Buckley, 2008: char. 289): In lateral view, surangular and dentary suture: simple, with little or no interdigitation (0); suture complex, with interlocking prongs from both surangular and dentary, three posterior prongs from dentary and two from surangular (1).

Character 290 (Turner & Buckley, 2008: char. 290): Prominent depression on palate near alveolar margin at level of sixth or seventh alveolus: absent (0); present (1).

Character 291 (de Andrade & Bertini, 2008: char. 103): Pterygoid, ventral surface of pterygoid flanges, parachoanal fossae: absent (0); present (1).

Character 292 (Turner & Sertich, 2010: char. 292): Pterygoid, in ventral view, participation in suborbital fenestra: pterygoid forms margin of suborbital fenestra (0); excluded from suborbital fenestra by ectopterygoid-palatine contact (1).

Character 293 (Turner & Sertich, 2010: char. 293): Maxilla, lateral surface along alveolar margin, conformation of the neurovascular foramina: foramina absent or form a single continuous row (0); gap in foramina between an anterior series and a posterior series (1).

Character 294 (Turner & Sertich, 2010: char. 294): Surface of tooth enamel: smooth or slightly crenulated (0); with ridges at base of crown (often extending apically) (1).

Character 295 (Turner & Sertich, 2010: char. 295): Posterior (molariform) teeth, wear facets: absent (0); present (1).

Character 296 (Turner & Sertich, 2010: char. 296): Tooth (with transitional morphology) present at premaxilla-maxilla contact: absent (0); present (1).

Character 297 (Turner & Sertich, 2010: char. 297): Basioccipital, midline crest on basioccipital plate below occipital condyle: absent (0); present (1).

Character 298 (Turner & Sertich, 2010: char. 299): Dorsal osteoderms, accessory ranges of osteoderms (sensu Frey, 1988): absent (0); present (1).

Character 299 (de Andrade & Bertini, 2008: char. 131): Maxillary tooth, size relative to maxillary palatal surface in palatal view: proportionally small teeth, occupying only marginal portion of ventral surface of maxilla (0); proportionally well-developed teeth, occupying large area of maxillary palatal surface (1).

Character 300 (Jouve, 2004: char. 68 & Jouve, 2009: char. 75): Ventral lamina of jugal: extends far anterior to ectopterygoid (0); ends at the level of the ectopterygoid (1).

Character 301 (Sereno & Larsson, 2009: char. 199, modified from Norell, 1988: char. 42 & Brochu, 1997: char. 51): Surangular extension toward posterior end of retroarticular process: along entire length (0); pinched off anterior to posterior tip (1).

Character 302 (Turner, 2015: char. 302): Muscle attachment scars on ventral surface of

quadrate ramus: form modest crests (0); prominent knobs (1).

Character 303 (Turner, 2015: char. 303): Pterygoid flange shape: mediolaterally broad, reaching laterally beyond medial margin of quadrate condyles (0); relatively narrow, does not reach laterally to medial margin of quadrate condyles (1).

Character 304 (Turner, 2015: char. 304): In ventral view, posterior process of maxilla relative to ITF excluded from ITF (0); forms part of ITF (1).

Character 305 (Turner, 2015: char. 305): Highly modified ectopterygoid, mediolaterally broad and flattened with greatly expanded: absent (0); present, robust anterior process larger than posterior process (1); present, anterior and posterior process roughly equal in size (2).

Character 306 (Turner, 2015: char. 306): In ventral view, palate medial to toothrow: forms a single continuous surface (0); ridge running on the palate medial to toothrow formed by maxilla and ectopterygoid (1).

Character 307 (Turner, 2015: char. 307): Maxillary toothrow, penultimate and ultimate maxillary teeth enlarged and highly modified crushing tooth: absent (0); present (1).

Character 308 (Turner, 2015: char. 308): Prefrontals: do not meet at midline (0); meet at midline (1).

Character 309 (Turner, 2015: char. 309): Pear shaped external naris: absent (0); present (1).

Character 310 (Turner, 2015: char. 310): Skull, dorsal surface at parietal-squamosal contact surface: continuous across suture (0); suture marked by groove or sulcus (1).

Character 311 (Turner, 2015: char. 311): Maxilla, lateral surface, continuous groove or sulcus extending from orbital margin towards narial opening: absent (0); present (1).

Character 312 (Turner, 2015: char. 312): Maxilla, posteromedial process curving posteriorly onto palatine formed nasopharyngeal passage: absent (0); present (1).

Character 313 (Turner, 2015: char. 313): Squamosal, posterior half, dorsal and ventral rims of groove for external ear valve musculature: thin or parallel sided (0); flared posteriorly (1).

Character 314 (Turner, 2015: char. 314): Lacrimal, in dorsal view, anterior extent on rostrum relative to prefrontal: prefrontal extends farther anteriorly (0); lacrimal extends farther anteriorly (1); lacrimal and prefrontal subequal in anterior extent (2).

Character 315 (Turner, 2015: char. 315): Lacrimal, in dorsal view, mediolateral width relative to prefrontal: equal to or less than width of prefrontal (0); wider than prefrontal (1).

Character 316 (Turner, 2015: char. 316): Premaxillae, degree of contact posterior to the incisive foramen: extensive contact (0); narrow contact (1).

Character 317 (Turner, 2015: char. 317): Posterior margin of the palatines where they form the floor of the nasopharyngeal passage, shape: V- or U-shaped (0); straight (1).

Character 318 (Turner, 2015: char. 318): Posterior margin of the choanal groove, location: anteriorly on the pterygoids (0); posteriorly on the pterygoids near the posterior margin of pterygoids (1).

Character 319 (Turner, 2015: char. 319): Pterygoid-palatine contact, ventral aspect of palate, shape of the suture: transverse, or nearly so (0); prong of pterygoid projects anteriorly (1).

Character 320 (Turner, 2015: char. 320): On palate, foramen located on premaxilla/maxilla suture near the alveolar border: absent (0); present (1).

Character 321 (Turner, 2015: char. 321): Ectopterygoid/pterygoid contact in ventral view: complex, anterior part of ectopterygoid forming suture whereas posterior part of ectopterygoid overlaps the pterygoid (0); sutured along entire contact, no part of ectopterygoid overlapping pterygoid (1).

Supplementary Material S5: Phylogenetic results

Changes made to the original matrix

Bernissartia fagesii:

Char. 5: ? ↦ 1

Char. 10: ? ↦ 2

Char. 11: ? ↦ 0

Char. 12: ? ↦ 0

Char. 21: ? ↦ 1

Char. 32: 0 ↦ 1

Char. 34: ? ↦ 1

Char. 39: ? ↦ 1

Char. 40: ? ↦ 0

Char. 62: 1 ↦ ?

Char. 64: ? ↦ 0

Char. 65: ? ↦ 0

Char. 69: ? ↦ 0

Char. 81: 1 ↦ ?

Char. 102: 1 ↦ ?

Char. 118: ? ↦ 0

Char. 119: ? ↦ 1

Char. 121: ? ↦ 0

Char. 122: ? ↦ 1

Char. 123: ? ↦ 0

Char. 124: ? ↦ 1

Char. 125: 1 ↦ 0

Char. 127: ? ↦ 0

Char. 128: ? ↦ 1 / 2

Char. 133: ? ↦ 0

Char. 135: ? ↦ 0

Char. 136: ? ↦ 1

Char. 138: ? ↦ 1

Char. 141: ? ↦ 1

Char. 143: ? ↦ 1

Char. 146: ? ↦ 0

Char. 150: ? ↦ 1

Char. 155: ? ↦ 0

Char. 158: ? ↦ 0

Char. 161: ? ↦ 0

Char. 169: 1 ↦ 0

Char. 171: ? ↦ 0

Char. 172: 1 ↦ ?

Char. 185: ? ↦ 0

Char. 186: ? ↦ 0

Char. 190: ? ↦ 0

Char. 193: ? ↦ 0

Char. 195: ? ↦ 1

Char. 197: ? ↦ 2

Char. 198: ? ↦ 0

Char. 201: ? ↦ 0

Char. 202: ? ↦ 0

Char. 206: ? ↦ 1

Char. 210: ? ↦ 0

Char. 211: ? ↦ 0

Char. 214: 0 ↦ ?

Char. 217: ? ↦ 0

Char. 218: ? ↦ 0

Char. 219: 0 ↦ 1

Char. 220: ? ↦ 0

Char. 229: ? ↦ 0

Char. 230: ? ↦ 0

Char. 231: ? ↦ 0

Char. 235: 0 ↦ 1

Char. 236: ? ↦ 0

Char. 238: ? ↦ 0

Char. 240: ? ↦ 0

Char. 241: ? ↦ 0

Char. 244: ? ↦ 0

Char. 245: ? ↦ 0

Char. 249: ? ↦ 0

Char. 253: ? ↦ 0

Char. 262: 0 ↦ 2

Char. 265: ? ↦ 1

Char. 270: 1 ↦ 0

Char. 278: ? ↦ 1

Char. 292: 0 ↦ ?

Char. 304: ? ↦ 0

Char. 306: ? ↦ 0

Char. 311: ? ↦ 0

Char. 314: 1 ↦ 1 / 2

Char. 316: ? ↦ 0

Char. 319: ? ↦ 0

Char. 320: ? ↦ 0

Char. 321: ? ↦ 0

Paralligator gradilifrons:

Char. 5: 1 ↦ ?

Char. 6: 1 / 2 ↦ ?

Char. 17: 1 ↦ 0

Char. 66: 0 ↦?

Char. 159: 0 ↦?

Char. 315: 1 ↦ 0

Char. 320: 1 ↦?

Paralligator major:

Char. 5:? ↦ 0

Char. 6: 1 ↦ 2

Char. 17:? ↦ 0

Char. 66:? ↦ 0

Char. 315:? ↦ 1

Batrachomimus pastosbonensis:

Char. 5:? ↦ 0

Char. 17: 1 ↦ 0

Char. 49: 0 ↦ ?

Wannchampsus kirpachi:

Char. 3: 3 ↦1

Char. 5: 0 ↦ ?

Rugosuchus nonganensis:

Char. 6: 1 / 2 ↦ ?

Char. 17: 1 ↦ 0

Char. 35: 1 ↦ 0

Char. 49: 0 ↦ ?

Char. 69: ? ↦ 0

Char. 311: ? ↦ 0

Char. 315: 1 ↦ ?

Aprosuchus ghirai:

Char. 35: 1 ↦ 0

Char. 69: 1 ↦ ?

Char. 315: ? ↦ 1

Shamosuchus djadochtaensis:

Char. 3: 3 ↦ 1

Char. 35: 1 ↦ 0

Char. 49: 0 ↦ 2

Char. 159:? ↦ 2

Knoetschkesuchus guimarotae:

Char. 6: 1 ↦ 2

Char. 22: 0 ↦ 1

Char. 35: 0 ↦ 1

Char. 49:? ↦ 0

Char. 69: 1 ↦ 2

Char. 140: 2 ↦ 1

Char. 279: 0 ↦ 1

Char. 311: 1 ↦ 0

Char. 315: 0 ↦ 1

Knoetschkesuchus langenbergensis:

Char. 6: 1 ↦ 2

Char. 22: 0 ↦ 1

Char. 66: 0 ↦?

Char. 69: 1 ↦ 2

Char. 143: 2 ↦?

Char. 279:? ↦ 1

Char. 315: 1 ↦ 0

Sabresuchus sympiestodon:

Char. 35: 1 ↦?

Char. 69: 1 ↦?

New Technology Search, full dataset:

41 trees of 1488 steps, consensus: CI: 0.26, RI: 0.59, 1500 steps

Synapomorphies and bootstrap scores:

Node 1 (77%): 33(1), 128(0), 143(1)

Node 2 (100%): 1(2), 16(1), 19(1), 24(1), 30(1), 45(2), 47(1), 51(1), 55(1), 67(1), 68(1), 82(1), 95(1), 99(1), 196(1), 197(2), 204(1), 205(1), 252(1)

Node 3 (85%): 2(1), 60(1), 106(2), 114(1), 127(0), 143(0), 212(1)

Node 4 (61%): 36(2), 49(2), 96(0), 139(1), 145(1)

Node 5 (99%): 1(1), 32(1), 75(1), 97(1), 206(0), 214(1), 215(1), 216(1), 217(1), 219(1), 220(1), 221(1), 222(1), 223(1), 224(1)

Node 6 (42%): 25(1), 37(2), 39(1), 41(1), 79(1), 103(0), 125(1), 150(1), 197(1)

Node 7 (27%): 192(1), 201(1), 211(1)

Node 8 (40%): 108(3), 160(1), 262(1)

Node 9 (25%): 55(0), 77(1), 143(1), 168(2), 203(0), 234(1)

Node 10 (18%): 19(0), 67(3), 107(0), 142(0), 194(1)

Node 11 (60%): 9(0), 10(2), 15(1), 17(1), 26(1), 45(1), 46(1), 83(1), 167(2), 193(0), 199(1), 208(0)

Node 12 (7%): 11(1), 23(1), 67(2), 96(1), 156(1), 157(1), 168(1), 182(1), 283(1), 320(1)

Node 13: 81(1), 103(1), 161(1), 289(1), 314(0)

Node 14: 56(1)

Node 15 (100%): 5(1), 6(2), 18(1), 126(3), 141(1), 155(0), 159(1), 176(1), 183(1), 197(0), 286(1), 287(1)

Node 16 (14%): 71(2), 76(1), 138(1), 143(2), 149(1), 170(1), 178(1)

Node 17 (34%): 44(0), 120(1), 154(0), 159(1), 162(1), 164(1), 183(1), 272(1), 318(0)

Node 18 (10%): 27(1), 67(1), 96(0), 106(2), 145(0), 192(1), 198(1), 212(0)

Node 19 (37%): 95(0), 105(2), 159(0), 167(0), 178(0)

Node 20 (42%): 1(1), 74(1), 79(0), 107(1), 226(1)

Node 21 (52%): 27(0), 91(1), 108(1), 295(1)

Node 22 (38%): 140(1), 165(1), 185(1), 232(1), 235(1), 279(1), 292(1), 318(1)

Node 23 (75%): 78(2), 111(1), 127(0), 208(1), 237(1), 265(0), 294(1)

Node 24 (43%): 108(2), 130(1), 148(1), 299(1)

Node 25 (46%): 78(3), 106(4), 121(1), 124(1)

Node 26 (77%): 127(0), 140(0), 170(0), 198(0), 225(1), 271(1)

Node 27 (34%): 5(1), 6(2), 56(1), 71(3), 79(0), 112(0), 147(1), 150(0), 169(1), 312(1)

Node 28 (2%): 100(1), 142(1), 165(1), 197(0)

Node 29 (5%): 13(1), 96(2), 140(0), 265(0)

Node 30 (52%): 3(2), 26(0), 36(1), 45(0), 63(0), 77(2), 107(1), 143(0), 236(2), 243(1), 270(0), 305(2)

Node 31: 33(1), 57(1), 64(1), 68(0), 128(0), 257(1)

Node 32: 252(0)

Node 33 (56%): 78(1), 163(1), 227(1), 239(1), 240(1), 265(1)

Node 34 (3%): 79(2), 178(1), 182(1), 183(1), 184(1), 264(0)

Node 35 (3%): 27(1), 70(0), 81(1), 142(0), 159(3), 173(1), 300(1), 315(0)

Node 36 (36%): 10(1), 44(0), 49(0), 71(4), 101(1), 207(1)

Node 37: 45(0)

Node 38: 315(1)

Node 39: 37(1)

Node 40 (36%): 5(0), 7(0)

Node 41 (1%): 69(0), 92(1), 96(1), 97(1), 171(1)

Node 42 (0%): 13(0), 65(0), 75(1), 153(0)

Node 43 (2%): 71(4), 162(1), 169(0), 266(1)

Node 44 (8%): 5(0), 11(1), 17(0), 22(1), 35(1), 56(0), 66(0), 259(1), 298(0)

Node 45 (23%): 3(1), 4(1), 49(0), 79(1), 96(2), 97(0), 140(2), 229(1)

Node 46: 11(0), 44(0), 100(0)

Node 47: 12(1)

Node 48: 18(1), 32(1), 69(2), 75(0), 126(2), 234(0), 266(0)

Node 49 (69%): 36(2), 47(0), 64(1), 160(0), 181(1), 193(1), 195(1), 199(0), 211(1), 249(1), 254(1), 262(2), 277(1), 318(0)

Node 50 (56%): 29(1), 45(0), 79(2), 145(0), 168(1), 207(1)

Node 51 (0%): 27(0), 170(1), 219(2), 260(1), 320(1)

Node 52 (90%): 80(1), 158(1), 184(0), 262(2), 317(1)

Node 53 (11%): 9(0), 168(1), 216(2), 275(1)

Node 54: 11(0), 49(0), 69(2), 92(0)

Node 55: 297(0), 315(1)

Node 56: 35(0), 44(0), 165(0), 171(0), 277(1)

Node 57: 128(0), 311(0)

Node 58: 44(2), 49(0), 79(1), 315(1)

Node 59 (49%): 9(0), 122(0), 126(4), 178(0), 183(0), 302(1), 303(1), 306(1), 321(1)

Node 60 (72%): 11(1), 278(0), 314(0), 315(0)

Node 61 (65%): 5(0), 74(1), 79(0), 105(1), 141(1), 168(1)

Node 62 (23%): 76(1), 117(0), 265(1), 268(1)

Node 63 (8%): 44(2), 98(1), 260(1)

Node 64 (73%): 3(2), 20(1), 57(1), 79(0), 178(0), 243(1), 267(0), 270(0)

Node 65 (74%): 126(2), 238(1)

Node 66 (15%): 13(0), 96(0), 97(2), 177(1), 223(1)

Node 67 (4%): 258(0)

Node 68 (18%): 264(1)

Node 69 (30%): 77(0), 169(0), 279(1)

Node 70 (19%): 82(2)

Heuristic search, full dataset:

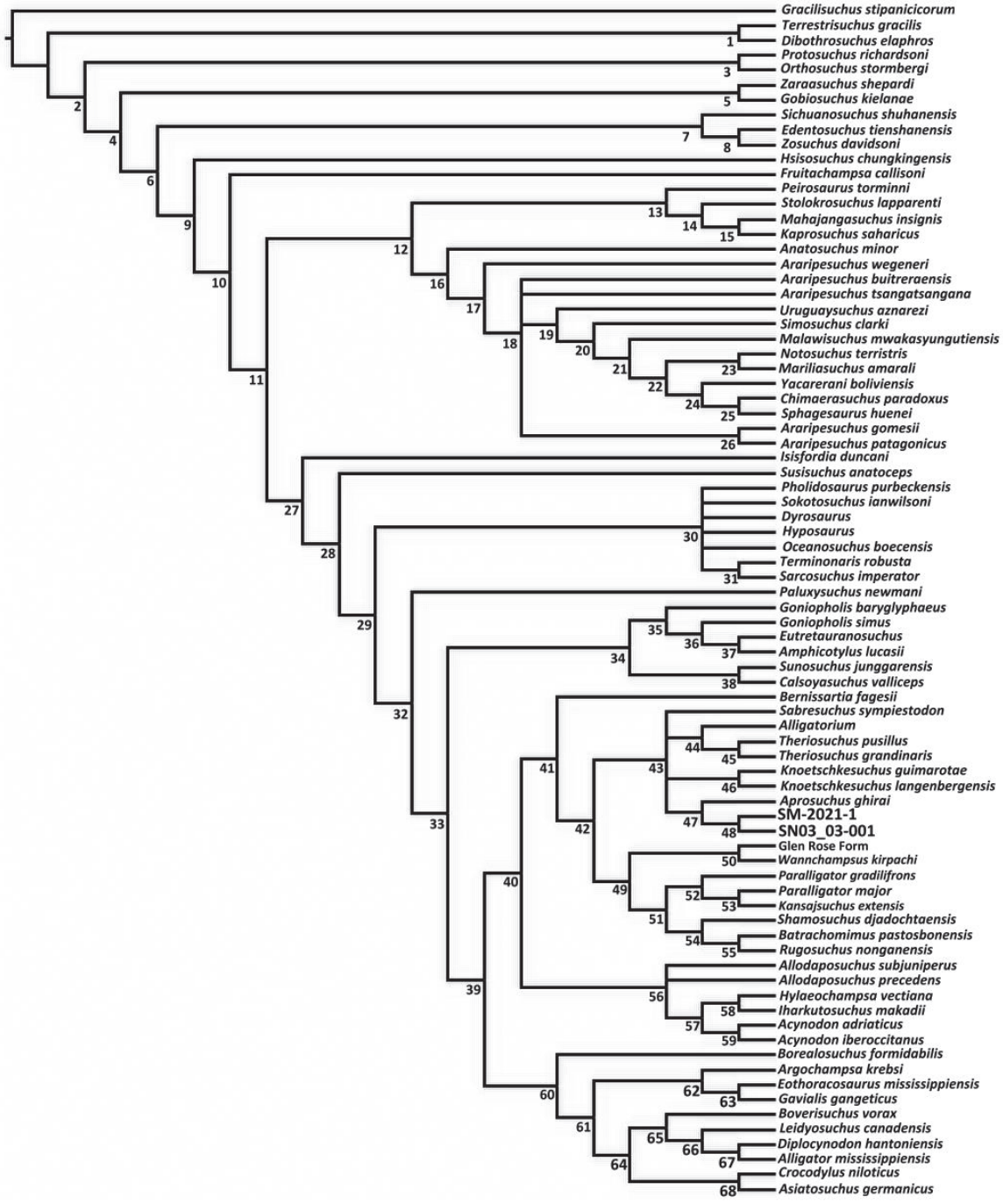

60 trees of 1488 steps, consensus: CI: 0.26, RI: 0.58, 1513 steps

Synapomorphies and bootstrap scores:

Node 1 (73%): 33(1), 128(0), 143(1)

Node 2 (100%): 1(2), 16(1), 19(1), 24(1), 30(1), 45(2), 47(1), 51(1), 55(1), 67(1), 68(1), 82(1), 95(1), 99(1), 196(1), 197(2), 204(1), 205(1), 252(1)

Node 3 (67%): 2(1), 60(1), 106(2), 114(1), 127(0), 143(0), 212(1)

Node 4 (64%): 36(2), 49(2), 96(0), 139(1), 145(1)

Node 5 (97%): 1(1), 32(1), 75(1), 97(1), 206(0), 214(1), 215(1), 216(1), 217(1), 219(1), 220(1), 221(1), 222(1), 223(1), 224(1)

Node 6 (37%): 25(1), 37(2), 39(1), 41(1), 79(1), 103(0), 125(1), 150(1), 197(1)

Node 7 (19%): 192(1), 201(1), 211(1)

Node 8 (39%): 108(3), 160(1), 262(1)

Node 9 (24%): 55(0), 77(1), 143(1), 168(2), 203(0), 234(1)

Node 10 (19%): 19(0), 67(3), 107(0), 142(0), 194(1)

Node 11 (74%): 9(0), 10(2), 15(1), 17(1), 26(1), 45(1), 46(1), 83(1), 167(2), 193(0), 199(1), 208(0)

Node 12 (11%): 11(1), 23(1), 67(2), 96(1), 157(1), 168(1), 182(1), 283(1), 320(1)

Node 13 (9%): 80(0), 103(1), 161(1), 289(1), 314(0)

Node 14 (8%): 56(1)

Node 15 (98%): 5(1), 6(2), 18(1), 126(3), 141(1), 155(0), 159(1), 176(1), 183(1), 197(0), 286(1), 287(1)

Node 16 (29%): 71(2), 76(1), 138(1), 143(2), 149(1), 170(1), 178(1)

Node 17 (46%): 44(0), 120(1), 154(0), 159(1), 162(1), 164(1), 183(1), 272(1), 318(0)

Node 18 (16%): 27(1), 67(1), 96(0), 106(2), 145(0), 192(1), 198(1), 212(0)

Node 19 (35%): 95(0), 105(2), 159(0), 167(0), 178(0)

Node 20 (55%): 1(1), 74(1), 79(0), 107(1), 226(1)

Node 21 (63%): 27(0), 91(1), 108(1), 295(1)

Node 22 (43%): 140(1), 165(1), 185(1), 232(1), 235(1), 279(1), 292(1), 318(1)

Node 23 (77%): 78(2), 111(1), 127(0), 208(1), 237(1), 265(0), 294(1)

Node 24 (45%): 108(2), 130(1), 148(1), 299(1)

Node 25 (50%): 78(3), 106(4), 121(1), 124(1)

Node 26 (77%): 127(0), 140(0), 170(0), 198(0), 225(1), 271(1)

Node 27 (35%): 5(1), 6(2), 56(1), 71(3), 79(0), 112(0), 147(1), 150(0), 169(1), 312(1)

Node 28 (3%): 100(1), 165(1), 197(0)

Node 29 (4%): 13(1), 96(2), 140(0), 265(0)

Node 30 (62%): 3(2), 26(0), 36(1), 45(0), 63(0), 77(2), 107(1), 143(0), 236(2), 243(1), 268(1), 270(0), 305(2)

Node 31 (70%): 78(1), 163(1), 227(1), 239(1), 240(1), 241(1), 265(1)

Node 32 (1%): 79(2), 178(1), 182(1), 183(1), 184(1), 264(0), 297(0)

Node 33 (0%): 27(1), 70(0), 81(1), 159(3), 173(1), 300(1), 315(0)

Node 34 (40%): 10(1), 44(0), 49(0), 71(4), 101(1), 207(1)

Node 35 (17%): 45(0)

Node 36 (18%): 315(1)

Node 37 (38%): 37(1)

Node 38 (30%): 5(0), 7(0)

Node 39 (0%): 69(0), 92(1), 96(1), 97(1), 171(1)

Node 40 (0%): 13(0), 65(0), 75(1), 153(0)

Node 41 (2%): 71(4), 162(1), 169(0), 266(1)

Node 42 (7%): 5(0), 11(1), 17(0), 22(1), 35(1), 56(0), 66(0), 259(1), 298(0)

Node 43 (19%): 3(1), 4(1), 49(0), 79(1), 96(2), 97(0), 140(2), 229(1)

Node 44 (23%): 11(0), 44(0), 100(0)

Node 45 (48%): 12(1)

Node 46 (84%): 18(1), 32(1), 69(2), 75(0), 126(2), 324(0), 266(0)

Node 47 (82%): 36(2), 47(0), 64(1), 160(0), 181(1), 193(1), 195(1), 199(0), 211(1), 249(1), 254(1), 262(2), 277(1), 279(1), 318(0)

Node 48 (70%): 29(1), 45(0), 79(2), 145(0), 168(1), 207(1)

Node 49 (4%): 27(0), 170(1), 219(2), 260(1), 320(1)

Node 50 (88%): 80(1), 158(1), 184(0), 262(2), 317(1)

Node 51 (5%): 9(0), 168(1), 216(2), 275(1)

Node 52 (16%): 11(0), 49(0), 69(2), 92(0)

Node 53 (9%): 297(0), 315(1)

Node 54 (14%): 35(0), 44(0), 165(0), 171(0), 277(1)

Node 55 (13%): 128(0), 311(0)

Node 56 (7%): 44(2), 49(0), 79(1), 315(1)

Node 57 (54%): 9(0), 122(0), 126(4), 178(0), 183(0), 302(1), 303(1), 306(1), 321(1)

Node 58 (75%): 11(1), 278(0), 314(0), 315(0)

Node 59 (61%): 5(0), 74(1), 79(0), 105(1), 141(1), 168(1)

Node 60 (28%): 76(1), 117(0), 265(1), 268(1)

Node 61 (8%): 44(2), 98(1), 260(1)

Node 62 (87%): 3(2), 20(1), 57(1), 79(0), 178(0), 243(1), 267(0), 270(0)

Node 63 (73%): 126(2), 238(1)

Node 64 (9%): 13(0), 96(0), 97(2), 177(1), 223(1)

Node 65 (6%): 258(0)

Node 66 (22%): 264(1)

Node 67 (38%): 77(0), 169(0), 279(1)

Node 68 (18%): 82(2)

New Technology Search, without characters associated with ontogenetic variation:

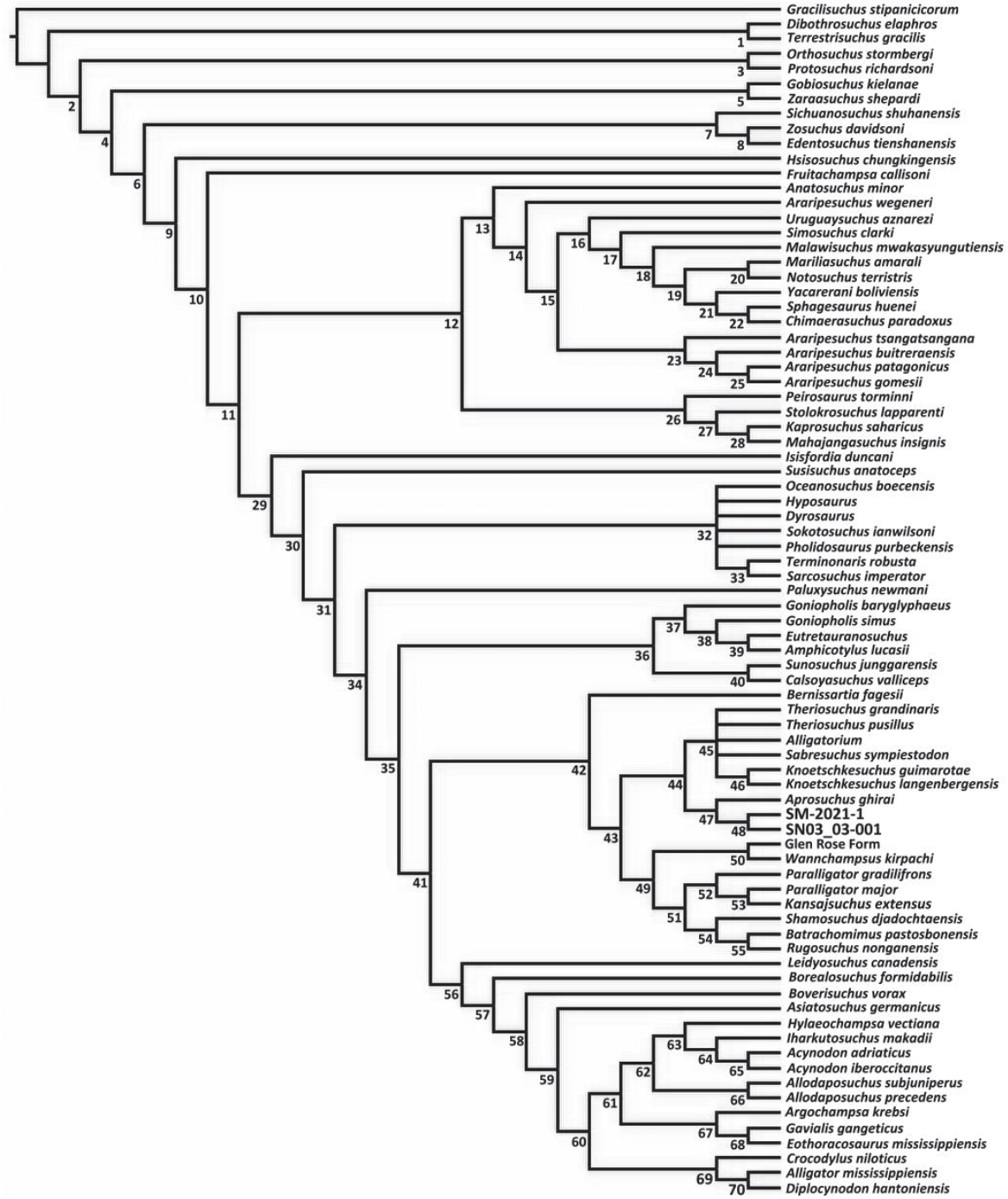

15 trees of 1444 steps, consensus: CI = 0.26, RI = 0.59, 1465 steps

Synapomorphies and bootstrap scores:

Node 1 (73%): 33(0), 128(0), 143(1)

Node 2 (100%): 1(2), 16(1), 19(1), 24(1), 30(1), 45(2), 47(1), 51(1), 55(1), 67(1), 82(1), 95(1), 99(1), 196(1), 197(2), 204(1), 205(1), 252(1)

Node 3 (79%): 2(1), 60(1), 106(2), 114(1), 127(0), 143(0), 212(1)

Node 4 (51%): 36(2), 49(2), 96(0), 139(1), 145(1)

Node 5 (98%): 1(1), 32(1), 75(1), 97(1), 206(0), 214(1), 215(1), 216(1), 217(1), 219(1), 220(1), 221(1), 222(1), 223(1), 224(1)

Node 6 (43%): 25(1), 37(2), 39(1), 41(1), 79(1), 103(0), 150(1), 197(1)

Node 7 (29%): 192(1), 201(1), 211(1)

Node 8 (56%): 108(3), 160(1), 262(1)

Node 9 (30%): 55(0), 77(1), 143(1), 168(2), 203(0), 234(1)

Node 10 (15%): 19(0), 67(3), 107(0), 142(0), 194(1)

Node 11 (68%): 9(0), 10(2), 15(1), 17(1), 26(1), 45(1), 46(1), 83(1), 167(2), 193(0), 199(1), 208(0), 301(1)

Node 12 (10%): 23(1), 67(2), 96(1), 157(1), 168(1), 182(1), 283(1), 320(1)

Node 13 (23%): 71(2), 76(1), 138(1), 143(2), 149(1), 170(1), 178(1)

Node 14 (42%): 44(0), 120(1), 154(0), 162(1), 164(1), 272(1), 318(0)

Node 15 (16%): 67(1), 96(0), 106(2), 192(1), 198(1)

Node 16 (32%): 105(2), 167(0), 178(0)

Node 17 (43%): 1(1), 74(1), 79(0), 107(1), 226(1)

Node 18 (61%): 91(1), 104(2), 108(1), 295(1)

Node 19 (35%): 140(1), 165(1), 185(1), 232(1), 235(1), 279(1), 292(1), 318(1)

Node 20 (75%): 78(2), 111(1), 127(0), 208(1), 237(1), 294(1)

Node 21 (36%): 108(2), 130(1), 148(1), 299(1)

Node 22 (48%): 78(3), 106(4), 121(1), 124(1)

Node 23 (23%): 104(1)

Node 24 (32%): 191(1), 271(1)

Node 25 (73%): 140(0), 198(0), 225(1)

Node 26 (11%): 81(1), 103(1), 161(1), 289(1), 314(0)

Node 27 (10%): 56(1)

Node 28 (97%): 5(1), 6(2), 18(1), 126(3), 141(1), 155(0), 159(1), 176(1), 183(1), 197(0), 286(1), 287(1)

Node 29 (38%): 5(1), 6(2), 56(1), 71(3), 79(0), 112(0), 147(1), 150(0), 169(1), 312(1)

Node 30 (5%): 100(1), 165(1), 197(0)

Node 31 (4%): 13(1), 96(2), 140(0)

Node 32 (52%): 3(2), 26(0), 36(1), 45(0), 63(0), 77(2), 107(1), 143(0), 236(2), 268(1), 270(0), 305(2)

Node 33 (49%): 78(1), 163(1), 227(1), 239(1), 240(1), 241(1)

Node 34 (1%): 79(2), 178(1), 182(1), 183(1), 184(1)

Node 35 (1%): 27(1), 70(0), 81(1), 159(3), 173(1), 315(0)

Node 36 (47%): 10(1), 44(0), 49(0), 101(1), 207(1)

Node 37 (19%): 45(0)

Node 38 (16%): 315(1)

Node 39 (52%): 37(1)

Node 40 (41%): 5(0), 7(0)

Node 41 (0%): 69(0), 96(1), 97(1), 162(1)

Node 42 (3%): 75(1), 169(0), 223(1), 266(1)

Node 43 (5%): 5(0), 17(0), 22(1), 56(0), 66(0), 171(1), 259(1), 298(0)

Node 44 (17%): 3(1), 49(0), 97(0), 140(2), 229(1), 312(0), 315(1)

Node 45 (40%): 100(0), 122(0), 124(0), 159(2)

Node 46 (77%): 18(1), 31(0), 32(1), 90(1), 234(0)

Node 47 (86%): 36(2), 47(0), 64(1), 160(0), 181(1), 193(1), 195(1), 199(0), 211(1), 249(1), 254(1), 277(1), 318(0)

Node 48 (84%): 29(1), 45(0), 145(0), 168(1), 207(1)

Node 49 (6%): 27(0), 170(1), 219(2), 260(1), 301(0), 320(1)

Node 50 (86%): 80(1), 122(0), 158(1), 184(0), 317(1)

Node 51 (4%): 9(0), 168(1), 216(2), 275(1)

Node 52 (13%): 49(0), 69(2)

Node 53 (18%): 297(0), 315(1)

Node 54 (14%): 44(0), 165(0), 171(0), 277(1)

Node 55 (29%): 128(0), 311(0)

Node 56 (5%): 43(1), 76(1), 182(2), 268(1)

Node 57 (0%): 171(1), 278(0)

Node 58 (0%): 23(1), 260(1), 297(0)

Node 59 (0%): 82(2)

Node 60 (0%): 77(0)

Node 61 (2%): 45(0), 81(0), 159(0), 162(0)

Node 62 (8%): 49(0), 65(0), 268(0), 312(0)

Node 63 (63%): 23(0), 165(0), 302(1), 303(1), 306(1), 307(1), 321(1)

Node 64 (22%): 297(1), 304(1)

Node 65 (64%): 5(0), 74(1), 105(1), 141(1), 168(1), 278(1), 315(1)

Node 66 (34%): 315(1), 320(1)

Node 67 (73%): 3(2), 13(1), 20(1), 57(1), 270(0)

Node 68 (71%): 126(2), 238(1)

Node 69 (28%): 96(0), 97(2), 177(1), 223(1)

Node 70 (31%): 169(0), 258(0), 264(1), 278(1), 279(1)

References

Brochu C. A. (1997). Morphology, fossils, divergence timing, and the phylogenetic relationships of *Gavialis*. *Systematic Biology*, 46(3): 479-522. https://doi.org/10.1093/sysbio/46.3.479

Brochu C. A. (1999). Phylogenetics, taxonomy, and historical biogeography of Alligatoroidea. *Journal of Vertebrate Paleontology*, 19(S2): 9-100. https://doi.org/10.1080/02724634.1999.10011201

Buckley G. A. & Brochu C. A. (1999). An enigmatic new crocodile from the Upper Cretaceous of Madagascar. *Special papers in palaeontology*, 60(60): 149-175.

Buckley G. A., Brochu C. A., Krause D. W. & Pol D. (2000). A pug-nosed crocodyliform from the Late Cretaceous of Madagascar. *Nature*, 405(6789): 941-944. https://doi.org/10.1038/35016061

Buscalioni A. D. & Sanz J. L. (1988). Phylogenetic relationships of the Atoposauridae (Archosauria, Crocodylomorpha). *Historical Biology*, 1(3): 233-250. https://doi.org/10.1080/08912968809386477

Clark J. M. (1994). Patterns of evolution in Mesozoic Crocodyliformes. In Sues H. D. (eds.) *The Shadow of the Dinosaurs: Early Mesozoic Tetrapods*. New York: Cambridge University Press: 84–97.

de Andrade M. B. & Bertini R. J. (2008). A new *Sphagesaurus* (Mesoeucrocodylia: Notosuchia) from the Upper Cretaceous of Monte Alto City (Bauru Group, Brazil), and a revision of the Sphagesauridae. *Historical Biology*, 20(2): 101-136. https://doi.org/10.1080/08912960701642949

Gasparini Z., Fernandez M. & Powell J. (1993). New tertiary sebecosuchians (Crocodylomorpha) from South America: phylogenetic implications. *Historical Biology*, 7(1): 1-19. https://doi.org/10.1080/10292389309380440

Gasparini Z., Pol D. & Spalletti L. A. (2006). An unusual marine crocodyliform from the Jurassic-Cretaceous boundary of Patagonia. *Science*, 311(5757): 70-73. https://doi.org/10.1126/science.1120803

Gomani E. M. (1997). A crocodyliform from the Early Cretaceous dinosaur beds, northern Malawi. *Journal of Vertebrate Paleontology*, 17(2): 280-294. https://doi.org/10.1080/02724634.1997.10010975

Jouve S. (2004). *Etude des Crocodyliformes fini Crétacé-Paléogène du Bassin des Oulad Abdoun (Maroc), et comparaison avec les faunes africaines contemporaines: Systématique, Phylogénie et Paléobiogéographie.* Unpublished PhD thesis, Muséum National d'Histoire Naturelle.

Jouve S. (2009). The skull of *Teleosaurus cadomensis* (Crocodylomorpha; Thalattosuchia), and phylogenetic analysis of Thalattosuchia. *Journal of Vertebrate Paleontology*, 29(1): 88-102. https://doi.org/10.1080/02724634.2009.10010364

Martinelli A. G. (2003). *Comahuesuchus brachybuccalis* (Archosauria, Crocodyliformes) from the Late Cretaceous of Río Negro Province (Argentina). *Ameghiniana*, 40(4): 559-572.

Norell M. A. (1988). *Cladistic Approaches to Paleobiology as Applied to the Phylogeny of Alligatorids.* Unpublished PhD thesis, Yale University, 264 p.

Ortega F., Buscalioni A. D. & Gasparini Z. (1996). Reinterpretation and new denomination of *Atacisaurus crassiproratus* (middle Eocene; Issel, France) as cf. *Iberosuchus* (Crocodylomorpha, Metasuchia). *Geobios*, 29(3): 353-364. https://doi.org/10.1016/S0016-6995(96)80037-4

Ortega F., Gasparini Z., Buscalioni A. D. & Calvo J. O. (2000). A new species of *Araripesuchus* (Crocodylomorpha, Mesoeucrocodylia) from the lower Cretaceous of Patagonia (Argentina). *Journal of Vertebrate Paleontology*, 20(1): 57-76. https://doi.org/10.1671/0272-4634(2000)020[0057:ANSOAC]2.0.CO;2

Pol D. (1999a). *El esqueleto postcraneano de Notosuchus terrestris (Archosauria: Crocodyliformes) del Cretácico Superior de la Cuenca Neuquina y su información filogenética*. Unpublished MSc thesis, Universidad de Buenos Aires, 158 p.

Pol D. (1999b). Basal mesoeucrocodylian relationships: new clues to old conflicts. *Journal of Vertebrate Paleontology*, 19(3): 69A.

Pol D. & Norell M. A. (2004a). A new gobiosuchid crocodyliform taxon from the Cretaceous of Mongolia. *American Museum Novitates*, 2004(3458): 1-31. https://doi.org/10.1206/0003-0082(2004)458<0001:ANGCTF>2.0.CO;2

Pol D. & Norell M. A. (2004b). A new crocodyliform from Zos Canyon, Mongolia. *American Museum Novitates*, 2004(3445): 1-36. https://doi.org/10.1206/0003-0082(2004)445<0001:ANCFCM>2.0.CO;2

Pol D. & Apesteguía S. (2005). New *Araripesuchus* remains from the early late cretaceous (Cenomanian–Turonian) of Patagonia. *American Museum Novitates*, 2005(3490): 1-38. https://doi.org/10.1206/0003-0082(2005)490[0001:NARFTE]2.0.CO;2

Pol D., Ji S. A., Clark J. M. & Chiappe L. M. (2004). Basal crocodyliforms from the Lower Cretaceous Tugulu Group (Xinjiang, China), and the phylogenetic position of *Edentosuchus*. *Cretaceous Research*, 25(4): 603-622. https://doi.org/10.1016/j.cretres.2004.05.002

Pol D., Turner A. H. & Norell M. A. (2009). Morphology of the Late Cretaceous crocodylomorph *Shamosuchus djadochtaensis* and a discussion of neosuchian phylogeny as related to the origin of Eusuchia. *Bulletin of the American Museum of Natural History*, 2009(324): 1-103. https://doi.org/10.1206/0003-0090-324.1.1

Pritchard A. C., Turner A. H., Allen E. R. & Norell M. A. (2013). Osteology of a North American goniopholidid (*Eutretauranosuchus delfsi*) and palate evolution in Neosuchia. *American Museum Novitates*, 2013(3783): 1-56. https://doi.org/10.1206/3783.2

Schwarz D., Raddatz M. & Wings O. (2017). *Knoetschkesuchus langenbergensis* gen. nov. sp. nov., a new atoposaurid crocodyliform from the Upper Jurassic Langenberg Quarry (Lower Saxony, northwestern Germany), and its relationships to *Theriosuchus*. *PLoS One*, 12(2): e0160617. https://doi.org/10.1371/journal.pone.0160617

Sereno P. & Larsson H. (2009). Cretaceous crocodyliforms from the Sahara. *ZooKeys*, 28: 1-143. https://doi.org/10.3897/zookeys.28.325

Sereno P. C., Larsson H. C., Sidor C. A. & Gado B. (2001). The giant crocodyliform Sarcosuchus from the Cretaceous of Africa. *Science*, 294(5546): 1516-1519. https://doi.org/10.1126/science.1066521

Turner A. H. (2004). Crocodyliform biogeography during the Cretaceous: evidence of Gondwanan vicariance from biogeographical analysis. *Proceedings of the Royal Society of London. Series B: Biological Sciences*, 271(1552): 2003-2009. https://doi.org/10.1098/rspb.2004.2840

Turner A. H. (2006). Osteology and phylogeny of a new species of *Araripesuchus* (Crocodyliformes: Mesoeucrocodylia) from the Late Cretaceous of Madagascar. *Historical Biology*, 18(3): 255-369. https://doi.org/10.1080/08912960500516112

Turner A. H. (2015). A review of *Shamosuchus* and *Paralligator* (Crocodyliformes, Neosuchia) from the Cretaceous of Asia. *PLoS One*, 10(2): e0118116. https://doi.org/10.1371/journal.pone.0118116

Turner A. H. & Buckley G. A. (2008). *Mahajangasuchus insignis* (Crocodyliformes: Mesoeucrocodylia) cranial anatomy and new data on the origin of the eusuchian-style palate. *Journal of Vertebrate Paleontology*, 28(2): 382-408. https://doi.org/10.1671/0272-4634(2008)28[382:MICMCA]2.0.CO;2

Turner A. H. & Sertich J. J. (2010). Phylogenetic history of *Simosuchus clarki* (Crocodyliformes: Notosuchia) from the late cretaceous of Madagascar. *Journal of Vertebrate Paleontology*, 30(sup1): 177-236. https://doi.org/10.1080/02724634.2010.532348

Wu X. C. & Sues H. D. (1996). Anatomy and phylogenetic relationships of *Chimaerasuchus paradoxus*, an unusual crocodyliform reptile from the Lower Cretaceous of Hubei, China. *Journal of Vertebrate Paleontology*, 16(4): 688-702. https://doi.org/10.1080/02724634.1996.10011358

Wu X. C., Sues H. D. & Dong Z. M. (1997). *Sichuanosuchus shuhanensis*, a new? Early Cretaceous protosuchian (Archosauria: Crocodyliformes) from Sichuan (China), and the monophyly of Protosuchia. *Journal of Vertebrate Paleontology*, 17(1): 89-103. https://doi.org/10.1080/02724634.1997.10010956

Zaher H., Pol D., Carvalho A. B., Riccomini C., Campos D. & Nava W. (2006). Redescription of the cranial morphology of *Mariliasuchus amarali*, and its phylogenetic affinities (Crocodyliformes, Notosuchia). *American Museum Novitates*, 2006(3512): 1-40. https://doi.org/10.1206/0003-0082(2006)3512[1:ROTCMO]2.0.CO;2

Appendix 5: Supplementary Material concerning the publication 'A multi-isotopic study reveals the paleoecology of a sebecid from the Paleocene of Bolivia'

Supplementary Material S1: Samples used in this study:

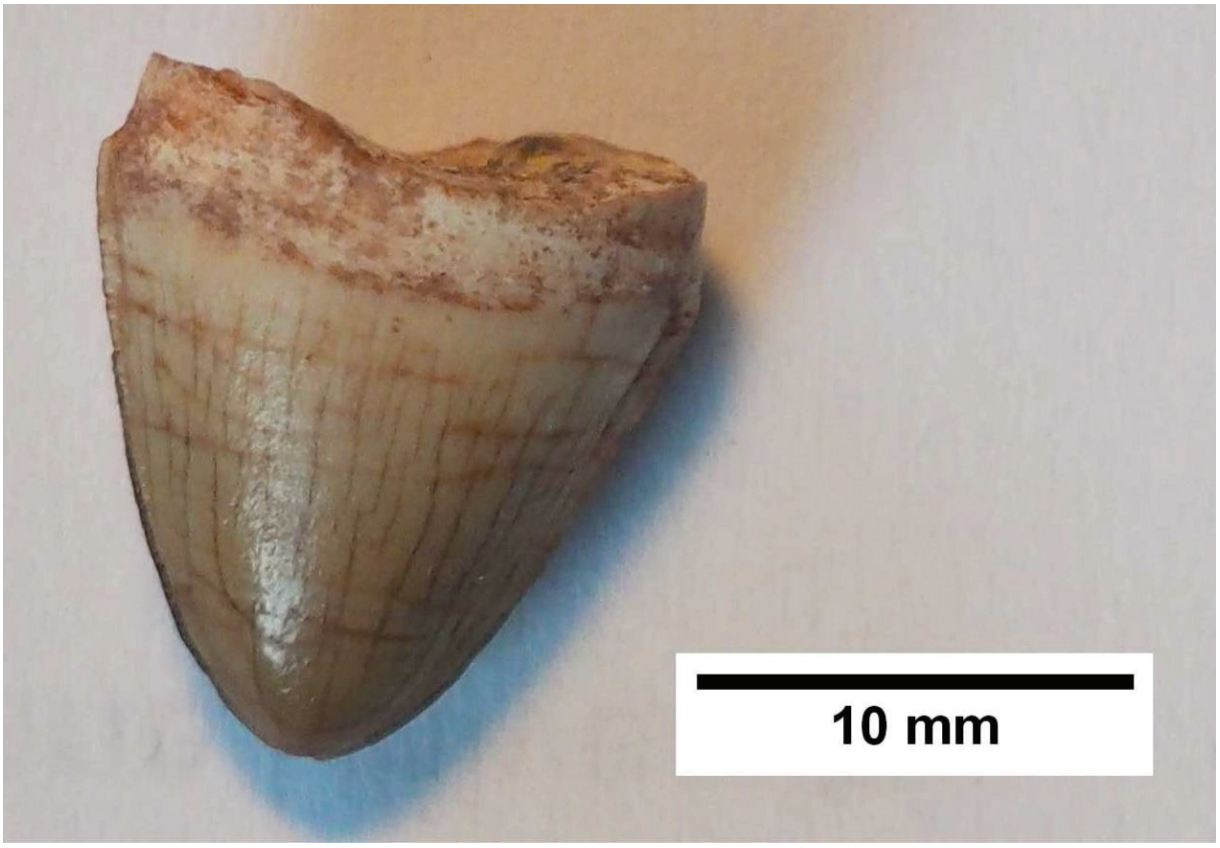

Figure V-1: Picture of sebecid tooth sampled, sample name S1.

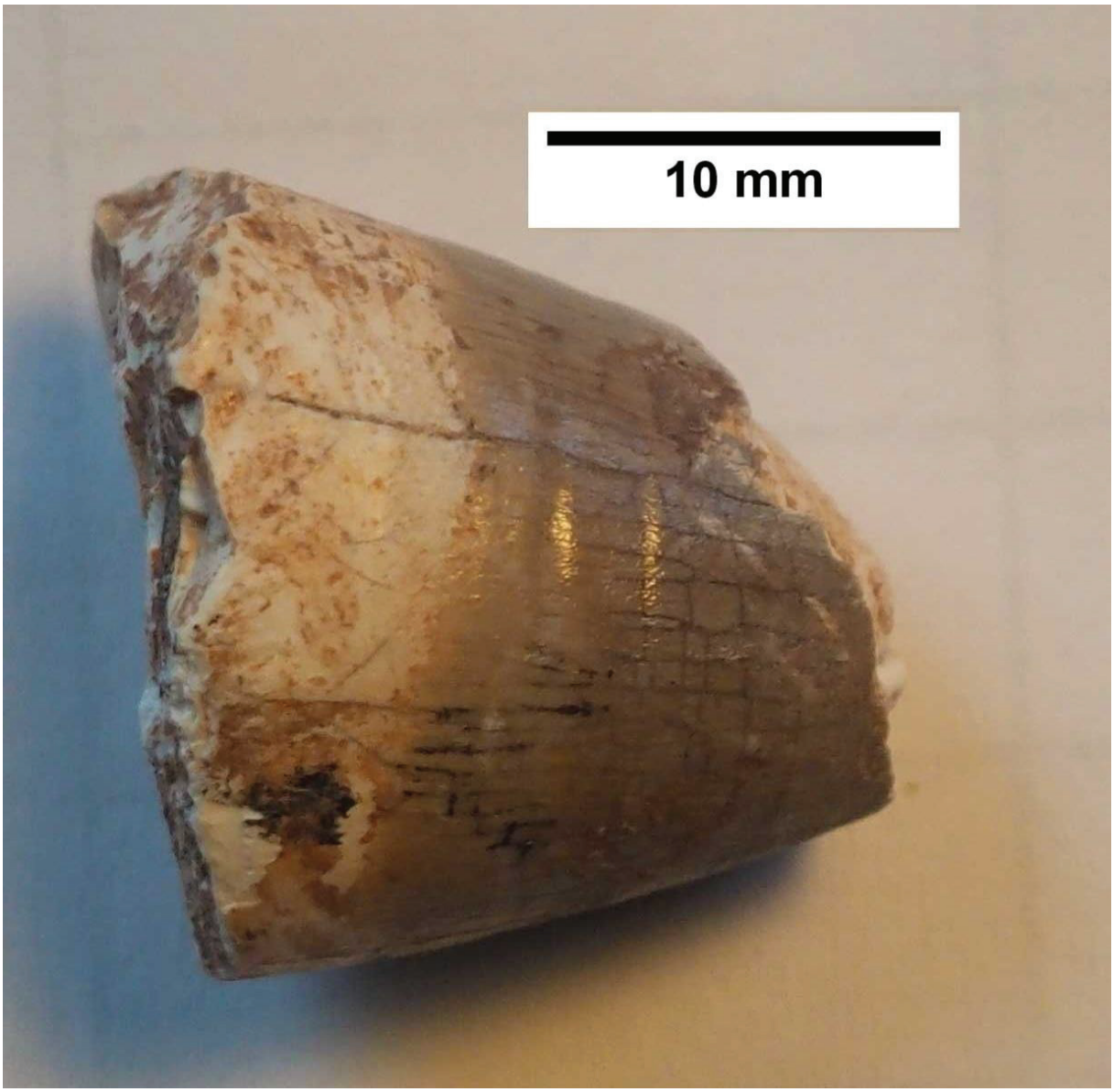

Figure V-2: Picture of sebecid tooth sampled, sample name S2.

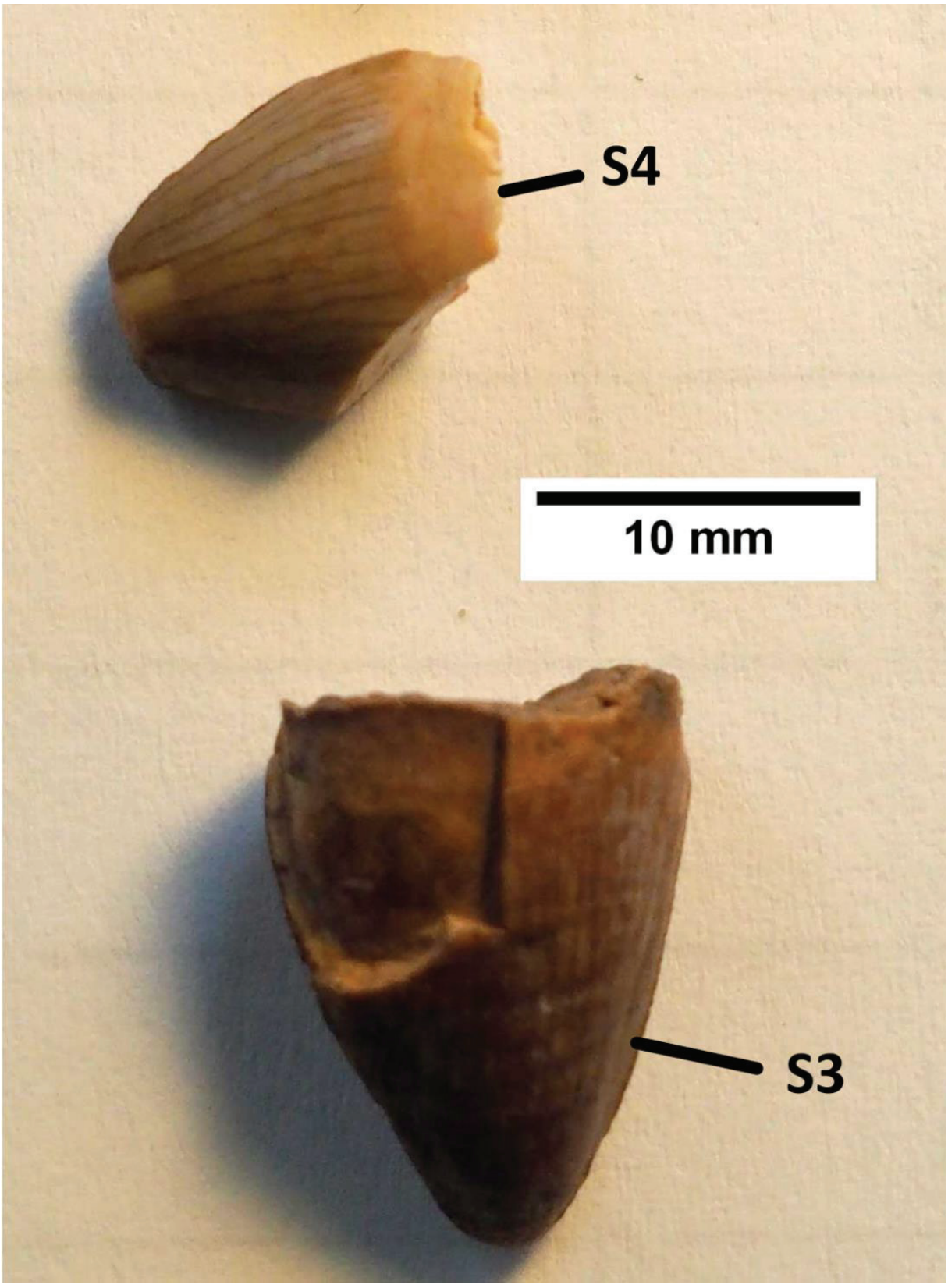

Figure V-3: Picture of sebecid teeth sampled, sample name S3 & S4.

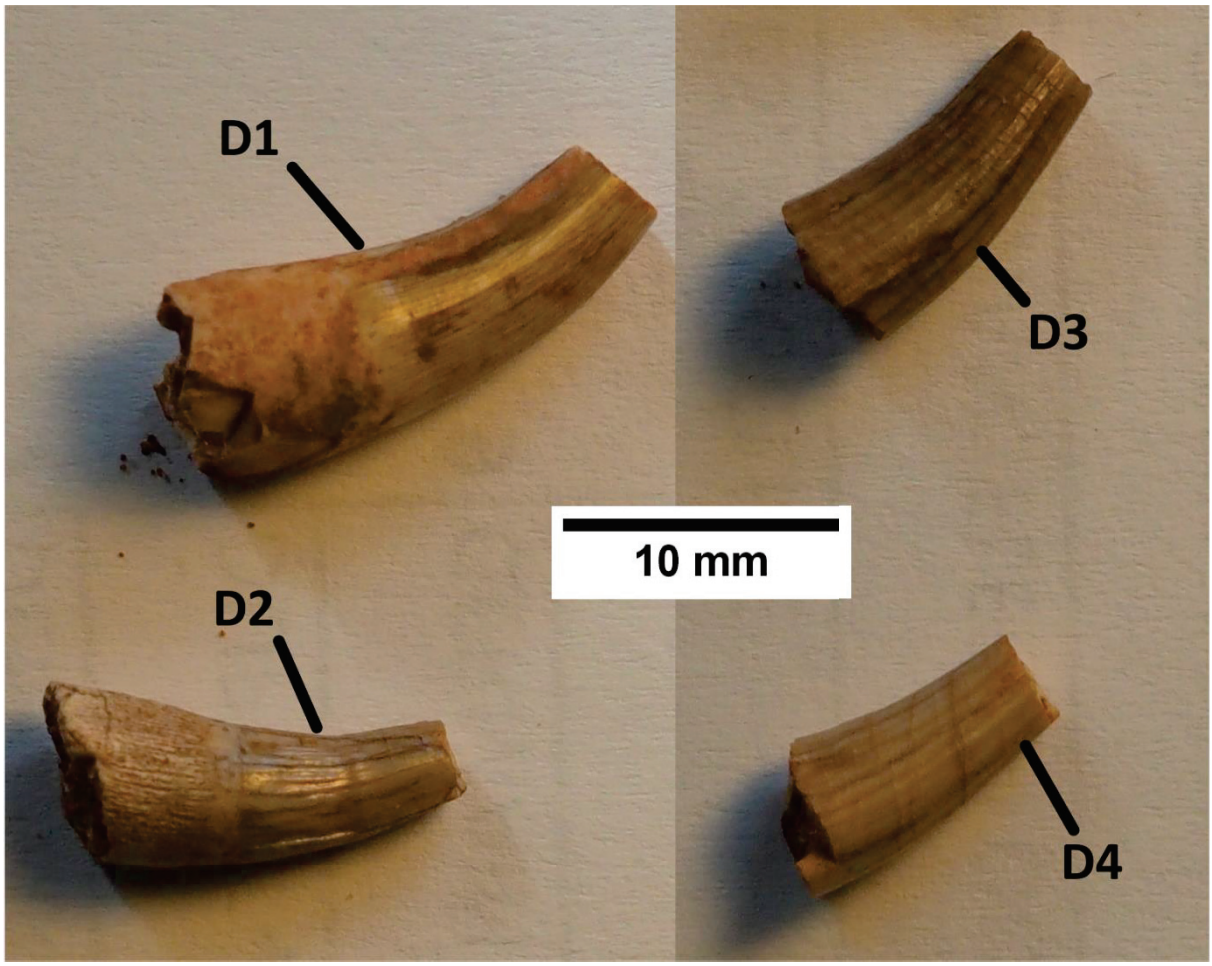

Figure V-4: Picture of dyrosaurid teeth sampled, sample name D1 to D4.

Figure V-5: Picture of fish remains sampled, sample name DE, GA1 & GA2.

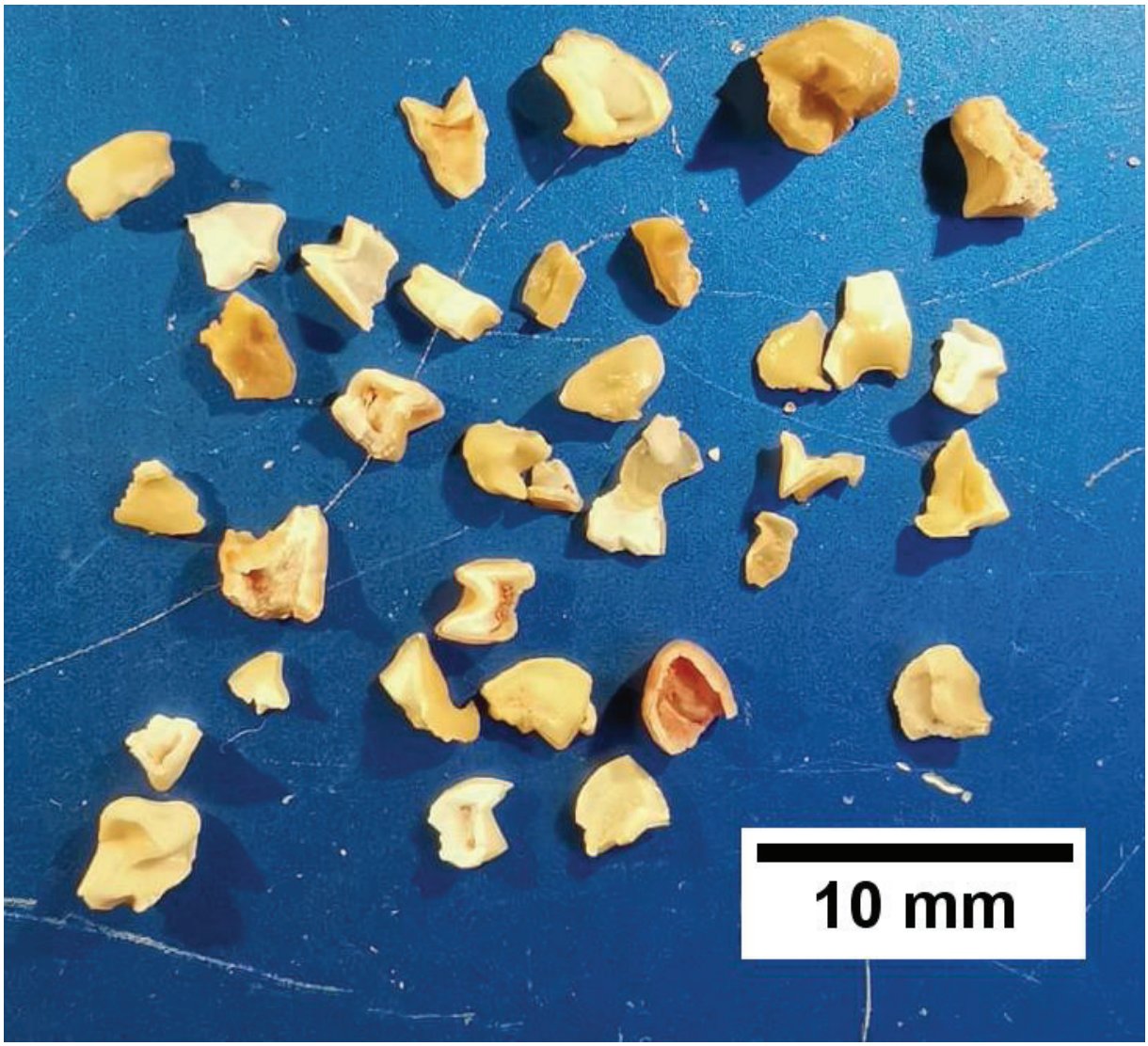

Figure V-6: Picture of mammal teeth sampled, sample name Mmf1 to Mmf4. The specimens were sampled in bulk to compose four different samples.

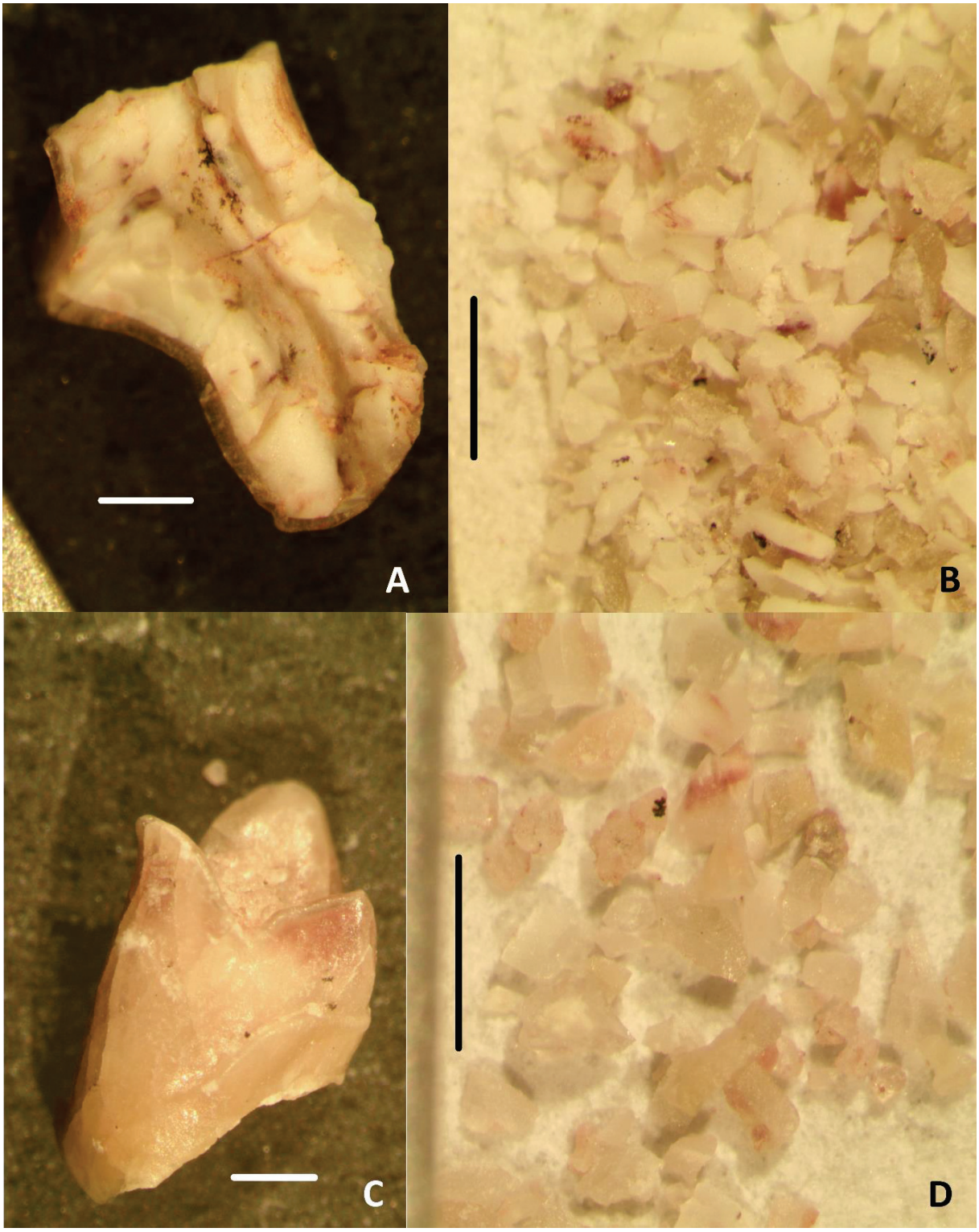

Figure V-7: Picture of mammal teeth sampled, sample name P1: before (A) and after (B) sampling and P2: before (A) and after (B) sampling. Scale bars are 1 cm.

Supplementary Material S2: Geographical and stratigraphical situation of Tiupampa. Red dot is the locality of Tiupampa. Maps is from Google Maps (2023) and Jouve *et al.* (2021; fig. 1), scale bar is 10 km. Stratigraphic scale is modified from Jouve *et al.* (2021; fig. 2):

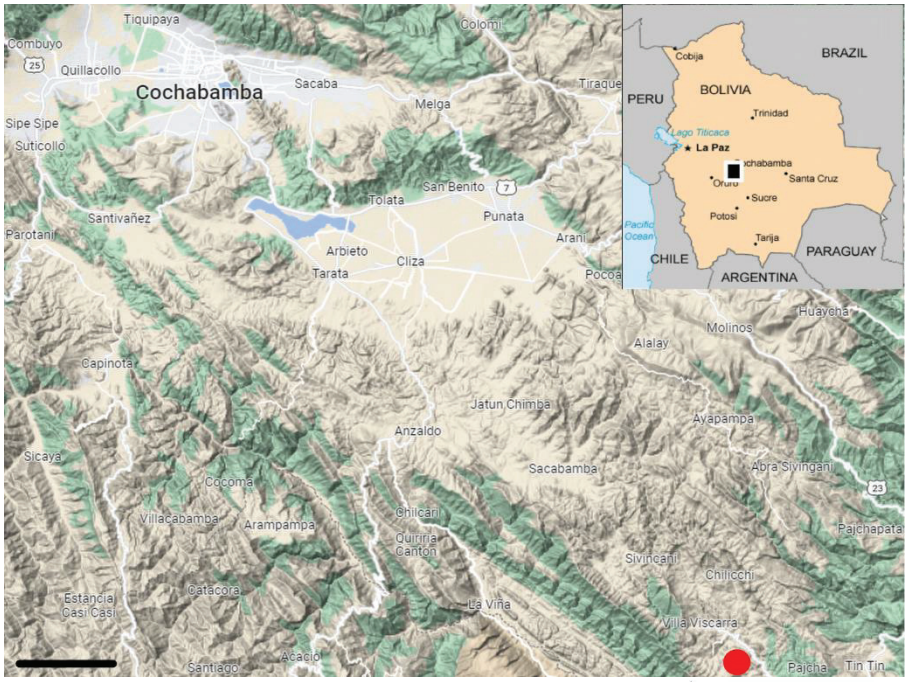

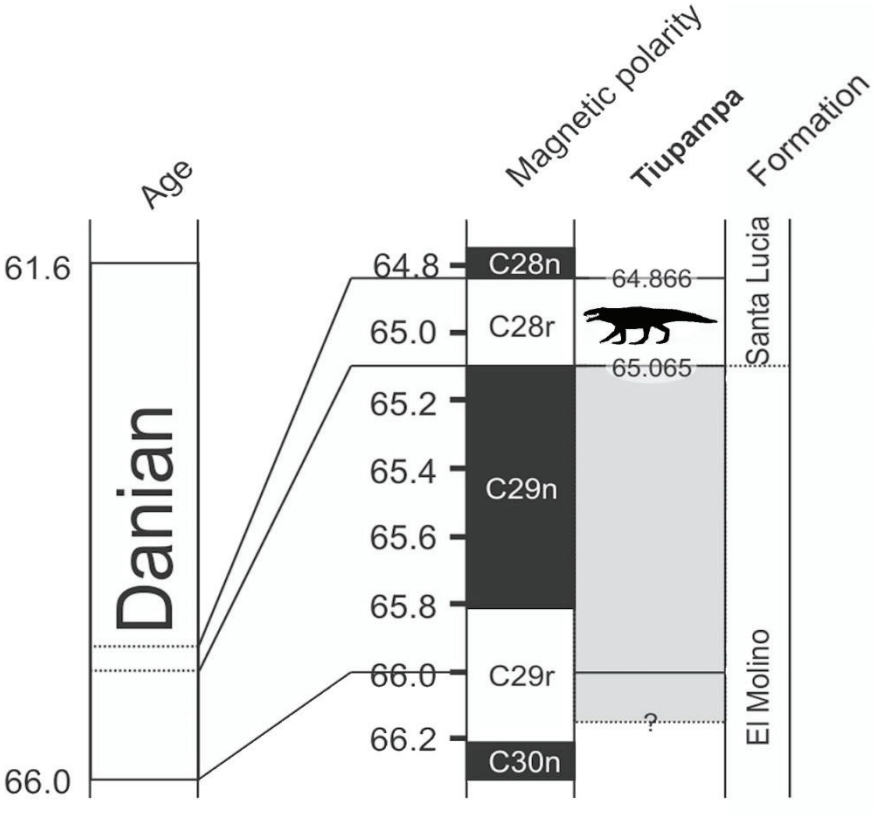

Supplementary Material S3: Detailed protocols and analytical techniques:

Oxygen isotope analysis of biogenic apatite phosphate

This protocol seeks to isolate the phosphate (PO_4^{3-}) from the vertebrate apatite as silver phosphate (Ag_3PO_4) crystals using acid dissolution and anion-exchange resin. For each sample, at least 10 mg of powder was dissolved in 2 mL of 2M HF. The CaF_2 residue was separated by centrifugation and the solution was then neutralized by adding 2.2 mL of 2M KOH. Amberlite™IRN78 anion-exchange resin beads were added to the solution to isolate the PO_4^{3-} ions. After 24h, the solution was removed, the resin was rinsed with double deionized water and eluted with 27.5 mL of 0.5M NH_4NO_3. After 4h, 0.5 mL of NH_4OH and 15 mL of an ammoniacal solution of $AgNO_3$ were added and the solution were placed in a thermostated bath at 70°C for 7h, allowing the precipitation of Ag_3PO_4 crystals, which were then analysed.

Oxygen and carbon isotope analysis of biogenic apatite carbonate

Following the protocol of Koch *et al.* (1997), vertebrate apatite powders were washed with a 2% NaOCl solution to remove organic matter, then rinsed and centrifugated four times with double deionized water. Afterwards, ultrapure acetic acid (0.1 M) was added and left for up to 24h, then the powders were rinsed and centrifugated again four times with double deionized water and air dried at 40°C. For both treatments, the powder/solution ratio was kept constant at 0.04 g/mL.

Calcium and strontium isotope analysis of vertebrate apatite

Leaching

Following the protocol of Balter *et al*. (2002), the samples was submitted to a leaching procedure as follows: the powders were transferred into microcentrifuge tubes (2mL polypropylene) and 500 µL of ultrapure acetic acid (0.1 M) was added and left for 25 min. The powders were then rinsed and centrifugated three times with double deionized water.

Ca and Sr purification and separation

In summary, after the acid attack described in the Material & Methods section, the samples were first loaded in chromatography columns with AG50W-X12 resin to collect only calcium, strontium and iron and discard all other matrix elements. Then, a second separation procedure was performed using chromatography columns with AG50W-X8 resin to collect only calcium

and strontium and remove iron elements. Finally, a third separation procedure using chromatography columns with Sr-Specific resin allowed to separate the calcium from the strontium in the samples. All these steps are explicated in detail in Table 1 below.

Table 1: Protocol for Ca and Sr purification and separation

Step	**Acid**	**Volume (mL)**
1- Matrix removal (using AG50W-X12 resin)		
Wash	6N HCl	4
Conditioning	0.4N HCl	2.5
Load	0.4N HCl	0.2
Elution	0.4N HCl	12.8
	1N HCl	3.5
Recover Ca, Sr, and Fe	6N HCl	2.5
2- Fe removal (using AG50W-X8 resin)		
Wash	H_2O (DD)	15
	0.5N HNO_3	5
	6N HCl	5
Conditioning	6N HCl	5
Load	6N HCl	0.2
Recover Ca and Sr	6N HCl	4.3
Elution	0.5N HNO_3	5

3- **Separation of Ca and Sr** (using Sr-Specific resin)		
Wash	0.5N HNO_3	4
Conditioning	3N HNO_3	2.5
Load	3N HNO_3	0.3
Recover Ca	3N HNO_3	3.2
Recover Sr	0.5N HNO_3	4

Supplementary Material S5: Estimation of mean annual precipitation (MAP):

MAP is estimated through the following equation (Rey *et al*., 2013):

(1) Log_{10} (MAP +300) = 0.092 Δ + 1.148

where MAP: mean annual precipitation (in mm/year).

Furthermore, after Kohn (2010):

(2) $\Delta = (\delta^{13}C_{atm} - \delta^{13}C_{leaf}) / (1 + \delta^{13}C_{leaf} / 1000)$

where $\delta^{13}C_{atm}$: carbon isotope composition of atmosphere (‰V-PDB, estimated using equations 3 to 7) and $\delta^{13}C_{leaf}$ carbon isotope composition of diet (C_3 plants in this study, -22 ‰ V-PDB).

Carbon isotope composition of the atmosphere was estimated through the following equations (Barral *et al*., 2017):

(3) $\delta^{13}C_{atm} = ((\delta^{13}C_{foram} + \varepsilon\ (^{13}C / {}^{12}C)_{DIC/CaCO3} + A + 10^3) / ((\varepsilon\ (^{13}C/^{12}C)_{DIC/CO2} / 10^3) + 1)) - 10^3$

where $\delta^{13}C_{foram}$: carbon isotope composition measured in benthic foraminifera (values taken from Cramer *et al*., 2009); $\varepsilon\ (^{13}C / {}^{12}C)_{DIC/CaCO3}$: carbon isotope fractionation between dissolved inorganic carbon (DIC) and the calcium carbonate of benthic foraminifera (-1‰; Romanek *et*

al., 1992); A: combined factor representing the sum total of disequilibrium effects on carbonate production by benthic foraminifera at high latitudes, associated with the biological pump, the surface water DIC and the subsurface bacterial oxidation of organic matter (2.8‰; Tipple *et al*., 2010) and ε $(^{13}C/^{12}C)_{DIC/CO2}$: carbon isotope fractionation between DIC and atmospheric CO_2.

(4) $\varepsilon\ (^{13}C/^{12}C)_{DIC/CO2} = (0.91\ \varepsilon\ (^{13}C\ /\ ^{12}C)_{HCO3/CO2}) + (0.08\ \varepsilon\ (^{13}C\ /\ ^{12}C)_{CO3/CO2})$

where ε $(^{13}C\ /\ ^{12}C)_{HCO3/CO2}$: fractionation factor for HCO_3^- regarding atmospheric CO_2 and ε $(^{13}C\ /\ ^{12}C)_{CO3/CO2}$: fractionation factor for CO_3^{2-} regarding atmospheric CO_2

(5) $\varepsilon\ (^{13}C\ /\ ^{12}C)_{HCO3/CO2} = -0.1141\ T + 10.78$ (Zhang *et al*., 1995)

where T: foraminiferal calcification temperature (in °C)

(6) $\varepsilon\ (^{13}C\ /\ ^{12}C)_{CO3/CO2} = 0.052\ T + 7.22$ (Zhang *et al*., 1995)

(7) $T = 17 - 4.52\ (\delta^{18}O_{foram} - \delta^{18}O_{H2O}) + 0.03\ (\delta^{18}O_{foram} - \delta^{18}O_{H2O})^2$ (Erez & Luz, 1983)

where $\delta^{18}O_{foram}$: oxygen isotope composition measured in benthic foraminifera (values taken from Cramer *et al*., 2009); $\delta^{18}O_{H2O}$: oxygen isotope composition of seawater (-1‰; Lécuyer *et al*., 2013; Martin *et al*., 2014).

References

Balter V., Saliège J. F., Bocherens H. & Person A. (2002). Evidence of physico–chemical and isotopic modifications in archaeological bones during controlled acid etching. *Archaeometry,* 44(3): 329-336. https://doi.org/10.1111/1475-4754.t01-1-00065

Barral A., Gomez B., Legendre S. & Lécuyer C. (2017). Evolution of the carbon isotope composition of atmospheric CO2 throughout the Cretaceous. *Palaeogeography, Palaeoclimatology, Palaeoecology*, 471, 40-47. https://doi.org/10.1016/j.palaeo.2017.01.034

Cramer B. S., Toggweiler J. R., Wright J. D., Katz M. E. & Miller K. G. (2009). Ocean overturning since the Late Cretaceous: Inferences from a new benthic foraminiferal isotope compilation. *Paleoceanography*, 24(4): 1-14. https://doi.org/10.1029/2008PA001683

Erez J. & Luz B. (1983). Experimental paleotemperature equation for planktonic foraminifera. *Geochimica et Cosmochimica Acta*, 47(6), 1025-1031. https://doi.org/10.1016/0016-7037(83)90232-6

Jouve S., Muizon C. d., Cespedes-Paz R., Sossa-Soruco V. & Knoll S. (2021). The longirostrine crocodyliforms from Bolivia and their evolution through the Cretaceous–Palaeogene boundary. *Zoological Journal of the Linnean Society*, 192(2): 475-509. https://doi.org/10.1093/zoolinnean/zlaa081

Koch P. L., Tuross N. & Fogel M. L. (1997). The effects of sample treatment and diagenesis on the isotopic integrity of carbonate in biogenic hydroxylapatite. *Journal of Archaeological Science*, 24(5): 417-429. https://doi.org/10.1006/jasc.1996.0126

Kohn M. J. (2010). Carbon isotope compositions of terrestrial C3 plants as indicators of (paleo) ecology and (paleo) climate. *Proceedings of the National Academy of Sciences*, 107(46), 19691-19695. https://doi.org/10.1073/pnas.1004933107

Lécuyer C., Amiot R., Touzeau A. & Trotter J. (2013). Calibration of the phosphate δ18O thermometer with carbonate–water oxygen isotope fractionation equations. *Chemical Geology*, 347, 217-226. https://doi.org/10.1016/j.chemgeo.2013.03.008

Martin J. E., Amiot R., Lécuyer C. & Benton M. J. (2014). Sea surface temperature contributes to marine crocodylomorph evolution. Nature communications, 5(1), 1-7. https://doi.org/10.1038/ncomms5658

Rey K., Amiot R., Lécuyer C., Koufos G. D., Martineau F., Fourel F., Kostopoulos D.S. & Merceron G. (2013). Late Miocene climatic and environmental variations in northern Greece inferred from stable isotope compositions (δ18O, δ13C) of equid teeth apatite. *Palaeogeography, Palaeoclimatology, Palaeoecology*, 388: 48-57. https://doi.org/10.1016/j.palaeo.2013.07.021

Romanek C. S., Grossman E. L. & Morse J. W. (1992). Carbon isotopic fractionation in synthetic aragonite and calcite: effects of temperature and precipitation rate. *Geochimica et Cosmochimica acta*, 56(1), 419-430. https://doi.org/10.1016/0016-7037(92)90142-6

Tipple B. J., Meyers S. R. & Pagani M. (2010). Carbon isotope ratio of Cenozoic CO2: A comparative evaluation of available geochemical proxies. *Paleoceanography*, 25(3): 1-11. https://doi.org/10.1029/2009PA001851

Zhang J., Quay P. D. & Wilbur D. O. (1995). Carbon isotope fractionation during gas-water exchange and dissolution of CO2. *Geochimica et Cosmochimica Acta*, 59(1): 107-114. https://doi.org/10.1016/0016-7037(95)91550-D

Appendix 6: Information related to the multi-isotopic studies of Réalmont, Aumelas and El Kohol

Réalmont (France)

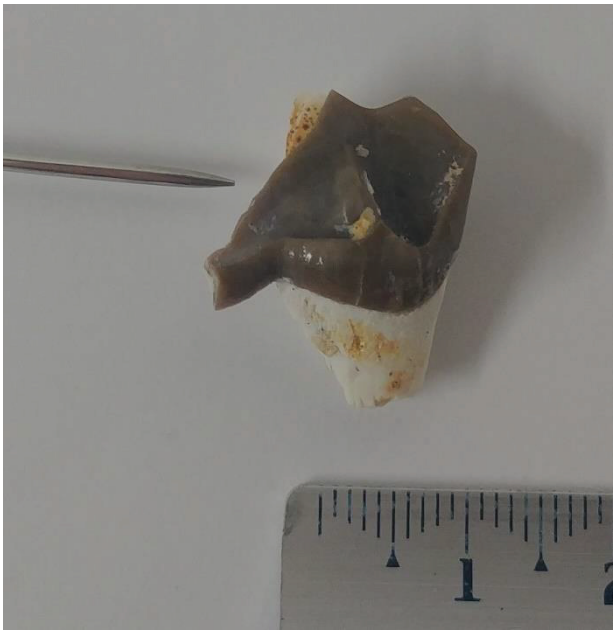

Figure VI-1: Rea 1 before sampling.

Figure VI-2: Rea 1 after sampling.

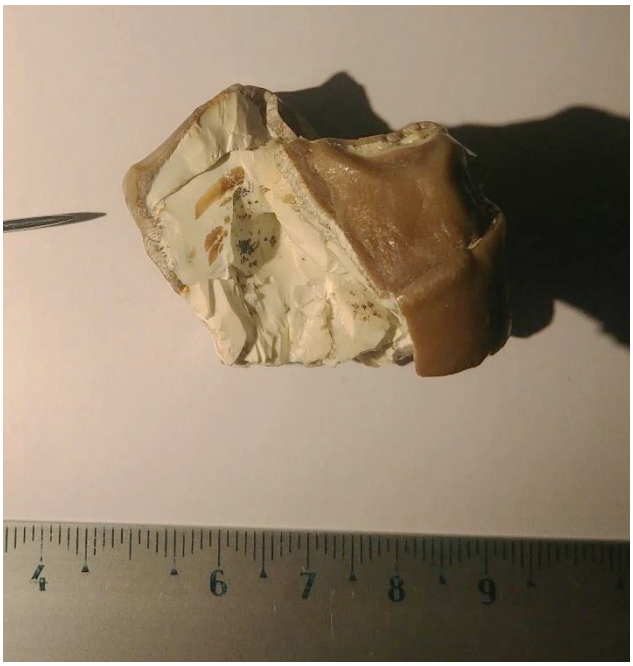

Figure VI-3: Rea 2 before sampling.

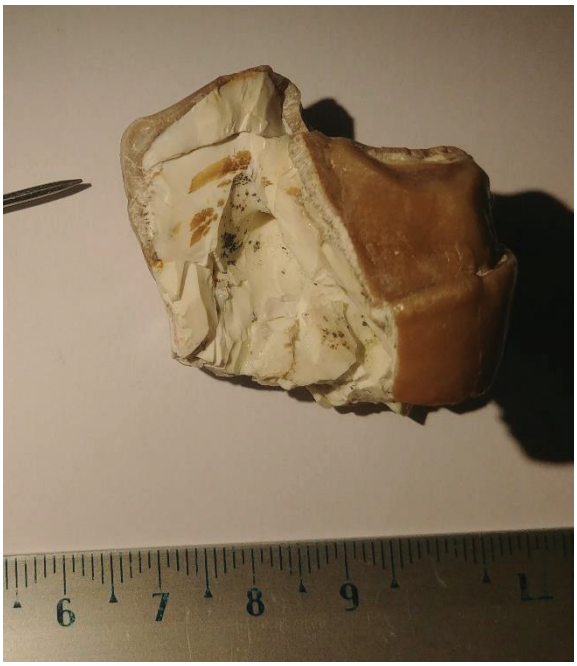

Figure VI-4: Rea 2 after sampling.

Figure VI-5: Rea 3 before sampling.

Figure VI-6: Rea 3 after sampling.

Figure VI-7: Rea 4 before sampling.

Figure VI-8: Rea 4 after sampling.

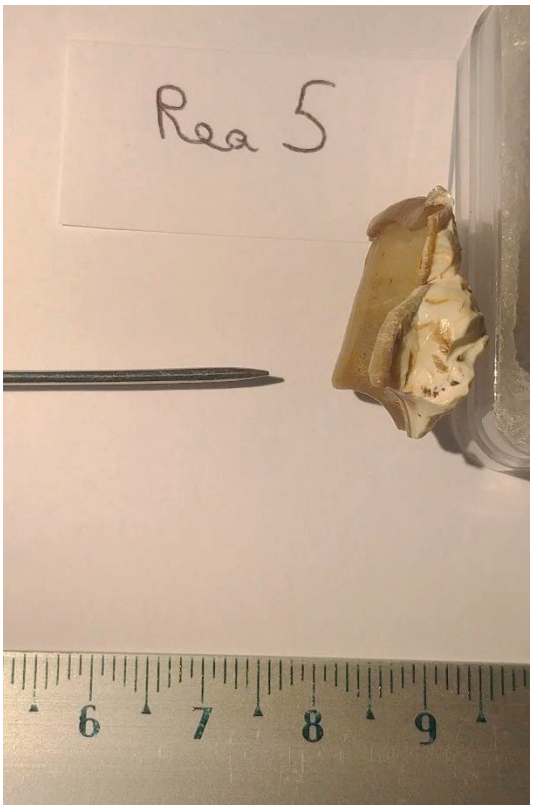

Figure VI-9: Rea 5 before sampling.

Figure VI-10: Rea 5 after sampling.

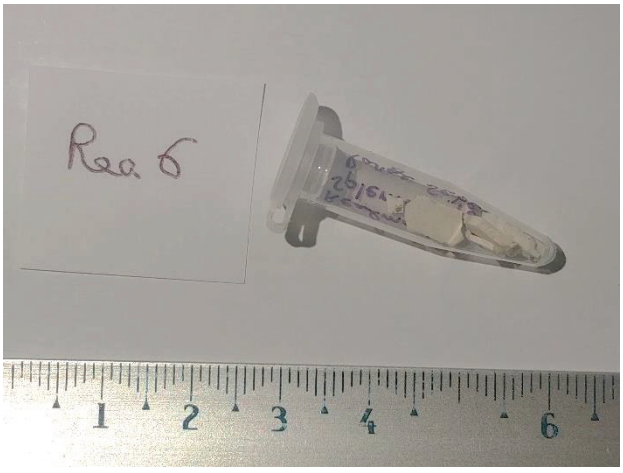

Figure VI-11: Rea 6 before sampling.

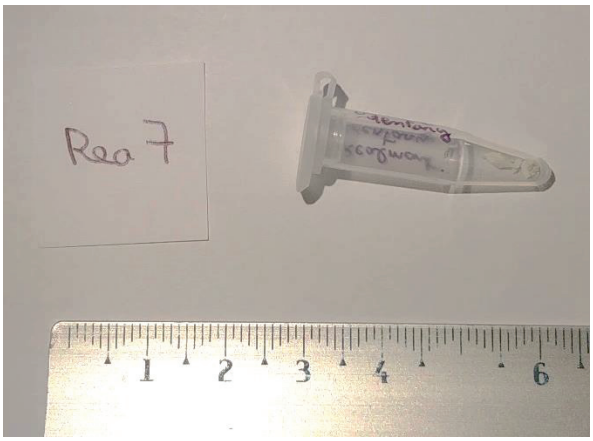

Figure VI-12: Rea 7 before sampling.

Figure VI-13: Rea 8 before sampling.

Figure VI-14: Rea 8 after sampling.

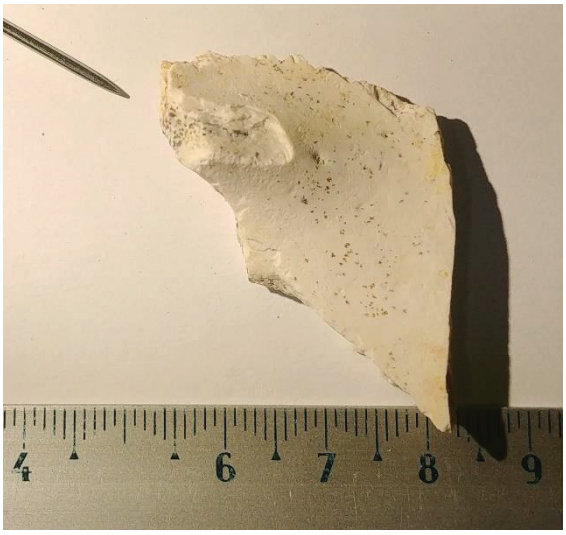

Figure VI-15: Rea 9 before sampling.

Figure VI-16: Rea 9 after sampling.

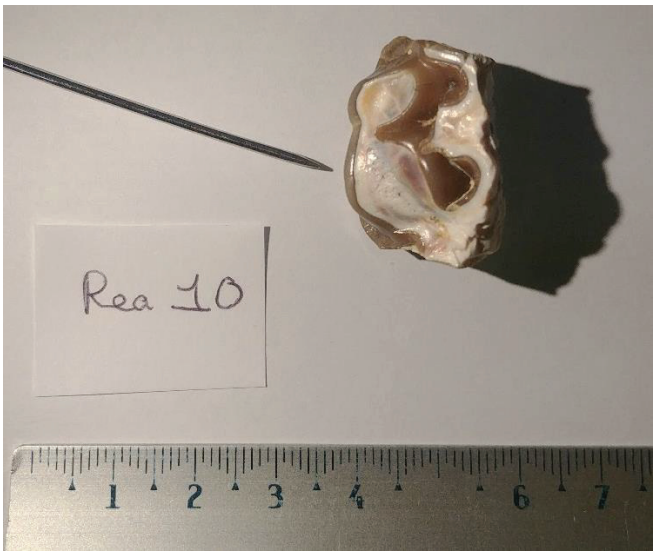

Figure VI-17: Rea 10 before sampling.

Figure VI-18: Rea 10 after sampling.

Aumelas (France)

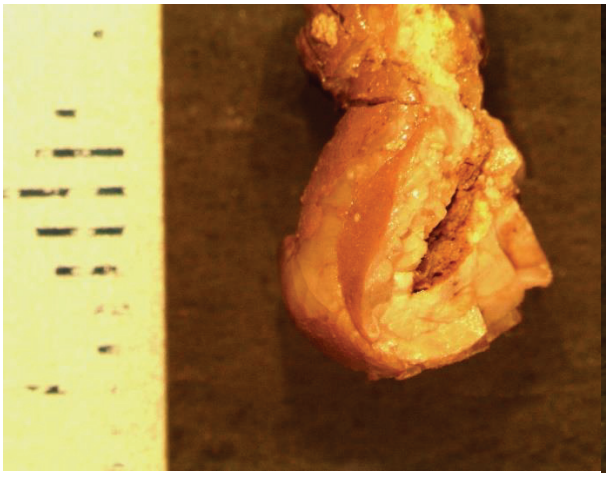

Figure VI-19: Aum180 before sampling.

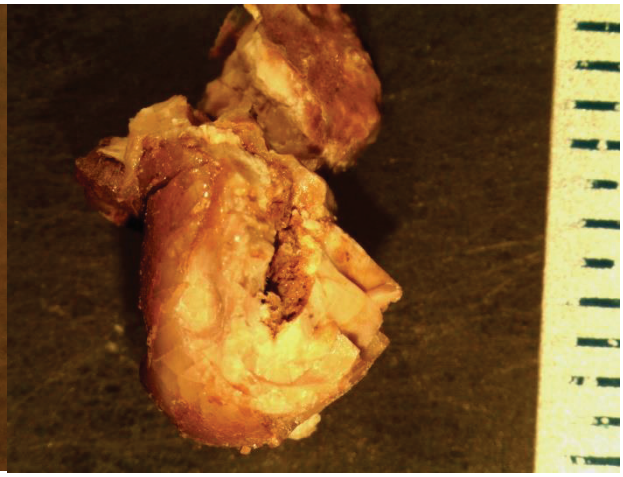

Figure VI-20: Aum180 after sampling.

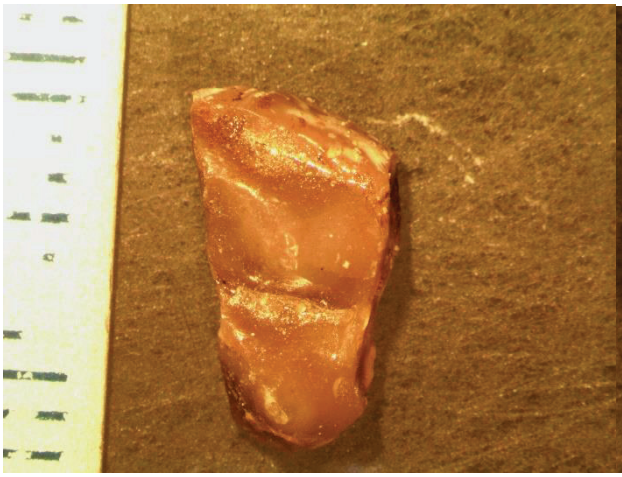

Figure VI-21: Aum1873A before sampling.

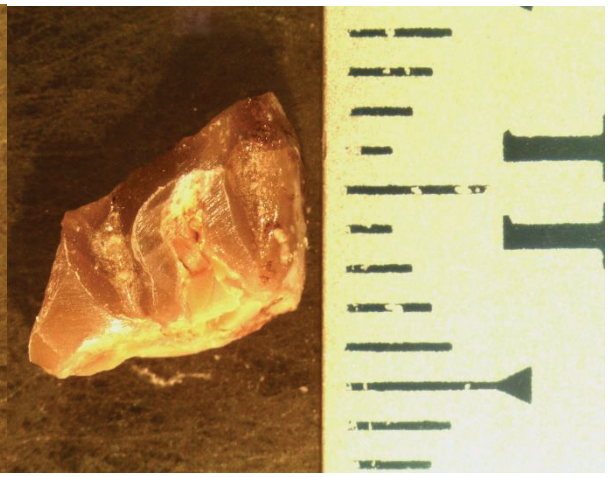

Figure VI-22: Aum1873A after sampling.

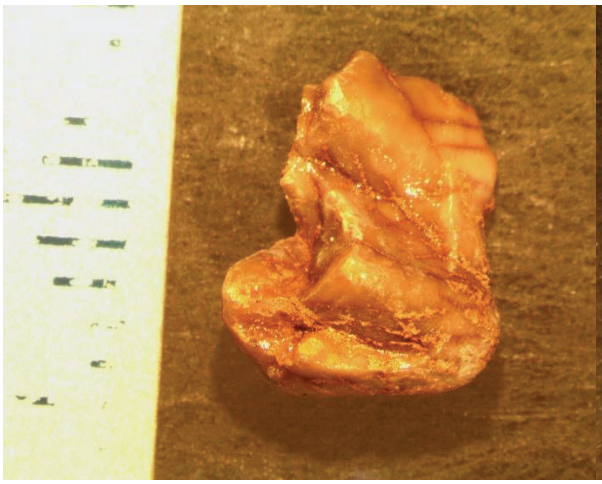

Figure VI-23: Aum1873B before sampling.

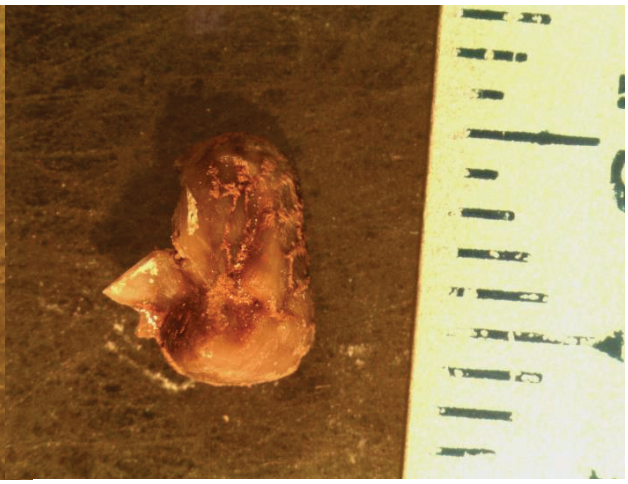

Figure VI-24: Aum1873B after sampling.

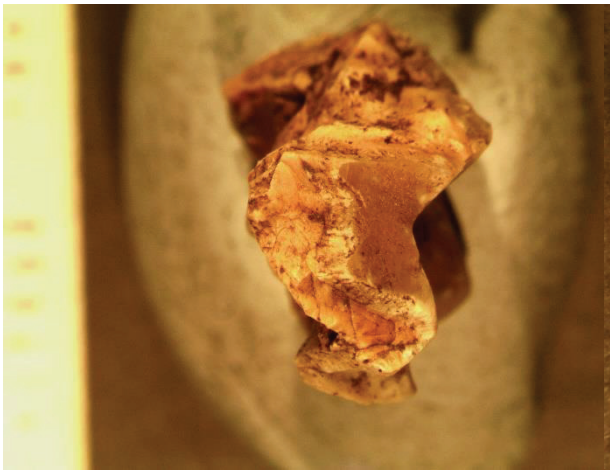

Figure VI-25: Aum1873C before sampling.

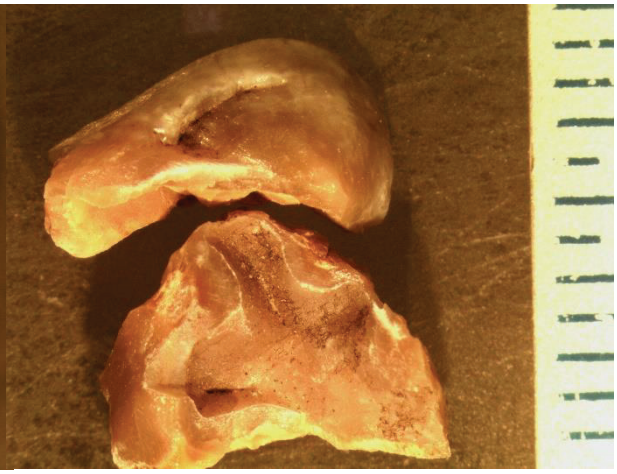

Figure VI-26: Aum1873C after sampling.

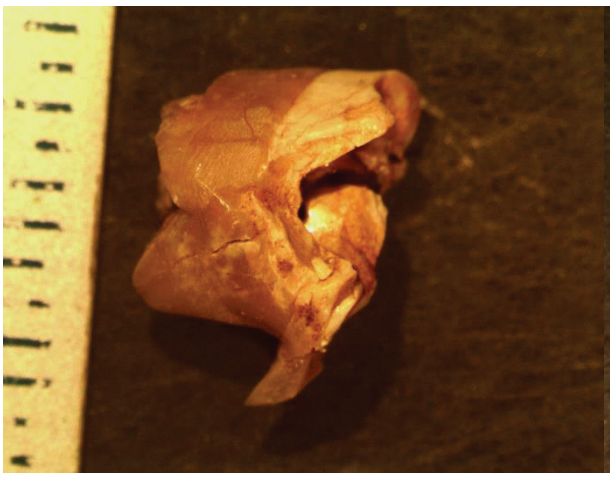

Figure VI-27: Aum1872 before sampling.

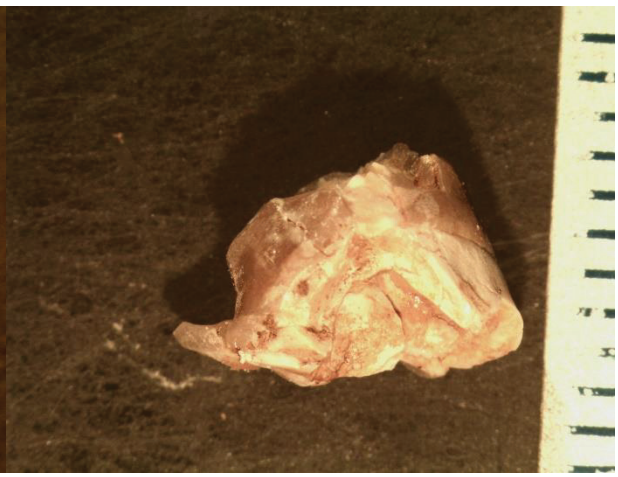

Figure VI-28: Aum1872 after sampling.

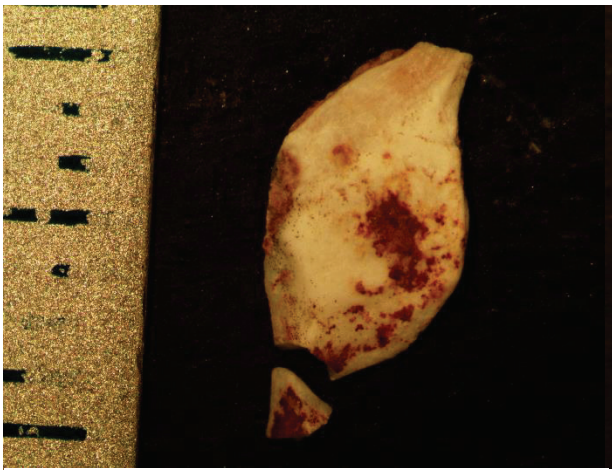

Figure VI-29: KD1 before sampling.

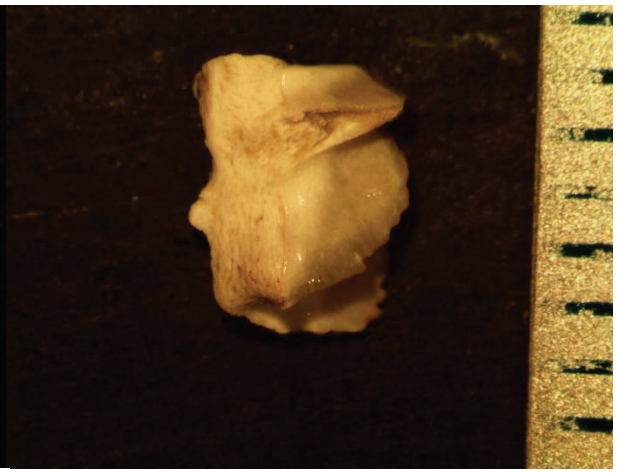

Figure VI-30: KD2 before sampling.

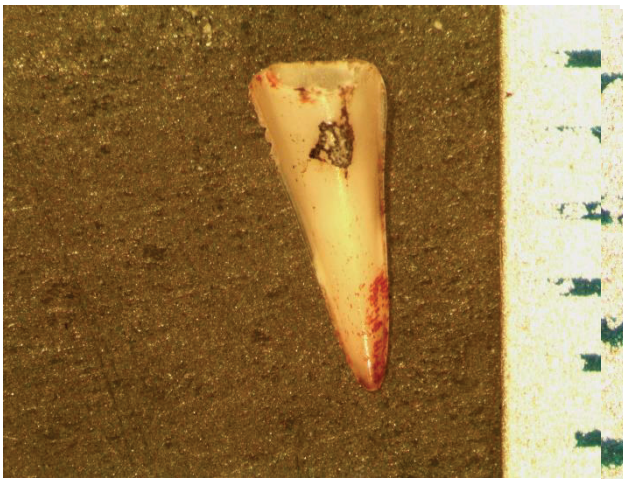

Figure VI-31: KD3 before sampling.

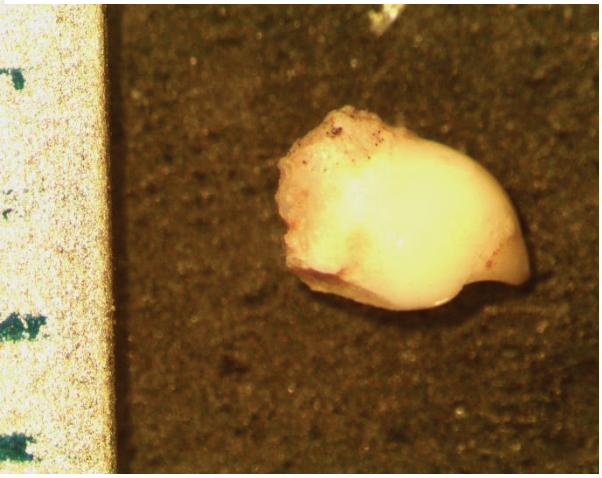

Figure VI-32: KD4 before sampling.

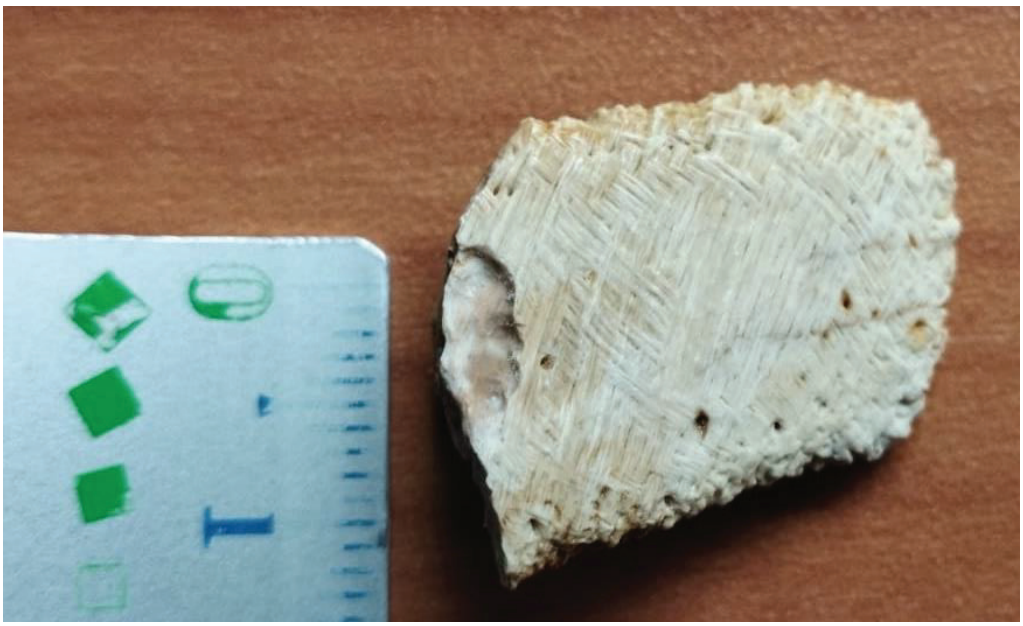

Figure VI-33: AI after sampling.

El Kohol (Algeria)

Figure VI-34: KABC-05 before sampling.

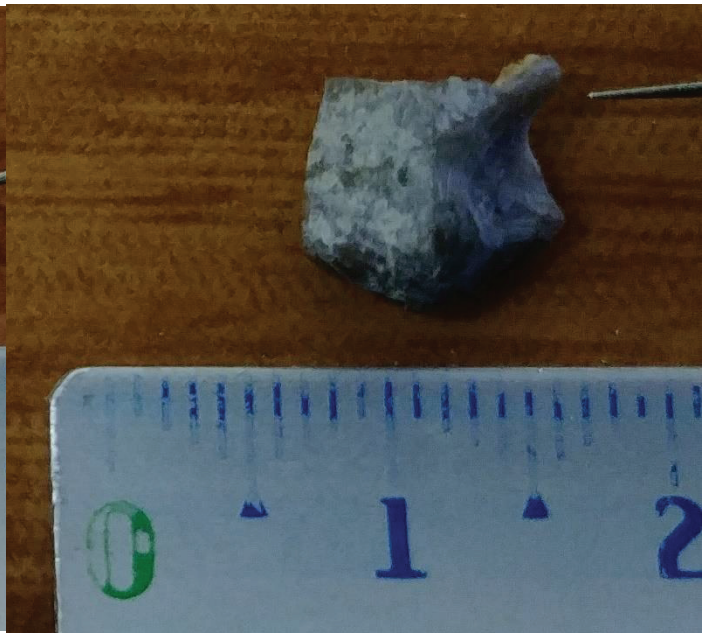

Figure VI-35: KABC-05 after sampling.

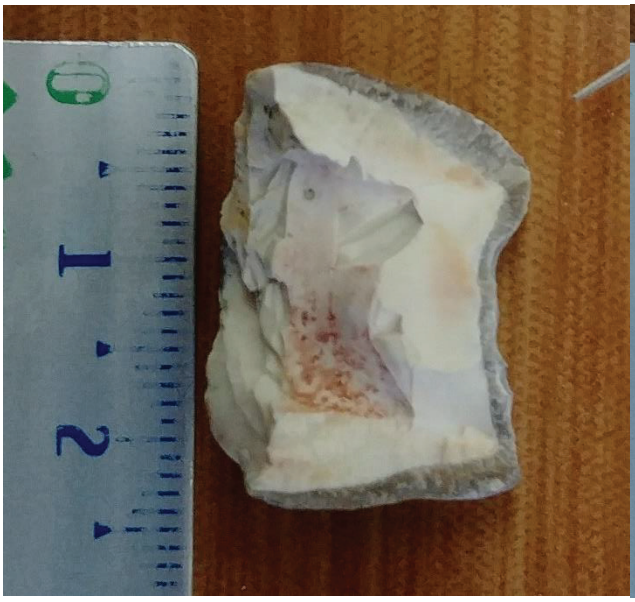

Figure VI-36: KABC-06 before sampling.

Figure VI-37: KABC-06 after sampling.

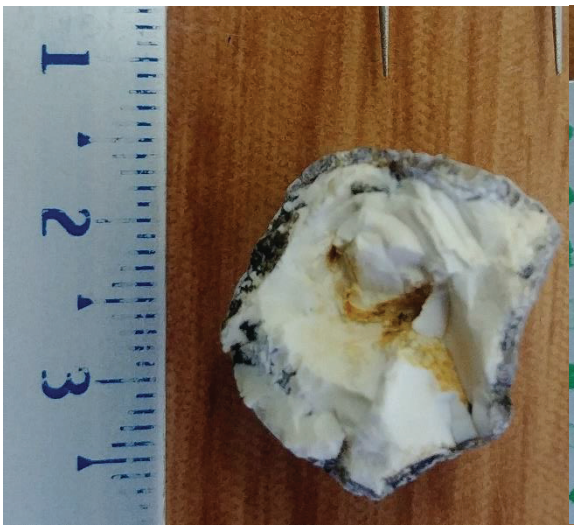

Figure VI-38: KABC-07 before sampling.

Figure VI-39: KABC-07 after sampling.

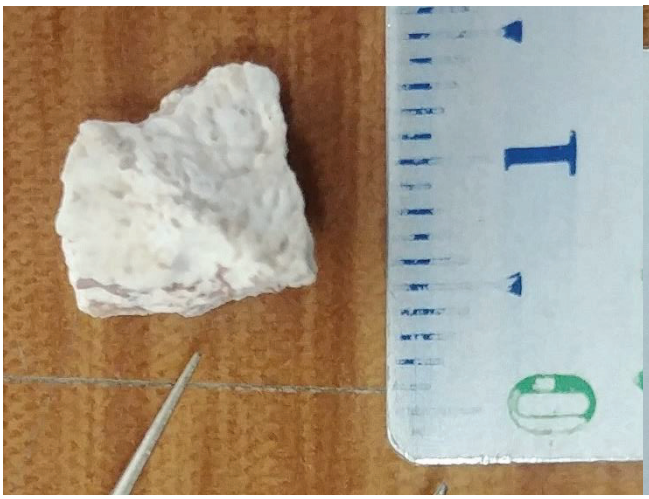

Figure VI-40: KDE before sampling.

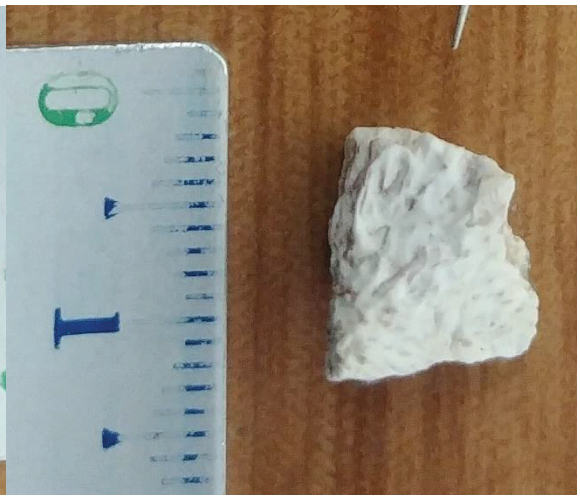

Figure VI-41: KDE after sampling.

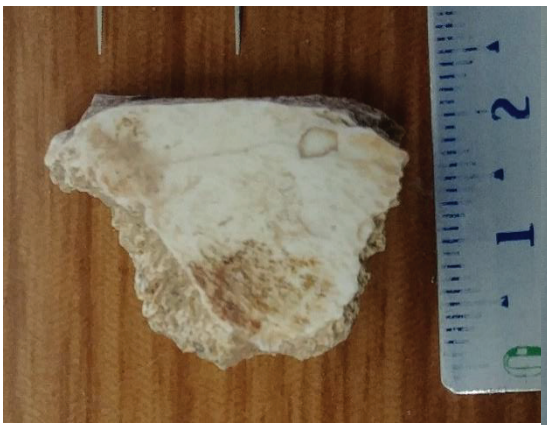

Figure VI-42: KDT before sampling.

Figure VI-43: KDT after sampling.

Appendix 7: List of specimens scanned and segmented in this thesis, with scan information

Taxon	Specimen	Scanner	Scan parameters	Voxel size	Worker*	Length/width of skull (cm)
Alligator mississippiensis	UCBL WB35	GE Phoenix X-Ray GmbH (INSA Lyon)	140 kV, 80 µA, 1500 projections with 0.667s exposure time	70 μm^3	Y. P., G. P. & D. C.	26.0/13.8
Alligator mississippiensis	MHNL 50002667	DTHE RX Solutions (INSA Lyon)	280 kV, 254 µA, 2240 projections	68 μm^3	Y. P.	13.3/7.1
Alligator mississippiensis	MHNL 50001401	DTHE RX Solutions (INSA Lyon)	280 kV, 282 µA, 2240 projections	78 μm^3	Y. P.	42.5/22.5
Alligator sinensis	IRSNB 3487	DTHE RX Solutions	280 kV, 283 µA, 2240 projections	75 μm^3	Y. P.	24.5/15.5
Alligator sinensis	NHMW-Zoo-HS-4219	YXLON FF 35 CT	100 kV, 310 µA, 3600 projections with 1s exposure time	81 μm^3	Y. P.	15.8/5.24
Alligator sinensis	NHMW-Zoo-HS-12511	YXLON FF 35 CT	120 kV, 140 µA, 3600 projections with 1s exposure time	37 μm^3	Y. P.	10.3/4.3
Alligator sinensis	NHMW-Zoo-HS-12512	YXLON FF 35 CT	121 kV, 141 µA, 3600 projections with 1s exposure time	42 μm^3	Y. P.	9/3.5
Alligator sinensis	NHMW-Zoo-HS-37966	YXLON FF 35 CT	140 kV, 130 µA, 3600 projections with 1s exposure time	84 μm^3	Y. P.	22.3/14.4

Taxon	Specimen	Scanner	Scan parameters	Voxel size	Worker*	Length/width of skull (cm)
Caiman crocodilus	UM unnumbered	RX Solutions EasyTom 150 (ISEM)	90 kV, 260 µA, 1440 projections	24 μm^3	Y. P.	4.9/2.3
Caiman yacare	IRSNB 13521	DTHE RX Solutions (INSA Lyon)	280 kV, 357 µA, 2240 projections	101 μm^3	Y. P.	22.5/13.0
Crocodylus acutus	MZS Cro055	GE Phoenix X-Ray GmbH (INSA Lyon)	140 kV, 80 µA, 1500 projections with 0.667s exposure time	87 μm^3	G. P., N. R. & D. C.	52.5/25.8
Crocodylus acutus	IRSNB 13235	DTHE RX Solutions (INSA Lyon)	280 kV, 282 µA, 2240 projections	82 μm^3	Y. P.	40.0/20.3
Crocodylus acutus	NHMUK 1964.1999-2002	Nikon Metrology XT H 225 ST (NHMUK)	90 kV, 200 µA	25 μm^3	Y. P.	5.6/2.7
Crocodylus acutus	NHMUK 1862.1.272	Nikon Metrology XT H 225 ST (NHMUK)	?	50 μm^3	Y. P.	16.8/NA
Crocodylus intermedius	MNHN-ZA-AC-1885-489	DTHE RX Solutions (INSA Lyon)	280 kV, 453 µA, 2240 projections	10 μm^3	Y. P.	63.5/32.5
Crocodylus intermedius	MNHN-ZA-AC-1885-490	DTHE RX Solutions (INSA Lyon)	280 kV, 453 µA, 2240 projections	10 μm^3	Y. P.	57.4/27.7

Taxon	Specimen	Scanner	Scan parameters	Voxel size	Worker*	Length/width of skull (cm)
Crocodylus intermedius	NHMUK 1856.2.18.3	Nikon Metrology XT H 225 ST (NHMUK)	90 kV, 200 µA	55 μm^3	Y. P.	10.0/4.3
Crocodylus johnstoni	NHMUK 1926.2.25.129	Nikon Metrology XT H 225 ST (NHMUK)	220 kV, 185 µA	98 μm^3	Y. P.	25.0/9.1
Crocodylus mindorensis	NHMUK 1877.12.13.20	Nikon Metrology XT H 225 ST (NHMUK)	200 kV, 450 µA	35 μm^3	Y. P.	8.0/3.8
Crocodylus moreletii	NHMUK 1973.24.96	Nikon Metrology XT H 225 ST (NHMUK)	?	55 μm^3	Y. P.	12.0/5.7
Crocodylus niloticus	MHNL 90001850	GE Phoenix X-Ray GmbH (INSA Lyon)	120 kV, 120 µA, 1200 projections with 0.5s exposure	50 μm^3	G. P. & Y. P.	12.5/6.2
Crocodylus niloticus	MHNL 90001851	GE Phoenix X-Ray GmbH (INSA Lyon)	140 kV, 80 µA, 1200 projections with 0.5s exposure time	50 μm^3	J. M., G. P. & Y. P.	10.1/4.4
Crocodylus niloticus	MHNL 90001855	GE Phoenix X-Ray GmbH (INSA Lyon)	140 kV, 80 µA, 1200 projections with 0.5s exposure time	60 μm^3	J. M., G. P. & Y. P.	13.4/5.9

Taxon	Specimen	Scanner	Scan parameters	Voxel size	Worker*	Length/width of skull (cm)
Crocodylus niloticus	UM 2001-1756-1-434NR	RX Solutions EasyTom 150 (ISEM)	80 kV, 380 µA, 1440 projections	78 µm^3	G. P.	21.1/9.8
Crocodylus niloticus	MHNL 50001405	DTHE RX Solutions (INSA Lyon)	290 kV, 340 µA, 2240 projections with 0.167s exposure time	102 µm^3	J. M., Y. P. & D. C.	61.0/38.5
Crocodylus niloticus	MHNL 50001397	DTHE RX Solutions (INSA Lyon)	290 kV, 294 µA, 2240 projections with 0.111s exposure time	90 µm^3	J. M., Y. P. & D. C.	45.0/28.0
Crocodylus niloticus	MHNL 50001395	DTHE RX Solutions (INSA Lyon)	290 kV, 329 µA, 2240 projections	102 µm^3	D. C. & Y. P.	20.5/9.3
Crocodylus niloticus	MHNL 50001399	DTHE RX Solutions (INSA Lyon)	290 kV, 320 µA, 4480 projections	102 µm^3	Y. P.	36.2/20.5
Crocodylus niloticus	MHNL 50001388	GE Phoenix X-Ray GmbH (INSA Lyon)	140 kV, 80 µA, 1500 projections with 1s exposure time	82 µm^3	G. P.	42.0/25.4
Crocodylus niloticus	NHMUK 1894.6.5.33	Nikon Metrology XT H 225 ST (NHMUK)	220 kV, 636 µA	90 µm^3	J. M., D. C. & Y. P.	56.0/38.5

Taxon	Specimen	Scanner	Scan parameters	Voxel size	Worker*	Length/width of skull (cm)
Crocodylus niloticus	MHNT.PAL.2013.0.1004.1	DTHE RX Solutions (INSA Lyon)	280 kV, 453 µA, 2240 projections	100 μm^3	Y. P.	NA/27.0
Crocodylus novaeguineae	BMNH 1886.5.20.1	Nikon Metrology XT H 225 ST (NHMUK)	155 kV, 171 µA	66 μm^3	Y. P.	25.0/13.1
Crocodylus palustris	MHNL 50001398	DTHE RX Solutions (INSA Lyon)	290 kV, 329 µA, 2240 projections	102 μm^3	G. P., D. C. & Y. P.	47.5/31.4
Crocodylus palustris	NHMUK 1905.3.25.1	Nikon Metrology XT H 225 ST (NHMUK)	90 kV, 200 µA	22 μm^3	Y. P.	5.0/2.4
Crocodylus palustris	BMNH 1848.2.5.9	Nikon Metrology XT H 225 ST (NHMUK)	?	66 μm^3	Y. P.	24.5/13.7
Crocodylus palustris	BMNH 1852.5.9.46	Nikon Metrology XT H 225 ST (NHMUK)	210 kV, 174 µA	76 μm^3	Y. P.	35.0/15.6
Crocodylus porosus	MHNL 50001402	DTHE RX Solutions (INSA Lyon)	290 kV, 329 µA, 2240 projections	100 μm^3	D. C., Y. P. & G. P.	52.0/27.2

Taxon	Specimen	Scanner	Scan parameters	Voxel size	Worker*	Length/width of skull (cm)
Crocodylus porosus	NHMUK 1882.1.267	Nikon Metrology XT H 225 ST (NHMUK)	?	41 µm^3	Y. P.	14.5/6.0
Crocodylus rhombifer	MHNL 42006506	GE Phoenix X-Ray GmbH (INSA Lyon)	120 kV, 120 µA, 1200 projections with 0.5s exposure time	86 µm^3	Y. P.	21.8/12.9
Crocodylus rhombifer	MHNL 42006507	GE Phoenix X-Ray GmbH (INSA Lyon)	120 kV, 120 µA, 1200 projections with 0.5s exposure time	86 µm^3	Y. P.	23.4/13.0
Crocodylus rhombifer	NHMUK 51.3.18.27	Nikon Metrology XT H 225 ST (NHMUK)	90 kV, 200 µA	29 µm^3	Y. P.	5.0/3.1
Crocodylus siamensis	MHNL 50001390	DTHE RX Solutions (INSA Lyon)	280 kV, 500 µA, 2240 projections with 0.167s exposure	100 µm^3	Y. P. & D. C.	43.0/23.4
Crocodylus siamensis	UCBL WB41	GE Phoenix X-Ray GmbH (INSA Lyon)	140 kV, 80 µA, 1500 projections with 1s exposure time	86 µm^3	C. S.	47.2/25.0
Crocodylus siamensis	MHNL 50001389	DTHE RX Solutions (INSA Lyon)	290 kV, 282 µA, 2240 projections	86 µm^3	B. D.	38.3/21.4

Taxon	Specimen	Scanner	Scan parameters	Voxel size	Worker*	Length/width of skull (cm)
Crocodylus siamensis	UCBL 2019-1-237	GE Phoenix X-Ray GmbH (INSA Lyon)	140 kV, 80 µA, 1500 projections with 1s exposure time	75 μm^3	C. S. & G. P.	34.5/17.6
Crocodylus siamensis	MHNL 50001404	DTHE RX Solutions (INSA Lyon)	290 kV, 320 µA, 2240 projections	102 μm^3	Y. P.	57.0/32.0
Crocodylus sp.	NHMUK PV R 2192	Nikon Metrology XT H 225 ST (NHMUK)	220 kV, 410 µA	90 μm^3	Y. P.	NA
Crocodylus sp.	MNHN-F.1908-5-2	DTHE RX Solutions (INSA Lyon)	290 kV, 319 µA	102 μm^3	G. P. & Y. P.	NA/31.0
Crocodylus sp.	MNHN QV14	GE Phoenix X-Ray GmbH (INSA Lyon)	140 kV, 80 µA	80 μm^3	C. S.	NA/21.6
Gavialis gangeticus	UCBL WB39	GE Phoenix X-Ray GmbH (INSA Lyon)	140 kV, 80 µA	80 μm^3	G. P.	53.9/20.3
Gavialis gangeticus	MHNL 50001406	DTHE RX Solutions (INSA Lyon)	290 kV, 258 µA	80 μm^3	Y. P. & D. C.	56.0/19.5

Taxon	Specimen	Scanner	Scan parameters	Voxel size	Worker*	Length/width of skull (cm)
Gavialis gangeticus	MHNL 50001407	DTHE RX Solutions (INSA Lyon)	290 kV, 319 µA, 2240 projections with 0.167s exposure time	102 μm^3	J. M. & Y. P.	69.7/29.4
Gavialis gangeticus	NHMUK 1846.1.7.3	Nikon Metrology XT H 225 ST (NHMUK)	120 kV, 415 µA	31 μm^3	J. M., Y. P. & D. C.	27.5/6.9
Gavialis gangeticus	NHMUK 1873	Nikon Metrology XT H 225 ST (NHMUK)	200 kV, 650 µA	52 μm^3	G. P., Y. P. & D. C.	45.0/13.4
Gavialis gangeticus	NHMUK 1935.6.4.1	Nikon Metrology XT H 225 ST (NHMUK)	200 kV, 800 µA	90 μm^3	Y. P. & D. C.	61.0/23.0
Mecistops sp.	UM N89	GE Phoenix X-Ray GmbH (INSA Lyon)	140 kV, 80 µA, 1200 projections with 1s exposure time	86 μm^3	Y. P. & G. P.	48.9/21.9
Mecistops sp.	SVSTUA 022001	GE Phoenix X-Ray GmbH (INSA Lyon)	140 kV, 80 µA, 900 projections with 0.667s exposure time	86 μm^3	C. S.	29.5/11.9
Mecistops sp.	AMU Zoo-04721	GE Phoenix X-Ray GmbH (INSA Lyon)	140 kV, 80 µA, 900 projections with 0.667s exposure time	86 μm^3	C. S.	39.4/15.3

Taxon	Specimen	Scanner	Scan parameters	Voxel size	Worker*	Length/width of skull (cm)
Mecistops sp.	MZS Cro083	GE Phoenix X-Ray GmbH (INSA Lyon)	140 kV, 80 µA, 1500 projections with 0.665s exposure time	80 μm^3	J. M., Y. P. & G. P.	35.0/14.3
Mecistops sp.	UCBL LF22	DTHE RX Solutions (INSA Lyon)	280 kV, 244 µA, 2240 projections	45 μm^3	Y. P.	9.6/4.3
Mecistops sp.	NHMUK 1924.5.10.1	Nikon Metrology XT H 225 ST (NHMUK)	200 kV, 800 µA	90 μm^3	Y. P.	61.0/23.3
Mecistops sp.	NHMUK 1907.5.2.11	Nikon Metrology XT H 225 ST (NHMUK)	90 kV, 200 µA	35 μm^3	Y. P. & D. C.	8.0/3.2
Melanosuchus niger	MZS Cro073	GE Phoenix X-Ray GmbH (INSA Lyon)	140 kV, 80 µA, 1500 projections with 0.667s exposure time	87 μm^3	Y. P., D. C. & G. P.	37.8/23.0
Melanosuchus niger	NHMUK 1872.6.4.1	Nikon Metrology XT H 225 ST (NHMUK)	200 kV, 800 µA	47 μm^3	J. M., Y. P. & D. C.	21.1/10.9
Melanosuchus niger	NHMUK 1965.1325-1329	Nikon Metrology XT H 225 ST (NHMUK)	90 kV, 200 µA	36 μm^3	Y. P.	10.0/?

Taxon	Specimen	Scanner	Scan parameters	Voxel size	Worker*	Length/width of skull (cm)
Osteolaemus tetraspis	UCBL 2019-1-236	DTHE RX Solutions (INSA Lyon)	140 kV, 80 µA, 1500 projections with 0.667s exposure time	70 μm^3	G. P.	24.5/15.2
Osteolaemus tetraspis	MZS Cro040	GE Phoenix X-Ray GmbH (INSA Lyon)	120 kV, 120 µA, 1500 projections with 0.5s exposure time	55 μm^3	G. P., N. R., D. C. & Y. P.	19.2/11.5
Osteolaemus tetraspis	NHMUK 1946.1.22.1	Nikon Metrology XT H 225 ST (NHMUK)	90 kV, 200 µA	25 μm^3	Y. P.	7.6/4.4
Osteolaemus tetraspis	NHMUK 1862.6.30.5	Nikon Metrology XT H 225 ST (NHMUK)	200 kV, 800 µA	54 μm^3	Y. P., G. P. & D. C.	23.5/13.6
Paleosuchus trigonatus	MHNL 42003939	DTHE RX Solutions (INSA Lyon)	280 kV, 282 µA, 2240 projections	77 μm^3	Y. P.	16.2/7.5
Paleosuchus trigonatus	MHNL 42006547	DTHE RX Solutions (INSA Lyon)	230 kV, 282 µA, 2240 projections	59 μm^3	Y. P.	10.6/3.4
Paleosuchus trigonatus	MHNL 42006719	DTHE RX Solutions (INSA Lyon)	120 kV, 261 µA, 1600 projections	52 μm^3	Y. P.	11.2/3.9

Taxon	Specimen	Scanner	Scan parameters	Voxel size	Worker*	Length/width of skull (cm)
Paleosuchus trigonatus	MHNL 42000543	DTHE RX Solutions (INSA Lyon)	120 kV, 353 µA	55 μm^3	Y. P.	8.2/3.1
Paleosuchus trigonatus	NHMUK 1866.8.14.212 -215	Nikon Metrology XT H 225 ST (NHMUK)	90 kV, 200 µA	28 μm^3	Y. P.	5.6/3.0
Paleosuchus trigonatus	BMNH 1868.10.8.1	Nikon Metrology XT H 225 ST (NHMUK)	?	68 μm^3	Y. P.	22.0/12.3
Paleosuchus trigonatus	NHMUK 1869.5.21.30	Nikon Metrology XT H 225 ST (NHMUK)	90 kV, 200 µA	76 μm^3	Y. P.	9.7/4.9
Tomistoma schlegelii	UM 1097	RX Solutions EasyTom 150	100 kV, 290 µA, 1440 projections	100 μm^3	C. S. & B. D.	20.7/7.3
Tomistoma schlegelii	NHMUK 1863.10.4.1	Nikon Metrology XT H 225 ST (NHMUK)	90 kV, 200 µA	44 μm^3	Y. P.	9.0/3.2
Tomistoma schlegelii	NHMUK 1893.3.6.14	Nikon Metrology XT H 225 ST (NHMUK)	200 kV, 800 µA	67 μm^3	J. M., D. C. & Y. P.	52.1/17.9

Appendix 7

Taxon	Specimen	Scanner	Scan parameters	Voxel size	Worker*	Length/width of skull (cm)
Tomistoma schlegelii	MZS Cro094	GE Phoenix X-Ray GmbH (INSA Lyon)	140 kV, 80 µA, 1500 projections with 0.665s exposure time	86 µm^3	J. M., D. C. & Y. P.	48.5/17.0
Diplocynodon ratelli	MHNL LA86	GE Phoenix X-Ray GmbH (INSA Lyon)	140 kV, 80 µA	86 µm^3	C. S.	? /14.5
Diplocynodon sp.	UCBL-FSL 531244-45	GE Phoenix X-Ray GmbH (INSA Lyon)	140 kV, 80 µA	40/86 µm^3	G. P. & Y. P.	NA
Voay robustus	NHMUK 36684	Nikon Metrology XT H 225 ST (NHMUK)	180 kV, 467 µA	90 µm^3	G. P.	38.0/23.3
Voay robustus	NHMUK 36685	Nikon Metrology XT H 225 ST (NHMUK)	180 kV, 889 µA	90 µm^3	G. P.	39.0/23.0
Voay robustus	NHMUK PV R 2204	Nikon Metrology XT H 225 ST (NHMUK)	210 kV, 315 µA	81 µm^3	Y. P. & G. P.	NA/26.0

Taxon	Specimen	Scanner	Scan parameters	Voxel size	Worker*	Length/width of skull (cm)
Arambourgia gaudryi	MNHN QU17155	GE Phoenix X-Ray GmbH (INSA Lyon)	140 kV, 80 µA	42 µm^3	C. S. & D. C.	10.7/5.8
Allodaposuchus precedens	MMS/VBN-12-10	DTHE RX Solutions (INSA Lyon)	145 kV, 448 µA	100 µm^3	Y. P.	NA
Atoposauridae?	CHE 02.15	DTHE RX Solutions (INSA Lyon)	291 kV, 291 µA & 290 kV, 58 µA	90 & 18 µm^3	Y. P.	NA/4.0
Varanosuchus sakonnakhonensis	SM2021-1-097	DTHE RX Solutions (INSA Lyon)	290 kV, 131 µA; 290 kV, 93 µA; 220 kV, 129 µA & 200 kV, 350 µA	40; 30; 30 & 80 µm^3	Y. P., N. R. & J. R.	17.1/12.0
Varanosuchus sakonnakhonensis	SM2021-1-098	DTHE RX Solutions (INSA Lyon)	290 kV, 197 µA	60 µm^3	Y. P. & J. R.	NA
Varanosuchus sakonnakhonensis	SM2021-1-100	DTHE RX Solutions (INSA Lyon)	290 kV, 197 µA	60 µm^3	Y. P.	NA
Varanosuchus sakonnakhonensis	SM2021-1-101	DTHE RX Solutions (INSA Lyon)	290 kV, 291 µA	90 µm^3	Y. P.	NA

Taxon	Specimen	Scanner	Scan parameters	Voxel size	Worker*	Length/width of skull (cm)
Hylaeochampsa vectiana	NHMUK PV R 177	Nikon Metrology XT H 225 ST (NHMUK)	?	48 μm^3	Y. P.	NA
Pholidosaurus laevi	NHMUK PV R 3414	Nikon Metrology XT H 225 ST (NHMUK)	?	90 μm^3	Y. P.	NA/?
Pholidosaurus sp.	CHE 112.3	DTHE RX Solutions (INSA Lyon)	290 kV, 291 µA	90 μm^3	Y. P.	NA/17.8
Rhabdognathus sp.	MNHN TGE 3859	GE Phoenix X-Ray GmbH (INSA Lyon)	?	75 μm^3	J. M. & G. P.	?
‘ *Metriorhynchus* ’ *brachyrhynchus*	MPV 2010.3.61U	GE Phoenix X-Ray GmbH (INSA Lyon)	140 kV, 80 µA	85 μm^3	G. P.	NA
Steneosaurus jugleri	SCR010-312	GE Phoenix X-Ray GmbH (INSA Lyon)	140 kV, 80 µA	50 & 86 μm^3	B. D.	?

Appendix 7

Taxon	Specimen	Scanner	Scan parameters	Voxel size	Worker*	Length/width of skull (cm)
Steneosaurus cf. *bouchardi*	SCR010-374	GE Phoenix X-Ray GmbH (INSA Lyon)	140 kV, 80 µA	86 µm^3	B. D.	?
Steneosaurus sp.	TCH006-1255	GE Phoenix X-Ray GmbH (INSA Lyon)	140 kV, 80 µA	50 & 86 µm^3	B. D.	?
Hamadasuchus rebouli	MDE C001	DTHE RX Solutions (INSA Lyon)	280 kV, 225 µA	40 µm^3	Y. P.	?
Hamadasuchus sp.	UCBL-FSL 532408	GE Phoenix X-Ray GmbH (INSA Lyon) & DTHE RX Solutions (INSA Lyon)	140 kV, 80 µA & 280 kV, 169 µA	86 & 30 µm^3	Y. P., C. S. & N. R.	32.5/18.0
Zulmasuchus querejazus	MHNC 6672	GE Phoenix X-Ray GmbH (INSA Lyon)	150 kV, 80 µA	30 & 75 µm^3	Y. P.	NA

*people who have taken part in the segmentation (all from Université Lyon 1): Benjamin Dailh (B. D.), Céline Salaviale (C. S.), Davide Conedera (D. C.), Gwendal Perrichon (G. P.), Jeremy Martin (J. M.), Jeanne Rolland (J. R.), Nicolas Rinder (N. R.) & Yohan Pochat-Cottilloux (Y. P.)

Appendix 8: List of other specimens used in this thesis, obtained from collaborations / open data

Taxon	Specimen	Provider / reference	Voxel size	Worker*	Length/width of skull (cm)
Alligator mississippiensis	OUVC 9761	Lawrence Witmer (Ohio University)	500 μm^3	Y. P. & G. P.	30.4/15.5
Alligator mississippiensis	OUVC 10606	Lawrence Witmer (Ohio University)	45 μm^3	Y. P. & G. P.	2.9/1.6
Alligator mississippiensis	OUVC 11415	Lawrence Witmer (Ohio University)	49 μm^3	Y. P. & G. P.	9.5/4.9
Alligator mississippiensis	TMM M-983	Timothy Rowe (University of Texas)	250 μm^3	Y. P. & G. P.	17.5/9.6
Alligator mississippiensis	SMNK-REP 164	Irena Raselli (Jurassica Museum)	29 μm^3	Y. P. & G. P.	3.7/2.0
Alligator mississippiensis	SMNK-REP 308	Irena Raselli (Jurassica Museum)	79 μm^3	B. D. & Y. P.	12.3/6.6
Alligator mississippiensis	SMNK-REP 309	Irena Raselli (Jurassica Museum)	79 μm^3	B. D. & Y. P.	11.0/6.0
Alligator mississippiensis	SMNK-REP 311	Irena Raselli (Jurassica Museum)	79 μm^3	B. D. & Y. P.	8.6/4.7
Caiman crocodilus	UMMZ herps 46112	Cody Thompson (University of Michigan)	121 μm^3	C. S. & G. P.	18.1/11.0
Caiman crocodilus	UMMZ herps 128024	Cody Thompson (University of Michigan)	121 μm^3	G. P. & D. C.	21.9/14.5

Taxon	Specimen	Provider / reference	Voxel size	Worker*	Length/width of skull (cm)
Caiman crocodilus	UMMZ herps 155282	Cody Thompson (University of Michigan)	68 μm^3	G. P.	10.1/5.8
Caiman latirostris	UMMZ herps 155283	Cody Thompson (University of Michigan)	90 μm^3	G. P.	13.4/8.5
Caiman latirostris	UMMZ herps 155284	Cody Thompson (University of Michigan)	48 μm^3	C. S. & D. C.	7.6/4.6
Caiman latirostris	UMMZ herps 155285	Cody Thompson (University of Michigan)	66 μm^3	C. S. & D. C.	10.1/6.2
Caiman latirostris	UMMZ herps 155286	Cody Thompson (University of Michigan)	109 μm^3	C. S. & D. C.	15.7/9.6
Caiman latirostris	UMMZ herps 155287	Cody Thompson (University of Michigan)	104 μm^3	C. S., G. P. & D. C.	21.8/14.9
Caiman latirostris	UMMZ herps 155288	Cody Thompson (University of Michigan)	100 μm^3	C. S. & D. C.	15.3/9.2
Caiman latirostris	SMNK-REP 314	Irena Raselli (Jurassica Museum)	29 μm^3	G. P. & Y. P.	3.1/1.9
Caiman latirostris	SMNK-REP 315	Irena Raselli (Jurassica Museum)	29 μm^3	G. P. & Y. P.	3.2/2.0
Caiman latirostris	SMNK-REP 316	Irena Raselli (Jurassica Museum)	29 μm^3	G. P., Y. P. & D. C.	3.0/2.0

Taxon	Specimen	Provider / reference	Voxel size	Worker*	Length/width of skull (cm)
Caiman latirostris	SMNK-REP 317	Irena Raselli (Jurassica Museum)	29 μm^3	G. P. & Y. P.	3.2/2.0
Caiman yacare	UMMZ herps 155289	Cody Thompson (University of Michigan)	121 μm^3	C. S. & D. C.	30.1/18.8
Crocodylus halli	UF herp 145927	David Blackburn (University of Florida)	112 μm^3	G. P.	28.4/17.4
Crocodylus johnstoni	OUVC 10425	Mario Bronzati (Universidade de São Paulo)	?	M. B.	?
Crocodylus moreletii	TMM M4980	Mario Bronzati (Universidade de São Paulo)	?	M. B.	?
Crocodylus porosus	OUVC 10899	Lawrence Witmer (Ohio University)	47μm^3	Y. P.	9.0/3.5
Gavialis gangeticus	UF herp 118998	David Blackburn (University of Florida)	147 μm^3	G. P.	51.7/18.9
Gavialis gangeticus	YPM herr 008438	Jessie Maisano (University of Texas)	25 μm^3	G. P.	8.2/4.2
Osteolaemus tetraspis	FMNH 98936	Jessie Maisano (University of Texas)	55 μm^3	C. S.	7.8/5.1
Tomistoma schlegelii	FMNH 98874	Jessie Maisano (University of Texas)	65 μm^3	C. S.	13.5/5.6

Taxon	Specimen	Provider / reference	Voxel size	Worker*	Length/width of skull (cm)
Tomistoma schlegelii	TMM M6342	Christopher Brochu (University of Iowa)	165 µm^3	Y. P. & G. P.	33.6/14.3
Voay robustus	MNHN-F.1908-5	Romain David (MNHN)	133 µm^3	G. P.	NA/29.1
Diplocynodon ratelli	MNHN-F-SG 557	Romain David (MNHN)	118 µm^3	G. P.	NA
Trilophosuchus rackhami	QMF16856	Jorgo Ristevski (University of Queensland)	51 µm^3	J. R.	? /6.9
Portugalosuchus azenhae	ML1818	Eduardo Puértolas-Pascual (Universidad de Zaragoza)	110 µm^3	E. P.	?/?
Dyrosaurus phosphaticus	MNHN-ALG1	Romain David (MNHN)	133 µm^3	G. P.	?
Thalattosuchus superciliosus	MNHN RJN 256	Romain David (MNHN)	104 µm^3	G. P;	NA
‘ *Steneosaurus*’ *bollensis*	BSPG 1984 I258	Julia Schwab (University of Manchester)	43 µm^3	Y. H.	NA
Cricosaurus araucanensis	MLP 72-IV-7-1	Julia Schwab (University of Manchester)	448 µm^3	Y. H.	NA
‘ *Metriorhynchus* cf. *brachyrhynchus*	NHMUK PV OR 32618	Julia Schwab (University of Manchester)	55 µm^3	J. S.	NA

Appendix 8

Taxon	Specimen	Provider / reference	Voxel size	Worker*	Length/width of skull (cm)
Macrospondylus bollensis	MCZA VPRA-1063	Christina Byrd (Museum of Comparative Zoology of Cambridge)	500 µm^3	E. W.	? /28.2
Aphaurosuchus escharafacies	LPRP 0697	Gustavo Darlim (Universidade de São Paulo)	500 µm^3	Y. P.	34.4/21.9
Mariliasuchus amarali	MZSP-PV50	Hussam Zaher (Universidade São Paulo)	69 µm^3	Y. P. & N. R.	10.8/8.4
Mariliasuchus amarali	MZSP-PV51	Hussam Zaher (Universidade São Paulo)	59 µm^3	Y. P. & N. R.	9.8/7.1
Protosuchus haughtoni	BP/1/4746	Mario Bronzati (Universidade de São Paulo)	?	M. B.	?
Junggarsuchus sloani	IVPP 14010	Julia Schwab (University of Manchester)	130 µm^3	J. S.	14.4/NA
Eopneumatosuchus colberti	MNA V2460	Keegan Melstrom (NHMLA)	97 µm^3	A. H.	12.0/NA

*people who have taken part in the segmentation: A. H. (Alan Turner, Stony Brook University), Benjamin Dailh (B. D., Université Lyon 1), Céline Salaviale (C. S., Université Lyon 1), Davide Conedera (D. C., Université Lyon 1), Eduardo Puértolas-Pascual (E. D.; Universidad de Zaragoza), Eric Wilberg (E. W., Stony Brook University), Gwendal Perrichon (G. P., Université Lyon 1), Jorgo Ristevski (J. R.; University of Queensland), J. S. (Julia Schwab, University of Manchester), M. B. (Mario Bronzati, Universidade de São Paulo), Y. H. (Yanina Herrera, Universidad Nacional de La Plata) & Yohan Pochat-Cottilloux (Y. P., Université Lyon 1)

Appendix 9: Supplementary Material concerning the publication 'The neuroanatomy and pneumaticity of *Hamadasuchus* (Crocodylomorpha, Peirosauridae) from the Cretaceous of Morocco and its paleoecological significance for altirostral forms'

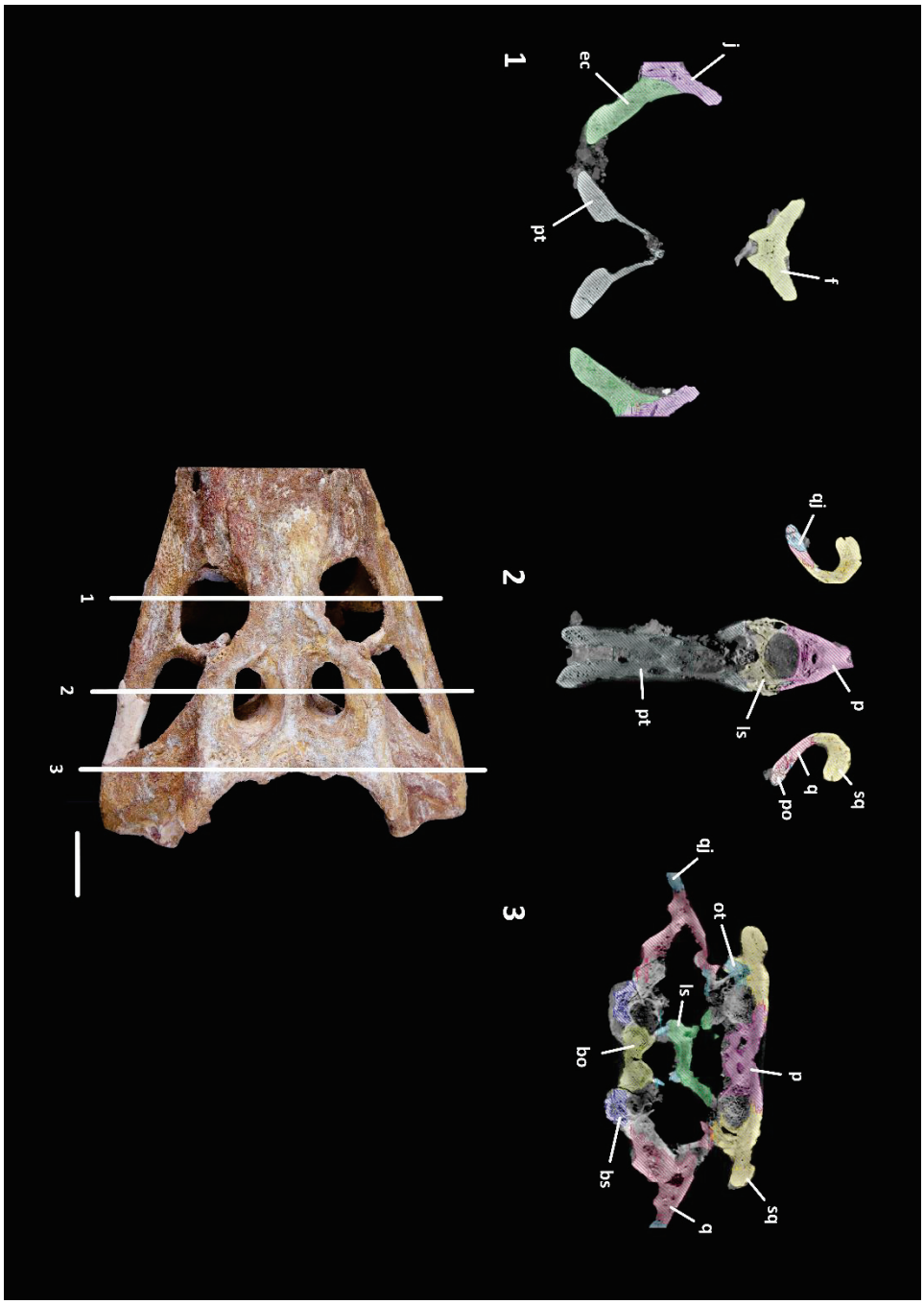

Supplementary Material S1: Figure showing transverse slices at different anteroposterior positions throughout the skull of *Hamadasuchus* (UCBL-FSL 532408). bo: basioccipital, bs: basisphenoid, ec: ectopterygoid, f: frontal, j: jugal, ls: laterosphenoid, ot: otoccipital, p: parietal, po: postorbital, pt: pterygoid, q: quadrate, qj: quadratojugal, sq: squamosal. Scale bar is 5 cm.

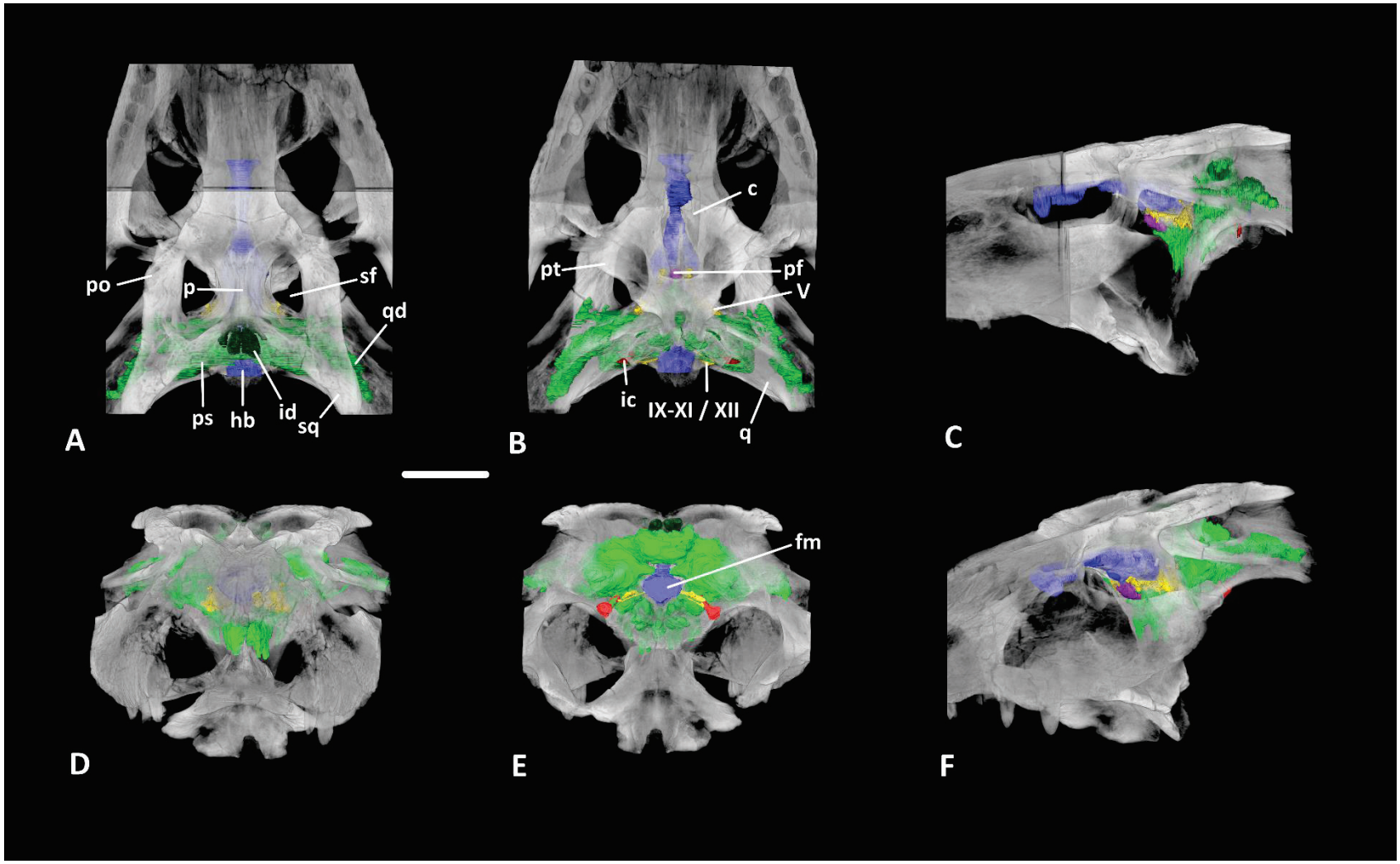

Supplementary Material S2: Figure showing three-dimensional reconstructions of the segmented parts of the skull of *Hamadasuchus* (UCBL-FSL 532408) with the skull rendered semi-transparent in dorsal (A), ventral (B), lateral (C), anterior (D), posterior (E) and anterior ¾ (F) views. V: cranial nerve V, IX-XI / XII: cranial nerve IX-XI and/or XII, fm: foramen magnum, hb: hindbrain, ic: internal carotid artery, id: intertympanic diverticulum, p: parietal, pf: pituitary fossa, po: postorbital, ps: pharyngotympanic sinus, pt: pterygoid, q: quadrate, qd: quadrate diverticulum, sf: supratemporal fenestra, sq: squamosal. Scale bar is 5 cm.

Appendix 10: Supplementary Material concerning the publication 'A survey of osteoderm histology and ornamentation among Crocodylomorpha: a new proxy to infer lifestyle?'

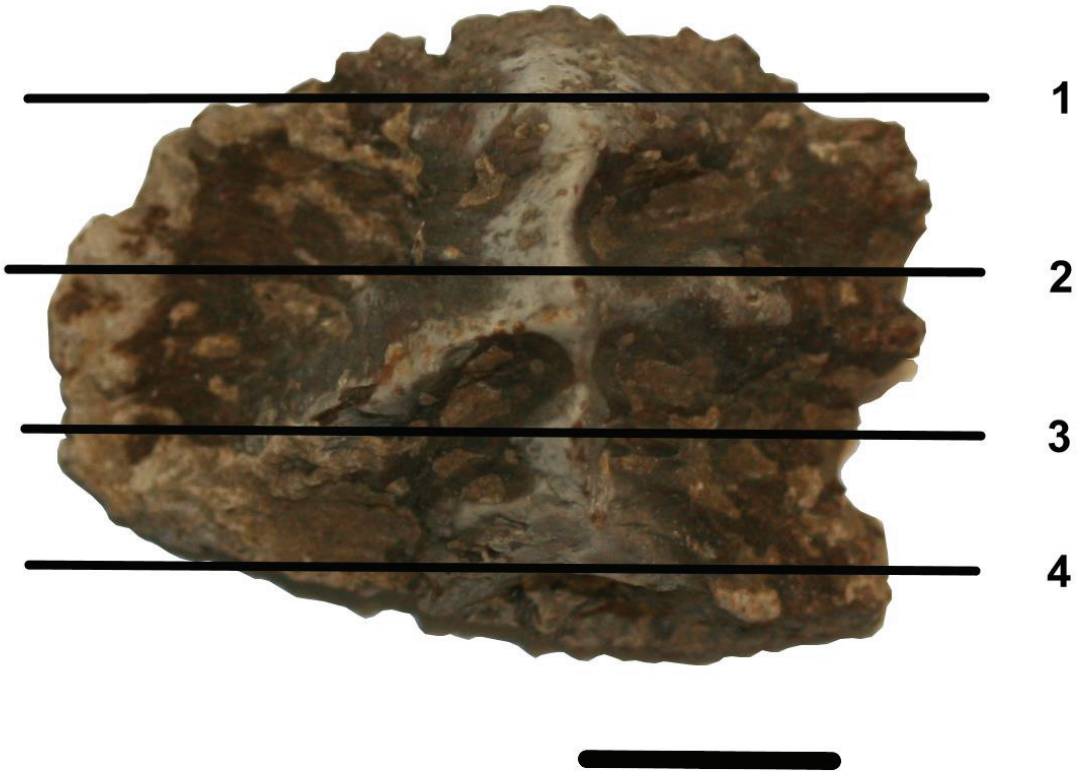

Supplementary Material S1: Four thin sections made from the osteoderm of *Iberosuchus* (UCBL-FSL 530948-90080 in dorsal view). Scale bar is 1 cm.